Per Thomas Moe

Pressure and Strain Measurement During Hot Extrusion of Aluminium

Volume I
An Overview of the Work and Articles

Trondheim, March 2005

Doctoral thesis for the degree of doktor ingeniør

Norwegian University of Science and Technology
Faculty of Engineering Science and Technology
Department of Engineering Design and Materials

NTNU

This thesis has been submitted to the Norwegian University of Science and Technology, Department of Engineering Design and Materials in partial fulfilment of the requirements for the Norwegian academic degree Doktor Ingeniør

Pressure and Strain Measurement During Hot Extrusion of Aluminium, Volume I
Trykk- og Tøyningsmåling ved Varmekstrudering av Aluminium, Bind I

Institutt for Produktutvikling og Materialer (IPM)
Norges Teknisk-Naturvitenskapelige Universitet (NTNU)

Doktor ingeniøravhandling (PhD thesis) 2005:50

ISBN 82-471-6967-3 (elektronisk/electronic)
ISBN 82-471-6968-1 (trykt/printed)

ISSN 1503-8181

To the memory of my father

Preface

This thesis is the result of an almost six year long study of aluminium extrusion and of various measurement techniques that can be used to gather information about the process. The work has been most interesting, but also very demanding. It could not have been carried out without the financial, professional, technological and moral support of a great number of contributors. Considerable economic resources have been provided by many divisions of Hydro Aluminium and the Norwegian Research Council through various research programmes. Funding provided by AMR Engineering AS has allowed me to improve my physical understanding in general and, therefore, also to establish models of various aspects of the extrusion process and sensor behaviour.

During most of my work with this thesis I have been employed by the Department of Engineering Design and Materials (formerly the Department of Machine Design and Materials Technology) at the Norwegian University of Science and Technology and enjoyed the full professional support of the metal forming group of the department and of SINTEF Materials and Chemistry (formerly SINTEF Materials Technology). My main supervisor, Prof. Sigurd Støren has been a most inspiring and visionary guide into the world of extrusion technology. His ingenuity has been a most valuable asset. He has initiated the sensor development process and has also shown great skill in finding the economic resources that have allowed the work to be completed. Prof. Ola Hunderi has been a most useful co-supervisor and helped me to better understand various aspects of measurement technology. Arnfinn Willa-Hansen, Hans Iver Lange and Robert Flatval of SINTEF Materials and Chemistry have provided invaluable assistance in the sensor development process and during experiments. Most of the technological advances have been the results of rewarding teamwork. Dr. Martin Lefstad and Dr. Shahriar Abtahi have been my mentors in the field of extrusion technology, while Prof. Henry Valberg introduced me to the technology of metal forming. The tool shops of the Department of Engineering Design and Materials and VerkstedPartner AS have skilfully manufactured complex tools that professional tool designers and tool manufacturers did not even dare to think of. Much of the later experimental activity and numerical study has been performed in close cooperation with Wojciech Wajda, and it has been a great pleasure for me to learn from our common work. I am most grateful that he has taken the time to teach me numerical modelling as well as Polish technical and everyday language.

Capacitec, Inc. has produced high-temperature capacitive displacement sensors of the best quality and provided customer support-services that have been very satisfactory. The Sounding Board of my study, consisting mainly of Hydro and SINTEF employees, has given me very valuable feedback. I am particularly indebted to Sigurd Rystad for arranging a most fruitful stay at the Hydro Raufoss Automotive extrusion plant in the early parts of the study. It gave me a clear understanding of some of the problems facing my industrial partners, and therefore created the necessary motivation for my work. I am also grateful that the director of Centre de Mise en Forme des Matériaux (CEMEF) at Ecole Nationale Supérieure des Mines de Paris, Prof. Jean-Loup Chenot, granted me an eight-month stay at the institution. The courses of the master and doctoral studies at

CEMEF that I followed introduced me not only to the physics and numerics of material forming, but also to French everyday and technical language. Prof. Maciej Pietrzyk of Akademia Górniczo Hutnicza in Kraków both reviewed and helped me in writing some of my articles and papers. I am thankful that he and other organizers of the 5th, 6th, 7th and 8th ESAFORM conferences as well as the 12th ICEM and Metal Forming 2004 conferences have both reviewed and accepted all our papers. I found it most inspiring to be invited to write extended articles for the International Journal of Material Forming Processes based on our contributions to the 5th ESAFORM conference. I would like to thank Prof. Wojciech Misiołek of Lehigh University who skilfully chaired the extrusion sessions at the ESAFORM conferences, and with whom I had very useful discussions. In the final phase of my study a scholarship from the Norwegian Research Council has allowed me to relate my work to the demands of the extrusion industry and to establish a first business plan draft. The scholarship was granted in relation to a competition arranged by the leader of the NTNU Entrepreneurship Center, Professor Sigmund J. Waagø. I thank the organizers and the panel of judges of the competition, who found our contribution worthy of the second prize. The fact that professional investors have taken an interest in our work and ideas has been very inspiring. I am also indebted to Nancy Bazilchuk. She has very effectively read most my thesis and made me aware of many of the grave grammatical errors that I have committed.

I would like to thank my mother, Helle Moe (siv. ing.), for the help she has offered. She has read the entire thesis and given me the most valuable feedback. She has also made it possible for me to focus on the work in the final part of the study. Furthermore, I simply cannot overestimate the professional help given to me by my father, Dr. Per Harald Moe, both before and during my PhD work. His excellent research and development work in the fields of forge welding and drilling over the last twenty years has been a constant source of inspiration. He has time and again shown how to skilfully combine creativity and critical analysis. His optimism and enthusiasm are to my mind the natural prerequisites for invention. It is most unfortunate that he was not able to experience the completion of my study of material mechanics/physics and measurement technology whose initiation he certainly contributed to almost twenty years ago. He lost a long and difficult battle against the cancer in March 2002. He never surrendered and never stopped inventing and planning ahead. My sole consolation has been that his many contributions to science and technology will never be lost.

Finally, I would like to thank all the members of my family for the moral support they have so generously offered me, for it was often needed. My wife Hanna deserves the greatest recognition. She has been the best possible partner both in life and work over the last nine years. She possesses a unique intellect as well as the noblest of personal qualities. She has given birth to and has cared for our child Julia Helene whose smile is sufficient to light up any dark day.

Per Thomas Moe

Table of Contents

VOLUME I: AN OVERVIEW OF THE WORK AND ARTICLES

PREFACE ..... **V**

ABSTRACT ..... **IX**

CHAPTER 1 INTRODUCTION **1**

CHAPTER 2 ALUMINIUM EXTRUSION TECHNOLOGY **3**

2.1 BACKGROUND 3
2.2 PRINCIPLES AND TERMINOLOGY 6
2.3 THE PHYSICS OF METAL FLOW 12
2.4 THE BASIC ASSUMPTIONS OF EXTRUSION MODELLING 17
2.5 CHALLENGES AND EXTRUSION RESEARCH 25

CHAPTER 3 THE OBJECTIVES OF THE STUDY **35**

3.1 THE TASK DESCRIPTION 35
3.2 COMMENTS ON THE MOTIVATION FOR THE STUDY 37
3.3 COMMENTS ON THE OBJECTIVES AND LIMITATIONS OF THE STUDY 43

CHAPTER 4 TRACTION MEASUREMENT TECHNOLOGY **47**

4.1 ON THE PRINCIPLES OF DISPLACEMENT MEASUREMENT 49
4.2 ON THE DESIGN OF TRACTION SENSORS FOR METAL FORMING 60
4.3 PIN SENSOR DESIGNS AND TRACTION MEASUREMENT DURING ROLLING 65
4.4 THE STATE OF TRACTION MEASUREMENT IN ALUMINIUM EXTRUSION 68

CHAPTER 5 AN OVERVIEW OF THE WORK **73**

5.1 ON THE PRESENTATION OF RESULTS 73
5.2 HIGH TEMPERATURE TESTING 77
5.3 COMPRESSION TESTING 80
5.4 LABORATORY ROD EXTRUSION EXPERIMENTS 87
5.5 LABORATORY SPLIT TUBE (PIPE) EXTRUSION 97
5.6 LABORATORY THIN-STRIP EXTRUSION 101
5.7 INDUSTRIAL U-PROFILE EXTRUSION 106

CHAPTER 6 GENERAL CONCLUSIONS AND FUTURE WORK **113**

6.1 THE MAIN CONCLUSIONS 113
6.2 FUTURE WORK 115

BIBLIOGRAPHY **117**

APPENDICES **135**

VOLUME II: A COMPREHENSIVE REPORT ON THE SECOND SET OF ROD EXTRUSION EXPERIMENTS

VOLUME I: LIST OF APPENDICES

COMMENTS

APPENDIX A:

A Technique for Measuring Pressure on the Die Face during Extrusion

APPENDIX B:

Thin Strip Aluminium Extrusion – Pressure, Temperature and Deflection Recordings of the Extrusion Die

APPENDIX C:

Experiments with Die Deflection during Hot Extrusion of Hollow Profiles

APPENDIX D:

A Study of the Limits of Self-Stabilization during Extrusion of Thin Strips

APPENDIX E:

Measurement of Temperature and Die Face Pressure during Hot Extrusion of Aluminium

APPENDIX F:

An Evaluation of Material Behaviour during Extrusion of AA6060 Rods

APPENDIX G:

An Analysis of Forge Welding of Steel Rods

APPENDIX H:

An Approach for Evaluating Constitutive Models for Hot Aluminium Extrusion – Rod Extrusion of AA6060 as a Case Study

APPENDIX I:

A Study of the Thermomechanical Response of a Die Face Pressure Sensor for Hot Aluminium Extrusion

APPENDIX J:

Visions of a System for Shape Control during Thin Strip Aluminium Extrusion

APPENDIX K:

Measurement of Temperature and Pressure during Thin Strip Extrusion

APPENDIX L:

An Experimental and Numerical Study of Induction Heating of Billets

APPENDIX M:

Abstract: An Evaluation of Errors in Extrusion Modelling and Experiments

Abstract

The aluminium extrusion process is based on simple principles, but allows profiles with the most complex cross-sectional shapes to be produced at a very high rate. One of the greatest challenges of aluminium extrusion is to control material flow and dimensional variability of thin-walled high-strength profiles, for which the demand is growing. The die outlet geometry and the temperatures of the billet and tools must be carefully tuned in order to secure satisfactory material flow conditions. Due to the high pressures in the container, the deformation of the extrusion dies and the distortion of the die outlet may be significant and must be compensated for. The thermal conditions in the extrusion press must also be controlled. Even in the age of numerical modelling much trial and error is needed to make certain that the product satisfies the customer requirements. If simple and effective process control could be implemented, the cost and dimensional variability of extruded profiles could be significantly reduced. This would not only secure the continued use of extruded profiles in old markets but also open new ones.

The main objective of this study has been to establish useful and simple methods for measuring the pressure at the interface between the die and the billet and the deformation of the die during hot extrusion of aluminium. Pressure measurement data may be used to establish a better understanding of the extrusion process and to carefully evaluate the many numerical extrusion models that are presently being developed and refined for the purpose of predicting profile shape and properties. A most important task is the evaluation of constitutive models used to describe bulk material and friction behaviour. The requirements for such models should be viewed in relation to common flow instability phenomena such as buckling. Sensors may in the future be integrated in intelligent extrusion dies in order to make certain that temperature and flow condition changes are as small as possible and to prevent overloading of extrusion dies during production. It is of the utmost importance that dimensional variability is detected early.

This study has consisted of many parts. The first step was a careful evaluation of sensor designs using the Capacitec HPC-75 high-temperature capacitive displacement probes and the Capacitec 4004 amplifier series. The feasibility of high- and low-temperature pressure measurement was demonstrated through various types of compression testing. The capacitive sensors were repeatedly tested in a hot air furnace to 650 ºC, and results were satisfactory for all but one of the sensors. The sensor sensitivity to temperature changes that occur during extrusion is usually less than 10 % of the full sensor response.

The pressure sensors have been repeatedly tested in several dies for aluminium rod extrusion. The feasibility of, and a method for, performing useful measurements in the high-temperature extrusion environment have been demonstrated. The measurement accuracy is better than ± 10 % of full scale of 200 MPa when the effects of temperature changes are compensated for. The measurement repeatability is of a similar magnitude for genuinely replicated measurements. The measurement resolution is better than 1 %. It is firmly believed that the measurement and calibration technology may be further improved, and that the measurement accuracy may be better than 5 % of full scale.

Rod extrusion experiments allowed the quality of the finite element modelling approach to be evaluated. The code ALMA2π was used, and material data of the Zener-Hollomon flow rule have been obtained by compression testing. Simulated and measured results of the ram force, die face pressure and liner force generally differed less than 10 %. The estimated die outlet temperature change was systematically 10 ºC too high. As there are significant differences between extrusion and compression testing, the use of material data from compression testing amounts to an extrapolation of data. Experiments did not demonstrate that the approach is unacceptable, but plots showing the deviation between experimental and estimated ram force and outlet temperature data indicated that there are a number of parameter combinations that are equally good as or even better than those obtained through compression testing. Very high accuracy determination of flow parameters may be difficult. Measurement errors significantly complicate matters.

The pressure sensors may be used to study practical extrusion problems and to establish a better understanding of metal flow and the significance of die deformation. Thin strip extrusion experiments were performed to gain insight into the thermo-mechanics of flow instability (buckling). The feasibility of performing pressure measurement during the extrusion of thin strips was demonstrated, but sensors were not properly calibrated. The first round of the experiments was run with a die outlet 78.5 mm wide and 1.7 mm thick, and a container diameter of 100 mm. During extrusion of AA6060 flow instability phenomena were not encountered. A second round of experiments was performed with non-instrumented dies and somewhat thinner profiles (1.1 and 1.4 mm). Flow instability in the form of buckling was provoked for high outlet temperatures, and many replicate experiments were performed. The shape of the buckled thin strip was also measured continuously with a laser triangulation technique during extrusion at high speed. Due to limitations related to the experimental set-up, neither the resolution nor the accuracy of the approach was entirely satisfactory. Nonetheless, the feasibility of the approach was demonstrated, and it is quite possible to improve the measurement technique.

Capacitive pressure measurement techniques have been combined with methods for measuring the deformation of the mandrel and the straining of the bridges to study the behaviour of dies during tube extrusion. Capacitec capacitive probes were used to measure bridge strains. High temperature Kyowa strain gauges were also used for the same purpose. The die mandrel deflection was measured by conventional displacement transducers connected to the mandrel and the die cap by rods. Only measurements by the capacitive sensors proved sufficiently reliable during measurements. The study revealed that the state of stress in dies for hollow profiles may be very close to critical. The die face pressure at the top face of the mandrel exceeded 500 MPa.

Two rounds of industrial experiments were performed with a U-profile that proved most difficult to extrude. In the first round of experiments, the flow stability was not satisfactory, and plugging of the outlet ruined experiments. The second round was more successful, and sensors were used to record the die face pressure on-line. The experiments demonstrated the feasibility of industrial experiments, but clearly indicated that further development of the sensors should be performed. It is important that sensors are made more durable, and that calibration techniques are further developed. Practical die designs that allow simple integration of sensors in the press should be developed.

Chapter 1

Introduction

The ancient Greek philosopher Aristotle defined all objects in nature by their shape and composition. While different groups of objects may be distinguished by their common geometry, single members of a group are recognised by the matter of which they are composed. This ancient discussion of matter is outdated and will not be pursued here, but Aristotle's views on geometry have certain relevance for the subject this thesis, the application of measurement techniques for displacement and pressure in hot aluminium extrusion. No other forming process matches the ability of extrusion to produce long profiles with the most complex thin-walled cross-sectional shapes. Hence, extruded profiles do constitute an easily recognisable group of objects in an Aristotelian sense. However, while their special shapes make profiles very useful for a large range of applications, geometry or rather the failure to meet requirements for shape variability, is a major concern for those seeking a more widespread use of aluminium profiles in the important automotive market, as one important example. Extrusion is based on a simple and intuitive principle, and serious problems related to dimensional variability are not necessarily apparent at first glance. Yet, the dimensions of extruded products may vary by more than a tenth of a millimetre both with regard to thickness and shape distortion. This seriously complicates or even prevents cost-effective mass production of complex structures consisting of processed aluminium profiles.

Excessive dimensional variability is a challenge extrusion probably has in common with most manufacturing processes. New inventions, however spectacular they may appear, are seldom immune to improvement. As new applications and tighter requirements for product quality emerge, process development may prove necessary. Mass production, in particular, is utterly reliant on a well-developed understanding of the main mechanisms of the process as well as a technology for measuring and controlling essential parameters. While two pieces are never equal, they may be made interchangeable for all practical purposes if they are produced within sufficiently narrow tolerances. Today, most developed and efficient processes do have some systems of on-line control of essential parameters. Metal rolling and subsequent sheet metal forming processes, for example, may produce the most complex products within a micrometre tolerance thanks to careful modelling and the successful employment of closed loop control systems. With the enticing perspective of gaining a larger share of the automotive market, aluminium profile producers seek to implement tighter control through more extensive modelling and measurement. The work presented here should be seen in relation to the

more general research objectives of the employer Hydro Aluminium Extrusion, which are to reduce dimensional variability by a factor of ten and to increase the tool lifetime.

The objective of this thesis is to convey results from a study where attempts have been made to measure the pressure at the face of extrusion dies as well as the resulting strains and die deflections. A high-temperature capacitive pressure sensor has been used for most purposes, but other measurement techniques were also tested. Although one of the main reasons for developing a sensor system is to provide valuable new information about the physics of metal flow, no new hypothesis or model has been proposed. The focus has rather been on the characterisation of the sensor behaviour as well as on the design of experiments performed in order to study the feasibility of measurement and the capabilities of sensor systems (accuracy, resolution, repeatability etc). This includes a discussion of methods of calibration and temperature correction. Rod extrusion was chosen as a main test case, since it may most easily and accurately be modelled. Results from experiments have earlier been presented at 5th and 7th ESAFORM conferences [Moe02] [Waj04] and at the Metal Forming 2004 conference [Moe04b] [Moe04c]. Within the framework of three research programmes funded by the Norwegian Research Council, the candidate has cooperated closely with both SINTEF Materials Technology and Hydro Aluminium Extrusion in order to implement measurement technology for a range of applications of interest to the employer. Financial support was found in the PROSMAT-programme for an experimental and numerical study of the loading and responses of a hollow profile bridge die. The objective was to facilitate later estimation of die lifetime and dimensional variability of profiles. The most important results have been presented at the 6th ESAFORM conference [Moe03a]. A study of the instability of metal flow during thin-strip extrusion was supported by the COMPFORM-programme and has been performed in cooperation with Wojciech Wajda. Presentations of some of the experimental and numerical results have been given at the 5th, 6th and 8th ESAFORM conferences [Lef02] [Waj03] [Waj05a], at the 12th ICEM conference [Moe04d] and in the International Journal of Forming Processes [Moe03b]. Finally, within the framework of the Hydro supported FREMAT-programme, two rounds of industrial experiments were performed at Hydro Aluminium Extrusion plant at Raufoss, Norway.

The thesis consists of two volumes. Volume I contains an introductory overview of the work as well as 12 conference papers and journal articles that describe the various parts of the experimental study and numerical analysis of data. Volume II includes a more comprehensive description of experiments and results from the study of rod extrusion. It has been added to simplify an evaluation of the pressure measurement techniques. Volume I commences with a description of the extrusion process and a more complete discussion of some of the relevant challenges and research objectives (Ch. 2). The scope of and some of the limitations of the current work are the subject of a closer focus (Ch. 3). An overview of relevant measurement techniques and sensor designs has also been provided (Ch. 4). The next chapter (Ch. 5) presents a more detailed outline of the work and the main conclusions from the various parts. Finally, general conclusions and suggestions for further work are provided (Ch. 6). The conference papers and articles have been added in the appendices. Reference [Stø03] is the product of an early self-study of aluminium extrusion under the guidance of Professor Sigurd Støren. It may serve as a more comprehensive and alternative introduction to the subject.

Chapter 2

Aluminium extrusion technology

Extruded aluminium profiles may today be found in a very large number of common products. They are, for example, widely used in the fields of construction and transport. The terms aluminium and extrusion are so closely related that those who work with metal forming, rarely pay attention to the fact that aluminium extrusion is a compound expression that was given a clear meaning only about 100 years ago. Hot aluminium extrusion is today regarded as a mature manufacturing process. It is based on relatively simple principles, but still suffers from a number of shortcomings. When deficiencies make themselves apparent in either the efficiency of the process or the quality of the product, they may have large economic implications, which in turn create an impetus for improvement. This section presents the background and principles for hot extrusion of aluminium, as well as some of the main challenges facing those who are seeking to increase their physical insight into the process and impose better process control. More complete descriptions of the aluminium extrusion process have been provided by Laue and Stenger [Lau81], Saha [Sah00], Sheppard [She99], Bauser, Sauer and Siegert [Bau01], Dieter [Die86], Hufnagel [Huf83] and Lange [Lan85]. Støren and Moe [Stø03] have also described the process along with product use. The PhD theses of Lefstad [Lef93], Abtahi [Abt95], Grasmo [Gra95] and Tverlid [Tve97] contain comprehensive introductions to the subject of extrusion technology and research.

2.1 Background

Aluminium or aluminum is one of the world's commonest elements and makes up more than 8 % of the earth's crust. Nonetheless, the very first grains of metal were isolated only in 1825 by H.C. Ørsted [EncW]. It then took another 60 years before Hall, Héroult and Bayer made industrial metal production feasible. The early decades of the 20th century saw the first widespread use of the metal, and by the 1960s it had risen to the position of being the most commonly used nonferrous metal. Low weight, high conductivity and respectable mechanical properties are some features that make it a strong candidate for many applications. Aluminium reacts easily and forms strong bounds, which can only be broken if considerable amounts of energy are expended. In nature it occurs in igneous rocks such as feldspar, feldspathoid and mica composed of aluminosilicates. The more fortunate geologists may find it in crystalline aluminium oxides such as rubies and sapphires. Most aluminium metal may be traced back to bauxite, a grey or white clay stone whose main constituent is aluminium hydroxide.

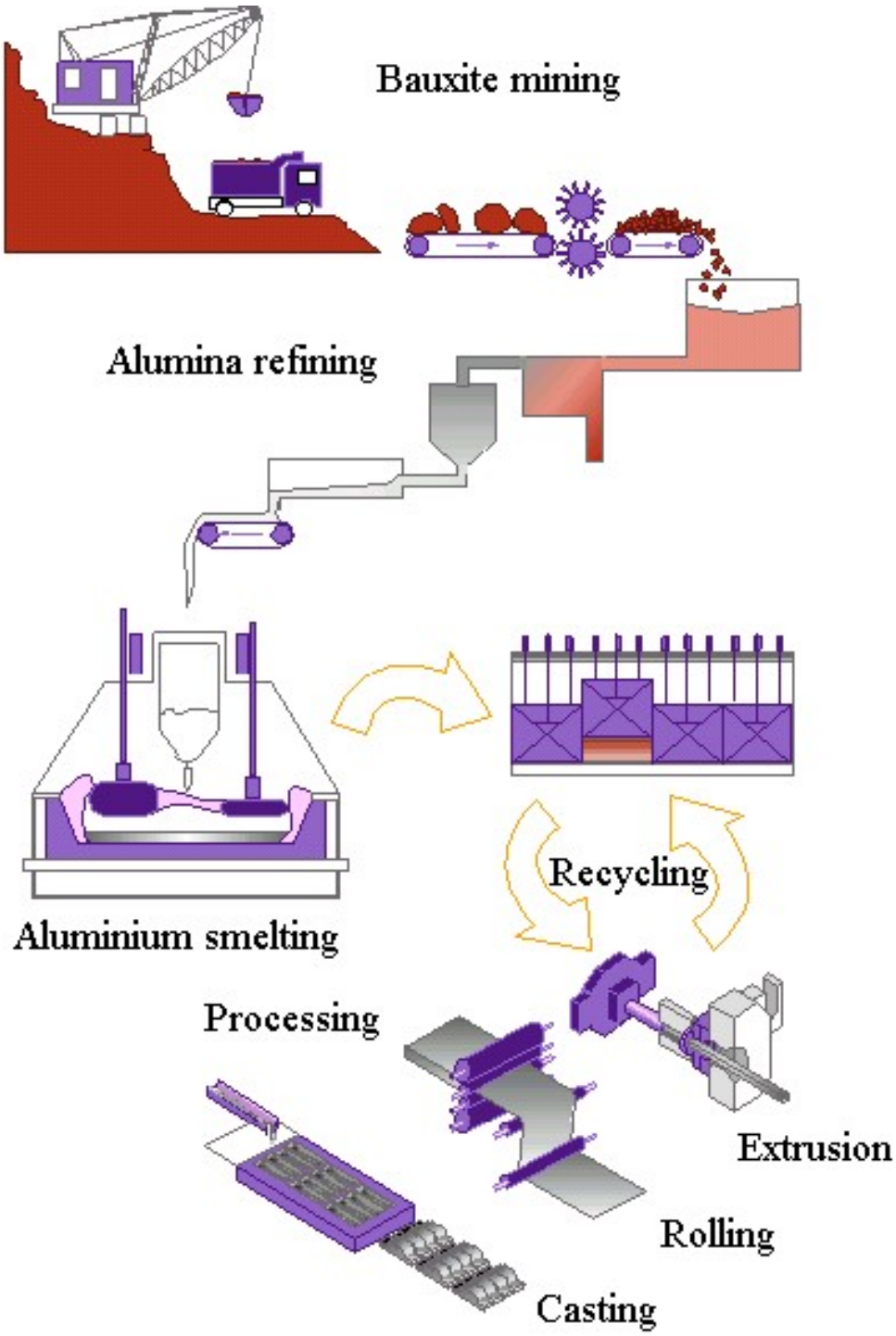

Figure 2.1. An idealized presentation of aluminium refinement from bauxite to an extruded, rolled or cast aluminium product [IaiW]

Aluminium metal may be regarded as an energy bank. The critical stage in the manufacturing process in terms of energy investment is the electrolysis, in which Al_2O_3 is reduced to aluminium metal with a purity of 99.4 to 99.8 %. The energy expended on melting and casting amounts to less than 10 % of that used in the first-time production

of aluminium metal. The cost of producing aluminium metal is significantly higher than that of steel. However, while corrosion may quickly render steel components unfit for use, a strong, and for many purposes, impenetrable membrane of aluminium oxides efficiently protects the energy investment from harsh environments. Hence, the use of aluminium not only necessitates, but in fact promotes recycling. For a large number of applications aluminium does not compete with steel, but when weight and appearance considerations predominate, aluminium often is the most appropriate choice. Economic and environmental gains can probably most easily be found in the field of transport as has long been recognised by the manufacturers of aircraft, buses, trucks, trains and light ships. It may seem somewhat surprising that aluminium products have still not fully penetrated into the automobile industry. This is probably mainly due to the inaccuracy of relevant production processes such as extrusion. Aluminium frames have been introduced in a number of cars, but automated assembly is significantly complicated and consequently made more expensive by excessive dimensional variability. Special profile shape calibrations often have to be introduced after down-stream forming.

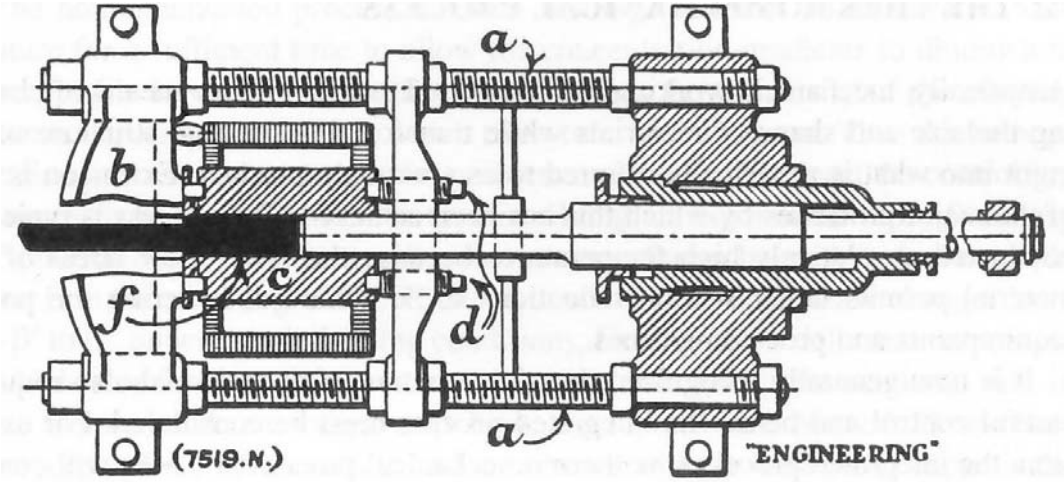

Figure 2.2. Alexander Dick's first hot working press from 1894 [She99].

The invention of material forming by extrusion preceded the discovery of aluminium, and it is doubtful that the early users of the process envisioned the large impact it was to have on the production of light metals in general. Extrusion is a medieval Latin noun from the 16th century. It originates from the Latin verb *extrudere,* which is composed of the words *ex-* (out of) and *trudere* (push, thrust) [MwW]. The definition today embraces all processes in which material pieces are plastically deformed and forced through a die opening with a cross-sectional shape similar to the desired shape of the extruded piece. Metals, polymers and even food may be extruded, making the very first application of the principle quite hard to identify. However, due to the large forces required to extrude most metals, progress in metal extrusion has been intimately linked to the general development of modern technology. The very first record of practical use in modern times dates back to the early part of the industrial revolution. Joseph Bramah was granted a patent on lead extrusion at the very end of the 18th century (1797) [She99]. During the 19th century there were a number of improvements to press designs, but it is fair to say that the introduction of the hot working press in 1894 by Alexander Dick probably marked the most important step in the development of presses. By first heating

the material to be formed and by controlling the temperature of the surrounding tools, he managed to reduce the required press force so that materials of significant strength could be extruded. The time was ripe for the extrusion of aluminium alloys. Extruded profiles of aluminium may be of the most complex shape while exhibiting completely satisfactory mechanical properties for a range of purposes. At temperatures close to 600 °C, the plastic flow of aluminium may be relatively easily provoked, and the ram force is moderate, even though the material flow is quite complex. Heat treatment may be performed after extrusion in order to provide sufficient strength to the aluminium alloy. One of the main objectives of alloy design in relation to the extrusion process is to make sure that the material is easily extrudable (low force requirement and high quality), but that it still exhibits sufficiently high mechanical strength at low temperature. The 6xxx-series of aluminium alloys, whose main alloying elements are magnesium and silicon, is the basic extrudable alloy. If parts are exposed to higher loads, it can be useful to add other combinations of alloying elements. The 7xxx-series is alloyed with magnesium and zinc while the 3xxx-series contains manganese. The extrudability of these alloys is usually poorer than of the 6xxx-series. Larger forces are needed, and the tool wear is therefore often more significant. Still, extruded aluminium profiles generally offer a unique combination of strength and freedom with regard to design solutions.

2.2 Principles and terminology

A forward extrusion press is composed of three main elements: the ram, the container and the tool package / tool stack. In addition, a hydraulic aggregate provides the force necessary to cause the material to flow plastically as the ram moves forwards. While industrial presses may apply a force of as much as 100 MN (equal to the weight of 10 000 medium sized cars), 10 MN is normally more than sufficient for laboratory presses. Standard industrial presses are usually in the range from 16 to 32 MN. In front of stem or ram is a cylindrical piece of steel, the dummy block, which is allowed some movement normal to the extrusion direction. It is exchangeable, and in many extrusion presses it is attached to the ram with a bolt. Practical solutions for the design may depend on the specific objectives of the press designer. The dummy block is generally meant to reduce the sensitivity to eccentricity with regard to the press line up and to simplify maintenance. In this work, stem and piston are expressions that have been used interchangeably when referring to the front part of the ram and its related parts, while the dummy block is usually regarded as a part of the ram or stem design.

The container may most easily be designed as a thick inner massive steel ring or liner surrounded by layers of induction coils and insulation. Containers are exposed to cyclic pressure loads of considerable magnitude. Early experience with fatigue cracking promoted a somewhat complex pre-stressed liner design which is still in common use today. Containers may be dismantled and exchanged when worn out. The induction coils that encircle the liner may be used to accurately control the container and billet temperature. In this work no great distinction has been made between the container and the liner, because the focus of this research is not on the container design. The force transferred from the ram to the liner by friction via the billet is here denoted by either container or liner force or load. The shear stresses between the billet and the container liner may be of very large magnitude since the aluminium sticks to the wall.

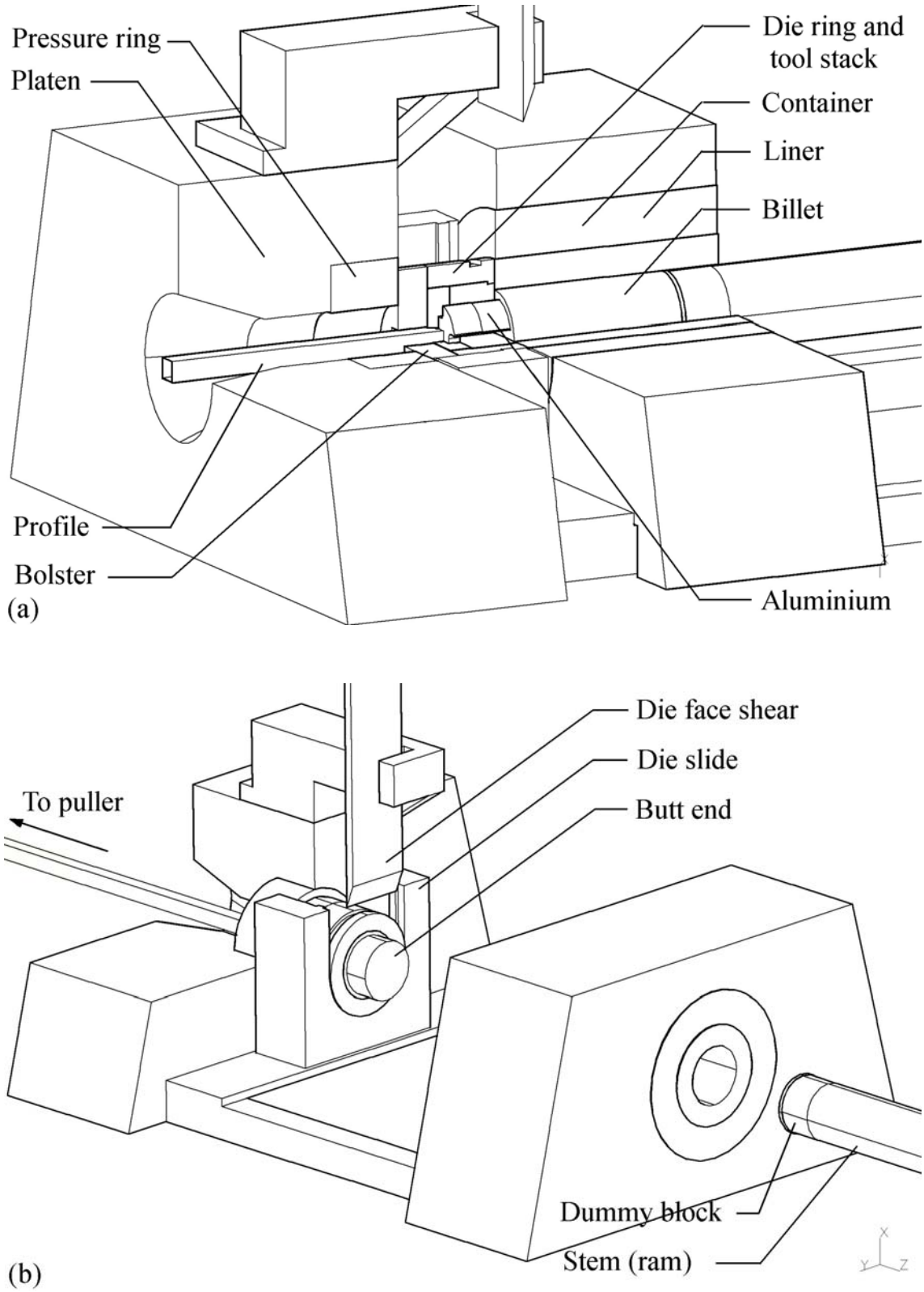

Figure 2.3. The main components of a horizontal extrusion press. A section of the press has been cut away. (a) shows the press during extrusion, and (b) shows the press directly before the butt end is cut.

Most tool stacks consist of a die, a backer, a die holder/ring and a bolster. There are, however, a number of different strategies and solutions when it comes to the details of design. One of the main objectives of the supporting tool design is to minimise die deformation and outlet shape distortion. The openings in the support tools must be as tight as possible. The designer must always consider, however, that industrial tools must be changed regularly since the orders very often are small and tools may be worn and/or broken. Additional costs are related to delays in production, both directly and indirectly. Delays slow down production and may cause undesirable thermal conditions and the production of excess scrap. Dies should be designed so that they may be changed as quickly and easily as possible. Industrial tools are also made so that the fewest possible parts and the smallest amount of material has to be changed when a die outlet is worn or production of a certain profile shape stops. Dies used in laboratory environments, on the other hand, may be made to fit the purpose of the experiment in question. The set-up used in most of the experiments of the present work, for example, included no backer and no tight-fitting die ring. Examples of die designs are given in subsequent sections.

There are important differences between the dies used for producing open and hollow profiles. The more complex hollow profiles require the flow to be split before being welded together close to the outlet of the die. The bridge, spider and porthole dies used for this purpose consist of two parts and differ considerably from the flat-faced dies used for open profile extrusion. Various philosophies exist regarding the control of material flow even for the extrusion of simple open profiles, and a carefully designed pre-chamber or feeder close to the die outlet is often used for this purpose. Feeders may be integrated in the die plate or in a separate plate placed in front of it. The feeder, die and backer plates are fitted into a die ring and constitute an exchangeable unit. The bolster is handled separately, and is not changed along with the die.

A geometric feature of disproportionately large importance for the surface properties and the shape of extruded profiles is the sometimes very narrow die outlet. Profiles may be in intimate contact with the die even after having entered the outlet, because most dies are designed with short and moderately choked contact surfaces at the outlet. The extruded profile is often slightly plastically modified after having left the container. The main purpose of the bearing surfaces is to impose contact and to control the material flow. The length of the bearings in the extrusion direction and the choking of the flow determine the resistance and retardation. The length of the bearing surfaces normally varies along the circumference of the die outlet. Bearings are often tapered and usually shortest close to the edges where the material has a tendency to flow more slowly. In the literature, the bearing surfaces are also referred to as the die lands. Once filled with aluminium, the aperture formed by the bearing surfaces is called the bearing channel. A channel that is not choked is either parallel or in release. The angle defining the degree of choke or release is the choke or release angle. Flow control may be enforced by changing the choke angle, since the material flow is retarded more where the choke is large. A die with a bearing channel that is completely in release is called a zero length bearing die. Since the radius at the inlet of the bearing channel, the inlet radius, never is exactly zero, there will in practice always be a finite bearing length. If the release angle is not sufficiently large, aluminium deposited close to the outlet may modify the surface of the profile. Surfaces that have been torn or scratched will be less pleasing to the eye.

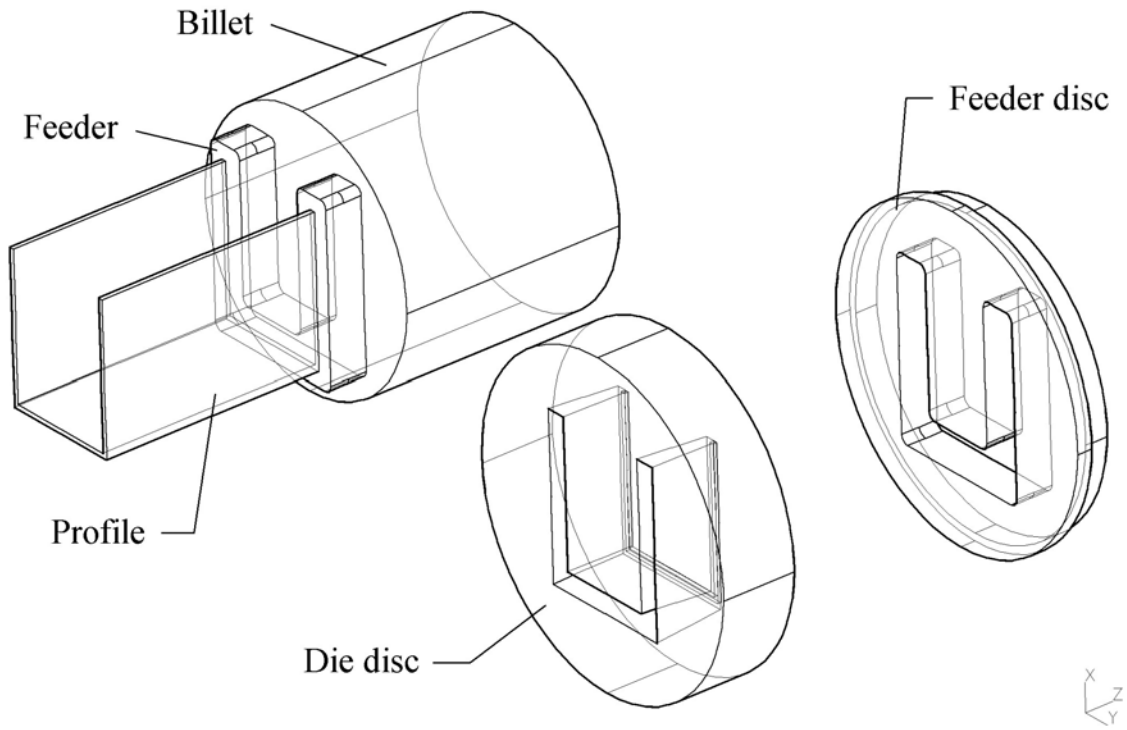

Figure 2.4. The principle of open profile extrusion. The feeder disc, the die disc and the partly extruded aluminium billet/profile are shown.

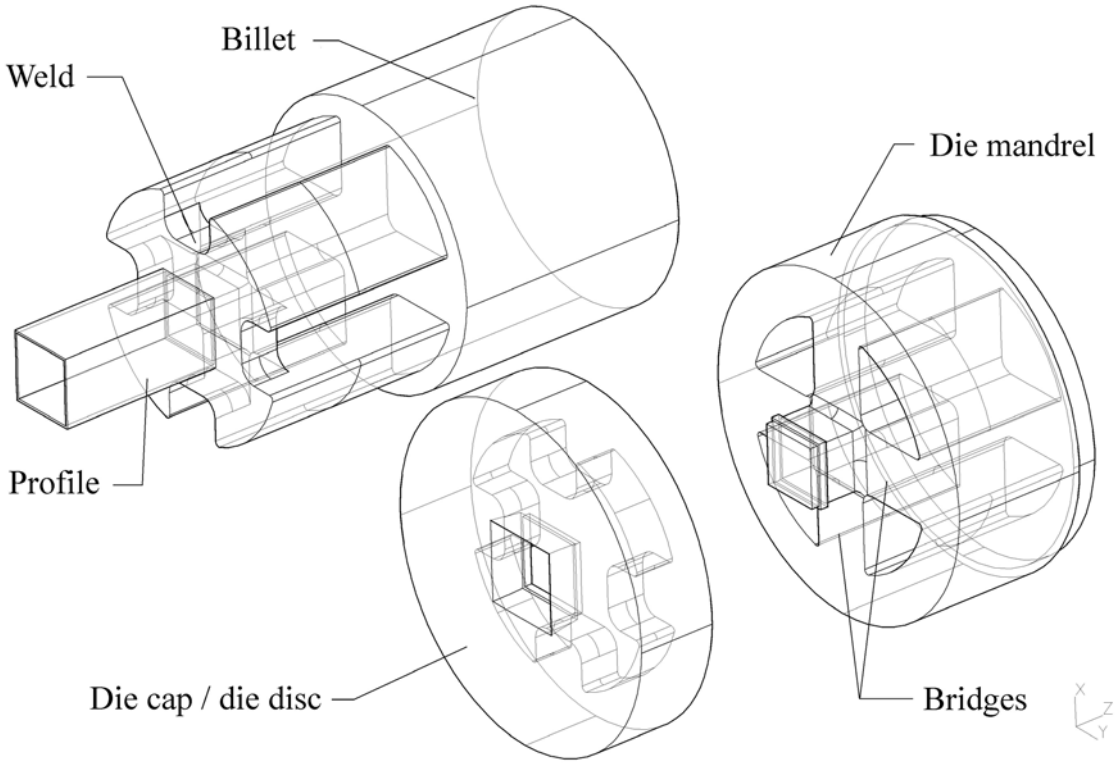

Figure 2.5. The principle of hollow profile extrusion. The die cap (die disc), the die mandrel and the partly extruded aluminium billet/profile are shown.

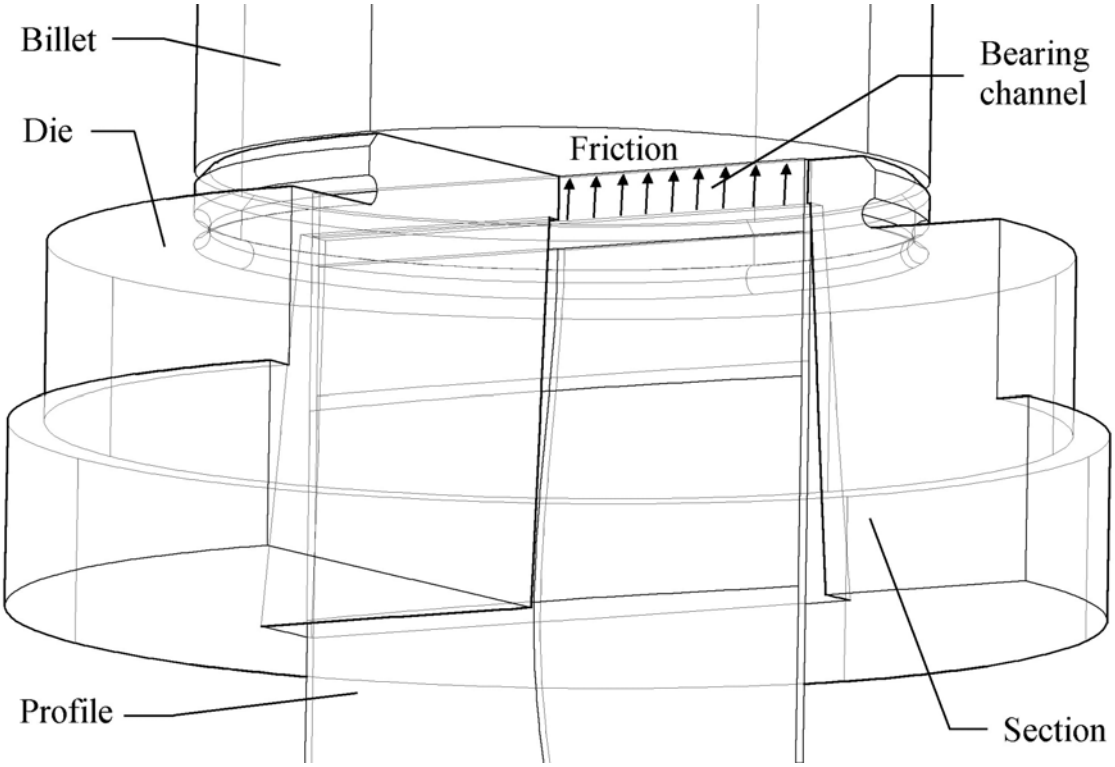

Figure 2.6. A die for extrusion of thin strips in the laboratory of SINTEF Materials Technology. A section of the die has been removed to allow the profile to be viewed also in the bearing channel. The bearing channel is here of uniform length along the circumference of the outlet.

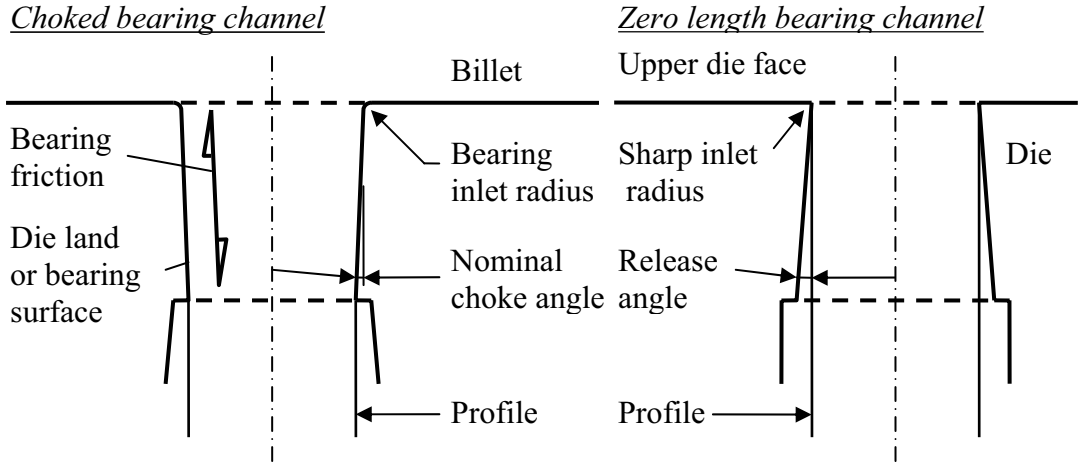

Figure 2.7. Cross-sections of bearing channel geometries for choked and zero length channels. The angle of choke is often very small, usually less than half a degree. The outlet geometry is modified due to elastic die deformations.

A definition of extrusion as a process in which a piece of material is pushed through a die outlet with a somewhat smaller cross-section is accurate, but not overly preclusive. The fact that there is no unique way of performing extrusion is confirmed by the relatively extensive system of designations describing the process. Extrusion may be

continuous or discontinuous, depending upon the way the material is fed into the press. Polymer extrusion may easily be performed in a more or less continuous manner with a screw pushing the material out of the container. High pressures and temperatures make the principle less applicable to the production of aluminium profiles, but there are, in fact, some continuous aluminium presses [She99]. The process may also be described as either direct or indirect, depending on whether the die/container or the ram constitute the movable parts. In order to control flow, all the parts may be moved simultaneously [Ber00]. Forward, in contrast to backward extrusion, refers to a situation where the profile flows in the direction of the ram movement. The direction of the ram movement also determines whether the extrusion press is called horizontal or vertical. Furthermore, when the temperatures of the billet and tools are kept high to simplify metal flow, the process may be referred to as hot extrusion. For aluminium, the term cold may be used when temperatures are below approximately 300 °C. Aluminium is usually extruded at high temperatures, although some hard alloys may require that initial billet temperatures be not significantly higher than 300 ºC. Aluminium extrusion is usually performed without lubrication since this may promote unfavourable flow and harm surface quality. In contrast, steel extrusion may often require the lubrication of the interface between the billet and the die/container. Finally, a distinction must be made between dies needed for producing hollow and open profiles and between dies for single and multiple profiles.

This thesis deals exclusively with the direct/forward aluminium extrusion. Experiments have been run at high temperature and without lubrication. In addition, comparatively short billets have been extruded in a discontinuous manner. The following presentation will therefore focus only on one extrusion technique, and will make no further reference to the other types mentioned above. The extrusion method described is probably also the most commonly used in commercial applications. A discontinuous forward extrusion process may be divided into six main steps:

1. The hot billet is loaded into the container after it has been heated by appropriate equipment (usually induction heating coils).

2. The ram is moved forward to set up the billet before being withdrawn to allow locked-in air to escape. This is called the burp cycle.

3. The profile is extruded as the ram again moves forward. The motion is halted when only a short discard remains. The discard is called the butt end.

4. The ram is withdrawn and the container is separated from the die. Since the surface of the dummy block usually has been smeared with carbon, the butt end should stick to the face of the die.

5. The butt end is sheared off of the die face by the die face shear. The process may involve using water as a cutting fluid.

6. Finally, the die and the container are brought together again and a new billet is loaded into the container.

An extrusion cycle may last from a minute to a couple of minutes. There are normally no delays between the runs. Profitability in extrusion requires down times to be kept to an absolute minimum. It is quite possible to extrude a new billet without removing the old butt end as described by steps 4 to 6. In fact, when feeders or bridge dies are used, a part of the butt end is left in the die and may only escape through the die outlet (billet-to-billet extrusion). The advantage of not removing at least parts of the discard is that the process assumes some of the properties of continuous extrusion. When the first profile in a batch is extruded, care must be taken to fasten it to a puller which guides it straight out on the run-out table. If the butt end is not removed, the next profile may be extruded without any interruption since it may be easily grabbed by the puller. If the discard is completely removed, each cycle is like the first. However, if the discard is not removed, the quality of the profiles may suffer from the weakening effect of oxide inclusions. There will then be oxides in the weld between the discard and the new billet, which consequently constitutes a curved plane of weakness. This situation is aggravated by the physics of flow, as a plane surface or cross-section of the billet in the container may turn into a paraboloid-shaped surface stretching several metres along the length of the profile. The main reason for removing the butt end is that it usually contains most of the oxides and other impurities originally attached to surface of the billet.

2.3 The physics of metal flow

When a piece of aluminium is extruded at high temperature, the material behaviour may be characterized as thermoelasto-viscoplastic. The material expands due to heating, but is at the same time compressed elastically. The plastic deformations are significantly larger than the elastic ones, however, and the work performed by the ram is essentially irreversible and a source of considerable heat dissipation. Permanent shear deformations are generally related to the movement of dislocations, but there may also be other active mechanisms such as grain boundary sliding. Hot aluminium behaves as a fluid when exposed to significant loads, but the response of the material is a non-linear function of strain, strain rate and temperature. The viscoplastic metal flow in the container may be studied experimentally by inserting pins or discs of marker material into billets, performing extrusion to various lengths, splitting the billets and profiles and etching the cross-sections [Val88]. Illustrative patterns emerge. What are known as emptying diagrams allow particle paths to be traced from the billet to the profile. The diagrams reveal that material particles in the various parts of the billet may experience very different temperature and deformation histories as they flow towards the outlet. The material closest to the die outlet in the beginning of the run may remain almost non-deformed. The material in the centre of the billet is mainly elongated, while the material close to the container walls may be both heavily sheared and elongated. In most cases, the deformations are extremely large. The ratio between the cross-sectional area of the container and the area of the die outlet is denoted the extrusion ratio (ER). The extrusion ratio is a measure of the average elongation of the material during plastic deformation, since it behaves almost incompressibly. Industrial ratios of extrusion normally exceed 40 and may sometimes even be greater than 100. Thus, the average straining of the material (logarithmic) is typically in the range from approximately 3.5 to 4.5. It should be noted that hot aluminium extrusion sometimes is performed with multihole dies that make possible the production of a number of profiles simultaneously.

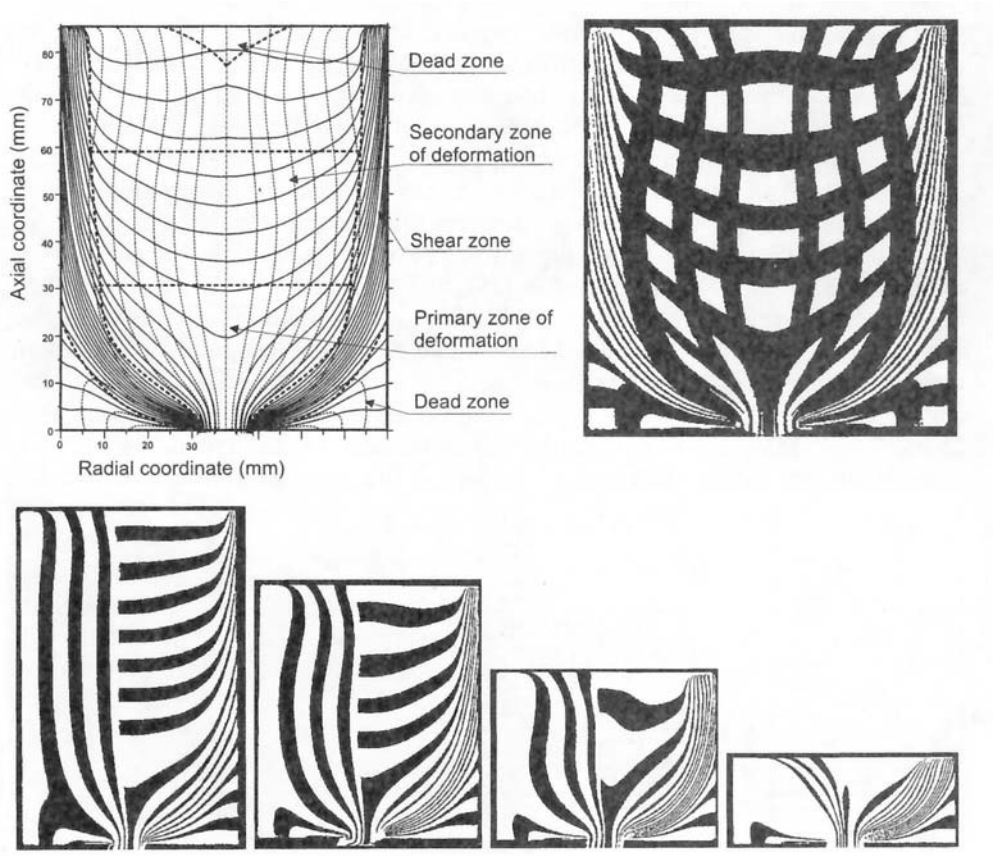

Figure 2.8. Flow patterns obtained with the marker material technique of Valberg. A regular grid of marker material was initially inserted in the billet. Some Characteristic regions of deformation have been identified. The transient nature of the process is evident. A further presentation of Valberg's technique and patterns is given by Støren and Moe [Stø03].

The flow patterns established through experiments with marker materials indicate that boundary conditions and die and press geometry probably are the factors that influence the velocity field the most. Since the die opening aperture is quite small, the hydrostatic component of stress in the container is large compared to the deviatoric one. There is intimate contact between the billet and the container wall. As a consequence, friction is usually of what is known as the sticking type. The material particles in direct contact with the container wall do not move, and deformation occurs mainly in the interior of the material. As the ram moves forward, the billet flows quickly in the middle, while the material is retarded or even brought to a standstill at the walls. This kind of flow is called a plug flow, and strain rates close to the outlet of the die may be very high (up to 10 000 s^{-1} close to the die outlet). The material at the container wall is detached and flows mainly towards the centre of the billet only when the ram is very close to the die. Oxides and impurities of the billet surface accumulate in the butt end, which is regarded as desirable, and extrusion is usually stopped before oxides flow into the profile. If the container is too hot, there is a risk that the outer layer of the billet may flow along the container wall and into the profile surface. The result may be blisters at the profile surface [Han96]. Lubrication is almost never used in aluminium extrusion, as it would greatly ease the undesired flow of contaminated material from the container surface to

the die outlet. The contamination of the extruded material by the lubricating fluid is another negative effect. Sticking friction also between the extrusion die and billet causes a retardation of flow close to the die surface. This forms what is called a dead zone close to the intersection between the die and the container. The material in the dead zone deforms plastically only to a very small extent [Kia96]. Close to the outlet of the die there must be a layer of intense shear between the dead zone and the central metal flow. The size of the dead zone is gradually reduced as the material in the shear layer flows out of the outlet and forms the surface of the profile. The reasons for using flat-faced dies rather than conical ones are that they promote the accumulation of contaminated material in the butt end and are significantly less expensive.

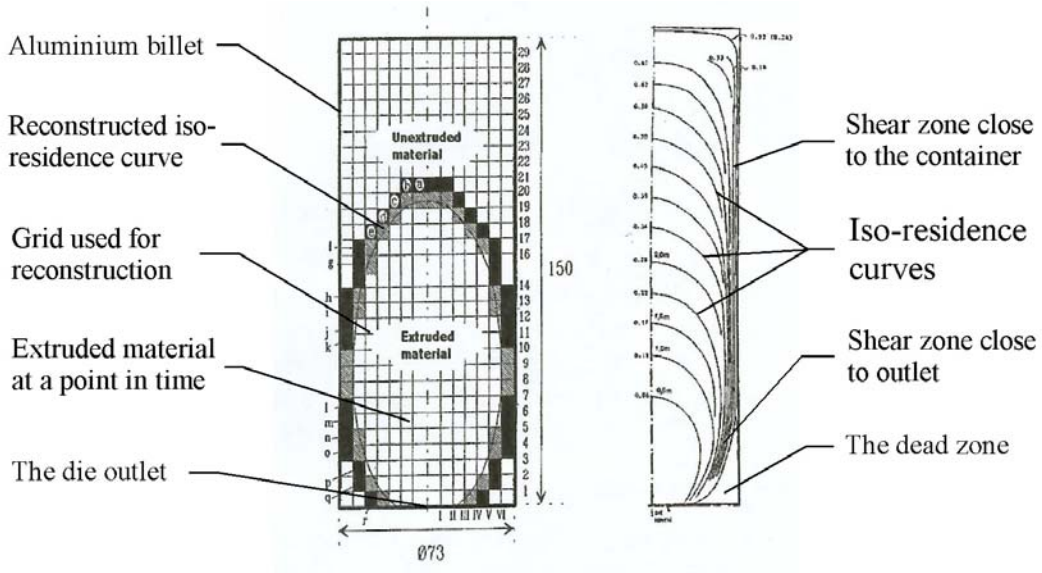

Figure 2.9. Emptying diagrams – diagrams showing the lines defined by material extruded at the same time (iso-residence curves). The figure to the left has been generated by Valberg. A further description is given in [Stø03].

It is possible to define or identify a number of zones in the billet that experience various types of deformation. The material is elongated mainly in the primary deformation zone in front of the die outlet. The dead zone in contact with the die face experiences almost no deformation in the early stages of extrusion. Intense shear deformation occurs at the inlet and outlet of the primary deformation zone and at the boundary between the dead zone and the primary zone of deformation. There is also significant shear deformation along the container wall. The deformation of the centre of the billet is very moderate, but close to the ram there may be some radial flow. The subdivision of the billet into smaller volumes may prove useful when certain analytical or semi-analytical techniques are used to study extrusion. However, the approach may also be somewhat artificial and should be handled with care. First of all, there may or may not be distinct boundaries between various flow regimes in the container. The problem with a simplified analysis is that it neither provides accurate answers nor makes it possible to assess the size of the errors inherent in the analysis. Second, extrusion is a transient process, and the patterns of flow gradually change as the ram moves towards the die face. The dead zone close to the die gradually diminishes until the very last stage of the process, when it flows

radially to the die outlet. At that point, however, ram movement is usually disrupted since the friction forces and consequently the ram force rather abruptly increase.

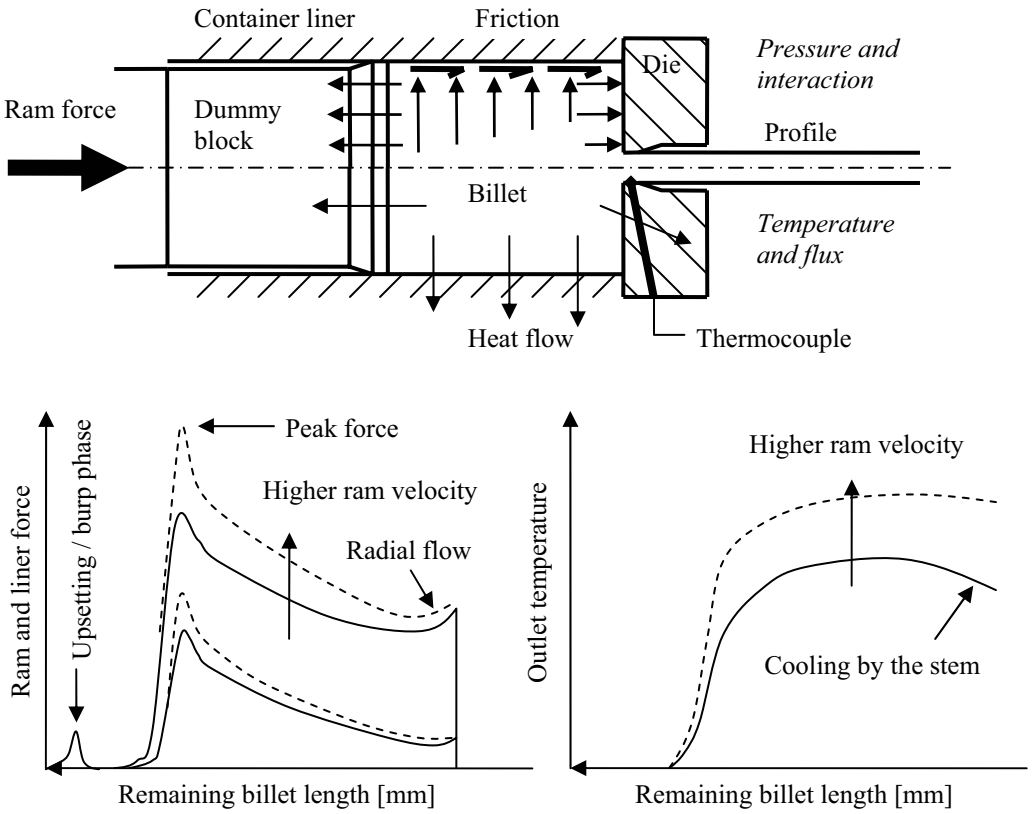

Figure 2.10. Typical curves for ram force and outlet temperature. The x-axis indicates the length of the billet remaining in the container. The extrusion run is usually interrupted when the ram force starts increasing. The component of the ram force transmitted through the container liner due to friction is also shown. The force component may or may not be applied on the die.

Measurement of temperature and ram force sheds further light on the transient nature of the process. In direct forward extrusion the ram force must be expected to decrease gradually, as the movement of the ram reduces the area of interaction between the billet and the liner. The ram force, however, is also altered by the gradual change in flow patterns described above and the changes in flow resistance due to heat dissipation and temperature increase. Plastic deformation initially causes the billet to heat up quickly. A consequence is a somewhat accelerated decrease in ram force after the initial peak force has been reached. There may, as will be further discussed, also be other causes for this initial sudden decrease in the ram force. The term quasi-static is extensively used to describe the extrusion process, since outlet temperatures usually stabilise at a higher level and since the transient effects on flow and microstructure are relegated to the very early and late parts of the run. This is particularly true for industrial extrusion, which is performed with relatively long billets. The length is three to six times the diameter. It is important to note in relation to the discussion on process control, that the first and last parts (some meters in all) of an extruded profile are usually discarded. Unsatisfactory

microstructure and profile shape and the presence of a diffusion weld make the material less desirable for use. The term quasi-static may be misleading in many cases, for it is seldom possible to secure completely uniform conditions along the length of the profile. The ram speed or the initial temperature of the billet may be controlled so that the outlet temperature is almost constant during the extrusion. The control strategy is often called isothermal extrusion and is widely used industrially.

The outlet temperature is the parameter that has received closest attention when microstructural properties of profiles have been assessed. The reason is that the highest temperature the material experiences must be known when phenomena such as melting and re-crystallisation are studied. Since convection usually dominates over conduction in extrusion, the temperature of a material particle steadily increases when it moves towards the outlet of the container until it reaches a point in the bearing channel where plastic dissipation has virtually ceased and heat generation related to friction is negligible. The press limit diagram, in its many different forms, may be used to map the process window for a particular press, profile shape and alloy. One of the limits of the diagram relates to the maximum capacity of the press. The other limit is determined by the maximum acceptable surface temperature. Surface fracture due to melting around precipitates, pick-up due to abrasion, re-crystallisation or die lines due to scratching by hard particles on the die lands may determine the shape of the second line. In all cases, however, experiments or careful modelling of material flow is needed to establish the link between the maximum temperature at the outlet and the billet temperature and the ram velocity. Hence, the press limit diagrams contain information not only about surface defect mechanisms, but also about the material flow behaviour. It is worth mentioning that the billet temperature need not be assumed to be initially constant. In order to compensate for uneven dissipative heating during extrusion as well as heat losses to the stem, the billet temperature is often tapered. The front end temperature of the billet is higher than that of the back end.

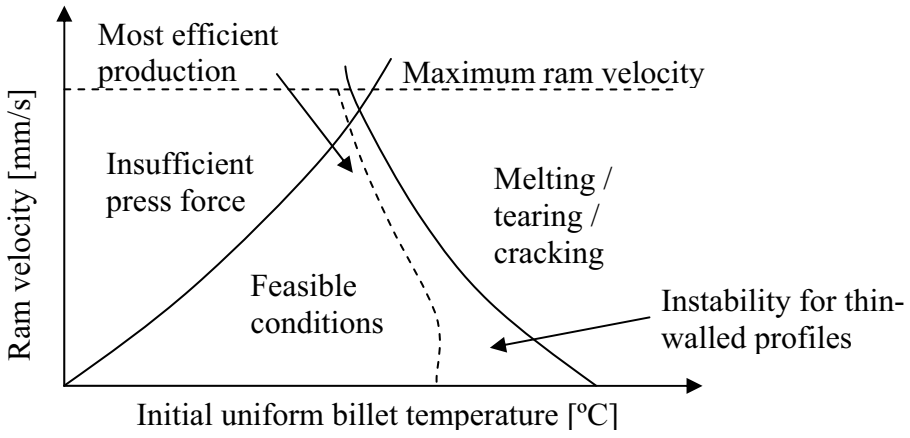

Figure 2.11. The press limit diagram for a specific extrusion press, alloy and profile geometry. The dashed line is usually not a part of the diagram, but has been added to indicate that there may also be temperature and velocity limitations related to flow instability phenomena such as buckling.

2.4 The basic assumptions of extrusion modelling

An accurate solution to the extrusion problem requires a careful study of all the laws of conservation (mass, momentum and energy). The equations are usually coupled. The dissipation of heat is caused by plastic deformation and causes the temperature to increase. Furthermore, the value of the flow stress depends on the temperature, since viscoplastic flow may be more easily provoked at higher temperatures. In order to actually solve the conservation equations, quantitative information on the mass and heat flow behaviour must be added in addition to the assumption of incompressibility. While there are a number of ways to solve the equations, the most commonly used modelling approach for extrusion is that of continuum thermo-mechanics [Mal69]. Deformation and stress fields are then assumed to be continuous except across clearly defined lines of discontinuity. The descriptions of material behaviour are called constitutive or material equations. In most cases one may assume that heat conduction occurs according to Fourier's law. Both the billet and tool materials are fairly isotropic with regard to conduction. Material data (heat conductivity, heat capacity and density) are usually temperature dependent, and the problem is highly non-linear. For cases of extrusion at a fairly high rate, convection (heat transport related to mass transport) is usually more important than conduction. The heat is effectively transported out of the container with the material flow, and there are large temperature gradients close to the outlet of the die where most of the heat is generated. Still, there may be a significant flow of heat from the billet to the surrounding tools by heat conduction. The die steel and aluminium are in intimate contact so the heat transfer is fairly efficient across the boundary.

Modelling of deformation is more complex than modelling of heat flow. The theory of plasticity allows a treatment of irreversible material behaviour in a systematic manner [Cha87] [Kha95] [Lem90] [Ric74] [Sch01] [Sch03] [Sim98]. The theory has also been extended to relevant cases of viscoplastic deformation [Lem90], and it is now possible to more closely link the continuum mechanical analysis and microstructure modelling [Raa98] [Yan93] [Est98]. The most advanced concept is probably that of multi-scale modelling, which assumes that deformation mechanisms at a number of length scales may be taken into account by a continuum-based flow/friction model. An advantage of continuum approaches is that they treat not only discrete discontinuities and localisation of strain [Pęc97] [Pęc98], but general anisotropic flow behaviour of materials. Materials with an anisotropic microstructure may often be more easily deformed in one direction than in another. It is well known, for example, that extrusion causes an elongation of the grain structure, and that extruded profiles behave anisotropically during downstream forming processes such as bending and hydroforming. To what extent it is necessary to consider anisotropic material behaviour when modelling extrusion is still not entirely clear. One-way coupled flow-microstructure calculations have been quite successful in predicting texture evolution [Auk96]. The flow and final material microstructure are to a large extent controlled by the geometry of the die and container. Still, the quality of the corresponding force estimates is not known. Neither is the quality of predictions of the flow velocity distribution. Based on very rudimentary evaluations of the resistance to deformation of the aluminium f.c.c. lattice in various directions it may be argued that ram loads should decrease as the material microstructure is allowed to orient itself in the most favourable direction [Gra95][Pet99]. At the same time, however, there are material hardening and softening effects related to the organisation and development of

dislocation networks. The microstructural phenomena occur at different length scales, but are clearly related and need to be considered in modelling. It is, as indicated, often assumed that the extrusion process is quasi-static, and that the extrusion microstructure mainly develops from the cast microstructure in the early phases of the run. One may also most easily observe the hardening and softening mechanisms on the ram force at the onset of extrusion.

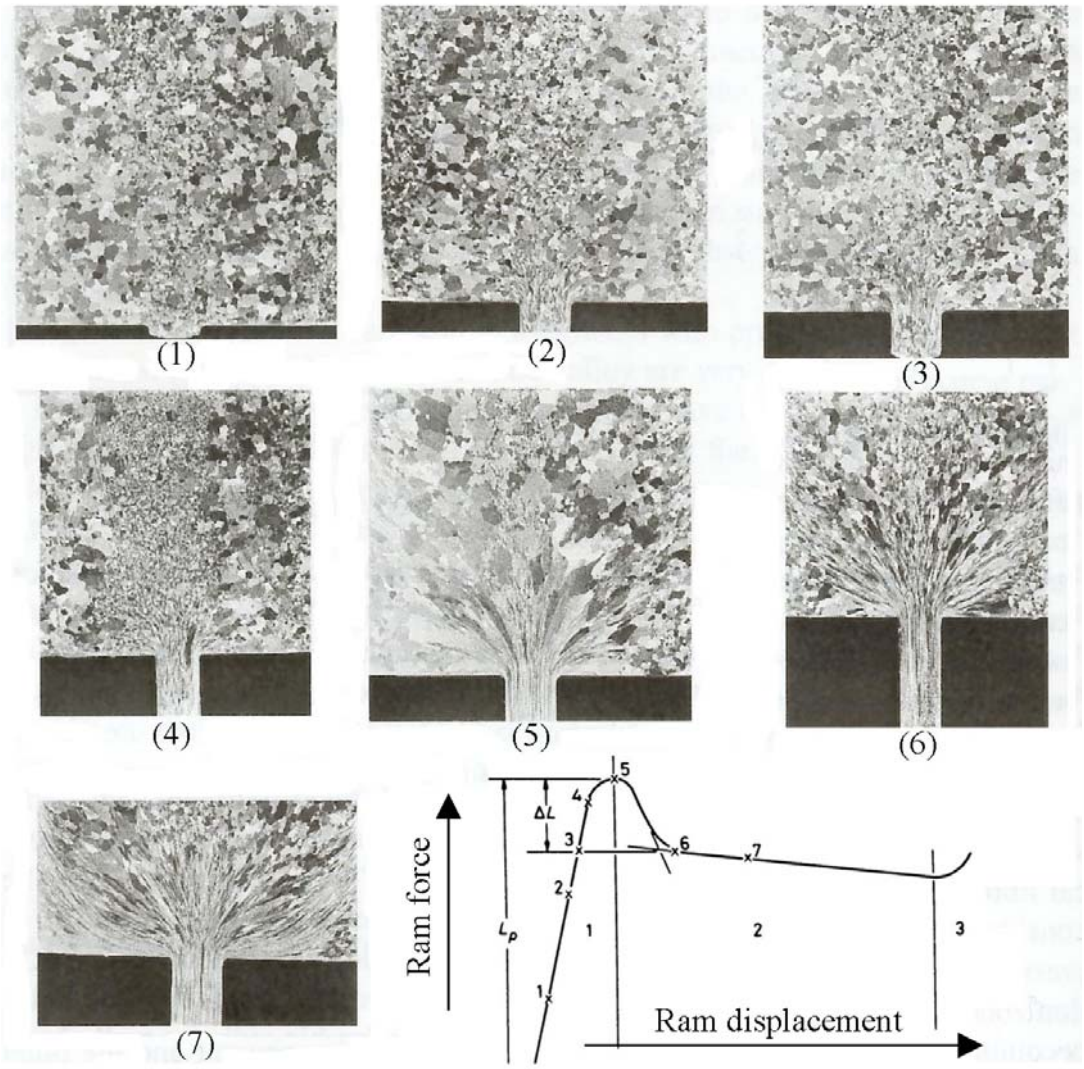

Figure 2.12. The evolution of the grain structure during the early phases of extrusion. Grains are initially quite equiaxed, but are much deformed close to the shear zones and in the profile [She99].

It should be understood that a piece of material or a material particle that flows through the container and out of the die outlet will be only gradually deformed. Each particle of the billet experiences a unique deformation and temperature history, and the material deformation is to some extent history dependent. Thus, the development of the material microstructure is complex. Both the elongation of grains and the organisation of sub-grain networks should be evaluated. Large amounts of energy are stored in the deformed lattice. Re-crystallisation of the dynamic kind during deformation is not so commonly

observed [She99]. However, in zones of intense shear and elongation the microstructure may be reorganised. Grains are elongated so much that the sub-grains are often pinched off and form the cores of a new fine grained structure [Ger04]. In some alloys diffusion may also contribute to the reorganisation. The need for detailed multi-scale modelling of stain localisation must be evaluated. It is not exactly known how successful the approaches that assume more smooth displacement fields and simpler material models are in predicting force requirements and microstructure development. Analytical calculations may be most useful for establishing a better understanding of the basic mechanisms of flow. It is quite clear, however, that numerical tools are needed in order to properly model the evolution of microstructure and flow during extrusion, and to produce useful estimates of forming loads and temperatures.

Most of the numerical simulation codes in use today are based on a large number of simplifications with regard to the description of the material behaviour. Multi-scale extrusion modelling is in its infancy. There are some numerical codes that include fully elasto-viscoplastic formulations, but calculations are usually time-consuming [Fli02] [Cha99] [Cha00] [Cha01]. It is therefore relatively common to entirely disregard the elastic deformations of the billet and to assume that aluminium behaves as a completely viscous material [Hol92] [Ren99]. Plastic deformations are usually much larger than elastic ones, and it is likely that acceptable estimates of forming forces and temperatures may be obtained with the viscoplastic material models. Most of the energy put into the ram movement is spent on viscoplastic deformation. The elastic component of the material response may, however, be important in studies of the limits of flow stability for extrusion of thin-walled profiles. The elastic response affects the contact mechanics in choked bearing channels and determines the friction in the bearing channel [Lof00] [Lof01]. Elasticity must also be considered when the behaviour of the extruded profile in air is considered. The most advanced continuum models should treat both the viscous behaviour of aluminium in the container and the solid behaviour of the extruded profile. The transition region in the bearing channel is the most difficult to describe. Bulk and fricion material behaviour is controlled by temperature, strain, strain rate and potentially also a range of other factors. The optimal numerical formulations may differ for the billet and profile. Even though there is a lower threshold for the initiation of viscoplastic deformations, it is probably low for high-temperature deformation of aluminium.

The concepts of yield surfaces in classical plasticity theory and flow surface in the theory of viscoplasticity are similar, but the viscoplasticity theory allows the calculation of rates of deformation on the basis of the state of stress [Sim98]. Very often it is simply assumed that the material is isotropic and purely viscous. The flow shear stress is regarded as a function of strain rate and temperature, but not strain. Strain hardening and softening that may occur for small deformations are simply neglected since the material that flows into the profile has undergone very large deformations. It is often assumed that the material, at least in an Eulerian sense, is in a steady state during most of the extrusion run [She99]. A relatively persistent grain and sub-grain network is in fact established in the primary zone of deformation soon after extrusion commences. The network may be somewhat modified towards the end of the run. However, when material behaviour is assessed, it is important that the material particles flowing through the container are studied. They may experience changes in loading conditions and the

activation of new dislocation systems [Pie02]. It may also be important to evaluate strain hardening behaviour. Still, one awaits a sufficiently thorough study of the subject.

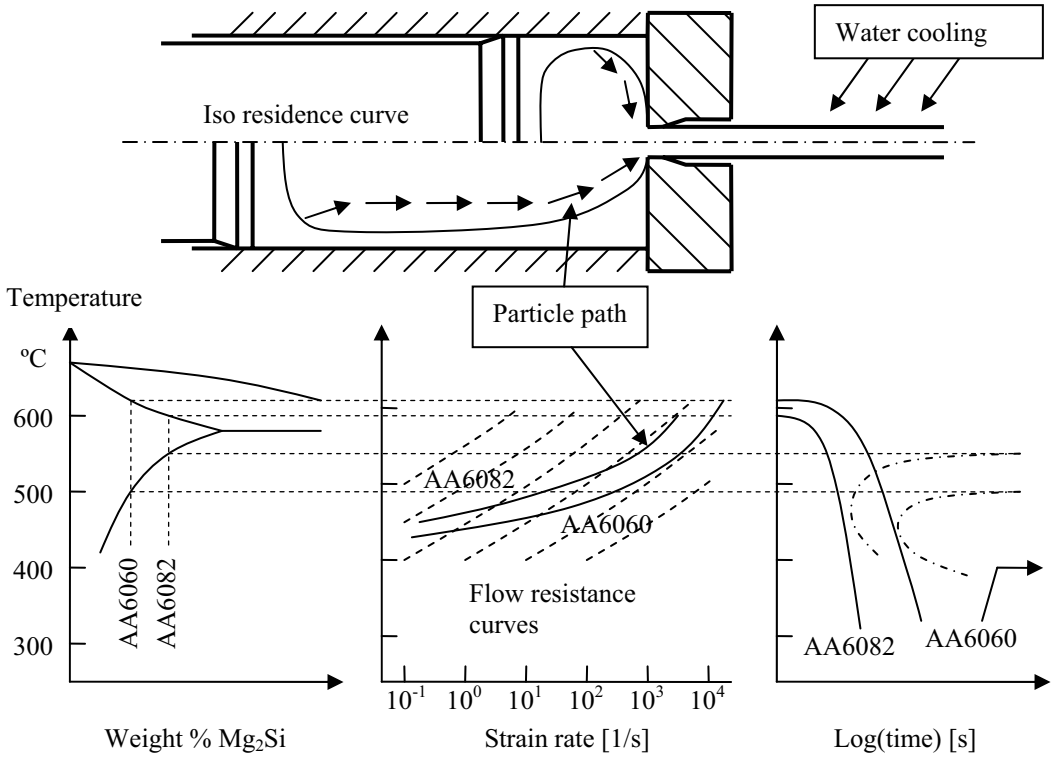

Figure 2.13. The presentation of the temperature and deformation history for a material element flowing through the container. The diagrams (phase, strain rate temperature and CCT) treat two generic alloys AA6060 and AA6082. Material data have been shown for only one of the two alloys.

The most commonly used phenomenological flow rule that describes the behaviour of aluminium is the Zener-Hollomon relation, introduced by Zener and Hollomon in order to fit data from forming of steel [Zen44]. Sellars and McGregor Tegart later found it to be most useful for fitting data obtained from aluminium materials testing [Sel72].

$$\sigma_f = \alpha^{-1} \operatorname{arcsinh}\left(Z/A\right)^{1/n} = \alpha^{-1} \ln\left(\left(Z/A\right)^{1/n} + \sqrt{\left(Z/A\right)^{2/n} + 1}\right) \qquad (2.1)$$

σ_f is the flow stress of the material, which must be compared to the equivalent stress $\bar{\sigma}$ at any point.

$$\bar{\sigma} = \sqrt{\frac{3}{2}\sigma_{ij}\sigma_{ij}} \qquad (2.2)$$

σ_{ij} are the various coordinate stresses. The summation rule of Einstein is used, and the notation is in accordance with that of Malvern [Mal69]. Z is called the Zener parameter, which is a temperature-compensated strain rate.

$$Z = \dot{\bar{\varepsilon}} \exp\left(\frac{Q}{RT}\right) \tag{2.3}$$

Q is the activation energy for self-diffusion. R is the universal gas constant (8.3144 J mol^{-1} K^{-1}) and T is the temperature of the material specimen. The equivalent strain rate $\dot{\bar{\varepsilon}}$ may be related to the components of shear stress $\dot{\varepsilon}_{ij}$.

$$\dot{\bar{\varepsilon}} = \sqrt{\frac{2}{3}\dot{\varepsilon}_{ij}\dot{\varepsilon}_{ij}} \tag{2.4}$$

If aluminium is treated as a viscous fluid, the viscosity $\eta(\dot{\bar{\varepsilon}},T)$ may be introduced. It relates either equivalent stresses to equivalent strain rates:

$$\bar{\sigma} = 3\eta\left(\dot{\bar{\varepsilon}},T\right)\dot{\bar{\varepsilon}} \tag{2.5}$$

or components of stress to components of strain:

$$\sigma_{ij} = 2\eta\left(\dot{\bar{\varepsilon}},T\right)\dot{\varepsilon}_{ij} = \eta\left(\dot{\bar{\varepsilon}},T\right)\dot{\gamma}_{ij} \tag{2.6}$$

While the Zener-Hollomon relation was initially introduced as a regression relation, it is to some extent supported by simple models treating dislocation movement on single slip planes [Cam75] [Nes98]. The rate controlling mechanism is usually assumed to be the climbing of dislocation jogs that occurs by diffusion. The athermal contribution to the flow stress increase is often neglected, since no significant changes in microstructure are expected during steady state deformation. There are versions of the Zener-Hollomon relation that include also the effect of strain hardening or softening. Additional material parameters and terms may be added. The main motivation for adding terms is usually that the relation may be better fitted to the data at hand. It is important to note that the Zener-Hollomon relation predicts that the flow stress is a logarithmic function of the Z parameter at high Z values and an exponential function at low values.

$$\sigma_f = \left(\alpha n\right)^{-1} \ln\left(Z/A\right) \qquad \text{for } Z/A >> 1 \tag{2.7}$$

$$\sigma_f = \alpha^{-1}\left(Z/A\right)^{1/n} \qquad \text{for } Z/A << 1 \tag{2.8}$$

The Zener-Hollomon relation mimics a strain rate and temperature dependency that is often observed experimentally. However, one should be careful when using material data to model extrusion if the data have been determined at rather low strain rates, such as by compression or torsion. The main reason is that the rate of deformation is very high close to the die outlet and bearings, and that it is not entirely certain that the material data obtained by conventional tests are fully representative. The mechanisms and mechanics of deformation need not be the same at high and low rates of deformation [Ast01] [Dja00], and extrapolation may produce erroneous estimates of

flow stress. The accuracy of the ram force and the temperature estimates depends on how much in error the constitutive relations are at high rates and how large volumes that actually deform at high rates. The importance of testing material behaviour at a high rate must be carefully assessed before flow codes may be effectively used to predict flow behaviour during extrusion. The task is a demanding one, because flow codes are based on a number of other assumptions that also must be carefully tested.

In order to solve the conservation equations one must supply information about all the boundary conditions. It is much harder to describe the mechanical interaction between the billet and the tools than the flow of the bulk material. Mechanical testing procedures are less accurate and developed, and it is less certain that the boundary conditions may be exactly recreated in a representative test. Furthermore, the material constitution need not be uniform, and useful micromechanical models are more difficult to establish. Sticking contact is usually assumed to dominate at the container-billet interface. The aluminium billets and the steel dies are in close contact at high temperatures, and only for low-temperature extrusion of high-strength alloys have indications of sliding friction been found [Fli02]. Full sticking boundary conditions may be applied by specifying a zero relative velocity at the boundary or a Tresca friction model with a high friction factor ($m = 1$).

$$\tau_f = mk \tag{2.9}$$

τ_f is here the friction stress, and m is the shear flow stress of the bulk material. The choice of friction relation is determined by the modelling approach. The wall shear stress is determined by the behaviour of the bulk material. In order to model more complex material behaviour in the boundary layer close to the tool-billet interfaces, viscoplastic friction relations may be introduced. Lubrication and impurities may affect flow and friction resistance, and so may tool surface texture. The viscoplastic friction relations are of a similar nature as the flow relations for the bulk material. The theory of friction modelling is a two-dimensional analog of the plasticity theory [Mon00], and anisotropic criteria may for instance be implemented if necessary.

The bearing surfaces close to the outlet of the die are usually fairly short, but are still vital tools for controlling the flow in extrusion. As discussed earlier, the flow may be retarded in parts of the extruded section by making the surfaces longer or by slightly choking the bearing channel. If the consequences of such modifications are to be predicted by a model, an accurate description of the friction at the bearing surfaces is necessary. Earlier research results, which will be treated more thoroughly in the next sub-section, indicate that there is less intimate contact between the aluminium and die at the outlet. This applies even if the bearing channel is choked. The consequence is that if the full sticking relation is implemented, the predicted build-up of pressure most certainly is too high. It would therefore appear as if the bearing channel is more effective in controlling flow than it actually is. If contact is less intimate, the interface shear resistance is most likely dependent on the pressure. If the pressure increases, there may be interaction over a larger portion of the surfaces of the steel and aluminium. The total friction force then increases. The simplest model describing such behaviour is the Coulomb model. If the interaction is treated in an averaged manner, the friction shear

stress, τ_f, may in a first approximation be regarded as proportional to the normal pressure, p_n, acting at the steel-aluminium interface.

$$\tau_f = \mu p_n \qquad (2.10)$$

μ is the friction factor. The normal pressure is the component of stress normal to the extrusion die face. It is related to the hydrostatic pressure in a simple manner (Mohr's circle). The normal pressure must be expected to be high when the hydrostatic pressure is high. Shear stresses are usually small compared to the hydrostatic pressure, although this may not be completely true close to the outlet of the bearing channel. Due to friction, both the hydrostatic and normal pressure increases in the direction opposite to that of extrusion. If μ is a constant, the friction shear stress should also increase. The friction shear stress will, at a certain point in the bearing channel, reach the flow shear stress if the bearing channel is sufficiently long. As long as the extruded material is of uniform composition, it should not be possible to further increase the wall shear stress. Sticking conditions prevail, and deformation occurs essentially in the interior of the material. The intimacy of contact would be as high as it possibly could be. Wanheim and Bay have introduced a friction relation that has been derived from a local slip-line model of adhesive friction [Pet97] [Wan74] [Tve97]. Large segments of the extrusion environment have adopted the term stick-slip friction to describe the situation in which a part of the bearing channel is in less intimate contact, and another part is in fully intimate contact. The term is used also in this work, but it may be misleading. Stick-slip friction is also often regarded as the erratic contact between two solid surfaces. The extrusion stick-slip friction is possibly an even more complex issue relating to the very high rate elasto-viscoplastic behaviour in a thin boundary layer close to the bearing surfaces. To what extent friction shear stress in the slipping area is temperature- and rate-dependent is not exactly known. There may potentially be a number of factors that affect friction in the very high rate region of deformation at the die outlet. Although the friction behaviour is called slipping, there are probably a number of asperities that deform viscoplastically. There may be significant profile surface modification, as such asperities are sheared off during the very high rate deformation. Satisfactory modelling of the micro-mechanisms of bearing channel deformation has not yet been performed. One should note that the problem is related to experiments rather than to mathematics.

The current sub-section has treated some of the most important and basic assumptions of extrusion flow modelling. There are also a number of other assumptions related to boundary conditions. When treating complex thin-walled high-strength profile shapes, one should consider extrusion tool deformation. In order to establish accurate and useful predictions of the extruded profile shape and microstructure, a mathematical deduction must be performed. Analytical techniques such as the slab method [Axm98] [Chi01], the upper bound method [Hal65] [Avi68] [Jia96] [Kak96] and the slip line method [Gei37] [Hil50] [Joh70] [Joh82] [Chi97a] [Chi97b] [Chi99] [Chi03] may produce estimates of ram forces and outlet temperatures. However, if practical problems are to be solved, one usually has to resort to numerical flow calculations. The solution of the conservation equations is not a trivial issue, even if it is assumed that the material behaviour is purely viscous. The conservation equations for the flow are coupled and must be solved simultaneously or at least in a staggered manner for the complete run.

Also the die deformation and the heat transfer to the tools must be considered. The main variables for the flow problem are usually the hydrostatic pressure, the flow velocity and the temperatures. The finite element method is the most widely used method for extrusion simulation. It is based on the Principle of Virtual Power [Zie91] and assumes that all the variables may be approximated by a piecewise polynomial function. When treating viscoplastic flow, it is important to carefully choose these functions in order not to impose too many linear restrictions on the velocity field from the incompressibility relation [Bel94]. There are a number of possible formulations [Che98b] [Bel00]. In the treatment of the equation for energy conservation it may be necessary to apply what is called an upwinding scheme, which mimics convection along streamlines [Zie91] [Fle91]. The objective of the discretisation is to establish sets of equations that may be solved by for example a Newton-Rapson approach and that may produce the nodal values of the main variables (e.g. pressure, velocity, temperature). The system is highly non-linear, so the solution approach must be an incremental one. Furthermore, time discretisation is performed, and solutions must be found for many time-steps. As the ram moves, the profile flows out of the die. Thus, the mesh must be updated, and the approach must be able to describe the physics of the profile in air. It is possible to relate the movement of the mesh directly to the movement of the material. This is called the Lagrangian approach. In order to avoid excessive mesh distortion and very frequent and very time-consuming re-meshing, the Arbitrary Lagrangian Eulerian (ALE) approach may be implemented [Aym01] [Gou98] [Haa00] [Hue86]. The ALE method allows the user to define the translation of the nodes. The close link between the movement of the material particles and the mesh is then lost, and it may be necessary to later convect material information about the state of stress by an independent scheme. Holthe et al. and van Rens have developed viscoplastic flow codes for the extrusion process [Hol91] [Ren99]. Lof et al. reports on a flow or extrusion code that allows the study of fully elastoviscoplastic material behaviour [Lof01].

It should be emphasized that even though the main difficulty in connection to material modelling is that of accurately establishing material models and data, there are still large challenges related to the development of numerical simulation codes. Calculation times are still significant and both formulations and solution procedures must be further improved. A special difficulty of extrusion is that material modelling should probably also be seen in relation to the discretisation approaches, for strain localisation requires a careful adaption of mesh and formulation. The flow of material during extrusion is not an elliptical problem ideally suited for numerical solution by the finite element method, but rather the composition of several hyperbolic ones. The task of verification is most difficult, especially in the case of three dimensional modelling. Not only must the codes be capable of predicting ram forces and outlet temperatures, they must also predict small changes in the profile shape and the deformation of the extrusion tools. The loads on the dies are immense during extrusion. The numerical simulation tool will first be of significant value when it may be used effectively as an aid in die design and trouble shooting processes. While one has experienced very important progress in the field of numerical modelling over the last decade, important work remains to be done.

2.5 Challenges and extrusion research

The industrial implementation of extrusion technology must be regarded as successful. Significant investments have been made in a vast number of plants worldwide. Profiles are used in many products, and the extrusion business is generally profitable. Extrusion is no longer a novel technology, and even though there still are resources available for technological development, the forces of inertia are large when it comes to industrial implementation [Pan00] [Pan02]. Recent improvements have been related to details rather than concepts. The main challenge facing plant managers is cost reduction, which primarily requires logistics to be streamlined, process control to be very effectively implemented and routines to be improved and followed. Few manufacturers are willing to risk their money and reputation on promising but unproven concepts. Of course, for some the picture may change if possible gains are sufficiently large. Today, the very enticing prospect of acquiring a larger share of the automotive market (or the fear of loosing the segments that have already been gained) provides a strong impetus for change. While there is a need for an improved capability to predict and accurately tune the material microstructure and properties, the largest challenge is probably to satisfy the industry's strict requirements to dimensional variability.

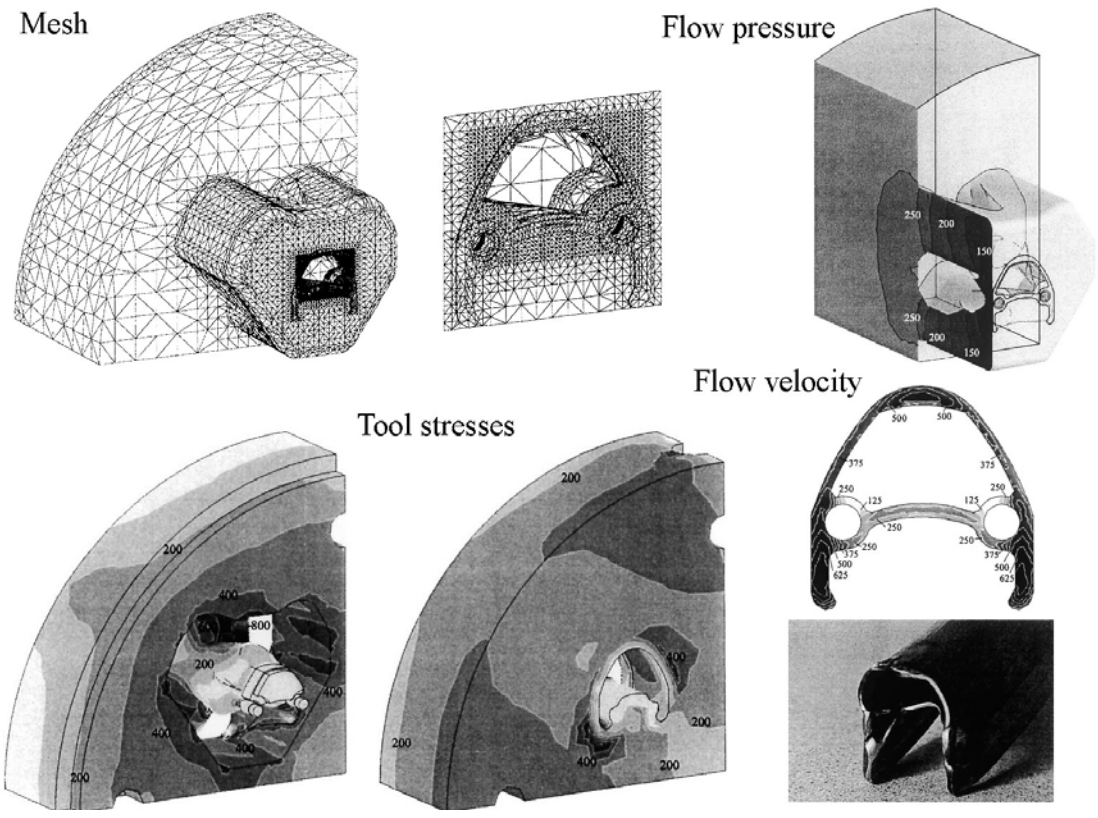

Figure 2.14. An example of FEM modelling of flow in extrusion [Lof01]. Calculations have been performed both to estimate the pressure build-up (top right), flow velocity (bottom right) and die deformation and stresses (bottom left).

The extrusion process was not initially designed to produce aluminium profiles with the very narrow geometrical tolerances in demand today. Some claim that problems related to excessive dimensional variability are closely linked to the press / tool design and the transient nature of the process and are therefore almost inevitable. Such a claim may be disputed, but one thing is quite certain. In order to control material flow and profile dimensions of thin-walled profiles, particular attention must be paid to the design of extrusion tools and die outlets and to the careful control of the temperatures of the billet and tools during the extrusion process. The nominal dimensions of the die outlet seldom match those that are desired for the profile. Both the thickness and the cross-sectional shape of profiles may deviate, and deviations may quite easily exceed a tenth of a millimetre. First, there is always an effect of the difference in thermal expansion of aluminium and die steel that has to be considered. Second, adhesive layers deposited on the die lands may cause the die opening to narrow. Adhesive layers are seldom very thick, but may still significantly affect flow conditions. Third, since the pressure at the upper die face may reach 500 MPa or more during extrusion, tools may be considerably deformed. The deformation is not uniform and may seriously affect the shape of the die outlet. The tool stacks are, as stated previously, usually designed to provide optimal support for the dies so that die deflections and outlet distortions are as small as possible. This may be achieved by designing the backer and bolster with as tight outlets as possible. Dies for extreme shapes such as U-profiles or hollow profiles may still suffer from large deformations, as the support cannot be optimal. Furthermore, there is seldom a die design that completely compensates for the effect of die deformations. When extrusion dies are used over long periods of time in hostile environments, they may creep and crack. Such phenomena are not always easily predictable, and effects may sometimes not be detected before quite significant lengths of profiles of unsatisfactory quality have been produced. The economic losses may then be significant.

Finally, in the case of thin-walled profiles, shape distortion and to some extent thickness deviations may be the result of flow instabilities. Skilled technicians, the die correctors, may tune bearing lengths and choke angles in order to ease flow where it is necessary so that the outlet velocity becomes as close to uniform as possible over the cross-section of the profile. Feeder design is performed with the very same objective. If resistance to flow along various flow paths differs, shear stresses are set up in the profile as it leaves the die in order to counter shear straining. As the parts of the profile that tend to flow faster exert a drag on other parts, compressive and tensile stresses also exist. This may cause both thickening and thinning of the profile. However, the flow is essentially stable, and the section shape may not be severely affected. The mechanism described above has been called the self-stabilisation mechanism in extrusion [Stø93]. The limits of stability may be exceeded if the die design and container flow promotes instability, the profile is extremely thin, or the material for some reason softens. In such cases velocity differences may give raise to deformations such as buckles or wrinkles [Zas00]. Profiles with asymmetric cross-sectional shapes may also curve as they leave the die. Given that the die was not designed to produce curved profiles [Bun02] such behaviour indicates that die correction is needed. In industrial extrusion, a puller is frequently used to guide the profiles to the run-out table. The low tensile force exerted by the puller may in many cases prevent unstable flow. However, if the flow is not stable at the onset of extrusion, it may be hard to extrude anything at all. The profile may stick to the tools,

and the die outlet may get plugged. Both time and money must be spent correcting die outlets or producing new dies. It must be added that the instability of flow is seldom an insurmountable problem when sufficiently thick-walled sections are extruded. The die designers and die correctors, aided by their personal experience and statistical data bases containing results from extrusion with similar profiles, often reach quite workable solutions over relatively few trial iterations. Only approximately ten percent of the profiles extruded may, according to sources in the extrusion industry, be expected to cause significant problems and are worthy of closer attention. However, with a greater focus on weight and strength considerations, material cost and quality, the percentage may be expected to increase significantly in the future if efforts are not made to improve process control. Today, it is generally accepted that procedures of trial and error are simply too costly and must be superseded by careful design based on insight.

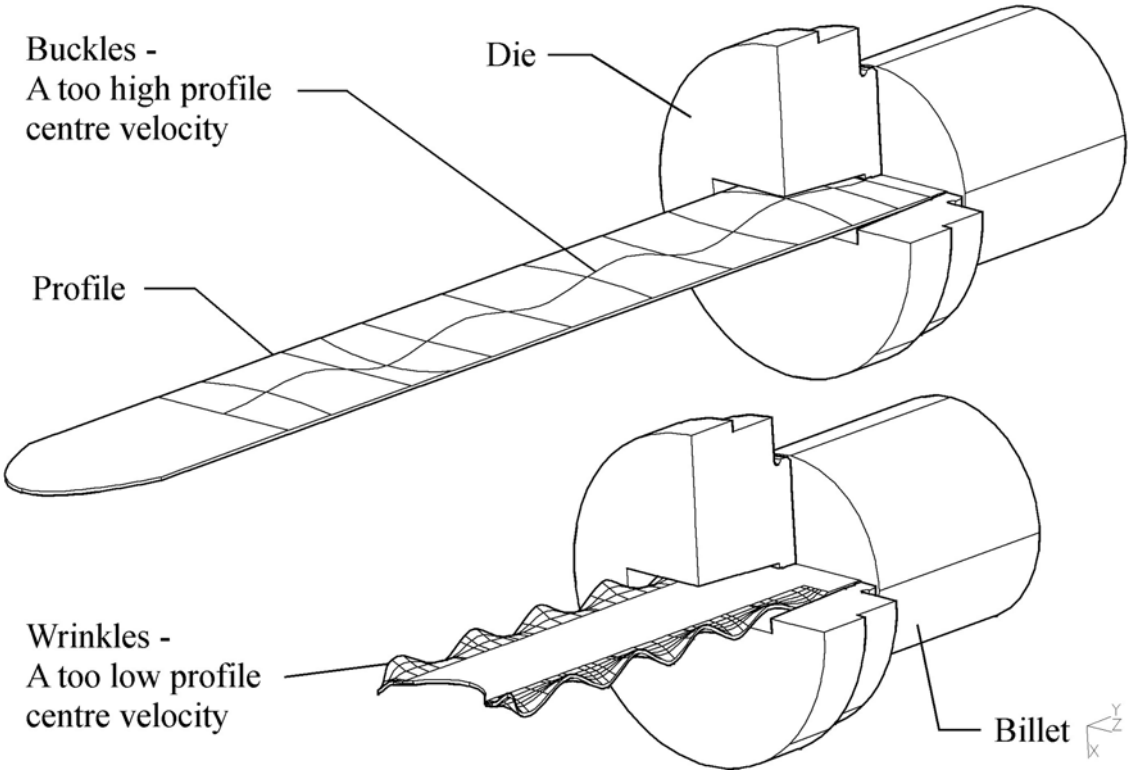

Figure 2.15. Buckles and wrinkles due to improper flow balance during the extrusion of a thin strip of aluminium. More complex profiles may experience even more serious distortions such as wryness.

Too much dimensional variability is a diagnosis which says everything and nothing at the same time. It is often a symptom of a general lack of process control rather than of any easily diagnosable malady for which there is an efficient cure. When assessing the geometrical variability in extrusion, one should keep in mind that the fundamental mechanisms controlling flow stability and shape variability are complex and far from completely understood. The effects that die deformations have on the outlet shape are easily predictable, but the interaction between the die deformation, the flow velocity and the pressure build-up is complex. Still, no model treats all essential effects and produces

predictions that have been verified through careful experiments. Statistical models based on data from experiments (phenomenological models) hardly give full insight into the mechanics of extrusion. Finite element or similar models of the complete extrusion system may be very complex, and they are still not used effectively to solve flow problems. While the first finite element models of metal forming date as far back as to the beginning of the 1970s [Lee73] [Zie74], it may still take some years before codes may accurately and reliably predict the profile shapes. Results must be very carefully evaluated, for the thin-strip extrusion process is a most complex and delicate system. A study of the flow stability requires a constitutive model that addresses not only the material flow in the container, but also the buckling and thinning phenomena in the outlet. The model must be sensitive to the important friction mechanisms of the bearing channel. A fundamental problem in the study of flow stability is that only a few minutes of rotation of the bearing surfaces due to die deformation may cause the bearing channel to turn from choke to release and, thus, influence flow drastically. This is not so much a modelling problem as a weakness of the extrusion process in general, for it requires the die outlets not only be extremely accurately made, but also hopelessly purposefully. Often no such exact sense of purpose exists on the part of the die designer, and the task must in the very end be solved by trial and error by the die correctors at the plant. It is therefore not at all easy to establish an understanding of the physics of the extrusion process and to build models that are actually of practical use.

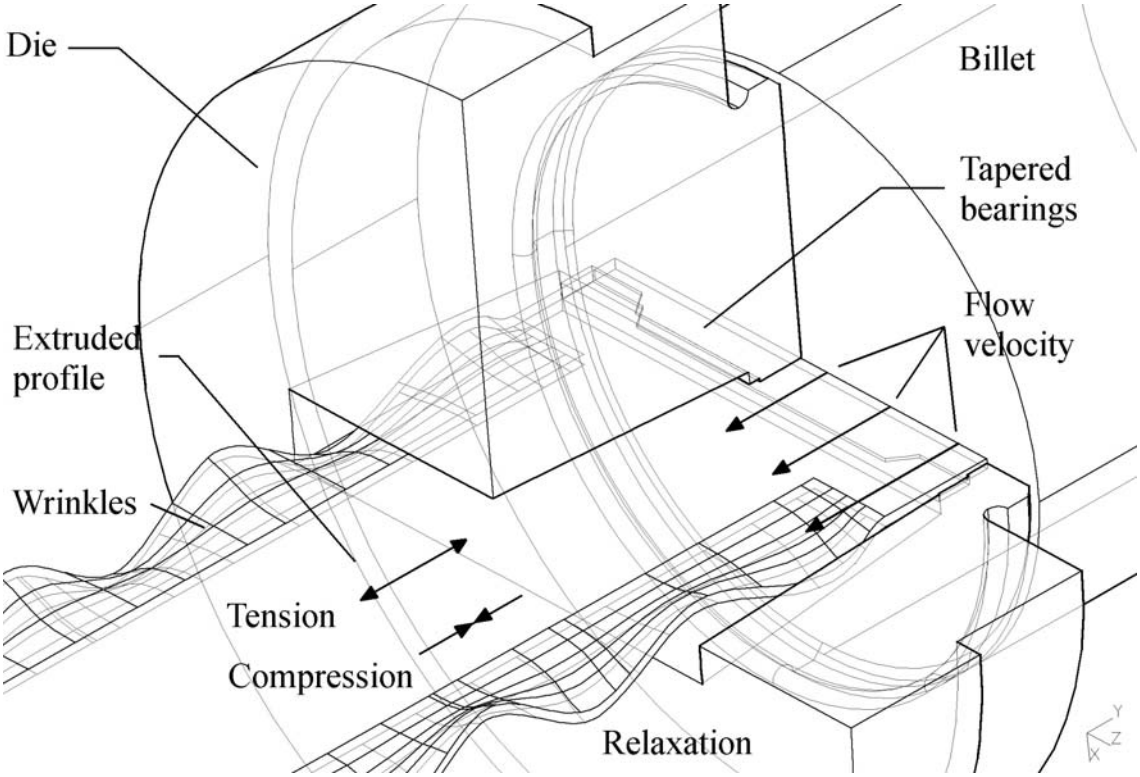

Figure 2.16. A tapered bearing channel used for extrusion of thin-strips. The flow close to the edges of the profile is too fast, and the profile is distorted close to the outlet. The wrinkling probably occurs as the stresses in the profile reach a critical level. The phenomenon is often observed and is further described by Grasmo [Gra95].

The current study is a part of a larger research effort whose main objective has been to establish a more fundamental understanding of the extrusion system and particularly of the physics of material flow and friction in and around the die outlet. Focus has been on the mechanisms of flow stability and on the possible causes of dimensional variability. This research activity commenced more than 15 years ago and has mainly been carried out by researchers at the Norwegian University of Science and Technology and SINTEF Materials Technology under the skilled guidance of Professors Sigurd Støren and Henry Valberg. Economic resources have been provided by the Norwegian Research Council and Norsk Hydro. The current section provides an overview of the activities and a brief summary of the main results. Related results obtained by other researchers are also referenced. Tverlid has provided a more complete presentation of early studies [Tve97].

The necessity of developing a unified theory and effective modelling tools for extrusion has been treated by Støren in the paper entitled *The Theory of Extrusion – Advances and Challenges* [Stø92]. It presents the long-term objectives of research on extrusion and underlines the necessity of developing a basic understanding of material behaviour and microstructure evolution, the mechanics of the complex extrusion system and relevant measurement methods for validation of results. The importance of actively applying insight to the forming process of extrusion and downstream processes to develop better products is stressed. Støren has focused on the fundamental mathematical descriptions of metal flow in extrusion and strain localisation phenomena [Stø89] [Stø91]. He was among the first to emphasize the need for process charts that allow one to focus on a number of aspects of the microstructure development of material particles flowing through the container. Some of the charts were presented in the previous section.

The parallel development of numerical codes and measurement methodology has been regarded as a fundamental building block in the study. Kjell Holthe and Lars Hanssen developed the ALMA2D and ALMA2π programs in the late 1980s and early 1990s with the objective of studying flow under the assumptions of plane strain and axisymmetric conditions [Hol91] [Hol92]. The work was supported by SINTEF, Hydro Aluminium and the Norwegian Research Council. The codes make use of models for viscoplastic material behaviour and full sticking container friction. During extrusion, the boundaries of the flow domain change and the mesh is compressed. The ALMA codes allow the temperature distribution in the tools to be evaluated and multiple cycles to be run [Hol96]. The task of improving the codes has been a continuous one, and later versions allow stick-slip bearing friction to be modelled [Hol99]. Efforts have also been made to implement a more effective element formulation to handle the large velocity gradients close to the bearing surfaces [Auk00]. The ALMA2D and ALMA2π codes have been extensively used by Hydro Aluminium, SINTEF and NTNU. Material data for a range of alloys have been established by torsion testing [Ped99], and the mechanics of the torsion test and the appropriateness of constitutive relations have been studied [Irg90] [Gra95]. An extensive set of rod extrusion experiments has been run in order to check the validity of results predicted by the code [Gra92]. The grid line technique of Valberg has in this relation been used to evaluate the related predicted flow fields. Valberg's technique has been extensively used also on other occasions to study more complex cases of extrusion [Val88] [Val90] [Val92a] [Val92b] [Val93] [Val96a] [Val96b] [Val96c]. Hanssen, Lefstad, Rystad, Reiso and Johnsen combined experiments with a

similar marker material with ALMA simulation to better understand the flow of material from the surfaces of the billet into the die outlet [Lef92] [Han98] [Han00].

Martin Lefstad has developed a technique for measuring the temperature of the metal flow at the die outlet and in the bearing channel [Lef96]. Pyrometers may be used to measure the temperature of the extruded profile on-line, but they are not able to measure the peak temperature at the outlet. Thermocouples may also be placed in extrusion dies close to the profile, but the temperature of the die material and aluminium usually deviate significantly. Lefstad therefore positioned thermocouples in direct contact with the aluminium flow. The penetration depth of the thermocouple tip into the flow of aluminium is set so that measurements are accurate. Calibration may be performed since the melting temperature of secondary phase Mg_2Si particles in the 6xxx alloys is known. This temperature measurement technique has been extensively used over the last fifteen years in studies of metallurgy and friction in relation to the extrusion process. Both Oddvin Reiso and Lefstad have used the measurement technique to evaluate the influence of melting of Mg_2Si particles on the extrudability of AA6xxx-alloys [Rei92] [Lef93]. Reiso has demonstrated that melting of secondary particles occurs almost spontaneously at the eutectic temperature, but also that extrudability may be optimised by tuning the alloy composition and the thermo-mechanical processing of the material. Lefstad investigated the tearing limits for AA6060 and AA6082 alloys. He observed that when there were no Mg_2Si particles in the profile, the surface was torn first when it reached the solidus temperature of the material. However, when there were Mg_2Si particles, tearing occurred at the eutectic temperature. Lefstad related the tearing to the melting of Mg_2Si particles. He also constructed special press limit diagrams that took into account the tearing mechanism in extrusion.

Geir Grasmo, Shahriar Abtahi and Steinar Tverlid focused on establishing models for flow and bearing friction during extrusion of thin aluminium strips. The thin strip shape they used was such that the extrusion ratios in two and three dimensions are equal. The two-dimensional extrusion ratio is then defined as the ratio between the billet diameter and profile thickness. In such cases it is expected that the deformation in the symmetry plane is plane strain and that two-dimensional codes (plane strain/axisymmetric) may be used to predict the outlet temperature and to study bearing channel flow. Grasmo made extensive use of the ALMA2D software and ran both torsion and extrusion experiments to evaluate the flow behaviour of aluminium [Gra95]. He experienced that ALMA2D, when used with the Zener-Hollomon flow rule, produced acceptable predictions of the main process responses. Furthermore, he also found that simulations with the common assumption of sticking friction through the entire bearing channel predicted temperature increases at the bearings that were too high. A similar observation was later made by Torgeir Welo et al. [Wel96]. Grasmo therefore proposed that the friction stress at the outer part of the channel is of a slipping or less intimate type.

Shahriar Abtahi performed careful experiments with a split die design to study adhesive layers in slightly choked bearing channels and the surface generation of extruded sections [Abt95] [Abt96]. A similar split die was used by Clode and Sheppard, who performed experiments with more or less the same objective [Clo90]. The practical interest of such studies relates not only to the challenges of establishing numerical

models, but also to the reduction of surface defects such as pick-up, die-lines and micro die-lines that often appear as easily confoundable grooves in the profiles stretching long distances. Micro die-lines cause a surface roughness, R_a, of approx 0.2 μm, while the characteristic dimension of die lines may be up to twice as much. Clode and Sheppard claim that pick-up and die-lines occur when the bearings are in release so that there is intermittent contact between steel and aluminium and continuous surface modification along the bearings. Micro die-lines, however, may also be observed when the bearing channel is known to be choked, and both Abtahi and Sheppard claim that they are caused by the abrasive action of third party particles residing in an adhesive layer at the die lands. In the case of extrusion of 6xxx-alloys, both researchers have identified the particles as α-AlFeSi, but their origin is uncertain. A natural assumption that has been advocated by Sheppard is that they come from the shear zone close to the dead zone of the billet, as does most of the profile surface material. The alternative view is that they originate from the bearings, but this seems less likely, since it has been shown by many authors [Sah98a] [She99] [The92] that material from the adhesive layer is regularly drawn out of the die and replenished. Similar observations have been made by Feder and co-workers, who have performed extensive optical experiments with transparent model materials and dies [Fed02]. The build up and preservation of the layer appears to be a dynamic mechanism depending on a number of parameters, with the initial die land surface texture and properties [Tok88], material temperature and properties as well as process parameters being important ones. According to Bjørk et al. [Bjø99] and Saha [Sah98a], the discontinuous nature of the extrusion process with its frequent stops and starts, plays a part and promotes wear as the adhesive layer is frequently torn off. Nitrided surfaces seem to be less affected and more resistant.

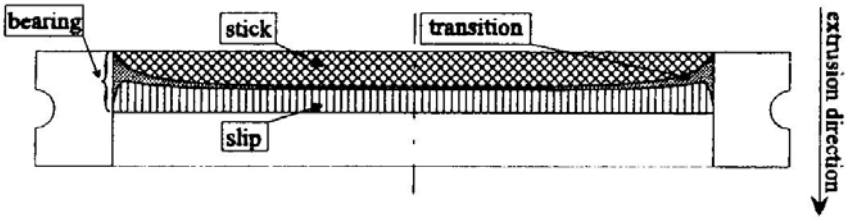

Figure 2.17. Friction domains at the bearing surfaces according to Abtahi [Abt95]. The experiments were run with split dies that allowed inspection of the bearings after extrusion.

The observations described above further indicate that the tribological conditions in the bearing channel are potentially poorly represented by a full-stick relation. The partition of the die land into regions with and without adhesive layers was interpreted as a proof of the existence of two distinctly different mechanisms of friction working in the outlet, namely that there is a region of stick, where the section material completely adheres to the die steel, and a region of slip, where the material glides on an adhesive layer. There is also a transition zone where the surface is built and the surface material is elongated as it flows outwards towards the profile surface. The existence of such flow has been demonstrated experimentally, although not incontestably, by extrusion experiments with Valberg's grid techniques [Val94]. Bjørk et al. also claim that a model with two different contact regimes is supported by the observation that wear on die lands seem to

be greatest in the transition zone. The adhesive layer is most firmly attached to the bearings in the transition zone. The pressure increases in the direction opposite to that of extrusion, and there is no or only a very thin adhesive layer in the sticking zone. Die wear is to a large extent related to stops and starts of extrusion. The adhesive layer and particles from the die may then be torn off the bearing surfaces. Bjørk et al. claim that the more firmly the adhesive layer is attached, the faster the surface is worn out.

(a) Extrusion with slightly choked (10-15') bearing channel

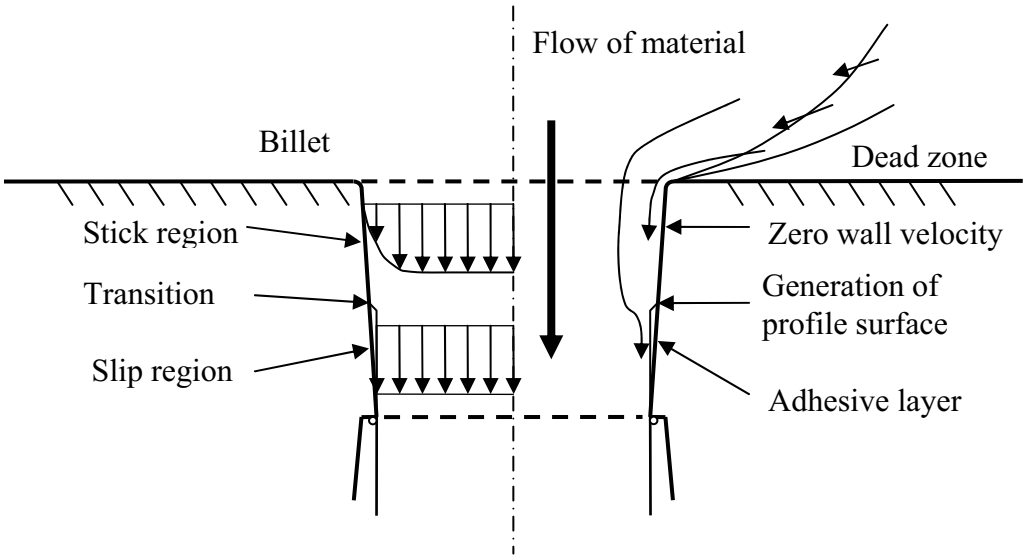

(b) Die and bearing deformation effects

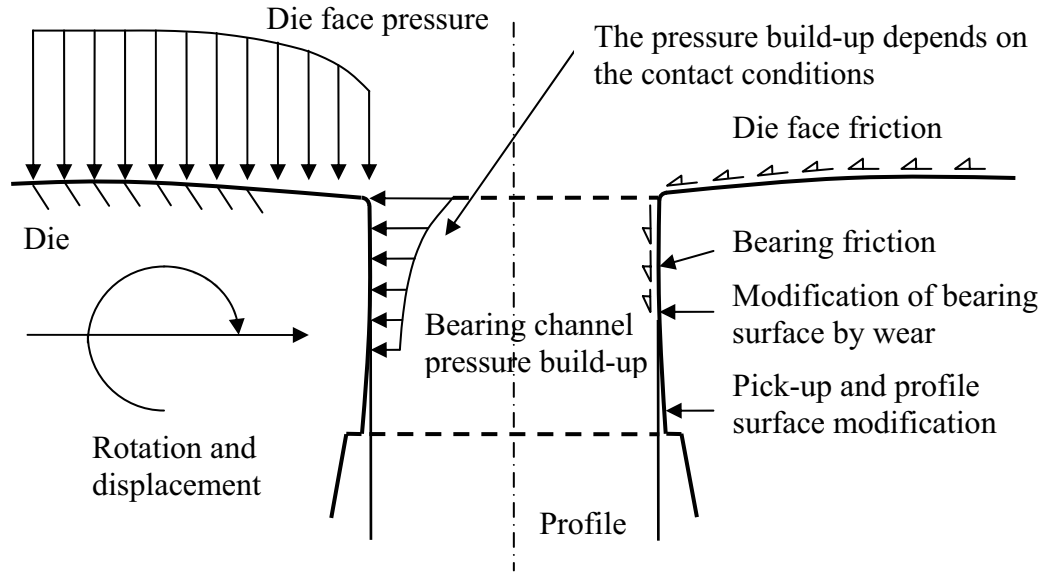

Figure 2.18. A model of flow and friction close to the outlet of the extrusion die. The bearing channel is nominally slightly choked (a), but deformation of the die and wear may cause it to become parallel or even in release (b).

In order to model the pressure build-up in a stick-slip bearing channel with the flow code FIDAP, Abtahi carefully measured the length of the adhesive region in the extrusion direction for all cases he had run. He then established an experimentally based friction relation. The pressure build-up was found to depend on the choke angle and was very sensitive to changes if the bearing channel was close to parallel. Tverlid performed further experiments with the split die designs in order to more closely model bearing friction [Tve97]. He made use of the Forge2® numerical code for metal forming, and implemented the Coulomb / Wanheim-Bay friction relation to model the pressure build-up in the bearing channel. The assumption was that the contact was less intimate in the part of the bearing channel with an adhesive layer. For a friction factor of approx 0.4 he found that Forge2® predicted positions of the slip point in fair accordance with the ones measured by Abtahi and himself. Experiments seemed to indicate, however, that the friction shear stress in the slipping area may be velocity dependent. The use of three-dimensional extrusion codes to study the problem was proposed, for although the plane strain approach may be satisfactory in predicting temperatures, it may in fact fail in describing friction phenomena in the bearing channel. When the flow and friction in the bearing channel are assessed, it is most important that differences in pressure build-up and flow velocity over the entire cross-section of the extruded profile are taken into account. The thermoelasto-viscoplastic behaviour of the extruded profile in air must also be evaluated and so must the deformation of the extrusion die.

A process for developing a numerical model for three-dimensional aluminium flow started in the late 1990s. A first incomplete version of the program Extrud3D was presented by Trond Kvamsdal in 2002 [Kva02], but further development was stopped or delayed due to insufficient funding. A viscoplastic flow model was implemented in Extrud3D, and temperature and flow problems have been coupled. Validation of the code has to a certain extent already been performed [Lef99] [Abt02]. Challenging tasks related to the modelling of the thermo-mechanics of the bearing channel remain. Similar development of 3D flow codes has been performed elsewhere [Eik97] [Ren00] [Moo99] [Lof00] [Lof01] [Lof02] [Sha02] [Wil02]. There are also a large number of examples of applications of commercial codes in the study of extrusion [Cha99] [Cha00] [Cha01] [Dua03] [Fli00] [Fli02] [Gas00] [Kim00] [Kim02] [Shi97] [Zho03]. Deform™ and Forge3® are two examples of programs dedicated to the study of material forming. They are based on the Lagrangian formulation and focus on forming processes that are somewhat simpler than extrusion, for example forging. Regular and time-consuming remeshing must be performed so that the mesh does not degenerate. ALE formulations are developed and will simplify the numerical study of extrusion. Larger finite element software producers now also focus on material forming processes. The companies that work with MARC, ABAQUS, LS-DYNA are examples of software developers that have made significant efforts to adapt codes to the study of aluminium extrusion and similar processes. Some of the simulation codes implement the stick-slip friction model and support the observations of Abtahi with regard to the sensitivity of the friction effects to small changes in the choke angle. Attempts are also being made in order to use flow codes to study flow control and die design optimisation [Jou98] [Lee00] [Uly02] [Zha00]. HyperXtrude by Altair Engineering is a commercial program that has been developed for sensitivity studies in relation to extrusion.

As modelling codes become more capable of tackling the complexities of the thermo-mechanics of the extrusion process, greater efforts are invested in modelling. Prof. Støren has in this respect proposed that thin-strip geometry may be used as a common test case, since it is the simplest geometry for which instabilities may be provoked. Two detailed studies of the flow instability during thin-strip extrusion have been performed partly in parallel with the study reported in the current thesis. Wojciech Wajda has treated flow stability during thin strip extrusion with flat-faced dies [Waj03] [Waj05b] while Frode Halvorsen rather has focused on extrusion with feeders. Both of these studies, along with the study presented in this thesis, are based on the many experiences gained in earlier phases of the research on extrusion that has just been summarized.

Chapter 3

The objectives of the study

This section presents and comments on the initial task description of the PhD work. The objectives of the work as defined by Prof. Sigurd Støren have generally proven realistic as well as relevant and therefore not been significantly altered. They are presented in the first sub-section of this chapter. Initially Prof. Støren and the candidate also proposed an approach for reaching the objectives of the study, and the plan has in fact been relatively closely followed. Some of the limitations of the work were apparent at the onset of the study, although they were not specifically mentioned in the task description. They are treated closely in the final part of the current section. Some important modifications and limitations have been introduced in the course of the work. The details of the research approach that has been followed will be more thoroughly treated in Chapter 5. The focus of the first parts of the current chapter is rather on the motivation for the work as well as on the final objectives. The discussion should necessarily be seen in relation to the presentation of the extrusion process and the related challenges of Chapter 2.

3.1 The task description

The problem setting, motivation and purpose of the study were initially presented by Prof. Sigurd Støren as follows:

One of the main challenges for the future of extrusion technology is to produce sections for optimal functional performance at the lowest possible material consumption with a variation in dimensions, shape, properties and surface appearance less than 10% of today's level at a competitive price per meter section delivered to the customer, giving satisfactory profitability along the whole value chain.

There has been a continuous evolution of extrusion technology in the last few decades, related to alloy development, extrusion press design, press parameter monitoring, automatic control, section design, die design and process planning. This evolution is mainly based on systematic improvement of each factor individually, whereas the method of trial and error is applied for improving the total performance with respect to productivity and consistence in section dimensions, shape, surface appearance and section properties. Only quite recently, based on the results from the ALMA-, the EXPOMAT- and the PROSMAT-programmes has a more system-oriented approach to the problem been adapted. Here, analytical and fundamental studies of basic

phenomena, laboratory studies of generic sections, 3D numerical analysis of heat flow, metal flow, stresses, strains and displacements in deforming material and dies, as well as systematic analysis of microstructural evolution, surface generation, operational practice and new die design principles are carried out simultaneously.

In the further development of this system-oriented and scientific approach, one critical "missing link" for obtaining a deeper process understanding and for development of actuators for controlling variability, is the development of a sensor/predictor system for continuous monitoring of variations in the flow, temperature and stresses in the die (and container?) during the press cycles.

The purpose of this PhD study is to contribute to the establishment of a fundamental base for such a sensor/predictor/actuator system.

The main objectives of the study were also set at the onset of the study by Prof. Støren. There were essentially three goals:

- *Develop a measurement system for the measurement of the pressure between the deforming aluminium alloy and the die at specific positions in the die with a precision better than ± 10 MPa. In combination with the measurement of temperature, monitoring of the variation of pressure and temperature during a press cycle with a precision better than respectively ± 3 MPa and ± 3 K.*

- *Combine this measurement with 3D simulation of metal flow through the die in order to predict the distribution of pressure, friction, temperature and heat flow in the interface between the deforming alloy and the die. This should be done in two steps:*
  - *Step 1: For a generic die in a laboratory set-up*
  - *Step 2: For a generic die in a commercial operating press*

- *Prepare the candidate for taking a leading role in the industrial implementation of the "Future Extrusion Technology Target: Factor 10 Reduction in Extruded Product Variability".*

Further evaluations and interpretations of the objectives of the study are given in the subsequent sub-sections. Volume II of the thesis presents a more detailed interpretation of the objectives related to measurement system properties. ALMA, EXPOMAT and PROSMAT are research programmes supported by the Norwegian Research Council during the 1990s. An important objective of the programmes has been to increase the general expertise in materials processing technology, and research on light metals has been an area of special concentration. The programmes focus mainly on Norwegian industry and research. Hydro Aluminium has contributed greatly throughout the decade to these research programmes and is still an initiative-taker with respect to the newer programmes called FREMAT and COMPFORM. Hydro Aluminium and SINTEF were represented in the Sounding Board for the study, and both took a very active part in the determination of goals as well as in the actual implementation of the technology.

3.2 Comments on the motivation for the study

The necessity for reducing dimensional variability of extruded aluminium sections is the main motivation for this PhD study's efforts to develop measurement techniques that allow better process control. Profiles, whose dimensions often deviate by more than a tenth of a millimetre from the nominal values [Stø03], may be acceptable for a number of purposes. However, when extruded profiles are used in more complex designs or in parts that are mass-produced, it is of the utmost importance that profile production is of sufficiently high precision. Downstream processes such as bending and hydroforming are complicated by the inaccuracies of the extrusion process. Variability in the cross-sectional shape and thickness of profiles affects the elastic springback during bending and consequently the shape of the bent products. Direct automatic assembly is then hampered. Later modification of profile shape and dimensions and excessive tuning of downstream forming processes in order to compensate for shape deviations may be extremely costly. An additional manufacturing step with profile shape tuning may increase the cost of products based on extruded profiles by as much as 60 % [Wel04]. Losses related to inaccurate manufacturing may also be large at the extrusion plant when tolerances are tight and profiles complex. Extrusion of thin-walled high-strength profiles cannot be efficiently performed without a satisfactory control of flow and tool deformation. Several trial-and-error iterations at the plant may be necessary to make certain that profiles are of satisfactory quality. Tools sometimes have to be scrapped and redrawn. If the profile is difficult to extrude, small changes in the process parameters during production may cause the quality of the product to become unsatisfactory. In the worst case, profiles have to be remelted and complete orders have to be rerun. Thus, the causes of variability in the extrusion process must be identified at an early stage and appropriate actions must be taken to implement better control. If a better understanding of the mechanics of extrusion is established, more complex profiles may be run and higher production rates may be reached. Process optimisation may also be performed to reduce start and end effects so that more of the extruded material may be used. Finally, better process control makes possible closer integration of extrusion and downstream process steps such as stretch-bending and the implementation of fully automated manufacturing systems for composite products. The positive consequences and the cost of improvement must be and most likely should be favourably related.

Advanced users of extruded profiles, such as the Audi, the automotive manufacturer, have experienced the need for better process control during extrusion. For more than a decade, Audi has sought to refine aluminium car technology so that it can compete with steel also in price. Audi has developed spaceframes for cars that are 40 to 50 % lighter than the traditional steel car structure. Fuel consumption and emissions are reduced, while handling and safety are improved. Aluminium has for a long time been the preferred choice for materials for bumpers or crash-boxes. One of the advantages of aluminium forming technology and extrusion in particular is that the cost of tools is low, and that the production of smaller series of cars may be profitable. The assembly of spaceframes may also be performed very effectively by welding, if the parts have been accurately produced. Still, a spaceframe of aluminium costs approximately 30 % more than a steel frame. The higher cost of aluminium material partly explains the difference, but the production technology is certainly lagging. The frames of the Audi A2 and A8 consist of 18 % and 25 % extruded aluminium profiles respectively. It would be

advantageous to use even more extruded profiles since they are cheap compared to cast parts. The weight of extruded parts that are used in bumpers and engine cradles is also significant. Hence, future cars may be expected to consist of considerably more than the 28 kg of extruded profiles as is the case of the A2 spaceframe. The cost of ready-to-assemble extruded parts for Audi is approx $10/kg, while the aluminium billet price is approx $1.5/kg. Profiles for less demanding applications such as bumpers are often purchased for less than $5/kg. Thus, there is a large potential for process improvement and cost reduction. The economic implications of significant improvements in the extrusion process are at the same time very large. Only limited quantity of aluminium cars are produced today. The annual production of the Audi A2 has in fact not exceeded 60 000, while the worldwide annual production of cars and vans is greater than 40 million. If the aluminium industry and car manufacturers manage to improve extrusion and downstream processes and establish aluminium-intensive car concepts that can fully compete with steel, sales of extruded profiles may increase significantly. If 5 million of the cars manufactured annually made use of aluminium spaceframes consisting of 50 kg of extruded profiles, revenues could reach $2.5 billion dollars annually. Today's prices will necessarily have to be cut, but this merely creates an enormous impetus for process improvement. A reduction of the price of profiles for spaceframes by say 20 % would in fact release approximately $500 million annually. It is not surprising that the president of the world's largest aluminium and profile producer, Alcoa, promised in 1996 that the first car manufacturer willing to produce a large series car will receive a reward of $1 billion. A more thorough discussion on the potential economical consequences of an improvement of the extrusion process has been given in reference [Moe04e].

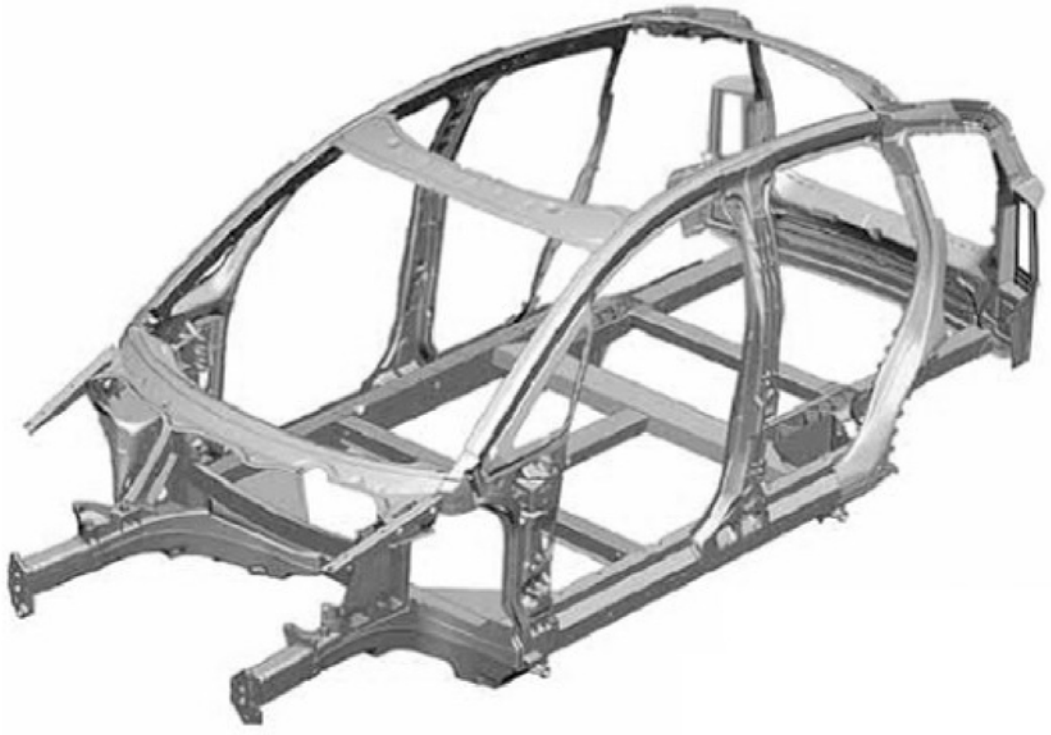

Figure 3.1. Audi A2 spaceframe consisting of extruded, cast and stamped aluminium parts. The Audi A2 and Honda Insight are the first smaller sized cars that make truly extensive use of aluminium in the body structure [Woo02].

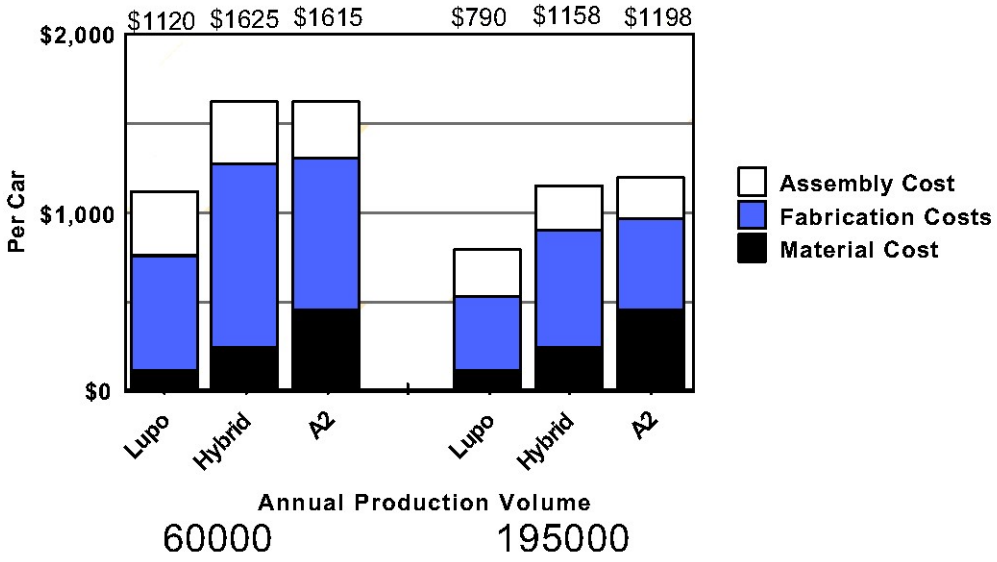

Figure 3.2. A comparison of material, fabrication and assembly costs for three small sized cars produced by the Volkswagen group. Two versions of VW Lupo are produced, a traditional steel frame car and a hybrid aluminium-steel version. The Lupo is a somewhat smaller car than the Audi A2 [Kel00].

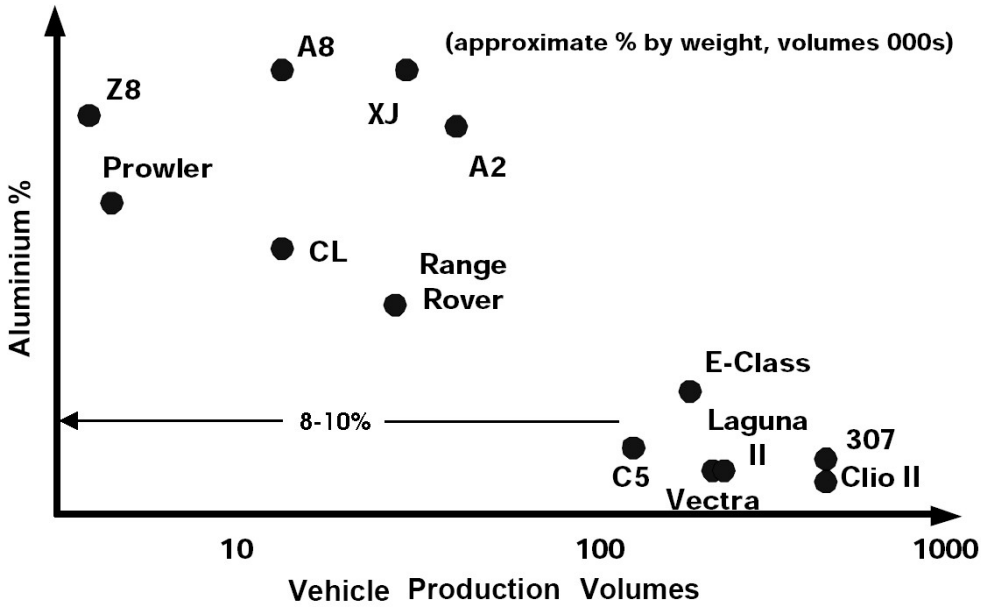

Figure 3.3. The production volumes versus the aluminium usage in some common cars. The car production volumes refer to the worldwide annual production. The annual production of some steel car types reach several hundred thousand yearly while aluminium cars are still produced in relatively small numbers. XJ refers to the Jaguar XJ while CL refers to the Mercedes CL-series. Both are luxury cars. Z8 is the BMW Z8 [Woo02].

The reasons for introducing new measurement techniques for the study of extrusion are easy to understand. Man's understanding of nature originates mainly from data obtained from measurements and physical observations. Mathematical models that mimic natural phenomena are sometimes developed in order to convey information about the nature of a system or to produce predictions of the responses of a process. The usefulness and beauty of mathematics cannot be disputed, and the strength of numerical simulation is probably evident to all. Mathematics allows the most complex systems in nature to be mimicked and advances comprehension. A view of a world governed by fundamental laws is in line with mankind's desire to control the surroundings. Still, models may be regarded as human artefacts that are based on numerous assumptions. Verification of the validity of models is an essential part of any research activity, and the basis of the hypothetical deductive approach that essentially is the systematisation of a sound scepticism. The central role of experiments in science has been emphasized by a number of scientists throughout history. Roger Bacon claimed as early as 1276 that "without experiment nothing can be known". Approximately two hundred years later Leonardo da Vinci urged: "Shun the precepts of those speculators whose thoughts are not confirmed by experience" [Pap04]. Galileo Galilei later introduced the experimental approach that is still in use today. Even in an age of very advanced mathematics and complex physical theories that treat particles that cannot be observed with the naked eye, a prominent scientist like Max Planck confidently stated "Experiments are the only means of knowledge at our disposal. The rest is poetry, imagination." Thus, the general need for experiments and measurement in the study of processes generally is deeply rooted and supported by the scientific community, past and present.

There is no doubt that the mathematical models of the aluminium extrusion process may potentially be important tools for process improvement. However, the models must be carefully controlled, especially since the continuum mechanical framework that often is used to study this process is entirely reliant on independent experimental determination of various kinds of material behaviour using representative tests. The most reliable support for constitutive or material relations such as that of Zener-Hollomon is not provided by multi-scale models, but usually rather by simple torsion and compression experiments. Due to the lack of better data, the results are often used indiscriminately in the study of extrusion. Since extrusion is a high rate transient process and standard materials tests are performed at a rather low rate, extrapolation of data is often regarded as both necessary and natural. The models that mimic friction are even more complex to accurately establish than those that mimic bulk deformation. Extrusion models are generally based on a number of bi-hypotheses that may not always be easily checked. Thus, in order to understand the material behaviour during extrusion, one is forced to perform systematic measurements of essential process parameters. Both modelling and measurement errors have to be considered. It would also be most valuable to measure the interactions between the various parts of the extrusion set-up in order to better understand nature of the extrusion system. The study of flow instability and dimensional variability during extrusion of thin-walled open and hollow profiles may be regarded as the most complex of tasks. As of today, the most important response of the extrusion system, and often the only one that is usually evaluated when assessing the quality of models, is the ram force. Accurate measurements of the die outlet temperature are also performed, but are not used in commercial presses. The extrusion system is one of a

very large number of degrees of freedom and potentially also one that may be quite sensitive to small gradients in the container pressure. It is easy to envision that two quite different models may predict the same ram force and outlet temperature, but not the same flow velocity distribution at the die outlet. By introducing sensors for the measurement of the die deformation, local die-face pressure measurements and profile shape, one may be able to better understand the relationship between flow stability and the process parameters. The sensitivity of the system to relatively small parameter changes may be determined. This would allow a better understanding of the limitations of the extrusion process and the various reasons for dimensional variability.

For a long time, finite element models have been regarded as promising tools for the analysis of flow and for the design of extrusion dies. However, in spite of the significant advances that have been made within the field of numerical modelling, finite element analysis is not effectively used. Computation times for practical problems are still fairly long, and the tasks of pre- and post-processing of data have not yet been sufficiently automated. The reliability of codes has still not been satisfactorily checked, and only expert use is usually recommended. More importantly, however, there are still many difficult and important questions relating to the appropriateness of modelling and numerical solution approaches as well as regarding requirements for the quality of material data. Very often it is neither natural nor possible to draw a distinction between the errors due to the modelling approach and the material data. The consequences of localisation of strain and material anisotropy have not been thoroughly considered. Refined models may be needed to study the phenomena. The importance of elastic deformation at the outlet must be assessed and seen in relation to the accuracy of the numerical approach and geometry descriptions. The development of new modelling tools requires a number of test cases to be run and results from simulation and measurements to be carefully compared. New and alternative accurate measurement techniques would then be very useful, if not entirely necessary.

As earlier suggested, finite element techniques could be most useful for relating profile-shape deviations to deviations in process parameters and the container flow conditions. It should be noted, however, that numerical simulation is not the only useful approach. Valuable information may be drawn from earlier industrial experience or from carefully planned experiments. Statistical analysis of data from a range of flow geometries would be a most useful tool. Models may, for example, be built with Artificial Neural Networks [Li00]. Information may be gathered from pressure and temperature sensors that have been placed in appropriate positions and compared to data on profile properties, shape and dimensions after extrusion. It is well known that the flow velocity is related to pressure gradients and that the pressure and velocity fields are related to the temperature fields. Thus, in principle, although perhaps not in practice, it should be possible to relate pressure differences close to the outlet to the flow resistance inside the bearing channel and close to the die outlet. Pressure sensors may potentially reveal whether there is a possibility of either latent or manifest flow instability and whether the die outlet is distorted more than initially expected. Since very small pressure changes may be related to changes in flow, measurement must be performed accurately and with a relatively high resolution. When a number of runs are performed, pressure and temperature measurements may be carefully monitored to make absolutely certain that

the flow conditions are optimal and do not change. On-line measurement of the profile or outlet shape may also be performed in combination with pressure measurements to establish a better understanding of flow. If the measurements indicate that the section quality is not acceptable, extrusion may be stopped and the necessary corrections may be implemented. In this way errors are identified at an early stage and economic losses may be limited. Bearing outlet wear and improper temperature control may be possible causes of deviations and variability in general. It could also be possible to use sensor technology to make certain that proper process conditions are established after a die has been changed. There is always the risk that small deviations in bearing geometry may seriously affect the profile shape and the flow stability. If the flow conditions change, and if the product quality deteriorates, the measurement system should produce a signal. Ideally, it should also be possible to introduce small actuators that directly compensate for changes in flow conditions and profile dimensions on-line or in between runs so that no manual tuning of the die outlet geometry should be necessary. The responses of the actuators should and must be related to the signals of the various measurement systems. One may envision an on-line system where the flow is continuously controlled in order to minimise the scrapping due to end and start up effects. Sensor and actuator systems may also be used to control the quality of the longitudinal weld during extrusion of hollow profile. The quality of the weld is controlled by the pressure in the weld pocket.

Another important motivation for developing pressure sensors is the need for a method of assessing die loads in relation the operating times for dies. The problem is intimately related to that of dimensional variability. Extrusion dies experience immense loads, and they are significantly deformed. Sometimes, plastic deformation occurs, and after some extrusion rounds, fractures may render the dies unfit for use. However, deficiencies may be difficult to reveal during or even after extrusion, and at first, the only consequence of plastic deformations or fracturing may be an excessive dimensional variability. It would be most useful if the die face pressures and the die responses could be continuously monitored so that that die defects could be spotted at an early stage. The problem is of particularly large importance for the extrusion of harder alloys and complex profiles.

The development of a system for effective die deformation and flow control for the extrusion process is not a straight-forward matter. The direct link between the flow outlet velocity and the die face pressure distribution has not been established, and quite demanding experimental and numerical studies are probably required. The efficiency of flow control through changes in process parameters or flow domain geometry has not thus far been sufficiently or thoroughly studied so as to allow one to determine the feasibility of the concept. The most important and difficult questions, however, relate to the profitability of the implementation of sensor and actuator technology. Dies and presses that incorporate sensors may be significantly more expensive to manufacture than the dies that are in use today. Thus, it must be demonstrated that the cost related to the development and implementation of sensor systems may be easily covered by the gains resulting from better process control. Intelligent dies with sensors and actuators must be easy to install in most presses, and special attention must be paid to the fact that there may be frequent die shifts due to wear or small order sizes. Sensors should be simple to mount and generally low cost. Alternatively, they should be placed in parts of the press that are not as frequently changed as most of the dies used today.

3.3 Comments on the objectives and limitations of the study

The study treated in this thesis was not intended to provide complete answers to the complex issues of flow control and shape variability. Neither was the main objective to establish intelligent die concepts that may be used industrially. The issues may first be satisfactorily treated when the necessary numerical modelling tools and measurement tools are available. The main objective of the present study was rather to demonstrate the feasibility of fairly accurate measurement of pressure or tractions at the billet - die interface in the environment of hot aluminium extrusion. Such a study is necessary if a satisfactory system for pressure measurement is to be developed. The temperature may be in the range of 400 to 600 ºC and may change by as much as 100 ºC in less than 10 seconds. The pressure at the die face may at the same time be in the range of 200 to 500 MPa depending on the profile shape, temperature, alloy and die geometry. The term pressure may be somewhat misleading and conceal some of the complexity of the measurement. During high-temperature extrusion, aluminium generally acts as a fluid with a high viscosity and with a low, but not insignificant threshold for the activation of flow. It is not always certain that there is perfect contact between the work piece and a sensor of finite size, especially if the aluminium has to flow into narrow crevices to reach the sensing area. The elastic material behaviour may also have an effect on the pressure distribution. However, the higher the temperature, the more easily the flow of the material is provoked. Still, it may be most difficult to distinguish between the sensor responses due to the components of traction forces acting normal to and parallel to the face of the tool. In this work, pressure is generally regarded as the normal component of traction acting at a surface. It deviates somewhat from the hydrostatic or isotropic stress.

Important steps in the study are the choices of appropriate principles of pressure measurement and sensor design and the development of effective calibration methods. Properties characteristic of the measurement technique such as accuracy, repeatability, temperature sensitivity and resolution must be determined by a series of appropriate extrusion runs. Experiments should also demonstrate the usefulness of the technique.

As will be further discussed in Chapter 4, there are a large number of approaches for measuring high pressures in demanding environments such as that of the aluminium extrusion process. It is not a straightforward matter to determine which one of the candidate measurement principles or sensor designs is the most suitable. Firstly, it is hardly possible to test all existing measurement techniques, and a real understanding of the vices and virtues of a specific technique may probably only be established through experiments. Secondly, if a technique fails to satisfy requirements after great efforts have been made to perform acceptable measurements, it is not quite certain that others will be equally unsuccessful in their attempts. Techniques may always be refined, and what may be regarded as design details may often separate success and failure. Thirdly, the advantages and disadvantages of various measurement techniques may not easily be compared. Often it may be difficult to determine which feature of a technique that is the most important. In the current study, it was decided at a very early stage that one was to focus mainly on one principle of displacement measurement, namely the capacitive. As an elastic member deforms when exposed to a pressure, two parts of a capacitor may be made to approach each other. The capacitance of the capacitor then changes. As will be further discussed, there are a number of ways to determine this change and consequently

the deformation of the elastic member and the pressure to which it is exposed. There were many reasons for choosing the capacitive displacement technique. First, capacitive sensors have earlier been used in high-temperature surroundings and their response has been reported to be fairly insensitive to temperature changes [Fos89]. The sensors may be of small size, and they may also accurately measure very small displacements (down to less than a tenth of a micron). Finally, they are only to a limited extent affected by noise and rough treatment. Thus, the choice of measurement principle is a natural one. The idea of using capacitive sensors was conceived almost at the same time and independently by a number of researchers related to or employed by the Hydro system. Prof. Sigurd Støren was the first to propose that the commercially available high-temperature capacitive sensors by Capacitec, Inc. should be used. The advantages of choosing commercially available sensors should be obvious. Capacitec has worked for many years with the refinement of capacitive measurement techniques and has gained much experience with industrial implementation. Capacitec is known to have worked extensively with extreme applications of the capacitive measurement principle [CpsW]. The company offers sensors that work up to 825 ºC and use materials whose properties are only to a relatively small extent affected by temperature changes. Thus, by using the commercial sensors it was expected that a long and expensive process of development of fundamental technology for high-temperature capacitive displacement measurement could largely be avoided. If modification of sensors should be necessary, Capacitec also provided the necessary assistance at reasonable prices. The choice of a commercial system contributed to a shift of focus towards the thermo-mechanical aspects of the sensor design and implementation of the technology in relation to the extrusion process. There are also disadvantages to choosing commercial sensors. These are mainly related to design freedom and can be further treated when the sensor principle has been tested.

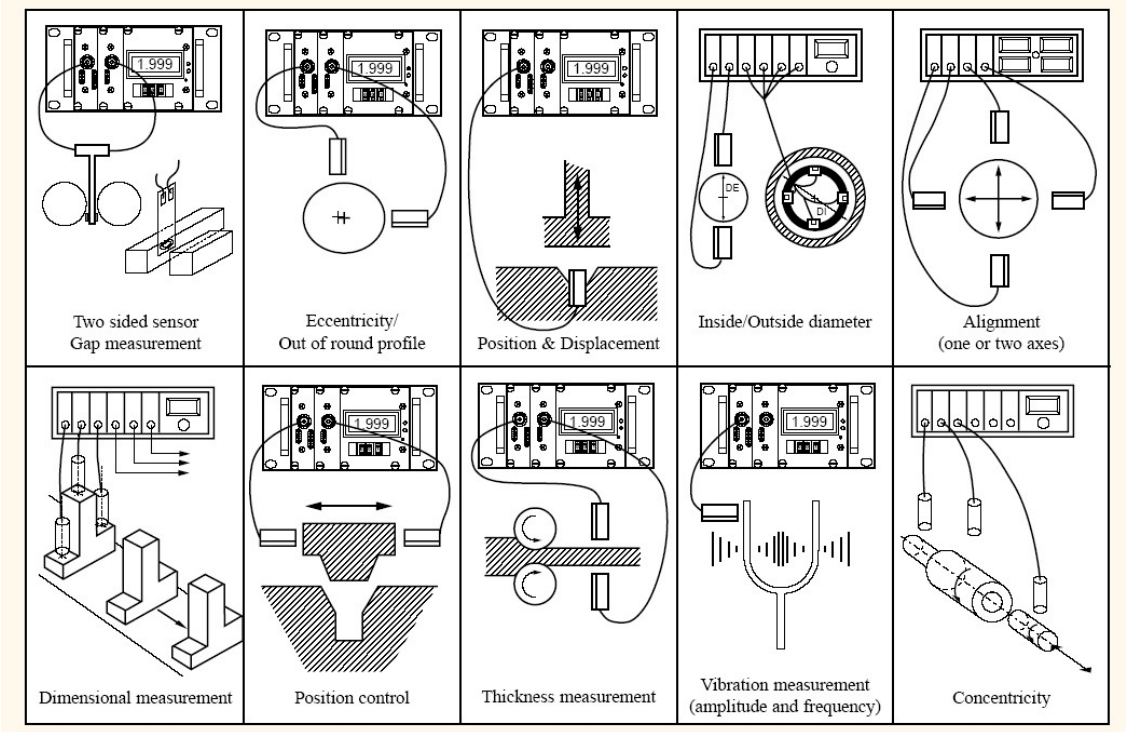

Figure 3.4. Different applications of capacitive displacement measurements [CapW].

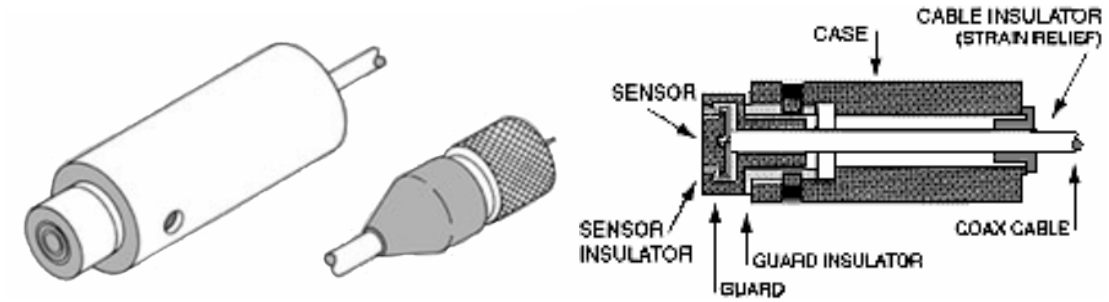

Figure 3.5. The Capacitec cylindrical (HPC) capacitive displacement probe [CapW].

Experiments were performed mainly to evaluate the characteristics of the sensors based on the capacitive measurement principle. It should be realised, however, that even in the case that commercial sensors are used, development of sensor measurement technology to be used in demanding environments is a rather expensive and time-consuming task. A number of iterations must usually be performed in order to reach a satisfactory design, and at each step extensive testing must be performed. It was therefore hardly possible within the framework of one PhD study to uncover the full potential of the technique. Hence, the main objective of the study was to demonstrate the feasibility of accurate pressure measurement and to lay the foundations for further development in the field. Hopefully, the thesis may breed creativity and allow others to make further progress. It may of course be said that the feasibility of measurement should have been evident even before the work commenced, and that the objectives of the study therefore simply were too modest. Capacitec has, as indicated, much experience with the instrumentation of sensors in similar environments and for similar purposes. The argument is undoubtedly relevant, for if a success was not anticipated in the first place, it would be wasteful to even attempt implementing. Still, one can never be certain that a technique will work before a demonstration has been performed. It was not completely clear initially that it would be possible to draw useful information from the experiments. In the literature there are plenty of examples of quite promising measurement techniques that have not performed satisfactorily or proven useful only after extremely large efforts have been invested. The details of the sensor design and the feasibility of properly mounting of the sensors caused the largest concerns. Experiments were the only means by which to gather certain information about the feasibility of this approach. It should be recognised that only by actually designing and testing sensors is it possible to make significant progress in the field of sensor technology. The development process is in fact very often more important than the result. It contributes to increasing the level of competence and is necessary for every industrial and academic research community.

Industrial experiments are most important as they effectively demonstrate to industrial partners the feasibility and relevance of measurement techniques. However, there is always a risk that the results from industrial experiments may not provide the adequate or anticipated answers. An industrial experiment is much more demanding and harder to control than the laboratory experiments. Industrial experiments are extremely time-consuming and fairly expensive. Regular production must be stopped, and a complete team of press operators must be employed. Therefore, the task of performing an industrial demonstration of the pressure measurement technique has not been one of the

main objectives within the framework of this PhD study. The reason was obvious already by the onset of the study. The resources and time at the disposal were simply not sufficient to allow a demonstration to be performed in a satisfactory manner. In total 300 kNOK were allotted to cover direct costs related to both laboratory and industrial experiments. The investment in the sensor equipment in fact consumed more than 150 kNOK. The production price of the laboratory dies were potentially of a similar magnitude, but significant costs could be cut as most parts could be produced by the tool shop of the Department of Engineering Design and Materials. The expense was then mainly one of time, another very scarce commodity. However, laboratory extrusion experiments were also quite expensive. SINTEF co-workers had to be hired, the SINTEF extrusion press had to be rented, and billet material had to be purchased. One day of experiments typically cost 15 kNOK, and only after some ten days of laboratory experiments all resources of the project were spent. Since the sensor design task is one that requires several iterations of trial and error, it was not realistic to assume that sufficient resources would also be available also for industrial experiments. The cost of industrial experiments are not exactly known, but may be expected to be more than five times higher than that of laboratory experiments. As will be further discussed in later sections, however, both the candidate and SINTEF co-workers actually took part in the preparations for and the execution of two rounds of industrial experiments that included the use of the capacitive die face pressure sensors. The experiments were performed within the framework of the FREMAT-project and in close cooperation with SINTEF Materials Technology and Hydro Aluminium Extrusion. The experiments were not dedicated to the task of industrial pressure sensor development, and therefore were not performed in complete accordance with the task description. Still, some conclusions on the feasibility of industrial pressure measurement could be drawn. Furthermore, very important experiences were drawn from the experiments, and many new ideas were generated, some of which will be presented in this thesis.

The objectives of this PhD study should be seen in relation to the objectives of the SINTEF co-workers with whom the candidate cooperated from the very outset of the study. The industrial implementation of both temperature and pressure measurement technology in a complex U-profile die was an important objective in the later parts of the study. In the early parts, however, the focus was not on one generic profile geometry as described by the task description, but rather on three different generic geometries. On-line die face pressure, bridge strain and mandrel displacement measurements were performed during tube (pipe) extrusion. The experiments were a part of the PROSMAT programme and performed in order to better understand the deformation of bridge dies and the criticality of the loading conditions. Thin strip extrusion was initially regarded as a relevant candidate case for the testing of pressure sensors. The complexity related to accurate modelling of flow, the cost of thin strip extrusion dies and the practical difficulties related to flow control made the case less relevant for the thorough study of sensor behaviour. Rod extrusion was the preferred alternative. However, the thin-strip geometry is still a most interesting case, since it is the simplest one that may exhibit instability phenomena. Therefore, several rounds of experiments were performed under the umbrella of the COMPFORM programme. The objectives were to examine the limits of instability of flow and to apply pressure and temperature sensors to establish a deeper understanding of flow instability mechanisms.

Chapter 4

Traction measurement technology

Measurement technology is the foundation of all modern research. Measurements open for an increase in the understanding of fundamental physical mechanisms and for the development of models that properly describe material behaviour and the often coupled nature of the systems of interest. Models of material forming processes are based on numerous assumptions, are of a complex nature and usually contain many parameters. A proper evaluation of the models requires sufficiently accurate data obtained from sufficiently many complementary measurement techniques. Furthermore, a thorough understanding of a process is a prerequisite for high quality and low cost production. The causes of process and product variability must be identified before the variability may be controlled and/or reduced. The implementation of actuator technology must be based on accurate measurement data and preferably on a model treating all physical mechanisms of relevance. In metal forming, the tool loads should also be limited, since overloads may cause plastic deformations and fracture, which may significantly change both the die and product shape and cause unforeseen stops in the production.

This section gives a basic overview of the state of traction measurement technology in material forming with particular focus on the process of aluminium extrusion. Schey included a more general description of traction measurement technology of relevance to metal forming in his classic book written more than twenty years ago [She83]. However, most techniques have since then been improved, and new ones have been introduced. Work is continuously being performed to adapt methods to new problems. Furthermore, the treatment of measurement data has been greatly simplified by the more widespread use of computers. Much better use of the potential of traction measurement techniques may be made today. Thus, many sensors may be used in the most demanding of environments, and the accuracy and resolution of measurement may be satisfactory.

It must be admitted that the current presentation of measurement techniques may hardly be complete. There are several reasons. First, sensor development is an issue of fairly large commercial interest, because sensors may be used to improve the quality of the process outputs. Publication of papers on the essential features of the sensor design or results from measurement may not always be in the best interest of the users of the sensors. The advantages of patenting measurement technology adapted to the study of metal forming processes may also be limited if patenting at all is possible. The details of pressure sensor technology may sometimes be best protected merely by limiting the flow of information. Thus, one should not completely rule out the possibility that even

the capacitive measurement method treated in this thesis already has been implemented on a limited scale in the extrusion industry. This does not make a study of such sensors less valuable. There is a significant difference between knowing about a technology and mastering it. Besides, there are a number of different solutions for design problems, and it is always valuable to compare new and old approaches to design and measurement.

Second, traction measurement technology is an interdisciplinary and broad subject. Advances in many relevant fields technology may come about allowing for new sensor designs for metal forming with improved capabilities. One should consider experiences from the use of sensors in processes that are similar to metal forming and aluminium extrusion in particular. An example is the polymer extrusion process, which occurs at lower temperatures and pressures. Pressure measurement is widely performed in order to study and control the process, since it may provide information on the constitution and the quality of the product. Porosity and delamination are examples of effects that pressure sensors may be used to assess. Commercial pressure sensors for studying casting of materials such as aluminium [KisW] are also available.

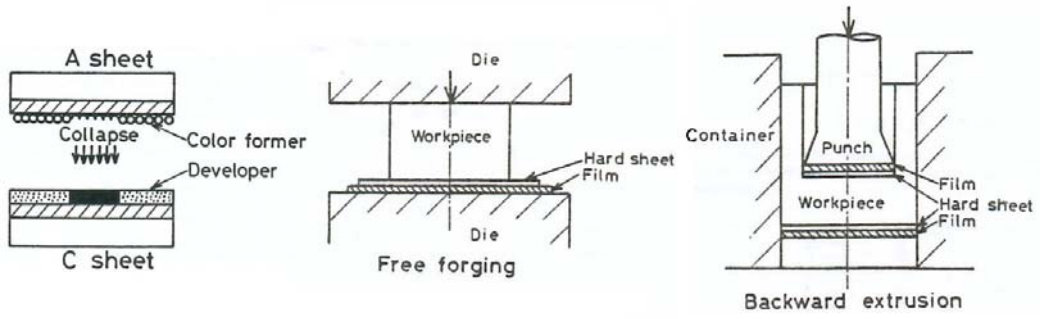

Figure 4.1. Pressure measurement by pressure sensitive films [Mor84]. The technique has been used to establish the interaction between the work piece and tools both during low temperature upsetting and extrusion.

Third, there are an enormous number of possible pressure sensor designs, and many have been tested in laboratory conditions and at moderate temperatures. Most sensor types measure traction only in an indirect manner. A pressure causes elastic deformation of a construction, and a displacement measurement sensor converts the information about the displacements to an electric signal. Some types of designs and displacement measurement principles are presented below. The focus is on techniques that eventually produce an electric signal that may be fed easily into a digital data logging system. There are also measurement approaches that do not require the displacement of parts or even electric signal treatment. Mori has, for example, used pressure sensitive films to study pressures during upsetting and backward extrusion of lead at low temperature [Mor84]. The films consist of a developer sheet and a sheet with bubbles of a colour former. When a sufficiently high pressure is applied at the top of the film, the bubbles break and there is a reaction that causes the colour of the developer sheet to change. If transparent dies and work pieces are used it is in principle also possible to use photo-elastic techniques to determine the stresses in the part of the sensor exposed to the loads. These techniques are less practical to use in relation to a system for process control.

4.1 On the principles of displacement measurement

Fortunately, the designer of traction sensors has a great many principles of displacement measurement or direct pressure measurement to choose from. De Sa [Sa97] provides a general classification of sensor principles. The presentation is of relevance also to this study. Fraden [Fra96] gives a general overview of the issue of measurement with descriptions of a very great range of measurement principles. Only the characteristics of some fundamental and much-used measurement methods are presented in this work. These are the fibre optic, the capacitive, the inductive, the piezoelectric and piezo-resistive. References are given to some of the sources that more thoroughly treat the capabilities of specific sensors. Volume II provides an overview of the most important expressions characterizing the response of sensors.

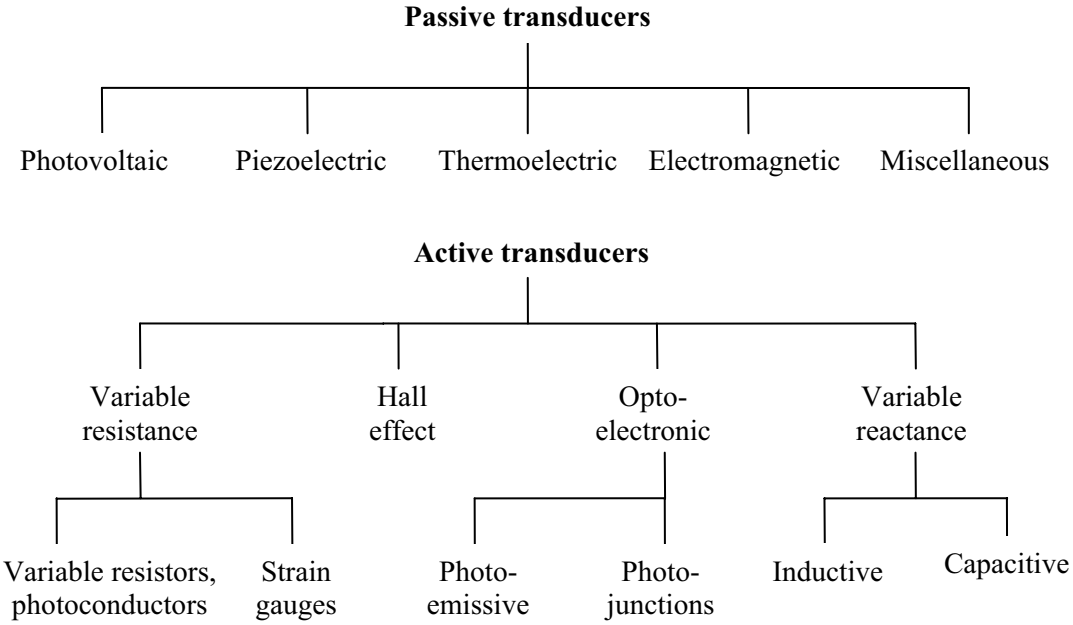

Figure 4.2. A general classification of transducer types. Passive transducers do not require an external power supply to effect the conversion of one form of signal to the other. Active transducers need an external supply [Sa97].

Although capacitive displacement measurements are performed in the current work, it need not be the one best suited for the purpose. The most critical requirements for the displacement measurement techniques are that they be useful at high temperature and insensitive to temperature changes. Most of the above mentioned approaches may fulfil these requirements if the sensors are properly designed and made of materials that are insensitive to temperature changes. While some measurement techniques today may be better than others, one should remember that there is an ongoing process of continuous improvement of sensor capabilities. New and better materials may be found, and more care may be taken to accurately compensate for temperature effects. The most important limitation in the use of sensor technology is usually the know-how of the user. It is very often an advantage to compare alternative methods through experiments.

4.1.1 Fibre optic displacement sensors

Optical displacement measurement techniques are among the most accurate ones that exist, and they may be used to measure not only the displacement of a point, but of complete surfaces. Two of the most critical requirements for optical measurements are that light must be allowed free passage to the object of interest and that the light beam must not be too seriously affected by the environmental conditions. Pressure sensors in metal forming tools cannot normally be observed during measurement, and in a high-temperature environment there may be density differences in air due to turbulence that may easily cause refraction of a light beam. Fortunately, it is possible to guide light to its destination and back through optical fibres, since a light travelling in the fibre is in most cases reflected from the surfaces rather than transmitted through the fibre wall. Optical fibres may be bent to radiuses of only 30 to 50 times their diameter and require generally very little space. The fibre diameter may only be 125 μm.

The optical fibre technology may be used in hostile environments. Silica and sapphire fibres work up to 800 and 1900 ºC respectively [Cla01]. Fibre optic sensors have been used up to 1600 ºC [Lfw92]. Additionally, proper fibre coatings for higher temperatures may be found. Gold coatings are commonly used to 600 ºC in oxidising atmospheres and nickel-chromium to 800 ºC. A further advantage of optical fibres is that the information they carry is not at all distorted by either electrical or magnetical noise.

Optical fibres are not only carriers of information. They may also be designed so that they effectively work as transducers. When a modification of the fibre itself causes a modulation of the light that may in some way be used in measurement, the fibre optic sensor is denoted intrinsic. If the modulation of light occurs outside the fibres, the sensor is extrinsic. The basic principle of optical measurements or any measurement technique using excitation signals (active transducers) is that the signals must somehow be modulated by the phenomenon that is studied. In the case of a light signal travelling in a fibre the intensity, phase, polarization angle, wavelength and spectral content may be altered by the transducer. Some of the principles of intensity modulation and fibre optic interferometry are presented in this section. Both Kersey [Ras97] and Lee [Lee03] provide updated overviews of the state of optical fibre measurement technology.

Fibre optic attenuation sensors

Fibre optic sensors based on intensity modulation are called attenuation sensors. They are very often designed to measure displacements in the range from 10 to 50 μm. An example of a sensor based on the intrinsic transducer principle is the micro bend sensor. The optical fibre may be placed between two plates, of which either one or both are corrugated. When a load is applied and the plates displace relative to each other, the fibre is compressed or bent. The intensity of the light exiting from the end of the fibre then changes. The reason is that the signal losses along the fibre increase if the light is forced to impinge on the fibre wall at higher angles.

An alternative extrinsic principle of measurement is that of reflection of light from the surface of an object moving towards the end of a fibre. The light that is leaving the fibre end is not focused but rather spreads out in a cone and is further scattered when it is

reflected from the surfaces placed at a distance from the fibre. If the optical fibre is at large distance from the surface only a small part of the light returns to the fibre. If the distance is very small, however, more of the reflected light returns. As will be further discussed, the principle may be and has been used to measure the deflection of a sensor disc [Yon93]. In an alternative version of the sensor, two fibres are used instead of one. One of the fibres emits and the other receives. It is also possible to transmit light from one fibre to the other through short air gap. The fibres are positioned parallel to each other. If one of the fibres is displaced normal to or along the direction of the fibre, the intensity of the transmitted light decreases. Finally, two receiving fibres may be used so that the position of the emitting fibre is given by the difference of the intensity of the light in each of the receiving fibres [Boc98].

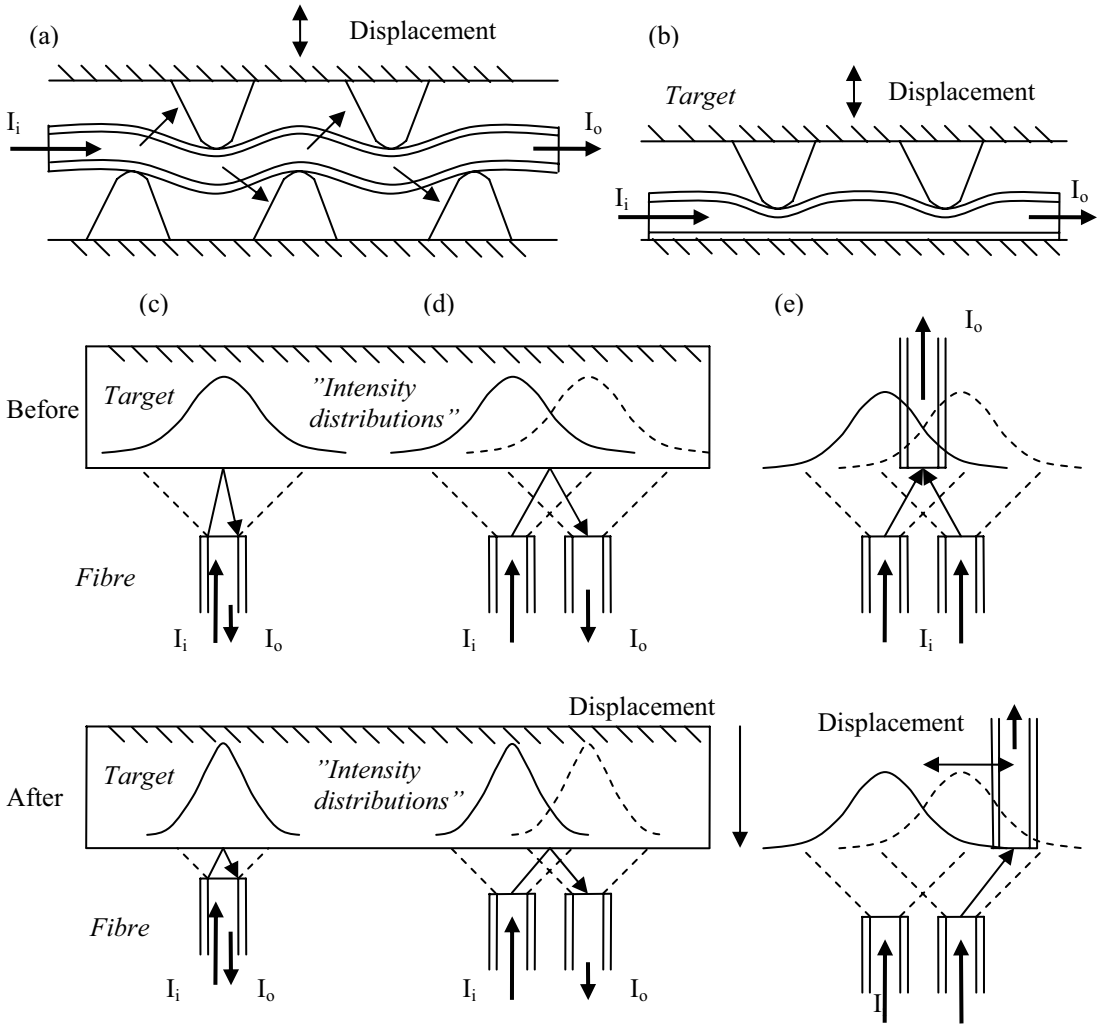

Figure 4.3. Various fibre optic attenuation displacement sensors. (a) and (b) are called micro bend sensors and are of an intrinsic type. (c), (d) and (e) are extrinsic sensors. The basic physical principle is the spreading of light from the end of an optical fibre. I_i is the intensity of the light transmitted into the fibre and I_o is the intensity of light leaving the fibre.

The intensity of the light may be modulated by polarisation phenomena. Light may be transmitted from the fibre through an input polarizer to a birefringent element. The birefringent element changes the state of the polarisation of the light according to the force that is applied on it. The light is then transmitted through a new polarizer oriented 45 º relative to the first and into a new optical fibre. The result is that the intensity of the light in the second fibre depends on the force applied on the birefringent material.

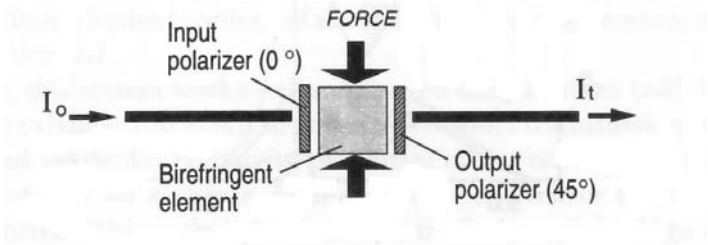

Figure 4.4. Attenuation displacement sensor using birefringent materials [Ras97]. I_o is the intensity of the input and I_t the intensity of the output light.

Fibre optic interferometric sensors

An interferometric technique for displacement measurement is the extrinsic Fabry-Perot interferometer (EFPI). Strain gauges and pressure sensors with deflecting membranes are regularly used. A fraction of the light transmitted through the fibre is reflected at the polished and often coated end of the fibre (less than 5 %) while a larger fraction is reflected from an exterior surface (the target) positioned at distance d from the fibre end. Most of the light reflected from the external surface is collected by the optical fibre since it travels within a Fabry-Perot cavity of very short length. The intensity of the light returning through the fibre is given by the intensity and phase difference for the two reflected light signals. The interference may be either constructive or destructive depending on the ratio between the wavelength, λ, and the extra distance travelled by the light returning from the target, the optical path difference ($2d$). In the ideal case there are no extra phase shifts due to reflection and the incidence of light is normal to the moving object, the phase difference is given by the relation $\varphi = 4\pi d/\lambda$ [Gan04]. During measurement the cavity length changes as the target approaches the fibre. The intensity of light of a given frequency then changes. A phase change of 2π corresponds to one fringe period (from maximum to maximum intensity). The change in the optical path difference is at the same time one wavelength, λ, or typically approx 0.8 μm.

When displacements larger than approx 0.4 μm are measured with an EFPI using light in a narrow frequency band, fringe counters must be applied. It is, however, also quite common that the incident light is distributed over a wide frequency range (white light). The reflected light signal is then modulated due to interference, and it is possible to deduce the actual gap distance from the output spectrum by using the Fast Fourier Transform [Cla01]. There are limits to the speed of the signal analysis.

Another critical issue for those using the EFPI techniques is to secure proper reflection at interfaces. Special Fabry-Perot cavities have been made. It is also possible to integrate the Fabry-Perot sensor in the fibre design itself, in which case it is called an

Intrinsic Fabry Perot Interferometer (IFPI). The advantage of intrinsic sensors as compared to extrinsic ones is that they are much more durable and less affected by environmental factors. It may also be easier to secure proper reflections of signals. The Fabry-Perot sensors have been used successfully at temperatures above 1000 ºC [Lfw92], but these kinds of measurement may not be regarded as trivial.

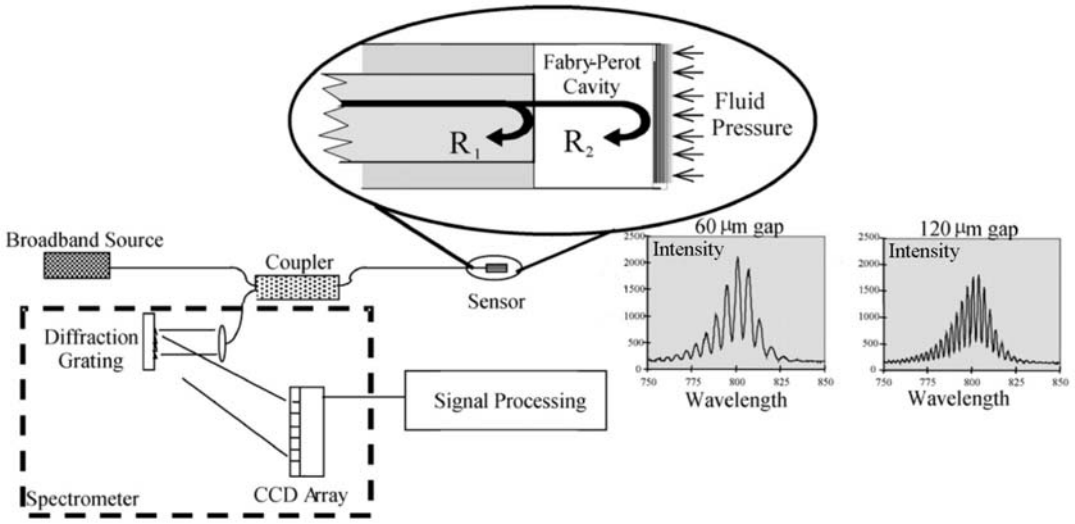

Figure 4.5. The principle of the extrinsic Fabry-Perot interferometer used to measure the pressure of a fluid [Kau03].

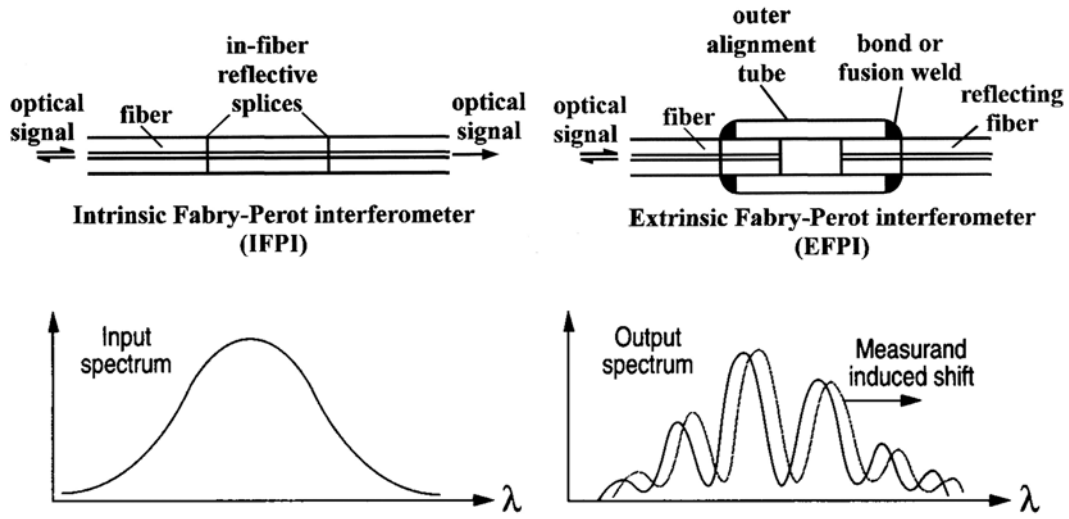

Figure 4.6. A comparison of some intrinsic and extrinsic Fabry-Perot interferometer designs. Input and output spectrums are compared [Ras97].

Advances in the technology of production and modification of optical fibres have made the introduction of more complex and reliable sensing methods possible. Fibre Bragg gratings (FBG) may now be introduced in fibres. These are bands of material with a

somewhat lower refraction index, and they reflect a certain part of the light signal. The wavelength of the reflected light wave is twice the effective refractive index multiplied by the grating period (according to Bragg's law) [Lee03]. The grating period may be modified by strain due to both mechanical loading and temperature increase, while the refractive index is mainly affected by temperature. Thus, if the white light is transmitted through the fibre, it should be possible to determine either the straining or temperature increases by studying the wavelength of the reflected light. If loads and temperature change simultaneously, it is also possible to measure both. One may, for example, place two optical fibres in the same environment. One should only be affected by the change in temperature while the other should also be mechanically strained. Compensated measurements may also be performed with only one fibre [Zha04].

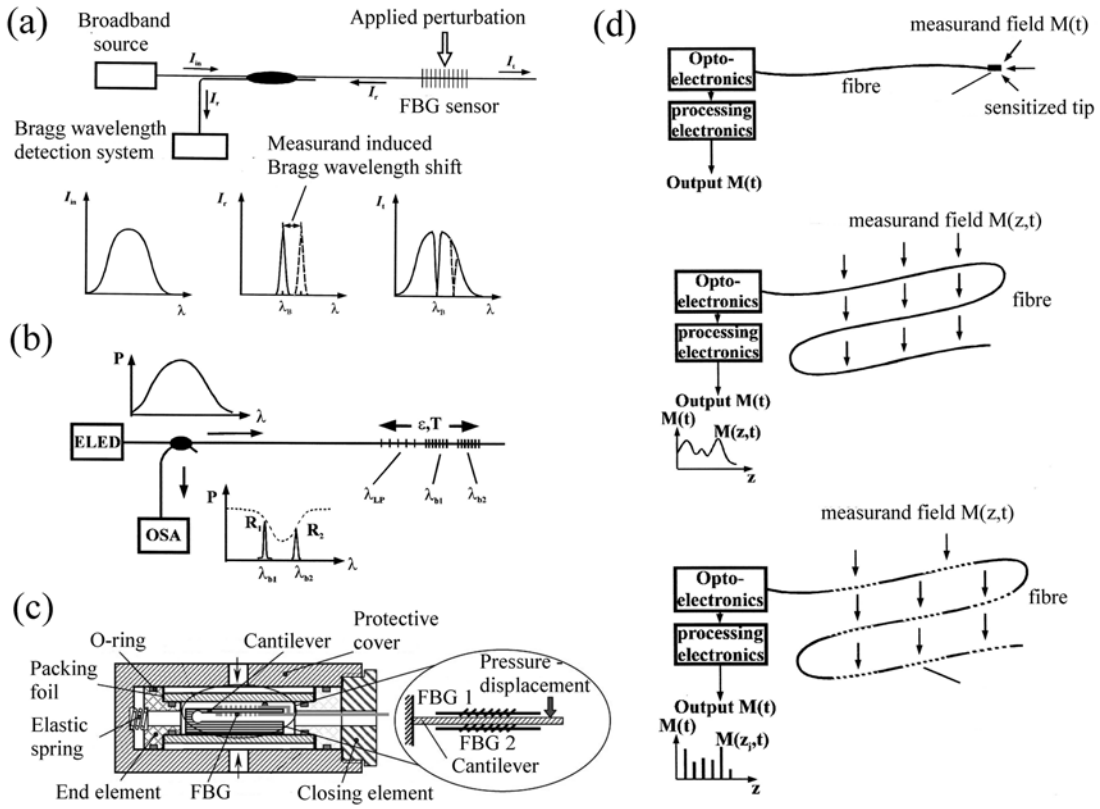

Figure 4.7. Fibre Bragg measurement: (a) principle of measurement, (b) principle of parallel measurements (c) temperature compensated cantilever sensor [Zha04], (d) the principles of point and distributed measurements [Gra00]. One optical fibre can be used to perform a great number of independent pressure and temperature measurements.

FBG may be used directly as Intrinsic Fabry Perot interferometers, and it is possible to combine various approaches [Rao02]. Fibre Bragg technology may be used in a range of pressure sensor designs. Fibre Bragg pressure sensors may be very compact and be parts of small point sensors. At the same time a number of sensors may be placed along the length of an optical fibre as long as the grating periods of the various sensors (or sensing areas) differ significantly.

4.1.2 Piezo-resistive sensors and strain gauges

A strain gauge is a sensor design rather than a sensor principle. Fabry-Perot and fibre Bragg sensors may in fact be used as strain gauges. Traditional strain gauges, however, work according to the basic principle that an elongation of the gauge, ΔL, causes a proportional change in the resistance, ΔR. The principle may be expressed as:

$$\frac{\Delta R}{R} = (1 + 2\nu)\frac{\Delta L}{L} + \frac{\Delta \rho}{\rho} \qquad (4.1)$$

ν is Poisson's ratio while R and L are the original resistance and L of the strain gauge. ρ is the resistivity of the material. $\Delta\rho$ is usually small for conventional strain gauges. If the material is piezoresistive, however, the resistivity may change considerably with the applied strain, and the last term may in fact be the dominant one. Most strain gauges are affected by temperature changes, but it is to a large extent possible to compensate by performing parallel measurements and by introducing well-known bridge circuit designs [Fra96]. Strain gauges of various types have been used extensively in the study of work piece and tool interaction in metal forming, and many applications will be presented in this section. Some of the largest challenges when using such sensors are temperature sensitivity, space requirements and mounting. There are relatively many producers of high-temperature strain gauges, and such gauges have been used in the current study.

4.1.3 Inductive displacement sensors

If two coils are in the vicinity of each other, one coil induces a voltage v_2 (emf) in the second coil proportional to the time derivative of the current in the first, i_1:

$$v_2 = -M_{21}\frac{di_1}{dt} \qquad (4.2)$$

M_{21} is the mutual inductance between two coils. It characterises the magnetic field that surrounds the coils and is determined by the geometry of the coils and the properties of the materials that surround the coils. Thus, if the first coil carries an AC excitation that induces an AC voltage in the second coil, the voltage of the second coil may be used to characterise a displacement. For example, the coils may be moved relative to each other, or a piece of ferromagnetic material positioned between or inside the coils may be moved. Linear variable differential transformers (LVDTs) are based on this principle of displacement measurement. LVDTs are widely used to control movements in industrial applications. They may, however, be somewhat vulnerable to various forms of electric and magnetic noise, and responses are also sensitive to temperature changes. Examples of application of LVDT to measure die face pressures in metal forming processes are not known to the candidate. Obviously, this does not mean that they cannot be used.

If a coil that carries an AC excitation is placed in close vicinity of a piece of conductive material, eddy currents are induced in the material. The eddy currents then produce a magnetic field that opposes the field set up by the coil. The total magnetic field differs for the cases when there is a piece of material close to the coil and when there is not.

Hence, if a sensing coil is introduced, it may be used to measure the displacement of any piece of conducting material relative to the coils. The emf induced in the second coil is affected by the presence of conductive material which alters the magnetic field. The eddy current sensors usually operate at relatively high frequencies (50 kHz to 10 MHz), as this is necessary to introduce eddy currents of significant magnitude. The closely related problem of induction welding of steel has been treated in [Moe04a]. The fundamental electromagnetical equations (Maxwell's equations) have been presented and solved for the specific problem. Eddy current sensors may be made fairly compact, even though the sensor design is quite complex. Sensors with diameters of 2 to 3 mm have been manufactured [Fra96]. A problem related to the use of all inductive sensors at high temperatures is the sudden drop in the permeability of ferromagnetic steels close to the Curie-temperature. The Curie temperature of steel is below 750 ºC. Permeability changes below 600 ºC are only moderate. However, the electric resistivity of sensor materials may also change significantly from room temperature to higher temperatures.

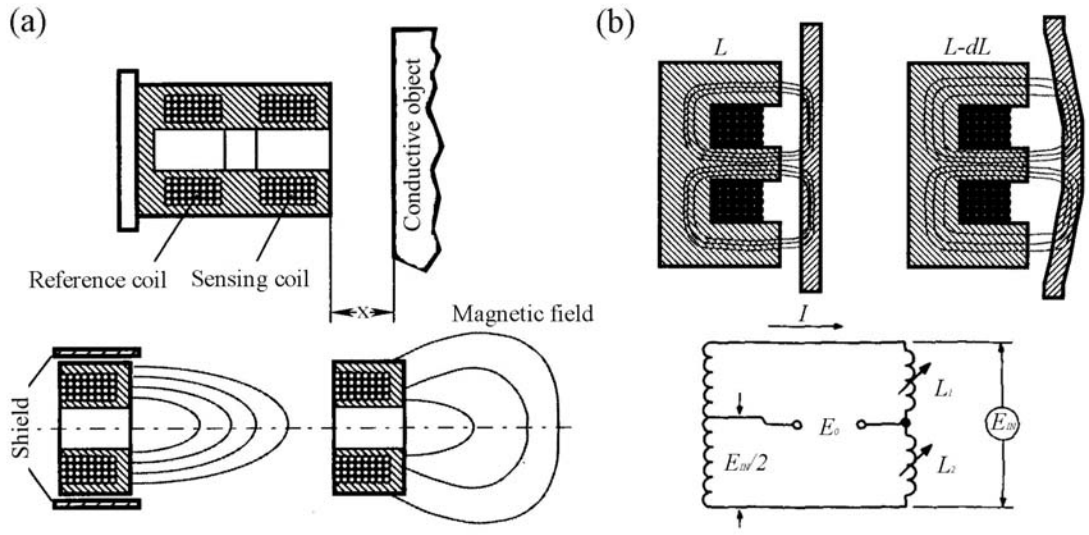

Figure 4.8. Two sensors based on the principle of induction: (a) an eddy current sensor with and without and external shield, (b) a Variable Reluctance Pressure sensor (VRP) with an equivalent circuit [Fra96].

Another example of the use of the principle of induction in measurement is the Variable Reluctance Pressure sensor (VRP). The sensor is a differential transformer consisting of a coil, an E-shaped magnetic core and a target (movable part). When a time-varying current is applied in the coil, magnetic fields are set up in the surrounding core, as well as in the target and in the air gap between the target and the core. The fields are modulated as the target moves. This modulation affects the inductance of the coil and the electrical signal in a circuit linked to it. The effect is large since the magnetical reactances across the air gaps are very high (the permeability of the core material is at least 1000 times higher than that of air). The sensor may be compared to the sensing half of a variable reactance bridge. There are two arms of the magnetic core. The output of the VRP sensor is proportional to the reluctance in each arm of the bridge and ideally inversely proportional to the gap distances [Fra96].

4.1.4 Capacitive displacement sensors

The capacitive sensors work according to a principle that is in a sense an analog to that of inductive sensors. If two bodies of opposite charges Q and $-Q$ are in the vicinity of each other, a stationary electric field is set up in the surrounding media. The potential difference of the bodies, V, is proportional to the charge:

$$V = \frac{Q}{C} \tag{4.3}$$

C is the proportionality factor, the capacitance, and is determined by both the geometry of the set-up and material properties of the surrounding media. The permittivity ε is the only material parameter of importance. The permittivity of vacuum ε_0 is $8.854 \cdot 10^{-12}$ F/m while the permittivity of air is slightly higher. The magnitude of the electric field in the space around two electric charges may be calculated. Maxwell's equations are also the basic equations for this problem. In the stationary case of capacitive measurement the equations simply reduce to Poisson's equation. The capacitance may be deduced if the electric field is known, since the capacitance is an expression of the energy stored in an electric field. Volume II discusses the fundamentals of capacitance analysis and presents some estimates of capacitance calculated by finite element analysis. If the charged bodies are two plates of surface area A positioned at a distance d from each other, a simplified analysis may produce a relatively good estimate of the capacitance:

$$C = \frac{\varepsilon A}{d} \tag{4.4}$$

The plates must be connected to a circuit in the measurement system. Q is then the time integral of the current. By changing the separation of the plates, one may change the capacitance of the circuit element. There are a number of ways to design a circuit so that changes in the distance d and the capacitance C produce a direct current output voltage or current change. Some details of circuit design have been treated in Volume II. The linearity of measurement may potentially be very good, especially if a guard is used. A guard is a piece of conductive material surrounding the electrode. It is at a carefully controlled potential that does not change when the distance between the sensor plates changes. The spreading of the electric field close to the edges of the capacitor plates is less important when a guard is used. The electric field across the gap of the capacitor is therefore more uniform, and the linearity of the sensor is improved by the guard.

The temperature sensitivity of capacitive sensors is usually small. The permittivity of air changes very moderately with the temperature, while insulation materials may be fairly insensitive to temperature changes. There are many useful techniques for temperature compensation [Pin96]. There are examples of applications of the capacitive sensors in harsh environments above 1000 ºC [Bai99]. The measurement accuracy and resolution may also be very good. For instance, capacitive sensor techniques are used in Atomic Force Microscopes (AFM) to characterise the surface topology of materials down to the atomic level. The accuracy of many industrial capacitive sensors is usually significantly better than a micron. The limitations are usually related to the calibration technique. The

resolution may be even better than the accuracy, and is often primarily limited by auxiliary equipment. A potential problem with capacitive sensors in very demanding environments is that there is a danger of short-circuiting the equipment. Furthermore, changes in the capacitive coupling between the various parts of the circuit may easily ruin measurements, so it is important to counter various forms of noise. The circuit design and insulation materials must therefore be carefully chosen. Volume II contains further information on the principles of capacitive displacement measurement.

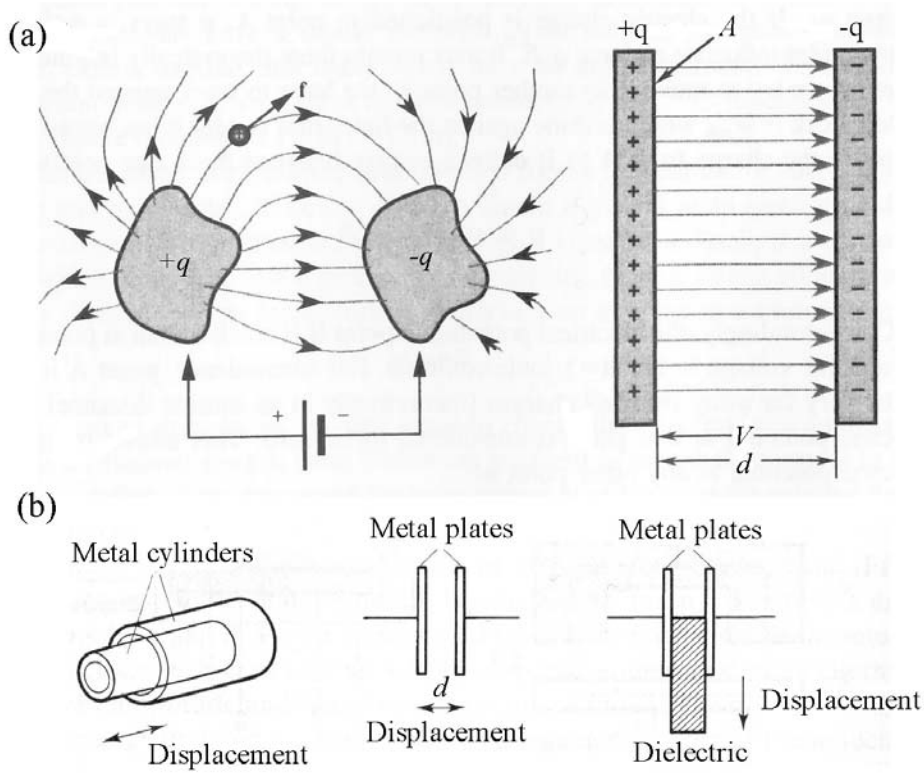

Figure 4.9: Capacitive displacement measurement: (a) the principle of measurement [Fra96], (b) possible capacitive displacement sensor designs [Bax97].

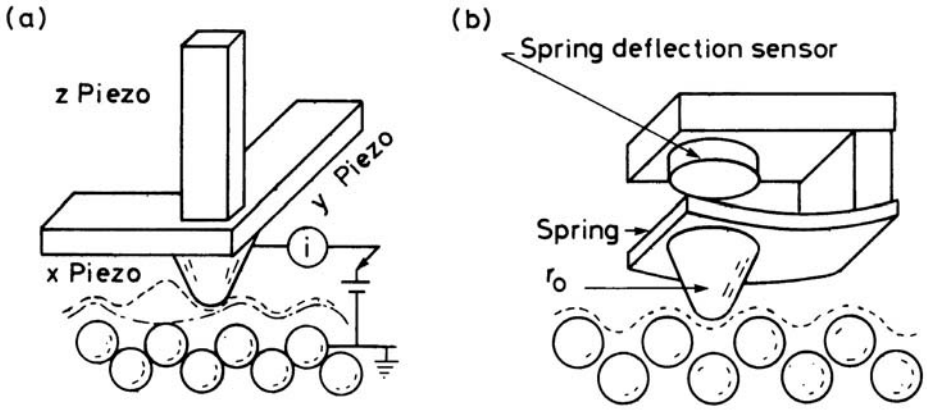

Figure 4.10. Measurements at the submicron and atomic level: (a) Scanning Tunneling Microscope (STM) and (b) Atomic Force Microscope (AFM) [Gar94].

4.1.5 Piezoelectric pressure sensors

When certain crystalline materials are subjected to stresses, they become polarized. One side of the crystal receives a net positive charge and the other a negative charge as a result of a reorganisation of the crystal structure. If both metallic electrodes and a circuit are attached to the crystal, an electric current may be measured during both loading and unloading. The principles of the piezoelectric stress measurement are described in detail by Luck and Agba [Luc98]. A charge amplifier may be used to produce a system output voltage different from zero during loading and unloading. The piezoelectric sensor is a capacitive circuit element with a high permittivity and the ability to generate a current. The voltage across a piezoelectric crystal capacitor is proportional to the applied force and inversely proportional to the capacitance and permittivity.

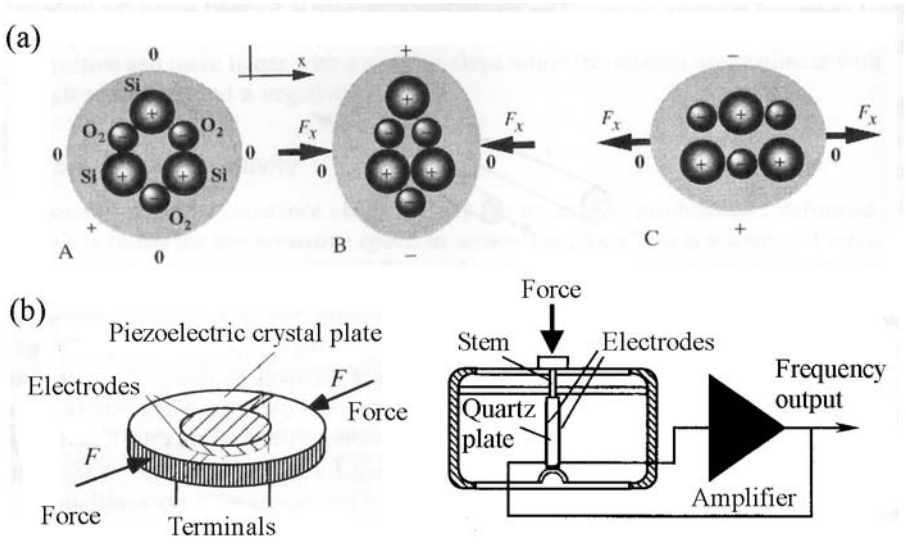

Figure 4.11. Piezoelectric sensors: (a) a simplified description of the piezoelectric effect, (b) two different piezoelectric sensor designs [Fra96].

The mode of operation described for the piezoelectric sensor is called a passive mode. No external excitation current is used, and only changes in the loads causes the sensor to respond. It is, however, possible to measure constant loads with piezoelectric crystals if they are used in the alternative active mode. Piezoelectric crystals may then be used as resonators in electric circuits, and the change in the fundamental frequency is linearly dependent on the applied load. Thus, by tracking the resonating frequency, the load may be determined. The first practical use of the piezoelectric effect was as early as in 1917 [Fra96]. Quartz crystal sensors were used to detect and study sound waves in water. The piezoelectric principle was also used by Siebel and Lueg [Sie33] to measure pressure in metal forming. Piezoelectric ceramics were developed in the 1950s. Today, there are numerous commercial pressure sensors that are based on piezoelectricity. Most sensors are made for low-temperature applications (< 300 ºC), but high-temperature use has also been reported [Seb02]. The reference gives an example of compression testing in which aluminium oxide is the piezoelectric material. There are also commercial piezoelectric melt pressure sensors that may be used in the study of material flow during polymer extrusion and aluminium casting [KisW]. Most of these sensors may function at higher temperatures only over shorter periods of time and require tools to be below 300 ºC.

4.2 On the design of traction sensors for metal forming

The choice of sensor design is more limited by the die designer's imagination than by any restrictions due to the choice of a specific displacement measurement method. Furthermore, the quality of the traction or pressure measurement results are often less determined by the general design of the sensor than by the details of the mounting solutions and the choice of materials. One of the largest challenges facing those who desire to design pressure sensors for accurate and repeatable measurements in the high-temperature extrusion environment is that of securing proper interaction between the various parts of the sensor. Only very small uncontrolled deformations of parts relative to each other may usually be tolerated (0.1 μm or less). This is most easily achieved by permanent connections such as for instance welds. Ideally, the sensor should be made of only one piece of material, but this is very often not practical. When the sensor consists of more than one part, one may wish to dismantle it to allow inspection and correction. If the parts of the sensors are connected by screws, for example, the parts may loosen during heating or loading. The difference between success and failure may sometimes be very small, but failure should not be altogether impossible to predict.

Since there are so many possible sensor designs, it may be worthwhile to define some characteristic groups of sensors. A distinction should first be made between sensors that constitute an integral part of the die and sensor units that may be inserted into the tools. The advantage of the integral sensors is that the tool surface facing the work piece remains intact. Depressions in the tool surface due to elastic deformation are also small, so there will be only insignificant marks on the work piece after forming. The insert sensor is probably easier to calibrate and manufacture accurately. It is also more user-friendly. An insert sensor is usually larger than an integrated one. If full use is made of modern measurement technology, this need not be a serious problem. The characteristic dimension of an insert sensor need not be larger than 5 to 10 mm.

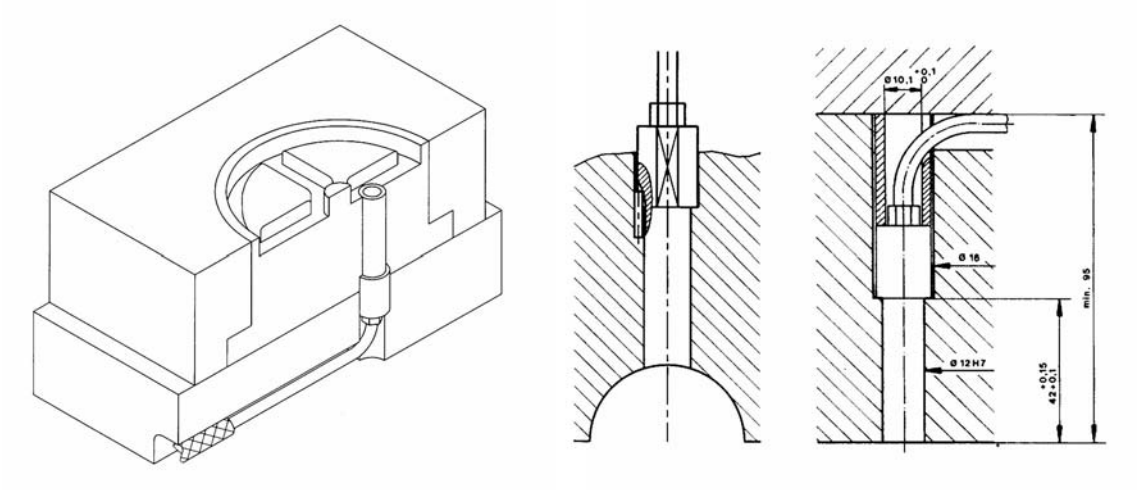

Figure 4.12. Kistler piezoelectric (quartz) high-temperature insert sensor for casting of aluminium (Type 6175A2) [KisW]. The sensor may be used in the range up to approx 200 MPa and to measure the pressure in aluminium melts up to 850 °C. The die temperature should not be higher than 300 °C.

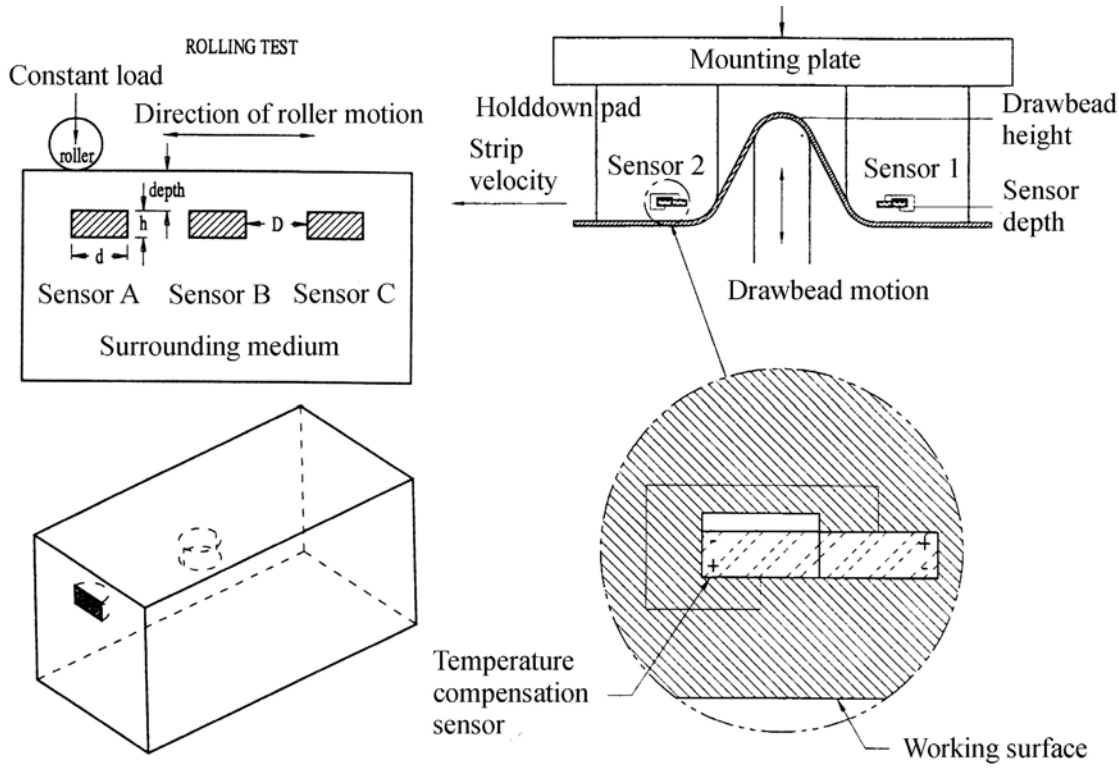

Figure 4.13. Insert and integral traction measurement sensors [Du99]. The sensors are of a piezoelectric kind and are baked into the die.

It is natural to draw a distinction between the two possible ways of inserting sensors, i.e. from the side of the die closest to the work piece or from the opposite side. In the first case it is important to add special features to the design that prevent the sensor from being pulled out of its space in the tool when the ram is retracted after the forming operation. It is also advantageous if the sensor is designed so that it may be parted from the tool to allow inspection. Sensors that are mounted from the side of the tool opposite to the tool-work piece interface (working surface) may be fairly easily dismantled. The modifications of the die must at the same time be larger, however. It may be difficult to inspect the geometry of sensor parts that are in the middle of the die. It should be noted, however, that it is quite possible to develop special tool designs that are better suited for measurement with sensors. Some of the designs used in the current work are examples.

One may also draw a distinction between sensor designs on the basis on the shape of the elastically deforming part of the sensor. Thin membranes are often used in low-pressure environments. In metal forming, one is forced to make use of fairly thick discs that are firmly attached to the surrounding die. The ratio between the disc thickness and disc diameter may typically be 1:3. The state of stress in the thick disc differs from that of a thin membrane. The thick disc deforms to a large extent by shear and is generally quite stiff. In high-pressure and temperature environments sensor deformations may be very small (typically 20 microns). Plastic deformations may be hard to avoid, so the task of designing the disc may be quite demanding. Still, deflecting disc sensors are commonly used [Du99] [Pin96] [Yon93]. An advantage of the thick sensor discs is that they are affected only to very small extent by shear loads. The shear tractions may cause some

eccentricity in the disc deflection and non-uniform disc straining. Yoneyama [Yon99] and Dellah et al. [Del02] have designed complex disc sensors that potentially may be used to both assess pressure and interface friction at the tool-work piece interface. The task is a difficult one, precisely because the sensitivity to shear tractions is much smaller than the sensitivity to normal tractions. Shear tractions are also of smaller magnitude.

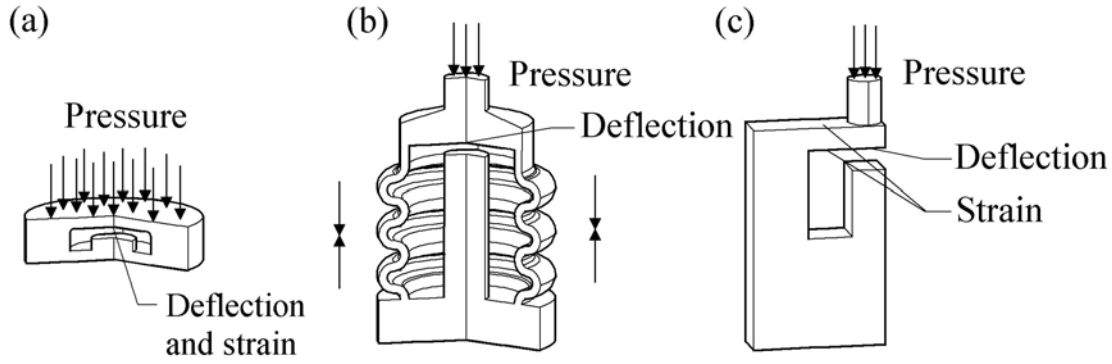

Figure 4.14. Some basic designs for elastically deforming parts: The disc, bellow and cantilever sensor designs. During loading all sensors are compressed.

The bellow designs pictured here are often used to measure low pressures. The design is less suitable for high-pressure applications, but may be used as long as only the end surfaces are exposed to the loads from the work piece. A bellow design may probably be designed so that it produces larger displacements than a disc design. Additionally, the end faces of the bellow are translated rather than bent as the case is for the disc. This may be an advantage for example when performing capacitive measurements. Bellow sensors are usually more sensitive to shear loads than disc sensors, for the construction is less stiff in the transverse direction. This is a clear advantage when shear stresses are measured, but it makes the task of accurately measuring normal pressure more difficult. Sensors that work in environments with transient temperature fields should be of short extension. Elongated sensors experience much thermal expansion. High-pressure bellow sensors are generally difficult to manufacture and are consequently expensive. No examples of use of bellow designs in metal forming are known, but a bellow design has been proposed below. The bellow sensor was an insert sensor of the pin type. A review of the state of pin-sensor design is also given below.

Cantilever designs have been extensively used for pressure measurements in relation to metal forming and other processes. While the disc and bellow sensors may be in direct contact with the work piece, cantilevers usually constitute a part of a more complex design and are often positioned at a certain distance from the tool surfaces. Cantilevers and deflecting discs are in some cases parts of the very same sensor design. The work piece exerts a pressure at the disc, which is in direct contact with the cantilever. A set of fibre Bragg sensors are often attached to the cantilever to measure strains [Zha04]. Fibre optical differential attenuation sensors may also be used [Boc98]. The cantilever and similar designs have also been relatively extensively used in new pin sensor designs. Conventional strain gauges have frequently been used to measure strains and thereby indirectly both normal pressure and shear stress.

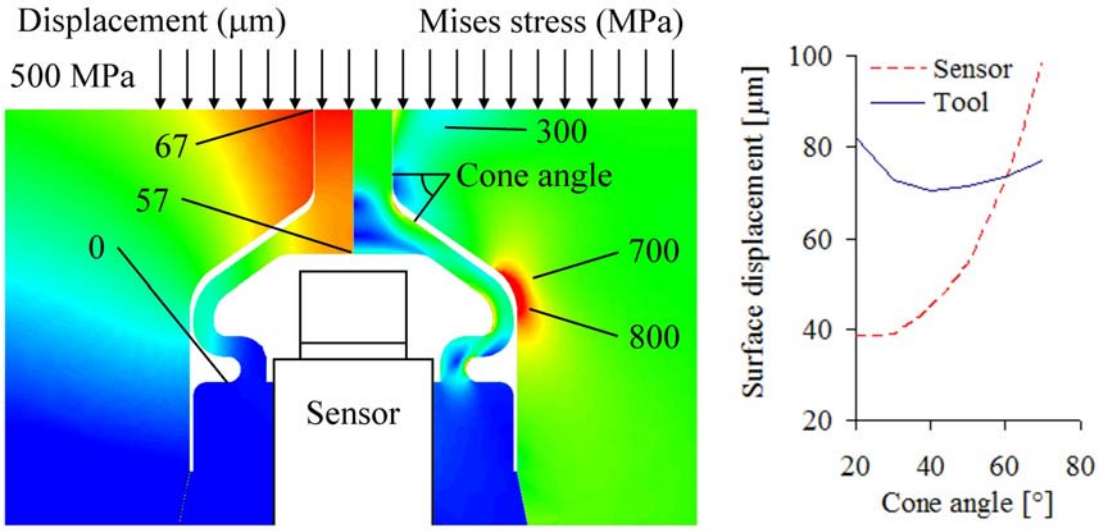

Figure 4.15. A bellow sensor design, with the vertical deformation (left) and the von Mises stress (right). The cone angle has been set so that the surfaces of the sensor and the tool remain flush during measurement. The cone angle is approximately 60 °. The level of stress in the sensor is acceptable while the tool experiences critical loading. The material behaviour is elastic. The material data are for steel at high temperature (E = 180 GPa).

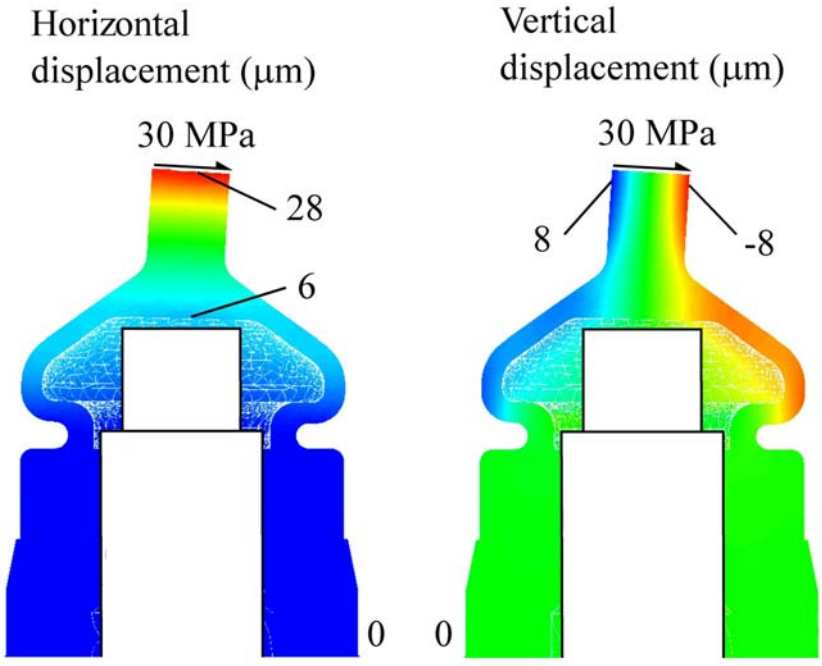

Figure 4.16. The effect of friction shear loading on the bellow sensor design response. The shear stress mainly causes the head of the sensor to tilt. The bellow design is more vulnerable to shear loading than the disc design.

The elastically deforming part of the sensor need not be of the types described here. Any type of deformation of the tool caused by either the normal pressure or the shear stress at a tool face may be measured. The integrated sensor of Du et al. presented above is an example of a sensor which is not actually a deflecting disc sensor, but rather one that measures the general deformation of the tool. The complexity of the evaluation of results will naturally depend on the design of the sensor. The farther away the sensor is placed from the surface of the tool, the less local the measurement, generally. Daneshi and Hawkyard [Dan71] measure the elastic compression of a split platen or block which constitutes one of the dies in a metal forming operation. Strain gauges have been used for the purposes. The gauges were attached close to the surface of the split platen, and they measured the general deformation of the tools. The work of Daneshi and Hawkyard contains a theoretically and experimentally based analysis of how various sensors react to spatially distributed loading. Approximate point loads have been applied at various distances from the position of the strain gauges to establish curves relating the strain response and the magnitude of the point load. They are in the current work called influence curves. The point loads were applied by a Brinell hardness indenter. When the influence curves have first been established, the superposition principle may be used to deduce data on the responses of the sensors to distributed loads. Most sensors should behave purely elastically, which makes the use of the superposition valid. The difficulty related to the use of the principle is that the pressure distribution may be unknown.

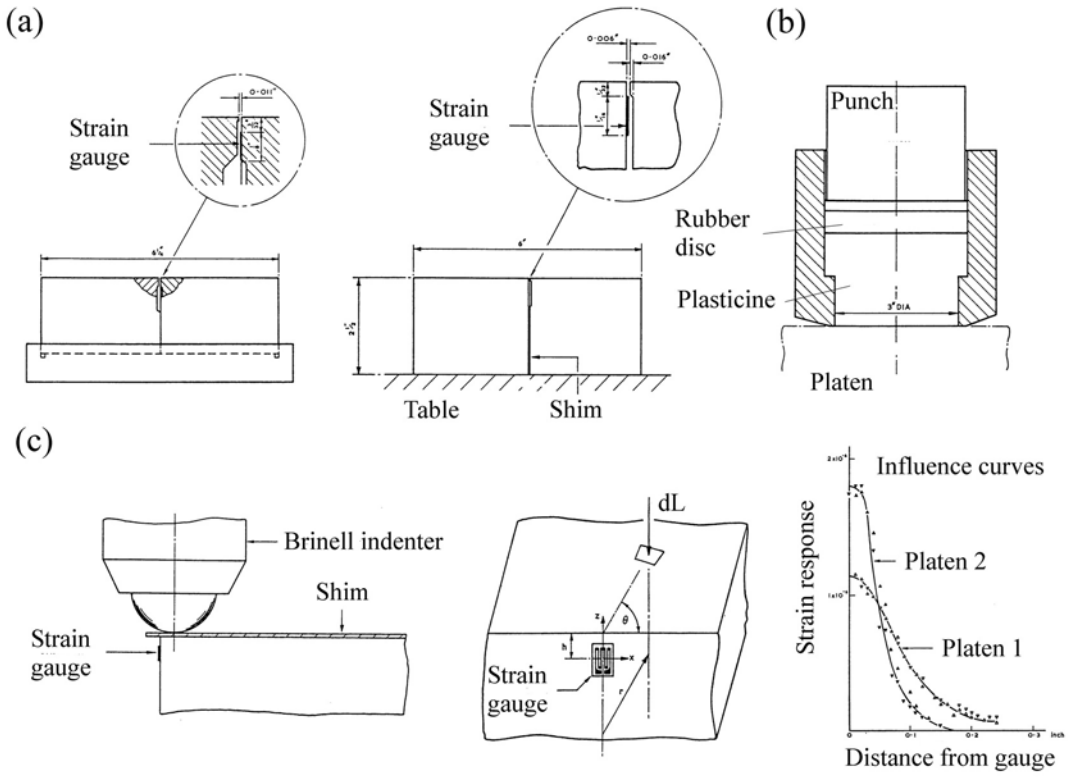

Figure 4.17. The split platen pressure cell by Daneshi and Hawkyard [Dan71]: (a) two sensor designs with strain gauges, (b) the principle of the hydrostatic compression calibration test and (c) point loading and the response of the sensors (influence curves).

4.3 Pin sensor designs and traction measurement during rolling

Pin sensors constitute a special sub-group of insert sensors. A common feature of almost all pin sensors is that the displacement (or tactile) measurement is performed at a certain distance from the tool surface. The pin transfers the forces from the work piece to the part of the sensor that deforms elastically. The pin sensor design was probably the first that was used to measure pressures during metal forming. Van Royen and Backofen [Roy57] [Roy60], who conducted very thorough investigations with strain gauges, refer to a number of early examples of pressure measurement in metal forming. Many of the early pin sensor designs made use of what may be regarded as more or less conventional strain gauges to measure the compression of a part of the pin. Experiments were usually performed at low temperatures (i.e much lower than 400 ºC). Van Royen and Backofen skilfully demonstrated how pin sensors could be used to measure not only the stress or traction component normal to the die face, but also the shear stresses. One pin was placed in a hole that was normal to the die face while another pin was fitted into a hole which was inclined from 30 to 60 degrees relative to the die face. In this way a part of the compression of the second pin was due to the tool-work piece shear stresses.

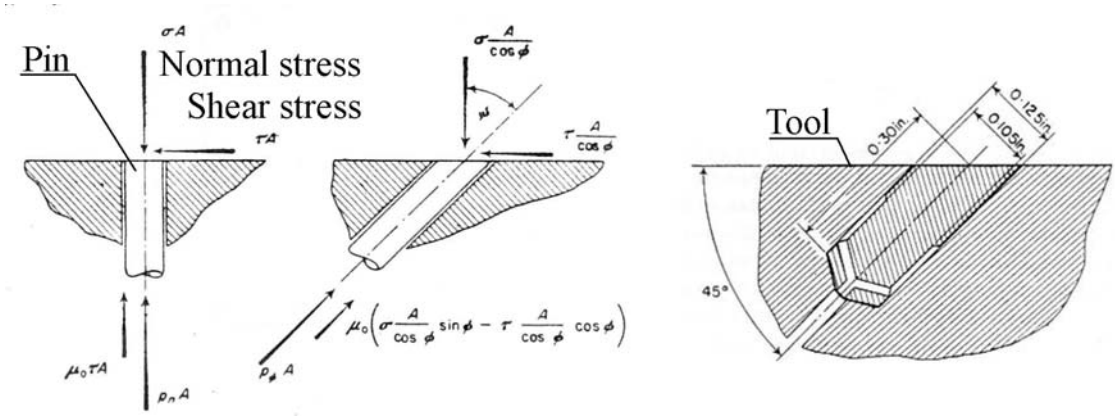

Figure 4.18. The pin sensors of van Royen and Backofen [Roy60]. Strain gauges were attached to the lowermost part of the pin to measure the pin compression.

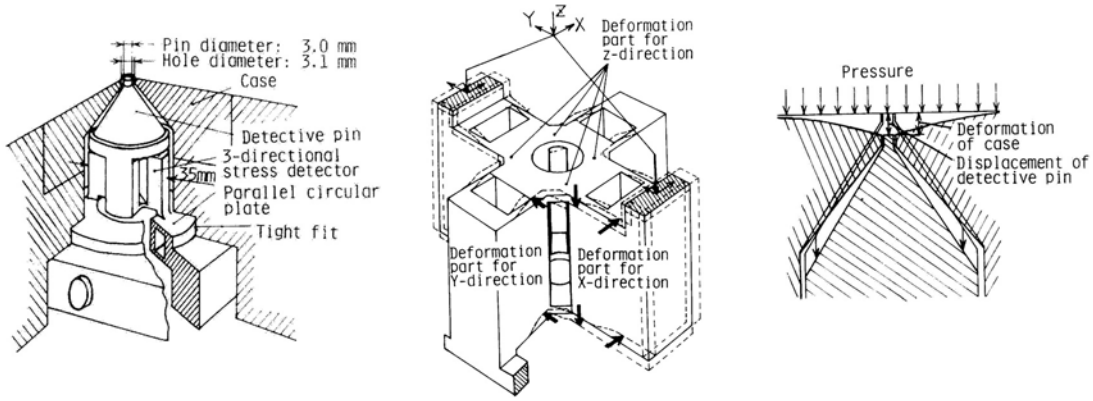

Figure 4.19. The pin sensors of Yoneyama et al. [Yon87]. Strain gauges were attached to the sensor to measure the deformation of the bridges. The sensor could be used to evaluate both pressure and shear stresses. The sensor was designed so that there is never any surface height difference.

The most important advantage of the pin sensor is the intuitive simplicity of the design. Furthermore, loads need never be critically large for a pin sensor, for the design may be very robust. The area of the top face of the pin may be small while the part consisting of the elastically deforming structures may be of a large cross-section [Yon87]. Another advantage of pin techniques is that the displacement measurement sensors may be placed far from the work piece, and that they may be artificially cooled [Han93]. A disadvantage of the pin design is that the mechanical interaction between the pin and the tool affects the measurement, and that the interaction may be complex. The friction between the pin and hole in the tool must be controlled. Lubrication may reduce the shear stresses, but may also complicate experimental procedures. Besides, if the layer of lubrication is broken, friction may be of random nature and difficult to assess [Roy60].

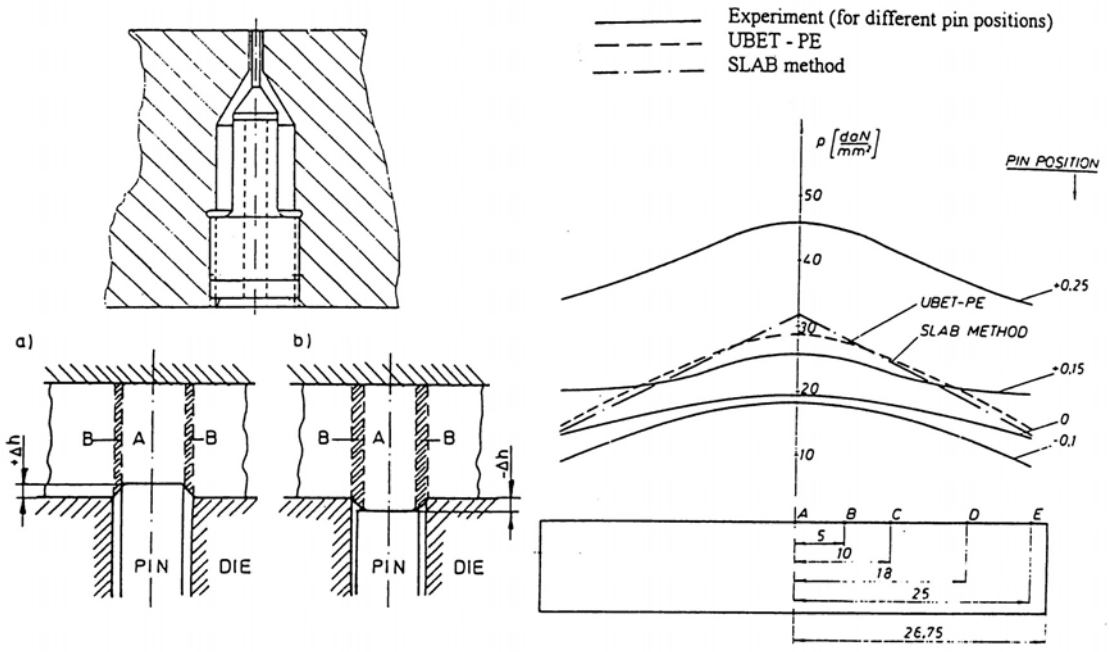

Figure 4.20. The effects of pin protrusion and depression considered by Plancak et al. [Pla96]. A simple compression test was used in the study, and pins were positioned so that there was an initial height difference Δh of -0.1, 0, +0.15 and 0.25 mm.

The contact between the pin and the work piece may be very difficult to determine and the source of inaccuracies. Calibration of the pin sensor is a simple matter, but one has to be careful when applying the calibration data in the analysis of data from subsequent measurements. The position of the top surface of the pin relative to the tool surface may significantly affect the response of the pin sensor. Plancak et al. [Pla96] have studied the effect of positioning the surface of the pin both above and below the tool surface. A displacement of 0.1 mm may significantly affect the sensor output during upsetting (20 %). The best results were obtained when the pin surface was positioned 0.15 mm above the tool surface. During upsetting, the pin may be depressed somewhat more than the surrounding tool, both due to the sometimes lower stiffness of the pin-construction and the inaccuracies from mounting. Thus, during upsetting, the offset should be smaller than 0.15 mm. If the top surface of the pin is below the tool surface, it is quite possible

that the material of the work piece does not completely cover the top surface of the pin. The sensor may indicate a load that is higher than the actual load if the pin protrudes from the surface, according to Plancak et al., because it also carries some of the load that should have been applied at the area directly surrounding it. During hot extrusion of aluminium, the problem is not as large as during cold compression testing. The material flows much more easily and pressure differences should be smaller. A larger problem during hot forming is, however, that the material may penetrate into the crevice between the tool and the pin. This may significantly affect the equilibrium calculations for the pin and the sensor output. Penetration of aluminium into the tool-pin crevice has an even larger negative effect on the shear measurement than on the pressure measurement.

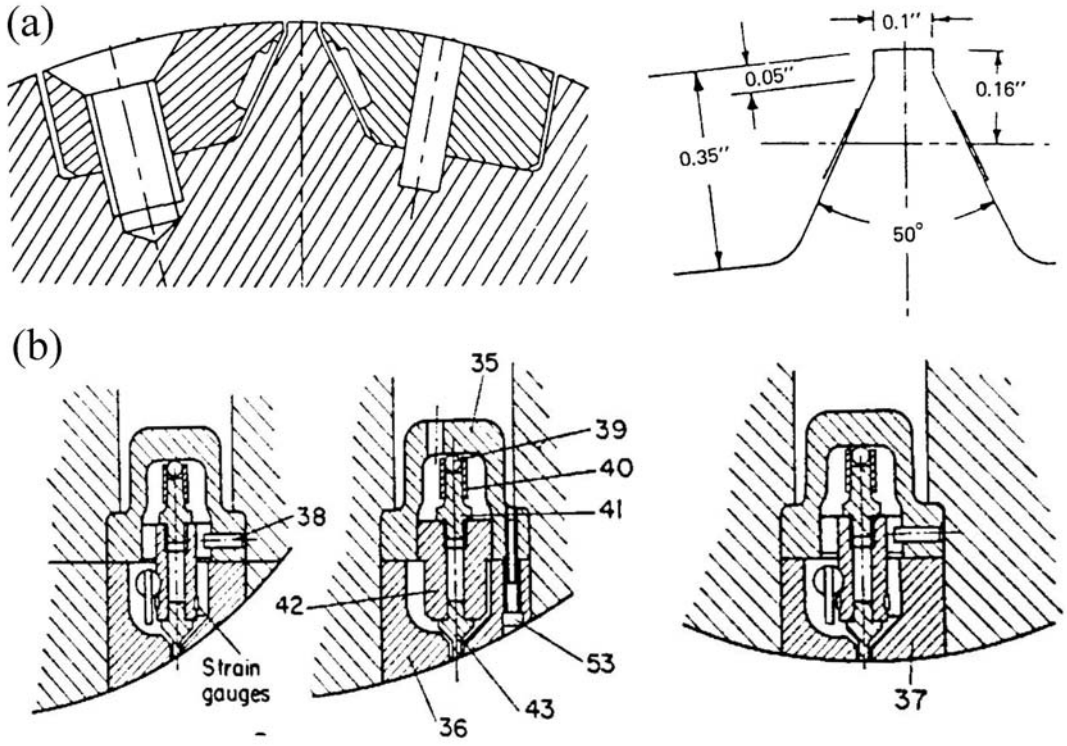

Figure 4.21. The pin sensors of (a) Banerji and Rice [Ban72] and (b) Al-Salehi, Firbank and Lancaster [Sal73]. Both sensors were inserted into rolls and strain gauges were used to measure deformations.

Pin sensors have been extensively used to study friction behaviour in cold rolling of various metals. The friction coefficient is generally regarded as the most important parameter in rolling. Rolling cannot be performed without friction. At the same time it is necessary to carefully control friction in order to secure optimal surface properties of the products. Both the rolling torque and the normal forces are continuously measured during rolling, so it is possible to directly control results from both pressure and shear measurement sensors. Both Siebel and Lueg and van Royen and Backofen studied the rolling process. Important improvements to the pin sensor design were proposed by Banerji and Rice [Ban72] and Al-Salehi, Firbank and Lancaster [Sal73]. The former group mainly integrated the pin in the roll construction, while the latter made use of a

fairly complex insert sensor. Both used strain gauges to measure the deformation of the pin. Further improvements to sensor designs based on the same technology have been proposed by many researchers. Great efforts have also been made to establish sensors that are able to accurately predict shear stresses. The most significant contributions are probably those of Yoneyama et al. [Yon87] [Yon89] [Yon99], Lenard et al. [Len91] [Len93] [Hum96] and Jeswiet et al. [Jes82] [Nya91] [Jes93] [Nya93] [Jes95] [Nya96] [Jes98]. High temperature rolling experiments with pressure measurement have been performed by Tieu et al. [Tie02] with the same pin-sensor that was used by Liu et al. [Liu01]. Schönert and Sander [Sch01] gave another example of the use of pin sensors and include references to work where sensors have been used to measure tractions during rolling of also other materials. Tong et al. [Ton02] have used fairly small pin sensors to study the process of casting of thin-walled hand phone components.

4.4 The state of traction measurement in aluminium extrusion

There are fewer examples of traction measurement in relation to the extrusion process than in relation to rolling. The reasons are most likely that rolling is a process of larger commercial importance and that it is still somewhat more difficult to make proper use of results from traction measurements in relation to extrusion. The experiences from the use of the measurement techniques developed for rolling should, however, be of some value to those who are studying aluminium extrusion. The pin sensor designs presented so far cannot in any way be regarded as optimal or very serious candidates for industrial implementation. Scrapping of dies due to fatigue cracking in the tool around the sensors and disruption of the production due to penetration of aluminium into the sensor cavity cannot be accepted. Some of the sensors are very large. Most of the sensors discussed that are used to study rolling only work at relatively low temperatures. The complexity of high-temperature measurement is much higher. It is of course not possible to rule out the prospect that much better pin sensors may be designed and that high-pressure high-temperature seals may be used to prevent flow of material into the sensor. However, the focus of the sensor designer should be on more reliable insert or integral sensor designs.

The most significant work on traction measurement for the extrusion process has been performed only quite recently. Yoneyama et al. have used both fibre optic techniques [Yon93] and conventional strain gauges [Yon99] to measure the container pressure during cold extrusion of aluminium. Experiments were performed with laboratory equipment of very small size. The equipment also contained sensors for measurement of the liner and ram forces so that the results from pressure measurement could at all times be compared to results from independent indirect measurement techniques. Calibration of the sensors was initially performed by a method of hydrostatic compression of a rubber cylinder. The press was designed so that the rubber disc could be moved in the direction of extrusion. This made it possible to establish influence curves similar to the type used by Daneshi and Hawkyard. Calibration experiments then revealed that both sensor designs were not very sensitive to loads that were not applied directly on top of the sensors. The strain gauge sensors have the potential to measure shear strains, but the task is much more complex because the pressures (normal stresses) are much higher than shear stresses during hydrostatic compression. Besides, elastic constructions are usually less affected by shear stresses than by normal stresses.

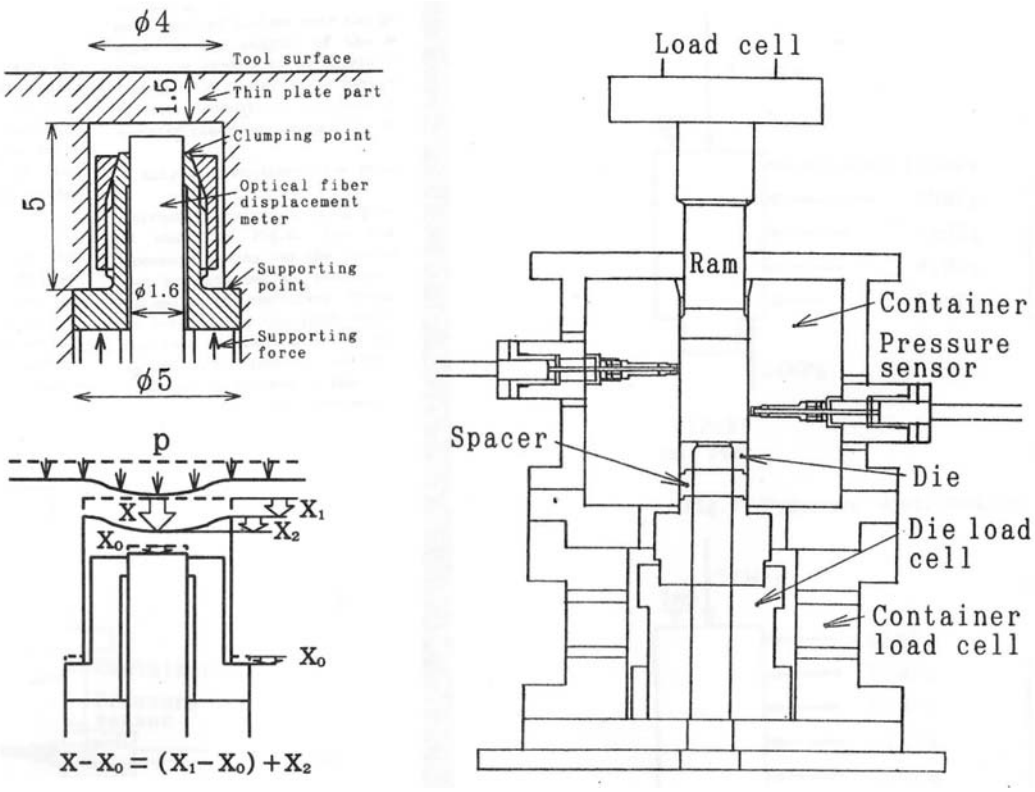

Figure 4.22. Fibre-optical attenuation sensor design used by Yoneyama et al. [Yon93] [Yon94]. Experiments were performed in a miniature press with an inner container diameter of only 20 mm. Experiments were only performed at low temperature, but the technique should be useful also at 600 ºC.

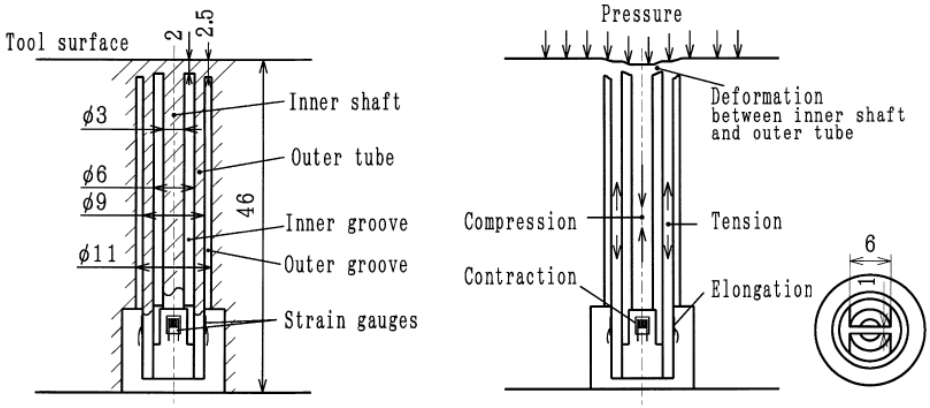

Figure 4.23. Integrated strain gauge sensor design used by Yoneyama [Yon99]. The sensors were used to study interface tractions during extrusion at low temperature. A small scale extrusion press was used.

Mori et al. have used commercial semi-conductor strain gauge pressure sensors by Kistler to measure die face pressures below 200 MPa at temperatures below 300 ºC during extrusion of AA1050. They have studied extrusion of rods [Mor01c] [Mor02a], thin strips [Mor02b] and hollow profiles [Mor03]. The objectives of their study seem to have been comparable to those of the study treated by this thesis. However, limitations

of conventional melt pressure sensors at the outset of the work made it necessary to seek measurement techniques that could be used at higher and more relevant temperatures. There was unfortunately no direct transfer of information between the NTNU/SINTEF research group and Mori et al. during preparations for the experimental work. Still, the approaches that have been followed appear to be similar. Mori et al. have performed measurements of the die face pressure with a relatively complex die design. The design made possible both easy dismantling and mounting of sensors and measurement of pressure at a range of distances from the die outlet. Mori et al. also introduced die displacement measurements to evaluate more overall deformation of the dies during extrusion. Kopp et al. have also used Kistler piezoelectric sensors to study processes similar to extrusion, namely thixo-forming [KopW]. Alternative methods for evaluation of local values at the interface between the billet and tools or the cases of hollow profile and backward extrusion have recently been presented by Kim et al. [Kim98] [Kim99] and Sato et al. [Sat02]. The approaches deviate from those used in the current study.

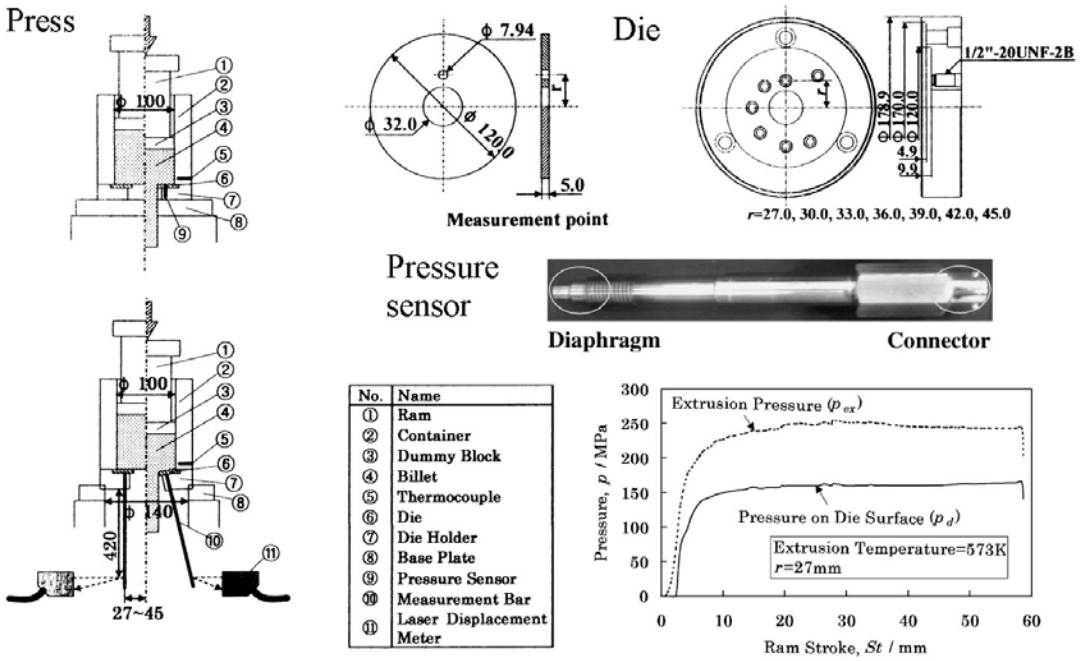

Figure 4.24. The die face pressure sensor design by Mori et al. [Mor02], with the rod extrusion press and the positions of the sensors (left), the extrusion die and sensor positions (top right), the pressure sensor (centre), the results (bottom left). Note that the extrusion press was of relatively large size.

Cvahte et al. have measured the overall die face load during extrusion and drawing processes with a specially designed load cell [Cva99]. Additionally, strain gauges were added to the pre-stressing ring surrounding the die to allow estimation of pressure inside the container. The experiments were performed at quite low temperatures (< 100 ºC). It is also possible and common during regular high temperature extrusion to estimate the average die face pressure on the basis of simultaneous measurements of the ram force and container liner force. The liner force is usually applied at the flanges of the die to seal off the container, but the liner may also be mounted on a specially designed liner

load cell arrangement [TubW]. The compression of the load cell may then be performed at relatively low temperatures and with almost any conceivable technique, even in the case of hot extrusion. In this thesis the focus is on local measures of force or pressure, and liner loads are only assessed for the purposes of verification.

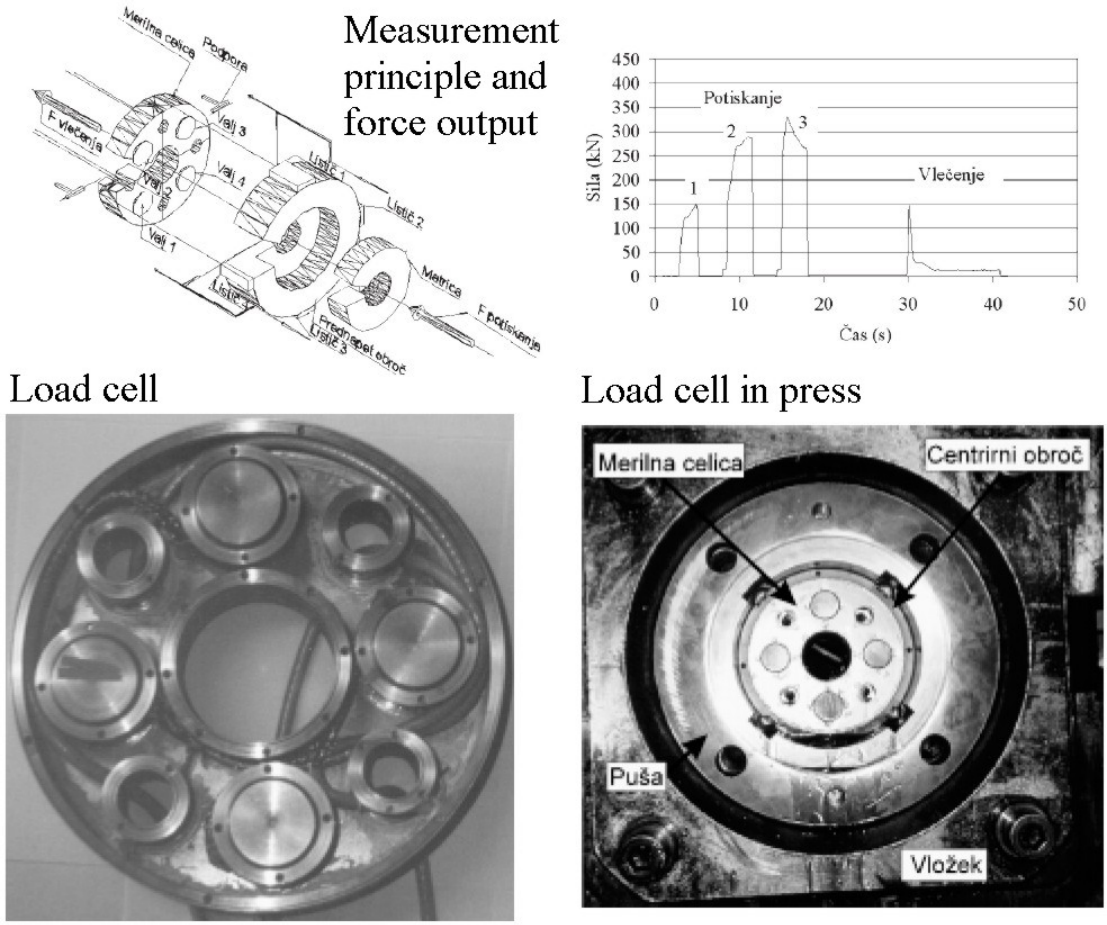

Figure 4.25. The extrusion-drawing tool load cell used by Cvahte et al. [Cva99]. The load cell makes use of strain gauges, and experiments were performed at low temperature (room temperature).

As previously discussed, pressure measurement is quite regularly performed in order to better control polymer extrusion processes. The pressure build-up is directly related to the physical properties of polymer melt (i.e. viscosity) and to the product quality. There are many suppliers of commercial pressure sensors, and the literature on the subject is rich. However, there are important differences between polymer and metal extrusion. Aluminium extrusion usually occurs at significantly higher temperatures and pressures, and the temperature increase due to plastic dissipation may also be higher. It is therefore seldom possible to directly apply pressure sensors for polymer extrusion in relevant studies of aluminium extrusion. On the other hand, the fundamental principles of measurement are the same and experiences drawn from polymer extrusion may be of rather large value in the process of designing aluminium extrusion pressure sensors. The purpose of this sub-section is not to provide a full review of the state of polymer melt pressure sensor technology, but rather to focus on a capacitive melt pressure sensor

design of particular relevance to the current study. Pinto et al. have designed a set of capacitive pressure sensors that integrate methods of direct temperature compensation and provide a useful presentation of the capacitive measurement technology in a US Patent Application [Pin96]. All sensors consist of a diaphragm or a thin disc/plate which deflects as a pressure is applied at its external face. The disc has been designed so that the highest occurring stresses cause neither fatigue cracking nor creep. The materials that have been used have optimal thermomechanical and electromagnetical properties. Furthermore, the sensors have been carefully designed so that the effects of temperature changes are balanced and so that the temperature sensitivity is kept as small as possible. Three thermal effects are important. The thermal expansion of the sensor housing material causes the capacitor gap to increase and the capacitance to decrease. The temperature increase affects the modulus of elasticity of the sensor disc material so that the gap distance may decrease although the pressure is constant during measurement. Finally, the temperature may affect the capacitance of the sensor. It is possible to compensate for the thermal effects by using a sensor with two capacitors measuring the disc deflection. An inner circular capacitor measures the capacitance of C_i across the shortest gap, and an outer annular capacitor measures the capacitance, C_o, across the gap at the periphery. The capacitors are affected similarly by the thermal expansion effect and changes in permittivity, but they respond differently to the disc deflection. A discriminator circuit has been designed that produces an output voltage, V_o, proportional to the difference in capacitance $C_i - C_o$ and to the frequency, F, and voltage, V_{REF}, of an applied reference voltage signal. The circuit also eliminates the effects of changes in parasitic capacitances associated with the cables connected to the capacitors, C_{is} and C_{os}. One of the most challenging tasks related to the design of capacitive sensors is to control the capacitive coupling between various elements in the circuit (wires, shields, housing and capacitor plates). The parasitic capacitances may easily be one or even two orders larger than the sensor capacitances, so small changes during measurement may easily completely ruin results.

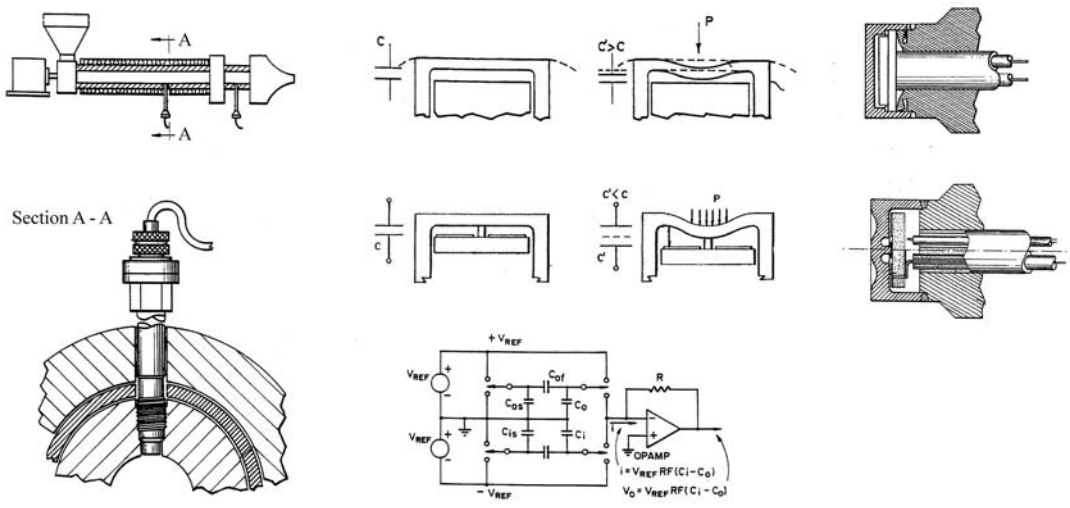

Figure 4.26. Capacitive melt pressure sensor developed by Pinto et al. [Pin96]: the process and sensor positioning (left), two different capacitive disc designs (top right), the electric circuit (bottom left).

Chapter 5

An overview of the work

The general objective of this study has been to develop, test and use pressure and strain sensors based on the capacitive principle of displacement measurement. Capacitive sensors were chosen as it was believed that they are fully capable of working at high temperatures, and because they produce outputs that are relatively insensitive to temperature changes. This does not mean, however, that the capacitive principle is more suitable than any of the other principles treated in the previous section. It is merely one of the many candidate sensor principles that should be carefully examined. Extensive testing of other techniques is needed before a fruitful comparison can be made. The current section presents the experimental approach followed during the course of this PhD study, and provides comments on the main objectives and results from each of the main stages or parts of the work. Detailed analyses of results from measurements have been provided in the appendices and in reports by co-workers referred to in the text.

5.1 On the presentation of results

The study of the behaviour of the capacitive die face pressure sensors and of related sensors consisted of several parts. Six experimental activities may be distinguished:

- high-temperature testing of capacitive sensors
- high- and low-temperature compression testing
- high-temperature laboratory rod extrusion
- high-temperature laboratory thin strip extrusion
- high-temperature laboratory split tube extrusion
- high-temperature industrial U-profile extrusion

The three first activities were mainly related to the establishment of the measurement technology, and their planning and experimental activity was entirely controlled by the candidate. The three last activities were to a larger extent applications of the technology related to the study of the thermo-mechanics of aluminium flow, and were performed in cooperation with researchers at SINTEF Materials Technology and Hydro Aluminium Extrusion. It would have been advantageous to perform rod extrusion before any other type of extrusion as this case, which essentially is two-dimensional, is the simplest to analyse. The evaluation of material flow for the most complex extrusion cases should be

performed with a well-established sensor technology. However, time was scarce, and SINTEF activities could not be delayed. Hence, the sensor technology has gradually improved and developed over the whole duration of the work. All types of experiments contributed to advancing the state of the fundamental measurement technology. The very last experiments with pressure sensors in the laboratory were performed with a second- or third-generation rod extrusion die and sensor concept.

The results of the research activities of the candidate within the framework of this PhD study may most rationally be presented as an ensemble of articles and reports. The main reasons are that the work has consisted of many semi-independent parts, and that the results from the different parts of the study have been shared with a wider audience both at conferences and through journal articles. The publication of the work enhanced the exchange of information with other researchers and made work simpler. Hopefully, it has also contributed to the advance of the general state of pressure measurement in aluminium extrusion research. The appendices contain the following journal articles, conference papers and reports:

Appendix A:

[Moe02] Moe P.T., S. Støren, *A technique for measuring pressure on the die face during extrusion*, Proc. 5th ESAFORM Conf. on Material Forming, April 2002, Kraków, pp. 463-466.

Appendix B:

[Lef02] Lefstad M., Moe P.T., Flatval R., Støren S., *Thin strip aluminium extrusion – pressure, temperature and deflection recordings of the extrusion die*, Proc. 5th ESAFORM Conf. on Material Forming, April 2002, Kraków, pp. 471-474.

Appendix C:

[Moe03a] Moe P.T., Lange H.I., Hansen A.W., Wajda W., Støren S., *Experiments with die deflection during hot extrusion of hollow profiles*, Proc. 6th ESAFORM Conf. on Material Forming, April 2003, Salerno, pp. 119-122.

Appendix D:

[Waj03] Wajda W., Moe P.T., Lefstad M., Støren S., *A study of the limits of self-stabilization during extrusion of thin strips*, Proc. 6th ESAFORM Conf. on Material Forming, April 2003, Salerno, pp. 267-270.

Appendix E:

[Moe03b] Moe P.T., Lefstad M., Flatval R., Støren S., *Measurement of temperature and die face pressure during hot extrusion of aluminium*, Intern. J. Forming Processes Vol. 6 (2003), No. 3, pp. 241-270.

Appendix F:

[Waj04] Wajda W., Moe P.T., Abtahi S., Støren S., *An evaluation of material behaviour during extrusion of AA6060 rods*, Proc. 7th ESAFORM Conf. on Material Forming, April 2004, Trondheim, pp. 245-248.

Appendix G:

[Moe04a] Moe P.T., *An analysis of forge welding of steel rods,* Proc. 7th ESAFORM Conf. on Material Forming, April 2004, Trondheim, pp. 399-402.

Appendix H:

[Moe04b] Moe P.T., Wajda W., Szeliga D., Madej L., Støren S., Pietrzyk M., *An approach for evaluating constitutive models for hot aluminium extrusion – Rod extrusion of AA6060 as a case study*, Proc. 10th Int. Conf. on Metal Forming, Sept. 2004, Kraków, pp. 723-730.

Appendix I:

[Moe04c] Moe P.T., Wajda W., Støren S., *A study of the thermomechanical response of a die face pressure sensor for hot aluminium extrusion,* Proc. 10th Int. Conf. on Metal Forming, Sept. 2004, Kraków, pp. 627-634.

Appendix J:

[Moe04d] Moe P.T., Wajda W., Couweleers F., Støren S., *Visions of a system for shape control during thin-strip aluminium extrusion*, Proc. 12th Int. Conf. on Experimental Mechanics, Sept. 2004, Bari, pp. 570-571 (extended abstract, full length article on the ICEM12 CD)

Appendix K:

[Waj05a] Wajda W., Moe P.T., Støren S., Lefstad M., Flatval R., *Measurement of temperature and pressure during thin-strip extrusion*, Proc. 8th ESAFORM Conf. on Material Forming, April 2005, Cluj, in press.

Appendix L:

[Moe05] Moe P.T., Wajda W., Støren S., Lefstad M., Flatval R., *An experimental and numerical study of induction heating*, Proc. 8th ESAFORM Conf. on Material Forming, April 2005, Cluj, in press.

Volume II:

[Moe04e] Moe P.T., A Comprehensive Report on the 2nd Set of Rod Extrusion Experiments, PhD thesis Volume II, Trondheim, 2005.

The paper [Moe04a] in Appendix G treats the modelling of the heating phase of an induction welding process. The fundamental equations of electromagnetism that are presented and solved in this work, the Maxwell equations, are the very same that govern the behaviour of both capacitive and inductive displacement sensors and the heating of aluminium billets prior to extrusion. There are very important differences between the physical behaviour of inductive and capacitive transducers [Sva99] [Chr00], but the point of origin for the analysis of such systems is the same. The objectives of the work presented in the paper were to establish a fundamental understanding of the nature of Maxwell's equation and electromagnetical phenomena and to learn how to implement the strongly coupled models of induction heating in the commercial finite element code ANSYS®. Induction heating modelling should also be used extensively in relation to the study of extrusion (Appendix L), as the initial temperature distribution of the billet at the onset of extrusion determines how deformation takes place during extrusion. Industrial experience has shown that it is vital to control the induction heating process to obtain profiles of satisfactory shape and quality [Nil02]. The main reason for including an analysis of induction heating in the current work is that quantitative studies of flow and sensor behaviour require that the uncertainties with regard to initial conditions be as small as possible. Appendix H includes a small study of sensitivities to changes in the

initial conditions, and it is vital that those who desire to further analyse the data from this thesis take into account possible errors in input data.

Two aspects of an article-based thesis may be particularly problematic. First, most of the articles are of limited size and do not provide a sufficiently complete presentation of the work. The current study focuses on experimental methods, and the description of the experimental activity must allow exact reproduction of results. Volume II has therefore been added. It provides a comprehensive overview of experimental and numerical results and a fairly detailed description of the experimental set-up for the last rounds of rod extrusion experiments. Evaluations of the experimental approach and the choices of sensor and experimental design are also given. The experiments are the most important of the study since they were performed in the most systematic manner and with the most refined versions of the capacitive pressure sensors and mounting solutions.

Second, in this article-based thesis, basic facts about the set-up of and results from important experiments are repeated a number of times. All parts of the thesis may be read as independent pieces, however, and some parts of the work are only meant to be used as references (Volume II). The current section and the papers contain the most important information. The article [Moe03b] provides a more detailed presentation of data first presented at the ESAFORM 2002 conference [Moe02] [Lef02]. It relates to experiments with both rods and thin-strips. It also provides a general discussion on sensor design and the objectives of the experiments. A further study of the instrumented rod extrusion experiments was presented at the Metal Forming 2004 conference [Moe04b] [Moe04c]. The latter of the articles focuses mainly on the temperature sensitivity of the sensors. The work detailed in [Moe04b] provides a more thorough treatment of inverse modelling concepts first presented in the article [Waj04].

A considerable part of the experimental results of the study, if not the largest part, have not been reported at all or only been reported by the candidate or co-workers in internal reports or memos. Not all experimental results were worthy of further analysis and not all analysed data were worthy of publication. This does not mean, however, that the experiments were of no value whatsoever. The study included more than two years of continuous and diverse experimental activity in the laboratory and at the Hydro Aluminium extrusion plant at Raufoss, Norway. There were several iterations of design, testing, analysis and redesign, and an understanding of the process, the capacitive sensor equipment and metal forming pressure measurement gradually improved. The most important results from the experiment were usually not the measurement data, but rather the conclusions that were drawn and the new ideas that were generated.

The rest of this section provides an overview of the experimental activity and analysis and communicates the objectives and most important conclusions of the various parts of the study. References to the SINTEF reports and memos of relevance are also given, for although the candidate has not been a part of the SINTEF system and thus is formally not a co-author of these reports, he has to a large extent contributed to their writing and fully supports most of their conclusions.

5.2 High temperature testing

All the Capacitec high-temperature capacitive displacement sensors used to measure the die face pressure were tested repeatedly in an electric hot air furnace up to 650 ºC. The main objective of the temperature testing was to verify that the temperature sensitivity of the sensor response was in accordance with the data provided by the manufacturer [Fos89]. Another goal was to check how well the solutions for mounting the capacitive probe work when heated to very high temperatures. Tools for upsetting / compression, including pressure sensors were therefore heated in an oven to 600 ºC.

Accurate data on temperature sensitivity provided by the manufacturer is presented in Volume II in relation to the description of the sensor equipment. When the sensor discs are positioned so that the initial DC voltage output of the system is approximately 8 V (full range: 0 to 10 V or 0 to 500 µm), a temperature change of 500 ºC should cause the voltage to decrease by 0.1 V. Furthermore, if the temperature changes by approximately 10 ºC during measurement at 500 ºC, the sensor output should be modified by less than 0.01 V. If calibration has been performed so that a voltage change of 1 V corresponds to a displacement of 50 µm (10 V ~ 0.5 mm), the effect of a temperature change of 10 ºC would be perceived as a displacement of less than 0.5 µm. During die face pressure measurement, the sensor disc response (movement) is in the range of 20 to 40 µm, so the reported temperature sensitivity of the capacitive sensors may be regarded as small. The data provided by the manufacturer have been established with a somewhat larger probe than the one used in the experiments (HPC-150 vs. HPC-75), but the temperature sensitivities of the probe types were not expected to differ significantly.

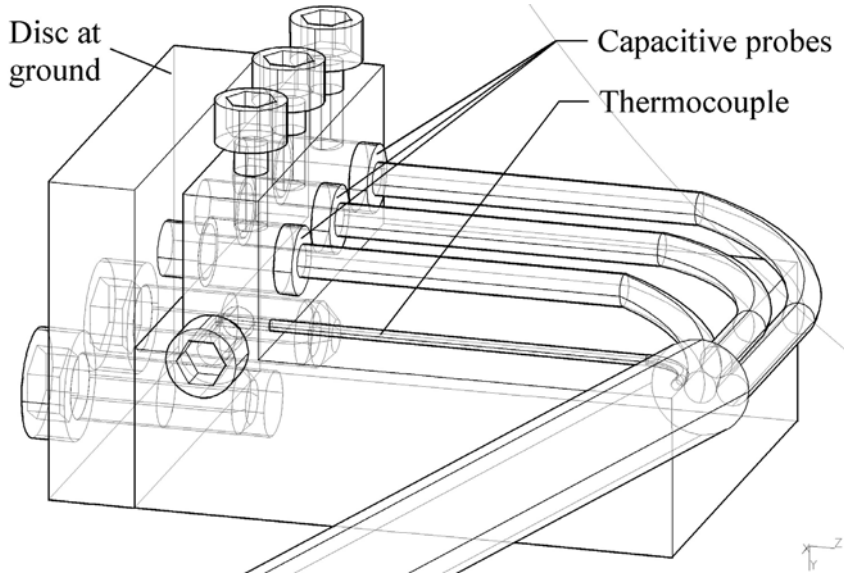

Figure 5.1. The set-up of the temperature test. The design has been slightly modified according to the experiences from testing. Three sensors may be tested while the set-up and air temperatures are measured.

In order to test the temperature sensitivity of the capacitive sensors, a special calibration stand was devised. The stand was made of Orvar Supreme H13 tool steel and had three spaces for capacitive probes. The distance between the probe heads and a disc was

fixed, but due to the thermal expansion of the stand material it could change during measurement (approx 0.05 µm/10 ºC). Two or three sensors were tested at a time to allow easier and more accurate comparison of results and to simplify testing. A fairly long and thick wire was attached to the stand so that it could be directly connected to the ground cable, which could not tolerate high temperatures. There was a hole in the electric furnace that allowed the sensor and ground cables to be guided to the amplifier rack. Thermocouples were also mounted in close vicinity to the stand to make possible parallel determination of the temperatures of the probe, the stand and the surrounding air. The heating was usually performed in steps of 50 to 100 ºC, and a steady state was reached at the end of each heating step. The output voltage of the sensors and the temperatures were continuously recorded. The steady state values are probably of the greatest interest and simplest to interpret.

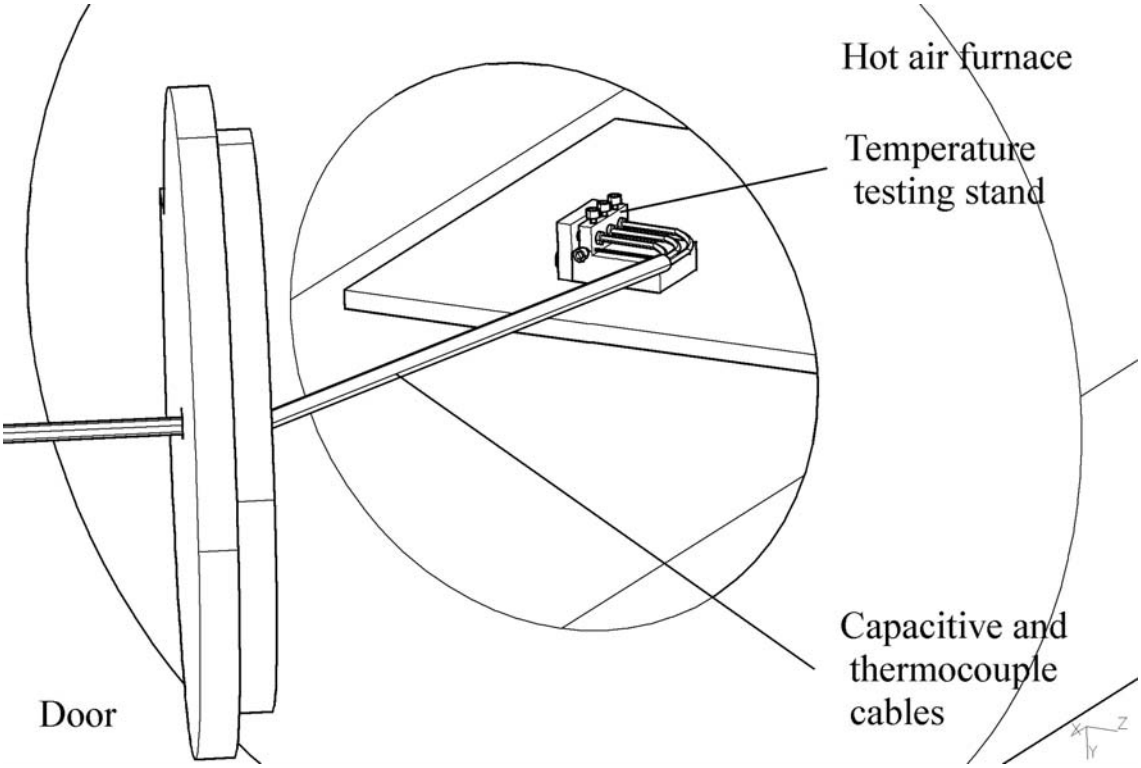

Figure 5.2. The experimental set-up for the temperature testing of the capacitive probes. The sensor was placed inside a hot air furnace, the door was then closed and heating commenced. There was a hole in the door for cables.

A general conclusion from the study was that the high temperature performance and the temperature sensitivity of the sensors were generally in relatively good agreement with the information provided by the manufacturer. The voltage changes recorded during heating from 25 to 500 ºC were in most cases smaller than approx 0.2 V. One of eight probes performed poorly, while the high-temperature performance of yet another one was questionable. The thermal response of the worst probe was approximately ten times larger than that of the other probes. The choice of amplifier was not important. After this behaviour had been thoroughly investigated and documented, the worst probe was replaced by a new one at no cost to the project. The reason for the very weak sensor performance was never explained by Capacitec. However, the poor measurement results

could be reproduced relatively accurately (approx within ± 25 %). After the equipment cooled down completely, the voltage reading was usually similar to the reading at the beginning of the experiment. Thus, it seems unlikely that the anomalous behaviour was due to improper mounting. A speculation is that a loose connection in the probe may have been the cause of the troubles. The candidate and Capacitec therefore worked out a new capacitive probe design with a better strain relief. It was extensively used in the subsequent experiments. A sketch of the new design is presented in Volume II.

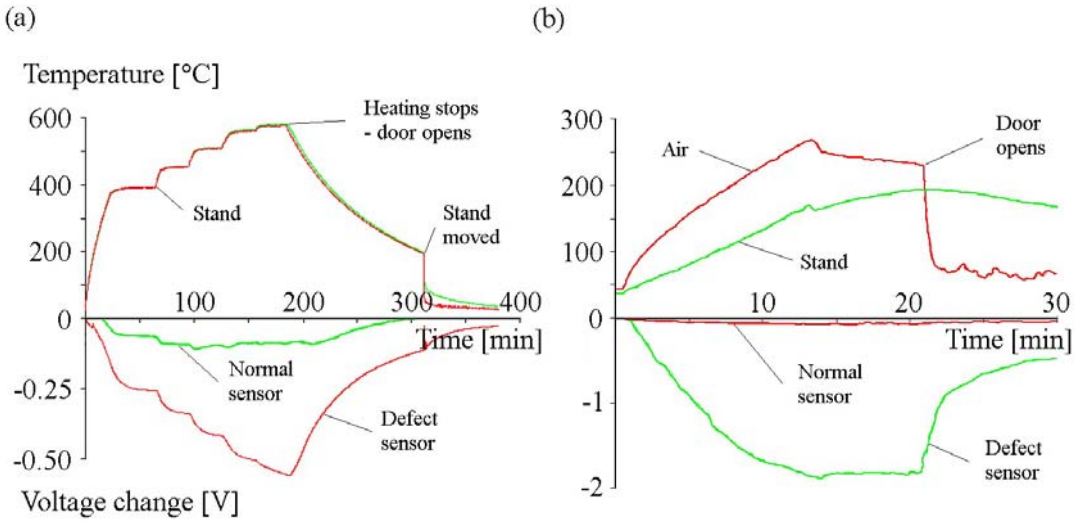

Figure 5.3. Two rounds of temperature testing of sensors: (a) parallel measurements with a defective and a properly functioning sensor up to 600 ºC, (b) parallel measurements with two other sensors up to 300 ºC. In both cases, the sensors were heated in a hot air furnace. The defective sensor proved extremely sensitive to changes in the temperature of the surrounding air.

The heating experiments were not performed in a sufficiently accurate and systematic manner to allow reliable conclusions on the details of thermal sensor behaviour to be drawn, and there was neither time nor resources to design satisfactory test set-ups and procedures. Besides, it is most difficult to determine reliable temperature compensation curves based on experimental results. First, the temperature effect is by itself rather small compared to the response of the sensors to mechanical loads. Second, the variability in the thermal response of the sensors is comparable to the magnitude of the response. Third, the temperature problem is of a transient nature, and the actual heat flow during extrusion should in any case be simulated physically and numerically to better understand the problem. Fourth, temperature sensitivity of the capacitive probe is usually only a part of the whole problem, and it is often the thermo-mechanical response of the deforming part of the sensor that causes the largest thermal deviations. The issue has been treated in Appendix I. The only reasonable conclusion to be drawn from the experiments is that the temperature effects are relatively small (2-5 % of the total sensor response), and that there is no reason to believe that the thermal responses are not fairly repeatable. The temperature testing of the mounting solutions did not reveal any loss of contact during measurement. Thus, it seemed reasonable to conclude that the sensors would probably not fail during the heating phase proceeding extrusion.

5.3 Compression testing

Both high- and low-temperature compression testing was performed in the early parts of the study. There were essentially three objectives. First, compression experiments allow the feasibility of pressure measurement in a hostile environment to be tested. Second, as compression testing is simpler and less expensive to perform than extrusion, it may be used to compare and evaluate promising sensor designs. Third, compression testing of various kinds may be suitable methods for calibration of sensors both at high and low temperature. The relatively small presses useful for the purpose have the potential to be much more accurately controlled than a large industrial or laboratory extrusion press.

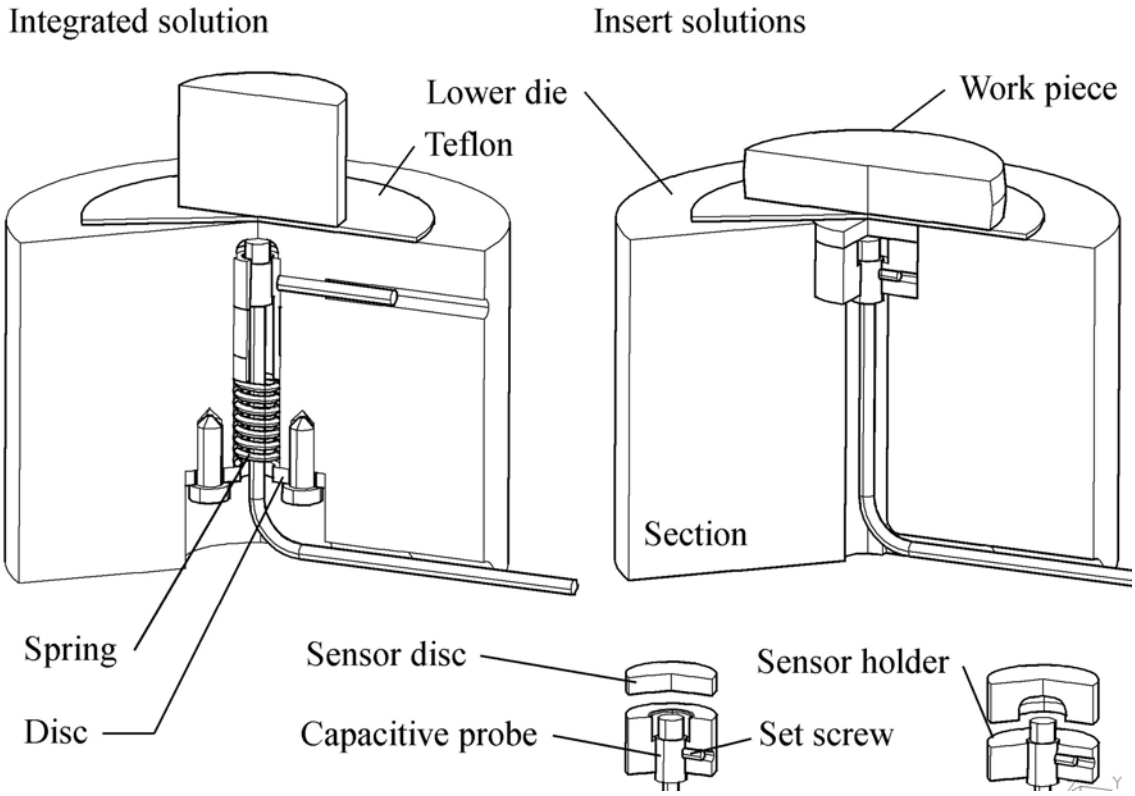

Figure 5.4. Compression test tool with integral and insert sensors (first, second and third tools). The integral sensor may be fastened either with a spring or with a set-screw. Three alternative insert sensor designs were tested.

All compression tests in the current PhD study were performed with the Dartec RE500 hydraulic press belonging to SINTEF Materials Technology. The accuracy of force measurement is better than 1 % within the complete load interval up to 500 kN. Ram force and displacement were continuously measured in addition to the sensor response and the temperature. Extensometer measurements, which may accurately determine the compression of the test specimens, were not performed even though such measurements would have allowed a closer study of material behaviour during compression testing. In total four tools with sensors were used, and five different sensor designs were assessed. Appendices C and E provide overviews of some possible sensor design strategies. The first design that was tested was a purely cylindrical insert sensor of 22 mm in diameter and 18 mm in height. The sensor was tightly fitted into a cylindrical hole in the tool.

The deflecting sensor disc and the probe holder, the cylindrical piece into which the probe was mounted, were separate parts. Two types of deflecting sensor discs were used. The first type was a cylinder 5 mm high and 22 mm in diameter. The second type was a disc 9 mm thick with a carefully machined cavity 5 mm deep. All edges of the sensor were rounded to limit the level of stress. The probes were fastened to the probe holders by two set screws (M2/M3). The force applied at the top face of the die was transferred from the sensor disc to the probe holder and into the die. The second tool for compression testing had a sensor of a similar design as the first tool. The sensor was of a somewhat smaller size, since a small sensor may be easily positioned close to the die outlet and in the mandrel of a bridge die. The diameter of the second insert sensor was 16 mm, and the height was 15 mm. The sensor disc was 3 mm thick.

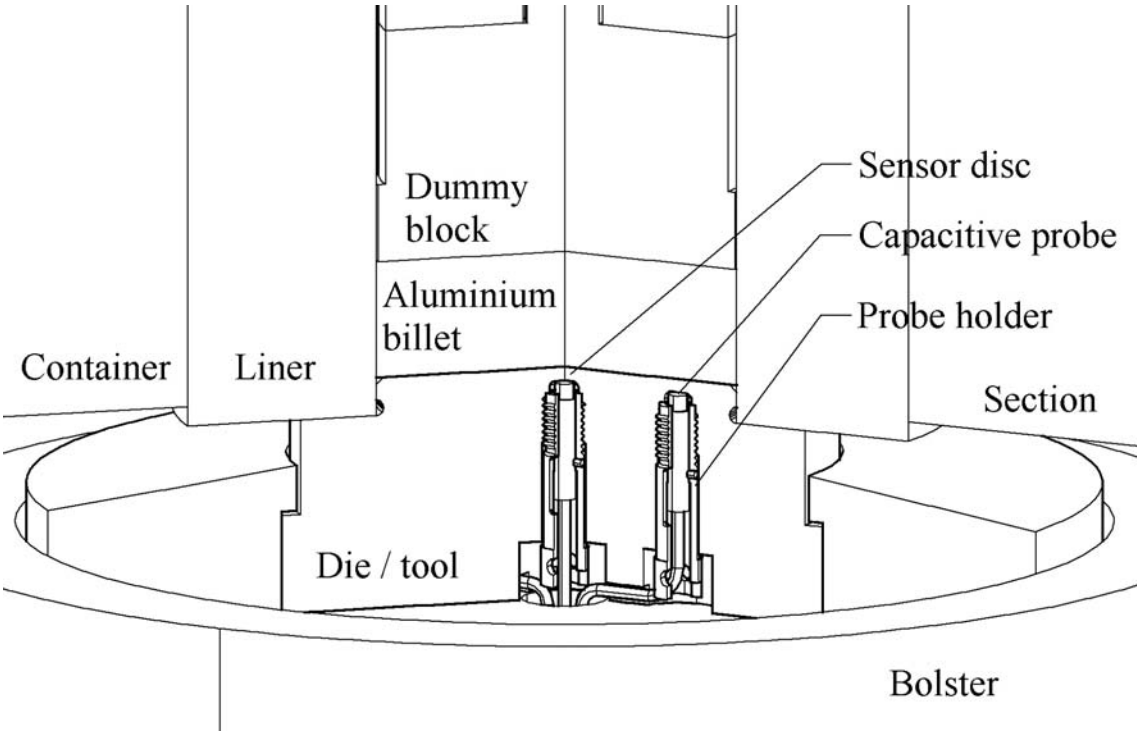

Figure 5.5. Integral sensor designs with finely threaded probe holder. Sensors could be fastened with a screw driver. A tight connection was established, but it was difficult to determine the nature of the interaction between the probe holder and the tool. The (fourth) die or tool was a laboratory extrusion die design without an outlet. The sensors could then be directly tested in the extrusion press. The die could later be modified and used for extrusion.

In the third die the sensor disc was an integral part of the tool design. A hole (Ø11 mm) was drilled from the bottom of the tool and almost to the top surface. A special cavity of 10 mm in diameter was then spark eroded close to the die face. The remaining integral sensor disc had a thickness of only 3.5 mm. The smallest diameter of the cavity was 9 mm. An important objective was merely to test the feasibility of manufacturing this sensor design. The capacitive probe was attached to a long cylindrical probe holder by a M2 set screw. Two solutions for mounting the probe holder to the die were tested. First, a M3 set screw was used to fix the holder to the wall of the cavity. The set screw was

inserted into a partly threaded hole that penetrated the tool in the radial direction. Second, the probe holder and probe were pressed toward an edge in the upper part of the sensor cavity by a specially designed Inconel® spring. Essentially the same solution was later used in most extrusion dies. The dimensions of the sensors were later changed, however, since it was desirable to make the sensors as small as possible.

The fourth tool used for compression testing was an extrusion die with three pressure sensors but no outlet. One sensor was placed in the centre of the die while two were placed 33 mm from the centre. The sensors were also of an integrated type, and the probe holders were of a similar design as those that were used in the previous upsetting experiments. The front of the holders consisted, however, of a finely threaded part. The innermost part of the sensor hole was therefore also threaded. During mounting, the probe holders were pressed towards an edge in the bottom of the sensor hole. Since two surfaces can never be perfectly co-planar, the contact between the probe holder and the edge in the cavity was not complete (and satisfactory). During loading it was therefore possible that the contact conditions inside the sensor hole changed abruptly, and that the sensor responded non-linearly to the load.

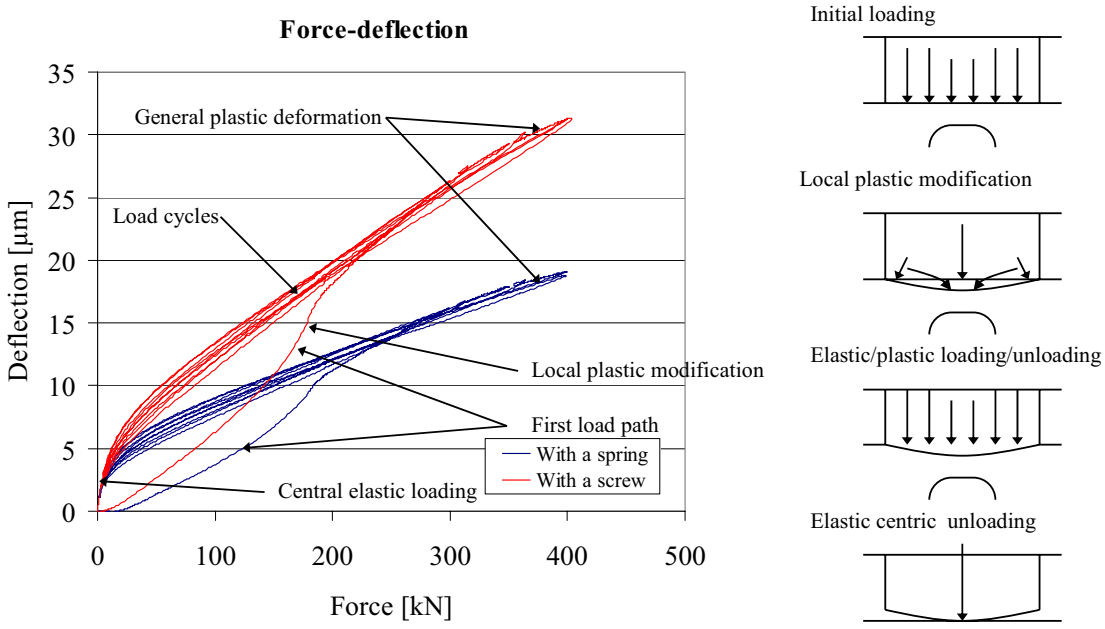

Figure 5.6. Results from low-temperature compression testing with specimens 35 mm in diameter and 30 mm high (left). A possible explanation for the non-linearity of the curves is given (right). Curves with the same appearance have been determined qualitatively. Non-linear behaviour may generally be related to the change in the effective loading area (due to plastic deformations during loading / unloading and probe expansion).

Three types of compression tests were run. First, cylindrical specimens 30 mm high and 35 mm in diameter were compressed at the top face of the sensors to various levels of strain. During high-temperature testing, the specimens were of either aluminium or steel. Low-temperature tests were only performed with AA6060 specimens. The high-

temperature tests were run in a specially designed electrical furnace at 500 ºC. The tests were very time-consuming and were difficult to perform with sufficient accuracy. Still, the results were encouraging, because they indicated that pressure measurement at high temperature was in fact feasible. During low-temperature testing, Teflon® sheets were placed between the work piece and the tool in order to reduce friction and to make the applied pressure more uniform. When the work piece was significantly deformed, the edges of the specimen penetrated into the Teflon® sheets and came into very intimate contact with the tools. Consequently the friction increased, and the specimen became more barrel-shaped. In addition, the specimens were usually slightly oval after testing. Experiments were usually stopped before significant ovalisation occurred.

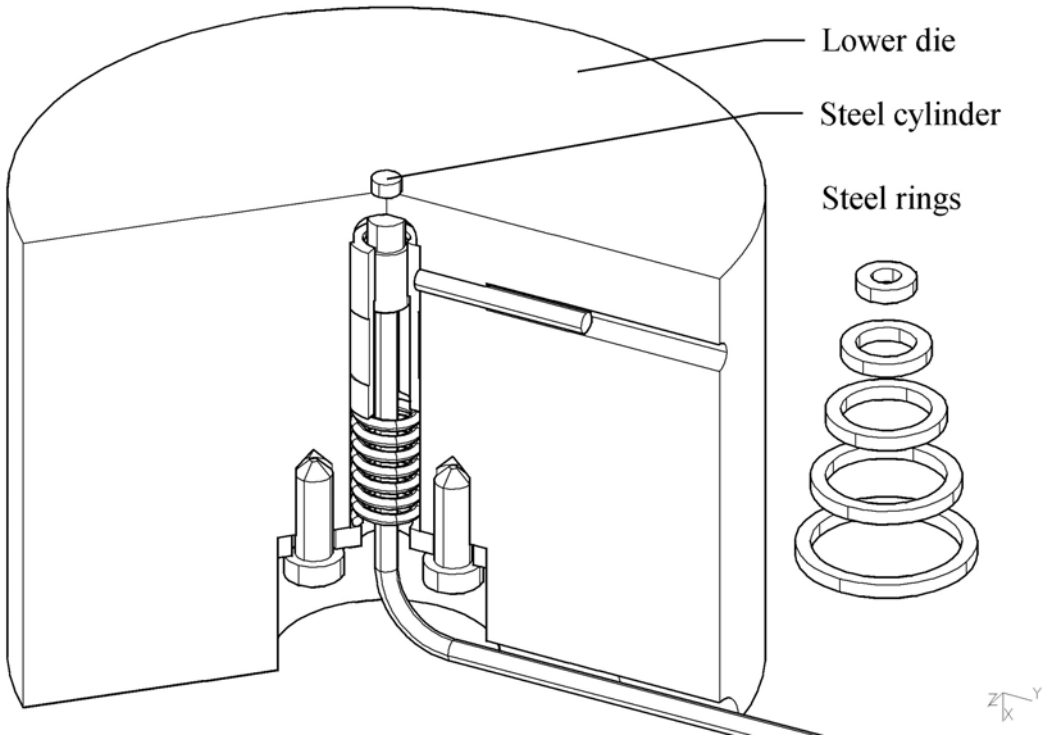

Figure 5.7. The integral sensor design with ring compression specimens. The smallest specimen is a cylinder with an outer diameter of 4 mm. The larger ones have outer diameters of 8, 12, 16, 20 and 24 mm.

The second type of compression testing was performed with hardened steel rings at low temperature. Both the height and the thickness of all rings were 2 mm. The outer diameters of the rings ranged from 4 to 24 mm. During testing, the rings only deformed elastically. If the rings are properly positioned relative to the centre of the sensor, they transfer approximate point loads or narrowly distributed line loads in the axisymmetric analysis. It would have been desirable to use thinner rings, but they would have been difficult both to manufacture and use. The objective of the experiments was to establish the influence curves (deflection vs. load at different positions) of the sensors. It is in principle possible to establish calibration factors for all alternative load distributions by adding (or integrating) the responses to all point loads [Dan71]. The approach is most relevant when the sensor disc constitutes an integrated part of the tool. The technique should in principle be easier to mimic and more accurate than the standard compression

test. Significant errors are introduced, however, by the method of integration and by the approximate nature of point load determination. Experiments were only performed at low temperature, as accurate positioning of the rings at high temperature is no simple task. The most important conclusion from the test, however, was that the sensor voltage output has a nearly linear relationship to the applied load. The tests also confirmed the conclusions from the numerical analysis of sensor behaviour (Appendix I), namely that only loads applied relatively close to the sensor cavity affect the sensor output. This is both a natural and important conclusion. Yoneyama has also found that loads applied far from similarly designed sensors are of limited importance [Yon99].

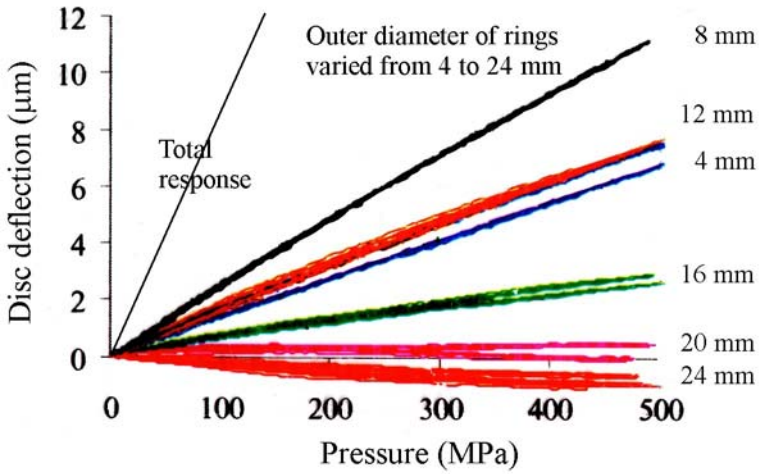

Figure 5.8. Results from elastic compression testing with cylinders of outer diameters from 4 to 24 mm. The experiment was run at room temperature with an integral sensor. The largest diameter of the sensor hole was 11 mm, and the disc thickness was 3.2 mm. Many experiments have been repeated.

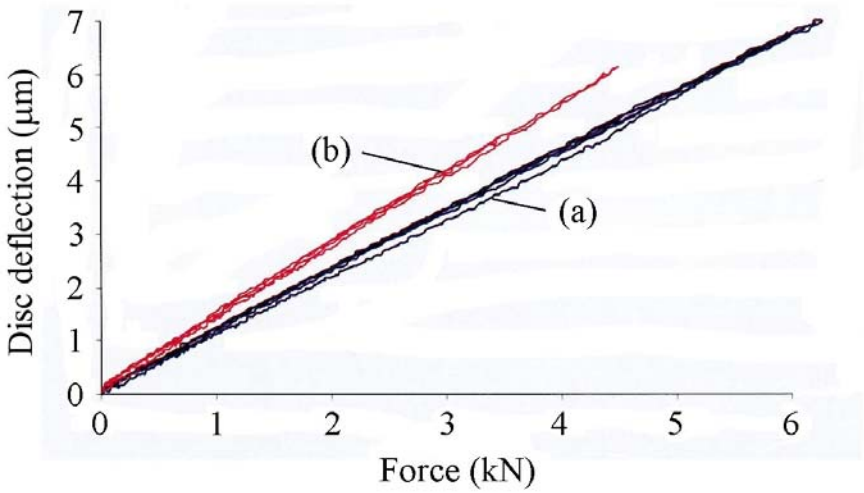

Figure 5.9. Results from elastic compression testing with cylinders of diameter 4 mm. Integral sensors of two dimensions are used: (a) disc thickness 3 mm and sensor hole diameter 10 mm, (b) thickness 3.2 mm and diameter 11 mm. Loading is performed almost until local plastic deformation of the sensor.

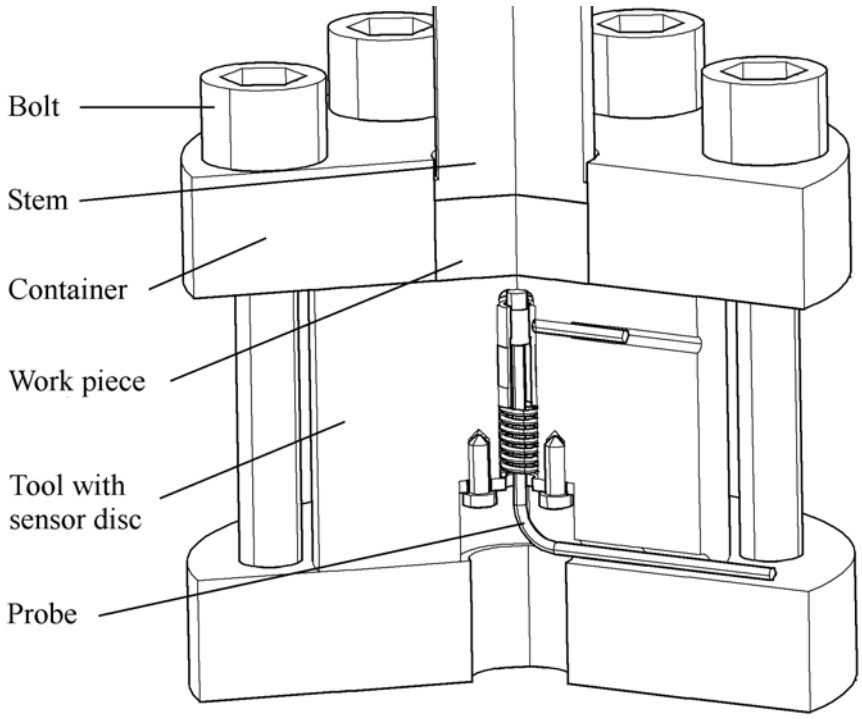

Figure 5.10. Hydrostatic compression testing with the integral sensor design.

The third and last type of compression experiment that was performed was hydrostatic compression inside closed containers. There are difficulties related to both types of compression previously described. During conventional upsetting, the size of the specimen is continuously increasing and the pressure distribution may also change. It is difficult to control friction, and the pressure applied at the top face of the die cannot be set freely by the experimenter, but is rather controlled by the material properties of the work piece. It may be difficult to establish sufficiently high pressures and at the same time recreate a sufficiently realistic type of interaction. The elastic ring compression test is inaccurate when perfect point loads are not used. It would be most advantageous to perform the integration of point loads physically through an experiment that provides a perfectly uniform load distribution. When performing hydrostatic compression testing, it is important that the material behaves plastically and that the tool-work piece interface friction is as low as possible. Lead and aluminium are appropriate choices of materials for the compressed specimen at low and high temperatures. A container with an inner diameter of 30 mm and a height of 40 mm was designed for the first experiments. This design may be placed on the top of all compression and extrusion tools and used to investigate the effect of distributed loading. An alternative to this off-line method of calibration is the in-situ calibration of sensors in the extrusion press. The technique is presented in Appendix E and Volume II. An advantage of the in-situ technique is that it should prevent changes in sensor response between calibration runs and experiments. A disadvantage is the often lower accuracy of force measurement, but remedies to this problem are available. The compression calibration techniques are complementary, and it is natural to use more than one technique in thorough studies of sensor behaviour. If the methods are used under similar conditions, they should produce consistent results. The accuracy obtained with the techniques may of course differ.

The compression experiments indicated that high-pressure measurement is feasible both at high and low temperatures. All of the sensor designs produced results that were worth analysing, and that appeared to be fairly accurate and repeatable. Plastic deformation and even fracture due to overloading may be the main causes of critical sensor failure. Sensor design analysis, aided by finite element modelling, was successful in revealing possible design weaknesses. An intuitive understanding of the limits of sensor design was developed as a result of the experiments. The inaccuracy of plastic material data at high temperatures is probably the main limitation, and better data should be sought.

Experiments with the smallest insert sensor (OD = 16 mm) clearly demonstrated that it probably should not be used during extrusion. For each new run, the sensor disc was pushed deeper into the hole in the die, and the sensor gave indications of new permanent deformations. After the experiments it was obvious that the disc had been plastically deformed to a considerable degree, and that small pieces of material had been sheared off both the sensor disc and the tool. The malfunction of the sensor may have been partly due to improper assembly. A numerical analysis revealed that the state of stress was locally close to critical. The sensor was manufactured because it was most important to explore the limits of the design space.

The quality of a sensor concept is often to a larger extent determined by small details of the mounting solution than by the more general sensor lay-out. One of the most important requirements for sensor design is user-friendliness. Sensors must not only function properly at high pressures. They should also be easy to use. The insert sensors mounted from the surface of the tool in contact with the work piece were, for example, extremely difficult to dismantle after experiments. Plastic deformation and oxidation made the contact between the sensor and the tools very intimate. A relatively large force had to be applied to eject the sensors, and there was the risk that the sensor could be damaged. The insert sensor design can be modified to allow easier dismantling of the sensor. It is, however, somewhat simpler to design a compact integrated sensor.

The design with the threaded probe holder worked properly both during off- and on-line calibration. There were some permanent deformations during the first cycle of loading to maximum loads, but this is to be expected for all sensors. After the tool was cooled to room temperature, however, it was extremely difficult to dismantle the sensors. High pressures and temperatures combined with oxidation caused sensors to get stuck. A chemical agent had to be used to reduce the surface traction and dissolve oxides.

Fastening the sensor with a spring was regarded as the solution that was the easiest to use and that produced the most satisfactory results. Yoneyama et al. have used a similar, but more complex and probably better solution [Yon93]. The solution requires more space, however, and was therefore not used in the current study. An important general conclusion from the early parts of the study was that die design should if possible be modified to allow simpler manufacture, mounting and use of the sensor. Designs with permanently mounted probes were regarded as the most reliable ones, but they are not necessarily the most easy to manufacture. Furthermore, permanent mounting of sensors made extensive testing of a range of sensor types difficult. Only four capacitive probes were available during most parts of the study.

5.4 Laboratory rod extrusion experiments

The rod extrusion experiments constituted the most important part of the work. The case was used to demonstrate the feasibility of capacitive pressure measurement and to study the nature and characteristics of sensor responses. Results from the experiments have been presented in a number of articles and papers (Appendices A, E, G, H and I), and an in-depth presentation has been provided in Volume II. There are numerous advantages related to the use of the simple and two-dimensional geometry of rod extrusion as a test case. First, numerical calculation techniques and experimental methods can be used to estimate the die face pressure and thereby the accuracy of measurement with relative ease. Second, it is feasible to perform parallel and replicate measurements of the die face pressure, and an accurate evaluation of the measurement variability and the quality of calibration techniques is then possible. Third, the effects that temperature changes have on the pressure sensor response may also be more easily assessed than for the full three-dimensional cases. Fourth, rod extrusion is probably the case best suited for the study of material flow and friction behaviour, even though the results obtained need not necessarily be applicable to more complex cases of extrusion. It is possible to use die face pressure sensors in combination with sensors measuring the liner load and other force and temperature measurements to critically check the fundamental hypotheses of the friction and flow behaviour of aluminium. The approach must quite necessarily be an iterative one, because neither the accuracy of the pressure sensors nor the numerical simulation tools are exactly known. An inverse analysis of flow behaviour based on parallel ram force and die outlet temperature measurements is a necessary first step.

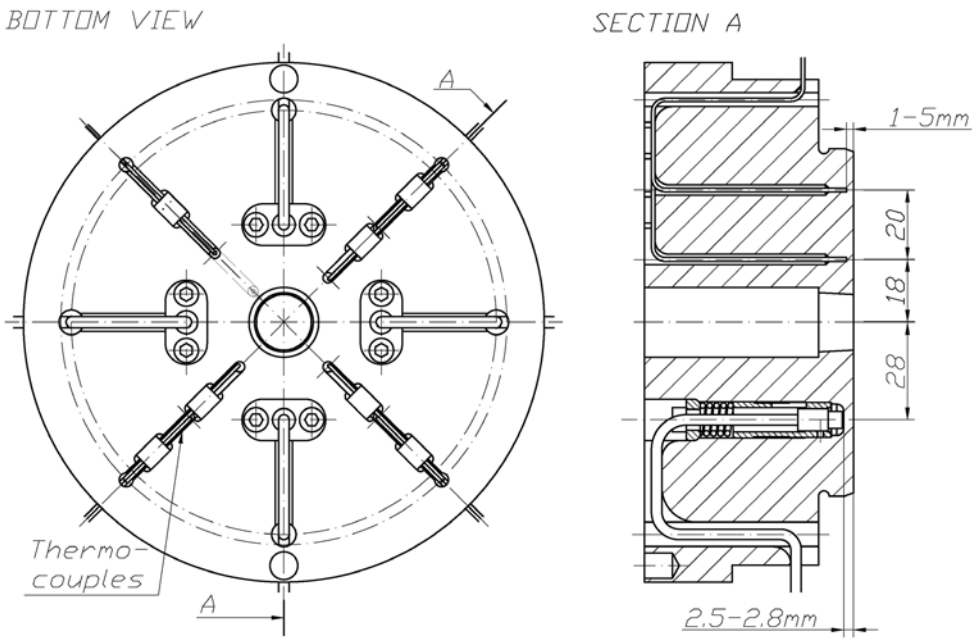

Figure 5.11. The simple rod extrusion die design used in the early rounds of high-temperature laboratory experiments with the pressure sensors. A similar die with sensors at other distances from the outlet was also used.

In total three rod extrusion dies were manufactured. The first two dies were of a type that is commonly used in the SINTEF 8 MN extrusion press in Trondheim. They are in this work called simple dies. Both dies had four holes for pressure sensors of the type that was used in the compression tools with integrated sensors. In the case of the first rod extrusion die, die A, the pressure sensors were positioned at three different distances from the centre of the die (one at 18 mm, two at 28 mm and one at 38 mm). The inner diameter of the die outlet and container diameters were 15.8 and 100 mm respectively for all experiments. In the case of the second die with a simple design, die B, all sensors were positioned 28 mm from the centre of the die. The sensors were placed 90º apart. Replication of measurements was generally regarded as important. Thermocouples that measured the temperature close to the surface of the dies were positioned at various distances from the die outlet. The results produced by the thermocouples made possible later evaluation of thermal effects and potentially on-line temperature compensation.

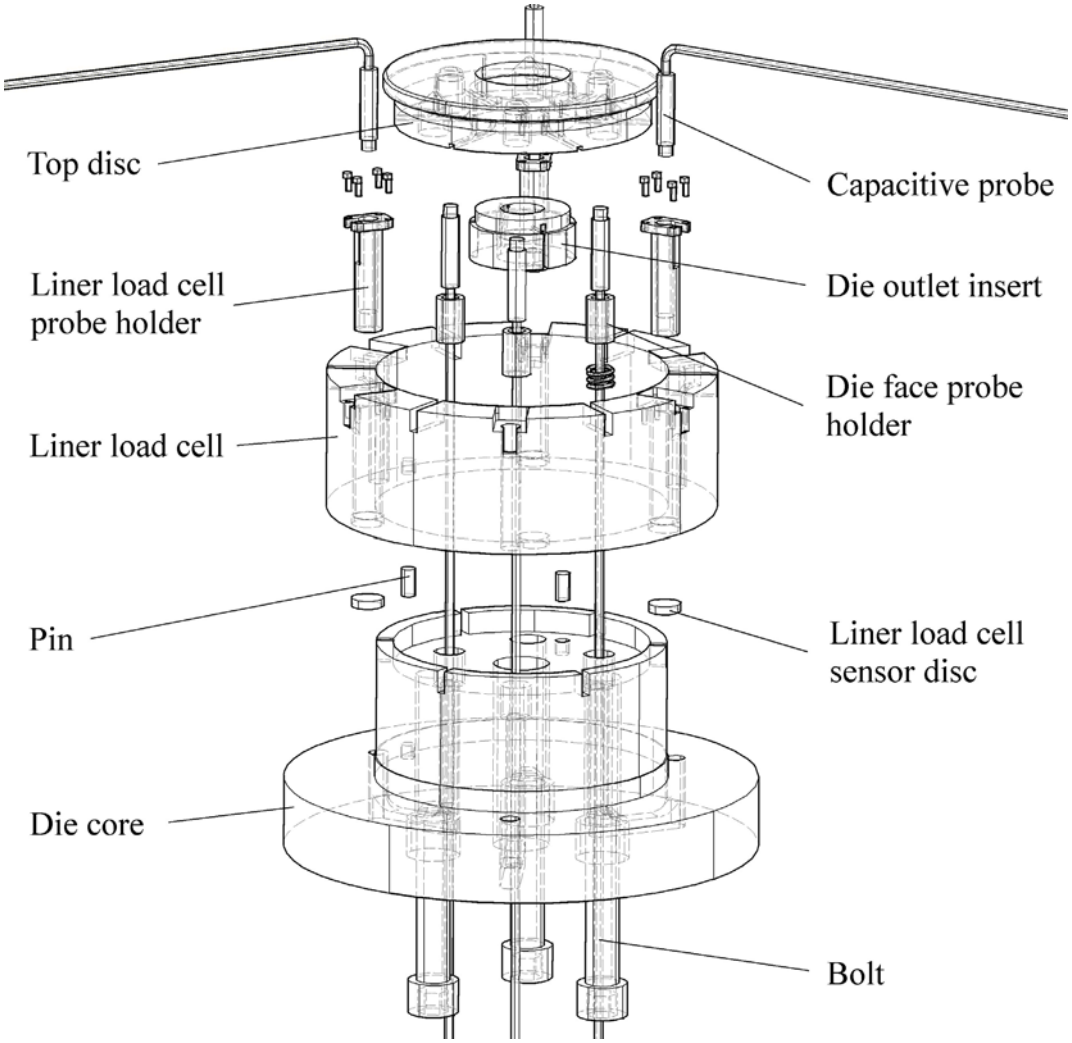

Figure 5.12. The complex rod extrusion die design used in the later rounds of high temperature extrusion experiments. The die has been disassembled and the most important parts are shown.

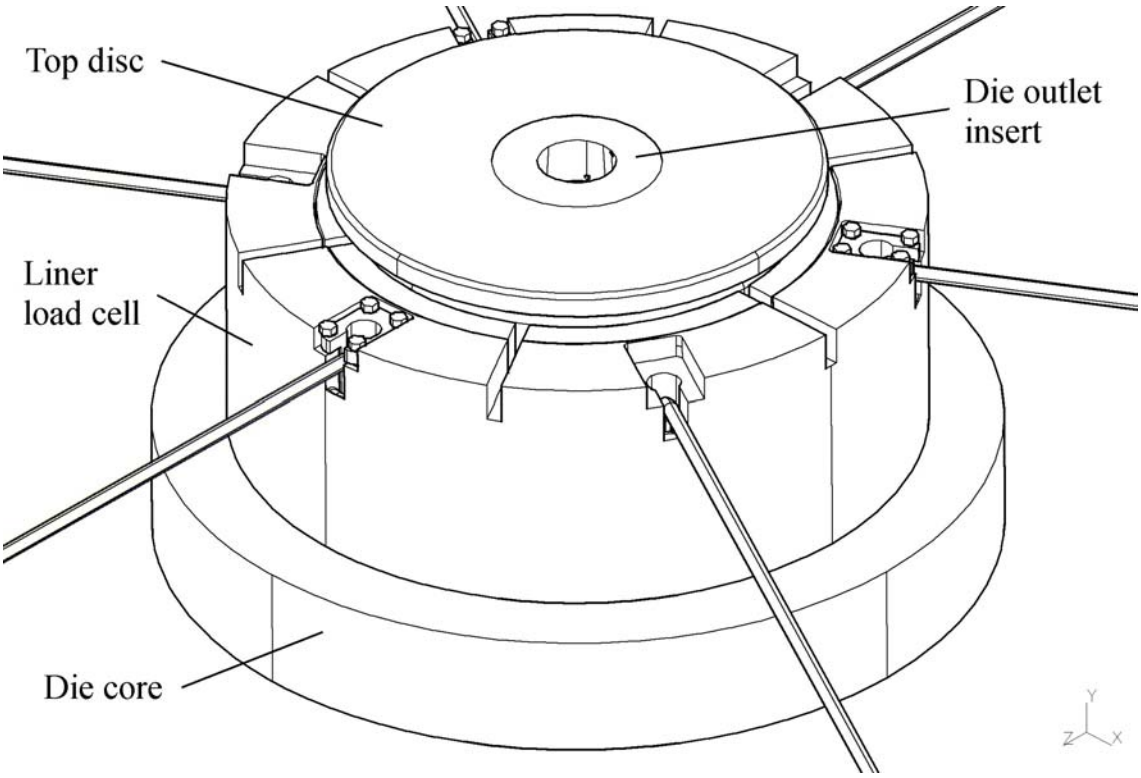

Figure 5.13. The complex rod extrusion die design used in the later rounds of high temperature extrusion experiments.

The third rod extrusion die, die C, was of a complex type. It was composed of several parts that had to be assembled before experiments could start. The die core was essentially a support die and was not in direct contact with the metal flow. The top disc had been split from the die to allow simple mounting of the probes of the die face pressure sensors. Three integrated sensors positioned 31 mm from the die centre and 120 º apart were used to measure the die face pressure. One of the capacitive probes was fastened in a similar way as the probes of the simple dies, by a spring. The remaining two probes were, however, fastened by a special arrangement with set screws. The solution was facilitated by the composite design of the die. Small outlet inserts could easily be shifted to allow the die face pressure to be varied over a large range for one set of sensors. Four inserts with outlet diameters of 11.2 and 15.8 mm (extrusion ratios of 80 and 40, respectively) were used. Two outlets were made with zero bearing lengths, and two were made with a bearing length-to-diameter ratio of 0.76 and a nominal choke angle of 40 minutes. By using outlets of different shape it was possible to systematically vary the die face pressure while using the same integral sensors. The composite design also made it possible to use the pressure sensors in a more detailed study of flow and friction. The last important part of the die design was a load cell that could measure the container liner load. Usually, the liner load is mainly due to the shear stresses between the billet and container. Liner load measurements made possible an evaluation of the magnitude of the shear stresses acting at the interface between the billet and container, and alternative estimation of the die face pressure measurements. The average pressure applied at the top face of the die can easily be calculated when the ram and the liner forces are known. The Capacitec capacitive sensors were also used in the liner load cell.

Laboratory extrusion experiments are relatively expensive, and there were sufficient resources for only approximately ten rounds of experiments. Thus, in order to reveal the most information about the sensor system and material flow behaviour from a relatively small number of experiments, systematic experimental approaches had to be adopted. During experiments with the simple extrusion dies, only two parameters were varied: the ram or profile velocity and the billet temperature. The experimental design was essentially a 2^2 factorial design [Box78], but some additional levels of ram velocity were in fact added during experiments. During some of the runs, the velocity was also step changed in order to provoke distinct step changes in pressure during extrusion. This would make it easier to distinguish the effects of temperature and pressure on the sensor response. All runs were randomised, and there were at least two replicate runs for each case. A case is defined as a combination of certain levels of the process parameters. A run is the extrusion of one billet. The billet length was 200 mm. Extrusion was stopped when the height of the butt end was only 19 mm. The butt ends were generally not removed between the runs. The complete experimental rounds with dies A and B were repeated after the extrusion equipment had been dismantled and reassembled. The press also had to be cooled and reheated between rounds. A replication of an experiment that was performed in such a manner was regarded as a genuine one. Genuine replications gave indication of the true measurement variability, as well as the accuracy of a specific set or round of measurements. The fact that all experiments were performed with dies with a number of sensors greatly simplified the replication of measurements.

Experiments with the complex die design were performed in a similar manner to those with the simple geometry. The experimental matrix was larger, however, since two parameters of the die outlet design were also changed systematically: the bearing length and the extrusion ratio. Thus, the experimental design was essentially a 2^4 factorial design with additional runs added to determine the lack of fit for both interpolation and extrapolation. The experiments lasted five days, but one of the days involved only replication of cases. The experiments were only partly randomised, since the die outlets could not be entirely freely changed during a day of experiments. Each day or round of experiment constituted an independent block (Volume II). Systematic and random errors in pressure, ram and temperature measurement were confounded with effects related to a change in die outlet shape. Nonetheless, significant efforts were made to accurately control input parameters, and the errors of the ram force measurement should be relatively small. A detailed assessment of the errors of pressure measurement should therefore be possible, for the ram force can always be related to the die face pressure.

Finite element (FE) simulation is a tool that may be effectively used to estimate force, temperature and pressure effects of input parameter changes, and to link die face pressure and force measurements. The FE models are based on many assumptions and produce predictions that should be very carefully checked. This is most important if die face pressure estimates are to be used in the evaluation of the die face pressure sensor behaviour. The experimental plan was designed so that it was possible to evaluate the quality of the descriptions of material behaviour at various levels of the process data. This should strengthen the analysis since it is based on more data points, and since pure model errors should be simpler to distinguish from the systematic errors in measurement or experimental procedures. The temperature effect on the pressure measurements is an

example of an error, whose magnitude depends on the values of the process parameters. Another reason for running experiments at a number of levels was that it allowed testing of the pressure sensors (alternatively simulation model) over a greater range of pressure. This was necessary to assess the linearity of the sensor response. An evaluation of the quality of simulation and measurement approaches must be based on measurement data obtained from real extrusion experiments. The outputs from established measurement techniques for ram force and die outlet temperature were the natural points of origin. It is always possible to evaluate the mean square deviation, E_F, of the type:

$$E_F \sim \sum_{i=1}^{n} \left(\frac{F_x - F_c}{\sigma_F} \right)^2 \qquad (5.1)$$

where F_x is the measured force and F_c is the calculated one. σ_F is a typical measure for the random variation. The number of measurement points is also considered. A similar expression may be established for the temperature error. A part of the error may be due to the model or the sub-models. Another part may be due to the numerical approach. Experiments may also be in error. Thus, the task of establishing an optimal model for extrusion is not a trivial one, and was not in fact an objective of the study. However, in order to evaluate pressure sensor behaviour, it was necessary to quantitatively evaluate the models that were in use and improve them if necessary. The issue is treated in Appendices F and H. It should be noted that Appendix F presents an introductory study and that errors in the simulation of the outlet temperature were later revealed.

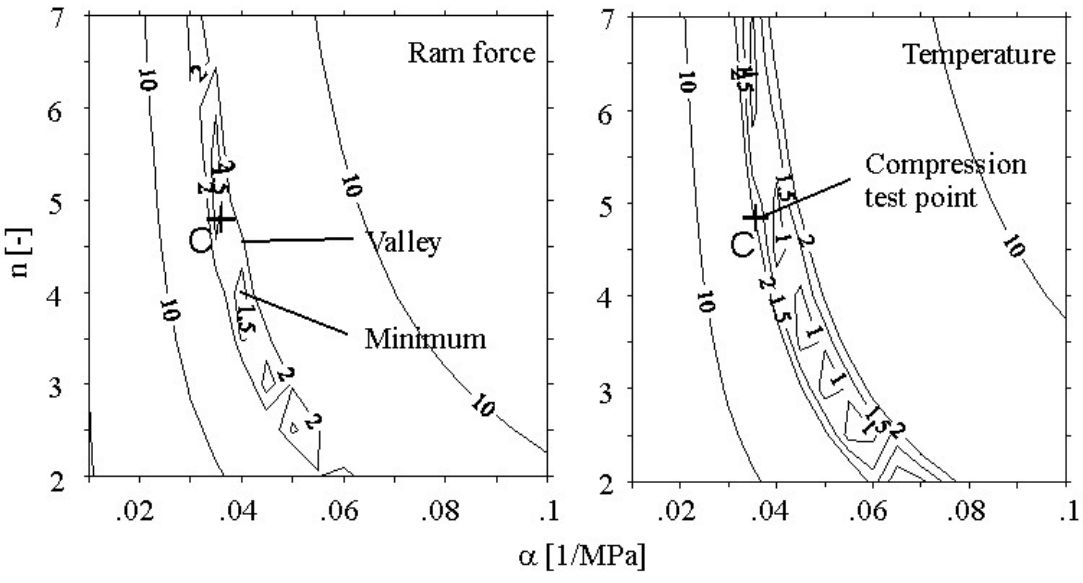

Figure 5.14. The error surfaces for force, E_F, and temperature, E_T. The surfaces have been calculated from the results from the experiments with complex dies that have zero length bearing channels. Only the parameters of the Zener-Hollomon flow model have been evaluated. The activation energy, Q, and the parameter A have been determined by compression testing. The α and n parameters have been systematically changed in a relevant range.

Many-dimensional plots of E_F and the corresponding temperature error, E_T, as functions of the parameters of the model are most useful tools. They reveal model sensitivities to changes in the material parameters, and in a way they reveal the nature of the extrusion system. Very often there is not a distinct minimum / optimum point, but rather a large number of parameter combinations that may be quite satisfactory. Such combinations may be said to be in a valley of low error values. It may be most useful to compare the surfaces of E_F and E_T. If models, experiments and codes are in order, the surfaces of E_F and E_T should produce fully consistent indications. On the other hand, if results are not consistent, both the experimental and modelling approaches need to be further assessed. If a bi-hypothesis is changed or a systematic measurement error is revealed, the outlook of the error surfaces change, hopefully in the right direction. The task of refining models is, however, an iterative one that should involve critical evaluation of all of the important and fundamental assumptions. The current thesis presents only the very first iteration of such a demanding study. Improvements to the simulation code ALMA2π is certainly possible, while the accuracy of the measurement techniques could be higher. Better temperature control during extrusion would also help. Finally, material models should be refined. When using material data obtained by compression testing, estimates and measurement of ram force deviate by less than 10 %. It is quite hard to spot systematic errors. Simulated die outlet temperatures are, however, approx 10 ºC higher than the measured ones. It is not known whether material data obtained by other techniques, such as torsion testing, are better suited to extrusion. The question is a most interesting one, but an answer will probably only be found by a more thorough approach to material modelling than has been attempted here. The error plots could of course also be used in such a study, but it would then be necessary to seek methods to evaluate many-dimensional surfaces. In the current study, only simple models with relatively few parameters have been assessed, and it has been assumed that container friction is of the sticking type. More complex phenomenological models and microstructure modelling should be combined with optimisation techniques in later studies. In relation to the current study it should be noted that the method of numerical analysis does not allow the demonstration of pressure measurement accuracy significantly better than 10 %.

Only results from extrusion runs with the complex die have been published. The main reason is that no physical in-situ calibration of the sensors was performed in the first five days of experiments. Finite element analysis was then used to establish calibration factors linking the die face pressure and the disc displacement. However, the accuracy and repeatability of the measurements are significantly better when in-situ or on-line calibration is performed in advance of the extrusion experiments. Experiences from the rod extrusion experiments with the dies of simple design in fact spurred the introduction of the in-situ calibration technique. The quality of the raw data from the experiments with the simple and complex dies did not differ much, however, and it was not possible to claim that the sensors used in the later rounds of experiments were superior to those used in earlier rounds. In both cases, sensors that were seemingly identical and exposed to the same pressure produced results that deviated by more than 10 % (20 MPa or 2 μm). The finite element approach may only reveal differences in responses when the dimensions of the sensors are known to differ. It is quite difficult to accurately measure the actual dimensions of the sensors. Additionally, the details of mounting may affect the sensor response. These issues are further treated in Appendix J. The on-line or in-

situ calibration technique described in the appendices, made it possible to determine the responses of individual pressure sensors. Both the accuracy and repeatability of pressure measurement could then in fact be improved. Note that there is an important difference between the repeatability of measurements for runs that have been genuinely replicated and for runs that have been repeated during an experimental round. The latter was much smaller (±2 % of full scale) than the former (< ±10 %). This is an indication of the strength of the measurement principle, and it shows that during extrusion experiments, results were generally not affected by the loosening of the sensors. The techniques for mounting the probes were far from optimal, but for many purposes acceptable. The experience with repeatability also seems to indicate, however, that that the calibration technique may be improved further. Deviations of approximately 5 % from one round of calibrated experiments to the next round may be explained by the inaccuracy of the ram force measurements during calibration (Volume II).

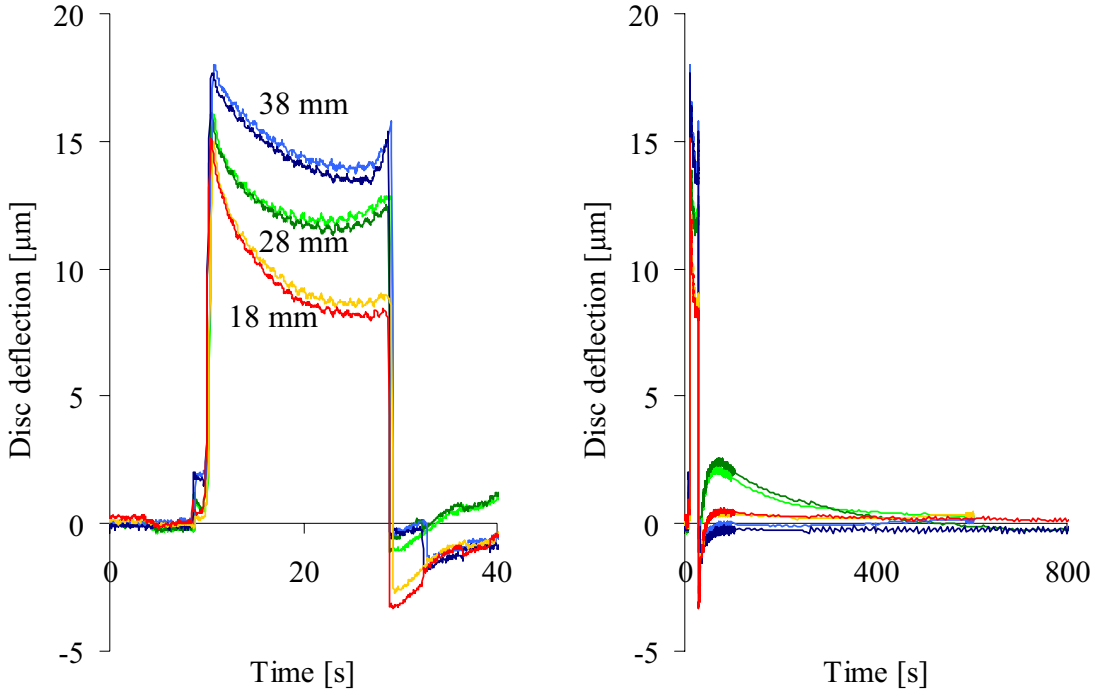

Figure 5.15. An example of raw data from pressure measurement with a simple die – die A. Experiments were performed with AA6060. The ram speed was 10 mm/s and the billet temperature was initially 450 ºC. The extrusion ratio was 40. The DC voltage output from the measurement system has been multiplied by 50 µm/V. A reference point has also been set. No calibration was performed before extrusion. Hence the actual pressure cannot be accurately determined. The sensors have been placed at various distances from the die outlet. A part of the response is due to the thermal response of the sensors (10 %). Its magnitude depends on the position of the sensor, on the sensor design and on the characteristics of the probes that have been used. Only a small permanent drift in the response was observed, but the temperature effects may be very long-lasting and needs to be corrected for. Replications, albeit not genuine, have been performed of all runs.

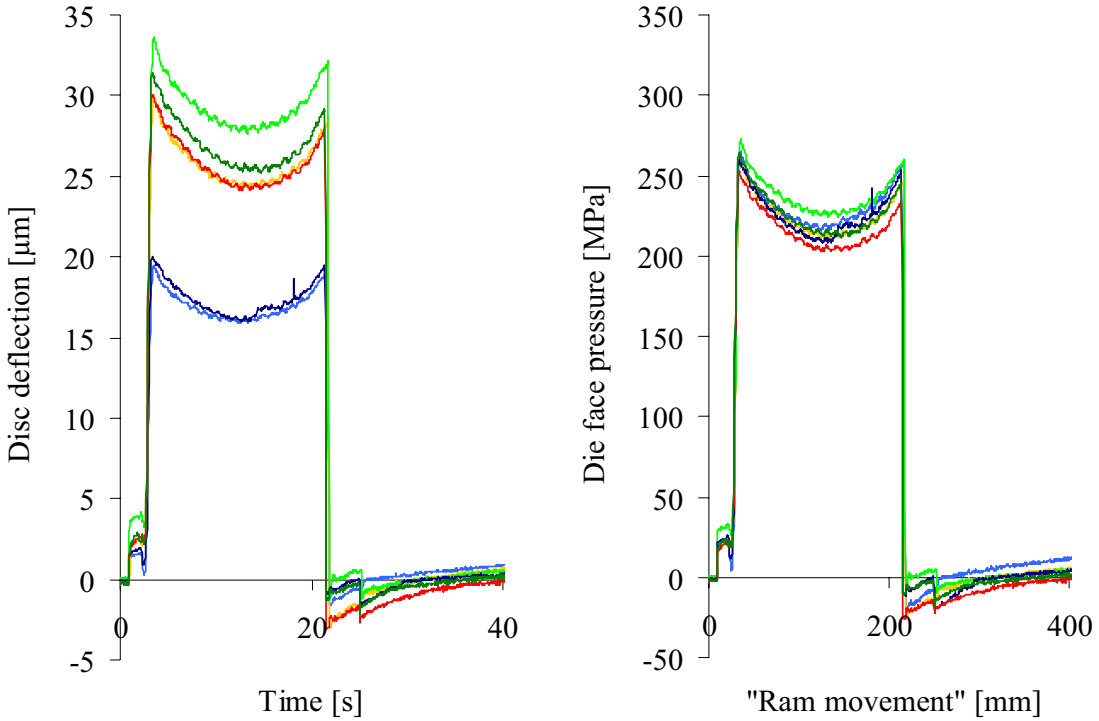

Figure 5.16. Raw data and calibrated data from experiments with the complex die – die C. Experiments were performed with AA6060. The ram speed was 10 mm/s and the billet temperature was initially 450 ºC. The extrusion ratio was 40. Three sensors and two sensor fastening solutions have been used to measure pressure. The experiments have been genuinely replicated. The calibration factors were established by hydrostatic compression testing before extrusion commenced. No compensation for temperature effects has been performed. After a sufficiently long period all responses returned to the zero point ± 0.2 µm. The "ram movement" is here only a measure of time multiplied by the ram speed, 10 mm/s.

The systematic approach to experiments makes a detailed assessment of the accuracy and repeatability of measurement possible, even though there is only a relatively limited amount of data available. Two types of comparisons are of particular interest.

First, predictions by the simulation code ALMA2π using material data obtained through compression testing have been compared with results from the pressure measurement. Only cases with zero-length bearing channel have been evaluated due to uncertainties related to bearing friction modelling. During measurement, the temperature of the die face pressure sensor disc changed significantly, and the sensor response was affected by thermal expansion and elastic and electromagnetic material parameter changes. The phenomenon has been studied closely with a two-way coupled die deformation and material flow model, and a temperature compensation method has been introduced. It contributes to some percentage of improvement of measurement accuracy, especially if extrusion is run at very high speed. Temperature compensation does not affect results at the onset of extrusion since there has been insufficient heat flow. Appendix J and Volume II of the thesis describe in detail the temperature effects and the compensation

technique. As indicated, the deviation between the simulated and measured results is generally smaller than 10 %. The accuracy of measurement is probably better than 10 %, but due to the limitations of the testing technique, it is not possible to determine the true value of the die face pressure with very high accuracy. The repeatability of genuine replications is of the same magnitude as the accuracy if calibration has been performed in between the rounds of experiment. A more detailed discussion of a comparison of simulated and measured results is given in Volume II.

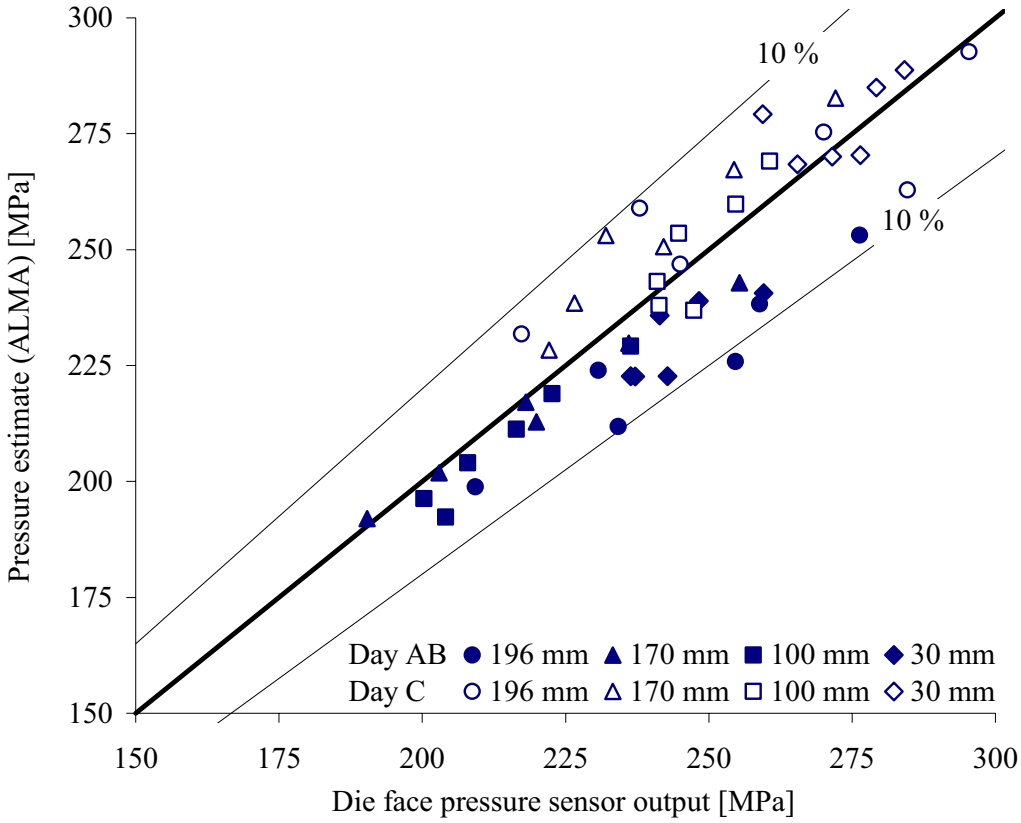

Figure 5.17. A comparison of the directly measured die face pressure and estimates calculated with the flow code ALMA2π. All measurement points have been taken into account. Average values for three sensors from the three first days of experiments (A-C) and a range of billet lengths are shown.

Second, output from the die face pressure sensors have been compared with estimates of die face pressure based on the ram force and liner load measurements. The pressure sensor of the complex die was positioned so that it produced an output that was approx 5 % higher than the average die face pressure during almost the entire run. Volume II presents the ALMA2π calculations that support this observation. The total force applied at the die face is simply the difference between the ram and liner force. The pressure estimate is not very sensitive to modelling assumptions, but it is affected by errors in the force measurement. The accuracy of the force measurement was approx 6 MPa, while the accuracy and repeatability of the liner load measurement was in fact no better than that of the die face pressure measurement. Hence, the second method for assessing sensor behaviour was also of limited precision. It is a most useful method, however, and

it may and should be further improved. The liner load cell design is not optimal, and greater efforts should be made to accurately calibrate ram and liner force measurements. The fact that the method is almost independent of modelling assumptions is an obvious advantage. Comparisons are not affected by inaccuracies in determination and control of input variables such as the billet temperature. An input parameter change should affect both direct measurement results and estimates to the same extent, so the technique may in fact be regarded as self-compensating. The only critical assumption of the analysis is that the pressure distribution is not that affected by the input data change. Numerical techniques are much more difficult to use. The task of accurately measuring input data and modifying a numerical analysis until it produces satisfactory estimates can be very time-consuming. Ram force and temperature data may be used to check the results.

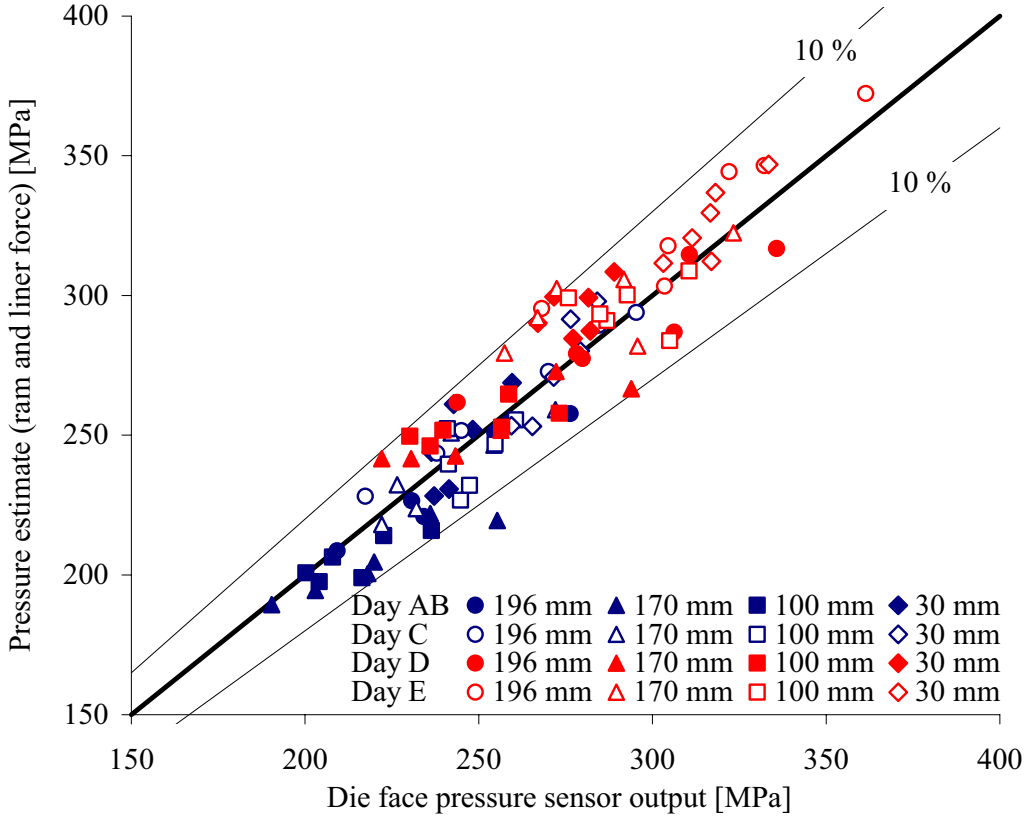

Figure 5.18. A comparison of the directly measured and temperature compensated die face pressure and an estimate based on data of the ram and liner force measurements (see Volume II). Average values for three sensors from all days of experiments (A-E) and a range of billet lengths are shown.

The second comparison of results reveals that the sensors produce outputs that generally deviate by less than 10 % in the entire measurement range, from 175 to 350 MPa. The main advantages of the sensor testing approach with the complex die presented here (and more thoroughly evaluated in Volume II), is that sensors can be tested over such a large range and that alternative estimates of the die face pressure may be established. By systematically changing the process parameters it has been possible to closely study the temperature sensitivity of the sensors and impose compensation (as discussed).

5.5 Laboratory split tube (pipe) extrusion

Split tube extrusion experiments and modelling were performed within the framework of the PROSMAT research programme and in close cooperation with Hans Iver Lange and Arnfinn Willa-Hansen of SINTEF Materials Technology, Trondheim. Results from the experiments have been presented at the ESAFORM conference (Appendix C) as well as in a SINTEF report [Lan02a]. Earlier work related to the study has also been presented in reports by Lange and Hansen [Lan99] [Lan00]. The main objective of the study was to establish techniques that allow measurement of the loads on the faces of hollow dies and the mechanical response of the die in terms of the displacement of the die mandrel and the strains in the bridges. It is well known that dies for hollow profiles (bridge, porthole and spider dies) are exposed to immense loads and consequently may deform significantly during extrusion. Plastic deformations occur, and so may creep and cracking after a relatively low number of cycles. Such behaviour often affects the dimensions of the die outlet and the dimensions of the extruded sections. The dies for hollow profiles are quite ingenious inventions that allow for the production of the most complex aluminium sections, but there are very strict limits for the precision of the shape of the profile. The true shape of the die outlet, is to a great extent controlled by the displacement of the fairly flexible die mandrel relative to the die cap and bolster. The mandrel displacement may be reduced by careful die design, but probably never completely eliminated. If bridges are made thicker, they are stiffer, but the pressures are also higher. In order to lower the loads, bridges must be made both thinner and less stiff. The mandrel mainly displaces in the extrusion direction, but the less symmetric the extruded profile is, the larger the possibility that there may be undesirable rotations and displacements in the direction normal to extrusion. In the rod extrusion study of this section, the focus has been mainly on mandrel displacements in the extrusion direction.

The extruded profile was a tube with an outer diameter of 38 mm and a thickness of 2.5 mm. The tube was split in the longitudinal direction during extrusion by special pins that had been placed in the bearing channel. This arrangement allowed measurement of the mandrel deflection relative to the bottom disc of the die. In addition to the standard ram displacement and ram force measurements there were five types of measurements:

- die face / mandrel top pressure measurements
- capacitive bridge strain measurements
- strain gauge bridge strain measurements
- mandrel and bottom disc deflection measurements
- various die and sensor temperature measurements

Relatively few runs were performed and the ram velocity was only varied in the range from 0.5 to 2 mm/s. The main reason that experiments were not run faster was the fear of overloading and die and sensor damage. With die face pressures reaching more than 500 MPa, some plastic deformation, especially in the bridges, could not be avoided, and there was a danger of fatigue and cracking after relatively few runs. Three-dimensional die simulations supported such an assessment. Fractures were also observed in parts of the equipment after the second day of experiments. However, these were not critical. Appendix C presents results from simplified calculations of the die response.

The capacitive displacement sensors were inserted into a hole in the mandrel of the die. The same spring mounting technique was used as in most of the other extrusion experiments. On the first day of experiments, the results were satisfactory. There were only very small (< 0.5 μm) abrupt output voltage changes during measurement, and the probes appeared to be properly fixed. The results from a replicate round of experiments, performed a half-year after the first, were unfortunately less positive. The measurement signal was then less stable, and there was significant scatter in the results. In addition, temperature changes seemed to affect results much more than on the first day or any other day of experiments with other types of dies. The poor sensor behaviour was not typical, and its causes remain unknown. Measured displacements during the loading were of the same magnitude on both days. It should be noted that the report on the rod extrusion experiments by Lange [Lan02a] only presents results from the second day of experiments, and therefore gives an unduly pessimistic view of the feasibility of die face pressure measurement at very high pressure.

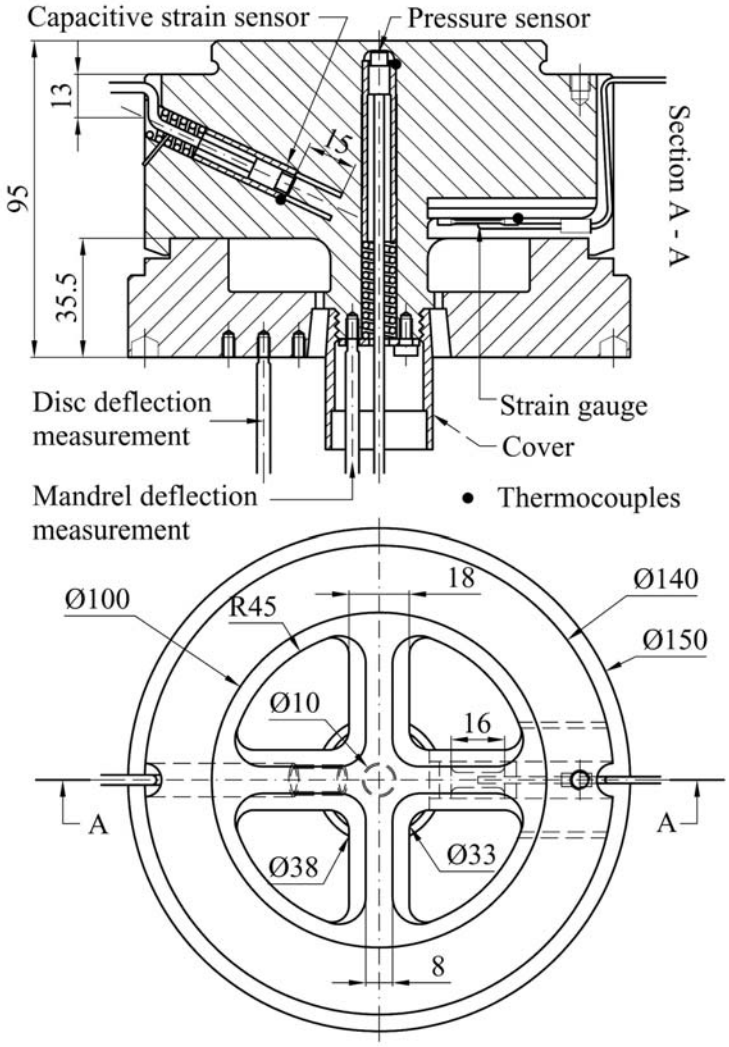

Figure 5.19. The die used for split pipe extrusion: a cross-section (A-A) showing the most important details of the design (top); the top view (bottom)

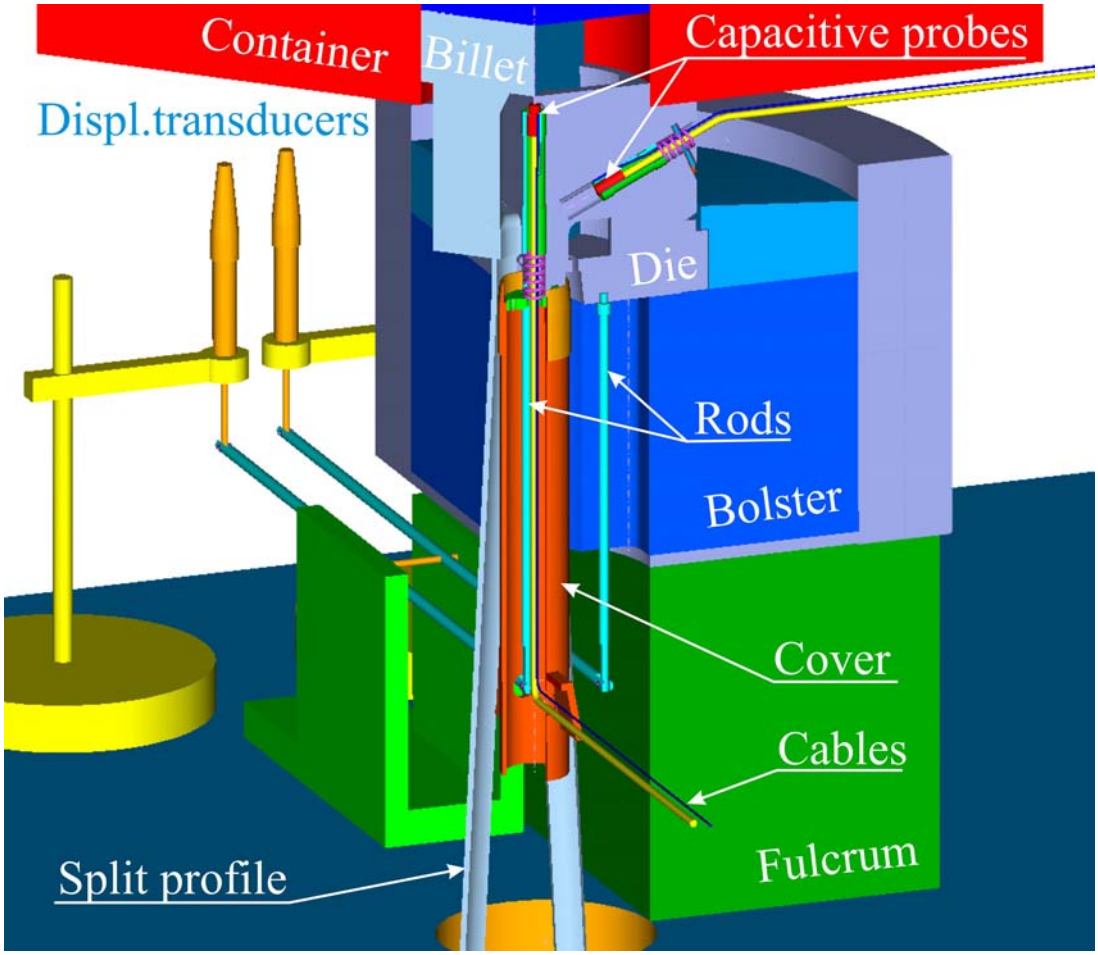

Figure 5.20. The experimental set-up for split pipe extrusion. Only a quarter of the tool stack, profile and billet is shown.

The straining of the die bridges was measured by two alternative techniques: high-temperature strain gauge and capacitive measurement. The capacitive technique was not used during the first day of experiments. The specially designed sensor holes that allowed measurement of relative displacements had not yet been produced. They were manufactured by spark erosion between the first and second round of experiments. The direction of the sensor hole was approximately that of the largest component of strain in the bridge. The relative elongation of the bridge compared to a non-deformed cylinder in the centre of the hole was measured. Strain measurement by Kyowa strain gauges was planned for the first experimental round. However, the strain gauges did not work at all, and it turned out that the strain gauge cable had broken during the assembly of the die. The gauge was mounted underneath the bridge and protected by a special cover. The arrangement was relatively fragile. The second attempt to perform measurement of the bridge strains was more successful than the first. Both systems for bridge strain measurement produced outputs of reasonable magnitude, and the responses usually returned to the original zero point after unloading (±5 %). There was, however, a significant amount of scatter in results. Furthermore, the strain gauges were not properly calibrated before the experiments. Only trends in the output during extrusion could be measured with the equipment. Absolute values of strain were not obtained.

One simply cannot draw certain conclusions on the quality of the strain measurement techniques solely on the basis of the split tube extrusion experiments. The capacitive sensors are to a very small extent temperature sensitive, and they seem to be both easier to use and more reliable than the strain gauges. On the other hand, they may require somewhat more space. This, however, depends on the details of the sensor design that is used. The holes for capacitive strain measurement were simpler and less expensive to manufacture than the special arrangement for the strain gauges. Lange's reports [Lan99] [Lan00] [Lan02a] provide more information on the type of high-temperature strain gauges that were used and on their behaviour during calibration experiments.

The displacement of the mandrel relative to the bottom disc of the die (the die cap) was continuously measured during both rounds of experiment. Only the large displacement component in the extrusion direction was considered. The first iterations of the mandrel deflection study of the PROSMAT programme were undertaken by Lange and Hansen with a somewhat simpler die design than the one used in the parts of the study that are described in this thesis. Displacement transducers have generally been used to measure the displacement of the mandrel and the die cap relative to the press board / ground. In the earlier iterations of the study, the rods were made of glass and were therefore fairly insensitive to temperature changes. The arrangement proved most impractical, however, for during extrusion there were significant vibrations that caused the brittle rods to fracture. In the two rounds of the experiments considered here, Invar rods were used instead. Mechanical vibrations still complicated measurements, and the output from the measurement system often changed abruptly and significantly. There was also a large amount of scatter in the results. The magnitude of displacement seems to be in fair accordance with estimates produced by numerical calculations. Mori et al. [Mor02b] and Wagener and Wendenburg [Wag01] have made similar measurements at lower temperatures with laser measurement techniques, which have the potential of being both much more accurate and simpler to use. Laser techniques were also assessed in this study, but the scattering of the laser beam due to hot air turbulence was regarded as a considerable problem. The positive experience drawn from other uses of the optical techniques indicate that the approach should be reconsidered (Appendix J).

The main conclusions from the split tube experiments were that the capacitive technique of distance measurement had indeed great potential. Strain measurement did prove to be feasible, but all of the measurement techniques had to be improved. Errors were as large as 20-30 % of full scale. Numerical analysis of die deformation indicated that there was a fairly good agreement between the applied pressure measured and the die response. Both experiments and models were probably in error. The interaction between the die and the billet is very complex and efforts should be made to establish a proper coupled flow and deflection model. In the current study, only two-dimensional visco-plastic flow was satisfactorily assessed with the flow code ALMA2π. A three-dimensional calculation by Forge3® provided a rough estimate of the maximum load distribution. A more thorough three-dimensional study is most time-consuming, however, and requires an automatic routine for at least one-way coupling of the codes for simulation of flow and die deformation. Such a routine has only been developed for the simple case of rod extrusion (Volume II). Many researchers have modelled hollow profile extrusion, and some references to relevant studies and codes have already been given in Chapter 2.

5.6 Laboratory thin-strip extrusion

The thin-strip extrusion experiments were performed in cooperation with Martin Lefstad and Robert Flatval of SINTEF Materials Technology. During the last rounds of experiments there was also extensive cooperation with Wojciech Wajda of NTNU. The measurement technology developed and refined by the research group was also for use in Wajda's PhD work. The objective of the thin-strip extrusion experiments was as earlier indicated to establish a better understanding of the thermo-mechanics of flow during extrusion, and to reveal the causes of shape variability for open profiles. When very thin-walled profiles are extruded, a satisfactory outcome cannot be guaranteed (Chapter 2). Significant efforts must sometimes be made to tune the dimensions of the die outlet, particularly the bearing surfaces and the feeder design. The deformation of the die must also be considered and accurately compensated for, so that the actual outlet and profile dimensions are as close as possible to the goal. The geometry of the die should be tuned to secure a uniform outlet flow velocity. If some parts flow faster than others, profiles may in the extreme cases buckle or curve. If the flow is only slightly unstable, there may be thickness variations, and residual stresses may be set up in the profile. This may be of some importance during later thermo-mechanical processing. It was assumed that when the limit of flow stability is reached, it would be possible to distinguish relatively small pressure changes close to the outlet both in the centre and at the edges of the profile. The task is a difficult one and probably requires sensors to be placed very close to the die outlet. However, the general flow conditions most certainly control the stability of flow, and they can more easily be assessed with pressure sensors. As the billet is compressed, the temperature and velocity fields change. The pressure should also be affected, and it would be most interesting to continuously and accurately measure the distribution of the pressure in many positions at the die surface. The thin-strip extrusion study should contribute to a better understanding of the limitations of the process, and to the establishment of refined criteria and models that may help predict instabilities on the basis of the pressure and temperature measurement.

Three stages of the study of thin-strip extrusion and flow stability may be identified. A fully instrumented strip extrusion die was first manufactured in order to evaluate the feasibility of measuring pressure and temperature in and close to the die outlet. The main challenge of the study was not to perform pressure measurements, but rather to design a die outlet of proper dimensions. If the strip is too thick, no instability effects are observed. If it is too thin, however, extrusion may prove completely impossible. The profile may get plugged in the die. The ideal profile design is one that allows instability to be provoked for some combinations of levels of easily variable process parameters such ram velocity and billet temperature, but not for others.

In the first part of the study the nominal die outlet thickness was 1.7 mm. The thin strip experiments were generally performed with the profile of width $W = (\pi/4)\cdot D = (\pi/4)\cdot 100$ mm = 78.5 mm, where D is the diameter of the container. The outlet of the first die was perfectly rectangular, but die deformation may have caused it to be somewhat concave during extrusion. Extrusion through such an outlet is no trivial task, but the profile was regarded as one that could be handled. This assumption was proven correct, for no flow instability could be provoked by changing the values of the process parameters. Two

rounds of experiments were performed, mainly because the sensors did not work properly during the first one. Three pressure sensors were in use during experiments, one close to the centre of the profiles and two close to the edges. The sensor concept used was the same as in most of the other extrusion experiments. Details on the die and sensor designs have been given by Lefstad et al. [Lef01] [Lef02a] and Moe et al. [Moe03b]. Only two of the three sensors are shown in the drawings. During the first experimental round, the probe holders did not fit properly into the sensor holes and did not move freely. This is an important requirement for the spring fastening solution. The holder's diameter was subsequently slightly reduced (0.05 mm), and during the second round of experiments all sensors worked much better. However, no on-line calibration of the type described earlier was performed, so only trends throughout the runs for the various sensors were compared with simulated results. Simulation was mainly of the simple two-dimensional plane strain viscoplastic type (ALMA2π). The research group has made only limited use of three dimensional models [Waj03]. Lefstad has written a more extensive SINTEF report on the results from the experiments [Lef02b].

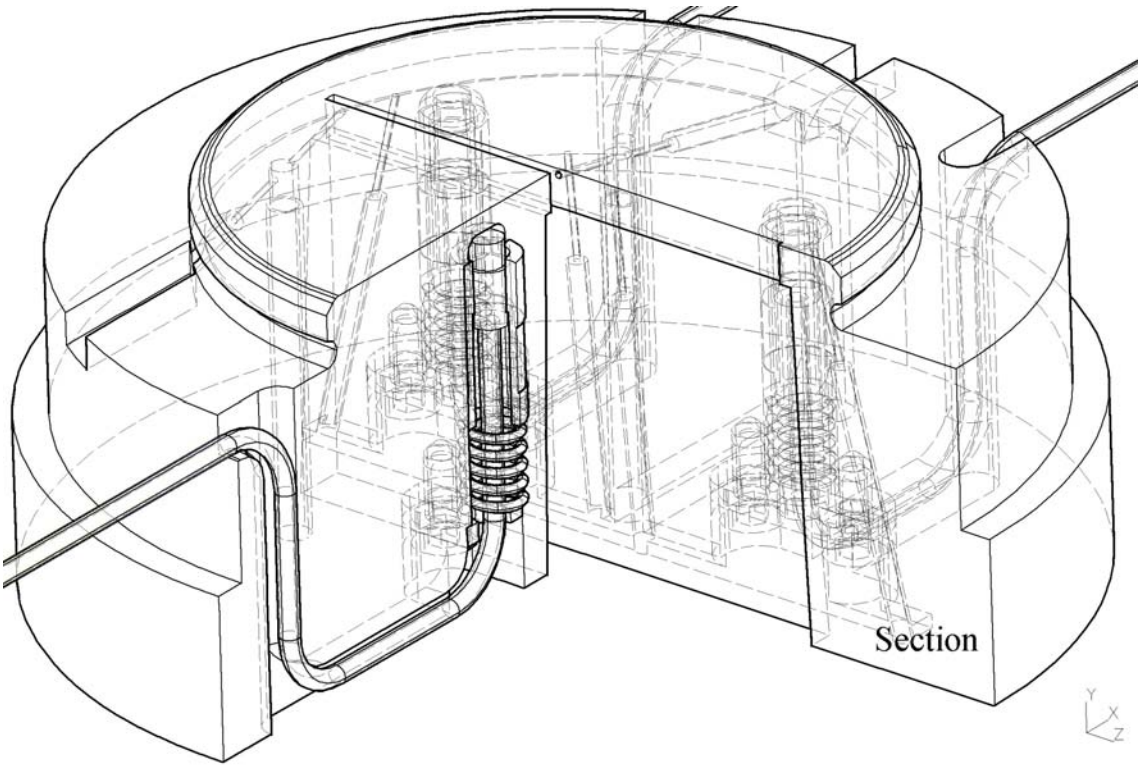

Figure 5.21. The first instrumented die used to measure die face pressure and outlet temperature during extrusion of thin strips (nominal outlet dimensions: 78.5 mm x 1.7 mm) of aluminium. Only three quarters of the die are shown, but interior details of the die are drawn with dashed lines.

No pressure sensors were used in the second part of the thin strip extrusion study. The objective was to determine the limits of flow stability and then to find the most proper die designs for later investigations. Fully instrumented dies are relatively expensive to manufacture and use. The profile width was still 78.5 mm, and the bearing lengths were as short as possible (shorter than 0.5 mm with a rounded inlet). The die outlet cross-

sections were slightly convexly shaped in order to compensate for the distortion of the die outlet due to die deformation. A first die was made with the largest outlet thickness of 1.55 mm and the smallest thickness of 1.3 mm. The corresponding values for the second die were 1.4 and 1.1 mm. Flow instability (buckling) was provoked only for the thinnest profile. It was possible to affect the buckling behaviour by changing the ram velocity and the billet temperature. When experiments were run at low temperature the flow was apparently stable, but at high temperatures the waviness of the profile was quite pronounced (amplitude of as much as 5 to 10 mm). The instability phenomenon was of a transient nature for all the cases or combinations of input data that were run. Buckling started as soon as after half a meter and ended approximately half-way through the run. The experiment, thus, gave valuable insight into the thermo-mechanics of aluminium flow and may be used as a test case for numerical modelling. The main results from the experiment have been reported in reference [Waj03]. The experiment was repeated once after the die had been cleaned and prepared for a new round. The same qualitative behaviour was observed, but the experiments indicated that a perfect replication may be hard to perform. Small changes in the temperature distribution or bearing surface constitution probably affected results. The shape and frequency of the buckles were measured on-line with a laser triangulation technique. The technique was used for the first time by the group. A high speed camera filmed the movement of a thin laser strip that illuminated the profile surface. The details of the experimental set-up and the main results have been reported in reference [Moe04d].

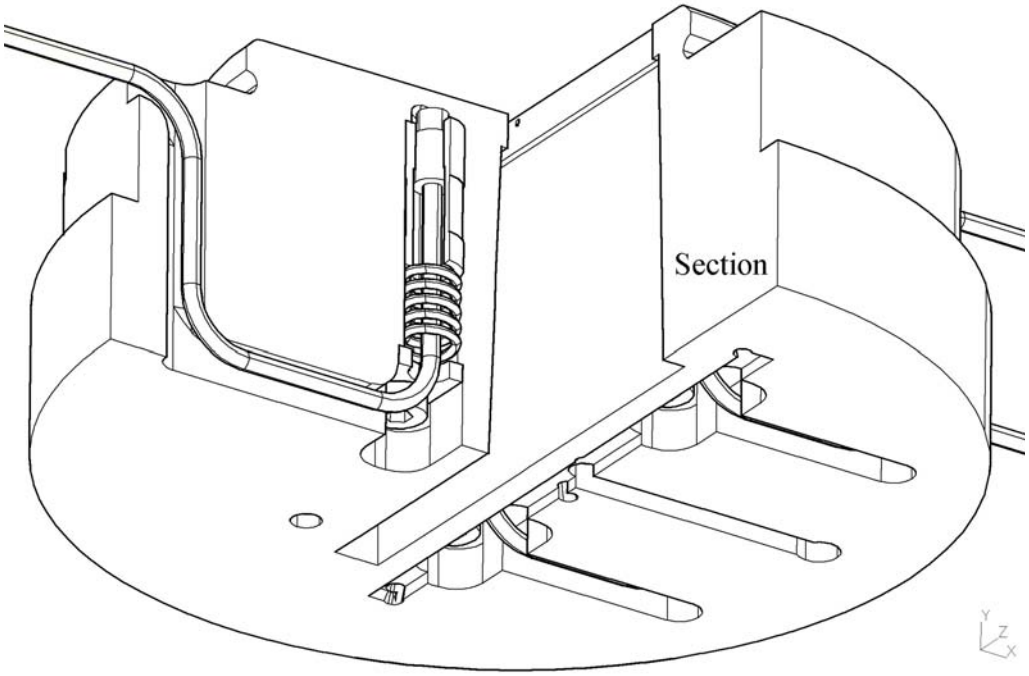

Figure 5.22. An alternative view of the first instrumented die used to measure die face pressure and outlet temperature during extrusion of thin strips.

The last part of the thin strip extrusion study was performed in relation to Wojciech Wajda's PhD study. The focus of this study was on material behaviour and instability mechanisms. A new set of instrumented thin strip extrusion experiments was planned

and carried out by the NTNU/SINTEF research group. As in the first round of thin-strip experiments, three sensors were used to assess flow instability during extrusion of very thin profiles. The design of the new insert type pressure sensor was one of the many that had been considered in the early phases of the sensor development study. An evaluation of the behaviour of the new sensor has been given in reference [Moe04d]. The paper treats the consequences of limited plastic sensor deformation. Plastic deformation of the deflecting disc of the sensor is hard to avoid and may in fact be accepted if a moderate overload is applied during the first calibration experiment. Then, residual stresses will be introduced, and as a consequence the elastic range of loading may be increased. It is important that the true capacity of the sensor is found, although in a high-temperature environment it would be dangerous to only use the onset of plastic deformation as a criterion for pressure sensor design. Note that only a limited amount of information on the high temperature plastic properties of the H13 tool steel is available [Udd04].

In a paper submitted to the 8th ESAFORM Conference on Material Forming (Appendix K) Wajda, Moe, Støren, Lefstad and Flatval report on the results from the last rounds of thin-strip extrusion. At this stage of the study of flow instability, it is not possible to draw conclusions on the nature of flow or on the usefulness of pressure sensors. It is believed, however, that the work performed thus far has contributed to an improvement of tools for analysis, and that the time is finally ripe for performing a thorough study of the problem. The thin strip extrusion experiments have proven the feasibility of pressure measurement, but have also clearly shown that sensor design must be improved. The new design proposed is more accurate and easier to use than earlier ones. The capacitive probe may be mounted in a semi-permanent manner, which makes it easier to reduce unwanted displacements. With the introduction of the new insert sensor, an important step has been taken in the direction towards commercialisation of the technology.

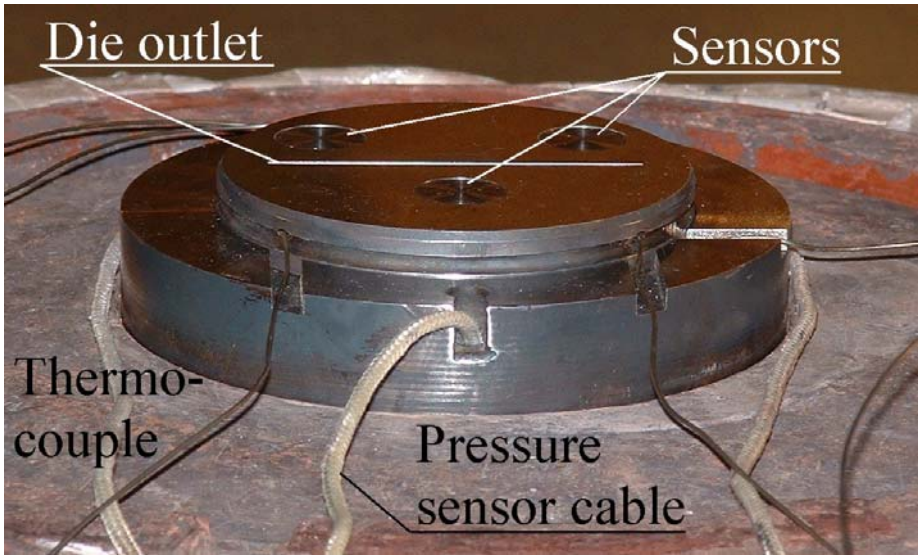

Figure 5.23. The extrusion die that was used in the last round of thin-strip experiments. The experiments were performed in relation to the PhD study of Wojciech Wajda. Three insert die face pressure sensors were positioned so that they measure pressure both close to the centre and the edges of the profile.

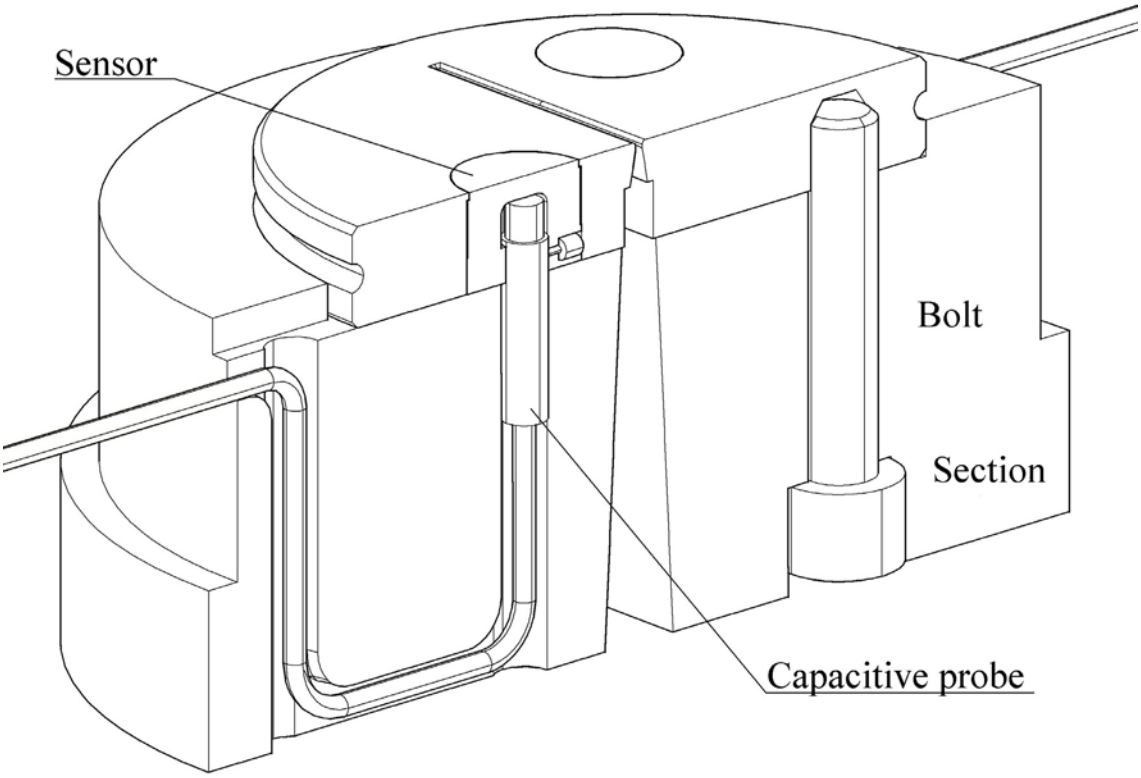

Figure 5.24. The extrusion die that was used in the last round of thin strip experiments. The probes were fastened to the housing by a set screw. It is also possible and probably preferable to mount the sensors permanently by soldering.

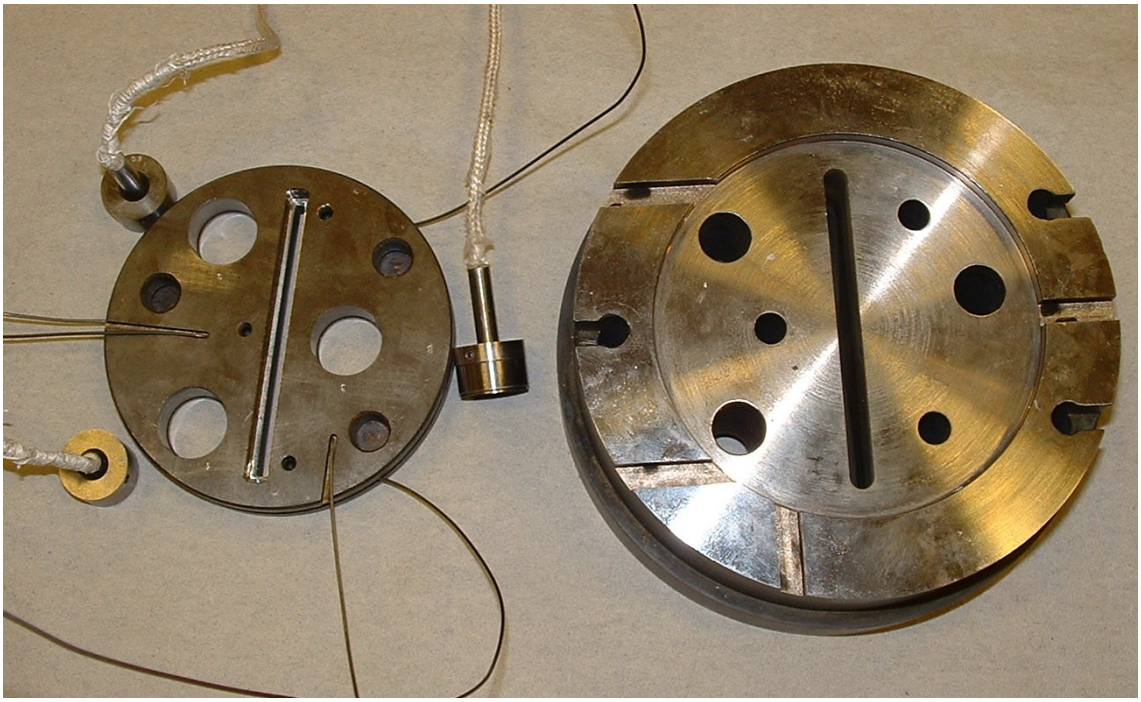

Figure 5.25. The extrusion die that was used in the last round of thin strip experiments. The die consisted of a top disc and die core (support) similar to the one used during rod extrusion with the complex die.

5.7 Industrial U-profile extrusion

Industrial experiments may, as discussed in Chapter 3, be necessary to demonstrate to industrial partners the feasibility of measurements. Hydro Aluminium clearly signalled very early on in the study that industrial tests would be desirable. Thus, two rounds of experiments were performed at the Hydro Aluminium Extrusion facilities at Raufoss, Norway. The experiments were performed in a 2200 metric ton industrial press, and an exacting semi-commercial U-profile was chosen as the test case. The height of the profile was approx 120 mm, the width 49.5 mm and the thickness 2.3 mm. The profile shape was not chosen because it was ideally suited for the pressure measurement feasibility study. In that case, a much simpler profile shape would have been preferable. The industrial experiments were performed in cooperation with various research groups at Hydro Aluminium Extrusion and with SINTEF groups both in Oslo and Trondheim. The overall objective of the study was not merely to measure pressure, but to better understand shape variability related to extrusion and subsequent thermo-mechanical processes. The hope was that the pressure measurements would provide valuable insight into the conditions of flow and the causes of variability. For those involved with the die face pressure measurement study, however, the demonstration of feasibility of industrial pressure measurement was quite naturally the most important objective. Notes on the preparations and results from the experiments have been written by Hans Iver Lange of SINTEF Materials Technology [Lan01] [Lan02b] [Lan02c]. The current presentation only provides a very short evaluation of pressure sensor behaviour during measurement. The candidate took part in the process of designing sensors, performing experiments and evaluating results, and the experiments constituted the natural final phase of the experimental activity related to his study. It should be noted, however, that the industrial experiments were actually performed in parallel with the rod extrusion study.

The industrial experiments were performed on two separate occasions and with two similar dies. The dies were in both cases designed by an affiliate of Hydro Aluminium Extrusion and manufactured by Extrusion Tools at Karmøy, Norway. The dimensions of the die outlets were determined by skilled die designers. The details of the pressure and temperature sensor designs were designed by the candidate and co-workers at SINTEF Materials Technology, Trondheim. During the first round of experiments sensors were inserted in the die disc. Pressure measurements were made both at the face of the tongue of the disc and outside the tongue. A conventional feeder disc could not be used, and this proved to be a disadvantage. Thus, in the second round, the sensors were integrated into the feeder disc (of conventional type), and the sensors were placed symmetrically outside the legs of the U-profile. There was no pressure sensor in the tongue of the die or feeder disc during the second round of experiments, mainly because there was not sufficient space. It was clearly preferable not to weaken the tongue unnecessarily with the introduction of a sensor cavity. Sensors were not placed in optimal positions for the study of material flow. In fact, the most difficult problem related to design was that of finding the sufficient space for the pressure sensor holes. The position that was chosen was probably the most natural one from this perspective. Since the experiments were the very first of their kind performed by the NTNU/SINTEF research group, replicate measurements of pressure was preferred to measurement of pressure differences. Only two sensors were available in the study. A large number of measurements were performed of both the flow temperature and the extrusion die temperature.

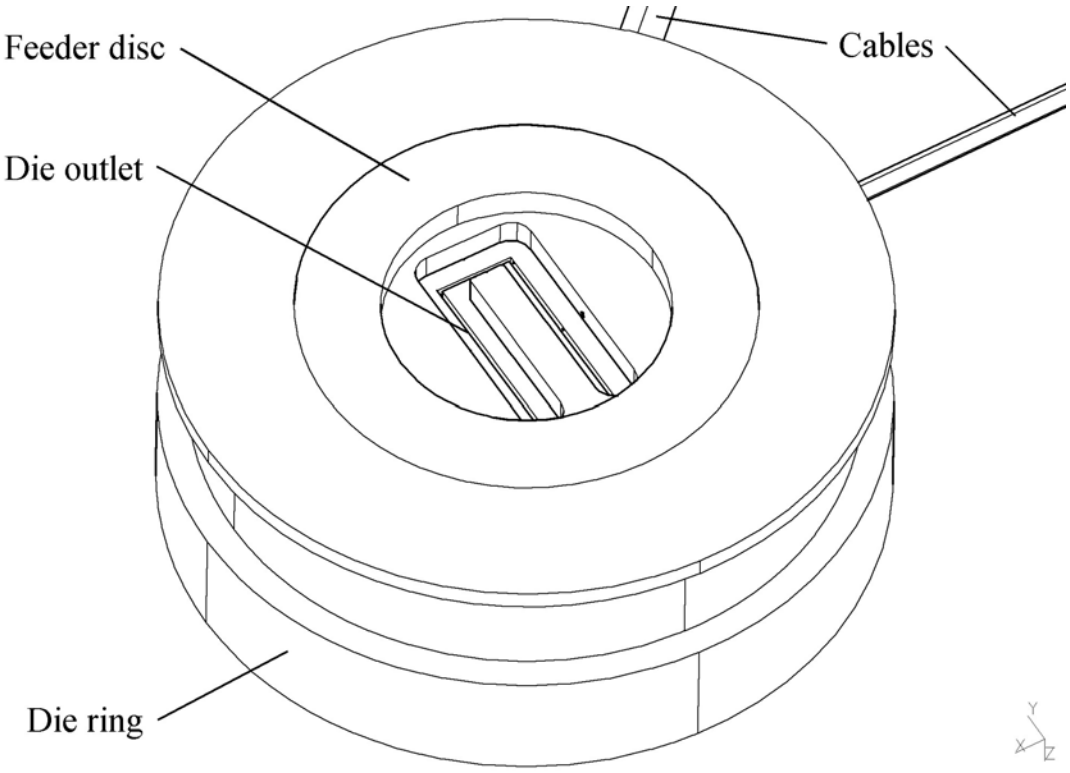

Figure 5.26. A top view of the tool stack used for industrial extrusion of a U-profile with a thickness of 2.3 mm, a height of 120 mm and width 49.5 mm.

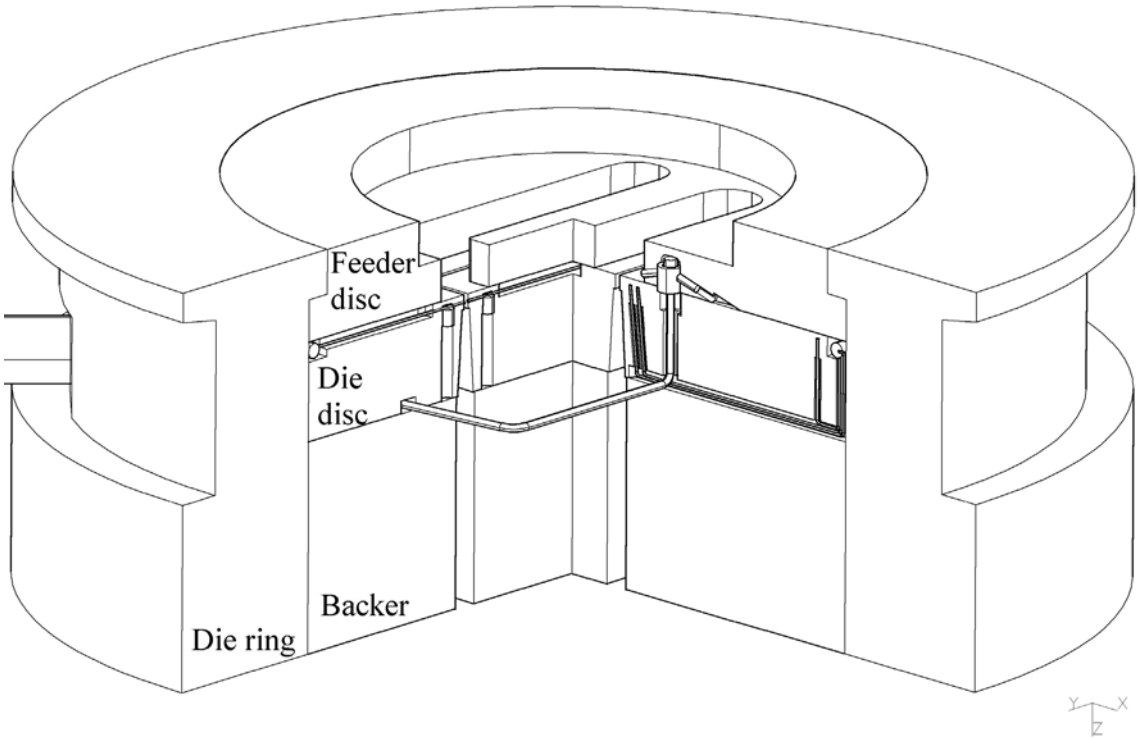

Figure 5.27. A side view of the tool stack used for industrial experiments. Only three quarters of the tool stack are shown. Thermocouples are also shown.

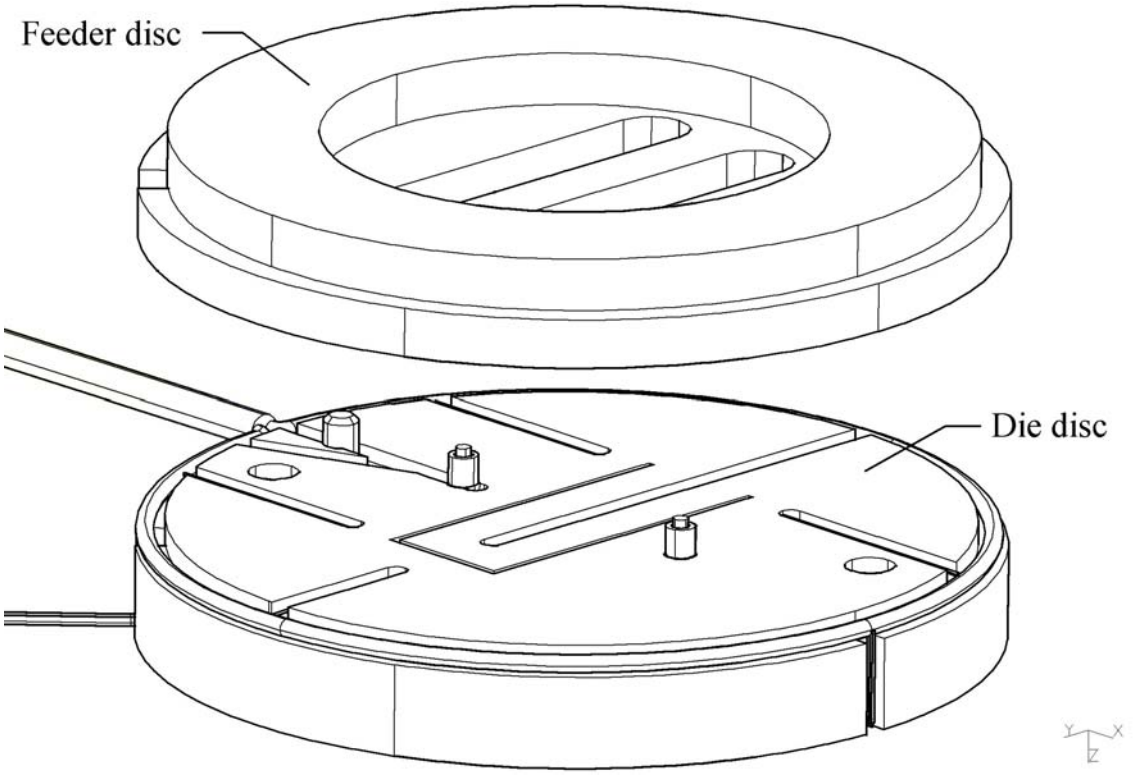

Figure 5.28. A view of the upper faces of the die disc and feeder discs with sensors used during industrial experiments. Slots for thermocouples may be observed.

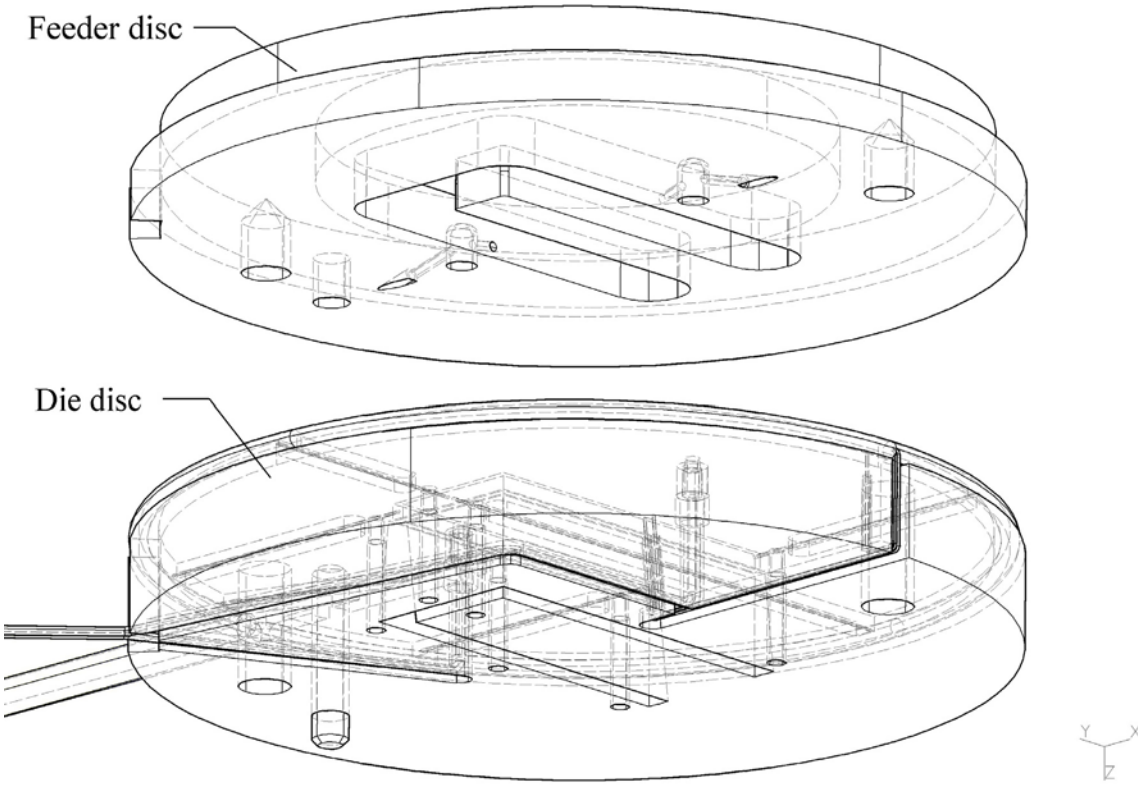

Figure 5.29. A view of the bottom faces of the die disc and feeder discs with sensors used during industrial experiments. Hidden lines have been added.

During both rounds of experiments the die face pressure sensors were integral parts of the tool rather than inserts. The reason was that sensors in this situation probably are more robust and smaller, and are less likely to weaken the general die design. Besides, no satisfactory insert sensor design had been developed. The sensors were fastened with a spring in the first rounds of experiments and with set screws in the second. The feeder disc, the die disc and the backer were inserted into a die ring after the sensors had been mounted. This operation was quite complex and there was a real danger that sensors could be damaged during assembly. There is obviously room for further improvement of the sensor and die designs so that assembly may be made easier. After assembly, the entire tool stack was heated in an electrical furnace over a longer period of time at high temperature before it was transported to the press and inserted in the die slide.

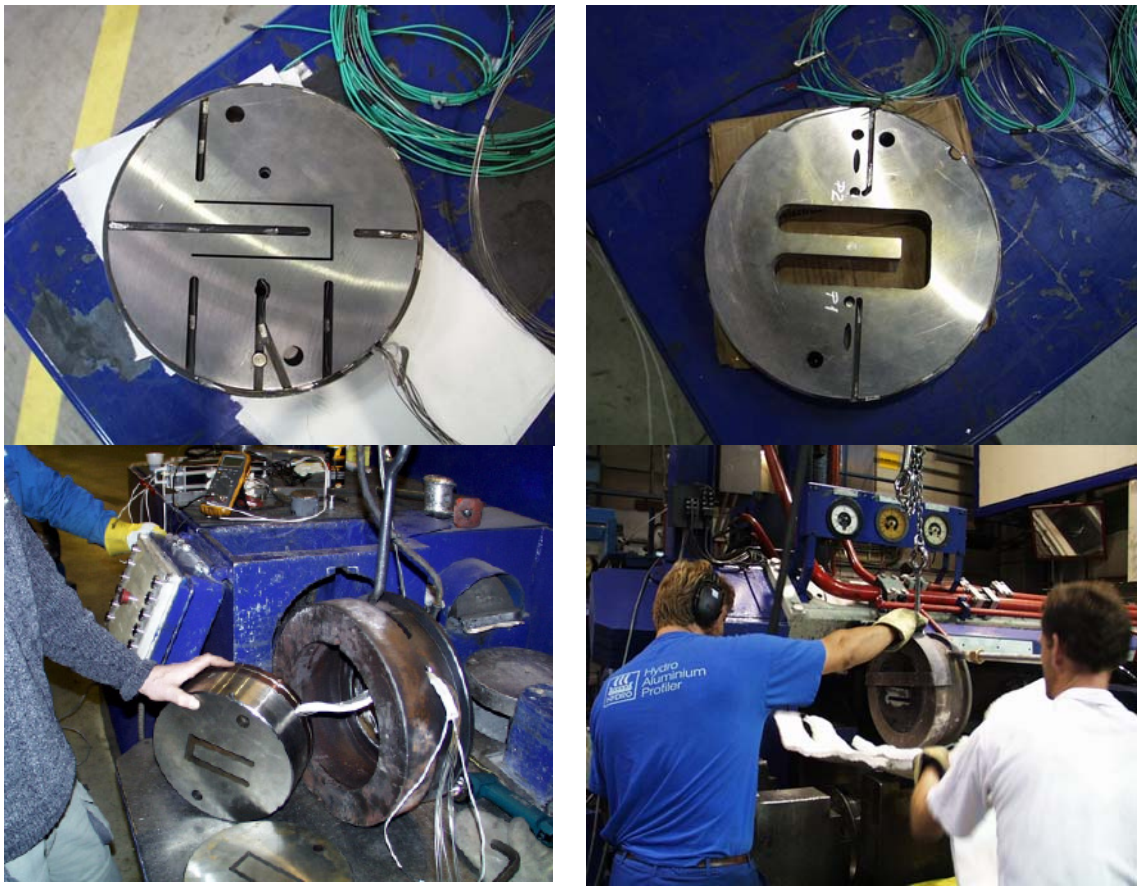

Figure 5.30. A top view of the die disc and a bottom view of the feeder disc of the tools used during industrial experiments. The die is assembled and inserted into the extrusion press (die slide) after having been heated and unpacked.

None of the experimental rounds were completely successful with regard to pressure measurement. During the first round, the flow stability was extremely poor. The reasons were probably improper temperature control and the fact that a non-conventional feeder was used. The legs of the U-profile were retarded. The result was plugging of the outlet. Only by applying a considerable overload were the press operators able to loosen the profile so that the experiment could continue. The tongue of the die was, however, plastically deformed during the overloading, and the die outlet was also much distorted.

What should have been a U-profile came out as an inverted V-profile (to the great amazement of those taking part in the experiments). The thickness of the legs deviated significantly (±0.5 mm) from the nominal value. The flow stability was improved by the use of a puller, but there was no remedy for the thickness deviations. The experiments had to be stopped after a few runs. The pressure sensors responded satisfactorily during the first experimental run. However, large amounts of water were poured on the billet to ease the cutting of butt end. Water then penetrated into the die and short circuited the sensor system. Since the die was very hot, the water gradually evaporated between the runs so that the output signal was regained. However, by that time, a new butt end had to be cut and water was again poured on the billet and die. The water spray could not be turned off or modified in any way since it would endanger the press operations.

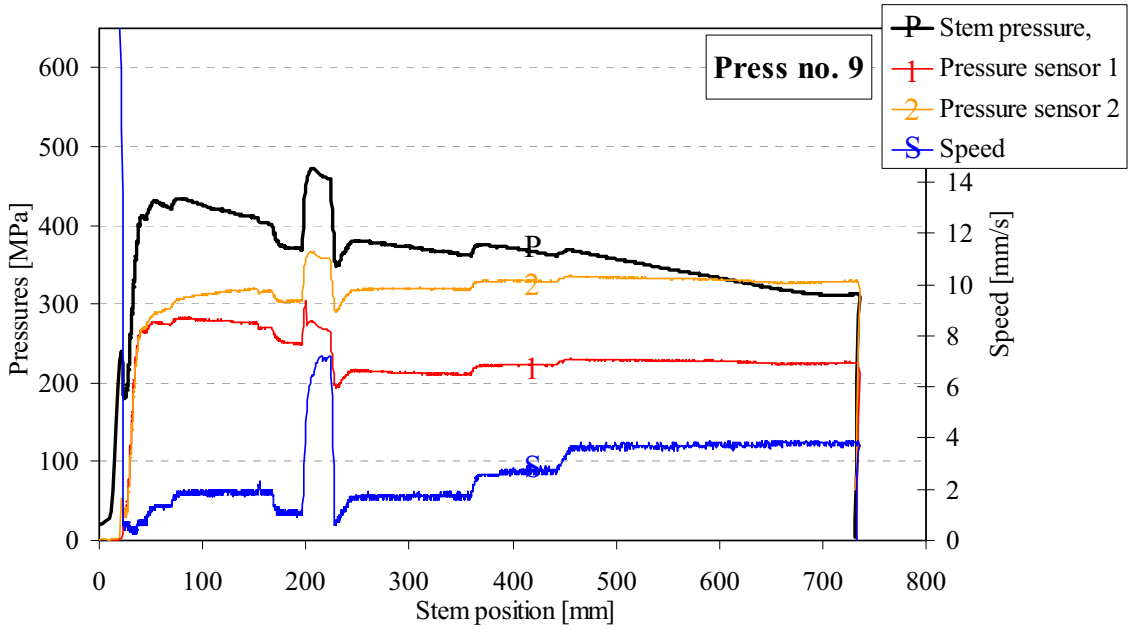

Figure 5.31. Results from the ninth press of the second round of industrial experiments. The ram (stem) pressure and die face pressures are plotted. On-line or in-situ calibration of the die face pressure sensors was not performed, and the calibration factors had to be determined by finite element modelling. The ram force was measured continuously at the extrusion press. The ram speed was changed on many occasions during measurement. The changes affected both the ram and die face pressure in a similar manner.

In the second round of experiments, better flow stability was obtained through the use of an appropriate feeder design and through better temperature control. Additionally, the pressure sensor equipment had been improved so that there would be no penetration of water into critical parts. The experiment produced interesting information about shape variability during the extrusion of U-profiles of the two alloys AA6060 and AA6082. Results have been reported in internal Hydro and SINTEF reports not available to the candidate and not of very great relevance to the subject of the current study. However, the industrial pressure measurement was unfortunately still not a complete success. The responses of the pressure sensors were of reasonable magnitude during the first five to

six runs, and the experiments demonstrated the feasibility of industrial measurement. Yet, the repeatability of measurement was not acceptable, and permanent displacements were observed after each run. It soon became obvious that at least one of the sensors did not function properly. After some additional runs the second sensor also produced results that were clearly unsatisfactory. The failure on the part of the sensors may be explained by plastic deformation of the sensor disc, improper mounting or some sort of a short-circuiting mechanism. After experiments, all the sensor discs were carefully inspected. No significant permanent deformations were then observed. The position and the mounting of the sensors after deformation could not be controlled as the probes were damaged at the extrusion plant during the disassembly of the die. It is possible that the mounting solution was a weak point of the sensor design, but it is more likely that the sensor measurements during the second round of experiments were also affected by the hostile environment of the industrial extrusion press. Results from measurements indicate that the degradation of the sensor response took place both in between and during the extrusion runs. Water was also used as a cutting fluid for removal of butt ends during the second round of experiments, and it appears that the special measures taken to protect the equipment were not sufficient.

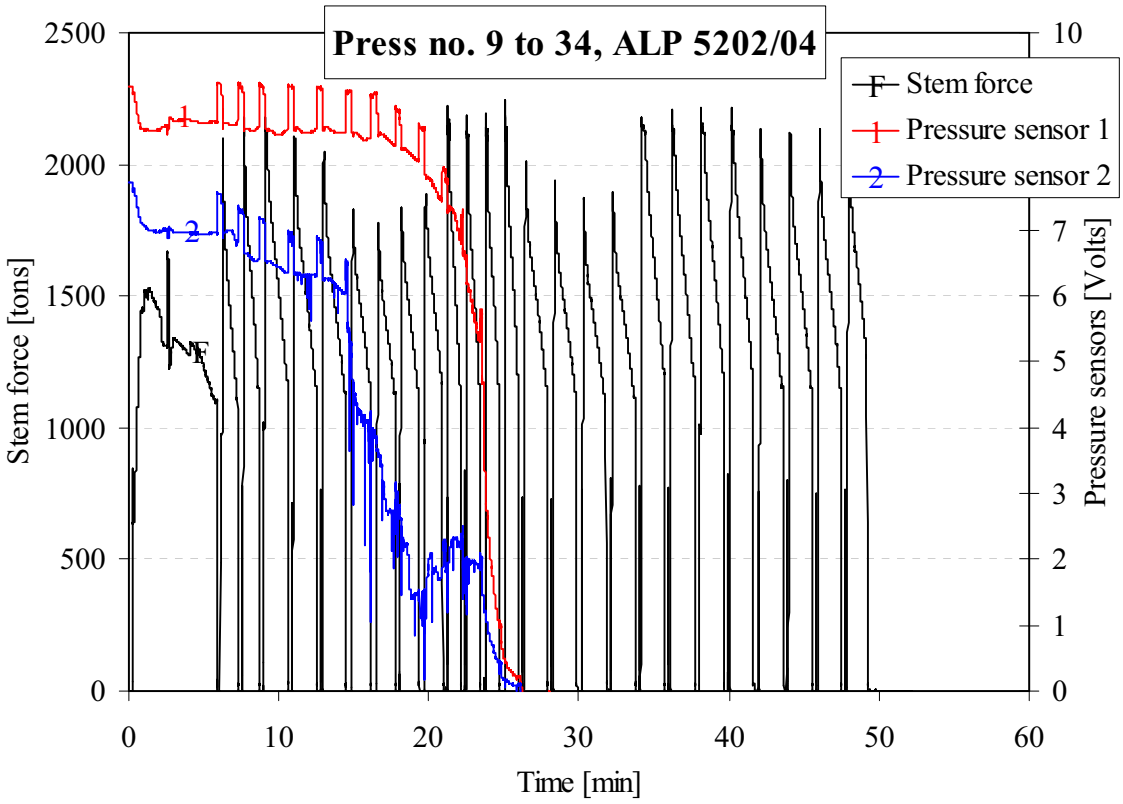

Figure 5.32. Results from all runs of the second round of industrial experiments. The ninth press was the first with the instrumented die. The earlier runs had been performed with a similar die without pressure sensors and thermocouples. The ram (stem) force was measured continuously. The output voltages of the sensor system are shown. Short-circuiting occurred after 13 runs, but detoriation of the signal was evident from the outset of the experiment. Sensor 1 produced somewhat better results than sensor 2.

The most important lesson learnt from the industrial experiments was obviously that the industrial extrusion environment must be regarded as very hostile, and that careful preparations are needed to implement new technology. This does not mean that the preparations were in any way faulty. The industrial case had been carefully studied by finite element modelling, and the equipment and methods had been thoroughly tested in the laboratory environment. Important adjustments had been made in order to adapt the technology to the more demanding industrial environment. Preparations were carefully performed. Still, it must be admitted that the experimental rounds were not great successes. In both cases, the sensors stopped working after a relatively small number of runs. It would, however, be completely wrong to regard the industrial implementation as a complete failure. Success in industrial measurements can never be guaranteed. Only two serious independent attempts were made in this study, and corrections could not be made when the equipment first had been installed in the press. The largely industrial procedure of installation of the instrumented dies in the press was violent and very difficult to control. The experiment was similar to an old-fashioned western duel, in which the duellists could only shoot from the hip. Luck was obviously needed, even if the revolvers were of the best quality and the preparations had been extensive. In this case the extrusion process probably got the better of the opponent, but somehow it was also proven that the process is not invincible. The experimental results clearly indicate that the capacitive measurement technology may be successfully implemented, but that a more systematic approach must be followed.

Two types of improvements should be carefully evaluated in relation to a new attempt with industrial implementation of the capacitive pressure measurement technology. First, a sufficiently robust instrumented die concept that may be easily implemented in industrial presses must be developed. The paper of Appendix J briefly discusses the possibility of developing a special feeder design that may be used together with a number of dies and that need not be changed when the die is worn out. If experiments are to be repeated and a proper die concept is developed, it is possible and preferable to mount capacitive probes permanently. The non-permanent mounting solution used thus far is most suitable for the laboratory environment, and sensor technology should generally be improved. The method of transmitting signals should also be reviewed. Ideally, information should be transmitted digitally without the use of wires. A simpler and maybe better alternative would be to use intelligent dies with rapid coupling.

Second, experiments must be performed purposefully, and one must allow oneself to go through a learning processes consisting not just of two iterations but several. It was early on quite obvious that the objectives of the U-profile study were too broad and ambitious. The profile shape was complex and not an ideal case for the feasibility study. A simpler test case, preferentially one of rod extrusion, should have been chosen, and the focus should have been on describing pressure sensor behaviour rather than flow and instability mechanisms and shape variability. The approach used in the laboratory rod extrusion study should be slightly modified and applied in the next attempt in industrial implementation. It should be clearly recognised that the implementation and commercialisation of pressure sensor technology are sizeable tasks. Yet, success has at least been brought a step closer by the successful implementation of capacitive sensor in the high-temperature – high-pressure laboratory environment.

Chapter 6

General conclusions and future work

6.1 The main conclusions

Measurement of the pressure between an aluminium billet and an extrusion die during high-temperature extrusion is feasible. Specially designed pressure sensors that integrate Capacitec HPC-75 high temperature capacitive probes connected to the corresponding 4000 series amplifiers have been used to determine the die face pressure and strains in dies during rod, thin-strip and tube (pipe) extrusion in the laboratory. The feasibility of measurement in an industrial environment has been demonstrated during the extrusion of a U-profile. Experiments were performed at the Hydro extrusion plant at Raufoss, Norway. The die face pressure sensors may be used to pressures of more than 500 MPa (5000 bar) and to temperatures of 600 ºC. The main characteristics of the sensors are:

- Characteristic size and spatial resolution of approximately 10 mm
- Measurement accuracy within 5 to 10 % of full scale
- Measurement repeatability for genuine runs of 5 to 10 % of full scale
- Measurement repeatability for a given set-up of approximately 3 % of full scale
- Measurement resolution better than 2 % of full scale (for short perturbations)
- Very short response times (significantly less than 1 second)
- Temperature sensitivity smaller than 15 % of full scale (no compensation)
- Temperature sensitivity smaller than 5 % of full scale (with compensation)

Further improvement of both the sensor design and performance of capacitive pressure sensors is possible and desirable. The sensors may be either integral parts of the die or inserts, depending on the application. The capacitive probes have so far not been fixed permanently to the sensor housing or die, but permanent mounting would contribute to a further improvement of the accuracy, repeatability and resolution of measurement. New insert sensors may be smaller, more durable and easier to use.

Accurate techniques of calibration and testing of the die face pressure sensors are vital. Rod extrusion experiments have been performed in order to characterise the response of pressure sensors in the range from 175 to 350 MPa. Both the process parameters and the die outlet geometry may be changed in order to test sensors at even higher pressures. The testing technique also made it possible to systematically change both the magnitude and the rate of sensor temperature change and the characteristics of the thermal sensor response. The most important features of the calibration and testing approach were:

- Finite element simulation of sensor response and sensor shape optimisation
- Off-line point compression testing to characterise the sensor response
- On-line isotropic compression testing to accurately establish calibration factors
- Alternative estimation of die face force by ram and liner force measurements
- Alternative estimation of die face force by numerical flow modelling
- A die design making possible replicate parallel measurement of pressure
- An experimental design allowing tractions to be varied systematically

The accuracy of the method of estimation of the die face pressure by ram and liner force measurement is approximately 10 %. Predictions of force and temperature by the finite element flow code ALMA2π are of similar accuracy. Inverse modelling of the extrusion process is a useful tool in the evaluation of the quality of force, temperature and pressure estimates and measurement data. An improvement of numerical techniques and measurement approaches is needed in order to demonstrate pressure measurement of accuracy better than 10 %. The approach should be an iterative one and focus both on measurement and on modelling. The pressure sensors are of great value in the analysis since they provide information the distribution of pressure during extrusion.

Capacitive pressure sensor technology has not yet been successfully implemented at extrusion plants. Sensor designs must as indicated be further developed, and important questions related to the application of the technology must be assessed. Experience from industrial experiments indicates that die face pressure sensors should be permanently implemented in “intelligent” dies for extrusion of thin-walled profiles. The sensors may provide valuable information on material flow, on the deformation of dies and on the state of stress in and the dimensions of the extruded profile. Optical sensors that measure the shape of the profile and critical dimensions on-line have been tested and may also be included in a commercial press set-up. Two extrusion cases of academic and commercial interest have been closely studied both experimentally and numerically. Tube extrusion experiments demonstrated that die deformations during extrusion of hollow profiles may be very large due to the high pressures applied at the top face of the die. Pressures, bridge strains and mandrel displacements may be measured on-line. During extrusion of aluminium thin-strips unstable flow and buckling may be provoked in a systematic manner. The distribution of the pressure at the die face and the shape of the extruded profile may be measured on-line. The case is probably the simplest one that may be used in the study of the limits and mechanics of flow stability.

Finally, the most important conclusion of the current study is simply that capacitive die face pressure measurement in the harsh environment of the extrusion process is feasible. The measurement accuracy is no poorer than the accuracy of the calculation models in use today. This main conclusion may seem trivial, but is by no means an obvious one. Alternative measurement techniques used in this and other studies, such as high-temperature strain gauge measurements, have in fact proven much less reliable and significantly more difficult to use. The successful application of pressure measurement technology in the high-temperature laboratory environment opens new opportunities in relation to extrusion process control. The candidate firmly believes that a capacitive measurement system in the near future can and should provide useful data on flow with an accuracy and repeatability better than 5 % of full scale of measurement.

6.2 Future work

The present study has only focused on a small number of profile shapes and produced a limited amount of results. More extensive testing of the measurement techniques could undoubtedly have been performed. Particular attention should be paid to calibration and to careful preparations, for the accuracy and repeatability of all the measurement techniques could have been significantly better. A case that should be rerun as soon as possible is that of thin-strip extrusion. Earlier experiments have proven the feasibility of both measuring small die face pressure changes and of purposefully provoking flow instabilities, but no measurements have been performed during the transition from instable to stable flow and vice versa. The time is ripe for acquiring information from both pressure and shape sensors about the mechanics of flow instability. This would make it easier to realise the significance of the introduction of measurement technology in the study of extrusion. Experiments should be combined with the numerical study of flow. This would probably require the development of computer programs that are able to predict flow instabilities and very small shape and dimension variations (10 micron). Most of the measurement techniques that have been assessed in the current study may be used in the evaluation of flow stability. It is then obviously most important that the deformation of dies is carefully controlled.

The present study is an early step towards the commercialisation of an intelligent extrusion die concept. Further improvement of both sensor designs and of the concepts of measurement and flow control are needed, however. First, a new and improved capacitive sensor design should be introduced. Today, the pressure sensors consist of essentially two parts, the capacitive displacement probe and the sensor disc/plate with housing. The sensor disc is in many cases a part of the extrusion die. It would be more sensible to closely integrate the two components of the sensor, because it would reduce the risk of unaccounted for displacements and therefore improve measurement accuracy and repeatability. Ready-to-use calibrated capacitive insert pressure sensors rather than displacement probes should in the future be acquired from the commercial probe manufacturer. The new insert pressure sensors should be significantly smaller than the sensors in use today. A cylindrical pressure sensor with a maximum diameter of 5 mm or less may be envisioned. Sensors should be easily and accurately mounted, and the details of the mounting should not influence the sensor response. It should be possible to calibrate the sensors off-line, but also the on-line techniques of calibration should be refined. The pressure sensors should integrate temperature measurement, and direct and accurate temperature compensation methods should be implemented. It would be most useful if pressure sensors for high temperature environments based on alternative measurement principles could be developed. Fibre optic techniques are as indicated in Chapter 4 particularly interesting due to the small size, high-temperature properties and the relatively low cost of the optical fibre itself. Alternative measurement techniques may provide results that may shed new light on the results that were obtained with the old techniques. It would then be possible to further develop old techniques or to work further with only the new ones if they are proven superior.

A second step in the work towards commercialisation of the measurement techniques is the development of intelligent dies that can be adapted to a large number of die outlet geometries and that can monitor and even control the flow of aluminium. If material

flow is to be controlled, however, it is important that the fundamental behaviour of the material be better understood. The importance of developing proper flow codes has already been stressed. It is also vital to develop appropriate combined experimental and numerical methods for evaluating flow and friction behaviour. A possible solution to this problem is to integrate a range of measurement techniques in a small size laboratory press, and to perform experiments with maximum control of temperature and other process parameters. The experiments must be representative, and both rod and thin-strip extrusion should be evaluated. The next step in the study of flow and process variability would be careful experiments with thin-strip geometry and intelligent dies. Focus should not only be on describing the mechanics of flow, but also on controlling the dimensions of the profile more closely. Die deformation and critical profile dimension measurements should be added in order to allow a very careful evaluation of the consequences of the billet-die face interaction. It would be useful if methods for directly measuring the die outlet geometry were also introduced. While the thin-strip should be the starting point for the study, it would be natural to extend the study to more complex profiles when extrusion with simpler geometries is well understood. The final stage in the development of intelligent dies would be one where knowledge about flow and deformation is actively used to develop general shape control strategies. The simplest one would involve the establishment of process limit diagrams and the introduction of methods for determining and warning of improper flow and dimension control. A more desirable approach may consist of the development of actuators that are less sensitive to die deformation or even completely new die designs.

The dimensional variability of the sections produced by the extrusion process should be seen in relation to the nature of and the requirements for downstream forming processes. Advanced users of extruded profiles perform a large number of operations to reach a product that is useful. Each process step is affected by the output of the earlier ones. The product shape and structure are gradually modified. The variability in the dimensions of the product after extrusion affects the precision of subsequent stretching and bending operations. It is sometimes necessary to introduce additional profile shape calibration or correction steps. While the quality of extruded aluminium products is sufficient for a number of products, less dimensional variability is needed if the prices of complex products are to be competitive. A possible solution to the problem is the introduction of entirely new press concepts that integrate intelligent die designs and systems for direct and high rate downstream forming of complex parts. Improved methods for dimension and flow control as well as better control of the die deformations must be implemented. New press concepts are most relevant for the large volume production of parts for the automotive industry. They are much needed if thin-walled extruded aluminium profiles are to compete with inexpensive substitutes made of steel.

Bibliography

Chapter 1

[Lef02a] Lefstad M., Moe P.T., Flatval R., Støren S., *Thin strip aluminium extrusion – pressure, temperature and deflection recordings of the extrusion die*, Proc. 5th ESAFORM Conf. on Material Forming, April 2002, Kraków, pp. 471-474.

[Moe02] Moe P.T., S. Støren, *A technique for measuring pressure on the die face during extrusion*, Proc. 5th ESAFORM Conf. on Material Forming, April 2002, Kraków, pp. 463-466.

[Moe03a] Moe P.T., Lange H.I., Hansen A.W., Wajda W., Støren S., *Experiments with die deflection during hot extrusion of hollow profiles*, Proc. 6th ESAFORM Conf. on Material Forming, April 2003, Salerno, pp. 119-122.

[Moe03b] Moe P.T., Lefstad M., Flatval R., Støren S., *Measurement of temperature and die face pressure during hot extrusion of aluminium*, Intern. J. Forming Processes Vol. 6 (2003), No. 3, pp. 241-270.

[Moe04a] Moe P.T., *An analysis of forge welding of steel rods – Heating phase modeling*, Proc. 7th ESAFORM Conf. on Material Forming, April 2004, Trondheim, pp. 399-402.

[Moe04b] Moe P.T., Wajda W., Szeliga D., Madej L., Pietrzyk M., Støren S., *An Approach for Evaluating Constitutive Models for Hot Aluminium Extrusion – Rod Extrusion of AA6060 as a Case Study*, Proc. 10th Int. Conf. on Metal Forming, Sept. 2004, Kraków, pp. 723-730.

[Moe04c] Moe P.T., Wajda W., Støren S., *A study of the thermomechanical response of a die face pressure sensor for hot aluminium extrusion,* Proc. 10th Int. Conf. on Metal Forming, Sept. 2004, Kraków, pp. 627-634.

[Moe04d] Moe P.T., Wajda W., Couweleers F., Støren S., *Visions of a system for shape control during thin-strip aluminium extrusion*, Proc. 12th Int. Conf. on Experimental Mechanics, Sept. 2004, Bari, pp. 570-571 (article on CD).

[Moe04e] Moe P.T., Intelligent Die Systems, Business plan, October 15th 2004.

[Moe05] Moe P.T., Wajda W., Støren S., Lefstad M., Flatval R., *An Experimental and Numerical Study of Induction Heating*, Proc. 8th ESAFORM Conf. on Material Forming, April 2005, Cluj, in press.

[Stø03] Støren S., Moe P.T., *Ch 8. Extrusion,* pp. 385-480, In: Totten G.E., Scott MacKenzie D. (Ed.), *Handbook of Aluminium*, Marcel Dekker, 2003, N.Y.

[Waj03] Wajda W., Moe P.T., Lefstad M., Støren S., *A study of the limits of self-stabilization during extrusion of thin strips*, Proc. 6th ESAFORM Conf. on Material Forming, April 2003, Salerno, pp. 267-270.

[Waj04] Wajda W., Moe P.T., Abtahi S., Støren S., *An evaluation of material behaviour during extrusion of AA6060 rods*, Proc. 7th ESAFORM Conf. on Material Forming, April 2004, Trondheim, pp. 245-248.

[Waj05a] Wajda W., Moe P.T., Støren S., Lefstad M., Flatval R., *Measurement of Temperature and Pressure during Thin-Strip Extrusion*, Proc. 8th ESAFORM Conf. on Material Forming, April 2005, Cluj, in press.

Chapter 2

[Abt95] Abtahi S., Friction and interface reactions on the die land in thin-walled extrusion, Doctoral thesis, Norwegian Institute of Technology, Trondheim, 1995.

[Abt96] Abtahi S., Welo T., Støren S., *Interface mechanisms on the bearing surface in extrusion*, Proc. 6th Int. Alu. Extr. Techn. Sem., Chicago (Ill.), 1996, Vol II pp. 125-131.

[Abt02] Abtahi S. and Lefstad M., Simulation of temperatures, profile speeds and forces during extrusion of aluminium using the FE code Extrud, Report STF24 F02335. SINTEF Materials Technology. Trondheim, Norway, 2002.

[Ake88] Akeret R., Stremel W., *Control of Metal Flow in Extrusion Dies*, Proc. 4th Int. Alu. Extr. Techn. Sem., Chicago, Ill., 1988, Vol II pp. 357-367.

[Ale01] Alexandrov S., Mishuris G., Miszuris W., Sliwa R.E., *On the dead-zone formation and limit analysis in axially symmetric extrusion*, Int. J. Mech. Sci. 43, 2001, pp. 367-379.

[Alt97] Altan T., Vazquez V., *Status of process simulation using 2D and 3D finite element method 'What is practical today? What can we expect in the future?',* J. Mater. Process. Technol. 71, 1997, pp. 49-63.

[Are00] Arentoft M., Gronostajski Z., Niechajowicz A., Wanheim T., *Physical and mathematical modelling of extrusion processes*, J. Mater. Process. Technol. 106, 2000, pp. 2-7.

[Ari03] Arif A. F. M., *On the use of non-linear finite element analysis in deformation evaluation and development of design charts for extrusion processes*, Finite Elements in Analysis and Design, In Press.

[Ast01] Astakhov V.P., Shvets S.V., *A novel approach to operating force evaluation in high strain rate metal-deforming technological processes*, J. Mater. Process. Technol. 80–81, 2001, pp. 226–237.

[Auk97] Aukrust T., Tjøtta S., Vatne H.E., Van Houtte P., *Coupled FEM and Texture Modelling of Plane Strain Extrusion of an Aluminium Alloy*, Int. J. of Plasticity Vol. 13 No 2., 1997, pp. 111-125.

[Auk96] Aukrust T. et al., *Texture and Grain Structure in Aluminium Sections*, Proc. 6th Int. Al. Extr. Techn. Sem., Chicago, Illinois, 1996, Vol. I pp. 171-177.

[Auk00] Aukrust T., LaZghab S., *Thin shear boundary layers in flow of hot aluminium*, International Journal of Plasticity 16, 2000, pp. 59-71.

[Avi68] Avitzur B., Metal Forming: Process and Analysis, McGraw-Hill, New York, 1968.

[Axm98] Axmann C., Mannl V., *Investigation of metal extrusion and axial compression of compressible media by means of a modified slab method*, Archive of Applied Mechanics 68, 1998, pp. 137-146.

[Aym01] Aymone J.L.F., Bittencourt E., Creus G.J., *Simulation of 3D metal-forming using an arbitrary Lagrangian-Eulerian Finite element method*, J. Mater. Process. Technol. 110, 2001, pp. 218-232.

[Bau01] Bauser M., Sauer G., Siegert K., *Strangpressen, Verfahren, Werkstoffe, Produktion*, Aluminium Verlag, 2001.

[Bel80] Bello L., *Die corrections for changing flow characteristics*, Proc. 2th Int. Al. Extr. Techn. Sem., Chicago (Ill.), 1980, pp. 89-115.

[Bel94] Bellet M., Chenot J.L., Fourment L., Massoni E., Montmitonnet P., Proc. Seminaire de Plasticité, Sophia Antipolis, 1994, Vol 1-3.

[Bel00] Belytschko T., Liu W.K., Moran B., Nonlinear Finite Elements for Continua and Structures, Wiley, New York, 2000.

[Ber00] Berezhnoy V. L., *Non-Traditional Process Techniques of Extrusion and Pressing*, Int. J. Adv. Manuf. Technol. 16, 2000, pp. 19–22.

[Bjø99] Bjørk T., Bergstrøm J., Hogmark S., *Tribological simulation of aluminium hot extrusion*, Wear 224, 1999, pp. 216–225.

[Bjø00] Bjørk T., Bergstrøm J., Hogmark S., *Optimization of Nitriding Parameters for Extrusion Dies, Evaluated in an Extrusion Simulation Test*, Proc. 7th Int. Al. Extr. Techn. Sem., Chicago (Ill.), 2000, Vol. II pp. 317-325.

[Bun02] Buntoro I.A., Müller K.B., Overview of various bending methods directly after extrusion process, Proc. 5th ESAFORM Conf. on Material Forming, Kraków, 2002, pp. 443-446.

[Cam75] Campbell J.D., Arch. Mechanics 27, 1975, p. 407.

[Cha87] Chakrabarty, J., Theory of Plasticity, McGraw-Hill, New York, 1987.

[Cha99] Chanda T., Zhou J., Kowalski L., Duszczyk J., *3D Fem Simulation of the Thermal Events During AA6061 Aluminum Extrusion*, Scripta Materialia, Vol. 41, No. 2, 1999, pp. 195–202.

[Cha00] Chanda T., Zhou J., Duszczyk J., *FEM analysis of aluminium extrusion through square and round dies*, Materials and Design 21, 2000, pp. 323-335.

[Cha01] Chanda T., Zhou J., Duszczyk J., *A comparative study on iso-speed extrusion and isothermal extrusion of 6061 Al alloy using 3D FEM simulation*, J. Mater. Process. Technol. 114, 2001, pp. 145-153.

[Che96] Chenot J.-L., Chastel Y., *Mechanical, thermal and physical coupling methods in FE analysis of metal forming processes*, J. Mater. Process. Technol. 60, 1996, pp. 11–18.

[Che98] Chenot J.-L., Bay F., *An overview of numerical modelling techniques*, J. Mater. Process. Technol. 80–81, 1998, pp. 8–15.

[Che02] Chenot J.-L., Fourment L., Mocellin K., *Numerical treatment of contact and riction in FE simulation of forming processes*, J. Mater. Process. Technol. 125–126, 2002, pp. 45–52.

[Chi97a] Chitkara N.R., Butt M.A., *Axisymmetric tube extrusion through a flat-faced circular die: Numerical construction of axi-symmetric slipline fields and associated velocity fields*, Int. J. Mech. Sci. 39, No. 3., 1997, pp. 435-454.

[Chi97b] Chitkara N.R., Butt M.A., *Combined rod and tube extrusion: Numerical solution of axi-symmetric slipline fields and associated velocity fields*, Int. J. Mech. Sci. 39, No. 4., 1997, pp. 435-454.

[Chi99] Chitkara N.R., Butt M.A., *Axi-symmetric tube extrusion through a smooth conical or cosine die and over a conical or ogival mandrel: numerical construction of axi-symmetric slip-line fields and associated velocity fields*, Int. J. Mech. Sci. 41, 1999, pp. 1191-1215.

[Chi01] Chitkara N.R., Aleem A., *Extrusion of axi-symmetric tubes from hollow and solid circular billets: a generalised slab method of analysis and some experiments*, Int. J. Mech. Sci. 43, 2001, pp. 1661-1684.

[Chi02] Chitkara N.R., Kim Y.J., *Development of an Adaptive Directional Reduced Integration Technique and its Application to Rigid-Plastic Finite-Element*

Analysis of Heading and Backward Extrusion, Int. J. Adv. Manuf. Technol. 20, 2002, pp. 581–588.

[Chi03] Chitkara N.R., Butt M.A., *Axisymmetric Rod Extrusion Through Smooth and Partially Rough Conical, Cosine, and Flat-Faced Circular Dies: Slip-Line Field Solutions Using Numerical Methods and Some Experiments*, Int. J. Adv. Manuf. Technol. 3, 2003, pp. 157–176.

[Cla00] Claves S.R., Misiołek W.Z., *Effect of Die Design on Microstructure of Extruded Aluminium*, Proc. 7th Int. Al. Extr. Sem., Chicago (Ill.), 2000, Vol. I pp. 225-231.

[Clo90] Clode M.P., Sheppard T., *Formation of Die Lines during Extrusion of AA6063*, Mat. Sci. Tech. 6, 1990, pp. 755-763.

[Die86] Dieter G.E., Mechanical Metallurgy, McGraw-Hill, New York, 1986.

[Dja00] Djapic Oosterkamp L., Ivankovic A., Venizelos G., *High strain rate properties of selected aluminium alloys,* Materials Science and Engineering A278, 2000, pp. 225–235.

[Dua03] Duan X., Sheppard T., *Simulation and control of microstructure evolution during hot extrusion of hard aluminium alloys*, Mat. Sci. and Eng. A351, 2003, pp. 282- 292.

[Eik97] Eikemo M.S., Espedal M.S., Fladmark G., *On the numerical solution of a three dimensional extrusion model*, Comput. Visual. Sci. 1, 1997, pp. 1–14.

[EncW] Encyclopedia Britannica Online Edition, Aluminum.

[Est98] Estrin Y., *Dislocation theory based constitutive modelling: foundation and application*, J. Mater. Process. Technol. 80-81, 1998, pp. 33-39.

[Fed02] Feder J., *Friction: a scientific and practical challenge*, Presentation at Conference Industry, Academia and Research, Friction, Plasticity and Fracture: Engineering problems that pose fundamental basic research questions.

[Fle91] Fletcher C.A.J., Computational Techniques for Fluid Dynamics Vol. 1 and 2, Springer, Berlin, 1991.

[Fli00] Flitta I., Sheppard T., *On the Mechanics of Friction during the Extrusion Process*, Proc. 7th Int. Al. Extr. Techn. Sem., Chicago, Illinois, 2000, Vol. I pp. 197-203.

[Fli02] Flitta I., Sheppard T., *Investigation of friction during the extrusion of Al-alloys using FEM simulation*, Proc. 5th Int. ESAFORM Conf. on Mat. Form., Krakow, 2002, pp. 435-438.

[Fur96] Furu T., Pedersen K., Abtahi S., *Microstructurally Based Modeling Applied to Cold Extrusion of Aluminum*, Proc. 6th Int. Al. Extr. Techn. Sem., Chicago, Illinois, 1996, Vol. I pp. 341-347.

[Gad99] Gadala M. S., Wang J., *Simulation Of Metal Forming Processes With Finite Element Methods*, Int. J. Numer. Meth. Engng. 44, 1999, pp. 1397-1428.

[Gas00] Gasiorczyk J., Richert J., *Application of FEM Modeling to Simulate Metal Flow Through Porthole Dies*, Proc. 7th Int. Al. Extr. Sem., Chicago (Ill.), 2000, Vol. II pp. 195-202.

[Gei37] Geiringer H., *Fundéments mathématiques de la théorie des corps plastiques isotrops*, Mémorial des Sciences Mathématiques 86, 1937.

[Ger04] van Geertruyden W.H., Misiołek W.Z., Wang P.T., Static vs. Dynamic Recrystallization in Extrusion of 6xxx Aluminium Alloys, Proc. 7th

ESAFORM Conf. on Material Forming, April 2004, Trondheim, pp. 183-186.

[Gou98] Gouveia B.P.P.A., Rodrigues J.M.C., Martins P.A.F., *Finite element modelling of cold forward extrusion using updated Lagrangian and combined Eulerian–Lagrangian formulations*, J. Mater. Process. Technol. 80–81, 1998, pp. 647–652.

[Gra92] Grasmo G., Holthe K., Støren S., Valberg H., Flatval R., Hanssen L., Lefstad M., Lohne O., Welo T., Herberg J., Ørsund R., *Modelling of Two-Dimensional Extrusion*, Proc. 5th Int. Alu. Extr. Techn. Sem., Chicago, Ill., 1992, Vol II pp. 367-376.

[Gra95] Grasmo G., Friction and Flow Behaviour in Aluminium Extrusion, Doctoral thesis, Norwegian University of Science and Technology, 1995.

[Gro00] Gronostajski Z.J., The *constitutive equations for FEM analysis*, J. Mater. Process. Technol. 106, 2000, pp. 40-44.

[Haa00] van Haaren M. J., Stoker H. C., van den Boogaard A. H., Huétink J., *The ALE-method with triangular elements: direct convection of integration point values*, Int. J. Numer. Meth. Engng. 49, 2000, pp. 697-720.

[Hal65] Halling J., Mitchell L., *An upper-bound solution for axi-symmetric extrusion*, Int. J. Mech. Sci., 7, 1965, p. 227.

[Ham02] Hambli R., *Influence of Material Properties Variation on Damage Evolution During Extrusion Processes*, Int. J. Adv. Manuf. Technol. 20, 2002, pp. 676–682.

[Han96] Hanssen L., Lindviksmoen P., Rystad S., *Effect of Blend and Extrusion Parameters on Material Flow*, Proc. 6th Int. Al. Extr. Techn. Sem., Chicago, Ill., 1996, Vol. II, pp. 11-21.

[Han98] Hanssen L., Lefstad M., Rystad S., Reiso O., Johnsen V., *Billet Surface Flow in Aluminium Extrusion using Half-Moon Dies*, Proc. 1st ESAFORM Conf. on Material Forming, March 1998, Sophia Antipolis.

[Han00] Hansen L., Lefstad M., Rystad S., Reiso O., Johnsen V., *Billet Surface Flow in Aluminium Extrusion using "Half-Moon Dies"*, ALUMINIUM Vol. 76, March 2000, pp. 138-141.

[Hec98] Hector L.G., Schmid S.R., *Simulation of asperity plowing in an atomic force microscope Part I: Experimental and theoretical methods*, Wear 215, 1998, pp. 247-256.

[Hei02] Heiberg G., Brechet Y., Jensrud O., Roven H.J., *Selection of aluminium alloys for extrusion profiles: methodology and development of a specialised software*, Materials and Design 23, 2002, pp. 505–509.

[Hen23] Hencky Z., Z. angew. Math. Mech. 3, 1923, p. 241.

[Hil50] Hill R., The Mathematical Theory of Plasticity, Oxford Claredon Press, Oxford, 1950.

[Hir68] Hirth J.P., Lothe J., Theory of Dislocations, McGraw-Hill, New York, 1968.

[Hol91] Holthe K., Numerical Simulation of aluminium extrusion: Volume 1: ALMA Theory manual, Report STF71 F91028. SINTEF Structural Engineering. Trondheim, Norway, 1991.

[Hol92] Holthe K., Hanssen L., Støren S., *Numerical simulation of the aluminium extrusion process in a series of press cycles*, Proc. NUMIFORM'92, Rotterdam 1992, pp. 611-618.

[Hol96] Holthe K., Tjøtta S., *The Heat Balance During Multiple Press Cycles*, Proc. 6th Int. Alu. Extr. Techn. Sem., Chicago, Ill., 1996, Vol I, pp. 387-392.

[Hol98] Holthe K., PROSMAT Research Program: Modelling of flow in the bearing channel Modelling of Coulomb Friction in ALMA, Report STF22 F98691. SINTEF Civil and Environmental Engieering. Trondheim, Norway, 1998.

[Hol02] Holthe K., Hanssen L., Giertsen E., ALMA User's manual, SINTEF Report, 2002.

[Hue86] Huetink H., On the Simulation of Thermo-mechanical Forming Processes – a mixed Eulerian-Lagrangian Formulation, Doctoral thesis, Technical University of Twente, Twente, 1986.

[Huf83] Hufnagel W., Aluminium Taschenbuch, Aluminium-Verlag, Dusseldorf, 1983.

[Hwa97] Hwan C.-L., Plane strain extrusion by sequential limit analysis, Int. J. Mech. Sci. Vol. 29 No.7, 1997, pp. 807-817.

[IaiW] www.world-aluminium.org - home of the International Aluminium Institute

[Irg90] Irgens F., Constitutive formulation for hot metal extrusion and the relation to the torsion test, SINTEF Project Memo (200375.20) 90-11-20.

[Jac96] Jackson A., Sheppard T., *Observations on Production and Limit Diagrams for the Extrusion Process*, Proc. 6th Int. Al. Extr. Techn. Sem., Chicago, Illinois, 1996, Vol. I pp. 209-216.

[Jia96] Jia Z. et al., *Application of Upper Bound Element Technique (UBET) for Aluminium Extrusion*, Proc. 6th Int. Al. Extr. Techn. Sem., Chicago, Illinois, 1996, Vol. II pp. 247-252.

[Joh70] Johnson W., Sowerby R., Haddow J.B., Plane-strain Slip-line Fields: Theory and Bibliography, Edward Arnold, London, 1970.

[Joh82] Johnson W., Sowerby R., Venter R.D., Plane slip line fields for Metal Deformation Processes, Pergamon Press, Oxford, 1982.

[Jou98] Joun M. S., Hwang S. M., *Die Shape Optimal Design in Three-Dimensional Shape Metal Extrusion by the Finite Element Method*, Int. Journal for Numerical Methods in Engineering 41, 1998, pp. 311-335.

[Kak96] Kakinoki T., Katoh K., Kiuchi M., *Application of Upper Bound Method to Extrusion Die Design*, Proc. 6th Int. Al. Extr. Techn. Sem., Chicago (Ill.), 1996, Vol. II pp. 5-9.

[Kha95] Khan A.S., Huang S., Continuum Theory of Plasticity, Wiley, New York, 1995.

[Kia96] Kialka J., Misiolek W.Z., *Studies of Dead Metal Zone Formation in Aluminum Extrusion*, Proc. 6th Int. Al. Extr. Techn. Sem., Chicago (Ill.), 1996, Vol. II pp. 107-111.

[Kim00] Kim Y-T., Ikeda K., *Flow Behavior of the Billet Surface Layer in Porthole Die Extrusion of Aluminum*, Metall. Mater. Trans. 31A, 2000, pp. 1635-1643.

[Kim02] Kim Y-T., Ikeda K., Murukami T., *Metal flow in porthole die extrusion of aluminium*, J. Mater. Process. Technol. 121, 2002, pp. 107-115.

[Koc93] Kocanda, A. et al., *Contact Pressure Distribution in Tool/Workpiece Interface in Forward Extrusion*, Proc. 4th Int. Conf. Techn. Plasticity, Bejing, China, 1993, Vol.I, pp. 587-592.

[Kor02] Korbel A., Short course on structural and mechanical aspects of plastic strains in metals, Compendium AGH, 2002, pp. 1-56.

[Kva02] Kvamsdal, T., Presentation at the Fremat project meeting, Oslo, 2002.

[Lan85] Lange K., Handbook of Metal Forming, McGraw-Hill, New York, 1985.

[Lau81] Laue K., Stenger H., Extrusion: Process, Machinery, Tooling, American Society for Metals, Metals Park, OH, 1981.

[Laz02] LaZghab S., Aukrust T., Holthe K., *Adaptive exponential finite elements for the shear boundary layer in the bearing channel during extrusion*, Comput. Methods Appl. Mech. Engrg. 191, 2002, pp. 1113-1128.

[Lee73] Lee C.H., Kobayashi S., *New solutions to rigid-plastic deformation problems using matrix method*, J. Eng. Ind., Trans ASME 95, 1973, p. 865.

[Lee99] Lee G.-A., Im Y.-T., *Finite-element investigation of the wear and elastic deformation of dies in metal forming*, J. Mater. Process. Technol. 89–90, 1999, pp. 123–127.

[Lee00] Lee C.M., Yang D.Y., *A three dimensional steady-state finite element analysis of square die extrusion by using automatic mesh generation*, Int. J. Mach. Tools Manuf. 40 (1), 2000, pp. 33–47.

[Lef92] Lefstad M., Reiso O., Johansen V., *Flow of Billet Surface in Aluminium Extrusion*, Proc. 5th Int. Al. Extr. Techn. Sem., Chicago (Ill.), 1992, Vol. I pp. 11-21.

[Lef93] Lefstad M., Metallurgical Speed Limitations during the Extrusion of AlMgSi-Alloys, Doctoral thesis, University of Trondheim, 1993.

[Lef96] Lefstad M., Reiso O., *Metallurgical Speed Limitations During the Extrusion of AlMgSi-Alloys*, Proc. 6th Int. Al. Extr. Techn. Sem., Chicago (Ill.), 1996, Vol. I pp. 11-21.

[Lef99] Lefstad M., Flatval R., Ekstrudering av skinne og U-profil i laboratorieverkstedet ved SINTEF som underlag for simuleringsprogrammet Ekstrud3D, Report STF24 F99602, SINTEF Materials Technology, Trondheim, Norway, 1999.

[Lem90] Lemaitre J., Chaboche J.L., Mechanics of solid materials, Cambridge University Press, 1990.

[Lof00] Lof J., Klaseboer G., Huétink J., *FEM Simulations of Aluminium Extrusion Using an Elasto-Viscoplastic Material Model*, Proc. 7th Int. Al. Extr. Sem., Chicago, Ill., 2000, Vol. II pp. 211-222.

[Lof01] Lof J., *Elasto-viscoplastic FEM simulations of the aluminium flow in the bearing area for extrusion of thin-walled sections*, J. Mater. Process. Technol. 114, 2001, pp. 174–183.

[Lof02] Lof J., Blokhuis Y., *FEM simulations of the extrusion of complex thin-walled aluminium sections*, J. Mater. Process. Technol. 122, 2002, pp. 344–354.

[Lüh97] Lührs G., Hartmann S., Haupt P., *On the numerical treatment of finite deformations in elastoviscoplasticity*, Comput. Methods Appl. Engrg. 144, 1997, pp. 1-21.

[Mal69] Malvern L.E., Introduction to the mechanics of a continuous medium, Prentice-Hall, New York, 1969.

[Mar01] Marthinsen K., Nes E., *Modelling strain hardening and steady state deformation of Al-Mg alloys*, Mat. Sci. and Techn., 17, 2001, pp. 376-388.

[Meh01] Mehta, B.V., Al-Zkeri I., Gunasekera J.S., Buijk A., *3D flow analysis inside shear and streamlined extrusion dies for feeder plate design*, J. Mater. Process. Technol. 113, 2001, pp. 93-97.

[Mis96] Misiołek W.Z., *Material physical response in the extrusion process*, J. Mater. Process. Technol. 60, 1996, pp. 117-124.

[Mon00] Montmitonnet P., Delamare F., Felder E., Marsault N., Cours de Tribologie de la Mise en Forme, Ecole des Mines de Paris, Centre de Mise en Forme des Matériaux, 2000.

[Moo95] Moon Y.H., Van Tyne C.J., Gordon W.A., *The use of multiple flow fields for continuous solutions from upper bound analysis*, J. Mater. Process. Technol. 52, 1995, pp. 561-569.

[Moo99] Mooi H.G., Koenis P.T.G., Huétink J., *An effective split of flow and die deformation calculations of aluminium extrusion*, J. Mater. Process. Technol. 88, 1999, pp. 67-76.

[MwW] www.m-w.com - Merriam-Webster Online Dictionary: extrusion

[Nak99] Nakanishi K., Koba H., Kamitani S., *Metal flow control in hot extrusion of aluminium alloy using the pocket hole dies - Die design aided by physical simulation system*, Proc. of the 6th ICTP, Nuremberg, 1999, Vol II, pp. 1833-1838.

[Nes98] Nes E., Modelling *of work hardening and stress saturation in FCC metals*, Progr. in Mat. Sci. 41 (1998), 129-193.

[Nes01] Nes E., Marthinsen K., Rønning B., *Modelling the evolution in microstructure and properties during processing of aluminium alloys*, J. Mater. Process. Technol. 117 (2001), 333-340.

[Nes02] Nes E., Marthinsen K., *Modeling the evolution in microstructure and properties during plastic deformation of f.c.c.-metals and alloys – an approach towards a unified model*, Mat. Sci. and Eng. A322 (2002), 176-193.

[Nil99] Nilsen K.E., Kals H.J.J., van Houten F.J.A.M., Vaneker T.H.J., *The development of a die design support system for aluminium extrusion*, Proc. of the 6th ICTP, Nuremberg, 1999, Vol I, pp. 309-314.

[Pan00] Pandit M., *Extrusion - Trends and perspectives concerning temperature measurement and control in aluminium extrusion*, Aluminium. 76, no. 7, 2000, pp. 564-572.

[Pan02] Pandit M., Rothweilwer V., *Aluminium semis industry - New measurement and automation system increases the productivity of extrusion plants.* Aluminium. 78, no. 3, 2002, pp. 130-138.

[Par96] Parson N.C. et al., *Surface Defects on 6XXX Alloy Extrusions*. Proc. 6th Int. Al. Extr. Techn. Sem., Chicago, Illinois, 1996, Vol. I pp. 57-67.

[Ped99] Pedersen K., Abtahi S., *Oversikt over materialkunnskap som kan brukes for å analysere (modellere) tilvirkningsprosesser*, SINTEF Report, 1999.

[Per71] Perzyna P., *Thermodynamic Theory of Viscoplasticity*, Advances in Applied Mechanics, vol. 11, Academic Press, New York, 1971.

[Pet97] Petersen S.B., Martins P.A.F., Bay N., *Friction in bulk metal forming: a general friction model vs. the law of constant friction*, J. Mater. Process. Technol. 66, 1997, pp. 186-194.

[Pet99] Pettersen T., A study of the deformation and recrystallization microstructures and textures in AA6060 and AA6082 – Experimental investigations and modelling, Doctoral thesis, Norwegian University of Science and Technology, 1999.

[Pęc97] Pęcherski R.B., *Macroscopic measure of the rate of deformation produced by micro-shear banding*, Arch. Mech. 49, 1997, pp. 385-401.

[Pęc98] Pęcherski R.B., *Macroscopic effects of micro-shear banding in plasticity of metals*, Acta Mechanica 131, 1998, pp. 203-224.

[Pie02] Pietrzyk M., *Through-process modelling of microstructure in hot forming steels*, J. Mater. Process. Technol. 125-126, 2002, pp. 53-62.

[Raa98] Raabe D., Computational Materials Technology, Wiley, 1998.

[Rei92] Reiso O., The Effect of Microstructure on the Extrudability of Some Aluminium Alloys, Doctoral thesis, Norwegian Institute of Technology, Trondheim, 1992.

[Rei96] Reiso O. et al., *The Effect of Cooling Rate After Homogenization and Billet Preheating Practice on Extrudability,* Proc. 6th Int. Al. Extr. Techn. Sem., Chicago, Illinois, 1996, Vol. I pp. 141-148.

[Ren99] van Rens B.J.E., Finite Element Simulation of The Extrusion Process – Shape prediction for complex profiles, Doctoral thesis, Technische Universiteit Eindhoven, 1999.

[Ric74] Rice, *Continuum mechanics and thermodynamics of plasticity in relation to microscale deformation mechanisms*, U.S. Atomic Energy Commission Contract No. AT (II-I)-3084 Technical Report No. 28, 1974.

[Sah96] Saha P.K., *Influence of Plastic Strain and Strain Rate on Temperature Rise in Aluminium Extrusion*, Proc. 6th Int. Al. Extr. Techn. Sem., Chicago (Ill.), 1996, Vol. I, pp. 355-359.

[Sah98a] Saha P.K., *Thermodynamics and tribology in aluminium extrusion*, Wear 218, 1998, pp. 179-190.

[Sah00] Saha P.K., *Aluminum Extrusion Technology*, ASM International, Metals Park, Ohio, 2000.

[Sah98b] Sahoo S.K., Kar P.K., Singh K.C., *Upper-bound analysis of the extrusion of a bar of channel section from square: rectangular billets through square dies*, J. Mater. Process. Technol. 75, 1998, pp. 75–80.

[Sah99] Sahoo S.K., Kar P.K., Singh K.C., *A numerical application of the upper-bound technique for round-to-hexagon extrusion through linearly converging dies*, J. Mater. Process. Technol. 91, 1999, pp. 105–110.

[Sch01] Scheidler M., Wright T.W., *A continuum framework for finite viscoplasticity*, Int. J. of Plasticity 17, 2001, pp. 1033-1085.

[Sch03] Scheidler M., Wright T.W., *Classes of flow rules for finite viscoplasticity*, Int. J. of Plasticity 19, 2003, pp. 1119–1165.

[Sel72] Sellars, C.M., Tegart, W.J.McG., *Hot workability*. Int. Met. Rev. 17, 1972, pp. 1-24.

[Sha02] Shanghvi J.Y., Michaleris P., *Thermo-elasto-plastic finite element analysis of quasi-state processes in Eulerian reference frames*, Int. J. Numer. Meth. Engng. 53, 2002, pp. 1533–1556.

[She99] Sheppard T., Extrusion of Aluminium Alloys, Kluwer, 1999.

[Shi97] Shi H., McLaren A.J., Sellars C.M., Shahani R., Bolingbroke R., *Constitutive equations for high temperature flow stress of aluminium alloys*, Mat. Sci. and Techn. 13, 1997, 210-216.

[Sib00] Sibilla S., Baron A., *Numerical Modeling of Three-Dimensional Aluminium Flow in Extrusion Dies*, Proc. 7th Int. Al. Extr. Sem., Chicago (Ill.), 2000, Vol. II pp. 203-210.

[Sim98] Simo J.C., Hughes T.J.R., Computational Inelasticity, Springer, 1998.

[Ska96] Skauvik I. et al., *Numerical Simulation in Extrusion Die Design*, Proc. 6th Int. Al. Extr. Sem., Chicago, Illinois, 1996, Vol. II pp. 79-82.

[Stø89] Støren S., Roadman R., Jackobsen Ø., Herberg J., Grasmo G., Solheim K.G., *ALMA, Mathematical modelling of material behaviour in light alloy extrusion*, SINTEF Report STF20 F89073. SINTEF Production Engineering, Trondheim, Norway, 1989.

[Stø91] Støren S., Grasmo G., *Hot extrusion of thin-walled aluminium sections*, MECAMAT'91, Paris, 1991. SINTEF Report STF20 A91105. SINTEF Production Engineering, Trondheim, Norway, 1991.

[Stø92] Støren S., Grasmo G., *High Velocity Extrusion of Thin-Walled Aluminium Sections*, Proc. 5th Int. Al. Extr. Techn. Sem., Chicago (Ill.), 1992, pp. 353-357.

[Stø93] Støren S., *Theory of extrusion – advances and challenges*, Int. J. Mech. Sci. 35, 1993, pp. 1007-1020.

[The92] Thedja W.W., Muller K.B., Ruppin D., *Tribochemical Process on the Die Land Area During Extrusion of AA6063 Alloy*, Proc. 5th Int. Al. Extr. Techn. Sem., Chicago (Ill.), 1992, pp. 467-474.

[Tib96] Tibbets B., Wen J., *Control Framework and Deformation Modeling of Extrusion Processes: An Upper Bound Approach*, Proc. 6th Int. Al. Extr. Techn. Sem., Chicago (Ill.), 1996, Vol. I pp. 375-385.

[Tok88] Tokizawa M., Takatsuji N., *Effects of the Die Condition and Billet Composition on the Characteristics of the Extruded 6063 Aluminium Alloy*, Trans. of the Japanese Institute of Metals 29, 1988, pp. 69-79.

[Tve97] Tverlid S., Modelling of Friction in the Bearing Channel of Dies for Extrusion of Aluminium Sections, Doctoral thesis, Norwegian University of Science and Technology, 1997.

[Uly98] Ulysse P., Johnson R. E., *A study of the effect of the process variables in unsymmetrical single-hole and multi-hole extrusion processes*, Int. J. Mech. Sci. 73, 1998, pp. 213–225.

[Uly99] Ulysse P., *Optimal extrusion die design to achieve flow balance*, Int. J. Machine Tools & Manufacture 39, 1999, pp. 1047–1064.

[Uly02] Ulysse P., *Extrusion die design for flow balance using FE and optimization methods*, Int. J. Mech. Sci. 44, 2002, pp. 319–341.

[Val88] Valberg H., The profile surface formation during the extrusion of metals, Doctoral Thesis, Norwegian Institute of Technology, Trondheim, 1988.

[Val90] Valberg H., *Metal Flow in Direct Axisymmetric Extrusion*, Proc. Int. Conf. Dev. Form. Techn., Lisbon, Portugal, 1990, Vol.2, pp. 1.11-1.38.

[Val92a] Valberg H., *Metal Flow in the Direct Axisymmetric Extrusion of Aluminium*, J. Mater. Process. Technol. 31, 1992, pp. 39 - 55.

[Val92b] Valberg H., Groenseth R.A., *Metal Flow in Direct, Indirect and Porthole Die Extrusion*, Proc. 5th Int. Al. Extr. Techn. Sem., Chicago (Ill.), 1992, Vol.I, pp. 337-357.

[Val93] Valberg H., Hansen A.W., Kovacs R., *Deformation in Hot Extrusion investigated by means of a 3-D Grid Pattern Technique*, Proc. 4th ICTP, Bejing, 1993, Vol.I pp. 637-645.

[Val94] Valberg H., Malvik T., *An Experimental Investigation of the Material Flow inside the Bearing Channel in Aluminium Extrusion*, Int. J. Mat. Prod. Techn. 9, 1994, 4/5/6, pp. 428-463.

[Val96a] Valberg H., Malvik T., *Metal Flow in Die Channels of Extrusion*, Proc. 6th Int. Al. Extr. Techn. Sem., Chicago (Ill.) 1996, Vol.II, pp. 17-28.

[Val96b] Valberg H., Coenen F.P., Kopp R., *Metal Flow in Two-Hole Extrusion*, Proc. 6th Int. Al. Extr. Techn. Sem., Chicago (Ill.), 1996, Vol.II, pp. 113-124.

[Val96c] Valberg H., *A Modified Classification System for Metal Flow Adapted to Unlubricated Hot Extrusion of Aluminum and Aluminum Alloys*, Proc. 6th Int. Al. Extr. Techn. Sem., Chicago (Ill.), 1996, Vol. II, pp. 95-100.

[Wag96] Wagoner R.H., Chenot J.-L., Fundamentals of Metal Forming, Wiley, 1996.

[Wag01] Wagoner R.H., Chenot J.-L., Metal Forming Analysis, Cambridge University Press, 2001.

[Waj05b] Wajda W., Unknown title, Doctoral thesis, Norwegian University of Science and Technology, Trondheim, 2005.

[Wan74] Wanheim T., Bay N., Petersen A.S., Wear 28, 1974, pp. 251-258.

[Wan97] Wang J., Gadala M.S., *Formulation and survey of ALE method in nonlinear solid mechanics*, Finite Elements in Analysis and Design 24, 1997, pp. 253-269.

[Wel96] Welo T., Abtahi S. and Skauvik I., *An Experimental and Numerical Investigation of the Thermo-Mechanical Conditions on the Bearing Surface of Extrusion Dies*, Proc. 6th Int. Al. Extr. Techn. Sem., Chicago (Ill.), 1996, Vol. II pp. 101-106.

[Wil02] Williams A. J., Croft T.N., Cross M., *Computational Modelling of Metal Forming Processes*, Proc. 5th Int. ESAFORM Conf. on Mat. Forming, Krakow, 2002, pp. 67-70.

[Wri98] Wright R.N., Paulson M.S., *Constitutive equation development for high strain deformation processing of aluminum alloys*, J. Mater. Process. Technol. 80–81, 1998, pp. 556–559.

[Wu02] Wu C.-Y., Hsu Y.-C., *Optimal Shape Design of an Extrusion Die Using Polynomial Networks and Genetic Algorithms*, Int. J. Adv. Manuf. Technol. 19, 2002, pp. 79–87.

[Xie95] Xie, J.X., Ikeda K., Murakami T., *UBA analysis of the process of pipe extrusion through a porthole die*, J. Mater. Process. Technol. 49, 1995, pp. 371–385.

[Yan93] Yang W., Lee W.B., Mesoplasticity and its applications, Springer Verlag, 1993.

[Yan00] Yang D.Y., Park K., Lee Y.K., Lee D.H., *3D FE analysis for industrial hollow section extrusion of multiply connected sections using mismatching refinement with domain decomposition*, Proc. of the 6th ICTP, Nuremberg, 1999, Vol III, pp. 1807-1812.

[Yeo01] H.T., Choi Y., Hur K.D., *Analysis and Design of the Prestressed Cold Extrusion Die,* Int. J. Adv. Manuf. Technol. 18, 2001, pp. 54–61.

[Zab00] Zabaras N., Bao Y., Srikanth A., Frazier W.G., *A continuum Lagrangian sensitivity analysis for metal forming processes with applications to die design problems*, Int. J. Numer. Meth. Engng. 48, 2000 pp. 679-720.

[Zas00] Zasadziński J., Libura W., Misiołek W.Z., *Minimal Attainable Wall Thickness in Aluminium Extruded Sections*, Proc. 7th Int. Al. Extr. Techn. Sem., Chicago (Ill.), 2000, Vol. I pp. 365-370.

[Zbi00] Zbib H.M., Diaz de la Rubia T., Rhee M., Hirth J.P., *3D dislocation dynamics: stress-strain behavior and hardening mechanisms in fcc and bcc metals*, Journal of Nuclear Materials 276, 2000, pp. 154-165.

[Zbi02] Zbib H.M., Diaz de la Rubia T., *A multiscale model of plasticity*, Int. J. of Plasticity 18, 2002, pp. 1133–1163.

[Zen44] Zener, C., Hollomon, J.H., *Effect of strain-rate upon plastic flow of steel*. J. Appl. Phys. 15, 1944, pp. 22-32.

[Zie74] Zienkiewicz O.C., Godbole P.N., *Flow of plastic and viscoplastic solids with special reference to extrusion and forming processes*, Int. J. Num. Meths. Eng. 8, 1974, p. 3.

[Zie91] Zienkiewicz O.C., Taylor R.L., *The Finite Element Method*, Fourth Edition, Volume 1 and 2, McGraw-Hill, London, 1991.

[Zha00] Zhang X., Heathcock J., *Modeling of Metal Flow for Bearing Design*, Proc. 7th Int. Al. Extr. Sem., Chicago (Ill.), 2000, Vol. II pp. 169-176.

[Zho03] Zhou J., Li L., Duszczyk J., *3D FEM simulation of the whole cycle of aluminium extrusion throughout the transient state and the steady state using the updated Lagrangian approach*, J. Mater. Process. Technol. 134, 2003, pp. 383–397.

Chapter 3

[CapW] www.capacitec.com

[CpsW] www.capsense.com

[Fos89] Foster R., Linear Capacitive Reactance Sensors for Industrial Applications, Proc. 40th Annual Earth-moving Industry Conference, Peoria, Ill., 1989.

[Kel00] Kelkar A., Strategies for Aluminium in the AutoBody, Presentation May 9 2000, msl1.mit.edu/msl/meeting_05082000/prz_pdf/BIW_2000.pdf.

[Li00] Li Y.Y., Bridgwater J., Prediction of extrusion pressure using an artificial neural network, Powder Technology 108, 2000, pp. 65-73.

[Pap04] Pappalettere C., advances in Experimental Mechanics, McGraw-Hill, 2004.

[Wel04] Welo T., Private communication, 2004

[Woo02] Woodrow A., *The Aluminium Spaceframe and beyond,*Metal Bulletin, 17th Int. Alu. Conf. Presentation, 2002.

Chapter 4

[Bai99] Bailleul G., Albijat S., *Capacitive sensor device for use at high temperature and pressure, including a coaxial cable with integrated end portion*, US Patent 5,892,365, 1999.

[Ban72] Banerji A., Rice W.B., *Experimental Determination of Normal Pressure and Friction Stress in Roll Gap during Cold Rolling*, CIRP Ann., 1972, pp. 53-54.

[Bax97] Baxter L.K., *Capacitive Sensors – Design and Applications*, IEEE Press, New York, 1997.

[Boc98] Bock W.J., Eftimov T.A. and Wisniewski R., *A differential fibre optic transducer for hydrostatic pressure measurement*, Sensors and Actuators A 70, 1998, pp. 238-242.

[Bri86] Britten D., Jeswiet J., *A Sensor for Measuring Normal Forces with Through and Transverse Friction Forces in the Roll Gap*, Trans. of SME/NAMRI 14, 1986, pp. 355-358.

[Bus99] Busch W., *Extrusion technology - On-line control of profile geometry by an optical coordinate measurement technique*, Aluminium. 75, no. 6, 1999, pp. 508-512.

[Cla01] Clarck P., Boriniski J., Gunther M. and Poland S., *Modern fibre optic sensors*, Smart Materials Bulletin, June 2001, pp. 8-11

[Cva99] Cvahte P., Dragojevic, V., Fajfar P., Rodič T., *Measurement of forces during extrusion and drawing of Al rods*, Kovine Zlitine Tehnologije, 33 (3-4), 1999, pp. 249-252.

[Dan71] Daneshi G.H., Hawkyard J.B., *A split-platen pressure cell for the measurement of pressure distribution in upsetting operations*, Int. J. Mech. Sci. 13, 1971, pp. 355-371.

[Del02] Dellah A., Wild P.M., Moore T.N., Shalaby M., Jeswiet J., *An Embedded Friction Sensor Based on a Strain-Gauged Diaphragm*, J. Manuf. Sci. Eng. 124, 2002, pp. 523-527.

[Du99] Du H., Klamecki B.E., *Force Sensors Embedded in Surfaces for Manufacturing and Other Tribological Process Monitoring*, ASME J. Manuf. Sci. Eng. 121, 1999, pp. 739-748.

[Fra96] Fraden J., Handbook of Modern Sensors 2nd ed., Springer-Verlag, New York, 1996.

[Gan04] Gangopadhyay T.K., *Non-contact vibration measurement based on an extrinsic Fabry-Perot interferometer implemented using arrays of single-mode fibres*, Meas. Sci. Technol. 15, 2004, pp. 911-917.

[Gar94] Gardner, J.W., Microsensors, Wiley, Chichester, 1994.

[Gra00] Grattan, K.T.V., Sun D.T., *Fiber optic sensor technology: an overview*, Sensors and actuators, 2000, pp. 40-61.

[Han92] Hansen, A.W, Valberg H., Welo T., Temperatursensor – Måling av kontakt-spenninger ved stukeprøving av sylinder, Project Memo (200523.01) 1992-07-13. SINTEF Materials Technology.

[Han93] Hansen A.W., Valberg H., Welo T., *A technique for measuring the pressure on the tool surface*, Proc. 4th Int. Conf. Technology of Plasticity, Bejing, 1993, Vol. I pp. 303-308.

[Han96] Hansen A.W., Valberg H., *Accurate Measurements Inside the Tool in Hot Working of Metals*, Proc. 6th Int. Al. Extr. Techn. Sem., Chicago, Illinois, 1996, Vol. II, pp. 11-15.

[Has99] Hasegawa K., Murata M., *Extrusion with changing closs section shape of tube*, Proc. of the 6th ICTP, Nuremberg, 1999, Vol I, pp. 677-680.

[Hat88] Hatamura Y., Yoneyama T., *Measurement of Actual Stress and Temperature on a Roll Surface during Rolling*, JSME Int. J. 31, 1988, pp. 465-469.

[Hum96] Hum B., Colquhoun H.W., Lenard J.G., *Measurements of friction during hot rolling of aluminum strips*, J. Mater Process. Technol. 60, 1996, pp. 331-338.

[Jes82] Jeswiet J., Rice W.B., *The Design of a Sensor for Measuring Normal Pressure and Friction Stress in the Roll Gap During Cold Rolling*, Transactions of SME/NAMRI 10, 1982, pp. 130-134.

[Jes93] Jeswiet J., Nyahumwa C., *A sensor for measuring metal deformation interface forces*, J. Mater. Process. Techol. 39, 1993, pp. 251-268.

[Jes95] Jeswiet J., *Aspect ratio, friction forces and normal forces in strip rolling*, J. Mater. Process. Technol. 53, 1995, pp. 846-856.

[Jes98] Jeswiet J., *A comparison of friction coefficients in cold rolling*, J. Mater. Process. Technol. 80-81, 1998, pp. 239-244.

[Kau03] Kaufmann K.R, Wavering T., Morrow D., Davis J. and Lieber R.L., *Performance characteristics of a pressure microsensor*, J. Biomechanics 36, 2003, pp. 283-287.

[Kim98] Kim Y.-T., Ikeda K., Murakami T., Nishimura K., *Pressure Distribution on Die in Porthole Die Extrusion*, Proc. 1998 Jap. Spring Conf. Technol. Plasticity, 1998, Osaka.

[Kim99] Kim Y.-T., Ikeda K., Murakami T., *Measurement of pressure distribution on dies in porthole die extrusion*, J. Jpn. Inst. Light Met. 49, 1999, pp. 296-301.

[KisW] www.kistler.com

[Koj96] Kojima Y., Kohga T., Mizuno T., Mizuno T., *Measurement of Contact Pressure in Experiment with Plasticine*, J. JSTP 37 (428), 1996, p. 951.

[KopW] Kopp R., Neudenberger D., Winning G., *Different concepts of thixoforging and experimentss for rheological data*, www.rwth-aachen.de/sfb289.

[Kot97] Kotera H., Shima S., Takayama R., Kanno I., Hirai F., Moriyama Y., *Development of Pressure Micro Sensor of ZnO Thin Film*, Proc. Jap. Spring Conf. Technol. Plasticity, 1997, Tokyo.

[Lee03] Lee B., *Review of the present status of optical fibre sensors*, Optical Fiber Technology 9, 2003, pp. 57-79.

[Len91] Lenard J.G., *Measurement of friction in cold flat rolling*, J. Mater. Shaping Technol. 9, 1991, pp. 171-180.

[Len93] Lenard J.G., Malinowski Z., *Measurement of friction during the warm rolling of aluminium*, J. Mater. Process. Technol. 3-4, 1993, pp. 357-371.

[Lor00] Di Lorenzo R.A., Filice L., Micari F., *Analysis of pressure distribution on the die in cold extrusion operations*, Wire. 50, 2000, pp. 36-39.

[Lfw92] Laser Focus World, *Virginia reasearchers work on sapphire-based sensors for high temperature (1600C) applications*, June 1992, p. 18.

[Li92] Li M., Klamecki B.E., Weinmann K.J., *SN-Gauge and Instrumented Pin: Devices to Measure Shear and Normal Tool Forces in Sheet Metal Forming*, Transactions of SME/NAMRI 20, 1992, pp. 103-107.

[Liu01] Liu Y.J., Tieu A.K., Wang D.D., Yuen W.Y.D., *Friction measurement in cold rolling*, J. Mater. Process. Technol. 111, 2001, pp. 142-145.

[Luc98] Luck R., Agba E.I., *On the design of piezoelectric sensors and actuators*, ISA Trans. 37, 1998, pp. 65-72.

[Mor84] Mori K., Osakada K., Fukada M., Measurement of Contact Pressure in Metal Forming by Pressure Sensitive Film, J. Eng. Materials and Techn. 106, 1984, pp. 127-131.

[Mor99] Mori T., Takatsuji N., Matsuki K., Murotani K., Aida T., Uetoko K., *Measurement of Pressure Distribution on Die Surface in Hot Extrusion, Study of Pressure Distribution on Die Surface and Metal Flow in Hot Extrusion*, Proc. 50th Jap. Conf. Technol. Plasticity, 1999, Fukuoka.

[Mor00] Mori T., Takatsuji N., Matsuki K., Murotani K., Aida T., Uetoko K., *Study of Pressure Distribution on Die Surface and Metal Flow in Hot Extrusion*, Proc. 51st Jap. Conf. Technol. Plasticity, 2000, Ichinoseki.

[Mor01a] Mori T., Takatsuji N., Matsuki K., Murotani K., Aida T., Uetoko K., *Measurement of Pressure Distribution on Die Surface on Hot Extrusion of Aluminium Alloy*, Proc. 52nd Jap. Conf. Technol. Plasticity, 2001, Fukui.

[Mor01b] Mori T., Takatsuji N., Matsuki K., Murotani K., Aida T.,Uetoko K., *A Study of Measurement of Extrusion Die Deformation in Aluminium Hot Extrusion*, Proc. 52nd Jap. Conf. Technol. Plasticity, 2001, Fukui.

[Mor01c] Mori T., Takatsuji N., Matsuki K., Aida T., Murotani K., Uetoko K., *Measurement of Pressure Distribution on Die Surface in Hot Extrusion of Pure Aluminium Rod – A study of Deformation of Extrusion Die in Aluminium Hot Extrusion I*, J. JSTP 42 (489), 2001, pp. 1080-1084.

[Mor02a] Mori T., Takatsuji N., Matsuki K., Aida T., Murotani K., Uetoko K., *Measurement of Deformation of Extrusion Die in Hot Extrusion of Aluminium – Deformation of Extrusion Die in Aluminium Hot Extrusion II*, J. JSTP 43 (501), 2002, pp. 968-972.

[Mor02b] Mori T., Takatsuji N., Matsuki K., Aida T., Murotani K., Uetoko K., *Measurement of pressure distribution on die Surface in hot extrusion of 1050 aluminium rod*, J. Mater. Process. Technol. 130-131, 2002, pp. 421–425.

[Mor03] Mori T., Takatsuji N., Matsuki K., Aida T., Murotani K., Uetoko K., *Measurement of Pressure on Die Surface and Deformation of Extrusion Die to Hot Extrusion of Plate and H-shape – Deformation of Extrusion Die in Aluminium Hot Extrusion III*, J. JSTP 44 (507), 2003, Part 4 pp. 452-456.

[Nya91] Nyahumwa C., Jeswiet J., van Lutterwelt C. A., Friction Sensor for Sheet Metal Rolling, CIRP Ann. 40 No. 1, 1991.

[Nya93] Nyahumwa C., Jeswiet J., *A Sensor for Measuring Metal Deformation Interface Forces*, J. Mater. Process. Technol. 39., 1993, pp. 251-268.

[Nya96] Nyahumwa C., *The evolution of a cantilever sensor to measure normal and frictional forces in the roll gap during cold rolling*, J. Mater. Process. Technol. 39, 1996, pp. 251-268.

[OmeW] www.omega.com/literature/transactions/volume3/trantocvol3.html

[Pin96] Pinto G.A., Lawhite L.E., Eggleston G., Carr R.B., Frusztajer B.B., Capacitive melt pressure measurement with center mounted electrode post, US Patent 5,492,016, 1996.

[Pla96] Plancak M., Bramley A.N., Osman F.H., *Some observations on contact measurement by pin load cell in bulk metal forming*, J. Mater. Process. Technol. 60, 1996, pp. 339-342.

[Roy57] van Royen G.T., Backofen W.A., *Friction in Cold Rolling*, J. Iron Steel Inst., 186, 1957, pp. 235-244.

[Roy60] van Royen G.T., Backofen W.A., A Study of Interface Friction in Plastic Compression, Int. J. Mech. Sci. 1, 1960, pp. 1-27.

[Rao02] Rao Y.J. et al., Simulataneous strain and temperature measurement of advanced 3-D braided composite materials using an improved EFPI/FBG system, Optics and Lasers in Engineering 38, 2002, pp. 557-566.

[Ras97] Rastogi P.K., Optical Measurement Techniques and Applications, Artech House, Norwood (MA), 1997.

[Rus03] Russell B.D., Lasenby J., Blackburn S., Wilson D.I., *Characterising paste extrusion behaviour by signal processing of pressure sensor data*, Powder Technology 132, 2003, pp. 233– 248.

[Sal73] Al-Salehi F.A.R., Firbank T.C., Lancaster P.R., *An experimental determination of the roll pressure distributions in cold rolling*, Int. J. Mech. Sci. 15, 1973, pp. 693-710.

[Sa97] de Sa A., Electronics for Scientists – Physical Principles with Applications to Instrumentation, Prentice Hall, 1997.

[Sat02] Sato M., Nishimura, K., Murakami T., Ikeda K., *Measurement of Pressure Distribution on Tool Surfaces of 3-D Backward Extrusion*, Proc. Jap. Spring Conf. Technol. Plasticity, 2002, Chiba, pp. 926.

[Seb02] Sebastian J.R., Stubbs D.A., Dutton R.E., *High temperature piezoelectric sensor*, US Patent Application Publication, US 2002/0043898, Apr. 18, 2002.

[Sch83] Schey J.A., Tribology in Metal Working, ASM, 1983, pp. 204-224.

[Shi97] Shida S, Hasegawa H., Komatsu Y., *Measurement of Contact Pressure between Rolls by Pressure Measuring Films*, Proc. Jap. Spring Conf. Technol. Plasticity, 1997, Tokyo.

[Sie33] Siebel E., Lueg W., *Üntersuchungen über die Spannungsverteilung im Walzspalt*, Mitt. KWI, no. 15, 1933, pp. 1-15.

[Tan03] Tan X., Bay N., Zhang W., *Friction measurement and modelling in forward rod extrusion tests*, J. Eng. Tribology 217, 2003, pp. 71-82.

[Tat02] Takashi Tatsukawa T., Morinaga K., Shida S., *Measurement of Contact Pressure Distribution between Rolling Rolls Using Pressure Measuring Film*, J. JSTP 43 (496), 2002, p. 46.

[Tie02] Tieu A.K., Jiang Z.Y., Lu C., *A 3D finite element analysis of the hot rolling of strip with lubrication*, J. Mater. Process. Technol. 125-126, 2002, pp. 638-644.

[Ton02] Tong K.K.S., Hu B.H., Niu X.P., Pinwill I., Cavity pressure measurements and process monitoring for magnesium die casting of thin-wall hand-phone component to improve quality, J. Mater. Process. Technol. 127, 2002, pp. 238-241.

[TubW] www.tu-berlin.de/fak3/wewi/metallische_werkstoffe/html_ger/Forschung

[Wei96] Weinmann K.J., Kernosky S.K., *Friction studies in sheet metal forming based on a unique die shoulder force transducer*, CIRP Ann. 45, 1996, pp. 269-272.

[Yon87] Yoneyama T., Hatamura Y., *Development of a die-sensor*. JSME Int. 30(262) 1987, pp. 670-677.

[Yon89] Yoneyama T., Hatamura Y., *Measurement of Actual Stress and Temperature on a Roll Surface during Rolling*, JSME Int. J. 32, 1989, pp. 113-117.

[Yon93] Yoneyama T., Kitagawa M., *Measurement of the contacting stress in extrusion*, Proc. 4th ICTP, Bejing, 1993, Vol II pp. 553-558.

[Yon94] Yoneyama T., Hatamura Y. et al, *Development of a pressure sensor using an optical fiber sensor*, J. JSTP no 35, 1994, pp. 158-163.

[Yon95] Yoneyama T., Takatsuka K., Kitigawa M., Hatamura Y., *Measurement of the Contact Pressure in Aluminum Hot Extrusion*, J. JSTP, 36 (419), 1995, pp. 1397-1402.

[Yon99a] Yoneyama T., *Development of a new pressure sensor and its application to the measurement of contacting stress in extrusion*, J. Mater. Process. Technol., 95, 1999, pp. 71-77.

[Yon99b] Yoneyama T., Yamada M., Yamada T., *Measurement of pressure and frictional stress on the roll surface during mandrel mill rolling*, Proc. 6th ICTP, Nuremberg, 1999, Vol II, pp. 1575-1580.

[Zha04] Zhao Y., Liao Y., *Discrimination methods and demodulation techniques for Fibre-Bragg grating sensors*, Optics and Lasers in Eng. 41, 2004, pp. 1-18.

[ZhaX] Zhao Y., Yu C., Liao Y., *Differential FBG sensor for temperature-compensated high-pressure (or displacement) measurement*, Optics & Laser Technology, In press.

Chapter 5

[Cap97] Capacitec Inc., Non-contact displacement standard products catalogue, Ayer, Mass. 1997.

[Cap98] Capacitec Inc., Operation / Maintenance Manual for Series 4000 Capacitec Amplifiers and Rack Accessories, Ayer, Mass. 1998.

[Chr00] Chari M.V.K, Salon S.J., Numerical Methods in Electromagnetism, Academic Press, 2000.

[Lan99] Lange H.I. and Hansen A.W., DieOpt '98: Deflection and deformation of extrusion tools – instrumentation and measurements, Report STF24 F98349, SINTEF Materials Technology.

[Lan00] Lange H. I., Måling av bevegelse av dor og skive under ekstrudering av et aluminium rørprofil, SINTEF Project Memo (424505.24) 2000-08-28.

[Lan01] Lange H.I., Plan for extrusion trials at HAP/Raufoss (P22) of deep U-profile (ALP5202), SINTEF Project Memo (240557) 2001-11-21.

[Lan02a] Lange H. I., Instrumented tube extrusions of Aluminium (AA6082) with focus on strain measurements, Report STF F24, SINTEF Materials Technology, Trondheim, Norway.

[Lan02b] Lange H.I., ALP5202 instrumented die trials at P22/HAP, November 2001, SINTEF Project Memo (240557.03) 2002-04-04.

[Lan02c] Lange H.I., ALP5202 instrumented die trials at P22/HAP, August 2002, SINTEF Project Memo (240557.12) 2002-09-17.

[Lef01] Lefstad M., Verktøy for pressing av skinne med trykksensorer og termoelementer. Prosjekt: Compform – ekstrudering. SINTEF Project Memo (242791.10) 2001-09-28.

[Lef02b] Lefstad M., Laboratorieforsøk utført i november 2001 med esktrudering av skinne der trykk-sensorer og termoelementer innsatt i verktøyet. Prosjekt: Compform ekstrudering, SINTEF Project Memo (242791.10) 2002.01.23.

[Nil02] Nilsen R. (Professor, Norwegian University of Science and Technology), Private communication, 2002.

[Sva89] Svaasand L.O., Elektrisitet og Magnetisme Vol I and II 6th print, Tapir trykk 1989.

[UddW] www.uddeholm.com/utab/pdf/facts/orvar_supreme english_020602.pdf

[Wag01] Wagener H.W. and Wendenburg A., Analysis system Prerequisite for automation in metal forming technology. J. Mater. Process. Technol. 116, 2001, pp 55-61.

APPENDICES

Comments

There are thirteen appendices, of which twelve contain full journal articles and papers presented at conferences. The last appendix describes a conference paper which is being prepared when this thesis is printed. It presents a possible and necessary next step in the work. The papers of Appendices K and L have been added to the thesis after it was first submitted to the committee. Appendix K provides information on the very last set of experiments that the candidate took part in. Capacitive pressure sensors were used. The experiments were run in December 2004 as a part of the PhD work of one of the candidate's colleagues, Wojciech Wajda. His work relates mainly to modelling of thin-strip extrusion and the use of the pressure sensor data. The candidate contributed both during the design work (mainly in relation to sensor design) and during experiment and analysis. He also wrote the full paper. The conference paper of Appendix L provides additional information about the temperature distribution in the billet after induction heating and before the billet is loaded into the press and extruded.

Most of the articles have been written in cooperation with co-workers at NTNU and SINTEF Materials and Chemistry. In Chapter 5 of Volume I of this thesis the roles of the various participants have partly been described, and the tasks have been related to specific research projects. As often is the case in relation to research and development work, it may be difficult and even unnatural to evaluate the contributions of individuals. Progress in research is often the result of the synergetic effects of human interaction. The sensor development task has required that participants with different backgrounds work closely together. However, the committee evaluating the work of the candidate has the right to receive information about the exact nature of the work of the candidate and co-workers. A specification of the tasks performed by the candidate in relation to all publications is given below.

Appendix A:
The paper contains the first analysis of capacitive pressure sensor design and testing, the main responsibilities of the candidate. He has planned and performed experiments, and he has analysed the results. He has also run the simulations and written the paper. Professor Støren has been a supervisor and reviewed the work. In addition, he has initiated the PhD-study and proposed the use of capacitive measurements. All sensor designs have been developed by the candidate.

Appendix B:
The candidate has planned and performed experiments and analysed results. He has also contributed to the design of the die, mainly the pressure sensor design. He has run all simulations and written most of the paper. Dr. Lefstad and Flatval have overseen the machining of the die and designed the details related to temperature sensors. They also took an active part in the experiments. The role of Prof. Støren was the same as for the paper of Appendix B and all other papers.

Appendix C:
The role of the candidate was as in the previous paper. Lange and Hansen contributed to the planning and played a significant role during experiments. They were also mainly responsible for the work related to strain gauges and displacement transducers. The overall design of the die was performed by Hydro, but all authors contributed to modifications. Lange and Hansen were mainly responsible for the contact with the die manufacturer. Wajda acted as a consultant and performed 3D simulations with Forge3.

Appendix D:
Experiments were planned and the die was designed by all participants of the NTNU and SINTEF group. The candidate took an active part in both planning and experiments and contributed significantly to the writing of the article. The experiments were what may be regarded as screening experiments for Wajda's PhD work. He performed most of the profile shape and dimension measurements and wrote the first draft. Abtahi has performed the three-dimensional flow simulation by Extrud3D.

Appendix E:
Appendix E presents the results of a further elaboration of the material presented in Appendices A and B. In addition, an analytical direct and inverse model for the pressure build-up in very long bearing channels has been added. The model has been developed solely by the candidate. He has written the entire journal article.

Appendix F:
The paper of Appendix F makes use of data from the candidate's experiments. The use of response surfaces to evaluate material data in extrusion is a concept that he also has worked out independently. It was first used in relation to analytical calculations in Appendix E. A Fortran script for running inverse simulations has been made by Wajda, but the guidelines were determined by the candidate. He wrote both the paper draft and the final paper. Abtahi's contribution to this specific work was negligible.

Appendix G:
The paper is a piece of independent work by the candidate and was performed to test the ANSYS induction heating simulation. A check of the code was performed (but has still not been reported) by using old experimental data from induction heating of steel pipes obtained from a third party.

Appendix H:
The paper presents a more thorough evaluation of the approach presented in Appendix F. Some initial errors related to temperature data from simulation were removed. The article has been written by the candidate. The data from his rod extrusion experiments were used, and he has also worked out most of the figures. Wajda's Fortran-script was used to assess the sensitivities. Prof. Pietrzyk has carefully reviewed and edited the paper. Dr. Szeliga and Madej have performed standard compression material testing and inverse analysis for AA6060. Wajda has further analysed the material data and has introduced the information into the response surface plots. He has also implemented a simplex routine for optimization, but it has not been assessed in the paper.

Appendix I:
The text is an independent piece of work by the candidate. He has worked out the script for the ANSYS simulations, coupled the die simulation to flow simulation by ALMA, evaluated results and written the article.

Appendix J:
The article has been written by the candidate. He has also proposed the specific concept for intelligent dies, but the issue has been thoroughly discussed with Prof. Støren. The concept is in many ways similar to the control system Prof. Støren has requested. Profile shape measurement by laser triangulation is a task that was originally proposed by Prof. Støren. Couweleers has evaluated the measurement concept and reported on a number of appropriate measurement techniques. The candidate was the main initiative taker in relation to the experimental testing to determine if laser triangulation measurement was at all feasible, and he has contributed during the preparations. Experiments were run in cooperation with Wajda and Couweleers. The data from optical measurements were analysed mainly by the latter. The evaluation of the thermo-mechanical behaviour of the new insert pressure sensor design has been performed by the candidate.

Appendix K:
The paper has mainly been written by the candidate. He performed a pre-study and optimization of sensor design (Appendix J). The die and sensor concepts were then worked out in close cooperation with both Flatval and Wajda, the latter later performed independent calculations in order to check data. Wajda also performed flow calculations so that the loads could be more accurately determined. The manufacture of the die has been overseen mainly by Wajda and Flatval. Assembly, compression and extrusion experiments were performed by all authors apart from Prof. Støren. The candidate then assisted in the subsequent analysis of data. The calibration method used earlier by the candidate was used. Wajda performed all measurements of profile dimensions and made most of the figures. The work is a part of Wajda's PhD study, which focuses more on the use of data from sensors and on the modelling of flow instability. The main reason for presenting the article in this work is to show yet another application of the capacitive pressure measurement technique. It is important to note that the development of sensors is an iterative task.

Appendix L:
The paper is an independent piece of work by the candidate. The experimental data have been adopted from a work of Dr. Lefstad and Flatval referenced in the text.

No paper has been written on industrial experiments, which constituted an important part of the study. As indicated in Chapter 5 a report has been written by H.I. Lange, and this thesis presents the main conclusions. The candidate performed the following tasks. He designed the pressure sensors and calculated calibration factors. He took part in all project meetings and in the planning of the experiments. He also mounted and tested the sensors prior to extrusion in cooperation with Lange. Other important preparations were also carried out. During the actual experiments he was partly responsible for logging and mounting of the die in the press. Finally, he analysed pressure measurement results.

Appendix A

Moe P.T., Strøen S.

A Technique for Measuring Pressure on the Die Face during Extrusion

Paper in Proceedings

5th ESAFORM Conference on Material Forming
April 20, Krakow, pp 463-466

A technique for measuring pressure on the die face during extrusion

P.T. Moe, S. Støren

Department of Machine Design and Materials Technology, The Norwegian University of Science and Technology – Richard Birkelandsvei 2B, 7491 Trondheim, Norway
e-mail:Per.T.Moe@Immtek.ntnu.no; Sigurd.Storen@Immtek.ntnu.no

ABSTRACT AND CONCLUSION: The article evaluates designs for sensors capable of measuring pressure applied to the upper face of aluminium extrusion dies. The technique chosen is that of measuring the deflection of a plate relative to some point to which a capacitive probe has been fastened. Typical maximum deflections are about 20-30 microns, corresponding to a pressure of 200-500 MPa when the sensor is properly tuned. Measurement of pressure on the die during rod extrusion has been chosen as a first test case. By a simple but effective general calibration method variability can be reduced significantly, and it seems probable that measurements can be undertaken with an accuracy of about ±10 MPa and a resolution of less than ±3 MPa. In such a case particular attention must be paid to transient thermal fields and localized heating of the plate, which will cause an additional sensor plate bending of some 10 % of maximum deflection.

Key words: Hot extrusion, aluminium, die, pressure measurement, capacitive sensors

1 INTRODUCTION

As extruded aluminium profiles are getting into more widespread use, focus is on reduction of shape variability. The implementation of a complete and predictive extrusion theory in simulation tools is regarded as an essential step towards better product quality as it will increase understanding of the interaction between die deflection, flow stability and shape. Yet, modelling must be complemented by appropriate techniques of measurement. Useful tools in a shape sensitivity study would be sensors able to determine local values of pressure on the die face and to quantify the forces of interaction between die, billet and container. Sensor design, testing with easily analysable die geometry and the establishment of methods of calibration are then the natural tasks.

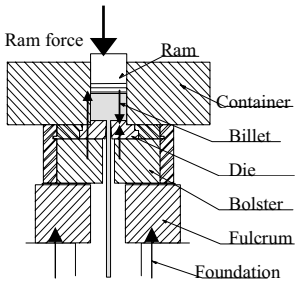

Fig. 1. Experimental 8 MN vertical extrusion press used

2 SENSOR DESIGN

2.1 Choice of measurement principle

Pressure measurement in materials forming has been an active field of research for years. A number of approaches have been followed [1,2]. Apart from the popular piezoresistive sensors, which relate stress directly to changes in resistivity, the most common methods are related to the conversion of pressure to relative displacement by some kind of an elastically deforming element such as a plate or a bellow. This allows the use of standard displacement transducers such as optical, inductive or capacitive ones. A technique also tested is the direct measurement of some strained element by strain gages. Capacitive sensors as well as Fabry-Perot optical sensors are probably the most interesting ones due to their small size and their functionality above 400°C. Capacitive sensors also display very small sensitivity to the expected sudden changes in temperature (40-80°C) and are ideal for the measuring ranges in question.

The principle of capacitive deflection measurement is merely that the reactance, $1/C=L/\varepsilon A$, of a properly designed flat plate capacitive circuit element is proportional to the distance, L, between the plates. In the case of measurement of displacement, one

capacitor plate (area A) is a part of the sensing probe while the other, being connected to earth, is a part of the deflecting construction. The separating medium is air whose dielectric coefficient ε will depend to a certain extent on temperature. A range of techniques for applying and assessing signals exists. The evaluation of high frequency signals (15.625kHz) by synchronous demodulation is normally regarded as the best with respect to noise.

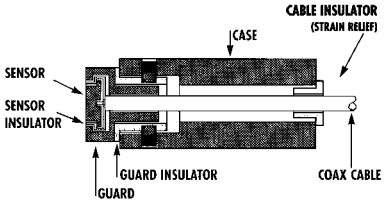

Fig. 2. The Capacitec capacitive probe used in experiments

Some characteristics of capacitive sensor equipment provided by Capacitec [3] are shown in table 1 and the design of a high temperature probe is displayed in figure 1. Small size is favoured as the sensitivity of the probe is inversely proportional to its size.

Table1. Sensor characteristics – Capacitec HPC-75A-V-N3

Property	Data
Typical calibration range	0 – 10V = 0 – 500 µm
Linearity	±0.2% of Full Scale = ±1 µm
Repeatability	±0.01% of FS = ±0.05 µm
Resolution	±0.01% of FS = ±0.05 µm
Max temperature	825°C
Temperature sensitivity 450°C	-0.2-0.3 µm/10°C

2.2 Evaluation of pressure sensor design

A die face pressure sensor design must fulfil certain requirements if the sensor is to be useful. Accuracy should be better than ±10 MPa and the resolution below ±3 MPa. Accuracy is mainly related to proper calibration procedures and the necessity of such while resolution mainly relates to table 1. Some further semi-quantifiable criteria are given in table 2.

Table2. Design criteria

Design criteria	Comment
Optimised form	Max deflection/stress-ratio
Low shear stress sensitivity	If shear not also measured
Small size	To be placed in narrow spaces
Local pressure measurement	From 2-15 mm diameter
Low die deflection sensitivity	Only to respond to direct load
Low temperature sensitivity	Preferably < 10 % of FS
Robustness	To stand industrial handling
Easy to mount/dismantle	Or proper permanent solution
Accurate and proper fitting	Not to loosen and move
Easy to manufacture	Low cost and accurately
To fit standard C-sensors	If special order not made
Easy to analyse	Minimum of assumptions
Easy to calibrate	Simple relevant test preferable

There is probably no optimal sensor solution, but specific design categories can be evaluated (table 3).

Table3. Sensor design evaluation and categories

Permanently fixed sensor	**Demountable sensor**
Technically preferable	Less expensive for repeated use
Insert into the die	**Integrated in die design**
Al may penetrate into crevices	Most robust
Height difference in surface	Difficult to check geometry
More difficult optimisation	More easily analysable
Insert from bottom face	**Insert from top face**
Shear causes much tilting	Locked in place by press rest
Standard calibration easier	Danger of unwanted pull out
Small force applied to sensor	Difficult to dismantle

Figure 3 displays some possible practical design solutions, of which most have been tested in hot compression and found more or less satisfactory.

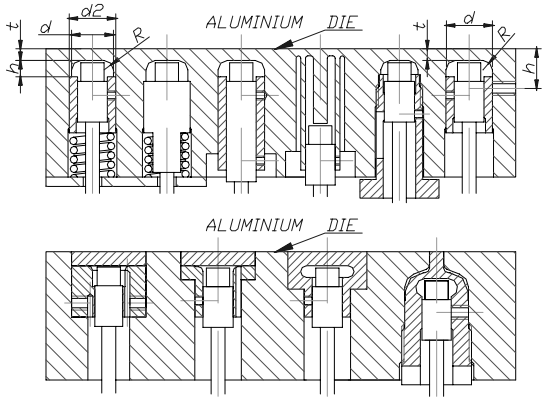

Fig.3. Examples of the sensor as an integrated part of the die and as an insert. Sensors are demountable.

Sensor design optimisation consists of maximising elastic plate deflection for parameters like plate thickness, t, upper edge radius R, hole diameter d and fastening point, h, and taking into account practical design limitations. Figures 4 present values of equivalent stress and deflection assuming elastic behaviour and R=3mm. For a maximum value of 800 MPa, the deflection is about 35 µm, which is a non-conservative value as the load is applied only locally. In the relevant range there is not one optimum, but rather some optimal combination of d and t. As the plate is thick and shearing is limiting, most is gained by increasing R or h.

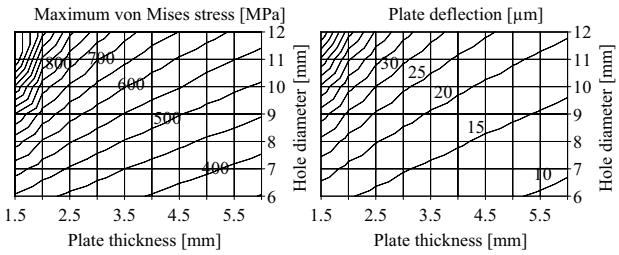

Fig. 4. Deflection and stress for rightmost sensor of figure 3 - E=180GPa, load of p=250MPa over an area of diameter 35mm

3 THE EXPERIMENTAL APPROACH

3.1 The experimental set up and parameters

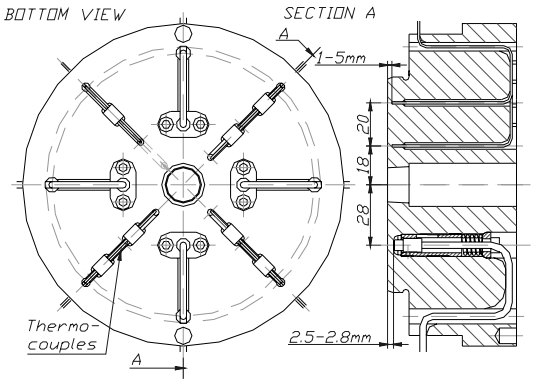

Fig. 5. Simple die geometry – rod extrusion

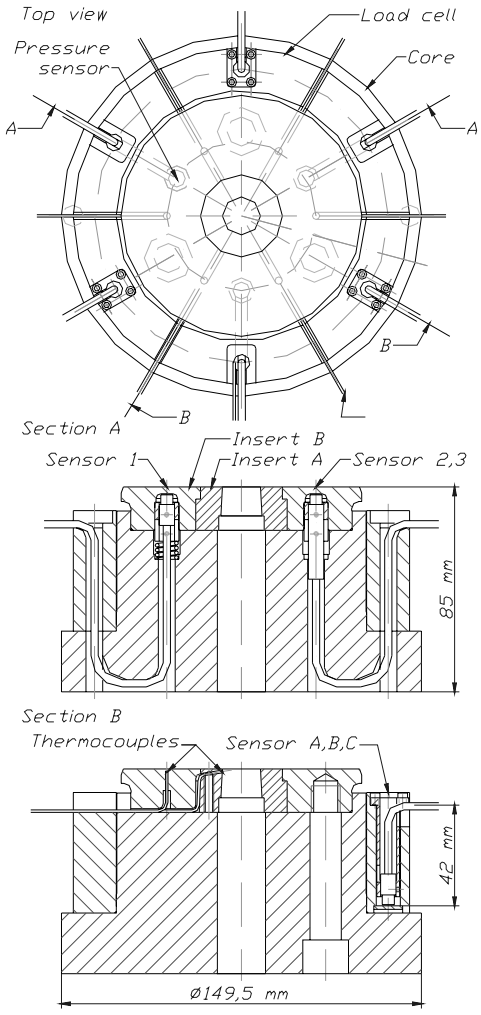

Fig. 6. Complex die geometry – rod extrusion

Experiments were performed at an 8 MN vertical experimental press as shown in figure 1. As focus was on determining the feasibility of measurement and on testing out sensor solutions, the most easily analysable case was chosen. Rod extrusion presents itself as the one best described by 2D simulation, and if sensors are properly placed on the die surface, results should directly indicate the forces at work. A further advantage is that a number of sensors and thermocouples may be placed in virtually the same position, simplifying replication. Figure 5 and 6 display die geometries and sensor solutions tested. As experiments with the two provided quite similar results, only those of the complex die geometry are treated. The die inserts used had zero bearing outlet geometry. Three die face pressure sensors were used. Of these, one probe was locked in position by a spring while the other were fastened by set screws. Replicate measurements were undertaken also by demounting the equipment and switching positions of the last two probes. Table 4 presents process data.

Table4. Data (Levels in bold presented in this paper)

Parameter	Value	Variation
Alloy	**6060.35**	
Press/extrusion ratios	**40**, 80 (**15.8**,11.2 mm)	±0.02 mm
Outlet velocities	200, **400**, 800 mm/s	±4 mm/s
Billet temperature	**450**, 500 °C	±5 °C
Billet dimensions	**Ø96x200** mm	±1 mm
Butt end (not removed)	**19** mm	±0.5 mm
Bolster temperature	**480** °C (Die <435 °C)	±2 °C
Container temperature	**430** °C	±2 °C
Ram temperature	**130** °C	±5 °C
Cycle period	**10** min	±1 min

A load cell for measuring the part of the load distributed by shear to liner and solely into the die was devised for the complex die. Capacitive probes sense the compression of a 42 mm high ring. The naive approach indicates that an upper limit to deflection at 1 MN load would be about 36 µm. In site calibration yields a value of about 30 µm which corresponds well with a detailed FEM analysis.

3.2 Results and discussion

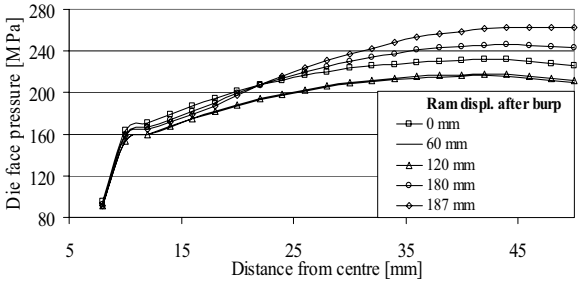

Fig. 7. The pressure distribution on the die face by Alma

A theoretical estimate of the pressure on the die face has been established by the extrusion code Alma [4] using a modified Zener-Hollomon model. Material parameters have earlier been obtained by hot torsion

testing. At the outlet an artificial bearing of 0.5mm was added in order to make calculation feasible, a further 1mm alters ram force by 1%. Alma and the material model have earlier been tested extensively, and results have been found to correspond well with measurements. The pressure distribution of figure 7 reveals that pressure is high in the very beginning and particularly in the end of the extrusion charge when the radial pressure build up is significant as the flow direction is mainly radial. Factors relating the pressure distribution to deflection have been calculated by FEM for the relevant load and geometry. Variability makes the method inaccurate.

Table5. Indirect (solely by FEM) calibration problems

Assumptions that not always will hold
Displacement-voltage calibration correct for test temperature
Displacement-voltage calibration correct for sensor geometry
Determination of sensor dimensional variability exact / easy
Correction due to sensor non-linearity can be applied
The maximum relevant plate deflection is actually measured
The details of mounting do not influence on results

Table6. Deflection sensitivity [µm] to sensor shape

	R=2		R=3	
	t=2.5	t=3	t=2.5	t=3
d=8	23.6	19.4	20.2	18.1
d=9	27.3	23.4	24.5	21.6

For d and t dimensional variability should be well below 0.05 mm, so this aspect is probably mostly related to R and h. A direct and simple method of calibration, consisting of plugging the outlet and undertaking hydrostatic compression in-site, was performed. The billet height used is of smaller importance as the static friction stress is low, but calibration must be undertaken under stationary relevant thermal conditions. Figure 8 indicates that mounting is an important source of variability.

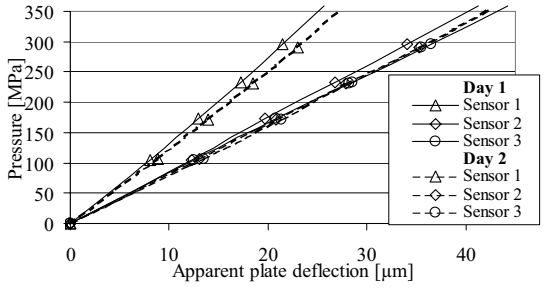

Fig. 8. Calibration curves obtained by hydrostatic compression

The limiting accuracy of force measurement is about ±50kN or 6 MPa. A plate bending effect of 1µm due to transient thermal state and thermal expansion is not taken into account in calibration. Yet, figures 9 and 10 show that reduction of variability due to calibration is significant (±15% to ±5%), and that different sensor design actually yield similar results.

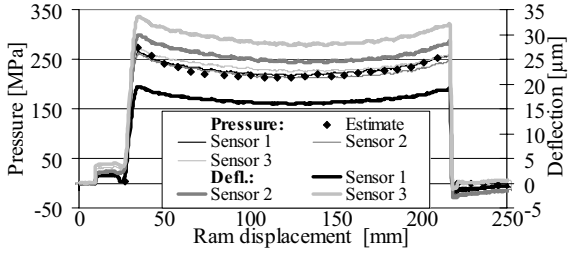

Fig. 9. Effect of calibration - run #1-2 - all sensors

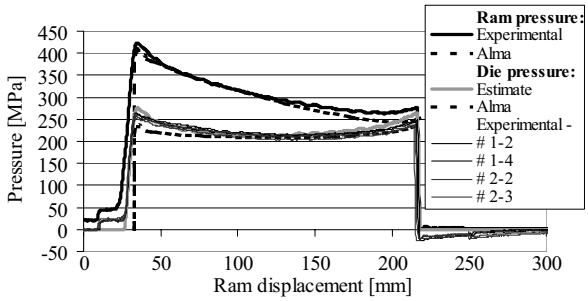

Fig. 10. Pressure measurements and simulation - sensor 2

Ram force data seem to be in fair accordance with Alma results. Measured die pressures are initially 40 MPa higher, but very close to an estimate based on the ram force and an assumed average container friction of 19MPa. Figure 11 shows that the estimate can be related to the force measured by the liner load cell. Ram force curves are only based on calibration and measurement data, but the variation in load cell data is somewhat larger than indicated by figure 11.

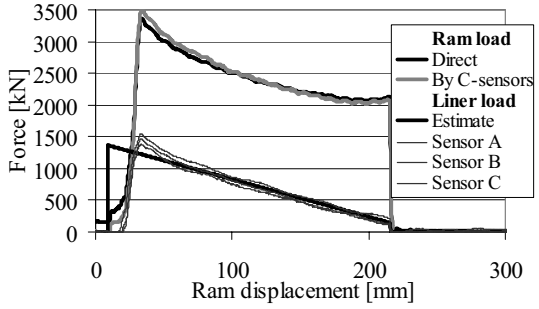

Fig. 11. Measurement of load through container liner and die

REFERENCE

1. A.W. Hansen et al., A technique for measuring stresses on the tool surface, In*: Proc. 4th Int.Conf. Technology of Plasticity*, Bejing (1993) Vol I : 303-308.
2. T. Yoneyama, Development of a new pressure sensor and its application to the measurement of contacting stress in extrusion, *J.Mat.Proc.Tech* 95 (1999) 71-77.
3. R.L. Foster, Linear Capacitive Reactance Sensors for Industrial Applications, In: *Proc. 40th Annual Earth-moving Industry Conference*, Peoria, Ill. (1989).
4. K. Holthe, L. Hanssen and S. Støren, Numerical simulation of the aluminium extrusion process in a series of press cycles, In: Proc. *NUMIFORM'92*, Rotterdam (1992).

Appendix B

Lefstad M., Moe P.T., Flatval R., Strøen S.

Thin Strip Aluminium Extrusion
–
Pressure, Temperature and Deflection Recordings of the Extrusion Die

Paper in Proceedings

5th ESAFORM Conference on Material Forming
April 20, Krakow, p. 471-474

Thin strip aluminium extrusion – pressure, temperature and deflection recordings of the extrusion die

M. Lefstad[1], P.T. Moe[2], S. Støren[2], R. Flatval[1]

[1]*SINTEF Materials Technology, R. Birkelands vei 2b, N - 7465 Trondheim, Norway*
e-mail: Martin.Lefstad@sintef.no; Robert.Flatval@sintef.no

[2]*Department of Machine Design and Materials Technology, Norwegian University of Science and Technology, R. Birkelands vei 2b, N - 7491 Trondheim, Norway*
e-mail: P.T.Moe@Immtek.ntnu.no, Sigurd.Storen@Immtek.ntnu.no;

ABSTRACT: The paper treats the extrusion of a thin strip of aluminium profile. The profile shape is relatively simple, and the case can be analysed relatively easily both experimentally and numerically. Since the problems concerning the stability of flow and die deflections are similar to those found with more complex profiles, this work is relevant to industry. The objective of the work has mainly been to establish measurement techniques that can determine the temperature and die face pressure along the width of the profile. Profile shape has also been studied and compared with numerical die deflection calculations based on pressures established both numerically and experimentally. Due to a relatively large profile thickness, the limits of flow stability as a result of buckling, for instance, were never reached. In future studies, the profile thickness will be reduced to reach the limits for flow stability and the influence of die deflection.

Key words: extrusion, aluminium, pressure, temperature, deflection, material forming

1 INTRODUCTION

When extruding thin-walled aluminium sections, there normally will be a tendency that different parts of the section flow faster or slower than other parts. Flow velocity gradients give rise to shear stresses between the parts, and normal stresses will build up at the outlet of the die. Then there are compressive stresses for parts that have a tendency to flow faster, and tensile stresses for parts with a tendency to flow slower. Due to the transient nature of the extrusion process, both with respect to the flow field and the temperature field, these stresses will vary during the press cycle. If this stress build-up influences the inflow of the metal from the die to the different parts of the section in such a way that unacceptable thickening, buckling, thinning, damage or rotation of the section is avoided, we can define this as ***self-stabilization.*** This mechanism is probably the most important characteristic of the thin-walled extrusion process, but is also the least understood from a scientific point of view. The intention of the present paper is to contribute to making a quantitative description of the dynamics of self-stabilization. The starting point will be experimental studies and numerical modelling of thin-strip extrusion. Variation in both flow temperature and pressure on the die face are measured for a complete cycle and the influence of die deflection on profile geometry is evaluated. In order to compare the experimental results with 2D simulations at the symmetry-line of the strip, the strip width B is selected such that the reduction ratio R is the same in both 2 and 3 dimensions. This means that if $R = \pi D^2/(4Bt) = D/t$, then $B = (\pi/4)D$ (D is the container diameter and t is the strip thickness) [1,2]. This geometry can be considered to be the generic section for the study of the phenomenon of self-stabilization.

2 EXPERIMENTAL SET-UP

The experiments were performed in an 8 MN vertical laboratory press, with a container diameter of 100 mm. A thin strip (1.7 mm x 78.5 mm) was extruded, and the width (B) was chosen according to the equation above. Figure 1 shows the die with pressure and temperature sensors. Along the whole periphery, the parallel bearings had an inlet radius of 0.5 mm and a length of 0.5 mm followed by a 3° release over a length of 4 mm.

Aluminium alloy 6060 was used (0.41 % Si, 0.47 % Mg, 0.18 % Fe). The billets were 96 mm in diameter and 150 mm long. As profiles longer than 8 m cannot be produced without being bent, rather short billets were used.

Table 1 presents the experimental matrix. This is designed to check the sensitivity of the techniques

for measuring forces, pressures, temperatures and the dimensions of the profiles. Several experiments were performed for each variant shown in Table 1. The parameter levels were chosen so that temperatures at the die bearings were similar to those obtained under industrial conditions (550 – 590 °C). The temperatures in the container and die were 430 °C in all experiments, whereas the stem was heated to 120 °C before extrusion.

Table 1. Variants of billet temperatures and extrusion speeds

Exp.	Tbillet (°C)	Stem speed (mm/s)
1	480	9
2	480	16
3	520	9
4	520	16

Capacitive pressure sensors were positioned at the centre of the die (P1) and at the corner of the profile (P2), both 15 mm from the die opening, see Figure 1. The technique is described in [3].

Thermocouples were inserted into the extrusion die as marked in Figure 1. The profile surface temperatures at the bearings [4] were measured at the middle of the width and at the corner of the profile. These are the positions with the highest temperatures to which the material is exposed during the whole extrusion cycle. Two thermocouples were also positioned in the die, at 4 and 9 mm from the die opening, in order to record temperature gradients close to the bearings and the temperatures close to the pressure sensors.

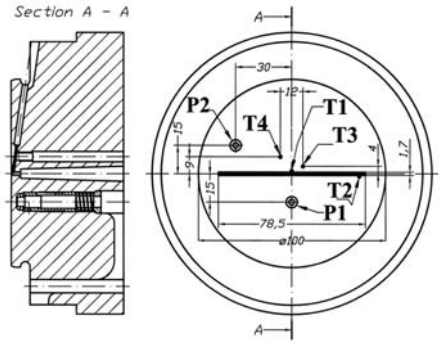

Fig 1. Die for strip extrusion with pressure (P1 – P2) and temperature sensors (T1-T4) indicated

3 RESULTS AND DISCUSSION

3.1 Ram force and temperature

Table 2 shows the characteristic values of force and temperature readings for all experiments. Figures 2 and 3 plot the forces and temperatures of Experiments 1 and 4 as a function of ram displacement. Table 2 shows that there are minor differences in ram force between the two extrusion speeds for a given billet temperature. Increasing the billet temperature from 480 to 520 °C reduces shear resistance and thus the ram force by approx. 10 %. The rather small difference between the maximum force at the start and end of the extrusion charge is due to the reduced container friction for the short billets that were used.

Table 2. Forces and temperatures for the variants 1 – 4.

Exp.	Force (kN) max - min	Max. temperature			
		T1	T 2	T 3	T 4
1	3170 – 2450	556	557	479	475
2	3340 – 2580	575	577	481	477
3	2780 – 2240	574	567	487	484
4	2920 – 2300	591	586	489	485

The maximum profile temperatures at the die bearings, T1 and T2, range from 555 °C for Experiment 1 to 590 °C for Experiment 4. The difference between T1 and T2 is up to 7°C. For both billet temperatures the profile surface temperature increases significantly when the speed is increased, although the ram force differs only moderately. The reason is probably that the temperature gradients in the profile are larger at the highest extrusion speed. The mean temperature increase in the profile is probably not very different for the two speed levels.

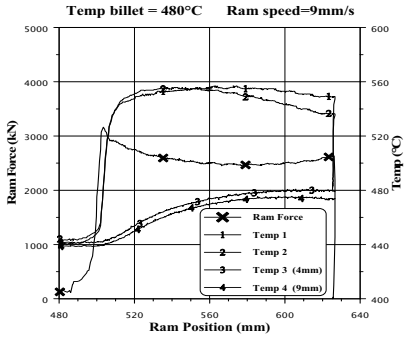

Fig 2. Force and temperatures T1-T4 for Experiment 1

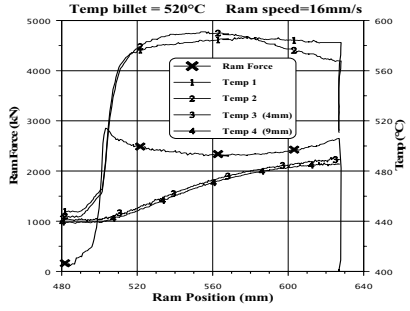

Fig 3. Force and temperatures T1-T4 for Experiment 4

The development of the profile temperatures differs somewhat for thermocouples T1 and T2, as seen in Figures 2 and 3. In the centre (T1) the temperature is highest at the start of the extrusion, and decreases by

20 °C towards the end. At the profile corner (T2) the temperature varies by only 5 °C with the highest temperature in the middle of the extrusion. The heat generation is probably largest close to the profile corner, where it is likely that the heat transfer to the die is at the start of extrusion. When the heat transfer evens out due to the overall heating of the die, the temperature at the profile corner catches up.

Simulation was performed with the 2D FEM code Alma [5] under the assumption of plane strain in the symmetry plane. A Zener-Hollomon model was used and the material parameters were determined by hot torsion. Force estimates will generally not be correct due to the geometrical simplification, but Figure 4 shows that Alma simulations are in fair agreement with measurements of the die bearing temperatures. The simulation gave somewhat higher temperatures than the measured ones (T3, T4) inside the extrusion die, probably due to poor contact between the die and the thermocouple. In any case, the temperature recordings in the die are at a much lower level than at the die bearing. This shows that the temperature gradient is very steep close to the die opening.

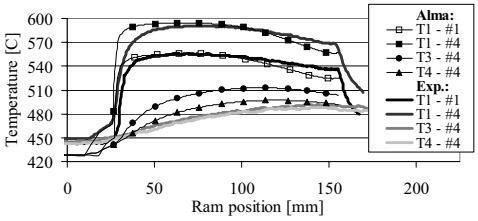

Fig. 4. Temperature by measurement and by Alma calculation

3.2 Pressure measurements

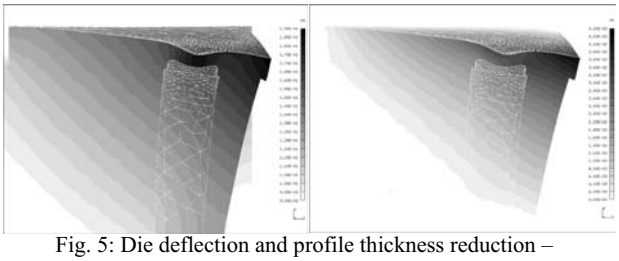

Fig. 5: Die deflection and profile thickness reduction –
1. Displacement || to extrusion direction: max 190, min 90µm
2. Displacement ⊥ to extrusion direction: max 44, min 0µm
Uniform load of 275 MPa, Young's modulus of 180 GPa

When sensors are placed close to the die outlet, the general die deflection should be taken into consideration. Even in the absence of sensor holes, level differences in the upper die face of more than 0.05 mm and much shear deformation was experienced close to the bearings (Figure 5). If the sensor is made as an integrated part of the die, sensor plate deflection will be influenced by the general die deflection. Asymmetry will complicate the analysis of the conditions for fastening the probe, and the measured deflection for a given load will depend on the point of contact. Measurements indicate that mounting may cause a variation in plate deflection of some ±2 out of 20 µm. A solution is calibration in-site by isotropic compression prior to experiments. This was not done as experience from the experiment in fact led to this conclusion. Yet, by initial moderate overloading, output was at least made to return to zero upon unloading.

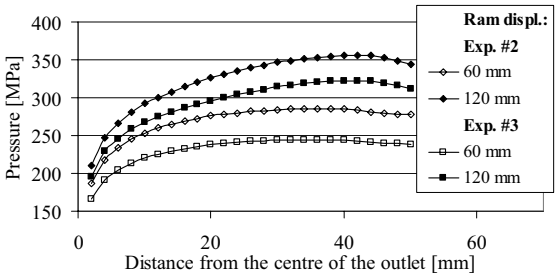

Fig. 6: Pressure sensitivity to velocity and temperature

The objective of this work was not so much the study of absolute values as that of variation with time and position using the parameters presented. Figure 6 shows Alma results for the load on the die face at the mid point and at the end of the charge for the two extreme cases, Experiments 2 and 3.

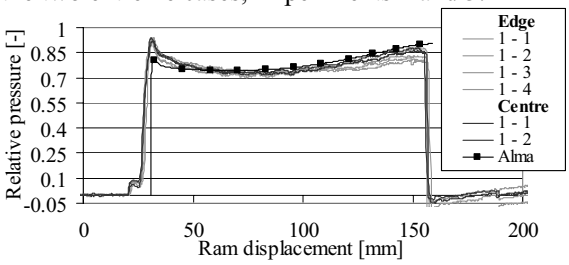

Fig. 7: Scaled pressure results for Experiment 1

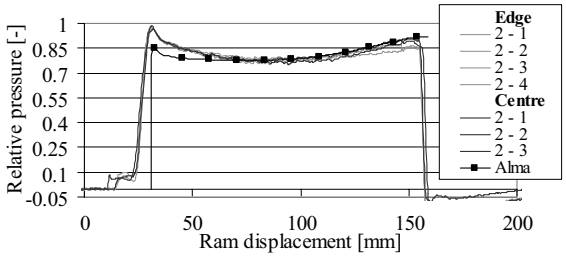

Fig. 8: Scaled pressure results for Experiment 2

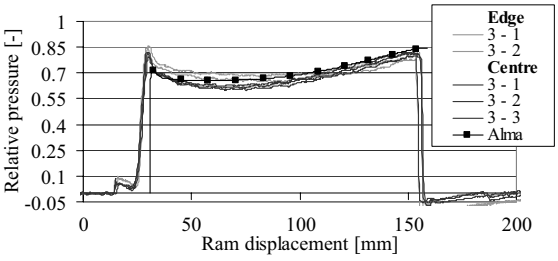

Fig. 9: Scaled pressure results for Experiment 3

Figures 7 to 9 compare experimental results for a number of runs with the Alma pressure calculations. All values have been scaled using the largest deflection measured for each sensor. All Alma results have been divided by the value 340 MPa, which has only been used to make the graphs comparable. The curves indicate that the pressure sensors and Alma calculations correspond fairly well with regard to pressure levels.

However, as in [3], the shapes of the curves differ, as the initialization peak is much lower for Alma. Some deviation may probably be due to the inability of the simulation code to indicate the actual pressure at initialization while most must be related to the effect of transient temperatures on sensor plate bending. The effect also causes the sensor output to return to zero only a matter of seconds after unloading. This indicates that the relative pressures for Alma are somewhat low and that a scaling factor of about 310 MPa probably is more appropriate. The temperature effect, which typically accounts for 5-10 % of the output, is also a source of variability.

As for the time variation of pressure with respect to the sensor position, there seems to be a small and repeatable difference between the probe placed in a central position and the one close to the edge of the profile. The central sensor may register a larger increase in pressure towards the end of the press. Given the variation in results the effect is probably not statistically significant, and as scaling is unique for each sensor, differences in values of absolute pressure cannot be deduced. Due to the large profile thickness, flow was self-stable, and no pressure effects directly linked to instability were observed.

3.3 Die deflection and profile geometry

Samples from the extruded profile were taken out 1 m from the front, the end, and at the middle, then the thickness was measured with a micrometer for the positions shown in Figure 10. Typical results for thickness measurements are shown in Figure 11. In each case the results are from two completely replicate runs.

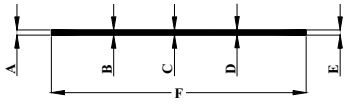

Fig. 10. Profile cross-section and positions of measurement

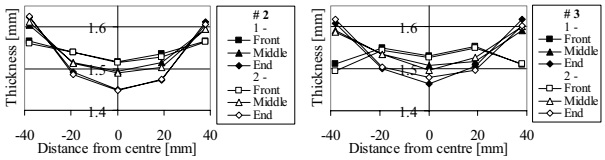

Fig. 11. Thickness measurements Experiments 2 and 3

A variation of profile thickness of about 0.1 mm corresponds well with deflection calculation results shown in Figure 5 and with calculations in which the pressure sensor is absent. Since pressure increases and the liner load decreases towards the end of the press cycle, an increase in thickness variation by some 20-30 % is expected. Experiments provided similar results.

The profile thickness close to the edges increases during the first half of the press cycle. The phenomenon has not been observed earlier, and the thickness was only expected to be affected by plate deflection and temperature effects to a negligible degree. A possible cause may be the presence of an oxide layer, which is probably only gradually worn down close to the corners of the outlet.

4 CONCLUSIONS

Thin-strip extrusion with width B=(π/4)D is an interesting generic case for the study of self-stabilization as it allows easy analysis, yet produces results that are also relevant to more complex extrusion cases. The future study of thinner profiles will reveal the limits of flow-stability and describe their interaction with die deflection. Important tasks in this context will include calibration and 3D modelling.

ACKNOWLEDGEMENT

The authors gratefully acknowledge and thank the Research Council of Norway and Hydro Aluminium for financial support and their permission to publish this work

REFERENCES

1. S. Støren, Theory of extrusion – advances and challenges. *Int.J.Mech.Sci. 35* (1993) 1007-1020.
2. S. Abtahi, T. Welo and S. Støren, Interface mechanisms on the bearing surface in extrusion, In: *Proc. 6th Int.Alu.Extr. Techn.Sem*, Chicago, Ill., (1996) Vol II: 125-131.
3. P.T. Moe and S. Støren, A technique for measuring pressure on the die face during extrusion, In: *Proc. 5th Int. ESAFORM Conf.*, Krakow (2002).
4. M. Lefstad, Metallurgical Speed Limitations during the Extrusion of AlMgSi-Alloys, PhD-thesis, University of Trondheim (1993).
5. K. Holthe et al., Numerical simulation of the aluminium extrusion process in a series of press cycles, In: Proc. *NUMIFORM'92*, Rotterdam (1992).

Appendix C

Moe P.T., Langø H.I., Hansen A.W., Wajid W., Strøen S.

Experiments with Die Deflection during Hot Extrusion of Hollow Profiles

Paper in Proceedings

6th ESAFORM Conference on Material Forming
April 20, Salerno, p119-122.

Experiments with die deflection during hot extrusion of hollow profiles

P.T. Moe[1], H.I. Lange[2], A.W. Hansen[2], W. Wajda[3], S. Støren[1]

[1]*Department of Machine Design and Materials Technology, Norwegian University of Science and Technology, Richard Birkelands vei 2B, N - 7491 Trondheim, Norway*
URL : www.ntnu.no e-mail: Per.T.Moe@Immtek.ntnu.no; Sigurd.Storen@Immtek.ntnu.no

[2]*SINTEF Materials Technology, Richard Birkelands vei 2B, N - 7465 Trondheim, Norway*
URL : www.sintef.no e-mail: Hans.I.Lange@sintef.no; Arnfinn.W.Hansen@sintef.no

[3]*Department of Computational Methods in Metallurgy, Akademia Gorniczo-Hutnicza, al. Mickiewicza 30, 30 - 059 Krakow, Poland e-mail: wwajda@metal.agh.edu.pl*

ABSTRACT: Aluminium extrusion dies are normally exposed to high pressures and experience significant elastic and even plastic deformation. Die deflection may affect outlet/profile dimensions, especially in cases where the profile is non-symmetric and temperature, flow resistance and pressure build-up change with time. Bridge dies for hollow profiles are usually more vulnerable than dies for open profiles since pressure build-up is larger and the die construction is less stiff. The paper focuses on techniques for measuring the pressure on the upper face of a bridge die and the resulting strain in the bridges and deflection of the mandrel. Capacitive displacement sensors are used to measure pressure, but also provide an alternative to strain gauges in the study of bridge strain. The deflection of the mandrel relative to the bottom face of the die is measured with inductive displacement transducers connected to the die with rods. Although sensors operate at temperatures up to 500 °C and experience temperature shocks of 60°C, all produce relatively accurate and repeatable data.

Key words: aluminium extrusion, high temperature, pressure, strain, deflection, measurement

1 INTRODUCTION

The bridge die for hollow profiles was introduced early in the history of aluminium extrusion. Today the ability to efficiently manufacture hollow profiles probably constitutes the process' main asset if not its raison d'être. While open profiles usually may be manufactured by a combination of other forming processes, hollow profiles also require a first-class method for longitudinal welding. The bridge die welding chamber, with complete absence of air, high temperature and large pressure, then provides ideal conditions. However, friction and area reductions, cause isotropic pressure to increase considerably in the direction opposite to that of extrusion and, thus, significant mandrel movement and straining of the bridges. The result may be a distorted outlet and profile shape. A component of displacement in the extrusion direction is probably inevitable. However, perpendicular displacement may also occur in the case of asymmetric profiles. The result is twisting as well as thinning/thickening of the profile (Figure 1). Shape deviation due to deflection may be reduced through die design, but probably never eliminated. First, extrusion is regarded as a transient. Second, a weakness of bridge die design in particular is that outlet dimensions are linked to the movement of a core experiencing an immense load. The load will be lower for dies with slender bridges, but stiffness is then also lower. A proper design may be found through fully coupled 3D flow and deflection calculations, but such an approach is still quite exigent in terms of computer time. This paper rather explores methods of verification, that is, techniques for measuring the pressure on the die face, strains in the bridges and deflection of the die mandrel or core.

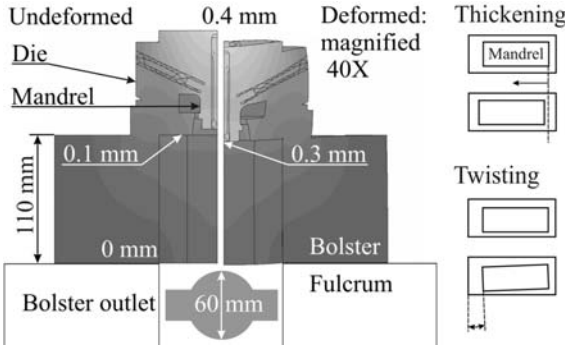

Fig 1. Deflection contours on undeformed/deformed geometry

2 EXPERIMENTS AND EQUIPMENT

As the objective of the study is to develop measuring techniques, a symmetric bridge die design (Figure 2) for pipe extrusion is well suited as a test case. Analysis is then made simpler as only displacement in the extrusion direction should be expected. Plugs placed in the outlet split the flow into two C-formed profiles and allow die deflection measurements.

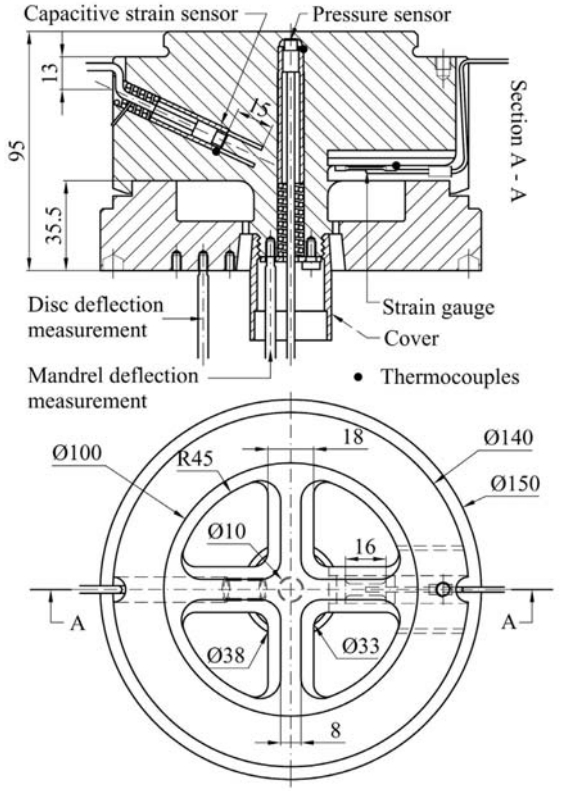

Fig 2. Hollow die geometry used in experiments

The die face pressure sensor consists of a Capacitec capacitive probe (Figure 3) measuring the deflection of an elastic steel plate. Typical max displacement is about 25 µm relative to the edge where the sensor is fixed. Sensor accuracy is less than a micron or about ±20-30 MPa. Sensor characteristics can be found in references [1] and [2] describing earlier applications.

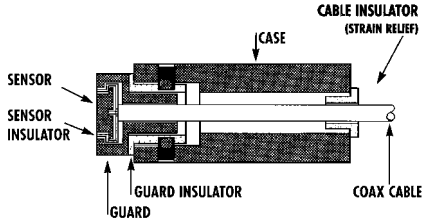

Fig 3. The Capacitec capacitive probe used in experiments [1]

Measurement of mandrel displacement relative to the fundament and disc was performed with rods connected to HBM ±5mm inductive transducers [3] (Figure 4). Glass and Invar steel with low thermal expansion may be used as rod material, but the last, being less brittle, has been found preferable. Proper design and fixation of the rods are the limitations rather than the accuracy of the transducer itself.

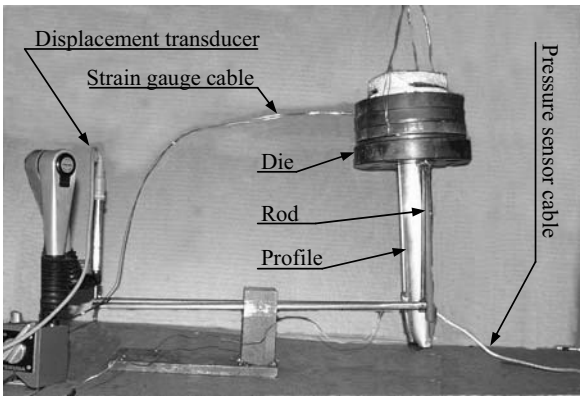

Fig 4. Die with mandrel deflection measurement equipment

Both a high temperature strain gauge, KYOWA KHC-20-120-G8-11 C2M, mounted in a covered slot below the bridge (Figure 5) and a capacitive sensor, inserted into a spark-eroded hole, can be used to give an indication of the strains in the bridges during loading. In the case of the last one, an inner mandrel is left non-deformed during loading.

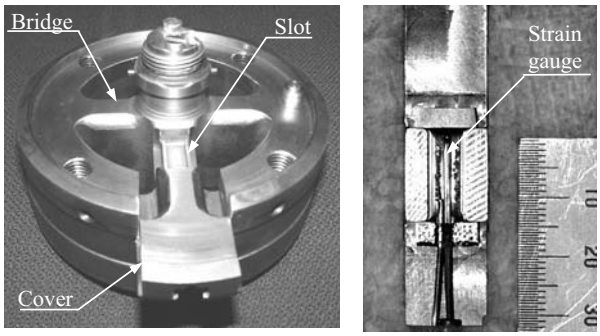

Fig 5. Die with slot for strain gauge and gauge mounted in slot

Two completely replicated rounds of experiments were carried out in an 8 MN vertical lab press with a container diameter of 100 mm. Billets of AA6082 (Ø96x200mm) were initially heated to 480°C. Ram and die/container temperatures were set to 130 and 430 °C. A 15 mm butt end was not removed between runs. Four billets were extruded at each ram speed of 0.5, 1 and 2 mm/s. The danger of overloading made experiments at higher ram speeds less desirable.

3 RESULTS AND DISCUSSION

Figure 6 shows the ram force as a function of ram displacement as well as ram speed. While the peak force increases with ram speed, differences at quasi-steady state are smaller. This can be explained by an increase in heat dissipation with rate. At 2 mm/s, there is close agreement between measured values and those obtained with Alma, a 2D extrusion code [4]. A Zener-Hollomon law is used, and geometry is such that both press ratios and friction surface are as in the 3D case (Figure 7). At lower speeds peak force is still similar to the one in experiment, but somewhat too high at the end of the press.

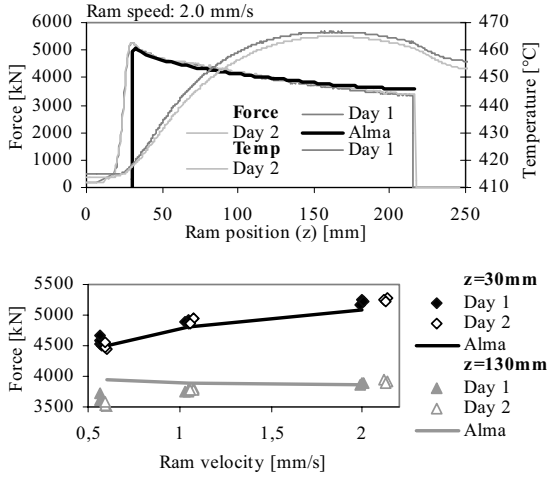

Fig 6. Ram force and mandrel temperature measurement

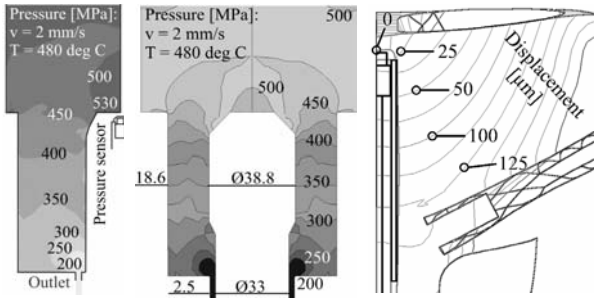

Fig 7. Forge3/Alma pressure distribution and plate deflection

Independent calibration methods are desirable. In the case of the pressure sensor such exists [1], but it was not used in this study. Instead FEM provides the conversion factor from measured plate deflection to pressure. The 3D Lagrangian code Forge3 and Alma supply the structural calculation with estimates of tractions. The vertical displacement of the mandrel relative to the sensor plate is shown in Figure 7. The conversion factor is 20 ± 1 MPa/µm. In Figure 8 this factor has been applied to raw data from the first day and temperature compensated data from the second. There is close agreement between the peak pressures of replicated runs at different days, but temperature sensitivity of the sensor used on the 2nd day causes some deviation in trends. A rational correction has been made with the help of measured temperature data. Raw data from day 1 differs somewhat from calculated results at z=130 mm. This is probably the result of temperature sensitivity and random error.

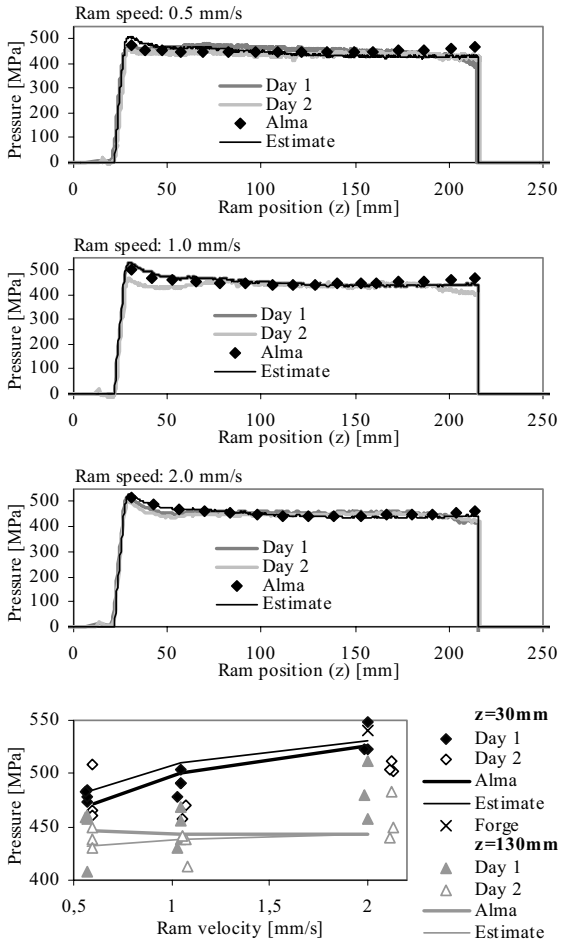

Fig 8. Estimated, calculated and measured die face pressure

Standard deviation was found to be about 20 MPa. Thus, while peak pressure at 0.5 mm/s cannot be judged significantly different from that of 1 mm/s, the sensor is able to distinguish between pressures at 0.5 and 2 mm/s. Figure 8 also includes an estimate of the die face pressure based on the ram load, liner friction and the effects of area reduction. Generally, pressure should change as material is first heated by dissipation and then cooled by the approaching ram.

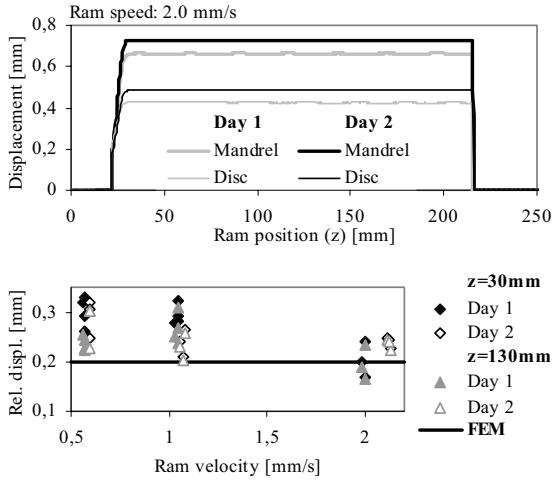

Fig. 9. Displacement of mandrel relative to the die bottom face

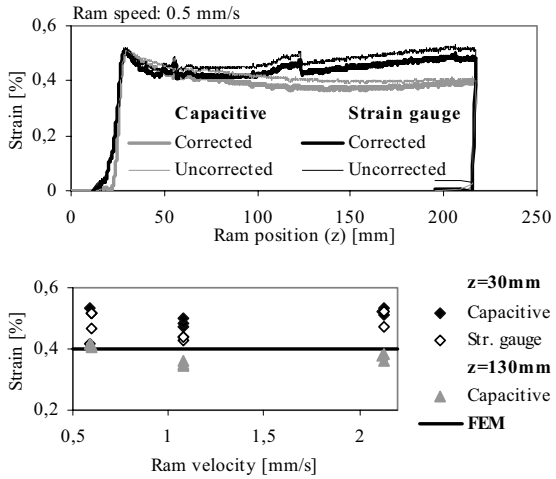

Fig. 10: Strains measurement in the bridge

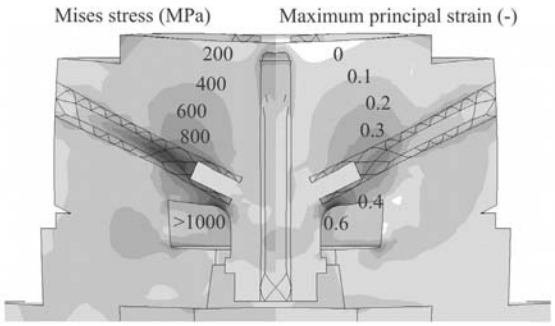

Fig. 11: Mises stresses and max principal strain and in bridges

Figure 9 shows that there is a 0.2 to 0.3 mm vertical movement of the mandrel relative to the disc. This may be compared to the die deflection calculation of Figure 1 and 7, which uses the load data of Figure 8. Measured results should be higher than calculated ones since the model neglects interfaces. Accuracy and repeatability are still not quite satisfactory, and improvements to the technique should be sought. Results from the two different strain measurements are shown in Figure 10. They are in fair accordance with FEM as shown in Figure 11, although strain distribution is very non-uniform close to the sensors. Repeatability is uncertain, as experiments have not been replicated. High temperature tests have earlier indicated that strain gauges are more sensitive to temperature changes than the capacitive sensors [3].

Both experimental and numerical methods are rather coarse, and accurate results are not to be expected. However, the study gives an indication of the large stresses and strains in a bridge die. Although the yield stress of H13 steel (900 MPa at 500°C) was exceeded locally, all sensors behaved satisfactorily. Crack growth was in the end observed in the strain gauge cover. Dies are normally not designed with as sharp notches as the one in this study, but crack development close to sites of stress concentration is usually a menace to die life.

4 CONCLUSION

Techniques for measuring applied load on a bridge die as well as the resulting strains in the bridges and mandrel deflection have been studied in replicated experiments. All experimental and simulated results are in fair accordance. The maximum load on the upper die face was about 530±30 MPa. The mandrel then deflected some 0.2±0.05 mm relative to the die plate, causing strains in the bridges of 0.45±0.05 %.

ACKNOWLEDGEMENT

The authors gratefully acknowledge and thank the Research Council of Norway and Hydro Aluminium for financial support and their permission to publish this work.

REFERENCES

1. P.T. Moe and S. Støren, A technique for measuring pressure on the die face during extrusion, In: *Proc. 5th Int. ESAFORM Conf.*, Krakow (2002).
2. M. Lefstad et al., Thin strip aluminium extrusion – pressure, temperature and deflection recordings of the extrusion die, In: *Proc. 5th Int. ESAFORM Conf.*, Krakow (2002).
3. H.I. Lange et al., Deflection and deformation of extrusion tools - instrumentation and measurements, SINTEF Report STF24 F98349, (1998).
4. K. Holthe et al., Numerical simulation of the aluminium extrusion process in a series of press cycles, In: Proc. *NUMIFORM'92*, Rotterdam (1992).

Appendix D

Wajid W., Lefstad M., Moe P.T., Abtahi S.,
Flatval R., Strøen S.

A Study of the Limits of Self-Stabilization during Extrusion of Thin Strips

Paper in Proceedings

6th ESAFORM Conference on Material Forming
April 28, Salerno, p267-270

A study of the limits of self-stabilization during extrusion of thin strips

W. Wajda[1*], M. Lefstad[2], P.T. Moe[1], S. Abtahi[2], R. Flatval[2] and S. Støren[1]

[1]*Department of Machine Design and Materials Technology, Norwegian University of Science and Technology, Richard Birkelands vei 2B, N – 7491 Trondheim, Norway*
URL: www.ntnu.no e-mail: Wojciech.Wajda@immtek.ntnu.n; Per.T.Moe@immtek.ntnu.no; Sigurd.Storen@immtek.ntnu.no

[2]*SINTEF Materials Technology, Richard Birkelands vei 2B, N – 7465 Trondheim, Norway*
URL: www.sintef.no e-mail: Martin.Lefstad@sintef.no; Shahriar.Abtahi@sintef.no

[*]*Previous address: Department of Computational Methods in Metallurgy, Akademia Gorniczo – Hutnicza, al. Mickiewicza 30, 30 – 059 Krakow, Poland*
URL: www.kmpm.agh.edu.pl e-mail: wwajda@metal.agh.edu.pl

ABSTRACT: This paper describes the second step in a study of flow instability and self-stabilisation during extrusion of a thin strip. In this work, a stable flow is regarded as one where the profile leaves the die with a close to uniform velocity. Instability is thought to occur when parts of the profile flow more easily than other parts so that the profile experience buckling or thinning when it leaves the die. The instability limit depends on profile geometry and process parameters, and the study shows how instability may be provoked by reducing the thickness of the thin strip and changing process parameters. An instability point was found when a 78.5 mm wide and 1.1 mm thick profile was extruded. The paper discusses characterisation methods as well as the nature and distribution of the buckles. The investigation was supported by 3D simulation, which appears to be a very useful tool for investigating self-stabilisation mechanism phenomena. The instability case for thin-strip extrusion is a proper generic test for qualifying numerical codes used in the study of extrusion.

Key words: thin strip extrusion, self-stabilization, aluminium, 3D simulation

1 INTRODUCTION

Cost and weight considerations encourage the use of sections with reduced wall thickness in products that are not highly stressed. Extruded aluminium profiles can be made very thin, but there are limits to the thickness to width ratio for a given set of process parameters. The thinner the profile is, the more vulnerable it is to flow instability mechanisms. An instable flow is one where the profile is leaving the die with a non-uniform velocity, and, thus, where some kind of buckling or thinning may occur. In the end, the outcome might be complete plugging of the outlet. Normally such behaviour is prevented by self-stabilization [1] mechanisms since parts of the section leaving with a higher velocity will attempt to pull the slower ones by shearing. However, if the profile is made sufficiently thin shear stresses put up will not be large enough to prevent instabilities. At the same time the forces that may cause the profile to buckle as it leaves the die need not be so large since thin profiles buckle more easily.

The problem is closely related to constitutive and frictional behaviour. The extrusion process is very complex and, thus, difficult to describe due to the non-uniform distribution and temporal changes of state parameters like e.g. temperature and strain rate. Deformation zones and friction conditions must then also be expected to change. Non-homogeneities present in the container and in the bearing channel may be another cause of instable flow. Instability is related among other things to non-uniform pressure distribution, different conditions along particle paths, slip point movement in bearing channel, non-uniform friction in bearing channel, die deflection and wearing, stick-slip phenomena in the sliding zone and sudden change of stress state after material leaves bearing channel. In order to understand and control such complexity all phenomena and their influence on material behaviour must be described both qualitatively and quantitatively. Accurate measurement is a necessity if the task is to be achieved, and techniques of temperature and pressure measurement were therefore presented in

previous papers [2,3]. Results from extrusion of a thin strip profile, 78.5 mm wide and 1.7 mm thick, have earlier been investigated. Analysis was supported in a simplified manner by 2D ALMA software simulation, and numerical results were compared with measurements of ram force, outlet temperature and die face pressure [3]. This paper treats new experimental runs with the thin strip geometry where profile thickness has been reduced to 1.4 and 1.1 mm in order to enforce instable flow. The following analysis focuses on the nature and conditions of the instable behaviour, but offers no complete explanation.

2 EXPERIMENT

In order to examine instability behaviour, 3 series of thin strip extrusion experiments were performed. The experiments were carried out in an 8 MN vertical laboratory press. Figure 1 shows the outlet geometries of the three dies used. As indicated in reference [2] the width, W, and thickness, t, of the outlet of die A were chosen in order to legitimate a plane strain analysis. 2D and 3D press ratios then should be equivalent, $R = \pi D^2/(4Wt) = D/t$. D, the container diameter, was 100 mm and the width, given by $W = (\pi/4)D$ was 78.5 mm. The thickness was set to 1.7 mm. The outlets of dies B and C were somewhat convex rather than purely rectangular. Minimum / maximum thickness were 1.1 / 1.3 and 1.4 / 1.55 mm. Thickness was varied to compensate for the thickness reduction due to the deflection of the die observed during extrusion with die A.

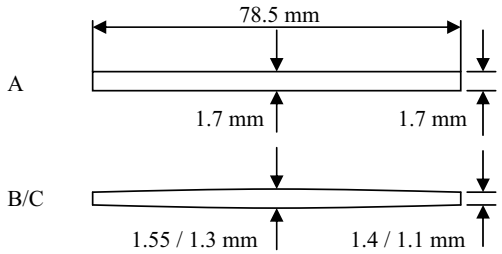

Fig. 1. Die outlet geometries for dies A, B and C

A short bearing channel (1 mm) was used for all dies in order to reduce the uncertainties related to bearing channel friction and to enforce instability. The entry to the opening was rounded with radius 0.5 mm. Extruded material was aluminium AA6060. Billet height and diameter were 150 and 96 mm. The ram, container and die temperatures were the same for each experiment, 150, 430 and 430 ^{o}C respectively.

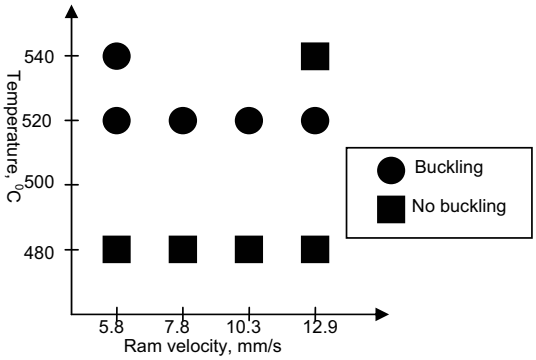

Fig. 2. Experimental matrix with indication of result for die C

The process parameters, that were varied in order to investigate the limits of self-stabilisation, were the ram speed and the initial billet temperature. Buckling did first occur when thickness was reduced to 1.1/1.3 mm. Figure 1 shows the levels of billet temperature (480, 520 and 540 ^{o}C) and ram speed (5.8, 7.8, 10.3 and 12.9 mm/s) for die C, and it indicates at which conditions buckling took place (marked with circles). It should be added that also in the cases where distinct buckles were not observed, there were indications of waviness with very small amplitude.

Parts of a strip experiencing instable flow at ram speed 5.8 mm/s and temperature 520 ^{o}C, are shown in Figure 3. The presented sections were taken 1 m from beginning (F), in the middle (M) and 1 m from back (B) of the strip. For all instable cases, no distinct buckles were initially observed. Buckling started after about a meter had been extruded and lasted some 2-3 meters.

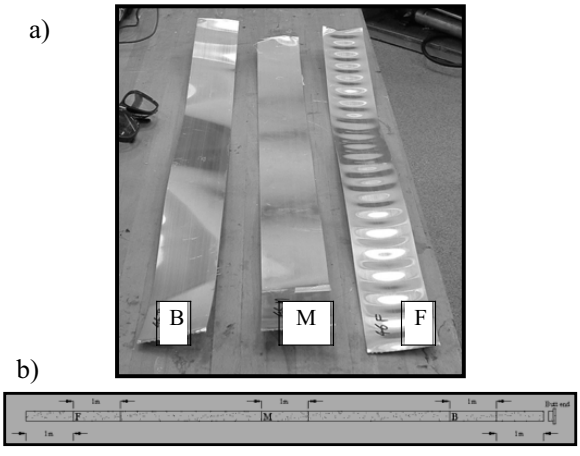

Fig. 3. (a) Sections of strip extruded at 520 ^{o}C for ram speed 5.8 mm/s, from right 1 m from beginning, in the middle and 1 from back of the strip, (b) marked places of taken sections

3 BUCKLING CHARACTERISATION

Measurement of the characteristics of buckling was performed at the NTNU laboratory. Extruded strips were attached to the moving table, and a inductive displacement transducer positioned above the table and in direct contact with strip measured height differences (Figure 4). So far only one line of data in one table pass has been stored, but parallel measurements would in principle also be possible. Later analysis refers to the height of buckles in the centre of the strip. Accuracy was about 20 μm. Ideally such measurements should be perfomed in line as the profile leaves the die. In that case, a non-contact high speed technique would be preferable.

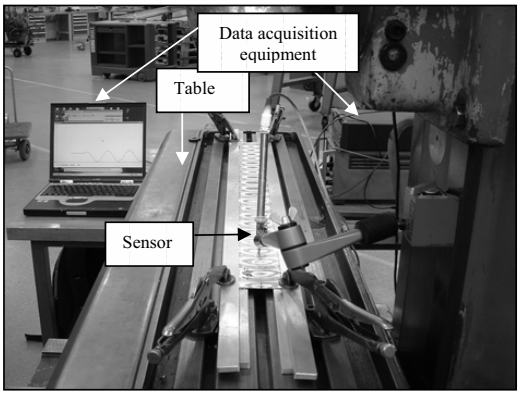

Fig. 4.Buckling measurement equipment at NTNU laboratory

The following quantities were used to illustrate instability development: the beginning and the end of buckling, the maximum height (amplitude) of buckling, the top distance, the elongation of the centre of the strip and the thickness of the strip. The top distance is the period or the length between two neighbouring maximum points, and is inversely proportional to the frequency. A sinusoidal wave equation is locally a fairly good approximation to measurement data, and the changes in amplitude and frequency with ram displacement may be used to characterize buckling changes. The length of the wave may be calculated and compared to length of the edge to estimate elongation of the strip centre by following formula:

$$\Delta L = \frac{L_{WAVE} - L_{EDGE}}{L_{EDGE}} \cdot 100\% \qquad (1)$$

where: ΔL = elongation in the centre of the strip, %; L_{WAVE} = length of the strip centre, mm; L_{EDGE} = length of the strip edge, mm;

4 RESULTS AND ANALYSIS

Figure 5 shows the length of the buckled region at all ram velocities. It reveals no particular trend and gives not unexpectedly the impression that the process is very unstable and sensitive to temperature and velocity perturbations. Although replicate runs give very similar results, no firm conclusions should be drawn on the basis of the limited data available. So far experiments only prove that thin strip extrusion is suitable for the study of flow instability.

a)

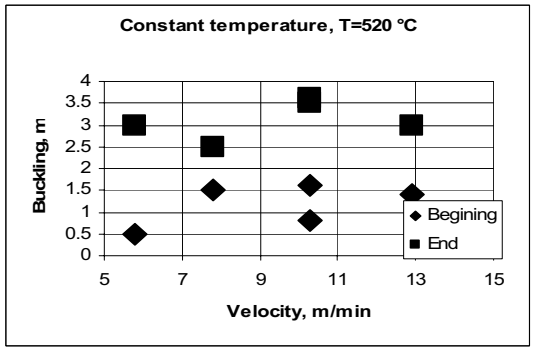

b)

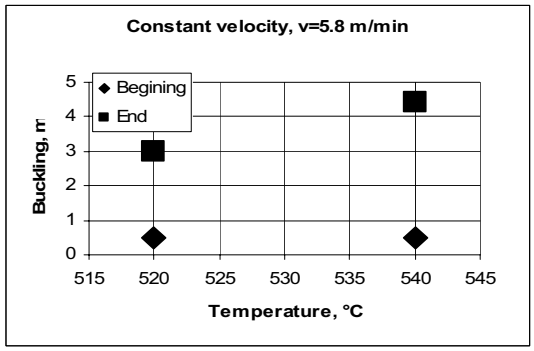

Fig.5 Length of buckling for die C. (a) Constant billet temperature 520 °C. (b) Constant ram velocity 5.8 mm/s (b)

Figure 6 and 7 present further data from buckling measurement and analysis. Changes in amplitude, top distance and elongation versus extruded strip length are shown in Figure 6. The ram speed is 5.8 mm/s. Both at 520 and 540 °C amplitude and elongation decrease while top distance increases as more strip is extruded. This is in accordance with observations during extrusion. Buckling started quite abruptly, and then a gradual smoothing out followed. Amplitude and top distance are, according to Figure 7, close to inverse proportional. Furthermore, values of amplitude and elongation are lower for lower temperature, and top distance is increasing when temperature is decreasing.

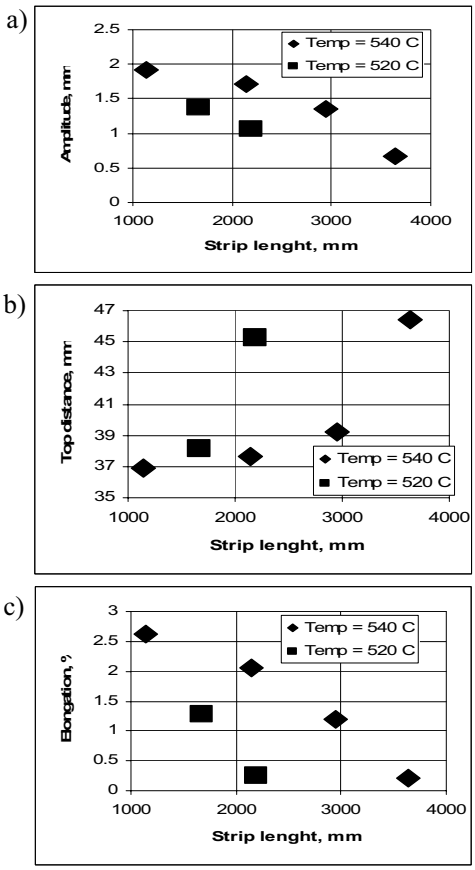

Fig. 6. Changes of a) amplitude, b) tops distance, c) elongation on the strip obtained from extrusion with ram speed 5.8 mm/s.

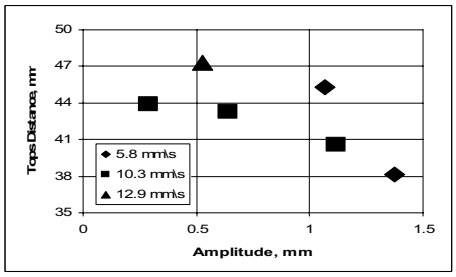

Fig. 7. Relation between amplitude and tops distance for different ram speeds and constant billet temperature 520°C

Profile thickness distribution must be found if the velocity distribution is to be determined. Accurate measurements are hard to perform, especially since the strips had to be bent just after leaving the die, and the thickness distribution then most probably was somewhat altered. Lack of space and the absence of a run-out table necessitated such bending. In order to compensate for the lacking thickness data 3D computer simulation of extrusion process was performed. A velocity distribution across the profile width for a number of ram positions is shown in Figure 8 [4]. The simulation was done with the Eulerian code, EXTRUD, which gives an indication of speed distribution, but still is unable to model buckling satisfactorily. A more uniform flow towards the end of the press is in accordance with observations.

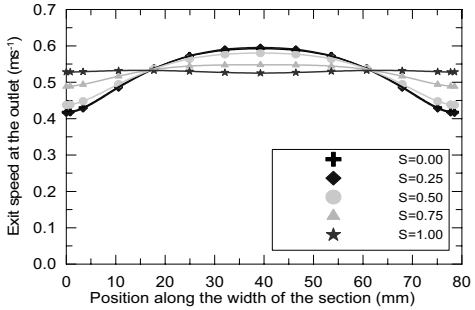

Fig. 8. Simulated exit speed at different ram positions S. Ram position was normalised to 1.

5 CONCLUSIONS

Flow instabilities may be enforced when extruding a 78.5 x 1.1 mm thick strip by choosing proper process parameters. Thin strip extrusion seems to be a useful test case for FE models since instabilities may occur although the geometry is quite simple. Analysis and characterisation of buckling shows the very unstable character of the phenomenon.

ACKNOWLEDGEMENTS

The authors gratefully acknowledge and thank to Research Council of Norway and Hydro Aluminium for financial support and their permission to publish this work.

REFERENCES

1. Støren, S.: Theory of extrusion – advances and challenges. Int.J.Mech.Sci., 35: pp1007-1020, Pergamon Press, 1993.
2. Lefstad M. et al., Thin strip aluminium extrusion – pressure, temperature and deflection recordings of the extrusion die, Proc. 5th Int. ESAFORM Conf. on Mat. Form., Krakow, pp. 471-474, 2002.
3. Moe, P.T. and Støren S.: Pressure measurement on the die face during aluminum extrusion, Proc. 5th Int. ESAFORM Conf. on Mat. Form., Krakow, pp. 463-466, 200
4. Abtahi, S., Lefstad, M. Simulation of temperatures, profile speeds and forces during extrusion of Aluminium using the FE code Extrud, SINTEF Report STF24 F02335, (2002)

Moe P.T., Lefstad M., Flatval R., Strøen S.

Measurement of Temperature and Die Face Pressure during Hot Extrusion of Aluminium

Journal article

International Journal of Forming Processes
Vol. 6 (2003) No. 3, p 241-270

Measurement of temperature and die face pressure during hot extrusion of aluminium

P.T.Moe* — M.Lefstad— R.Flatval**— S.Støren***

** Norwegian University of Science and Technology*
Richard Birkelandsvei2B
N-7491 Trondheim
Norway
Per.T.Moe@immtek.ntnu.no
Sigurd.Storen@immtek.ntnu.no

*** SINTEF Materials Technology*
Richard Birkelandsvei2B
N-7465 Trondheim
Norway
Martin.Lefstad@matek.sintef.no
Robert.Flatval@matek.sintef.no

ABSTRACT: *This article discusses the value of measurement techniques in laboratory studies of hot aluminium extrusion and evaluates the requirements to their accuracy. An established technique for measuring the profile surface temperature at the die outlet is combined with a die face pressure measurement technique. The article evaluates possible pressure sensor designs. The selected technique measures the deflection of a plate relative to a point where a capacitive probe has been attached. An in-site calibration technique provides accuracy of about ±10 MPa. The measurement technique can be applied to temperatures above 600℃ and is only influenced by temperature changes to a limited extent. Rod extrusion serves as a test case for the sensor, and good agreement with simulation has been obtained. The sensors are also used in a study of dimensional variability during extrusion of a generic thin-strip.*

KEYWORDS: *aluminium extrusion, pressure, temperature, measurement, capacitive sensor.*

1. Introduction

Aluminium extrusion is an appealing process since it appears to be so simple yet produces the most complex and useful profiles. At the same time, it is to some degree still a craft and conceals a number of complexities that are eventually reflected in the product quality. Dimensional variability prevents the use of tight tolerances and causes a substantial percentage of scrap. Poor temperature control leads to variability in the microstructure and necessitates posterior heat treatment in order to reproduce material properties. The fine surface properties, which make aluminium profiles so appealing, depend on strict control of the process parameters as well as die geometry. Cost is strongly affected by the great variability in die life.

Extrusion has two main weaknesses when used as a method of mass production. First, it is a transient process, for which temperature, forces, die-deflection and product dimensions vary continuously with the ram position. Second, flow is normally controlled by very short and almost parallel so-called bearing surfaces at the die outlet. If the profile does not leave the die with a uniform velocity, it will bend or buckle. In the severest case, no extrusion is possible as the outlet gets plugged. The remedy is usually a gradual modification of the bearing surfaces by hand grinding until a satisfactory result is obtained. However, by extruding sufficiently thick specimens, one can avoid the problem altogether. The faster moving parts of the profiles will actually pull the slower ones so that outlet velocity is uniform. A consequence of this self-stabilization mechanism is the generation of residual stresses in the profile. It is also noted that mass production is significantly simplified by the fact that mechanical pullers normally suppress flow instabilities.

For a great number of applications the process variability one sees today is acceptable. However, problems emerge when customers need to specify even tighter tolerances, thinner wall thickness or lower cost. The traditional solution sought is one of trial and error where die correction is brought to its limits. An alternative and often not linked path that is favoured by engineers, consists of finding satisfactory process conditions through theoretical models. The trial and error method eventually provides answers, but at high cost. A descriptive and predictive theory usually treats simplified cases and not the complex practical problems. For more than a decade FEM has been regarded as a solution. A number of 3D codes have emerged (van Rens, 1999, Williams et al., 2002), but evaluation is a necessity. Fundamental questions relate to constitutive and friction modelling, the use of continuum mechanics and choice of numerical scheme. A multi-scale theory of extrusion implemented in an adequate numerical framework probably will emerge within a decade. Focus must then be on validation or rather rejection of the codes and hypotheses through properly planned experiments with simple but representative generic profile shapes. Two geometries that have been thoroughly studied are shown in Figure 1 (Støren, 1993). Even such simple cases as the rod and the thin strip extrusion are, however, extremely underdetermined as models contain an abundance of parameters, and alternative methods of measurement seem to be the sole remedy.

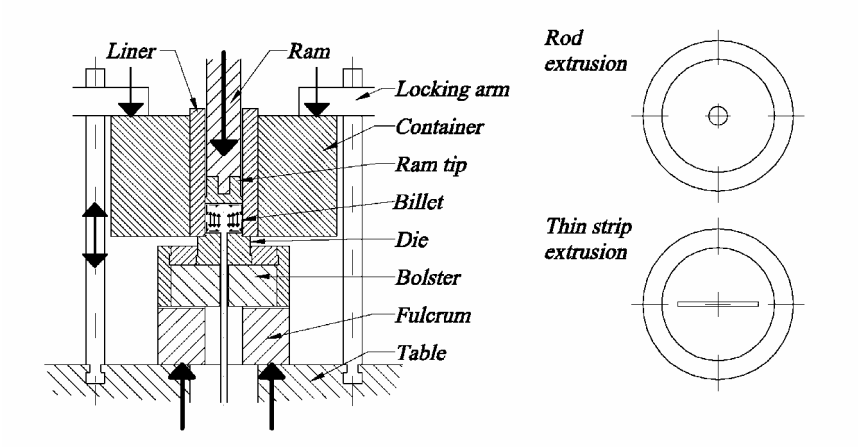

Figure 1. *Extrusion set-up with forces indicated and generic die geometries*

This article focuses on dimensional rather than microstructural variability. The large forces at work during extrusion cause considerable and gradually varying elastic deformation of the tooling. As the die is poorly supported centrally, it will bend or deflect much like a thick plate. The most direct and significant consequence of this die deflection is the alteration of die outlet dimensions followed by a variation in profile thickness. Flow stability and pressure build-up will also be affected by the deviation of outlet geometry. In the extreme cases of very thin-walled extrusion self stabilization will be put to a test. Figure 2 displays some of the complexity of the extrusion process and the close relationship between various aspects. An increase in an input variable such as velocity or billet temperature will affect profile shape, but not necessarily in an easily predictable manner.

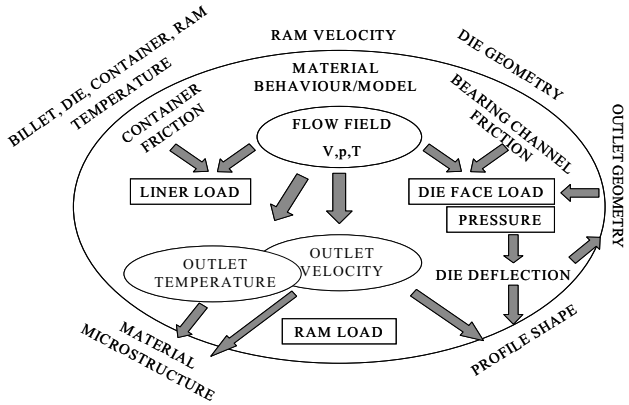

Figure 2. *Simplified process description*

Profile shape prediction is a natural task for the next generation of numerical simulation tools, but methods of direct measurement are still highly desirable. The

direct load on the die cannot be distinguished from the part led through the liner merely from ram load measurements, and therefore assumptions made with regard to friction on the liner wall cannot be verified. Measurement of liner load has been performed as it makes assessment of the load on the die face possible. Yet, direct local measurement of the entire die face load distribution would be of even greater value to calculations of die deflection and profile shape. This article treats such a pressure sensor and thereby also provides information on the friction conditions on the container wall and the flow patterns in the container in general. Such sensors in their most refined form may also be used to evaluate pressure build-up through the bearing channel, material and bearing channel friction models at high strain rates and eventually the mechanics of self-stabilization. In such a study, the method is complemented by an established technique for recording the temperature on the bearings. However, these are difficult tasks as it will be shown that extreme measurement accuracy and resolution are needed. Accuracy in measurement is, however, a key issue for even for the simpler cases mentioned above and in-site code-independent calibration and simple but representative test cases are necessities.

2. A study of the requirements to measurement accuracy

If measurement techniques are to provide information on the quality of physical models and numerical results, there are certain requirements concerning sensor accuracy. Even if calibration methods are used one must assume the existence of some bias in addition to unavoidable random errors. A consequence of an excessive uncertainty in measurement is simply that no model or hypothesis can actually be rejected with any real confidence. If so the value of measured results is limited.

Regression analysis may be used as a statistical tool in an inverse analysis that is performed in order to fit measured data to models or to rule out improper models. In order to establish the requirements for measurement accuracy, one must study a case in which the model is assumed to describe nature perfectly and errors only are related to the act of measuring itself. The question is then whether a measurement technique with a certain error may provide worthwhile information on material behaviour. This depends not only on the measurement error, but also on the model and the number of parameters. Such a study may be relatively complex in the case of extrusion, especially if many parameters are assumed unknown. Therefore only a simplified analytic case treating a region of high pressure and full stick in an axially symmetric 60 mm long bearing channel of radius 7.9 mm is treated. Though the case seems to be of limited practical value, an interesting experimental study has been performed with such geometry (Valberg, -). The deposition of an adhesive layer in the outermost 20 mm of the channel is reported when the choke is 1°. This layer is similar to the one found by Abtahi in the slipping zone during thin-strip extrusion and where a low contact pressure makes assumptions of a Coulomb-like friction law seem reasonable (Abtahi et al., 1996). Full stick is assumed in the remaining channel where a high pressure causes more intimate contact. In this region, one assumes

rather optimistically that point measurements of pressure and temperature can be made 20 and 40 mm from the outlet (Figure 3). As a rough approximation, flow is assumed to be fully developed generalized Newtonian in the sticking region and of uniform velocity in the slipping region. Bearings are assumed parallel.

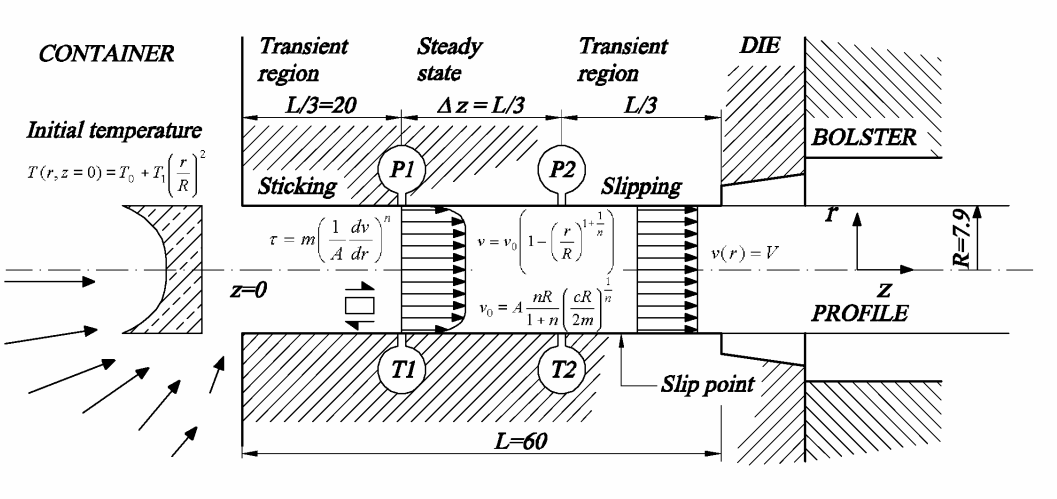

Figure 3. *Experimental set-up with sensor positions T1, T2, P1, P2.*

In Figure 3, τ is the rz-shear stress and v the flow velocity. The standard inverse analysis is to determine material parameters m and n of the expression for a generalised Newtonian fluid, while in this study m and n are viewed as constants. A only serves to make the strain rate expression dimensionless and is set to 1 s^{-1} in the analysis. No temperature dependence is assumed, and the energy and equilibrium equations therefore are partially decoupled. The equilibrium equation may then be solved in a standard manner giving the velocity distribution in Figure 3. R is the bearing channel radius and c is the gradient in pressure in the flow direction. c may be found by assuming conservation of mass. The result is Equation [1].

$$\Delta p = -\frac{2m}{R} F\left(n, A\right)\Delta z \qquad F\left(n, A\right) = \left[\frac{\bar{v}}{AR}\frac{1+3n}{n}\right]^n \qquad [1]$$

The relation also determines the sensitivity of the pressure build-up between two measurement points to the parameters m, n and A as friction is constant in the sticking zone. The absolute value of pressure will throughout the bearing channel be affected by the slipping zone friction coefficient, μ, as shown by Equations 2 and 3.

$$p\left(z\right) = \frac{\tau_0}{\mu B} f\left(z;\mu,B\right) \qquad f\left(z;\mu,B\right) = \exp\left(\frac{2\mu B}{R}\left(L-z\right)\right) \qquad [2]$$

$$p(z) = \frac{2m}{R} F(n, A)(L - z) + \frac{m}{\mu B} F(n, A)\left(1 - \ln\left(\frac{m}{\tau_0} F(n, A)\right)\right) \qquad [3]$$

L is the bearing length and τ_0 is the minimum shear stress in the bearing channel. τ_0=5 has been found to give reasonable results (Tverlid, 1997). Figure 4 shows pressure build-up and friction through the bearing channel for velocities 50 to 200 mm/s. μ=0.4, m=15 MPa, n=0.11, A=1 and B=1, which corresponds roughly to the 6060 alloy, is assumed. The slip point is then situated 14 to 17 mm from the outlet.

The development of an analytical expression for the temperature increase from one measurement point to another probably cannot be done without making simplifying assumptions. All dissipation of heat is assumed to take place on the bearing surface, which is reasonable in the case of a plug flow. In addition, convection is assumed to dominate in the extrusion direction, and a Lagrangean approach is adopted through a slab analysis. Such simplifications seem justified when the profile velocity is above 5-10 mm/s and shear deformation is localized to thin boundary layers. Again material parameters are set independent of temperature.

One is thus left with the task of solving the one-dimensional heat conduction equations for a slab moving downstream with given initial and flux boundary conditions. In the sticking region the flux can be assumed constant while in the slipping region one must take into account the reduced dissipation due to a reduction in pressure. As a rough approximation the initial temperature field or the field at the inlet to the bearing channel, z = 0, can be assumed to be parabolic (Figure 3). T_0 and T_1 could be taken as functions of the extrusion velocity. This complicates the inverse analysis somewhat. In reality, the inlet temperature must be expected to change with time since the extrusion process is a transient one. Again, a simplification is made under the assumption that small changes can be expected in the quasi-transient phase of the charge. The analytical solution to the heat conduction problem in the sticking region for the parabolic initial condition is given by Equation 4. Only the change in temperature from a point at z_1 to another at z_2 at the bearing r = R is evaluated.

$$\Delta T = \frac{2m\alpha}{kR} F(n, A)\Delta z + 4\left(T_1 - \frac{m\bar{v}R}{2k} F(n, A)\right) \sum_{n=1}^{\infty} \frac{1}{a_n^2}\left(\exp\left(-\alpha \frac{a_n^2 z_2}{R^2 \bar{v}}\right) - \exp\left(-\alpha \frac{a_n^2 z_1}{R^2 \bar{v}}\right)\right) \qquad [4]$$

Here α is the diffusivity, k the conductivity and $J_1(a_n) = 0$ where J_1 is a Bessel function (Carslaw et al, 1959). For all practical cases the transient effect terms are insignificant if z > 20mm, that is in the measurement region. Hence, the change in

temperature from one measurement point to another can be expected to be linear according to the parabolic temperature field. The same solution would be obtained if extremely fast redistribution of heat is assumed, and only energy equations and boundary conditions are sought to be satisfied. Figure 4 shows the temperature distribution at the bearing faces for velocities 25, 50, 100 and 200 mm/s. One immediately observes that heat generation is substantial and that there are practical limits to the extrusion rate. In fact, for a 7000-alloy Valberg observed a phenomenon called "bambooing". At exit velocities above 150 mm/s cyclic variation in profile diameter occurs as ram force oscillates abruptly. Figure 4 indicates that this may be a stick-slip phenomenon in relation to cyclic local melting of the profile surface.

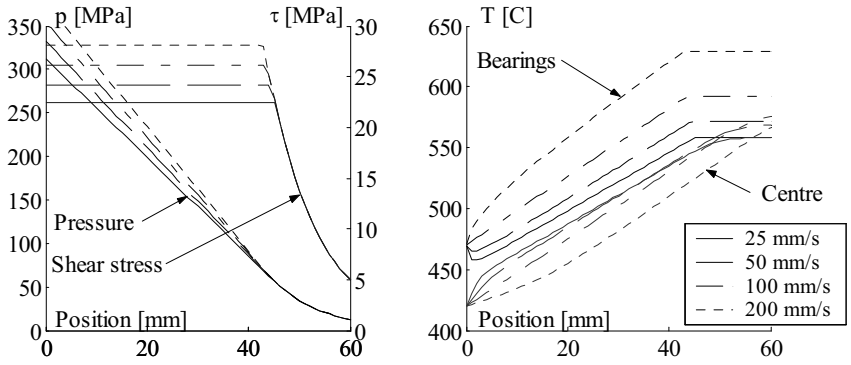

Figure 4. *Pressure build-up, friction and temperature on the bearings*

The established model for pressure and temperature change is the starting point for the inverse analysis. By choosing different levels of profile velocity (25 to 200 mm/s) one generates an experimental matrix. Also the channel diameter could have been changed in order to extend the analysis to either higher or lower strain rates. However, although the elected values of velocity are low, they cover most realistic and interesting cases for a long bearing channel geometry. A weighted least squares error gives a measure of fit between measured and calculated temperature change:

$$S(m,n,A)=\sum_{i=1}^{k}\frac{\left(\Delta p^{x}\left(v_i\right)-\Delta p^{c}\left(v_i\right)\right)^2}{\sigma_p^2}+\frac{\left(\Delta T^{x}\left(v_i\right)-\Delta T^{c}\left(v_i\right)\right)^2}{\sigma_T^2} \qquad [5]$$

$\Delta p^{c}(v_i)$ is a calculated value of pressure change for velocity v_i whereas $\Delta p^{x}(v_i)$ is the corresponding measured one. σ_P and σ_T are then standard errors of pressure and temperature measurement. In this ideal case, a perfect model is assumed so errors are related only to measurement techniques. Furthermore, it is assumed that no bias exists since proper calibration is performed. Simulated measurement results may then be generated by simply adding a random error with distribution $N(0, \sigma_P)$ and

N(0, σ_T) to the calculated result. A case with m=15 MPa, n=0.11 and A=1 is chosen here as these data are representative for AA6060. If σ_P is set to 5 and 20 MPa and σ_T to 1 and 5 K, measured results could very well look like those in Figure 5.

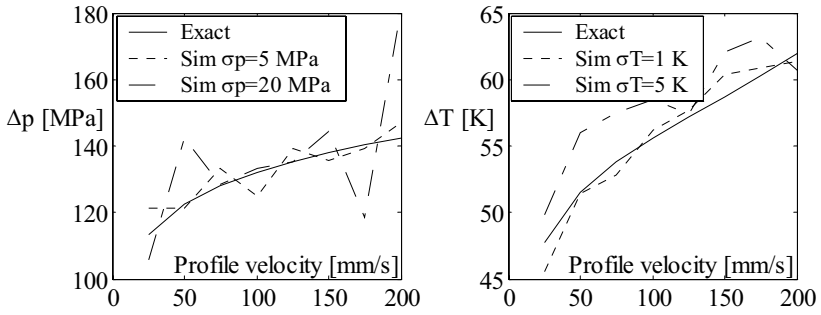

Figure 5. *Generated measured and exact results – pressure and temperature*

The objective of the inverse analysis is to perform critical hypothesis tests rather than to fit experimental data to neat models. In the case where only one model is under investigation the objective is to reject choices of m, n and A that are less probable. Low accuracy reduces confidence when the models are rejected. In the extreme case, one model is just as good as any other. By studying simulated results and perfect models one puts focus on measurement criteria. Figure 7 shows S calculated for a number of values of m and n when the measured values are assumed to have σ_P = 5 and 20 MPa and σ_T = 1 and 5 K. One observes that a large standard deviation related to measurement makes the retrieval of the initial values of m and n difficult. The minimum of S does not single out the real values of m and n, and a large variation produces a surface with small gradients. There are a number of optimization techniques that can be used in order to find the most probable solution (Özisik et al., 2000). Analytical equations are found by setting partial derivatives with regard to m and n equal to zero, but they must be solved iteratively.

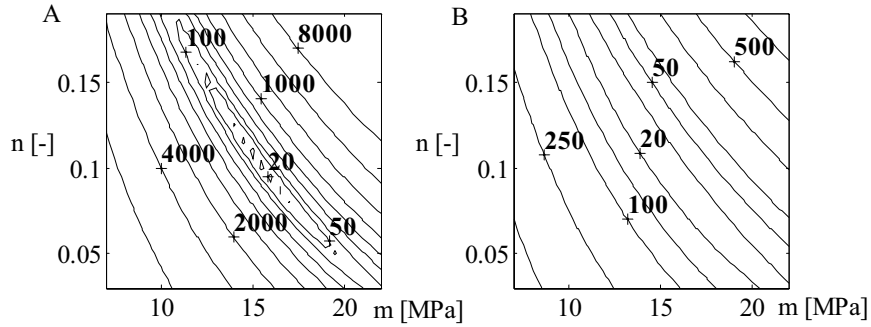

Figure 6. *S(m,n,A) plotted for A: σ_P = 5 MPa/σ_T = 1 K, B: σ_P = 20 MPa/σ_T = 5 K*

Figure 6 shows that measurement standard deviation should be close to σ_P = 5 MPa and σ_T = 1 K if the objective to use measurement techniques in the study of material models. The requirement is probably stricter since a number of simplifying assumptions have been made. Certainly, no model can be assumed to describe nature perfectly. Measurement errors are also seldom completely random. Furthermore, the number of unknown variables is much larger than indicated by this analysis. The constitutive equation is temperature dependent, and the container and bearing channel friction introduce a multitude of new variables. Finally, the energy equation introduces diffusivity as well as interface heat transfer coefficients as parameters. Although alternative tests may be used to determine many of these parameters, the errors in the tests still influence the extrusion analysis. One should also note that the assumptions of laminar flow and no elasticity simplify inverse modelling while unbiased measurement is hard to perform.

In the present study, the objective has rather been to perform measurements of pressure on the upper die face. If a study of self-stabilization effects is to be performed, pressure differences equal to those caused by variable bearing lengths or chokes must be identified. As the pressure build-up in the bearing channel might be less than 50 MPa, a natural requirement to the measurement accuracy is about 5 MPa. If the intension only is to give an indication of the loads on the dies and die deflection, requirements to accuracy may be somewhat reduced. The pressure on the upper die face may be expected to be in the range from 200 to 500 MPa. A requirement of 5 % accuracy would correspond to 10 to 25 MPa.

3. Measurement techniques and numerical simulation

3.1. *Temperature measurement techniques*

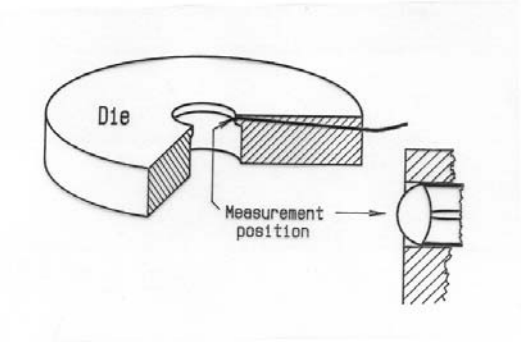

Figure 7. *Thermocouple measurement of profile temperature (Lefstad, 1993).*

Proper temperature control is essential to all material forming processes, the extrusion of aluminium being no exception. A high billet temperature is desirable since it allows the use of lower ram force. Yet, if it is too high, the consequence will be a cracked or uneven profile surface as a result of melting. Thermocouple or pyrometer measurement of the both billets and extruded profiles can be performed as a routine. However, the temperature in the bearing channel is of greatest interest since it is the highest. Lefstad has shown that thermocouples in direct contact with the profile (Figure 7) measure the profile surface temperature with an accuracy of 2-4 °C (Lefstad, 1993). Calibration is mainly related to scraping depth and can be performed as it is known that melting of Si-particles and subsequent profile surface tearing occurs above 577 °C for an Al-1.2%Si alloy. Another important aspect is the response time of the thermocouple. For the depicted set-up it has been found to be about 2 seconds. The use of this measurement technique is limited to experimental activity as the thermocouple leaves a groove in the profile surface.

3.2. *Die face pressure measurement*

Measurement essentially consists of converting and interpreting signals so that a greater understanding of nature is obtained. Although the human body is sensitive to pressure, it lacks the ability provide the brain with accurate quantitative measures. Pressures in forming processes are also normally extremely high. Hence, alternative methods must be used to transform pressure to comprehensible signals. When using a computer the final output is normally an electric one. Calibration is necessary if such a signal is to be interpreted in terms of pressure. One should note that pressure measurement always includes some kind of averaging since pressure is defined as a pointwise measure of force divided by area. All pressure sensors are in reality force sensors, and the size of the equipment will determine the spatial resolution.

Development in the field of pressure, force and friction measurement in metal forming has been going on for at least the last 70 years (Siebel et al., 1933). The objective has been to gain insight and improve process control. General problems relate to the development of reliable sensors, the establishment of proper methods of calibration and the reduction of sensor size. In the case of hot forming processes, the main challenges are the extremely high pressures, the high working temperature and the sensitivity to sudden temperature changes. For the extrusion process one must expect an increase in temperature from about 450 to about 600 °C close to the bearings. The conditions are detrimental to both accuracy and sensor operating time.

3.2.1. *Alternative measurement principles*

Various physical principles have been and may be applied to the measurement of pressure in metal forming. Most sensors used in polymer forming industry make use of the piezoelectric principle, which states that there is a direct link between charge distribution in and the applied pressure on a piezoelectric crystal. However,

standard piezoelectric sensors usually are limited to temperatures and pressures below 300 °C and 30 MPa due to material considerations.

Piezoelectric sensors are among the very few ones with the ability to convert pressure directly to an electric signal such as a voltage. The most popular alternative consists of using a displacement sensor to measure an elastic membrane, plate or bellow deflection caused by the applied pressure. Piezoresistive sensors have the property that resistance increases with load or straining. Hence, they may measure the stresses in a deflected membrane and thereby the applied load. Again temperature represents the main problem. High temperature strain gauges exist, but they are often sensitive to temperature changes. Fastening of the strain gauge poses an additional problem as normal glue does not suffice at high temperature. Various pressure sensors for extrusion at lower temperatures using traditional strain gages to measure elastic deflection have been developed (Yoneyama et al., 1993, Yoneyama, 1999). A sensor and the complete experimental set-up are shown in Figure 8. An ingenious calibration method reveals a linear relationship between the pressure and the output signal. The calibration is performed in the extrusion set-up or in-site.

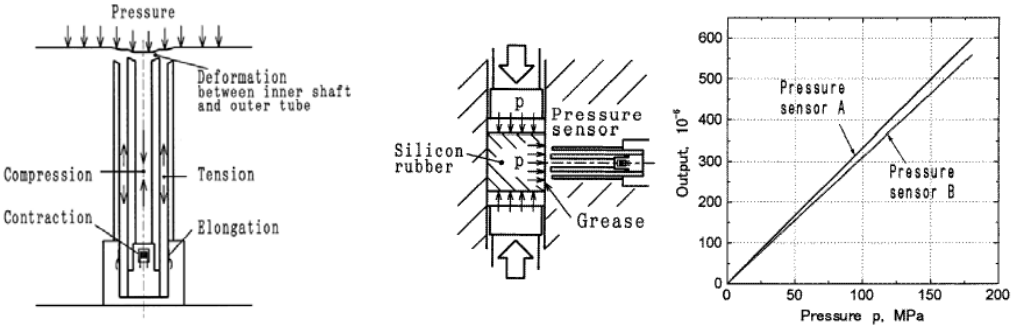

Figure 8. *Strain gauge pressure sensor developed by Yoneyama (Yoneyama, 1999)*

An elastic deflection may also be measured by some optoelectronic method. Fibre-optic strain gauges may be used in the very same way as traditional ones, but they give can withstand very high temperatures. The two most popular ones are the Fabry-Perot (FP) interferometer and the Bragg-interferometer. The first is probably best suited since the deflection of a small elastic membrane may be measured directly. The sensor system assesses the reflected light from a fixed semi-transparent surface and from a deflecting mirror. The principle is that the wavelength modulation of reflected and transmitted light depends on the width of the gap between the surfaces. The advantages are small equipment size, high accuracy and high resolution. Actually such sensors are most effectively used in the measurement range of a wavelength, which is a very small measure, also for this application.

Alternative fibre-optic sensors relate measured intensity to displacement. In the case of the dual fibre intensity sensor, light emitted from one fibre is reflected by a

plate and absorbed by another fibre. The intensity then relates to the distance between the plate and fibres. Reflection properties of the bottom side of the deflecting plate must be satisfactory, and coating or insertion of a reflecting plate is probably a complicating necessity. Microbend sensors work on the principle that light escapes the fibre and the intensity falls if the fibre is bent. The principle is not ideally suited to this application. Another completely different group of sensors are the inductive ones. These consist of coils and permanent magnets and are therefore relatively large and normally show a poorer high temperature performance.

3.2.2. *Description of the Capacitec capacitive sensor*

This article focuses on capacitive sensors (Baxter, 1997) as they are accurate, temperature insensitive, very small and user-friendly. Capacitive measurement is simply a determination of potential differences and can be used in studies from the atomic level up to the macroscopic level. The potential difference, V, relates to the charge, q, of two interacting bodies as V=q/C where C is the capacitance. When measuring distance with a properly designed capacitive sensor consisting of two flat plates, the capacitance is close to inversely proportional to their separation (d). The analytic relation $C=\varepsilon A/d$ holds very well if plate separation is significantly smaller than plate extension. A is the surface of a plate and ε is the dielectric coefficient of the medium which in this case is air. One should note that the main reason for deviations from the above relation is the spreading of the electric field close to the edges. By adding a guard ring to the sensor, the edge effect is suppressed.

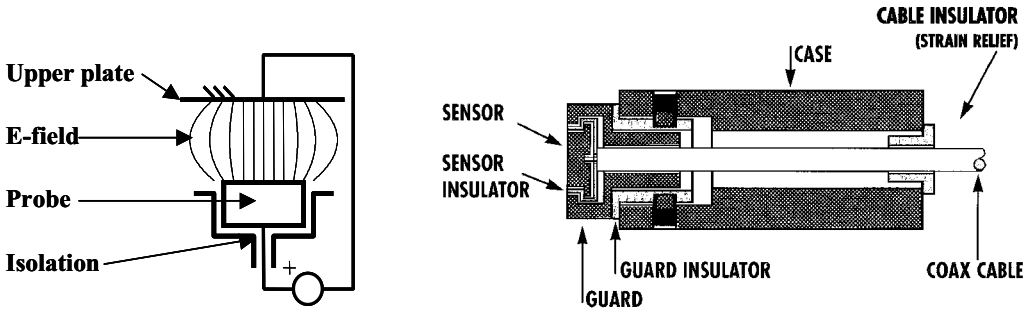

Figure 9. *Capacitive sensor principle and Capacitec probe used (Capacitec, 2000)*

Table 1. *Sensor characteristics – Capacitec HPC-75A-V-N3 (Capacitec, 2000)*

Property	Data
Typical calibration range	0 – 10V = 0 – 500 µm
Linearity	±0.2% of Full Scale = ±1 µm
Repeatability	±0.01% of Full Scale = ±0.05 µm
Resolution	±0.01% of Full Scale = ±0.05 µm
Max temperature	825 °C
Temperature sensitivity at 450 °C	-0.2-0.3 µm/10 °C

In this study a high temperature probe produced by Capacitec Inc. has been used (Figure 9). A probe constitutes one of the plates in a capacitor and is built into a guard and the case. A deflecting plate is the other sensor plate, which is at ground level. Signal conditioning of the Capacitec 4100 amplifier is described by Foster (Foster, 1989). The main characteristics of the measurement system are shown in Table 1. Although capacitive sensors may be used in a number of ways, the evaluation of high frequency signals (15.625 kHz) by synchronous demodulation is normally viewed as preferable with regard to noise. The output is simply a direct current signal very close to proportional to sensor plate separation. The calibration is normally undertaken with a micrometer with an accuracy of less than ±0.5 μm.

3.2.3. *Evaluation of pressure sensor design*

Although capacitive probes may register very small signal changes, a realistic requirement to resolution is ±3 MPa. The preceding inverse analysis set the requirement to accuracy to about ±5-10 of 250 MPa. Table 1 indicates that the non-linearity of the equipment is the main limitation. In principle, the effect could be taken into account when measuring or reduced by operating with a smaller range. However, as long as the accuracy of the calibration method is limited to ±0.5μm, there is a limit to the accuracy obtainable by the pressure sensor without any other means of calibration. A direct calibration method for pressure shown below will improve accuracy, but the above values may still be used in the design phase. A requirement to the sensor is thus that it should yield a displacement of at least 0.5·250/10 μm = 12.5 μm. The sensor optimization task then consists of changing design in order to maximize deflection while stresses are kept below the yield limit.

A fundamental requirement to pressure measurement is that it should have a high spatial resolution. If the sensor is to measure close to the outlet or other details of interest, it must itself also be small. As container diameters may range from a 100 mm in experimental presses to ten times larger in industrial ones, the sensor diameter should be no more than about 10 mm. One should note that dies deflect significantly during extrusion and that displacement of the sensor plate and consequently a small non-zero output may be experienced even in the absence direct loading of the sensor. Remedies must be found either through design or calibration.

Simplicity is a key requirement. Sensor design should be simple to analyse and build on a simple principle. Furthermore, sensor design should allow simple and accurate machining. The use of a ready-made capacitive sensor system reduces development time. Yet, a high sensor price necessitates reuse. A method allowing easy, accurate and reproducible mounting and dismantling should therefore be sought. The probe must not be allowed to move permanently at any stage. Rough handling is especially a problem under industrial conditions, and fragile components should be properly protected during assembly.

The criteria above are probably fulfilled by an infinite number of possible designs solutions, some of which have been thoroughly studied. Table 2 has been

found productive as it reveals some general advantages and disadvantages of groups of design solutions. One should note that it does not assume the use of a special measurement principle. However, in the following sections the pressure sensor consists of a probe measuring an elastically deflecting loaded plate.

Table 2. Sensor design evaluation and categories

Demountable sensor	**Permanently fixed sensor**
+ Less expensive if used repeatedly	+ No permanent displacements during loading
The sensor as an insert in the die	**The sensor integrated in die design**
- Al may penetrate into crevices	+ Most robust
- Height difference in surface	- Difficult to check dimensions accurately
- Difficult to analyse numerically	+ Simple optimization of sensor design
⇓⇒	
Insert from bottom face	**Insert from top face**
- Shear causes a lot of tilting	- Locked in place by press rest
+ Standard calibration easier	- Danger of unwanted pull out
+ Small force applied to sensor	- Difficult to dismantle

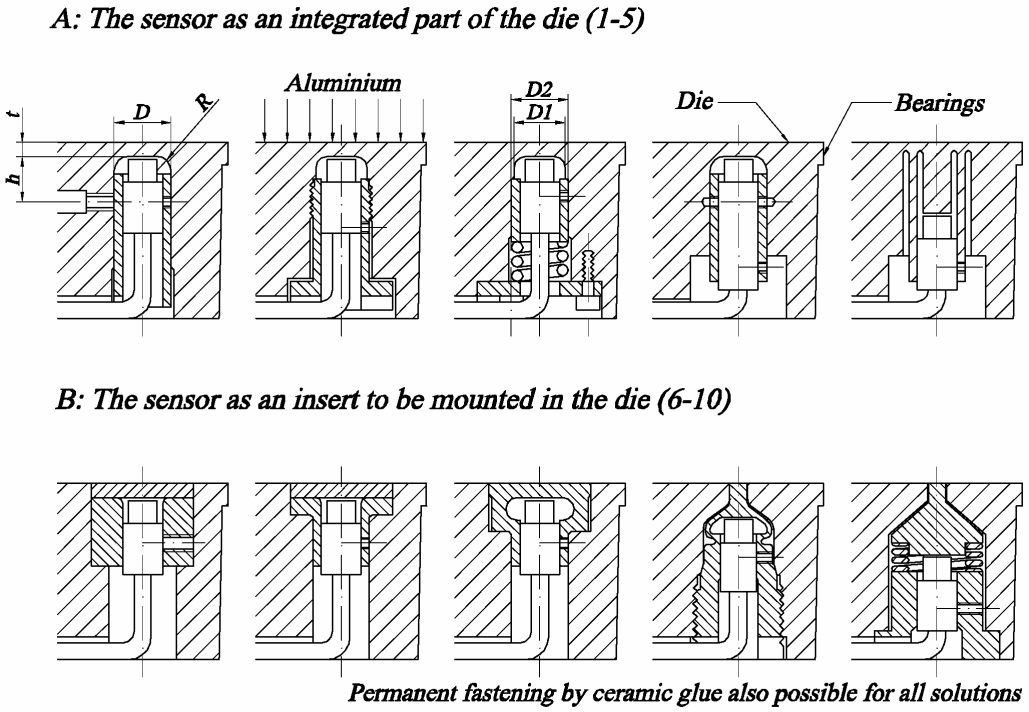

Figure 10. S*ensor design examples – integrated (A) and insert(B) solutions*

Some practical design solutions related to the categories above are presented in Figure 10. Most alternatives have been tested either in hot compression or extrusion

and found quite satisfactory. An insert sensor seems to be an ideal solution as it gives the impression of being a unit, sensitive only to the load applied to it and easily calibrated in advance. However, this is hardly the case if it is in the form of a plug mounted from the upper side of the die as it quite necessarily is in intimate contact with the die and thus affected by the interface conditions. An insert sensor mounted from the bottom side may be somewhat less influenced by the deflection of the die. Most sensors used in materials forming have until now been of this type. So-called pin sensors consisting of a hole in the die filled with a pin and an elastic element, have been popular (Hansen et al., 1993). The displacement may be logged by for instance a capacitive probe. By using also a tilted sensor both pressure and shear traction may be measured. A very accurate pressure and friction sensor for low temperature forming processes has been developed (Yoneyama et al., 1993). A fundamental disadvantage with all such sensors is, however, that hot aluminium penetrates into and fills even the narrowest crevices in the surface. Furthermore, the sensor proposed by Yoneyama et al. is much too large, and many of its virtues are lost when it is made smaller and modified so that it can be used with the capacitive sensor in question. Figure 10 shows possible design solutions (sketches 9 and 10).

A sensor integrated in the die is probably the most robust solution, but sensitivity to the overall distribution of load on the die must be taken into account. In order to avoid manufacturing a cavity of such a large depth, a die consisting of several parts has been designed (Figure 15). A number of simple and accurate mounting solutions then exist, yet the upper surface of the die need not be broken. The very same design solution may be and has been applied to typical industrial dies.

3.2.4. *Optimization of sensor geometry*

Pressures applied on the die may range from less than 150 to more than 500 MPa in aluminium extrusion. At the same time, the yield stress of typical H13 die steel at the relevant temperature is somewhat above 800 MPa (Uddeholm, 2002). The optimization task consists of maximizing plate deflection while preventing yield and permanent displacements. At the higher stresses, the mere existence of a cavity may cause stresses to exceed the yield stress at least locally. The level of stress may be limited by increasing the plate thickness (t) or by reducing the diameter of the cavity (D)(Figure 10). For thick plates, however, the largest effect is obtained by increasing the radius of the cavity (R), as the level of shear stress will be most critical. The displacement measurement also depends on the distance from the bottom side of the plate to the point where the probe is fixed to the wall of the cavity (h).

Figure 11 shows die deflection and maximum von Mises stress as a function of plate thickness and cavity diameter. R is has been set to 3 mm. Only elastic behaviour is assumed with a Young's modulus of 180 MPa. A uniform load of 250 MPa is applied over an area with diameter 35 mm. One observes that the optimum is represented by a line rather than a point. Typically, the largest deflections to be expected would be about 30 μm, or about 60 times the linearity of the system.

One should note, however, that practical considerations limit the design space. The smallest high temperature probe provided by Capacitec has a head and case diameter of about 5 and 6.3 mm respectively. Furthermore, the method of optimisation presented does not take into account radically different design solutions and other design criteria. An additional restriction is that measurement of deflection should be insensitive to shear tractions. These are expected to be relatively small and are not measured. Yet they cause tilting of the sensor plate and more critical loading.

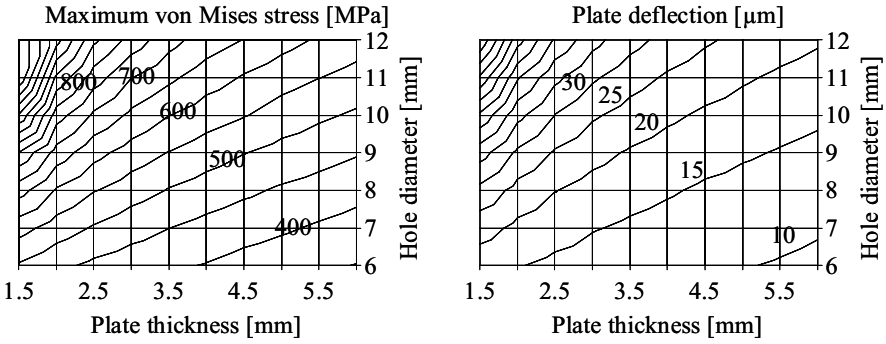

Figure 11. *Von Mises stress and plate deflection-plate thickness and cavity diameter*

3.2.5. *Calibration and temperature correction*

According to the supplier's instructions the capacitive sensors are calibrated at room temperature so that an output of 10 V indicates a distance of 500 μm. A 30 μm deflection corresponds to a voltage change of 0.6 V, which is sufficient at least when compared to the 1 mV resolution of the system. Measurement accuracy is, however, limited by the 1μm linearity, but even more so by issues related to fastening of the probe, variability in manufacture (Figure 3), overall die deflection, high temperature behaviour and sensitivity to sudden changes in temperature of about 60-70 °C. Early experiments indicate that these effects limit accuracy to about ±2 μm / 20 μm. Under such circumstances an indirect calibration by FEM is corrupted by poor input data.

Table 3. *Sensitivity of deflection [μm] to variations in geometrical parameters*

	R=2		R=3	
	t=2.5	t=3	t=2.5	t=3
d=8	23.6	19.4	20.2	18.1
d=9	27.3	23.4	24.5	21.6

In-site pressure calibration is a necessity. Approaches using smaller specimens and point loads have been found inaccurate and impractical though they may reveal the spatial sensitivity of the sensor. Calibration can be performed most easily in the relevant temperature range by plugging the outlet and compressing a hot aluminium billet (Figure 12). As static friction is low, pressure can be expected to be isotropic and homogeneous. This is confirmed by tests with billets of various lengths. The

pressure is then easily calculated and can be compared with signal output. The three sensors occupy the same positions, and the difference between sensor 1 and the two other sensors can be explained by a somewhat different design. One should note that the load distribution on the die in this case is not too different from that experienced during extrusion, and the effects of die deflection will therefore be included in the calibration. Furthermore, the influence of the liner load can be checked separately. The limiting accuracy of the press force measurement is ±50 kN or about ±6 MPa.

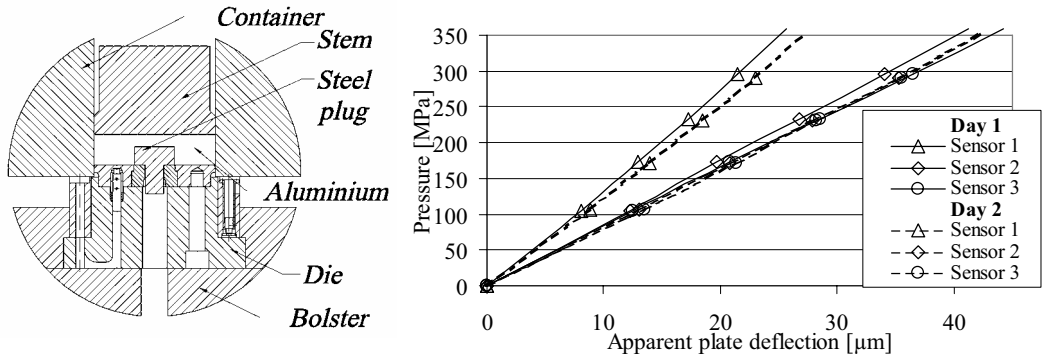

Figure 12. *In-site calibration of pressure sensors in the die*

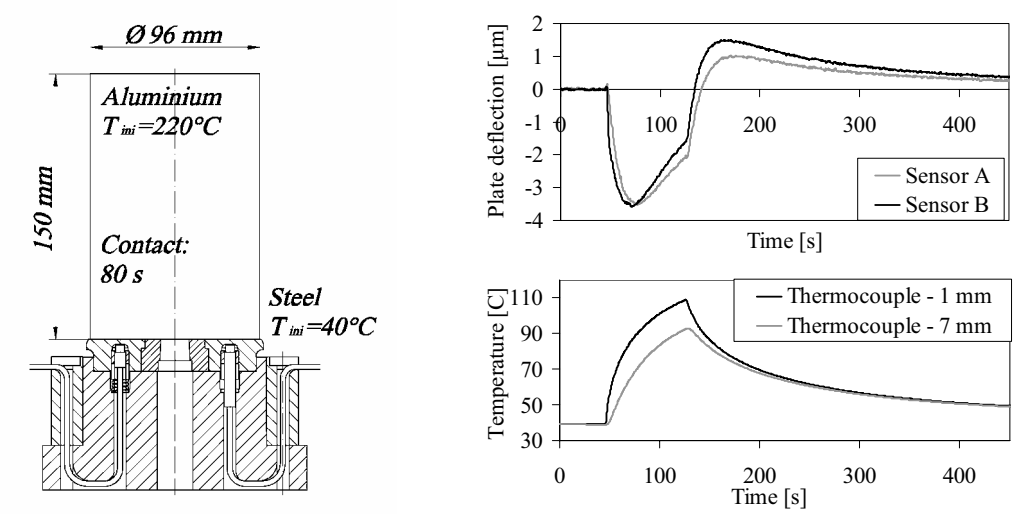

Figure 13. *Temperature test set-up and typical results (no mechanical load applied)*

Calibration is performed in the lower range of the temperature interval experienced during extrusion, and isothermal conditions are sought so that no transients are present. The thermal characteristic of the probe as well as lowering of the E-modulus are thereby taken into account. Even so, temperature changes during extrusion will provoke two effects. First, changes in dielectric properties of the

material will cause a fall in output of approximately 5 mV (0.25 μm) for each 10 °C of temperature increase. Second, sensor plate heating will cause thermal expansion and a slight plate bending. This effect is transient as it is related to the non-uniform temperature distribution. A simple test where a hot billet is placed on top of the die reveals the transient behaviour at room temperature (Figure 13). This serves as a test case when temperature effects during extrusion are modelled numerically (Moe, 2003). One should note that the two effects mentioned above affect the output in opposite directions, but their transient nature and their relative sizes prevent complete cancellation. However, temperature effects account for less than 10% of the output signal, and a proper correction scheme brings this number down to 1-2%.

3.3. *Numerical simulation*

Extrusion geometries have been specifically chosen so that they can be studied more or less satisfactorily under the assumptions of axisymmetry and plane strain. This allows the use of 2D programs, which are more accurate and practical than 3D packages. The Lagrangean software Forge2 has been found able to model bearing channel phenomena (Tverlid, 1997), but has only been used in the design stage. Alma has been used extensively since it is a dedicated aluminium extrusion code (Holthe et al., 1992), which has been thoroughly tested out on relevant cases. The program is in essence Eulerian, but allows mesh compression due to movement of the ram. A Zener-Hollomon constitutive relation has been applied:

$$\bar{\sigma} = \frac{1}{\alpha} \arcsin h\left[\left(\frac{Z}{A}\right)^{1/m}\right] \qquad Z = \dot{\bar{\varepsilon}} \cdot \exp\left[\frac{Q}{RT}\right] \qquad [6]$$

σ and ε are measures of equivalent stress and strain. Material parameters (m, α, A) have been obtained through torsion testing. T is the temperature, Q the activation energy and R the universal gas constant. A limitation with the code is that it assumes full stick at the container walls at all instances. The program treats heat flow of all parts at all stages of the extrusion cycle. By keeping heat transfer parameters constant, it probably exaggerates the intimacy of contact in the stage in front of the upsetting. A correction has therefore been made. Ideas and Abaqus have been used in the studies of die deflection and heat transfer. Material constants of the die steel correspond to those of an H13 quality (Uddeholm, 2002).

4. Extrusion experiments and discussion

The two simplest profile geometries are probably those of rod and thin-strip extrusion, and they therefore serve as test cases in this study. In addition to being

simple to analyse these profiles have much common with industrial open profile shapes. Rod extrusion allows the most thorough study of general friction conditions both in the container and in the bearing channel as axial symmetry reduces the computational costs, increases accuracy and simplifies the evaluation of results. In addition, it provides the simplest test or calibration case for measurement techniques and allows a larger number of replicate measurements than any other geometry.

Flow stability and tool deflection considerations are of smaller interest for rod extrusion, but will play an important role when extruding very thin aluminium strips. In that case, the profile thickness will vary with both ram position and along the width of the cross-section due to changing die load conditions and die deflection. The same will be the case with the bearing channel angle, which controls friction (Abtahi et al., 1996). By reducing the profile thickness the limit of self-stabilization is ultimately found. It should be noted that if the thin strip is sufficiently wide deformation in the central part of the strip is close to the plane strain and can be studied relatively well by 2D simulation. It has been found that a plane strain assumption also applies well to practical cases where the reduction in the symmetry plane is equal to the overall one. This means that $Re=\pi D^2/(4Bt)=D/t$ or $B=(\pi/4)\,D$. Re is the reduction, D the container diameter, B and t the strip width and thickness.

4.1. *Rod extrusion – Axially symmetrical extrusion case*

4.1.1. *Experimental set-up*

All experiments reported on were performed in an 8 MN vertical laboratory press, with a container diameter of 100 mm (Figure 1). Figure 14 presents two different die designs used in the study of rod extrusion. Experiments with the two provided quite similar results, but the complex die allows the simplest mounting of sensors. Two probes were fastened with setscrews while one was kept in place by an inconel spring. In addition, the complex die can be used with insert outlets with different extrusion ratios and bearing channel angles and lengths. This allowed the study of bearing channel friction without having to manufacture new dies and sensors. Only some of the results of a larger experimental matrix are presented here.

In case of the complex die, the capacitive sensors have also been integrated in a load cell, which measures the liner load. The mean pressure on the die can then be deduced from the ram load and the liner load. The load cell is designed so that it is only compressed by the load from the liner and not sheared. As a rather rough approximation, the liner load, F, is related to measured compression, d, as $d = (L/AE)\,F$, where A is the cell area, E the mean elastic modulus and L the height of the load cell. A typical load of 1 MN would then yield a displacement of about 30 μm. A more accurate relation was obtained by FEM or by performing calibration through compression testing. One should note that the load cell is not more accurate than the pressure sensor. A better solution would be to mount the container

permanently on top of much longer rods as has been done elsewhere. Such a solution, however, could not easily be integrated in the extrusion equipment at hand.

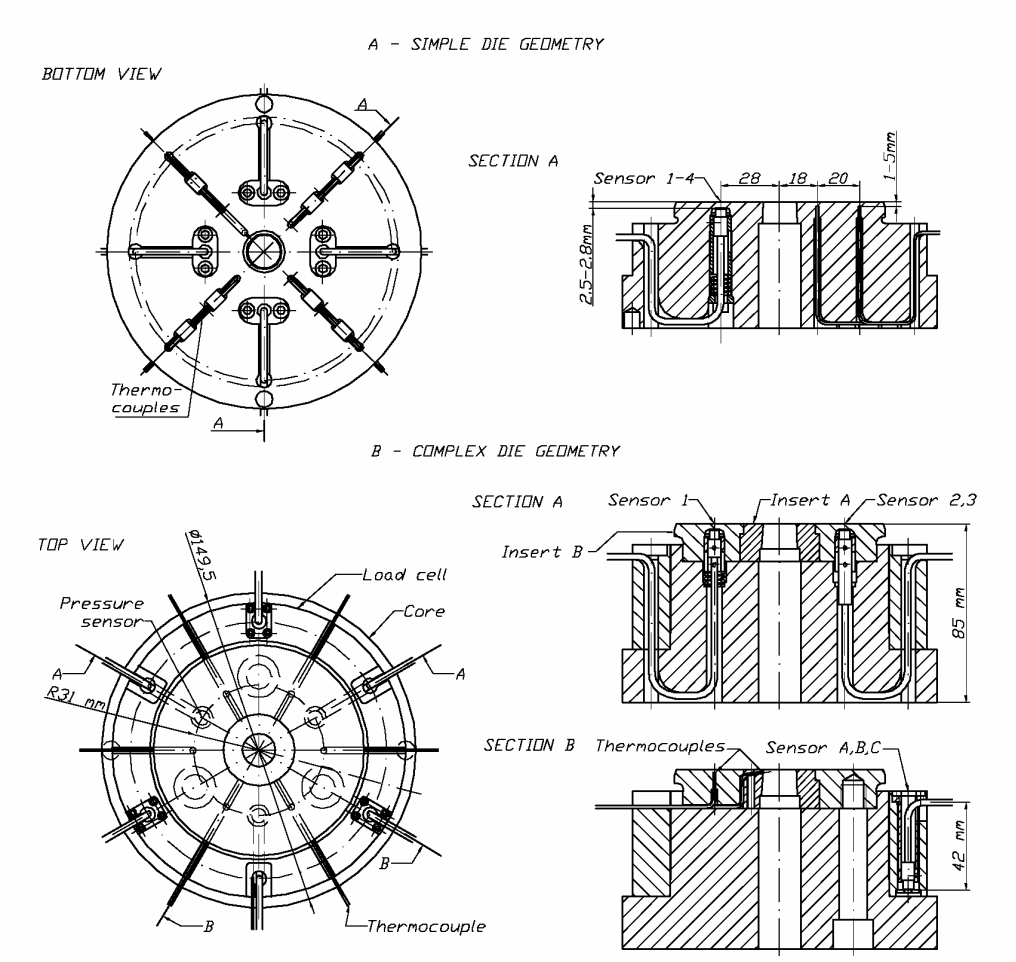

Figure 14. *Simple (A) and complex (B) die geometry for rod extrusion experiments*

Table 4. *Process parameters – rod extrusion case*

Parameter	Value	Variation
Alloy	**6060.35**	
Press/extrusion ratios	**40**, 80 (**15.8**,11.2 mm)	±0.02 mm
Outlet velocities	200, **400**, 800 mm/s	±4 mm/s
Bearing channel geometry	**Zero bearing** / 40’ choke	5’
Billet temperature	**450**, 500 °C	±5 °C
Billet dimensions	**Ø96x200** mm	±1 mm
Butt end (not removed)	**19** mm	±0.5 mm
Bolster temperature	**480** °C (Die <435 °C)	±2 °C
Container temperature	**430** °C	±2 °C
Ram temperature	**130** °C	±5 °C
Cycle period	**10** min	±1 min

In the experiments, four different outlet geometries were used. As indicated by the bold letters in Table 4 only the case of extrusion ratio 40 and approximately zero bearing is presented in this article. Replicate measurements were undertaken in two ways. First, all sensors were positioned at the same distance from the outlet 120° apart. Second, the whole experimental series was repeated after the equipment first had been dismantled and then reassembled. Probe positions for sensors 2 and 3 were switched while the same probe was used in sensor 1 on both days. Although no firm conclusion can be drawn from the sparse data, Figure 12 seems to indicate that the calibration curve depends just as much on the mounting as on the probe used.

4.1.2. *Results and discussion*

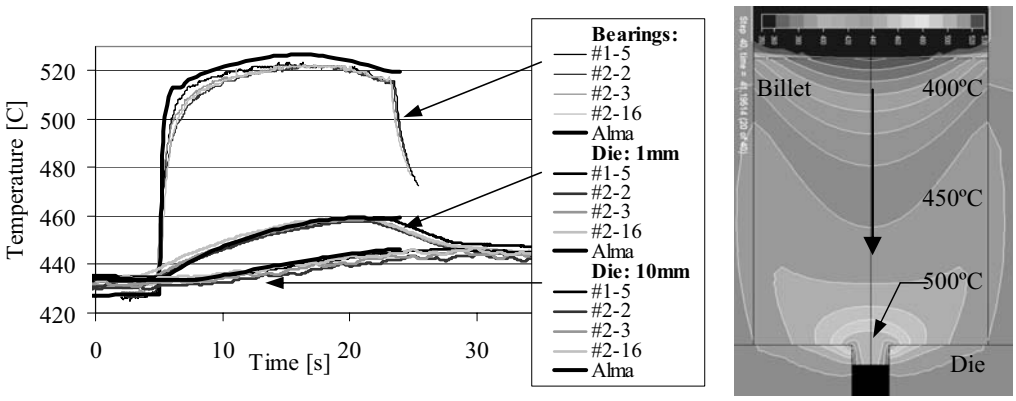

Figure 15. *Calculated and measured temperature histories and Alma plot after 10 s*

During extrusion two thermocouples measure the profile temperature at the outlet of the die. At the same time the temperature at different depths at the very same position as the pressure sensor was measured (Figure 15). The close agreement between numerical and measured data supports the choice of material model and heat transfer parameters. A much larger temperature change is experienced in the flow at the outlet close to the probes. A change of less than 50 °C causes a transient thermal plate bending effect, but experience from Figure 13 indicates that this should not be larger than about 2 μm or 10 % of the total pressure output signal.

Figure 16 shows the load output signal before and after the calibration curves of Figure 12 have been applied. Apart from determining the conversion from voltage to pressure calibration serves to reduce measurement variability from about 15 % to 5 % of full scale. The pressure estimate given in Figure 16 is obtained by subtracting a force corresponding to a 19 MPa container friction from the ram force and dividing by the actual die face area. The choice will be discussed below.

All x-axes are time axes, but an approximate ram displacement is obtained by multiplying time with mean ram velocity. One observes that displacement signal does not return to zero immediately after unloading, but rather approaches the value

asymptotically. This is most likely due to transient plate bending effects. The sudden change in output after unloading occurs as the ram is torn off the press rest.

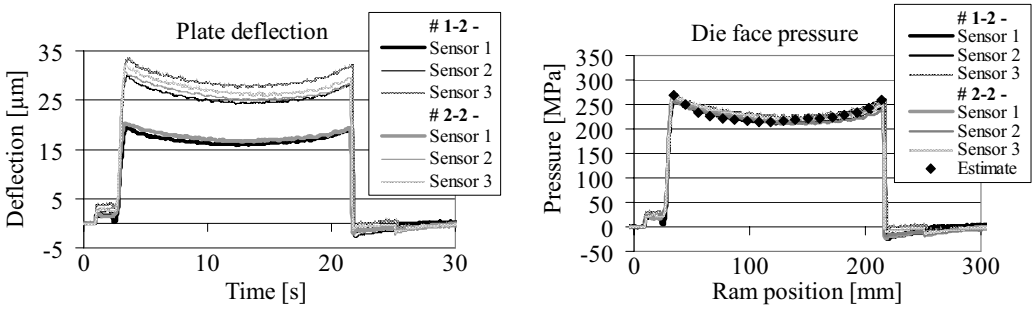

Figure 16. *Estimated and measured sensor plate deflections and pressure*

During extrusion the pressure distribution on the die surface will change as the flow becomes more radial at the end of the charge. Figure 17 displays this development. The pressure sensors have been placed at a distance from the outlet where the pressure is approximately the average of the pressure on the die thus making the comparison of ram force and pressure measurements more justified. Figure 18 with ram force, measured liner load and the estimate presented above motivates the choice of 19 MPa as the shear stress towards the container. The liner load is observed to be approximately proportional to the length of the billet. This indicates that the shear stress is almost constant. There is close agreement between the ram load curve measured directly and the one calculated on the basis of measured die face pressure and liner load. No curve fitting has been performed. A somewhat larger difference was anticipated since data have not been corrected for thermal effects and the assumptions are rather course.

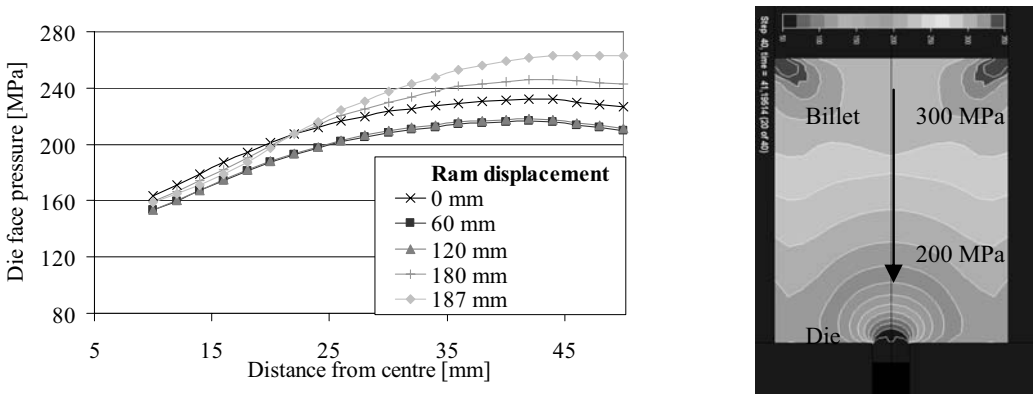

Figure 17. *Die face pressure and pressure distribution calculated by Alma*

Pressures calculated by Alma and measured ones are compared in Figure 19. The agreement is also quite good in this case. Apparently the peak pressure is somewhat underestimated by Alma. This may be explained by the fact that the calculation assumes full stick at all times, while probably some sliding may occur in the early phases of the charge. Flitta et al. argue that the container friction coefficient will depend on strain rates in addition to temperature (Flitta et al., 2002). A low strain rate initially may give a low container friction and a somewhat higher die pressure. One should note, however, that no temperature corrections have been performed for the curves of Figure 19. While the initial pressure probably is quite correct, the decrease in pressure is to a certain extent due to the upwards plate bending phenomenon. Both the estimate and the fact that the pressure curves do not return directly to zero upon unloading indicate a 10 MPa higher pressure towards the end of the charge. This indicates that the Alma curves are somewhat too low at all times.

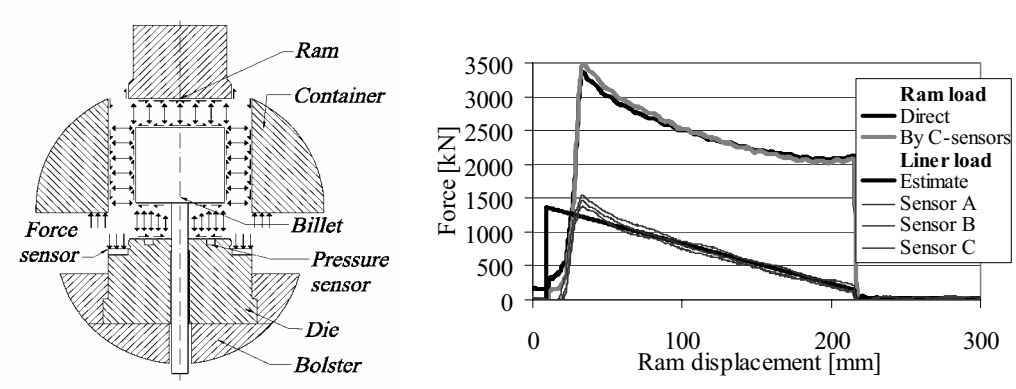

Figure 18. *Force components and measured and estimated ram and liner load*

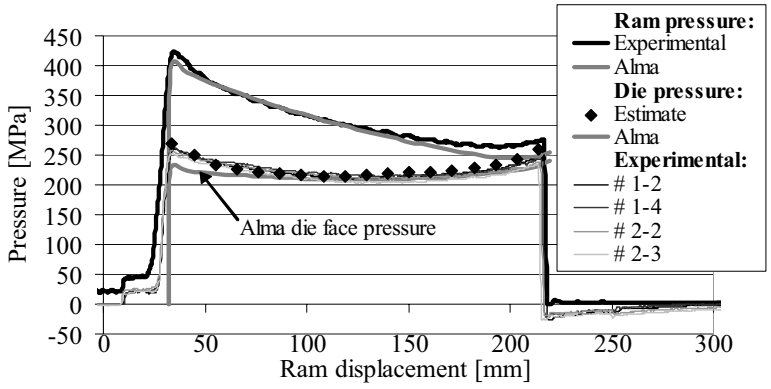

Figure 19. *Mean pressure on the ram and pressure on the die face*

4.2. *Thin strip extrusion – Plane strain extrusion case*

4.2.1. *Experimental set-up*

The thin strip die geometry used in the study of flow stability is given in figure 20. The outlet dimensions are 78.5 mm x 1.7 mm. Along the whole periphery of the parallel bearings the inlet radius is 0.5 mm and the length 0.5 mm followed by a 3° release over a length of 4 mm. Capacitive pressure sensors are positioned at the centre of the die (P1) and at the corner of the profile (P2), both 15 mm from the die opening. Thermocouples are inserted in the die as marked in Figure 20. The profile surface temperatures at the bearings were measured at the middle of the width and at the corner of the profile. These are the positions with the highest temperatures, to which the material is exposed during the whole cycle. Two thermocouples are also positioned in the die, 4 mm and 9 mm from the die opening in order to record gradients close to the bearings and temperatures close to the pressure sensors.

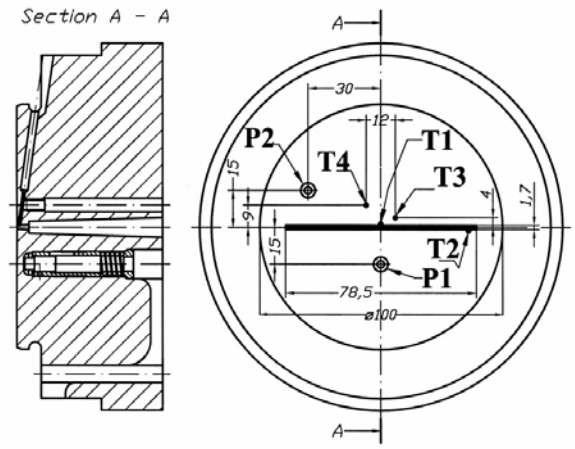

Figure 20. *Mean pressure on the ram and pressure on the die face*

Conditions that were very similar to those in Table 4 were chosen. The billet length was reduced to 150 mm as considerations with regard to space required profiles longer than 8 m to be bent. According to Table 5 somewhat higher billet temperatures were also set so that the temperatures at the bearings were similar to those obtained under industrial conditions (550 – 590 °C). If instabilities occurred, they would only be expected at higher velocities and temperatures.

Table 5. *Variants of billet temperatures and extrusion speeds*

Exp.	T - billet (°C)	Ram speed (mm/s)	Profile speed (m/min)
1	480	9	31
2	480	16	56
3	520	9	31
4	520	16	56

4.2.2. *Results and discussion*

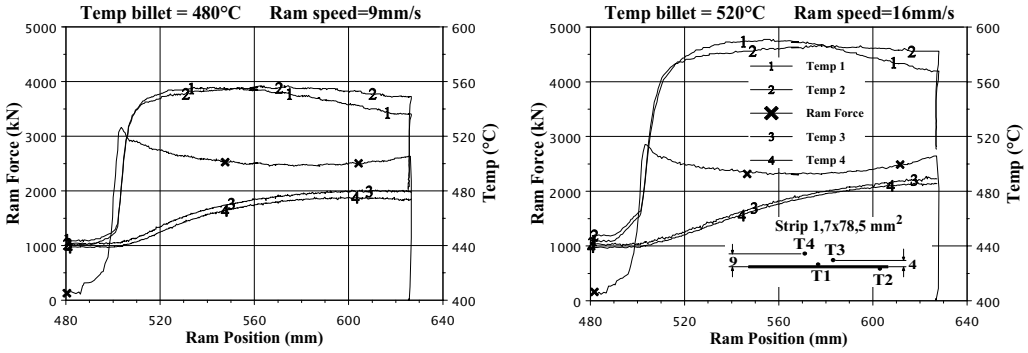

Figure 21. *Mean pressure on the ram and pressure on the die face, run 1 and 4*

Table 6 shows the characteristic values of force and temperature readings for all experiments. The forces and temperatures in Experiments 1 and 4 as a function of ram displacement are plotted in Figure 21. As relatively short billets are used and variation in liner load is small, there is a rather small difference between the ram force at the start and at the end of the extrusion. As to be expected, a high ram velocity and low billet temperature gives the highest force. The experimental matrix provides a variation in force of ±300 kN or ±10 % and in temperature change of ±10 °C or 15 % of the change. Such variation should be detectable with the sensors at hand, and the set up provides a good test case. However, even for extremely high billet temperature and ram velocity, flow instabilities could not be provoked.

Table 6. *Forces and temperatures for the runs 1-4*

Run no.	Force(kN) max – min	Maximum temperature [°C]			
		T1	T2	T3	T4
1	3170 – 2450	556	557	479	475
2	3340 – 2580	575	577	481	477
3	2780 – 2240	574	567	487	484
4	2920 - 2300	591	586	489	485

The development of the profile temperature differs somewhat for thermocouples T1 and T2, as seen in Figure 21. In the centre (T1) the temperature is highest at the start of the extrusion, and decreases by 20 °C towards the end. At the profile corner (T2) the temperature varies by only 5 °C with the highest temperature in the middle of the extrusion. The difference may be explained by a higher heat generation close to T2 and spatial variation related to heat transfer to the die. Temperatures T1, T3 and T4 for the different experiments have been calculated by the Alma plane strain module. In Figure 22 one observes that there is close agreement between the measured and calculated temperature on the bearings. Probably due to poor contact

between T3/T4 and the die there is a 5 °C difference between measurement and calculation. Figure 21 still indicates a certain temperature change around the probes.

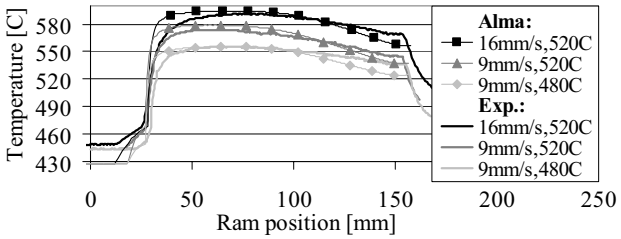

Figure 22. *Measured and calculated temperature for experiments 1, 3 and 4*

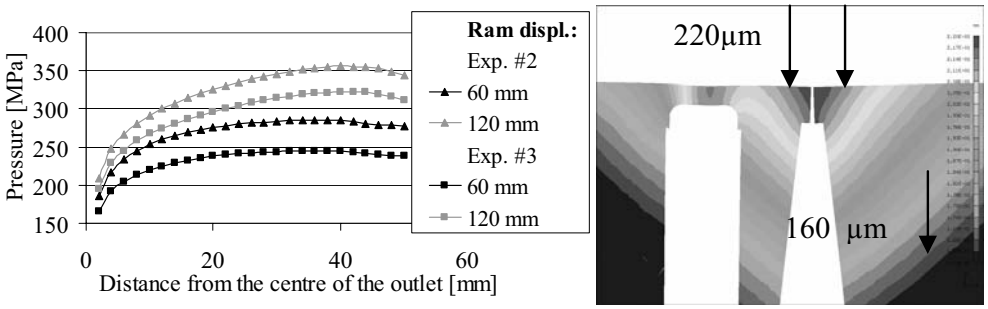

Figure 23. *Calculated pressure distribution on the die face in the centre plane and displacement in the extrusion direction (max: 220 µm, min: 160 µm)*

Alma also provides the pressure in the symmetry plane, and Figure 23 shows the die face pressure at the mid point and at the end of the charge for the extreme cases, runs 2 and 3. Since the program is only 2D, ram force estimates generally do not agree with the measured values. Since no in-site calibration was performed, pressure measurement accuracy was only about ±10 %. Deflection calculations using the data of figure 23 show that displacements other than those related directly to the deflection of the sensor plate makes analysis of contact between the probe and the die very difficult. An independent calibration scheme as described above is regarded as a necessity as measured deflections measurements depends on contact conditions.

However, the objective of this study is not so much to determine absolute values of pressure as to test the sensors' ability to determine pressure variation with regard to time and position. According to Figure 23 one may expect that there will be a 20 % variation in pressure between the runs. Hence, the case is a test of the material model and ability of the sensors to detect changes caused by variation in input variables. Figure 24 shows the centre line pressure, P1, throughout the charge for three different combinations of variables. All experimental values have been scaled for each sensor so that the largest overall deflection and pressure measured is equal

to 1. Also Alma results have been scaled so that a non-dimensional pressure of 1 corresponds to 340 MPa. The choice only serves to make graphs comparable. However, the curves indicate that Alma and measurement correspond fairly well with regard to pressure levels. As the case was with rod extrusion, Alma seems to predict a much lower initialization peek. Again, this may be partly due to the choice of boundary conditions and to the fact that thermal transients influence sensor output. Also in this case, the output returns to zero asymptotically after unloading. This indicates that the relative pressures for Alma probably are somewhat low and that a scaling factor of about 310 MPa is probably more appropriate. As for the time variation of pressure with respect to the sensor position, there seems to be a small but repeatable difference between the probe placed in a central position, P1, and the one close to the edge of the profile, P2. P1 registers a larger but probably not statistically significant increase towards the end of the press. As the difference between the output of P1 and P2 is smaller than the accuracy, it is difficult to determine if the absolute pressure is highest at P1 or P2.

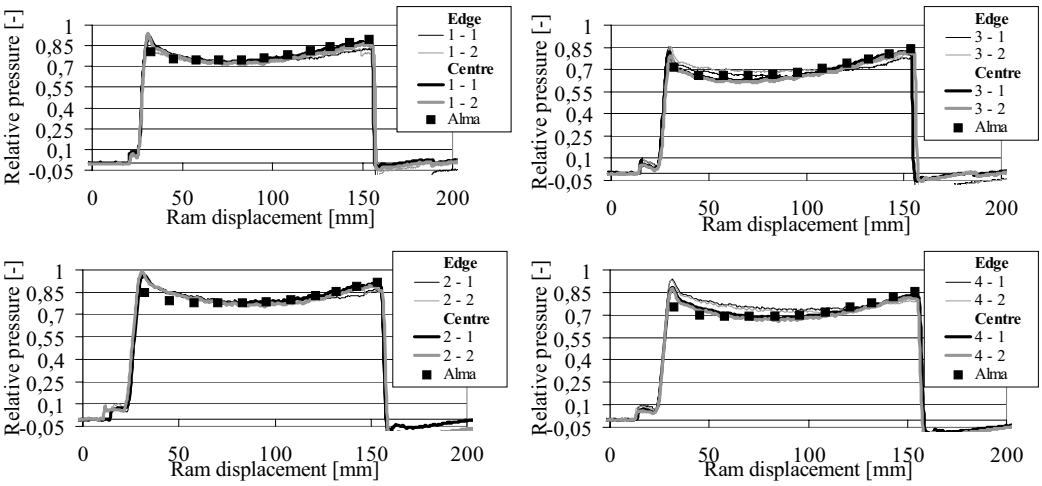

Figure 24. *Scaled pressure results for experiments 1 to 4*

Samples from the extruded profile were taken out from the front and end and at the middle. The thickness was then measured with a micrometer at five positions across the width. Figure 25 presents typical results thickness measurement results. The data are from two replicate runs. Unequal thermal expansion of steel and aluminium, material deposition on the bearings and thinning effects cause profile thickness to be significantly less than 1.7 mm. A variation of profile thickness of about 0.1 mm corresponds well with deflection calculation results shown in Figure 26. Since the pressure increases and the liner load decreases towards the end of the press cycle, an increase in the thickness variation by some 20-30 % is expected. Calculated and measured results correspond fairly well, even though thermal gradients in the die have not been considered.

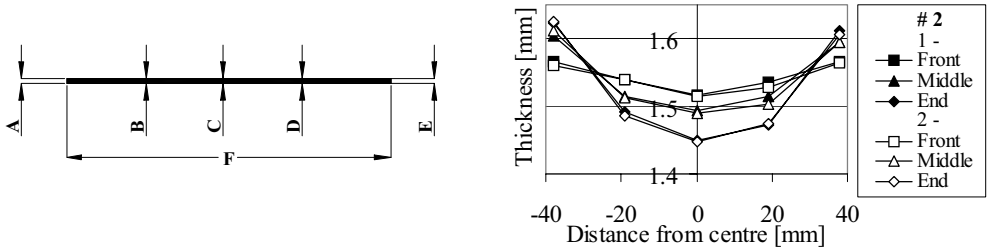

Figure 25. *Positions of measurement on the profile cross-section and thickness at three points along the profile length. Results are from 2 replicate runs.*

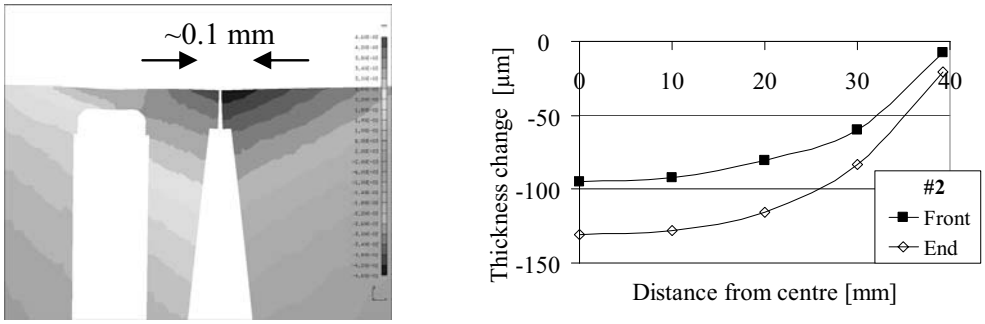

Figure 26. *Die deflection calculations showing the closing of the outlet, both in the symmetry plane (max: 48 µm, min: -48µm) and for the whole outlet.*

An unexpected increase of the thickness close to the outer edges during the first half of the press cycle is observed in Figure 26. In the case of earlier similar experiments thickness variation at the edge has been negligible. Calculations also indicate that neither load nor temperature changes during the press cycle may explain the phenomenon. A possible cause may be that an adhesive layer has been deposited and probably only gradually worn down in the area between thermocouple T2 and the edge during extrusion. The remnants of such were observed after experiments. In general, effects not directly related to the general thermomechanical behaviour of the die complicate the prediction absolute thickness values.

5. Conclusions

Aluminium extrusion is a complex process governed by a number of parameters. An important group is the one related to material behaviour. The development of alternative measurement techniques is a necessity when the appropriateness of models is assessed. However, due to the inevitable inaccuracy of measurement and

the abundance of parameters, statistically significant conclusions are hard to draw. Usually a number of parameter combinations will work equally well.

Bearing channel temperature sensors and die face pressure sensors are valuable tools in the study of aluminium extrusion. Such will typically have an accuracy of ±2-4 °C and ±10 MPa if the described methods of calibration are used. Typical resolution of the pressure sensor is less than ±3 MPa, but special attention must be paid to transient thermal effects. The extrusion of rods provides the simplest test case and allows a number of replicate measurements as well as the most accurate study by FEM. In addition the case provides valuable information on friction phenomena both in the container and in the bearing channel.

Thin-strip extrusion with width chosen to obtain plane strain conditions is an interesting generic case for the study of self-stabilization as it allows easy analysis, yet has features in common with more complex geometries. The study revealed no flow-instability or non-uniform exit velocity although significant profile thickness variation could be related to the deflection of the tooling package. A 0.1 mm thinning of the centre part of the section relative to the edge (1.6 mm) was recorded. The future study of extrusion with even thinner profiles will reveal the limit flow-stability and relate this to die deflection and pressure build-up in the die. Greater attention should then be paid to calibration and 3D FEM modelling.

Acknowledgements

The authors gratefully acknowledge and thank the Research Council of Norway and Hydro Aluminium for financial support and their permission to publish this work. They would also like to thank their colleagues at NTNU and SINTEF for support during the study, and the participants and organizing committee of the 5th ESAFORM conference for showing a genuine interest in the findings.

12. Bibliography/References

Abtahi S., Welo T., Støren S., *Interface mechanisms on the bearing surface in extrusion*, Proc. 6th Int. Alu. Extr. Techn. Sem., Chicago, Ill., 1996, Vol II pp. 125-131.

Baxter L.K., *Capacitive Sensors – Design and Applications*, IEEE Press, New York, 1997.

Capacitec Inc., *Non-contact displacement standard products catalogue*, Ayer, Mass. 1997.

Capacitec Inc., *Operation / Maintenance Manual for Series 4000 Capacitec® Amplifiers and Rack Accessories*, Ayer, Mass. 1998.

Carslaw H.S., Jaeger J.C., *Conduction of Heat in Solids 2nd ed.*, Clarendon, Oxford, 1959.

Flitta I., Sheppard T., *Investigation of friction during the extrusion of Al-alloys using FEM simulation*, Proc. 5th Int. ESAFORM Conf. on Mat. Form., Krakow, 2002, pp. 435-438.

Foster R., *Linear Capacitive Reactance Sensors for Industrial Applications*, Proc. 40th Annual Earth-moving Industry Conference, Peoria, Ill., 1989.

Hansen A.W., Valberg H., Welo T., *A technique for measuring the pressure on the tool surface*, Proc. 4th Int. Conf. Technology of Plasticity, Bejing, 1993, Vol I pp. 303-308.

Holthe K., Støren S., Hanssen L., *Numerical simulation of the aluminium extrusion process in a series of press cycles*, NUMIFORM'92, 1992, pp. 611-618.

Jeswiet J., Nyahumwa C., *A sensor for measuring metal deformation interface forces*, J. Mats. Proc. Tech. 39, 1993, pp. 251-268.

Lefstad M., Metallurgical Speed Limitations during the Extrusion of AlMgSi-Alloys, Doctoral thesis, University of Trondheim, 1993.

Lefstad M., Moe P.T., Støren S., Flatval R., *Thin strip aluminium extrusion – pressure, temperature and deflection recordings of the extrusion die*, Proc. 5th Int. ESAFORM Conf. on Mat. Form., Krakow, 2002, pp. 463-466.

Moe P.T., Støren S., *A technique for measuring pressure on the die face during extrusion*, Proc. 5th Int. ESAFORM Conf. on Mat. Form., Krakow, 2002, pp. 463-466.

Moe P.T., Doctoral thesis to be published, 2003.

Nyahumwa C., *The evolution of a cantilever sensor to measure normal and frictional forces in the roll gap during cold rolling*, J. Mats. Proc. Tech. 39, 1996. pp. 251-268.

Özisik M.N., Orlande H.R.B., *Inverse Heat Transfer*, Taylor & Francis, New York, 2000.

van Rens B.J.E., Finite Element Simulation of The Extrusion Process – Shape prediction for complex profiles, Technische Universiteit Eindhoven, 1999.

Siebel E., Lueg W., *Üntersuchungen über die Spannungsverteilung im Walzspalt*, Mitt. KWI, no. 15, 1933, pp. 1-15.

Støren S., *Theory of extrusion – advances and challenges*, Int.J.Mech.Sci., no. 35, 1993, pp. 1007-1020.

Tverlid S., Modelling of Friction in the Bearing Channel of Dies for Extrusion of Aluminium Sections, Doctoral thesis, The Norwegian University of Science and Technology, 1997.

www.uddeholm.com/utab/pdf/facts/orvar_supreme english_020602.pdf

Valberg H., unpublished work, Norwegian University of Science and Technology.

Williams A. J., Croft T.N., Cross M., *Computational Modelling of Metal Forming Processes*, Proc. 5th Int. ESAFORM Conf. on Mat. Form., Krakow, 2002, pp. 67-70.

Yoneyama T., Kitigawa M., *Measurement of the contacting stress in extrusion*, Advanced Technology of Plasticity, 1993, pp. 553-558.

Yoneyama T., Hatamura Y. et al, *Development of a pressure sensor using an optical fiber sensor*, J. JSTP no 35, 1994, pp. 158-163.

Yoneyama T., *Development of a new pressure sensor and its application to the measurement of contacting stress in extrusion*, J.Mat.Proc.Tech. no 95, 1999, pp. 71-77.

Appendix F

Wajid W., Moe P.T., Abtahi S., Strøven S.

An Evaluation of Material Behaviour during Extrusion of AA6060 Rods

Paper in Proceedings

7th ESAFORM Conference on Material Forming
April 20, Trondheim, pp 245-248

An evaluation of material behaviour during extrusion of AA6060 rods

W. Wajda[1], P.T. Moe[1], S. Abtahi[1] and S. Støren[1]

[1]*Department of Engineering Design and Materials, Norwegian University of Science and Technology*
Richard Birkelandsvei 2B, N – 7491 Trondheim, Norway

URL: www.ntnu.no *e-mail: Wojciech.Wajda@ntnu.no; Per.T.Moe@ntnu.no*

ABSTRACT: Extrusion is one of the most complex material forming processes to model due to the large strains, the high strain rates and the large temperature gradients involved. Although numerical modelling now makes it possible to study the most complex thin-walled profile shapes, useful results may only be obtained if the description of the material behaviour is accurate. While it is common to establish material data through standard material testing by compression or torsion, one is not guaranteed that such data will be applicable to extrusion, which is a process that involves much more involved deformation. The current paper discusses a possible experimental set-up and an approach for analyzing how well material relations obtained through torsion testing perform when they are used to predict extrusion pressure and outlet temperature.

Key words: aluminium extrusion, constitutive model, Zener-Hollomon, AA6060

1 INTRODUCTION

Recent advances in the art of numerical modelling of elasto-viscoplastic deformation have significantly improved our understanding of and ability to control forming processes. As finite element codes allow us to simulate the most complex material behaviour, we tend to perceive the limit between models and nature itself as less distinct. Metal plasticity research is then also often viewed as a converging process, in which constitutive relations are gradually refined in order to explain new physical observations on micro- or macro-level. However, modelling errors may never be completely eradicated. Models are by definition only simplified representations of nature, and their dependence on empirical data is the cause of random and systematic errors. The conventional approach to modelling of forming processes includes a step of standard materials testing, usually by compression or torsion, which is to qualify constitutive relations for later use. While such relations very often are applied as if they were generally valid, any use on cases other than that of the original test set-up constitutes in fact a potentially inaccurate extrapolation. The limits of a material relation's applicability are often just as important to its user as the relation itself, and it may be argued that just as important as proposing a hypothesis is the task of testing and rejecting it.

Aluminium extrusion is unarguably one of the most complex forming processes to study and to control. FE calculations may be very time-consuming due to the large deformations and the coupled nature of the problem. Still, the results may be of limited value to those attempting to find the reasons for and predict the occurrence of excessive dimensional variability or flow instability phenomena such as buckling. For if a formulation is to be truly predictive, there must be special emphasis on quantitative descriptions of flow and on frictional behaviour. While problems related to recreating the frictional conditions of the bearing channel by some standard test such as pin-on-disc may seem evident, one may easily overlook the errors introduced when accepting flow relations established by standard material testing. The paper introduces error plots that allow careful assessment of the applicability of such material data to rod extrusion. An alternative estimate of the parameters for the Modified Zener-Hollomon flow rule based on results from extrusion of AA6060 is also presented.

2 MODELLING ASSUMPTIONS

The starting point of any evaluation of constitutive relations should be an analysis of the characteristics and requirements of the process of interest. For even though there is a common basic mechanism of metal plasticity (dislocation movement), the rate of strain in any material element is determined by the state of the material and the loading conditions, which may vary from one process to another. While torsion testing, for instance, usually is performed at strain rates lower than 50 s^{-1} and at constant temperature, material particles in extrusion may experience very high strain rates, large strains and a changing state of stress. Figure 1 shows the flow paths of two particles in the billet and corresponding histories of strain rate and temperature. Calculations are rigid visco-plastic, and the flow relation of Eq. 4 has been used with coefficient set # 1 of Table 1. History dependence has not been considered. Strain hardening is rarely observed in standard material testing to large strains. It is often assumed that microstructural parameters such as the dislocation density or cell size remain almost unaltered in material elements after the initial deformation. However, standard testing procedures seldom fully take into account changes in loading conditions and the possible activation of alternative dislocation systems during extrusion. Anisotropic flow behaviour may be of importance, especially in relation to strain localisation, a phenomenon which is hard to recreate in standard tests and FEM. The quality of a modelling approach should always be checked by comparing predictions and experimental results for a set of representative extrusion cases.

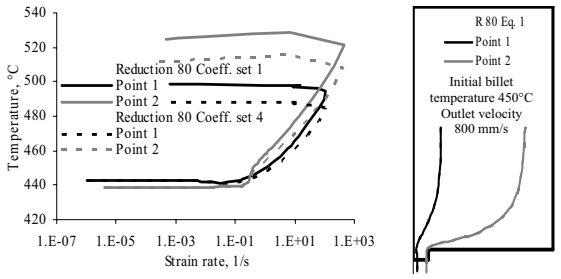

Fig. 1. Changes in strain rate and temperature along flow paths

Continuum mechanics makes a distinction between supposedly universal conservation laws and material dependent descriptions of flow behaviour, of which there is almost an infinite number. Thermodynamics and dislocation theory may give some indication of the appropriateness of formulations. It is for instance common, on the basis of simple studies of thermally activated deformation, to introduce a temperature compensated strain rate, the Zener-parameter Z or ζ (Eq. 1) to simplify flow rules such as the Power-Law (PL) (Eq. 2), the Zener-Hollomon (ZH) (Eq. 3), or the Modified ZH (MZH) (Eq. 4) [1]. Q is here the effective activation energy and R the universal gas constant. α, A, n and C are the flow rule coefficients.

$$\zeta = (Z/A) = \left(\dot{\bar{\varepsilon}}/A\right)\exp(Q/RT) \tag{1}$$

$$\sigma_f = \alpha^{-1}\zeta^{1/n} \tag{2}$$

$$\sigma_f = \alpha^{-1}\sinh^{-1}\left(\zeta\right)^{1/n} = \alpha^{-1}\ln(\zeta^{1/n} + \sqrt{\zeta^{2/n}+1}) \tag{3}$$

$$\sigma_f = \alpha^{-1}\sinh^{-1}\left(\zeta\right)^{1/n} + C\zeta^{1/n}\Big/\sqrt{\zeta^{2/n}+1} \tag{4}$$

While Eq. 3 is supported by steady state dislocation studies, the adherents of a hypothetical-deductive approach would focus on the regressive rather than the mechanistic interpretation of flow rules. Table 1 presents four sets of parameters, which have been established by standard materials testing. Eq. 3 is a special case of Eq. 4 (C = 0). Eq. 2 is the first order term in the Taylor-expansion of Eq. 3. Flow stress estimates based on Eqs. 2-4 deviate only for quite large Z-values (Figure 2). This may be important to extrusion modelling, although the sensitivity of the ram force to the flow rule formulation may be small due to the coupled nature of the problem. High strain rate deformation mechanics may differ from that of low rate, and the extrapolation of data from testing to extrusion conditions by the use of the Z-parameter may be questioned. Eq. 3 should also be checked.

Table 1. AA6060 and AA6063 (# 4) parameter sets for Eq. 4

#	Ref	α [MPa^{-1}]	n	A [s^{-1}]	Q [J/mol]	C
1	[1]	0.0430	4.530	$9.39\cdot10^{11}$	180 900	1.7
2	[1]	0.0671	3.310	$5.89\cdot10^{10}$	180 100	1.5
3	[1]	0.0512	4.240	$1.28\cdot10^{12}$	191 300	1.5
4	[2]	0.0400	5.385	$5.91\cdot10^{9}$	141 550	0

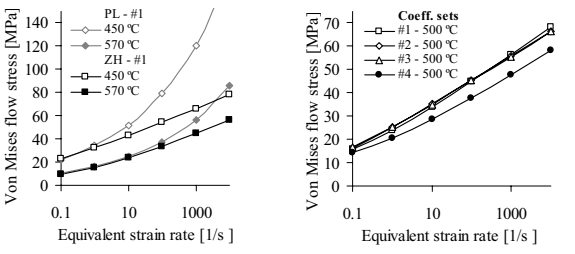

Fig. 2. A comparison of flow stresses predicted by Eq. 2 and 3

It is not trivial to test a flow rule hypothesis by rod extrusion analysis. Extrusion models contain many parameters and are based on numerous hypotheses such as the continuum hypothesis and others related to the material behaviour. Moreover, measurements may be affected by random and systematic error.

3 DESCRIPTION OF EXPERIMENTS

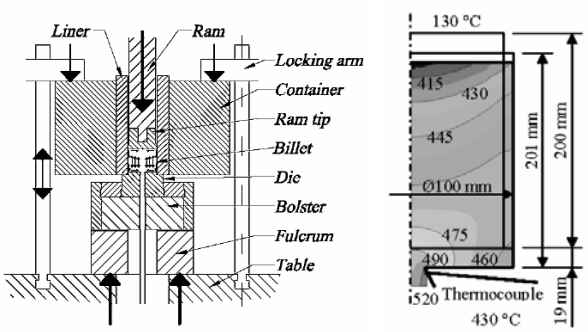

Fig. 3. Press design, experimental set-up and billet temperature

A set of rod extrusion experiments was run in an 8 MN vertical laboratory press for billets of diameter of 100 mm. Figure 3 presents the geometry of the set-up, and the experimental matrix with key results is given in Table 2. At least three replications were run at each level, and the variation in ram force and outlet temperature was less than ±100 kN and ±3 ºC. The accuracy of measurements was about the same. Experiments were run in a completely randomised manner, and in order to secure well-defined thermal conditions, there was a 10 min pause between each run. The experimental practice of welding the new billet to the old butt end (of length 19 mm) was adopted. While this approach may not be described as optimal from a materials testing point of view, it was all in all viewed as the most favourable solution since the experimental set-up, which also included die face pressure sensors, was complex and fragile [3]. The results from the current study are, at least as far as the outlet temperature and ram force is concerned, fully consistent with those of Grasmo et al. [4]. They also treated AA6060, but removed the butt end between each run. Still, one is here not to claim general validity of the results of the study. The paper is merely to demonstrate an approach. A zero length bearing design was adopted in order to avoid the uncertainties introduced by bearing friction. Ref. [3] provides further information on experiments.

Table 2. Experimental matrix and characteristic results: Ram force [kN] and temperature [ºC] for 100 mm butt end.

Extrusion ratio		40 (15.8 mm)		80 (11.2 mm)	
Billet temp. [ºC]		450	500	450	500
Profile speed [mm/s]	200	2139[A] *504*	1974[B] *515*	2320[G] *516*	2218[H] *523*
	400	2268[C] *523*	2039[D] *534*	2492[I] *537*	2310[J] *549*
	800	2392[E] *538*	2148[F] *552*	2631[K] *563*	2424[L] *574*

4 NUMERICAL ANALYSIS

A simplified description of viscoplastic flow at high temperatures is here adopted. Elastic effects are not assessed since elastic deformation generally will be small, and since stick-slip behaviour in the outlet is avoided through the use of zero length bearings. In this first study, a non-linear purely viscous isotropic flow behaviour according to Eq. 4 is adopted. Strain-hardening and other history dependent effects are not assessed. Heat conduction is also assumed to be isotropic. The heat conduction coefficient at 400 ºC is 32 for steel and 228 W/mK for aluminium. The steel-aluminium heat transfer coefficient is set to 3.5 kW/m^2K on the container and die surfaces and 5.5 kW/m^2K on the billet-ram interface. The MZH flow rule has been implemented in ALMA, a computer code for extrusion [5]. The estimates of ALMA and of the more general but similar code ANSYS/Flotran are consistent. One case of high and another of low level of force and temperature are shown in Figure 4. Force and temperature estimates by ALMA are too low when material data have been established through torsion testing, like set # 1 of Table 1. The shapes of the temperature curves in the initial phase of the run depend on the thermocouple's response time. Data are only compared at quasi-steady state.

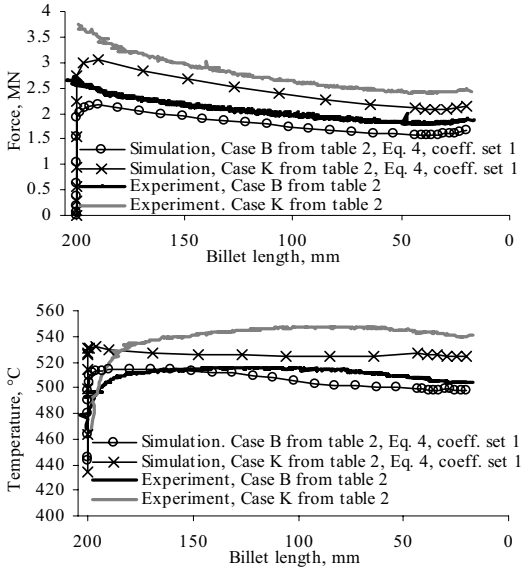

Fig. 4. Measured/simulated ram force and outlet temperature.

The next natural step is to evaluate the reasons for deviations and to seek the flow rule and coefficient set that gives the most consistent results. Systematic errors related to measurement should be smaller than

100 kN and 5 ºC. Both in relation to modelling and experiment it is important to carefully control the duration of billet handling steps and thereby the billet temperature to secure satisfactory replication.

Useful tools for analyzing error sources are plots of square error (Eq. 5) of temperature ($M = T$) and ram force ($M = F$) (Figure 5). If systematic errors are neither related to measurement nor model, the plots should display surfaces with coincident minima. Measured and simulated values, M_x and M_c, should only differ by about σ_M, the characteristic purely random measurement error. One should then expect $E_F \approx E_T \approx 1$. In the current study σ_F and σ_T have been set to 100 kN and 5 ºC. E_M uses data from all levels and p^{ijk} points in time at quasi-steady state.

$$E_M(\alpha,n,Q,A) = \frac{1}{12\sigma_M^2}\sum_{i=1}^{2}\sum_{j=1}^{2}\sum_{k=1}^{3}\frac{1}{p^{ijk}}\sum_{l=1}^{p^{ijk}}\left(M_x^{ijk}(t_l) - M_c^{ijk}(t_l)\right)^2 \qquad (5)$$

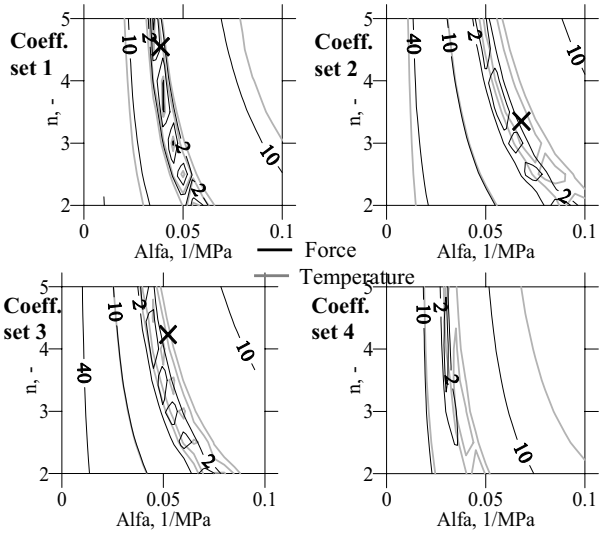

Fig. 5. Force and temperature error surfaces. Values of A, Q and C are given in Table 1. **X** are the torsion testing results.

Figure 5 displays four cross-sections of the (α, n, A, Q, C) parametric spaces for temperature and force error. They have been chosen so that the A, Q and C parameters are the same as in coefficient sets # 1-4 of Table 1. This makes it possible to check if any of the sets is an optimal choice. The most characteristic feature of the error plots is the valley running more or less diagonally, in which the points of minimum error are located. Many combinations of parameters may in fact be used to establish equally acceptable estimates of temperature and force. This flexibility is partly due to the random error in the experiments and partly due to the characteristics of the flow rules and the extrusion system. An essential question, which is left for later analysis, is whether the same flexibility exists when one is to assess other responses of the process such as flow instability.

Another important question is whether the system is flexible enough to allow parameters to be estimated by torsion testing. If that is the case, the curves of Figure 6 should be similar to those for the torsion test. Here, one merely observes that the parameter sets of Table 4 are not optimal. It seems as the most sensible choice for A, Q and C, would be that of set # 1. Still, Figure 5 shows that (α,n) = (0.043,4.53) are not the coordinates of the minimum point. A significantly smaller overall error is for instance obtained when (α,n) = (0.035,5.0). The point has been found by visual inspection. An even better fit can be found by using optimisation techniques in the full five-dimensional parameter space. Figure 6 displays E_F and E_T for all runs of Table 2 (A-L)

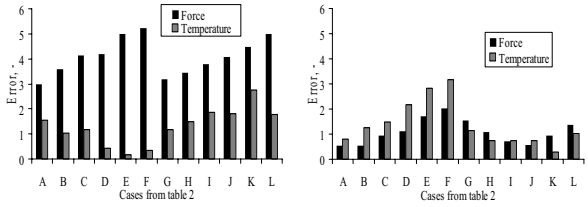

Fig. 6. Force and temperature error for runs A-L (see Table 2) Left: (α,n) = (0.043,4.53) (Set 1), Right: (α,n) = (0.035,5.0)

5 CONCLUSION

An approach, in which the coefficients of the MZH flow rule are determined by torsion testing and thereafter applied in rigid viscoplastic simulation of extrusion, may not produce optimal estimates of ram force and outlet temperature at the same time.

ACKNOWLEDGEMENTS

The authors gratefully acknowledge and thank the Research Council of Norway and Hydro Aluminium for their support.

REFERENCES

1. K. Pedersen, S. Abtahi, Oversikt over materialkunnskap, SINTEF Report, Trondheim (1999).
2. T. Sheppard, *Extrusion of Aluminium Alloys*, Kluwer, Boston (1999).
3. P.T. Moe, S. Støren, A technique for measuring pressure on the die face during extrusion, In: *Proc. 5th ESAFORM Conf. on Material Forming*, Krakow (2002) 463-466.
4. G. Grasmo et al., Modelling of Two-Dimensional Extrusion, In: *Proc. 5th International Aluminium ET Seminar*, Chicago (Ill.) (1992) Vol. II 367-376.
5. K. Holthe, Numerical simulation of aluminum extrusion Vol 1: ALMA Theory Manual, SINTEF Report (1991).

Appendix G

Moe P.T.

An Analysis of Forge Welding of Steel Rods
–
Heating Phase Modelling

Paper in Proceedings

7th ESAFORM Conference on Material Forming
April 2004, Trondheim, pp. 399-402

An analysis of forge welding of steel rods – Heating phase modelling

P.T. Moe[1]

[1]*Department of Engineering Design and Materials, Norwegian University of Science and Technology*
Richard Birkelandsvei 2B, N – 7491 Trondheim, Norway

URL: www.ntnu.no *e-mail: P.T.Moe@ntnu.no*

ABSTRACT: Shielded Active Gas Forge Welding is a joining technique for tubes and rods. It is characterised by the attention which is paid to reducing bevel surface oxides prior to welding, to establishing a best possible temperature distribution through either resistance or induction heating and finally to shaping bevels that give optimal thermo-mechanical conditions during welding. The current paper discusses a possible application of the technique, namely the joining of rods by annular welds only. Focus is on modelling of the induction heating phase. The restriction to annular welding makes the design and handling of the coil simpler, and a sensitivity analysis is performed in order to establish an understanding of the effect a change of geometrical parameters of the rods and the coil have on the joule heating and consequently the temperature distribution.

Key words: induction heating, forge welding, finite element modelling

1 INTRODUCTION

Most mechanical designs of practical interest consist of multiple components, which have been joined in some manner, very often by welding. Relatively low investment cost, wide applicability and fairly high reliability are the most important virtues of the arc welding (AW) methods, while other methods such as forge welding (FW) prove most cost-effective when the parts to be joined are quite large and/or many. Longitudinal seam welding of pipes is one of the earliest and best known FW applications using induction heating. However, FW may also be used for high-quality/low-cost joining of pipe segments. For instance, Shielded Active Gas Forge Welding (SAG-FW) was originally a technique developed to render possible simple high-rate J-laying of offshore pipes [1]. Today, SAG-FW stands out as one of the most advanced general approaches to FW of pipes and rods. The technique is primarily defined by the focus which is placed on optimisation of welding conditions and the set of measures taken to establish such conditions. It is acknowledged that if two pieces of material are to merge so that the surface separating them is virtually undetectable in all respects, bevel surfaces must be clean and free from oxides, and the thermo-mechanical conditions in the vicinity of the weld (temperature, contact pressure, state of stress) must enhance both diffusion and plastic deformation within the relevant timeframe. SAG-FW includes techniques for designing bevel shapes, establishing temperature distributions prior to forging, setting the parameters of the process and reducing the bevel surfaces so that satisfactory welding conditions are obtained and so that the weld assumes a specified final shape and no finishing is necessary after welding. Careful temperature control is essential for a number of reasons. As SAG-FW in essence is an enhanced diffusion welding technique, melting is neither necessary nor desirable. While a high bevel face temperature promotes diffusion and reduction of oxides, one should avoid too excessive heating and particularly melting as this in most cases produces poorer material properties and complicates microstructure control. Equipment and procedures for electro-magnetical (EM) heating (high frequency resistive heating (HFR) or induction heating) in relation to welding and heat treatment constitutes a vital part of SAG-FW technology. In order to secure

a uniform temperature on the bevel surfaces, it is important to understand and to control the EM fields in and around the pieces to be welded. HFR SAG-FW of pipes has been extensively studied experimentally and incorporates today a number of patented techniques for controlling heating.

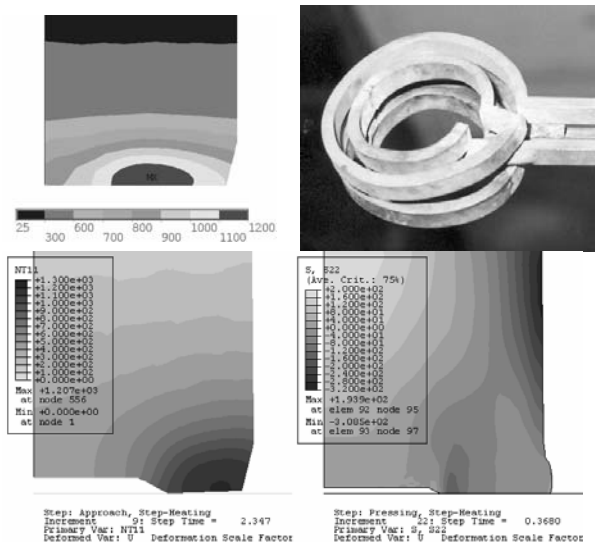

Fig. 1. Coil designs and temperature distributions for through thickness welding and example of rod annular forge welding

The current paper focuses on forge welding of thick rods (Ø180 mm) and assumes that an annular weld of 30 mm width for various reasons is sufficient. An important advantage of FW compared to AW is that through-thickness welds in fact may be produced just as fast as annular ones, and it might appear as if a restriction to the latter type only favours AW-techniques and brings no real benefits to FW. For the relevant rod dimensions, however, FW is about 10 times faster than AW. Furthermore, the annular welding restriction makes it possible to reduce press force and heat input requirements and therefore also cost. Coil design and welding procedures may also be simpler for annular than for through thickness welding. In order to establish an almost uniform and sufficiently high temperature (typically 1000 ± 100 ºC) through the complete cross section of the rod, it may be necessary to place a complex coil in the weld gap (Figure 1). Yet, the coil must be removed before the forging movement starts if it is not to fuse with the rods. This is a complicating step which consumes time that could be better spent on forging, for during the first half second after heating ends, the temperature drop may be as large 200 ºC if temperature gradients are steep (Figure 6).

2 MODELLING APPROACH

Due to the highly non-linear and coupled nature of the FW process, it may be quite difficult to assess the consequences of changes in design and process parameters, not to mention to optimise weld quality. For instance, it is possible to tune the bevel shape in order to increase the contact stresses on a certain part of the bevel or the overall plastic deformation during forming. However, a consequence may in the most extreme case be that also the induction heating phase and temperature distribution at the onset of the forging movement is altered. This may affect plastic deformation and contact stresses in another direction than expected. There are a number of interactions both between the various phases of the FW process (heating, approaching, forging, cooling) and between different physical aspects (thermal, electro-magnetical, mechanical). For this very reason, multi-physics finite element analysis presents itself as a useful tool for studying the overall sensitivities to changes in parameters and to gain insight into the physics of the welding process. A FE model could in combination with carefully designed experiments be used to establish empirically based contact models and process windows and to optimise the process.

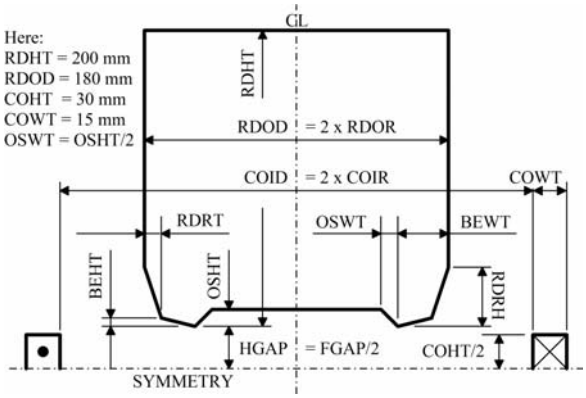

Fig. 2. Geometry of the rod and coil in the sensitivity study

The current study is merely to give some insight into the physics of forge welding and provide a first numerical analysis of sensitivities to design changes for the mentioned case of annular welding of thick rods. The work is performed in two steps. While, the thermo-mechanics of FW will be treated in another paper, the objective is here to give some insight into the induction heating phase and an assessment of temperature distribution's dependence on process parameters and on the geometrical parameters of the bevel and the double coil (Figure 2).

3 THEORETICAL ASPECTS OF INDUCTION

Surrounding any flow of electric charge there is a magnetic field of a magnitude determined by the law of Ampere (Eq. 1). *I* is the coil current, **J** the current density vector, **D** the displacement current and **H** is the magnetic field. Furthermore, if a piece of some conducting material is placed in a magnetic field of varying magnitude, another of Maxwell's equations, Faraday's law (Eq. 2), predicts that an electric field is set up in the material and that eddy currents will flow. Since heat dissipation is normally related to the movement of electric charges, nature provides us with a very useful method for heating up for instance metals. While Gauss' law (Eq. 3) states that there are electric monopoles, Eq. 4 rules out magnetic ones. Eq. 5 is a statement of electric charge conservation. Eqs. 1 and 5 assume that the time derivative of **D** need not be considered. This quasi-static assumption is acceptable if the AC wavelength is fairly large, as is the case here ($\lambda > 10^3$ m) [2].

$$\text{curl}\,\mathbf{H} = \mathbf{J} + \frac{\partial \mathbf{D}}{\partial t} \approx \mathbf{J} \qquad \oint \mathbf{H}\mathrm{d}\mathbf{s} = I \tag{1}$$

$$\text{curl}\,\mathbf{E} = -\frac{\partial \mathbf{B}}{\partial t} \qquad \oint \mathbf{E}\mathrm{d}\mathbf{s} = -\frac{\partial \Phi}{\partial t} \tag{2}$$

$$\text{div}\,\mathbf{D} = \rho \qquad \oiint \mathbf{D}\,\mathbf{n}\mathrm{d}A = Q \tag{3}$$

$$\text{div}\,\mathbf{B} = 0 \qquad \oiint \mathbf{B}\,\mathbf{n}\mathrm{d}A = 0 \tag{4}$$

$$\text{div}\,\mathbf{J} + \frac{\partial \rho}{\partial t} = \text{div}\left(\mathbf{J} + \frac{\partial \mathbf{D}}{\partial t}\right) \approx \text{div}\,\mathbf{J} = 0 \tag{5}$$

ρ is the electric charge density while Q is the electric charge. If Eqs. 1-5 are to be used to model induction heating, constitutive relations that describe material behaviour and link the magnetic flux density vector, **B**, and **H** and the electric field density vector, **E**, and **J** must be introduced. A common assumption is that the permeability of air is equal to that of free space, μ_0. As for the rod material, the simplest approach is merely to assume proportionality, i.e. $\mathbf{B} = \mu_0\mu\mathbf{H}$ and $\mathbf{J} = \sigma\mathbf{E}$, where μ is the material relative permeability and σ the conductivity. Given the somewhat limited objective of the current analysis, the simplifications above seem acceptable. Still one should bear in mind possible effects of material hysteresis as well as saturation at large values of flux density. A first order effect included in the analysis is the influence of temperature on σ and μ. The material data of the analysis are presented in Figure 3. At the so-called Curie temperature ferritic steels are demagnetised.

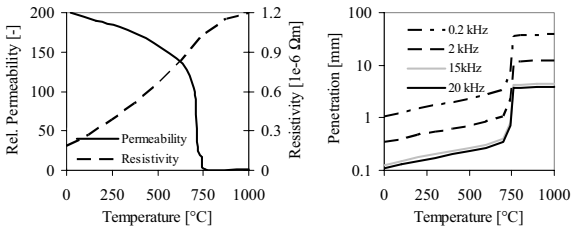

Fig. 3. EM material data and penetration

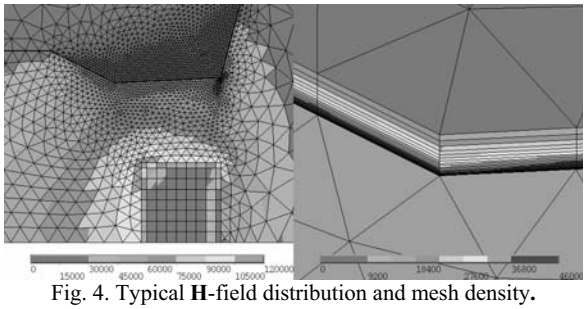

Fig. 4. Typical **H**-field distribution and mesh density.

When μ is set constant in air, **B** satisfies Laplace's equation, $\nabla^2\mathbf{B}=0$, and the intensity of the field will, thus, only gradually decrease with the distance. This makes it necessary to introduce elements mimicking infinite geometry, but places small requirements on the element formulation in the air surrounding the coil. However, in the steel rod, the distribution of the EM fields may be extremely non-uniform, and eddy currents seldom penetrate deep into the material. Eq. 2 and Figure 4 provide an explanation. If the **B** field varies with time, curl **J** ≠ 0 and current distribution is not uniform. It may be shown that if μ and σ are constants, the field distribution is given by Eqs. 6–7.

$$\nabla^2\mathbf{B} - \mu_0\mu\sigma\frac{\partial \mathbf{B}}{\partial t} = 0 \tag{6}$$

$$|B_z| = \mu B_0 \exp\left(-\frac{x}{\delta}\right) \text{ where } \delta = \sqrt{\frac{2}{\omega\,\mu_0\,\mu\,\sigma}} \tag{7}$$

If a sinusoidally time-varying **B**-field has amplitude B_0 in air and frequency, FREQ, the magnitude of the **B**-field in the rod is given by Eq. 7. x is the distance from the surface, and δ is the penetration depth. For a frequency FREQ = $\omega/2\pi$ = 20kHz, δ may be very small and extreme mesh refinement is desirable near the rod surface (Figure 4). Due to demagnetisation of ferritic steels penetration depends on temperature (Figure 3). ANSYS provides a staggered approach for solving both the EM harmonic and the transient thermo-mechanical problems. Ref. [3] discusses how the magnetic vector potential, **A** (**B** = **∇**×**A**), may be introduced to simplify Eqs. 1-5.

4 SENSITIVITY ANALYSIS

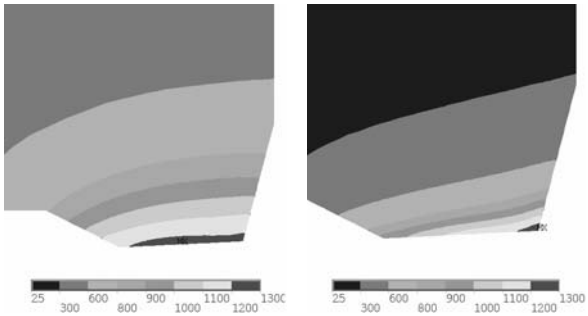

Fig. 5. (COIR, FREQ, CREG) is (65, 15, 0.1) and (70, 20, 0)

The objective of the heating phase is to introduce a temperature field which allows the weld to attain the desired shape and properties after welding. Requirements to the gradient into the rod can only be found by assessing elasto-viscoplastic deformation during forging. The surface temperature must be uniform and sufficiently high. Optimal conditions are most easily obtained when the average diameters of the coil and bevel are similar (Figure 5). However, since the temperature may decrease significantly during removal of an internal coil, it would be desirable to use a coil that is external to the weld gap or at least one that may be very easily removed. The essential question is then whether one may tune rod geometry and process parameters so that spreading of the EM field or heat conduction may compensate for a radial offset between the bevel and the coil. ΔT_M, the maximum temperature difference on the bevel face, ΔT_G, the gradient normal to the surface to a depth of 10 mm, and the heating time are assessed as bevel shape (0–5) and process parameters (6–9) are varied.

Table 1. Levels of parameters [mm]

#	Name	-1	+1		#	Name	-1	+1	
0	RDRH	10	**20**	mm	1	RDRT	**5**	10	mm
2	BEHT	0	**1**	mm	3	BEWT	25	**30**	mm
4	OSHT	**3**	6	mm	5	FGAP	**50**	60	mm
6	COIR	**70**	80	mm	7	FREQ	15	**20**	kHz
8	CURR	4	**5**	kA	9	CREG	**0**	0.1	-

In order to reduce the computing time the analysis is split in two parts. First, the influence of bevel shape is assessed while parameters 6–9 are fixed at levels indicated by bold characters. The conclusion is that the bevel should be narrow and carefully angled to counter larger coil diameters. A larger gap distance gives a more uniform **H**-field, a slower heating and smaller temperature differences. The average main effects (when going from –1 to +1) are shown in Table 2. Interactions between different variables are small, and higher order effects were not assessed.

Table 2. Effects of changing shape and process parameters

Shape	MEAN	0	1	2	3	4	5
ΔT_M [ºC]	483	78	36	-110	187	-3	-50
ΔT_G [ºC]	983	30	32	-67	-8	-4	-83
t_{HEAT} [s]	6.4	-0.9	-0.3	0.8	0	0.1	1.8
Process	MEAN	5	6	7	8	9	-
ΔT_M [ºC]	619	-81	303	55	72	-115	
ΔT_G [ºC]	773	-81	152	78	122	-233	
t_{HEAT} [s]	32.1	19.6	-8.6	-19.8	-29.6	39.1	

The temperature gradient across the bevel surface is much too large, and it would be desirable to remedy the situation by altering process parameters, such as the AC frequency, FREQ, the AC amplitude, CURR, and the current regulation exponent, CREG. If CREG > 0, the current in the coil is reduced when the maximum temperature of the rod, T_M, gets close to a set point T_{SP} = 1250 ºC. According to Figure 6, the value of CREG affects ΔT_M. Similarly, with a smaller FREQ and CURR a longer heating cycle is needed which allows more redistribution of heat.

$$I = CURR\left(1 - T_M / T_{SP}\right)^{CREG} \quad (8)$$

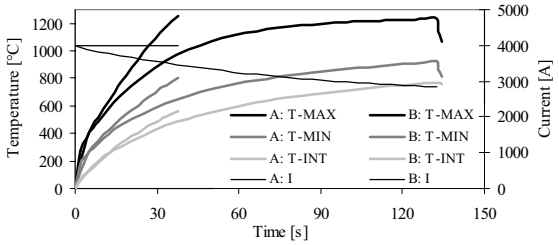

Fig. 6. Max, min and internal temperatures with CREG of 0/0.1

5 CONCLUSIONS

FEM provides a method for studying SAG-FW and optimizing the induction heating sequence. When fairly thick annular welds are to be produced, a coil placed between rods may be a necessity. Yet, a more uniform surface temperature may be obtained by tuning bevel shape and process parameters.

ACKNOWLEDGEMENTS

The author has received extensive technical support from AMR Engineering AS, a Norwegian firm that has worked with forge welding concepts for more than 20 years. A special tribute is paid to the former director of AMR, the inventor of SAG-FW and the father of the author, the late Per Harald Moe, PhD.

REFERENCES

1. P.H. Moe, Offshore Pipelaying, PhD-thesis, Norwegian Institute of Technology (1987) (in Norwegian).
2. Ansys Inc., Theory Manual, Ver 6.1.
3. M.V.K. Chari, S.J. Salon, Academic Press (2000).

Appendix H

Moe P.T., Wajda W., Szeliga D., Madej L.,
Støren S., Pietrzyk M.

An Approach for Evaluating Constitutive Models for Hot Aluminium Extrusion
–
Rod Extrusion of AA6060 as a Case Study

Paper in Proceedings and Journal Article

10th International Conference on Metal Forming
September 2004, Krakow, pp 723-730

STEEL-GRIPS 2 (2004)
Suppl. Metal Forming 2004, pp 723-730

Per Thomas Moe, Wojciech Wajda, Lukasz Madej, Danuta Szeliga, Sigurd Støren and Maciej Pietrzyk:

An approach for evaluating constitutive models for hot aluminium extrusion – rod extrusion of AA6060 as a case study

Constitutive relations are approximate mathematical descriptions of fundamental material behaviour and essential parts of all continuum models of physical systems. Testing and documentation of the accuracy and limitations of material models is a prerequisite for successful simulation. Although many material models may be given mechanistic interpretations, the primary source of knowledge is empirical data from well-defined representative experiments. The current article discusses constitutive modelling of flow in extrusion of aluminium. The complexity of the material deformation complicates both experimental and numerical studies. Conventional materials testing procedures for metal forming cannot fully reproduce extrusion conditions i.e. high strain rates, large strains, large temperature changes and high hydrostatic stresses, while high rate testing techniques do not give complete insight into the deformation history of material elements flowing through the system. Rod extrusion in carefully controlled laboratory conditions appears to be a simple method for testing the ability of flow rules implemented in a modelling tool to predict system responses during extrusion, such as the ram force, the outlet temperature and the die face pressure. The article presents comprehensive results from such experiments with AA6060 as well as compression testing experiments performed in order to establish material data for the same alloy. An evaluation is performed of the deviation between results from extrusion experiments and from simulations with the Zener-Hollomon constitutive relation and material data from the compression tests. Simulations with the Arbitrary Lagrangian-Eulerian code ALMA produce estimates of force in fair accordance with measured results, but somewhat too high temperatures. It is shown that better estimates of temperature can be obtained without considerably altering the ram force estimate. Yet, proper control of temperature before and during extrusion is essential if the verification of models is to be trusted. Differences between experimental and simulated data may at least partly be explained by errors in the measurement of input or output parameters. Furthermore, the error plots reveal that the non-linear and coupled extrusion system is such that equally acceptable estimates of the output parameters may be produced when extruding with a different sets of material data.

Aluminium extrusion is a metal forming process of large commercial importance, but also one that is requiring both to model and control. In essentially one step, a ram forces a cast billet to flow through a narrow die opening. There is a full transformation of both the shape and microstructure of the work piece, as the ratio between the cross section areas of the billet and the profile, the extrusion ratio, may in some cases exceed a hundred. The deformation is at the same time very non-uniform, and each material element or particle in an extruded section has experienced a unique deformation history. While some particles in the front end of the profile may remain nearly non-deformed, others in the boundary layer close to the bearings are both elongated and heavily sheared. Strain rates may exceed 1000 s^{-1}. Dissipation of heat is considerable, and temperatures may locally increase from 400 to melting above 600 °C.

There is no standard material testing procedure that fully recreates extrusion conditions. Torsion and compression tests are normally performed at low rate and to relatively moderate levels of deformation, whereas high-rate testing such as the Hopkinson Split bar method does not by itself reveal the effect of the large changes in microstructure. As will be further discussed, material modelling contributes to bridging the gap between materials testing and extrusion. Still, the application of material data obtained by standard tests in the study of extrusion should be regarded as an extrapolation, and results must be carefully checked.

The current article provides a short survey of objectives, principles and requirements of modelling of aluminium extrusion and materials testing. Results from compression testing at high temperatures of aluminium alloy 6060 are presented. Inverse material modelling is used to extract data. In order to investigate how applicable such data are to the study of extrusion, a series of rod extrusion tests have been run. While the ram force and outlet temperature are the main output data to be used in the current study, also measurement of die face pressure and container shear stress have been performed and presented in [1] and [2]. Output data estimates have been produced by the FE code ALMA [3]. Error surfaces showing the deviation between measured and numerically estimated response were first introduced in ref. [4]. The approach is further studied in order to evaluate the applicability of compression testing results and to reveal an optimal set of material parameters.

Objectives and principles of extrusion modelling

Model building for extrusion may occur at a number of levels depending on objectives of the user. A first goal may merely be to relate ram force or outlet temperature to outlet dimensions, billet material properties and process parameters such as the ram velocity or the temperatures of the billet and tooling. Sufficiently useful expressions or tables for most industrial purposes may be established simply through

*Per Thomas Moe, M.Sc.; Wojciech Wajda, M.Sc.,*Department of Engineering Design and Materials, Norwegian University of Science and Technology, Trondheim, Norway; *Lukasz Madej, M.Sc.; Danuta Szeliga, PhD;* Department of Computer Methods in Metallurgy, Akademia Górniczo Hutnicza, Kraków, Poland; *Prof. Sigurd Støren;* Department of Engineering Design and Materials, Norwegian University of Science and Technology, Trondheim, Norway; *Prof. Maciej Pietrzyk;* Department of Computer Methods in Metallurgy, Akademia Górniczo Hutnicza, Kraków, Poland

regression analysis of data from extrusion experiments. Another possibility, which is assessed in the current article, is to introduce analytical and/or numerical models based on more fundamental physical experience with metal plasticity and heat transfer. The most common approach, the continuum mechanical, deals with average and generally continuous measures of internal forces and displacements. Whereas the conservation laws for mass, momentum and energy are implicitly satisfied, specific descriptions of the material behaviour must be established through materials tests. It is assumed that when a piece of a material is loaded in a certain way, its response will be determined mainly by its composition and microstructure. It therefore seems natural to introduce material dependent equations that may be used in the prediction of forces and temperatures for all cases in which a piece of material is loaded in a similar manner and under similar conditions. The essential question, especially in relation to extrusion, is how one is to establish similarity.

A second objective of extrusion modelling is to predict the development of material microstructure and properties. For instance, in order to control the subsequent operations of material forming such as bending or hydroforming it is important to predict and control the development of an anisotropic microstructure during extrusion. Moreover, by coupling microstructure and flow models one may obtain a better understanding of the mechanics of extrusion and in more general cases reach more accurate estimates of ram force and temperature or other process parameters.

The starting point for most models is a description of the basic mechanism of plasticity, i.e. dislocation movement. It is often assumed that the deformation rate is controlled by thermally activated diffusion mechanisms such as the climbing of dislocation jogs [5]. In microstructure models the flow stress is split into a rate/temperature dependent part, τ_t, and an athermal one, τ_a:

$$\tau = \tau_t + \tau_a = \tau_t + K_1\sqrt{\rho_i} + K_2\left(1/\delta + 1/D\right) \qquad (1)$$

τ_a is assumed to depend on the internal variables of the model, typically the grain size, D, the subgrain size, δ, and the dislocation density, ρ_i. While history dependence may be introduced through special evolution equations for the different variables, it is often claimed that during extrusion a steady state is reached for all particles and that the rate of generation will be equivalent to the rate of dislocation storage [5]. Another observation is that even though grains may be extremely elongated, subgrain networks remain almost stable and of uniform size [6]. As a consequence, changes in τ_a for particles that move through the container should be expected to be fairly small compared to changes in τ_t. It may be shown [5] that τ_t may be expressed as a function of the temperature, T, and the shear strain rate, $\dot{\gamma}$:

$$2\sinh\left(\tau_t V_t / kT\right) = \left[b^2 \rho_m B_t \nu_D\right]^{-1} \dot{\gamma} \exp\left(Q/kT\right) \qquad (2)$$

ρ_m is the density of mobile dislocations, b Burgers vector, ν_D the Debye frequency, V_t the activation volume and k Boltzmann's constant. The activation energy, Q, is the one required for climbing of jogs and related to self-diffusion. The last terms constitute the Zener-Hollomon parameter, Z, a temperature compensated strain rate. While equation (2) is essentially a model for single slip planes, it closely resembles the Zener-Hollomon flow rule (ZH), equation (3), established through macroscopic materials testing. A non-dimensional Zener parameter, $\zeta = Z/A$, is introduced:

$$\sigma_f = \alpha^{-1}\,\mathrm{asinh}\left(\zeta\right)^{1/n} \qquad (3)$$

$$\sigma_f = \alpha^{-1}\zeta^{1/n} \qquad (4)$$

$$\sigma_f = \alpha^{-1}\,\mathrm{asinh}\left(\zeta\right)^{1/n} + C\,\zeta^{1/n}\Big/\sqrt{\zeta^{2/n}+1} \qquad (5)$$

Equation (4) expresses a flow rule of the Power-Law type as a function of the ζ parameter while equation (5) is the Modified Zener-Hollomon (MZH) expression, which was initially introduced to simplify analysis of torsion testing data [7]. The Power-Law is a first order Taylor-expansion of the ZH-relation, and probably gives a too high estimate of flow stress at high strain rates (**Fig. 1**). The validity of the extrapolation may be questioned, and one should be careful when applying data obtained by standard materials testing in extrusion studies. At high strain rates there may be other mechanisms of deformation [8]. Furthermore, the model presented above is too simple to be expected to reveal all complexities of plasticity. For instance, the need for an anisotropic plasticity criterion should be evaluated. Particles that flow towards the die outlet may experience changing loading conditions and, therefore, also activation of new dislocations and possibly temporary softening. The mechanics of flow in areas of high strain rates or close to velocity discontinuities has not been given much attention. There are only a few examples of anisotropy being treated in a coupled manner in relation to extrusion at all [9]. As dedicated simulation codes and faster computers emerge the necessity of multi-scale models may be assessed.

The third and potentially most important objective of extrusion modelling is to predict outlet flow velocity and profile dimensions. As long as the flow resistance in the different parts of the outlet is similar and profiles not too thin, the parts of the cross-section that tend to flow faster will pull the dragging ones. This is the self-stabilisation mechanism of extrusion. When profiles are made thinner and wider, there will be a risk that profiles will buckle or bend as they

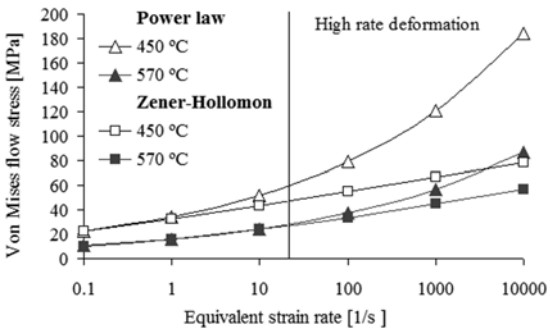

Fig. 1: Flow stress for two different constitutive relations (AA6060)

leave the die. To control flow manufacturers of dies carefully tune bearing lengths or feeder sizes. It is important to properly compensate for outlet distortion as it may alter the profile shape and the friction conditions. Flow stability also seems to be sensitive to the changes in average flow speed and billet temperature and probably to the characteristics and properties of the material [10]. Both the mechanics of flow in the container and the behaviour of the profile in air need to be taken into account. Thus, the self-stabilisation mechanism is one that concerns the complete extrusion system and one that may be sensitive to small perturbations. Modelling of extrusion of thin-walled profiles is a most demanding task. The first step in such a study would merely be to evaluate the requirements to and nature of reliable quantitative material models.

Compression testing results and analysis

The current article focuses on the generic aluminium alloy 6060, delivered by Hydro Aluminium Sunndalsøra. The composition is presented in **Table 1**. The material was cast and homogenised before testing and extrusion.

To estimate material parameters compression tests were performed at temperatures of 450, 500, 550 and 590 ºC and strain rates of 0.15, 1.5, 15, 20 s^{-1}. Experiments were performed on the Gleeble 3800 machine of the Institute for Ferrous Metallurgy in Gliwice, Poland. An inverse analysis approach based on finite element modelling was used to improve the accuracy of the material data. The approach, which is described in ref. [10], makes it possible to distinguish the component of force needed to overcome friction from the one causing plastic deformation. It also takes into account the fact that friction may cause non-uniform distributions of strain, stain rate, temperature and stress in the specimen. After the inverse analysis, a small strain-softening effect is still evident. Experiments were only run to logarithmic strains of approximately 1.

Strain independent equation (3) was selected to describe flow stress behaviour. An average value of the flow stress for strains of 0.2 to 1.0 was used. The activation energy was calculated for five constant levels of flow stress:

$$Q = -R\left.\frac{\partial \ln \dot{\varepsilon}}{\partial(1/T)}\right|_{\sigma} \qquad (6)$$

R is the universal gas constant (8.314 J/(mol K)), T is the temperature and $\dot{\varepsilon}$ is the equivalent strain rate. The average value of Q was 180 943 J/mol. While the activation energy is related to the osmotic force of diffusion and, hence, the state of stress, it was not possible to draw any conclusions on the stress dependency from the experimental data. All values were within ± 5000 J/mol. The simplex method was applied to determine the other parameters of equation (3) [12]. The result is set C of **Table 2**.

Set A has earlier been established through torsion testing with a slightly different and older variant of AA6060 [13]. Set B was established by an inverse rod extrusion analysis treated in [4] and below. **Fig. 2** compares experimental equivalent stress-equivalent strain rate data with estimates by equation (5) for sets A to C of Table 2. Set C of course produces the best fit for all temperatures. It is interesting

Table 1: AA6060.35 composition

Mg	Si	Fe	Ti	Mn	Ga	Other	Al
0.472	0.413	0.214	0.015	0.013	0.012	0.032	Rest

Table 2: MZH parameter sets for AA6060

Set	Ref	α [MPa^{-1}]	n	A [s^{-1}]	Q [J/mol]	C
A	[14]	0.0430	4.530	$9.39 \cdot 10^{11}$	180 900	1.7
B	[2]	0.0350	5.000	$9.39 \cdot 10^{11}$	180 900	1.7
C	-	0.0368	4.800	$3.90\ 10^{11}$	180 943	0.0

that similar values for the activation energy have been obtained by torsion and com

pression. One should add that 180 kJ/mol may regarded as a large energy for the 6000-series. Significantly lower values (approx 160 kJ/mol) are reported in for instance ref. [6]. In the current work only values of Q given in Table 2 are used since the focus is on evaluating data obtained by compression testing. Ref. [4] provides further analysis of parameter sets found in [6].

Rod extrusion experiments

A set of rod extrusion experiments were run in an 8 MN vertical laboratory press with a container diameter of 100 mm (**Fig. 3**). Measurement of the ram force and the outlet temperature was performed continuously. The accuracy of the force measurement was approx ±100 kN. Temperature measurement was performed with thermocouples that had been inserted into the die and plough the profile to a depth of approx 0.1 mm (Fig. 3). The technique and calibration methods are described in [14]. At least two thermocouples were used simultaneously. When properly mounted they provide results differing less than 2-3 ºC. Ref. [2] gives further information on the die design, as well as on a new pressure measurement sensor integrated in the tool.

The objective of the experiments was to produce a range of force and temperature responses that would allow later evaluation of material models. 24 different cases, defined by various combinations of levels of the four parameters shown in **Table 3,** were performed. Cases 1 to 12 were run with zero bearing lengths, whereas in cases 13 to 24 very long ones were used (12 mm for extrusion ratio (ER) 40 and 8 mm for ER 80). For both cases the nominal choke

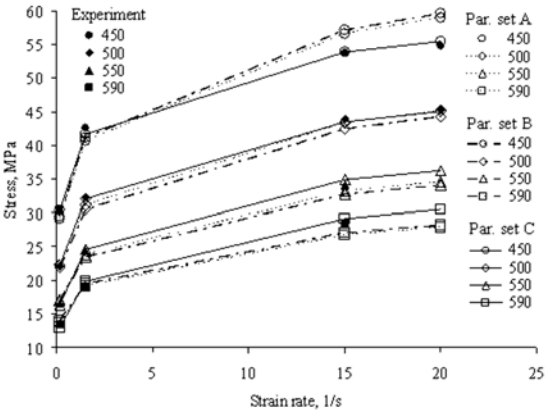

Fig. 2: Compression testing results – stress versus strain rate

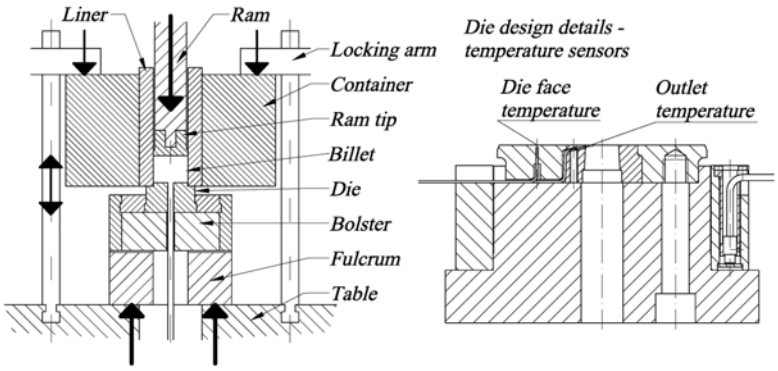

Fig. 3: The SINTEF 8 MN vertical laboratory press and die design

was 40'. Still, contact should be of the less intimate or the so-called slipping type in the whole bearing channel [15].

All cases were run at least twice. In addition, cases 1 to 6 were run on two different days to check the replicability, and in some cases there were in all 6 replicated runs. PV is the profile velocity, RV the corresponding ram velcity and BT the nominal temperature of the billet. The actual billet temperature was approx 5 ºC lower than BT. In addition, the temperature was slightly altered by the approximately 30 s delay between the billet loading and extrusion. All billets measured Ø96x200 mm. The butt end/press rest of length 19 mm was not removed between the runs. This practice simplifies experiments, but may be regarded as suboptimal from the point-of-view of materials testing. Later finite element calculations do consider the special initial thermal conditions. Further, the experimental results are in fair accordance with those of ref. [16], which were obtained when the butt end was removed between the runs. The total billet length after the upsetting and initial elasto-plastic compression was approx 201 mm.

To ensure stationary conditions with die and container temperature of about 430 °C, experiments were performed at a slow rate of about one every 10 to 12 min. The bolster temperature was 480 °C. The initial temperature of the ram was set to 130 ± 10 °C. Since the thermal conditions need not to be optimal, results from the first run in every round of experiments were disregarded.

Tables 3 and 4 provide results from measurement of ram force and outlet temperature for all cases. The values are the average values for all runs of a case. Results from the individual runs were in all cases within ±50 kN and ±5 °C. Results for four characteristic values of the remaining billet height have been considered. A 350 kN difference in ram force between the cases of zero and long bearings is mainly due to bearing friction. It is not recommendable to deduce the bearing friction directly from this number since thermal conditions differ for the two cases as a result of the additional dissipation caused by the bearing friction.

Table 3: Extrusion cases and measured ram force [kN]

CASE	ER	BT	RV	195 mm	170 mm	100 mm	30 mm
	-	°C	m/s	kN	kN	kN	kN
1/13	40	450	0.2	2948 / 3315	2589 / 2935	2114 / 2490	1882 / 2289
2/14	40	450	0.4	3188 / 3536	2784 / 3086	2247 / 2575	2043 / 2376
3/15	40	450	0.8	3462 / 3804	2982 / 3298	2387 / 2677	2204 / 2488
4/16	40	500	0.2	2535 / 2873	2289 / 2606	1975 / 2325	1825 / 2225
5/17	40	500	0.4	2734 / 3107	2416 / 2675	2051 / 2358	1955 / 2278
6/18	40	500	0.8	3014 / 3254	2573 / 2800	2140 / 2402	2095 / 2367
7/19	80	450	0.2	2993 / 3544	2706 / 3154	2295 / 2727	2057 / 2495
8/20	80	450	0.4	3301 / 3573	2947 / 3257	2485 / 2805	2268 / 2611
9/21	80	450	0.8	3606 / 4025	3174 / 3503	2628 / 2940	2423 / 2760
10/22	80	500	0.2	2663 / 3045	2479 / 2822	2224 / 2590	2023 / 2418
11/23	80	500	0.4	2902 / 3242	2621 / 2928	2303 / 2620	2160 / 2504
12/24	80	500	0.8	3156 / 3411	2786 / 2995	2413 / 2657	2318 / 2622

Table 4: Extrusion cases and measured outlet temperature [°C]

CASE	ER	BT	RV	195 mm	170 mm	100 mm	30 mm
	-	°C	m/s	°C	°C	°C	°C
1/13	40	450	0.2		498 / 518	503 / 520	495 / 512
2/14	40	450	0.4		512 / 537	522 / 543	517 / 537
3/15	40	450	0.8		526 / 556	543 / 568	545 / 568
4/16	40	500	0.2		513 / 534	515 / 533	505 / 521
5/17	40	500	0.4		525 / 552	535 / 557	528 / 547
6/18	40	500	0.8		533 / 568	553 / 580	553 / 577
7/19	80	450	0.2		497 / 514	498 / 513	489 / 504
8/20	80	450	0.4		517 / 535	521 / 537	514 / 527
9/21	80	450	0.8		537 / 556	545 / 562	541 / 556
10/22	80	500	0.2		510 / 527	508 / 523	498 / 512
11/23	80	500	0.4		530 / 549	533 / 549	524 / 537
12/24	80	500	0.8		548 / 569	556 / 574	551 / 565

Material flow and simulation

Rod extrusion is the simplest of extrusion cases, and the rod is the only geometry that may be modelled accurately in 2D within a reasonable timeframe. Hence, it is also the only geometry that may serve as a case for detailed sensitivity studies and inverse material modelling. ALMA is a numerical code dedicated to the study of 2D rigid-viscoplastic flow during extrusion. The MZH flow rule is implemented. ALMA results have earlier been found to be in accordance with those of extrusion experiments, but thorough studies of errors (modelling and measurement) are few. Since the finite element codes are by nature only approximate, it must be assumed that there may be finite and not

necessarily insignificant errors. These may relate to incomplete descriptions of strain localisation or bearing friction or to the underlying continuum hypothesis itself.

Fig. 4 presents both measured and simulated results for cases 1 and 9. The simulation has been performed with material data established through compression testing, i.e. set C. **Fig. 5** shows the corresponding output by the outlet temperature sensors. A further comparison of results from cases 1 to 12 is presented in **Fig. 6**. The temperature measurement is for all runs and billet heights significantly lower than the estimate by ALMA. The deviation in force seems less significant. It may seem as if ALMA somewhat exaggerates changes in container force. This may be due to the full sticking assumption or to a poor description of the temperature distribution. It is interesting to note that errors are smaller at high rate of deformation than at a low.

It is not obvious that errors are entirely due to model deficiencies. The results from the experiments should also be critically assessed. The ram force measurement may be somewhat too high as the friction between the container and the ram is not taken into account in the flow model. Thermocouples may indicate too low temperatures when not accurately mounted and manufactured. They may also locally affect flow and cause extra plastic heat dissipation. However, measurements are in accordance with ref. [12], and results from different sensors are in fair agreement.

General information given in Fig. 6 about the deviation between the results from simulation and experiment may also be expressed by indicators such as the error functions for force and temperature, E_F and E_T respectively.

$$E_M = \frac{1}{12\sigma_M^2} \sum_{i=1}^{12} \frac{1}{p^i} \sum_{j=1}^{p^i} \left(M_x^i(t_j) - M_c^i(t_j) \right)^2 \qquad (7)$$

M_x and M_c are the measured and corresponding calculated values of force ($M = F$) or temperature ($M = T$). σ_F and σ_T are typical measures of random error, 100 kN and 5 K. p^i is the number of measurement points for case i. t_j is the time at measurement point j. Due to the 1 s response time of the thermocouples the initial phase of the run should be disregarded. E_M and M_c depend on the parameters of the MZH flow rule (α, n, A, Q, C). If proper values of σ_F and σ_T are chosen, the value of E_M should approach 1 when the estimated and measured results are in accordance.

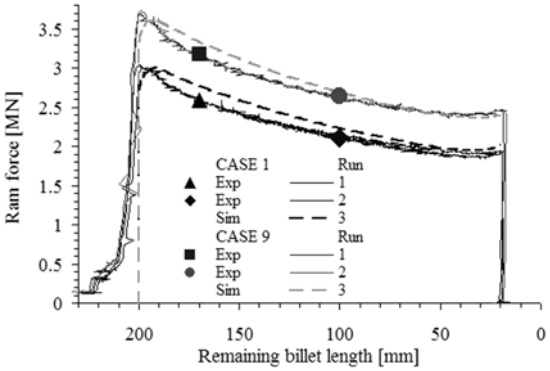

Fig. 4: Examples of measured and estimated ram force

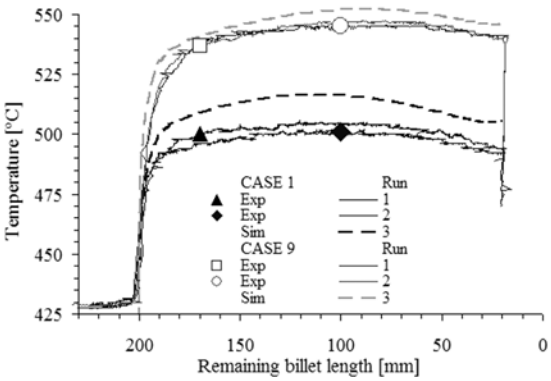

Fig. 5: Examples of measured and estimated outlet temperature

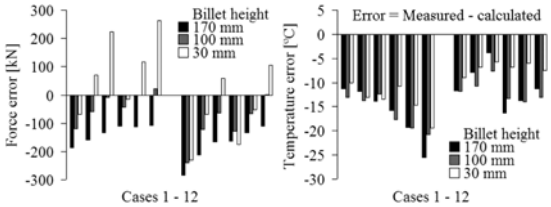

Fig. 6: Force and temperature errors for cases 1 to 12 – set C

Force and temperature errors for cases 1 to 12 have been plotted as a function of α and n in **Fig. 7**. One has adopted values of A and Q of the compression test. C is equal to zero (a pure ZH-model). The plots are useful since they reveal the characteristics of the extrusion system and some difficulties related to inverse modelling of extrusion and coupled non-linear thermo-mechanical processes. Similar surfaces may be obtained when the MZH flow rule is used to model either compression or torsion testing. A problem is then that there are numerous combinations of α and n that produce quite acceptable estimates of temperature and force. Valleys of low error stretch across the plots, and the position of the minima is not obvious due to the statistical errors in measurement. The estimation problem is even more complex in 5D. Similar cross-sections have been found for completely other values of A, Q and C [4].

An important feature of Fig. 7 is the offset between the valleys of minimum force and temperature. Ideally, the

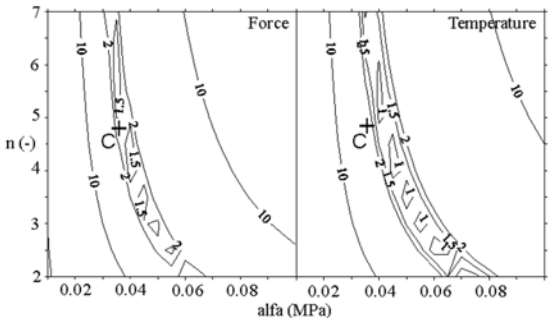

Fig. 7: Force and temperature error plots for uncorrected data from measurement (A = $3.90 \cdot 10^{11}$ s^{-1}, Q = 180 943 J/mol, C = 0)

points of minimum error should coincide and also be in the close vicinity of the point defined by parameter set C if the compression test is truly representative. The deviation in Fig. 7 may be due to errors related to measurement or simulation. The discrepancies may also occur as a result of the extrapolation of compression test data obtained at low rates to the study of extrusion. Even if strain hardening, anisotropy etc may be disregarded and one would expect a common minimum in the parameter space to exist, it need not at all be close to the point defined by parameter set C. In order to obtain better estimates of temperature, the value of A is changed from $3.90 \cdot 10^{11}$ to $9.39 \cdot 10^{11}$ s^{-1} in **Fig. 8**. The value of A then corresponds to one that has been estimated in AA6060 torsion tests with [13], but it is evident that the (α, n) – coordinates of the torsion test data (set A) are not those of the minimum point. For example, parameter set B gives a better overall fit. Fig. 8 reveals a further characteristic of the extrusion system that requires some attention when measurement techniques are devised and material data evaluated. Even if the distance between points such as A and B may be small, measures of error may differ significantly. One is moving out of the valley.

The change of the value of the A parameter has brought force and temperature valleys closer, but no optimal or general model has been established. **Figs. 9 and 10**, which compare experiment results with simulation estimates based on different sets of material data, indicate that there still is some room for improvement. If no errors are related to measurement data, compression data implemented in the ALMA flow code produce results that may be useful, but non the less suboptimal. However, measurement errors do exist and may explain some of the deviations between measured and simulated results. **Fig. 11** is a plot of error surfaces obtained when that it is assumed that temperature and force measurements are systematically 5 ºC and 100 kN too high. The values of Q, A and C values are the same as those of Fig. 7, while the measurement data have been corrected. As a result, the optima have moved closer to the compression testing point, and the offset between the force error and temperature error valleys is smaller.

Errors may also appear if the input data of the model do not correspond to those of the experiment. For instance, extrusion modelling requires an accurate description of heat transfer because of the coupled nature of the problem**. Tables 5, 6 and 7** show how the force and temperature errors

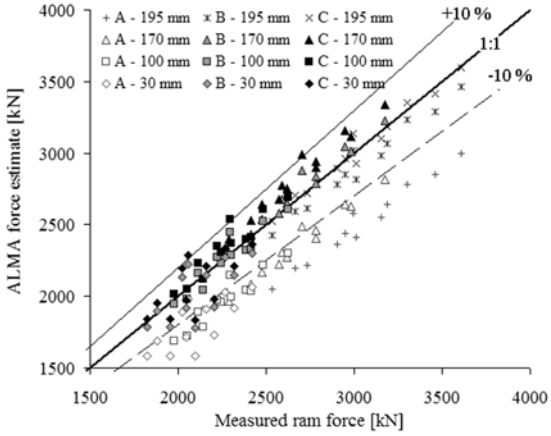

Fig. 9: Comparison of measured and simulated force. Results are for various parameter sets and billet lengths.

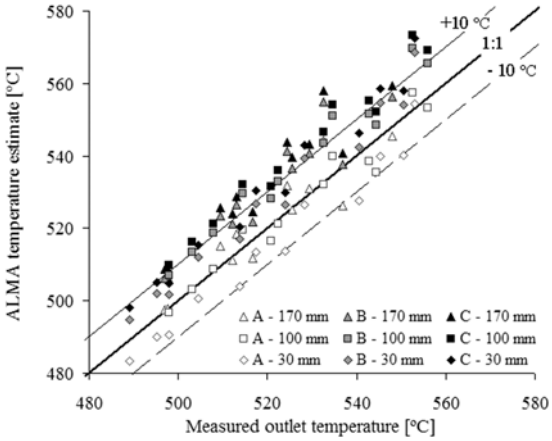

Fig. 10: Comparison of measured and simulated temperature. Results are for various parameter sets and billet lengths.

depend on the initial temperature of the ram (130 ºC), the deviation of from the nominal billet temperature (450 and 500 ºC) and the duration of waiting time (30 s) from the billet is loaded till extrusion actually commences. Only one of the parameters is changed at a time. For the nominal values of the parameters possible force errors are reasonable, but the tables indicate that better estimates of the tempera-

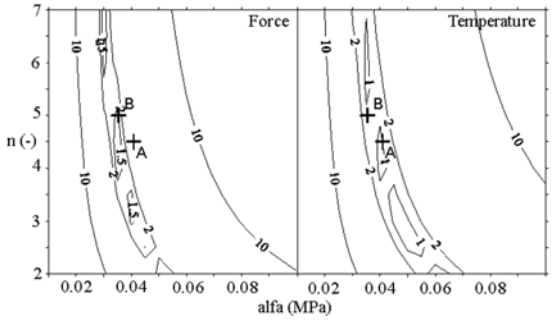

Fig. 8: Force and temperature error plots for uncorrected data from measurement (A = $9.39 \cdot 10^{11}$ s^{-1}, Q = 180 900 J/mol, C = 1.7)

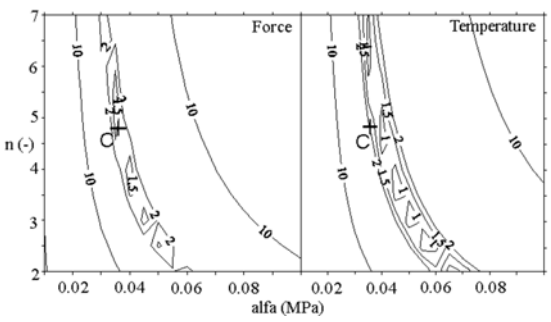

Fig. 11: Force and temperature error plots for corrected data from measurement (A = $3.90 \cdot 10^{11}$ s^{-1}, Q = 180 943 J/mol, C = 0)

ture could be obtained by decreasing the temperature of the system. While this is in accordance with observations from experiments, a lower temperature would probably cause an increase in the force estimates which already are too high. Further, it is not reasonable to expect temperatures to vary by more than 10 ºC and the waiting time by more than 15 s. These changes should not affect error estimates to a large extent.

Table 5: Force and temperatures errors and ram temperature

Ram temp. [°C]	25	50	75	100	125	150	175	200
Force error [-]	1.3	1.2	1.2	1.1	1.1	1.0	1.0	1.0
Temp. error [-]	1.9	2.0	2.2	2.3	2.4	2.6	2.7	2.9
Average error [-]	1.6	1.6	1.7	1.7	1.7	1.8	1.9	1.9

Table 6: Force and temperatures errors and billet temperature

Billet temp. dev. [°C]	-50	-10	-5	0	5	10	50
Force error [-]	3.0	1.4	1.2	1.1	0.9	0.8	2.0
Temperature error [-]	0.7	1.9	2.1	2.5	2.8	3.1	5.5
Average error [-]	1.9	1.6	1.7	1.8	1.8	1.9	3.7

Table 7: Force and temperatures errors and waiting time

Waiting time [s]	1	5	30	60	120	240	480
Force error [-]	0.9	0.9	1.0	1.2	1.6	2.5	4.6
Temperature error [-]	3.0	3.0	2.6	2.3	1.6	0.7	2.0
Average error [-]	1.9	1.9	1.8	1.7	1.6	1.6	3.3

Finally, the heat transfer coefficient between aluminium and steel and the heat conduction coefficients may both be in error. However, the system is not particularly sensitive to changes in these parameters within reasonable bounds. This is an advantage in relation to materials testing.

Conclusion

Plots of deviation between measured and calculated data for ram force and outlet temperature may be used to check the parameter sets established through standard materials testing. One has found that simulations using material data from compression tests produce fairly accurate estimates of ram force, but less so for outlet temperature. Deviations between experimental and simulated data may be due to both modelling and experimental error. Further studies will focus on closer temperature control during extrusion experiments and on high speed materials testing.

References

[1] P.T. Moe, M. Lefstad, R. Flatval, S. Støren, Intern. J. of Forming Processes Vol. 6 (2003) No. 3, p. 241/270.

[2] P. T. Moe, W. Wajda, S. Støren, A study of the thermo-mechanical response of a die face pressure sensor for hot aluminium extrusion, Proc. Metal Forming 2004, Sept. 2004, Kraków, In press.

[3] K. Holthe, L. Hanssen, S. Støren, Numerical simulation of the aluminium extrusion process in a series of press cycles, Proc. NUMIFORM'92, 1992, Sophia Antipolis, p. 611/618.

[4] W. Wajda, P.T. Moe, S. Abtahi, S. Støren, An evaluation of material behaviour during extrusion of AA6060 rods, Proc. 7th ESAFORM Conf. on Material Forming, April 2004, Trondheim, p. 245-248.

[5] E. Nes, Progress in Materials Science Vol. 41 (1998), p. 129/193.

[6] T. Sheppard, Extrusion of Aluminium Alloys, Kluwer, NY, 1999.

[7] G. Grasmo, Friction and Flow Behaviour in Aluminium Extrusion, Trondheim, 1995 (PhD-thesis).

[8] L. Djapic Oosterkamp, A. Ivankovic, G. Venizlos, Mat. Sci. and Eng. A278 (2000), p. 225/235.

[9] T. Aukrust, S. Tjøtta, H.E. Vatne, P. Van Houtte, Int. J. of Plasticity Vol. 13 (1997) No. 1/2, p. 111/125.

[10] W. Wajda W., P.T. Moe, M. Lefstad, S. Støren, Study of the limits of self-stabilization during extrusion of thin strips, Proc. 6th Esaform Conf. on Metal Forming, April 2003, Salerno, p. 267/270.

[11] Szeliga D., Pietrzyk M., Identification of Rheological and Tribological Parameters, Metal Forming Science and Practice, A State-of-the-art Volume in Honour of Professor J.A. Schey's 80th Birthday, ed., Lenard J.G., Elsevier, Amsterdam, 2002, p. 227-258.

[12] J.A. Nelder, R. Mead, Computer Journal Vol. 7 (1965), p. 308/313.

[13] B. Rønning, Hot torsion testing of 6063.50, 6060.10, 6060.75 and 6060.90, SINTEF Metallurgy Report STF34 F93237, 1993.

[14] M. Lefstad, Metallurgical Speed Limitations During the Extrusion of AlMgSi-Alloys, Trondheim, 1993 (PhD-thesis).

[15] S. Abtahi, Friction and interface reactions on the die land in thin-walled extrusion, Trondheim, 1995 (PhD-thesis).

[16] G. Grasmo, K. Holthe, S. Støren, H. Valberg, R. Flatval, L. Hanssen, M. Lefstad, O. Lohne, T. Welo, J. Herberg, R. Ørsund, Modelling of Two-Dimensional Extrusion, Proc. 5th Intern. Aluminium Extrusion Technology Seminar, 1992, Chicago, Vol. II p. 367/376.

Moe P.T., Wajid W., Strøen S.

A Study of the Thermomechanical Response of a Die Face Pressure Sensor for Hot Aluminium Extrusion

Paper in Proceedings and Journal Article

10th International Conference on Metal Forming
September 20, Krakow, p627-634

STEEL GRIPS 2 (2010)
Sp Metal Forming 2010, p627-634

Per Thomas Moe, Wojciech Wajda and Sigurd Støren:

A study of the thermo-mechanical response of a die face pressure sensor for hot aluminium extrusion

Die face pressures up to 500 MPa may cause large elastic and even plastic deformations of the tool stack during aluminium extrusion. As a result, both the die outlet and the profile shape may be significantly distorted. In the extreme case also the stability of the flow is affected, so that the profile may buckle or curve. Particularly when extruding thin-walled sections it is essential to control the outlet shape by careful die design, by introducing self-compensating mechanisms or by measuring shape or other essential parameters and correcting, preferably on-line. In order to establish a better understanding of extrusion and to improve control, it is important to study all relevant physical responses of the process. The article presents a pressure sensor that may be used to assess the pressure distribution on the die face and potentially also the stress distribution in the profile. It uses the capacitive principle for distance measurement to determine the elastic deformation of a disc in contact with the aluminium billet. The 2.75 mm thick sensor disc is an integral part of the extrusion die. The study focuses on the thermo-mechanical response of the sensor during extrusion. The disc deflection is approx 30 µm, and the linearity of the capacitive sensor is approx 1 µm. An in-situ calibration technique makes it feasible to measure pressure to an accuracy of approx ± 5 %. The most significant effect that is not captured by the calibration technique is the thermo-mechanical response of the sensor when it is heated during extrusion. One has found that thermal expansion may cause deviation in maximum response of approximately 10 %. At the same time, however, a reduction in the elastic modulus and changes in capacitance of the system due to the temperature increase, counteract the thermal expansion effect. A simple method of temperature compensation is presented as well as a rod extrusion case study of pressure measurement.

Extruded aluminium profiles may potentially be of the most involved cross-sectional shape and integrate features and functionality of importance to the user. Today, thinner and wider profiles are demanded. The main challenge in relation to extrusion of thin-walled profiles is to accurately control dimensions and to secure stable flow and uniform outlet velocity. Instabilities are manifest as sections buckle or bend, and latent if there are no shape changes but residual tensile/compressive stresses in the sections. As of today, the tuning of flow is mainly based on the visual observations and handwork of skilled die correctors. Their main instrument is the friction or bearing surfaces close to the die outlet. Much time is spent on preparing, testing and correcting the die geometry. When the dies are put into production, there is a careful and continuous control of key shape parameters of the sections in order to prevent scrap production. Rerunning of orders and re-melting of material is not unusual. Excessive variability in shape may in the case of large volume production, cause significant losses related to downstream processing. Yet, the greatest loss is probably that of possibilities. More extensive use of aluminium profiles in cars may be desirable, but the cost of the extruded product is high when tolerances are tight.

A solution to the shape variability problem may be the introduction of an altogether new process or die concept. It is more likely, however, that there will be many small but important improvements of tool and press design and auxiliary equipment for process control. Such progress is facilitated by advances in many fields of technology. First, numerical simulation now offers the possibility to closely study the details of the extrusion process and to predict the flow field and profile dimensions. Traditionally, the main focus of numerical modelling has been on quantifying the elastovisco-plastic properties of aluminium. However, die correctors and manufacturers also pay close attention to the deformation of the dies and the distortion of the outlets caused by the large tractions between die and billet and by the temperature changes due to plastic dissipation. Friction forces acting between the container and the billet may also play a part when they are guided through the die since the friction surface decreases during extrusion. Models make it possible to evaluate the involved coupled nature of the process, but it is vital that they are carefully validated.

There is also a steady progress in the field of sensor and actuator technology. In high precision forming processes, it is important to limit or compensate for the deformation of the tools. In some cases automatic compensation may effectively be established. In others on-line closed loop control may be performed as sensors and actuators may be integrated in the tools. During rolling for instance sheet thickness may be controlled down to micrometer accuracy. There are many reasons why process control with sensors and actuators may be less effective in extrusion. Still, one should not disregard shape control. Steady progress has been made over the last twenty years in the field of on-line measurement of key parameters of the extrusion process. So far, the main objective has been to increase insight and to establish models. The bearing channel temperature was measured in ref. [1], and ref. [2] supplies a recent example of a die deflection and strain measurement technique. On-line techniques for high-speed profile shape measurement have also been studied [3], and different research groups have developed sensors for measurement of the pressure at the billet-die or billet-container interface [4-7].

The current article treats a technique for estimating the die face pressure based on displacement measurement by capacitive sensors. As has been shown in ref. [4], one of the main advantages of these sensors is that they only to a

Per Thomas Moe, *M.Sc.*; *Wojciech Wajda, M.Sc.; Prof. Sigurd Støren,* Department of Engineering Design and Materials, Norwegian University of Science and Technology, Trondheim, Norway

small extent are affected by the temperature changes of the extrusion environment. The current article provides a full review of results from a set of rod extrusion experiments. The main objective of the work was to assess the thermo-mechanical response of sensors and to establish techniques for calibration and temperature compensation.

Sensor and die design

In the current study, capacitive high-temperature probes of the type Capacitec® HPC-75A-V-N3 (**Fig. 1**) were used to measure the elastic deformation of the material around a cavity in the die caused by a pressure applied at its upper face (**Fig. 2**). Two different solutions for fixing the sensor to the die were used. The probe may be pushed towards an edge in the sensor cavity by an Inconel spring (solution A). Alternatively, two set screws may fix the sensor to a point in the wall of the cavity (solution B). The die design and the mounting solutions are shown in **Fig. 3**. The die consists of a top disc, a die outlet insert, a die core and a liner load cell, which also makes use of capacitive probes. The composite design has a number of advantages. Sensor holes are simple to manufacture, and sensors may easily be mounted. Besides, it is possible to use the same sensor when extruding with different outlet dimensions.

The die is attached to a return cable to the amplifier of the capacitive equipment and, thus, is an integral part of the electric circuit of the capacitive sensors. The probe is connected to the amplifier by an isolated coax cable. For an alternating current of frequency 15.625 kHz the main potential drop will be across the gap between the top face of the probe and the bottom face of the sensor disc. When a pressure is exerted on the top face of the die by the flowing aluminium, the gap distance is reduced and so is the recorded voltage. In the ideal case of the measurement of pure translation, the linearity of the equipment by Capacitec® is approx ± 0.2 % of full scale. Since there are

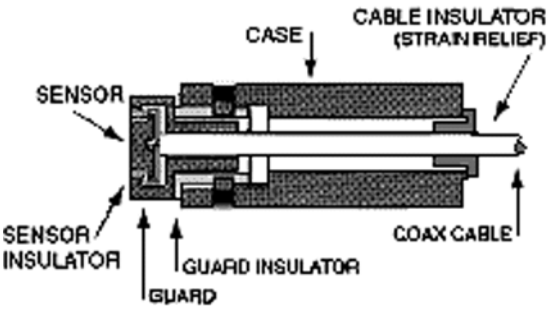

Fig. 1: Capacitec® HPC-75A-V-N3 probe with cable [8]

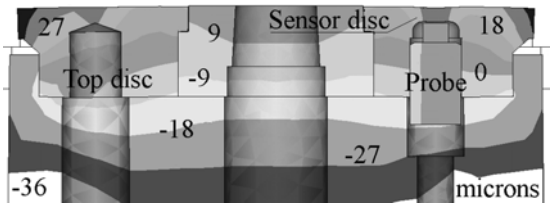

Fig. 2: Calculated displacement of the pressure sensor

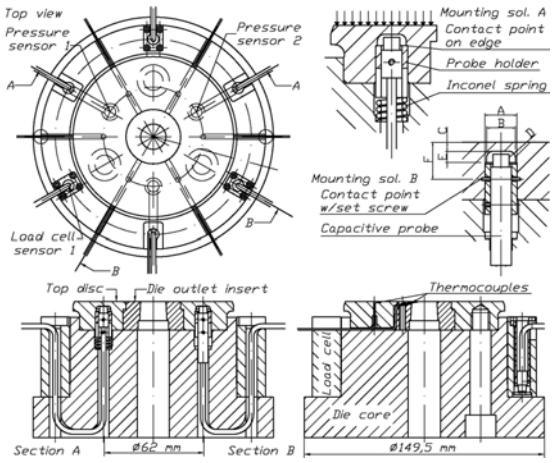

Fig. 3: Die design used in experiments with die inserts

limits also to the accuracy and linearity of the calibration viameter (0.5 µm), a full scale much smaller than 0.5 mm is not practical. This gives a linearity of ca ± 1 µm. The resolution/repeatability is significantly smaller (± 0.01 %).

Calibration

When the capacitive probe is integrated in a die pressure sensor, pressure-voltage (displacement) calibration curves should be established by independent and representative physical tests rather than deduced from the displacement calibration and FE models. There are a number of reasons for this. First, it is probably not feasible to produce purely elastic displacements significantly larger than 30 µm with the design of Fig. 2 [4]. The non-linearity of the capacitive measurement is then considerable and difficult to assess. Second, the sensor disc is bent and may even tilt during loading. As the actual sensing area is quite small (3 mm in diameter), the response is probably still repeatable, but it is not certain that it may be easily predicted. Third, it is difficult to determine and model the mechanics of contact between the sensor and the die. In the case of mounting solution A one may find that the point of contact changes during loading. Fourth, the accuracy of machining affects the thermo-mechanical response of the sensor. Each sensor will respond according to a unique calibration curve.

Table 1 presents typical sensor dimensions, the average calibration factor for the two mounting solutions and some effects of the shape variability. The shape factors A-F are shown in Fig. 3. The calibration factor is defined as the ratio between the pressure applied on the die surface and the apparent displacement. Both 2D and 3D sensitivity analyses have been performed with the FE code ANSYS. **Fig. 4** reveals to which extent a uniform load applied at a given distance from the sensor affects the sensor output. During extrusion the complete top surface of the die is in intimate contact with aluminium. However, if aluminium starts to flow at a distinct finite yield stress, the sensor disc deflection may locally affect the pressure distribution and of course vice versa. This coupling is evident during cold compression of aluminium and steel, but is less likely to be of significance during hot aluminium extrusion.

Table 1: The effects of machining errors (axisymmetric study)

Factors - all values, expect for G are in [mm]	-1	0	+1
A – Largest diameter of the sensor hole	9.90	10.00	10.10
B – Smallest diameter of the sensor hole	8.85	9.00	9.15
C – Thickness of the deflecting disc	2.60	2.75	2.90
D – Radius of corner close to disc	1.75	2.00	2.25
E – Distance: disc to contact point sol A	3.30	3.50	3.70
F – Distance: top disc to contact point sol B	11.20	11.50	11.80
G – Modulus of elasticity [GPa]	170	175	180

Effects	Solution A factor	Solution B factor	Stress intensity
Average	12.40 MPa/µm	7.57 MPa/µm	2.60
A	+ 0.11 (0.88 %)	- 0.03 (0.43 %)	- 0.02
B	- 0.61 (4.95 %)	- 0.14 (1.84 %)	+ 0.14
C	+ 0.69 (5.53 %)	+ 0.33 (4.35 %)	- 0.15
D	+ 0.55 (4.47 %)	+ 0.19 (2.55 %)	- 0.37
E	- 0.26 (2.08 %)	+ 0.70 (0.27 %)	+ 0.04
F	- 0.00 (0.01 %)	- 0.12 (1.64 %)	+ 0.01
G	+ 0.35 (2.86 %)	+ 0.22 (2.86 %)	+ 0.00

Two techniques of calibration have been found useful. In the first approach, steel rings of diameters 4 to 40 mm and cross-sections of 2 x 2 mm^2 are pressed towards the top face of the sensor. The experiments indicate that the relationship between pressure and voltage change deviates less than 1 % from linearity and support the conclusions drawn from Fig. 4 with regard to the area of influence. It is easier and better, however, to calibrate the sensors in-situ at relevant temperatures by compressing a thin billet repeatedly at various levels of ram force (**Fig. 5**) after the outlet has been plugged [4]. When a moderate overload is applied initially, permanent displacements do not occur later during calibration or extrusion. Overloading causes plastic deformations, and the elastic range is extended as a result. An overload may also contribute to better fastening of the probe. If the sensor response is to return to zero upon unloading, a steady state temperature distribution must be reached before calibration is performed.

The outcome of the calibration tests was not affected by the length of the billets. Hence, the state of stress probably was homogeneous and purely isotropic during calibration, and the die face pressure distribution was almost uniform.

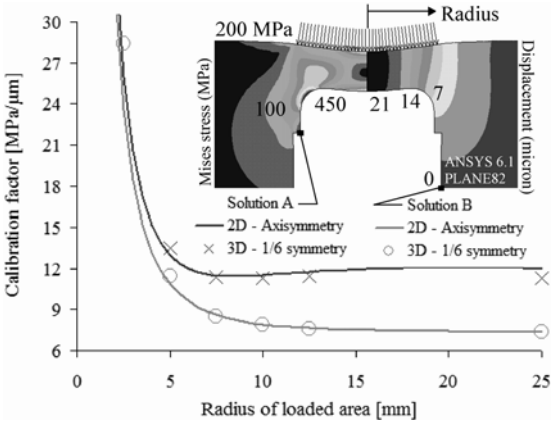

Fig. 4: The dependence of the sensor response on loading area

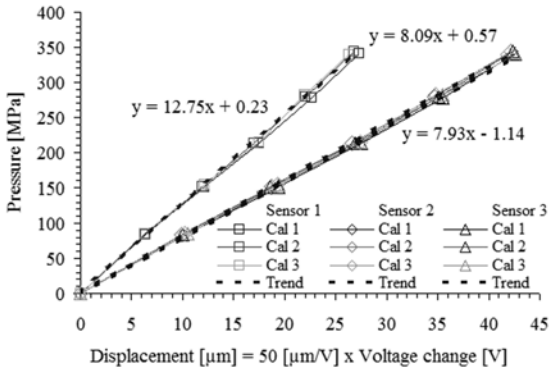

Fig. 5: Results from calibration through hydrostatic compression

It is important that the calibration case relates to a known well-defined load distribution, which may deviate from the one experienced during extrusion. In ref. [10] the relevant cases of rod extrusion have been studied with the flow code ALMA. **Fig. 6** presents estimates of the die face pressure at the start and end of extrusion. When the billet length is short, the flow direction will mainly be radial, and the pressure gradient along the surface will be large.

Since the sensor is of finite size and is an integral part of the die construction, one may expect systematic errors to occur when the loads on the die deviate from those of the calibration case. In order to evaluate the sensor response for different load configurations, a 3D thermo-mechanical model of the tool stack has been established in ANSYS 6.1 (Fig. 7) [11]. The thermal and/or mechanical loads may be imported from ALMA. **Table 2** displays essential data for the Uddeholm Orvar Supreme tool steel.

Table 3 shows that the displacement of the bottom point of the disc relative to the probe-die contact points is not significantly affected by the load distribution. The relative tilting of the disc may differ by approx 1 µm (a positive tilt is defined as one which causes the distance between the disc and the probe to be shortest on the side closest to the die centre). As the absolute distance between the disc and sensor is more than 300 µm, the capacitance should not be

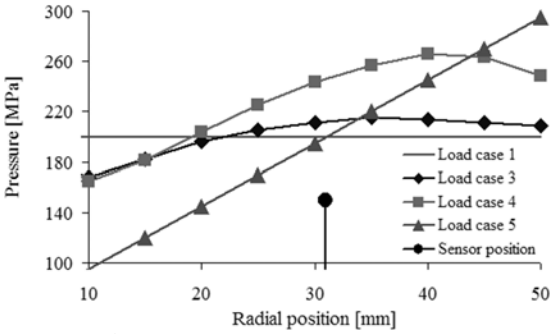

Fig. 6: Die face pressure distribution - calibration and extrusion

Table 2: Orvar Supreme (HRC 45) – properties [12]

Temperature [°C]	20	400	450	500	550	600
E-modulus [MPa]	210	180	170	160	150	140
Poisson's ratio [-]	Set to 0.3 at all temperatures					
Yield stress [MPa]	1220	1000	920	820	730	600

Table 3: Calibration factors [MPa/µm] / tilt [µm] of disc from model

Sensor solution A	0°	30°	60°	90°
CASE 1: Uniform load	11.82 / 1.3	11.83 / 1.4	11.85 / 1.3	11.83 / 1.1
CASE 2: With liner load	11.80 / 1.2	11.79 / 1.4	11.85 / 1.3	11.82 / 1.1
CASE 3: ALMA start load	11.84 / 0.9	11.83 / 1.0	11.85 / 1.0	11.86 / 0.7
CASE 4: ALMA stop load	11.76 / -0.1	11.76 / 0.0	11.77 / 0.0	11.77 / 0.0
CASE 5: Gradient load	11.38 / -2.3	11.35 / -2.1	11.37 / -2.3	11.41 / -3.9
Sensor solution B	**0°**	**30°**	**60°**	**90°**
CASE 1: Uniform load	7.55 / 0.5	7.58 / 0.9	7.60 / 0.8	7.56 / 0.3
CASE 2: With liner load	7.52 / 0.5	7.56 / 0.9	7.60 / 0.8	7.55 / 0.3
CASE 3: ALMA start load	7.56 / 0.0	7.58 / 0.34	7.60 / 0.27	7.57 / -0.2
CASE 4: ALMA stop load	7.49 / -1.1	7.52 / -0.8	7.54 / -0.8	7.52 / -0.8
CASE 5: Gradient load	7.30 / -3.9	7.31 / -3.6	7.33 / -3.7	7.32 / -4.1

much affected by the tilting. It should be noted that even if the pressure is uniform, the disc will be inclined. The reason is that the tool stack does not provide perfect support for the die. Deformations are far from uniform (**Fig. 7**). In fact, since die deflections may be quite large, it would not be completely unreasonable to assume that the sensor may respond to changes in loads applied on parts of the die not in close vicinity of the sensor. An example of such a load change is the decrease of the liner load from approx 1000 kN to 100 kN during extrusion. Fortunately, according to Table 3 such a change does not affect the sensor response significantly. It should in this relation be noted that also the position of the sensor relative to the symmetry plane (given in degrees) is less important.

Table 4: Calibration factors [MPa/µm] recorded on different days

ER	Day 1	Day 2	Day 3	Day 4	Day 5
Sensor 1	13.2	13.2	12.8	12.0	12.4
Sensor 2	8.5	7.9	8.1	8.4	7.8
Sensor 3	8.1	8.4	7.9	8.3	7.4

Table 4 presents the results from hydrostatic calibration on different days/for different rounds of experiments. It is assumed that 1 V change corresponds to a displacement of 50 µm. Only the probe of sensor 1 was fixed according to solution A. A complete dismantling of the equipment was performed after each round. The sensor disc thickness was also reduced by 0.05 mm before the fourth round. The variability observed in Table 4 may be due both to actual differences in sensor characteristics and to the limitations of the calibration technique itself. The accuracy of the ram force measurement is not better than ± 50 kN (± 2.5 %). For properly fixed probes deviations between calibration curves established on different days were smaller than 2.5 %. This applies also to the comparison of calibration data established before and after the experiments. Only on one occasion of fifteen did a probe loosen during extrusion.

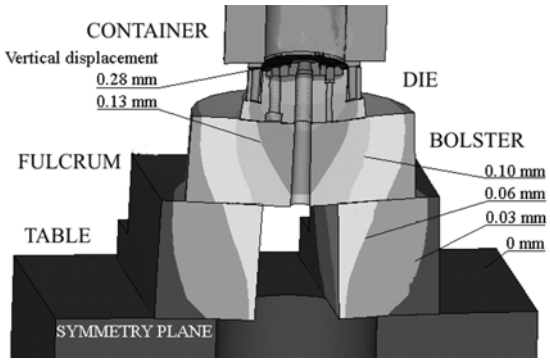

Fig. 7: Model of the 8 MN SINTEF press tool stack in ANSYS

Table 5: Extrusion cases and average measured pressure [MPa]

CASE	ER	BT	RV	195 mm	170 mm	100 mm	30 mm
	-	°C	m/s	MPa	MPa	MPa	MPa
1/13	40	450	0.2	231 / 280	213 / 253	204 / 244	229 / 270
2/14	40	450	0.4	260 / 313	234 / 271	212 / 249	233 / 267
3/15	40	450	0.8	279 / 337	256 / 292	230 / 265	247 / 274
4/16	40	500	0.2	210 / 251	182 / 216	186 / 223	220 / 263
5/17	40	500	0.4	237 / 282	199 / 227	185 / 215	216 / 246
6/18	40	500	0.8	257 / 298	219 / 234	198 / 219	225 / 245
7/19	80	450	0.2	239 / 291	227 / 277	235 / 280	254 / 297
8/20	80	450	0.4	272 / 313	251 / 277	243 / 269	269 / 294
9/21	80	450	0.8	296 / 347	269 / 307	249 / 285	268 / 302
10/22	80	500	0.2	217 / 261	211 / 239	234 / 262	258 / 282
11/23	80	500	0.4	247 / 295	220 / 250	224 / 255	256 / 279
12/24	80	500	0.8	288 / 321	239 / 258	226 / 247	256 / 283

The calibration factors of Table 3 are lower than those of Table 4. This may to some extent be attributed to an inaccurate description of the sensor geometry. It has also been observed that during calibration, the temperature was some 15 ºC lower than at the onset of the extrusion runs. This is mainly because additional cooling is caused by the ram during calibration runs. When a number of billets are extruded, the temperature of the die will also gradually increase. In this case the effect was small (less than 5 ºC).

Rod extrusion experiments

In order to check the feasibility of performing die face pressure measurement during extrusion, rod extrusion experiments were run in a vertical 8 MN laboratory press of SINTEF Trondheim. AA6060.35 billets were of length 200 mm and diameter 96 mm. The container diameter was 100 mm. The 19 mm butt end was not removed between runs, and the total height of the billet after the burp phase and at peak pressure was ca 201 mm. The pause between each run lasted ca ten minutes, and the die and container temperatures almost returned to the initial level of 430 ºC in front of each run. The ram temperature was 130 ºC.

Four parameters were changed during the experiments in order to produce different levels of die face pressure. By replacing the outlet inserts the extrusion ratio (ER) and the bearing length (BL) could be altered. The experiments were also run at three different levels of ram/profile speed

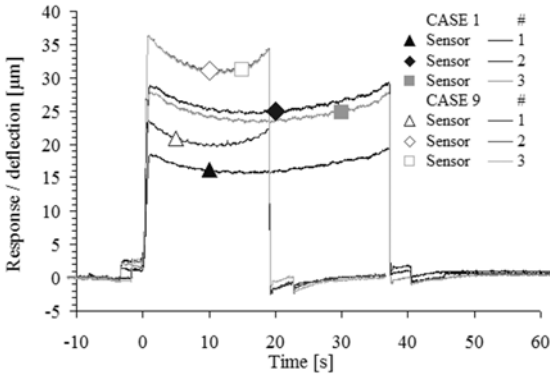

Fig. 8: Apparent displacement measurement for cases 1 and 9

(RV/PV) and two levels of initial billet temperature (BT). **Table 5** defines the 24 cases. For each case there were at least two replicate runs. In addition, cases 1-6 were run on two days (1 and 2) in order to check accuracy. Further, in each run pressure was measured by 3 independent sensors in essentially the same position. Ref. [10] reveals further information about the experimental set-up and key output data such as the ram force and the outlet temperature.

Fig. 8 presents experimental results from two different cases, 1 and 9. Small fluctuations may first be registered when the billet is loaded and the ram shears of the material along the container wall (0.2 µm). Then during the burp phase a displacement of some 3 µm is recorded before the actual extrusion is performed. The sensor responds to load changes as the ram is pulled of the butt end. The sensor output does not immediately return to zero after extrusion, but rather converges slowly. This behaviour is related to a transient thermo-mechanical sensor response. Techniques for temperature compensation are discussed below.

Values of die face pressure at billet heights 195, 170, 100 and 30 mm have been listed in Table 5. The values are based on results from all sensors and runs. In all but one case did the sensors produce estimates within approx ±20 MPa from those of Table 5. This seems to be a reasonable value given the accuracy of the calibration technique. The data have not been corrected for any thermal effects.

An analysis of experimental results

The current analysis focuses on the thermo-mechanical response of the pressure sensors to the heat shock caused by the heat dissipated during plastic deformation. Fig. 8 indicates that heating causes a systematic error which may be addressed at least in an approximate manner. Finite element flow modelling may provide further information on the pressure measurement accuracy. Rod extrusion is then an appropriate test case since it may be easily and accurately modelled. In **Fig. 9** uncorrected measurement results from one of the pressure sensors are compared with pressure estimates by ALMA. The flow model assumes full sticking at the container walls and that the aluminium alloy behaves according to the Modified Zener-Hollomon flow rule. The material data have been established by high temperature compression testing [10]. Force estimates are quite accurate, and estimates of pressure also seem to be in fair agreement with measurements. The calibration factor of case 1 seems to be too low. The transient thermal effect appears to affect the sensor output by less than 10 %.

The thermo-mechanical behaviour of the pressure sensor may be evaluated by introducing thermal loads from flow simulations in the 3D ANSYS 6.1 tool stack model. Both simulation and measurement indicate that the maximum temperature change 1 mm below the surface close to the sensor is approx 30 ºC (**fig. 10**). The surface temperature change is less than 5 °C larger, while the capacitive probes are significantly less affected since they are positioned at a certain depth and since there is an interface between the probes and the die. The cavity radiation is insignificant.

Two effects must be included in a model of the thermal response of the pressure sensor. First, as the temperature of the probe is lower than that of the die itself, thermal expansion may cause the gap between the disc and probe to increase. An additional increase is caused by a slight upwards bending of the sensor disc, which is due to the temperature differences in the disc and the die. The second effect relates to the temperature dependency of the elastic properties. When the temperature of the disc increases, the elastic modulus decreases. The deflection increases, and it will appear as if the pressure is larger than it actually is.

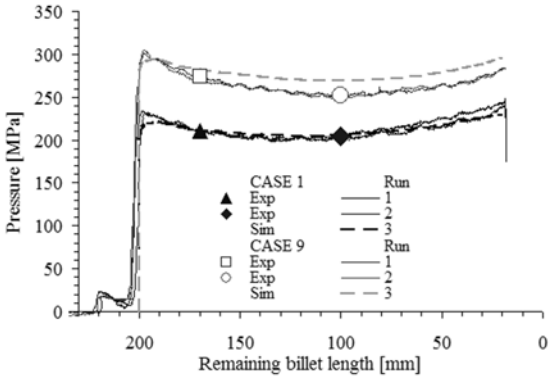

Fig. 9: A comparison of measured and estimated pressure

In **Figs. 11 and 12** the various components of the sensor response are compared. A uniform (200 MPa) and time-independent pressure distribution has been applied on the top of the die face. While the load distribution may differ

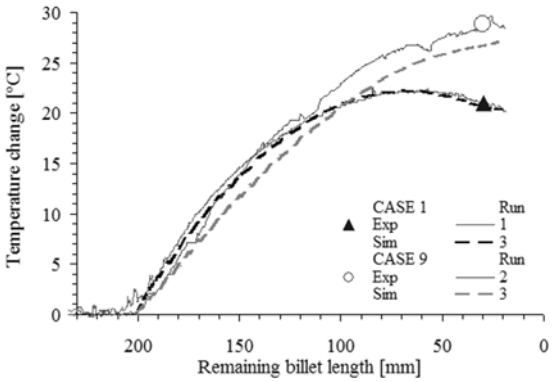

Fig. 10: The sensor temperature 1 mm below the die surface

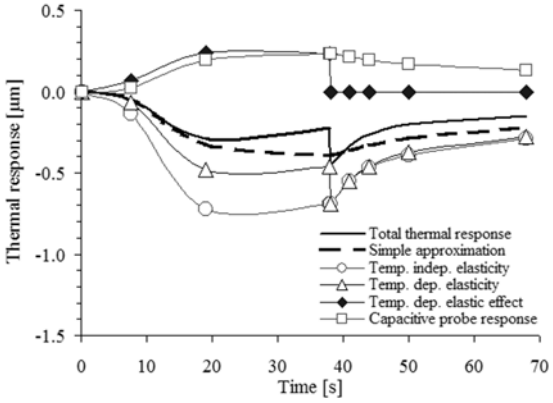

Fig. 11: The thermal response of sensor A – case 1

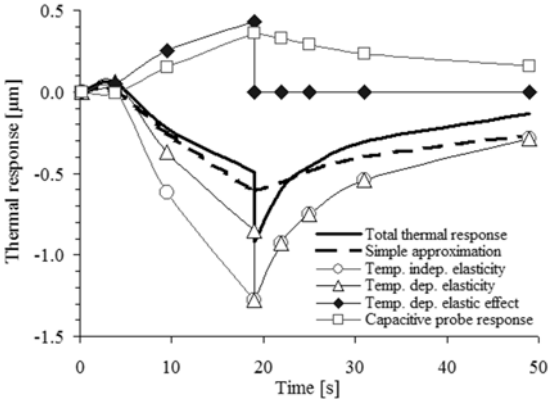

Fig. 12: The thermal response of sensor A – case 9

from the one actually experienced during extrusion, it may be useful in the study thermal effects. Note that a positive response is defined as one that would make it appear as if the distance between the sensor disc and probe is reduced and as if the pressure is too high. Note that if the elastic modulus is assumed temperature dependent, the total error of measurement may actually increase upon unloading. An increase of the load during extrusion would also cause the total thermal effect during extrusion to be less significant.

Heating of the capacitive probe alters the properties of the insulation materials and lowers the voltage output from the measurement system. The change is similar to the one caused by an increase of the die face pressure. As shown in Figs. 11 and 12, the effect contributes to a reduction of the total thermal transient response as long as it is small. It is difficult to produce accurate estimates. According to ref. [9], the thermal response is approx - 0.03 µm/ºC in the relevant temperature range. However, heating experiments indicate that every probe exhibits a unique characteristic, and one has found that the thermal response may in fact be several times larger than indicated above. Determination of repeatability of such small effects in a transient thermal environment is a relatively complex task.

Experimental results such as those presented in Fig. 10 imply that the calculations that have produced Figs. 11 and 12 are fairly correct with regard to the magnitude of the thermal effect. The sensor deflection due to temperature shocks appears to be almost twice as large for mounting solution B as for solution A. The effects on the pressure measurements are more similar as the total disc deflection also is larger for mounting solution B. In both cases the thermal effect causes deviations of less than 10 %.

Temperature compensation may be performed in various ways. Ideally, a method of automatic compensation could be implemented. Parallel measurement with two probes, one sensing only the thermal effect and the other sensing both the thermal effect and the mechanical load, would in principle be possible, but is difficult to perform given the size of the probes relative to the die. Other types of relative measurement, of which there are some examples in the literature, may also be assessed. However, since the size of the systematic error caused by the thermal effect is fairly small, quite simple remedies based on temperature measurements may be sufficient for most purposes. Both measures of temperature gradients close to the die and transient temperature changes should be assessed. In Figs. 11 and 12 results from a simplified compensation scheme have been displayed. The basic assumption is that the most influential thermal effect is the one related to differences in temperature and thermal expansion of the probe and the die. In fact, the probe is assumed not to be affected. Only the thermal expansion of the die over a distance from the bottom of the disc to the point where the probe is fixed is assessed. The characteristic temperature measurement is performed close to the edge which serves for fixing the sensor according to mounting solution A. Even though the model disregards a number of first order effects, it seems to produce acceptable results for most cases studied and for both fixing solutions. Of course, one must consider the uncertainties related to modelling of the thermal response.

Fig. 13 compares pressure estimates by ALMA for the cases 1 to 12 with corresponding measured values which have not been corrected for thermal effects. Data from all three pressure sensors have been added in order to give an indication of the accuracy of the measurement approach. By plotting results at various ram positions/billet lengths, it should be possible to spot systematic errors of transient nature. Fig. 13 seems to confirm that the thermal response causes an artificial reduction of the measured pressure.

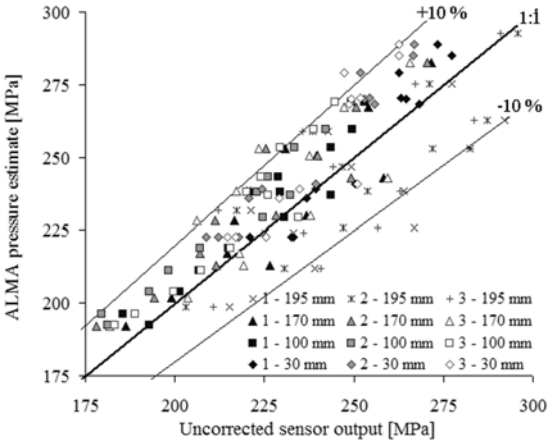

Fig. 13: Uncorrected pressure measurement and ALMA estimates

Note that systematic errors may be due to flow modelling inaccuracy, and that there is some scatter in the results.

In **Fig. 14** results from ALMA have been compared with measurement data that have been modified according to the simplified thermal compensation approach. Calibration factors of Table 4 have also been reduced by 1 % in order to compensate for the error introduced when calibration was performed at temperatures somewhat below the one recorded at the onset of extrusion. These measures bring results in better accordance with those predicted by the flow model. The mean value of the absolute deviation between measured and simulated data has been reduced by 30 to 50 %, depending on the ram position. Still, there is a certain degree of scatter in results. The standard deviation of the difference between the measured and the simulated response has been reduced by approx 20 %.

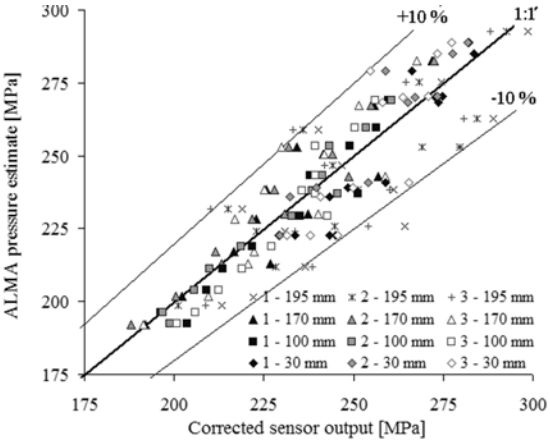

Fig. 14: Corrected pressure measurement and ALMA estimates

Conclusions

The capacitive principle of displacement measurement is one that may be successfully used to measure the pressure applied on the top face of extrusion dies. Sudden increases of the die temperature caused by heat dissipation during extrusion were found to affect the sensor output by less than 10 %. A simple temperature compensation technique based on the response of thermocouples placed in close vicinity to the sensor may be used to reduce errors.

Future work will focus on improving the accuracy of the calibration techniques, establishing methods of on-line temperature compensation and making sensors smaller and easier to use. The possibility of predicting variations in the section shape and thickness and instability of flow by using pressure measurements should also be assessed.

References

[1] M. Lefstad, Metallurgical Speed Limitations During the Extrusion of AlMgSi-Alloys, Trondheim, 1993 (PhD-thesis).

[2] P.T. Moe, H.I. Lange, A.W. Hansen, W. Wajda, S. Støren: Experiments with die deflection during hot extrusion of hollow profiles, Proc. 6th ESAFORM Conf. on Material Forming, ed., V. Brucato, Salerno, 2003, p. 119-122.

[3] P.T. Moe, W. Wajda, F. Couweleers , S. Støren, Visions of a system for shape control during thin-strip aluminium extrusion, Proc. 12th Int. Conf. on Experimental Mechanics, Sept. 2004, Bari, In press.

[4] P.T. Moe, M. Lefstad, R. Flatval, S. Støren, Intern. J. of Forming Processes Vol. 6 (2003) No. 3, p. 241-270.

[5] T. Yoneyama, J. Mat. Proc. Techn. 95 (1999), p. 71-77.

[6] T. Yoneyama, M. Kitigawa, Measurement of the contacting stress in extrusion, Proc. 4th ICTP, May 1993, Bejing, Vol II p. 553-558.

[7] T. Mori, N. Takatsuji, K. Matsuki, T. Aida, K. Murotani, K. Uetoko, J. Mater. Process. Technol. 130-131 (2002), p. 421-425.

[8] Capacitec Inc. (www.capacitec.com), Non-contact displacement standard products catalogue (1997), Ayer (Mass.).

[9] R. L. Foster, Linear Capacitive Reactance Sensors for Industrial Applications, Proc. 40th Annual Earthmoving Industry Conference, 1989, Peoria (Ill.).

[10] P.T. Moe, W. Wajda, D. Szeliga, L. Madej, S. Støren, M. Pietrzyk, An approach for evaluating constitutive models for hot aluminium extrusion – Rod extrusion of AA6060 as a case study, Proc. Metal Forming 2004, Sept. 2004, Kraków, (in press).

[11] www.ansys.com

[12] utab.uddeholm.com – orvar_supreme-english_020602.pdf

Moe P.T., Wajid W., Couleers F., Strøen S.

Visions of a System for Shape Control during Thin-Strip Aluminium Extrusion

Paper in Proceedings

12th International Conference on Experimental Mechanics
September 20, Bari, pp 57-71
and on the ICEM12 CD

ICEM12- 12th International Conference on Experimental Mechanics
29 August - 2 September, 2004 Politecnico di Bari, Italy

VISIONS OF A SYSTEM FOR SHAPE CONTROL DURING THIN-STRIP ALUMINUM EXTRUSION

P.T. Moe[a], W. Wajda[a], F. Couweleers[b], S. Støren[a]

[a] *Department of Engineering Design and Materials, Norwegian University of Science and Technology, Richard Birkelandsvei 2B, 7491 Trondheim, NORWAY, Per.T.Moe@ntnu.no*
[b] *SINTEF ICT, OS Bragstads plass 2A, 7465 Trondheim, NORWAY*

ABSTRACT
Hot aluminium extrusion is a process of large commercial significance, but still also one that is relatively poorly understood and controlled. This is mainly due to the complexity of the material flow and to the process' coupled nature. Mechanical loads and heat shocks cause the entire tool stack to deform considerably and the die outlets to distort during extrusion. Profile shape deviations may often exceed several tenths of a millimetre. When thin-walled and wide profiles are extruded, poor shape control may also relate to flow instabilities such as thinning, thickening, wryness, buckling and in the most extreme cases even full plugging of the outlet. The article presents die face pressure and profile shape measurement techniques that have been successfully applied in a laboratory environment, and discusses how they may be used in industrial test tools to analyze and more accurately control material flow and, thus, to reduce shape variability. A new pressure sensor design with capacitive probes is also presented. Emphasis is placed on minimising plastic sensor deformation and the transient thermal response.

1. INTRODUCTION
Properties such as a relatively high strength-to-weight ratio, excellent heat conductivity and an appealing surface texture make aluminium a preferred material for a number of designs and applications. It is a unique material since it may be extruded into sections of the most complex open or hollow shape. In the case of direct extrusion a ram pushes the aluminium billet, which is otherwise confined by the container walls, through a die opening of a specified shape. The billet is of a finite length and pre-heated to facilitate visco-plastic deformation. The extrusion ratio, i.e. the ratio between the billet cross sectional area and the outlet area (ER), may exceed a hundred. As plastic flow is incompressible, the considerable elongation of the work piece is given by ER. The microstructure is then completely transformed. Grains are elongated in the extrusion direction and sheared along tool surfaces. Particles break up. Re-crystallisation may or may not occur, depending on the deformation history and the billet preparation. Thus, modelling of flow is a complex task requiring effects on a multitude of scales to be taken into account. It is also a task of some significance, for it allows both the mechanical properties and the shape of the extrudate to be determined. It is widely acknowledged that the variability in shape has to be reduced and the process' accuracy increased if extruded aluminium sections are to come into widespread use in complex designs produced in large volumes. Since the flow may seem very restricted by the tools, the sources of profile shape variability may not directly be evident. However, as will be discussed, the forces acting on the interfaces between the tools and the work piece are of significant magnitude. As tool stacks deform, die openings distort. Outlets may then either open or close. At the same time friction conditions close to the outlet may also change. The most common method for controlling the flow, the residual stress

distribution and the profile shape is by carefully rendering the geometry of a slightly choked so-called bearing channel at the die outlet. Bearing friction surfaces may be of variable length and inclination along the circumference of the profile to compensate for flow speed variations. In the case of thick-walled profiles, the outlet velocity will be uniform even when bearings surfaces are not used since the faster moving parts of the profile tend to drag the slower ones and since the profile is stiff enough to counter buckling. Yet, when profiles are made thinner, bearing lengths and choke angles must be properly tuned to prevent flow instabilities. While a slight or latent instability may only manifest itself as a local thinning or thickening or a mild waviness, extruded profiles may in the extreme cases buckle and bend (Fig. 2). As dies deform and outlets distort, instable flow may either be provoked or suppressed. Thermal dissipation due to deformation and friction as well as surface wear affect the pressure build-up, the flow behaviour and instability phenomena.

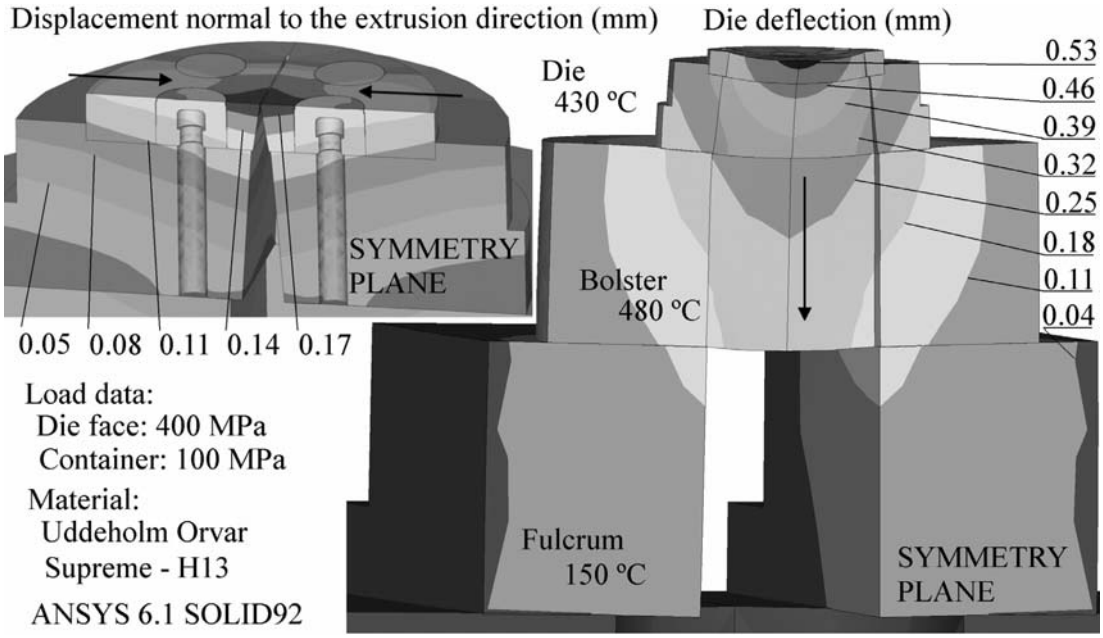

Fig.1. Deformation of the tool stack and outlet distortion

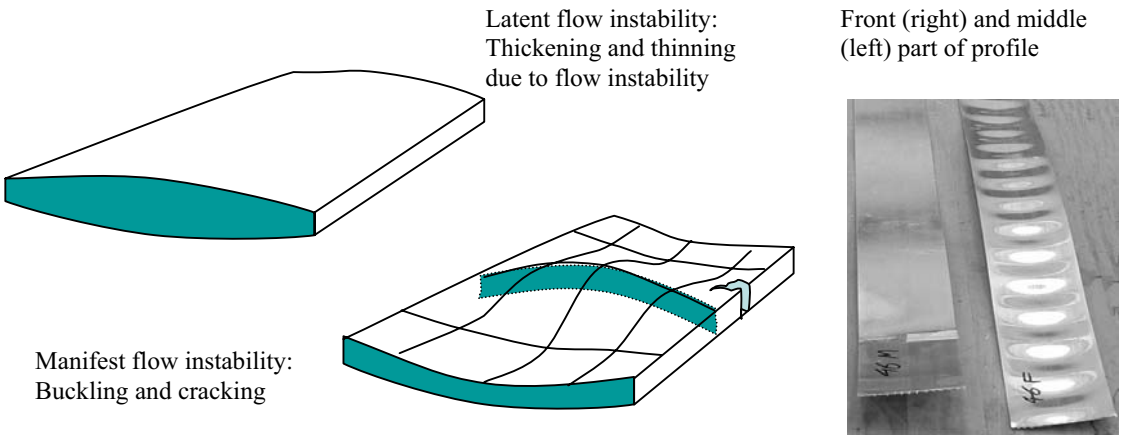

Fig. 2. Extruded buckled profile shape

Material flow control is still more of an art than a science. Modelling of flow instabilities is a difficult task both from a theoretical and practical point of view. A widely accepted modelling approach for the flow problem of extrusion is still lacking, and due to the large deformations occurring during extrusion calculations are time-consuming and potentially inaccurate. The problem is complicated by the fact that there is a significant difference between the flow behaviour of the material in the container and the thermoelasto-viscoplastic response of the profile as it leaves the die. Finally, the scarcity of accurate on-line measurements of essential process parameters makes verification difficult. The current work assesses the possibility of establishing intelligent dies that incorporate equipment for on-line measurement of shape and local values of die face pressure. Examples of practical sensors are also presented.

2. PROCESS CONTROL

The objective of implementing systems for controlling the extrusion process is to reduce the variability in profile microstructure, properties and shape. Causes of variability are intimately linked to the nature of the process itself. Continuous extrusion techniques are not common, so extrusion of aluminium may be regarded as essentially a transient process. The temperature of the billet and the die may increase significantly due to plastic dissipation and friction during extrusion. As a result the material softens and flows more easily. In the early phase of the extrusion run the material structure also starts to orient and elongate in the extrusion direction. On the nano/micro-scale dislocation networks evolve. The intermediate phase of the run is often denoted quasi-steady because from a spatial or Eulerian perspective both the microstructure and temperature fields change less. However, there will be gradual changes to the flow field, as the stagnant or dead zone close to the die face gradually shrinks. In the final phases both the pressure gradient and flow are generally in the radial direction, and material that has been cooled by the ram approaches the outlet. Thus, the temperature, microstructure and properties of the extruded section evolve through the run. Further, there may be changes to the velocity distribution close to the outlet the container friction force as the loads exerted on the dies and the outlet distortion change. To further complicate the situation, tools are frequently shifted in the extrusion plant. Since bearing surfaces are worn down and dies crack and creep, regular inspection is necessary. Besides, order sizes are often relatively small, even for large volume applications, for the extrusion industry adheres to a Just-In-Time philosophy. Tuning of process parameters for a given profile shape is therefore a most demanding task that must often be repeated. Control systems of any value must be easily implemented.

The simplest and most common method for reducing the variability in material properties and section shape is to cut and discard the front and back end of the profile. Point checks of shape are also performed downstream in the extrusion plant, and may bring about extensive pre-consumer scrapping. Further, in between the runs a sufficiently long butt end containing contaminated/impure material is sheared off the die and scrapped. To make the changes in the outlet temperature over the run smaller and, thus, to reduce the length of the front end discard, billets with tapered temperature distributions are often utilised. A related approach denoted isothermal extrusion, is to gradually reduce the ram speed during the run. Heat dissipation then decreases, and more heat conduction is allowed. Melting is avoided while the production rate is optimal. The temperature of the profile may be measured on-line by pyrometers or IR-cameras, but it is not always necessary to introduce a closed loop system to achieve acceptable results. Simple models that link velocity and outlet temperature for a particular cross-section may first be calibrated and used to set an optimal ram velocity.

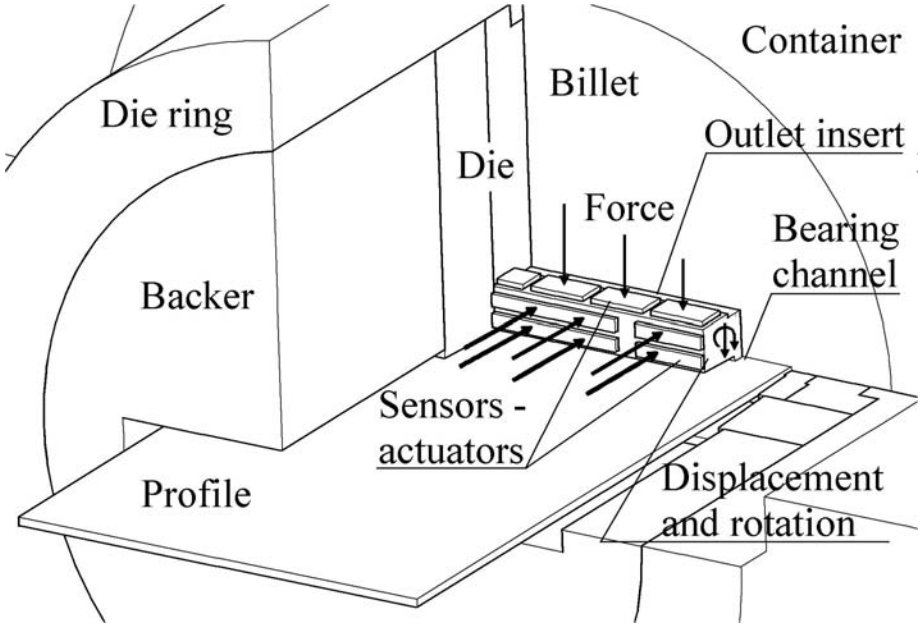

Fig. 3. Thin strip bearing channel actuator

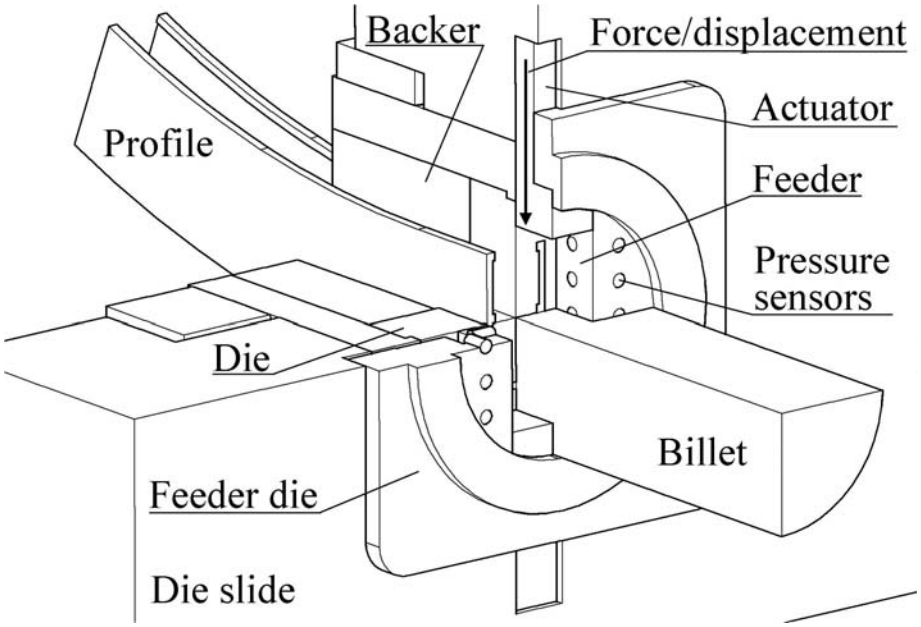

Fig. 4. U-profile feeder geometry actuator

It is significantly harder to control the shape of the profile than the temperature. First, on-line thickness measurement is complicated by a high extrusion speed and a complex profile shape. Second, few have performed extensive and reliable studies of flow stability and the causes of thickness variations. Third, it is not at all trivial to compensate for geometrical variability. The most commonly used instruments for flow/dimension control are the bearing surfaces (Fig. 3) and the pre-chamber/feeders (Fig. 4). Die outlet modification is a manual operation performed in between runs by a guild of skilled die correctors using their intuitive understanding of flow. It would be useful to automatically perform on-line corrections to the outlet geometry based on exact data on flow behaviour, just as is done for the rolling process. However, actuator design for the extrusion environment is a demanding task especially if the objective is to

control the minute details of the bearing channel geometry. When the bearing surfaces are close to parallel, as usually is the case, friction forces and surface properties of the profile may change considerably even for the smallest distortion of the outlets. In such a case, poor control may introduce rather than suppress instability. Besides, for most profiles it may be impractical to change the geometry of the bearing channel. A more feasible solution may be to alter the general flow field by closing some parts of a feeder and opening up others. Both for good and for bad the material flow is much less sensitive to changes in the geometry of the feeder than the bearings. Future studies of flow and actuator design may reveal if flow control by on-line modification of feeder shape is practical. There is of course also the question if it is necessary to introduce a closed-loop control system at all. Merely a system for on-line measurement of the profile shape and pressure would be of great value since it would aid the technical staff in determining the causes of instability and variability. Most instability problems may probably be solved without an analysis system, but it is not evident that optimal solutions may be easily spotted. An analysis tool may be used before production starts to speed up the iterative tuning approach, and it may be used continuously during extrusion to detect flow behaviour changes. Die bearing wear and creep may permanently alter the geometry of the die, and there are both systematic and random errors linked to the input variables of the extrusion process. Instability phenomena are sensitive to changes in process parameters such as billet temperature and ram velocity [1]. When the process drifts out of control, dimensional variability and the state of residual stress in the profiles are affected. It is important then that deviations are detected and corrective action taken as soon as possible.

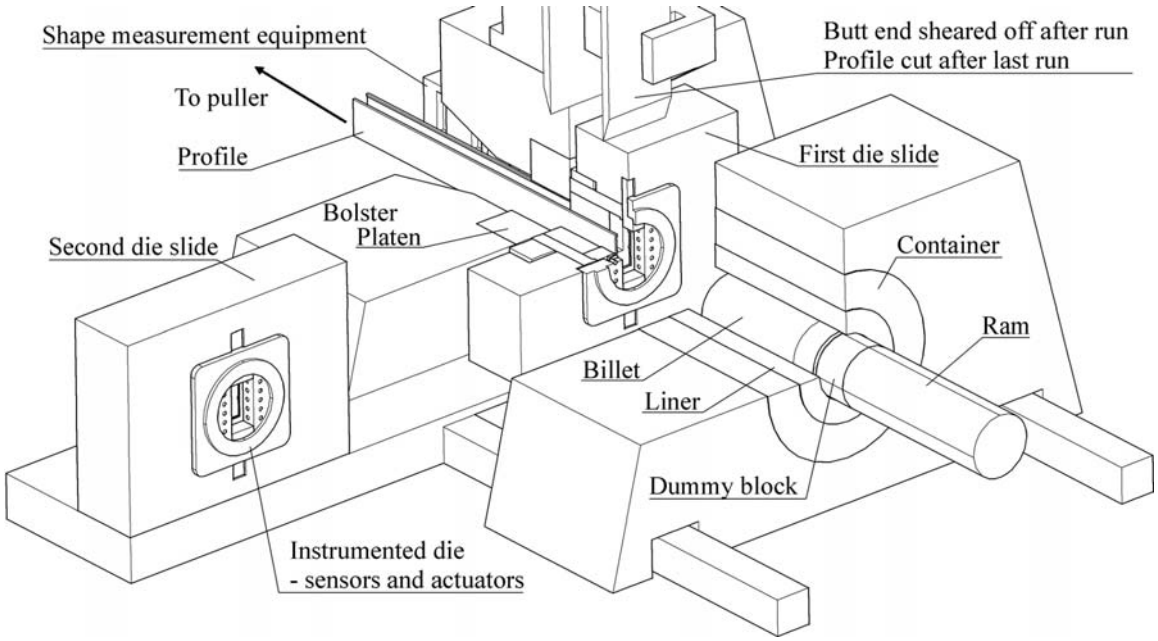

Fig.5. Conventional extrusion press with die integrating pressure and temperature sensors

Figs. 4 and 5 present a possible test and surveillance die concept for large series production of similar profiles, typically for the automotive industry. Extrusion dies for open sections are often of a composite design consisting of a die, backer and feeder plate in addition to a die ring that keeps the parts together. Since bearing surfaces are worn out after some hundred runs in the most severe cases, it is not practical to place sensors in the die plates. Further, frequent tool shifts make die sensors complex to handle. Instead, sensors should be fitted into special feeder plates to be used with different dies and not so frequently replaced. The sensors give an indication of the pressure and temperature distributions in and around the feeder, and it should

from these data be possible to draw conclusions about the flow field and the residual stresses of the profile. A better understanding of the system may be obtained if key dimensions of the profiles also are measured on-line or if at least an indication of flow instabilities is given.

3. PROFILE SHAPE MEASUREMENT AND FLOW INSTABILITY INDICATION

Knowledge about acoustic, electric, magnetic and optical phenomena may be used in the study of profile shape and thickness variations during extrusion. Satisfactory techniques should be able to distinguish thickness changes of approx 10 μm from profile movement of approx 10 mm in all directions due to vibration, twisting and buckling. It would be highly desirable to map the entire shape of the section, but it may prove difficult for complex profiles. Especially when either buckling or thinning/thickening at the onset of flow instability is to be quantified, relatively high sampling rates are required (1000 per second or more). The profile velocity may exceed 1.5 m/s while the buckling wavelength is typically approximately 100 mm.

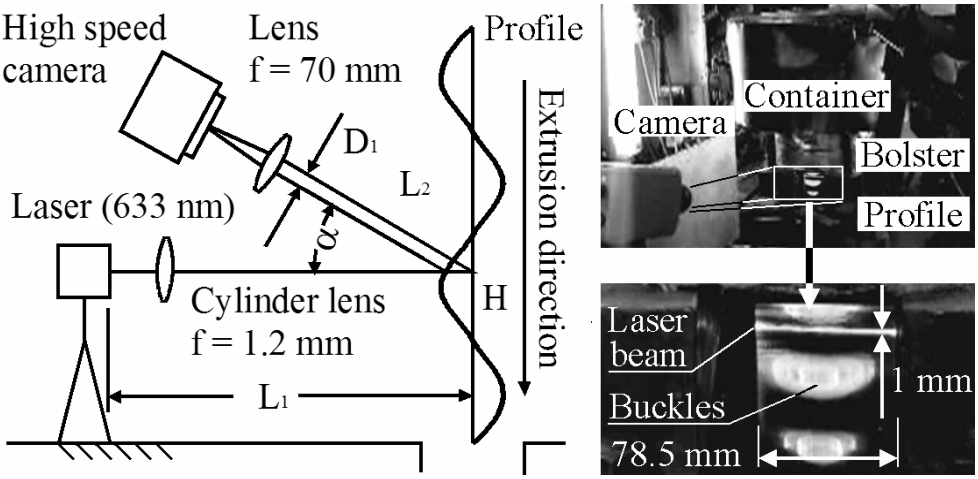

Fig.6. Profile shape principle and measurement set-up (a laser triangulation technique)

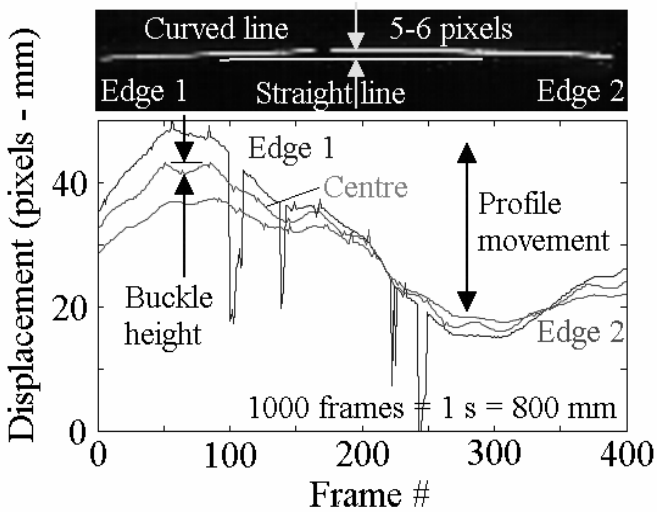

Fig. 7. Measured shape distortion. Measurements have been performed close to the profile edges and centre

A laser triangulation method was used in a first study of the limits of flow stability for thin strips (78.5x1.1 mm^2). The general principle of triangulation is shown in Fig. 6. A laser beam is focused on the surface of the profile and the spot is imaged onto either a CCD chip or a

position sensitive device (PSD), i.e. a lateral photo effect detector. A change in the profile height leads to a displacement of the image on the detector. If sensors are placed on both sides of the profile it is in principle possible to measure variations in the strip thickness down to micrometer accuracy for a full range of 20 mm. The objective of the current study, however, was rather to measure the shape of the surface of a thin strip after the onset of buckling. For this reason the full width of the profile was illuminated by a laser beam (Fig. 6). A high speed image converter camera, Ultranac FS501 [2], was positioned at a distance L_2 = 1150 mm and, due to space limitations, at an angle α of only 17 º. In the present study, the camera filmed an area measuring 130 x 130 mm^2 with a pixel size of ca 16 µm and through a lens (f = 70 mm). Hence, a buckle height, H, of 1 mm appears in the camera as a movement of 1 pixel or 18 µm (= 1 mm · sin(17) · 70/1150). It is possible to distinguish displacements down to 0.2 pixels (≈ 0.2 mm) by interpolation techniques. The camera sampling speed was 1000 frames/second. Due to storage limitations only 4 s sequences could be shot. Fig. 7 shows an image of a buckle detected by the camera as well as 0.4 s of continuous height measurements taken in the centre of the profile and at the edges. The largest oscillations are due to lateral translation (70 mm) and rotation of the strip. As long as the side edges of the profile are straight (Fig. 2), buckles appear only in the central part (Fig. 7). This must be regarded as a prerequisite for accurate measurement of the buckle height. A value of 5 mm (5 pixels) seems to correspond well with measurements performed off-line [1]. While the wavelength was approx 100 mm for all levels of ram speed in the limited set of experiments, the buckle height seems to depend both on the billet temperature and the ram speed. Further, buckling usually started approx 1 m from the front end and ended gradually after some further 3-4 meters. At the same time, the buckle height changed continuously [1]. A further development of the technique and an assessment of alternative methods are future tasks. It is in principle possible to improve the accuracy of the optical measurements, but the main difficulties are space limitations and turbulence of hot air.

4. DIE FACE PRESSURE MEASUREMENT

Pressure is a measure of the average force over an area of infinitesimal extension. However, most pressure sensors assess force distributions over a small but finite extension. Further, due to a significant interface friction in metal forming, one should make a distinction between the isotropic pressure, which is a variable in many flow codes, and the tractions normal to the die interface. Still, the principles of measurement are common to most fields of research. While piezoelectric sensors are commonly used in low temperature applications, high temperature types have only fairly recently been developed and used in relation to metal forming [3]. Conventional strain gauges are popular, and high temperature gauges have been to measure the straining of extrusion dies [4] and pressure [5]. Fibre optic sensors based on the principles of Bragg and Fabry-Perot may also be used in strain gauges or to directly measure deflections of elastic constructions. The current article discusses how a capacitive sensor system may be used to measure the displacements of a steel disc in contact with the aluminium billet and, thus, the pressure on the billet-die interface. Capacitive probes of the type Capacitec® HPC-75A-V-N3 have been used extensively in earlier experiments [6][7]. The deflecting disc of the sensor has so far been an integral part of the die (Fig. 8). When the disc is loaded, deforms by bending and approaches the top face of the probe, the capacitance of the system increases (Fig 9). The response may deviate from that of the case of pure translation of two plates, but for a 50 µm displacement the inverse of the capacitance is still a linear curve. An electric signal oscillating at 15.625 kHz is applied in a circuit consisting of a coax cable, the probe, the gap, the die and a return cable to the amplifier. A DC voltage signal proportional to the distance

between the probe and disc is found by demodulation. Calibration was performed so that a full scale of 10 V is equal to a displacement of 500 μm. The linearity is approx 0.2 % of full scale.

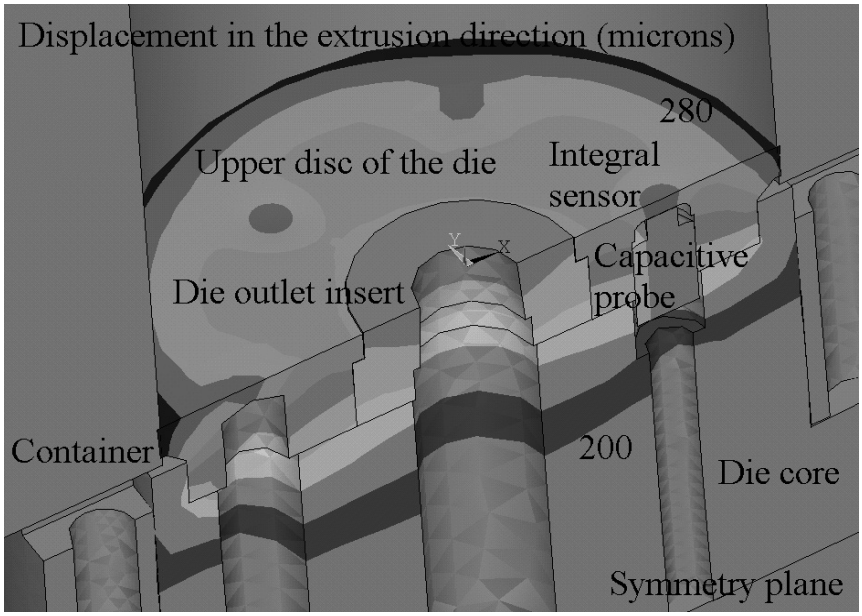

Fig.8. A pressure sensor integrated in the die design (displacements in the extrusion direction [μm])

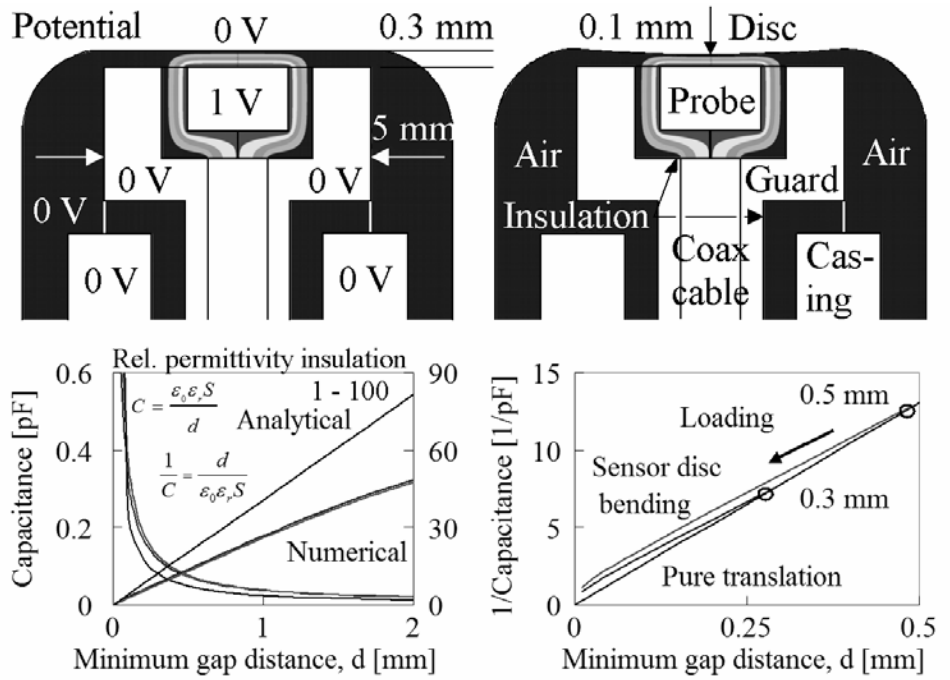

Fig. 9. Electric field and capacitive probe (the effect of translation and bending of the sensor disc)

The feasibility of measuring extrusion die face tractions has been demonstrated through the use of sensors that were integral parts of dies [4]. A further improvement of sensor design and its usefulness, especially in relation to thin-strip extrusion, is sought. Insert type sensors (Fig. 10) are potentially more accurate since the connection between the capacitive probe and the housing may be of a more permanent kind and the distinction between the pressure sensor and the die itself is clearer. Furthermore, calibration is a simpler task since it need not necessarily be done in-situ, but rather in a similar but more easily controllable environment. According to

ANSYS calculations [8] the response of the sensor design of Fig. 10 increases only by 1-2 % if the state of contact between sensor and die changes from intimate to none. The difference in disc deflection for sensors tightly fit into the actual extrusion die and into an axi-symmetric test die is also only 1 %. The main difference between Figs. 10 and 11 is the rotation of the sensor due to die deflection. Skew disc deflection caused either by a skew load, shear friction or general die deflection is small for all relevant cases of loading for the current sensor design, i.e. less than a micron. Penetration of aluminium into the crevice between the die and the sensor will occur and affects the output by approx 2 % for the shown solution. It is in principle possible to eliminate the effect by tuning the height, EDHT, of the sensor part with a reduced diameter. EDHT should then be slightly larger than the disc thickness, DITH (Fig. 10).

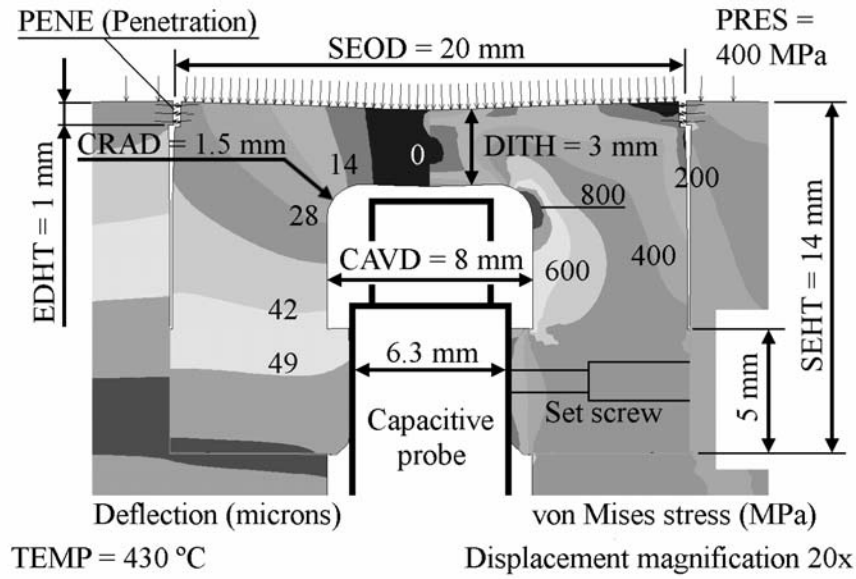

Fig.10. Insert sensor design (2-D axisymmetric ANSYS® model with uniform load of 400 MPa)

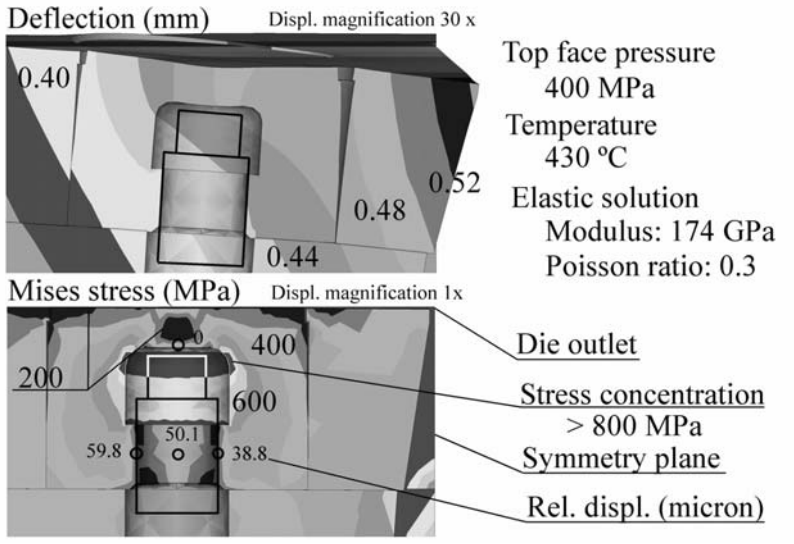

Fig. 11. Sensors placed in a thin-strip extrusion die (3-D axisymmetric ANSYS® model with uniform load of 400 MPa)

A possible disadvantage of the insert compared to an integral sensor is that it is more critically stressed for all types and levels of load (Fig. 12). The larger the diameter of the sensor, the larger is also the design space, defined by the thickness of the disc, DITH, and the radius of

the corner close to the outer edge of the disc, CRAD (Fig. 13). During thin strip extrusion die face tractions may reach 400 MPa. At 500 ºC few materials have an elastic range extending higher than 800 MPa (Fig. 14). Thus, for all relevant sensor designs some plastic deformation must be expected close to the edges of the sensor disc or, if the disc is thin, in its centre. In the latter case there is a risk of cyclic plastic deformation and complete sensor failure. Limited plastic deformation close to the disc edges, however, need not be entirely detrimental. After the first loading cycle one may observe permanent deformation of as much as half a micron, but since there are residual stresses, the elastic range is also extended. The kinematic model for hardening of Fig. 14 is of a simple kind and only serves to explain a phenomenon that has been observed during experiments [7]. The somewhat unlikely situation of plastic deformation during unloading should be avoided, since it causes a hysteresis. Pressure sensors may and should tolerate significantly higher pressures than those needed to initiate local plasticity. However, creep and fatigue must be considered in relation to cyclic loading, and one should remember that there may be a relaxation of residual stresses at higher temperatures. In addition, temperature increases during extrusion causes the yield stress to decrease (Fig. 13).

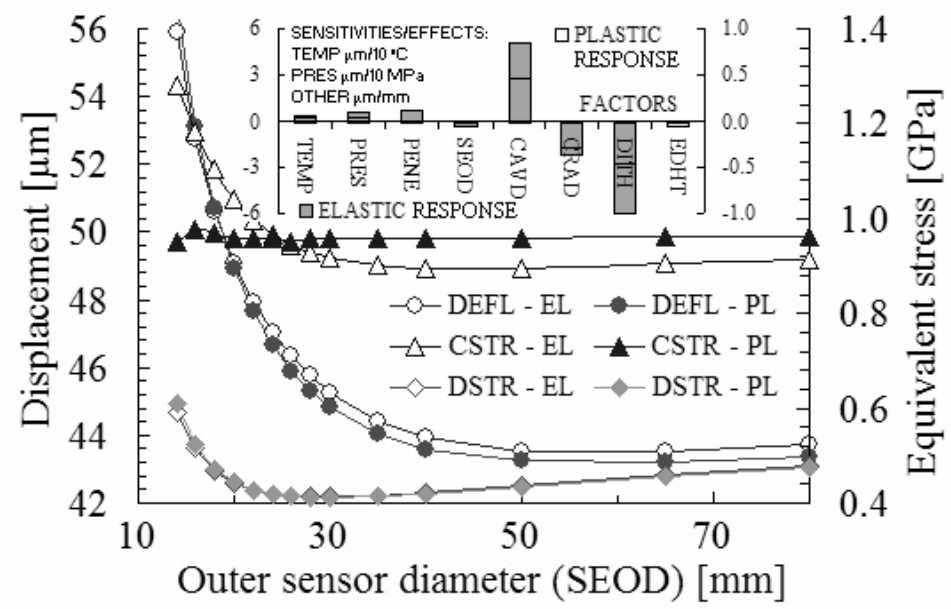

Fig.12. Stresses and deflection versus sensor diameter and the effects on response of changes in load and geometry (Fig.10)
DEFL – Deflection, CSTR / DSTR – Corner / disc stress

Furthermore, the temperature increases due to heat dissipation during extrusion do not only affect the yield stress of the material, but also the actual response of the sensor in the linear range. One effect is related to the thermal expansion of the material which also causes a slight upwards bulging of the sensor disc. An opposite effect is caused by the lowering of the elastic modulus of the material. According to Fig. 15 the thermo-elastic response is a transient one and usually makes it appear as if the load is lower than it actually is. Displacements caused by temperature shocks amounts to approx 10 % of the total sensor response, for at some distance from the die outlet temperature changes are moderate. Fig. 15 is based on a 2D axi-symmetric model which also indicates that there is an almost linear relationship between the thermo-mechanical response and the magnitude of the temperature increase. The described response is countered by a decrease in the voltage reading from the capacitive system due to heating of the probe. The effect corresponds to closing of the capacitor gap of ca 0.03 µm/ºC. It is

possible to somewhat modify the thermo-mechanical response by changing sensor design. In this relation one has found that the choice of sensor OD is less important (<1 μm).

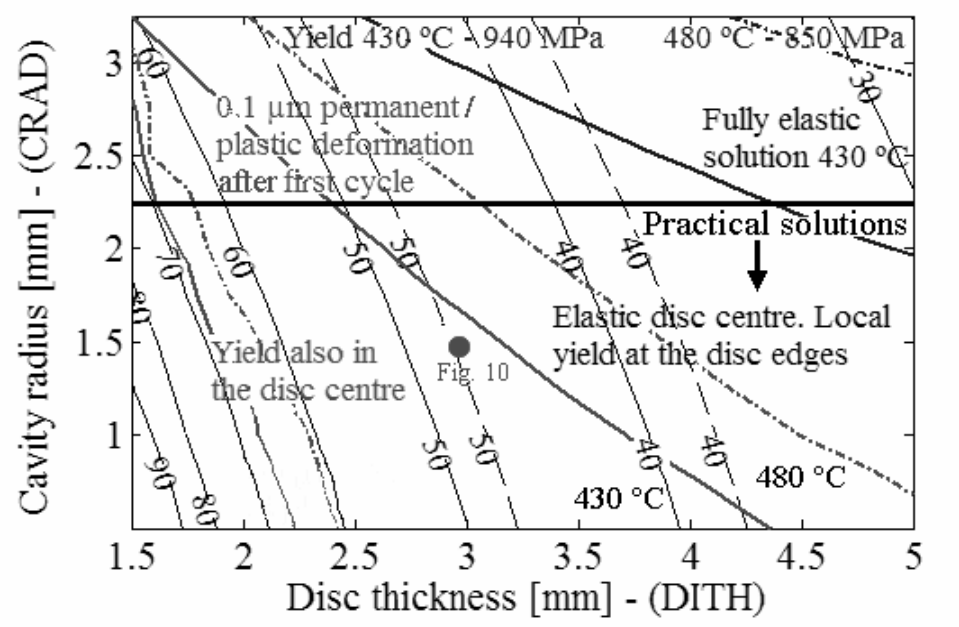

Fig. 13. Design optimisation for sensor of Fig. 10.
Thin lines – sensor deflection, thick lines – plastic limits. Full lines – at 430 ºC, dash lines – at 480 ºC

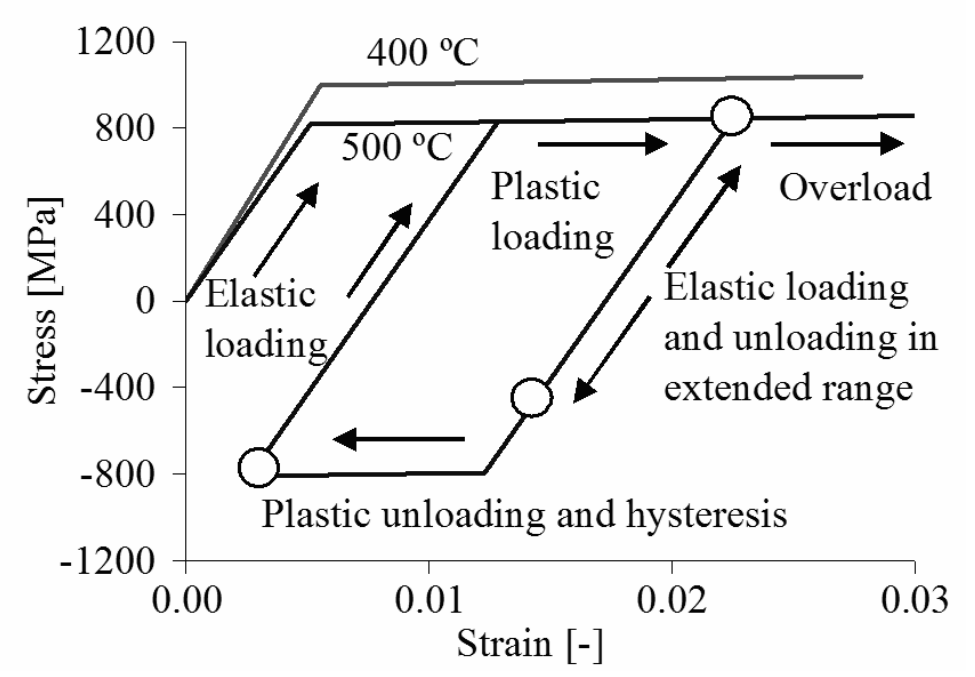

Fig.14. Possible modes of elasto-plastic sensor loading. Data are only approximate for Orvar Supreme H13 tool steel [9]

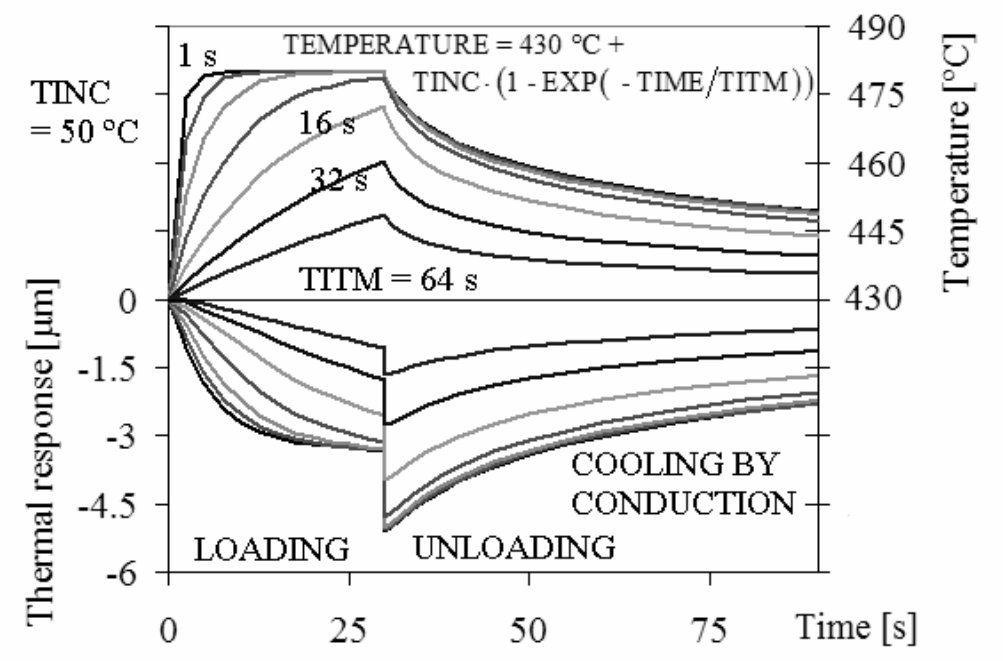

Fig. 15. Typical thermo-elastic response of insert sensor. The applied die face temperature is given in the upper part.

5. CONCLUSIONS AND FURTHER WORK

High speed on-line measurement of profile shape and die face pressure during extrusion is feasible. One may still question whether such techniques may be integrated in a fully-fledged control system for extrusion, but they may prove to be very useful tools for those studying the causes of flow instability and shape variability. Future work is to focus on improving sensor design and on increasing the understanding of material flow in extrusion.

BIBLIOGRAPHY

[1] W. Wajda et. al., "A study of the limits of self-stabilization during extrusion of thin-strips", Proc. 6th ESAFORM Conf. on Mat. Form., April 2003, Salerno, pp. 267-270.
[2] www.bygg.ntnu.no/ktek/simlab/simlab/resurser(index).htm
[3] J.R. Sebastian et al., "High Temperature Piezoelectric Sensor", US Patent Application US 2002/0043898, Apr. 18, 2002.
[4] P.T. Moe et al., "Experiments with die deflection during hot extrusion of hollow profiles", Proc. 6th ESAFORM Conf. on Mat. Form., April 2003, Salerno, pp. 119-122.
[5] T. Yoneyama et al., "Development of a die-sensor", JSME Int. J. 30, 1987, pp. 670-677.
[6] www.capacitec.com
[7] P.T. Moe et al., Intern. J. Form. Processes, Vol 6., 3, 2003, pp. 241-270.
[8] www.ansys.com
[9] utab.uddeholm.com – orvar_supreme-english_020602.pdf

Appendix K

Wajid W., Moe P.T., Strøen S., Lefstad M.,
Flatval R.

Measurement of Temperature and Pressure During Thin-Strip Extrusion

Paper in Proceedings

8th ESAFORM Conference on Material Forming
April 26-28, Cluj-Napoca

Measurement of Temperature and Pressure During Thin-Strip Extrusion

W. Wajda[1], P.T. Moe[1], S. Støren[1], M. Lefstad[2], R. Flatval[2]

[1]*Department of Engineering Design and Materials, Norwegian University of Science and Technology – Richard Birkelandsvei 2B, N-7491 Trondheim*
URL: www.ntnu.no *e-mail: Wojciech.Wajda@ntnu.no; Per.T.Moe@ntnu.no; Sigurd.Storen@ntnu.no*

[2]*SINTEF Materials and Chemistry – Richard Birkelandsvei 2B, N-7491 Trondheim*
URL: www.sintef.no *e-mail: Martin.Lefstad@sintef.no; Robert.Flatval@sintef.no*

ABSTRACT: The objective of the work has been to examine temperature and pressure changes on die face and in bearing channel during thin strip extrusion of AA6060 for stable and unstable material flow conditions. The obtained data are expected to provide information that may be useful for establishing thermo-mechanical models of material flow. Dies with slightly convexly shaped strip outlets of thickness 1.2 and 1.4 mm and width 78.5 mm were used. The billet diameter and initial length were 100 and 200 mm respectively. Sensors measured the die outlet temperature and the die face pressure. For initial billet temperatures in the range from 480 to 540 ºC and ram speeds from 5.8 to 12.9 mm/s the outlet temperature was in the range from 500 to 600 ºC. Die face pressures were in the range from 250 to 400 MPa. The repeatability and accuracy of pressure measurement were within approximately ± 10 %. Flow instability (buckling) was successfully provoked only during extrusion of the thinnest profiles for initial billet temperatures above 520 ºC. The shape and extension of the buckles changed continuously during a run and could differ significantly for the various runs. A very important goal was to assess reproducibility, and experiments were genuinely replicated. Results indicate that while the instable behaviour could be reproduced, the limits of stability and appearance of the strip could change. The mechanism appears to be sensitive to small changes in interface friction and thermal conditions.

Key words: aluminium extrusion, buckling, instability, pressure measurement

1 INTRODUCTION

Users of extruded aluminium profiles are demanding thinner and stronger profiles at lower prices. At the same time, dimensional variability must be reduced if extruded sections are to be economically used in complex high volume applications that require fully automated production and assembly. An important objective of the research on aluminium extrusion and downstream processes is to establish effective and reliable techniques and tools for process control. For example finite element modelling has long been regarded as a potentially useful aid. Even though important progress has been made with regard to the development of efficient codes, much work remains to be done. A most important step is the verification of codes by closely controlled experiments.
The objective of this study of aluminium extrusion has been to more closely investigate the limits of flow stability. There is necessarily a limit to how thin profiles that may be extruded. During extrusion material that flows along various paths are to different extents retarded. The bearing channels / die lands and feeders of extrusion dies are the main instruments for flow control. They may be designed and modified so that there will be a larger tendency of a uniform flow velocity. When flow control is imperfect, however, the material that moves faster pulls the slower. When the profiles are very thin or the material resistance is low, this self-stabilization mechanism is weak, and the extruded profile shape may be distorted. Waviness or buckles may appear. During industrial die design it is important that the limits of flow instability are known. Hence, many rounds of thin-strip extrusion have been run, and the conditions at the die face have been measured. All experiments have been carefully repeated. Properly calibrated pressure sensors [1,2,3,4] have for the first time been used during thin-strip extrusion.

2 EXPERIMENTAL SET-UP

Three rounds or days of extrusion experiments were run in the 8 MN vertical laboratory press of SINTEF Materials and Chemistry (Fig. 1). The container and die temperatures were approx 430 ºC while the bolster was externally heated to 480 ºC. The initial temperature of the ram tip was approx 130 ºC. The ram temperature was quite necessarily non-uniform, but careful control of temperature was performed before extrusion. In contrast to industrial practice no puller was used. Pullers cause tensile stressing of the profile and suppress instabilities. A future extension of the study should include also the use of pullers.

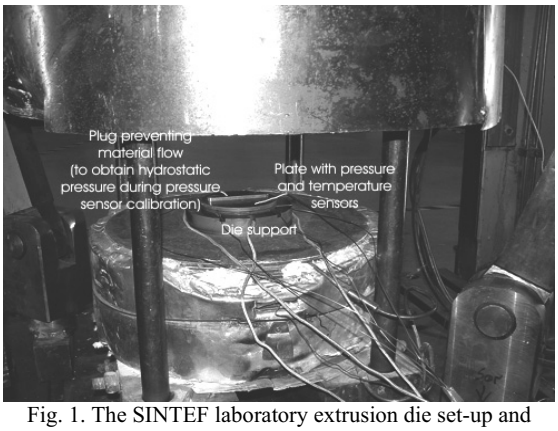

Fig. 1. The SINTEF laboratory extrusion die set-up and pressure sensor calibration technique

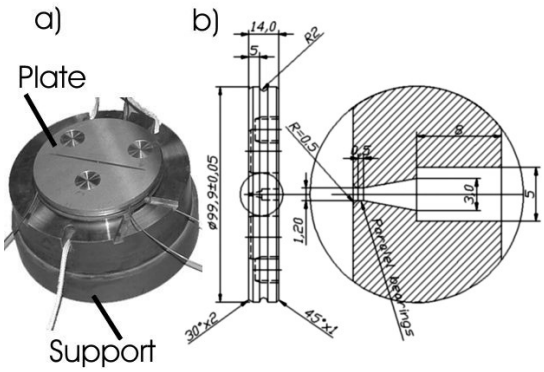

Fig. 2.a) Assembled die (plate and support), b) detailed drawing of the plate (top disc) and bearing channel

A composite extrusion die was used. It consisted of a top disc, a disc support and three capacitive die face pressure sensors (Fig. 2). Four thermocouples mounted in the top disc continuously measured the die outlet and die face/pressure sensor temperatures. The thermocouples in the outlet scratched the profile surface, and the groove depth was approximately 0.1 mm. Sensors have been carefully calibrated [4].

The die outlets were not perfectly rectangular, but rather convex (both with radiuses of 15.4 m). During extrusion the die deformed elastically and the die outlet shape was distorted. The thickness of the die outlet and profile became smaller in the centre than at the edges [1]. The top discs/plates were fastened with bolts and could be replaced. Two die outlets were used. The minimum die outlet thicknesses were nominally 1.4 and 1.2 mm. The width of the thin-strip was 78.5 mm.. The extrusion ratio is equivalent to the ratio between the billet and profile thicknesses in one of the symmetry planes. The bearing surfaces of the die outlets were of constant length around the whole circumference (0.5 mm) and the die bearings were designed to be parallel.

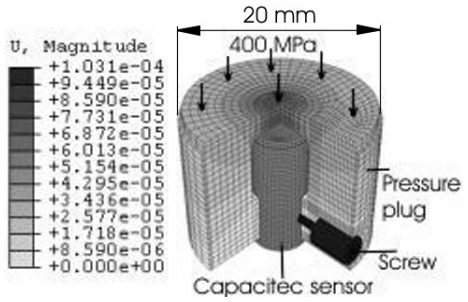

Fig. 3. The capacitive insert pressure sensor. Magnitude of displacement due to load (400 MPa) on top of plug (scale in [m]). An E-modulus of 180 GPa (at 430 ºC) has been used..

A new and improved capacitive pressure design was used in the study. In contrast to earlier designs used by the authors [1] the sensor was of a type that could be inserted into an appropriate hole in the top disc. It consisted of a capacitive probe and a sensor housing (Fig. 3). The capacitive displacement measurement system was purchased from Capacitec. A thorough description of the system has been given in [5]. The HPC75-type sensors measures displacements even at a temperature of 850 ºC. Accuracy, repeatability and linearity are all better than 0.5 µm. During extrusion the pressure sensor top disc deformed elastically in response to the immense load from the billet. The elastic sensor behaviour has been closely studied and optimised in [4]. A pressure of 400 MPa causes a maximum deflection of the sensor disc of approx 50 µm. In situ-calibration by careful experiments with hydrostatic compression (Fig.1) is needed to secure an acceptable measurement accuracy ($\pm 3\sigma \approx \pm$ 0.5 MPa/µm (10 %)). An improvement of the accuracy may probably be achieved by permanently fusing the capacitive probe to the sensor housing.

3 EXPERIMENTS AND RESULTS

The first experimental round was run with the die outlet of minimum thickness 1.4 mm. The thinner outlet was used during the second and third rounds. Two additional unsuccessful attempts with the thin outlet were made after the second round. Complete plugging of the outlet prevented experiments from being run. The flow was at the limit of stability, and lubrication (oil and copper) of the die face and die outlet appeared to be necessary in order to secure a safe start-up. The exact effect of lubrication is not known. It may affect the container flow, and it is known to prevent the profile from sticking to die support. However, it was not necessary to lubricate during the first round of experiments with new dies. The difficulties related to plugging made it natural to extrude billet-to-billet without cutting the butt end.

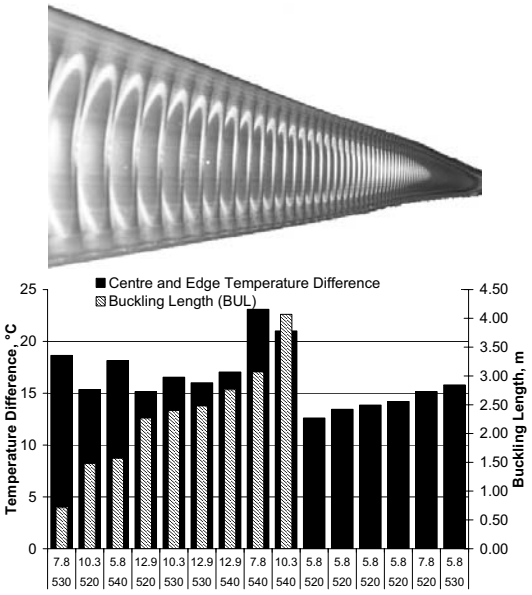

Fig. 4. A description of runs and results and a buckled profile. Edge and centre bearing channel temperature difference (black) and buckling length (hatched). The abscissa indicates the ram velocity (mm/s) and the initial billet temperature (°C).

The height of the remaining butt end was 20 mm. At the onset of the extrusion cycle (billet loading), the butt end temperature was probably similar to that of the surrounding container and die since runs were performed as much as 5 to 7 minutes apart. The total initial length of the fused billet was approx 202 mm after the initial burp phase. A round of experiments consisted of many extrusion runs. Two process input variables, the initial billet temperature and the ram velocity, were systematically changed during the experiment. There were five and four levels of the variables (480, 500, 520, 530, 540 ºC and 5.8, 7.8, 10.3, 12.9 mm/s). Figure 4 presents a profile with buckles. Buckling is here regarded as a distinct waviness of the profiles. It usually started after approx 1 meter of the profile had been extruded and lasted some meters (Fig.4). Thus, it was not a start-up effect, and it was related to temperature changes and the conditions of flow both in the container and the outlet. In figure 4 the length of the buckled part of the profile is compared with the difference between the centre and edge profile temperature during extrusion with the 1.2 mm thick die outlet. It seems that buckling is more likely to occur when the profile temperature is high and non-uniform. An uneven distribution of material properties may also contribute to the flow imbalance. Instabilities were observed even though profiles were extruded in a billet-to-billet manner. The amplitude and length of the buckles changed only gradually. In many cases, a slight waviness was observed. The flow instability was latent as opposed to manifest. The amplitude of the buckles changed continuously.

Table1. Results from experiments – Round 1

Case	BT	RV	FRC	OTC	OTE	PRC	PRE	BUL
8	480	10.3	3440	543	526	308	323	X
2	520	5.8	2887	542	524	259	270	X
3	520	10.3	3058	554	529	276	282	0.42
6	520	10.3	3079	555	528	272	287	X
7	520	12.9	3142	555	525	283	299	X
5	540	5.8	2763	555	527	240	256	X
4	540	10.3	2852	563	527	254	263	X

Table2. Results from experiments – Round 3

Case	BT	RV	FRC	OTC	OTE	PRE	BUL
21	520	5.8	3202	554	542	297	X
23	520	5.8	3246	560	547	302	X
25	520	5.8	3265	557	543	296	X
22	520	5.8	3209	560	545	298	X
26	520	7.8	3382	567	552	310	X
27	520	10.3	3367	575	559	321	1.48
28	520	12.9	3381	578	563	318	2.27
32	530	5.8	3116	564	549	290	X
33	530	7.8	3189	574	555	297	0.71
34	530	10.3	3239	577	561	305	2.4
35	530	12.9	3293	583	567	309	2.48
29	540	5.8	3064	567	548	282	1.57
30	540	7.8	3131	578	555	292	3.07
24	540	10.3	3148	578	557	288	4.07
31	540	12.9	3219	581	564	301	2.76

Table 1 and 2 provide data on the values of the main input variables and responses of all cases of the experiment. BT is the billet temperature (°C), and RV is the ram speed (mm/s). FRC is the ram force

(kN). OTC and OTE are the centre and edge outlet temperatures (^{o}C). PRC and PRE are corresponding die face pressures (MPa). BUL is the total buckling length (m). In Table 2 the PRC column was omitted due to centre sensor failure. The output data have been shown for a remaining billet length of 180 mm. Figures 5 and 6 present temperature and pressure curves for cases 24 (buckling) and 25 (no buckling). Changes in temperature caused pressure signals to be at most 10 % in error. Temperature compensation based on simulation and temperature measurement data is possible [3]. However, when extrusion is performed relatively slowly, as in the present case, the temperature effect is usually small (< 5%).

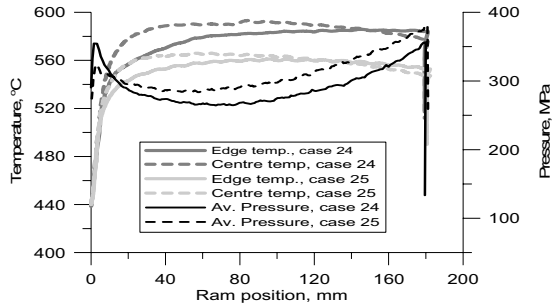

Fig. 5. The centre/edge outlet temperatures and die pressure – cases 24 and 25

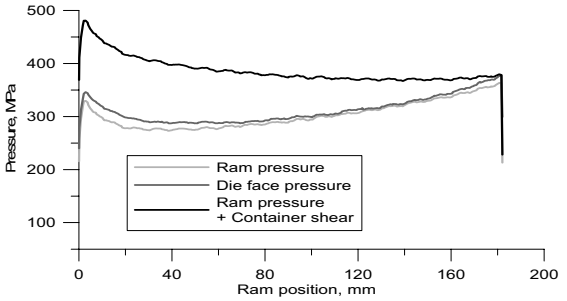

Fig. 6. A comparison of the ram pressure, die face pressure and total ram pressure and container shear (experiment no. 22).

The pressure sensors are most useful for the general evaluation of flow and friction during extrusion. An important question, however, relates to whether the sensors may be used to more or less directly indicate the imminence or occurrence of manifest instability. A large pressure and temperature gradient across the width of the outlet combined with high temperature could be an indication. Relatively small oscillations in the pressure could signal instabilities. When there is a latent instability, there must be compressive and tensile stresses in the profile. One envisions that they are partially released at the onset of buckling, which may potentially lead to pressure oscillations in the container. The results do not directly reveal such a phenomenon. It may be that the effects are too small or that the sensors due to their relatively large size (OD = 20 mm) were placed too far from the outlet. Small pressure differences may easily be completely smoothed out. Earlier experiments have shown that the pressure measurement resolution may be better than 5 MPa when transient effects are evaluated [5]. Further numerical modelling and experiments are needed to establish proper instability criteria. Still, the present set of thin-strip experiments has clearly demonstrated that the task is complex. The influence of environmental conditions (thermal, lubrication) is very hard to quantify, but must quite necessarily be included in a model of flow.

4 CONCLUSIONS

Extrusion of thin strip profiles through short bearing channels has proven to be a most useful and suitable case for the investigation of the flow instability. Instabilities may easily be provoked in a systematic manner. Further work on modelling and experiments are needed to establish useful criteria for instability based on on-line measurement of both temperature and pressure. Smaller and more accurate capacitive pressure sensors are needed.

ACKNOWLEDGEMENTS

The authors gratefully acknowledge and thank the Research Council of Norway and Hydro Aluminium for financial support and their permission to publish this work.

REFERENCES

1. P.T. Moe, M. Lefstad, R. Flatval, S. Støren, Measurement of temperature and die face pressure during hot extrusion of aluminium, Intern. J. Forming Processes Vol. 6 (2003), No. 3, pp. 241-270.
2. P.T. Moe, W. Wajda, S. Støren, A study of the thermo-mechanical response of a die face pressure sensor for hot aluminium extrusion, Proc. 10th Int. Conf. on Metal Forming, Sept. 2004, Kraków, pp. 627-634.
3. W. Wajda, P.T. Moe, M. Lefstad, S. Støren, A study of the limits of self-stabilization during extrusion of thin strips, Proc. 6th ESAFORM Conf. on Material Forming, April 2003, Salerno, pp, 267-270.
4. P.T. Moe, W. Wajda, F. Couweleers, S. Støren, Visions of a system for shape control during thin-strip extrusion, Proc. 12th Int. Conf. on Experimetal Mechanics, Sept. 2004, Bari, pp. 570-571 (abstract).
5. P.T. Moe, Pressure and Strain Measurement during Hot Extrusion of Aluminium, PhD thesis, Norwegian University of Science and Technology 2004.

Appendix L

Moe P.T., Wajda W., Støren S., Lefstad M., Flatval R.

An Experimental and Numerical Study of Induction Heating of Billets

Paper in Proceedings

8th ESAFORM Conference on Material Forming
April 2005, Cluj-Napoca

An Experimental and Numerical Study of Induction Heating

P.T. Moe[1], W. Wajda[1], S. Støren[1], M. Lefstad[2], R. Flatval[2]

[1]*Department of Engineering Design and Materials, Norwegian University of Science and Technology – Richard Birkelandsvei 2B, N-7491 Trondheim*
URL: www.ntnu.no *e-mail: Per.T.Moe@ntnu.no; Wojciech.Wajda@ntnu.no; Sigurd.Storen@ntnu.no*

[2]*SINTEF Materials and Chemistry – Richard Birkelandsvei 2B, N-7491 Trondheim*
URL: www.sintef.no *e-mail: Martin.Lefstad@sintef.no; Robert.Flatval@sintef.no*

ABSTRACT: The subject of this paper is electromagnetical induction heating of billets prior to hot extrusion of aluminium. The objective of the work has been to establish a numerical tool that may be used to evaluate the heating process and to assess the temperature distribution in the billet at the onset of extrusion. Proper temperature control is of large significance during commercial extrusion, and is particularly important in combined numerical and experimental studies of the extrusion process. AA6060 billets of height 300 mm and diameter 97 mm were used in experiments. The billets were heated by an induction coil connected to an EFD-Induction MINAC 50 transformer. The amplitude and frequency of the alternating current in the coil was approx 18.5 Hz and 700 A. Heating to 450 ºC lasted approx 6 min. Consistent results were obtained from a carefully tested coupled thermal-electromagnetical model established in ANSYS. At the end of the heating process there were temperature differences in the billet of approx 10 ºC. During the period of billet loading, which lasted approx 30 s, the temperature of the billet decreased approx 5 ºC, while temperature gradients were significantly reduced. Due to radiation and convection the billet centre is hottest at the start of extrusion.

Key words: aluminium extrusion, induction heating

1 INTRODUCTION

The great progress of numerical modelling over the last three to four decades has made possible detailed studies of the aluminium extrusion process. Hence, numerical simulation may be used directly for die design and for the implementation of better process control. There are difficulties, however. Extrusion is a strongly coupled process, both mathematically and physically. Tool deformations affect flow and profile shape and vice versa. Furthermore, the solution of the thermal and mechanical (flow) problems must be performed in parallel. Aluminium flow resistance is determined by the temperature, and heat dissipation is controlled by the viscoplastic deformation. Proper temperature control is essential for the control of the final material microstructure, the material properties of the extruded product and the profile shape. High-strength thin-walled profiles are in great demand, but very tight temperature control may be required to secure stable flow and satisfactory quality of such products.

Constitutive modelling is an important element in finite element modelling of material behaviour. A critical evaluation of friction and bulk deformation formulations is needed as quantitative data are to be deduced about the process. The requirements to the data must be evaluated, and methods for obtaining data must be checked. A key question is whether the data obtained by conventional material testing may be used in the study of a high-rate of deformation processes such as extrusion. The answer may most likely be obtained by carefully designed, controlled and monitored laboratory extrusion experiments [1]. A key issue is once again temperature control, and a fundamental requirement is that the temperature distribution at the onset of extrusion be known. The objective of the work presented in this paper has been to establish and test a numerical tool for the evaluation of billet induction heating and to evaluate the temperature distribution at the onset of extrusion during a typical round of experiments [1].

2 EXPERIMENTS AND SET-UP

An important piece of auxiliary equipment for the 8 MN vertical laboratory press of SINTEF is the billet induction heater equipment displayed in Figures 1 and 2. It consists of a MINAC 50 transformer (2 x 9 turns) by EFD-Induction (formerly ELVA) [2] and a water-cooled secondary coil for heating with 16 turns. The secondary coil height is 200 mm and the inner and outer diameters are 102 and 118 mm respectively. The cross-section of each of the turns is of rectangular shape with height 12 mm and width 8 mm. The turns are separated from each other by a layer of insulation. There is no insulation, however, between the billet and the coil. The billets placed in the coil should be of diameter smaller than 100 mm and of height of approx 200 mm. Also shorter billets may be heated if placed at the top of an appropriate cylinder. The temperature of the billet is measured continuously by a thermocouple that is brought into contact with the coil at the onset of heating.

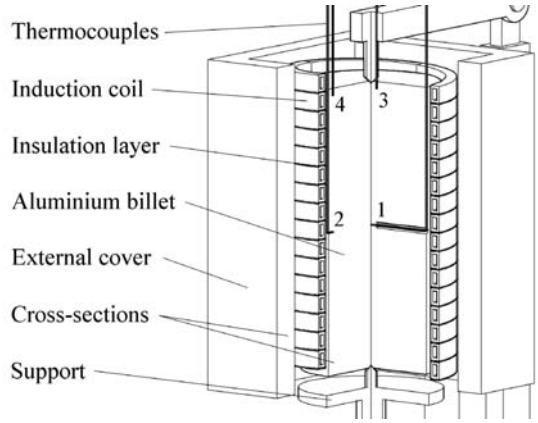

Fig. 1. The induction coil of SINTEF Materials and Chemistry

Fig. 2. EFD-Induction MINAC 50 transformer [2]

The MINAC 50 can provide a peak power of 80 kW, but during experiments the applied effect was below 20 kW. The magnitude of the current is determined by the impedance of the secondary coil and may in fact change during heating. As the billet temperature increases, electric resistivity increases. Electric and magnetic fields consequently penetrate deeper into the billet (Table 1). δ is the skin or penetration depth of the currents. The net effect of the property change is an increase of the total resistance. However, the heating rate need not increase since the magnitude of the applied current may decrease during heating. P_A of Table 1 is the applied surface flux equivalent to the heat generation in the billet. The assumption is that the current in the coil is constant an equivalent to 700 A. The frequency of the applied AC current is 18.5 kHz. A harmonic analysis to be described in the next section has been used to deduce results.

Table 1. Material data aluminium [3] (frequency 18.5 kHz)

Temperature ºC	K W/mK	$c\gamma$ J/m^3K	ρ $\mu\Omega m$	δ mm	P_A kW/m^2
20	211	2.52	0.027	0.61	69.6
100	219	2.59	0.036	0.71	80.8
200	224	2.65	0.048	0.81	92.6
300	223	2.71	0.060	0.91	103.7
400	216	2.78	0.073	1.00	114.5
500	209	2.84	0.087	1.09	125.0
600	200	2.89	0.104	1.19	136.7

Figure 3 presents results from a set of experiments that were performed with long billets and coils (300 mm). The temperature in the centre of the billets during heating was ca 10 ºC higher than at the edges, and differences were even smaller during the subsequent cooling phase. The billet temperature increase close to linearly with time. The moderate temperature increase at higher temperatures may be explained by a reduction of the current intensity, but also by the increasing effects of both natural heat convection and radiation. Simulated curves obtained from an ANSYS 7.1 model to be further described indicate the effects of radiation and convection.

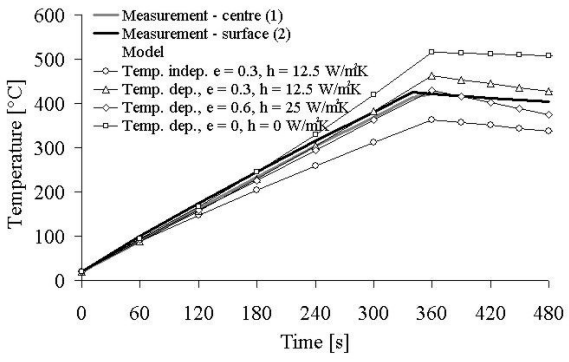

Fig. 3. Results from heating experiments [4] and simulation

3 MODELLING OF INDUCTION HEATING

The fundamental laws governing induction heating are Maxwell's equations and the conservation laws for energy and charge [3]. According to Ampere's law, the intensity of a magnetic field, **H**, surrounding a flow of charges, **I**, (for example in a coil) is:

$$\oint \mathbf{H} d\mathbf{s} = \mathbf{I} \tag{1}$$

Furthermore, according to Faraday's law the electric field, **E**, induced in a material is proportional to the time derivative of the magnetic flux, **Φ**:

$$\oint \mathbf{E} d\mathbf{s} = -\frac{\partial \mathbf{\Phi}}{\partial t} \text{ where } \mathbf{\Phi} = \int \mathbf{B} dA \tag{2}$$

B is the flux density vector and related to **H** by a constitutive relation. For the non-magnetic material aluminium one may simply assume that $\mathbf{B} = \mu_0 \mathbf{H}$. μ_0 is the permeability of vacuum, $4\pi \cdot 10^{-7}$ A/m.

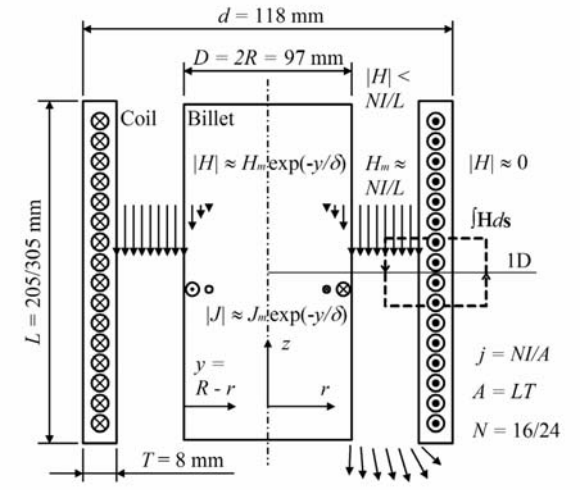

Fig. 5. The simplified induction heating model

A proper test case for numerical models may be obtained if it is assumed that an infinitely long and perfectly insulated cylindrical billet is heated by a surrounding coil with a current density of $j = NI/A$ where N is the total number of turns (Fig. 5). I is the amplitude of the alternating current whereas A is the total area of a cross-section of the coil. The length of the coil is L. The magnitude of the magnetic flux in the gap between the coil and the billet is according to [3] uniform and given by Ampere's law:

$$H_m = NI/L \tag{3}$$

The intensity of the magnetic field outside the coil is regarded as negligible. Assuming a sinusoidal time-varying applied current of frequency f one may calculate both the magnetic field $H_z(r,t)$ and the eddy current $J_\theta(r,t)$ in the billet from a diffusion equation directly deduced from Maxwell's equations:

$$\frac{d^2\mathbf{H}}{dr^2} + \frac{1}{r}\frac{d\mathbf{H}}{dr} - k^2\mathbf{H} = 0 \text{ where } k^2 = \frac{i\mu_0\omega}{\rho} = \frac{2i}{\delta^2} \tag{4}$$

ρ is the permeability and ω is the angular frequency ($2\pi f$). The skin depth, δ, is the essential parameter. The solution may be expressed in terms of Bessel's functions, but since the radius of the billet, R, is much larger than δ, one may actually look upon the problem as plane, in which case:

$$H_z(r,t) = H_m \exp(-y/\delta)\cos(\omega t - y/\delta) \tag{5}$$

$$J_\theta(r,t) = J_m \exp(-y/\delta)\cos(\omega t - y/\delta + \pi/4) \tag{6}$$

Here, $y = R\text{-}r$ and $J_m = \sqrt{2}\, H_m/\delta$. The expression for the total I^2R heat generation divided by the surface area of the billet is then simply:

$$P_A = J_m^2 \frac{\rho\delta}{4} = \frac{\rho H_m^2}{2\delta} = \frac{\rho}{2\delta}\left(\frac{NI}{L}\right)^2 \tag{7}$$

The temperature distribution may be calculated from the energy equation and Fourier's law. It may be assumed that all heat is generated at the surface, and that there are no losses to air. Due to the cylindrical symmetry of the billet, the solution is also one that includes Bessel's functions. However, heating takes place over a long time, and a parabolic temperature distribution is allowed to develop, in which case:

$$T \approx T_0 + \frac{P_A R}{2k}\left(4\tau + \left(\frac{r}{R}\right)^2 - \frac{1}{2}\right) \tag{8}$$

k is the heat conduction coefficient and $c\gamma$ is the heat capacity per m^3. The calculation is performed under the assumption of temperature independent material properties and constant heat flux. In reality, one may observe significant changes in both. Table 1 presents all material data that have been used in the study.

Although for instance radiation may be included in an analytical analysis, satisfactory answers for 2 and 3 dimensions are only obtained numerically. The FE code ANSYS has been used to calculate temperature increases in a staggered manner. The solution for a 1 dimensional non-linear problem of induction heating is described in detail in the ANSYS Users Manual. Results from analytical and numerical calculations are compared in Figure 6. It has been assumed that

there are no heat losses to the surroundings. Results from 1D analytical and numerical calculations with temperature independent material properties differ only marginally. Both predict temperature gradients smaller 10 ºC when the heating ends. A fine mesh in the boundary layer close to the surface of the billet is needed to obtain acceptable data (within ±2 ºC). In the outermost 2 mm of the billet the thickness of the linear elements (PLANE13) was only 0.15 mm. A comparison of the results from 1D and 2D models with temperature dependent material properties are also presented in Figure 6. In order to capture the effects of temperature changes time steps should be made fairly small (< 5s ~ 5 ºC). When billets are sufficiently long (500 mm), the 1D and 2D models produce similar results. In the case of billets of length 200 and 300 mm there is a significant flow of heat in the axial direction. The magnetic fields are weaker close to the edges of the billet. Thus, the edges are heated less than the central parts of the billet. When heat convection and radiation is included in the model, there is an even greater gradient in the temperature. Figure 7 presents the temperature distributions of the billets at the end of the heating phase and after a cooling period of 30 s. Emissivity and heat transfer coefficients of 0.2 (a rough surface) and 10 W/m^{2}K have been used.

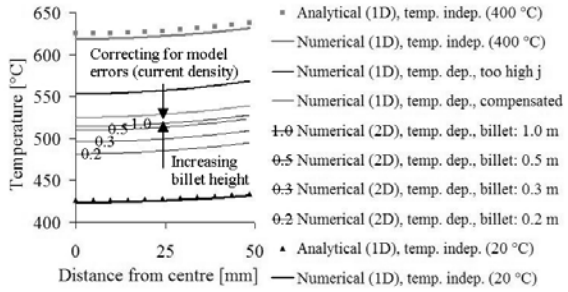

Fig. 6. Centre and surface temperatures for 1D and 2D analysis

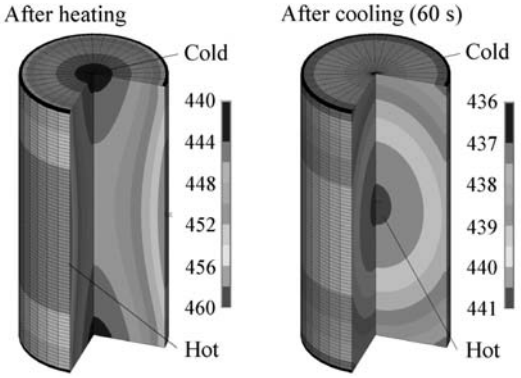

Fig. 7. Temperature distributions [ºC] after heating and cooling

4 DISCUSSION

The important question in relation to extrusion is to what extent uncertainties related to the temperature distribution in the billet affect process data. Figure 8 indicates that the temperature distribution at the end of the slow induction heating process is relatively uniform in most cases. During subsequent loading of the billet into the container (which lasts approx 30 s) heat losses are small. Due to the high conductivity of aluminium and the inefficient heat transport due to natural convection and radiation, the temperature of the billet quickly becomes uniform. During cooling the temperature decrease is only approx 10 ºC/min. The effect of a 10 ºC billet temperature change on the ram force is approx 3 % of maximum ram force during rod extrusion with a ratio of 40. The outlet temperature is altered by 2 to 3 ºC [1].

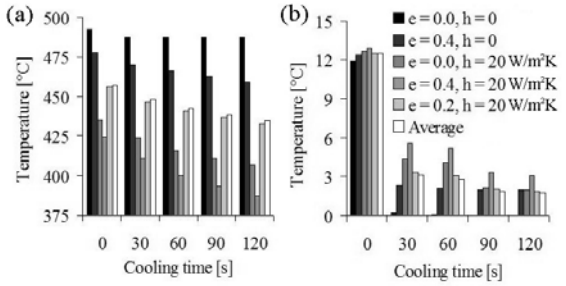

Fig.8. The effects of convection, h, and emissivity, e, changes. (a) The maximum temperature, (b) the maximum temperature differences in the billet at the end of heating and during cooling

5 CONCLUSIONS

Induction heating of billets for aluminium extrusion may be successfully simulated by the finite element code ANSYS. Simulations and experiments indicate that the temperature of the billet is uniform and should not deviate from the maximum value by more than 5 ºC if it is loaded into the container less than 30 seconds after heating ends.

REFERENCES

1. P.T. Moe, Pressure and Strain Measurement During Hot Extrusion of Aluminium, PhD thesis, Norwegian University of Science and Technology, 2005.
2. www.efd-induction.com
3. J. Davies, P. Simpson, Induction Heating Handbook, McGraw-Hill, London, 1979.
4. M. Lefstad, R. Flatval, Utprøving av induksjonsovn, SINTEF Internal Report STF24 A94341, 1994-11-23.
5. ANSYS® Inc., Theory Manual, Ver. 7.1.

Wajid W., Moe P.T., Abtahi S., Strøm S.

An Evaluation of Errors in Extrusion Modelling and Experiments

Abstract submitted to Conference

8th International Conference on Techology of Plasticity
October 26, Verona

Numerical modelling of hot extrusion of aluminium has become practical only during the last few years. Within less than ten years, however, computer simulation will become a vital tool for the designers of extrusion dies and for the engineers at the extrusion plants. Numerical modelling may increase production efficiency and allow more complex thin-walled profiles to be produced. If simulation codes are to provide accurate predictions, however, it is most important that fundamental assumptions as well as numerical codes are carefully assessed. Hot extrusion is a most complex process to model, and there are many sources of errors. The current paper presents an experimental approach including continuous measurement of ram forces, outlet temperatures and die face pressures. The errors related to measurement are carefully assessed. Furthermore, flow simulation has been performed with three simulation programs commonly used to model extrusion: Forge2®, Deform™ and Abaqus Explicit. The simulation program ALMA2π, dedicated to extrusion, has also been extensively used. An important objective of the study has been to compare predictions of the various codes and to assess the causes of deviations. All simulations have been performed under the assumption of isotropic material behaviour according to the Zener-Hollomon and Potential Law flow rules. The material data have been determined independently by compression and torsion testing. An evaluation of the errors related to material modelling is performed.

References:

[1] Moe P.T., S. Støren, *A technique for measuring pressure on the die face during extrusion*, Proc. 5th ESAFORM Conf. on Material Forming, April 2002, Kraków, pp. 463-466.

[2] Lefstad M., Moe P.T., Flatval R., Støren S., *Thin strip aluminium extrusion – pressure, temperature and deflection recordings of the extrusion die*, Proc. 5th ESAFORM Conf. on Material Forming, April 2002, Kraków, pp. 471-474.

[3] Moe P.T., Lange H.I., Hansen A.W., Wajda W., Støren S., *Experiments with die deflection during hot extrusion of hollow profiles*, Proc. 6th ESAFORM Conf. on Material Forming, April 2003, Salerno, pp. 119-122.

Per Thomas Moe

Pressure and Strain Measurement During Hot Extrusion of Aluminium

Volume II
A Comprehensive Report on the Second
Set of Rod Extrusion Experiments

Trondheim, March 2005

Doctoral thesis for the degree of doktor ingeniør

Norwegian University of Science and Technology
Faculty of Engineering Science and Technology
Department of Engineering Design and Materials

NTNU

This thesis has been submitted to the Norwegian University of Science and Technology, Department of Engineering Design and Materials in partial fulfilment of the requirements for the Norwegian academic degree Doktor Ingeniør

Pressure and Strain Measurement During Hot Extrusion of Aluminium, Volume II
Trykk- og Tøyningsmåling ved Varmekstrudering av Aluminium, Bind II

Institutt for Produktutvikling og Materialer (IPM)
Norges Teknisk-Naturvitenskapelige Universitet (NTNU)

Doktor ingeniøravhandling (PhD thesis) 2005:50

ISBN 82-471-6967-3 (elektronisk/electronic)
ISBN 82-471-6968-1 (trykt/printed)

ISSN 1503-8181

Preface

The thesis *Pressure and Strain Measurements During Hot Extrusion of Aluminium* consists of two volumes. The first gives an overview of the challenges of extrusion, the general objectives of the PhD study, the state of traction measurement in metal forming and the work performed in relation to the study. The first volume also contains twelve articles and papers that have been published as the work has progressed. It constitutes the main part of this thesis.

The second volume of the thesis is a comprehensive presentation of the final set of rod extrusion experiments performed in association with the study. It is admittedly quite uncommon to publish a thesis consisting of two volumes, and the motivations for the choice should probably be clearly explained. I should first call attention to the fact that the process of developing pressure and strain sensors for the extrusion process has been one of relatively many steps. Sensor designs have been proposed, analysed and tested experimentally. Results have been analysed and conclusions have been drawn. New iterations with better sensor and die designs have then been initiated. At the time this thesis was written, we were in fact taking a new step, and yet another step is most likely necessary before full-scale industrial implementation. Thus, the work presented in this thesis consists of many parts, but it is also only a part of the larger development work necessary to improve the extrusion process.

After years of experimental activity we possess a large amount of experimental data, which I only to a very limited extent have found space for in the first volume of the thesis. The objective of the first volume is primarily to convey the main conclusions and describe the general motivation behind them. Accurate capacitive pressure and strain measurement in dies during hot extrusion of aluminium is feasible, but there are still challenges related to industrial implementation. Sensor designs may be improved, and a method for effectively using the sensors may be developed. The objective of the second volume is mainly to provide the necessary support for the conclusions presented in the first volume. All data available cannot and should not be presented. The selection of data and information should make it possible for the potential user of the technology to trust the conclusions that have been drawn, and to continue the work if desired. It is most natural to present the last set of experiments since they have been performed in the most systematic manner, according to the most clearly defined goals and with the most refined sensor technology.

It would probably have been possible to present the experimental set-up and matrices, the results and the statistics in a conventional appendix. This was also my initial plan, but I very soon realised that it would be better to write a full report. Commentary is necessary to explain the choices of technical solutions and the results from the study. Furthermore, the systematic approach adopted is an essential part of the PhD work, and should be carefully justified. The approach may also be used in studies of new sensor designs to be used both in the laboratory and industrial environments. The analysis of data is not an innovation of the current study, but still needs satisfactory explanation.

The second volume discusses the assumptions of the numerical calculations, and it more closely treats both experimental and numerical results. Although the report is written as a more or less continuous piece of work, I neither expect nor advise the audience to read it as one piece. It is in many ways an independent piece of work, but is, as indicated, primarily a compilation of the most important information. Admittedly, it repeats much of the information presented in the first volume of the thesis, and is not written in the most concise manner.

Finally, I would like to draw attention to the preface of the first volume, which contains the necessary acknowledgements. I would again like to thank the Norwegian Research Council and Hydro Aluminium for the necessary economic support. I would also like to emphasize the important role played by my main supervisor, Professor Sigurd Støren, who has greatly contributed also to this second volume of the thesis.

Per Thomas Moe

Table of Contents

VOLUME I: AN OVERVIEW OF THE WORK AND ARTICLES

VOLUME II: A REPORT ON ROD EXTRUSION EXPERIMENTS

PREFACE ..... **III**

SYMBOLS AND TERMINOLOGY ..... **VII**

ABSTRACT ..... **XI**

CHAPTER 1 INTRODUCTION **1**

CHAPTER 2 SENSOR AND DIE DESIGN **3**

2.1 THE EXTRUSION PRESS 3
2.2 THE EXTRUSION DIE 7
2.3 CAPACITIVE PRESSURE MEASUREMENT SYSTEM 31

CHAPTER 3 EXPERIMENTAL PLAN **47**

3.1 SOME REQUIREMENTS FOR THE EXPERIMENTAL PLAN 47
3.2 THE EXPERIMENTAL PLAN FOR ROD EXTRUSION 49
3.3 FLOW AND DIE DEFORMATION MODELLING BY THE FINITE ELEMENT METHOD 60

CHAPTER 4 CALIBRATION EXPERIMENTS **89**

4.1 REQUIREMENTS FOR THE MEASUREMENT EQUIPMENT 89
4.2 CALIBRATION OF CAPACITEC DISPLACEMENT SENSORS 92
4.3 APPROACHES TO CALIBRATION OF THE PRESSURE SENSORS 103
4.4 ON-LINE CALIBRATION EXPERIMENTS 111
4.5 ON-LINE CALIBRATION OF THE LINER LOAD CELL 137

CHAPTER 5 EXPERIMENTAL RESULTS **145**

5.1 AN OVERVIEW OVER EXPERIMENTAL CASES AND RUNS 145
5.2 RAM FORCE AND OUTLET TEMPERATURE MEASUREMENT 147
5.3 DETERMINATION OF ZERO POINT FOR DIE FACE PRESSURE MEASUREMENTS 149
5.4 REDUCTION OF NOISE DUE TO INTERACTION BETWEEN SENSOR SYSTEMS 155
5.5 SOME OBSERVATIONS ON THE DYNAMIC SENSOR BEHAVIOUR 160
5.6 RESULTS FROM RUNS 168

CHAPTER 6 ANALYSIS AND DISCUSSION **253**

6.1 ANALYSIS OF VARIANCE 254
6.2 AN EVALUATION OF THE ACCURACY OF MEASUREMENT 264
6.3 THE EFFECT OF A BEARING CHANNEL 290
6.4 TEMPERATURE COMPENSATION 300
6.5 FINAL REMARKS ON THE MAIN OBSERVATIONS OF THE STUDY 317

CHAPTER 7 CONCLUSIONS **319**

REFERENCES **321**

Symbols and terminology

No systematic use of symbols has been made, since the thesis contains only a limited number of equations. When a new equation is introduced, all terms are generally treated thoroughly. The use of symbols is in accordance with common practice in the various fields of science. Note that some symbols may be used to describe different variables. The exact meaning of the symbols should be seen in relation to the context in which they are presented. A short list of examples is here provided:

α	-	an angle (for example the choke angle) a parameter of the Zener-Hollomon relation the diffusivity
ε	-	permittivity mechanical strain (ε_{ij} for the various components)
σ	-	the standard deviation (a stochastic variable) mechanical stress (σ_{ij} for the various components)
R	-	the electrical resistance of a circuit element a radius (for example of the die outlet or container)
A	-	an area (of for example a capacitor plate) a coefficient of a regression relation a parameter of the Zener-Hollomon relation a day or round of experiments
B	-	a factor linking various components of stress a coefficient of a regression relation a day or round of experiments
C	-	the capacitance the heat capacity a coefficient of a regression relation a parameter of the Modified Zener-Hollomon relation a day or round of experiments
D	-	a diameter (for example of the die outlet or container) the displacement current a coefficient of a regression relation a day or round of experiments
E	-	the modulus of elasticity the electric field
k	-	the number of a factor the heat conduction coefficient
Q	-	an electric charge the activation energy for diffusion (of the Zener-Hollomon relation)
OD	-	outer diameter of a piece

The following terms have been adopted from the textbook of de Sa [Sa97]:

Transducer
An input device that transforms one signal type to another. It may be a genuine energy converter (passive) or require an auxiliary source of energy (active). Transducers may be sensors or actuators.

Sensor
Instrument transducer used for measuring physical quantities by electrical means.

Accuracy
A term used to relate the output of an instrument to the true value of its input, with a specified standard deviation.

Repeatability
The closeness of agreement of a group of output values for a constant input, under given environmental conditions.

Resolution
The smallest increment in the input that can be detected with certainty by the transducer.

Sensitivity – calibration factor
The ratio of the magnitude of the output to the corresponding change in the magnitude of the input.

Linearity
A measure of the constancy of the sensitivity of the transducer over the entire useful range of input values.

Hysteresis
The algebraic difference between the average output errors corresponding to input values, when the latter is approached from the maximum and minimum possible input settings.

Drift
The unidirectional variation in the transducer's output that is not caused by any changes in its input.

Zero stability
The ability of the transducer to restore its output to zero when its input is returned to zero.

Chapter 2 of Volume I of this thesis presents a number of terms commonly used in the extrusion community. It has also been necessary to introduce a number of new or less commonly used terms to simplify understanding.

Die face pressure or **tractions**
The component of stress that acts normal to the extrusion die face (a distribution).

Die face force
The total force acting normal to the extrusion die face (an integral of the pressure).

Ram force
The force applied by the ram at the aluminium billet during extrusion.

Liner shear stress or **container (liner) shear stress**
The component of shear stress acting at the interface between the aluminium billet and the container or liner and in the direction of extrusion. The terms liner and container are used interchangeably in the current work. The liner is viewed as a part of the container.

Liner load or **liner force**
The total force acting between the aluminium billet and the liner or container and in the direction of extrusion. The liner force is the integral of the liner shear stress over the area of contact between the billet (and dummy block) and the liner.

Liner load cell
An instrument for measuring the liner force / load.

Container or **liner friction**
The interaction between the aluminium billet and the liner or container. The friction is generally not related to a value of the shear stress.

Bearing channel friction
The interaction between the aluminium profile and the bearing surfaces or die lands.

Calibration
The determination of calibration factors linking the sensor system voltage output and die face pressure or liner force. Also displacements may be evaluated.

On-line or **in-situ calibration**
Calibration of the die face pressure sensors or the liner load cell in the environment of the extrusion process and directly in relation to the extrusion experiments.

Off-line calibration
Calibration of the pressure sensors or the liner load cell by an independent method not directly in relation to the extrusion experiments or in the extrusion environment.

Finite element calibration
Determination of calibration factors solely by finite element calculation.

The experimental approach that has been followed in the current work has largely been adopted from the classical text book of Box, Hunter and Hunter [Box78] *Statistics for Experimenters*. The factorial approach they advocate has been somewhat modified, but the terminology that has been used in the book and in the current work is similar.

Factor or **input variable**
A process parameter that is systematically changed to produce an effect.

Run or **extrusion run**
Extrusion of one aluminium billet (deviates from the definition of reference [Box78]).

Level
The value of the input variable (i.e. low and high, -1 and 1 etc).

Case
A specific combination of levels for all factors. There may be several runs in a case.

Effect
The result of a change of the levels of one or more factors.

Variability
An expression of the degree of randomness in measurement results or input data.

Replication
An attempt to reproduce an extrusion run.

Genuine replication
A replication that requires that all relevant sources of variability are revealed.

Round or **day of experiments**
All runs performed on one day of experiments (only one set-up of the equipment).

Block
A set of experiments performed under similar conditions. A block in the current study is a round of experiments. A detailed description of the experimental approach is given.

Block effect
An effect related not to a change of the factors of the experiment, but rather to a change in conditions that should remain fixed during experiments. The block effect may occur if environmental conditions during experiments are not satisfactorily reproduced.

Randomisation
The running of cases and runs in a random order during a round of experiments or for the entire experimental plan.

Note that the term **sensor disc** is often used to describe the part of the sensor which is in intimate contact with the billet and deforms primarily elastically during measurement.

Abstract

A new die face pressure sensor design concept for the aluminium extrusion process has been developed. The sensors make use of Capacitec high-temperature capacitive displacement probes of the type HPC-75 and the Capacitec 4004 series amplifiers. The sensors are integral parts of a special extrusion die that may be used to study flow and friction mechanisms during extrusion of rods and similar geometries. The extrusion die has been designed so that the die outlet geometry may be easily changed in order to allow comparative studies.

The sensors may be accurately calibrated on-line by hydrostatically compressing a billet of small height. A set of experiments have been performed to evaluate the quality of the sensor design and calibration technique and to determine the capabilities of the sensors. Extrusion was performed at extrusion ratios 40 and 80. Die outlet inserts with bearing length-to-diameter ratios of 0 and 0.76 were used. The initial billet temperature was in the range from 450 to 500 ºC, and the profile velocity was varied from 200 to 3000 mm/s. Consequently, the die face pressure was systematically varied in the range from approximately 175 to more than 350 MPa.

Measurement of the ram force, the die outlet temperature and the die face temperature was performed in addition to three parallel replicate recordings of the die face pressure. Measurement of the liner load was also performed with capacitive displacement sensors in order to allow independent estimation of the die face pressure. The measured and simulated values of pressure deviated less than 10 %. The accuracy of measurement was probably better, but this may only be demonstrated if the calibration and verification techniques are refined. The repeatability was usually better than ± 10 % of full scale for genuinely replicated runs. Repeatability within a round of experiments was better than 3 %. Pressure oscillations of amplitude smaller than 3 MPa were successfully detected.

The sensors may be used at the highest temperatures experienced during aluminium extrusion. The pressure sensors are affected by changes in temperature. In none of the cases run was the thermal effect larger than 15 % of full scale. Simple temperature compensation schemes based on temperature measurement may be used to significantly reduce the effect. The sensors were successfully used to study material flow and to test assumptions related to container and bearing channel friction.

Chapter 1

Introduction

This report provides a comprehensive presentation of both the experimental set-up and results from rod extrusion experiments performed with a second generation or complex die, integrating replicate measurements of the die face pressure, the profile temperature at the outlet, the die face temperature and the force acting between the die and liner of the container. The results and the main conclusions from these experiments have earlier been treated in journal articles and conference papers [Moe02] [Moe03b] [Moe04b] [Moe04c] [Waj04]. However, due to the length limitations of these publications it has only been possible to focus on certain aspects of the experiments described, and to present a limited selection of the data material that has been gathered. The objective of this report is to provide a more thorough analysis of experiments. Ideally, it should be a reference for those who wish to assess the capacitive pressure measurement technique more thoroughly and to better understand the complexity and advantages of accurately recording and assessing data in relation to extrusion.

The complex rod extrusion experiments were run at a point in time when the feasibility of measuring the pressure acting at the die face by capacitive displacement sensors and elastically deflecting discs had already been demonstrated. Capacitive probes had been inserted into dies for hollow profiles [Moe03a], dies for thin strips [Lef02a], simpler dies for rods, and even industrial dies for U-profiles. Earlier rounds of rod extrusion had also been carried out. The repeatability of the pressure measurement seemed to be fairly satisfactory (±5 %) as long as the experimental set-up was not altered between runs. Yet, when sensors were dismantled and remounted, or even when the tool stack was simply cooled and then re-heated, voltage readings from the measurement system could differ by more than ±10 % for completely replicate runs. A similar difference in output could be obtained when different sensors measured pressures in same position. The following conclusions were drawn from the early experiments:

- It was not sufficient to merely establish a calibration curve linking the displacement and the voltage change for the capacitive probe and then work out the displacement pressure conversion factor by finite element modelling. Calibration curves had to be established experimentally for each individual sensor if a measurement accuracy of 5 % or better was required. High-temperature isothermal and hydrostatic in-situ calibration performed in relation to calibration experiments constituted a promising approach. Furthermore, it was of the greatest importance that proper corrections for the temperature changes during extrusion are made.

- A sensor design allowing better fastening of the probes should be sought. It is vital that there are no permanent displacements during extrusion and that the sensor remains properly fixed during both heating and cooling of the die and the tool stack. For the early die and sensor designs, mounting of probes was difficult to control and manufacturing inaccuracies were hard to spot. Dies were essentially of a standard type. Holes had been added that were 10 mm in diameter and that reached from the bottom side of the dies and almost 50 to 60 mm to the upper die face.

- It is important to perform alternative measurements allowing careful control of the results obtained with the pressure sensors. During extrusion the ram force is usually measured continuously. A component of the ram force is applied directly at the die face while another component is led through the liner, since friction forces act at the interface between the liner and the billet. A common assumption is that there is full sticking and, thus, significant shearing. Liner force measurements would provide valuable information about the constitutive behaviour and on the sensor response. While such measurements are regularly performed elsewhere, the press used for the early experiments did not incorporate the necessary equipment.

Thus, the main objectives of the experiments were to develop and test a simpler sensor design, to examine a method for on-line calibration of the probes and to establish data material through extrusion experiments that would allow a critical evaluation of the experimental approach. Numerous replicated extrusion experiments with a profile geometry that was easy to analyse had to be run, as the accuracy and repeatability of the measurements were among the most interesting aspects. A further objective related to the problem of calibration was to establish useful compensation techniques for changes of the sensor temperature. It was well known that the changes of die surface and sensor temperatures during extrusion are significant and affects the behaviour of the sensor.

As will be shown, the sensor of the current study was an integral part of the die. When sensors are not of this type, but are rather inserts, there are crevices in the top die face, and aluminium may penetrate into them. This may to some extent affect the sensor output [Moe04d]. The integral sensor is a somewhat safer solution, but it is also one that gives the experimenter less freedom to play with the shape parameters of the outlet and profile. Thus, it is also potentially one that is less useful. It would be most practical if sensors could be calibrated and tested on a simple case such as rod extrusion and then used in more complex studies such as the extrusion of thin strips [Lef02] [Waj03] [Moe04d]. An important objective of this study has been to develop and test a die design with an integrated sensor that would render possible the running of experiments with a range of different outlet geometries for the rod extrusion case. This would allow sensor designs to be tested at a greater range of mechanical and thermal loads. Furthermore, a tool for studying flow and friction behaviour for a generic case would then be available. The issue has been further treated in the references [Waj04] and [Moe04b]. Finally, an integrated pressure sensor would be very useful if it could be implemented as an analysis tool for studying flow stability and related dimensional variability of extruded profiles [Moe04d]. The tool may then be used to evaluate flow during industrial extrusion (Volume I).

Chapter 2

Sensor and die design

This section contains a description of the equipment that was used in the set of rod extrusion experiments performed to test a new die face pressure sensor design. The section commences with a general description of the extrusion press, but then focuses on the new sensor and die design concept. In the final part of the section the principle of capacitive measurement is reviewed, while the main characteristics of the Capacitec sensor equipment used in the experiments are presented.

2.1 The extrusion press

All rod extrusion experiments were performed with the 8 MN vertical laboratory press belonging to SINTEF Materials Technology, Trondheim, Norway (Figure 2.1 and Figure 2.2). The brand-name of the press is Hydraulico, and the press was acquired from Hydroform, Denmark in 1988 [Lef01a]. The press has 4 hydraulic cylinders that may be used simultaneously and independently for many purposes. During extrusion, the main ram cylinder was used. It has a maximum stroke length of 830 mm, and the ram velocity can be controlled automatically or manually in the range from 0.2 to 31 mm/s. The hydraulic pressure may reach 300 bar and may be measured continuously by a pressure sensor. The hydraulic systems are controlled by a Programmable Logic Controller (PLC), and the main process data are both shown on a display and given as voltage signals ranging from -10 to 10 V. Data gathering of up to 32 analog signals is performed by a PC running LabTech Notebook. An analog/digital converter allowed 12 bits sampling of the 32 signals at a rate of 20 per second. The logging equipment was improved after the rod extrusion experiments were performed, so that 15 bits analog-to-digital conversion was made possible. Lefstad provides further technical documentation concerning the press and procedures for aluminium extrusion in use at the time of experiments [Lef01a]. Calibration routines are treated in [Lef01b] and discussed further in Chapter 4 of this volume.

During extrusion, the tool stack consisted of the die, a bolster (die support), a glimmer plate and a pair of beams (fulcrums). The outer diameter of the bolster was 200 mm, while the diameter of the centre hole was 22 mm for all the experiments of interest. It was of greatest importance that the bolster provided maximum support for the die. Therefore, the bolster outlet was made as small as possible. The tool stack was placed at a press table/board with a cross-section of 1250 mm x 1000 mm. The press board is

sufficiently thick and firmly attached to the foundations of the building. In the centre of the press board, there was a hole of 200 mm in diameter leading from the ground floor to the basement and subsequently to a more than 6 m deep well. Whereas thicker and shorter profiles were guided directly into the well, thinner profiles were coiled up in the cellar. No puller was used during the experiments. The only pulling force exerted on the profiles was that of the weight of the extruded section. No arrangements had been made for cooling of the profiles since metallurgical testing after extrusion was not to be performed.

Figure 2.1. The SINTEF 8 MN vertical laboratory press in Trondheim, Norway. The diameter of the ram and container bore is approximately 100 mm. The container and tool support rest on the lower press board. The equipment may be dismantled to allow other kinds of experiments (such as forging).

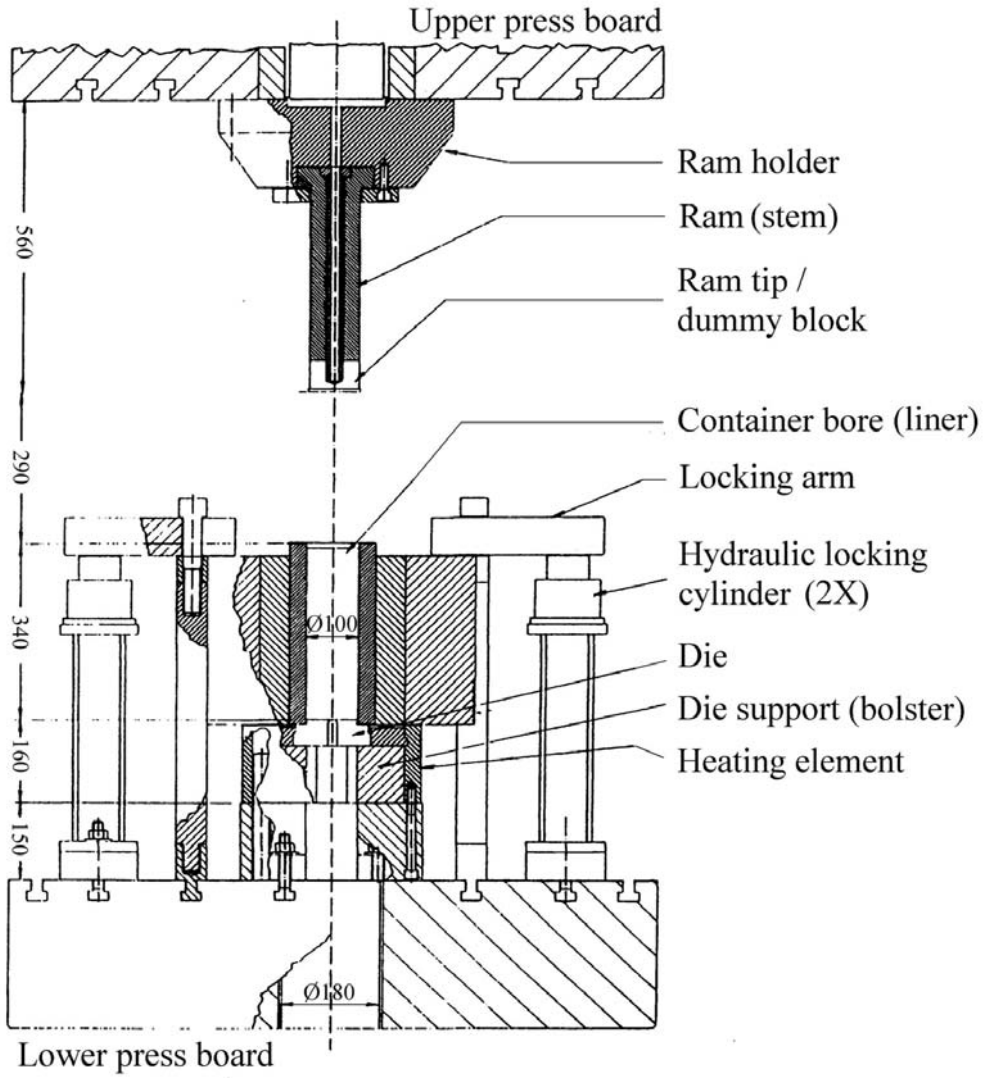

Figure 2.2. A drawing of the SINTEF 8 MN vertical laboratory press [Gra95].

The inner diameter of the standard container was 100 mm, while the container height was 350 mm. The container was supported only by the flanges of the extrusion die (Figure 2.3). During extrusion, the container or liner force due to the sticking friction between the billet and container is guided through the die and onto the die support. As will be further discussed, it would have been possible to introduce a special arrangement for guiding the liner force directly onto the die support or press board through a load cell. The deflection of the extrusion die is then less affected by changes in the container friction force, and estimates of the various components of the ram force would be directly available. However, an advantage of the current design is that the force guided through the liner contributes to sealing off the crevice between the die and the liner and to keeping the container and die in position. Two hydraulic locking cylinders apply an additional force lower than 200 kN at the top face of the container before, during, and after extrusion. At the same time, the maximum friction force may amount to more than 1000 kN at the onset of extrusion.

Figure 2.3. An extrusion die mounted in the container. The die is instrumented, but is not of the complex kind described in the current report.

Aluminium extrusion is usually performed at elevated temperatures. SINTEF Materials Technology has at its disposal induction heating equipment that allows billets to be heated to more than 400 ºC in approximately 4 minutes. The induction coil consists of 16 turns and has outer and inner diameters of 118 and 103 mm respectively. The applied effect is smaller than 20 kW. The temperature of the billet was measured continuously with a thermocouple. It was not completely uniform during and after heating. Induction heating causes the temperature to be highest at the die face. Convection during cooling in air caused the central part of the billet to be hottest. The billet surface temperatures were usually measured before the billets were dropped into the container. Both the container and the bolster were also heated by induction. During the heating phase, the temperatures were continuously measured by thermocouples of type K, and the effect was carefully tuned in order not to cause overheating of the tool materials. In order to establish steady state thermal conditions in the tool stack and container, pre-heating started approximately eight hours before the experimental activity commenced. The container was usually sealed off to prevent convective heat losses. Both the bolster and container were properly insulated. As opposed to industrial practice, the extrusion dies were mounted before the tool stack was pre-heated (Figure 2.3). Furthermore, tools were not shifted during a round (i.e. a day) of experiments. The reason was that the extrusion die was so complex that it could not easily and safely be removed from the tool stack when hot. There were in all six cables to the capacitive pressure measurement system and seven thermocouple cables. To further reduce heat losses from the tools, the dies were wrapped in insulation mats.

2.2 The extrusion die

Figure 2.4 to Figure 2.7 show the extrusion die that was used in all the experiments described in this report. The die is here called a complex or composite rod extrusion die as opposed to the dies of simpler geometry that were used in earlier rounds of rod extrusion experiments (Figure 2.3). The complex die consisted of four main parts:

- The **top disc** with 3 die face capacitive pressure sensors and 6 thermocouples
- The **die outlet inserts** with 2 to 4 bearing channel thermocouples
- The **container/liner force load cell** with 3 capacitive sensors and a thermocouple
- The **die core** with 3 bolts and a pin for mounting the top disc.

In addition, sensor holders, screws and springs were used to keep the capacitive probes in position. All the larger parts were made from AISI H13 hot working tool steel quality Uddeholm Orvar Supreme [UdeW]. The composition and the most important properties of the material are displayed in Table 2.1 and Table 2.2. Figure 2.8 presents important hot working properties of Orvar Supreme. After manufacturing of the various parts, the dies were heat-treated by quenching and tempering according to the recommendations of the manufacturer. A hardness of HRC 48 was obtained.

Figure 2.4. A view of the upper face of the complex rod extrusion die. An insert with outlet diameter 11.2 mm (ER = 80) has been used.

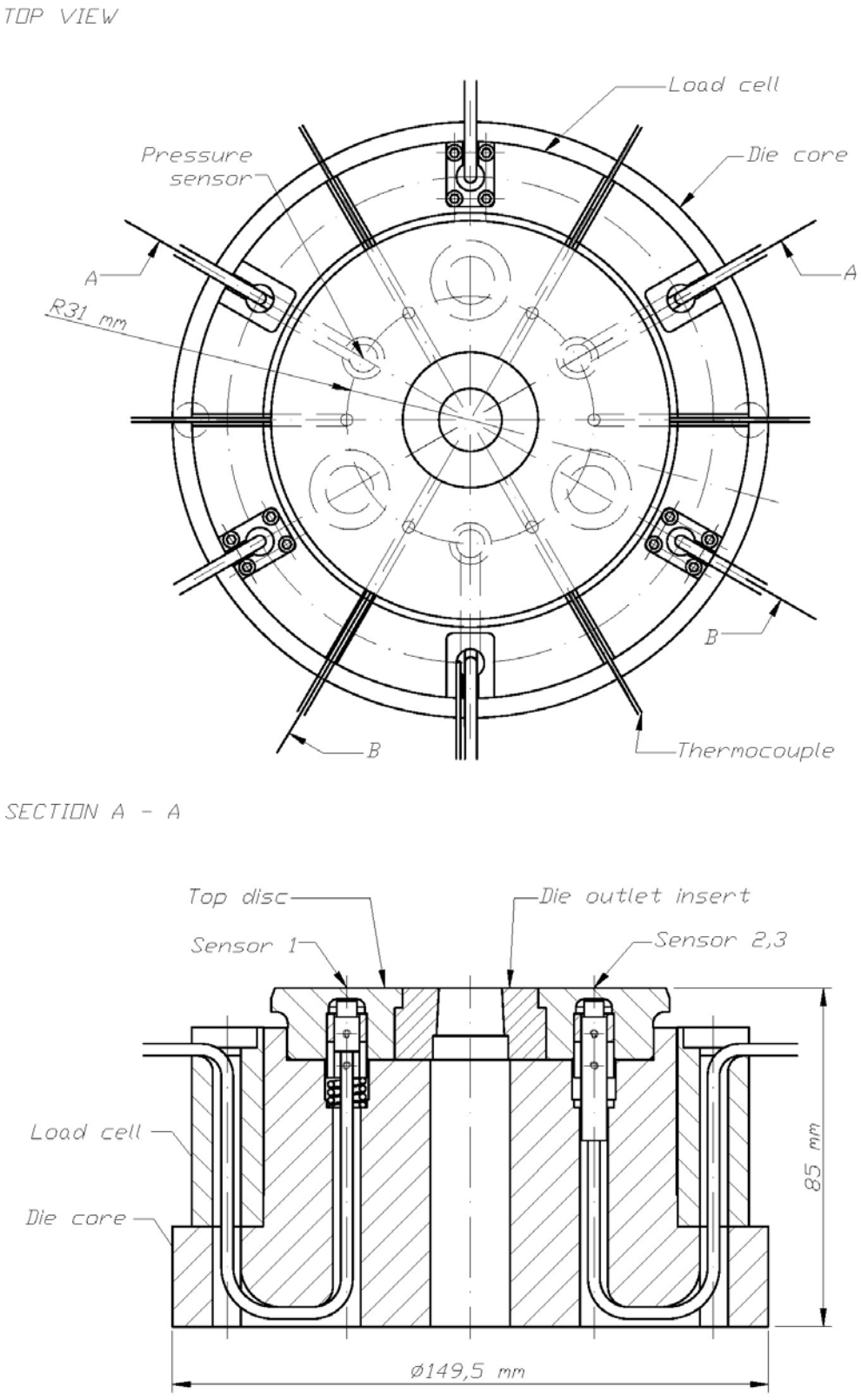

Figure 2.5. Assembly drawing of the complex rod extrusion die (not to scale).

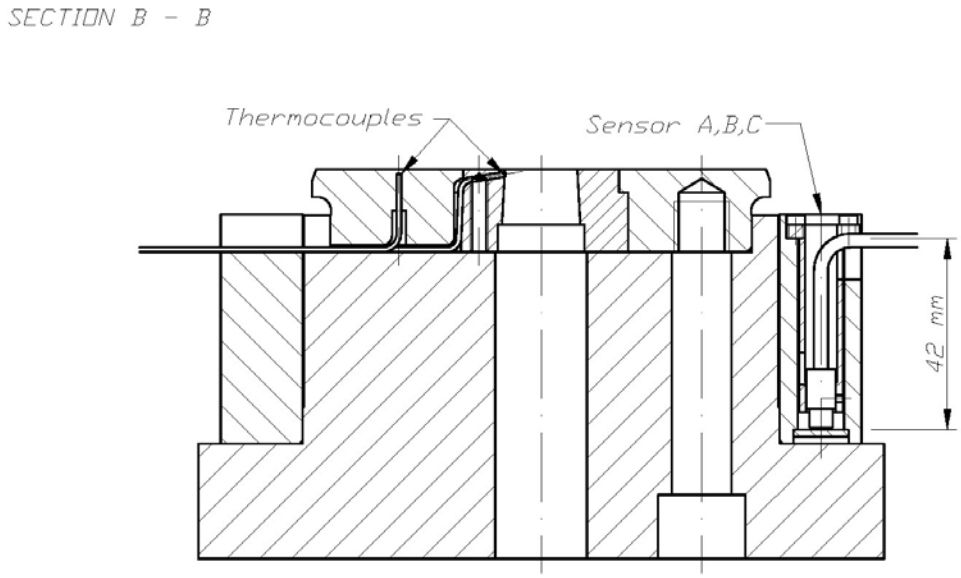

Figure 2.6. Assembly drawing of the complex rod extrusion die (continued).

Figure 2.7. A view of the bottom face of the complex rod extrusion die.

Table 2.1. Uddeholm Orvar Supreme hot working steel – alloying elements

	C	Si	Mn	Cr	Mo	V
Typical analysis weight %	0.39	1.0	0.4	5.2	1.4	0.9

Table 2.2. Uddeholm Orvar Supreme – thermo-mechanical properties

Temperature	20 ºC	400 ºC	600 ºC
Density [kg/m^3]	7800	7700	7600
Modulus of elasticity [GPa]	210	180	140
Poisson's ratio [-]	-	-	-
Coefficient of thermal expansion from 20 ºC [ppm/K]	-	12.6	13.2
Thermal conductivity [W/mK]	25	29	30
Specific heat capacity [J/m^{3}K]	-	-	-

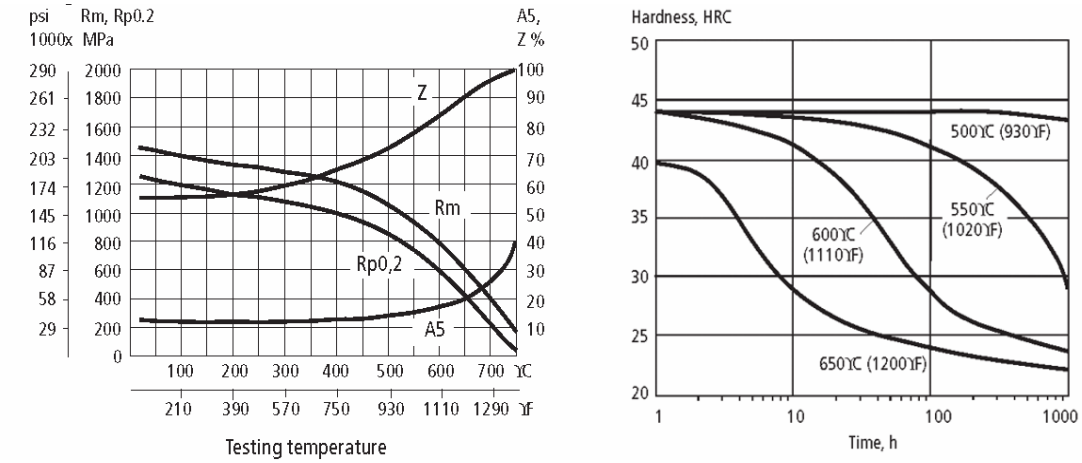

Figure 2.8. Left – tensile test data over a range of temperatures. Hardness HRC45. Right – effect of time at high temperatures on hardness. Both curves are found in the Uddeholm Orvar Supreme product data sheet [UdeW].

2.2.1 The die outlet insert design

As indicated earlier, the purpose of using a complex die was to allow experiments with a number of different die outlet geometries, but with the same integrated die face pressure sensors. There were essentially three reasons for changing the outlet geometry of the die.

First, it was though to be of greatest interest to test the response of the pressure sensors at a greater range of mechanical and thermal loads. This was made possible by the use of die outlet inserts with different diameters and bearing lengths. A similar effect could have been produced if the billet material or temperature had been changed. However, a second reason for using a set of inserts was to demonstrate a method for evaluation of friction and flow in the bearing channel. The third reason was to deduce material flow and friction data for a specific aluminium alloy over a large range of outlet temperatures and strain rates. The extrusion ratios of the study were of industrial relevance.

Figure 2.9 displays the four die outlet inserts used in the experiments. The container diameter was 100 mm, and the outlet diameters of the inserts were approximately 15.8 and 11.2 mm, which corresponded to industrially relevant nominal extrusion ratios of approximately 40 and 80. At 500 ºC, thermal expansion may have caused the outlet dimensions to be from 0.05 to 0.1 mm larger than at room temperature. If nominal dimensions are used in the evaluation instead of actual ones, pressure estimates should not be more than approximately 0.5 % in error. The die face pressure is then assumed to be proportional to the natural logarithm of the extrusion ratio [Stø03].

The inlet radius was made almost completely sharp for all the die outlets (< 0.2 mm), since the shape is easiest to manufacture and reproduce. Industrial dies are often made with inlet radiuses significantly larger than 0.2 mm. The geometry of the inlet affects the material flow and the way the material is sheared close to the outlet. For that reason, it would be best to choose an inlet geometry that could be very accurately defined and manufactured. It is at the same time a well-known fact that a perfectly sharp inlet corner may be difficult to model in most of today's numerical simulation codes. Lefstad has also observed that the flow stability of complex thin-walled profiles may in some cases be affected by small changes in the inlet geometry [Lef01c]. However, the differences in the pressure build-up due to the details of the inlet shape are probably not very large.

Two of the die outlet inserts were manufactured with very close to zero length bearings while the other two had bearings of significant length in the extrusion direction. The bearings of the latter were deliberately made artificially long to produce a detectable increase in the die face pressure. The actual friction phenomena of the bearing channel were also taken into consideration during the design work. Friction in the outermost part of the bearing channel is, according to Abtahi [Abt95], of the slipping type, which means that the contact is less intimate and pressure dependent. Closer to the inlet of the bearing channel the material is assumed to stick to the die. The deformation occurs in the aluminium rather than at the interface between the tool and the work piece. Since the pressure and shear stress increase in the direction opposite to that of extrusion in the slipping zone, the transition region between stick and slip is located where friction shear stresses approach the shear flow stress, τ_{flow}. Equation (2.1) is an analytical expression for the extension of the slip zone, L, based on a simple slab model and the Coulomb friction law. The simplifications made in the deduction of the formula are further treated in relation to the analysis of data (Chapter 6) and in [Moe03b].

$$\frac{L}{D} = \frac{1}{4\mu}\ln\left(\frac{\tau_{flow}}{\tau_0}\right) = \frac{1}{4\cdot 0.4}\ln\left(\frac{20}{5}\right) = 0.866 \qquad (2.1)$$

μ is the friction coefficient of the Coulomb law in the slipping zone. Based on studies of extrusion with almost parallel bearings, Tverlid [Tve97] has proposed a coefficient of approx 0.4. The value probably depends on both the flow velocity and the temperature at the interface, but such considerations are less important in relation to die design. τ_0 is the minimum shear stress in the bearing channel, and it is here assumed to be 5 MPa. The value is adopted from Abtahi. 20 MPa is a lower estimate of the shear flow stress of the material in the bearing channel. D is the diameter of the bearing channel.

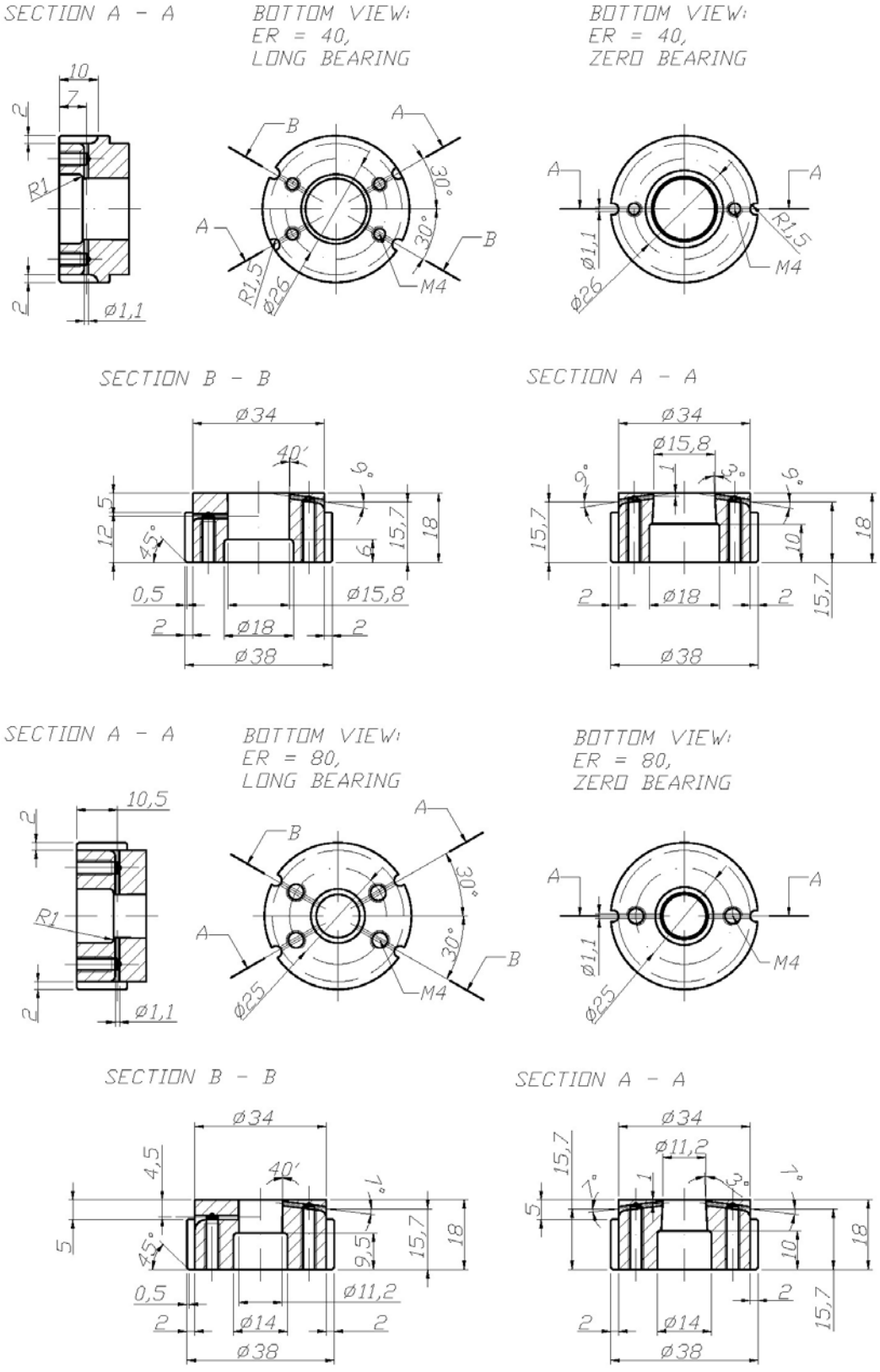

Figure 2.9. The die outlet inserts: Right – zero bearing inserts, Left – long bearing inserts, Top – extrusion ratio 40, Bottom – extrusion ratio 80.

The results are obviously inaccurate, but seem to be in fair accordance with an initial extrusion simulation by Forge2® based on the same model [TraW]. In the present work the *L/D* ratio has been set to approx 0.76. For *D* equal to 15.8 mm, *L* is 12 mm. For a *D*-value of 11.2 mm, *L* is 8.5 mm. When *L/D* is 0.76, there should be a Coulomb-type of friction in the entire bearing channel, as the friction shear stress should not be higher than the flow stress of the material anywhere. At the same time, however, pressure increases are significant. The slab calculation used above indicates that the pressure at the inlet to the bearing channel was approximately 42 MPa or typically 10 to 20 % of the total die face pressure. Such a pressure difference should be detectable for both the die face pressure sensors and ram force measurements.

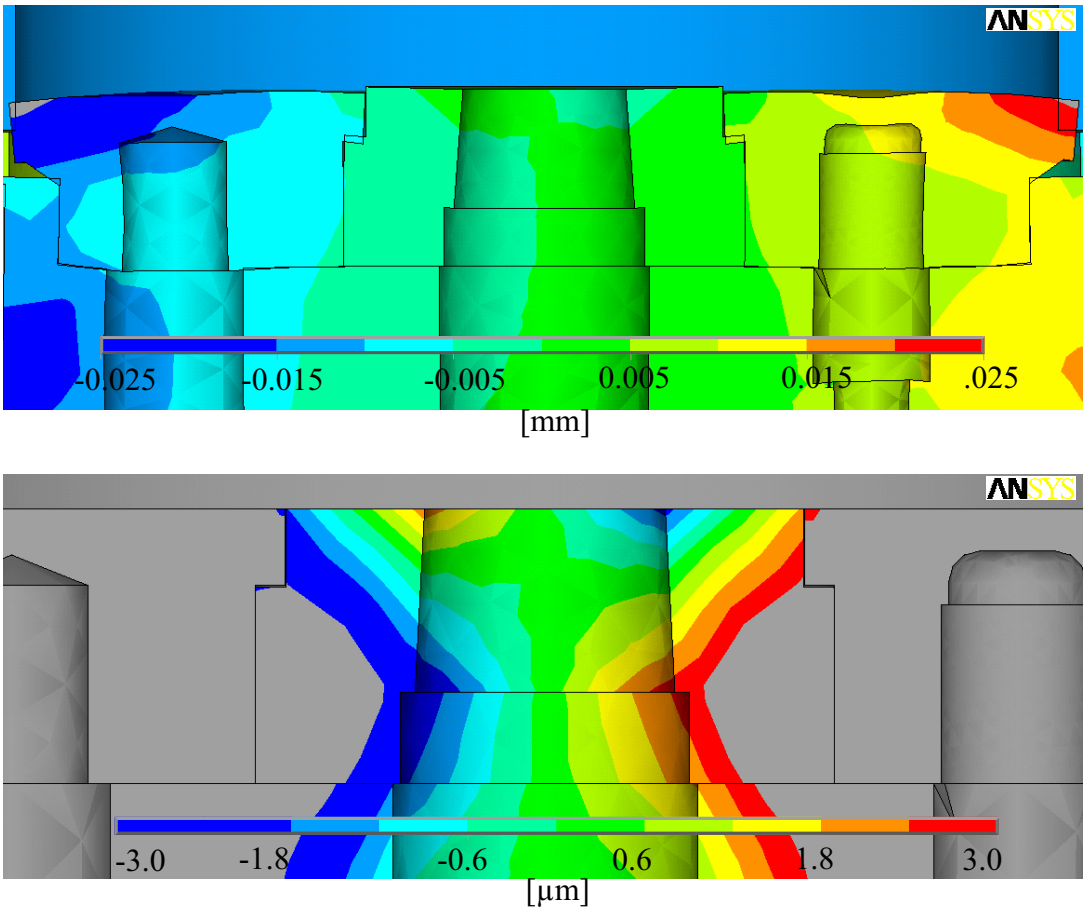

Figure 2.10. An example of deformation of a die outlet (ANSYS® 7.1). Both figures show the deformation in the direction normal to that of extrusion. The die face load is a uniform one of 200 MPa. The top figure shows the entire top disc and die outlet (minimum deformation: 25 µm to the left, maximum: 25 µm to the right). The bottom figure shows only the die outlet (minimum: 3 µm to the left, maximum 3 µm to the right)

The stick-slip phenomenon is affected by the choke angle of the bearings, but mainly when the angle is close to zero, typically less than 20 minutes [Abt95] [Lof01]. Then, the bearing channel may open so that there is almost no friction at all, and elastic effects may affect flow. Stick-slip may be observed even for a bearing channel of 1º choke, although the friction coefficient may differ from the case of slightly choked dies. In the

current study, the nominal choke of the long bearings was 40', which actually is a relatively large value. The die and the die outlet insert deformed significantly elastically during extrusion. Figure 2.10 presents results from calculations where the top die face has been exposed to a uniform load of exactly 200 MPa. Shear loads were not considered. The model includes the entire tool set-up of the SINTEF extrusion press and has been performed with ANSYS® 7.1. The details of the calculations are treated in Chapter 3. When the load is applied, there is less than a 0.01 mm reduction of the die opening as well as a 2 minutes tilt of the bearing surface. The tilt is artificially large due to the composite design of the die. Estimates may be inaccurate due to the complexity of modelling contact. For example, it has been assumed that the die inserts were tightly fitted into the sensor disc. Anyway, since the nominal value of the choke angle was so large, bearings should remain choked during extrusion. The zero bearing channels were of a release angle of 3º. During experiments there was some deposition of aluminium at the zero-length bearings, but the deposits probably did not cause significant additional pressure build-up. Experimental results seem to support this last assumption.

The surfaces of the long bearing channel inserts were neither ground nor polished after machining. This means that there were grooves in the surface normal to the extrusion direction and that there was significant surface roughness. The bearing surfaces were not hardened by nitriding, although this is a common industrial practice. The reason why nitriding was not performed was mainly that the number of runs to be performed with a die outlet would not be so large that there was a risk of significant wear. It should be realised, however, that friction conditions during the experiment may not have been completely equivalent to those experienced during industrial extrusion. One should note that the most important objective of the experiments was to generate a detectable effect.

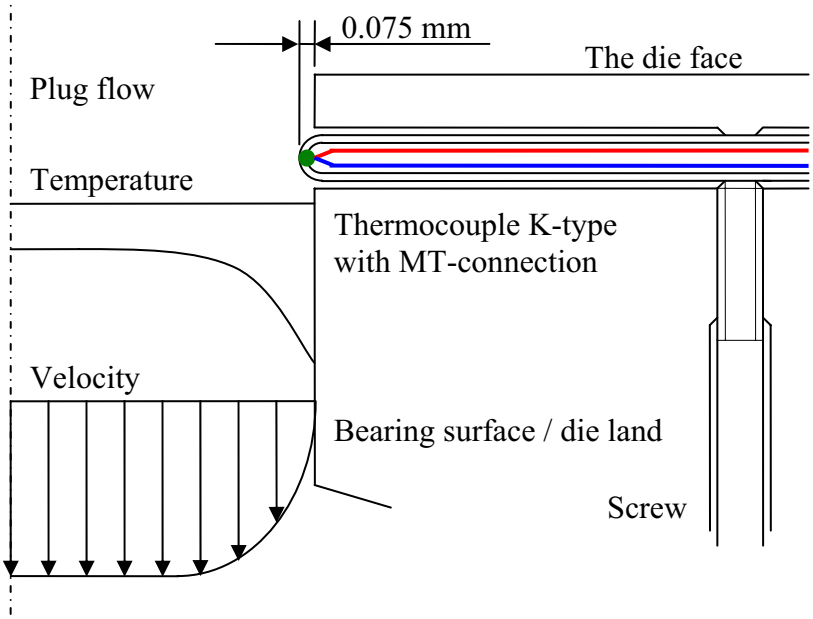

Figure 2.11. The principle of bearing channel temperature measurement method used in the study. The thermocouples were fixed in position by set screws.

In order to measure the temperature of the material leaving the die, two to four thermocouples were mounted in the die insert. The work was performed by Robert Flatval of SINTEF Materials Technology. The temperature measurement technique for extrusion has been developed by Lefstad [Lef93]. The thermocouples are in direct contact with the flow, and they scratch the profile surface. The depth of penetration affects the result measured. On one hand, the thermocouple obstructs flow and causes heating. On the other hand, the actual measurement point of the thermocouple is in its interior. Lefstad has found through extensive calibration studies that a penetration depth into the flow of approx 0.1 mm is optimal. The technique is very sensitive to the quality of the thermocouples, and the issue of probably the greatest importance is the position of the welded connection between the dissimilar metal wires. Lefstad has observed that if the position of the connection is not in the centre of the thermocouple, temperature measurements may be several degrees in error. The connections of the thermocouples may be checked with X-ray techniques. In all extrusion runs conducted for the present study, there were two thermocouples performing replicate measurements of the temperature at the outlet of the bearing channel. This allowed a closer check of the quality of measurement. However, if all thermocouples had been improperly manufactured, there might have been systematic errors that could not be easily uncovered without careful calibration. The thermocouples were of a type that has been thoroughly tested and are regarded as the best for die outlet temperature measurements. The exact thermocouple designation was Thermocoax K 2ABi10/1500mm/TM/MDi/2AB25.NN/2m [TheW]. The diameters of the thermocouples were 1 mm. Figure 2.11 shows the principle behind the flow temperature measurement thermocouple used in the experiments.

The thermocouples were mounted at the inlet, the outlet, and in the middle of the long bearing channels. The objective was to measure not only the outlet temperature, but also the temperature increase from the inlet to the outlet. This was an ambitious task. Earlier studies have shown that the temperature increase in the bearing channel may be smaller than 20 ºC, while the measurement accuracy typically is 5 ºC [Lef93] [Wel96]. The temperature change through the bearing channel is, however, a measure of dissipation due to friction, and therefore of the friction shear stress and the pressure build-up. The latter is the subject of the present study, and it would be most useful to perform parallel measurements based on completely different principles.

2.2.2 The top disc and sensor design

The objective of introducing a separate top disc was mainly to simplify manufacturing of the pressure sensor cavity and the assembly of the capacitive probes. A detailed drawing of the top disc design is shown in Figure 2.12. In order to prevent movement of the outlet during extrusion, the connection between the die outlet insert and the top disc was designed as a moderate shrink fitting. The top disc was heated to approx 100 ºC before the parts were assembled. Dismantling required a small force to be applied at the top face of the die insert in order to push it out. Hot aluminium was allowed to penetrate into the crevice between the die outlet insert and top disc, but not farther than 5 mm.

There were three cylindrical pressure sensor cavities (with maximum diameter 10 mm). The distance from the centre of the die outlet to the centre of any of the sensor cavities

was 31 mm. The pressure sensors were intended to perform essentially equivalent measurements since this would allow the characteristics of the sensors, such as accuracy and repeatability, to be carefully studied. Geometrical considerations mainly determined the positions of the sensors. The presence of the die outlet insert prevented sensors from being positioned very close to the outlet. The sensors were placed far from the edges of the top disc in order to prevent skew deformation of the sensors. Furthermore, sensors positioned approximately midway between the die outlet and the container wall give a relatively good indication of the average die face pressure. A more detailed evaluation of the issue is given in Chapter 3. It is known that the pressure distribution at the upper die face is non-uniform during extrusion and that it changes with time [Tve97].

Undoubtedly, it would have been advantageous to mount the probes either permanently or semi-permanently to the die, for it is vital that all displacements experienced during extrusion be reversible and accurately reproduced. Examples of methods for permanent or semi-permanent connections are gluing, soldering and welding. In the fairly high temperature environment of extrusion there are a number of limitations on the use of the techniques. Appropriate agents for gluing may be difficult to find, while there is the risk that the die material may soften during heating in relation to soldering and welding. Another approach discussed in reference [Moe04d] consists of drilling a hole in the sensor surface so that a pin and a set screw fix the position of the sensor. In the current study, however, it was decided that the probes should be fastened in ways that would allow easy dismantling and subsequent reuse in dies of completely different geometries. Furthermore, the probes were not to be considerably modified so as to simplify mounting. The price of the capacitive probes was relatively high, approx 15 000 NOK a piece, and damage and replacement of sensors could not be afforded.

The challenges of designing sensors for hot environments are as much related to details as to principles. The proverb “The devil lies in the details” is for the purposes of this work 100 % accurate. It is important that the contact between the sensor and the top disc of the die be well-defined and of small extension in the extrusion direction. High extrusion pressures cause considerable compression of the entire top disc, while temperature shocks provoke thermal expansion. At the same time, the capacitive probe experiences only a moderate temperature increase and remains almost non-deformed. If the point of contact between the probe and the top disc is not well-defined, permanent deformations most probably may be observed. Strained bonds may break, and contact may slip. Since the deflection of the sensor disc only amounted to 20 to 30 μm, all unaccounted-for permanent displacements are significant. Experiments with threaded-type Capacitec probes, HPT-75 [CapW], clearly demonstrated that even a relatively fine threading did not suffice to fix the probe properly. In the current study, Capacitec probes with cylindrical casings (HPC) were used. A description of the capacitive measurement system with probes is given below. The capacitive probes were fitted into a probe holder (Figure 2.13) and then fastened tightly to the holder by either one or two set screws. Neither the holder nor the probe experienced significant mechanical loading during extrusion. However, in order to prevent the connection from loosening due to thermal expansion, the thermal expansion properties of the probe material, Inconel®, and the holder, Orvar Supreme tool steel, should be similar. Fortunately they are not too different. Most Inconel®-alloys have thermal expansion coefficients of ca 10 ppm/K.

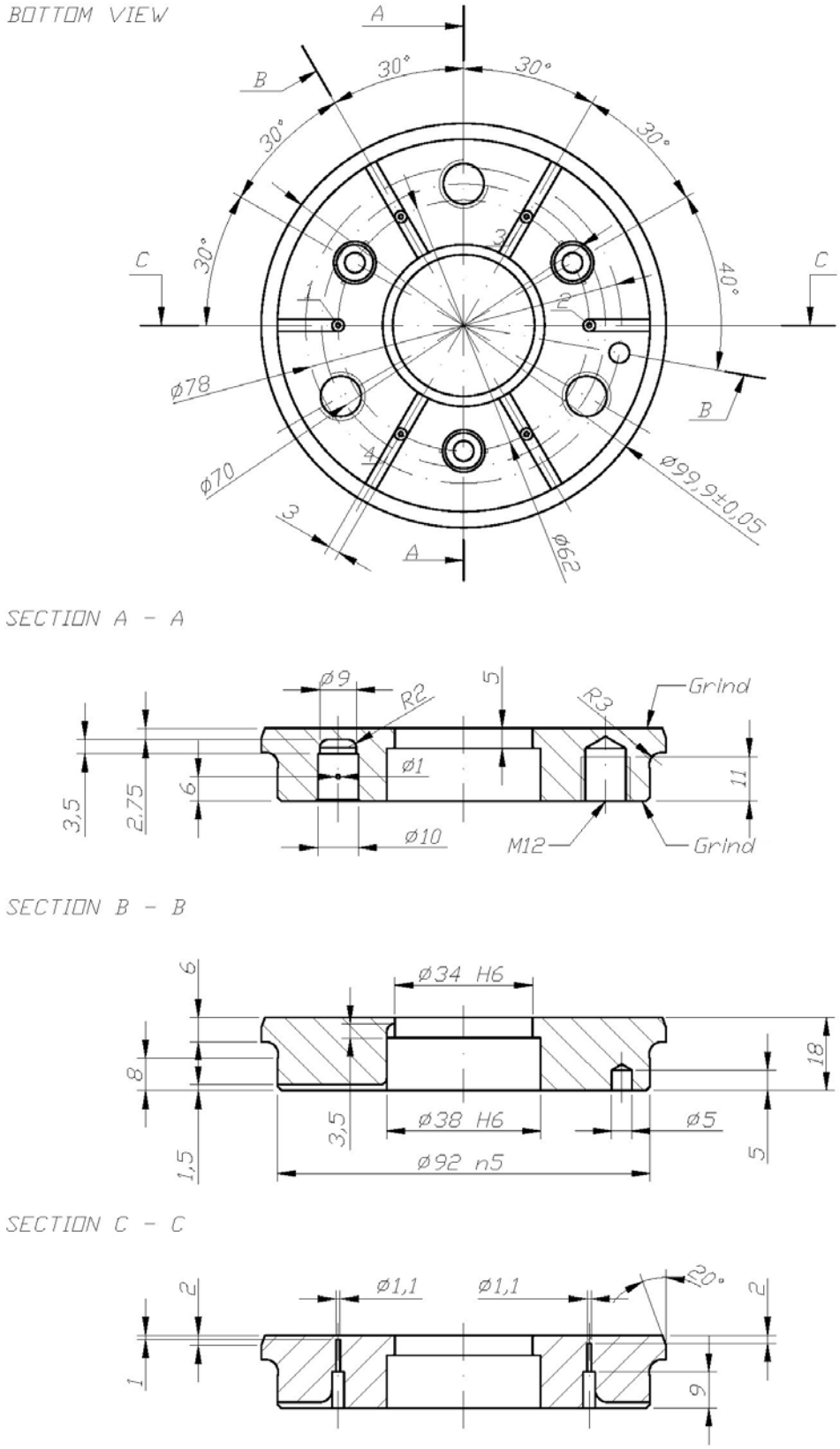

Figure 2.12. A detail drawing of the top disc design (not to scale).

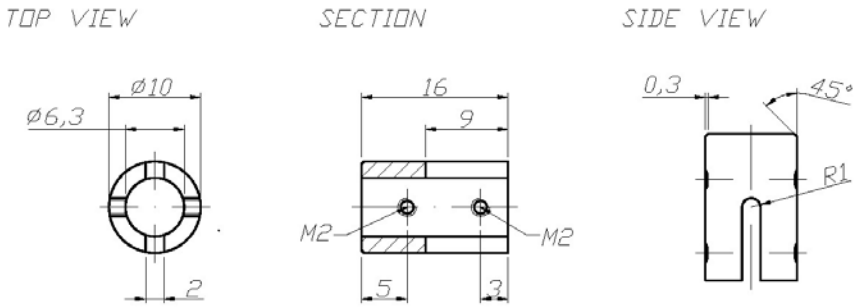

Figure 2.13. A detail drawing of the probe holder design (not to scale).

Figure 2.14. The bottom view of the top disc. A capacitive probe and two probe holders have been mounted. There are in all six holes for thermocouples. A hole for a pin has been added to prevent rotation of the disc relative to its support. The sensor holes were polished before extrusion and between each round of experiment. It was later found that this precaution was not necessary. The capacitive measurement is of an averaging kind.

Two solutions for fixing the holder to the top disc were tested (Figure 2.15):

A. A spring solution

The probe holder was fitted into the hole in the top disc and pressed toward an edge close to the sensor disc by a spring. The spring was made of a 1 mm thick Inconel® 618 filler rod, and coiled up manually with one turn approximately every 2 mm. The Inconel® material was chosen as it is designed for very high-temperature applications. The force applied by the spring was relatively small, and its actual magnitude did not seem to affect the measurement results significantly. Creep during extrusion contributed to a small permanent shortening of the length of the spring. The spring force was at no point in time so low that there was any danger of a complete loss of contact.

B. A set screw solution

An alternative and probably simpler way of mounting the probe holder is to fix it to the wall of the sensor hole with a pair of shortened set screws with dimensions of M2 (or M3). This was done when the probe had not yet been mounted. A somewhat modified Allen key was guided into the sensor hole and used to tighten the connection. In order to prevent any sliding of the parts relative to each other during pressing, the set screws were pressed into two shallow holes 1 mm in diameter that had been spark-eroded into the side of the sensor holes. The direction of both of these holes was normal to that of the sensor hole and parallel to the periphery of the top disc. There was a danger that the probe and the probe holder could rotate on an axis defined by the screws during measurement. The probe holder was, however, fitted tightly into the sensor hole (a tight slide fit). The probes were mounted in the holder after the holder had been connected to the top disc. Set screws were used also for this purpose.

Obviously, the proposed probe fastening solutions were neither perfect nor optimal. An important objective of the experiments was to test how well the different alternative designs worked in practice. The capacitive probe may more easily and accurately be mounted with set screws, but it is not at all easy to judge whether the connection stays tight after the sensor parts have been heated to 400 ºC. One way of securing a proper connection is to use screws of a material that expands more than the die steel when heated. It would have been most useful if the screws could be fitted into small holes or grooves in the casing of the capacitive probe. During tightening of the connection with set screws, some plastic modification of the casing occurred. As for the sensor response, it is evident that a capacitive probe mounted by set screws observes a larger deformation than a probe fastened by a spring as shown in Figure 2.15, since it also registers a larger part of the elastic deformation of the top disc. A disadvantage is that the measurement is at the same time less local [Moe04c]. The sensor responds to any load causing a general deformation of the top disc, even if the load applied directly at the surface of the sensor disc is zero. While it would be easier to devise a solution for mounting the probes close to the bottom face of the die outlet [Yon87], it was believed that it was important to minimise the effect of the overall top disc deformation. For that reason, the connection points were placed as deep into the sensor hole as possible. A similar, but somewhat more refined solution has been devised by Yoneyama et al [Yon93].

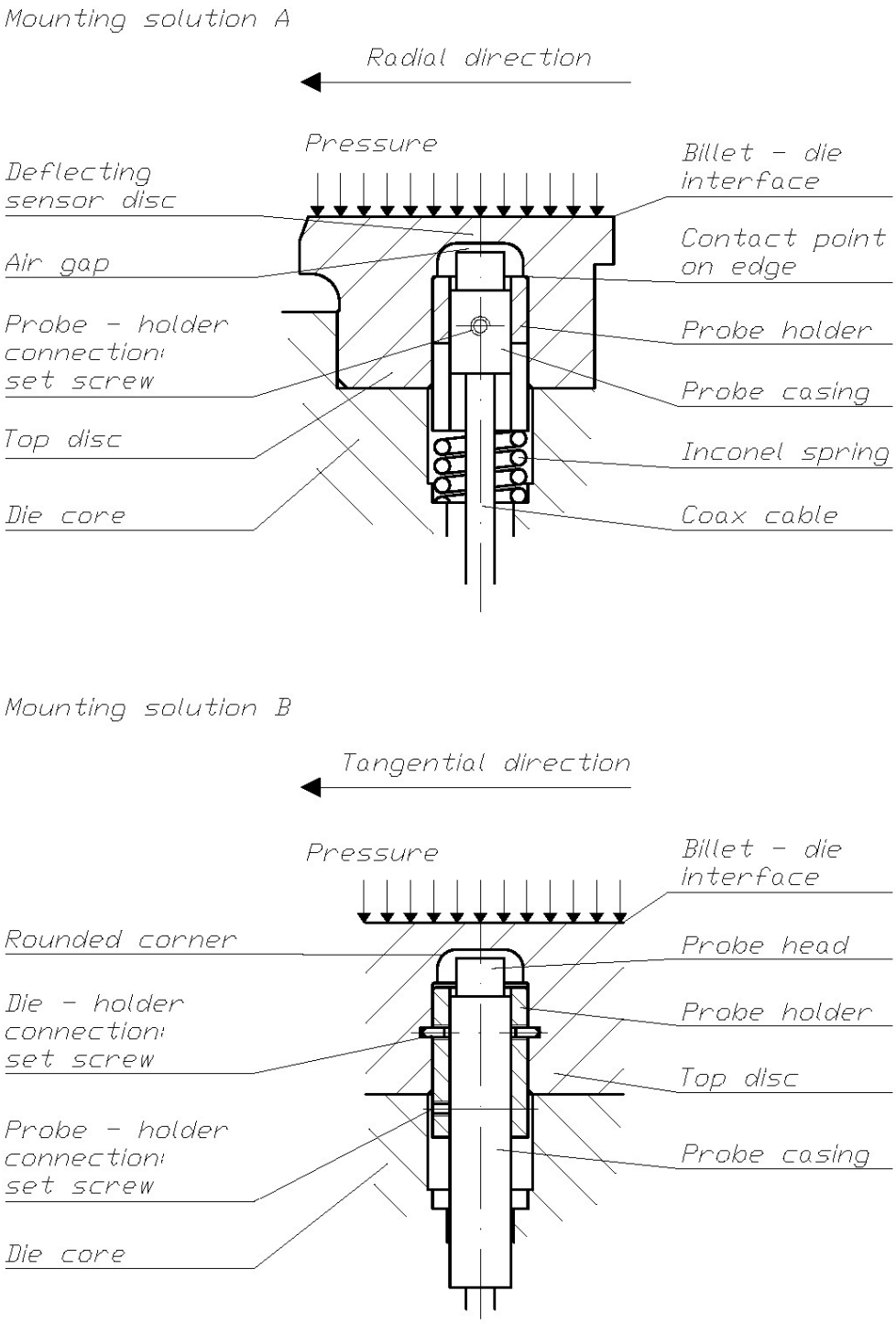

Figure 2.15. Two solutions for fixing the holder to the top disc of the die.

During extrusion, the pressure sensors experienced sudden temperature increases. As a result, the die material expanded, and there was an upwards bulging of the sensor plate as it became hotter than the surrounding sensor and die material. Since the temperature field is of a transient nature, the capacitive probe stayed colder and expanded less than the surrounding material. It would be possible in principle to design a capacitive sensor

that automatically compensates for thermal expansion effect [Pin96]. Two capacitive sensors could, for example, be used simultaneously. One of them could measure the die face pressure and temperature shock, while the other sensor should be affected only by the temperature shock. An alternative approach would be to use two sensors to measure the pressure. The sensors should, however, to different extents, be affected by the temperature increase. The sensor solutions used in the current study in fact allowed such compensation. However, the deformations of the sensor discs during extrusion were quite small, and the accuracy of the methods for compensation was therefore limited.

An alternative approach for temperature compensation is based upon continuous die face temperature measurements. In all, five thermocouples were mounted in the top disc shown in Figure 2.10. Measurements were performed at nominal distances from the die face of 1, 2, 3 and 4 mm as well as at the bottom face of the top disc. The reason for performing multiple measurements was to allow for the determination of the surface temperature and heat flux. It must be admitted that the accuracy of such estimates was limited. First, even though the thermocouple holes were manufactured by spark erosion, which is more accurate than drilling, the depths deviated somewhat from the nominal values, typically by more than 0.1 mm. This was mainly due to the use of inappropriate electrodes. For reasons that need not to be further discussed, it was not easy at the time to use better alternatives of manufacturing. Second, it is hard to secure and control the positioning of the thermocouples in the holes. No solder was added to secure proper contact. Instead, thermocouples were forced towards the bottom of the hole and fastened by strips welded to the bottom face of the top disc. As long as there was proper contact between the thermocouple tip and the die, measurement results were acceptable. A loss of contact affected results significantly. There are techniques that allow much better estimation of heat fluxes [Ber99]. These usually require that a plug be mounted in the surface of the die. Since the objective of the study was not primarily to measure temperatures, but rather forces, one could not defend adding further complexity to the die design. As will be shown, the temperature measurements performed were in fact quite useful for assessing temperature compensation schemes for the pressure sensors.

The pressure sensor holes were manufactured in three steps. Holes of 9 and 7 mm in diameter were drilled to sufficiently large depths. Then, specially designed electrodes were used to spark-erode the desired shape of the holes. The surfaces were made as smooth as possible. Finally, the bottom surfaces of the sensor discs were finely polished. The last operation was a manual one, but a drill press was used for the purpose so that surfaces would be as flat as possible. Although tight tolerances of ± 0.02 mm were initially set with regard to the dimensions of the sensor holes, it is doubtful that all dimensions need to be this accurately manufactured. The sensor response is determined by the shape of the sensor, but careful calibration must in any case be performed for each of the sensors before they are used. Inaccurate machining of the sensor disc may be accepted as long as the sensor produces a repeatable signal, whose linear response may accurately be determined. The most important tolerances were those of the sensor hole – probe holder fitting. The diameters of the probe holders were therefore carefully tuned until a tight sliding fit was obtained. It was also important to accurately control the position of the point of contact between the die and the holder. When using the spring solution the holder was pressed towards an edge of the sensor hole. Yet, it was almost

impossible to secure contact along the whole circumference of this edge. Both the surface of the holder and the edge were probably skew, and when the die and the sensors were deformed, the point of contact may have changed. Therefore, the die holders were manufactured with pivots that enforced only local contact (not shown in Figure 2.13). Given the limitations of machining accuracy, it is quite possible that only one pivot was in contact at a time. Additionally, the design for fastening with set screws may have been of accuracy significantly poorer than ± 0.02 mm. Practical experiments had to be performed in order to determine whether the sensors worked properly. The solutions presented here were admittedly of the simplest kind, but they were possible to manufacture in the not so well-equipped tool shops of NTNU and SINTEF. Simplicity is a virtue in relation to sensor design, especially when there are space limitations. There are, however, reasons why it is worthwhile to develop a more complex sensor designs.

2.2.3 The container liner load cell

No lubrication is usually used during aluminium extrusion to avoid contamination of the material and undesirable flow patterns. Thus, a significant part of the ram force was applied merely to overcome the friction between the billet and the container. Usually it is assumed that there is a state of full sticking, i.e. zero relative velocity at the boundary, and shear stresses at the interface are determined by the flow stress of the material. The shear stresses are typically in the range form 15 to 25 MPa, depending on the ram speed, the temperature, the material and the tool dimensions. For a container of diameter D = 100 mm and a billet length L = 200 mm, the total liner force F_c may approximately be:

$$F_c = \tau_c \cdot (\pi DL) = 20 \text{ MPa} \cdot (\pi \cdot 100 \text{ mm} \cdot 200 \text{ mm}) = 1257 \text{ kN} \qquad (2.2)$$

It is assumed that the constant shear stress, τ_c, acts at the entire interface between the billet and the container, which need not be entirely correct. Experiments showed that the maximum container or liner force easily exceeded 1000 kN. As a comparison, the total extrusion force may initially be approximately 3000 kN. The ram force is the sum of the liner force and the force exerted at the upper die face. In addition, there may be small contributions from friction at the die outlet (≈10 kN) and friction between the ram and the container (≈50 kN). The last component may in fact be regarded as a part of the liner force. As the billet length decreases during extrusion, the ram and liner forces decrease. When extrusion ends, the length of the butt end may be only 10 % of the initial billet length. The liner force has then similarly decreased. In order to keep the container in position, an additional force smaller than 200 kN was exerted at the top face of the container by two hydraulic cylinders.

Since the flanges of the die are of limited size, the contact pressure between the liner and the die, p_c, is of considerable magnitude. In the present case, the force of 1257 kN caused axial compressive stresses of almost 200 MPa. In Equation (2.3), D_o is the outer diameter of the area that is loaded, and D_i is the inner diameter.

$$p = \frac{4 \cdot F_c}{\pi \left(D_o^2 - D_i^2 \right)} = \tau_c \frac{4 \cdot DL}{D_o^2 - D_i^2} = \frac{4 \cdot 1257 \text{ kN}}{\pi \cdot \left(139.7^2 - 104^2 \right) \text{mm}^2} = 184 \text{ MPa} \qquad (2.3)$$

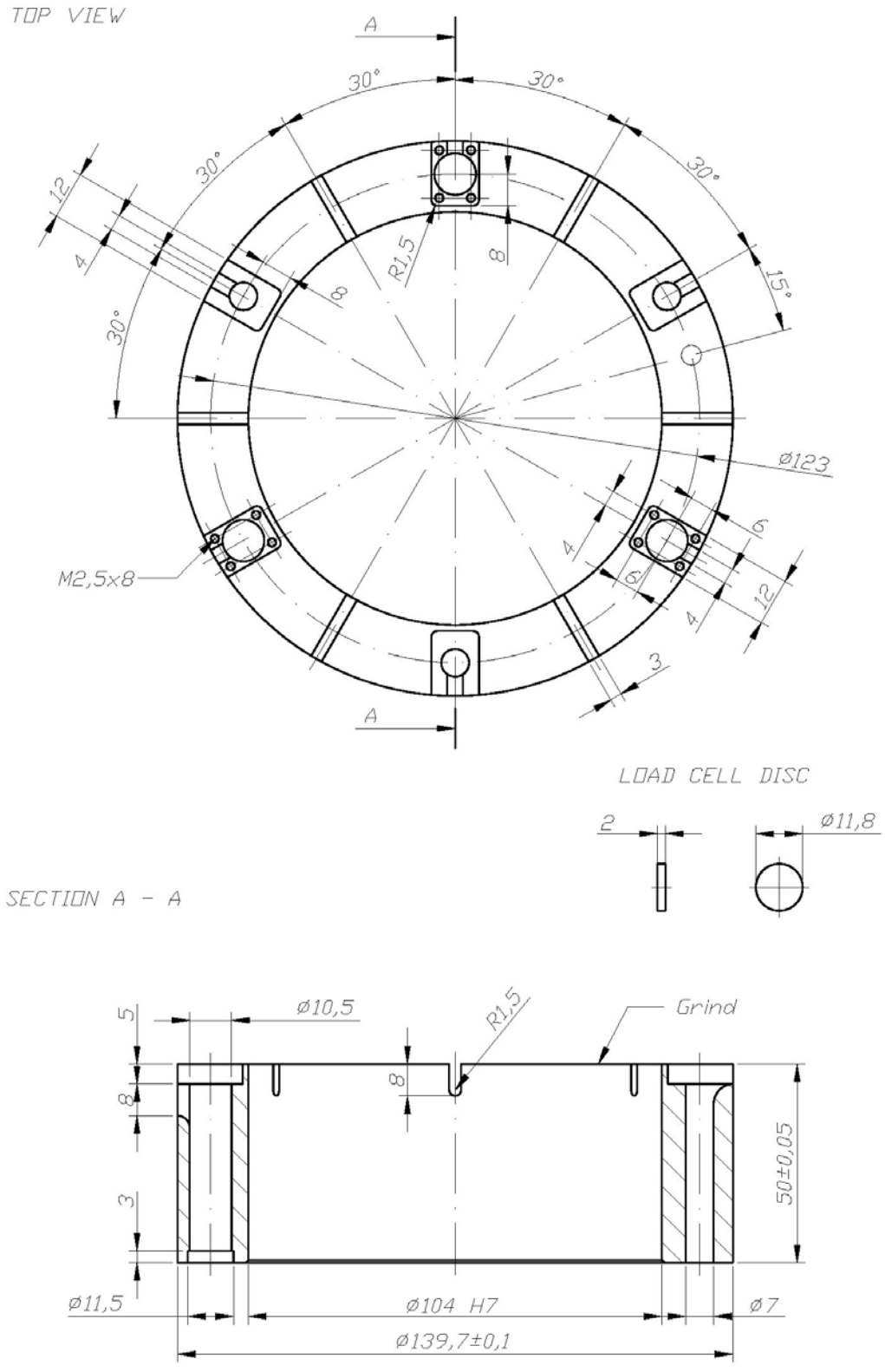

Figure 2.16. A detail drawing of the liner load cell with load cell discs (not to scale).

The current study focuses on the measurement of local values of die face pressure rather than global measurement of the liner force. However, since the ram force is known, measurements of liner force also reveal the total force applied at the upper face of the die. The die face force is the integral of the pressure at the die face. This force may also be measured directly with a load cell placed beneath the die, but this is not possible with the die designs used thus far in the SINTEF extrusion press. The reason is that the dies are exposed to both the die face and liner forces. A solution to this problem would be to mount the container on a set of pillars connected directly to either the bolster or the press table. This would not only render possible direct measurement of the die face force, but also the direct measurement of the container or liner force by an independent system. Such a system for liner force measurement has been devised and is in use for example at the Technical University of Berlin [TubW]. It has the potential of being extremely accurate, since very large and easily measurable elastic deformations may be achieved (> 0.1 mm), and since temperatures are not too high and change only to a very small extent. It would then be possible to use almost any available type of displacement measurement principle.

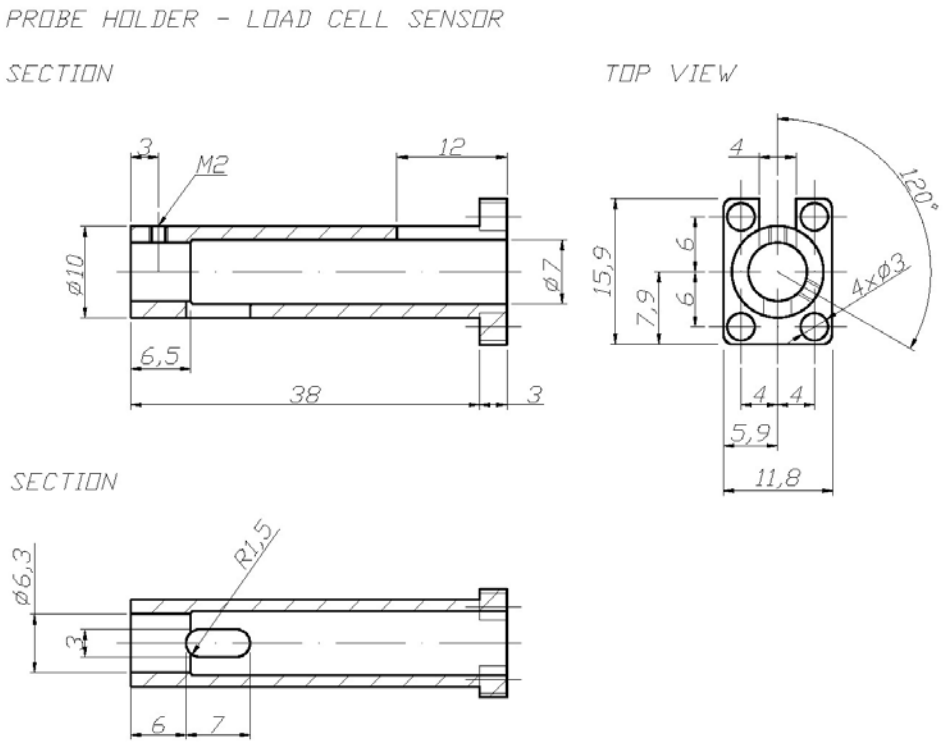

Figure 2.17. A detail drawing of liner load cell probe holder (not to scale).

The possibility of developing an external liner force measurement system was seriously considered. Such a system would undeniably have been a great help in the study of pressure sensor characteristics. However, significant changes to the set-up of the SINTEF extrusion press would have been necessary, and there were neither sufficient resources nor time for development. Focus would have been diverted from the pressure sensor design. Therefore, a slightly simpler but also less satisfactory solution was chosen. A liner load cell was integrated in the design of the extrusion die. This was

achieved by splitting the die into two parts, a die core and a surrounding load cell ring. The load cell is only affected by the load applied by the liner and not by the load at the top of the die face. At the same time, it is important that the cell be neither bent nor sheared, but rather experiences pure compressive deformation. As will be discussed in relation to calibration, these requirements were not at all trivial to achieve.

The load cell design is shown in Figure 2.16. The load cell was completely penetrated in the length direction by six holes in all. Three of these were for the cables of the pressure sensors in the top disc. The other three were for the probe holders shown in Figure 2.17 and for capacitive probes that measure displacement due to the compression of the load cell ring. The probes were of the same type as those used in the die face pressure sensors. The total height of the load cell was determined by the requirements of the measurement system. Capacitive sensors are potentially extremely accurate, but in the very harsh environment of the extrusion process it is by no means easy to distinguish noise from the pressure responses that cause deformations of 1 μm. Therefore, a full range of 25 to 30 μm should be regarded as a minimum requirement. A simplified expression for the total compression of the load cell during measurement is given by:

$$\begin{aligned}\Delta L_L &= \frac{4 \cdot F_c \cdot L_L}{\pi E\left(\left(D_{Lo}^2 - D_{Li}^2\right) - 3 \cdot D_{Ao}^2 - 3 \cdot D_{Bo}^2\right)} \\ &= \frac{4 \cdot 1257\ \text{kN} \cdot 42\ \text{mm}}{\pi \cdot 180\ \text{GPa} \cdot \left(\left(139.7^2 - 104^2\right) - 3 \cdot 10.5^2 - 3 \cdot 7^2\right)\text{mm}^2} = 45.4\ \mu\text{m}\end{aligned} \qquad (2.4)$$

L_L is the length of the measurement part of the load cell. ΔL_L is the change of the length and the response to be measured. F_c is again the liner force. E is the modulus of elasticity of steel at approximately 400 ºC while D_{Lo} and D_{Li} are the outer and inner diameters of the load cell. D_{Ao} and D_{Bo} are the diameters of the holes in the load cell. The actual response of the cell to a force of 1257 kN may have deviated from the value given above, since the deformation of the load cell was not completely uniform. The issue is treated in relation to the discussion on calibration of the load cell (Chapter 4). Another important issue treated in the numerical analysis of the sensor response relates to whether there was any contact between the die core and load cell during deformation. Such contact should, as much as possible, be avoided since it may disturb or complicate measurements. The load cell was designed so that it was in contact with the die core only close to the lowermost face of the cell. A fairly tight fitting prevented movement in the directions normal to that of extrusion. If the gap between the inner wall of the load cell and the outer wall of the die core is not sufficiently large, the cell may bend or shear and make contact with the die core. This was avoided with the current die design. Shearing effects were generally small.

The load cell disc of Figure 2.16 plugged the bottom of the load cell hole and worked as the second plate of the capacitor of the measurement system. It is important that there are no permanent displacements of the disc during measurement. If the disc is not properly mounted, it may displace when the load cell deforms. In the current study, the disc was shrunk-fit into the hole in the load cell. The disc solution was chosen mainly

because it was simple to manufacture. An alternative would have been to let the disc be a part of the load cell, and to spark-erode the geometry in the bottom of the hole. Both solutions may work, but the latter is probably the best and the safest. It is usually best to make sensors out of as few pieces of material as possible.

Each of the probe holders was fastened by four screws to the upper part of the load cell. There was no contact between the probe holders and the walls of the holes in the load cell into which they were initially fitted. The probe holders were not deformed during experiments. They may tilt somewhat during measurement.

2.2.4 The die core

The die core was a support tool rather than a die. Its main purpose was to keep the die outlet and top disc in position. Figure 2.19 shows the design. Extrusion dies for the SINTEF press are usually about 50 to 60 mm tall. The complex die used in the current study was 85 mm in total. It was made taller partially because there then would be more space between the container and the bolster to the pressure and thermocouple cables. Another reason was related to the requirements for the load cell design described above.

The geometry of the die core was, to a large extent, determined by the geometry of the surrounding parts. However, relatively few limitations were imposed on the design of the connection between the die core and the liner load cell. An alternative to the die design that was used in experiments was one with a quite simple cylindrical die core and a surrounding tall cylindrical load cell. The advantages of this solution are that it probably would be simpler to manufacture and that the load cell deformation may be larger. An advantage of the core design used in the current study was that the die was kept firmly in place by the container.

The top disc was fastened to the die core by three bolts with dimensions of M12. The reason for doing so was to prevent the top disc from being pulled off the core when the ram retracts after an extrusion run. The ratio between the die face surface and the cross-sectional surfaces of the bolts is given by Equation (2.5).

$$r = \frac{D_{To}^2 - D_{Ti}^2}{3 \cdot D_B^2} = \frac{100^2 - 11.2^2}{3 \cdot 11^2} = 27.2 \qquad (2.5)$$

D_{To} and D_{Ti} are the outer and inner diameters of the top disc and die insert while D_B is the approximate effective load carrying diameter of the bolts. If the material has a yield stress of 550 MPa, tensile stresses higher than 20 MPa cannot be not tolerated. Loads should be kept even lower, as there are stress concentrations in the threaded part of the bolt. At the same time, the elastic deformation of the bolts is significant:

$$\Delta L_B = \frac{\sigma_B}{E} L_B = \frac{550 MPa}{174 GPa} \cdot 53 mm = 0.17 mm \qquad (2.6)$$

It is absolutely necessary that the front end of the ram be lubricated during extrusion so that it may be easily pulled off the butt end after extrusion. Furthermore, great care must

be taken when the ram is retracted. It would probably also be advantageous not to remove the butt end between runs, but rather to extrude in a billet-to-billet manner. If the billet sticks to the ram, bolts may be permanently deformed and loosen. In the worst case, bolts may rupture. An additional problem is that the top disc and the die core are in practice connected by some sort of a spring connection. When the discard is released from either the top disc or the ram, the connection is closed abruptly and the sensors are shaken. This has to be taken into account when designing sensors. The result of the shaking related to the pulling-off of the butt ends was usually merely a slight movement of the zero-point for measurement. In one case, however, the probe also loosened.

The situation described above was obviously not desirable. The fact that there was an easily detectable mechanism that could have caused sensor failure indicates that there is much room for improvement of the sensor and die designs. An important measure that was stressed in the existing design was that the sensors must be fastened to the top disc and not to the die core. The spring solution may work properly only as long as the spring is stiff and there is no loosening of the connection with the top disc. Further steps may be to make the sensors smaller and more compact. The top disc may also be fastened in a more appropriate way by a die ring. Ideally, the composite design should be dropped completely and insert sensors should only be pushed into small cavities in the die surface and fixed tightly. In any case, the sensor response should in no way be dependent on the more general deformation of the die, whether it occurs during extrusion or after. The extrusion environment is very demanding, but not to such an extent that sensors may not be expected to work there. Although the die and pressure sensor designs were imperfect and should not be used in an industrial environment without modification, the designs were regarded as suitable for demonstration of the feasibility of measurement and for a study of flow and friction during extrusion. It is much simpler to take the necessary precautions in a laboratory environment than in an industrial one. During extrusion experiments no catastrophic failures occurred.

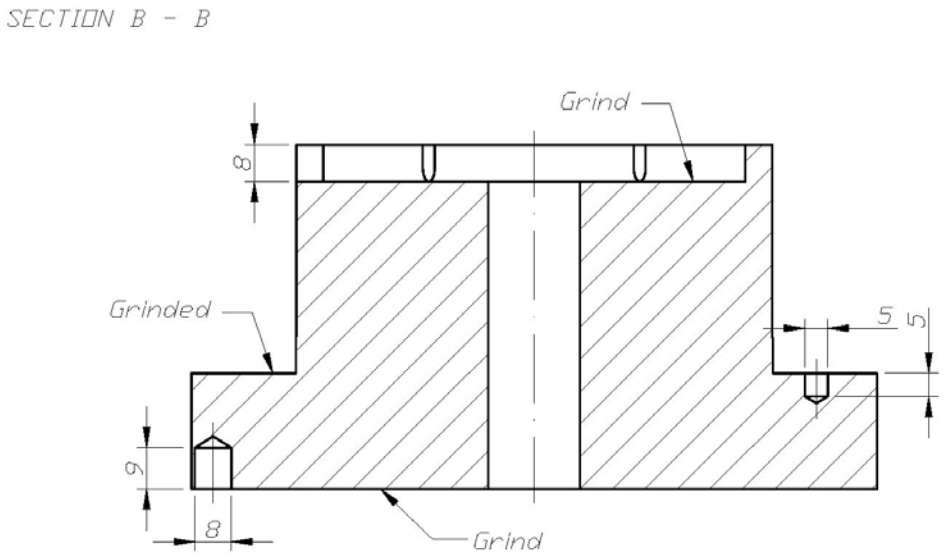

Figure 2.18. A detail drawing of the die core design (not to scale).

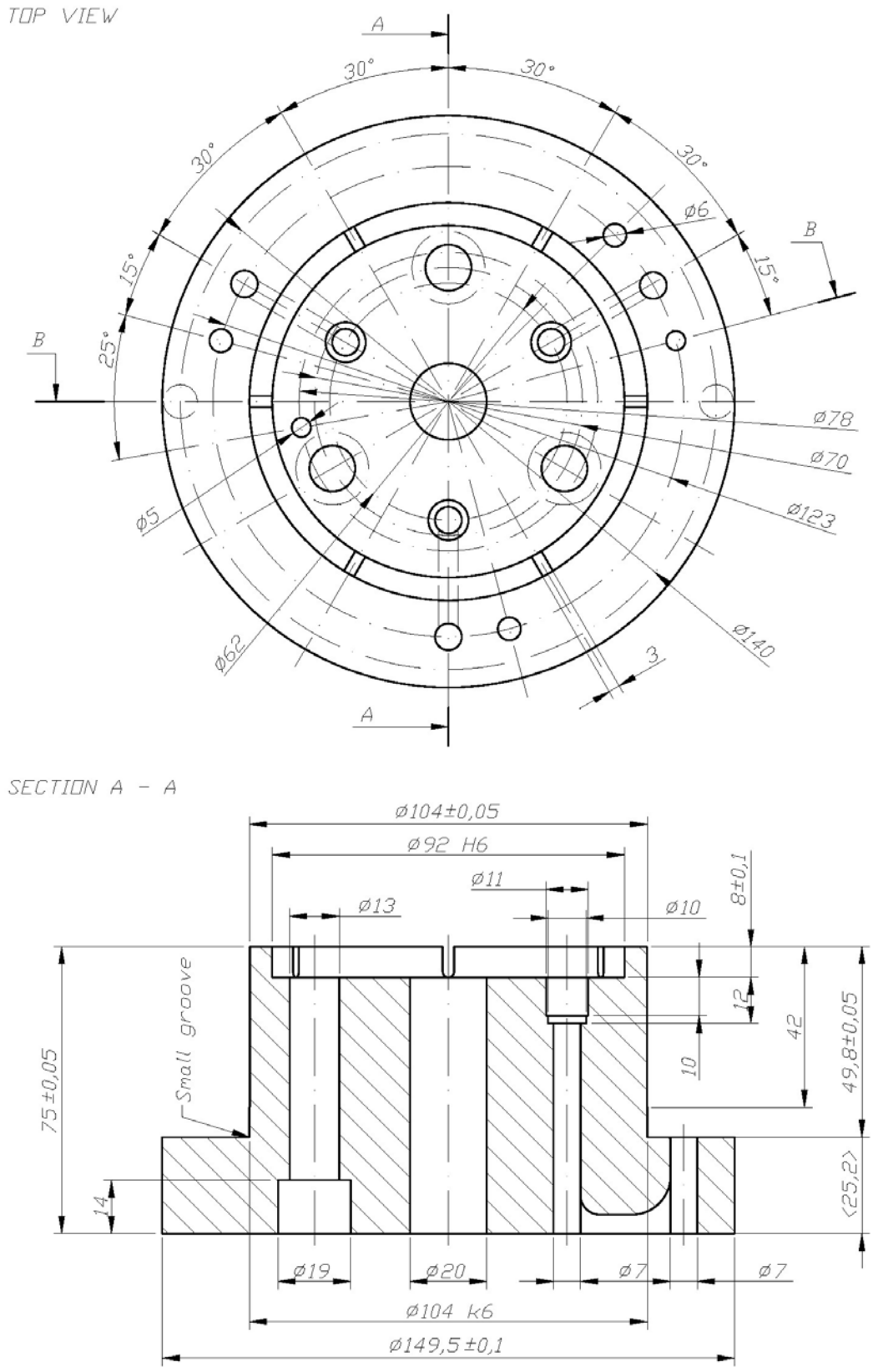

Figure 2.19. A detail drawing of the die core design (not to scale).

2.2.5 Assembly

Figure 2.21 shows the bottom face of a partly assembled die, and Figure 2.20 shows the top side. The top disc was tightly fitted into the die core and the connection was closed by tightening the bolts. After extrusion a certain force was applied to the bolts in order to loosen the connection between the parts. The connection between the die core and the load cell was also tight, but as indicated, only the lowermost part of the load cell was in contact with the die core. A small hydraulic press was used to mount the liner load cell. After it had been positioned it was neither a trivial undertaking nor in fact necessary to dismantle it. The probes and probe holders could be placed in the liner load cell after the load cell had been mounted. The positions of the liner load cell probes could even be corrected between extrusion runs, but this was seldom done.

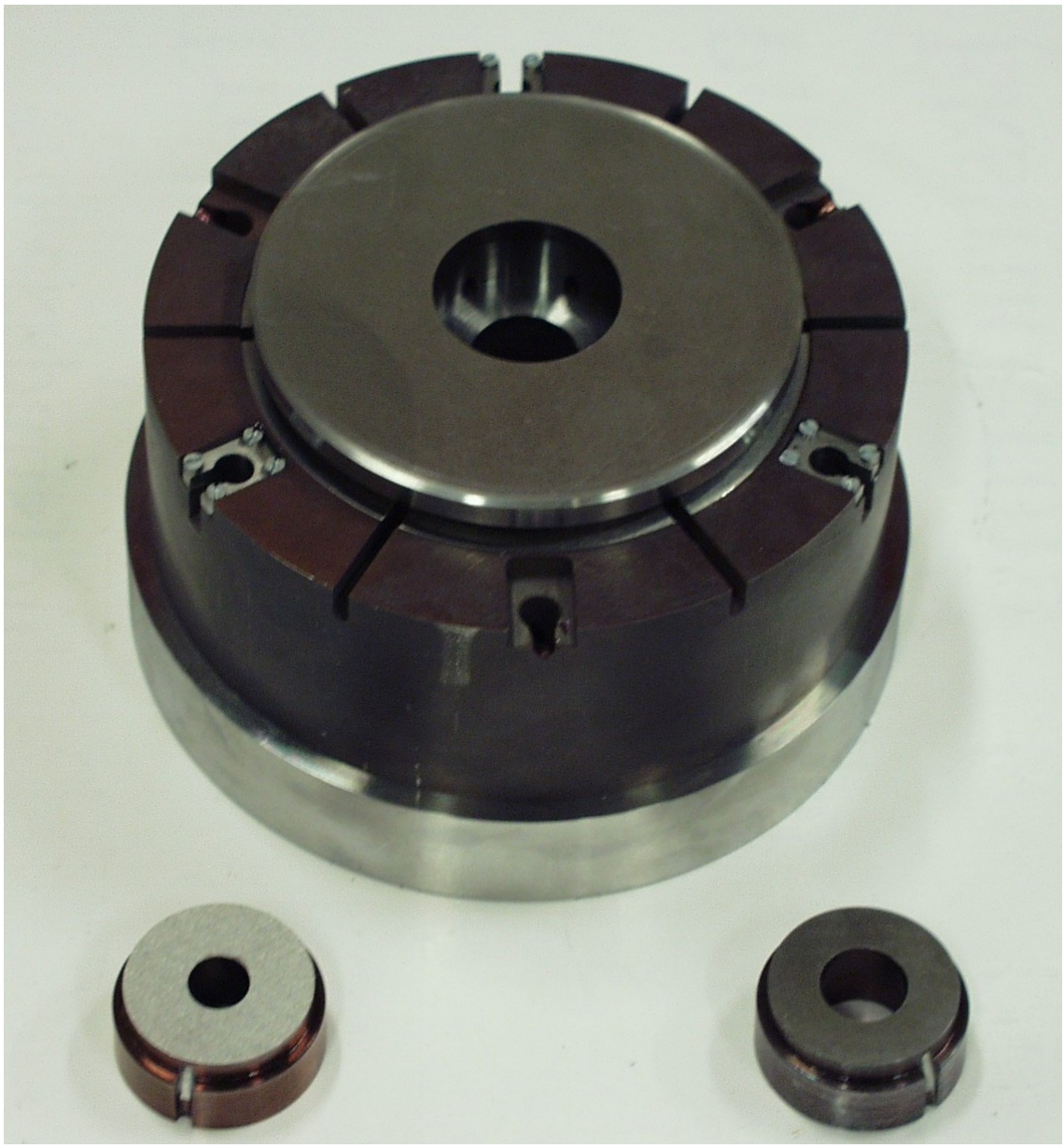

Figure 2.20. Top view of the complex extrusion die with two of the die outlets.

The capacitive probes of the die face pressure sensors were placed deep inside the die during experiments. No method that allows easy correction of the position of the probes during experiment had been devised. If the sensors did not work properly, and if it was believed that improper mounting was the cause, the experiment had to be discontinued. The die had to be removed from the tool stack and allowed to cool for some hours. Then the top disc had to be dismantled before corrections could be made. It was of great importance that there be a sufficient clearance between the probes and the holes in the die core. If the probes come into contact with the die core during assembly of the top disc and the core, they may loosen and stop working properly. The holes in the die core were first 7 mm in diameter, but were later enlarged by 0.5 mm to allow more secure mounting. The outer diameter of the casing of the capacitive probes was 6.4 mm. The reason the holes were not made larger in the first place was that the design needed to meet the requirements of the spring fastening solution for the probes. In later designs, the holes should be made wider in order to simplify the assembly of the die. All sensor responses were tested after assembly and prior to the insertion of the die into the press. In order to check if the probes worked properly, tests were also performed after the die had been inserted into the die and before heating.

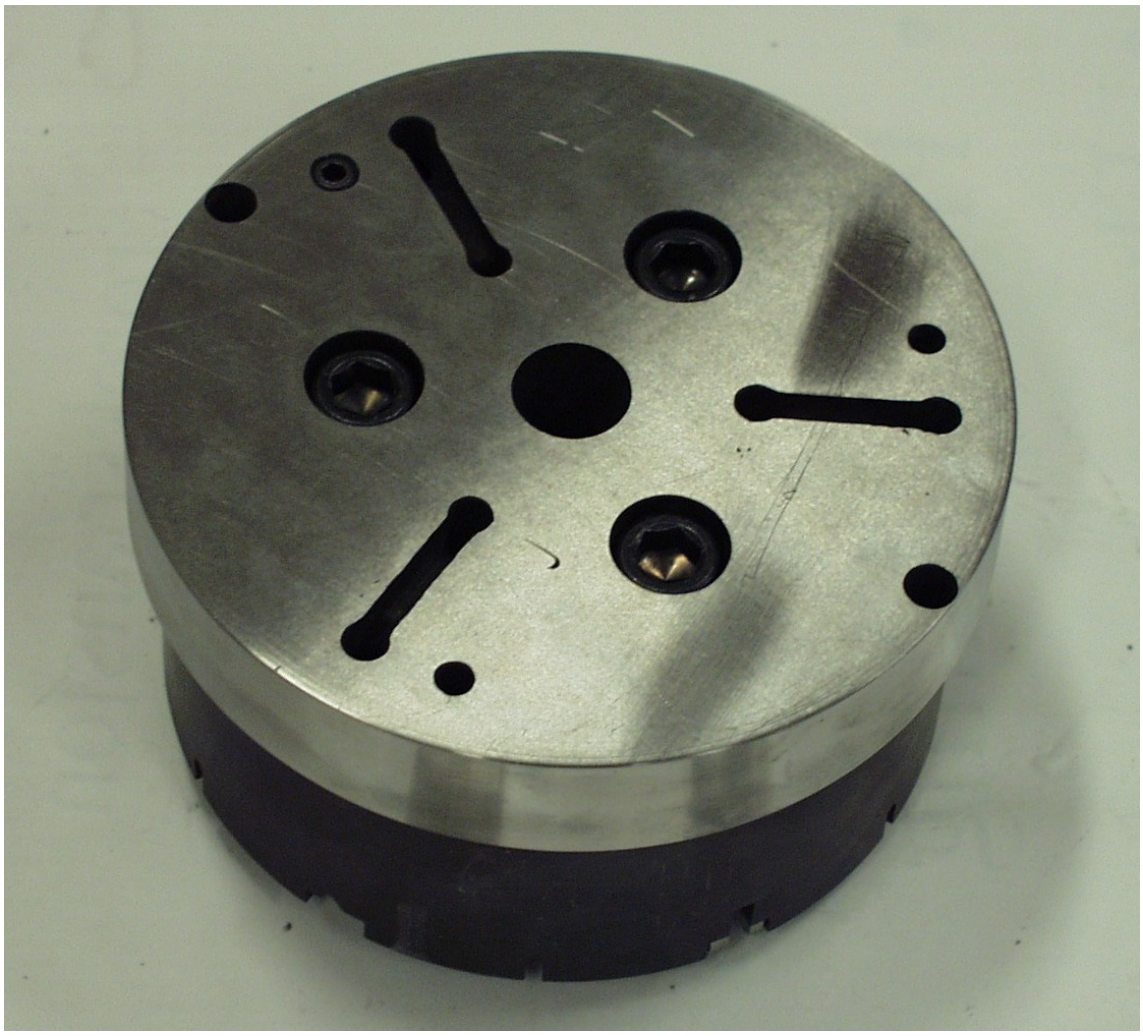

Figure 2.21. Bottom view of the complex rod extrusion die.

2.3 Capacitive pressure measurement system

2.3.1 The fundamentals of capacitive measurement

The fundamental physical mechanism that makes capacitive displacement measurement possible is expressed by the law of Coulomb for two point charges:

$$F = \frac{Q_1 Q_2}{4\pi\varepsilon_o \varepsilon_r r^2} \tag{2.7}$$

Between any two charges Q_1 and Q_2 a force F acts. If the sign of the charges are of opposite kind, the force attempts to bring the charges closer together. If the charges are of the same kind, they repel each other. The larger the distance, r, between the charges, the smaller is the force. The fundamental physical constant of the system is the permittivity. ε_0 is the permittivity of vacuum ($8.854 \cdot 10^{-12}$ F/m). ε_r is a relative number (relative permittivity or relative dielectric constant) characterising the properties of the material filling the space between the charged particles. The relative dielectric constant for air is usually close to 1. Most dry materials have values in the range from 2 to 10 while it may be much larger for some liquids. Proper use of Coulomb's law in relation to the study of capacitive sensors may be made if the law is properly reformulated.

In order to bring two particles of the same charge from infinity into a configuration where they occupy positions at a finite distance from each other, work must be done. As long as they remain in these positions, energy is conserved in the system. The same is the case if charges of opposite sign are deliberately kept apart by a force. If a new particle of positive or negative charge is introduced, it is attracted to one of the old charges and repelled from the other. If it is kept in place by a force, it has the potential to do work. The voltage, V, is an expression of the electric potential. The gradient of the voltage is the electric field, **E**. **n** is a differential element perpendicular to the equipotential surface. When a particle moves along an equipotential surface, no work needs to be done, since the force is acting in a direction normal to that of the movement.

$$\mathbf{E} = -\nabla V = -\frac{dV}{d\mathbf{n}} \text{ or } V_{ab} = \int_a^b -\mathbf{E} d\mathbf{n} \tag{2.8}$$

Coulomb's law assumes that there are point charges, while in reality electric conductors may have very different shapes. Still, it may be used to evaluate the energy of a system, but the principle of superposition must be used. A more refined concept is expressed through Maxwell's equations [Sva89]. There are in all four equations describing the interaction between electric and magnetic fields. High-frequency wave phenomena may require a solution of the complete system of equations. However, when relatively low frequency problems such as that of determining the essentially quasi-stationary electric field surrounding a capacitive measurement systems are evaluated, only one of the equations need to be evaluated, namely Gauss' law (the other of Maxwell's equations, being of general validity, must also be satisfied, at least in an approximate manner).

$$div(\mathbf{D}) = \rho \text{ or } \oiint \mathbf{D}\ \mathbf{n} dA = Q \tag{2.9}$$

Gauss' law states that there are electric monopoles with total charge Q (charge density ρ) and further, that there is such a thing as a displacement current emanating from it. The displacement current is related to the electric field **E** by a constitutive equation. If the material has a high dielectric constant, which is typically the case for materials containing electric dipoles, the displacement current is large. It is often assumed that a purely linear relationship may describe this observation, $\mathbf{D} = \varepsilon_r \cdot \varepsilon_0 \mathbf{E}$. The vector **n** is the normal to the surface, over which the integral of the displacement current is calculated.

Gauss' law is extraordinarily well suited for both analytical and numerical solution. It is the archetypical elliptic equation. If the equation is solved for a domain with a zero charge density, it is denoted Poisson's equation. If the charge density is zero, which is usually the case for the air region surrounding the charges, it is equal to the Laplace's equation. This is evident when the electric potential V is introduced, as one then may simply write $\nabla^2 V = 0$. The boundary conditions of the simplest kind consider only the potential of bodies (i.e. work that has been done to put them in a certain configuration). In the case of the example of two charged particles, only the charges of the particles are known and the potential difference must be determined by analysing the geometry of the system. In the case of an electrical circuit, however, it is in fact both in principle and in practice possible to define the voltages of the capacitor plates. The analysis of the electric field distribution then reveals the charge density of the plates and in air and the energy stored in the complete system.

In reality, the most interesting value to deduce is the capacitance, which describes how a certain capacitor configuration responds if either a voltage or a charge is applied. The capacitance is defined as the ratio between the charges of two bodies and the potential difference between them, $C = Q/V$. Stated differently, it is a measure of a system's ability to store energy, E:

$$E = \frac{1}{2} C V^2 = \frac{1}{2} \frac{Q^2}{C} \tag{2.10}$$

An example of great relevance to the current study is the case of two wide plates of surface area A separated by a gap of width d. An exact analytical deduction may not be performed, but since the plates are wide and the electric field is most concentrated in the gap between them, an approximation may prove to be fully adequate for a number of purposes. The approximate relation is:

$$C = \varepsilon_0 \varepsilon_r \frac{A}{d} \tag{2.11}$$

More accurate deductions of the capacitance of sensor system of relevance are presented below in relation to calibration techniques. When the distance between the discs is very large, the electric field between the capacitor plates is less uniform. The stray field

outside the capacitor is then more important, and a change of plate distance no longer causes a proportional change of capacitance.

There are three mechanisms of the capacitive principle of displacement measurement. If the capacitor plates are brought closer together, the sensor capacitance increases. The same effect is obtained if surfaces areas of the plates are made larger (overlaps to a larger extent). Finally, it is also possible to change the medium occupying the gap between the sensor discs so that the dielectric constant changes. In the current study, only the first mechanism is used. If the potential difference is kept constant, a decrease in the distance between the capacitor plates and an increase in the capacitance cause an increase in the energy of the system. At the same time, the charge density of the capacitor plates increases (and a current must flow). If the plates have fixed charges of opposite signs, both the voltage and the energy of the system decrease as the plates are brought closer together. They attract each other and may at the same time do work.

Measurement is usually a conversion of energy. Sensors usually consist of transducers, which convert signals of different natures. In the case of pressure measurement on the extrusion process a force is applied at the surface of the die, a disc deforms and causes a distortion of the electrical field of a capacitor and a change of the energy stored by it. The changes may cause a current to run in an electrical circuit or more commonly a modulation of a current already running in the system. Then, the signal is processed and usually digitalised so that the information it contains may be stored in the memory of a computer. Further conversion of energy occurs as the results from measurements are processed by a researcher, published and read by an audience. The remaining part of this subsection treats mainly the signal conditioning part of the system.

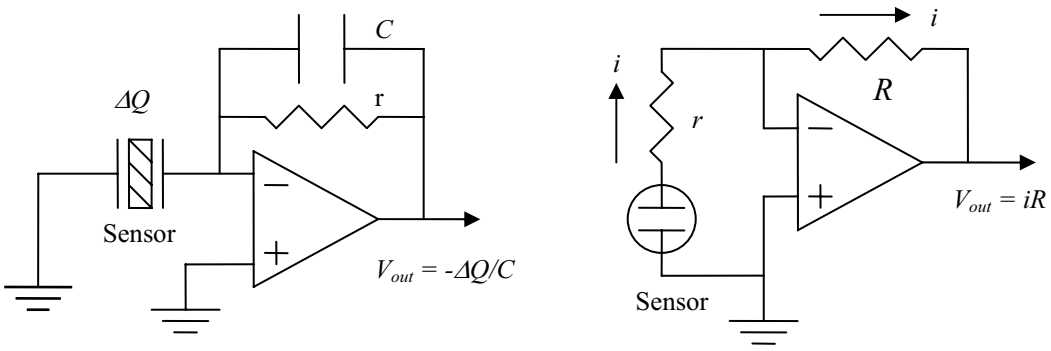

Figure 2.22. Charge amplifier designs used in piezoelectric sensors [Fra96].

Sensors or transducers are essentially of two kinds. Some are passive, which means that they need no external power to work. Piezoelectric sensors, which for some purposes are belonging to a subcategory of capacitive sensors, may be of this type. When a force is applied, capacitor plates placed at both sides of the piezoelectric material are charged. The effect is related to an orientation or a polarization of the material structure upon loading. In order to generate a useful measurement signal, charge amplifiers may be used. Some basic and imperfect designs are shown in Figure 2.22. One should realise that when there is a change in the charge of the capacitor plates there must also be a current flow in the system. A resistor may be used to convert the current signal to a

voltage signal. Very small currents may flow so the resistor should be a large one. When piezoelectric pressure sensors are used as described they detect changes in load rather than absolute levels.

The second group of sensors consists of active ones that require external power to work. An excitation signal is applied, and the transducers modify the signal when they respond to an external load. This is usually the way capacitive pressure sensors work. The excitation signal may be a constant voltage, a constant current, sinusoidal or pulsing currents. The simplest design is that of the direct DC circuit (Figure 2.23). A voltage V is applied so that there is a large charge Q on each of the capacitor plates. The resistance R is made so large that the magnitude of the charges of the capacitor plates does not significantly change during measurement. Then, as the capacitance of the sensor changes, the sensor output voltage may be described by $E_O = V\,(C_i/C_x)$, where C_i is the initial capacitance and C_x is the capacitance in the deformed state. A disadvantage of the circuit is the errors related to the low frequency response of the sensor. The circuit is also vulnerable to disturbances such as cable noise, thermocouple voltages, power frequency crosstalk and semiconductor noise [Bax97].

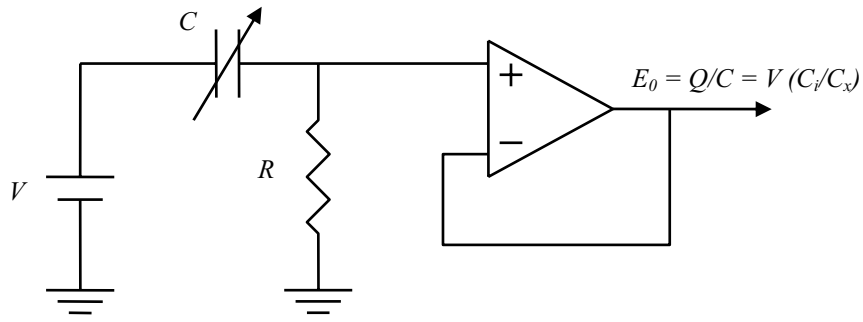

Figure 2.23. A capacitive sensor system based on the direct DC circuit [Bax97].

An alternative circuit design for capacitive pressure sensors is the *RC* oscillator circuit shown in Figure 2.24. The circuit operation is the classic Schmitt-trigger with *RC* feedback. The frequency of the oscillating signal is proportional $1/RC$ and may be determined with a frequency counter. An unguarded *RC* oscillator may have problems with leakages and stray capacitance [Bax97]. Furthermore, bridge circuits may not be directly devised, but fortunately a ratio metric response may be configured.

The most flexible and accurate methods of measuring changes in the capacitance of a pressure sensor are of similar nature to the synchronous demodulator circuit shown in Figure 2.25. A fairly high frequency signal (10 kHz – 100 MHz) is applied in a circuit containing the pressure sensor and a capacitor of known capacitance. The voltage at a point between the two capacitors is affected by changes in the reactance of the pressure sensor. The signal is amplified and compared with the excitation signal. An inverter may be used so that both positive and negative half-cycles contribute to measurement. High-frequency noise such as spikes may be filtered out with a low-pass filter. The output signal is a DC voltage proportional to the excitation voltage and the ratio of the capacitances $(C_1/(C_1+C_2))$. It is also possible to device bridge and feedback circuits

based on demodulation techniques. Figure 2.25 shows an example of the principle. The circuit is incomplete since DC bias on the amplifier input must be controlled. The response of the circuit is proportional to the excitation voltage and the ratio of the capacitances. If C_2 is the capacitance of the sensor, the output voltage is proportional to the displacement.

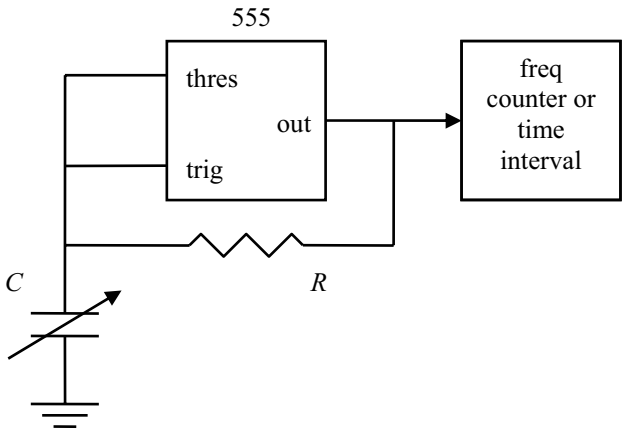

Figure 2.24. A capacitive sensor system based on the RC oscillator circuit [Bax97].

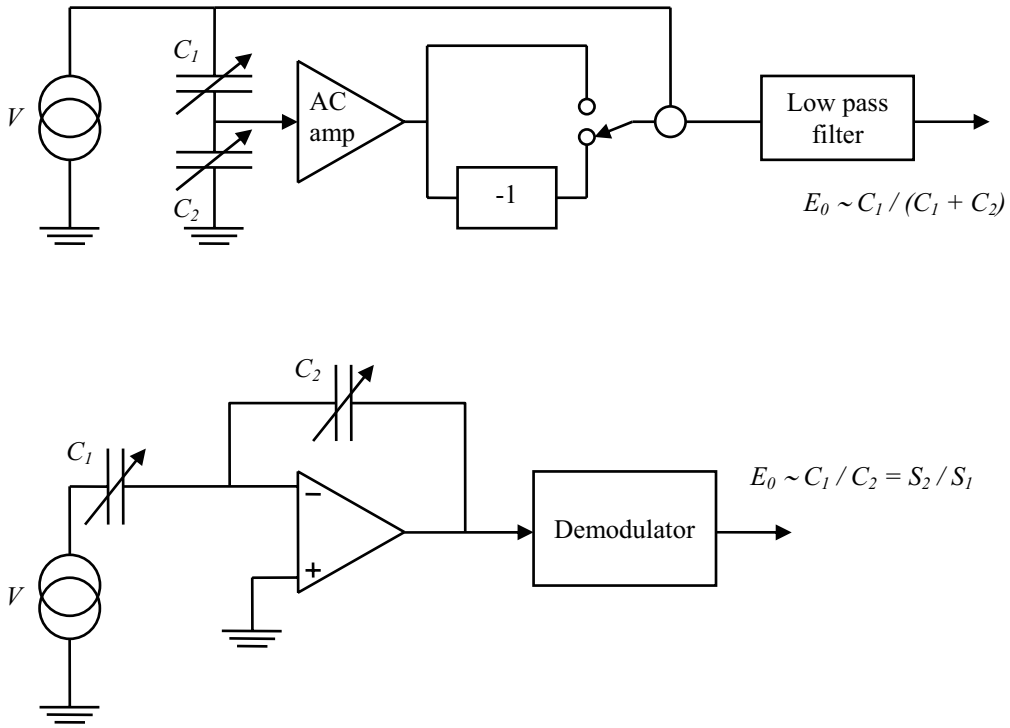

Figure 2.25. The principle of a synchronous demodulation circuit and feedback circuit.

2.3.2 The Capacitec capacitive displacement sensors and logging system

The capacitive sensor systems used to measure both the die face pressure and the liner loads were purchased from Capacitec, Inc. Capacitec, Inc. specializes in the design of capacitive displacement sensors for very hostile environments and for high-temperature applications. Capacitec sensors have been used in the production of glass and metal, in space applications and environments where there are extremely strong magnetic fields [CapW]. All applications of the sensors have not been revealed to the candidate.

The main office of the company is located in the US, but there is also a sales office in France, from which the equipment used in the experiments was purchased:

Capacitec, Inc.
87 Fitchburg Road
Ayer
Massachusetts
01432 USA

Capacitec sarl
P.O. Box 819 Capacitec sarl
16 rue Sojourner 94044
CRETEIL cedex
FRANCE

The Internet home page address for the company is www.capacitec.com [CapW].

A 4000-series sensor system with the capacity of performing three displacement measurements in parallel was purchased by the candidate on behalf of NTNU in the autumn of 1999. The total price of the system with three amplifier cards and sensors was approximately 100 kNOK. Three additional probes were later purchased. The price of a single probe with coax cable was approx NOK 15 000. During the summer of 2001 Hans I. Lange of SINTEF Materials Technology purchased yet another system with three sensors to be used for industrial testing of the concept in relation to the FREMAT programme. Both systems were used in the experiments described in the current report. The NTNU equipment was used to measure the die face pressure while the SINTEF system was used to measure the liner load. For reasons that will be clarified shortly, the two systems should not be used simultaneously in the same environment.

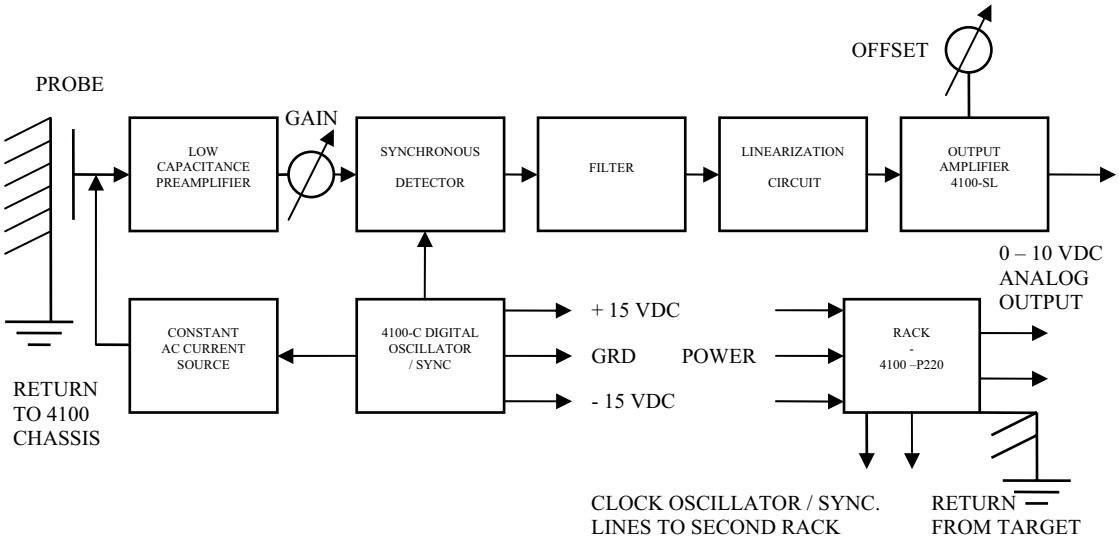

Figure 2.26. Capacitec 4100 series functional block diagram [Cap98].

The Capacitec series 4000 circuit system is of the type described above that makes use of synchronous demodulation to rectify an alternating current signal. The measurement system produces an analog voltage proportional to the distance between the capacitive probe and an electrically conductive surface connected to ground. The capacitive reactance of the sensor capacitor is proportional to the distance between the capacitor plates that are parts of the ground and the probe. Figure 2.26 shows a functional block diagram adopted from the *Operation/Maintenance Manual for Series 4000 Capacitec Amplifiers and Rack Accessories* [Cap98]. The system specifications given in the same source are listed in Table 2.3.

Table 2.3. Specifications 4100 series – main points [Cap98].

Input probe:	HPC, HPT, HPB or HPS Series
Input cable:	Low Noise Coaxial Cable, 100 % Shield. Max length 30 ft.
Input connector:	Microdot 10-32 miniature coaxial or BNC
Standard probe:	Capacitec HPC with 5 ft cable and connector
Linear range:	0.100 inches with HPC-150 and 4100-SL, 4100-L
Linearity:	± 0.2 % of full scale
Resolution:	± 0.01 % of full scale or ± 1 mV
Measuring surface:	Electrically conductive (100 ohms/cm)
Probe excitation:	Alternating current
- Voltage	- Proportional to gap, maximum 3V peak to peak
- Frequency	- 15.625 kHz ± 0.01 %
Linearization:	2 positive slope corrections with adjustable break points and slope
Analog output:	0 – 10 volts DC signal proportional to gap
Output impedance:	100 ohms
Offset adjustment:	- 10 volts to + 10 volts
Frequency response:	- 3 dB at 200 Hz
Operating temperature:	-15 ºC to + 35 ºC
Power requirements:	± 15 VDC @ 850 MA –P240 230-245 VAC at 50-60 Hz
Physical dimensions:	
- 4004 rack	11.5” deep x 5.0” wide x 3.54” high
Weight	
- 4004 rack	5.0 pounds

Three different input probe designs were evaluated, namely the cylindrical HPC (Figure 2.27), the threaded HPT (Figure 2.28) and the button HPB types (Figure 2.29). The cylindrical type was eventually used in all experiments described in the current report. The button-type sensor was difficult to mount tightly and required a non-symmetric sensor design. It was also simpler to handle insulation problems when dealing with the HPC and HPT probes. The casings of the cylindrical and the threaded probes may be in direct contact with the die at ground as they are satisfactorily insulated from the guard. The capacitive coupling between the guard and ground should not affect the sensor response, but the guard itself is important since it makes the field across the sensor gap more uniform, suppresses edge effects (stray field) and therefore contributes to making the sensor response more linear. The reason for this will become clearer in relation to the discussion on calibration. There is a strong capacitive coupling between the guard

and the sensor disc itself. It is therefore extremely important to accurately control the potential of the guard. When the guard is connected to ground, the potential difference across the sensor gap is very small, and measurements cannot be performed. Methods for fastening the button probe tightly to the pressure sensor housing while preventing the guard from getting in direct contact with it were evaluated. As the task was not sufficiently simple, it was abandoned. It should be added, however, that there are also advantages related to the use of button probes. They require little space, and a groove for the cable may easily be made in the die surface.

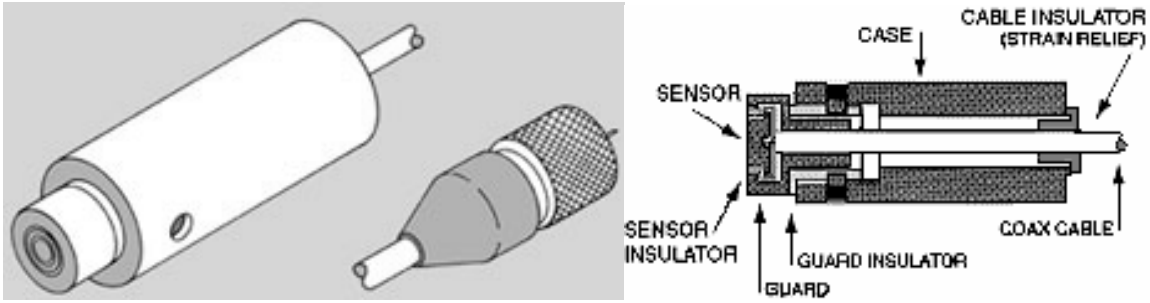

Figure 2.27. Capacitec HPC cylindrical probe (with microdot connector)[CapW].

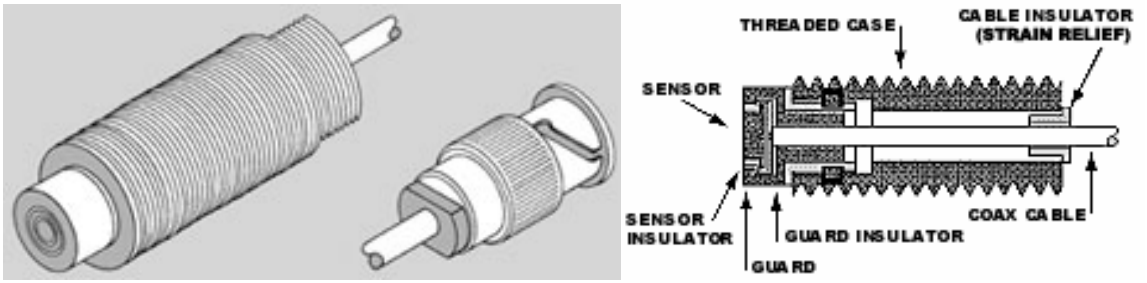

Figure 2.28. Capacitec HPT threaded probe (with BNC connector) [CapW].

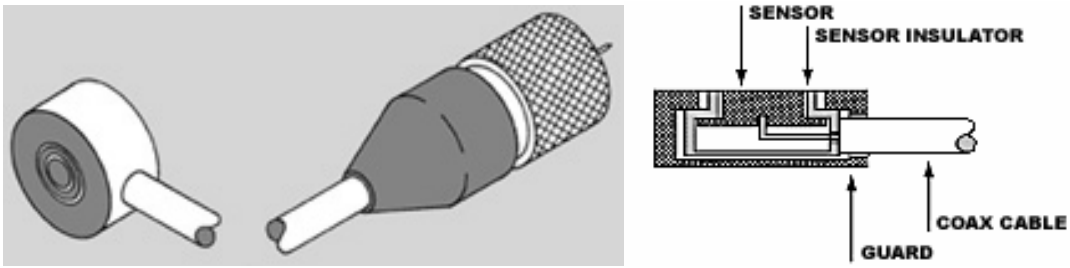

Figure 2.29. Capacitec HPB button probe (with microdot connector) [CapW].

The threaded type of probes, HPT, was also tested. An advantage of this type, apart from the insulated guard, is that a simple method for mounting the sensor exists. If the connection is not sufficiently tight, however, measurements may easily be ruined. A displacement of merely one-tenth of a millimetre in either the axial or lateral direction must be regarded as large when compared to a displacement measurement of only 20 to 30 microns. Threaded connections were tested in compression test experiments. A set screw had to be used to accurately fix the position of the sensor. It was then found that a cylindrical probe could be much more accurately positioned than the threaded one. While there always will be some slack in a threaded connection, the cylindrical probe

may be extremely tightly fitted. Furthermore, it is not easy to determine the exact point of contact between the sensor and its surroundings for a threaded connection. This may potentially be a problem for the evaluation of the sensor behaviour and during actual measurements. In the case of the cylindrical probes, the contact point is better defined. If a small conical hole is drilled in the side of the cylindrical casing, the set screw may prevent the probe from sliding relative to the probe holder. While any straining of the sensor cable is highly undesirable and should be avoided, there is always the risk that a tensile force may be exerted on the coax cable, such as during assembly. While a probe holder connection should not loosen when moderately strained, it should give in to a larger force to prevent probe damage. In the case of the threaded connection, the probe is allowed no freedom of movement even if a large force is applied.

During the very first rounds of experiments of this PhD study (compression and high-temperature testing) the fastening of the coax cable to the sensor disc was found to be a serious weakness of the probe design. As probes were mounted and dismantled and dies were moved in and out of the extrusion press, the sensor cables proved vulnerable to straining. Therefore, there was the risk that the cable could loosen and that the sensor signal could be distorted and even completely lost. One of the capacitive sensors proved to be extremely temperature-sensitive. When all sensors were placed in an oven and heated to 500 ºC, the thermal response of the defect sensor was approximately 10 times larger than that of the standard sensors. Capacitec proposed as a possible explanation that there might have been a bad connection between the sensor disc and the coax cable. The implication might have been that the fault was not theirs but rather the customer's. The probes had, however, been handled with the utmost care, and Capacitec decided to replace the poorly functioning items after the candidate spent weeks of troubleshooting. No explanation for the malfunction was later given. However, Capacitec designed a new cylindrical probe with strain relief (Figure 2.30). The sensor design was similar to one that had earlier been proposed by the candidate.

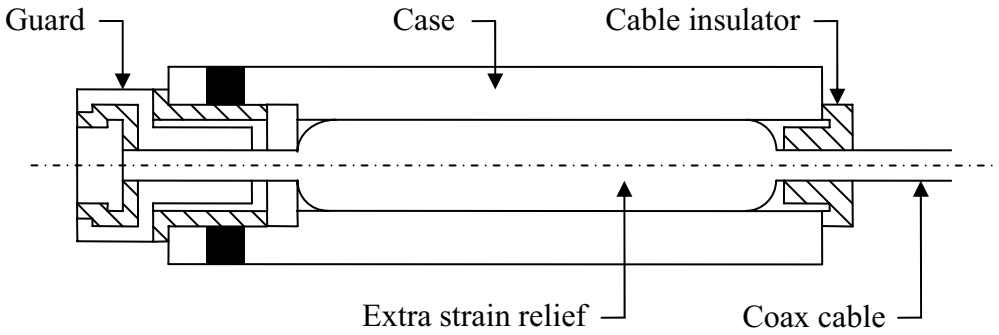

Figure 2.30. Special design Capacitec HPC cylindrical probe used in experiments

The special cylindrical probe designed for the application by Capacitec was named HPC-75-V-N3-3'-M-5506-6404-SD. The designation of the standard high-temperature sensors that were also used in the experiments is HPC-75-V-N3-3'-M. A description of the probe designation system is given in Table 2.4. It should be noted that Capacitec high-temperature probes are made of an Inconel® alloy. One advantage of the material is that there is very little corrosion at high temperatures.

Table 2.4. The Capacitec probe and cable designation system

A	-	B	-	C	-	D	-	E	-	F
HPC	-	XXX	-	X	-	X	-	XX	-	X

A	Probe type: HPC, HPT or HPB
B	Sensor diameter (mils): 40, 75, 150, 375, 500
C	Operating temperature range: A: 32 to 300 ºF, E: -100 to 500 ºF, H: A: -100 to 1400 ºF, V: -100 to 1600 ºF
D	Cable type (only for high temperature applications): N2: 99% double shielded 0.140 inch outside diameter flexible braided Inconel 600/Alumina Boria Silica insulators. Approx 20 pF/foot. T: 100 % single shield, 0.063 inch outside diameter Inconel® 600 tube / MGO filled powder insulator. Approx 60 pF/foot. U: 100 % single shield, 0.125 inch outside diameter Inconel® 600 tube / MGO filled powder insulator. Approx 36 pF/foot.
E	Cable length (feet)
F	Connector type: B: BNC, M: Microdot

The smallest high-temperature sensors available at the time of experiments, the HPC-75, were used. The sensor disc diameter was 75/1000 inch, or approximately 1.905 mm. The outer diameter of the guard and casing are 5 and 6.35 mm (0.25") respectively. The OD of the casing of the probes at hand actually varied from 6.25 to 6.35 mm, which meant that each and every probe and probe holder had to be specially fitted. The reason for choosing the smallest possible sensor was mainly that the dies used in the SINTEF laboratory press were quite small (characteristic dimension 100 mm), and that it was desirable to perform something that at least resembled a point measurement. Small sensors are also more sensitive to load changes, but at the same time they may be less stable. A small sensor must also be placed closer to the sensor disc than a large one. The maximum displacement measurement range of the sensor is approximately equal to the sensor diameter, for at larger distance the capacitor looks less and less like a flat plate capacitor. The non-linearity of the response then becomes more important.

The first sensors purchased were rather short, approximately 0.5" or 12.7 mm. Due to space limitations this was quite practical when industrial experiments were run. In the current study, the short sensor length proved to be not much of an advantage. It is significantly easier to mount probes with long casings than with short ones. At the same time, there was also enough space for long sensors in the dies that were in use. Only during assembly of the die was the use of long probes somewhat impractical. The total length of the new probes was approx 30 mm. Capacitec also provides standard probes of the same length as well as a range of other lengths.

The sensor cable N3 is not a standard Capacitec high-temperature cable as specified in Table 2.4. The most important requirements for the sensor cables relate to insulation and capacitive coupling. However, three additional requirements were of importance:

- The cable should be easily bendable so that it may reach any place in the die
- The cable should be robust, and it must be possible to use it several times
- The cable should not occupy much space (should be a thin cable)

The robustness requirement is of the utmost importance since sensors were to be used in a large number of dies and had to be re-calibrated several times. When thermocouples are used at high temperature, they usually become extremely brittle and may very easily fracture during dismantling. The same material behaviour would be completely intolerable for the capacitive sensor cable. The price of the sensor is approximately 20 times greater than that of the thermocouple, and the problem of re-calibration is also much more involved. Even if heating causes no brittleness, it is not at all desirable to bend cables plastically as they will be worn out quite quickly. Both the N2 and the T cables may be bent to relatively small radiuses, but not without causing plastic deformation and material degradation. In addition, the N2 cable has Alumina Boria Silica spacers that are very brittle and require much space. Since there are tractions of significant magnitude acting at the surfaces of the die, the holes that penetrate the die must be as small as possible. Thus, the rather flexible N3 cable was introduced (Figure 2.31). The exact specifications of the cable are not known. It satisfies the requirements for high-temperature cables, but the capacitive coupling with the surroundings is more significant than that of the N2 cable. For that reason its length should according to Capacitec be limited to approximately 1 meter.

The outermost insulation of the N3 and T cables is a woven fibreglass cover. This is undoubtedly one of the most annoying details of the Capacitec probe design. After the sensor has been used a couple of times at high temperature, the high-temperature tape or band at the ends of the cover pulverizes, and the fabric starts unwinding. The decay cannot be stopped easily, and the user is forced to continuously make efforts to repair damages and replace lost material. Another problem with the fibre glass cover is that it does not completely prevent the coax cable from making contact with the walls of the holes in the die. It is therefore important to be very careful when mounting probes and arranging the cables. Cables should always be allowed sufficient space and never be compressed. Additional spacers may in some cases be necessary.

Worn-out covers have continuously been mended, but a better solution for the insulation problem has not been found. In the early phases of the study, an entirely different cable solution was evaluated. The coax cable of the sensor should be made very short, only some 10 to 20 mm. It should be properly connected to a sufficiently well-insulated high-temperature cable leading all the way to the exterior of the tool stack. The connection between the two cables probably cannot be a standard microdot connection, since it is made of materials that cannot stand the high temperatures of the extrusion die. It should, however, be possible to develop an alternative connection. The high-temperature extension cable should be bent plastically if necessary, and it may be allowed to become brittle. It should not cost much more than a thermocouple and may therefore be easily replaced. It was realised that the solution would require some development work, and it was not worthwhile to delay the project in order for Capacitec to reach a solution. Later permanent pressure sensor solutions should probably be integrated and permanent parts of intelligent die designs. Cable wear will then be a less important problem.

Figure 2.31. The mounting of the capacitive probes (simple die).

Figure 2.31 shows the die at the final stage of the assembly and testing of sensors before the die was placed in the extrusion press. The die is not of the complex type, but rather of a simpler type that made use of four sensors for measuring the die face pressure at different distances from the inlet. The testing phase was not too different for the simple and complex die designs. The bottom face of the die is at the figure facing upwards so that the sensor positions may be adjusted. In the case of the complex die, this operation could only be performed when the top disc and die core were parted.

The high-temperature coax cables in Figure 2.31 are connected to low-temperatures Teflon®-clad cables through a microdot connection. The reason why the microdot was preferred to the BNC was mainly that it was of a significantly smaller size. As a result, it may more easily be guided through narrow channels in the die. An example is shown in Figure 2.5, where the coax cable is guided through a hole in the die to the flanges of the die, so that it may exit from the tool package through the gap between the container and the bolster (Figure 2.32). The solution was a complex one. It would have been possible to modify also the bolster design to simplify measurement, but this would be a more expensive solution. It would also be possible to guide the sensor cables through the bolster outlet parallel to the path of the extruded profile. This would be a less advantageous solution since the profile may have come into contact with the cables.

The designation of the low-temperature extension cables was EC-C-L2-7'. The cables were Teflon® clad and were placed outside the tool stack. The extension cables were connected to the rack with the signal processing system through a BNC connector. The

ground cable, which was not intended to withstand high temperatures, was connected to the rack by a banana jack and to the lower press board (Figure 2.2).

Figure 2.32. The extrusion die (simple type) was placed in the press and the various cables were guided out of the assembly between the bolster and container.

The main characteristics of the measurement system are given in Figure 2.26 and Table 2.3. All signal electronics components were gathered in the Capacitec 4000-series electronic rack. Both the NTNU and SINTEF equipment made use of the smallest type of racks, the 4004-P220, which allowed measurement with at maximum four channels. The rack contained a ±15 VDC regulated power supply at 350 mA. Each rack had a 4100-C digital oscillator card. The card was supplied with the direct current from the power supply of the rack and generated the sinusoidal excitation signal of frequency, 15.625 kHz and peak-to-peak voltage of less than 3 V. The system used a crystal oscillator as a reference. More detailed information about the circuit design is given in the *Operation / Maintenance Manual for Series 4000 Capacitec Amplifiers and Rack Accessories* [Cap98]. The excitation signal was common for all of the channels of the rack in order to avoid crosstalk. If two systems were placed in the same room, they interacted. Excitation frequencies deviated by a couple of hertz, and the DC output signals were affected by low frequency beats. The beats could sometimes not easily be removed by standard high-, low- or band-pass filtering since they were of almost the same frequency as the extrusion load response (Chapter 5). It was possible, however, to remove the oscillations manually, although it was a quite labour intensive task. The frequency of the beats could change during measurement, but changes were often easily detectable. In all cases where the two systems were run in parallel, it was possible to

verify, through replication of the experiments with only one of the systems active, that the results obtained after removing the beats for most purposes were acceptable. Still, the running of two systems in parallel as described is not recommended and was thus generally avoided. Most experiments were replicated to allow individual measurement of both die face pressure and liner load. This is quite obviously an awkward way to perform experiments, but not a completely inappropriate one. Ram force and outlet temperatures were registered for all runs. It should in this respect be added that the *Operation / Maintenance Manual* indicates that it is possible to synchronize the excitation signals of two clock cards so that beats are avoided and systems may be run in parallel. However, when first asked about the possibility, Capacitec customer service gave the impression that it would not be possible to run the systems in parallel as described in the manual. If new experiments requiring more than one measurement system are to be run, more thorough inquiries should be made.

In addition to the clock cards, the 4004 racks contain the low capacitance modular pre-amplifiers (PC-201B) and the synchronous detectors shown in Figure 2.26. It is possible to read out the sinusoidal measurement signal directly, but the demodulated DC output signal is usually of greatest interest. A Butterworth filter was used to effectively remove high-frequency noise (-3dB at 232 Hz, roll-off: 18 dB/octave). Most of the information of interest from the extrusion system was of a frequency lower than 20 Hz and was unaffected by filtering, but it is quite possible that information about such as stick-slip friction in the bearing channel might have been lost. However, such high-frequency information would in any case be very hard to analyse. Capacitec also install low pass filters with the -3dB point at either 3.1 or 5 kHz. The output is then more affected by high frequency noise, which may conceal valuable information about small physical effects. For that reason the standard filter was used.

Finally, for each of the channels there must be an amplifier card. In the current case, cards designated 4100-SL were used. A linearization circuit may improve the linearity of the signal from approx ± 2 % to ± 0.2 % of full scale. The maximum output voltage of 10 V may, in the case of the HPC-75 sensor, correspond to as much as 2 mm. As will be further discussed with respect to calibration, the optimal full scale was for the current case smaller, approximately 0.5 mm. The linearity was then approximately ± 1 μm or even better (i.e. the non-linearity is smaller than 1μm). Further linearization of the signal may according to Capacitec in some cases be performed manually since the non-linear behaviour is highly repeatable.

The resolution of the Capacitec system is ± 0.01 % of the full scale or 1 mV. For a full scale of 0.5 mm, this corresponds to ± 0.05 μm (50 nm). This value is often assumed to represent the repeatability of the system. Capacitive measurements may be extremely accurate, and as long as the measurement set-up is not altered, it is probably possible to recognise and repeat changes of 50 nm. In the most extreme cases, displacements of a fraction of 1 nm may be found (Volume I). However, as will be further discussed in relation to calibration (Chapter 4), the nominal values of repeatability presented seldom give a good indication of the ability of the system to reproduce a measurement during the actual extrusion experiments. One then has to take into account the fact that the equipment may be dismantled and that reference points may change.

2.3.3 The analog/digital converter and computer

An analog/digital converter had to be used together with a digital computer in order to register and store data. The AD converter had to fulfil certain requirements both with regard to rate, accuracy and resolution. First, the profile speed may be as high as 2.5 m/s during extrusion, and a run may last only 6 seconds. If only an estimate of the die face load is of interest, 5 samples per second may be sufficient. However, if the objective is to spot high-frequency load perturbations due to stick-slip behaviour or flow instability, the sampling rate should be considerably higher. When a profile buckles, for example, the typical wavelength may be as short as 50 mm or 1/50 second at the highest speeds. A proper representation of the pressure changes would require sampling rates of several hundred per second. When using the low-pass filter described above, load perturbations at a frequency higher than 200 Hz may not be spotted anyway. Since an outlet speed of 2.5 m/s is an extreme, a maximum sampling speed of 100 to 200 per second would probably be sufficient. It is, however, important that the system be able not only to process one measurement, but rather three or even six in addition to the ram force, the ram displacement and several important measurements of temperatures (die face and outlet). Measurements were performed with a total of 16 channels.

The objective of the study was to perform measurements of die face pressure with an accuracy of typically ± 10 MPa and a resolution of some ± 3 MPa. For a total die face pressure of 300 MPa, this would correspond to ± 3.3 % and ± 1 % respectively. If the total sensor deflection is approximately 30 μm, an accuracy of measurement of ± 1 μm and a resolution of ± 0.3 μm is needed. The capacitive displacement measurement system was fully capable of fulfilling these requirements. Analog-to-digital conversion should in principle not be a problem since an accuracy of ± 3 % and a resolution of ± 1 % are only moderate requirements. The problem is, however, that the capacitive system is usually calibrated so that a change from zero to maximum pressure only causes the voltage to change by approximately 0.6 V, for example from 8 V to 7.4 V. A suitable requirement for accuracy is then ± 20 mV, while the resolution should be better than approximately ± 6 mV. It is not completely unrealistic to require the accuracy of the logging equipment be close to ± 1 mV and that the resolution be significantly better. It is possible to offset and amplify the signal so that it is better adapted to standard analog-to-digital converters and so that the requirements are less stringent. However, errors may also be introduced during amplification, and amplification should be regarded as an unnecessary complication.

The data logging system of the SINTEF press has a sufficient number of channels to include press and liner force measurements. It was able to handle 20 samples per second with a resolution of 12 bits or ± 5 mV, which was not regarded as sufficient. Therefore, an additional measurement system was used to log the die face pressure and liner load. Parallel logging of the ram displacement and ram force was also performed. The temperature at the outlet was recorded by the SINTEF press system while the die face temperatures were handled by the additional system. Figure 2.33 shows the complete die face pressure and liner load measurement system. The Capacitec racks may be seen on the lower shelf. The analog/digital converter, a Fluke NetDAQ® (Networked Data Acquisition Unit) 2640A, has been placed at the left side on the upper shelf of the table.

The computer used during logging was an Acer Travelmate Pentium 3 laptop computer. The NetDAQ® logger may be run in a general network consisting of a large number of computers or in an isolated network with only one host computer. The last alternative was chosen. The operating system of the laptop was Windows NT4.0, and logging was performed with the program NetDAQ Logger for Windows [Flu94].

Figure 2.33. The SINTEF extrusion press and the die face and liner load pressure measurement system. The logger was at the left side at the top of the table while the amplifiers were placed on the shelf below the table.

Table 2.5. Fluke NetDAQ® 2640A capabilities in the DC mode.

Property	Slow	Medium	Fast
Sampling rate (20 channels)	6 per sec	45 per sec	143 per sec
Resolution – voltage	0.1 mV	-	0.3 mV
Accuracy (3·σ) – voltage	2.7 mV	4.2 mV	5.6 mV
Accuracy (3·σ) – temperature	0.65 ºC	-	0.90 ºC

The NetDAQ® logger may either be run in a slow, a medium or a fast mode. Table 2.5 provides information about sampling rates, accuracy and resolution for the equipment when recording signals from 20 channels. The accuracy is the value corresponding to three times the standard variation. It is assumed that the system has been used for more than a year, and that the equipment was at room temperature during experiments. The measurement range is ± 30 V, while the measured voltage is assumed to be only 8 V. During measurements, the sampling rate was approximately 30 per second, which for the time being was considered to be sufficient for the rod extrusion problem.

Chapter 3

Experimental plan

This section presents an experimental design of limited size that was used to critically test the behaviour of the die face pressure sensors. The design made possible a careful study of flow and friction in the extrusion process through simulation and experiment. The most important hypotheses of the flow simulation and die deformation calculations are presented, and estimates of the ram force, outlet temperature, die face pressure and liner force are deduced with the code ALMA2π. The experimental plan made possible a careful assessment of the effects of input parameter changes.

3.1 Some requirements for the experimental plan

The most important reason for performing the rod extrusion experiments was to test the new pressure sensor design concept presented in Chapter 2. Two types of information were sought. First, it was important to demonstrate the feasibility of measurement with the current sensor design. The new design made use of a new method for mounting and a totally new complex die design concept. Success was not guaranteed, and the process of ameliorating the design was regarded as the probably most important part of the study. Second, in the cases where the sensors seemed to work properly, it would be of interest to establish quantitative measures of the sensor's main capabilities. The most important were probably the measurement accuracy, repeatability and resolution. A further description of these measures and of the requirements is given in the section on calibration (Chapter 4). Definitions have also been provided in the terminology list. One should here merely note that experiments should be performed in a way that allows a critical assessment of both the quantitative and qualitative behaviour of the pressure sensors. The behaviour of the liner load sensors should be assessed in a similar manner.

A first requirement for the experimental plan was that it includes a sufficiently large number of replicate runs. This would allow a careful study of the repeatability of measurement. As will be further discussed in relation to the analysis of results, there are various forms of replications. In the current study of extrusion one should distinguish between runs that were repeated on a particular day (during a particular round) of experiments and runs that were repeated after the die had been completely disassembled and reassembled. The fact that there were three parallel measurements of pressure (three sensors) during all runs greatly simplified or enhanced the study of sensor repeatability and accuracy.

A second requirement for the experimental plan was that it be possible to estimate the die face pressure in alternative ways. As will be discussed, the ram force and liner load measurements could be used to estimate the die face force in most cases. It would, however, be most valuable if numerical simulations could be used not only to establish estimates of the main responses of the process, but to improve the understanding of the extrusion process. Later parts of this section examine some of the challenges of mathematical modelling of the extrusion process. It is important that the cases that were run ought to be suitable for numerical simulation or even for analytical studies.

A third requirement for the experimental plan was that it should allow sensors to be tested over a large range of pressures and thermo-mechanical conditions. The feasibility of measurement may be established by a few experiments run in a non-systematic manner. Even estimates of accuracy and repeatability may be determined. However, when measurement results are compared with estimates of pressure from other sources, it is not possible to completely trust the results from individual runs. Both estimates and measurements may be in error. It is better to change the loads in a systematic manner and to compare responses. Models are very often better suited to estimate effects than absolute values, and as will be shown, the effects may also in many cases be more accurately measured than absolute values. Effects are also often more interesting.

A fourth requirement for the experimental plan was that it should be suited to both the process and the die design. Furthermore, the experimental plan was limited by the resources available. For example, experiments could not be performed in a perfectly randomised manner, which in most cases is desirable. A change of one of the die outlets presented in the previous section would have required a one-day pause in the activity. Aluminium extrusion is usually performed in a hot environment, and the change of an instrumented die is no simple task. There were only resources available for one die to be manufactured and five days of experimental activity to be performed.

The importance of performing experiments in a systematic way cannot be exaggerated. If the sensors work and results are to be properly analysed, the most important and most difficult challenge is related to the determination of the actual value of the die face pressure. Alternative indirect measurement techniques cannot be expected to provide more accurate estimates than the pressure sensors. The results from finite element modelling (or any analytical or numerical technique) of flow must always be critically checked. The choice of rod extrusion as a test case made matters simpler, as the flow problem was of only two dimensions and as there was no buckling. The use of die outlets with practically zero length bearings was a very important simplification since the problem of bearing friction is a research issue of current interest. Still, the problem of numerical simulation was not trivial. For that reason, in-depth studies of the rod extrusion flow problem have been performed [Waj04] [Moe04b]. The objective of the studies has been to establish estimates of the modelling error based on more accurate measurements of ram force and die outlet temperature. In order for a detailed study of flow to be useful, the experimental plan should cover a relevant and sufficiently broad range of the input parameters of interest. In relation to both the evaluation of material models and the measurement of pressure, it was important that the changes to the input parameters be large enough to cause detectable effects.

3.2 The experimental plan for rod extrusion

3.2.1 Process responses

In the following text, the extrusion process is regarded as a system, which produces responses to changes in a set of input variables [Moe03b]. The relevant responses of the rod extrusion system have been presented in relation to the discussion on sensor design:

- The ram force
- The outlet temperature (point measurement)
- The die face pressure (local measurement of force)
- The die face temperature (point measurements)
- The liner load
- The liner load cell temperature
- Temperatures in the bolster and container

All the output data were continuously logged at a sampling rate of 20 to 30 per second. The shape and microstructure of the material could also be studied, as well as the profile shape. When the product is a rod, the shape of the extruded profile is characterised by one parameter, the diameter. No significant diameter variations were observed during experiments, except for one case when there was plugging. There was unfortunately no time for more detailed studies of the microstructure. A last source of output data is the gridline technique of Valberg [Val88]. It is possible that if such a technique had been effectively used to deduce quantitative data, significantly fewer experiments might have been needed in order to evaluate the material data. However, Valberg's technique probably must be regarded as one that provides mainly qualitative information about the material flow. The main reason for this is that the experiments are very time-consuming and that the resolution is relatively poor when cases of extrusion of industrial relevance are run (large extrusion ratios). The technique has been used by Grasmo et al. [Gra92] in a study of rod extrusion that was not too different from the one that is described in this thesis. The results were not used in a truly quantitative inverse analysis.

3.2.2 Input variables and parameters

An input variable for the extrusion process may loosely be defined as any aspect of the extrusion system whose change may potentially affect the system responses. A variable is by definition something that varies. The current study focuses primarily on four input variables or factors:

- The profile dimensions / the extrusion ratio / the outlet diameter
- The bearing length-to-diameter ratio
- The initial uniform billet temperature
- The ram velocity or profile velocity

The variables define the experimental matrix that was used to run the experiments. The billet temperature and ram velocity were by far the simplest variables to change. The profile dimensions and bearing geometry were mainly changed to demonstrate a sensor concept, which was one of the main objectives of the study.

The aluminium alloy

Only generic AA6060 was used in this study (Table 3.1). A change of alloy represents a simple way of causing a system response, but the four input variables above already define a sufficiently large experimental matrix. Furthermore, it is important that the properties of the materials used be well-known. The choice of AA6060 is a natural one, for it is a very commonly used (generic) alloy. Reference [Moe04b] reports on results from compression testing and compares the results with data from other authors. The material data for the Zener-Hollomon flow relation are presented in Table 3.2. The compression experiments were performed in close cooperation with Wojciech Wajda and the Academy of Mining and Metallurgy (AGH) in Kraków.

Table 3.1. AA6060 alloying constituents – data from four burns used in experiments.

	Mg	Si	Fe	Ti	Mn	Ga	V	Pb	Zn	Cu
Avg	0.472	0.413	0.215	0.015	0.013	0.012	0.008	0.005	0.003	0.003
St.dev.	0.003	0.001	0.001	0.001	0.000	0.001	0.001	0.001	0.001	0.000

Table 3.2. AA6060 parameter values of the Modified Zener Hollomon relation.

Source	Alloy	α [MPa]	A [s^{-1}]	n [-]	C [-]	Q [J/mol]
[Moe04c]	6060.35	0.0368	$3.90 \cdot 10^{11}$	4.800	0.0	180 943

Thermal conditions

In order to obtain satisfactory material properties and profile shapes during extrusion the system temperature must be closely controlled. The initial billet temperature is only one of many parameters that could have been changed. In the current study the container temperature at the onset of extrusion was always set to 430 ºC. The bolster temperature was 480 ºC. The bolster had a non-uniform distribution of temperature at the onset of the extrusion experiments, as heating was only performed at the outer surface of it. The temperature of the core of the bolster beneath the die was much closer to 430 ºC. ANSYS® calculations show that the die face temperature at the onset of extrusion was approximately equal to the container temperature, and that the temperature differences in the die were not larger than 20 ºC. A possible cause of variability in measurements is the change in container and die temperature due to the plastic heat dissipation during the extrusion. The time interval should be carefully controlled between runs. In the current study, the interval was set large enough (10 to 12 minutes) so that the steady state was re-established before the next extrusion run commenced. Both the thermo-mechanics of deformation and the pressure sensor behaviour may be affected by temperature changes.

The initial ram temperature must also be carefully controlled, as it affects the back end temperature of the billet and therefore the flow resistance, especially close to the end of the run. The slower an extrusion is performed, the more important the heat flow to the colder ram. The dummy block was moved into the container some time before extrusion commenced and heated to approx 130 ºC. If it had been heated further, one would have risked having the billet stick to the dummy block after extrusion. It should be noted that the temperature of the dummy block quite necessarily changes considerably during extrusion. The temperature was not measured on-line, but temperature measurements for a similar case have been performed by Grasmo et al. [Gra92].

Note that the term initial billet temperature is inaccurate. The billet was heated by an induction coil before it was moved through the air to the container. In the current study the nominal billet temperature was varied from 450 to 500 ºC. The bottom and top face temperatures were measured before the billet was dropped into the container. Usually there was a small deviation from the nominal temperature, and there may also have been a small undesired taper (< 5 ºC). After induction heating, the surface of the billet was hotter than the interior. In the subsequent pause, which lasted approx 30 seconds, the billet temperature changed due to heat transfer to the air and the container. The butt end (press rest) was generally not removed between the runs for reasons that will subsequently become clearer. The butt end temperature was initially similar to the container temperature. The billet temperature was at no time uniform or at steady state, and there was a continuous flow of heat to the surroundings after induction heating started. It was therefore important to control the duration of the different steps. Time should ideally not be a variable in the study. The sensitivity of both the outlet temperature and ram force to relevant loading time changes was found to be relatively small [Moe04b]. The reason is probably that the temperature gradients are moderate when the billet first is in the container. A more detailed study is needed (Appendix L).

The billet dimensions

The response of the extrusion system also depends on the billet dimensions. A longer billet usually causes the container friction and the ram force to be larger. The maximum temperature at the outlet and the die face pressure need not be affected much. The outer diameter of the billet cannot be larger than the inner diameter of the container, i.e. 100 mm. The nominal diameter of the billets was actually somewhat smaller, approx 95.5 mm, so that they would fit easily into the container. During the burp phase, the billets were compressed elasto-viscoplastically until they completely filled the container and the extrusion run started. The outer surfaces of the billets were not machined before extrusion and were relatively rough (as cast). Prior to heating, the billet length was approx 200 mm, but deviations could be as large as 0.5 mm. The butt end or press rest was not removed between the runs. The exceptions to this rule were the first run in the rounds and the first run after the butt end got stuck to the dummy block. Data from these runs were generally not used in the sensitivity analysis. As will be shown, however, the runs were important because they rendered possible a comparison of the responses of the system when experiments were run with and without a butt end. There are a number of reasons why the material may respond differently when there is a butt end in front of the billet and when there is not. First, the material in the butt end is pre-deformed and has a microstructure that may significantly deviate from that of the virgin billet. Second, the composition of the butt end and billet may differ, as surface contamination is stored in the butt end. Third, the butt end consists of material from all the previously extruded billets separated by oxidized welds. It is not known how weld interfaces affect the flow resistance and flow patterns. Finally, the total billet length is shorter in the first run when there is no butt end, and this may have an effect on the temperature history. As will be shown below, the differences in measured force and temperature for the different cases were not as large as feared. The advantage of running billet-to-billet in the way that has been described, is primarily that the experiments were simpler to perform since the butt end was not cut. This was of some importance since focus should not be shifted from the measurements task. It made also the task of measurement simpler.

The length of the butt end was approx 19 mm. Deviations were as large as 0.5 mm. The butt end was rather tall, and the interface between the butt end and container large. This caused it to stick to the die rather than the ram during the retraction of the ram. After the burp cycle the total height L_{BT} of the butt end and the compressed billet was:

$$\begin{aligned} L_{BT} &= L_{BE} + \left(1+\alpha\cdot\Delta T\right)\cdot L_{B0}\cdot\left(D_{B0}/D_C\right)^2 \\ &= 19\text{ mm} + \left(1+20\cdot10^{-6}\cdot430\right)\cdot200\cdot\left(95.5/100\right)^2\text{ mm} \\ &= 19\text{ mm} + 184\text{ mm} = 203\text{ mm} \end{aligned} \qquad (3.1)$$

L_{BE} is the height of the butt end, L_{B0} is the height of the billet at room temperature, D_{B0} is the diameter of the billet at room temperature and D_C is the inner diameter of the container. α is here the approximate thermal expansion coefficient for aluminium, and ΔT is the temperature change. The peak force was usually recorded when the distance from the front end of the ram to the upper die face was approximately 201 mm.

The die outlet shape

Extrusion was performed with outlets of nominal diameter of 15.8 and 11.2 mm, which correspond to extrusion ratios of 40 and 80. The actual diameter of the extruded rod when cold was less than 0.2 mm, or 2 % larger than the nominal diameter of the die outlet. Since the extrusion pressure is a function of the logarithm of the extrusion ratio, it was not much affected by such small deviations (less than approximately 1 %). The difference in the thermal expansion properties of the die and billet may have been the cause of about half of the deviation in shape. Errors may also be due to inaccurate machining. Die deformation does not significantly affect the shape of the die outlet, for the die support is quite good. The bearing channel is usually the main instrument for flow and surface texture control. In the case of the rod extrusion, the bearing channel geometry is only described by two parameters in addition to the outlet diameter. The bearing length, or rather the ratio between the bearing length and the outlet diameter, is regarded as an input variable in the study. If it is assumed that the bearing channel is of a constant outer radius, R, the build-up of the average pressure, $\Delta\sigma_z$, over a small length, ΔL, is approximately proportional to the ratio of the length to the radius. The wall shear stress, τ_w, may or may not depend on the tractions normal to the wall, σ_r.

$$\Delta\sigma_z^{avg}\cdot\pi\cdot R^2 = \tau\left(\sigma_r\right)\cdot2\cdot\pi\cdot R\cdot\Delta L \quad\Rightarrow\quad \Delta\sigma_z^{avg} = 2\tau_w\left(\sigma_r\right)\cdot\left(\frac{\Delta L}{R}\right) \qquad (3.2)$$

Hence, when operating with outlets of different diameters, it seems quite logical to scale the bearing length. As shown in the previous section, die outlets were either made with a zero length bearing channel or with rather long bearing channels. The first type made it possible to focus on the details of material flow in the container. The second type made it possible to test the assumption that the friction is pressure dependent even in a choked bearing channel. Force, pressure and temperature measurements should also make possible the estimation of the parameters of the friction relation. The assumption of parallel bearings was not completely incorrect. The nominal choke angle of all outlets was 40' ± 5'. The die deflection calculations of the previous section show that the real

choke angle was probably approximately 35' ± 5'. The choke angle was so small that it did not invalidate analytical calculations, but so large enough to ensure proper contact conditions. Commercial dies may be made with angles of only a few minutes. Note that the bearings have been made with no curvature whatsoever to simplify the study.

The length-to-diameter ratio for the bearing channels denoted as long was approx 0.76. The bearing lengths for extrusion ratios 40 and 80 were 12 and 8.5 mm respectively. While the bearings were of considerable length, the length-to-diameter ratio was in fact not very large compared to ratios of many industrial dies. Extrusion of thin strips with thicknesses of 2 mm, for example, is often performed with bearings significantly longer than 2 mm. Thus, the bearing channel pressure build-up in the rod extrusion dies and in industrial dies should not be too different. There may be other reasons, however, why results from rod and thin-strip extrusion may not be directly comparable. The most important is that the temperature conditions may be very different for the two cases. Another reason is that the friction mechanisms at micro-scale may affect bearings with lengths of 2 and 12 mm differently. The scaling of the micro-scale friction problem may differ from the scaling of the macroscopic flow problem. The consequence may be that constitutive relations with parameter values that work for rod extrusion may not work for thin-strip extrusion. Still, a study of friction in relation to rod extrusion probably would provide valuable insight into the problem of bearing channel friction anyway. It also gives an indication of the ability of the pressure sensor to measure small differences in pressure levels. The "scaling up" of the problem becomes an advantage.

3.2.3 The experimental matrix

As in most cases, the lack of time and resources limits the number of experiments that may be performed. 2^k factorial experiments and response surfaces techniques are often regarded as the most powerful tools of the experimenter when there are relatively many input variables [Box78]. The 2^k factorial design is a regression technique that allows characterisation or mapping of the responses of a process with a fairly small number of experiments. In the first step, only a high and a low level of each factor, which may be an input variable to the process, were defined. A specific combination of levels of all factors defines an experiment, which herewith is denoted a case. In most of the literature the term run is used, but in relation to extrusion it is more natural to define a run as the extrusion of one billet. There may be several replicate runs in a case. When there are k factors, there are 2^k possible combinations of the factors or cases. When all these are performed in an experiment, the 2^k factorial design is denoted full. If some of the factors are unimportant or cause responses that may be predicted on the basis of the other experiments, one may either deduce information about errors from the full design or perform fewer experiments according to a fractional factorial design. Experiments may be run in a manner that allows redundancy to be detected before all experiments have been performed. Another advantage is that although the technique is only of first order, it allows the assessment of the effects caused by all kinds of first-order interactions between the different factors to be assessed. The 2^k factorial technique may also be the starting point for a more thorough analysis of higher order effects or of an optimisation search. A final advantage of the 2^k factorial designs or any other two-level orthogonal design is that they provide both optimal and independent estimates of all coefficients in

the regression equation. Coefficients are estimated with the least amount of variance [Box78]. When an experiment is randomised, cases are run in a completely random order. This makes it possible a reduction of the influence of systematic errors on effects.

In the current study, the factorial design and the response surface methodology may be used in two ways. The most obvious application is the design of extrusion experiments to map the actual and simulated responses of the system over a range of input data. One may only wish to establish estimates of force, pressure and temperature. By comparing the measured and calculated responses, the limits of a specific model's validity may be better understood (Figure 3.1). The response surface methodology may, however, also be used when parameter optimisation is carried out on the basis of the experimental results (Figure 3.2). The factors may then be the parameters of the flow and/or friction relation. The response is the combined modelling and random error of the experiment. Computer simulation is performed instead of experiments to generate responses, even though a larger set of extrusion experiments should also be the point of origin for the study. The objective may be to assess how much the error changes as a result of the change of one parameter. The 2^k factorial approach may also be used to perform parameter optimisation, but it may then not be the most efficient design [Wal91]. Instead, use has been made of the simplex routine to search for the optimum point of two-dimensional response surfaces [Moe04b]. The analysis of experimental results is also treated more thoroughly in the last sections of this report.

Table 3.3. Levels of various input variables (with profile velocity).

Input variable	- 1 level	0 level	+ 1 level
A - Bearing length	Zero	-	Long
B - Extrusion ratio	40	-	80
C – Billet temperature	450 ºC	475 ºC	500 ºC
D - Profile velocity	200 mm/s	500 (400) mm/s	800 mm/s

Table 3.4. Levels of various input variables (ram velocity option A).

Input variable	- 1 level	0 level	+ 1 level
A - Bearing length	Zero	-	Long
B - Extrusion ratio	40	-	80
C – Billet temperature	450 ºC	475 ºC	500 ºC
D - Ram velocity	5 mm/s	12.5 (10) mm/s	20 mm/s

Table 3.3 and Table 3.4 show two alternative choices of factors and levels that were used in the experiments. The point of origin for the experimental design was a full 2^4 factorial. The reason why two alternative 2^k experimental designs were introduced was that either the ram or the profile velocity could be regarded as a factor. Since the die outlets are of different extrusion ratios, one has to take into account the extrusion ratio when linking the profile and ram velocities. The choice of variable depends to some extent on the objectives of the study. When the flow in the container is the most interesting issue, it is natural to use the ram velocity. When bearing channel friction is assessed, one may prefer to focus on the profile velocity. The choice is a subjective one, however, and it will be shown that it is always possible to deduce information about the effects of ram velocity changes from the effects of profile velocity changes and vice versa. The choice of billet temperature and ram velocity levels is justified below.

Factors (input variables): the process parameters

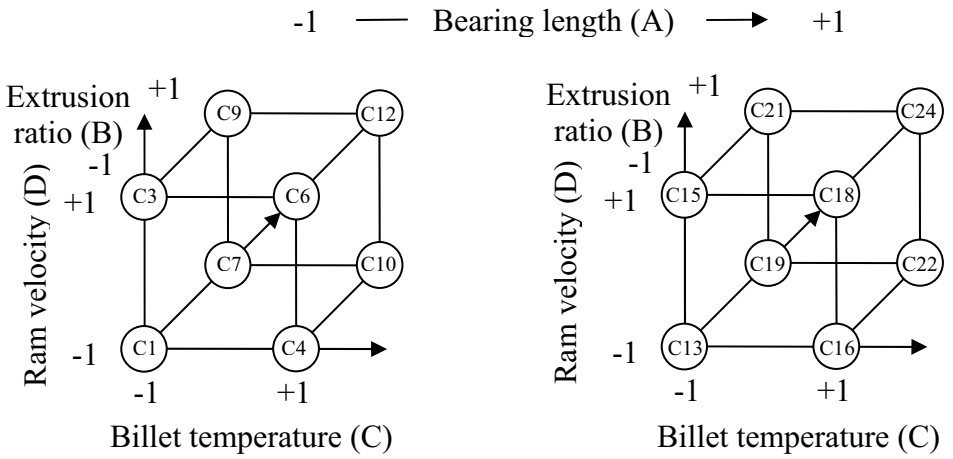

Results (all cases) – ram and liner force, outlet temperature and die face pressure

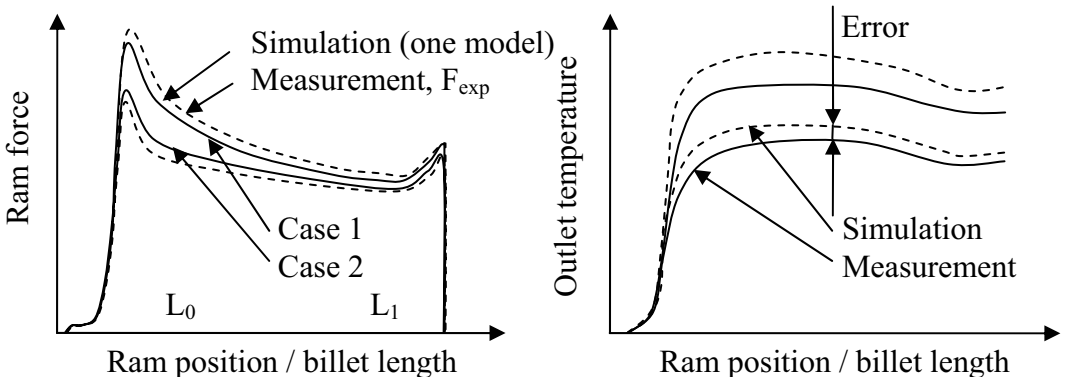

Error surfaces: Measured minus calculated force, temperature and pressure

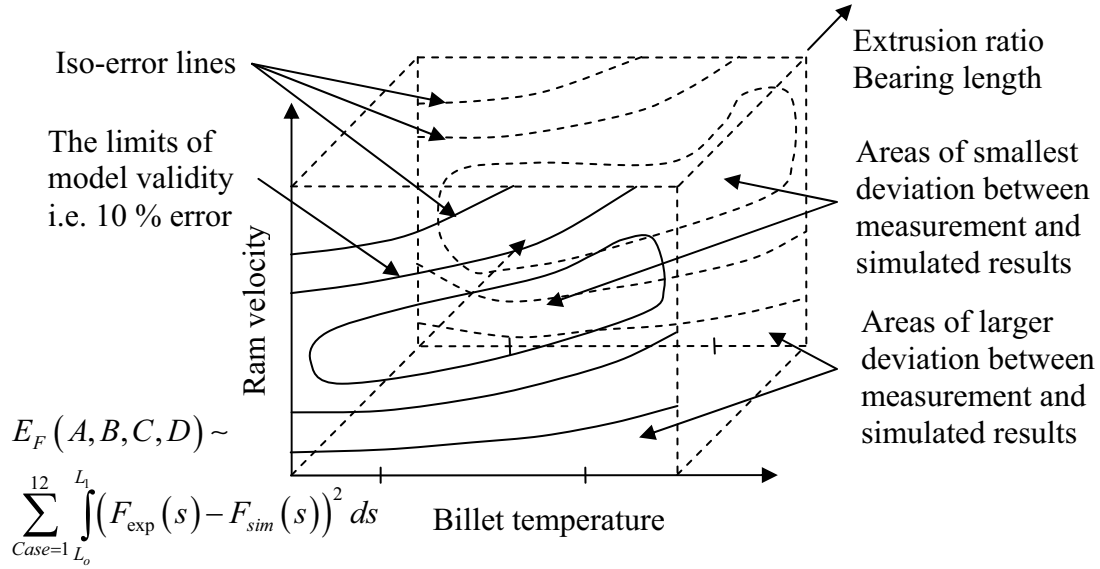

Figure 3.1. The experimental design and response surfaces used to investigate the responses of the extrusion system and the accuracy of one flow model.

Factors (input variables): the parameters of the extrusion flow and friction models

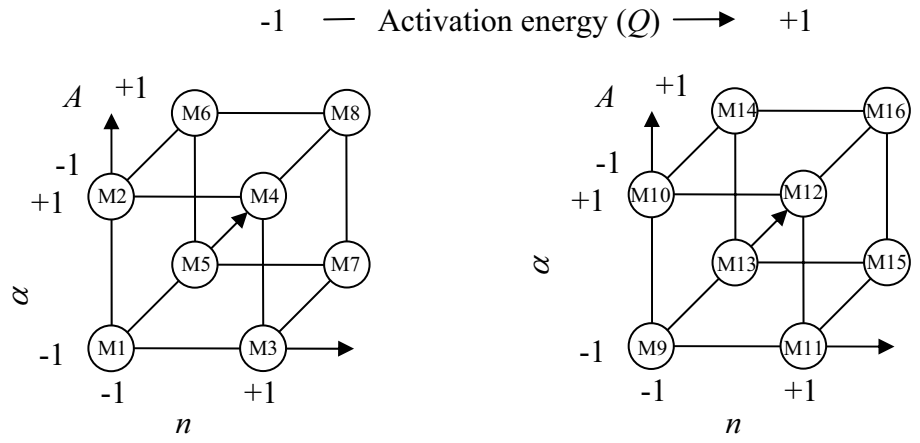

Results (all cases) – ram and liner force, outlet temperature, die face pressure

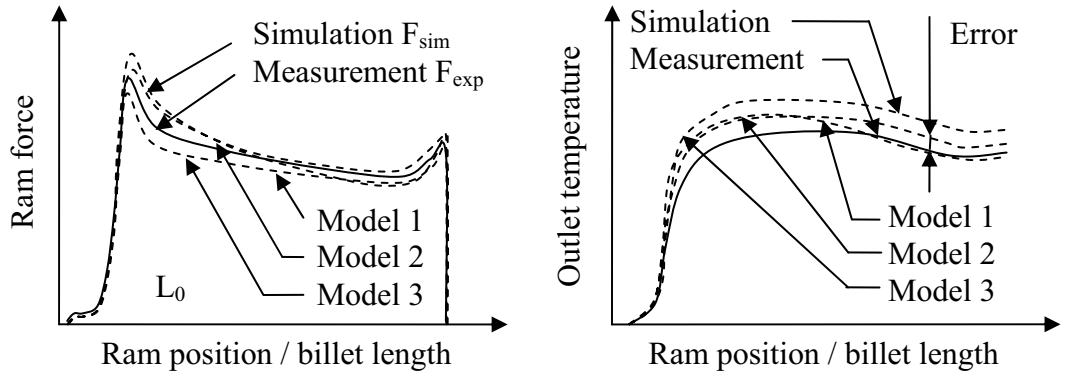

Error surfaces: Measured minus calculated force, temperature and pressure

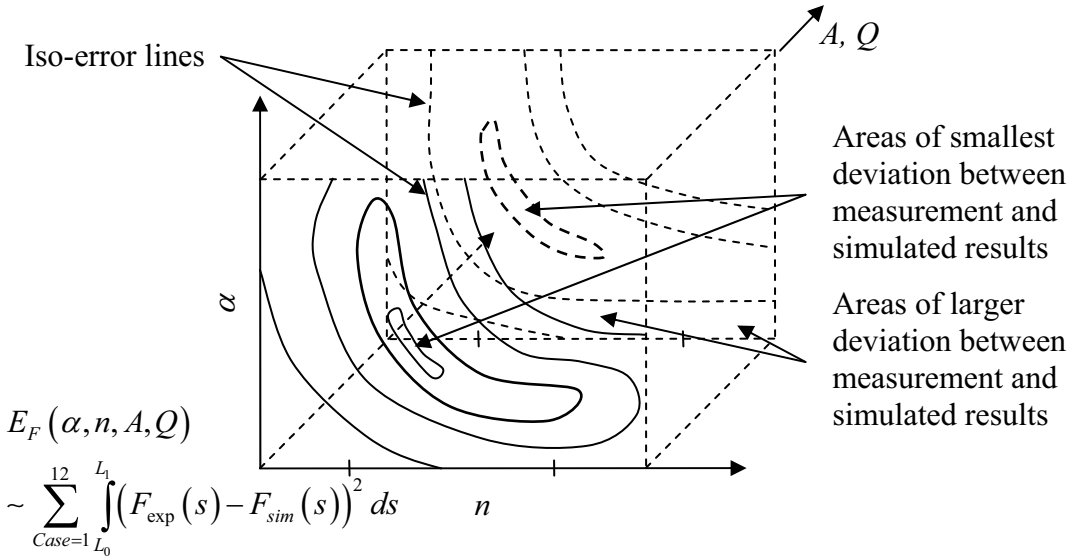

Figure 3.2. The experimental design and response surfaces used to seek the model that was in best accordance with experimental data – inverse analysis.

The 2^k factorial design presented is not ideally suited for the extrusion experiments. The reason is that it is much simpler to provoke an effect by changing either the ram velocity or the billet temperature than the details of the die outlet geometry. In order to change the die outlet experiments had to be interrupted and the die completely dismantled. Besides, the project only had enough funds for four extrusion die outlets. Therefore, it was not possible to perform a full higher-order regression analysis by simply adding a midpoint to the experimental set-up. This is the favoured solution since it would have preserved the orthogonality of the experimental design. Non-linear responses could have been studied, however, by adding levels of billet temperature and velocity. It is also possible to regard the experiments with each of the die outlets as full 2^2 factorial designs. In the case of the experiments with the die outlets with long bearing channels, additional midpoints were added to the design.

Table 3.5. Definition of cases - input variables and levels for each case.

Case	BL	ER	BT	PV	RV	BL	ER	BT	PV	RV
	A	B	C	D	D*	A	B	C	D	D*
1	0	40	450	200	5	-1	-1	-1	-1	-1
2	0	40	450	400	10	-1	-1	-1	-1/3	+1
3	0	40	450	800	20	-1	-1	-1	+1	+5
4	0	40	500	200	5	-1	-1	+1	-1	-1
5	0	40	500	400	10	-1	-1	+1	-1/3	+1
6	0	40	500	800	20	-1	-1	+1	+1	+5
7	0	80	450	200	2.5	-1	+1	-1	-1	-2
8	0	80	450	400	5	-1	+1	-1	-1/3	-1
9	0	80	450	800	10	-1	+1	-1	+1	+1
10	0	80	500	200	2.5	-1	+1	+1	-1	-2
11	0	80	500	400	5	-1	+1	+1	-1/3	-1
12	0	80	500	800	10	-1	+1	+1	+1	+1
13	L	40	450	200	5	+1	-1	-1	-1	-1
14	L	40	450	400	10	+1	-1	-1	-1/3	+1
15	L	40	450	800	20	+1	-1	-1	+1	+5
16	L	40	500	200	5	+1	-1	+1	-1	-1
17	L	40	500	400	10	+1	-1	+1	-1/3	+1
18	L	40	500	800	20	+1	-1	+1	+1	+5
19	L	80	450	200	2.5	+1	+1	-1	-1	-2
20	L	80	450	400	5	+1	+1	-1	-1/3	-1
21	L	80	450	800	10	+1	+1	-1	+1	+1
22	L	80	500	200	2.5	+1	+1	+1	-1	-2
23	L	80	500	400	5	+1	+1	+1	-1/3	-1
24	L	80	500	800	10	+1	+1	+1	+1	+1
25	L	80	450	1600	20	+1	+1	-1	11/3	+5
26	L	80	500	1600	20	+1	+1	+1	11/3	+5
27	L	80	500	2400	30	+1	+1	+1	19/3	+9
28	L	40	475	500	12.5	+1	+1	0	0	+2
29	L	80	475	500	6.25	+1	+1	0	0	-0.5

Table 3.5 presents all the cases run in the experiments. As indicated earlier, the full experimental matrix could not be run in one day and with only one die outlet. There were five rounds of experiments in all (Table 3.6). The first two rounds were run with the very same die outlet, and the objective of performing the second round was mainly to check repeatability. There are several reasons why results from one round of experiments may significantly differ from those of another round. The temperature of the extrusion set-up may not be the same in all the experimental rounds. The pressure sensors may not have been properly calibrated, and the thermocouples may not penetrate to a sufficient depth into the flow. Note that the last rounds of experiments were performed six months after the first ones. A change of process parameters that were not input variables may have occurred if the experimental conditions were not properly recreated. In the analysis of experiments performed according to a 2^k factorial design, the rounds are denoted blocks. The block is a set of cases performed under similar conditions. The blocks should be designed so that the blocking does not affect important effects. In the current study, the effects of the extrusion ratio and the bearing length were confounded with the block effects. It is very unfortunate that first-order effects are affected in this manner, but it is not possible to avoid the problem without using a number of more easily exchangeable die outlets during experiments. This is not possible with the current die design.

Table 3.6. Die outlet inserts and sensor positions at all days/rounds of experiment.

	Date	Outlet	Bearing length	Extrusion ratio	Cases
Round 1	2002.01.08	# 1	Zero	40	1 – 6
Round 2	2002.01.10	# 1	Zero	40	1 – 6
Round 3	2002.01.14	# 2	Zero	80	7 – 12
Round 4	2002.07.10	# 3	Long	40	13 – 18, 28
Round 5	2002.07.12	# 4	Long	80	19 – 27, 29

The objective was to run three replications of each case in a round of experiments. Two of the runs were performed with die face pressure sensors and one with the liner force sensor. Only during a few occasions were all sensors used simultaneously (Chapter 5), since the interaction between the systems made the analysis of results more difficult. It was not reasonable to perform more than three runs of each case, but some exceptions were made. Many of the cases run during round one were in fact genuinely replicated during round two. The ram force and outlet temperatures were measured during all runs.

A randomisation of the runs within a round of experiments may help in reducing the influence of changes in systematic errors occurring during a round. An example is the movement of the pressure sensors during experiments. Another cause of measurement errors is a possible transient heating of the set-up during extrusion. Only a partial randomisation was performed during the two first rounds of experiments. The order in which the cases were run was randomised, but all the runs or replications of a case were performed sequentially. This should allow a closer comparison of the runs of a case, but may impair estimates of effects. During the two last rounds of experiments, complete randomisation was performed. There was no or only a small systematic change of the ram force or the temperature measurements during a single round of experiments. This is probably due to the fact that the waiting time between the experiments was rather long. However, there may be one exception. During the very first experimental run of a

round the responses of the process were seen to deviate from those recorded later in the round. The data from the first runs were never used.

Table 3.6 contains a number of cases that are not a part of the standard factorial design. These cases may be used to test the regression formulas, or they may be included in the regression analysis with a non-orthogonal design. As indicated, one may also establish regression formulas that are only valid in sub-domains. The advantage of the 2^k factorial design is, however, that it is the simplest and most intuitive type of regression analysis. The effect of changing a factor from a high to a low value may be calculated merely by subtracting the average response at a low value of a factor from the average value of the responses at a high value. It may, for example, be assumed that the force is described by the function $f(x_1, x_2, x_3, x_4)$. x_1, x_2, x_3 and x_4 are the factors of the experiment. A scaling has been performed so that the high level is +1 and the low level is -1. Equation (3.3) is an expression of the main effect A_F from a change of the first factor, x_1.

$$A_F = \sum_{\substack{k=-1 \\ k\neq 0}}^{1} \sum_{\substack{j=-1 \\ j\neq 0}}^{1} \sum_{\substack{i=-1 \\ i\neq 0}}^{1} \frac{f(1,i,j,k) - f(-1,i,j,k)}{8} \tag{3.3}$$

Interaction effects such as AB_F, AC_F etc may be calculated in a similar way. The effects may be used in a linear regression formula (Equation (3.4)) to estimate the ram force or any other response of the system. F_0 is the average value of the force.

$$\begin{aligned} F(x_1,x_2,x_3,x_4) = {} & F_0 + \frac{A_F}{2}x_1 + \frac{B_F}{2}x_2 + \frac{C_F}{2}x_3 + \frac{D_F}{2}x_4 \\ & + \frac{AB_F}{2}x_1x_2 + \frac{AC_F}{2}x_1x_3 + \frac{AD_F}{2}x_1x_4 + \frac{BC_F}{2}x_2x_3 + \frac{BD_F}{2}x_2x_4 + \frac{CD_F}{2}x_3x_4 \\ & + \frac{ABC_F}{2}x_1x_2x_3 + \frac{ABD_F}{2}x_1x_2x_4 + \frac{ACD_F}{2}x_1x_3x_4 + \frac{BCD_F}{2}x_2x_3x_4 \\ & + \frac{ABCD_F}{2}x_1x_2x_3x_4 \end{aligned} \tag{3.4}$$

The scaling of the input variables may be suited to the problem at hand. Very often there may be a close to linear relationship between the x_i values and the non-scaled values of the input variables. The bearing length ratio, BL, may be scaled according to Equation (3.5).

$$x_1 = \frac{BL - 0.38}{0.38} \tag{3.5}$$

It is assumed that the bearing length-to-diameter ratio for the long bearing channels is exactly 0.76. Alternatively, one may just look upon the bearing channel as on / present (+1) or off / absent (-1). Outlet dimensions may either be expressed by the extrusion ratio, ER, or the diameter of the rod, OD.

$$x_2 = \frac{ER - 60}{20} \quad \text{or} \quad x_2 = \frac{-OD + 13.5}{2.3} \tag{3.6}$$

It is possible and probably best to express forces and pressures as a logarithmic function of the extrusion ratio. Such a relation would be in greater agreement with the results from earlier experiments and analytical expressions. The set of experiments described in the current report does not allow conclusions on the quality of the approximations to be drawn. The linear scaling of the billet temperature, *BT*, is given as:

$$x_3 = \frac{BT - 475}{25} \tag{3.7}$$

The linear scaling of either the profile velocity, *PV*, or the ram velocity, *RV*, may be expressed in several ways depending on the choice of midpoint of the design.

$$x_4 = \frac{PV - 500}{300} \qquad x_4 = \frac{RV - 12.5}{7.5} \tag{3.8}$$

It is also possible to scale the velocities in a non-proportional way.

$$x_4 = \frac{\ln(PV/100)}{\ln 2} - 2 \qquad x_4 = \frac{\ln(BV/2.5)}{\ln 2} - 2 \tag{3.9}$$

As a consequence $x_4 = 0$ when $PV = 400$ mm/s and $BV = 10$ mm/s, which may or may not be more appropriate. However, the scaling will not help in making the experimental design orthogonal.

3.3 Flow and die deformation modelling by the finite element method

One of the reasons for developing pressure sensors was to establish a tool that allows testing of the fundamental hypotheses of extrusion models. The extrusion models may be inaccurate even when applied to relatively simple problems. However, in an assessment of the pressure sensor behaviour, the deduction of pressure estimates by the extrusion flow models may prove necessary. This situation may at first be regarded as a highly unfavourable one, but it should be realised that this is by no means an uncommon problem in science. There are almost always errors related to measurement and models of the kind treated in the current study. This may very often not be fully comprehended before significant and seemingly unexplainable discrepancies appear and must be explained. A series of modifications of both the experimental techniques and the hypotheses of the models may then follow. The advances in modern science have been closely linked to the advance of measurement technology and vice versa. Research is in many ways an iterative process, in which experiments provide physical data and assumptions are made and tested. Whether the starting point should be a set of physical observations or a hypothesis of some kind is a question that is open for discussion. The question may in the end not be very important.

Estimates of force, temperature and pressure are first calculated by the finite element code ALMA2π according to assumptions that will be more thoroughly discussed. The starting point is a natural one. In order to design sensors both the mechanical loads and the temperature changes must be known, and in order to plan experiments a sense of the responses that could be expected had to be established. In order to test a hypothesis estimates that could be evaluated first had to be deduced. Even though there are large uncertainties related to the measurements of the die face pressure, it is at a minimum possible to use the pressure sensors to evaluate the accuracy of numerical simulation codes and vice versa. The ram force and the outlet temperature of the die were measured independently with fairly well established techniques. A minimum requirement for the simulation code is that it should be able to estimate these process responses with sufficient accuracy. The issue has been treated in reference [Moe04b].

3.3.1 Hypotheses of flow and die deformation simulations

The fundamental hypotheses of aluminium extrusion codes relate to how the material flows at high temperatures and how it interacts with the surrounding tool. However, one also has to make assumptions with regard to heat transfer both in the aluminium and to the surrounding tools. Assumptions are also made with regard to the thermo-mechanical behaviour of the tools. The extrusion steel die is usually regarded as either perfectly rigid or able to deform elastically. However, dies may plastically deform and creep if they are exposed to high loads and temperatures.

During extrusion, aluminium behaves both thermoelastically and viscoplastically. As is further discussed in Volume I, this means that the material expands thermally and is compressed elastically while it flows by shear deformation. At high temperatures it is often assumed that there is no threshold for the initiation of viscoplastic flow. The material flows like a fluid even when exposed to the very smallest deviatoric stresses. More thorough approaches make possible the implementation of more complex flow criteria and anisotropic material behaviour. Yet, in the current section it is assumed that at high temperatures the flow is simply purely viscous, and furthermore, that elastic deformations may be disregarded. The flow stress, σ_f, is assumed to be determined by the Modified Zener-Hollomon relation:

$$\sigma_f = \frac{1}{\alpha}\operatorname{asinh}\left(\left(\mathrm{Z}/\mathrm{A}\right)^{1/n}\right) + C\frac{\left(Z/A\right)^{1/n}}{\sqrt{\left(Z/A\right)^{2/n}+1}} \qquad (3.10)$$

A, α, m and C are the parameters of the flow rule. σ_f is the flow stress, which should be compared with an equivalent measure of stress. Z is the Zener parameter, which is a temperature-compensated measure of equivalent strain rate.

$$Z = \dot{\bar{\varepsilon}}\exp\left(Q/RT\right) \qquad (3.11)$$

Q is an activation energy related to self-diffusion in aluminium. R is the universal gas constant, and T is the material temperature. The material data used in the Modified

Zener-Hollomon relation have been determined in [Moe04b] and are presented in Table 3.2. The original Zener-Hollomon relation has at least partly been validated in studies of dislocation mechanics, but is mainly used because it is suitable for curve fitting. It may with some success be applied to fit experimental data over a relatively large range of strain rates and temperatures. As has been discussed in [Moe04b] and in Chapter 2 of Volume I it is not certain that it may be used to describe all aspects of flow during extrusion. The use of material data established in compression and torsion testing constitutes an extrapolation of data that has to be controlled. Note that when $C = 0$ the Zener-Hollomon relation and the Modified Zener-Hollomon relations are identical.

A second fundamental assumption of the current study relates to the nature of friction between the die and aluminium flow. Since the material is hot and flows easily, it has a tendency to stick to the walls of the container. It is commonly assumed in the study of extrusion that the velocity of aluminium particles parallel to the container wall is zero. The hypothesis is adopted for the current study, but it may be tested by the use of the liner load cell. The popularity of the full sticking assumption is not unreasonable. The assumption seems to be in fair agreement with experience. It is easy to implement in some codes and makes it unnecessary to introduce more parameters in the model. The friction stresses are completely controlled by the flow of the material in the billet and therefore by the parameters of the Zener-Hollomon relation. There is, however, a risk that shear stresses may be exaggerated, because there are reasons why shearing occurs at lower stresses than the flow stress. One reason is that the material is of a different composition in the boundary layer than in the interior of the billet. Another is that the strain rate and temperature dependency of deformation may differ in the high-rate regions close to the walls and in the interior of the material. A third reason may be a less intimate contact at boundaries. There is in such cases the possibility that shear stresses may also be pressure-dependent. Appropriate friction relations are available (Volume I).

Deviations from the full sticking assumption are most likely to occur at the die outlet even when there are choked bearing channels. One envisions that in the outer part of the bearings there is slipping or pressure-dependent friction, while there may be full sticking in the inner part of the bearings. The surface of the profile is assumed to be generated somewhere in between. The issue is treated in more detail by Abtahi [Abt95] and Tverlid [Tve97]. In the current study no numerical calculations on the pressure build-up in the die outlets with long bearing channels are performed. The experiments have, however, been designed so that the various assumptions with regard to bearing channel friction may be tested. The analysis presents relevant analytical calculations based on both the full sticking and stick-slip hypotheses (Chapter 6).

Temperature calculations are based on the assumption that heat conduction is isotropic and according to Fourier's law in all domains. The heat conductivity of aluminium is assumed to be 200 W/mK while the specific heat capacity and density have rather roughly been set to 900 J/kgK and 2700 kg/m^3. The material properties of the tool steel have been given in Table 2.2. The heat transfer coefficient between the billet and the surrounding steel parts has generally been set to 20 000 W/m^{2}K, while the heat transfer coefficient of 5000 W/m^{2}K is used between the various steel parts of the tool package. Sensitivity studies have been run. A glimmer plate placed between the bolster and the

fulcrums to prevent heat from escaping has been modelled as an interface with a very low heat transfer coefficient (50 W/m^2K). When the die is assumed to behave only elastically, the temperature-dependent material properties of Table 2.2 have been used. In relation to pure flow calculations, the tools may be regarded as completely rigid.

The extrusion process may not be expected to be perfectly described by a model based on the hypotheses presented above. Errors in results of typically 10 % or even more must be expected. Most of the material data that have been used to model the problem are only approximate. The calculations constitute merely a first iteration. There are also more serious limits to the ability of the codes to describe nature's mechanisms. In the current case one is mainly interested in estimates of the die face pressure, ram force and die outlet temperature. A continuum model using the Zener-Hollomon flow relation may then be regarded as probably the simplest one that can be expected to produce acceptable predictions for a wider range of process conditions. More complex models may also be developed to better describe the processes occurring during aluminium extrusion. Continuum-mechanical models may be coupled with models for evolution of the microstructure. Such models should be expected to better describe strain hardening and softening that may occur especially in the early phases of the process. They may also better describe flow localisation, high speed deformation and friction mechanisms. It would probably be possible to introduce particle-based models to more closely study such phenomena. However, a pragmatic approach to the problem is adopted, for it is not the objective of this study to establish new models. It would in fact be best if the model contains a known and fairly easily identifiable error, which the sensors could uncover. Neither the Zener-Hollomon flow rule nor the full sticking hypotheses may be expected to be completely in error. An assumption of isotropic material behaviour might work quite well. As has been discussed in reference [Moe04b], there may be a number of modelling approaches that may produce quite acceptable estimates of force and outlet temperature. The question is whether or not they may be used to describe and predict more complex phenomena related to flow instabilities or microstructure evolution. As will be further discussed in Chapter 6, the only hypothesis that seems to be contradicted by experimental results is one that predicts full sticking friction in the complete bearing channel. It therefore serves as an appropriate test case, and the experiments have been designed accordingly.

3.3.2 Numerical simulation codes

Flow simulation

There are numerous numerical approaches available in the study of material flow, but there have been few thorough comparisons of simulated and measured results. In the current study, only the finite element method has been used. Different formulations may be adopted to assess the flow and die deflection problems. The flow may be described for example in an Eulerian or an updated Lagrangian manner. In the Eulerian approach, the mesh is fixed in space while the material flows through it. The Lagrangian approach assumes that the mesh convects or flows along with the material. It is more difficult to describe history dependence with the Eulerian technique and the boundaries are by definition fixed in space. The Lagrangian technique has been used extensively to model material forming processes to moderate levels of deformation. The implementation of

elasto-viscoplastic material models is usually simpler using the Lagrangian framework, and it may in addition be easier to model contact and friction mechanisms. The main disadvantage of the Lagrangian approach is the need for relatively frequent re-meshing when deformations are large. During extrusion the material may easily be elongated as much as 80 times, and there is extensive shear deformation. If the elements are allowed to be distorted with the material, their aspect ratios and performance quickly degrade. The problem is greatest in the close vicinity of the die outlet. When the standard codes for forging analysis are used to study extrusion, the amount of time spent on re-meshing and the solution of equations may be considerable. It is possible to improve routines for re-meshing, and they may be adapted to the extrusion problem. Still, calculation times may be extremely long. There is also the problem that the mesh need not be perfectly compatible with the boundaries of the billet domain, and that force estimates may change somewhat immediately after re-meshing. The fact that there are both advantages and disadvantages related to each of the formulations makes it natural to seek the best in both. The Arbitrary Lagrangian Eulerian (ALE) approach allows the user to specify the convection of the mesh. This may be very useful in the study of the extrusion process. The mesh may be gradually compressed to compensate for the billet length reduction due to the ram movement. Close to the outlet, however, the mesh may be of the Eulerian type, since shape distortions are large, and since it is necessary to very accurately define the geometry of the die outlet. In or after the bearing channel, the mesh may again be convected to allow for a better description of the thermo-mechanics of the profile in the air and in contact with the bearings. A proper description of elastic deformation may be of importance in the study of stick-slip behaviour in slightly choked bearing channels. If history dependence is to be described by the ALE codes, they must implement some method of convecting information as the mesh moves. In the case of the Lagrangian approach, this is simpler as the mesh and material move together. During re-meshing, however, the information must be transferred from the old to the new mesh. Fully elasto-viscoplastic behaviour, yield-surface-like concepts and anisotropy may be implemented in all formulations, but the ease with which it is done may differ.

The estimates of ram force, outlet temperature, die face pressure and other responses of the current study have been deduced with the dedicated finite element code ALMA2π. The code was developed in the beginning of the 1990s by the extrusion research group at the Norwegian University of Science and Technology and SINTEF. ALMA2π treats a two dimensional axi-symmetric geometry. It takes into consideration the movement of the ram like any ALE code, but it does not consider the thermo-mechanical behaviour of the extruded profile in the air. The material behaviour is assumed to be purely viscous, and the most relevant flow relation implemented is the Modified Zener-Hollomon (Equation (3.10)). The Zener-Hollomon relation is a special type of Modified Zener-Hollomon relation ($C = 0$). The latest versions of ALMA allow modelling of pressure-dependent friction in the bearing channel. An advantage of the ALMA group of programs is that they more or less automatically take into consideration the heat transfer to the tools. It is therefore possible to study effects related to the gradual heating-up of the tools caused by the heat dissipation during extrusion. This may be relevant in industrial cases when the pause between each run is very short. In the current study, there is sufficient time for the heat to flow away from the container and die in between the runs. ALMA2π considers both the loading phase and the burp phase, but only in a

rather approximate manner. There is no increase in the diameter of the billet due to plastic deformation, so the prescribed billet dimensions should be those of the billet after the burp phase. The initial transient phase of extrusion is also not considered since it would have required a description of the movement of the newly generated surface. It is simply assumed that there is a butt end in the container when the new billet is loaded. Heat transfer between the butt end and the new billet is taken into account. It is possible to make the butt end very thin as if it was almost not present, but this is only an approximation. One of the reasons for not removing butt ends in between runs was that this type of extrusion may be most accurately modelled with ALMA2π. It should be added that it in fact may be somewhat harder to model extrusion with a butt end in a commercial software package. One has to consider heat flow prior to extrusion and the special geometry of the billet. There are also, as discussed earlier, other disadvantages related to this type of billet-to-billet extrusion.

Figure 3.3 and Figure 3.4 present estimates of the temperature distribution in the billet and bearing channel for a total billet height of 130 and 20 mm. The simulation has been performed for an extrusion ratio of 40, and there was virtually no bearing channel. The initial billet temperature was 450 ºC and the profile velocity was 400 mm/s. The initial ram temperature was as in the experiment 130 ºC. During extrusion the front end of the ram is slowly heated while the back end of the billet is cooled. The highest temperature in the bearing channel is close to 530 ºC. When the ram is close to the outlet, the cooling of the billet also has a distinct effect on the profile temperature. Figure 3.5 and Figure 3.6 present the isotropic pressure in the container for remaining billet lengths of 130 and 20 mm. When the billet is long, the dead zone close to the die face is large and the die face pressure is fairly uniform. When the billet is very short, the material flow is mainly in the radial direction, and there is a large pressure gradient. Close to the end of the run, there are similar pressure distributions at the die face and the ram face. The ram pressure is somewhat higher than the die face pressure due to the friction between the billet and container. Since the pressures are so high, the hydrostatic pressures deviate only slightly from the component of stress normal to the tool surfaces. It may therefore be relevant to talk about pressure measurement for what actually is the measurement of forces normal to the die surface or of tractions in general.

Some other commercial finite element packages have also been tested. Forge2® [TraW] by Transvalor® was used in the early parts of the study to aid in the sensor design work, but the Lagrangian formulation was to be found somewhat awkward to use in relation to the inverse modelling work. Calculations were very time-consuming, and sensitivity analyses were for that reason difficult to perform. Forge2® and ALMA2π produce force and temperature estimates that are similar, but no thorough analysis of differences has thus far been performed. One of the objectives of the reporting of the results from the experiments has been to stimulate comparative studies of flow. An extrusion flow model has also been built in ANSYS® Flotran in cooperation with Wojciech Wajda. The formulation is similar to that of ALMA2π, but it is not limited to 2D and allows the user to closely combine flow and die deflection calculations. Another advantage of the ANSYS® package is that the user is allowed much more control with the mesh displacement than in ALMA2π. The main disadvantage is that the calculation times are significantly longer than for ALMA2π. The force and temperature estimates from the

two programs were quite similar, at least in the early phases of the runs. In the later phases, differences were observed. These may be due to improper modelling of heat flow in the ANSYS® Flotran package. Note that the implementation of the Zener-Hollomon flow relation in ANSYS® Flotran is a user-controlled feature, which has not been properly checked yet. At the same time, ALMA2π has been used extensively for more than ten years by the extrusion communities at Hydro Aluminium, NTNU and SINTEF. Therefore, in this study results are only calculated with ALMA2π. Appendix M describes a planed comparative study.

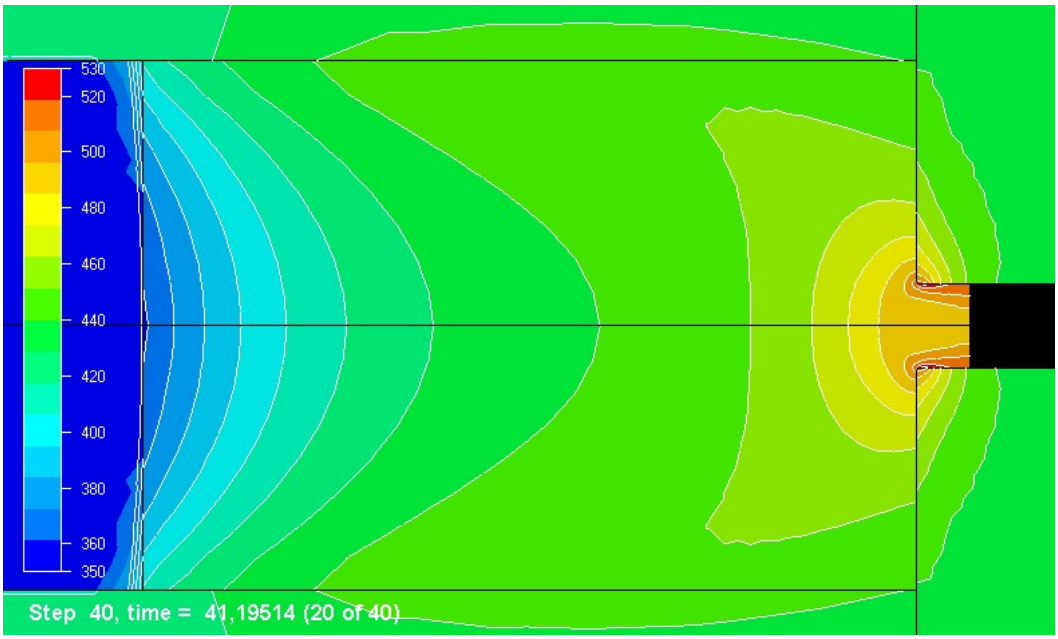

Figure 3.3. ALMA2π flow simulation – the temperature in the billet and tools

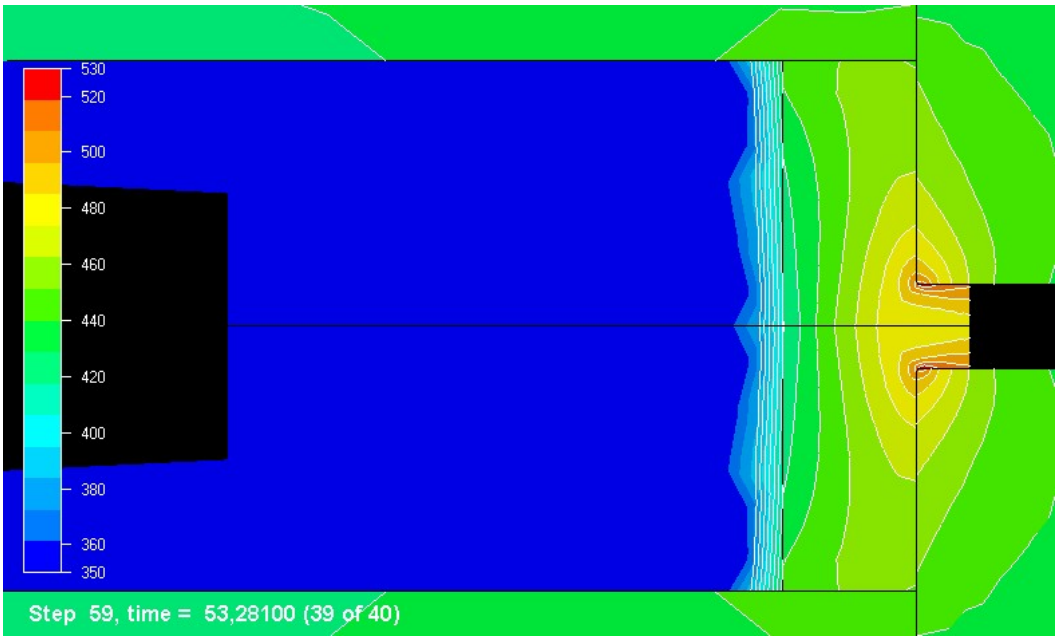

Figure 3.4. ALMA2π flow simulation – the temperature in the billet and tools

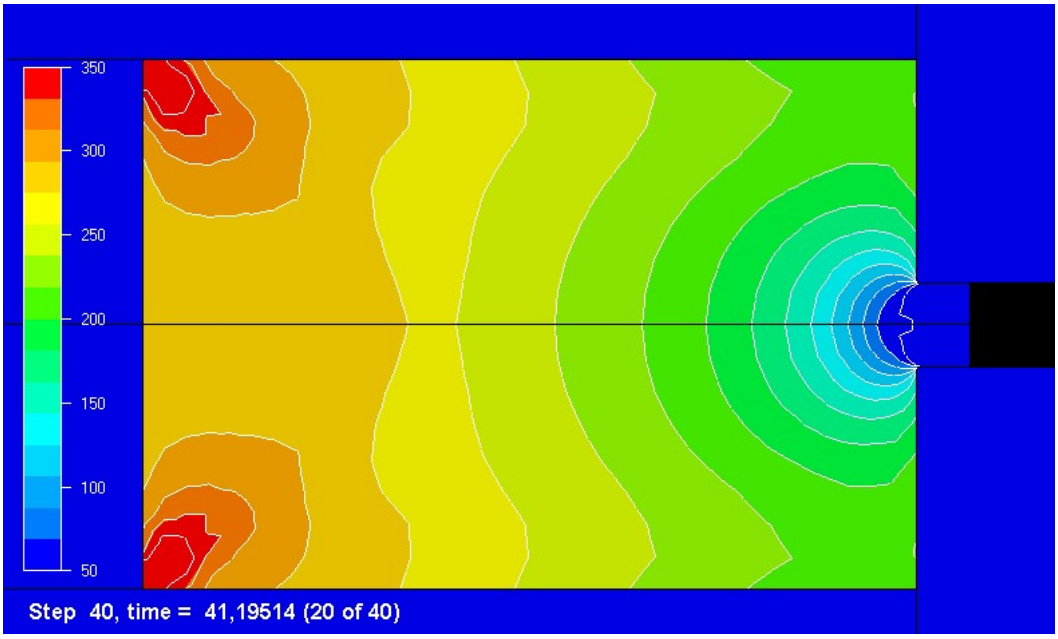

Figure 3.5. ALMA2π flow simulation – the hydrostatic pressure in the billet

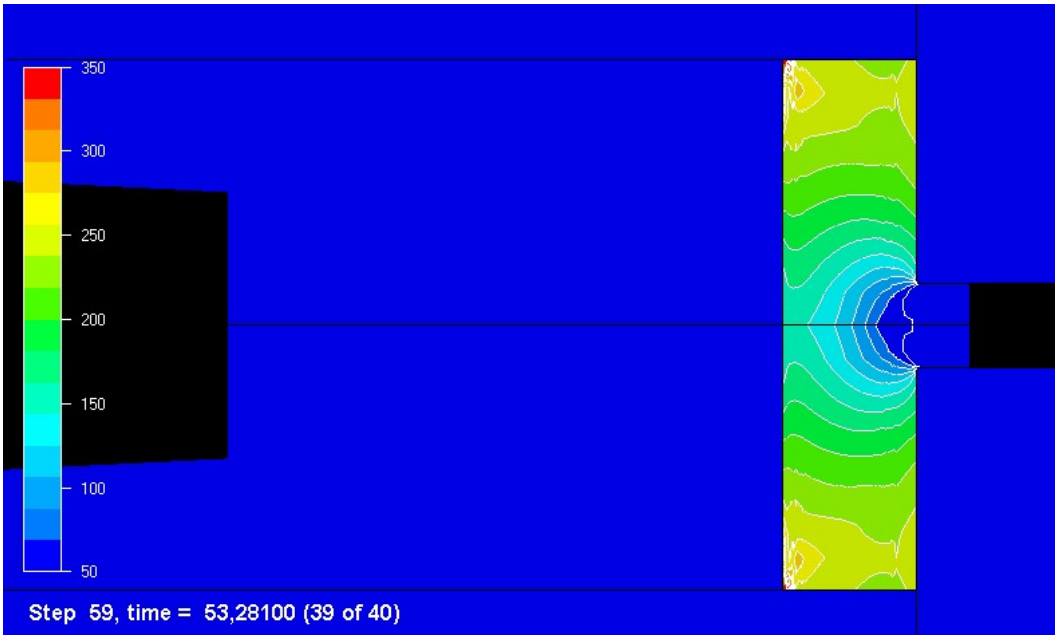

Figure 3.6. ALMA2π flow simulation - the hydrostatic pressure in the billet

Die deformation calculations and coupling of codes

In the current study, ANSYS® 7.1 has been used for the die deformation calculations. The analysis is one of small strains, and the Lagrangian approach has been used. The effect of non-linearities caused by geometrical changes may usually be disregarded since the deformation of the die is only moderate. Purely thermo-elastic material models are mainly used, but in order to better understand the behaviour of the sensor it has been necessary to make use of isotropic and kinematic hardening models of the simplest types. Unfortunately, only very basic information about the plastic behaviour of the tool

steel at high temperatures has been obtained from the steel manufacturer (Figure 2.8). Elements of the type SOLID92 and SOLID95 have been used in the three-dimensional analysis. The elements are based on interpolation functions of second order since they are more capable of modelling the bending of thick discs. A characteristic element size of 1 to 1.5 mm close to the sensor disc was sufficient to estimate displacements. This corresponded to 2 to 3 elements across the thickness of the disc. Slightly smaller elements were also needed to evaluate the state of stress. Figure 3.7 presents the entire tool stack model as well as the details of the meshing of the extrusion die.

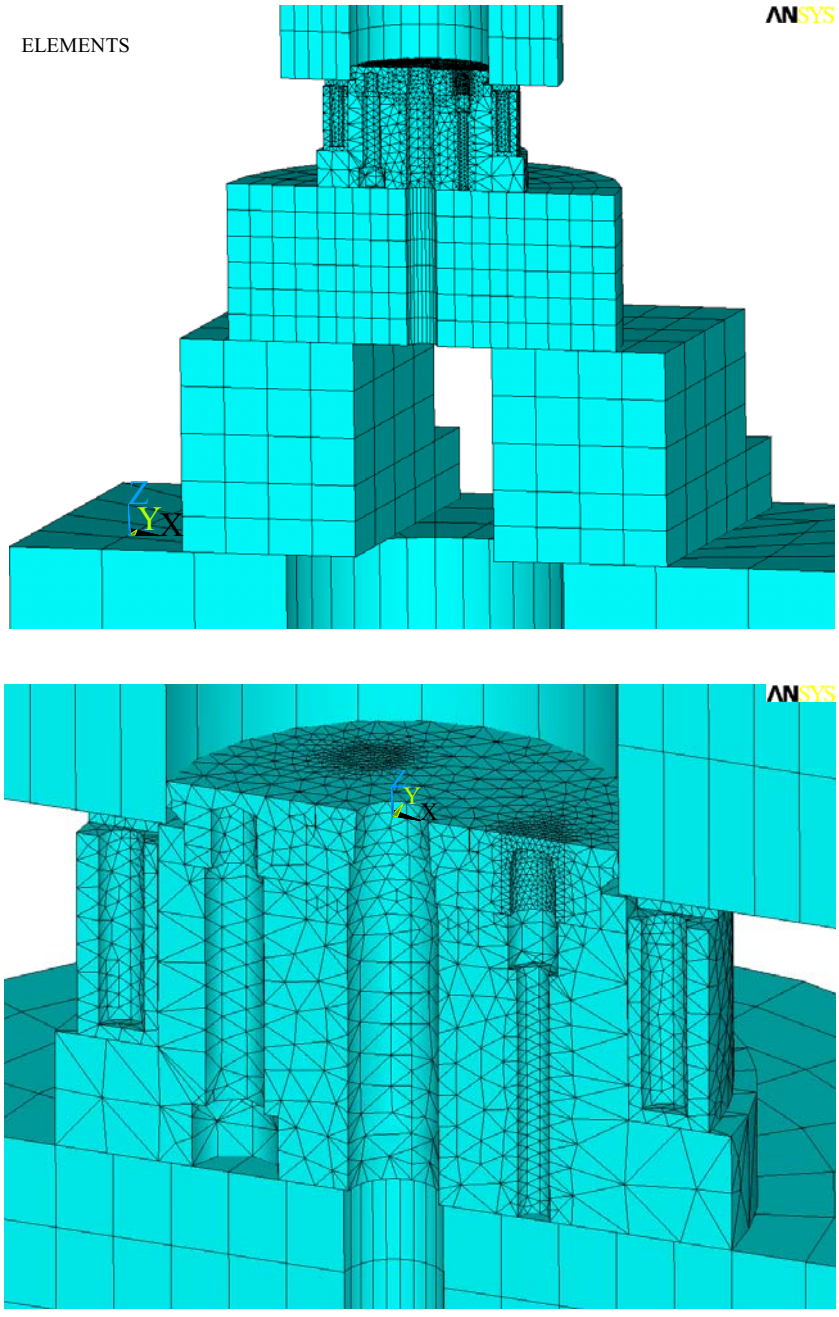

Figure 3.7. The finite element mesh of the extrusion die model in ANSYS® 7.1.

In order to model the contact between various parts of the tool package, the TARGE170 and CONTA174 second-order elements were used. The contact friction between the parts was assumed to be rough (with friction), and friction factors in the range from 0.1 to 0.3 were used. In fact, the magnitude of the friction factor did not significantly influence the results. It is important that a friction factor be sufficiently large to prevent tools from displacing in a direction normal to the extrusion direction. The contact between the fulcrum and the press board was of the no-separation type. The reason was that the fulcrums are firmly fastened to the press board by bolts, which are not modelled directly. Due to the special design of the tool stack, one half of the geometry had to be evaluated. However, when only the sensor behaviour is of interest, acceptable results may be obtained with a simpler model [Moe04c]. If only the die, bolster and container are included in the die deformation model, it is sufficient to treat a piece spanning an angle of 60º, i.e. 1/6 of the geometry. The probe and probe holder were included in some models and not in others. It is a fairly complex matter to model the interaction between the probe holder and top disc, so inaccuracies must be expected to be large. In some cases it may be better to estimate the relative movement for the bottom of the sensor disc and the fixing points for the probe holder.

Essentially, two types of calculations were performed. The simplest type was a study of the sensor behaviour under steady state conditions. It was assumed that the temperature of the die is uniform or that the temperature could be calculated from a set of boundary conditions. The second type was the transient analysis of the sensor behaviour during extrusion. The method of estimation for the sensor response to temperature changes is shown in Figure 3.8. ALMA2π was first used to estimate both the temperature at the die face and the tractions. ALMA2π also calculated the temperature of the tools, but the tool geometry was described only in a very approximate manner. The description is axi-symmetric while a three-dimensional model was necessary to properly describe the thermo-mechanical aspects of the sensor behaviour. Therefore, the die surface/interface temperatures calculated by ALMA2π were applied as boundary conditions in a more exact ANSYS® 7.1 tool stack temperature analysis. For most purposes it was sufficient to treat only the die, container and bolster in this analysis. The steady state temperature distribution that existed before experiments started was first calculated. The tools in contact with air lost heat mainly by heat convection. The bolster and container were continuously heated so that their temperatures were 480 and 430 ºC respectively. After extrusion the flow of heat from the billet to the die was not exactly known. Generation of heat by plastic deformation stopped when extrusion was halted, but the butt end was at an elevated temperature. On the other hand, it was in close contact with the colder dummy block, and after the retraction of the ram it lost heat to the air. It has merely been assumed that there after extrusion was convection from the die face to the surroundings. The convection coefficient was assumed to be roughly 200 W/m^2K. The assumption is most probably far too simple. The consequences of the simplification are treated in relation to the analysis of the experimental results (Chapter 6). It should here only be noted that the focus of the analysis was on the extrusion phase. The ANSYS® 7.1 thermal analysis makes use of the element SOLID85, which is second order. It was mainly chosen because it is compatible with the second order elements for the part of the analysis relating to mechanical calculations.

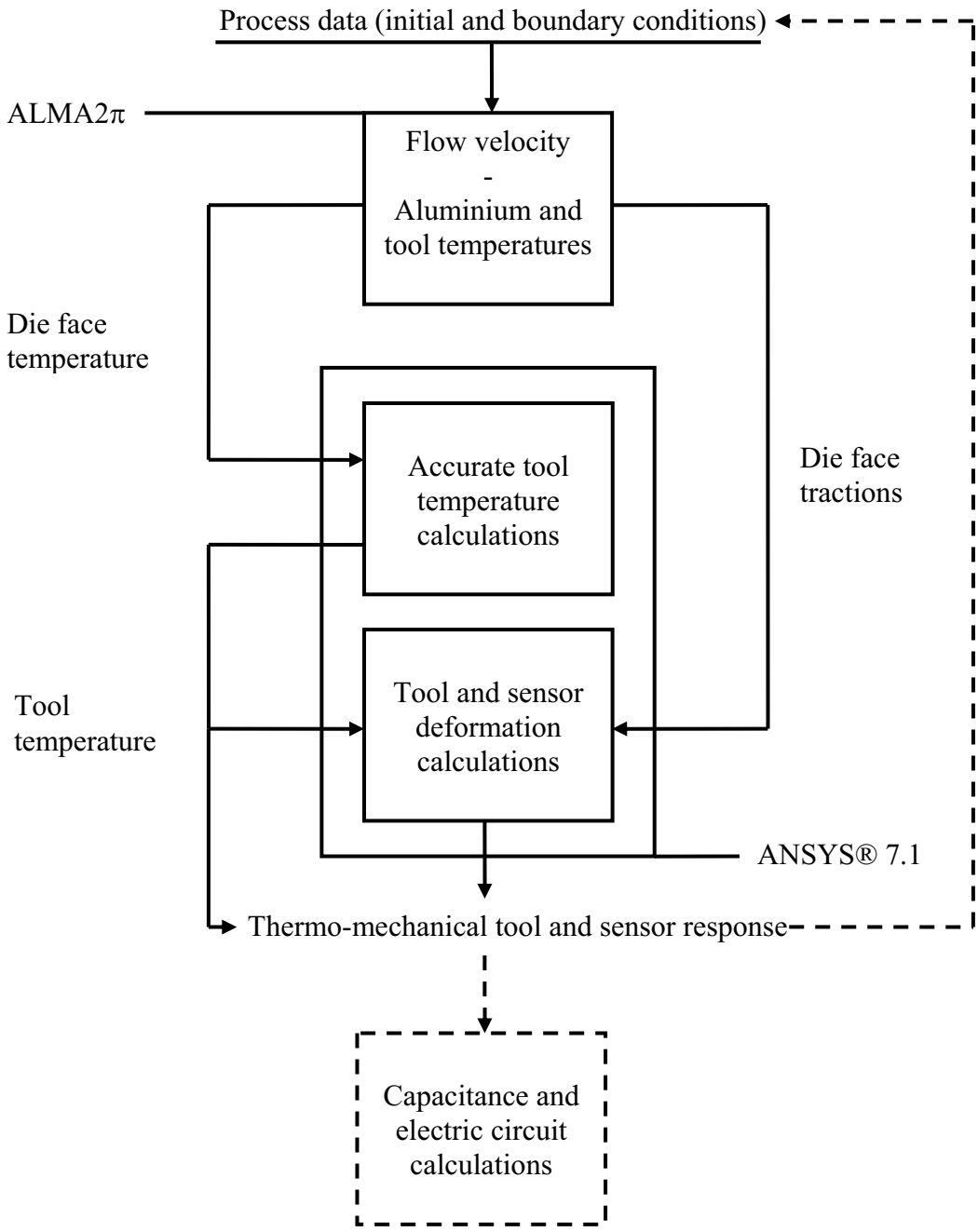

Figure 3.8. The principle underlying the thermo-mechanical (and electromagnetical) sensor response calculation. The figure describes the ANSYS® script.

Thermal and mechanical calculations were performed separately. The temperature was evaluated at a number of time steps. Heat expansion caused the die to deform. Tractions may be transferred from the ALMA2π calculations. However, in order to better understand the temperature effect, a constant uniform die face pressure or no pressure at all was applied. The focus has been on the pressure distribution since interface shear tractions were small. The thermal and mechanical calculations with ANSYS® 7.1 were decoupled, as no or very little heat generation was related to the tool deformation. In the analysis of flow in extrusion, it may be natural to perform iterations at each step in time.

The shape of the die may change, and the flow calculation may be affected. The need for an iterative approach is, however, relatively small in a study of rod extrusion. Nonetheless, the necessity of performing a coupled analysis in relation to the detailed study of sensor behaviour should be considered. There may be interesting effects related to the dynamic response of sensors. Additionally, the flow of heat around the sensor and the thermal response may deviate somewhat for the coupled and decoupled analyses.

In relation to the study of temperature effects, it may be natural to integrate a final step with the simulation of capacitance changes. This may be performed in ANSYS® 7.1. There are at least two advantages of such a calculation. First, it allows a closer study of the effects of changes in electromagnetic properties. Second, it allows a more accurate determination of the effects of sensor deformation. In the current analysis the disc deflection changes due to pressure and temperature changes were converted to pressure changes by the use of calibration factors for deformation and pressure to be deduced in the next section. A better understanding of the problem may be established through capacitance calculations even though the accuracy of measurement need not improve. An accurate description of probe geometry and sensor properties was not available, and there were serious questions related to the details of probe mounting. The measurement variability is very large, and it is difficult to take into account the random phenomena related to thermo-mechanical and electromagnetic behaviour.

3.3.3 Deduction of absolute values and effects by finite element models

In this work, ALMA2π was used to calculate estimates of the various responses for runs 1 to 12. The experiments with the long bearing channels were not considered. There were several reasons. First, the stick-slip bearing channel friction model had only fairly recently been implemented in ALMA2π, and the performance of the code had not yet been properly checked [Abt03]. Furthermore, the objective of the current study has primarily been to evaluate pressure sensor behaviour, and the inclusion of the bearing friction modelling at the present stage would primarily serve to complicate matters. A qualitative evaluation of the experimental results from extrusion cases 13 to 24 has been performed in the final analysis on the basis of calculations for the cases with the zero length bearing channel geometry. Finally, the numerical calculations were only meant to give an indication of what could be expected to be observed during experiments and as a starting point for the analysis.

Figure 3.9 and Figure 3.10 show the ram force predictions for the cases 1 to 6 and 7 to 12 respectively. The initial billet length was assumed to be 200 mm, and the final billet length was 19 mm. The remaining billet height of the abscissa was the vertical distance from the bottom face of the ram to the top face of the die. No distinction is here made between the terms billet height and length. Characteristic values of the system responses are more closely evaluated at billet heights 196, 170, 100 and 30 mm. The positions, from which data are taken, are indicated by symbols in the figures. Table 3.7 shows the force responses and the effects of changing the three factors of the regression model, the extrusion ratio, the billet temperature and the profile velocity. Two different choices of interpolation schemes are assessed. D^1 assumes that the relationship between the factor x_4 and PV is linear, while D^2 assumes a logarithmic function (Equation (3.9)).

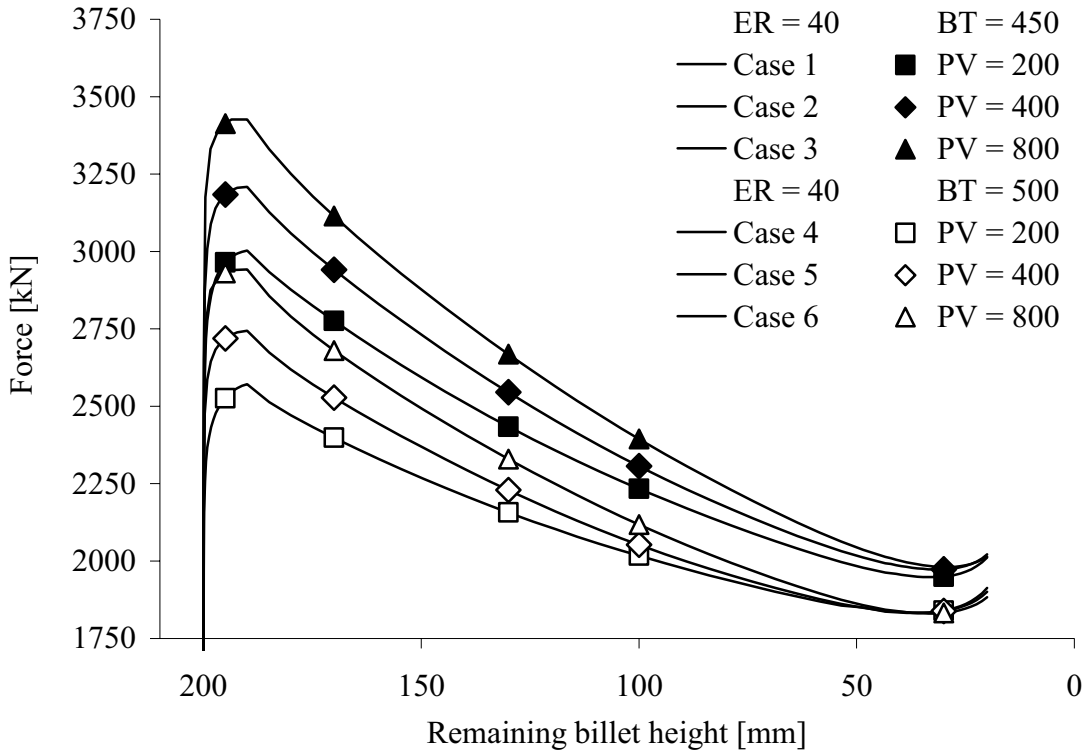

Figure 3.9. Estimates of ram force by ALMA2π - extrusion ratio 40.

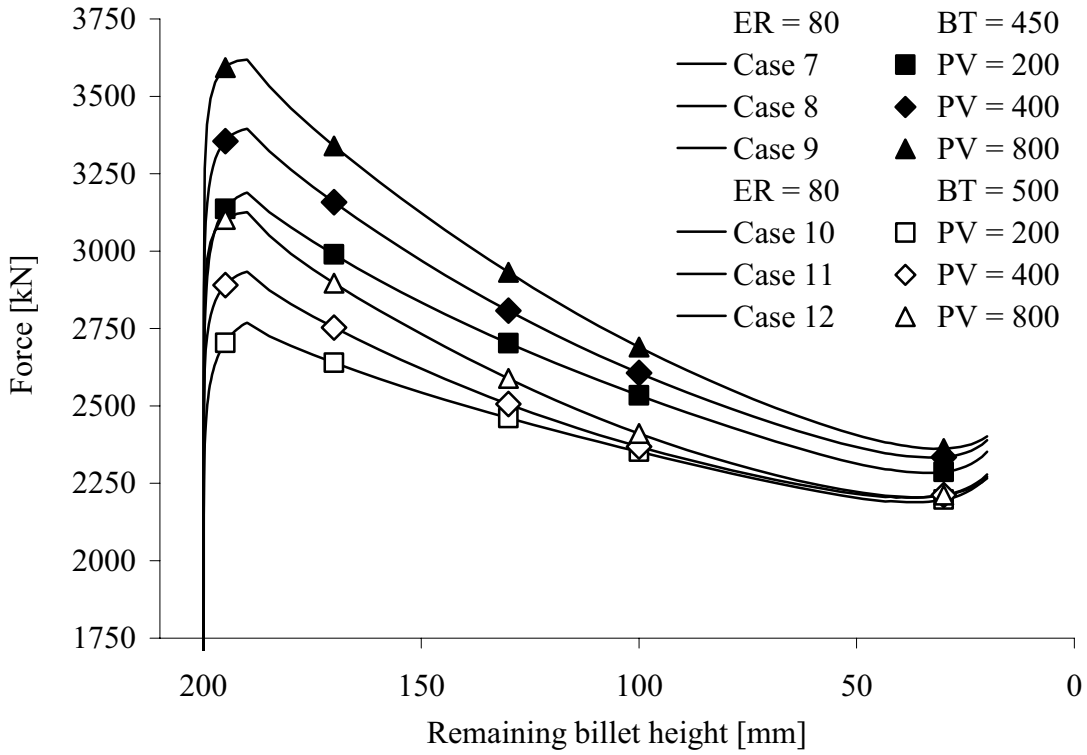

Figure 3.10. Estimates of ram force by ALMA2π - extrusion ratio 80.

Table 3.7. Force response [kN] predicted by ALMA2π (profile velocity as a factor).

Case		*ER*	*BT*	*PV*	*PV*	Billet length [mm]			
	AVG	B	C	D^1	D^2	196	170	100	30
1	1	-1	-1	-1	-1	2965	2776	2234	1950
3	1	-1	-1	1	1	3413	3114	2395	1981
4	1	-1	1	-1	-1	2526	2398	2017	1840
6	1	-1	1	1	1	2930	2680	2118	1833
7	1	1	-1	-1	-1	3136	2989	2534	2287
9	1	1	-1	1	1	3593	3340	2690	2363
10	1	1	1	-1	-1	2704	2640	2352	2197
12	1	1	1	1	1	3102	2897	2411	2212
2	1	-1	-1	-1/3	0	3184	2941	2307	1973
5	1	-1	1	-1/3	0	2719	2528	2053	1839
8	1	1	-1	-1/3	0	3356	3158	2607	2335
11	1	1	1	-1/3	0	2891	2753	2369	2212

Effects	Billet length				Estimated forces for cases 2, 5, 8 and 11				
	196	170	100	30	#	196	170	100	30
							D^1		
AVG	3046	2854	2344	2083	2	3115	2889	2287	1960
B - ER	175	224	306	364	5	2660	2492	2051	1838
C - BT	-461	-401	-239	-125	8	3288	3106	2586	2312
D - PV	427	307	119	29	11	2837	2725	2372	2202
							D^2		
BC	0	5	8	4	2	3189	2945	2314	1965
BD	1	-3	-12	17	5	2728	2539	2068	1836
CD	-26	-37	-39	-25	8	3364	3165	2612	2325
BCD	-4	-9	-9	-6	11	2903	2768	2382	2204

Cases 1, 3, 4, 6, 7, 9, 10 and 12 have been used to establish the data for the regression equations. While all the main effects, *B*, *C* and *D*, are clearly significant, some of the interaction effects may be disregarded. When the extrusion ratio is increased from 40 to 80 the ram force increases, but ALMA2π predicts that there is no significant interaction between the extrusion ratio and the other factors. The fact that Figure 3.9 and Figure 3.10 have more or less the same appearance, indicates that *BC*, *BD* and *BCD* are small. *BD* is of significance when the billet height is small. The two-factor interaction effect, *CD*, is more important. The effect of a velocity change is smaller at high than at low temperature. An approximate regression equation at billet height 170 mm is then:

$$F\left(x_2, x_3, x_4\right) = 2854 + 112x_2 - 201x_3 + 154x_4 - 19x_3x_4 \qquad (3.12)$$

Alternatively the force may be related directly to *ER*, *BT* and *PV*:

$$F\left(ER, BT, PV\right) = 5307 + 5.6ER - 6.5BT + \frac{\ln\left(PV/100\right)}{\ln 2}\left(515 - 0.76BT\right) \qquad (3.13)$$

Equations (3.8) to (3.9) have been used to deduce Equation (3.13). Factor x_2 has been expressed as a linear function of the extrusion ratio and not of the outer diameter of the rod. A logarithmic relation might have been more appropriate. Further simulation runs would be necessary to decide the relationship that is most appropriate, but since experiments are only performed at one of two levels, the results of such an analysis are not very important. As earlier indicated, it may be interesting to use the ram velocity as a factor rather than the profile speed. Some possible levels of the ram velocity are shown in Table 3.4. An alternative non-linear regression equation may also be obtained simply by inserting $PV = ER \cdot BV$ into Equation (3.13).

A logarithmic rather than a linear function has been used to relate x_4 and PV. The two approaches may be tested by running simulations at profile velocities of 400 mm/s. The cases 2, 5, 8 and 11 may be regarded as test cases. The logarithmic relationship seems to be the best. The estimates of Table 3.7 have not been calculated with Equation (3.12), but rather with equations including all the possible relevant terms. Results obtained with Equation (3.12) may deviate by ±20 kN from the more accurate ones.

The most important information to be drawn from Figure 3.9 and Figure 3.10 is that ram force response changes by almost 1000 kN may be caused by changing the three factors of the experimental matrix. The differences in the response are the largest in the initial phase of the run. When extrusion is run at a high rate, the strain rate is obviously higher, but the temperature also increases more due to the larger heat generation and smaller conduction to the surroundings. The effect of a profile velocity change is small towards the end of the run (assuming that two cases run at constant velocity are compared). When running an inverse analysis one should probably consider both the early and late phases of the run. However, estimates of force calculated by ALMA2π and results from experiments may deviate somewhat in the very beginning. The reason is that the ram speed need not be constant. During experiments the ram speed is very often increased only gradually. The calculations assume that the velocity increases linearly from zero to full velocity over a length of 10 mm. This partly explains why there was no distinct load peak in the early phases of the run. The velocity ramp has been used in the simulation, as it is simplest to simulate. As will be shown in Chapter 5 of this volume, however, the measured ram velocity was actually almost constant from the onset of extrusion.

Figure 3.11 and Figure 3.12 present estimates of the die outlet temperature obtained from the same ALMA2π calculations that produced the ram force estimates. The outlet temperature was initially approximately 425 ºC, but the temperature soon increased by 75 to 150 ºC. As indicated in the previous sub-section, the shape of the temperature curves depended to a great extent on the extrusion velocity. If extrusion was run fairly slowly (with a profile velocity of 200 mm/s), the ram significantly cooled the back end of the billet so that the temperature decreased towards the end of the run. Additionally, the heat conduction to the container and die was less important if a high-rate extrusion was performed. Note that the heat dissipation may in the very last part of the run change due to a change towards a more radial flow pattern. The ram force requirements and the dissipation of energy may increase significantly towards the end of the run.

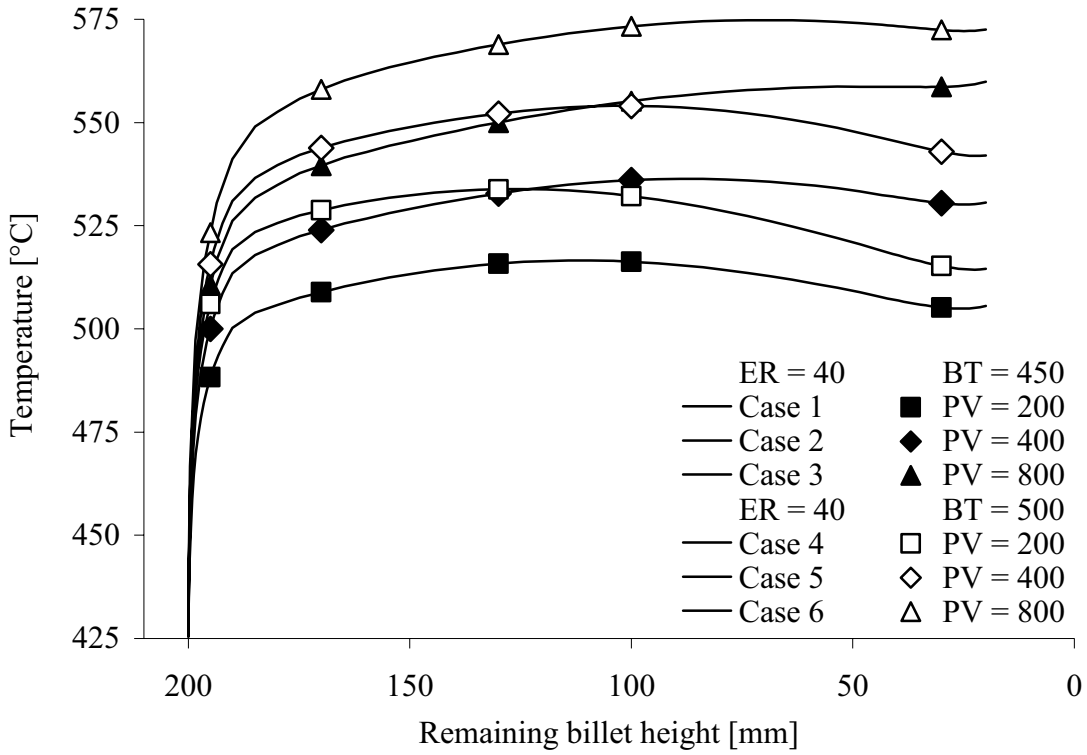

Figure 3.11. Estimates of outlet temperature by ALMA2π - extrusion ratio 40.

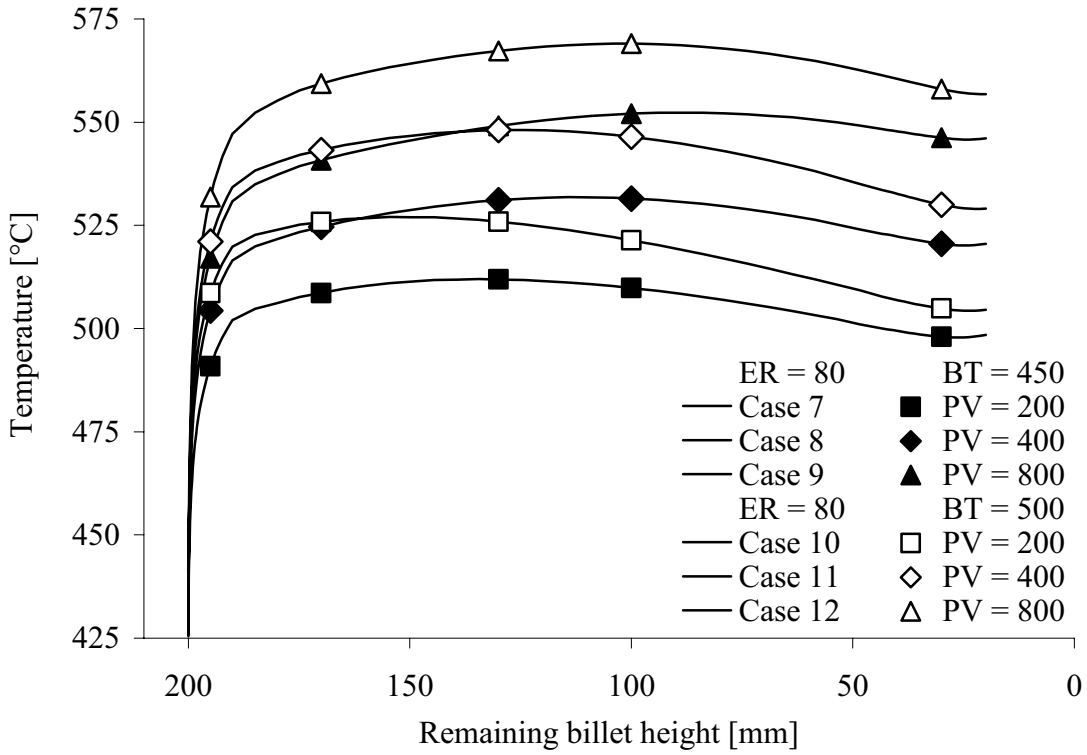

Figure 3.12. Estimates of outlet temperature by ALMA2π - extrusion ratio 80.

Characteristic temperature data from the temperature calculations are presented in Table 3.8. The information about the temperature for a billet height of 196 mm should not be used. The response is very sensitive to the height of the billet and to the heat flow in the upsetting phase. Furthermore, temperature measurements are seldom accurate in the early phases of the run due to the 1- to 2-second response time of the thermocouple. In the later stages of the run the temperature changes considerably less.

Table 3.8. Temperature response predicted by ALMA2π (profile velocity as a factor).

Case		*ER*	*BT*	*PV*	*PV*	Billet length [mm]			
	AVG	B	C	D^1	D^2	196	170	100	30
1	1	-1	-1	-1	-1	488	509	516	505
3	1	-1	-1	1	1	511	539	555	559
4	1	-1	1	-1	-1	506	529	532	515
6	1	-1	1	1	1	523	558	573	572
7	1	1	-1	-1	-1	491	509	510	498
9	1	1	-1	1	1	517	541	552	546
10	1	1	1	-1	-1	509	526	521	505
12	1	1	1	1	1	532	559	569	558
2	1	-1	-1	-1/3	0	500	524	536	530
5	1	-1	1	-1/3	0	516	544	554	543
8	1	1	-1	-1/3	0	504	525	531	521
11	1	1	1	-1/3	0	521	543	546	530

Effects	Billet length [mm]				Estimated temperatures for cases 2, 5, 8 and 11				
	196	170	100	30	#	196	170	100	30
							D^1		
AVG	510	534	541	532	2	496	519	529	523
B - ER	5	0	-6	-11	5	512	538	546	534
C - BT	16	19	16	11	8	500	519	524	514
D - PV	22	31	42	53	11	516	537	537	523
							D^2		
BC	1	-1	-1	-1	2	499	524	536	532
BD	2	1	2	-2	5	515	543	553	544
CD	-2	0	2	2	8	504	525	531	522
BCD	0	1	1	0	11	520	543	545	531

A regression equation similar to Equation (3.11) may be deduced by using the calculated effects of Table 3.6. Again it seems most appropriate to relate the input variable x_4 to the velocity through a logarithmic relationship. Only the main effects are of significant magnitude. The extrusion ratio seems to have a small and even negative effect on the die outlet temperature. This may be explained by the choice of the profile velocity as the input variable rather than the ram velocity. When the extrusion ratio is increased, the ram velocity quite necessarily decreases. The effect of a change in the profile velocity from a low to a high level is from 30 to 50 ºC, depending on the ram position. If the ram velocity is doubled and everything else is kept constant, an effect of approximately 15 to 20 ºC should be expected. If the billet temperature is increased by 50 ºC, the outlet temperature should increase by only 15 to 20 ºC. Some heat is lost to the surroundings, and there is also less generation of heat.

The die face temperature has been calculated at the same distance from the centre of the die as the die face pressure. Thermocouples have been placed at distances of 1 to 4 mm below the die surface. The objective was to measure not only the temperature, but also the temperature gradient and the heat flow. The temperature increases much less and much more slowly at the die face than in the die outlet. Figure 3.13 shows how the temperatures of both the die and the aluminium billet at the die billet-interface should increase towards the inlet. The temperature may change with time and ram position. The distributions shown are valid when the billet height is totally 100 mm.

Figure 3.14 shows how the temperature of the aluminium and the die at a distance 31 mm from the centre of the die changes with ram displacement. The ram velocity is 200 mm/s, and the initial billet temperature is 450 ºC. Since conditions are not steady state, and since there is a flux of heat between the billet and the die, the temperature of the die and billet may significantly differ. The temperature gradient inside the die may be very small and difficult to measure. One should note that it is again possible to observe a decrease in the temperature of the aluminium at the die face towards the end of the run.

Figure 3.15 and Figure 3.16 present the die face temperatures for the twelve cases of extrusion described above. The maximum temperature change of the die face pressure sensor disc is expected to be approximately 30 ºC. Note that the magnitude of the temperature change differs only moderately for the zero bearing cases that have been studied. The largest temperature changes need not be very much higher at low speed than at high speed, for in the latter case the heat may be transported out of the die by convection rather than to the tools by conduction. There is a certain slowness related to the transfer of heat through the die-billet interface. The estimates of the die face temperature are used to assess the sensor response to transient temperature changes.

Figure 3.17 and Figure 3.18 present estimates of the liner load. The liner load may be calculated by integrating the linear shear stresses over the length of the container or by subtracting the die face force from the ram force. The last option was chosen here. The liner force may be expected to be affected by the ram velocity to a relatively small extent after about half of the billet has been extruded. When the billet is very short, the initial billet temperature is of lesser importance. When the billet is very short, the liner force no longer decreases close to proportionally with the billet height. This may both be due to the change in material flow and to the change in thermal conditions. The extrusion run was always stopped just after the ram force started to increase and the material started to flow mainly in the radial direction.

If it is assumed that the shear stress distribution on the interface between the billet and the liner is uniform, a rough estimate of the shear stress may be obtained by dividing the liner force by the area of the interface. When the billet height is 170 mm and the surface area $2 \cdot \pi \cdot 50 \cdot 170 = 53407$ mm^2, the liner force may be in the range from 1000 to 1350 kN. The shear stresses are then typically from approximately 18 to 26 MPa. In the case of pure shear, equivalent stresses are in the range from 30 to 45 MPa, which are typical levels of flow stress for the aluminium at strain rates typical for the extrusion process.

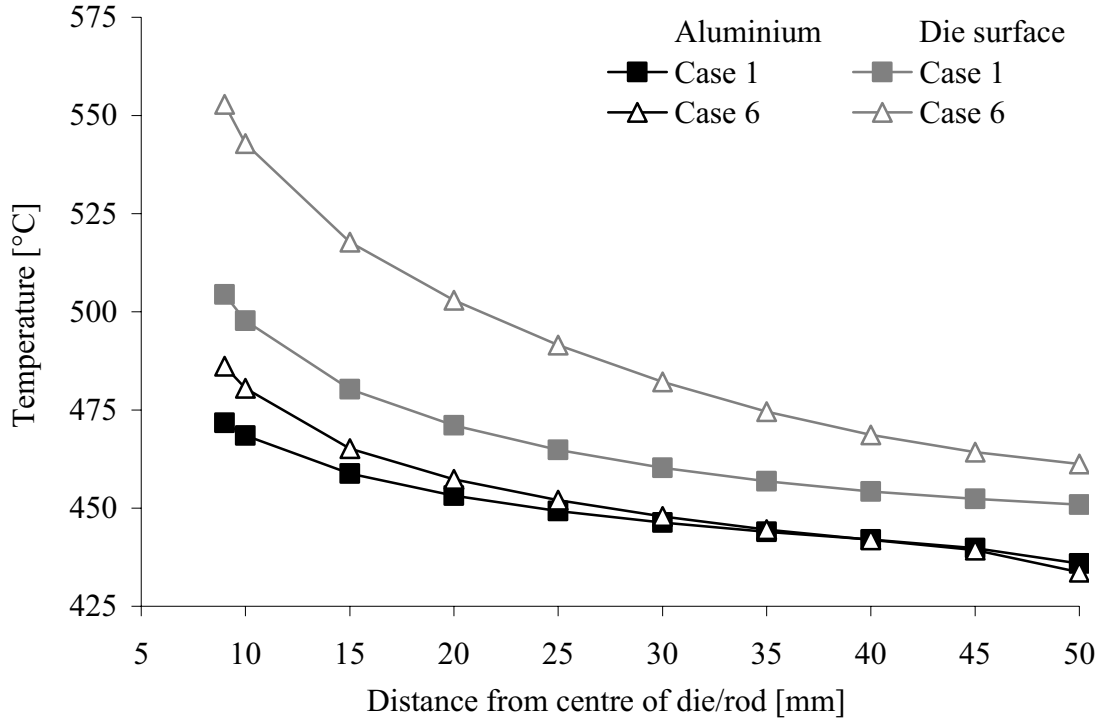

Figure 3.13. Estimates of aluminium-die interface temperature distributions for cases 1 and 6. The distribution has been determined at the very end of the run.

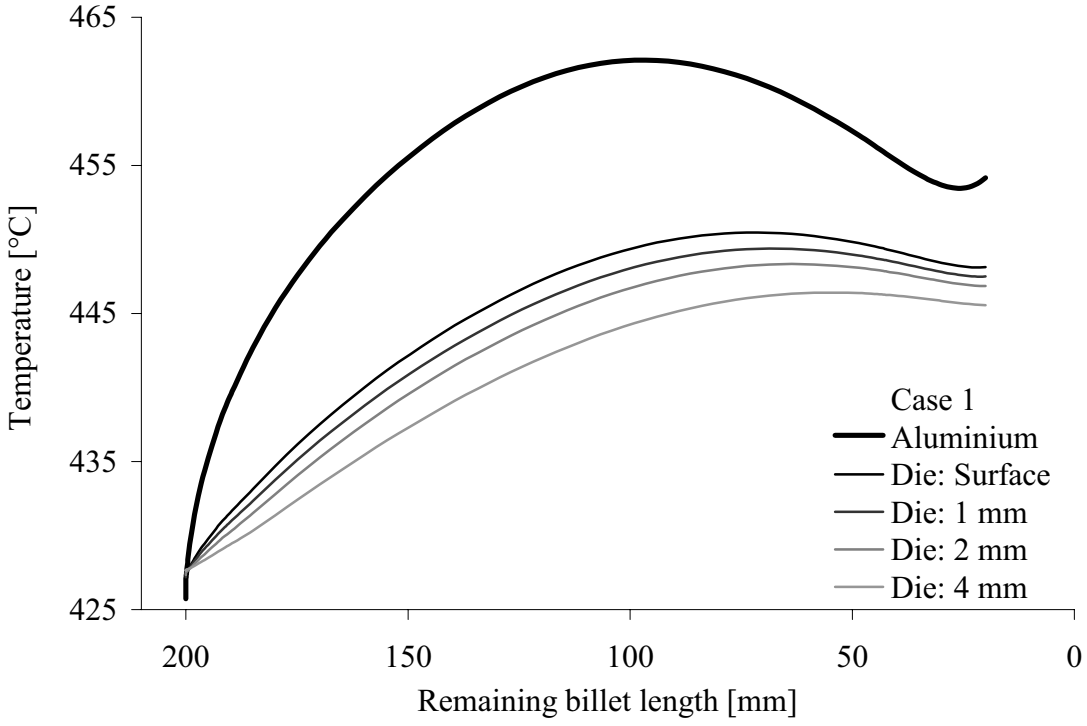

Figure 3.14. Estimates of the temperature of the aluminium and die at the interface and temperatures 1, 2 and 4 mm below the surface (31 mm from the centre).

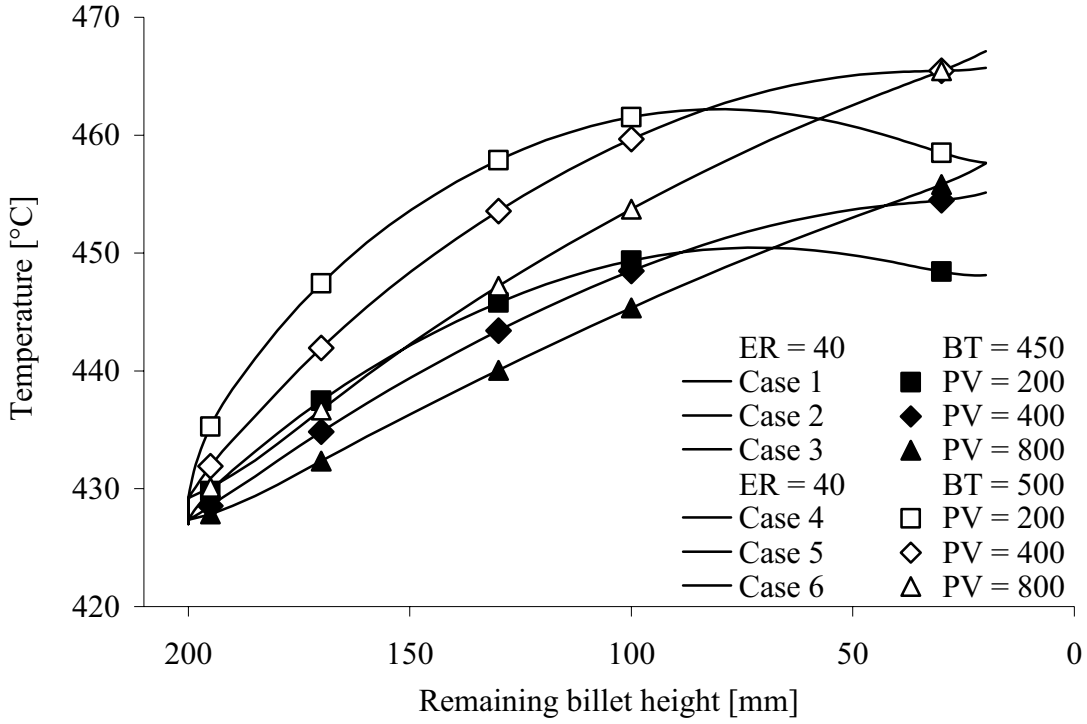

Figure 3.15. Estimates of the die face temperature at the sensor position (31 mm from centre) for extrusion ratio 40.

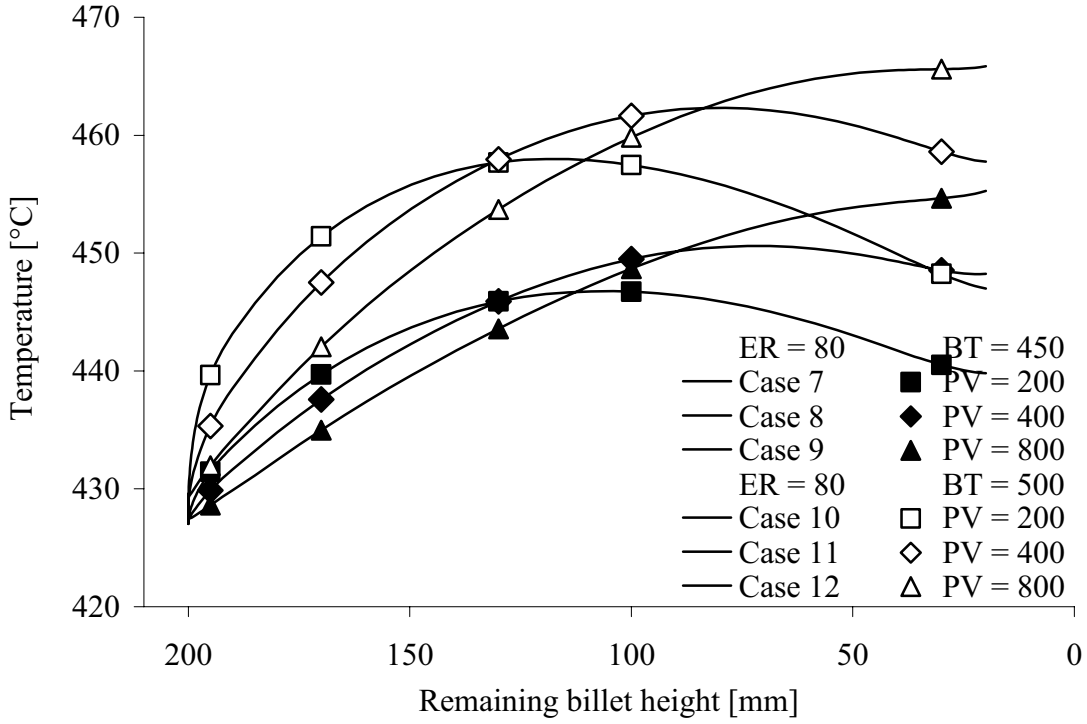

Figure 3.16. Estimates of the die face temperature at the sensor position (31 mm from centre) for extrusion ratio 80.

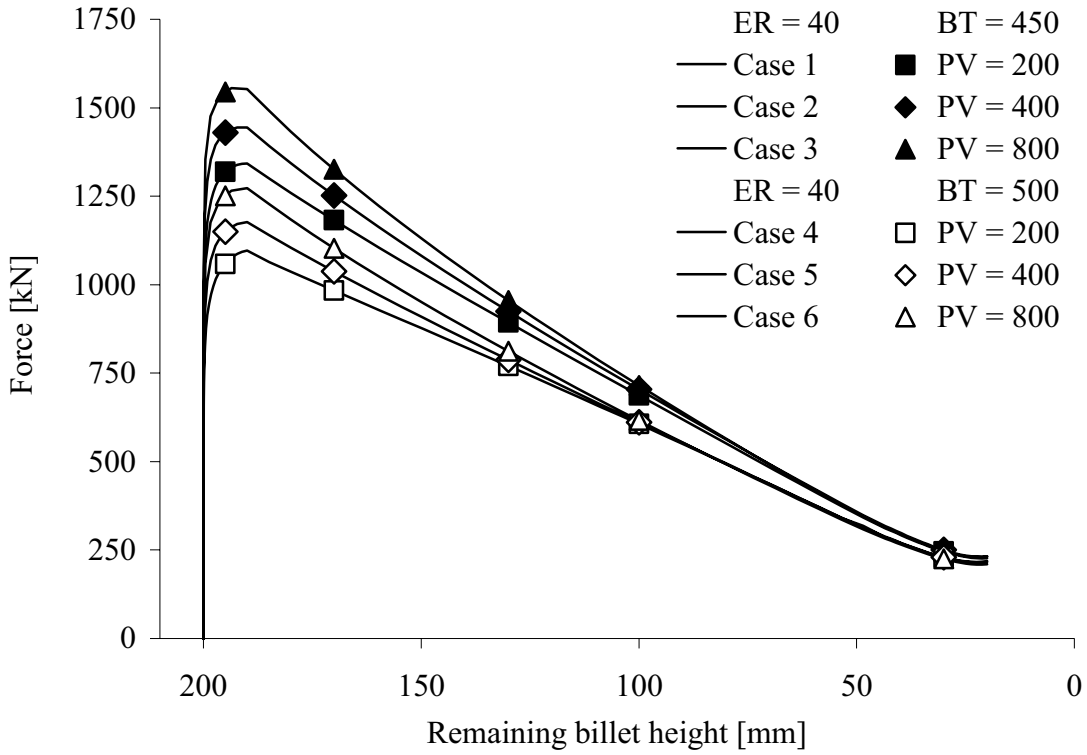

Figure 3.17. Estimates of the liner force/load by ALMA2π - extrusion ratio 40.

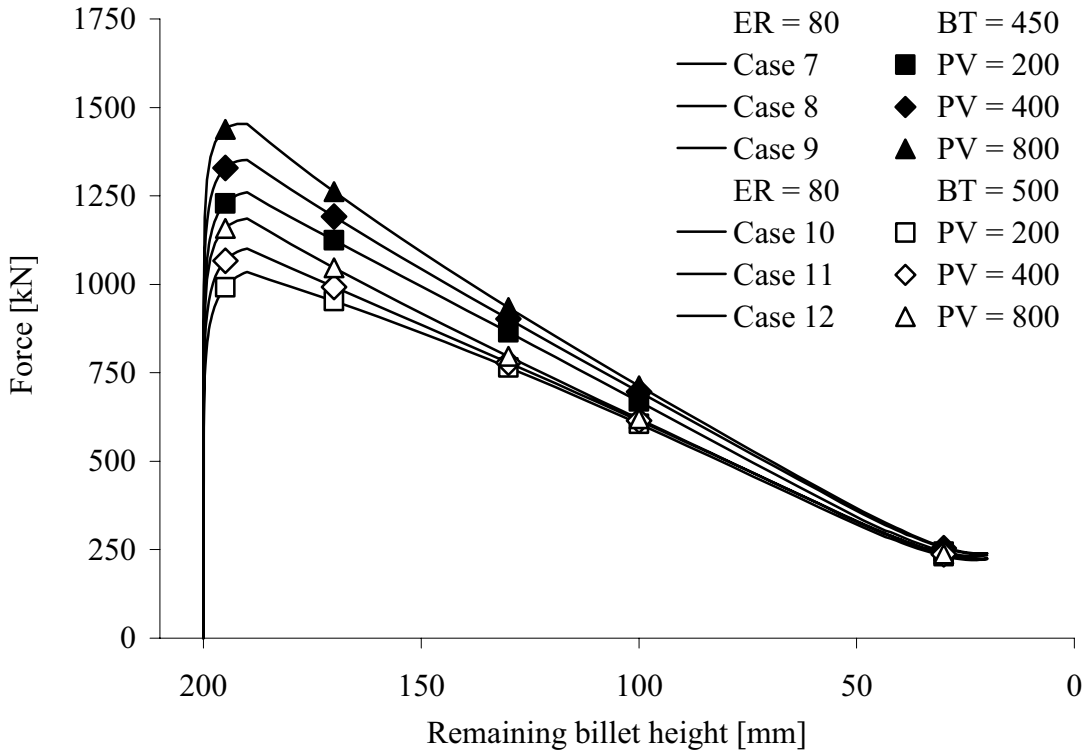

Figure 3.18. Estimates of the liner force/load by ALMA2π - extrusion ratio 80.

Figure 3.19 and Figure 3.20 show the die face pressure distribution for a billet height of 100 mm. Figure 3.21 and Figure 3.22 present similar distributions for billet heights of only 30 mm. The die face pressure is actually the coordinate stress normal to the die face, σ_z. z is the coordinate in the extrusion direction. Analytical models of plasticity theory usually predict a close to uniform pressure distribution at the die face. However, they are usually based on a somewhat simplified description of flow. The surface of the die is assumed to be completely covered by a dead zone, which experiences almost no plastic deformation, and which is heterogeneous with regard to the state of stress. In reality, there is probably a flow of material close to the outlet, and even relatively deep in the dead zone there may be a very moderate material flow in the radial direction. Since aluminium has very high viscosity, there is always a significant gradient in the hydrostatic pressure when there is flow. As the billet shortens, the radial component of the flow becomes more important, and the die face pressure gradient increases. Since the sensor is placed a certain distance from the outlet it should register an increase in the pressure towards the end of the run.

The shear stress, τ_{rz}, opposing the flow of material is highest close to the outlet. Figure 3.23 presents estimates of the shear stress for billet lengths of 100 mm. At the end of the run, the level of stress increased only moderately. There is some sensitivity in the input variables of the study, but the shear stress is of a much smaller magnitude than the component of stress normal to the surface. Hence, the value of the coordinate stress normal to the die face is, as earlier indicated, quite similar to the value of the hydrostatic pressure. Shear stresses lower than 30 MPa are not expected to significantly affect the response of the die face pressure sensor.

It has earlier been suggested that it may be useful to compare the average die face pressure with the die face pressure measurements. An estimate of the die face load may be obtained simply by subtracting the liner load from the ram load. The average pressure is obtained by dividing the die face load by the die surface area. It is then assumed that the stress component parallel to flow is zero at the die outlet or that the outlet is very small. Note that the cross-section area of the compressed billet is $\pi \cdot (50\ \text{mm})^2 \approx 7853\ \text{mm}^2$ while the area of the die outlet is either $\pi \cdot (5.6\ \text{mm})^2 \approx 98\ \text{mm}^2$ (1.2 %) or $\pi \cdot (7.9\ \text{mm})^2 \approx 196\ \text{mm}^2$ (2.5 %). ALMA2π predicts that the average pressure is approximately 10 to 15 MPa lower than the pressure measured by the sensor. Figure 3.24 shows that there is almost a perfect linear relationship between the calculated average die face pressure and the calculated sensor pressure. The length of the remaining billet is not of great importance unless the billet is very short (20 mm). A simple compensation technique of somewhat limited accuracy consists of multiplying the measured value of average pressure by 1.05. The technique makes it possible to determine the die face sensor pressure on the basis of alternative measurements and to evaluate the response of the die face pressure sensors without any further numerical analysis. The technique is probably not restricted to the analysis of results from extrusion with zero bearing channels. The die face pressure distributions for the cases run with a long bearing channel should most likely be quite similar to those presented here. The absolute value of pressure is higher since the bearing channel contributes to a pressure build-up.

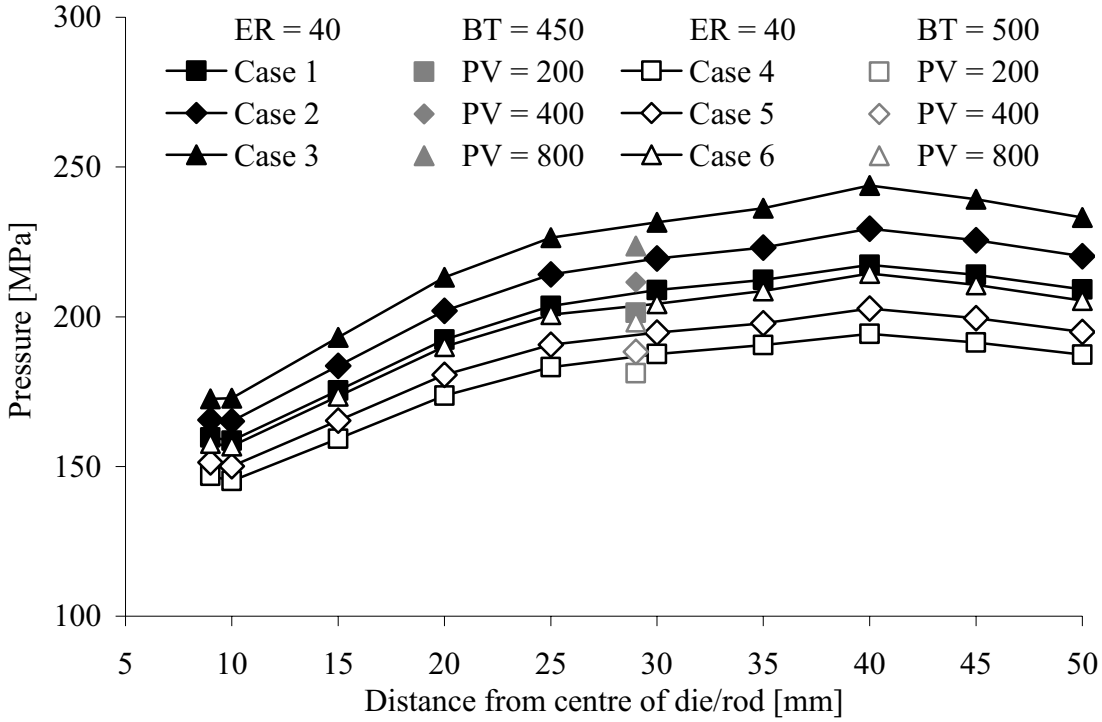

Figure 3.19. Estimates of die face pressure distribution (black) and average pressure die face pressure (grey) - extrusion ratio 40, billet height 100 mm.

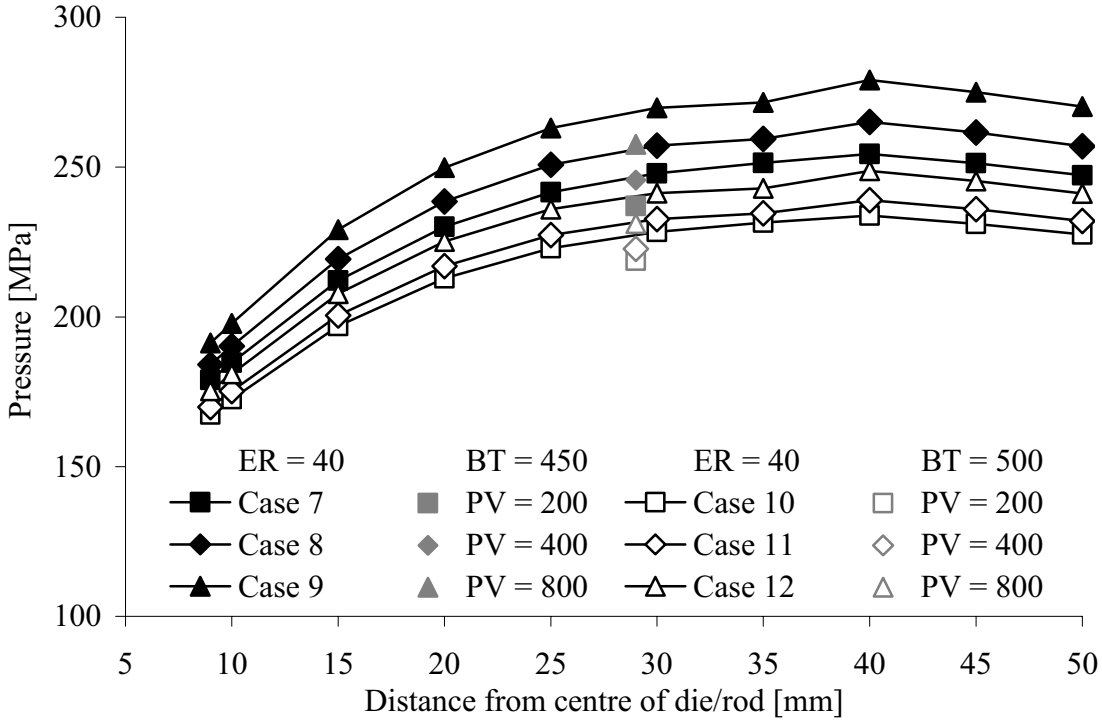

Figure 3.20. Estimates of die face pressure distribution (black) and average pressure die face pressure (grey) - extrusion ratio 80, billet height 100 mm.

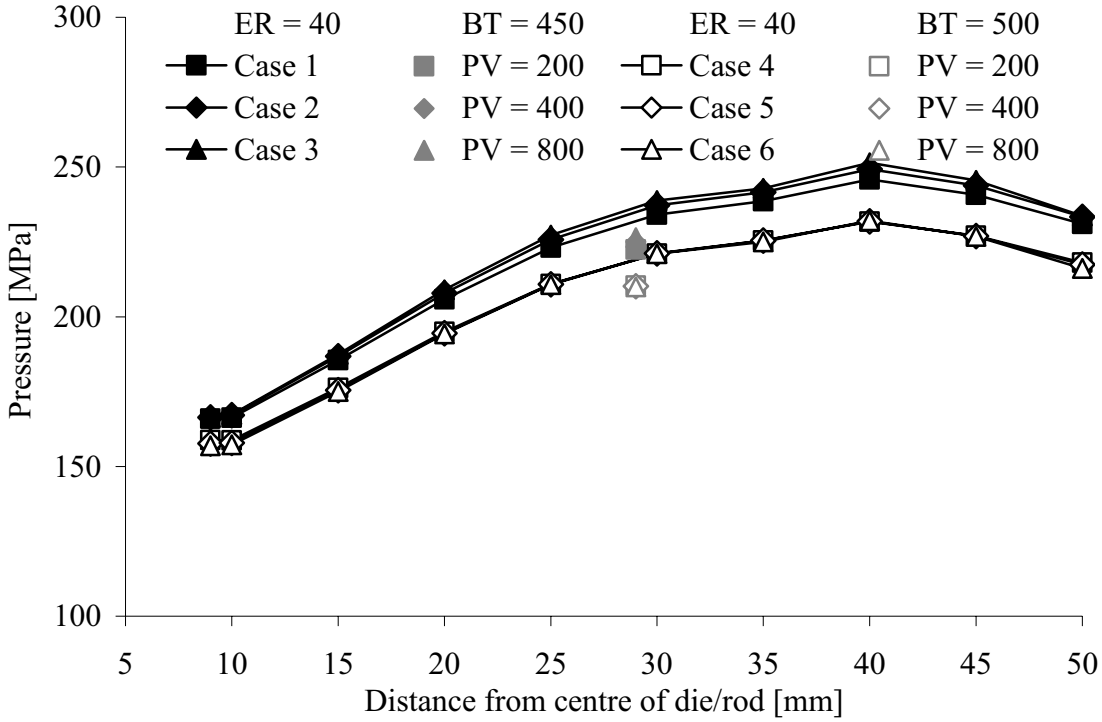

Figure 3.21. Estimates of die face pressure distribution (black) and average pressure die face pressure (grey) - extrusion ratio 40, billet height 30 mm.

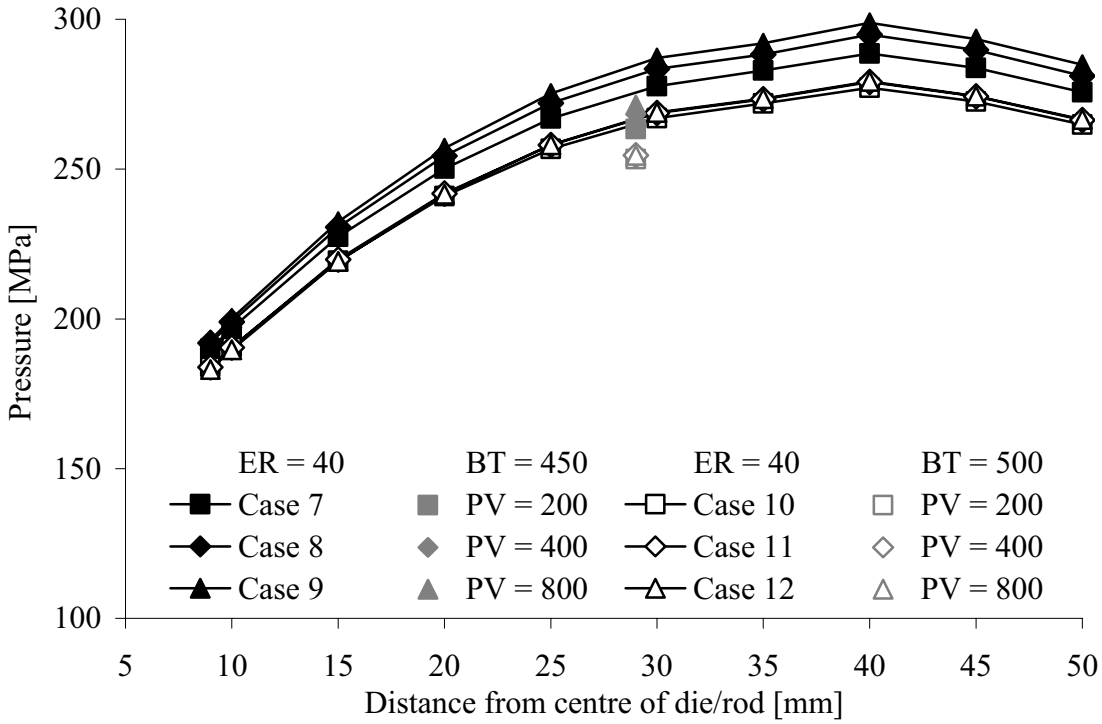

Figure 3.22. Estimates of die face pressure distribution (black) and average pressure die face pressure (grey) - Extrusion ratio 80, billet height 30 mm.

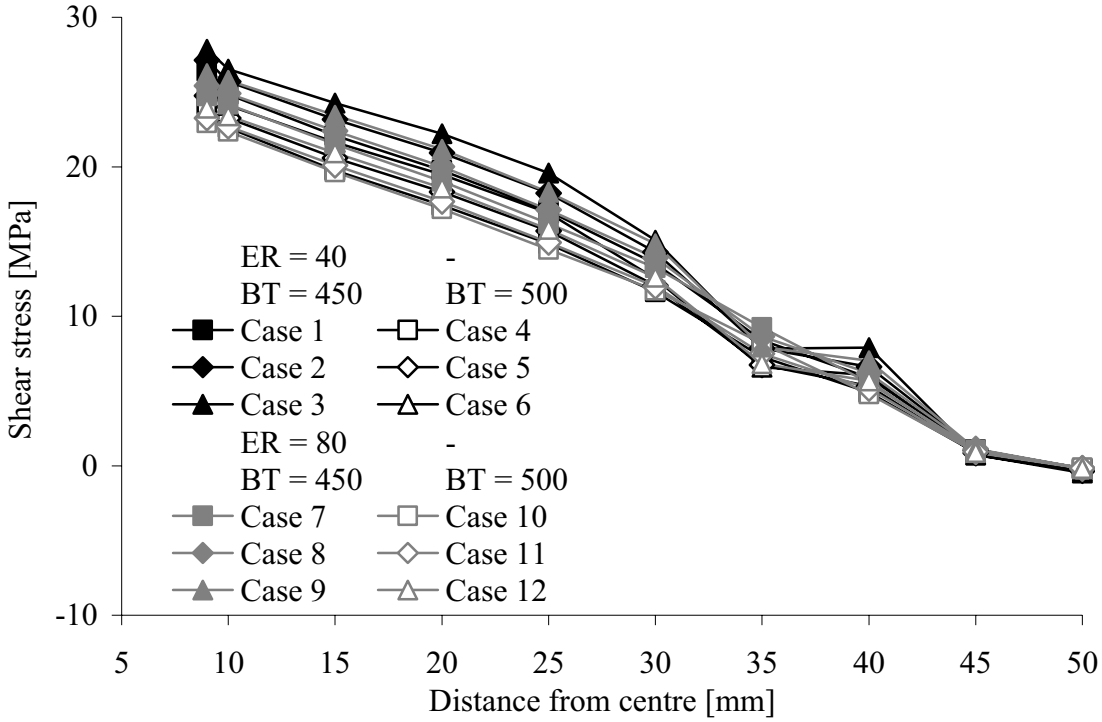

Figure 3.23. Estimates of die face shear stress distribution for extrusion ratios 40 and 80, remaining billet height 100 mm.

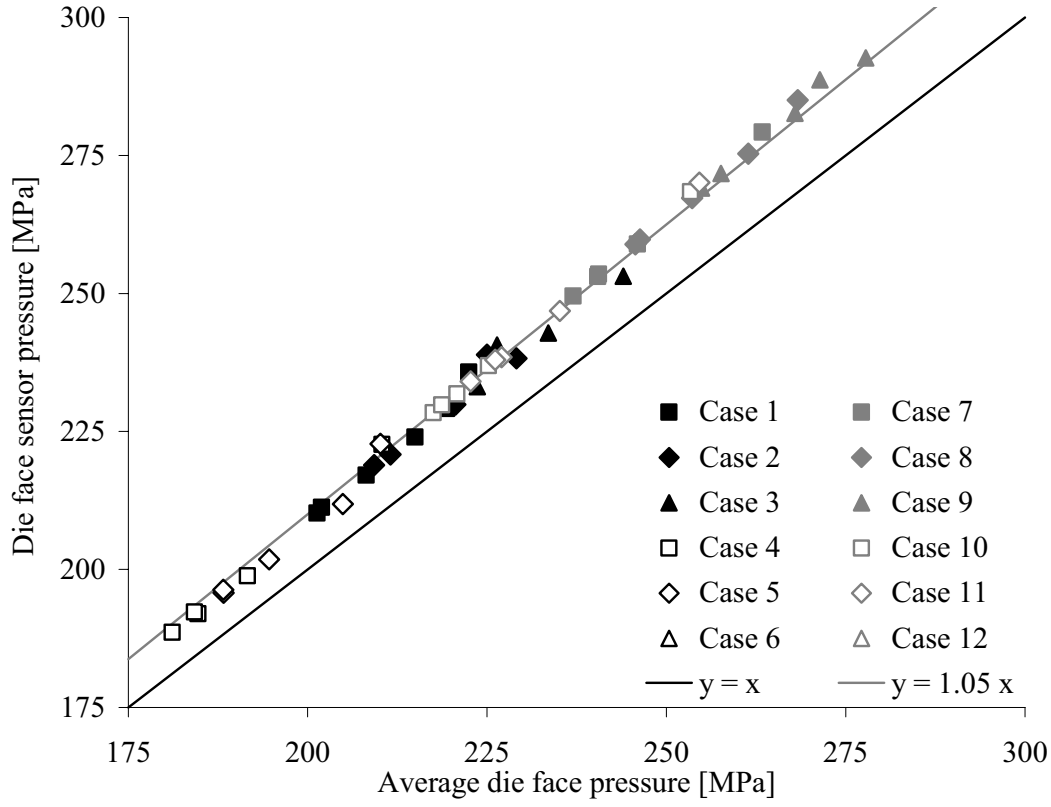

Figure 3.24. Relationship between the average pressure and the sensor pressure.

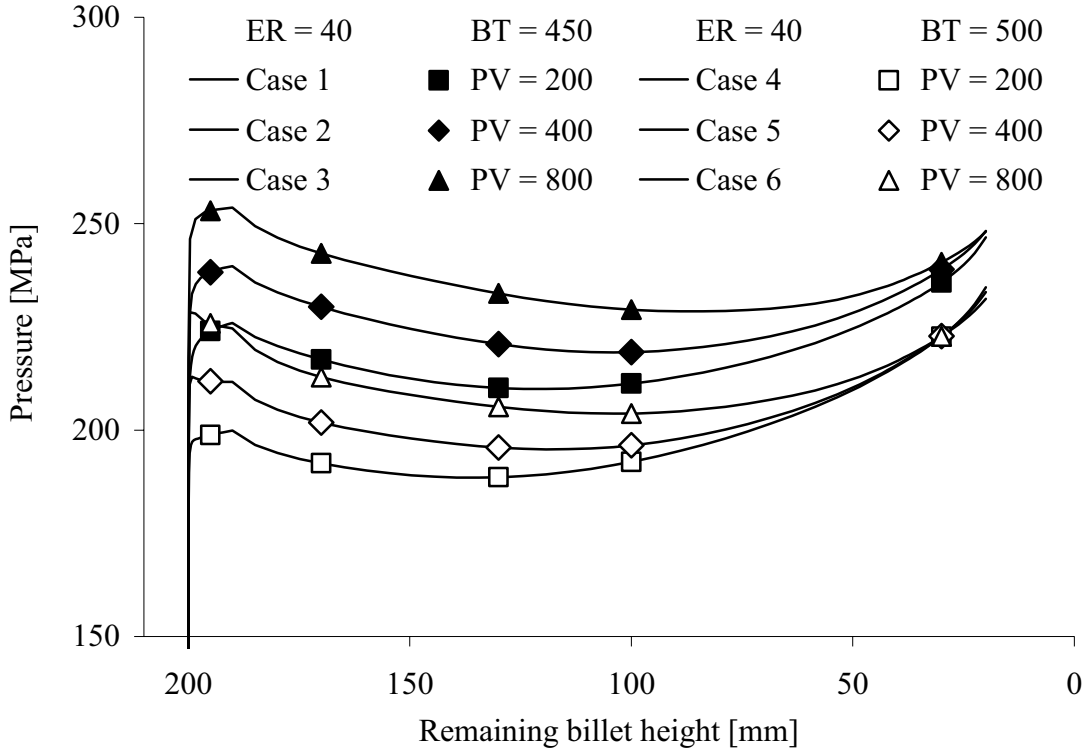

Figure 3.25. Estimates of die face pressure by ALMA2π - extrusion ratio 40.

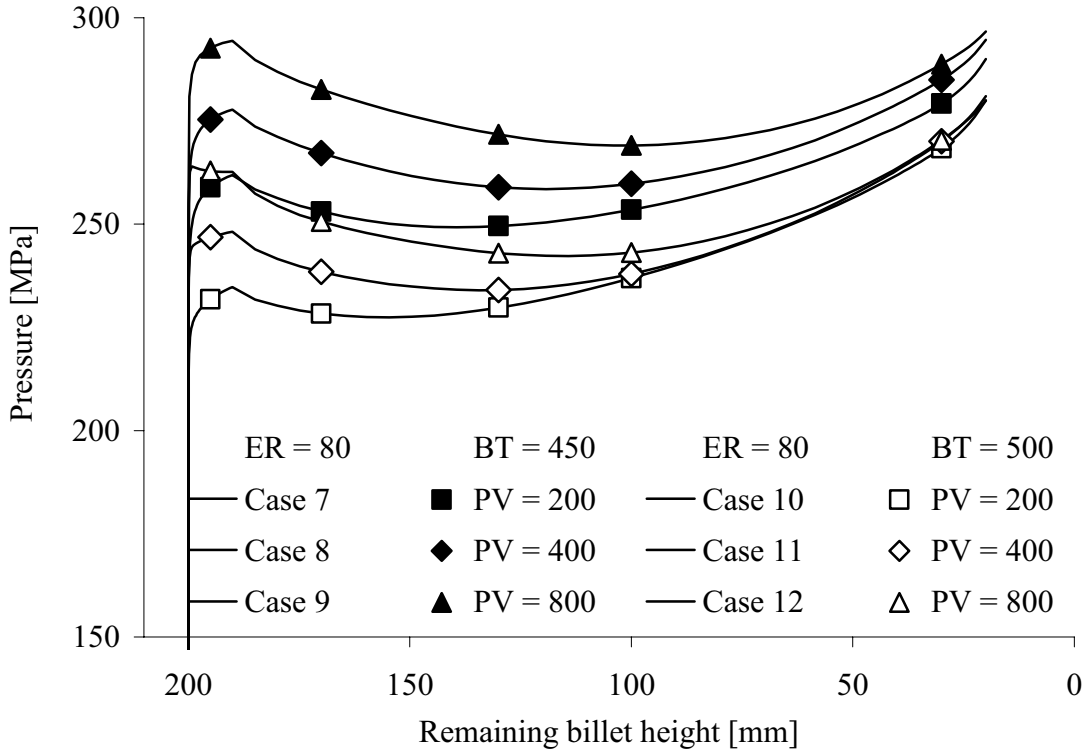

Figure 3.26. Estimates of die face pressure by ALMA2π - extrusion ratio 80.

Figure 3.25 and Figure 3.26 show estimates of the die face pressure at a distance 31 mm from the die centre (the sensor position) for all 12 cases. The die face pressure is high when the extrusion ratio is high, when the billet temperature is low and when the ram velocity is high. When the remaining billet is short, however, ALMA2π predicts that the profile/ram speed is of lesser importance. It is interesting to note that ALMA2π predicts that the die face pressure at the sensor position is almost insensitive to changes in initial billet temperature and ram velocity for a billet height of 30 mm.

Table 3.9 shows how changes of the input variables may affect the pressure response. All the main effects are significant while the interaction effects are generally small. The regression equation should be similar to that of the force. The logarithmic relationship between x_4 and the profile velocity is better than a linear one. Note that even though the profile velocity is regarded as an input variable in the analysis, there is a significant effect of changing the extrusion ratio. If the ram velocity is held constant and the extrusion ratio is changed, the effect may be larger than 50 MPa during the initial part of the run. There is probably a logarithmic relationship between the die face pressure and the extrusion ratio. The assumption has not been tested experimentally since extrusion has not been performed for any intermediate level of the extrusion ratio. Simulations may be performed in order to further evaluate the pressure dependency.

Table 3.9. Die face pressure predicted by ALMA2π (profile velocity as a factor).

Case		ER	BT	PV	PV	Billet length [mm]			
	AVG	B	C	D^1	D^2	196	170	100	30
1	1	-1	-1	-1	-1	224	217	211	236
3	1	-1	-1	1	1	253	243	229	241
4	1	-1	1	-1	-1	199	192	192	223
6	1	-1	1	1	1	226	213	204	223
7	1	1	-1	-1	-1	259	253	253	279
9	1	1	-1	1	1	293	283	269	289
10	1	1	1	-1	-1	232	228	237	268
12	1	1	1	1	1	263	251	243	270
2	1	-1	-1	-1/3	0	238	230	219	239
5	1	-1	1	-1/3	0	212	202	196	223
8	1	1	-1	-1/3	0	275	267	260	285
11	1	1	1	-1/3	0	247	238	238	270

Effects	Billet length [mm]				Estimated pressure for cases 2, 5, 8 and 11				
	196	170	100	30	#	196	170	100	30
					D^1				
AVG	243	235	230	254	2	234	226	217	237
B - ER	36	37	41	46	5	208	199	196	223
C - BT	-27	-28	-22	-15	8	270	263	259	282
D - PV	30	25	13	4	11	242	236	239	269
					D^2				
BC	-1	0	0	0	2	239	230	220	238
BD	2	1	-2	2	5	212	202	198	223
CD	-1	-3	-4	-3	8	276	268	261	284
BCD	0	-1	-1	-1	11	247	239	240	269

Steady state analytical calculations indicate that the die face pressure may not change much, at least in the early phases of the run. ALMA2π predicts that it may change and that the change depends on both the initial billet temperature and on the profile velocity. Extrusion is not a steady state process. The billet is of a finite length. It is heated during deformation, and it is cooled by the ram. The flow resistance and the pressure build-up are affected by the thermal conditions. In the final stages of the run the changes in the flow pattern may also cause a significant increase in the die face pressure. It should be noted that the ALMA2π simulations may in fact underestimate the die face pressure changes in the initial stage of extrusion. First, the ram speed is only gradually increased to a constant predefined level. Second, ALMA2π does not consider how microstructure changes affect the material flow stress. Initially, the billet has a cast microstructure, but develops an anisotropic elongated microstructure during extrusion. An increase in the dislocation density may first cause the flow resistance to increase, but softening soon takes place. There are important mechanisms of recovery, and the anisotropic extrusion microstructure is better adapted for deformation. Usually there is a distinct peak in the force and pressure at the onset of extrusion. A final effect that is not considered by ALMA2π is a possible redistribution of force that may occur if the nature of the billet-container interaction changes in the very beginning of the run. If proper contact is not initially made between the billet and container, the die face force may initially be higher than expected. The system responses are further assessed in relation to the analysis of experimental results.

Chapter 4

Calibration experiments

This section focuses on calibration of the pressure sensor equipment. The requirements for the sensor system with regard to properties such as accuracy and repeatability of measurement are first evaluated. The displacement calibration technique of Capacitec is then reviewed, and results from the rounds of displacement calibration are presented. A discussion on the differences between displacement calibration and extrusion pressure measurements is provided. Various methods for direct calibration of pressure sensors are treated. An on-line method for direct calibration was chosen and tested in relation to the extrusion experiments. A description of the results is given, and calibration factors are deduced. The measurement data are compared with similar data obtained from finite element calculations. Finally, results from calculations treating the deformation of the liner load cell and results from calibration measurements are presented.

4.1 Requirements for the measurement equipment

The measurement signal from the Capacitec 4000-series amplifiers is a DC voltage in the range from 0 to 10 volts. The objective of establishing a calibration curve is to link the voltage signal to the pressure acting at the top face of the extrusion die or the liner force. It would be best if the relation was a linear one, but in the age of computers linearity is not an absolute requirement. It is significantly more important that the transformation is one-to-one, in the sense that every value of the DC voltage output corresponds to only one value of die face pressure or ram force. In the case there is an excessive hysteresis, the task of measuring may become very complex. While it may be possible to use data from the first round of loading, the relationship between the pressure and the voltage during unloading and later load cycles may depend on the history of loading. There are a number of reasons for a hysteresis in relation to pressure measurement in metal forming. Friction between parts in the sensor is one, while another is the elasto-plastic deformation of the work piece or, in a more serious case, the sensors. The issue will be treated more in detail below.

Calibration relates primarily to the characteristic of the sensor denoted accuracy. The accuracy is a measure of the sensor's capability to indicate the true or actual value of the response of interest. If one wants to relate a number to the accuracy, one may choose the maximum difference between the measured value and the actual value that would have been obtained for a perfect measurement. One may also choose an average value of

error for all measurements. In this work, only some typical and very approximate values of accuracy are treated. The problem of determining the accuracy is primarily related to the fact that the actual value of the measurement signal is not known, and usually cannot be determined from the measurements on the process of interest. It must be estimated by alternative techniques and alternative approaches. Often one has to resort to estimates and probabilities based on statistical data. The calibration set-up has been introduced so that the response of the sensor may be measured in an environment where all influences are controlled. It is of great importance that the calibration case is similar to the process of interest so that the sensor responses during measurement and calibration are similar. The accuracy may be given as a relative value (compared to the full scale sensor response) or as an absolute value (voltage/displacement/pressure).

The objectives of the current study were initially stated by Professor Sigurd Støren as:

> *Develop a measurement system for measurement of the pressure between the deforming aluminium alloy and the die at specific positions in the die with a precision better than ± 10 MPa. In combination with the measurement of temperature, monitoring the variation of pressure and temperature during a press cycle with a precision better than respectively ± 3 MPa and ± 3 K.*

The requirements must be seen in relation to the objective of pressure measurement in extrusion. The NTNU/SINTEF extrusion group envisions sensors being used to gain detailed information about the flow of material and in a system for process (flow and die deformation) control. It is of importance that the sensors are capable of measuring small spatial and temporal differences or changes in pressure at the die-billet interface. The measurement accuracy is of particular importance when the sensor response is compared with absolute values of simulated data. However, a satisfactory repeatability of measurement is perhaps even more important when pressure differences are being evaluated. There are different types of repeatability. The most interesting is probably the one related to perfectly genuine replication of measurements. A completely new set of experiments should then be performed. A new, but similar extrusion press may be used, another group of researchers may perform experiments and new sensors may be applied. Alternatively, one may envision that a number of pressure sensors are used to measure the pressure differences in the container. In such a case the sensors should be made and calibrated so that they produce comparable results. The results may be inaccurate or biased, but the repeatability should at least be acceptable. Also another kind of repeatability should be evaluated. It is related to replication of measurement with one sensor and during only one round of experiment. The repeatability of measurement is then a measure of the stability of pressure measurement. It is obviously desirable that the sensor response is not degraded during a set of experiments, and that the first results obtained in a set of experiments are comparable to the last results.

In this work the terminology of de Sa has been adopted [Sa97]. It is presented in the terminology list. It may deviate somewhat from the terminology of the initial statement of requirements for the sensor system. The first sentence of the statement is regarded as a requirement for both the accuracy and repeatability of measurement. The sensors should be capable of producing an output that does not deviate more than 10 MPa from

the actual value, and a typical value for the scatter in measurements should be 10 MPa. The requirements are logical, but also very strict. It would be more natural to make use of relative values. The die face pressures may range from 200 MPa to almost 600 MPa, depending on the material that is being extruded, the profile geometry, the billet temperature, the ram speed and the position of the sensors. An accuracy of ± 5 % at 200 MPa is obviously easier to achieve than an accuracy of less than ± 2 % at 600 MPa. As is discussed in reference [Moe04d], it is significantly more complex to design sensors for die face pressures in the upper range than in the lower range of the scale. When pressures are high, plastic deformation is difficult to avoid. Anyway, the deformation or deflection of the sensor disc is not much larger than 30 μm. Displacement measurement should be performed with an accuracy and repeatability of approximately 1 μm.

The second sentence of the description of requirements refers to the system's ability to indicate changes in pressure during extrusion. Often, the term precision is regarded as a measure of the degree of measurement reproducibility [Fra96]. It indicates how much one measurement may deviate from another performed in exactly the same manner. It is related to statistical errors and scatter in measurements. In the current case, ±3 MPa corresponds to ± 1 to 1.5 % of full scale or ± 10 to 15 mV for the Capacitec system. It is natural to see the requirement in relation to the resolution of the system, which is an expression of the smallest change of an input parameter that may be detected. It would also be interesting to detect small pressure changes during extrusion that may be related to flow instability and stick-slip friction. Producers of measurement systems often claim that the resolution corresponds to the smallest change that may be shown by a standard voltmeter, typically 1 mV. Usually, this assessment is quite optimistic, if not completely misleading. In the case of the capacitive displacement measurement system, 1 mV corresponds to a displacement of 50 nm. Capacitive measurement systems may be very accurate (they are used to measure surface topology at the atomic level), but in order to be able to distinguish a displacement of 50 nm from pure noise, the circuit design must be finely tuned. While the task may not be impossible with the system of Capacitec, it is not at all trivial. Note that it is often also claimed that the repeatability of the system is equal to the resolution. This is for certain not the case for the pressure sensors.

During studies of flow instability and shape deviation it may be interesting to determine the magnitude of small pressure changes. The above interpretation of the requirements does not consider accuracy of small pressure change measurement. It merely states that the system should be capable of detecting pressure changes smaller than ± 1 to 1.5 % of full scale. It seems natural that the accuracy of measurement of the "absolute" pressure and of the pressure changes should be quite similar. The reason is essentially that all pressure measurements in relation to extrusion are relative. The difference between load change measurements from 0 to 200 MPa and from 195 to 200 MPa is merely that the range is 40 times larger. It may be that it is somewhat easier to calibrate accurately over a shorter range, but this need not be the case. Furthermore, deviations from linearity as well as inaccuracy should be largest at the highest pressures. The problem of pressure measurement differs from that of temperature measurement. A temperature change may be accurately determined even if the absolute value is not exactly known. In the case of the pressure measurement, the zero point may be found by simply unloading the sensor.

4.2 Calibration of Capacitec displacement sensors

4.2.1 A description of the calibration procedures and results

There is most probably no standard method for calibrating capacitive pressure sensors for aluminium extrusion, although various methods for directly linking pressure to the output voltage of the Capacitec amplifiers are treated below. However, a standard type of calibration of the capacitive displacement sensor system may and should regularly be performed. The Capacitec system was purchased in the autumn of 1999, and all sensors had then been carefully calibrated according to Capacitec specifications. The current report describes the very last rounds of experiments. They were performed in January and June 2002. The equipment had been used more or less continuously for two years, and the initial probes had even been replaced. The calibration curves for two probes using the same channel may differ significantly. Furthermore, the linearity of the system response degrades with time. Regular calibration checks and re-calibration are therefore necessary. The current subsection describes the results from the re-calibration that was performed in relation to the rod extrusion experiments with the complex dies.

The Capacitec sensors were initially calibrated so that there should be a close to linear relationship between the displacement and the DC output voltage in the range from 0 to 0.5 mm. The choice is a sensible one. The deviation from linearity should be smaller than ± 1 μm, which should be acceptable for measurements and possible to control with available displacement gauges. Furthermore, it is advantageous to place the probes at a certain distance from the deflecting disc of the pressure sensor housing. Direct contact between the probe and the sensor disc is then avoided. The relative disc deflection is usually only 20 to 40 μm, but if overloading occurs, the displacements may be much larger. The special sensor disc design makes direct contact more likely, if the sensor gap is very small. During earlier extrusion experiments, short-circuiting was experienced, probably as the sensor guard made contact with the upper corner of the sensor cavity. The fact that the top faces of some of the probes were slightly inclined (actually as much as 0.05 mm / 5 mm in the worst case) complicated matters. Therefore, the width of the capacitor air gap should initially be 0.3 to 0.5 mm. If calibration is performed as described, the sensor may also be used to measure the gap width during positioning.

The *Capacitec Operation/Maintenance Manual for Series 4000 Capacitec Amplifiers and Rack Accessories* [Cap98] describes recalibration procedures in detail. It suggests that the standard Capacitec calibration stand is used (Figure 4.1). A similar stand was made for temperature tests, but the design was not compatible with the available length gauge. For that reason, a somewhat different set-up was used for the initial displacement calibration. Figure 4.2 shows the basic outline of the SINTEF calibration equipment. The probe was fitted in a probe holder, and the position was fixed with a set screw. Before the system was switched on the probe was brought into contact with the second disc, which was connected to ground and constituted the second capacitor plate. When the probe was retracted, a Heidenhein Metro MT60 [HeiW] high-accuracy strain gauge continuously measured the distance between the discs of the capacitor. The accuracy of measurement was ± 0.5 μm. The MT60 was based on optical measurement technology. The measuring step may be in the range from 0.1 to 1 μm. In the current case it was set

to 0.5 μm. The zero point of the displacement measurement was set when the probe and the disc were in intimate contact. The contact conditions determined the reference point of the displacement measurements. An offset should in principle have no effect on the accuracy of measurement, for pressure measurement is based on relative displacement measurements. The non-linearity of the voltage displacement curve may complicate matters, because it is of the same magnitude as the desired accuracy of measurement.

Figure 4.1. The Capacitec standard calibration stand and capacitive probe [CapW].

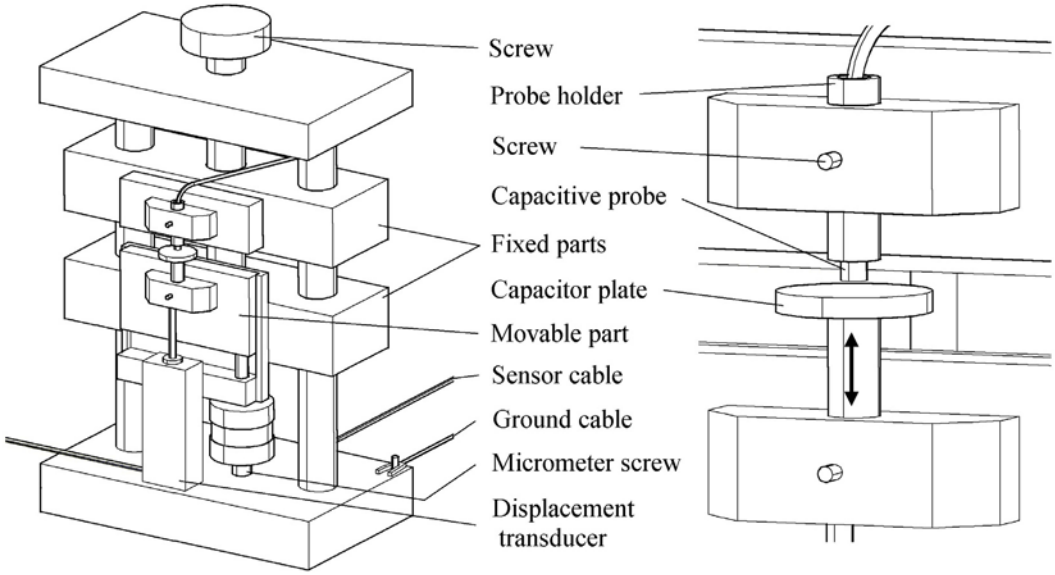

Figure 4.2. The calibration set up and the Heidenhein Metro MT60 strain gauge.

The four adjustable potentiometers of the Capacitec amplifiers were reset before re-calibration commenced. The equipment was switched on, and it was allowed at least 30 minutes warm-up time. Then, an iterative tuning procedure that has been more closely described in the Operation Manual was performed until the signal was sufficiently linear. Figure 4.3 shows the almost linear calibration curves of the different sensors together with the target curve. Since the deviations from linearity are very small, the

differences between the various calibration curves and the target curve have been plotted in Figure 4.4 to Figure 4.12. In the relevant measurement range, from 0.25 to 0.5 mm, the deviations from linearity are typically smaller than ± 0.5 µm or 0.1 % of full scale. Three or four independent checks were performed and some scatter in the results was detected. The $3 \cdot \sigma$ value is approximately 0.3 µm, which corresponds very well with the expected variability of strain gauge measurements. The data scatter is mainly an expression of the limitations of the calibration equipment. It is possible to improve both the linearity of the calibration curve and to reduce the amount of scatter by performing measurements in a well-defined manner. The influence of the lost motion is reduced if the wheel controlling the movement of the probe is either only turned clock-wise or only anti-clockwise direction during the sampling operation. Note that the curves of Figure 4.4 to Figure 4.12 have been obtained in this manner.

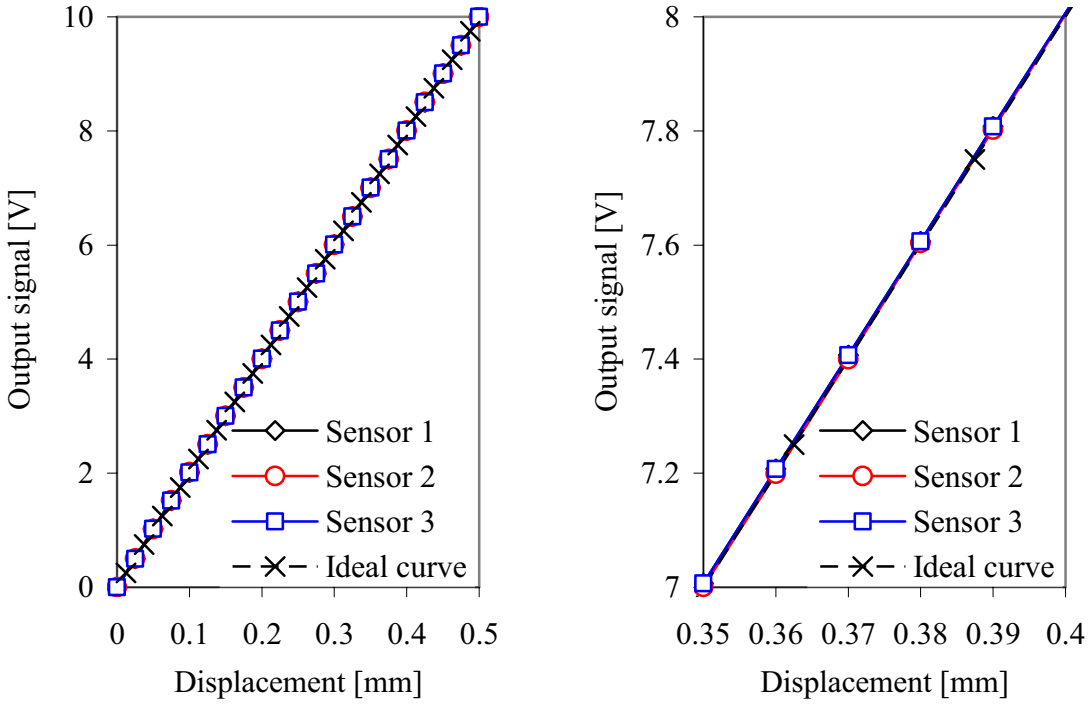

Figure 4.3. The linear calibration curves linking displacement and voltage.

Figure 4.13 presents average calibration data for all sensors and both re-calibrations. The first re-calibration was performed in January of 2002, while the second was made in June of the same year. Before the second re-calibration, the linearity was carefully tested. The slope of the calibration curve had changed by approx 0.1 %, but the linearity was satisfactory. The maximum deviation from the linear curve was 1 µm. Still, re-calibration was performed. The capacitive sensors of the liner load cell were calibrated in a similar way to the die face sensors. One of the liner load sensors was calibrated with a full range of 1 mm. The sensor was originally to measure relatively large strains in the bridges of dies for hollow profiles. The displacement calibration revealed that the sensor was also affected moderately (0.1 % of FS) by changes of the responses of the other sensors of the rack. The reason for the interaction has not been found.

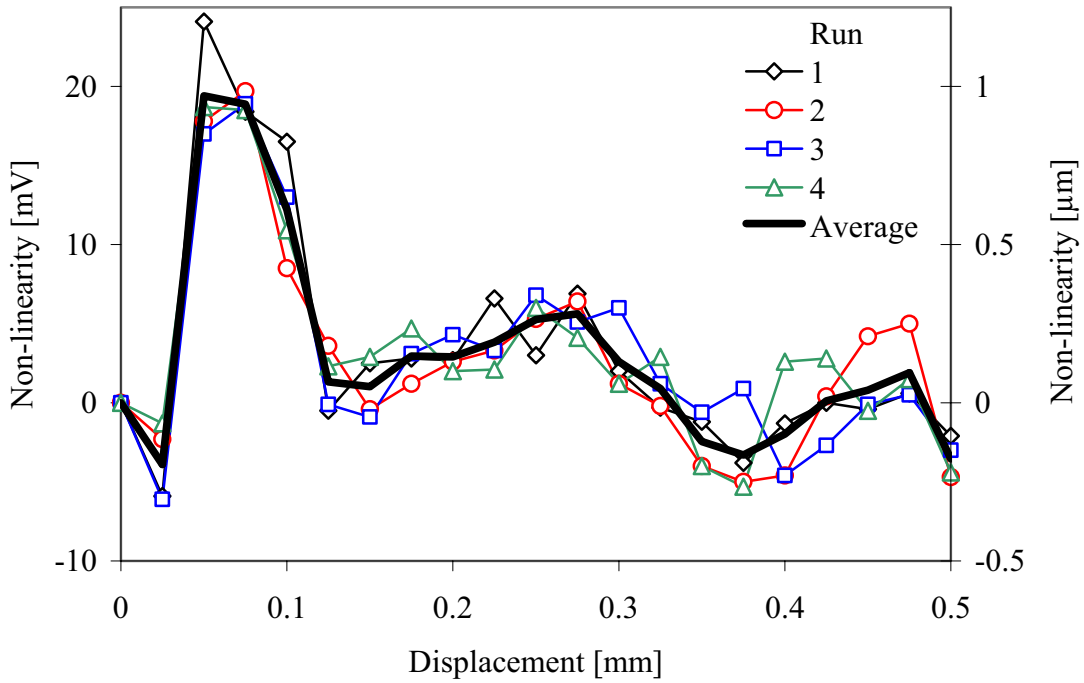

Figure 4.4. Deviation from linearity (voltage – 50 x displacement) – Full range check: Sensor 1 – Probe 17661, extension cable 3161, channel 1 NTNU.

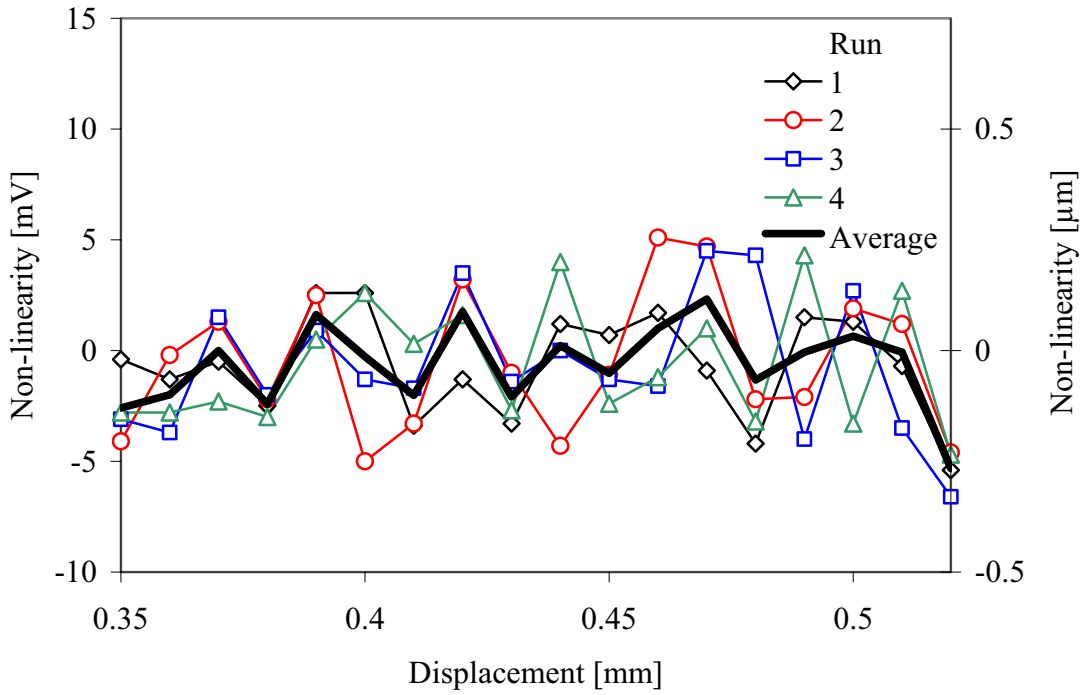

Figure 4.5. Deviation from linearity (voltage – 50 x displacement) – Reduced range check: Sensor 1 – Sensor 17661, extension cable 3161, channel 1 NTNU.

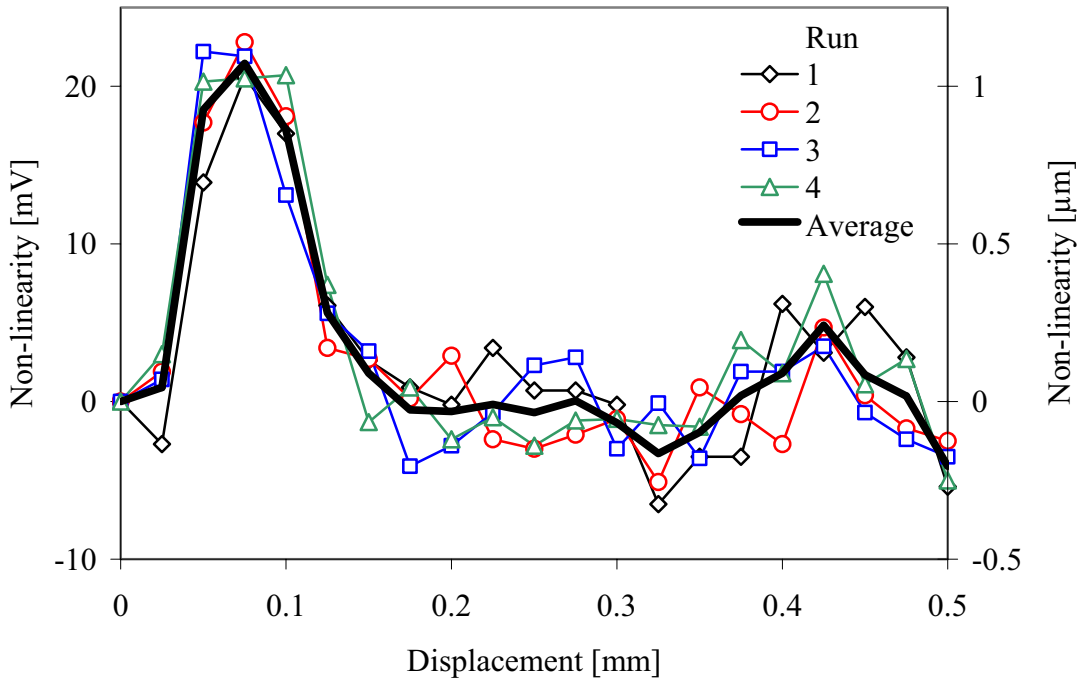

Figure 4.6. Deviation from linearity (voltage – 50 x displacement) – Full range check: Sensor 2 – Sensor 18097, extension cable 2582, channel 2 NTNU.

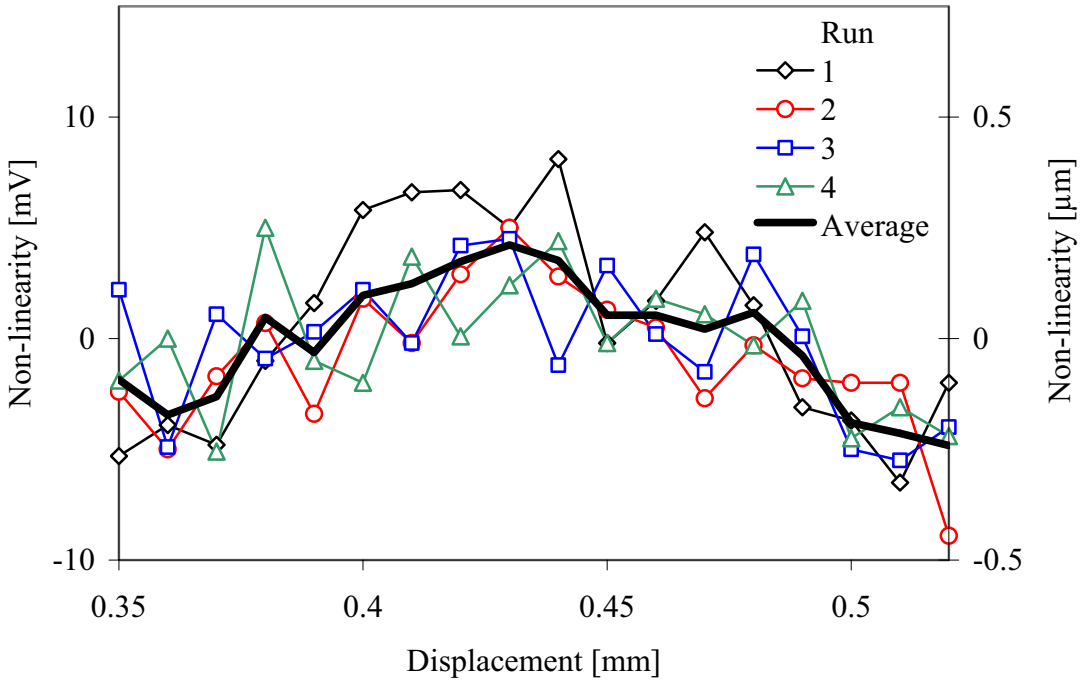

Figure 4.7. Deviation from linearity (voltage – 50 x displacement) – Reduced range check: Sensor 2 – Sensor 18097, extension cable 2582, channel 2 NTNU.

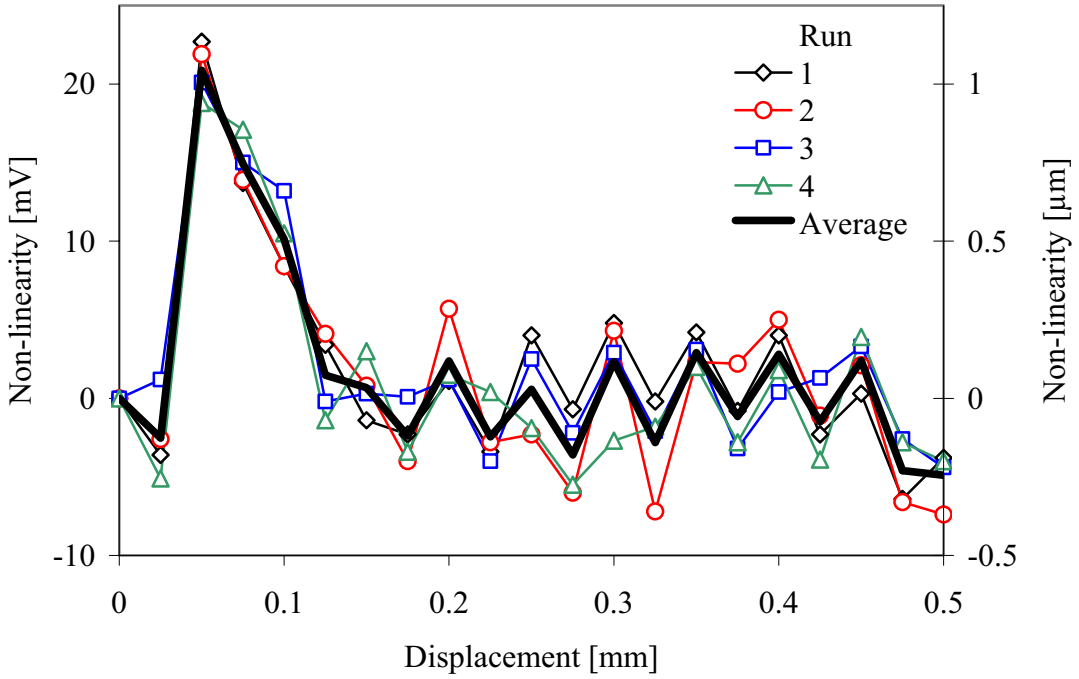

Figure 4.8. Deviation from linearity (voltage – 50 x displacement) – Full range check: Sensor 3 – Sensor 18098, extension cable 2581, channel 3 NTNU.

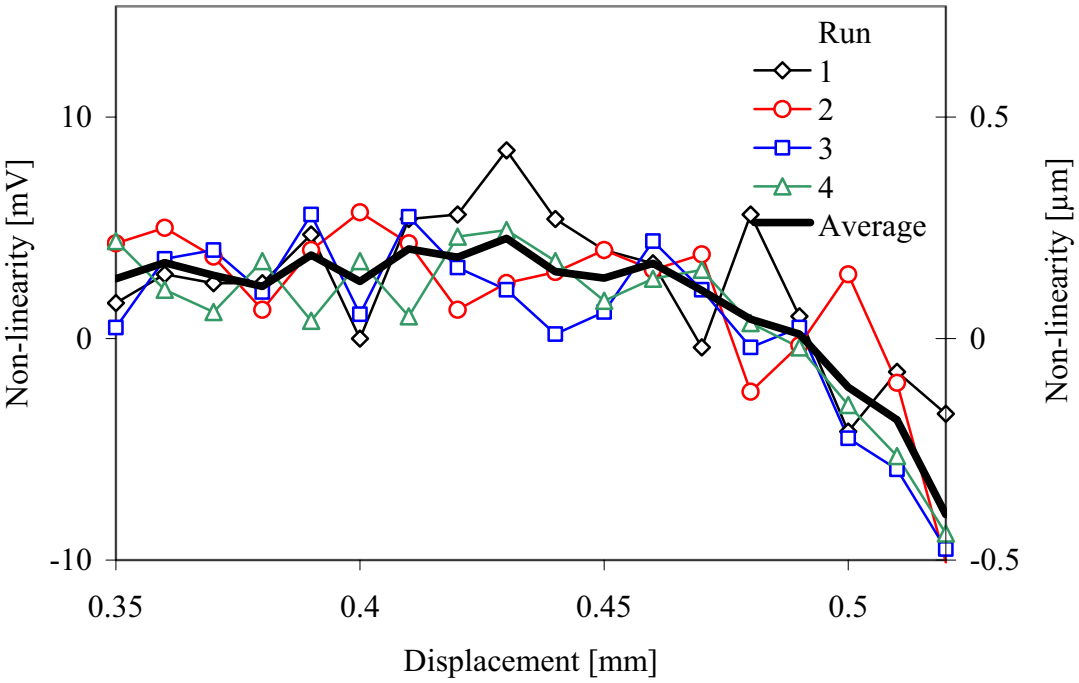

Figure 4.9. Deviation from linearity (voltage – 50 x displacement) – Reduced range check: Sensor 3 – Sensor 18098, extension cable 2581, channel 3 NTNU.

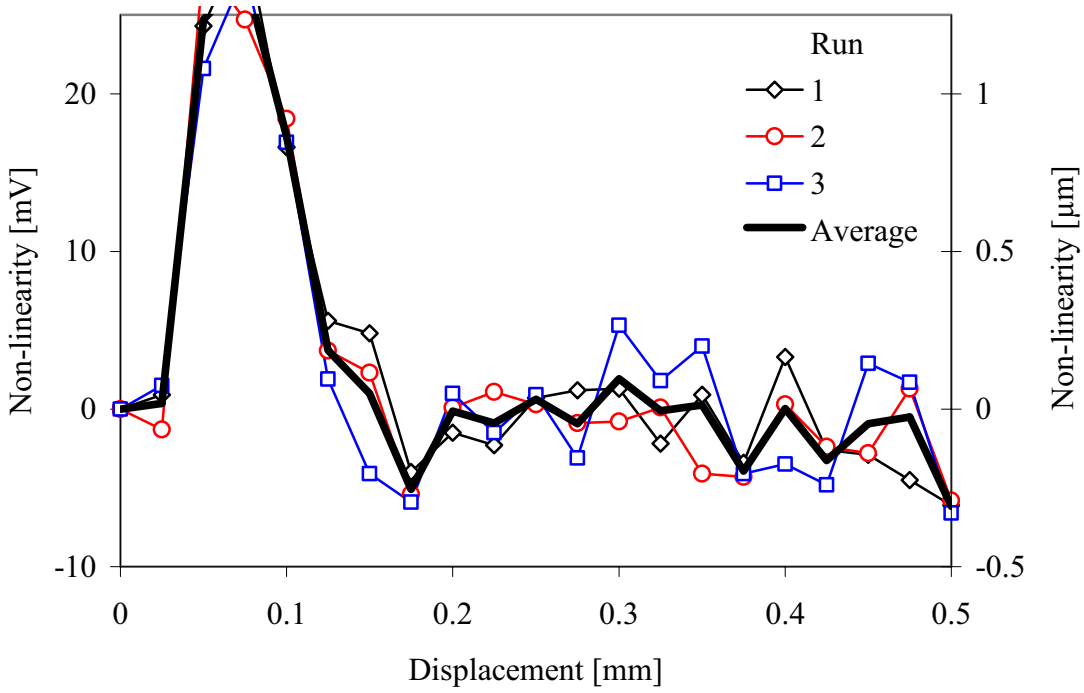

Figure 4.10. Deviation from linearity (voltage – 50 x displacement) – Full range check: Sensor 1 – Sensor 17661, extension cable 3161, channel 1 NTNU.

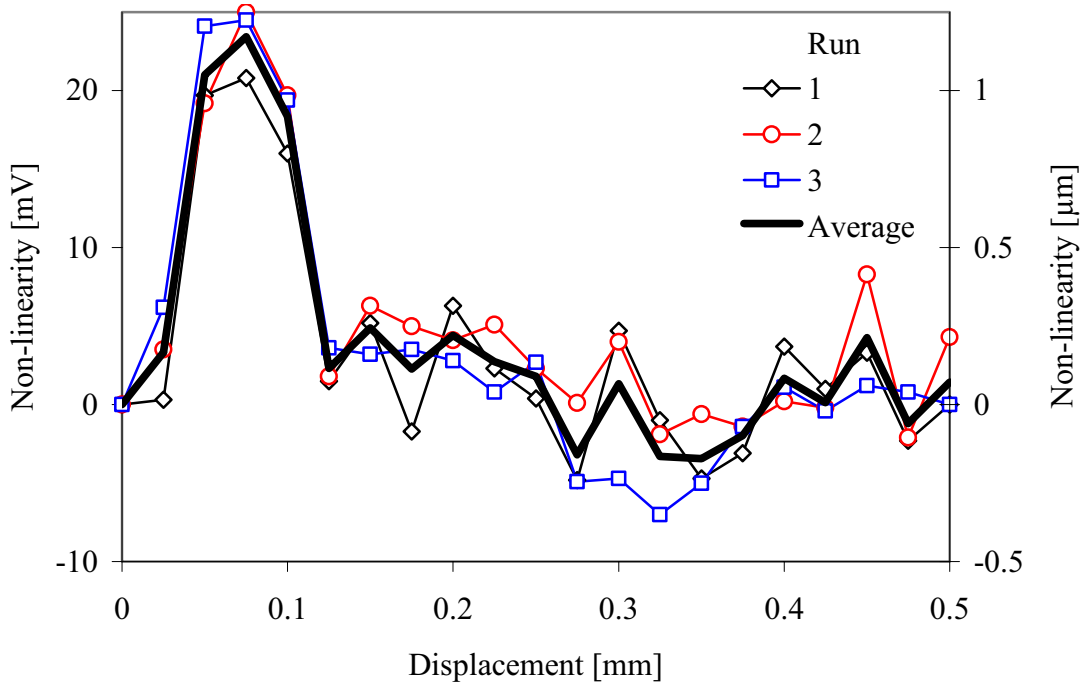

Figure 4.11. Deviation from linearity (voltage – 50 x displacement) – Full range check: Sensor 2 – Sensor 18097, extension cable 2582, channel 2 NTNU

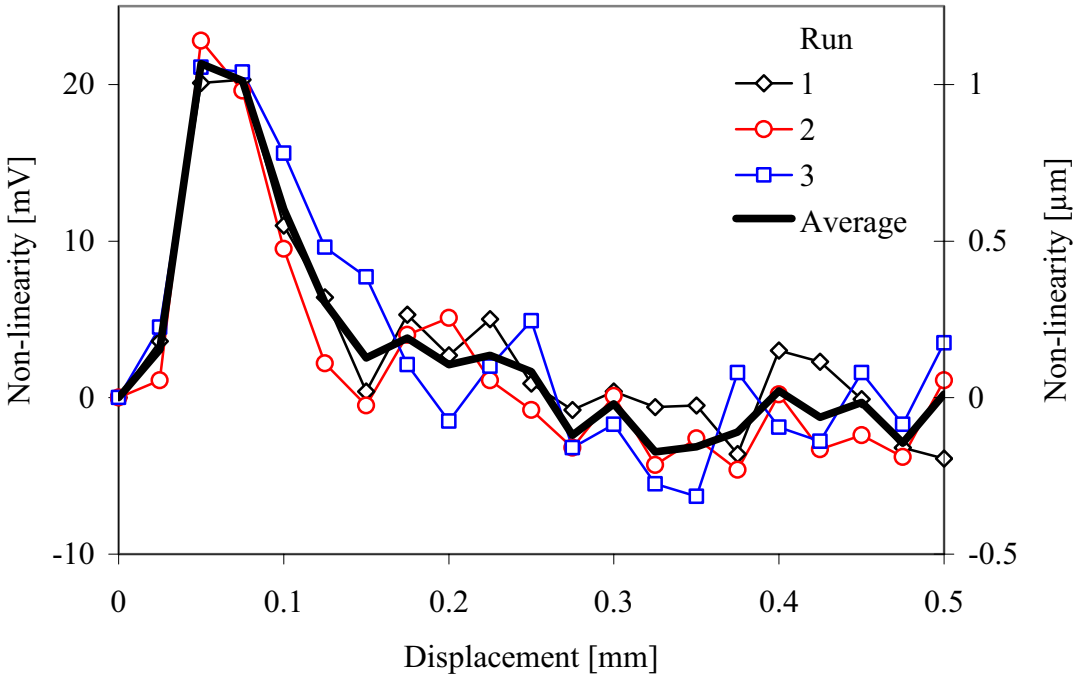

Figure 4.12. Deviation from linearity (voltage – 50 x displacement) – Full range check: Sensor 3 – Sensor 18098, extension cable 2581, channel 3 NTNU.

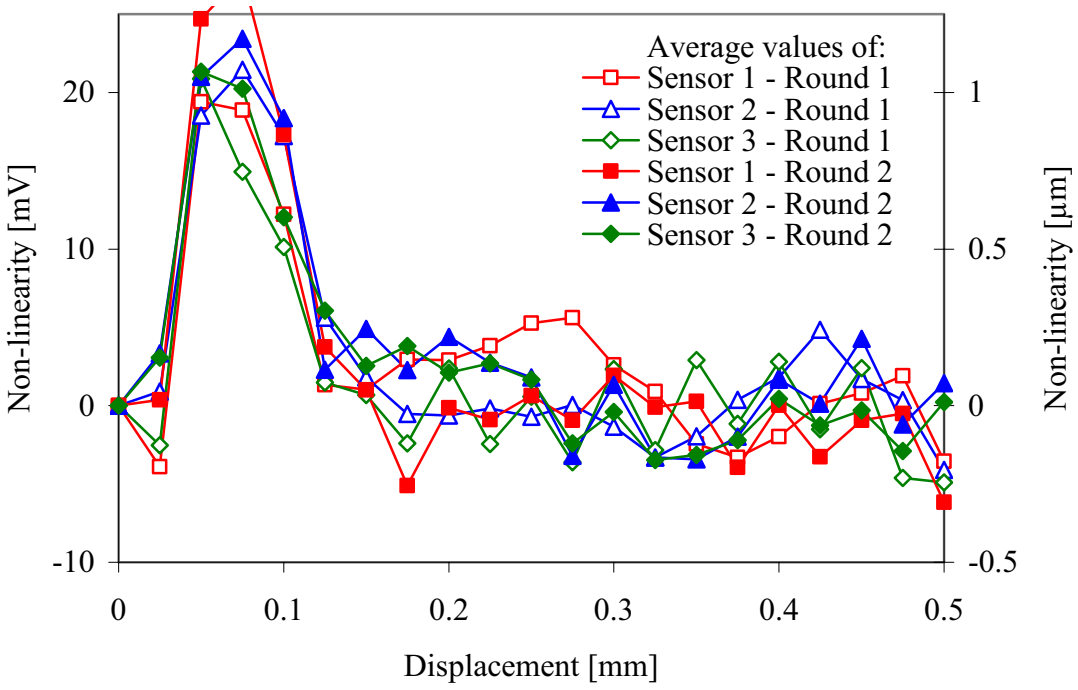

Figure 4.13. Comparison of calibration data for all capacitive displacement sensors and rounds of calibration (Round 1: January 2002, Round 2: July 2002). A round of displacement calibration differs from a round of extrusion.

4.2.2 Interpretation and use of results

The DC output voltage of the Capacitec displacement measurement system should be proportional to the capacitive reactance of the air gap of the sensor. According to the analytical or approximate expressions for the parallel plate capacitor, the inverse of the capacitance should change proportionally with the gap distance. If the plates of the capacitor are separated by a distance $d = 0.5$ mm, the capacitance is approximately:

$$C = \varepsilon_0 \varepsilon_r \frac{A}{d} = \varepsilon_0 \varepsilon_r \frac{\pi D^2}{4d} = 8.854 \frac{pF}{m} \cdot 1 \cdot \frac{\pi \left(1.9 \cdot 10^{-3}\right)^2 m}{4 \cdot 0.5 \cdot 10^{-3} m} = 0.0502\ pF \qquad (4.1)$$

The true capacitance may deviate from this value during measurement. First, the relative permittivity, ε_r, of air is not exactly 1, but slightly larger (1.000264) [Bax97]. Due to the rounding off performed in relation to the above calculation, the effect is not shown in Equation (4.1). As the air is heated the capacitance of the system may also change. The effect is usually very small, which partly explains why calibration curves determined at room temperature may work quite well also at high temperatures. For changes smaller than 5 ºC close to room temperature, the permittivity changes by only 5 ppm/ºC for dry air [Bax97]. This corresponds to 0.25 % / 500 ºC, but extrapolation of this type should never be performed. No separate high-temperature calibration procedure is proposed by Capacitec. Foster [Fos89] has mapped the sensitivity of high-temperature HPC-150 sensors to temperature changes (Figure 4.14). The changes in output voltage may not only be due to the changes in the capacitance of air. The thermal expansion of sensor parts is also of some significance. Still, the capacitive displacement measurement must be regarded as relatively insensitive to temperature changes.

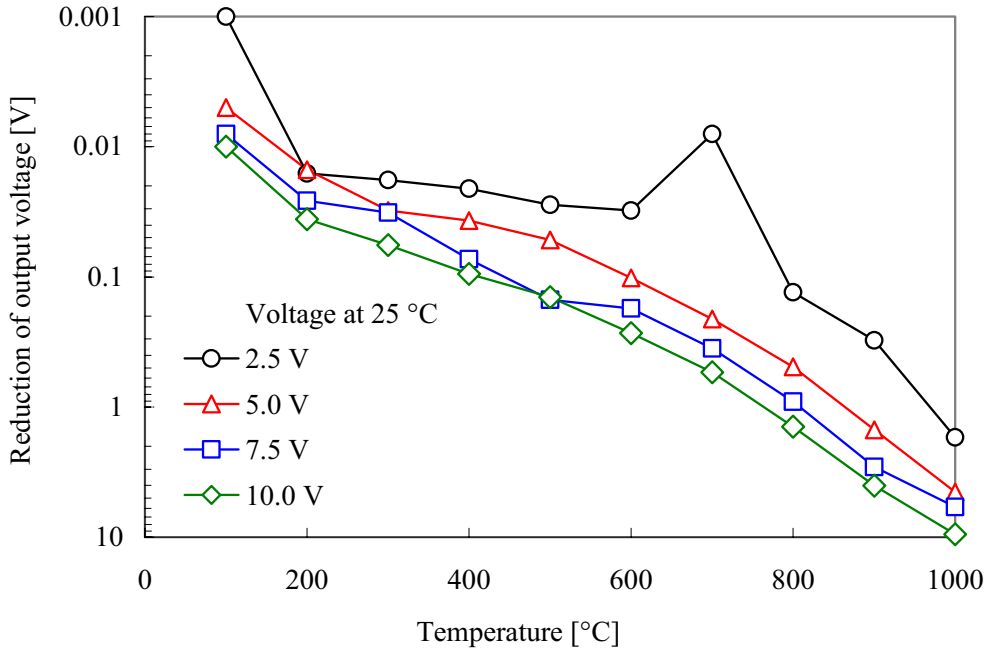

Figure 4.14. Temperature effect on sensor output [Fos89]. The values 2.5, 5.0, 7.5 and 10.0 V are the initial DC voltage levels (at room temperature).

Another reason why the true capacitance may deviate somewhat from the one calculated by Equation (4.1) is that the expression is only approximate. It does not take into account the spreading or fringing of the electric field, **E**, close to the outer edges of the capacitor. For the simplest thin plate capacitor design the effect may be quite significant (>10 %). The effect becomes more important as the ratio between the gap and the diameter of the capacitor, *d/D*, becomes larger. The response of a real capacitive sensor is non-linear. Matters may be improved by using a guarded sensor design like the one provided by Capacitec. Figure 4.15 displays the electrical field for a typical guarded capacitive displacement sensor. The guard contributes to making the electric field more uniform close to the plate edges. The guard may be at ground level or at any other well-defined voltage, which is the case for the Capacitec sensors. There is a strong electric field between the guard and the sensor disc of the probe. The disc of the probe is much stronger capacitively coupled to the surrounding guard than to the sensor plate at ground level, especially if the insulation material that separates the plate and the guard exhibits dielectric properties. However, the capacitance for the probe disc and the guard should not change much when the distance between the capacitor plates is altered, and it should therefore not influence measurements. The capacitance of a guard sensor is usually smaller than that of the ideal parallel plate capacitor. The figure on the left hand side of Figure 4.16 shows the capacitance and the inverse of the capacitance of the ideal and the guarded types (numerical) of sensors as a function of the gap distance. All calculations assume that the probe capacitor plate is circular and of diameter D = 1.9 mm. The relative permittivity of air is set to exactly 1 in the calculations. Note that the distance from the bottom of the sensor disc to the probe is usually smaller than 0.4 mm, while the capacitance curve is close to linear for sensor gaps that are smaller than 1 mm. The Capacitec equipment includes special circuit components that considerably improve the linearity of the sensor response (from 2 to 0.2 %).

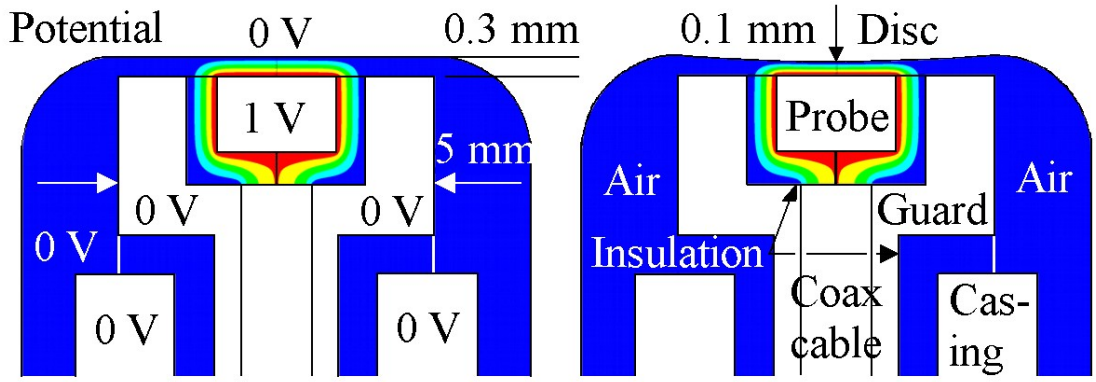

Figure 4.15. Calculation of the potential for sensors with electric fringe fields at the edges. Two types of simulations have been performed. One considers pure translation of the disc, while the other considers the sensor disc bending. Calculations are only approximate and have not been used in calibration.

A last reason why the capacitance may deviate from the value indicated by Equation (4.1) and even the value obtained through calibration, is that the deflecting disc does not move merely by translation towards the probe surface, but rather bends and even tilts. In the case the disc bends, it is natural to define the gap distance as the minimum distance

between the two discs. However, the capacitance change is smaller for a given change in gap distance when the disc bends than when it translates (assuming that the minimum gap distance is considered). If a finite element analysis is used to establish a relationship between the die face pressure and the movement of the centre point of the sensor disc, the experimental displacement calibration curves cannot be used directly to convert displacement data to voltage signals. The definition of the gap distance must first be changed. Figure 4.16 shows capacitance as a function of the gap width for discs that translate and bend. The curves have been calculated with the finite element package ANSYS® 7.1 and for sensors with an outer guard. The curve that is very close to linear in the entire interval from 0 to 0.5 mm displacement has been calculated for two flat capacitor plates separated by a distance d and moving towards each other by pure translation. The other curves have been calculated for sensor discs that bend. The initial distances between the two capacitor plates were either 0.3 or 0.5 mm before loading. The upper discs of the sensors deflect as they are exposed to loads. The shapes of the discs are spheres with radius R given as a function of the deflection, d, and the diameter, D_p, of the deflecting sensor disc. The diameter is here 8 mm. Note that the relationship between the capacitance and the inverse of the gap distance is still almost linear for a large range, even when a load is applied at the disc face. However, the curves for bending and translation differ, and calibration factors should also differ significantly. The non-linearity is most important when the gap distance is small.

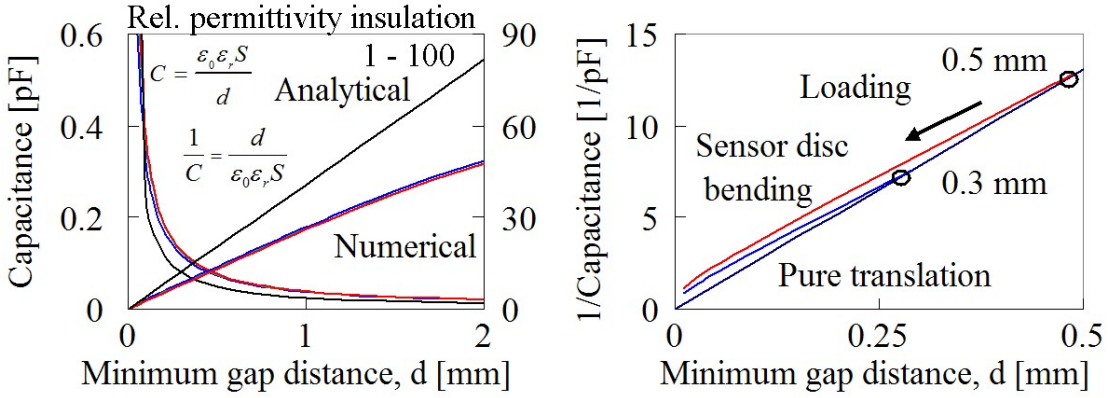

Figure 4.16. Capacitance as a function of the gap distance. The figure on the left hand side compares analytical results with numerical ones for a guarded sensor. The figure on the right hand side shows the change in capacitance as the sensor disc bends as it is exposed to a pressure.

Obviously, the offset of the centre of the sensor relative to the centre of the hole also determines the outlook of the true calibration curves. Tilting of the sensor disc relative to the capacitive probe and a line determined by its fixing points may be caused either by a non-uniform load distribution, by friction or by the overall die deflection. The effect is not very large compared to the total air gap distance or the deflection of the sensor disc. According to calculations performed with ANSYS® a tilt of typically 1 μm or less may be expected.

4.3 Approaches to calibration of the pressure sensors

4.3.1 Some basic calibration principles

The Capacitec equipment relates displacement of an object relative to the probe to the output voltage of the amplifier. The objective of the calibration analysis is to establish relationships between the pressure applied at the die face or at the faces of the liner load cell and the DC output voltage of the Capacitec measurement system. There are two possible types of approaches, the indirect and the direct. The first consists of two parts. A relationship between the output signal and the displacement of the elastically deforming sensor part is first established. Another calibration curve is then needed to link displacement and pressure. In this work, the second curve is generally determined by finite element modelling. The second approach, the direct one, assumes that a calibration set-up may be designed so that the relationship between the DC output signal and the die face pressure or the liner load may be established directly by experiment. The direct approach is probably the most accurate. Given the uncertainties related to measurement of the deflecting sensor disc, it is rather doubtful that the second approach may be used to establish a curve for calibration with accuracy much better than ± 1 μm.

The task of relating the deformation of either the die face pressure sensor disc or the liner load cell to pressure is not a trivial one. The task may be solved experimentally, but simulation is perhaps simpler. When the material behaves elastically, calculation methods may be very accurate. However, there are a number of questions related to the input data to the analysis. First, accurate descriptions of elastic material properties at higher temperatures are rare. There is at least a ± 2 to 5 % error in the values of the elastic modulus provided by the supplier of the die steel. High-temperature material testing may be performed to improve accuracy, but it may not at all pay off since there are a number of other uncertainties related to the analysis. For example, the shape of the sensors need not be as specified. A small sensitivity analysis of the consequences of relatively small deviations in shape has been performed [Moe04c], and it reveals some of the problems related to establishing calibration curves through FEM. As will be shown below, matters may be improved by careful sensor design, but not completely solved. There are questions related also to effects that are not integral parts of the FE models, such as the contact conditions of the various parts of the sensor. Where is the exact point of contact between the sensor holder and the die? What is the exact nature of the contact during measurement? Will there be any relative deformation not included in the FE model? In order to answer such questions a method of direct calibration is needed. This does not mean, however, that the indirect methods and FE analysis are entirely useless. They constitute an alternative and complementary approach and may be and have been used as tools for analysis of sensor behaviour and sensor design.

An accurate method of calibration has to fulfil certain criteria. Ideally, sensors should be calibrated by a completely independent test so that all possible effects may be carefully considered. The measurement set-up should be very easy to analyse. However, the test case should also be similar to the extrusion case. It is probably best to calibrate using a simple loading case, but the question is how to modify results so that they apply to the problem at hand. The present sensor study serves as an example. An insert sensor may

be mounted in a small press and compression tests may be performed both at high and low temperatures. The interface may be lubricated to reduce the influence of shear stresses. A calibration factor may then be established. The problem is, however, that in reality, shear interaction plays some part, and perhaps even more importantly, the mounting of the sensor in the calibration set-up may deviate from the mounting in the extrusion die. The die deformation is of significant magnitude during extrusion and contact conditions between the die and the sensor may be difficult to determine. As a result, the sensor response may differ somewhat from that of the simple calibration case [Moe04c]. It is possible to analyse such differences with finite element models, but this does not mean that accuracy of measurement necessarily is improved. It is usually necessary to test how applicable results are through experiments. For that reason, this study introduces a stepwise approach to test different aspects of the sensor behaviour.

Finally, it should be noted that the problem of calibration is closely linked to the sensor design issue. There are essentially two different types of sensor designs, the insert and the integrated type. The former has a well-defined area of influence and is probably less affected by the overall deformation of the die. The integral sensor has a limited area of influence [Moe04c], but the entire die must necessarily be included in the off-line tests. Besides, the determination of the load curve becomes more involved since the area of the die surface that is exposed to the load must be determined. In practice it is usually easiest to apply the pressure at the entire die face when the sensors are of the integral type. The same approach may be followed in order to evaluate die sensor interaction for the insert type of sensors, but if the interaction is well-defined, it may not be necessary. Another problem of both types of sensors is that they may be of large size. The pressure may not be uniform at the entire sensor surface, and the pressure distribution (not only the average pressure) must be found in order to determine the sensor response. It may seem that the solution would be the pin-sensor design (Volume I), but there are problems related also to measurement with such sensors. Friction between the pin and work piece and between the pin and the die must be compensated for. It may also be necessary to tune the deformation of the pin and its surroundings so that the tool surface remains completely flush during extrusion. If the pin is allowed to retract into the hole in the die face, measurements may be affected. Besides, penetration of aluminium into the sensor may cause it to stop working and measurement results to be in error.

4.3.2 Off-line calibration of pressure sensors

There is no standard method of performing direct calibration of the die face pressure sensors, but there are many methods that may be regarded as useful. The first idea was to use a technique that made it possible to establish a calibration curve by an off-line test, i.e. a test that is not performed in the extrusion environment. An off-line calibration test should in principle be easier to perform and potentially more accurate than an on-line test. The main problem of the off-line test is to generate conditions that resemble those that may be experienced during extrusion. Typically, the die face pressure may reach 200 to 500 MPa, while the sensor temperature may be in the range from 400 to 500 ºC. An approach that was initially considered consisted of applying a uniform pressure through a fluid with a moderate viscosity, such as oil. The technique is less appropriate at the high temperatures and high pressures of extrusion, however, and the

design of the hydraulic system would have been a quite demanding task that would have drawn much attention away from the true objective of the study, to analyse the loads on and the deformations of dies during extrusion. It might have been somewhat simpler to perform such calibration if sensors were of a type that could be inserted into dies.

The elasto visco-plastic compression test

An alternative method of calibration is the standard compression test. The compression test is simpler and cheaper to perform than extrusion. Smaller samples (OD 30 - 40 mm) and a more accurate press can be used. The compression test is also somewhat simpler to model than extrusion, and better estimates of the die face pressure may be obtained. However, it is not a perfect calibration test. First, the friction conditions at the interface between the work piece and the tool are never accurately known. There is a strong coupling between the distribution of pressure and friction at the interfaces. If the work piece is thin, the pressure builds up towards the centre of the compression specimen as a consequence of the resistance to flow due to friction. This is the "friction hill" pressure distribution. If the friction is of the Coulomb type, which most often is the case at low temperatures, shear stresses are pressure dependent through the constitutive relation. Thus, the distribution of the pressure or the tractions normal to the surface of the die face pressure sensor may be relatively complex. The ideal case of a uniform distribution may either be obtained by reducing the friction shear stress with lubrication or by choosing ideal combinations of specimen height and diameter. During compression testing, the specimen dimensions and the pressure distribution change gradually. This complicates the determination of the actual load applied at the sensor surface. A large number of compression tests were performed in the early parts of the study (Volume I). Teflon® mats were placed between the work piece and the tools in order to limit the effects of friction. The compressed specimens were not significantly barrel-shaped after deformation as would have been the case if friction stresses had been large. However, the friction coefficient may have changed during the experiments. The Teflon® mats were stretched and sheared off at the edges at a certain point during experiments. As a consequence, friction conditions changed and the pressure increased. The lubrication problem is even more complex to handle during high-temperature testing.

During low-temperature compression testing and high-temperature compression testing for high-strength materials, the elasto-viscoplastic nature of the material behaviour may complicate analysis. When the sensor disc deforms (deflects), the work piece material should adapt to the new shape of the die surface. For an incompressible and perfectly viscous material, this is not a problem as long as pressure changes are not of a too high frequency. However, in the case of compression testing with a material that may either deform purely elastically or elasto-plastically, it is by not certain that the surfaces of the die and work piece fit perfectly. After a sequence of loading and unloading, there may be a slightly convexly shaped bulge protruding from the surface of the specimen that has been in contact with the pressure sensor. During loading the work piece material first deforms only elastically, but as the loads increase it also flows plastically and fills the gap that parts it from the sensor surface. During unloading, however, it first adapts as the die surface straightens out, but at a certain point the bulge that was formed during loading may stop deforming plastically. The described effect most probably causes the curve that relates load and output voltage to be non-linear and non-unique. If the exact

pressure distribution had been known, it would probably have been possible to establish a linear relationship between a measure of the pressure (traction normal to the die face) and the sensor disc deflection. The non-linearity of the curves is probably primarily related to a change in the distribution of pressure. The effect has also been observed during simulation with ANSYS®, but only qualitative data have been obtained. If the diameter of the specimen changes due to plastic deformation, a somewhat different type of non-linearity may be observed. This type is simpler to analyse. Generally, one should use compression test specimens that are so large that the sensor response is not affected by a work piece diameter change. An alternative calibration method consists of loading a compression specimen confined by the walls of a short container. An increase of the area of loading is then prevented. The approach is treated in relation to the discussion on on-line calibration techniques.

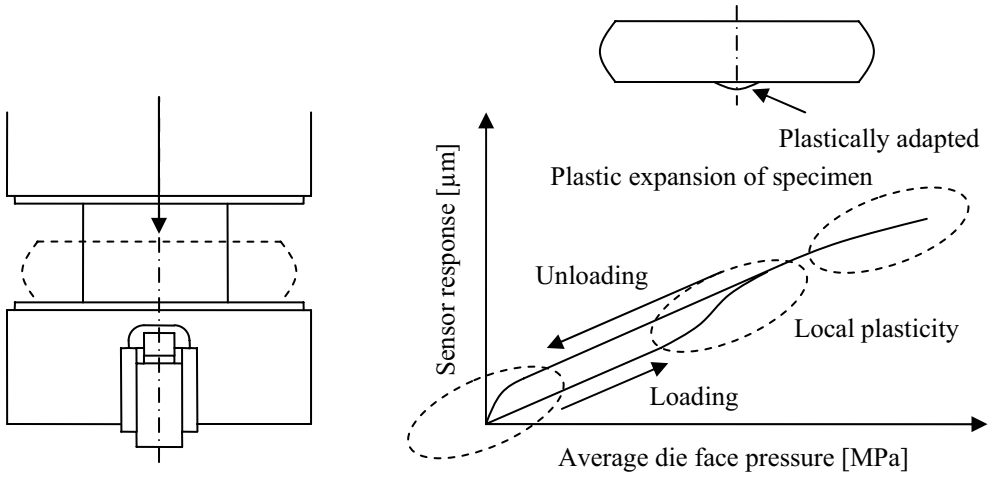

Figure 4.17. Calibration of pressure sensors by compression testing. The figure gives an indication of a possible cause of non-linear behaviour during tests. The mechanisms are further discussed in Chapter 5.

A problem related to off-line compression testing in general is that both the set-up and the calibration curve may be altered when the die and sensors are mounted in the press and subsequently heated to 400 to 500 ºC. Such changes may occur for example if the probes move somewhat. The calibration curves reveal that the change in output voltage may depend on the choice of zero point for the pressure measurement. Figure 4.7 may be used to display the problem. One may study two cases of measurement of essentially the same pressure. In the first case the sensor is mounted in such a way that the distance between the capacitor plates is approx 0.42 mm. In the second case the distance is 0.50 mm. As a force is applied the sensor disc may be assumed to deflect exactly 30 µm, i.e. from 0.42 to 0.39 mm or from 0.50 to 0.47 mm. Due to the deviations from linearity of the system, it will in the first case appear as if the deflection is 0.25 µm larger than it really is, while in the last case it will appear as if it is 0.25 µm smaller. If a non-linear curve is used for calibration, it may be possible to reduce such errors, but there are strict limits to the accuracy of measurement. Movements of the probes should obviously be avoided through proper sensor design. If the probe completely loosens, the experiment is ruined. However, the measurement task is not at all a trivial one due to the fairly rough handling of the die during assembly, the considerable loads at the die faces, the

significant elastic deformations and the large temperature changes. Hence, it is most important that the calibration curve is well-defined and to a small extent affected by noise.

The ring compression test

The uncertainties related to the boundary conditions of the standard plastic compression test complicate the analysis of results. As has been indicated, the disadvantages of the compression test make it less useful as a calibration case. An alternative approach that has been found more useful consists of compressing only elastically rings of a range of outer diameters on the upper face of the pressure sensors. The thickness of the rings should be very small in order to avoid the problems discussed in relation to the ordinary compression test. Point or line loads should ideally be applied. A practical thickness that has been used in experiments is 2 mm. Outer diameters may typically be 4, 8, 12, 16, 20 and 24 mm. The height of the specimen should not be much larger than the thickness in order to avoid buckling of the ring during experiment. The height of the specimens that were used in the current study was 2 mm.

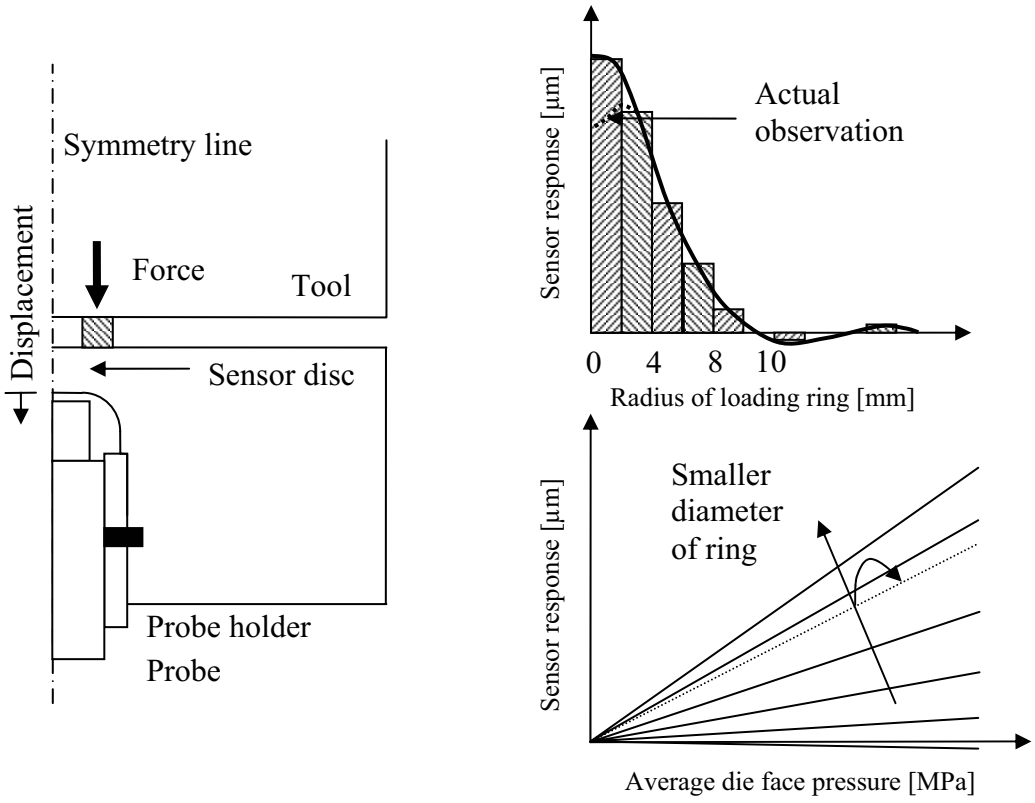

Figure 4.18. Calibration of pressure sensors by ring compression testing. The figure shows how results from experiments with rings of a range of diameters may be used to establish calibration curves for the sensors.

If the ring that is used for testing is sufficiently large, one should not expect the sensor disc to deform when the load is applied. Deflections only occur when the load is applied in fairly close vicinity of the sensor cavity. The larger the distance from the centre of the sensor, the smaller is normally the influence of the load. The influence curve may be

defined as a curve linking the deformation of the sensor to the radius of the die surface area within which a load is applied. The curves may be generated by integration of the results from many ring compression tests. The results obtained by integration to infinity may be used to characterise the behaviour of the sensor when a pressure is applied at the entire surface of the die. This assumes that the die is extremely large or at least that the sensor is placed at a sufficient distance from the edges of the die. There are, however, a number of reasons why such a procedure may be inaccurate. The rings must be placed accurately. It may also be necessary to check whether there is actually a proper contact between the surfaces of the ring and the die and to check the assumptions with regard to the pressure distribution. In practice, integration of the pressure may be very inaccurate, and it is doubtful that the approach may be used to determine very exact calibration curves (Volume I). However, it is likely that the results from a single ring compression experiment may be used to examine the characteristics of the sensor behaviour. The elastic ring compression method has been useful mainly since it has been applied to experimentally investigate the nature of the influence curve and to clearly demonstrate the linearity of the sensor behaviour.

4.3.3 On-line calibration of the die face pressure sensors

An on-line calibration test is regarded as one that is performed in the extrusion press immediately before and/or after extrusion experiments. On-line calibration may be very difficult to perform, and there are limits to the accuracy of techniques in an industrial environment. However, there are obvious advantages of testing the characteristics of the sensors in close connection to the extrusion experiments. The problems of predicting the high-temperature response of the sensors and the effects of the undesirable movement of sensors during assembly are largely overcome. Besides, during full scale on-line testing, the extrusion dies experience load conditions that are very similar to those experienced during extrusion. It should be realised that the loads applied on the extrusion die during extrusion are of enormous magnitude (in the present case, they correspond to the weight of 200 to 300 medium sized cars), and that the deformation of dies is significant. The complete tool set-up is in the present case of laboratory rod extrusion compressed elastically approximately 0.3 mm. Furthermore, the deformation is not uniform. Due to the special design of the set-up, the die is also distorted through shear and bending. This affects the shape of the die outlet, and more importantly, the non-uniform deformation may cause the sensor discs to distort even in the cases where no load is applied directly at the top face of the die. Figure 4.19 shows a thin-strip extrusion die that makes use of six insert sensors. A similar die has been used experimentally (Volume I). Only a part of the die is shown, and the die deformation is exaggerated. If the insert sensors are left out of the model and the load is applied directly at the top surface of the die core, the hole in which the sensor is placed becomes slightly oval. If the sensor is included in the model, traction forces act at the interface between the sensor insert and the top disc. To what extent the tractions actually affect the response of the sensor depends on the design of the sensor. Ideally, the lower part of the sensor should be very rigid in order to prevent distortion, while the sensor disc should easily deform. However, since the pressures are high, a very thin sensor disc cannot be used. Furthermore, space limitations may prevent the die support from being sufficiently rigid. Both in the case of insert and integral sensors, the die deformation may in practice play some part, typically $\pm$ 0.5 μm. The

issue has been treated in reference [Moe04c], and it has been found that the sensors used in the study were only to a limited extent affected by the general die deformation. Still, it should be considered during calibration testing.

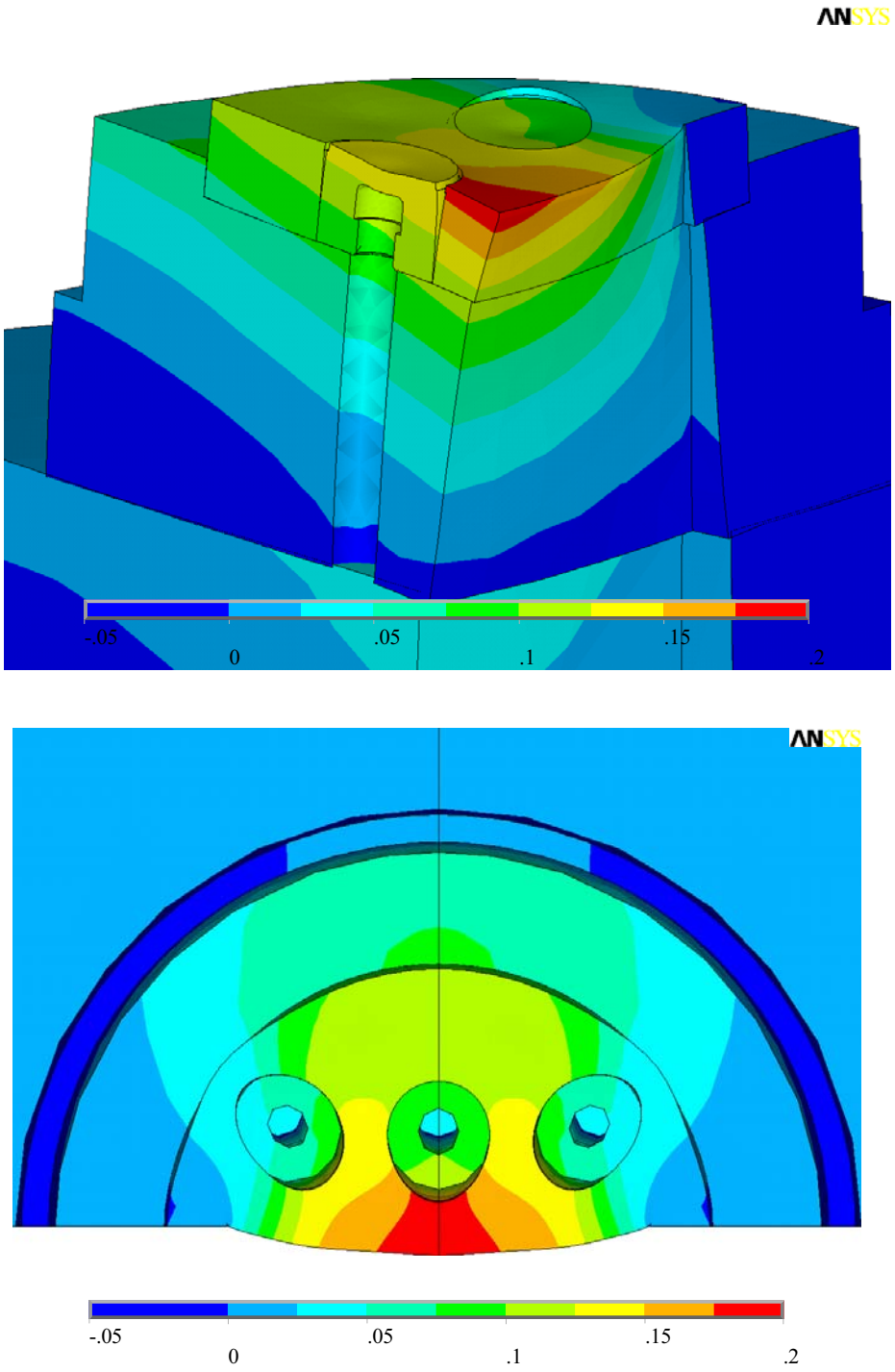

Figure 4.19. The ovalization of die-sensor holes (calculation with and without sensors). The values refer to displacements in a direction normal to extrusion [mm]. The deformation of the die has been magnified 30 times to show the effect of a uniform load of 400 MPa. The sensor design was shown in [Moe04d].

There are a number of reasons why on-line calibration may be quite difficult to perform. Extrusion of aluminium takes place at rather high temperatures. This complicates the handling of the equipment that may be necessary in relation to calibration. It would be possible, at least in principle, to perform compression testing of smaller specimens in the extrusion environment and with the same ram used for the extrusion process itself. The calibration would, however, be most impractical and potentially very inaccurate. In an industrial environment on-line calibration with very small specimens may probably be viewed as infeasible. If satisfactory extruded products are to be manufactured, it is essential that proper temperature control is secured. If the dies cool too much during calibration before extrusion, the flow may be affected during extrusion and so will also the metallurgy of the product. Thus, there is no time to do much adjustment when the dies first have been inserted into the extrusion set-up. An on-line calibration technique for integral sensors placed in the die should be both swift and accurate. If the pressure sensors are mounted permanently to the container or to an intelligent feeder design [Moe04e], calibration need not be performed that regularly. More time may be spent on calibration, and a range of techniques may be used.

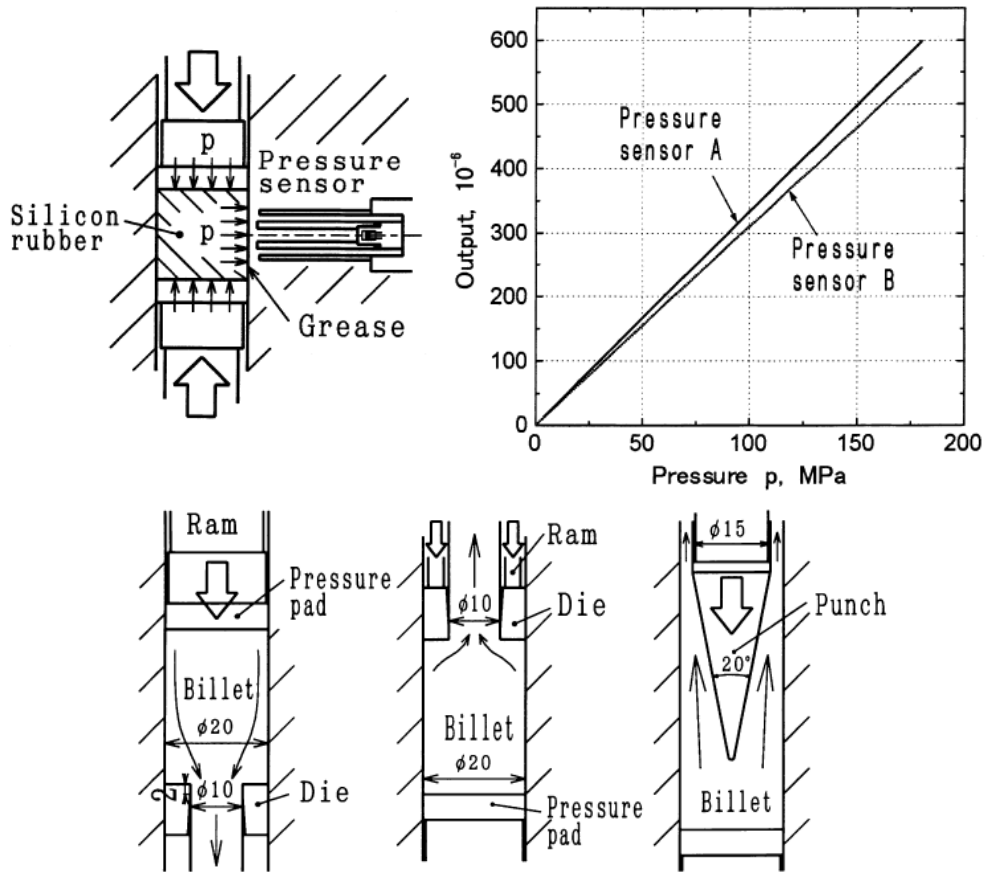

Figure 4.20. The small scale extrusion experiments of Yoneyama [Yon99] and the method of on-line calibration. The calibration of a sensor by hydrostatic compression testing is shown in the upper part of the figure. Both rams are moveable. Forward, backward and pierce extrusion with measurement are demonstrated in the lower part of the figure.

4.4 On-line calibration experiments

4.4.1 Experimental set-up

A technique for on-line calibration through hydrostatic or isotropic compression has earlier been presented [Moe03b]. The technique has been developed during the study, but since it is a quite intuitive one, it has much in common with techniques developed independently by other researchers. Yoneyama has performed a very interesting set of extrusion experiments [Yon99] with a miniature extrusion press at room temperature. The container diameter was only 20 mm while the outlet diameter was 10 mm. A piece of silicon rubber was first inserted in the container and both outlets were sealed off by two movable rams (Figure 4.20). The position of the rubber piece could be changed in order to establish an influence curve for the container pressure sensors. When the rubber piece was compressed, it expanded in the radial direction, exerted a force at the top face of the sensor and caused the strain gauges of the sensor to respond. A calibration curve could then be established. The state of stress in the rubber piece was most probably very close to hydrostatic during calibration. Friction was reduced by layers of grease at all the interfaces. The material could not escape, and there were no pressure gradients in the container. After calibration, the rubber piece was removed from the container and the set-up was configured so that different types of extrusion could be performed. It was possible to determine the pressure distribution at the billet container interface and the shear friction. The force on the die was measured continuously.

It is not simple to make use of the calibration technique of Yoneyama [Yon99] in a full-scale high-temperature industrial or laboratory environment. The silicon rubber and the grease should be replaced by materials that retain their properties up to 600 ºC while tolerating very high pressures. The only replacement for the rubber considered in the current study was aluminium, but there may be other acceptable alternatives. During the extrusion of steel, a process that usually takes place at much higher temperatures, glass may be used to lubricate. There may be alternatives more appropriate for the range 400 to 600 ºC. A paste consisting of oil and copper particles is often applied at the back end of the billet during laboratory extrusion in order to prevent the billet from sticking to the dummy block. At high temperature the oil burns, and only copper and carbon particles remain at the interface. Still, the paste may contribute to a reduction of the interface friction. Since calibration is performed on-line, it is vital that the lubricant may be easily removed before extrusion. During aluminium extrusion lubrication is seldom used. The lubricant would cause the material from the billet surface to flow into the outlet and the profile. The impurities of the billet surface would also end up in the profile. This would ruin both material and surface properties of the extruded product. While it is possible to clean the container after calibration and before extrusion, the use of a lubricant would only serve to complicate experiments unnecessarily. Furthermore, during hydrostatic compression it may not be necessary to lubricate at all. First, the billet may be made very thin, and the effect of the container friction should in any case be small. Second, if the material is prevented from flowing out of the outlet by a steel plug, there is no reason why there should be a gradient in pressure. A deviatoric state of stress in a fluid like hot aluminium is mainly related to the flow of material and velocity gradients. Calibration experiments should essentially be static.

Figure 4.21 shows the experimental set up used for calibration of the die face sensors, and Figure 4.22 is a picture of the different parts of the set-up for the calibration experiments. The same die was used for extrusion. The largest outer plug diameter was slightly smaller than 34 mm, i.e. the smallest outer diameter of all the die inserts. The smallest outer diameter of the plug was either 11.1 or 15.7 mm depending on the die outlet diameter. The lowermost part of the plug was added in order to prevent the plug from moving sideways. A problem with the plug is that it may damage the outlet. For that reason the steel plug was not hardened. Its lowermost part was also removed before the last rounds of extrusion experiments with long bearing channels. The result was a somewhat larger sideways movement of the plug, and after extrusion there were marks on the innermost edge of the top disc. This indicates that it had been in contact with the steel plug. However, the die outlet was properly sealed off at all times. It should be noted that with the original plug design, the thermocouples in the bearing channel may either be damaged or become retracted.

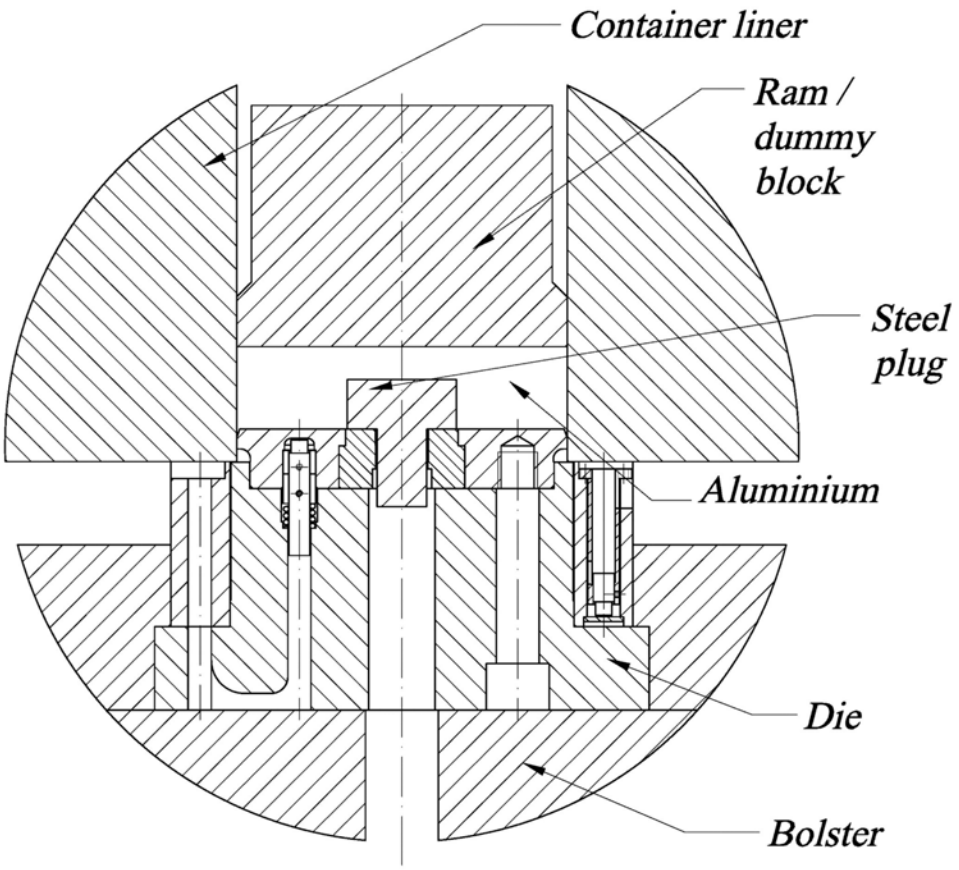

Figure 4.21. A cross-section view of the extrusion calibration set-up.

The steel plug is probably not the most elegant solution for sealing off the die outlet, nor is it very useful when performing industrial experiments. It may also be hard to use the steel plugs when profiles with relatively complex cross-sections are extruded and/or when the sensor is placed very close to the die outlet. There is always the danger that the calibration test billet may stick to the top face of the die and cannot be torn off. The

experiments must then be stopped and the test billet parted from the die, mechanically or chemically (by etching). When a steel plug (Figure 4.21) is used, it may be difficult to part the billet from the die with a die-shear. An alternative to using the simple plug design adopted in the current study is to either integrate the plug in the die design, or to use some kind of instrument to insert the plug from the bottom or top side of the die. In the case the plug is inserted from the bottom side, the loads applied on the plug have to be carried by tools supporting it. It would not be difficult to design such a plug for the bolt extrusion die, but the task may be much more demanding for cases of thin-walled complex profiles. A solution could be to change the complete design of the tool so that the top disc of the die may be adjusted more freely both in between runs and rounds of experiment. The plug design may also be simplified if feeder dies are used, since it then is possible to seal off the entire feeder during calibration. The simple plug presented above worked satisfactorily for the experiments with the laboratory rod extrusion die.

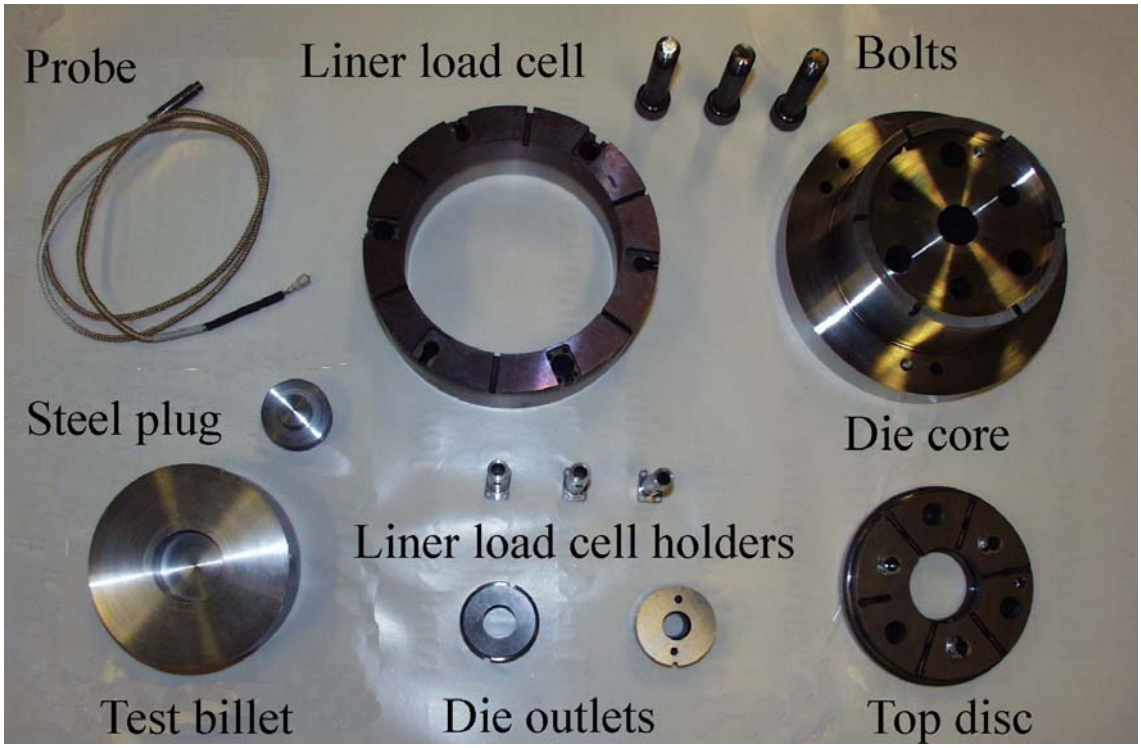

Figure 4.22. The parts of the extrusion and calibration set-up. The test billet and the steel plug are shown on the left hand side.

4.4.2 The accuracy of ram force measurements

During measurement new observations are made and related to an established standard for that type of measurement. When the Capacitec sensor system is used to measure the deflection of a sensor disc, the system must first be properly calibrated. The point of origin for any type of calibration is the definition of the relevant measurement unit, in this case the metre. The metre is now defined as the length of the path travelled by light in vacuum in 1/299,792,458 of a second. The second is equal to 9,192,631,770 periods of the radiation related to a specific change of state of the ^{133}Cs atom. Calibration of pressure sensors requires or essentially is a method for comparing the response of the

sensor with the standard. As was discussed above, the first step consisted of comparing the response of the Capacitec system with the response of the Heidenhain optical displacement gauge. The Heidenhain equipment is calibrated relatively frequently. This is usually done by relating the thickness of a set of orifice plates to output signal from the system. The orifice plates are also regularly checked. In every step, both bias and randomness may be introduced. Although capacitive measurements may be extremely accurate, the real accuracy of the pressure measurement is essentially determined by the method of calibration. If the on-line hydrostatic method of calibration is used, the limit is determined by the accuracy of the ram force measurements. The real measurement accuracy should in fact be poorer than the ram force measurement accuracy since the assumptions with regard to isotropy and uniformity probably are somewhat inaccurate.

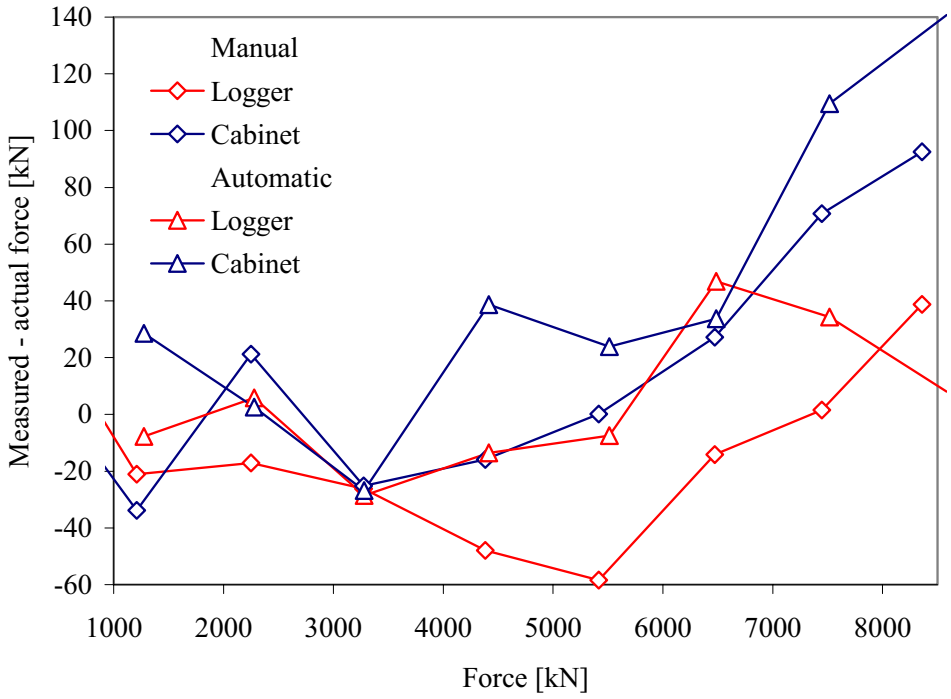

Figure 4.23. Calibration curve load measurements press [Lef01]. The "actual force" is the force indicated by the load cell used for calibration.

An output signal almost proportional to the ram force may be obtained by measuring the pressure of the oil in or close to the main hydraulic cylinder. The measurement should be performed in steady state, since the ram force pressure measurement system has a finite response time. In order to relate such a measurement to the ram force, a standard load cell is used. It relates the ram force to displacement during load cell compression. It would be a simple task to include a standard load cell in the press set-up, and the possibility has been seriously considered. However, load cells have only been used to calibrate the existing system for ram force measurement. Figure 4.23 shows a set of calibration curves that was obtained during the last calibration round before experiments were performed. Only the difference between the value of force indicated by the system and the value provided by the calibration load cell is shown. There are in all four curves. The SINTEF press may be run in either an automatic or a manual mode, and calibration

curves were obtained for both cases. The deviation between readings from the load cell and sensors is smaller than 50 kN. The measured or indicated force by the system is too high, when the force is larger than 6000 to 7000 kN. In the extrusion study, the ram force did not exceed 4500 kN. The force measurement is, however, most inaccurate for very low values (i.e. 500 kN and less). The ram force is indicated by a PC logger and by a display in the control cabinet. Systematic differences are of the same magnitude as the inaccuracy in measurement. The measurement repeatability for genuine replications (performed after a new set-up and on a new day) has not been established. Based on experience, it may be fair to assume, however, that the standard variation times three is smaller than 50 kN. Lefstad reports on the full set of calibration runs performed in January 2001 and treats more thoroughly ram force measurements at low levels of force [Lef01]. The described calibration runs were the very last ones that were performed prior to the second round of rod extrusion experiments.

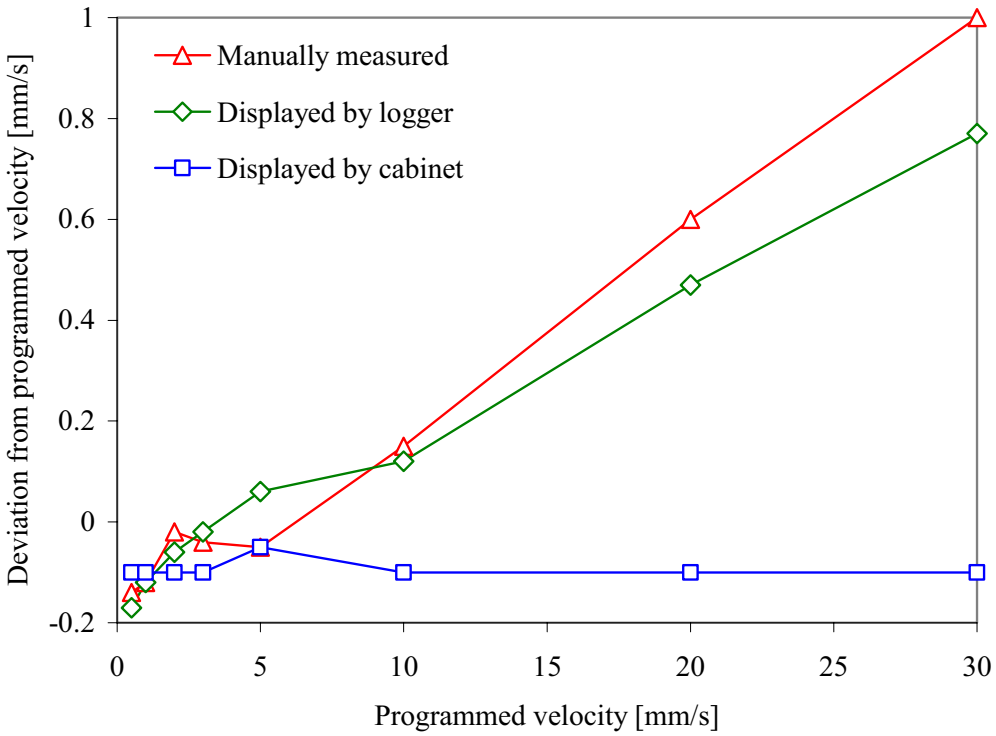

Figure 4.24. The calibration curve for the ram velocity. All values are compared with the requested value through the control system [Lef01].

The annual calibration of the extrusion press also includes a check of the position and the velocity indicated by the system. The position is accurately indicated by the display placed on the PLC cabinet (±0.1 mm). The error of the value provided by the PC logger of SINTEF may be somewhat larger (±0.5 mm). The ram velocity was measured manually by a length gauge and a clock. At the same time, the velocity indicated by the press system was continuously logged by the PC and displayed by the control cabinet. The most accurate measurement is the one performed manually. The PC logger seems to give a good indication (0.5 % deviation) of the actual velocity while the programmed or requested velocity and the displayed velocity may be as much as 3 % too low.

4.4.3 Results from pressure sensor calibration

This volume treats results from extrusion obtained on five days. Both the objectives of and the plan for the experiments were treated more thoroughly in Chapter 3. A new die outlet insert was used on each of the days apart from the second (Table 4.1). After a day of experiments the complex extrusion die was disassembled. The used die outlet insert was pushed out of the top disc before a new one was inserted. All the probes were removed from the sensor holes before the die inserts were dismantled. This made the dismantling operation simpler and safer. However, the probes were dismantled mainly because genuine replication of the experiments was desirable. In some cases changes were also made to the combinations of sensor hole and probe. This was done in order to better understand the sources of variability in measurement. If the method of calibration works satisfactorily, such sensor switches should not affect measurement results. In the following text the term "sensor hole" refers to a specific cavity in the top disc of the die. The term "sensor" refers to a combination of probe, extension cable, and amplifier of the Capacitec equipment. The nominal dimensions of all sensor holes were the same, and with the available measurement equipment, it was not at all easy to uncover any significant differences in actual sensor dimensions. The shape measurement accuracy was 0.01 mm for the diameters and 0.05 mm for the thickness of the sensor disc. The radiuses of the corners close to the sensor disc could not be accurately determined. It is possible that the measured deformations may have differed somewhat when the probes were used in different sensor holes (> 10 %). The issue has been treated in reference [Moe04c]. Table 4.2 displays the various calibrated combinations of sensor holes, probes, sensor cables and amplifiers.

Table 4.1. Die outlet inserts and sensor positions during all rounds of experiment.

Day	Die outlet insert	Sensor hole 1	Sensor hole 2	Sensor hole 3
A	ER = 40, zero bearing	Sensor 1	Sensor 2	Sensor 3
B	ER = 40, zero bearing	Sensor 1	Sensor 3	Sensor 2
C	ER = 80, zero bearing	Sensor 1	Sensor 3	Sensor 2
D	ER = 40, long bearing	Sensor 1	Sensor 3	Sensor 2
E	ER = 80, long bearing	Sensor 1	Sensor 3	Sensor 2

Table 4.2. Die outlet inserts and sensor positions during all rounds of experiment.

	Probe number	Extension cable number	Amplifier
Sensor 1	17761	3161	Channel 1
Sensor 2	18097	2582	Channel 2
Sensor 3	18098	2581	Channel 3

On-line calibration of die face pressure was performed immediately before and after extrusion experiments. The calibration sequence lasted approximately 20 to 30 minutes. The container and tool stack had been heated for approximately eight hours. In order to get access to the die face, the container was first lifted by hydraulic jacks. The steel plug was placed above the die outlet insert, and the test billet was placed on top of the die. The diameter of a new test billet was significantly smaller than the inner diameter of the container. The subsequent lowering of the container caused no difficulties. However, when the test billet was used repeatedly and plastically deformed, the outer diameter of the billet was only marginally smaller than the inner diameter of the container. The geometry of the billet was reduced by turning. New test billets were also manufactured.

The test billet and steel plug were first heated in the container to the same temperature as the die and container by heat conduction. It would have been possible to preheat the billet by the induction heating equipment of SINTEF Materials Technology. This makes mounting more difficult. As the volume of the test billet is very small, the heating time in the container is in any case very short (Equation (4.2)). The heat transfer coefficient of the aluminium-steel interface, h, is assumed to be 4000 W/m^{2}K. The density, ρ, and heat capacity, c, of aluminium is 2700 kg/m^3 and 880 J/kgK. The material data are only approximate, and the calculation only serves to give an indication of the magnitude and rate of heat transfer. The test billet diameter and length were 100 mm and 30 mm. After 10 seconds the temperature should be 390 ºC. Since neither heat conduction nor poor contact on the interface is considered, the actual heating time may have been somewhat longer. Also the steel plug was present, and the billets were sometimes longer than 30 mm. During the experiments, the test billet was heated for some minutes.

$$T = T_c + \left(T_0 - T_c\right) \cdot \exp\left(-\frac{2h}{\rho c}\left(\frac{2}{D} + \frac{1}{L}\right) t \right) = 430 + (30 - 430) \cdot \exp\left(-0.225 \cdot t\right) \qquad (4.2)$$

The above calculation does not consider the influence of the ram. After the billet had been inserted, the ram was moved downwards. It had first been pre-heated as much as possible in the container, but the ram temperature was probably not higher than 250 ºC. After the test billet had been heated to 430 ºC, the ram compressed the billet so that the billet deformed plastically and covered the complete surface of the die. At this point the temperature distribution was highly non-uniform since the ram cooled the billet, die and sensor. The complete system was allowed to reach something that resembled a steady state before calibration was performed. If experiments were run too early, the results were difficult to interpret. The temperature of the die face was continuously measured by thermocouples (Chapter 2). A change in the temperature affects the elastic properties of the sensor disc and may also cause deformations due to the thermal expansion. The heating of the different parts took much more time, since the ram was an effective heat sink. In the current study the warm up time of the described phase was usually some minutes. An example with results from calibration experiments performed after a too short heating phase is given below.

After the initial heating phase calibration experiments commenced. In order to establish a satisfactory calibration curve several cycles of loading and unloading were performed. Figure 4.25 shows the ram force and disc deflections of a typical loading cycle. It was neither the first nor the last in the series. The test billet had already expanded to fill the cross-section of the container. However, the shape of the test billet need not have been a perfect cylinder before the ram force was applied. The surface that should be in contact with the die face became slightly lens/disc-shaped probably when the ram was retracted after a calibration run (Figure 4.26). When contact between the ram and billet was made, the top surface of the die and the bottom surface of the test billet were probably not in contact at the entire interface. As a result there was initially a burp cycle, in which only a moderate ram force was applied. The billet material then deformed visco-plastically and filled the interior of the container. An intimate contact between the die and billet was established.

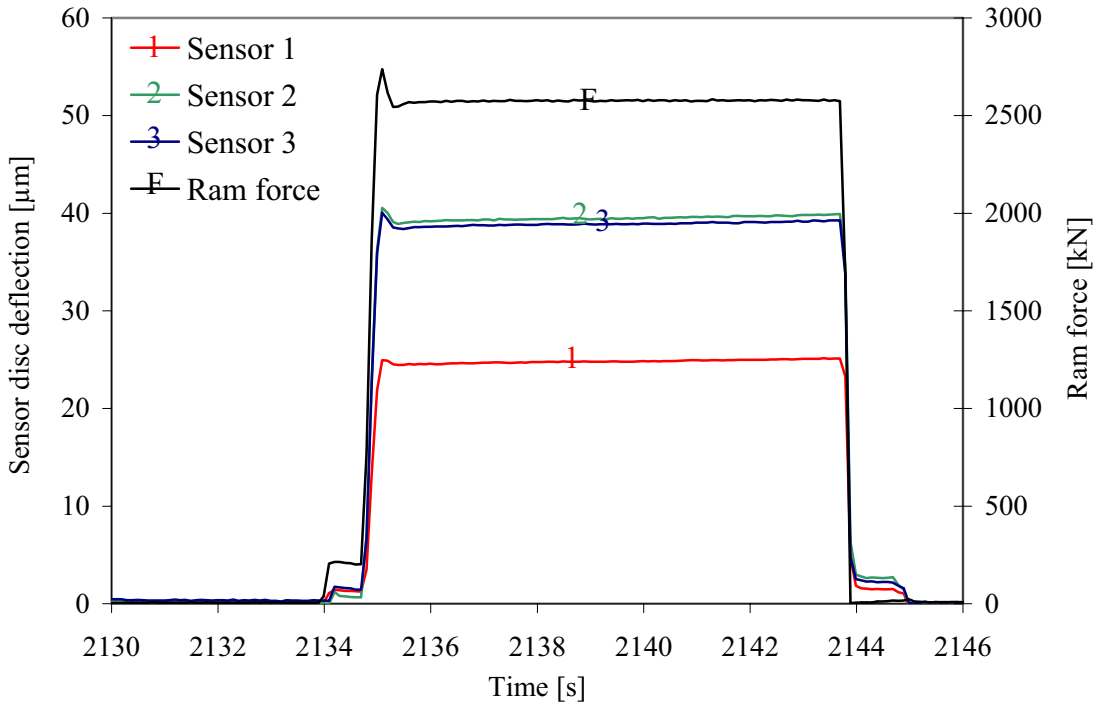

Figure 4.25. Load curves from calibration on day B recorded before extrusion started.

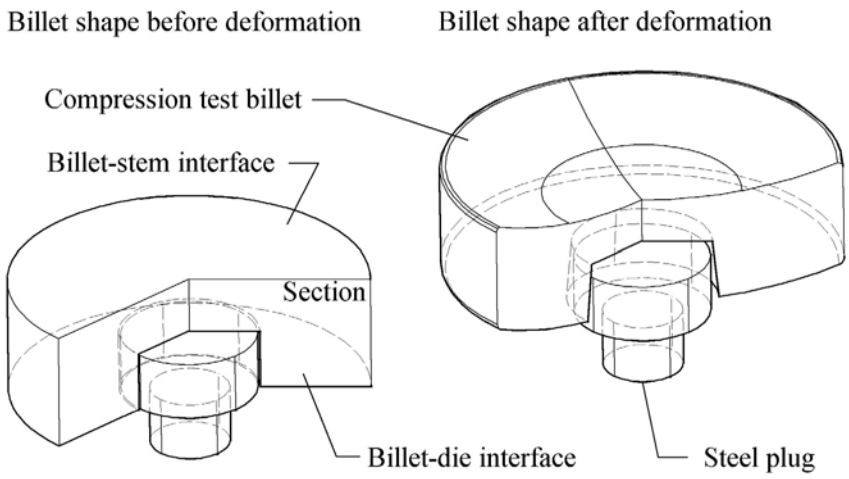

Figure 4.26. Typical shapes of the billet before and after compression testing.

When the burp cycle ended, the ram force increased to a pre-defined level since the motion of the ram was force controlled. Due to the slowness in the control system and the stiffness of the billet (no further plastic deformation could occur), it was difficult to avoid overshooting the pre-defined value of ram force. There were also limits to how accurately the force could be set. The force indicated to the control system may have been somewhat in error. At the same time, small ram displacements may have caused the force to change significantly. The force was kept at a high level for ten seconds or more until thermal transients disappeared. Figure 4.25 shows that the three capacitive

pressure sensors responded somewhat differently to the load. The mounting solution of sensor 1 differed from those of sensors 2 and 3 (Chapter 2), and the displacement measurement included less of the global compression of the top disc. The difference in the responses of sensor 2 and 3 were due to effects that may not be controlled or at least must be examined by the experimenter. In the current case, the difference was approx 1 µm or 2.5 %, which is quite small. A ram force of 2500 kN corresponds to a uniform die face pressure of 318 MPa, which here must be regarded as a relatively high pressure. A sensor disc deflection of almost 40 µm for sensors 2 and 3 is considerable, but the finite element analysis indicates that sensor deformations should be mainly elastic.

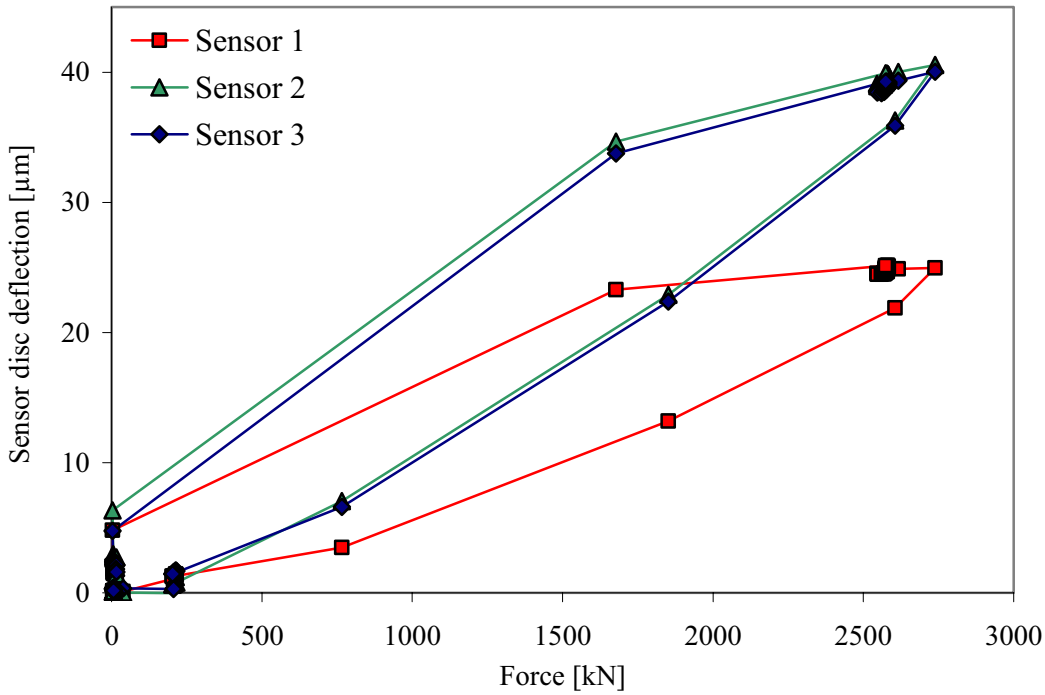

Figure 4.27. Load curves from calibration on day B recorded before extrusion started.

When the ram force was reduced to zero, the output signal of the pressure sensors still differed from that of the zero point. One should realise, however, that the ram was still in contact with the billet, and that the weight of the ram prevented the billet from deforming completely freely. Thus, the sensor discs were prevented from returning to the initial configuration. When the ram was completely retracted, the billet once more became lens-shaped, and the sensor discs to return to the initial zero point. Figure 4.27 shows the force-deflection curves that were logged during extrusion. The hysteresis may probably be attributed to lack of synchronism of measurements, slowness in the sensor systems and to the viscous material behaviour of the aluminium. Loading and unloading was performed very quickly (almost instantaneously). Measurement points are marked with symbols. The loading and unloading phases contain only four and two points respectively, while most of the sampling occurs at either the zero or high level of force. It is not believed that the hysteresis of the loading curves has a significant effect on measurement during extrusion, which occurs mainly at quasi-steady state.

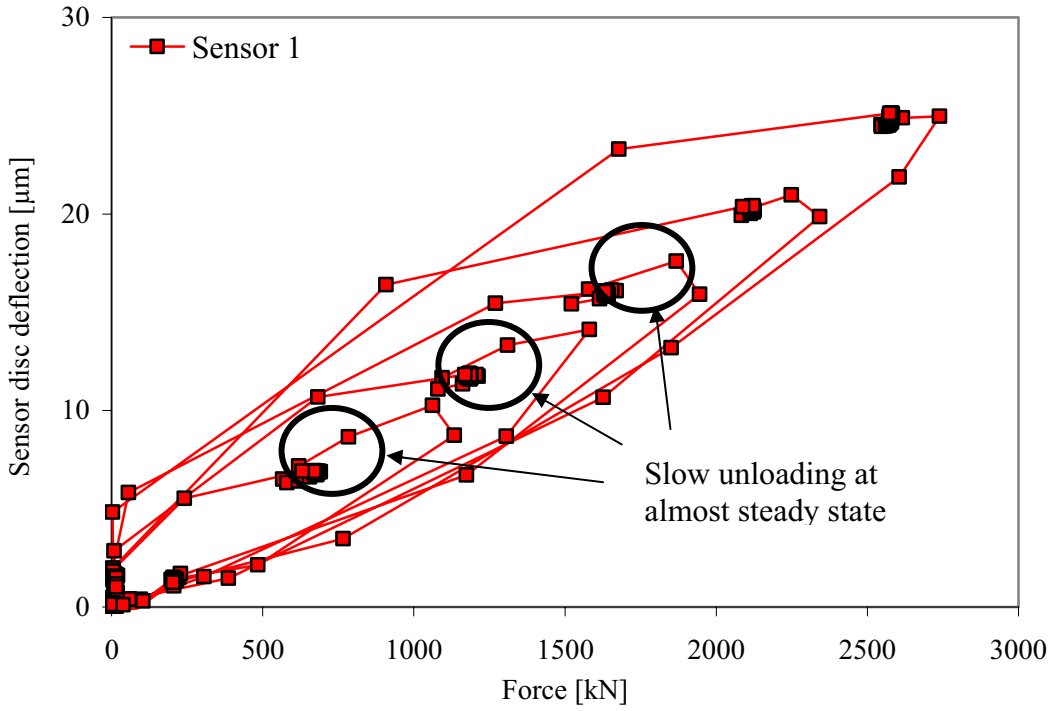

Figure 4.28. Load curves from calibration on day B recorded before extrusion started. The sensor disc deflection is the output voltage multiplied by 50 µm/V.

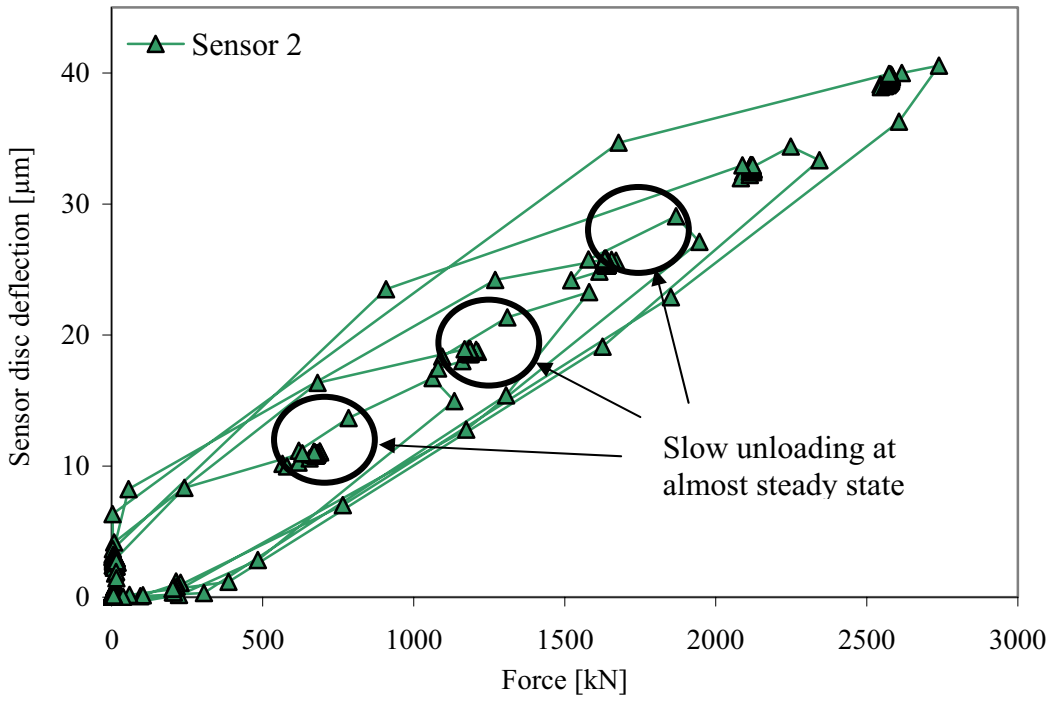

Figure 4.29. Load curves from calibration on day B recorded before extrusion started. The sensor disc deflection is the output voltage multiplied by 50 µm/V.

Figure 4.28 and Figure 4.29 show that even though there was a hysteresis for all loading and unloading curves, there was a close to linear relationship between ram force and die deflection at steady state. It is, as indicated, possible that the slowness of visco-plastic deformation may have caused some deviations from the desired linearity during hurried loading and unloading. When the sensor disc deflects, the material has to flow so that no cavity is formed between the work piece and the die. The issue is further treated in relation to the analysis of data from extrusion (Chapter 5). When studying the results of the current section, one should realise that the material has a finite response time. The deviation from linearity probably depends on the magnitude and velocity of the load change. A large change of the applied force may cause large deviatoric stresses and high strain rates. However, if the disc deflection is large, a relatively large amount of material must also flow. A very low level of deviatoric stress is needed to cause hot aluminium to flow, so very low-rate loading and unloading should leave no permanent deflection of the sensor disc. According to this assessment, a relatively slow change of the general load level during extrusion should most likely take place according to a linear curve established at steady state. Figure 4.28 and Figure 4.29 show results from a number of load and unloading cycles to various levels of pressure. The values that have been established at steady state lie on a line crossing either the x- or y-axis close to origo. The line may be regarded as a calibration curve. During the relatively slow unloading from the peak pressure to the steady state value, it should be possible to use the curve to determine pressures. There may be a small hysteresis determined by the rate of loading and the sensor design.

A typical calibration sequence consisted of several steps of loading and unloading, as shown in Figure 4.30. The values of ram force and the output voltage at steady state were recorded at each level of applied force, and calibration curves were plotted. Some further examples of loading curves and calibration curves are shown later in this section. The whole calibration procedure was usually repeated several times in order to check whether the calibration curves could be exactly reproduced. Although a significant amount of time was spent on calibration both after and before extrusion experiments, more research into the subject should be performed. Calibration should be run in a more systematic manner, and regular calibration checks should be performed in between extrusion experiments. This should reveal possible changes in the sensor response during extrusion and contribute to an increase of the accuracy of the measurements. Generally, larger efforts should be spent on determining accurately the scatter in results and the accuracy of the calibration method. From earlier experiments, it was known that even for nominally identical sensors responses could deviate as much as 10 to 20 %. An important objective of calibration testing was not only to establish calibration factors and improve measurement accuracy, but also to reduce the variability of genuinely replicated measurements. If experiments are performed with many sensors, a significant part of variability in results is related to differences in sensor shape, mounting, material properties, etc. An important reason for performing calibration is to compensate for such differences. Therefore, the calibration is also related to the sensor property denoted repeatability. Ideally, calibration experiments should contribute to an improvement of the repeatability of genuinely replicated measurements. If the calibration is very poorly performed, however, the use of the calibration factors may be counterproductive.

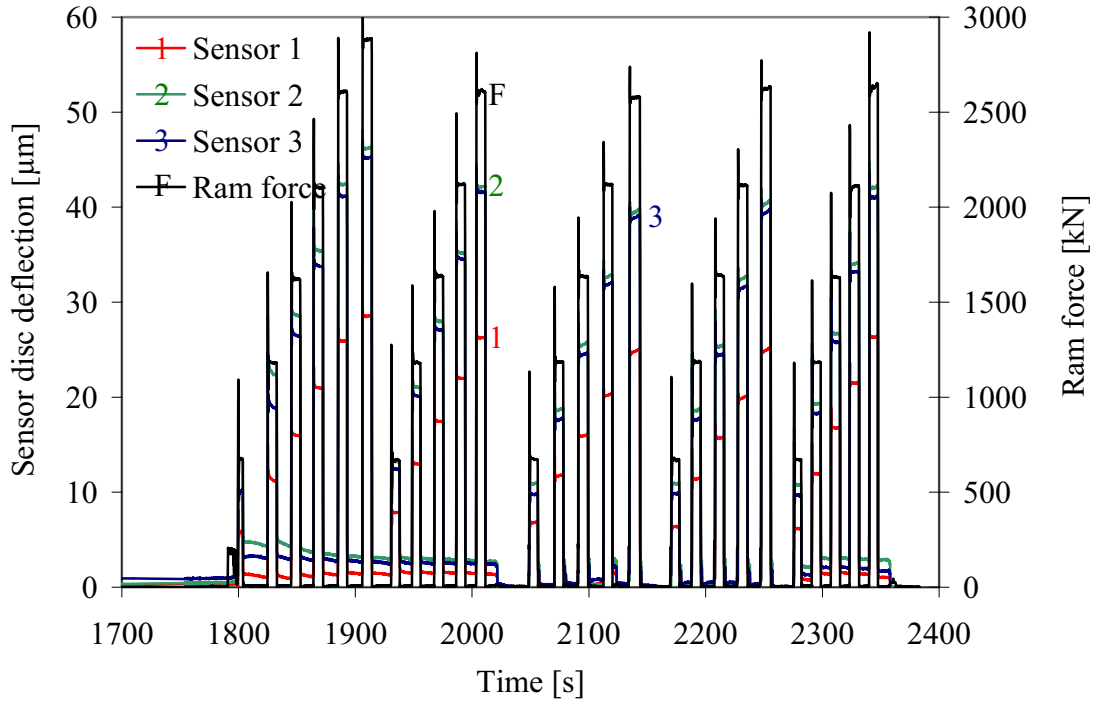

Figure 4.30. Load curves from calibration on day B recorded before extrusion started. The sensor disc deflection is the output voltage multiplied by 50 µm/V.

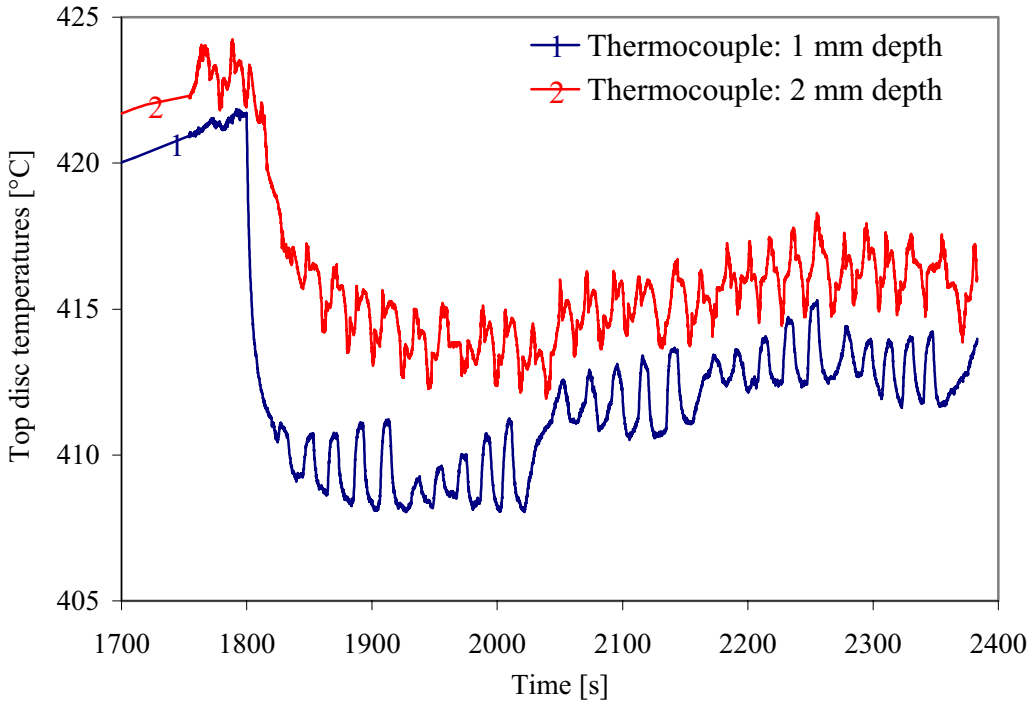

Figure 4.31. Top disc temperature curves from calibration on day B recorded before extrusion started. Both thermocouples were position 31 from the centre.

Even though the current set of experiments neither revealed the full potential nor the limitations of the calibration technique, some important observations were made. The accuracy cannot be better than that of the ram force measurement, in this case approx ± 2 %. There are, however, also some additional aspects to consider:

Plastic deformation

During calibration to extremely high pressures, sensors may deform plastically. Plastic or permanent deformations cannot be accepted during measurement. The response of the sensor is no longer linear and is determined by the plastic properties of the material, which may be more difficult to determine than the elastic ones. Furthermore, loading curves differ from unloading curves, and there may not be a one-to-one relationship between the pressure that is applied at the die face and the deflection of the sensor disc. The distance between the sensor disc and the probe may be shorter after unloading than before the loads were applied. Sensors should of course be designed so that the effects of plastic deformation are as small as possible. The die face pressure during extrusion may be in the range from 200 to 500 MPa or approximately 25 to 60 % of the yield stress. This makes it very hard to avoid plastic deformations close to the sensor cavities. The following should be noted. After plastic loading and elastic unloading, there should be a state of residual stresses in the material. If the material hardens according to the kinematic rule, the elastic range should also be extended after an overload. When the die face pressure is brought to the same level in the second load cycle, the response should only be elastic (see figure in [Moe04d]). Therefore, the recording of calibration curves should usually be performed after a round of moderate overloading. Figure 4.30 shows an example where the overload was approximately 300 kN higher than the load applied during calibration. It should be noted that the material volume deforming plastically and plastic deformations are usually small. However, at very high temperatures the material behaviour is viscoplastic and creep may be difficult to avoid. At the same time residual stresses may be relaxed, and the elastic range may be reduced. An increase in the temperature during extrusion causes a reduction of the yield stress and more plastic deformation to occur. If the unloading causes plastic deformation, load-displacement hysteresis is unavoidable. The safest solution is obviously to design the sensors so that plastic loading is more or less completely avoided.

Temperature effects

The temperature of the sensor discs and their surroundings should be monitored during calibration. It is known that the billet and top disc temperatures change significantly during extrusion. However, the calibration should be performed when the temperature field is steady state. Temperature changes may affect results in several ways. First, the elastic modulus is temperature dependent (Table 2.2). The sensor disc deflection is approx 10 % larger at 500 than at 400 ºC [UddW]. Second, when the sensor material expands thermally, the distance between the sensor disc and the probe increases. A temperature related transient sensor disc bending effect, which is further studied in the analysis, may play some part. Third, the response of the capacitive sensor is affected by temperature changes. The response during the first loading cycles of Figure 4.30 was affected by the die face temperature change shown in Figure 4.31. The initial sudden decrease in temperature occurred as the cold ram came into contact with the calibration

test billet. During the first two calibration rounds the ram was not completely retracted. As a result the pressure sensor disc was somewhat deformed after the unloading. When the sensor disc was cooled, the distance between the sensor disc and the capacitive probe gradually became smaller. After some two to three minutes of experiments a quasi-steady state was established and the zero point was fixed. Due to the cooling effect of the ram, the calibration runs in Figure 4.30 were carried out at a temperature that was 15 ºC lower than at the onset of extrusion. The calibration factor should therefore be modified accordingly (1 %). The small temperature oscillations occurring during calibration are not believed to have affected the calibration results significantly.

Container friction

The importance of container friction should be assessed. During the calibration runs it is desirable that the container friction is as small as possible so that the force applied at the upper face of the billet is completely transferred onto the face of the top disc of the die. Unfortunately, the liner force was not systematically measured during the calibration runs due to the crosstalk problems treated in previous sections. However, calibration was performed with billets of a range of heights (30 to 60 mm). Figure 4.32 reveals no systematic differences that could have been caused by container liner friction. The assumption that the friction plays no significant role during calibration is therefore probably correct. During extrusion, on the other hand, a large part of the ram force is guided through the liner. This should not invalidate the use of the calibration curves.

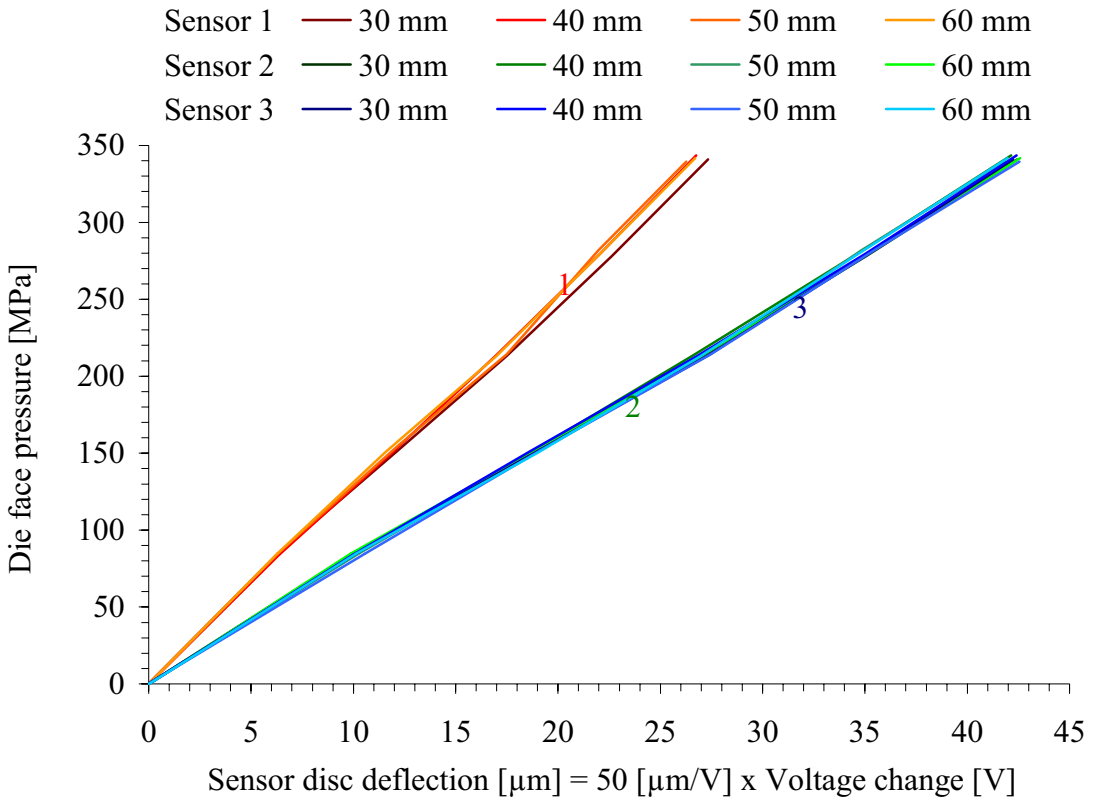

Figure 4.32. Calibration curves for experiments with billets of different lengths. The experiments belonged to round / day C of the extrusion experiments.

The calibration technique actually makes it possible to perform measurements of the die face pressure that are unaffected by assumptions about friction. Special attention has to be paid to the friction between the ram and the container walls during extrusion. Also this effect should be very small during calibration. No significant back extrusion was observed although there was a clearance of some tenths of a millimetre between the ram and the container wall. During extrusion the friction between the dummy block and the container wall may be more important. If it is assumed that the shear stress, τ_g, is 20 MPa, and the length of the contact surface, L_g, is 10 mm then the total friction force is:

$$F_g = \pi D_c L_g \tau_g = \pi \cdot 100 \text{ mm} \cdot 10 \text{ mm} \cdot 20 \text{ MPa} = 63 \text{ kN} \qquad (4.3)$$

D_c is the diameter of the container. 63 kN is less than 3 % of the total ram force. When the ram is running downwards along the wall of the container, before it comes into contact with the billet, a somewhat larger force, 200 to 300 kN, may be measured. This force may at least partly be due to ram-liner interaction. However, work is probably also performed as the aluminium is sheared off the container wall. The material is deposited on the back face of the billet. The thickness and constitution of the aluminium layer at the container walls may vary from one run to another. The shearing effect is probably not of importance during extrusion, but the friction effect may cause a somewhat higher ram force. The problem with this effect is that it is seldom included in models of flow and estimates of ram force. The back-extrusion effect is often neglected as it is believed that it has only a small effect on the required ram force. During calibration none of the described effects are believed to be of importance. However, a small error may be committed when it is assumed that the dummy block diameter is equal to the inner container diameter. It is usually somewhat smaller. As a result the sensor disc deflection – pressure calibration factors is somewhat to low. The effect is small (< 0.5 %).

Sensor design

The apparent inaccuracy in measurement may be just as much due to poor sensor design as to the limitations of the calibration technique. The possibility that there may be permanent displacements due to improper contact between the probe, probe holder and die has already been discussed. During most of the runs permanent displacements were not observed. There were very few instances of the distinct discontinuities in the output signal that may occur when the die is heavily shaken. Shaking is undesirable since it in the severest case may cause the probe to loose contact with the die. At the same time even a moderate displacement may, as has been discussed, alter the probe characteristic. However, the discontinuous response may to some extent be corrected for. In the set of experiments treated in this report the probe holder and die connection loosened only on one occasion, and the cause was probably hurried and improper mounting in the first place. Still the mounting solution is a cause of variability and should be improved.

Figure 4.33 to Figure 4.45 show some examples of loading-unloading curves for all sensors. For rounds 4 and 5 the curves from calibration performed after extrusion are also shown (Figure 4.38 and Figure 4.40). The curves show that Sensor 2 did not work properly at the end of round 5. The same observation was made during the extrusion experiments. The extrusion results shown in the next sections give a similar indication.

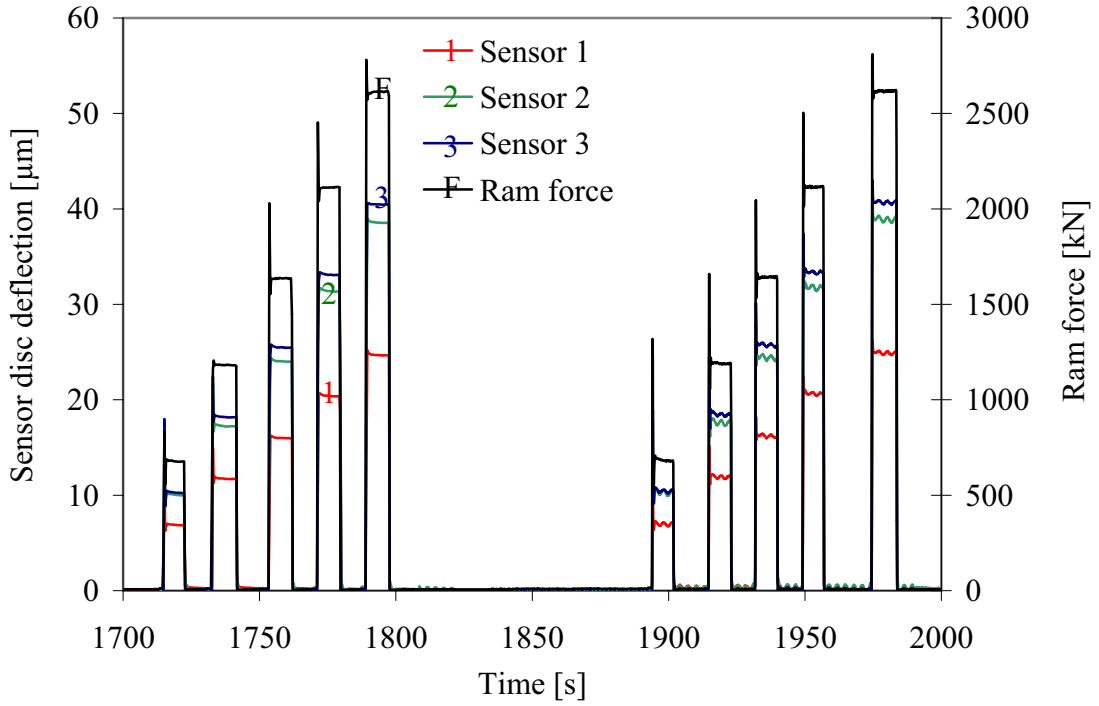

Figure 4.33. Load curves from calibration on day A recorded before extrusion started. The sensor disc deflection is the output voltage multiplied by 50 µm/V.

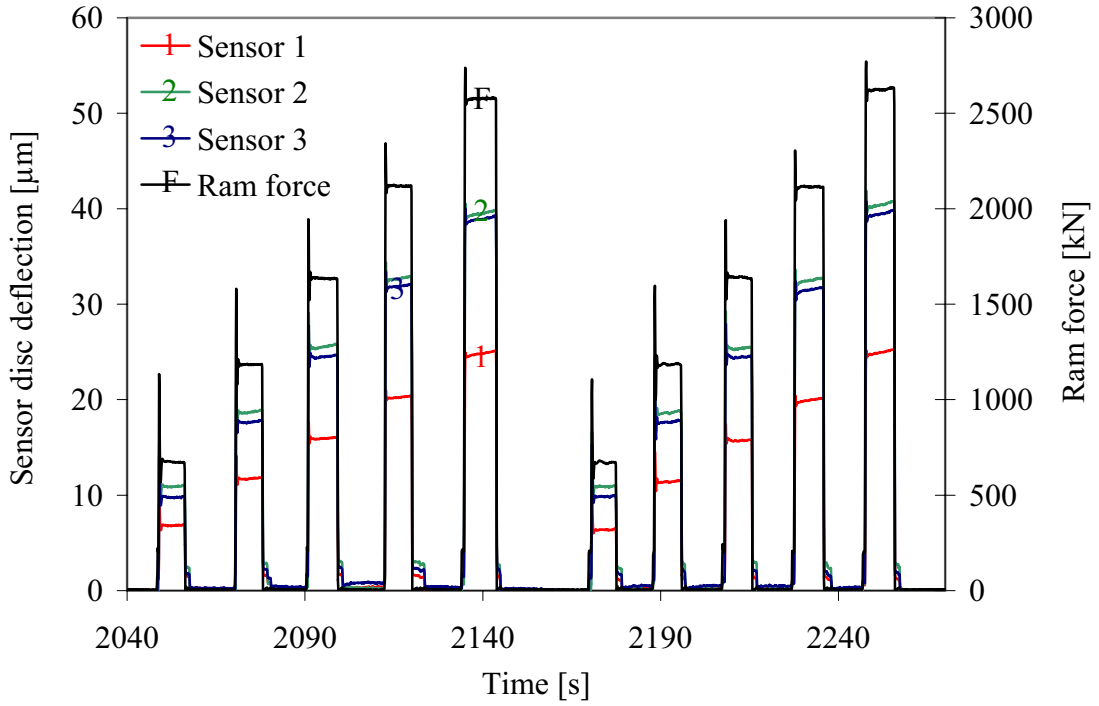

Figure 4.34. Load curves from calibration on day B recorded before extrusion started. The sensor disc deflection is the output voltage multiplied by 50 µm/V.

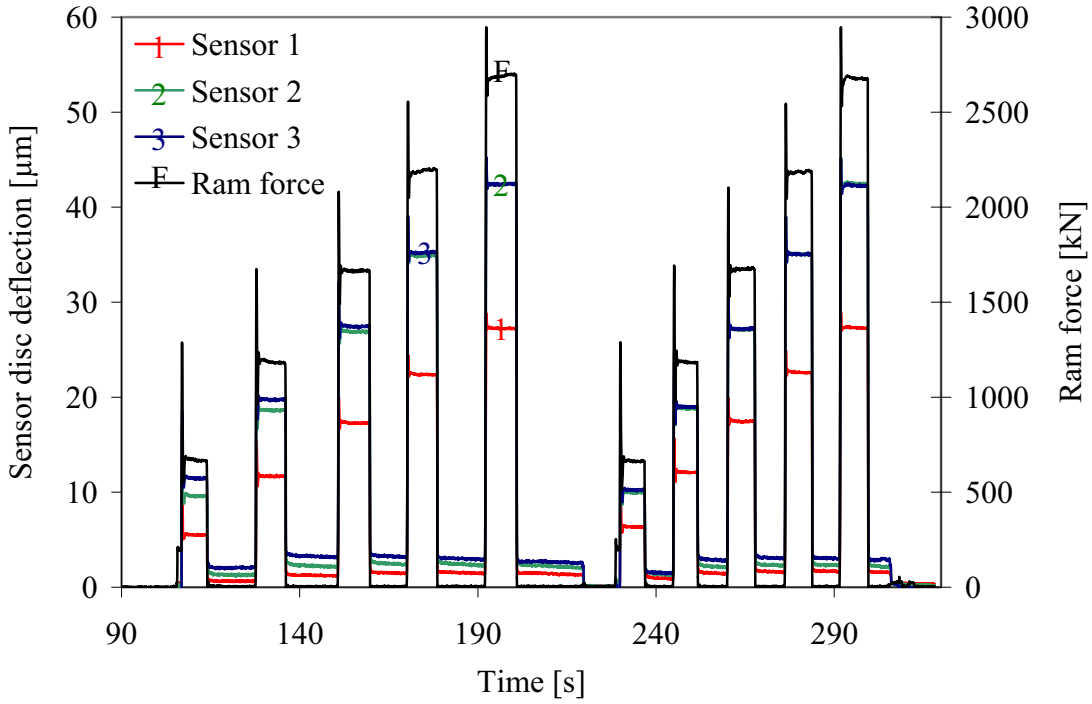

Figure 4.35. Load curves from calibration on day C recorded before extrusion started. The sensor disc deflection is the output voltage multiplied by 50 µm/V.

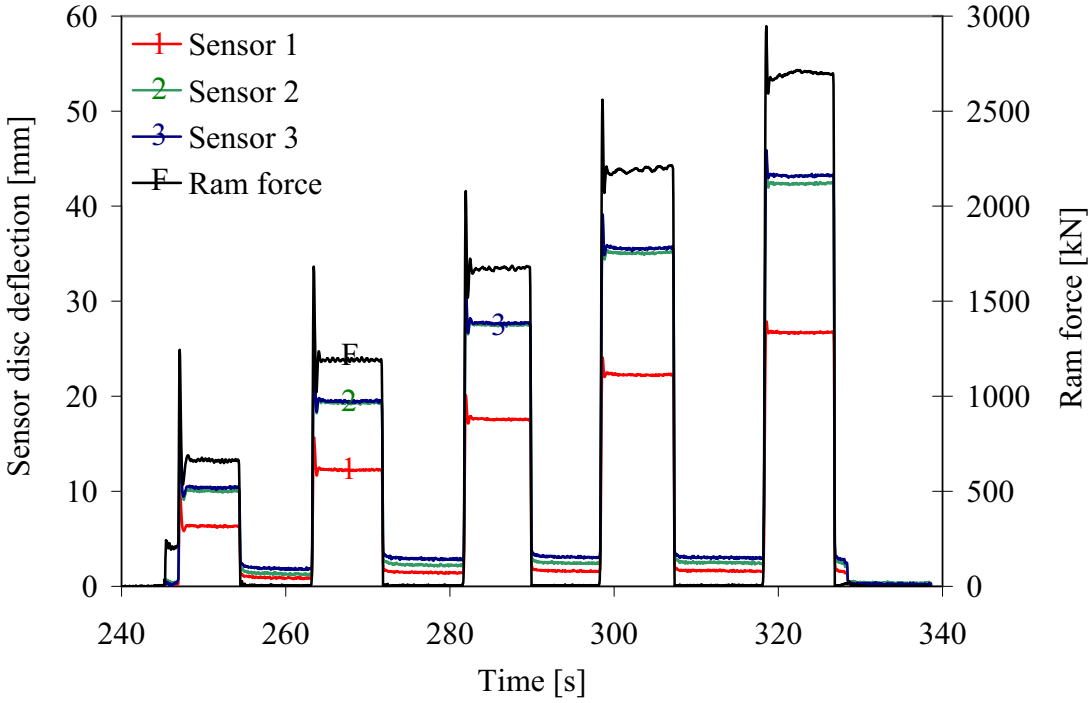

Figure 4.36. Load curves from calibration on day C recorded after extrusion ended. The sensor disc deflection is the output voltage multiplied by 50 µm/V.

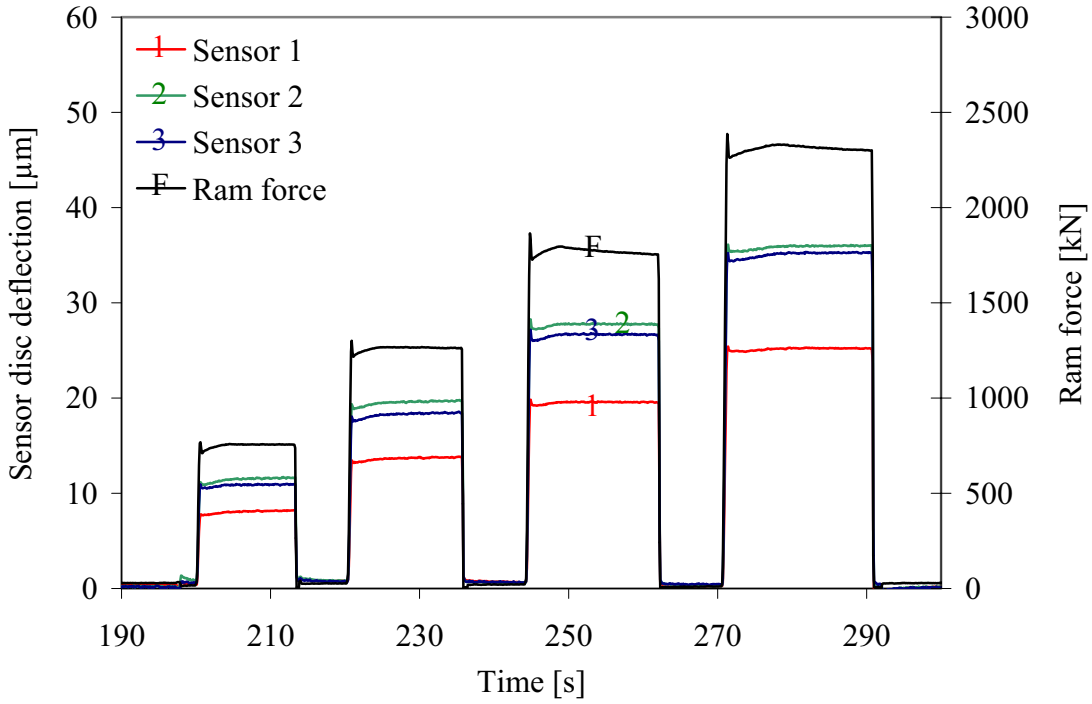

Figure 4.37. Load curves from calibration on day D recorded before extrusion started. The sensor disc deflection is the output voltage multiplied by 50 µm/V.

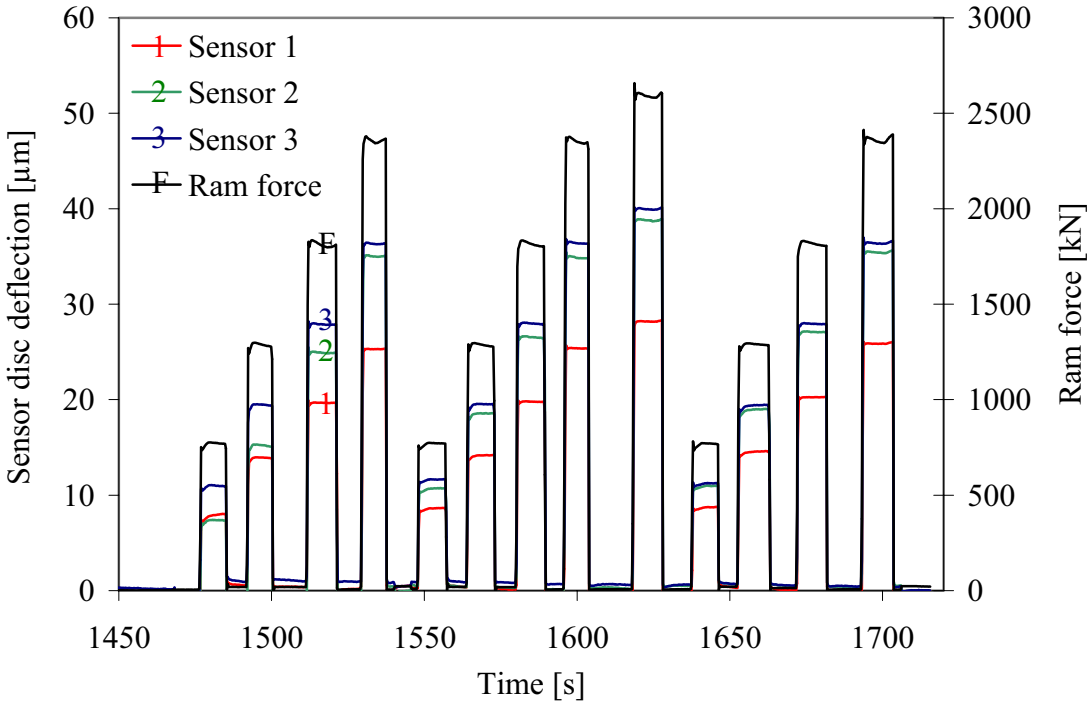

Figure 4.38. Load curves from calibration on day D recorded after extrusion ended. The sensor disc deflection is the output voltage multiplied by 50 µm/V.

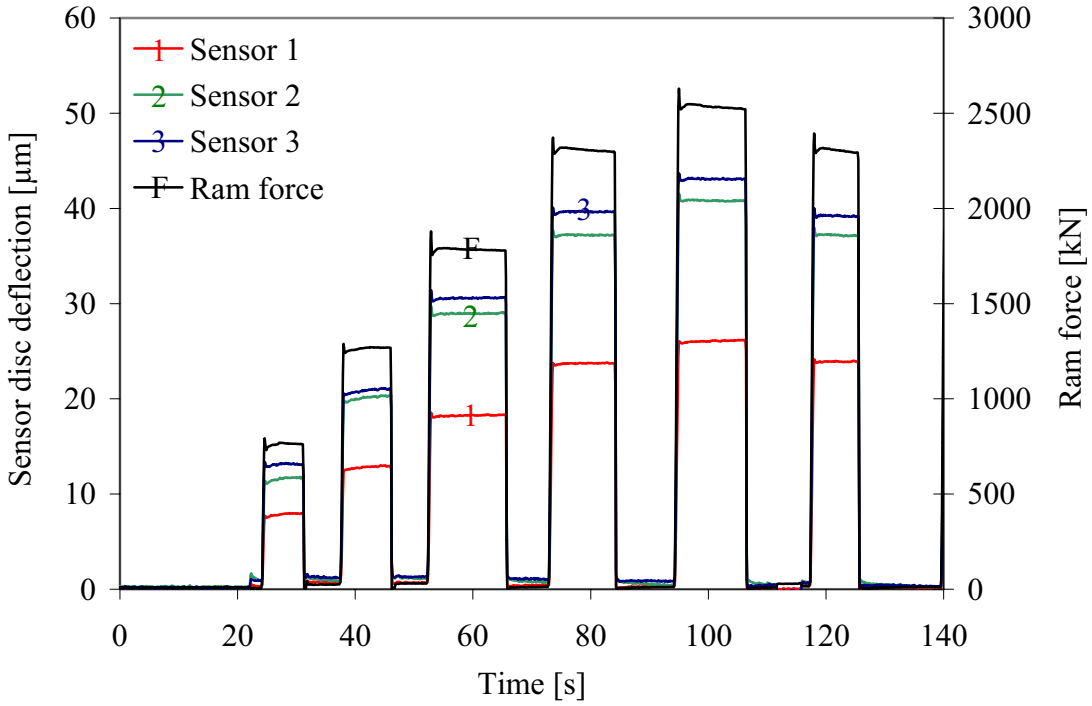

Figure 4.39. Load curves from calibration on day E recorded before extrusion started. The sensor disc deflection is the output voltage multiplied by 50 µm/V.

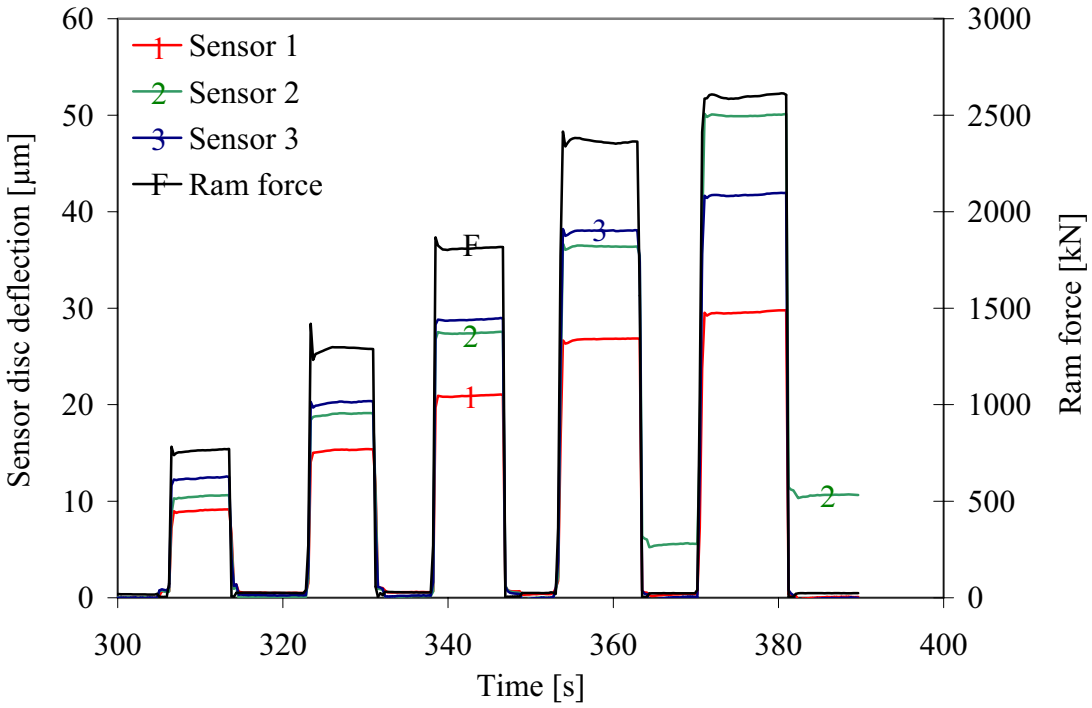

Figure 4.40. Load curves from calibration on day E recorded before extrusion ended. The sensor disc deflection is the output voltage multiplied by 50 µm/V.

Figure 4.33 to Figure 4.40 are quite characteristic for the calibration measurements. At very low pressures neither the ram force nor the pressure sensor measurements were very accurate. After unloading the measurement signals usually returned to zero output, but there was significant scatter in the results. In some cases the sensor disc deflection appeared to be as large as ± 0.3 μm after unloading. It could not be easily determined whether such deviations were due to permanent displacements or due to more random effects. While the output in some cases did not indicate a zero relative displacement after the first unloading, it could still do so after the second. Permanent displacements of 0.2 μm could also occur even though the probes were properly fastened. No extensive detailed study has been performed to reveal the drift of the zero point for displacement over time, but Chapter 6 gives an indication. The difference between the output signal before heating and after cooling was in some cases larger than 0.5 V, which corresponds to a displacement of 25 μm. Most of the change probably occurs during heating, cooling and the first round of calibration. In addition, oxidation of the sensor disc may also play some part. Probes may, however, also move if the top disc of the die moves (Chapter 2).

A careful study of the various responses of Figure 4.33 to Figure 4.40 at high levels of pressure revealed that there are limits to the accuracy of measurement. Calibration curves from a number of runs and all days are presented in Figure 4.41 to Figure 4.45. On each day of experiment several sequences of loading and unloading like the one shown in Figure 4.30 were performed. Usually the results from the last series of runs were chosen for plotting. All the data were collected after a steady state temperature distribution had been reached. An important initial observation is that the curves are very close to linear. A second observation is that most of the curves are very close to parallel although they may be offset somewhat in the vertical direction. The results for sensor 1 on day 4 and 5 give an example. An offset is usually due to a poor choice of reference point for the measurement of displacement. It may also be due to inaccuracy in force measurement. It is to a certain extent possible to correct for the offset.

There is a significant amount of scatter in the calibration factors estimated on the basis of data presented in Figure 4.41 to Figure 4.45. There is probably insufficient data for a completely satisfactory statistical analysis. The issue is further treated in relation to the use of the data in the study of extrusion (Chapter 6). However, the calibration figures give a good indication of the scatter in the measurement results for the described sensor design and calibration method. Figure 4.41 indicates that the calibration factor of sensor 2 was larger than that of sensor 3 in round 1. Figure 4.42 indicates that the situation was the other way around in round 2. However, in the last case the two distributions of slopes overlap, and it is not known whether the difference was truly significant. A study of all the available data indicated that the sample standard deviation of the slope of the calibration curves was close to 0.2 to 0.3 MPa/μm. As will be further discussed, this obviously affects the accuracy of single measurements. If the die face pressure is 200 MPa (which causes a deflection of typically 20 μm), the measured pressure may deviate as much as 10 to 15 MPa from the actual one. The trend lines that have been added to the figures indicate the best choice of calibration curve. Admittedly, the choices are to a certain extent subjective, but they are based on a thorough study of all experimental results. Table 4.3 presents calibration factors for all days and sensors. The use of two decimal places may be characterised as artificial and optimistic.

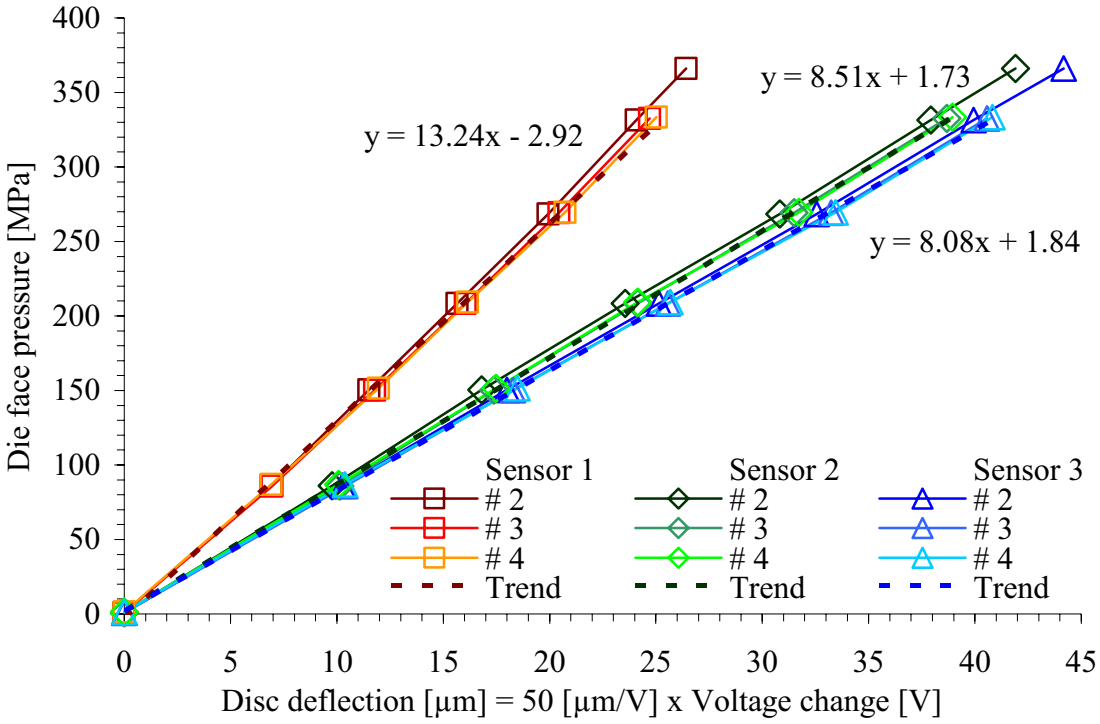

Figure 4.41. Calibration curves - round / day A of extrusion.

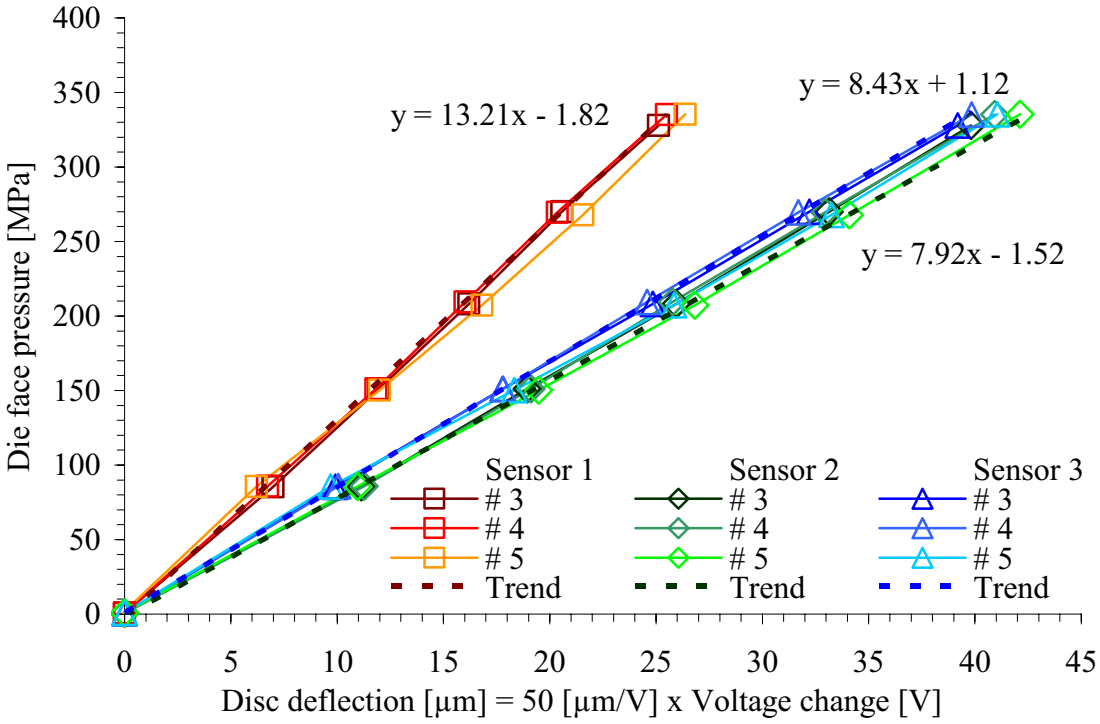

Figure 4.42. Calibration curves - round / day B of extrusion.

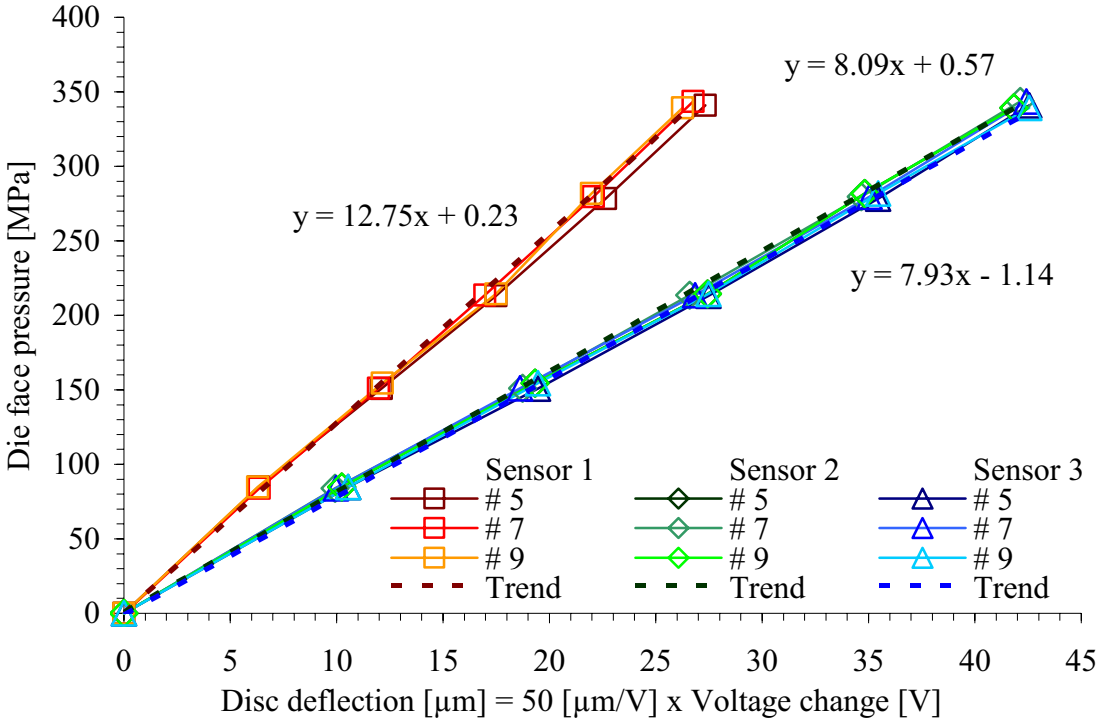

Figure 4.43. Calibration curves - round / day C of extrusion.

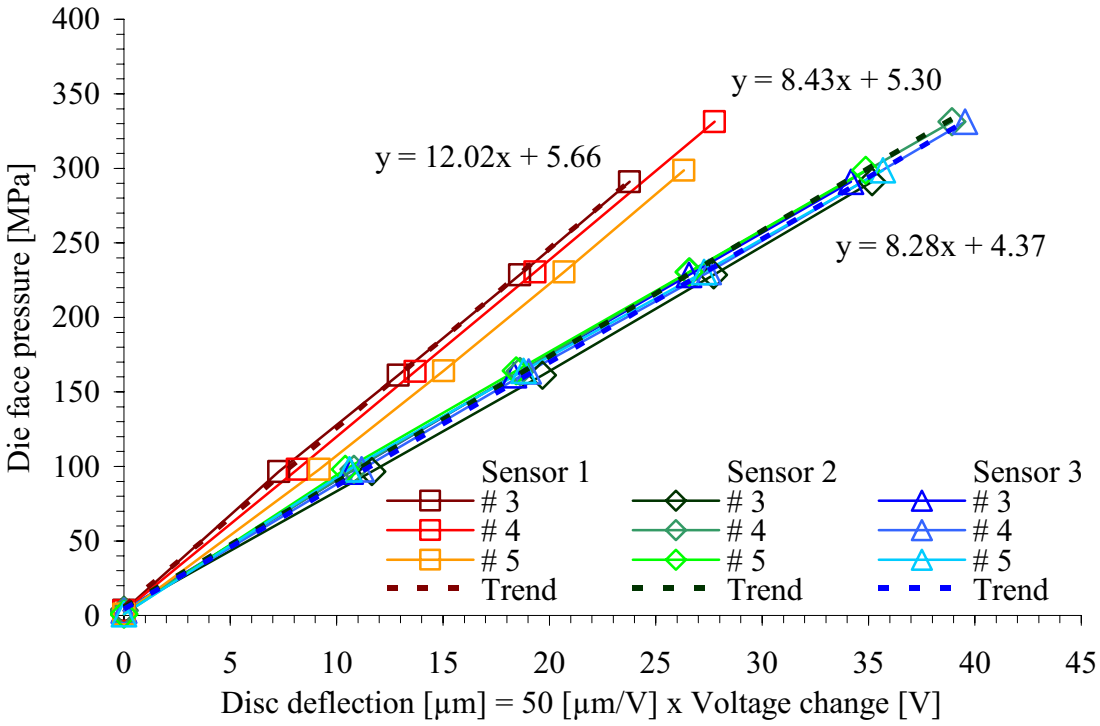

Figure 4.44. Calibration curves - round / day D of extrusion.

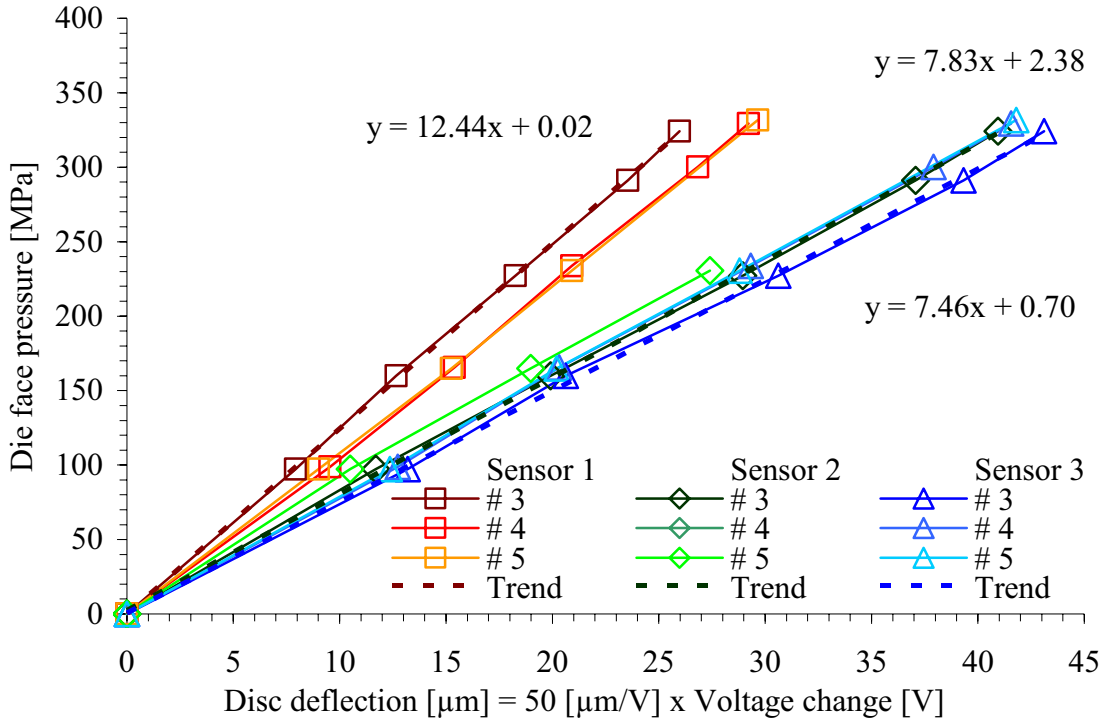

Figure 4.45. Calibration curves - round / day E of extrusion.

Table 4.3. The experimentally determined calibration factors [MPa/µm].

Round #	Date	Outlet geometry	Sensor 1	Sensor 2	Sensor 3
A	2002.01.10	Zero, ER = 40	13.24	8.51	8.08
B	2002.01.12	Zero, ER = 40	13.21	7.92	8.43
C	2002.01.15	Zero, ER = 80	12.75	8.09	7.93
D	2002.07.10	Long, ER = 40	12.02	8.43	8.28
E	2002.07.12	Long, ER = 80	12.44	7.83	7.46

4.4.4 Calibration factors established by the finite element method

If physical calibration is not performed, calibration factors must be calculated. The limitations of such an approach have been discussed above. The principles of finite element calculation by ANSYS® 7.1 have also been presented. A detailed analysis of various aspects of calibration has been performed in [Moe04c]. The full geometry of the 8 MN extrusion press of SINTEF Materials Technology has been studied (Figure 4.46 and Figure 4.47). A refined mesh that combines accuracy and short calculation times has been used. The material data of the H13 steel presented earlier have been adopted. The actual distribution of the temperature in the tool stack was calculated. It was assumed that the container and bolster were heated to 430 and 480 ºC respectively. The load at the die face was assumed to be uniform during calibration.

An important issue in relation to the use of the results from calibration is whether the calibration factors obtained during loading with a uniform pressure may be used for the extrusion case. It is known that during extrusion there may be a fairly steep gradient in the die face pressure in the radial direction [Tve97]. At the same time the deflection of

the sensor disc may be somewhat different for uniform and skew load distributions. The analysis in [Moe04c] indicates, however, that for the relevant cases of extrusion such differences are only marginal. Die face shear loading should also be considered in relation to the study of sensor behaviour. Shear loads may cause a small tilt (less than 1 µm) and straining of the sensor disc. However, the die face shear stresses are very small (15 – 30 MPa) compared to the die face pressure (200 – 300 MPa). Furthermore, the sensor disc is thick and not very flexible. Shear loading of a more flexible pin design has been treated in Volume I. The global deformation of the die due to a large liner load could have affected the response of integrated die face pressure sensors. However, the finite element analysis shows that the sensor disc behaviour only to a very limited extent is affected by the general deformation of the die.

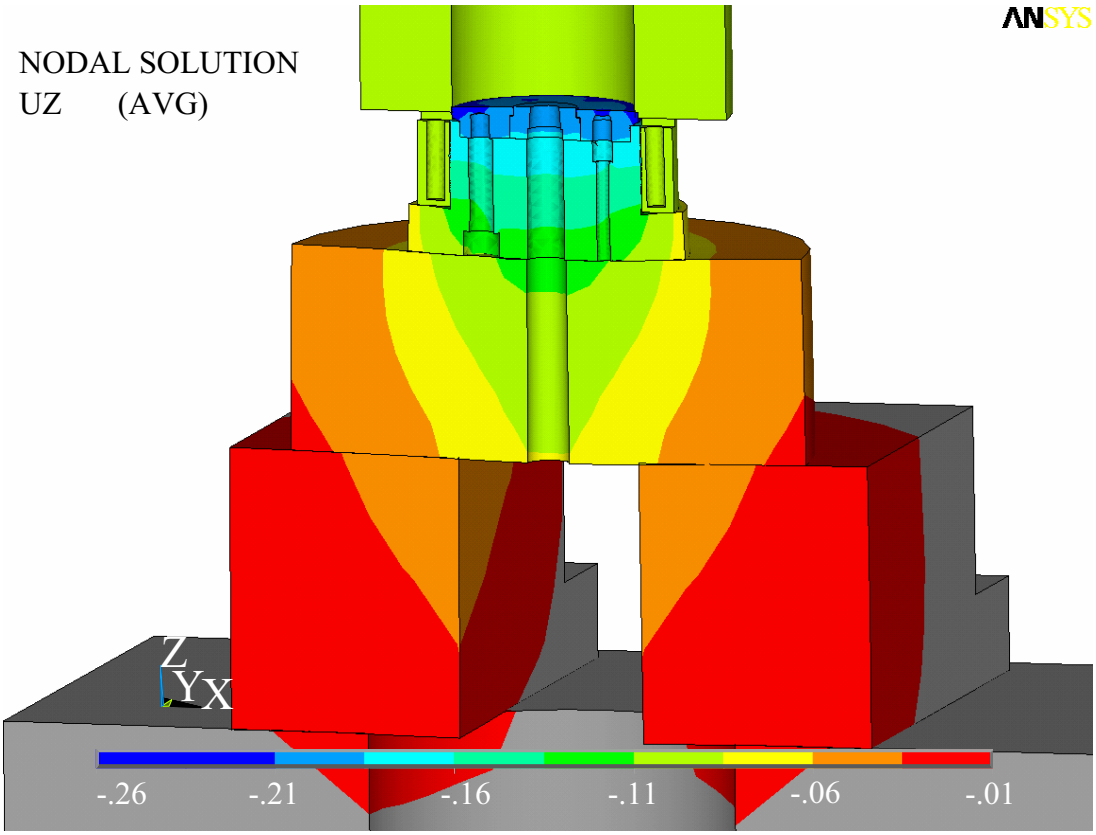

Figure 4.46. The die deflection calculated by a finite element model. The die deflection is the component of deformation of the die in the extrusion direction (Z). All presented values in the figure are in [mm].

The finite element model predicts a calibration factor of 11.8 MPa/µm for sensor 1 and 7.6 MPa/µm for Sensors 2 and 3. The responses of sensors 2 and 3 should not differ, since the sensors were made with the same nominal dimensions. The experimentally determined calibration factors of Table 4.3 are as much as 10 to 15 % larger than the factors calculated by the finite element method. It may first appear as the actual sensor disc deflection for a given pressure is smaller than the calculated one. The deviation is of a magnitude that may not easily be explained by the random errors in measurement.

The deviation is due to the somewhat different definitions of sensor disc deflection. It has been shown that there is an almost linear relationship between the gap distance and the output voltage. This is true also if the sensor disc bends rather than translates, but the calibration factor may be different. The value of the calibration factor depends on the definition of deflection or change of capacitor gap distance. The derivation of the experimental pressure-displacement calibration factors of Table 4.3 and Figure 4.41 to Figure 4.45 is based on the assumption that the displacement-voltage calibration factor is exactly 50 μm/V. If the gap distance is rather defined as the minimum air gap distance between the deflecting sensor disc and the probe, this is probably a too small value. A translation of a disc of 50 μm may cause the voltage to change by 1 V, but in order for a bending deflection to cause a change of 1 V, the change of the minimum gap distance must be larger. Thus, if the displacement-voltage factor is assumed to be 50 μm/V, the pressure-displacement calibration factor should be larger than the ones calculated by FEM. Equation (4.4) shows the alternative choices of calibration factors. The data have been taken from the first round of experiments with sensor 1. $K_{p/V}$, $K_{p/d}$ and $K_{d/V}$ are the calibration factors linking pressure and voltage, pressure and deflection and deflection and voltage. A difference in displacement-voltage calibration factors of 10 % may be easily explained by differences in capacitance changes of the translating and bending discs and the somewhat different definitions of capacitor gap (Figure 4.15). In the current study the die face pressure has been related to a measure of deflection in order to make the measured values easier to relate to. However, calibration experiments are essentially intended to relate the output voltage changes to the die face pressure. Nevertheless, it may be regarded as acceptable to use a factor 50 μm/V to calculate some kind of a characteristic value for the sensor disc deformation.

$$K_{p/V} = K_{p/d}K_{d/V} = 13.24\frac{MPa}{\mu m}\cdot 50\frac{\mu m}{V} = 11.8\frac{MPa}{\mu m}\cdot 56.1\frac{\mu m}{V} = 662\frac{MPa}{V} \qquad (4.4)$$

The response of the die face pressure sensor to the changes in temperature that may occur during extrusion is an important issue that also has been treated in reference [Moe04c], and that will be discussed further in relation to the analysis of extrusion results. All calibration experiments have been carried out at approximately 415 to 420 ºC, which is 10 to 15 ºC lower than the initial temperature during extrusion. It would have been useful also to know the response of the sensor at even higher temperatures, for the die and sensors are significantly heated during extrusion. The complete tool set-up should then have been heated in order to establish a steady state before calibration was performed. Figure 4.30 and Figure 4.31 clearly demonstrate this point. Testing at a range of temperatures may be extremely time-consuming, as the entire extrusion set-up has to be heated or cooled between the calibration runs. However, even though it almost always is desirable to perform tests at steady state, one may not be certain that such tests are actually representative. The temperature distribution is as indicated transient and non-uniform during extrusion. Furthermore, the sensor responses may be affected by effects not only related to changes in the material data, but also to the mechanics of the thermal expansion of the sensor. Physical reconstruction of such phenomena is hard to perform accurately. An example of a simple physical test has been provided in reference [Moe03b]. The finite element technique may be a very useful tool, since may be easily used to perform sensitivity studies.

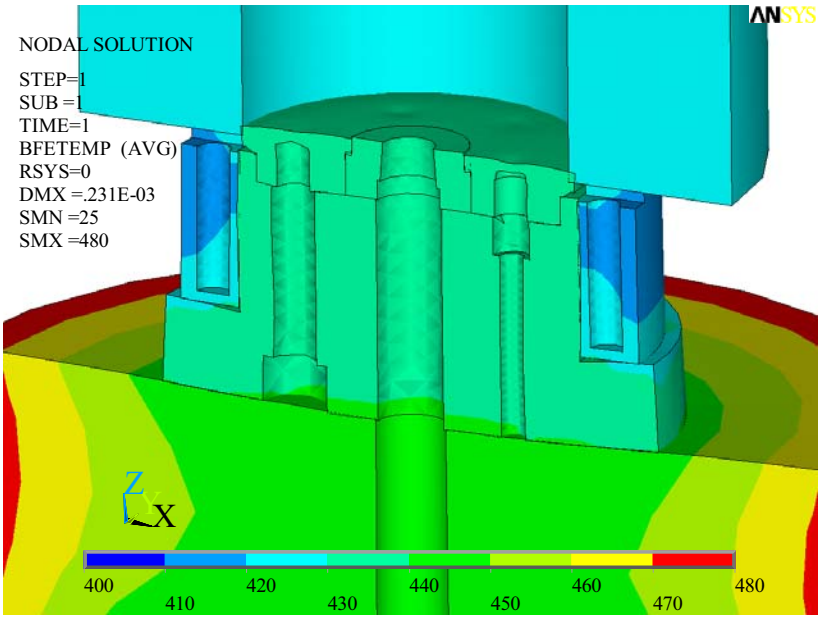

Figure 4.47. The temperature distribution of the extrusion set-up during calibration. It is assumed that the die face temperature is 430 ºC.

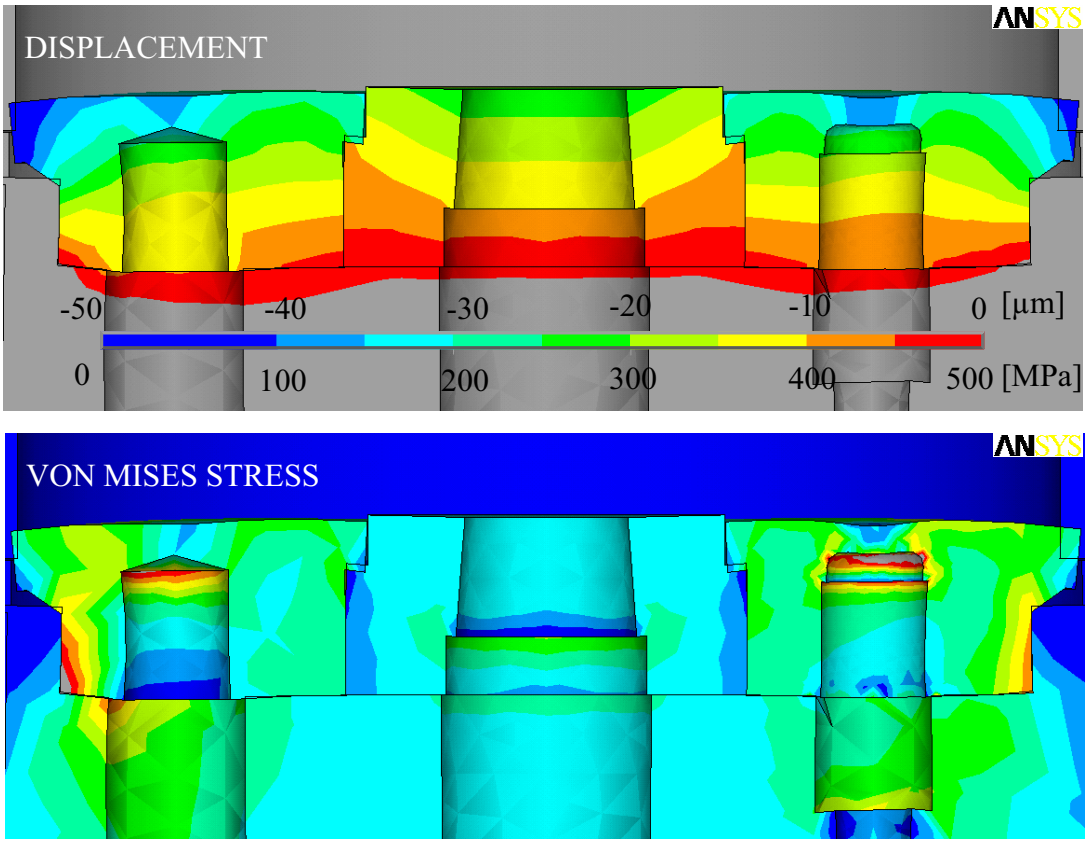

Figure 4.48. The axial component of the displacements and the von Mises stress of the top disc during calibration. The die face pressure is 200 MPa.

4.5 On-line calibration of the liner load cell

The liner load cell was introduced in order to render possible the measurement of the part of the ram force that is transferred through the container liner to the flanges of the die. The liner force is mainly due to the interface friction between the billet and the container, so experimentally established liner load data may be used to estimate shear stresses and test the full-sticking hypothesis in common use. The most important reason for performing liner force measurement is, however, that it is essentially an alternative indirect method of measuring the die face load, the integrated die face pressure. The ram force is equal to the sum of the liner force and the die face force.

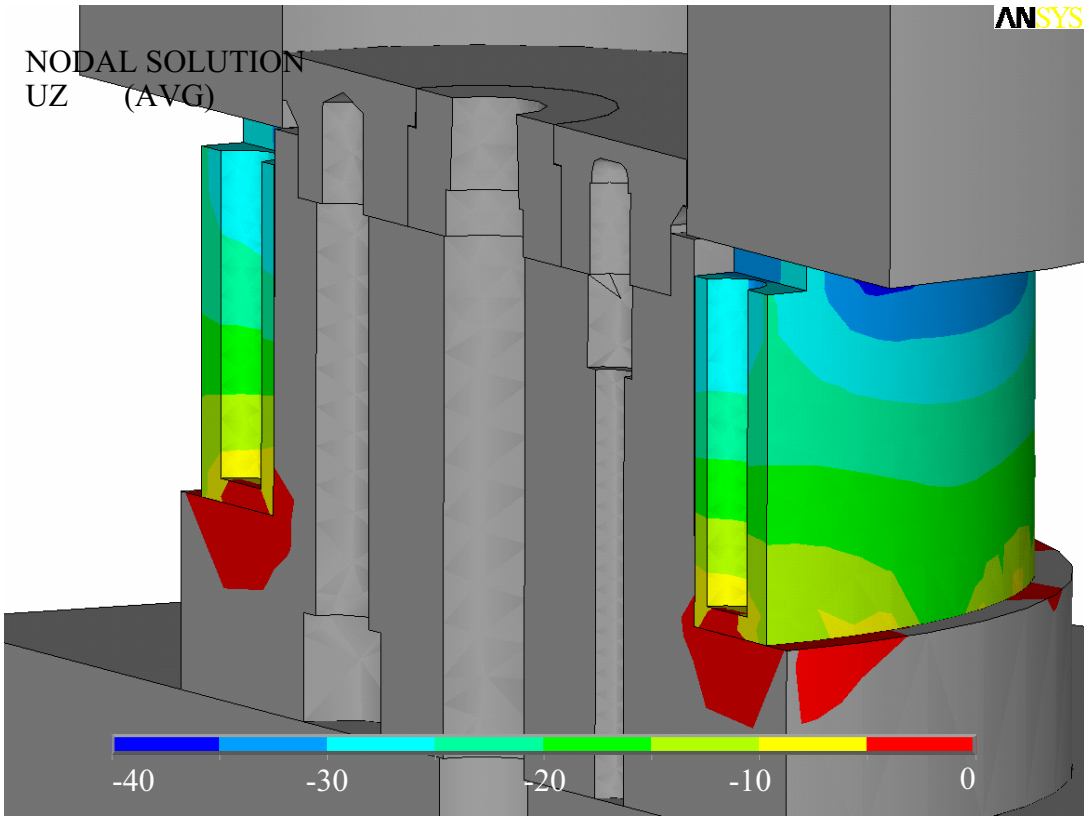

Figure 4.49. Elastic compression of liner load cell during calibration calculated by ANSYS® 7.1. The figure shows the axial compression. The liner load is 683 kN. The pressure is 100 MPa. Displacements are in [µm].

The liner load cell works according to a simple principle. When the liner load is applied, the load cell is compressed elastically. The length reduction is measured continuously by the capacitive displacement sensors that have been attached to rods extending almost through the whole liner load cell. The approximate calculations presented in Chapter 2 indicate that a liner force of 1000 kN may cause sensors to measure displacements of approx 36 µm. The calculations assume that the compression is perfectly uniform, but neither the load cell design nor the application of load is perfectly axisymmetric. The displacement field is non-uniform close to the upper end of the load cell. Figure 4.47 displays results from the very same ANSYS® 7.1 model that was first presented in the

last sub-section. The model predicts a sensor response corresponding to a displacement of approx 34 µm. Due to the special design of the sensor close to the top end (close to the liner), the compression of the material close to the sensor holes is slightly smaller than indicated by the analytical calculation. The numerical model indicates that the load cell may also experience limited bending and shearing due to the deformation of the die support, but this does not seem to affect the sensor output significantly. The stiffness of the container liner contributes to keeping the top faces of the load cell straight.

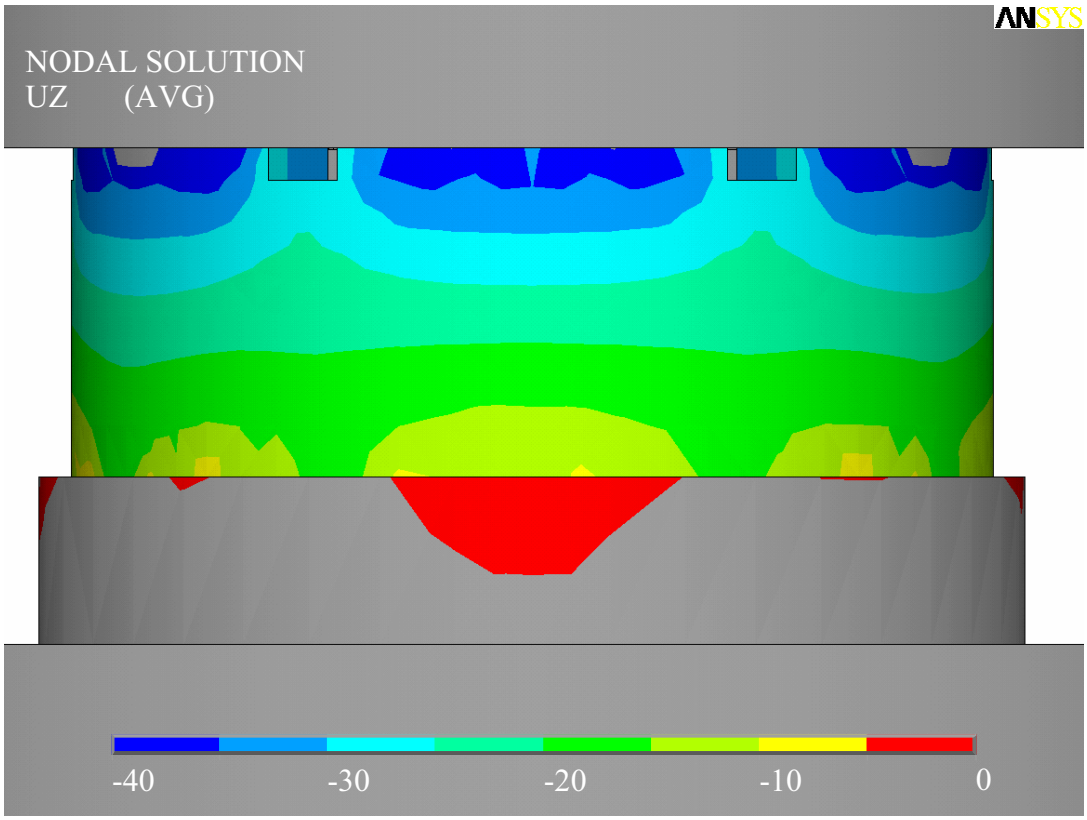

Figure 4.50. Elastic compression of liner load cell calculated with ANSYS 7.1®. The figure shows the axial compression. All data are in [µm].

The method used for calibration of the liner load cell was similar to, but simpler than the one used to calibrate the die face pressure sensors. Figure 4.51 shows the principle. A thick disc was placed on the top of the container liner, which had been brought into contact with the load cell. The ram was lowered onto the thick steel disc before the load was applied. The actual calibration procedure consisted of several rounds of loading and unloading to various levels of force. Figure 4.52 shows the results from one of the rounds of loading and unloading. Measurements were performed under steady state conditions. There was no test billet in the container during liner load calibration, and the cool ram was not in direct contact with the measurement system, as was the case during calibration of the die face pressure sensors. Thus, the temperature field of the extrusion die was not significantly altered during calibration experiments.

The liner load cell calibration experiments were performed during four of the five days of extrusion experiments. On some occasions calibration tests were run both before and after the extrusion runs. As in the case of the die face pressure calibration, it would have been highly desirable to run a larger number of experiments in a more systematic way. The experiments indicated that the calibration method works, but they neither provided a calibration curve of satisfactory accuracy nor revealed the potential weaknesses of the sensor design. The experiments that are described in the current report were the first of their kind, and they were performed when there was a scarcity of time and resources.

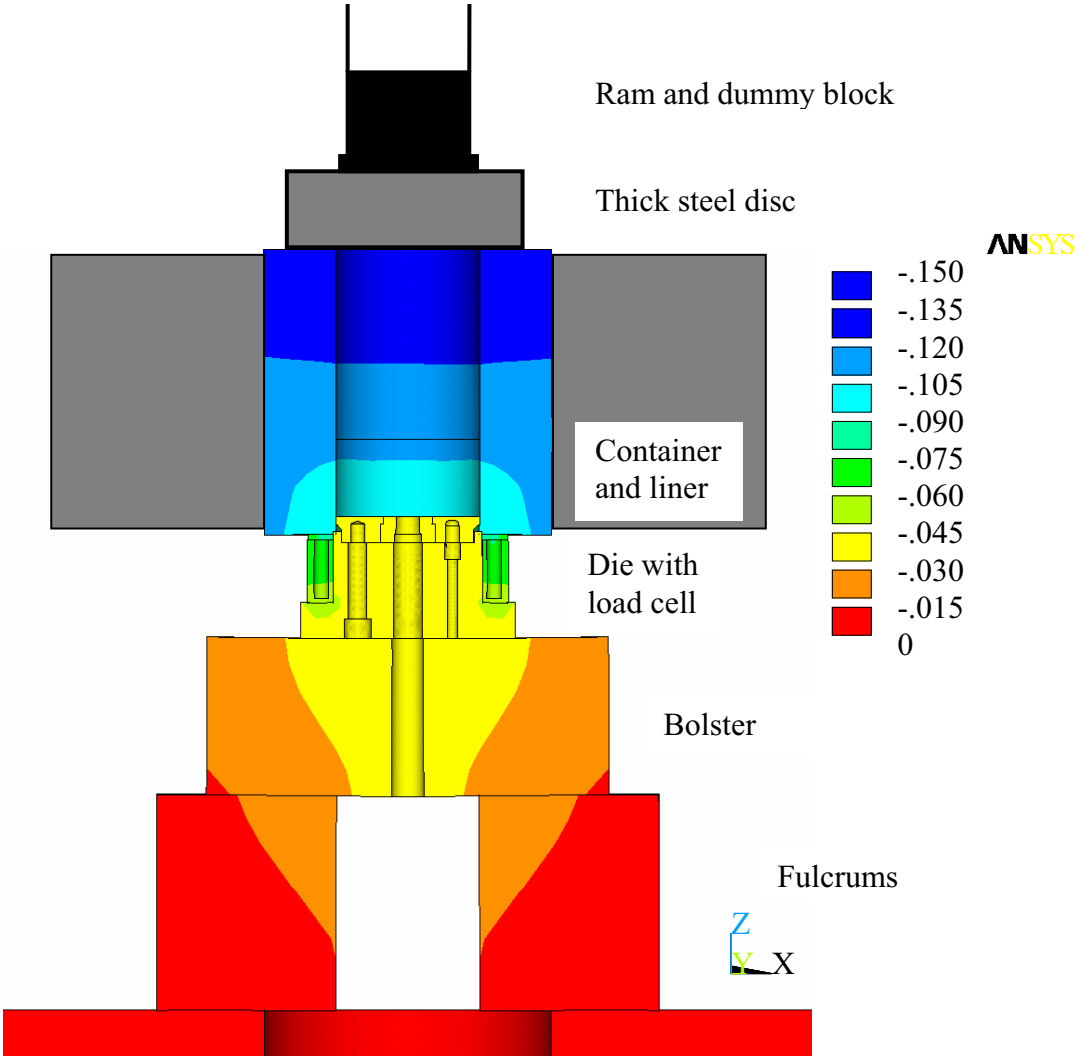

Figure 4.51. Method of liner load sensor calibration. The component of deformation in the extrusion direction is shown. All values are in [mm].

Curves like the one shown in Figure 4.52 indicate that even for two consecutive rounds of experiments, there may be some variability in the results. As in the case of the die face pressure measurements, an initial round that included a moderate overload was run in order to prevent further permanent deformations and to reveal unacceptable sensor behaviour. Plastic deformations were probably not provoked, but there was a risk that

the connection between the probe holder and liner load cell could loosen or change permanently during measurement. The most common cause of variability seemed to be lost motion in this or other connections, typically 0.5 µm. After unloading the output voltage could differ by as much as 10 to 20 mV from the zero point voltage. Note that for two of the sensors used in the liner load cell, a voltage change of 10 V corresponds to a sensor gap change of 0.5 mm. In the case of sensor 3 of Figure 4.52, the full range was 1.0 mm.

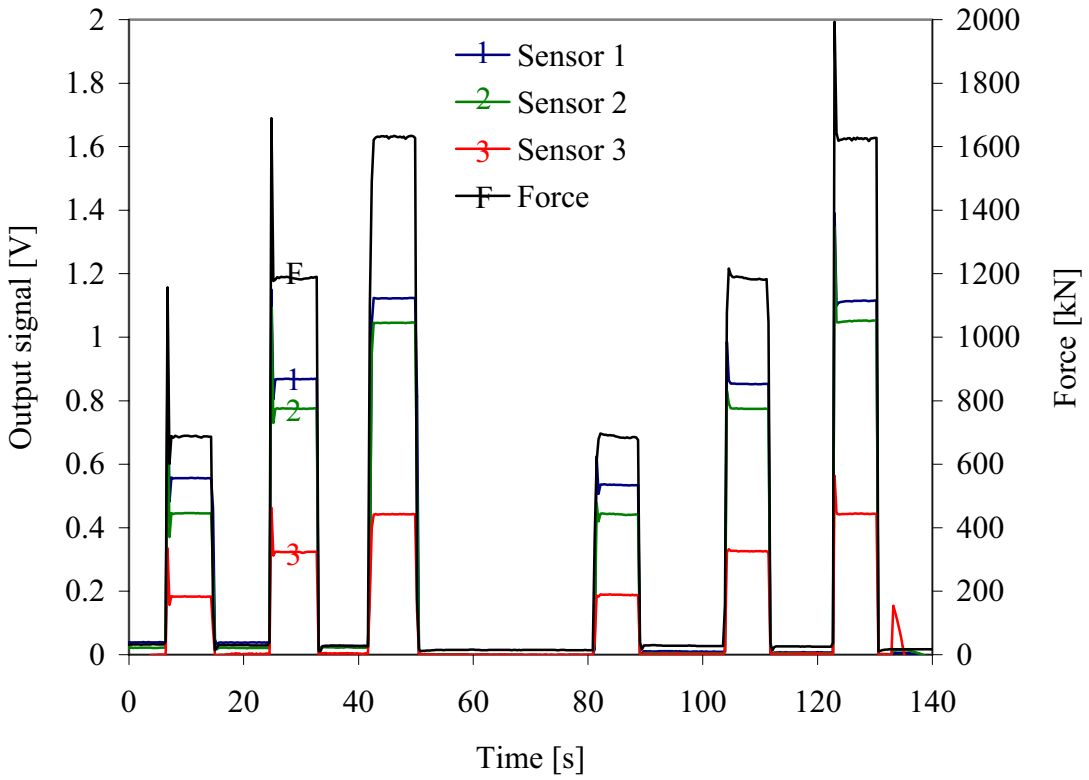

Figure 4.52. Results from a round of liner load cell calibration

A possible reason for the relatively large variability in sensor responses and also for the deviations between the analytical/numerical and experimental calibration curves was non-uniform loading. The load applied on the top of the die flanges was a distributed one, and the assumption has so far been that it, like the deformation, was uniform during experiment. However, this is an idealization that would require the surfaces of the liner and die in contact, to be perfectly co-planar and compatible. If the die and the liner were only in contact on parts of the die face, the compression of the load cell could easily have been non-uniform. The contact conditions were to a large extent determined by the geometry of the die and the liner, but the details of the mounting and clamping of the container appeared to be of some importance. The connection between the die and the container was a tight fit. However, when and if aluminium penetrated into the interface, mounting became difficult and the contact conditions for the liner load cell could be far from optimal. An aluminium layer covered one part of the flanges after extrusion, and it may have caused the deformation to be non-uniform.

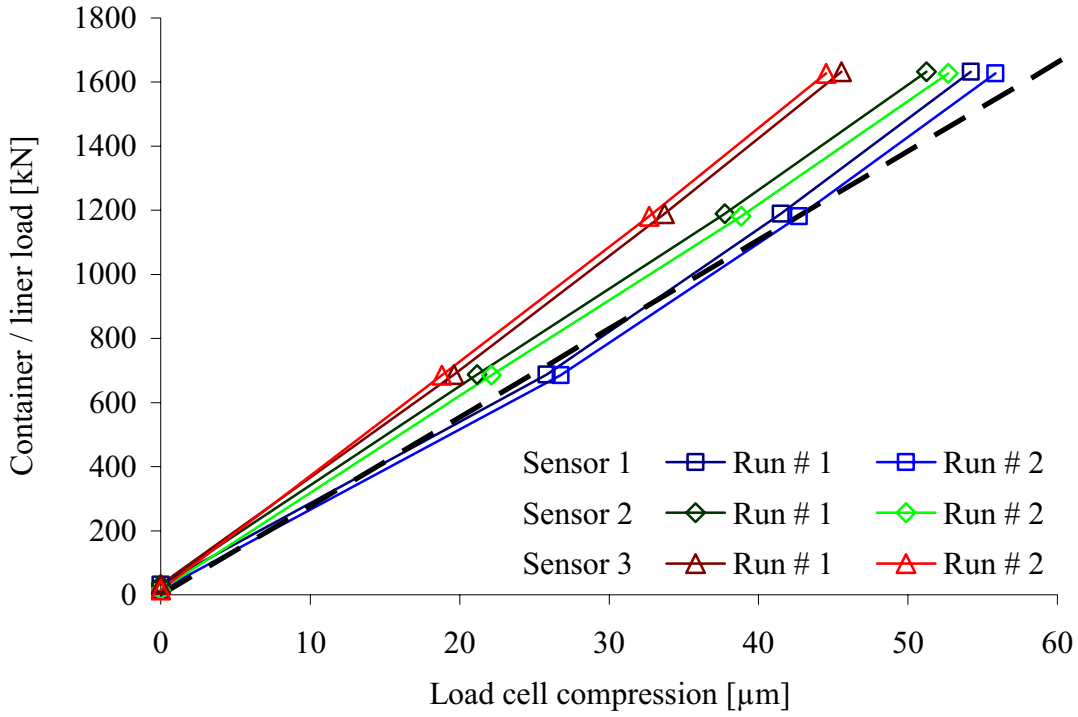

Figure 4.53. Liner load calibration curves (round A). The results are from two runs and three liner load sensors.

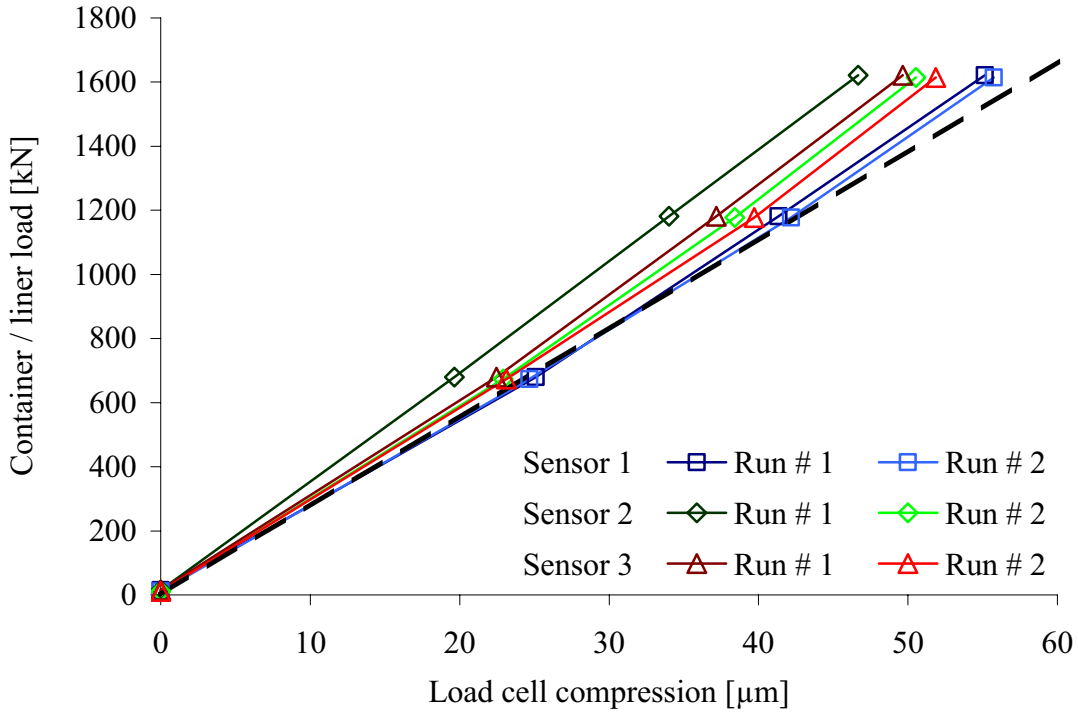

Figure 4.54. Liner load calibration curves (round B). The results are from two runs and three liner load sensors.

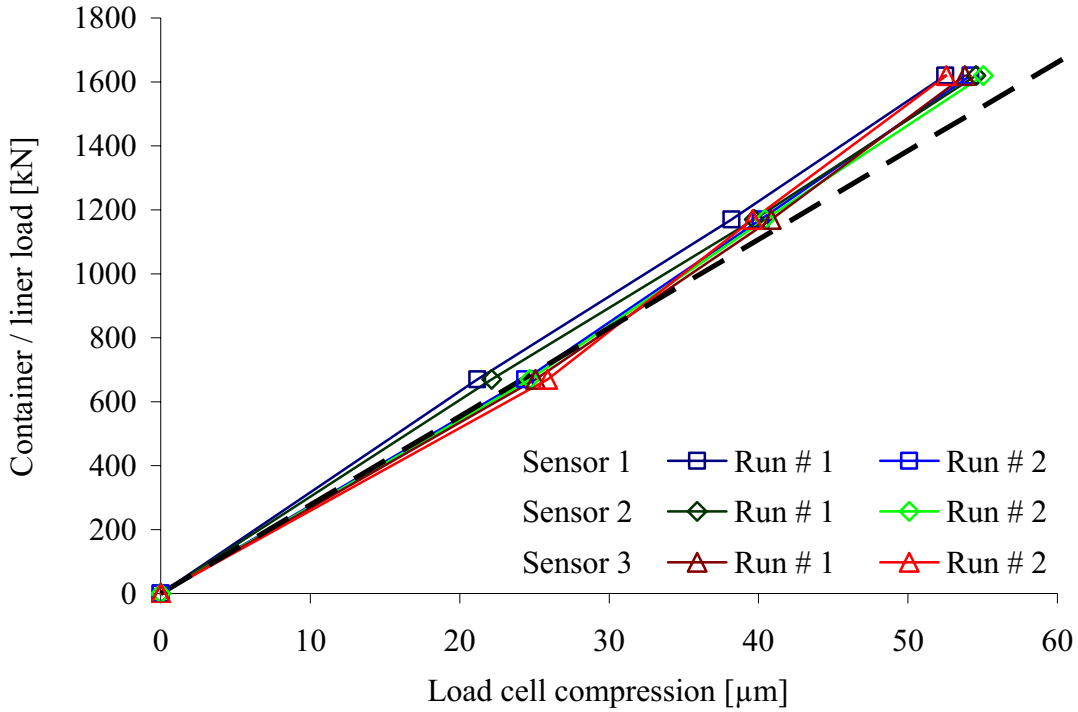

Figure 4.55. Liner load calibration curves (round C). The results are from two runs and three liner load sensors.

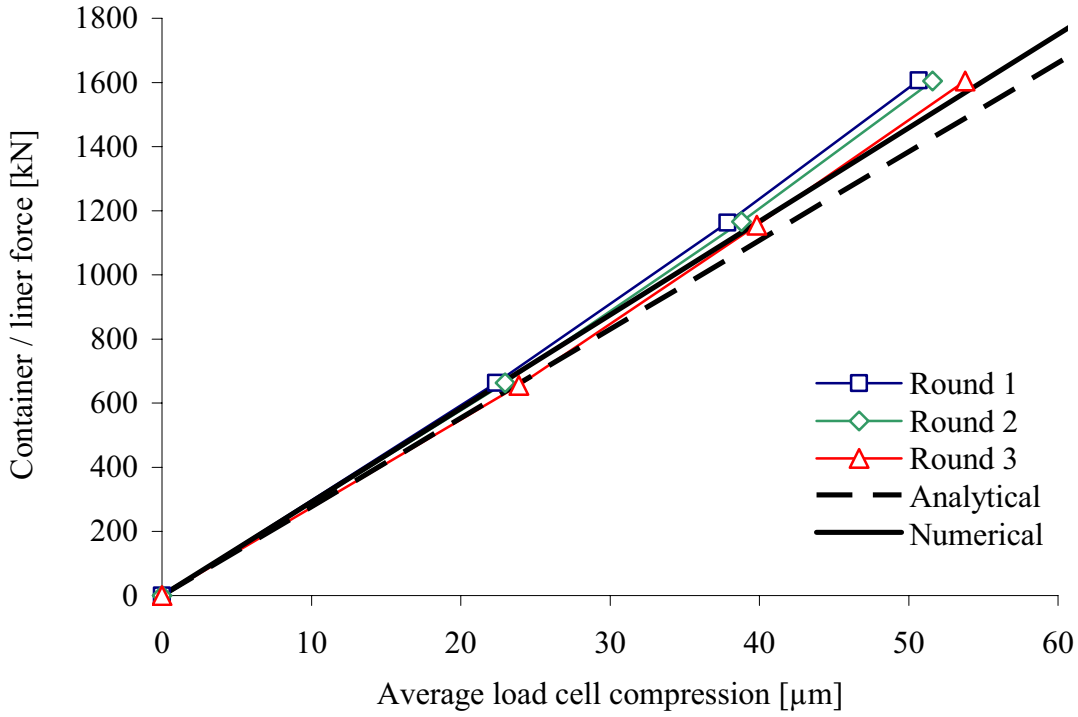

Figure 4.56. Liner load calibration curves – average of rounds A to C. The results are based on data from all sensors and experiments.

The possibility of skew loading was foreseen, and the solution to the problem was to place the three load cell sensors 120 º apart. While one of the sensors may indicate a too high load and another a too low load, the average value of compression for all the sensors should give a proper indication of the liner force. Figure 4.53 to Figure 4.55 display results from calibration of Sensors 1 to 3 for rounds 1 to 3, the rounds of extrusion with zero bearing length. For each round and sensor two replicate runs were performed. In between the runs the ram was retracted and contact conditions were re-established. The responses were fairly linear and not very different from analytical and numerical predictions. As was expected, the scatter in results was significant. In Figure 4.56 the average values of deflection and force are shown. The average for all sensors and runs of a round has been calculated.

Table 4.4. Calculated and experimental calibration factors for the liner load cells.

Round	A	B	C	D	E	Analytical	Numerical
kN/µm	31.61	31.00	29.83	NA	32.68	27.69	29.16
µm/V	50	50	50	50	50	50	50
kN/V	1581	1550	1492	NA	1633	1385	1458

Table 4.4 shows both the displacement-load and voltage-load calibration factors for all rounds except from the fourth. The displacement-load calibration factors obtained through experiment and calculation may be more easily compared for the liner load cell than for the die face pressure sensors. When the liner load cell is compressed, the probes move towards the sensor discs of the load cells much like during the standard Capacitec sensor displacement calibration. There is very little bending deformation, and it should be simpler to secure proper mounting of the sensors. Possible effects of temperature have not been considered, and neither has the magnitude of the lateral movement of the probe holder. Still, the analytical and numerical calculations should provide a better estimate of the liner load cell response.

The scatter in the results from the load cell calibration is, however, larger than for the die face pressure calibration. There is a large difference between the analytical estimate of the calibration factors and the measured factor, but it is more difficult to reject the numerically calculated factor on the basis of experimental data. The average force-displacement calibration factor obtained from measurements is 31.3 kN/µm, while the estimate of the standard deviation is 1.2 kN/µm. It is not reasonable to assume that the actual average calibration factors differed significantly at the different days. This means that the accuracy of measurement was far from perfect. The results may differ as much as 5 to 10 % from the actual values. At the same time, there was a significant variability in measurement both from one round to the next and even for a round of measurement.

The fact that the accuracy and repeatability of the liner load sensors are not better than those of the pressure sensors may at first seem somewhat strange, but may be explained by the difficulties related to controlling displacements smaller than 1 µm. In the case of liner load measurement, the problem may be overcome by designing a cell that experiences much larger deformations. It is also possible to compensate for the non-uniform loading and deformation. Experiments first of all demonstrate the feasibility of measurement and the potential of the capacitive pressure sensors.

Chapter 5

Experimental results

This section presents the results from the rod extrusion experiments with the complex instrumented die. Further details about the experimental activity are provided, and the principles of the treatment of the data from experiments are reviewed.

5.1 An overview over experimental cases and runs

Five rounds of rod extrusion experiments were performed. A round is identical to a day of experiment. The days are denoted A to E. At least six cases were run on each day (except from on day A), and there were at least two replicate runs for each case. Cases 1, 2, 3 and 5 were run on two days to allow a careful evaluation of the repeatability of measurement. There were as many as eight replicate runs of case 2.

Table 5.1. An overview of the cases of the experiment (ER – extrusion ratio, BT – billet temperature, BL – bearing length ratio, PV – profile velocity)

Zero Bearing (BL = 0)					
ER = 40	BT [ºC]		ER = 80	BT [ºC]	
PV [mm/s]	450	500	PV [mm/s]	450	500
200	Case 1	Case 4		Case 7	Case 10
400	Case 2	Case 5		Case 8	Case 11
800	Case 3	Case 6		Case 9	Case 12

Long bearing (BL = 0.759)					
ER = 40	BT [ºC]		ER = 80	BT [ºC]	
PV [mm/s]	450	500	PV [mm/s]	450	500
200	Case 13	Case 16		Case 19	Case 22
400	Case 14	Case 17		Case 20	Case 23
800	Case 15	Case 18		Case 21	Case 24
1600				Case 25	Case 26
2400					Case 27
	475			475	
500	Case 28			Case 29	

Table 5.1 gives an overview of cases, while Table 5.2 relates runs and cases. The run designation is a combination of a letter and a number. The letter indicates on what day the run was performed. The number is the serial number of the run on a specific day. A01, B01 and C01 are the very first runs on days A to C, while the first runs on the last days were named D00 and E00. Prior to the first run of a day, there was no butt end in the container. The results from the first runs were not intended for use in later analysis.

In some cases the butt end stuck to the dummy block rather than to the die face. The subsequent run was performed as the very first run of a day. An example of such a run is E20 of case 22 (Figure 5.95). The run has been added in the analysis since it serves to show that the results from the experiments are not significantly affected by the addition of the pre-deformed butt end. Run E20 is not an atypical run.

Table 5.2. Cases and runs (in standard letters: only die face pressure measurement, in italic letters: only liner load measurements, in bold letters: both types)

Day	Case	#	Run	Case	#	Run
A	1	3	A09, **10**, *11*	4	0	
B		2	B06, **07**		2	B12, 13
	2	5	A02, **03**, **04**, *05*, **14**	5	2	**A12**, **13**
		3	B02, **03**, **04**		4	B08, 09, *14*, **15**
	3	3	A06, **07**, *08*	6	0	
		2	B04, **05**		2	B10, 11
C	7	3	C02, 03, **04**	10	2	**C09**, 10
	8	4	C05, 06, **15**, **16**	11	2	C11, **12**
	9	2	C07, **08**	12	2	**C13**, 14
D	13	3	D02, 09, 14	16	3	D01, 08, 11
	14	3	D16, 17, *21*	17	2	D04, 05
	15	3	D06, (13), 15	18	3	D07, 10, 20
	28	4	D03, 12, 18, 19			
E	19	3	E01, 03, **13**	22	3	E05, 06, **20**
	20	2	**E17**, **18**	23	2	E11, **14**
	21	3	E02, 12, **19**	24	3	E04, 09, **15**
	25	1	E21	26	1	E22
	27	1	E23	29	4	E07, 08, 10, 16

There were in all 14 runs on day A, 15 on day B, 16 on day C, 22 on day D and 24 on day E. It proved difficult to perform more than 25 runs during a round due to calibration and the necessary pauses. Table 5.2 indicates which types of measurements that were performed during each of the runs. The ram force and as well as the die outlet and die face temperatures were measured during all runs. The die face pressures and the liner loads were measured with two separate Capacitec systems. For reasons that were discussed in Chapters 2 and 3, the systems should not be used simultaneously in close vicinity of each other. The consequence was that a beating signal is superposed on the DC output voltage of systems. There are, as earlier indicated, solutions to the problem, but at the time of the experiments, they were unfortunately not known. It was therefore decided that most of the runs should be performed with only one of the systems active at a time during most of the runs. The die face pressure measurement was obviously most important and performed during most (more than 2/3) of the runs. The approach must be characterised as suboptimal. One day's hire of press and operator cost at the time of the experiments more than NOK 10 000. A billet of length 200 mm cost approx 250 NOK. This brought the cost of one run to approximately 750 NOK. The savings related to the use of shorter billets are small, and the results may be less interesting to the industry and of lower value in an inverse analysis. Besides, the greatest costs were related to the design and manufacture of the extrusion die, the purchase of the capacitive equipment, the preparations for the experiments and the analysis of results. Thus, the cost of each run was in fact probably closer to NOK 10 000. It would be most unfortunate if sufficient information about the sensor and extrusion system behaviour could not be

obtained due to a problem that should be manageable. During earlier experiments it was possible to post-process measurement signals so that valuable information could be drawn also from the runs performed with both capacitive displacement measurement systems. Many runs were therefore performed with the two systems operating in parallel (Table 5.2). The signal processing approach is treated below.

5.2 Ram force and outlet temperature measurement

Ram force and outlet temperature measurement results presented in this section have not been modified in any way after they were recorded by the measurement system of the SINTEF laboratory extrusion press. The standard force, position and velocity calibration techniques of SINTEF have been described in the previous section. The sampling rate was 20 per second. The ram force was also logged by the independent system for the die face pressure measurements. Results do not significantly differ from those presented in this section. There were, as indicated in Chapter 2, two replicate measurements of the die outlet temperature. In the case of the long bearing channels (used on days D and E) the material flow temperature was measured close to both the inlet and the outlet of the bearing channel as well as in the middle of the channel. There were two thermocouples at the outlet of the bearing channel. In the case of the zero length bearing channels, two thermocouples were mounted as close to the die outlet as possible. Figure 5.1 presents results from case 2, which was run on days A and B. Outlet temperature sensor 2 produced similar results on both days. On day B, however, outlet temperature sensor 1 indicated that the temperature was approximately 20 ºC lower than on the previous day. The same observation was made for all the other cases that were run on that day. The explanation is that the thermocouple had been retracted during the experiments or in relation to the dismantling of the die immediately after day A. It was therefore no longer in close contact with the flow (Chapter 2). The results from temperature sensor 1 on day A should therefore not be used in the analysis of flow.

The temperature curves of Figure 5.1 give an indication of the measurement variability. As long as the thermocouples were properly positioned, results differed by less than 5 ºC. During all runs performed on days D and E the temperature at the inlet to the bearing channel was approximately 10 ºC lower than at the outlet, while the temperature in the middle of the bearing channel did not significantly differ from that at the outlet. An example is given by Figure 5.2. Welo et al. [Wel96] have made similar observations for somewhat different outlet geometries. It has earlier been proposed that friction shear stresses are pressure dependent and of relatively small magnitude in the outer part of the bearing channel. It is therefore often concluded that the pressure build-up is smaller in the outer than in the inner part of the bearing channel. Only the inlet and outlet temperature results are presented in this section of the report. The main objectives of performing experiments with long bearing channels were to use the pressure and temperature sensors to assess the friction behaviour and the pressure build-up in choked bearing channels. This should not only contribute to a better understanding of friction mechanisms, but it should also allow a closer evaluation of pressure sensor behaviour. Chapter 6 contains a further assessment of results.

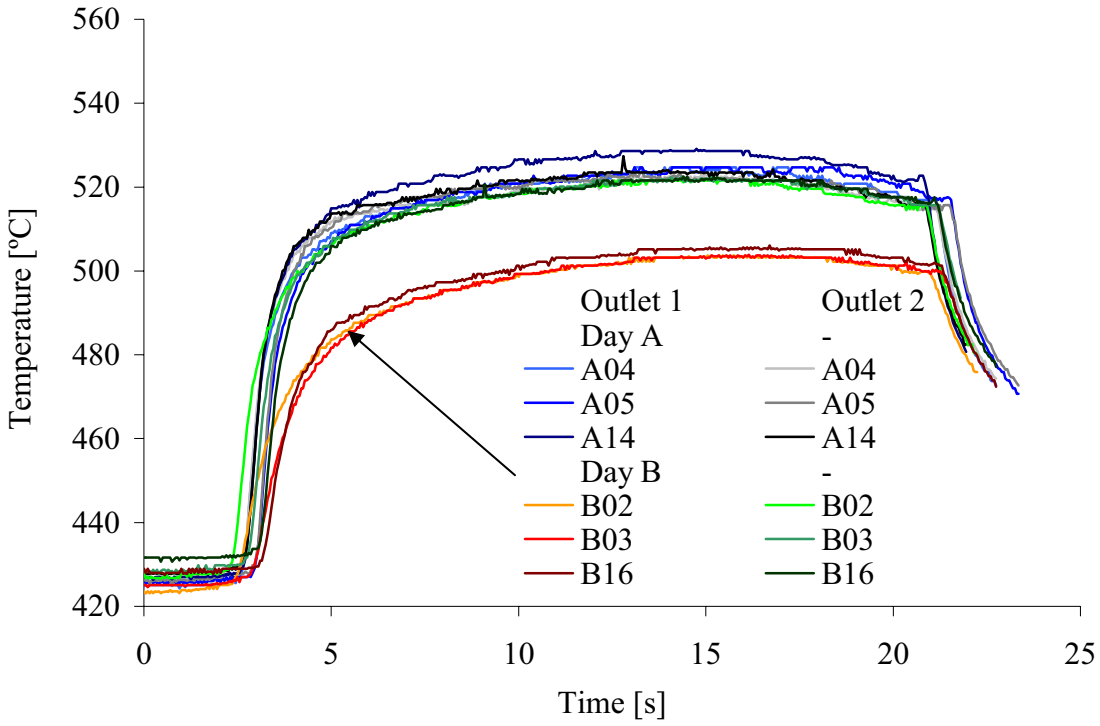

Figure 5.1. Die outlet temperature measurement for case 2 (runs A04, A05, A14, B02, B03 and B16). Two temperature sensors were used.

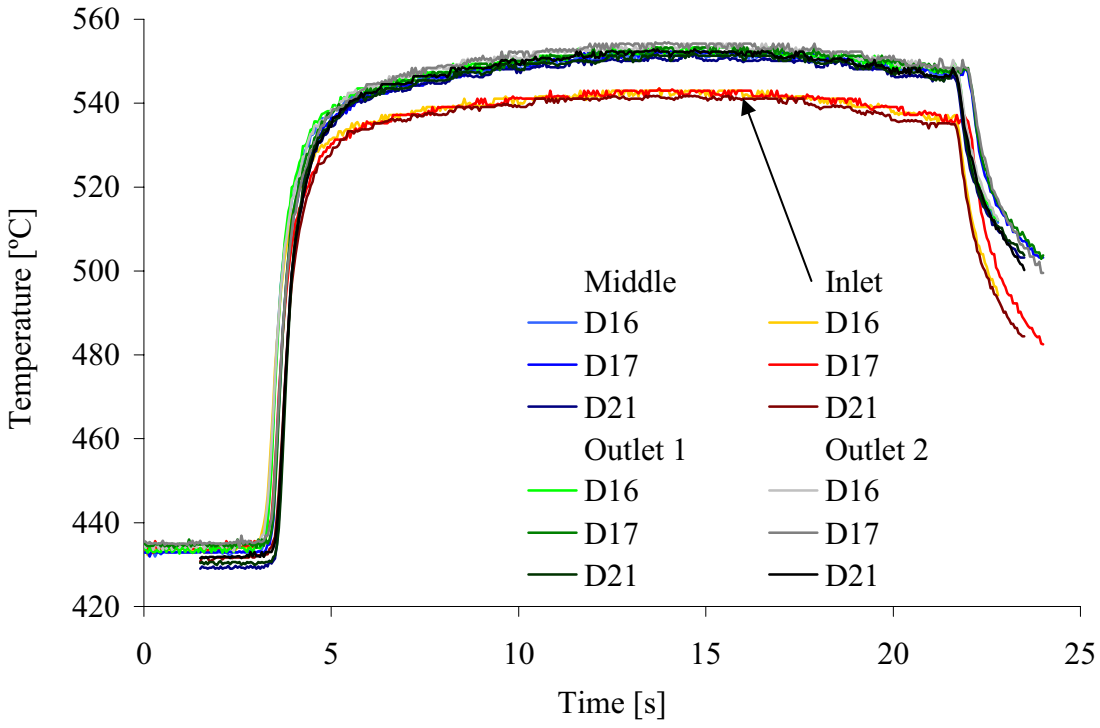

Figure 5.2. Die outlet temperature measurement for case 14 (runs D16, D17 and D21). Four temperature sensors were used.

5.3 Determination of zero point for die face pressure measurements

The output signal obtained from the capacitive displacement measurement system is, as indicated in Chapter 3, a DC voltage in the range from 0 to 10 V. An output signal of 10 V corresponds to a gap distance of approximately 0.5 mm. The initial gap distance was usually set to 0.4 mm (8 V). During measurement, voltage changes were typically in the range from 0.4 to 0.8 V, which corresponded to displacements of 20 to 40 μm. Since the change in the capacitance was caused by a bending deformation of a pressure sensor disc rather than a pure translation of one parallel plate of a capacitor, calibration curves established by the Capacitec displacement calibration method could not be used to accurately determine the sensor disc deflection or gap distances in the deformed state. This is not a serious problem, for in-situ calibration was performed in order to directly link die face pressure and voltage changes (Chapter 4). However, it may be much easier to assess approximate disc deflection (deformation) than voltage changes. The nominal calibration factor of 50 μm/V has been used to obtain a characteristic values. Figure 5.3 presents typical pressure measurement results. The run designation is B06 (Case 1). The mounting solution of sensor 1 differs from that of sensor 2 and 3, which explains the significant difference in response. The curves consist of essentially five parts:

- The initial phase after billet loading (–30 – 0 s)
- The burp phase (0 – 4 s)
- The loading phase (4 – 40 s)
- The unloading phase (40 – 45 s)
- The final recovery phase (45 – 120 s)

Figure 5.4 shows the signals of sensors 2 and 3 in the initial and burp phases. In order to accurately determine the sensor disc deflection, a zero point for the measurement had to be set. When the container was clamped, the billet dropped into the container or the ram was moved into the container, there was sometimes a small response from the sensor system (ca. 4 mV ~ 0.2 μm ~ 1.6 MPa). At this point, no significant force was applied directly at the top face of the die. However, there was mechanical interaction between the die and the ram through the container, and there was heat transfer from the billet to the die. A sensor response may have been related to the deformation of the die due to the liner load. As the ram moved through the container, it continuously sheared off the aluminium deposited on the container wall. The ram force typically reached 200 to 400 kN depending on the contact conditions in the container. The clamping forces were of a similar magnitude. Finite element analysis has indicated, however, that liner loads only to a very small extent affected the actual sensor disc deflection. It is more likely that loads applied through the liner caused the die to move and the sensor cables to get strained. If only a small force was applied on the capacitive probe through the cable, it would have been almost impossible to prevent the probe from moving 0.2 μm. If cables moved, they may have become somewhat differently capacitively coupled to the die at ground level. This may have been a problem particularly if the cables were in close contact with the die and improperly insulated. Since the sensor response prior to the burp phase seems neither to be due to direct mechanical loading nor thermal effects, it is natural to set the zero point for the pressure measurement at a point in time after the ram had entered the container and before extrusion commenced.

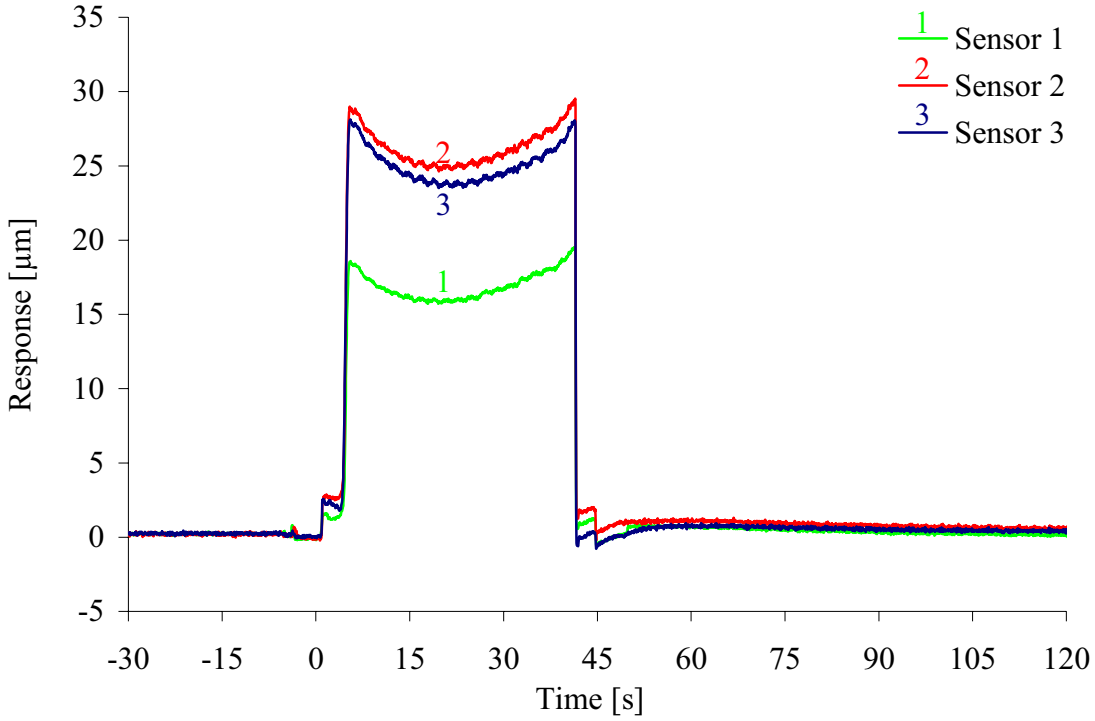

Figure 5.3. Measurement of the sensor disc deflection for all pressure sensors. The results are from case 1 and run B06.

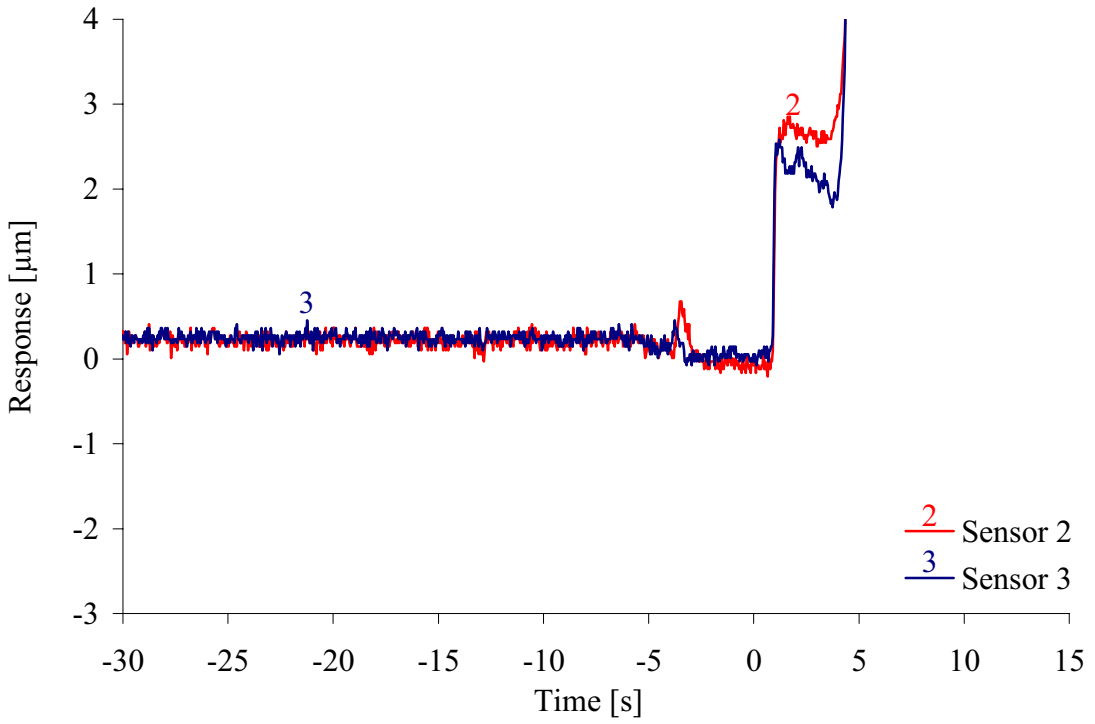

Figure 5.4. Measurement of the sensor disc deflection in the initial phase after billet loading. The results are from case 1 and run B06 and sensors 2 and 3.

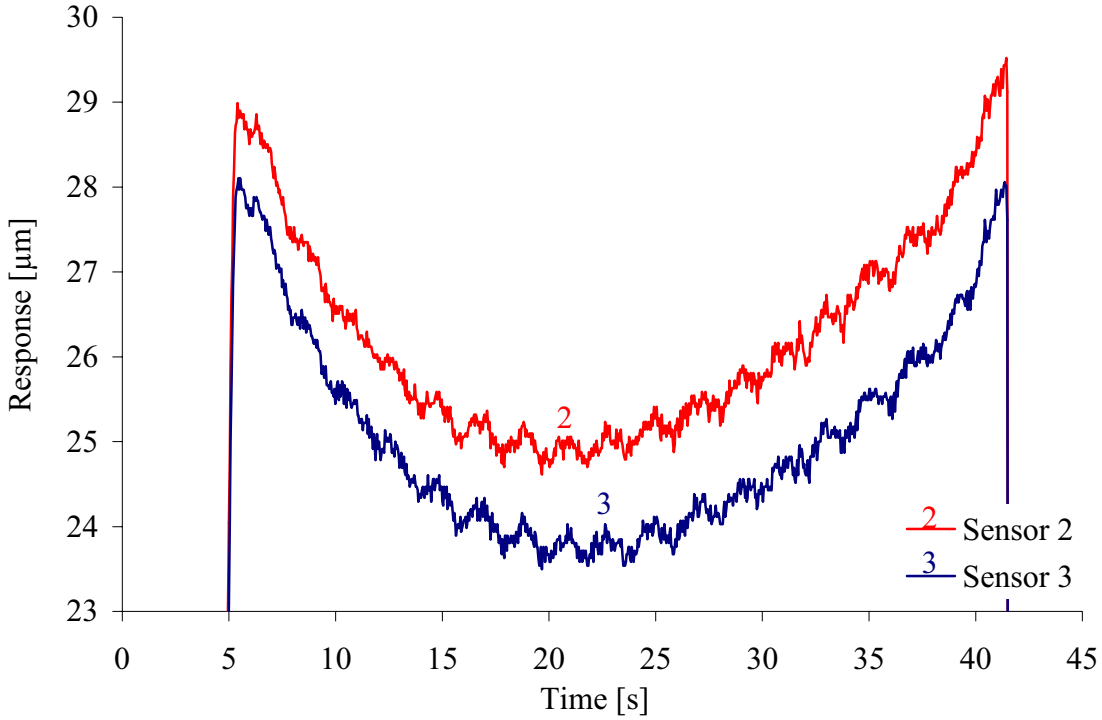

Figure 5.5. Measurement of the sensor disc deflection during extrusion. The results are from case 1 and run B06 and sensors 2 and 3.

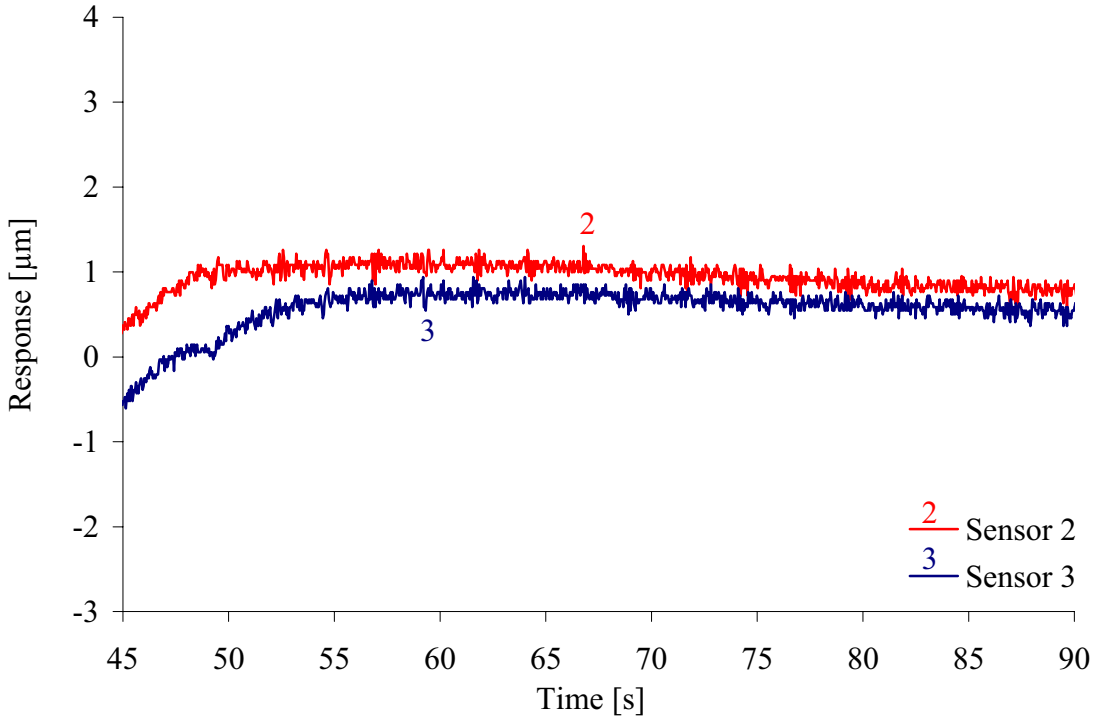

Figure 5.6. Measurement of disc deflection in the phase after unloading. The results are from case 1 and run B06 and sensors 2 and 3.

Figure 5.3 shows that the output of the pressure sensors did not return directly to the zero point after unloading but rather converged slowly. As will be discussed in the next section, temperature changes caused mainly by plastic dissipation affected the pressure measurements to various extents both during (Figure 5.5) and after the runs (Figure 5.6). It should here merely be noted that the sensor responses differed more after than before extrusion. An explanation may be that the sensors were to different extents affected by temperature changes. There may also have been small displacements during extrusion that may not be easily predicted. Plastic deformation of the sensor disc has already been discussed, but sensors had generally been designed for the demanding conditions. The contact between the probe holder and die may have been imperfect, and permanent displacements may have occurred. On days A to D, very few jumps or discontinuities in the responses of the pressure sensors were observed during, directly before or after measurement. During the last round of experiment, however, measurement signals were much less stable. The main reason for the poor results obtained on day E was improper sensor mounting during preparations for experiments. Sensors may have come into contact with the die core and coax cables may have been strained. On day E, it very soon became evident that sensor 2 did not function properly. Calibration curves could not be accurately reproduced (Chapter 4). After calibration compression testing and extrusion, the sensor output often indicated a positive pressure of significant magnitude. When the tool stack had first been heated, however, it was very difficult to improve sensor behaviour (Chapter 2). The tool stack had to be cooled, and the die had to be completely disassembled and reassembled.

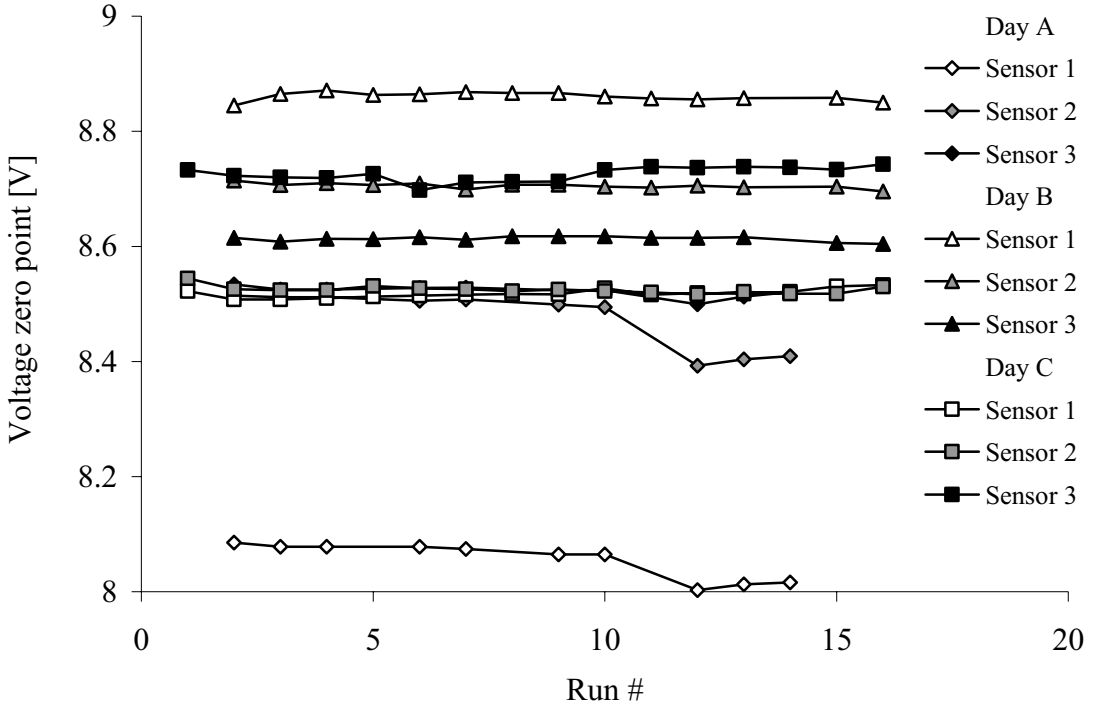

Figure 5.7. The DC voltage value defined as zero point for pressure measurement for all runs and all sensors on days A to C (an indication of the zero drift).

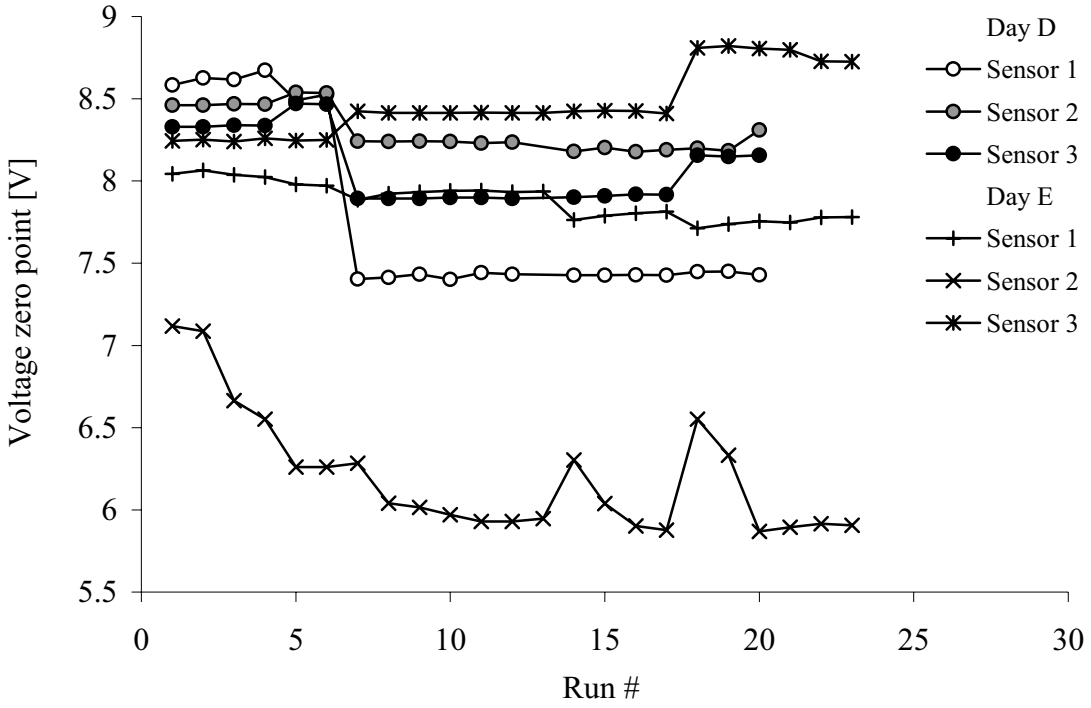

Figure 5.8. The DC voltage value defined as zero point for pressure measurement for all runs and all sensors on days D and E (an indication of the zero drift).

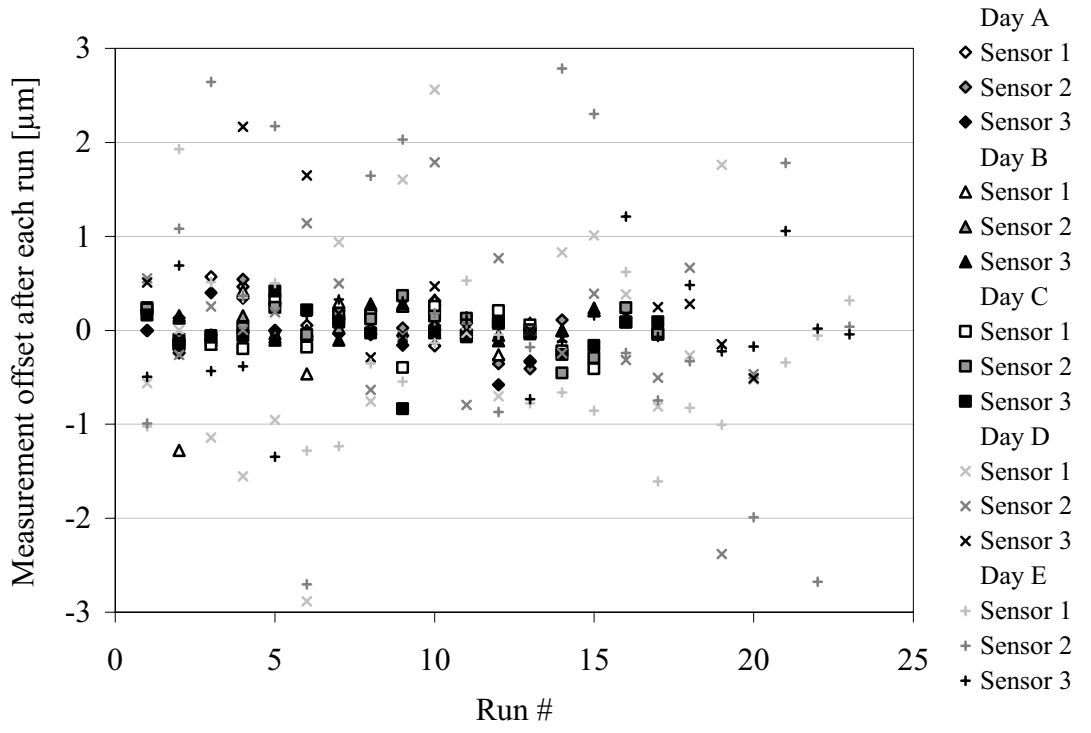

Figure 5.9. The remaining disc displacement 120 seconds or more after measurement of pressure. Results for all runs and sensors are shown.

Figure 5.7 and Figure 5.8 present the values of the zero point voltage for each of the runs and all pressure sensors. They seem to confirm that the zero stability was much poorer on day E than on the other days of experiment. There were also some changes in the voltage of the zero point on day D, but the repeatability of measurement was still quite good (as will be shown). The only significant change of zero point value in Figure 5.7 occurred after the 10^{th} run on day A. All sensors were affected. The 11^{th} run was performed with measurement of only the liner load. All the later runs on that day were performed with both systems working simultaneously. Whether the crosstalk and warm-up of the second sensor system affected the zero point readings is not known for certain. Pressure measurement results were in any case only to a very small degree affected.

Figure 5.9 presents the voltage change (converted to an equivalent displacement) from the start to the end of the run. Measurements were made immediately before and more than 100 s after extrusion. In some cases the logging was stopped relatively early, and the results presented in Figure 5.9 may be slightly affected by temperature changes. Still, these data seem also to support the conclusions drawn regarding the measurement zero stability. Even though there were a number of abrupt voltage changes on days D and E, results were far from useless. It was evident only for sensor 2 on day E that there had been a complete loss of contact between sensor and top disc during measurements. In the other cases the abrupt voltage changes were generally followed by periods of stability. Contact conditions probably did not change during such periods. During extrusion there were frequent cracking noises, and shock waves propagated in the tools. The last days of the experiment proved that the shocks may affect the sensor output in the most severe cases. The abrupt voltage changes were usually small (corresponding to displacements of less than a micron), but when the sensors were not properly mounted, there were also changes larger than 50 μm. When the output signal changes abruptly in the middle of the run, compensation may relatively easily be performed and defended. However, additional displacements are more likely to take place during loading or unloading. In such cases, compensation was generally not performed in the current study. The most critical phase of the extrusion run was when the ram was pulled off the butt end. The bolts connecting the top disc and the die core were elongated as the ram was pulled back. When the ram loosened, the top disc was quickly pulled back. This spring effect was further treated in relation to the die design (Chapter 2). If the probes or the coax cables were in contact with the die core, movements could affect measurement. The described mechanism is obviously a weakness of the die design, but it had the most serious negative effect when sensors were not properly mounted in the first place. Note that the results from experiments with the dies made of one piece of material (simple dies) were not significantly better than the results presented in the current study. Small unaccounted for displacements were in both cases observed and are difficult to avoid.

Data provided by the liner load sensors have been treated in a similar way as the data from the pressure sensors. Figure 5.10 shows the results from run A11 (Case 1) when only liner load measurements were performed. The nominal calibration factors were 50 μm/V for sensors 4 and 5 and 100 μm/V for sensor 6. The quality of the experimental liner load data could probably have been better. The best results were obtained during the first days of measurement. It seemed easier to accurately measure the changes of the liner load than the absolute values.

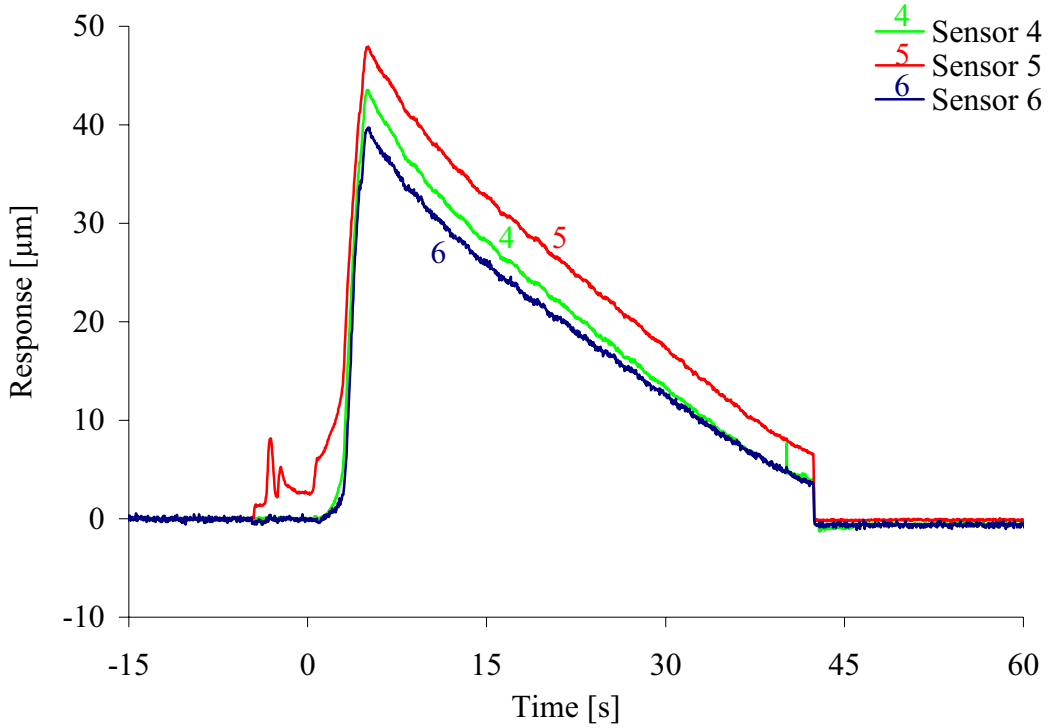

Figure 5.10. Measurement of the liner load cell compression by all sensors. The results are from case 1 and run A11. Only liner load measurements were made. The causes for the liner force fluctuation of sensor 5 before extrusion is not known, and this type of response was not typical.

5.4 Reduction of noise due to interaction between sensor systems

Figure 5.11 shows results from extrusion run B07, which was performed under the very same conditions (Case 1) as run B06 and during the same round (the next run). The results presented in Figure 5.3 and Figure 5.11 should be comparable. However, only measurements of the die face pressure were performed during run B06, while the liner load was also recorded during run B07 (Figure 5.12). The two measurement systems used to measure pressure and liner load interacted, and as a consequence a sinusoidally time varying signal was added to the sensor output signals. This was the crosstalk effect. During run B07 the sinusoidal signal was of a period of approx 7.18 s. It has been observed, however, that the period may in fact vary from 3 to 80 seconds only from one run to the next. If measurements were performed directly after one of the systems has been switched on, the period of the superposed signal varied during measurements. The amplitude of the signal was usually between 0.15 and 0.45 µm, while the total response of the pressure and liner load sensors was approximately 30 µm. As is evident from Figure 5.12, one of the liner load cell sensors, sensor 6, was more severely affected than the others. The amplitude of approx 28 µm was quite typical, and it is of a similar magnitude as the measurement signal. During calibration, the response of sensor 6 was also affected (1-2 %) by the responses of the sensors connected to the same rack. This indicates there were some problems related to signal processing. However, the results obtained from sensor 6 were largely in agreement with results from other sensors.

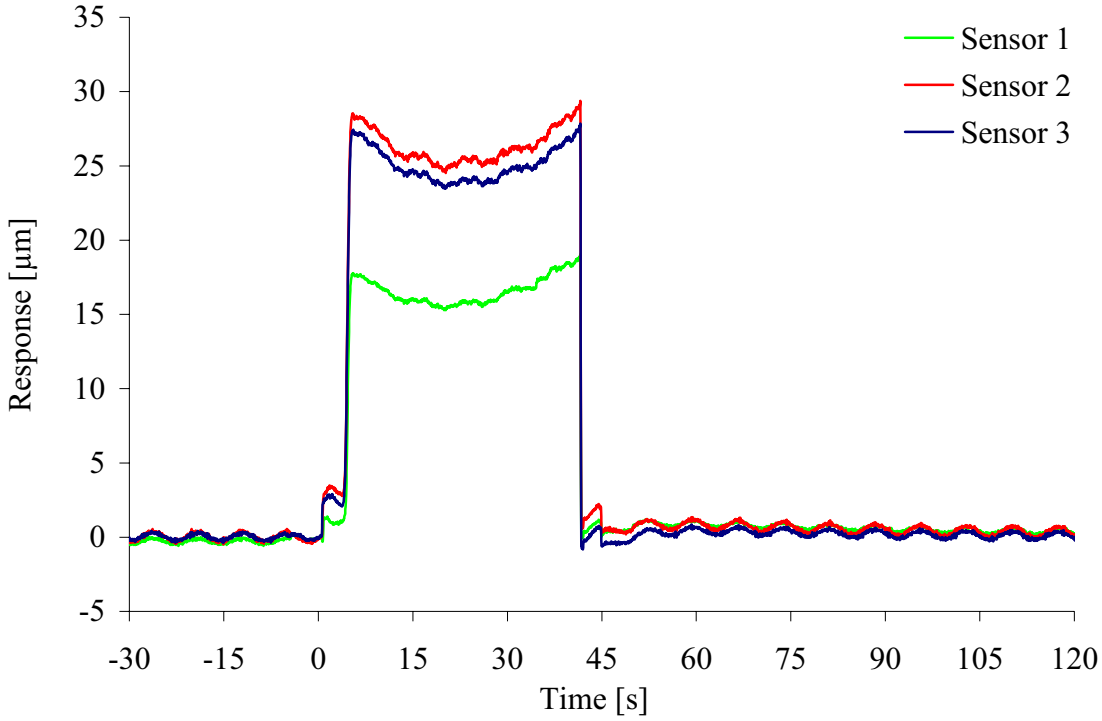

Figure 5.11. Measurement of the sensor disc deflection (voltage change times 50 µm/V) for all pressure sensors. The results are from case 1 and run B07.

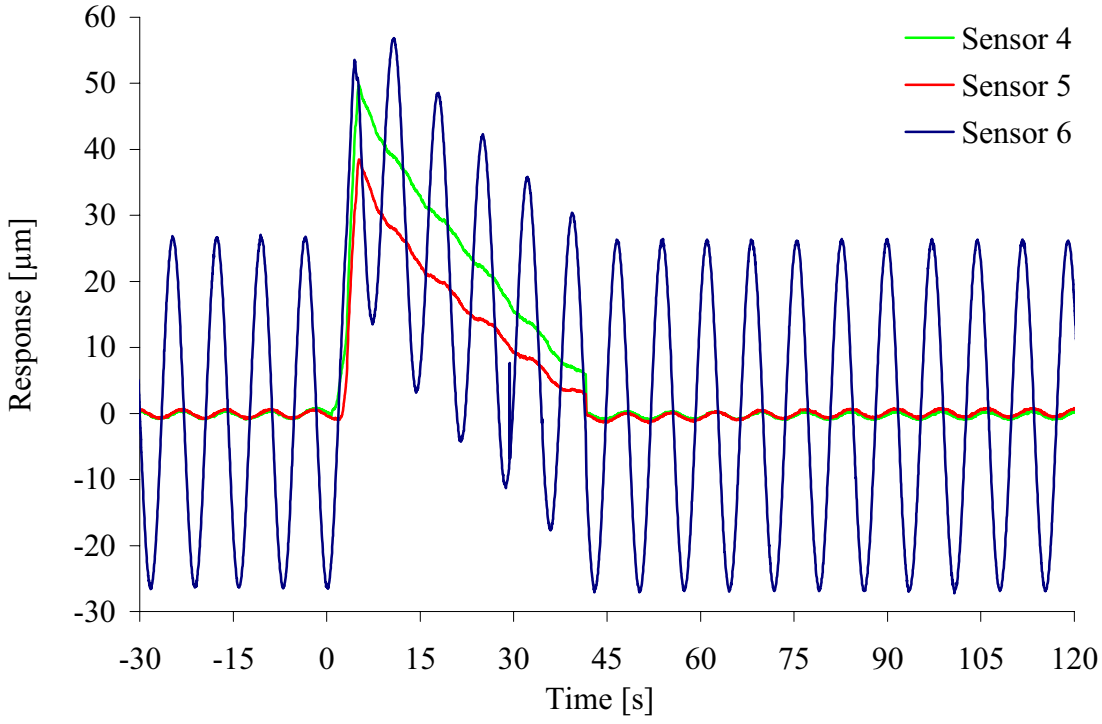

Figure 5.12. Measurement of the liner load cell compression (voltage change times 50 µm/V) for all sensors. The results are from case 1 and run B07.

Run B07 was not merely a replication of run B06, for it included an additional type of measurement. It provided valuable data from simultaneous measurement of liner force and die face pressure. For that reason it would be most interesting to make use of some of the information included in the measurement signals. Removal of the sinusoidally time-varying signal with constant frequency and amplitude is a feasible task. It is quite probable, however, that changes in the capacitor gap distance may not only have caused the DC voltage level to change, but also a change of the frequency, amplitude and phase of the beating signal. The problem of removing noise is an artificial one, for new experiments should be performed with synchronised clock cards. Hence, only a short presentation of the two techniques that have been used to reduce the influence of the beating signal is provided. First, if the superposed signal closely approximates a sinusoidal curve, a sinus wave may simply be subtracted from the output signal. The approach should cause the smallest loss of potentially useful information, for the filtering is applied for only one frequency. However, the task is a time-consuming one. Furthermore, the characteristics of the superposed signal sometimes changed during measurements and the approach may be inaccurate. The second much less used method is a standard technique of filtering. Matlab Signal Processing Toolbox has been used, as it allows a range of stop band filters to be used to reduce the influence of signals within a certain range of frequencies [MatW]. First, the frequency of the superposed signal may be determined by a Fourier analysis. While a Fourier series may approximate any function *f(t)* of time within an interval *[-T,T]*, the Fourier transform may be applied as *T* approaches infinity. The forward transform links the frequency distribution *Y(k)* to the measurement signal, while the backward transform may be used to determine the frequency distribution of the signal *y(t)*. Here, *k* is the oscillation frequency which is continuously distributed.

$$y(t) = \int_{-\infty}^{\infty} Y(k) e^{2\pi i k t} dk \qquad (5.1)$$

$$Y(k) = \int_{-\infty}^{\infty} y(t) e^{-2\pi i k t} dt \qquad (5.2)$$

When dealing with measurement signals that have been sampled at time steps, $t_k \equiv k\,\Delta$, it is more natural to use the discrete Fourier transform (DFT). k may assume the integer values 0,1,2,…,N. Δ is the sampling period. $y(t_k)$ is a discrete function. The frequency distribution Y_n must be determined.

$$y_k = \frac{1}{N} \sum_{n=0}^{N-1} Y_n e^{2\pi i k n / N} \qquad 0 \le k \le N-1 \qquad (5.3)$$

$$Y_n = \sum_{k=0}^{N-1} y_k e^{-2\pi i n k / N} \qquad 0 \le n \le N-1 \qquad (5.4)$$

If all y_k are real, the last equation may be expressed simply as a sum of cosine and sine functions, which closely relates to the traditional expression of the Fourier series.

$$y_k = \frac{1}{N}\sum_{n=0}^{N-1} a_n \cos\left(\frac{2\pi kn}{N}\right) + b_n \sin\left(\frac{2\pi kn}{N}\right) = \frac{1}{N}\sum_{n=0}^{N-1} a_n \cos\left(2\pi f_n \Delta k\right) + b_n \sin\left(2\pi f_n \Delta k\right) \quad (5.5)$$

$$a_n = real\left(Y_n\right), b_n = -imag\left(Y_n\right) \qquad 0 \le k \le N - 1 \quad (5.6)$$

n/N is the normalised frequency. f_n is then defined as $n/(N \cdot \Delta)$. The lowest frequency that may be described, apart from the $f_0 = 0$, is $f_1 = 1/(N \cdot \Delta) = 1/T$. T is then the length of the sampling interval. The highest frequency component is $f_{N-1} = (N-1)/(N \cdot \Delta)$. If N is sufficiently large $f_{N-1} \sim 1/\Delta$. According to the sampling theorem [MatW], the highest periodic waveform frequency that may be fully described is $f_{max} = f_{N-1}/2$. f_{N-1} is the Nyquist frequency, $f_{Nyquist}$ or f_{max}. In the current study the sampling period, Δ, of the die face pressure measurement system was approx 1/(25 Hz) or 0.04 s. Thus, it is not feasible to satisfactorily describe waveforms of frequencies higher than approx 12.5 Hz. The filter of the Capacitec system suppresses signals of higher frequencies than approx 200 Hz. The lowest frequency evaluated is usually that of the die face pressure or liner load measurement signal. When the ram velocity is 2.5 mm/s and the billet height is 200 mm, the measurement period is longer than 80 s. The output signal may or may not be viewed as a periodic signal, and there may be different way to process it, depending on the objectives of the study. Here, only the frequency of the signal that has been added due to the interaction between the measurement systems is evaluated.

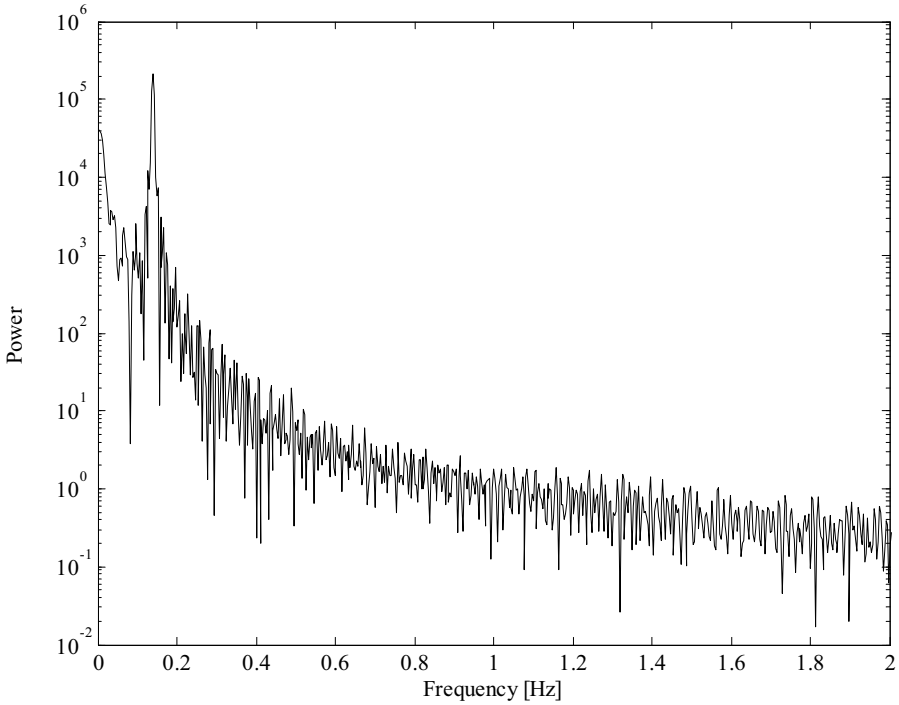

Figure 5.13. The power spectrum in the frequency range from 0 to 2 Hz for liner load measurements of run B07 and sensor 6.

Figure 5.13 shows the power spectrum (i.e. the magnitudes of the various frequency components) of the liner load signal of sensor 6. The Fast Fourier Transform has been used to produce the spectrum [MatW]. In all 8192 sampling points were used. Only the lower frequency range is shown. The peak of the distribution is at approx 0.1392 Hz, which corresponds to a period of approx 7.18 s. While the same observation was made by manual inspection of the response in the time domain, the results from the discrete Fourier analysis may far more easily be used in automated signal processing. It is much more difficult to distinguish the superposed undesired waveforms for the other sensors, since they are of smaller amplitude. The frequencies of the superposed signals always seem to be similar for the different sensors. In such a case, it is probably possible to use only the results from sensor 6 to distinguish the frequencies that should be removed.

Matlab uses the Z-transform, of which the discrete Fourier transform is a special case, to filter signals. The Matlab theory reference provides a description of the mathematical theory of filtering. The relationship between the filtered, $Y_o(z)$, and non-filtered transforms $Y_i(z)$ may be written as:

$$Y_o(z) = H(z)Y_i(z) = \frac{b(1) + b(2)z^{-1} + \ldots + b(n+1)z^{-n}}{a(1) + a(2)z^{-1} + \ldots + a(n+1)z^{-m}} Y_i(z) \qquad (5.7)$$

H(z) is the filter function, and the coefficients *a(i)* and *b(i)* should be tuned to optimise it. Matlab provides users with many techniques for establishing the coefficients *a(i)* and *b(i)*. In the current study, only the Finite Impulse Response (FIR) filter has been evaluated. It is a non-recursive moving average filter. The denominator of the filter function is a constant, i.e. $m = 0$. The *filtfilt* function processes the data both in the forward and reverse directions and performs zero phase digital filtering. It uses the filter function in Matlab, but suppresses effects at the start and the stop of the series. The stop band is in the range from 0.12 to 0.16 Hz.

Figure 5.14 compares the original and the filtered signals. The filter is obviously not optimal, but the waveform that has been added due to the interaction between the measurement systems has to a large extent been suppressed. Results from manual filtering are also shown. A purely sinusoidal curve has been tuned so that it as closely as possible approximates the superposed signal. The sinusoidal curve is subtracted from the measurement signal. The outcome could probably in this case have been better. If proper suppression is to be achieved in the full time range, frequencies have to be determined with three digit accuracy at least. It is possible that the signal amplitude, phase and frequency may change during measurement. When filtering is performed for the other sensors, the outcome may be more satisfactory, because the sensor responses are in the first place much less affected by the crosstalk. The original amplitude of the beating signal is usually smaller than 0.3 μm. After filtering, it may be only 0.05 μm or approx 2 to 3 % of full scale for the measurements. For many purposes, this may be completely acceptable. It should be realised, however, that the unphysical components have been added to measurement signals. Therefore, the results that have been obtained during measurement with two sensor systems have not been used to study effects of very small magnitude.

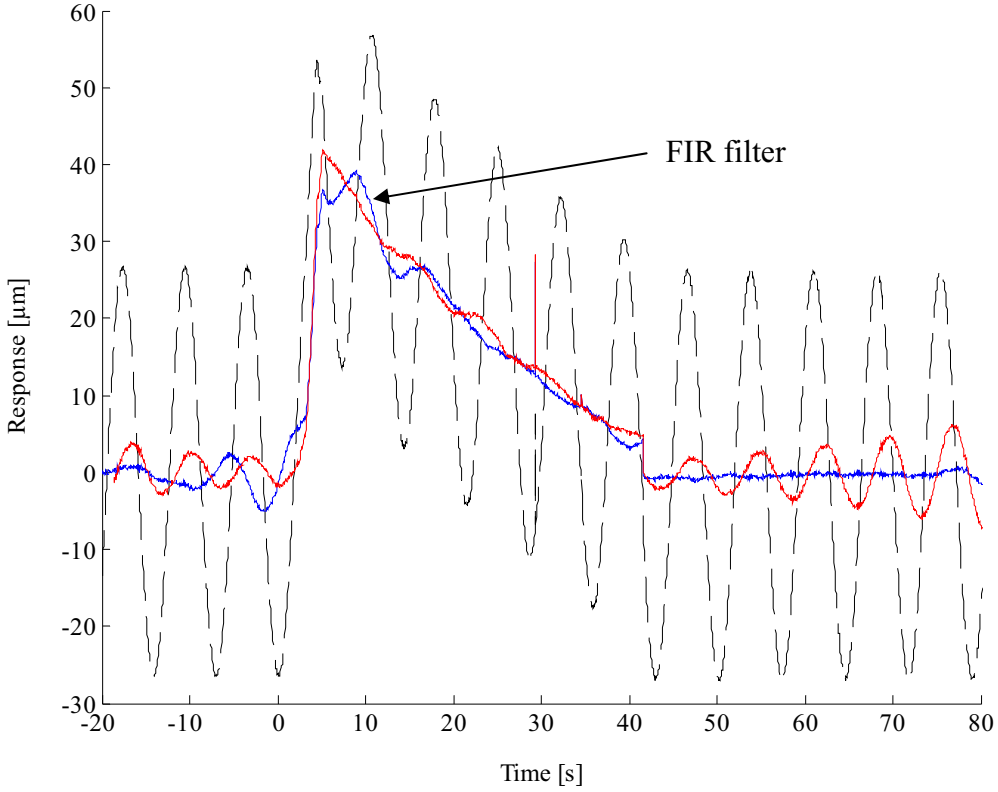

Figure 5.14. Liner load measurement results for sensor 6 and run B07. The dashed lines represent the raw data. The FIR filter gives the best suppression of the undesired waveform in the phase after unloading.

5.5 Some observations on the dynamic sensor behaviour

When a range of waveforms are suppressed by filtering, no distinction is in principle made between the responses of physical origin and pure noise. In the previous example, all signal components of frequency between 0.12 and 0.16 Hz were suppressed. The frequency of the superposed signal was, however, often very similar to the frequencies of the various physical responses of the system. The wavelength of the superposed signal is sometimes comparable to the loading time. In this sub-section an example of a load perturbation, whose cause may be relatively easily found, is first presented, and a pressure oscillation phenomenon that requires more accurate studies, is then assessed.

There were three reasons for running high-rate extrusion experiments as defined by the cases 25 to 27 (Table 5.1). The profile velocity was 1600 and 2400 mm/s. If the ram velocity is regarded as an input variable, cases 25 and 26 are both a part of the factorial design. If the profile velocity is the input variable, the cases may be used to check the validity of regression relations at very high outlet velocities. The most important reason for performing high-rate extrusion, however, was to provoke load/pressure oscillations. Such oscillations may occur if the material melts in the bearing channel, or if the profile sticks to the die after having left the die outlet. The two phenomena are often closely related. When the profile sticks to the die, the extrusion pressure may increase rapidly

and the outlet may get plugged. While plugging may be hard to avoid when extruding complex thin-walled profiles, it is not easy to provoke during rod extrusion.

Figure 5.15 and Figure 5.16 present results from ram/extrusion pressure and the average die face pressure measurements from case 27 and run E23. The ram velocity was 31.7 mm/s, the initial billet temperature was approx 500 ºC, the extrusion ratio was 80, and there was a bearing of length 8.5 mm. Only measurement of the die face pressure was performed, and the signals were not filtered or modified in any way.

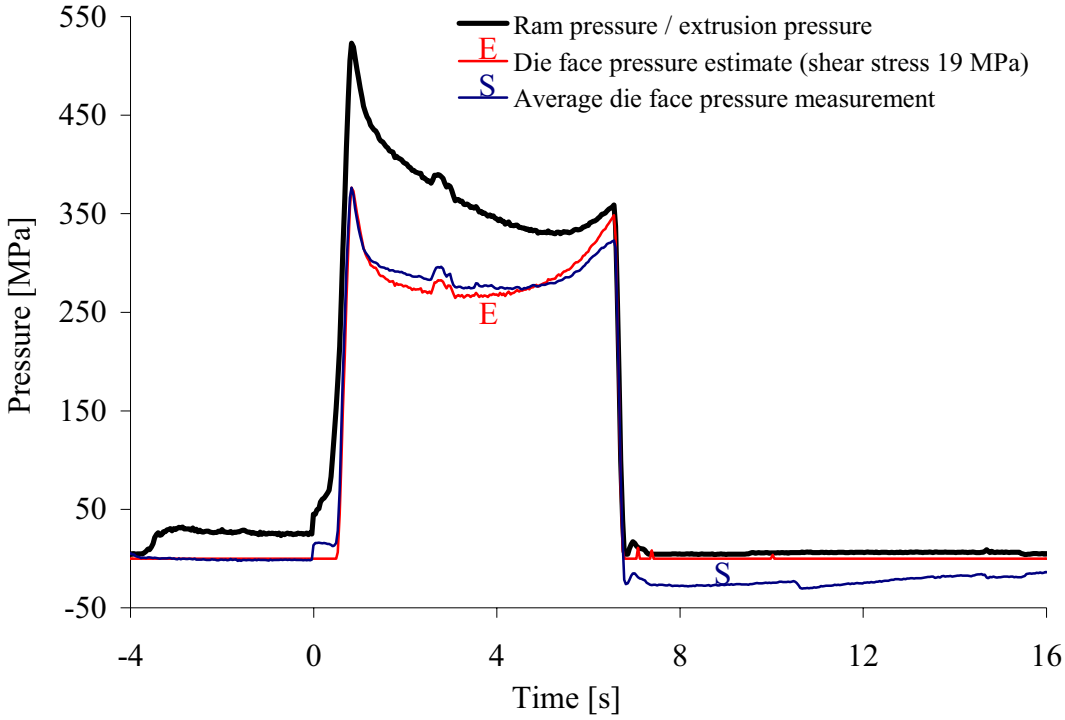

Figure 5.15. Results from ram force and die face pressure measurement for case 27 (run E23). The average pressure is based on results from all sensors.

At time 2.5 s there was a quite sharp increase in the load. The perturbation lasted approx 0.5 s. Figure 5.16 presents a magnified view of the loading phase of Figure 5.15. A die face pressure estimate has been established by subtracting a liner load corresponding to a mean container-billet interface shear stress of 19 MPa from the ram force. Thus, the estimate contains the very same information as the ram force / extrusion pressure curve. A shear stress of 19 MPa is merely an approximate value. It is in fair accordance with the results from the experiments run at other levels of the input parameters. The issue is treated more thoroughly below. Here, it is important that the choice makes possible a comparison of the pressure measurement data and ram force-based estimates.

Figure 5.16 contains interesting information about the pressure sensor response. While the trends in die face pressure estimate and measurement may differ due to thermal effects, predictions of step changes should be quite similar. The pressure change was approximately 15 MPa, and the extrusion and die face pressures did not significantly

differ. The same observation was made when performing experiments with the simple die design. The experiments were not repeated with the complex die design, but the current plugging example is probably a better and more interesting test of the sensor capabilities. The magnified picture of die face pressure curves shows that even smaller pressure perturbations may be observed with the die face pressure measurement system. However, it may be hard to distinguish changes in pressure significantly smaller than 3 MPa. This corresponds to a sensor disc deflection of approximately 0.3 µm. One should consider the effect of noise on measurements. The directly measured die face pressure curve has a smoother appearance mainly due to the fact that it is based not upon results from measurement with one sensor, but with three (an average value).

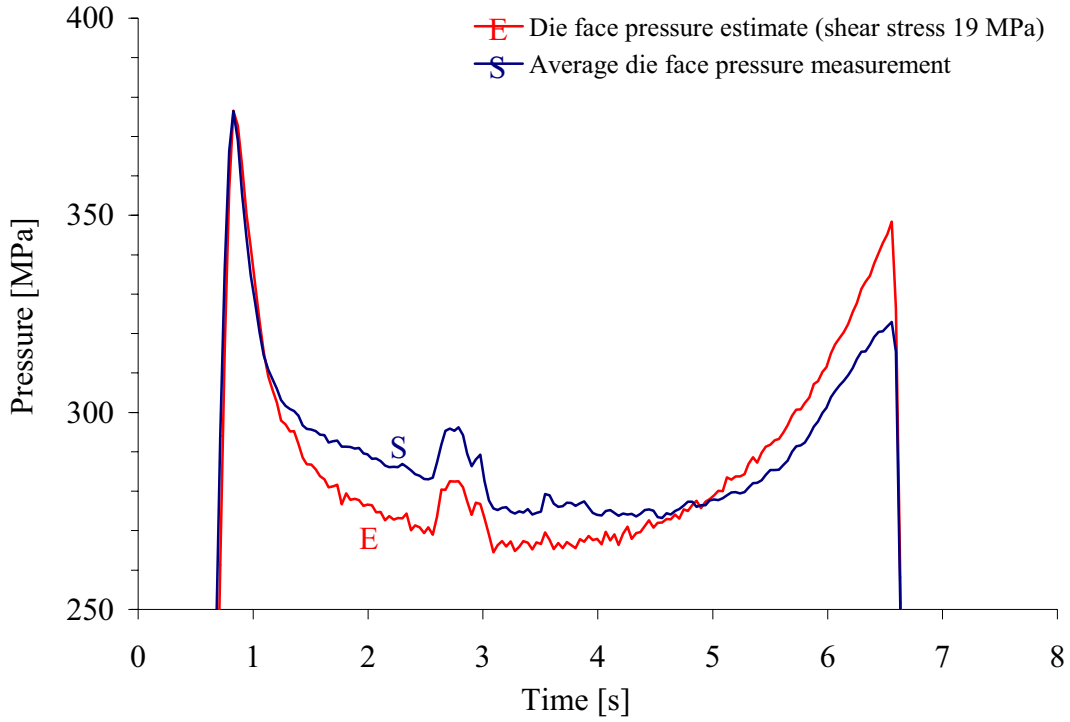

Figure 5.16. Results from the ram force and die face pressure measurement for case 27 (run E23). The average pressure is based on results from all sensors.

Two additional comments should be made with regard to the appearance of Figure 5.15. First, the increase in load at time t = - 4 s is mainly due to the movement of the ram along the container wall and to the upsetting of the billet. Aluminium is scraped off and accumulated at the end of the billet. The magnitude of the force depends on how tightly the ram fits into the container and on the thickness, temperature and constitution of the aluminium layer. Second, after unloading the sensor response does not return directly to zero, but rather indicates that the pressure is approximately -25 MPa. This is probably mainly due to the fact that the sensor response is affected by the temperature increase due to plastic dissipation during the flow of aluminium. While some sensors did not function properly on day E, results were in fact quite satisfactory during run E23. After some time the sensors again indicated a pressure of approximately zero pressure. Figure 5.8 displays the relative movement of the zero point.

The second example of load oscillations that may be suppressed if a filter is used, are shown in Figure 5.17 and Figure 5.18. Both figures present the results from run B06, which was performed with only the die face pressure measurement system. The ram speed was 5 mm/s, and the extrusion ratio was 40. Zero length bearings were used.

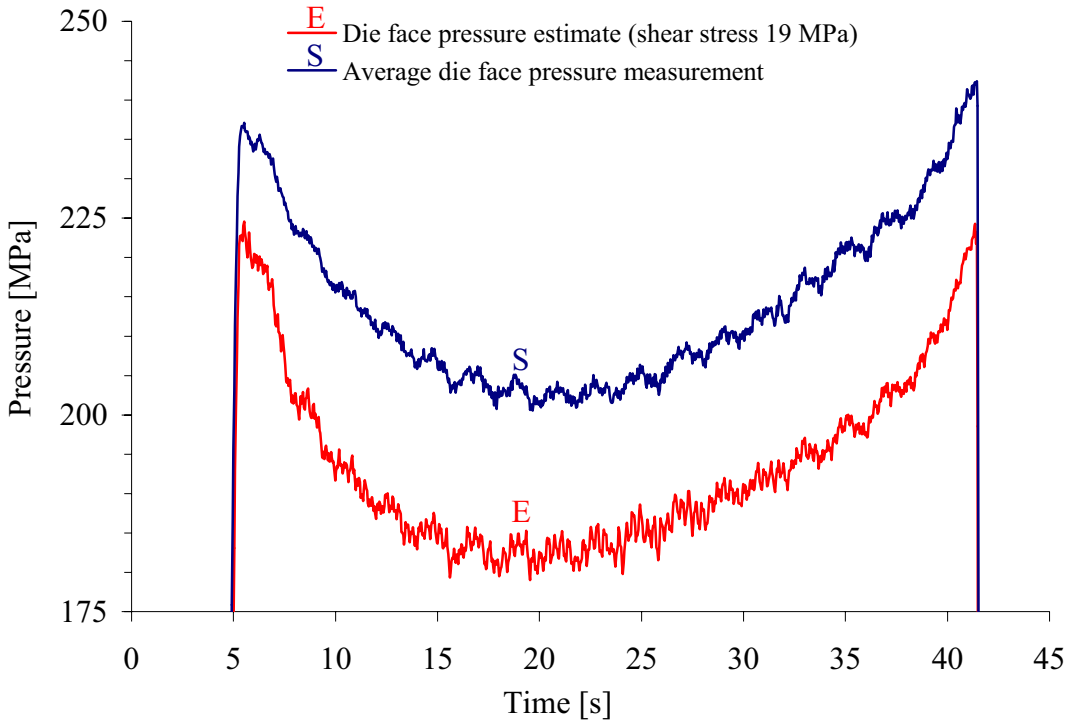

Figure 5.17. Results from ram force and die face pressure measurement for case 1 (run B06). The average pressure is based on results from all sensors.

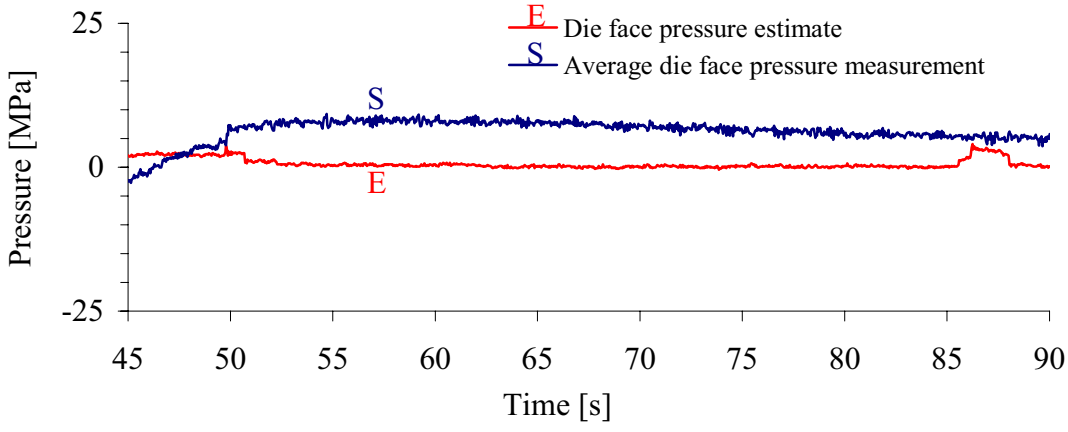

Figure 5.18. Results from ram force and die face pressure measurement for case 1 (run B06). The average pressure is based on results from all sensors.

The interesting features of the graphs are the pressure or load oscillations of frequency of approx 0.5 Hz and amplitude of approx 3 MPa (or 0.3 µm). The oscillations of the extrusion pressure and die face pressure curves were of the same magnitude and

frequency. They were also in phase. The possibility that the oscillations were due to noise may not completely be ruled out. Figure 5.18 shows, however, that there were no oscillations after extrusion. Oscillations were observed during all rounds and for most cases, but were slightly less significant on the last days of experiment. In Figure 5.16, for example, they were hardly visible. Figure 5.19, which shows results from run B04 run at ram velocity 20 mm/s and billet temperature 450 ºC (Case 3), indicate that they occurred during high-rate extrusion. However, they were less distinct than for extrusion at low rate, and the pressure sensor signal was less similar to the ram pressure signal.

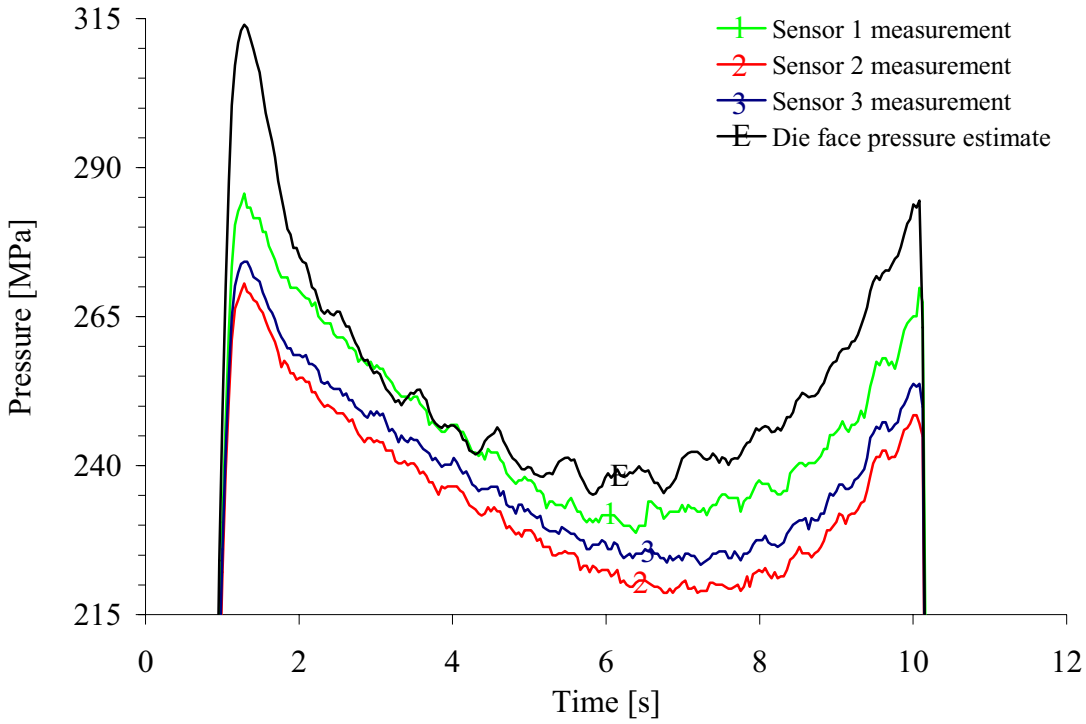

Figure 5.19. Results from ram force and die face pressure measurement for case 3 (run B04). The average pressure is based on results from all sensors.

It is quite likely that oscillations in the pressure sensor responses were due to physical changes in the distance between the sensor disc and the capacitive probe. As ram force and die face pressure signal oscillations generally were closely correlated, it also seems reasonable that they were both caused by real pressure changes. There may be a number of reasons for pressure oscillations. Friction conditions in a choked bearing channel may change during extrusion. Feder and co-workers [Fed02] have performed experiments with transparent model materials and dies, and therefore been able to optically study the flow in bearing channels and in the outlet region. The boundary between the sticking and slipping regions was not static, but was rather continuously modified. While there are random motions, friction mechanisms and flow behaviour are at the same time strongly linked. Pressure oscillations were observed when there are no bearing surfaces and stick-slip phenomena. Shearing of the material at a sharp die outlet both require and cause thermo-mechanical waves in the deforming material [Ast01]. Extrusion is in this respect similar to metal cutting, a process in which the mechanical vibrations are more

evident. Neither at the microscopic nor at the macroscopic level should extrusion of aluminium be regarded as a static process. One should consider the possibility that the extrusion die to some extent responds dynamically to loads and that the die deflection and flow problems are coupled. During rod extrusion, however, changes to the outlet shape should be of moderate magnitude and effect. The causes and effects of pressure oscillations in relation to plastic deformation will not be further discussed. It may, however, be important to understand completely the nature of such oscillations when treating the problem of flow stability for complex profiles.

One should not completely rule out the possibility that the mechanical behaviour of the pressure sensor itself causes signals to oscillate or at least modifies oscillating signals. First, the probe may have some freedom to move relative to the die and the sensor disc. Connections are never perfect, and a pressure change of 3 MPa corresponds to relative displacements of only 0.3 μm. With the current sensor design such small displacements may not be accurately controlled. Sensor 1 was fastened with a spring, and even though the probe holder was tightly fitted into the sensor hole, there may have been relative movements that were not properly controlled. Second, the die face pressure sensor disc may have behaved dynamically when exposed to load changes. Since the disc was very stiff and had a relatively small mass, it probably responded rather quickly. However, the pressure sensor disc and the surrounding elasto-viscoplastic medium were parts of one system. When the pressure increased, a further deflection of the sensor disc occurred. Then, the material of the billet close to the sensor had to flow. Even though deflections were very small, there was a delay in the response of the system. Most sensors have a response time of a finite duration. Therefore, the measurement signals may be out of phase, and pressure oscillations may not be properly represented by the sensor system. The figures presented so far indicate, however, that the response of the die face pressure sensor is not significantly poorer than that of the ram force measurement. The reason is probably that hot aluminium flows easily when exposed to deviatoric stresses of large magnitude. The response time of the system should be very small.

As indicated in the previous chapter the sensor behaviour may be quite complex at low temperature when the behaviour of aluminium must be characterised as fully elasto-viscoplastic. Deviatoric stresses must exceed a lower limit to cause the material to flow. During loading there may be a load redistribution causes the response of the sensor to deviate from that observed when there is a uniform die face pressure. Figure 5.20 displays a simple model describing elasto-viscoplastic sensor behaviour during the loading phase. Only the part of the billet closest to the sensor deforms plastically, and then along thin slip bands (width d). Only a simplified and non-physical type of sensor disc deflection is here described. First, the load is applied mainly close to the periphery of the sensor disc. It causes the disc to deform. As the deviatoric stresses increase, slip bands are activated closer to the centre of the disc. One may envision that there is only one slip band that moves radially towards the centre of the sensor disc as a wave when the deviatoric stresses are sufficiently high. In reality, there is probably no distinct cavity, but the contact is initially less intimate close to the centre of the disc. Deformation may occur simultaneously along many slip bands. The proposed elasto-viscoplastic model seems to be of some relevance during low temperature compression

testing. The problems related to the use of low temperature compression testing as a test or calibration case for the sensor have been treated in both Chapters 3 and 4.

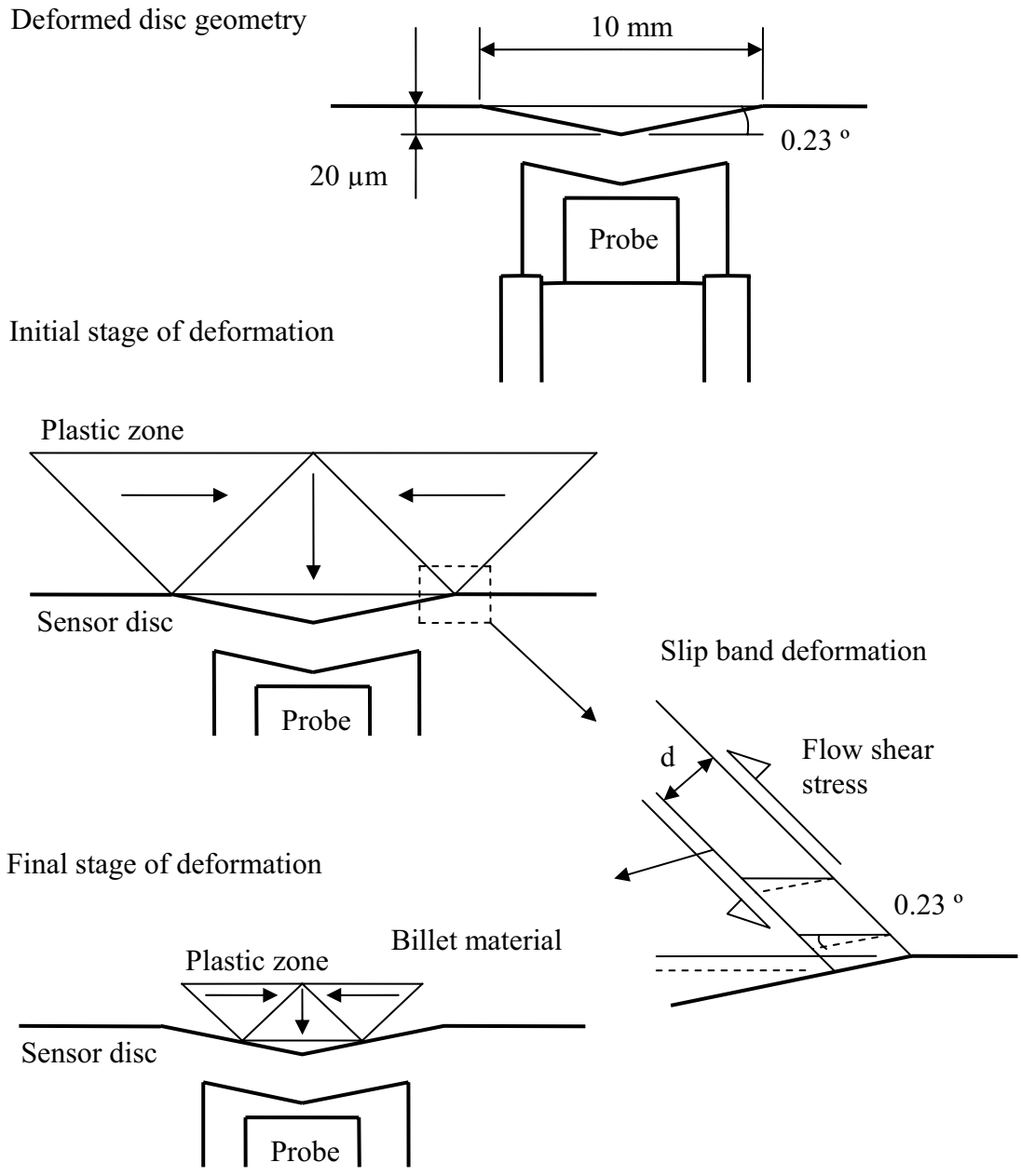

Figure 5.20. A possible mechanism of elasto-viscoplastic deformation. An upper bound analysis may be used to evaluate the some aspects of the problem.

The proposed model is less relevant for pressure measurement during extrusion since the temperature and loads are very high. The pressure is probably uniform at all times, and there is always an intimate contact between the billet and the container. The model

is, however, interesting because it provides an estimate of the strains that are caused by the sensor disc deflection. Also the response time of the sensor may be estimated. It may be assumed that the material deforms merely by shearing, as shown in Figure 5.20. If the total deflection of the disc is 20 μm, and the disc surface is depressed inside a circle of radius 10 mm, the maximum accumulated shear strain of a material element would be approximately 0.0040. The corresponding equivalent shear strain is 0.0023.

In order to estimate the time that is required to cause such a deformation, the material may be assumed to deform visco-plastically according to the Zener-Hollomon flow rule. Relevant material data have been presented in [Moe04b]. α = 0.0368 MPa^{-1}, Q = 180943 J/(molK), $A = 3.90 \cdot 10^{11}$ s^{-1} and m = 4.8. The initial temperature of the billet is higher than 400 ºC. In order to determine the strain rate, the flow stress must be known. Both strain rates and stresses may be deduced from the equation of conservation of momentum, the boundary conditions and the Zener-Hollomon equation. Only a rough estimate of the strain rate is here produced, and it is assumed that the equivalent flow stress is approximately 25 MPa. Much smaller stresses may probably cause the billet material to adapt to the changes in the topology of the tool surface. The calculation corresponds to a situation in which an element is stressed and suddenly allowed to deform. The strain rate should in an approximate manner be given by Equation 5.8:

$$\begin{aligned} \frac{\Delta\bar{\varepsilon}}{\Delta t} \approx \dot{\bar{\varepsilon}} &= \left(\sinh\left(\alpha\sigma_f\right)\right)^m A \exp\left(-\frac{Q}{RT}\right) \\ &= \left(\sinh\left(0.0368 \cdot 25\right)\right)^{4.8} \cdot 3.90 \cdot 10^{11} \exp\left(-\frac{180943}{8.314 \cdot 673.15}\right) s^{-1} = 0.0046 s^{-1} \end{aligned} \qquad (5.8)$$

If the strain rate is constant during deformation, a single slip band shears within a time interval of approx Δt = 0.0023/0.0046 s = 0.5 s. If the material deforms in the hot state, all slip bands deform more or less simultaneously as the sensor disc deflects. It would not be correct to regard 0.5 s as the response time of the sensor. The calculation is only approximate and based on a number of assumptions that have not been properly tested and are probably not entirely valid. The pressure measurement curves seem to indicate that the response time is shorter than 0.5 s. Furthermore, when the die face pressure only changes moderately, very small amounts of material have to flow, and the time required would be less significant. The important conclusion to be drawn from the above analysis is, however, that there may be some slowness in the sensor response due to very special nature of the flow of aluminium. The delay in the response of sensors mainly seems to affect loading and unloading phases during extrusion, and the effects may probably be neglected even then. The section on calibration experiments (Chapter 4) provides an example where the response time may affect measurement results during loading and unloading. It should be realised, however, that also the ram force measurement system has a finite response time. During the phases of loading and unloading, hydraulic oil flows in the press system. As a consequence, there are pressure differences, and the transducers may not accurately show the hydraulic pressure applied on the ram. Hence, during dynamic loading one must probably expect some differences in die face pressure data based on direct measurement and ram force measurement.

5.6 Results from runs

The remaining part of this section provides an overview of all essential results obtained during extrusion experiments with the complex rod extrusion die. Cases are presented in ascending order. It has been found natural, however, to directly compare results from runs performed with zero and long bearing channels. Thus, results from cases 1 and 13, 2 and 14 etc are presented in the same figures.

The presentation of results from a run contains a table that displays both nominal and actual values of the input parameters as well as a first statistical treatment of the output data. The billet temperature was measured with a thermocouple both in the front and back end of the sensor immediately before the billet was placed in the container. The temperature of the dummy block was measured immediately afterwards. The variability in the temperature data must be regarded as moderate.

Characteristic data from all runs have been deduced for remaining billet heights of 196, 170, 100 and 30 mm. Also maximum and minimum values of the ram force are shown in the tables. The maximum value of force was registered at the outset of the extrusion run. Since the remaining butt end was relatively long (19 mm), the minimum force value was usually measured just before the extrusion ended. As earlier indicated, no distinction is made between the terms “billet height” and “billet length” since extrusion was performed in the vertical direction.

Data from each individual run as well as estimates of the average and standard deviation values for each case are shown. The measure of variability used in the current work is generally the sample variance s^2. If the result from each run is denoted y_i and there are in all n runs, the sample variance is expressed by:

$$s^2 = \frac{\sum_{i=1}^{n}\left(y_i - \bar{y}\right)^2}{n-1} \quad \text{where} \quad \bar{y} = \frac{1}{n}\sum_{i=1}^{n} y_i \tag{5.9}$$

The tables do not present the results for each individual pressure sensor, but rather the average value for all three pressure sensors for every run. When treating the pressure measurement results, a distinction should be made between the measure of variability of the data from all sensors during a single run (calculated below the average value for each run) and the variability of the averaged data for all runs of a case (shown in the rightmost column of the sheets). The main purpose of performing three parallel replicate measurements of the pressure was to expose sensors to equivalent thermo-mechanical conditions. The variability of sensor output data for a single run is mainly related to the calibration. Differences in the pressure sensor output from one run to next may be due not only to the sensor behaviour, but also be caused by real differences in the pressure due to poor process control. Figure 5.21 and Figure 5.22 present the applied ram speed of all cases and runs. As indicated by the data for the variability in force measurements the replication of the runs was usually quite satisfactory. The tables present the average values and standard deviation for all input data. The billet temperature was generally 5 ºC lower than the nominal value, but only surface measurements were performed.

The treatment of the liner load data is similar to that of the die face pressure data. Only curves for average values are presented. No description of the measurement variability is provided in the tables, but the figures give an indication. The variability in absolute values is, as indicated in the discussion on calibration techniques, quite significant. The most appropriate approach is to treat only average values of liner load for all capacitive sensors of the cell. The mean value of the container shear stress has been calculated on the basis of the average liner load measurements for the billet length is totally 170 and 100 mm. The estimate is most probably too high, because the friction between the ram and the container has not been considered. The clamping force has also been neglected.

For all cases, there are figures showing the main responses of the system as a function of the remaining billet length:

- the ram force
- the die outlet temperature (bearing inlet)
- the die face temperature (at a depth of 1 mm and in the pressure sensor position)
- the average value of the liner load with scatter
- the output from all three pressure sensors

Additionally, the average die face pressure has been plotted as a function of the time. The purpose is to give an indication of the response of the sensor immediately before and after extrusion. The advantage of using the average pressure rather than the results from any individual pressure sensor is that systematic errors are more prominent than the random ones. The discussion on systematic and random errors was started in Chapter 4 and is continued in Chapter 6.

Results from a number of runs have been presented in all figures in order to give an indication of the scatter in results. Various symbols have been added to make it easier to identify graphs and to indicate where measurement data presented in the tables have been found. The die face pressure and container liner force data have been treated as described above. The results from the runs in which both measurement systems were used, have also been presented. Table 5.3 makes it possible to identify the runs.

Results from the simulations with ALMA2π presented in the previous section have been added in most of the figures. The reason is mainly that the curves simplify a comparison of various measurement data. The ALMA2π model has a number of weaknesses, and the deviation between the simulated and experimental results should not be regarded only as an expression of the measurement error. Both simulated and measured results are most probably in error. Estimates from ALMA2π are presented with a thick dashed line. Only the cases of zero bearing have been studied. When a bearing channel is added the ram force, die face pressure and outlet temperature increase. The build-up of pressure and the temperature change in the bearing channel may be evaluated by comparing results from cases 1 to 12 with results from cases 13 to 24. However, one should take into consideration the fact that the thermal conditions in the die outlet may considerably differ for the cases with and without a bearing channel. A much more thorough assessment of the use of pressure sensors is presented in Chapter 6.

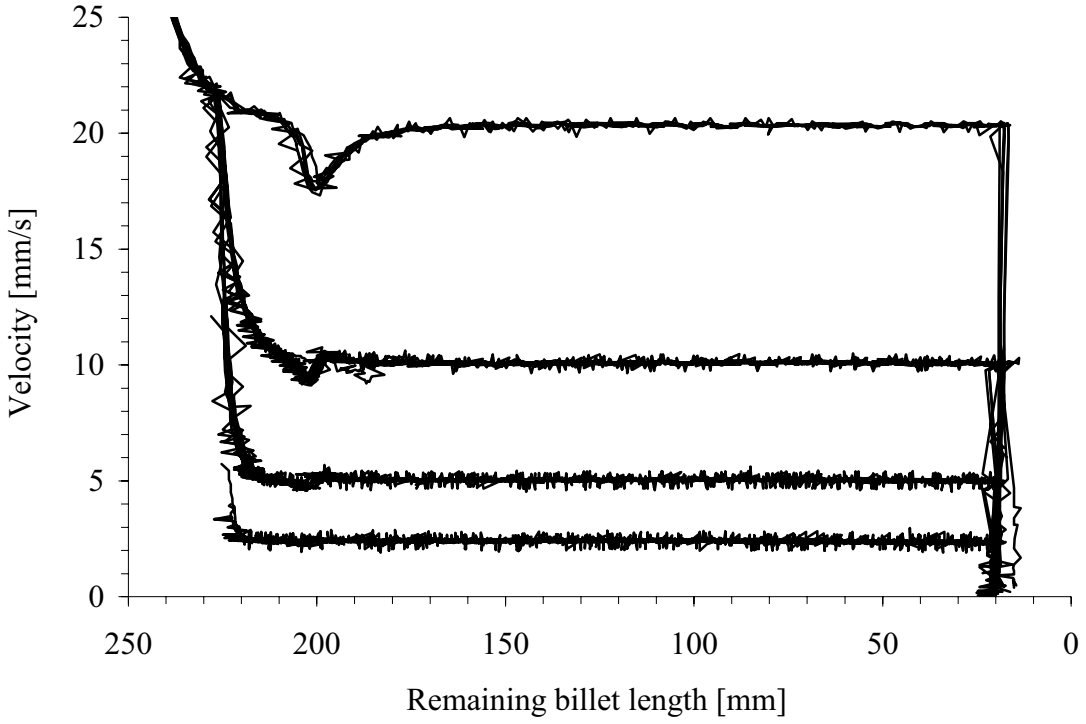

Figure 5.21. Measurement of the ram velocity for cases 1 to 12 (extrusion ratio 40).

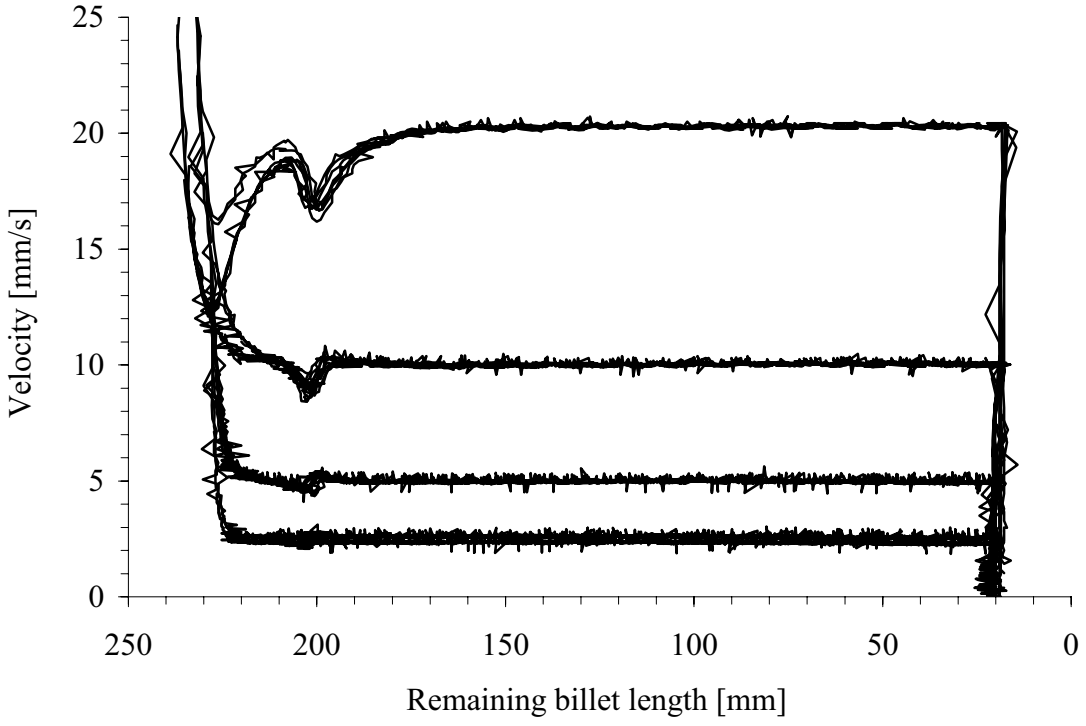

Figure 5.22. Measurement of the ram velocity for cases 13 to 26 (extrusion ratio 80).

Table 5.3. Case 1 – input and output data

SPECIFICATION	CASE	1							
Nominal extrusion ratio		40	-		Die outlet diameter		15.8	mm	
Nominal bearing length		0	mm						
Nominal ram velocity		5	mm/s		Profile velocity		200	mm/s	
Nominal billet temperature		450	ºC						
INPUT DATA	Day/run #	A09	A10	A11	B06	B07		Avg.	St.dev.
Actual velocity [mm/s]	Ram	5.0	5.0	5.0	5.0	5.0	-	5.0	0.0
	Profile	200	200	200	200	200	-	200	0.0
Initial billet surface temperature [ºC]	Front	450	440	442	445	445	-	444	3.8
	Back	446	439	444	443	440	-	442	2.9
	Average	448	440	443	444	443	-	443	3.1
Ram temperature [ºC]	Front	138	149	150	120	123	-	136	14.1
RESPONSE		1	2	3	4	5	6	Avg.	St.dev.
Ram force [kN]	Maximum	3019	3040	2982	3019	3028	-	3018	21.7
	Minimum	1899	1670	1745	1881	1881	-	1815	102.1
	196 mm	2970	2993	2884	2960	2950	-	2951	40.9
	170 mm	2590	2580	2575	2592	2610	-	2589	13.5
	100 mm	2120	2101	2100	2118	2130	-	2114	13.0
	30 mm	1910	1850	1850	1899	1900	-	1882	29.3
Bearing inlet temperature [ºC]	Maximum	506	503	503	504	505	-	504	1.3
	Minimum	428	428	424	429	429	-	428	2.1
	170 mm	500	496	496	498	498	-	498	1.7
	100 mm	505	501	502	504	504	-	503	1.6
	30 mm	497	495	495	494	495	-	495	1.1
Bearing outlet temperature [ºC]	Maximum	-	-	-	-	-	-	-	-
	Minimum	-	-	-	-	-	-	-	-
	170 mm	-	-	-	-	-	-	-	-
	100 mm	-	-	-	-	-	-	-	-
	30 mm	-	-	-	-	-	-	-	-
Die face pressure avg. value [MPa] for all 3 sensors	196 mm	233	232	-	235	228	-	232	3.1
	170 mm	215	212	-	215	214	-	214	1.3
	100 mm	206	204	-	205	204	-	205	0.9
	30 mm	233	224	-	230	231	-	229	3.9
Die face pressure st. dev. value [MPa] for all 3 sensors	196 mm	7.5	8.4	-	7.5	5.5	-	7.3	-
	170 mm	8.0	9.3	-	6.5	4.6	-	7.1	-
	100 mm	8.5	8.0	-	7.1	5.3	-	7.2	-
	30 mm	6.6	8.8	-	12.4	11.5	-	9.8	-
Container / liner force avg. value [kN]	196 mm	-	1320	1296	-	1294	-	1303	103.4
	170 mm	-	1032	992	-	977	-	1000	97.0
	100 mm	-	565	556	-	533	-	551	71.9
	30 mm	-	206	174	-	163	-	181	44.2
Liner friction [MPa]		-	21.2	19.8	-	20.2	-	20.4	0.7

Table 5.4. Case 13 – input and output data

SPECIFICATION	CASE	13						
Nominal extrusion ratio		40	-		Die outlet diameter		15.8	mm
Nominal bearing length		12	mm					
Nominal ram velocity		5	mm/s		Profile velocity		200	mm/s
Nominal billet temperature		450	ºC					

INPUT DATA	Day/run #	D02	D09	D14	-	Avg.	St.dev.	C13 - C1
Actual velocity [mm/s]	Ram	5.0	4.9	4.9	-	4.9	0.1	-0.1
	Profile	200	196	196	-	197.3	2.3	-2.7
Initial billet surface	Front	442	451	448	-	447.0	4.6	2.6
temperature [ºC]	Back	435	442	445	-	440.7	5.1	-1.7
	Average	439	447	447	-	443.8	4.6	0.4
Ram temperature [ºC]	Front	107	147	138	-	130.7	21.0	-5.3

RESPONSE		1	2	3	4	Avg.	St.dev.	C13 - C1
Ram force [kN]	Maximum	3367	3575	3468	-	3470	104.0	58
	Minimum	2119	2246	2243	-	2203	72.5	49
Effect C13 - C1:	196 mm	3270	3310	3326	-	3302	28.8	45
Pressure [MPa]	170 mm	2902	2960	2942	-	2935	29.7	44
	100 mm	2480	2500	2489	-	2490	10.0	48
	30 mm	2304	2295	2269	-	2289	18.2	52
Bearing inlet	Maximum	520	523	524	-	522	2.1	18
temperature [ºC]	Minimum	427	432	432	-	430	2.9	3
	170 mm	516	520	518	-	518	2.0	20
	100 mm	519	522	520	-	520	1.5	17
	30 mm	510	513	512	-	512	1.5	16
Bearing outlet	Maximum	527	530	530	-	529	1.7	-
temperature [ºC]	Minimum	427	432	432	-	430	2.9	-
	170 mm	521	525	523	-	523	2.0	-
	100 mm	526	529	528	-	528	1.5	-
	30 mm	519	521	521	-	520	1.2	-
Die face pressure	196 mm	271	289	280	-	280	9.0	48
avg. value [MPa]	170 mm	248	255	255	-	253	4.1	39
for all 3 sensors	100 mm	243	246	247	-	245	1.9	41
	30 mm	273	271	268	-	271	2.6	41
Die face pressure	196 mm	5.6	6.8	4.0	-	5.5	-	-1.8
st. dev. value [MPa]	170 mm	5.6	6.7	3.3	-	5.2	-	-1.9
for all 3 sensors	100 mm	7.0	7.0	4.0	-	6.0	-	-1.2
	30 mm	9.3	5.1	4.4	-	6.2	-	-3.6
Container / liner force	196 mm	-	-	-	-	-	-	-
avg. value [kN]	170 mm	-	-	-	-	-	-	-
	100 mm	-	-	-	-	-	-	-
	30 mm	-	-	-	-	-	-	-
Liner friction [MPa]		-	-	-	-	-	-	-

.

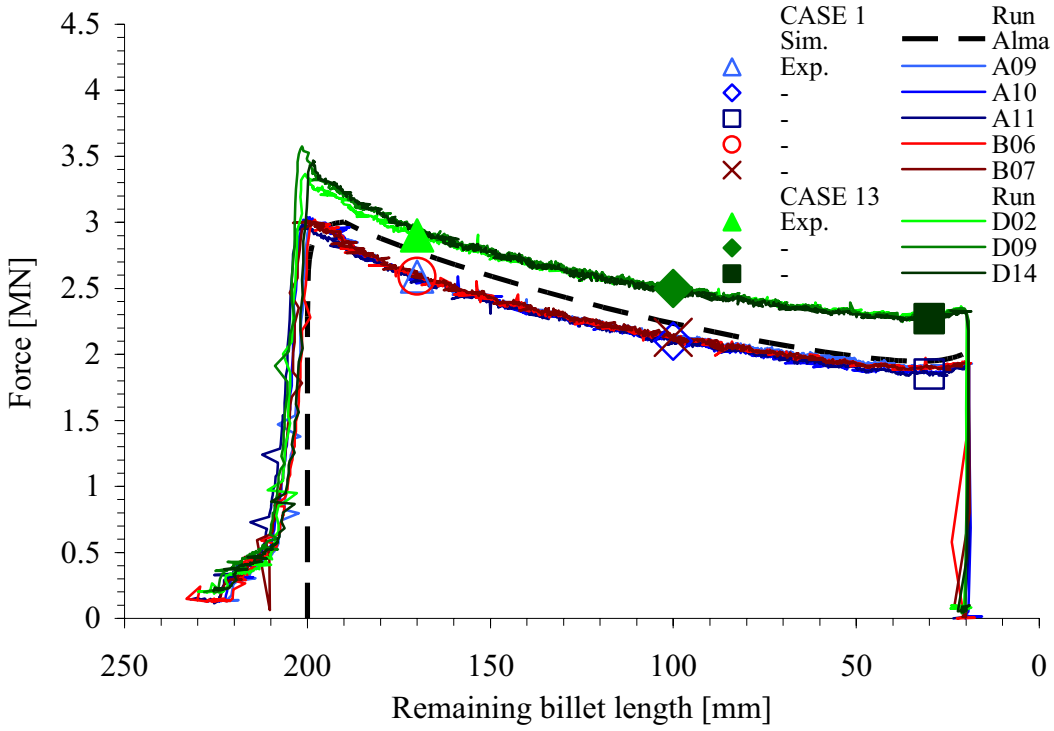

Figure 5.23. Measurement of the ram force - cases 1 and 13 (zero/long bearing).

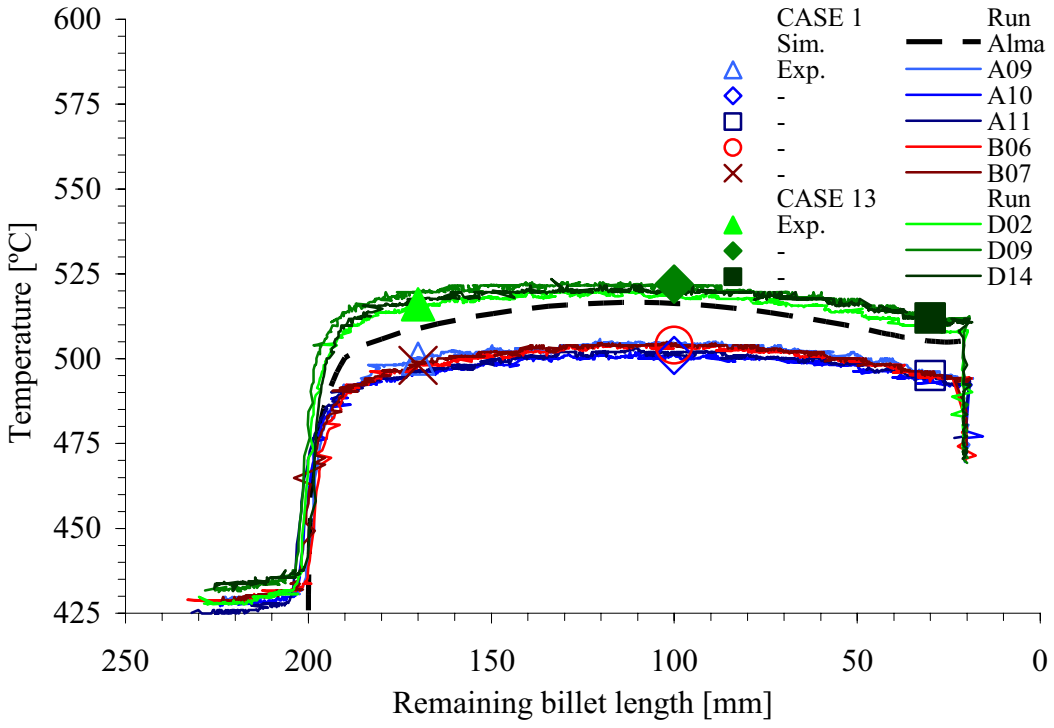

Figure 5.24. Measurement of the outlet temperature (bearing inlet) - cases 1 and 13.

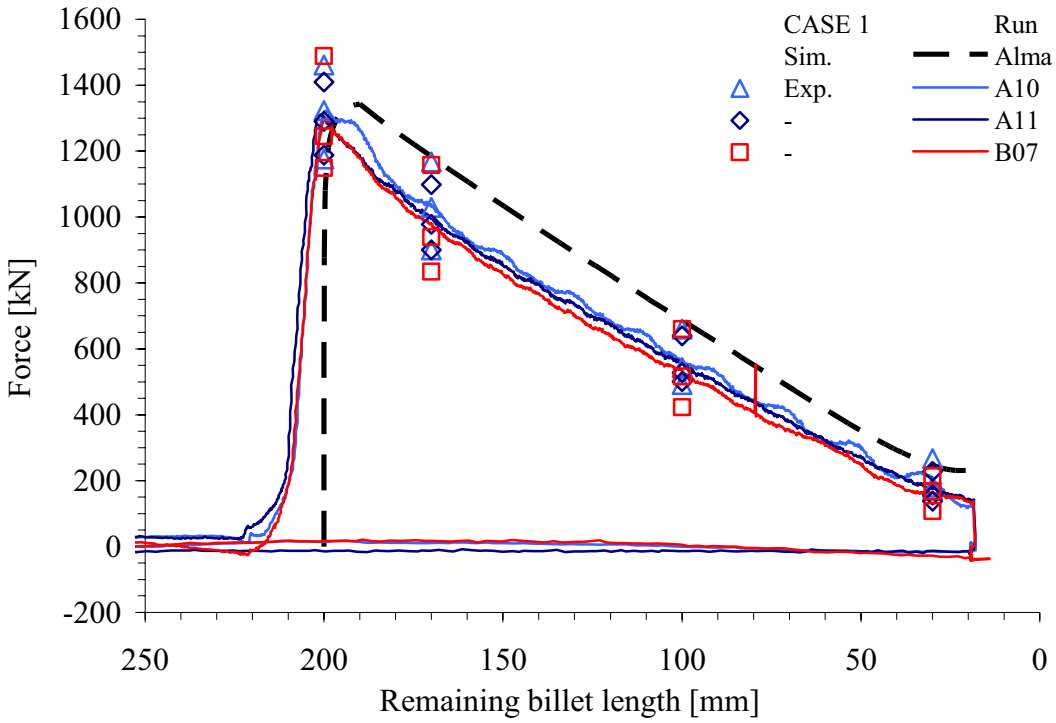

Figure 5.25. Averaged measurement of the container liner force - case 1.

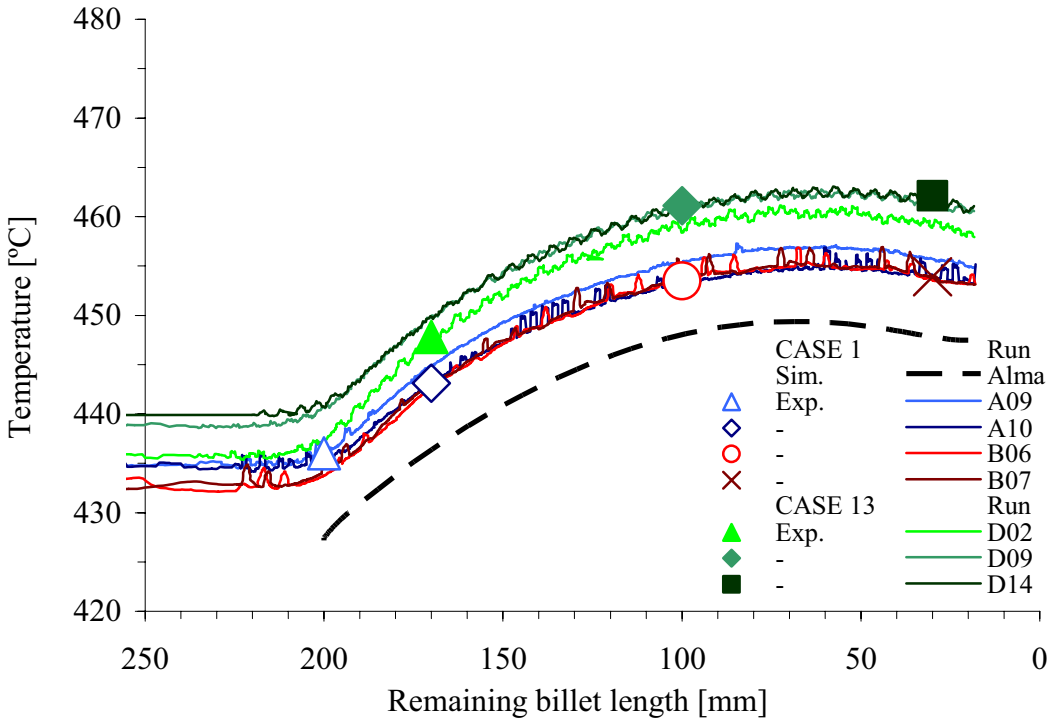

Figure 5.26. Measurement of the die face temperature - cases 1 and 13.

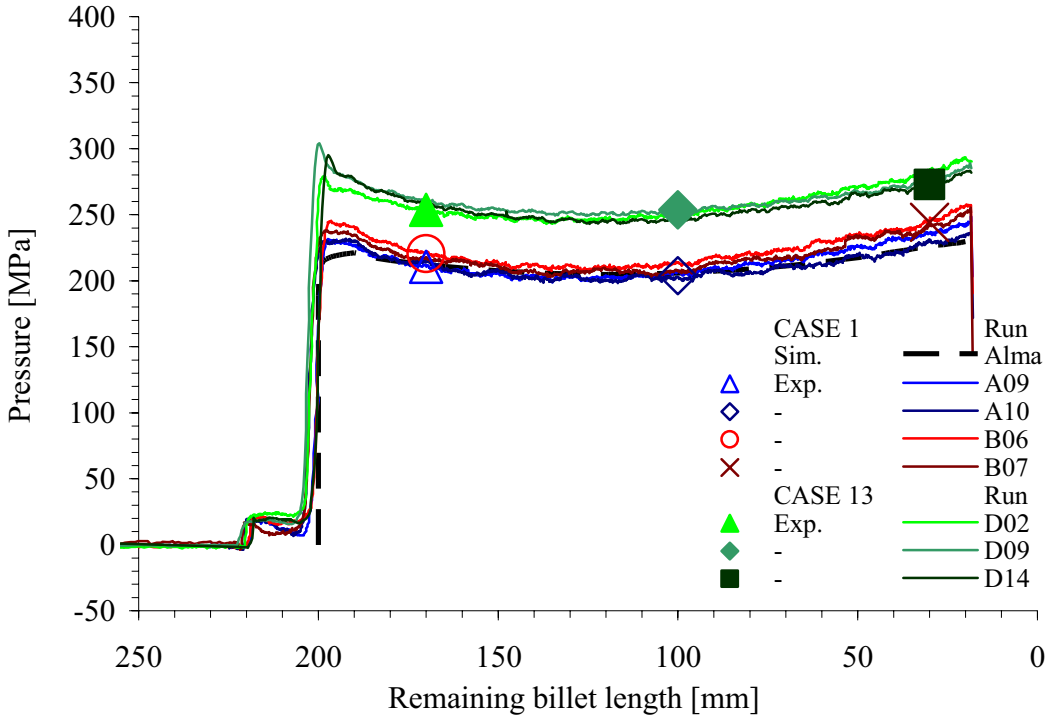

Figure 5.27. Measurement of the die face pressure by sensor 1 - cases 1 and 13.

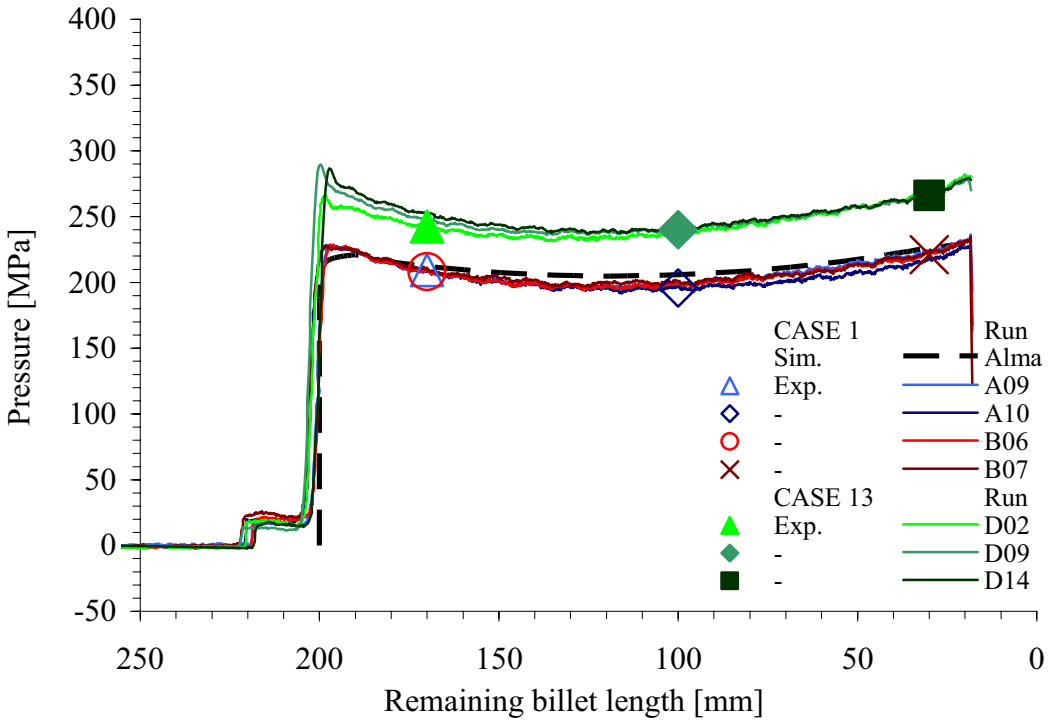

Figure 5.28. Measurement of the die face pressure by sensor 2 - cases 1 and 13.

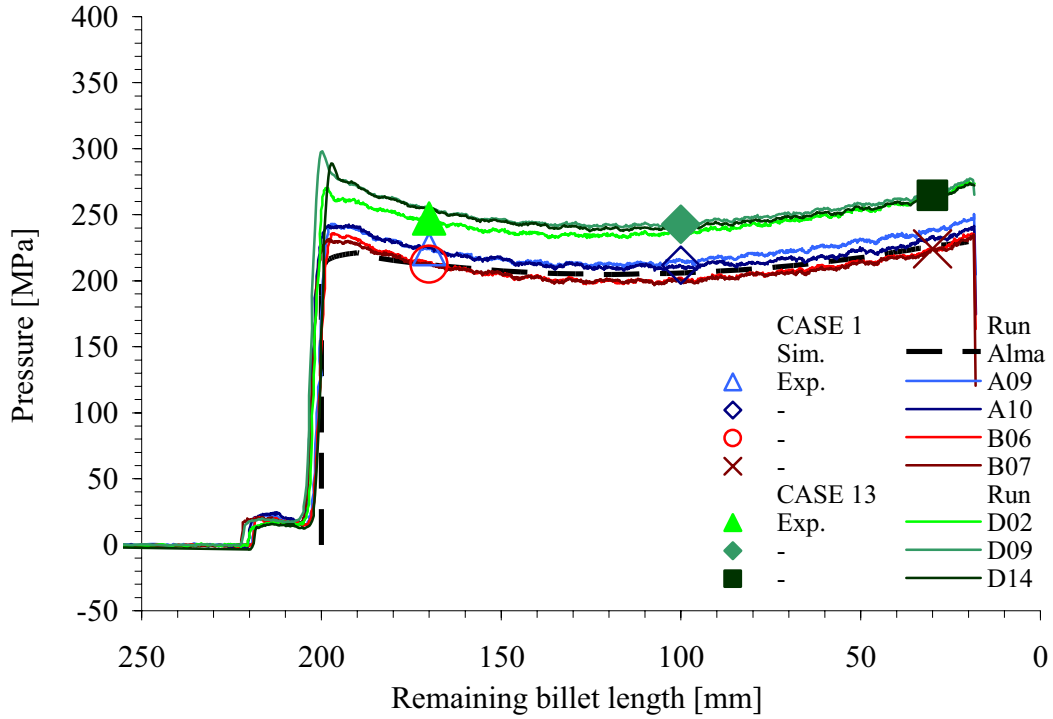

Figure 5.29. Measurement of the die face pressure by sensor 3 - cases 1 and 13.

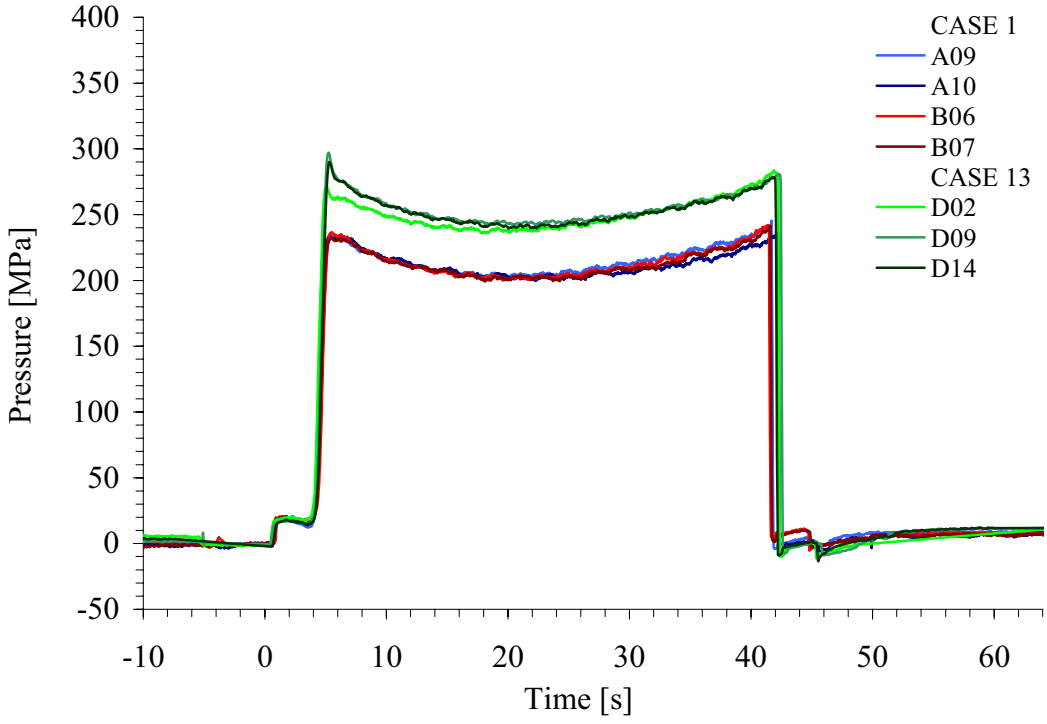

Figure 5.30. Measurement of the average die face pressure - cases 1 and 13.

Table 5.5. Case 2 – input and output data

SPECIFICATION	CASE	2							
Nominal extrusion ratio		40	-		Die outlet diameter		15.8	mm	
Nominal bearing length		0	mm						
Nominal ram velocity		10	mm/s		Profile velocity		400	mm/s	
Nominal billet temperature		450	ºC						
INPUT DATA	Day/run #	A03	A04	A14	B02	B03	B16	Avg.	St.dev.
Actual velocity [mm/s]	Ram	10.1	10.1	10.1	10.1	10.1	10.1	10.1	0.0
	Profile	404	404	404	404	404	404	404	0.0
Initial billet surface	Front	447	450	449	449	449	449	449	1.0
temperature [ºC]	Back	440	443	444	445	447	443	444	2.3
	Average	444	447	447	447	448	446	446	1.5
Ram temperature [ºC]	Front	138	143	130	144	142	115	135	11.2
RESPONSE		1	2	3	4	5	6	Avg.	St.dev.
Ram force [kN]	Maximum	3320	3310	3343	3326	3320	3334	3326	11.7
	Minimum	2020	2000	1826	2037	2017	1916	1969	82.2
	196 mm	3196	3164	3175	3210	3227	3224	3199	25.8
	170 mm	2800	2754	2765	2821	2803	2759	2784	27.8
	100 mm	2255	2240	2220	2297	2240	2228	2247	27.4
	30 mm	2050	2010	2040	2060	2050	2050	2043	17.5
Bearing inlet	Maximum	525	525	528	522	523	523	524	2.2
temperature [ºC]	Minimum	425	426	428	427	429	432	428	2.5
	170 mm	513	514	516	509	510	511	512	2.6
	100 mm	523	522	525	522	521	521	522	1.5
	30 mm	517	517	520	516	516	518	517	1.5
Bearing outlet	Maximum	-	-	-	-	-	-	-	-
temperature [ºC]	Minimum	-	-	-	-	-	-	-	-
	170 mm	-	-	-	-	-	-	-	-
	100 mm	-	-	-	-	-	-	-	-
	30 mm	-	-	-	-	-	-	-	-
Die face pressure	196 mm	261	261	259	261	254	263	260	3.1
avg. value [MPa]	170 mm	244	236	234	236	232	231	236	4.6
for all 3 sensors	100 mm	219	216	213	214	206	209	213	4.6
	30 mm	241	235	236	234	229	231	234	4.4
Die face pressure	196 mm	8.9	11.8	6.7	7.7	6.9	8.6	8.5	-
st. dev. value [MPa]	170 mm	10.1	7.0	6.9	6.4	6.0	7.5	7.3	-
for all 3 sensors	100 mm	9.6	7.0	7.1	6.7	4.8	5.9	6.8	-
	30 mm	9.7	8.4	7.6	10.5	11.5	7.5	9.2	-
Container / liner force	196 mm	1440	1428	1439	-	1356	1098	1352	168.9
avg. value [kN]	170 mm	1086	1098	1072	-	1070	958	1057	108.9
	100 mm	631	609	615	-	582	526	593	92.28
	30 mm	221	201	221	-	191	165	200	53.62
Liner friction [MPa]		20.7	22.2	20.8	-	22.2	19.6	21.1	1.1

Table 5.6. Case 14 – input and output data

SPECIFICATION	CASE	14						
Nominal extrusion ratio		40	-	Die outlet diameter		15.8	mm	
Nominal bearing length		12	mm					
Nominal ram velocity		10	mm/s	Profile velocity		400	mm/s	
Nominal billet temperature		450	ºC					

INPUT DATA	Day/run #	D16	D17	D21	-	Avg.	St.dev.	C14 - C2
Actual velocity [mm/s]	Ram	10.0	10.0	10.0	-	10.0	0.0	-0.1
	Profile	400	400	400	-	400.0	0.0	-4.0
Initial billet surface	Front	446	450	452	-	449.3	3.1	0.5
temperature [ºC]	Back	446	442	440	-	442.7	3.1	-1.0
	Average	446	446	446	-	446.0	0.0	-0.3
Ram temperature [ºC]	Front	140	128	128	-	132.0	6.9	-3.3

RESPONSE		1	2	3	4	Avg.	St.dev.	C14 - C2
Ram force [kN]	Maximum	3760	3771	3823	-	3785	33.7	58
	Minimum	2335	2341	2344	-	2340	4.6	47
Effect C14 - C2:	196 mm	3549	3494	3633	-	3559	70.0	46
Pressure [MPa]	170 mm	3088	3075	3095	-	3086	10.1	38
	100 mm	2570	2575	2580	-	2575	5.0	42
	30 mm	2373	2375	2380	-	2376	3.6	42
Bearing inlet	Maximum	544	544	542	-	543	1.2	19
temperature [ºC]	Minimum	433	433	433	-	433	0.0	5
	170 mm	537	537	536	-	537	0.6	25
	100 mm	543	543	430	-	505	65.2	-17
	30 mm	538	537	536	-	537	1.0	20
Bearing outlet	Maximum	553	554	553	-	553	0.6	-
temperature [ºC]	Minimum	433	433	433	-	433	0.0	-
	170 mm	545	544	543	-	544	1.0	-
	100 mm	553	552	551	-	552	1.0	-
	30 mm	548	548	547	-	548	0.6	-
Die face pressure	196 mm	315	311	-	-	313	2.7	53
avg. value [MPa]	170 mm	272	270	-	-	271	1.1	36
for all 3 sensors	100 mm	248	249	-	-	249	0.7	36
	30 mm	266	268	-	-	267	2.0	34
Die face pressure	196 mm	6.2	4.4	-	-	5.3	-	-2.3
st. dev. value [MPa]	170 mm	6.3	3.4	-	-	4.8	-	-2.6
for all 3 sensors	100 mm	4.3	1.2	-	-	2.7	-	-4.0
	30 mm	4.7	3.5	-	-	4.1	-	-5.5
Container / liner force	196 mm	-	-	1139	-	1139	-	-192
avg. value [kN]	170 mm	-	-	1021	-	1021	-	-32
	100 mm	-	-	584	-	584	-	-3
	30 mm	-	-	224	-	224	-	30
Liner friction [MPa]		-	-	19.9	-	19.9	-	-1.3

.

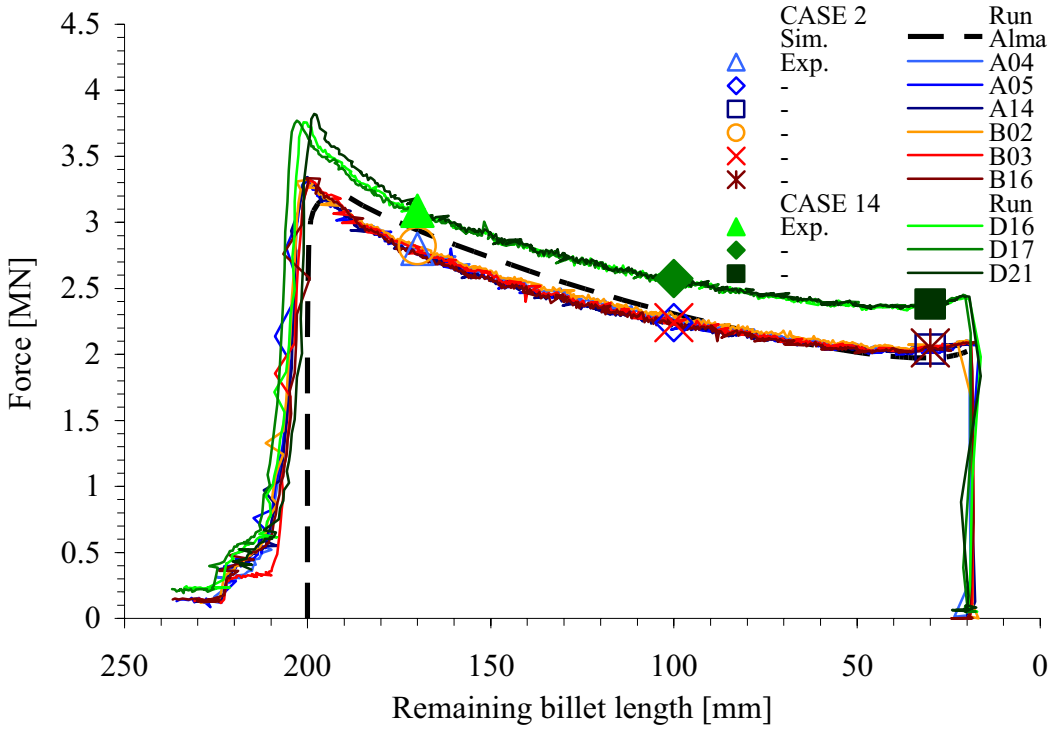

Figure 5.31. Measurement of the ram force - cases 2 and 14 (zero/long bearing).

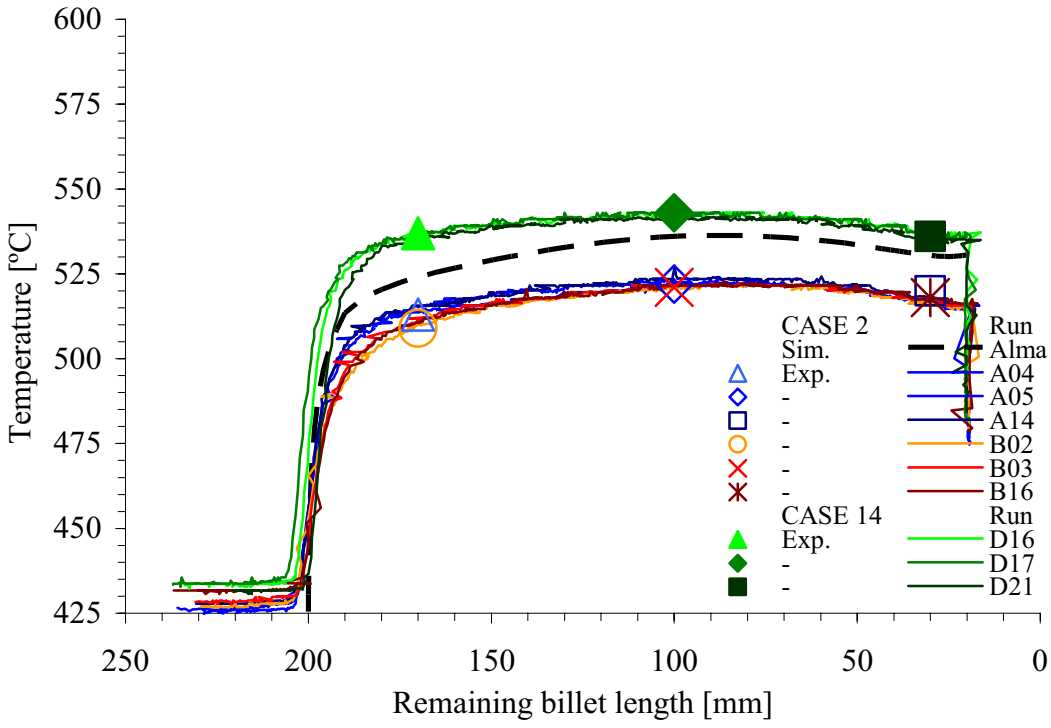

Figure 5.32. Measurement of the outlet temperature (bearing inlet) - cases 2 and 14.

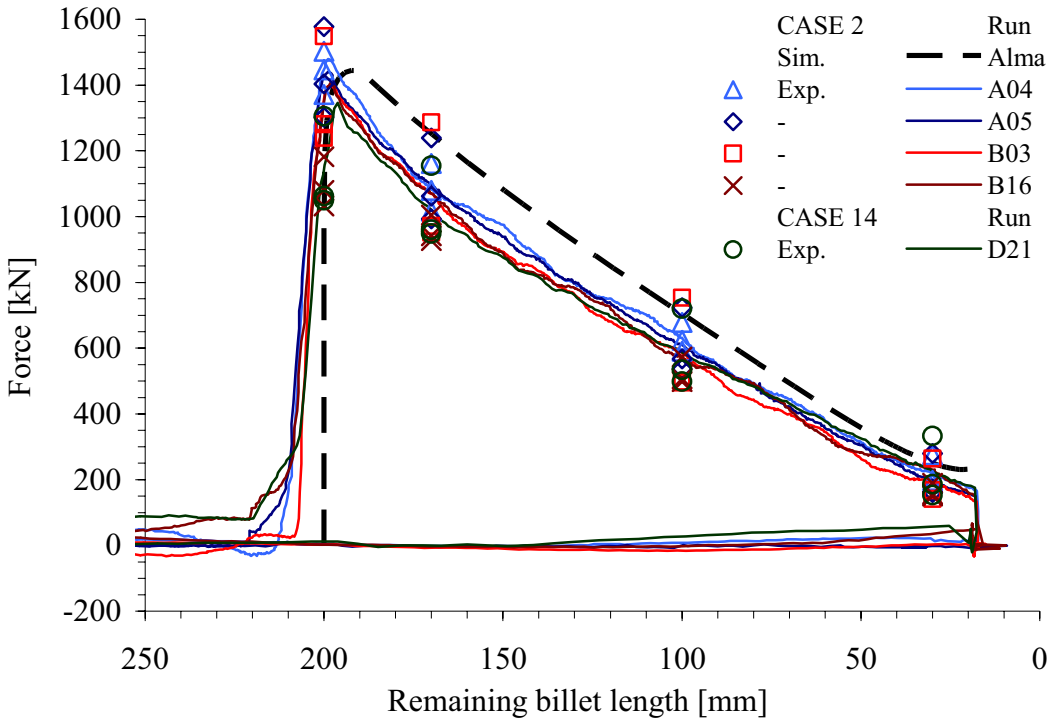

Figure 5.33. Measurement of the average container liner force - cases 2 and 14.

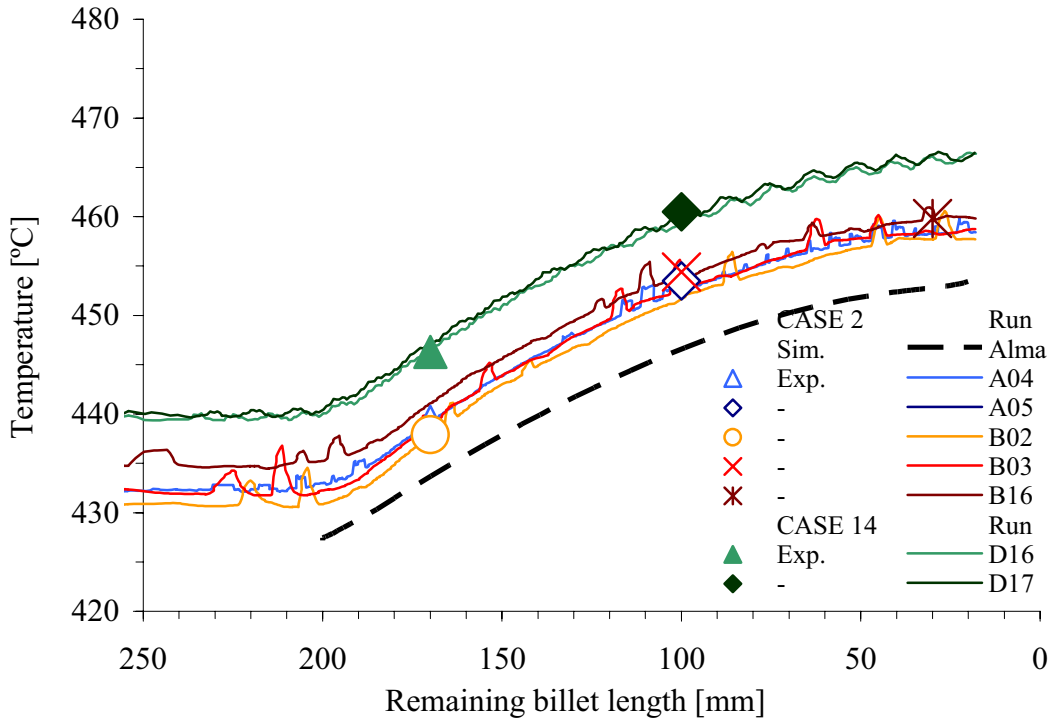

Figure 5.34. Measurement of the die face temperature - cases 2 and 14.

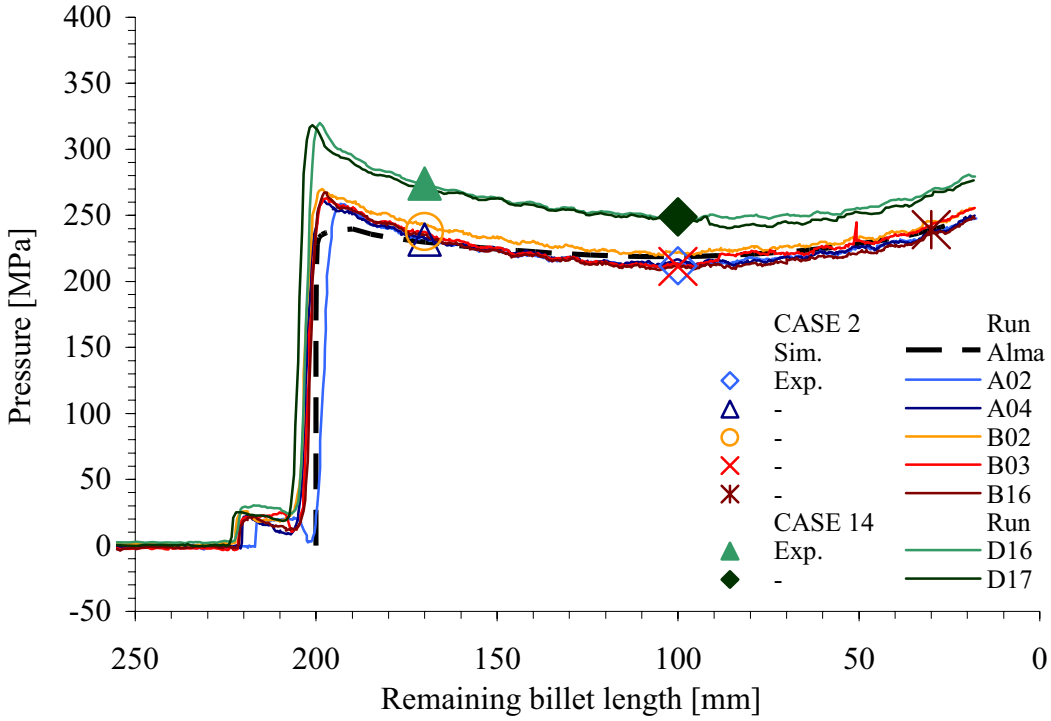

Figure 5.35. Measurement of the die face pressure by sensor 1 - cases 2 and 14.

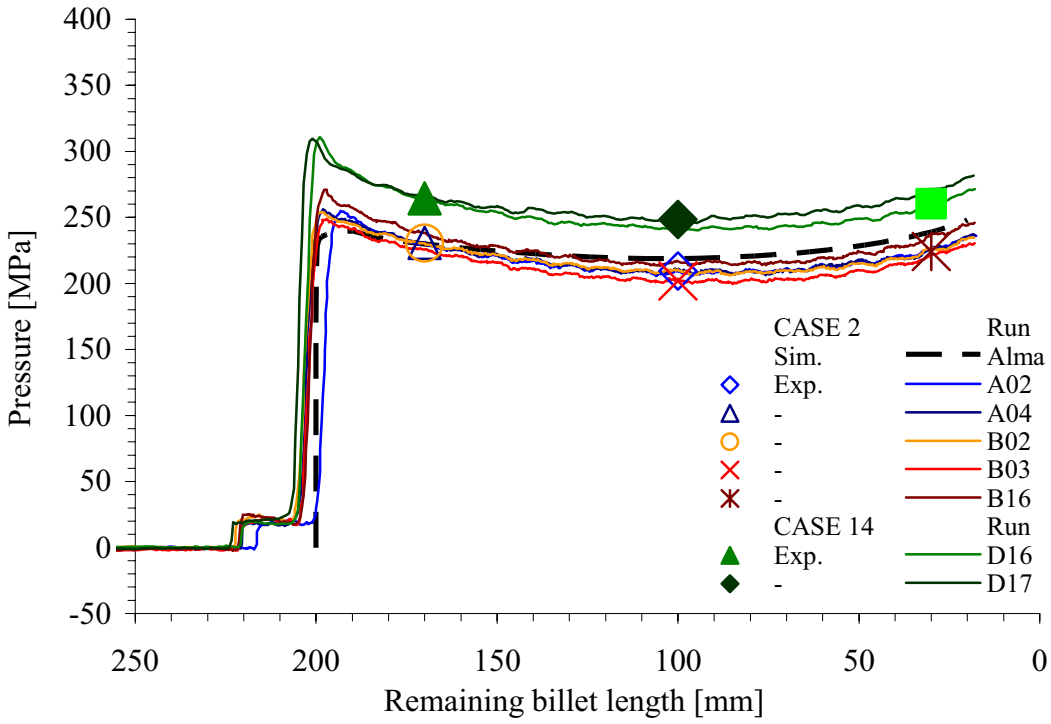

Figure 5.36. Measurement of the die face pressure by sensor 2 - cases 2 and 14.

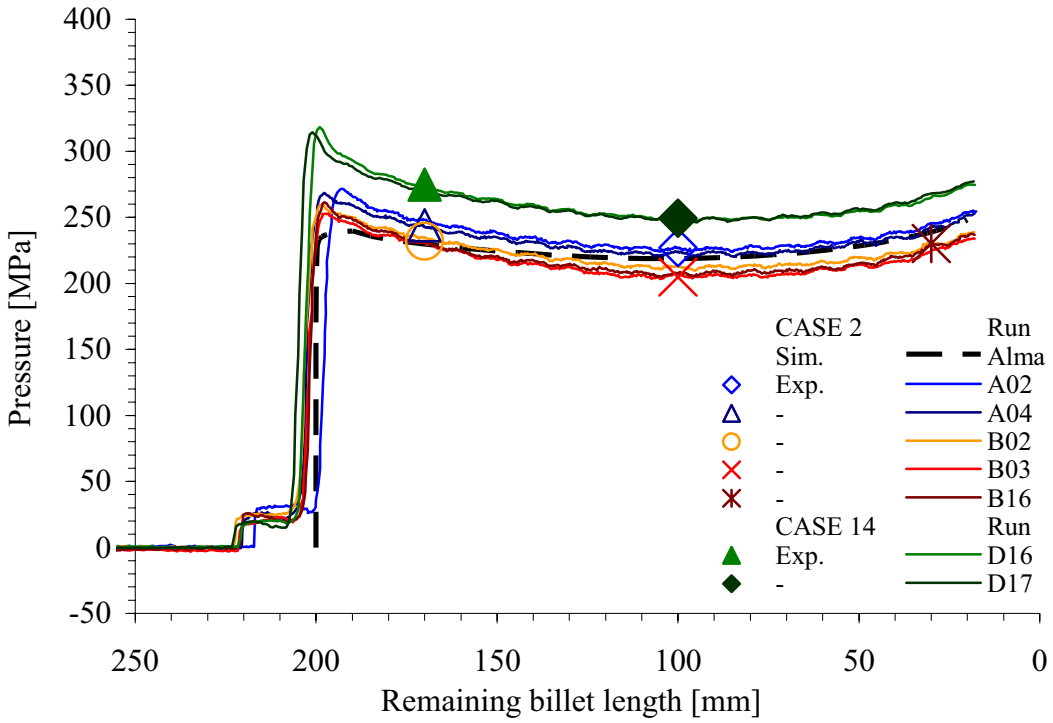

Figure 5.37. Measurement of the die face pressure by sensor 3 - cases 2 and 14.

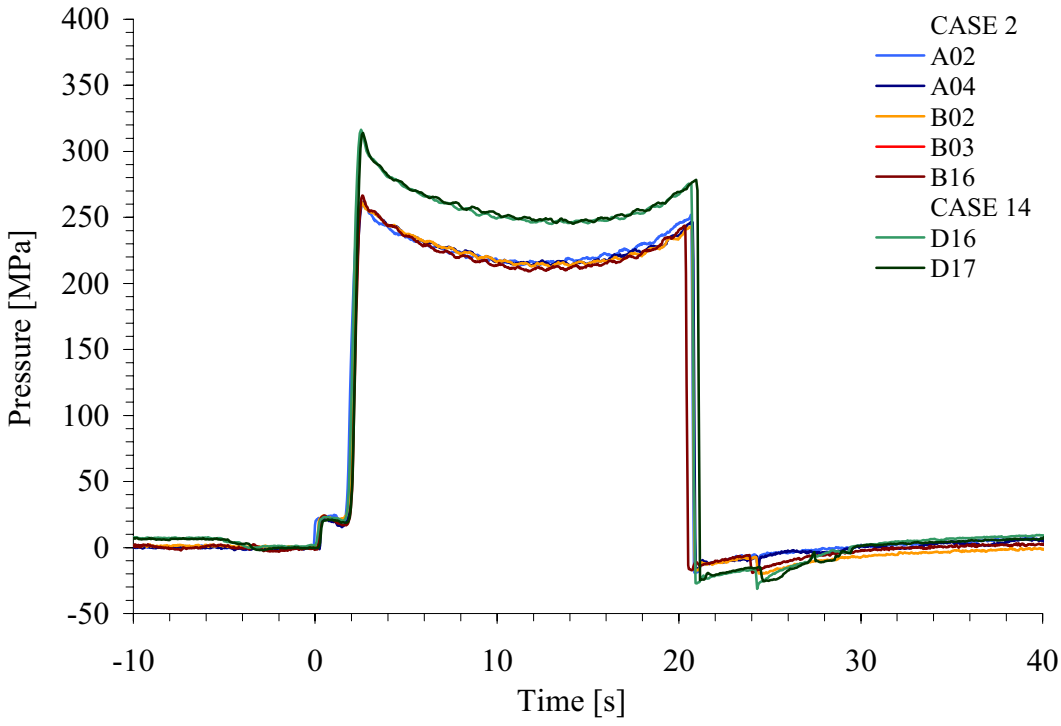

Figure 5.38. Measurement of the average die face pressure - cases 2 and 14.

Table 5.7. Case 3 – input and output data

SPECIFICATION	CASE	3							
Nominal extrusion ratio		40	-		Die outlet diameter			15.8	mm
Nominal bearing length		0	mm						
Nominal ram velocity		20	mm/s		Profile velocity			800	mm/s
Nominal billet temperature		450	ºC						
INPUT DATA	Day/run #	A06	A07	A08	B04	B05	6	Avg.	St.dev.
Actual velocity [mm/s]	Ram	20.4	20.4	20.4	20.4	20.4	-	20.4	0.0
	Profile	816	816	816	816	816	-	816	0.0
Initial billet surface	Front	451	449	450	450	447	-	449	1.5
temperature [ºC]	Back	448	445	443	445	443	-	445	2.0
	Average	450	447	447	448	445	-	447	1.6
Ram temperature [ºC]	Front	152	140	128	116	120	-	131	14.8
RESPONSE		1	2	3	4	5	6	Avg.	St.dev.
Ram force [kN]	Maximum	3490	3536	3562	3571	3603	-	3552	42.3
	Minimum	2118	2130	2159	2161	2173	-	2148	23.1
	196 mm	3375	3440	3500	3505	3540	-	3472	65.1
	170 mm	2950	2960	3010	2970	3020	-	2982	31.1
	100 mm	2340	2381	2400	2395	2419	-	2387	29.6
	30 mm	2176	2170	2205	2228	2240	-	2204	30.9
Bearing inlet	Maximum	550	549	551	542	544	-	547	4.0
temperature [ºC]	Minimum	423	428	428	426	430	-	427	2.6
	170 mm	526	531	530	519	522	-	526	5.1
	100 mm	545	543	545	540	541	-	543	2.3
	30 mm	547	547	549	541	542	-	545	3.5
Bearing outlet	Maximum	-	-	-	-	-	-	-	-
temperature [ºC]	Minimum	-	-	-	-	-	-	-	-
	170 mm	-	-	-	-	-	-	-	-
	100 mm	-	-	-	-	-	-	-	-
	30 mm	-	-	-	-	-	-	-	-
Die face pressure	196 mm	275	281	-	277	283	-	279	3.8
avg. value [MPa]	170 mm	255	257	-	254	257	-	256	1.2
for all 3 sensors	100 mm	229	232	-	227	232	-	230	2.5
	30 mm	246	251	-	247	243	-	247	3.1
Die face pressure	196 mm	8.0	8.0	-	7.6	9.7	-	8.3	-
st. dev. value [MPa]	170 mm	8.5	8.1	-	6.6	8.1	-	7.8	-
for all 3 sensors	100 mm	9.3	8.0	-	4.3	4.6	-	6.6	-
	30 mm	9.4	7.7	-	7.2	8.6	-	8.2	-
Container / liner force	196 mm	-	1420	1450	-	1441	-	1437	96.2
avg. value [kN]	170 mm	-	1150	1169	-	1167	-	1162	104.2
	100 mm	-	615	625	-	595	-	611.7	82.4
	30 mm	-	170	196	-	202	-	189.3	45.0
Liner friction [MPa]		-	24.3	24.7	-	26.0	-	25.0	0.9

Table 5.8. Case 15 – input and output data

SPECIFICATION	CASE	15						
Nominal extrusion ratio		40	-	Die outlet diameter		15.8	mm	
Nominal bearing length		12	mm					
Nominal ram velocity		20	mm/s	Profile velocity		800	mm/s	
Nominal billet temperature		450	ºC					
INPUT DATA	Day/run #	D06	D13	D15	-	Avg.	St.dev.	C15 - C3
Actual velocity [mm/s]	Ram	20.3	20.3	20.3	-	20.3	0.0	-0.1
	Profile	812	812	812	-	812	0.0	-4.0
Initial billet surface	Front	446	448	448	-	447	1.2	-2.1
temperature [ºC]	Back	437	442	445	-	441	4.0	-3.5
	Average	442	445	447	-	444	2.6	-2.8
Ram temperature [ºC]	Front	186	132	140	-	153	29.1	21.5
RESPONSE		1	2	3	4	Avg.	St.dev.	C15 - C3
Ram force [kN]	Maximum	4011	4014	4034	-	4020	12.5	59
	Minimum	2411	2465	2457	-	2444	29.1	38
Effect C15 - C3:	196 mm	3875	3895	3841	-	3870	27.3	51
Pressure [MPa]	170 mm	3283	3310	3300	-	3298	13.7	40
	100 mm	2650	2700	2680	-	2677	25.2	37
	30 mm	2445	2520	2500	-	2488	38.8	36
Bearing inlet	Maximum	569	570	570	-	570	0.6	22
temperature [ºC]	Minimum	432	433	433	-	433	0.6	6
	170 mm	556	557	556	-	556	0.6	31
	100 mm	568	567	568	-	568	0.6	25
	30 mm	568	568	569	-	568	0.6	23
Bearing outlet	Maximum	581	580	580	-	580	0.6	-
temperature [ºC]	Minimum	432	433	433	-	433	0.6	-
	170 mm	566	565	565	-	565	0.6	-
	100 mm	577	576	576	-	576	0.6	-
	30 mm	580	579	577	-	579	1.5	-
Die face pressure	196 mm	343	-	335	-	339	5.5	60
avg. value [MPa]	170 mm	293	-	297	-	295	2.7	39
for all 3 sensors	100 mm	267	-	267	-	267	0.4	37
	30 mm	274	-	279	-	277	3.7	30
Die face pressure	196 mm	19.1	-	4.7	-	11.9	-	3.6
st. dev. value [MPa]	170 mm	14.7	-	3.8	-	9.2	-	1.4
for all 3 sensors	100 mm	8.3	-	0.9	-	4.6	-	-1.9
	30 mm	8.4	-	1.8	-	5.1	-	-3.1
Container / liner force	196 mm	-	-	-	-	-	-	-
avg. value [kN]	170 mm	-	-	-	-	-	-	-
	100 mm	-	-	-	-	-	-	-
	30 mm	-	-	-	-	-	-	-
Liner friction [MPa]		-	-	-	-	-	-	-

.

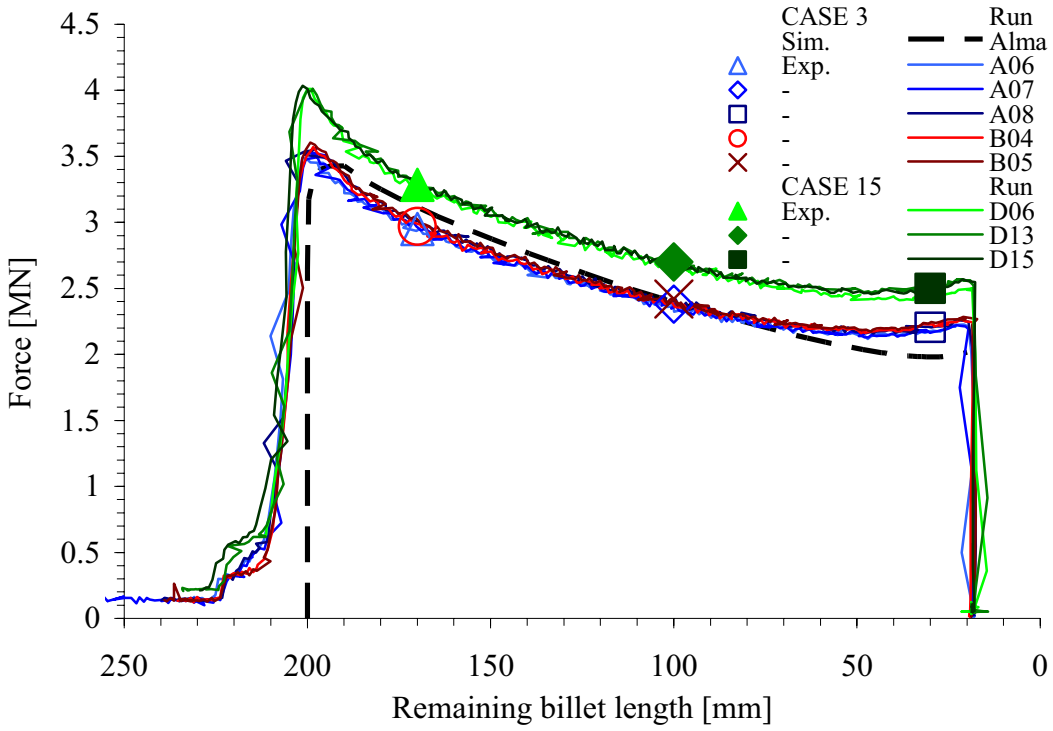

Figure 5.39. Measurement of the ram force - cases 3 and 15 (zero/long bearing).

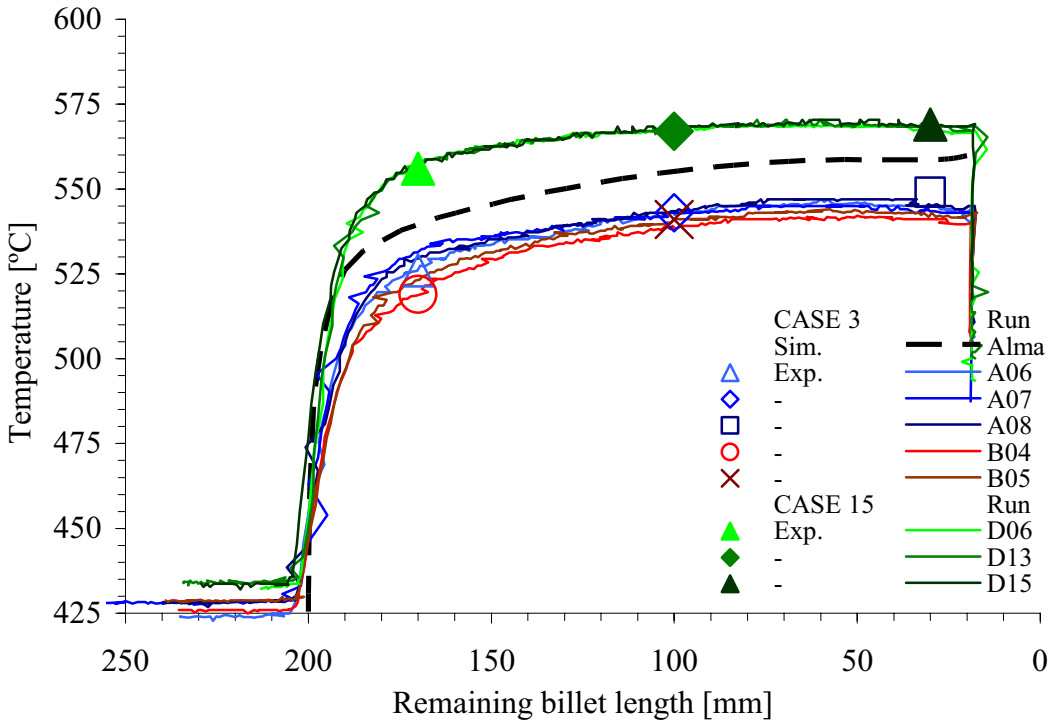

Figure 5.40. Measurement of the outlet temperature (bearing inlet) - cases 3 and 15.

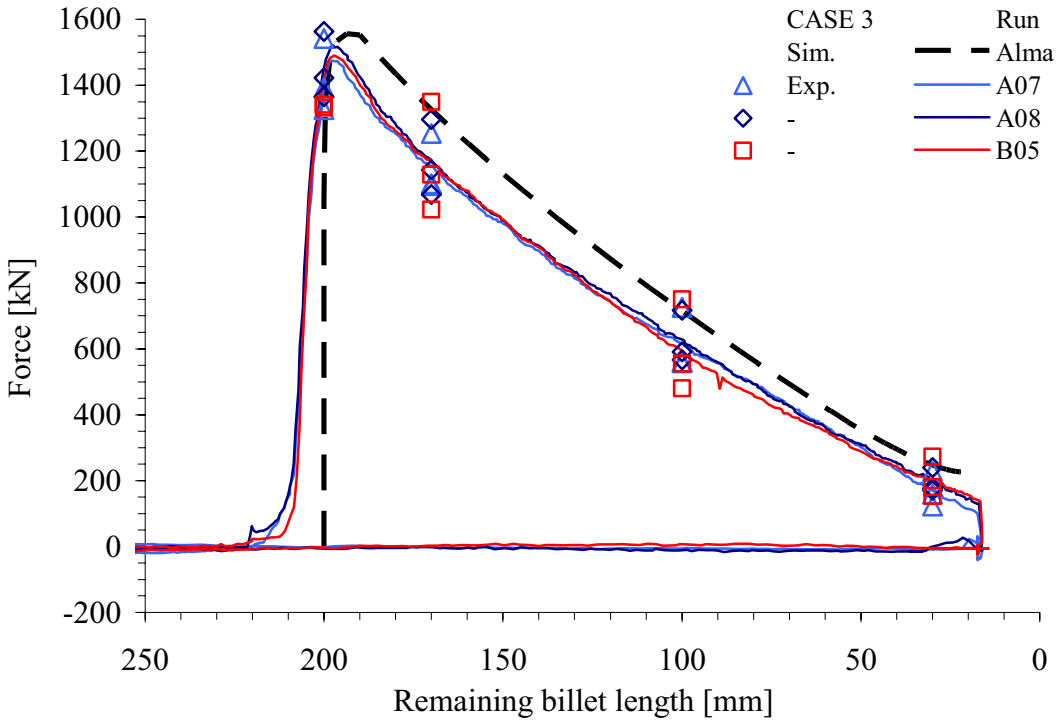

Figure 5.41. Measurement of the average container liner force - case 3.

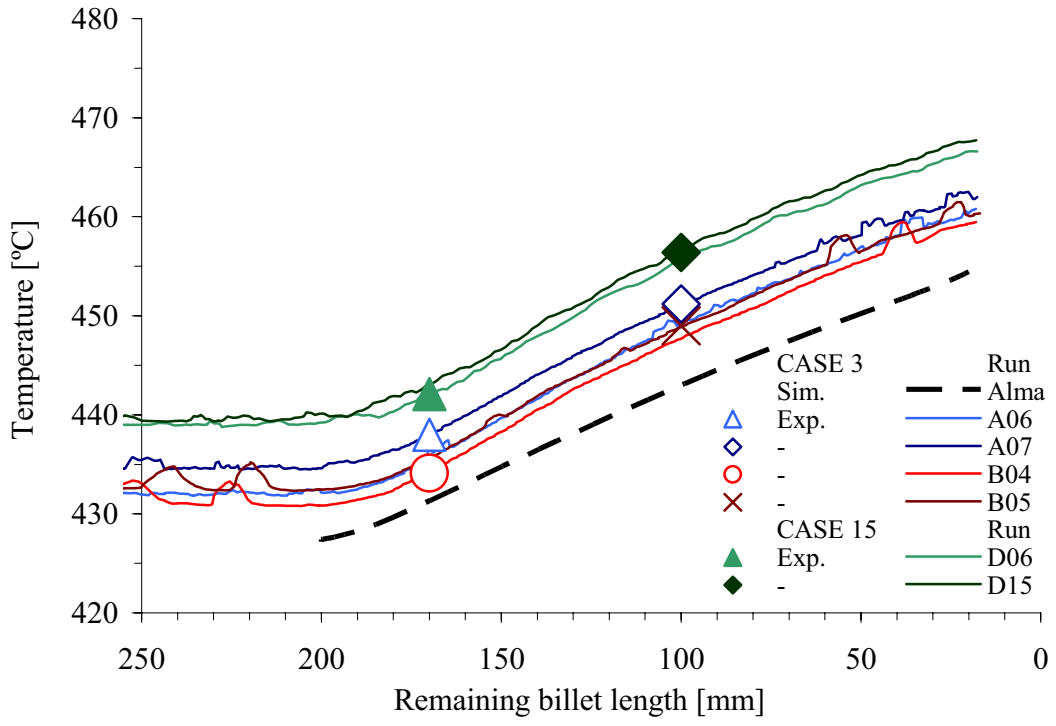

Figure 5.42. Measurement of the die face temperature - cases 3 and 15.

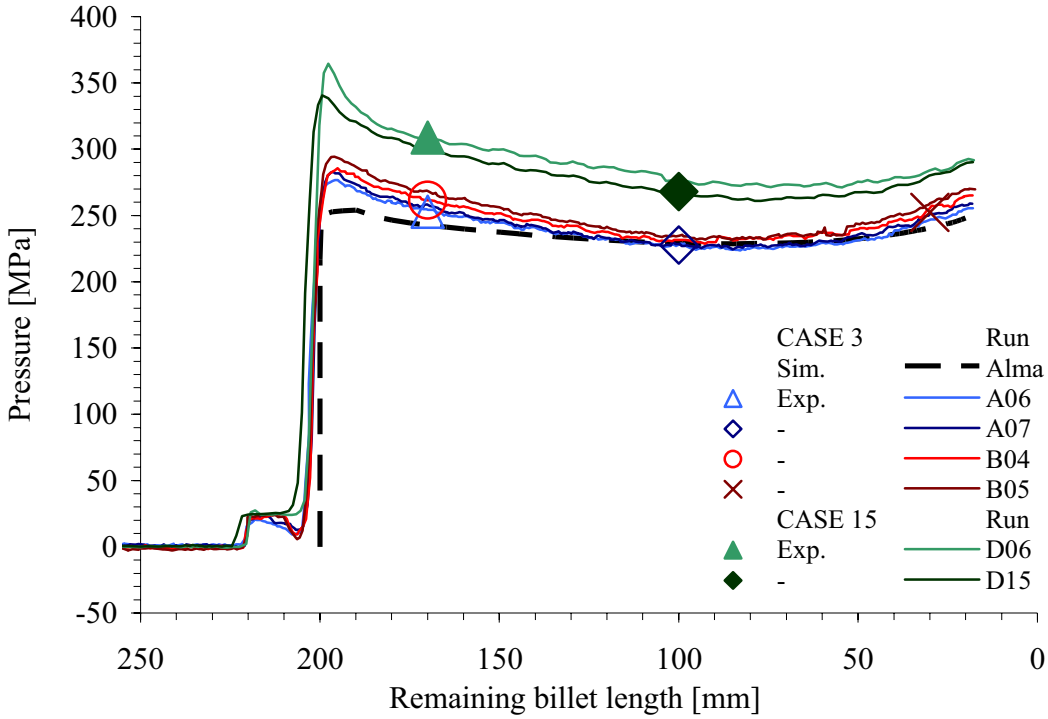

Figure 5.43. Measurement of the die face pressure by sensor 1 - cases 3 and 15.

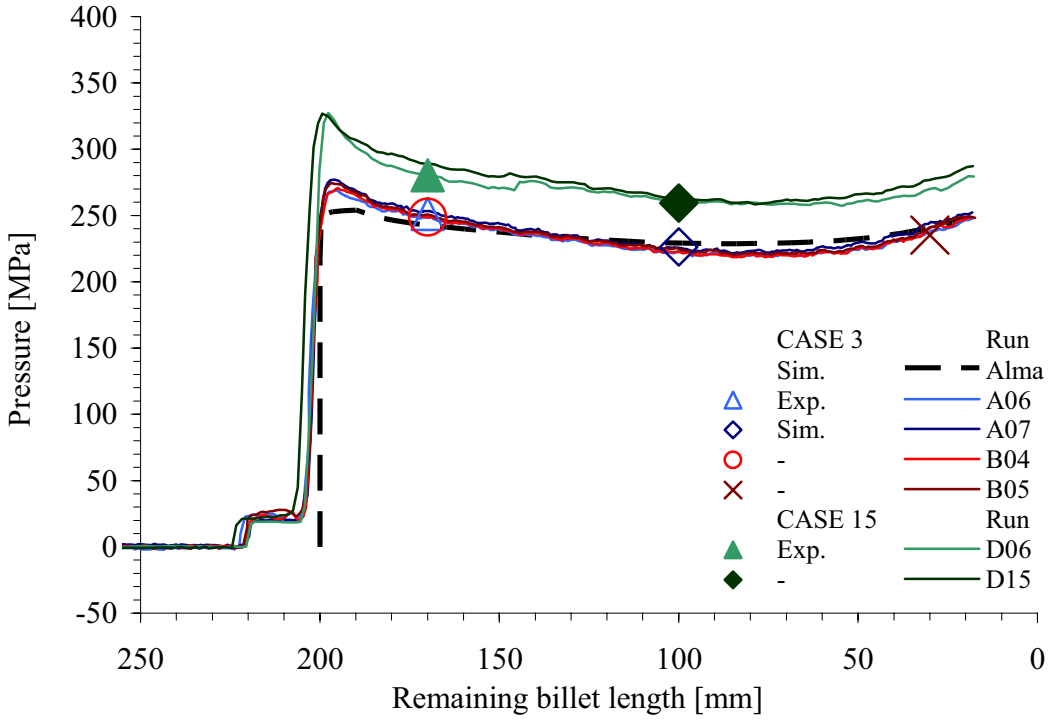

Figure 5.44. Measurement of the die face pressure by sensor 2 - cases 3 and 15.

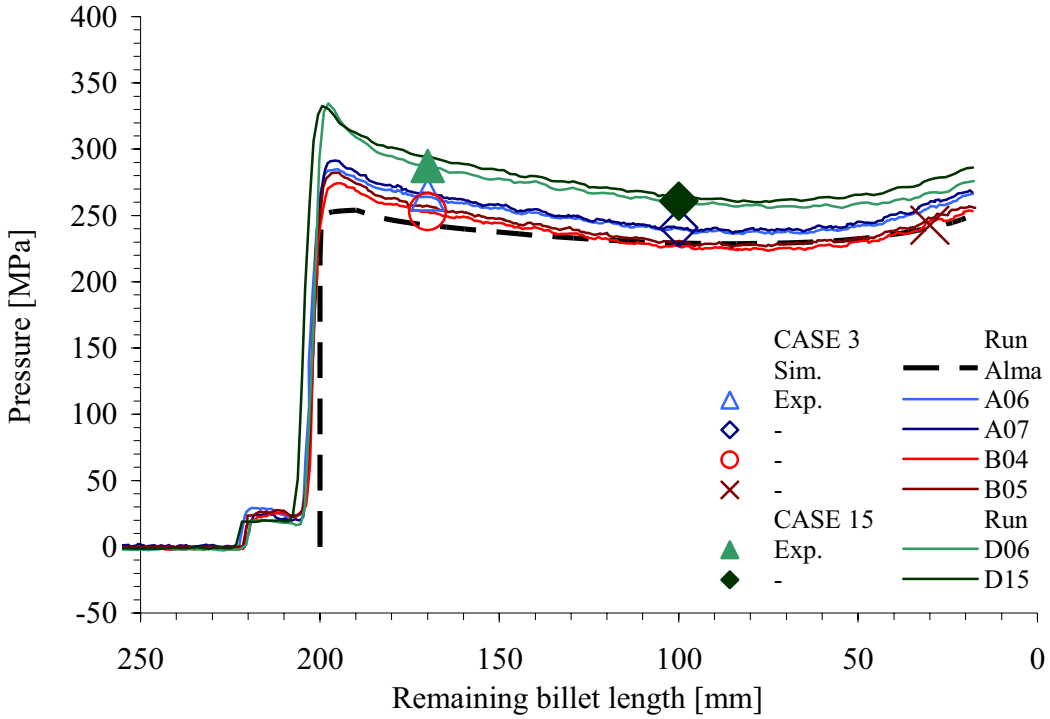

Figure 5.45. Measurement of the die face pressure by sensor 3 - cases 3 and 15.

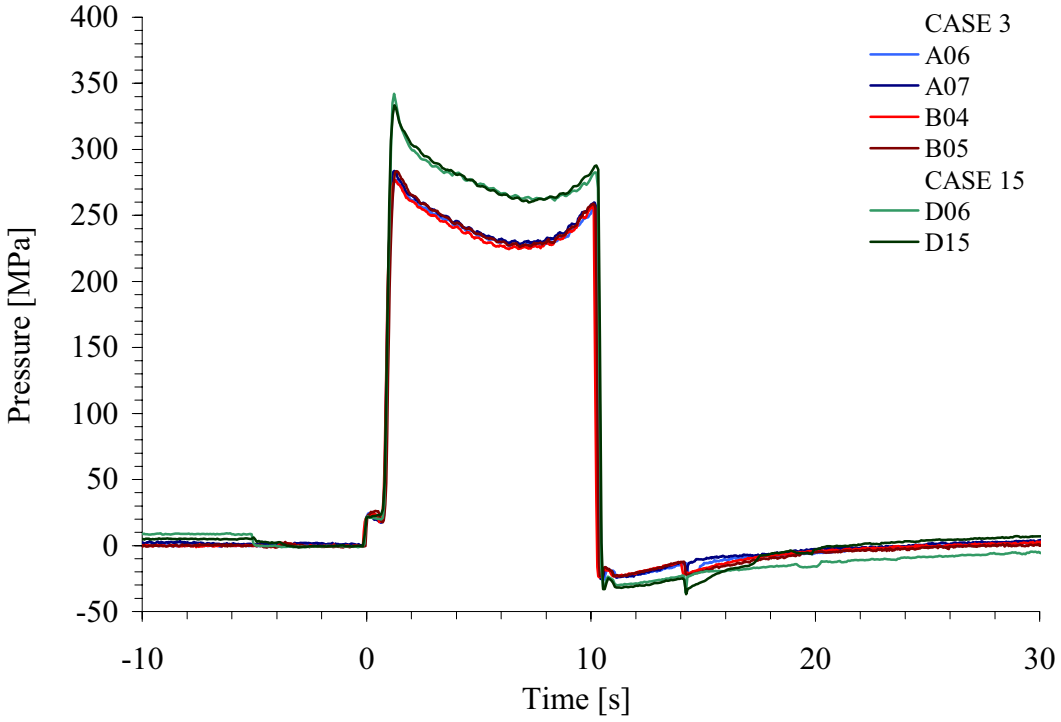

Figure 5.46. Measurement of the average die face pressure - cases 3 and 15.

Table 5.9. Case 4 – input and output data

SPECIFICATION	CASE	4							
Nominal extrusion ratio		40	-		Die outlet diameter			15.8	mm
Nominal bearing length		0	mm						
Nominal ram velocity		5	mm/s		Profile velocity			200	mm/s
Nominal billet temperature		500	ºC						
INPUT DATA	Day/run #	B12	B13	-	-	-	-	Avg.	St.dev.
Actual velocity [mm/s]	Ram	5.0	5.0	-	-	-	-	5.0	0.0
	Profile	200	200	-	-	-	-	200	0.0
Initial billet surface	Front	491	493	-	-	-	-	492	1.4
temperature [ºC]	Back	488	487	-	-	-	-	488	0.7
	Average	490	490	-	-	-	-	490	0.4
Ram temperature [ºC]	Front	125	128	-	-	-	-	127	2.1
RESPONSE		1	2	3	4	5	6	Avg.	St.dev.
Ram force [kN]	Maximum	2719	2707	-	-	-	-	2713	8.5
	Minimum	1771	1783	-	-	-	-	1777	8.5
	196 mm	2590	2546	-	-	-	-	2568	31.1
	170 mm	2300	2277	-	-	-	-	2289	16.3
	100 mm	1980	1970	-	-	-	-	1975	7.1
	30 mm	1840	1810	-	-	-	-	1825	21.2
Bearing inlet	Maximum	516	516	-	-	-	-	516	0.0
temperature [ºC]	Minimum	430	430	-	-	-	-	430	0.0
	170 mm	513	513	-	-	-	-	513	0.0
	100 mm	514	515	-	-	-	-	515	0.7
	30 mm	504	505	-	-	-	-	505	0.7
Bearing outlet	Maximum	-	-	-	-	-	-	-	-
temperature [ºC]	Minimum	-	-	-	-	-	-	-	-
	170 mm	-	-	-	-	-	-	-	-
	100 mm	-	-	-	-	-	-	-	-
	30 mm	-	-	-	-	-	-	-	-
Die face pressure	196 mm	210	210	-	-	-	-	210	0.3
avg. value [MPa]	170 mm	184	180	-	-	-	-	182	3.2
for all 3 sensors	100 mm	187	185	-	-	-	-	186	1.8
	30 mm	221	219	-	-	-	-	220	1.7
Die face pressure	196 mm	7.6	5.2	-	-	-	-	6.4	-
st. dev. value [MPa]	170 mm	5.4	2.9	-	-	-	-	4.1	-
for all 3 sensors	100 mm	7.3	5.0	-	-	-	-	6.2	-
	30 mm	11.0	11.9	-	-	-	-	11.5	-
Container / liner force	196 mm	-	-	-	-	-	-	-	-
avg. value [kN]	170 mm	-	-	-	-	-	-	-	-
	100 mm	-	-	-	-	-	-	-	-
	30 mm	-	-	-	-	-	-	-	-
Liner friction [MPa]		-	-	-	-	-	-	-	-

Table 5.10. Case 16 – input and output data

SPECIFICATION	CASE	16						
Nominal extrusion ratio		40	-		Die outlet diameter		15.8	mm
Nominal bearing length		12	mm					
Nominal ram velocity		5	mm/s		Profile velocity		200	mm/s
Nominal billet temperature		500	ºC					

INPUT DATA	Day/run #	D01	D08	D11	-	Avg.	St.dev.	C16 - C4
Actual velocity [mm/s]	Ram	5.0	4.9	4.9	-	4.9	0.1	-0.1
	Profile	200	196	196	-	197	2.3	-2.7
Initial billet surface	Front	489	503	497	-	496	7.0	4.3
temperature [ºC]	Back	494	494	487	-	492	4.0	4.2
	Average	492	499	492	-	494	3.9	4.3
Ram temperature [ºC]	Front	146	139	128	-	138	9.1	11.2

RESPONSE		1	2	3	4	Avg.	St.dev.	C16 - C4
Ram force [kN]	Maximum	3124	3167	3167	-	3153	24.8	56
	Minimum	2208	2188	2182	-	2193	13.6	53
Effect C16 - C4:	196 mm	2902	2890	2902	-	2898	6.9	42
Pressure [MPa]	170 mm	2650	2601	2610	-	2620	26.1	42
	100 mm	2373	2330	2320	-	2341	28.2	47
	30 mm	2231	2230	2220	-	2227	6.1	51
Bearing inlet	Maximum	531	535	535	-	534	2.3	18
temperature [ºC]	Minimum	428	432	435	-	432	3.5	2
	170 mm	529	534	534	-	532	2.9	19
	100 mm	529	533	533	-	532	2.3	17
	30 mm	519	521	521	-	520	1.2	16
Bearing outlet	Maximum	536	540	540	-	539	2.3	-
temperature [ºC]	Minimum	428	432	435	-	432	3.5	-
	170 mm	535	537	536	-	536	1.0	-
	100 mm	535	538	538	-	537	1.7	-
	30 mm	528	529	528	-	528	0.6	-
Die face pressure	196 mm	232	250	252	-	245	11.2	35
avg. value [MPa]	170 mm	210	212	220	-	214	5.6	32
for all 3 sensors	100 mm	218	220	227	-	222	4.4	36
	30 mm	256	261	265	-	260	4.3	40
Die face pressure	196 mm	6.4	5.4	5.9	-	5.9	-	-0.5
st. dev. value [MPa]	170 mm	6.9	5.2	6.3	-	6.1	-	2.0
for all 3 sensors	100 mm	4.2	6.4	7.6	-	6.1	-	-0.1
	30 mm	5.4	5.4	7.3	-	6.1	-	-5.4
Container / liner force	196 mm	-	-	-	-	-	-	-
avg. value [kN]	170 mm	-	-	-	-	-	-	-
	100 mm	-	-	-	-	-	-	-
	30 mm	-	-	-	-	-	-	-
Liner friction [MPa]		-	-	-	-	-	-	-

.

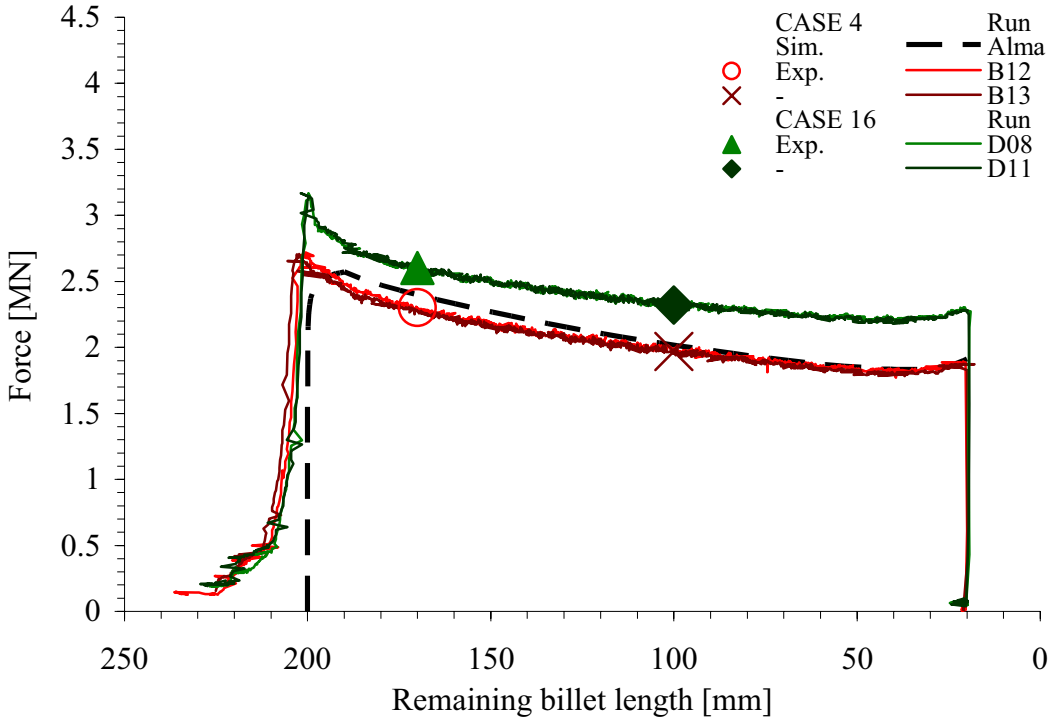

Figure 5.47. Measurement of the ram force - cases 4 and 16 (zero/long bearing).

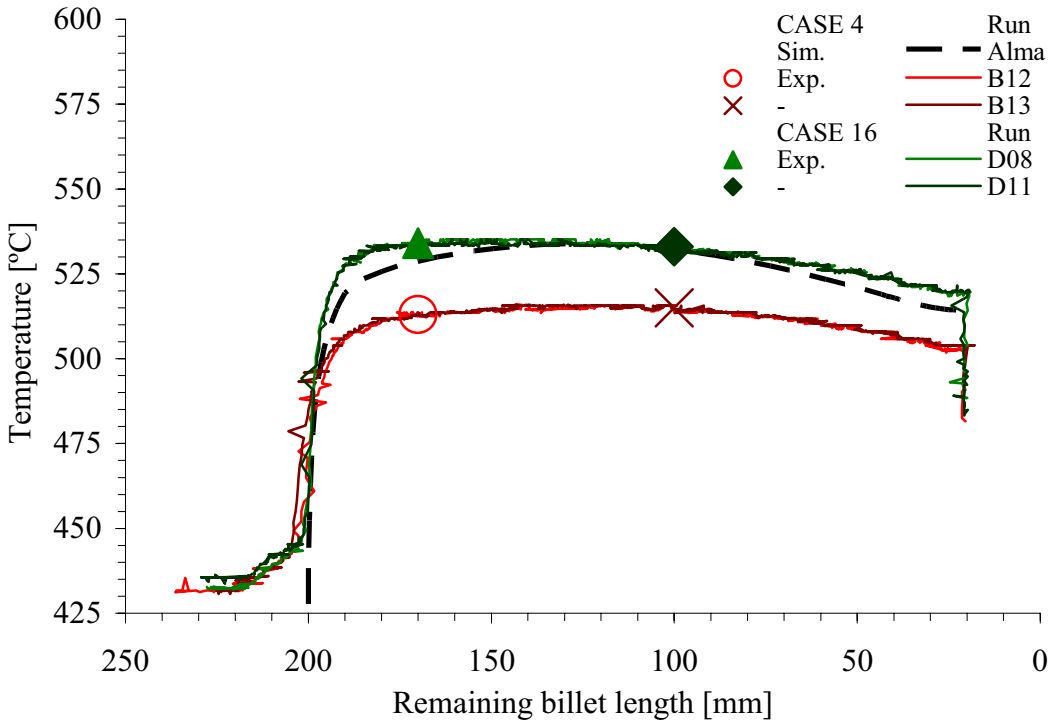

Figure 5.48. Measurement of the outlet temperature (bearing inlet) - cases 4 and 16.

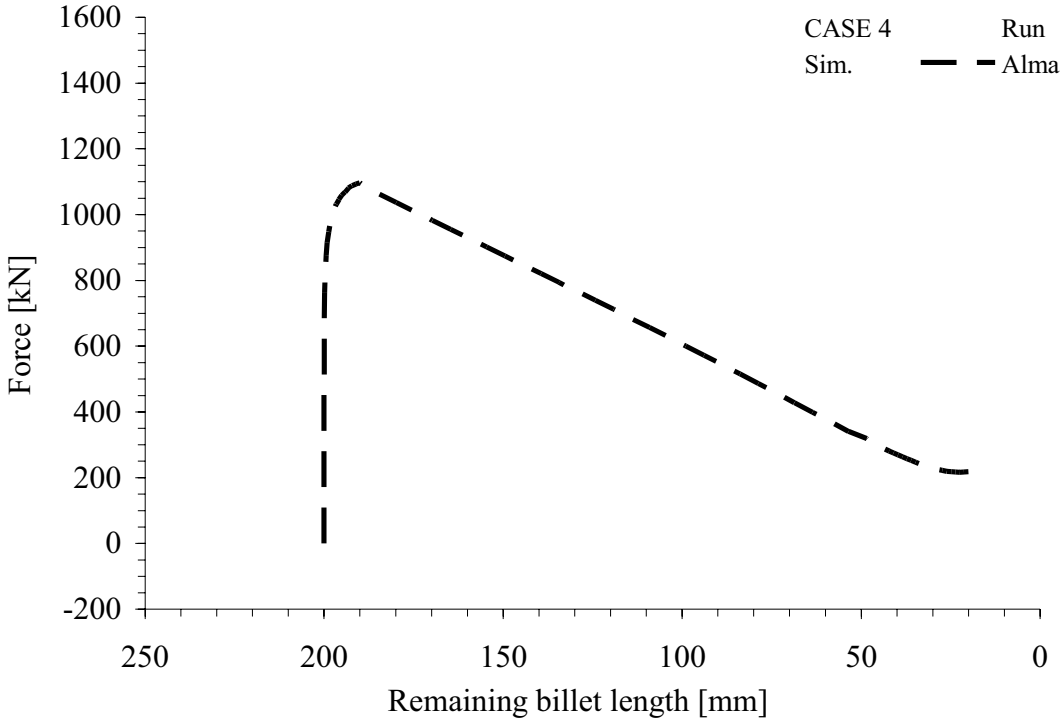

Figure 5.49. Measurement of the average container liner force - cases 2 and 14.

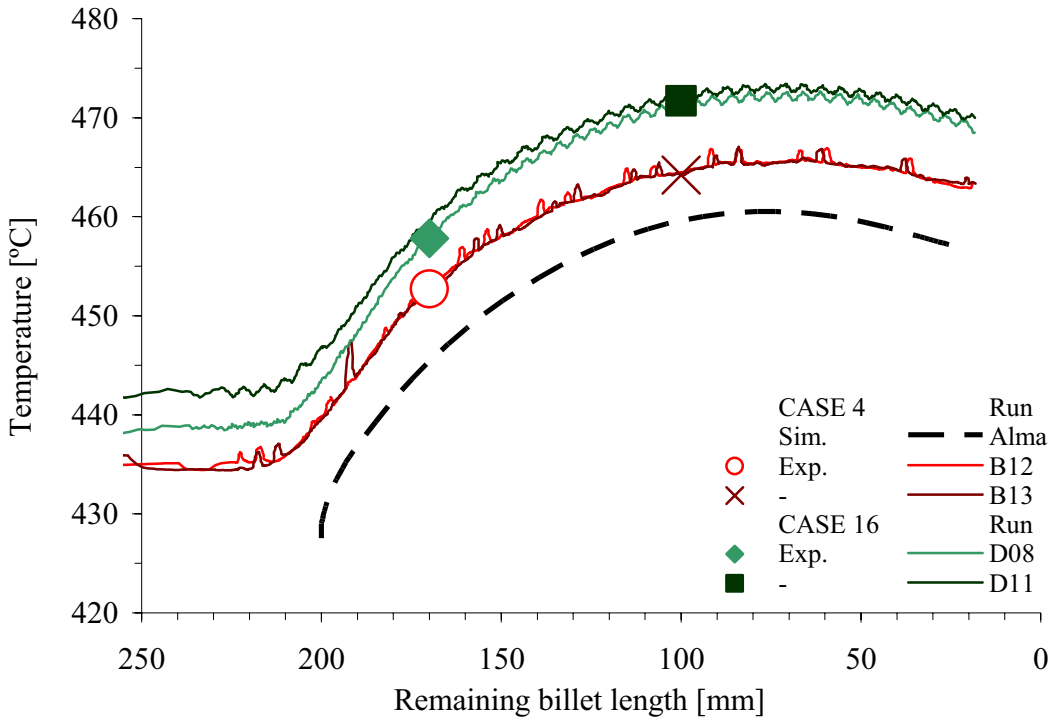

Figure 5.50. Measurement of the die face temperature - cases 4 and 16.

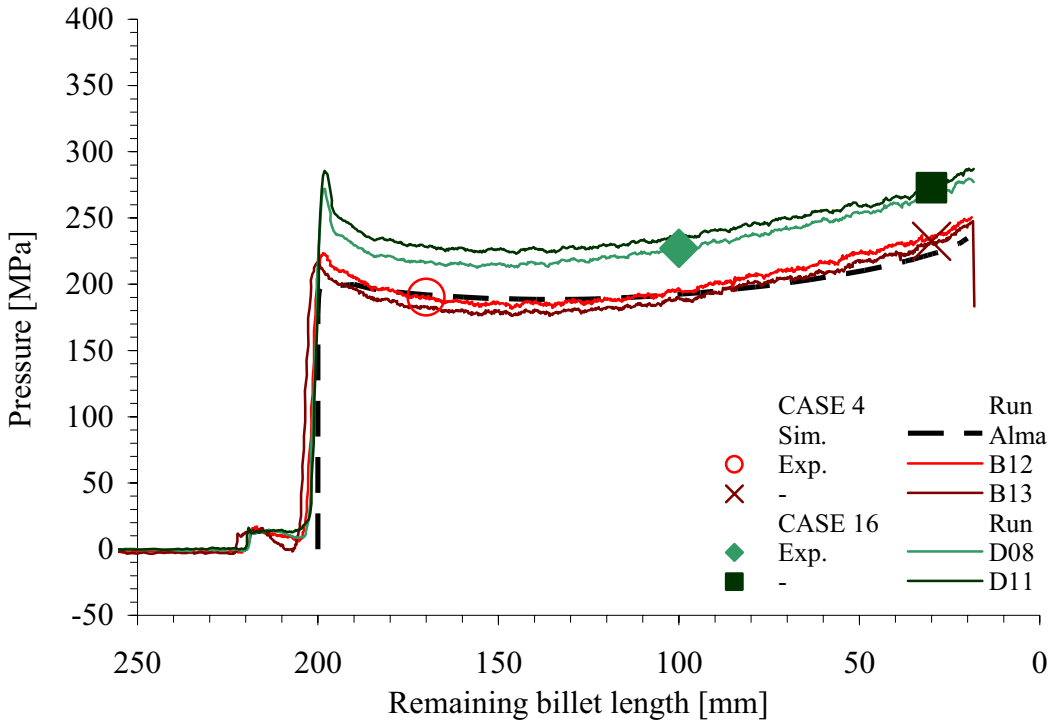

Figure 5.51. Measurement of the die face pressure by sensor 1 - cases 4 and 16.

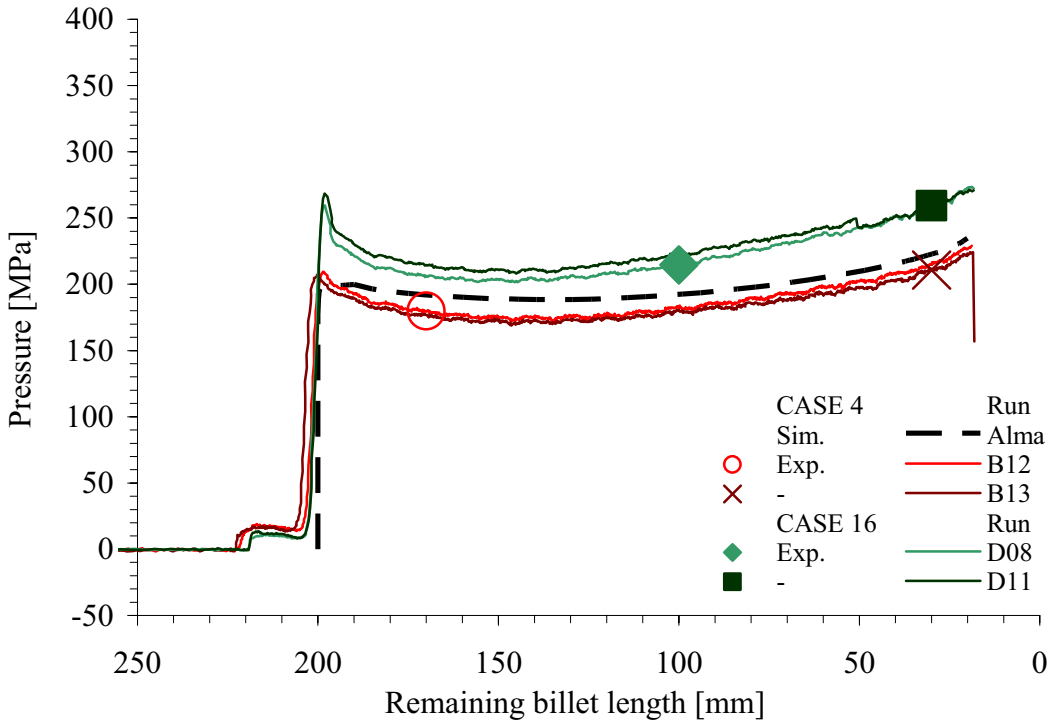

Figure 5.52. Measurement of the die face pressure by sensor 2 - cases 4 and 16.

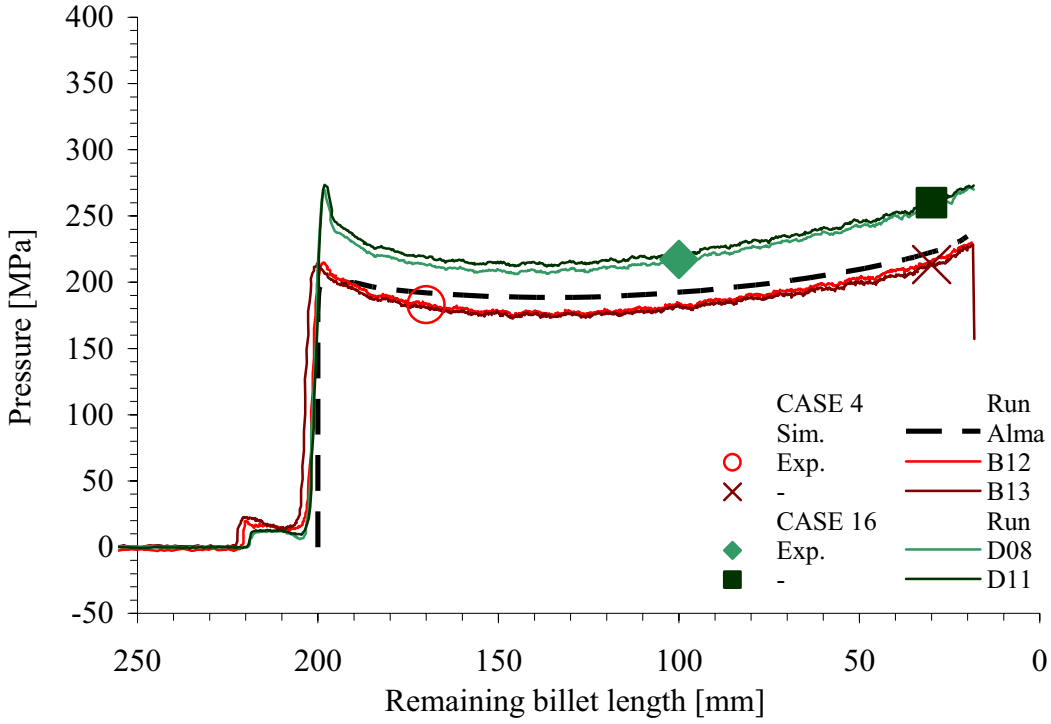

Figure 5.53. Measurement of the die face pressure by sensor 3 - cases 4 and 16.

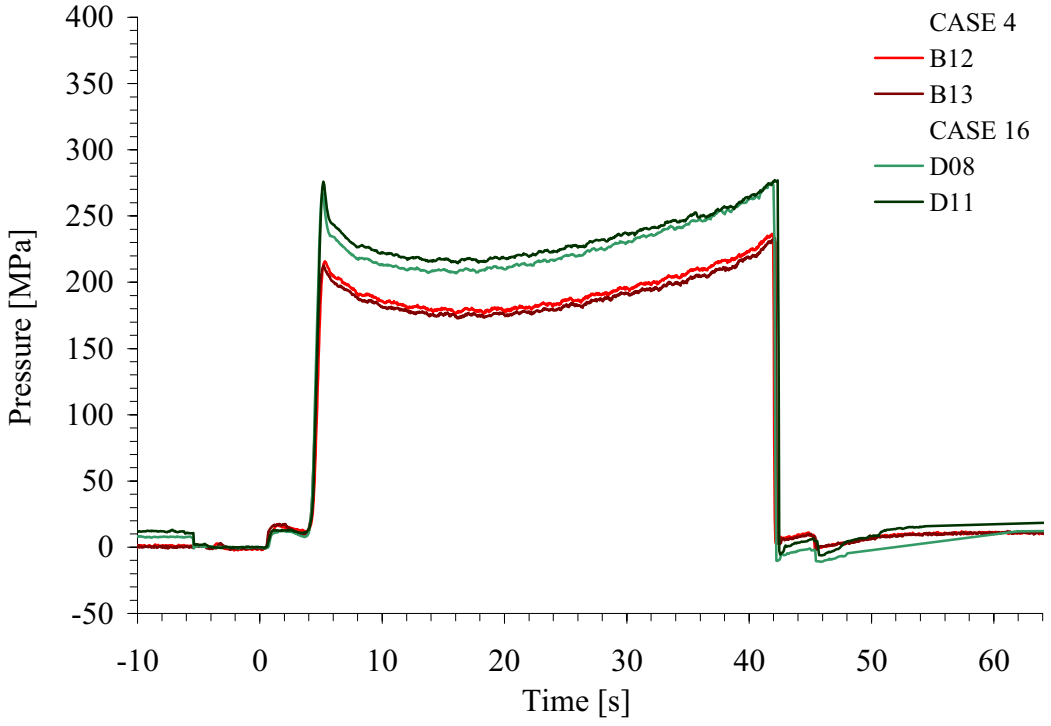

Figure 5.54. Measurement of the average die face pressure - cases 4 and 16.

Table 5.11. Case 5 – input and output data

SPECIFICATION	CASE	5							
Nominal extrusion ratio		40	-		Die outlet diameter		15.8	mm	
Nominal bearing length		0	mm						
Nominal ram velocity		10	mm/s		Profile velocity		400	mm/s	
Nominal billet temperature		500	ºC						
INPUT DATA	Day/run #	A12	A13	B08	B09	B14	B15	Avg.	St.dev.
Actual velocity [mm/s]	Ram	10.1	10.1	10.1	10.1	10.1	10.1	10.1	0.0
	Profile	404	404	404	404	404	404	404	0.0
Initial billet surface	Front	495	488	498	492	493	495	494	3.4
temperature [ºC]	Back	496	491	491	490	490	490	491	2.3
	Average	496	490	495	491	492	493	492	2.2
Ram temperature [ºC]	Front	140	135	135	125	129	122	131	6.8
RESPONSE		1	2	3	4	5	6	Avg.	St.dev.
Ram force [kN]	Maximum	2950	2996	2898	2993	2999	2927	2961	42.3
	Minimum	1639	1826	1899	1780	1901	1875	1820	100.2
	196 mm	2740	2777	2705	2826	2762	2754	2761	40.3
	170 mm	2420	2427	2395	2433	2439	2380	2416	23.2
	100 mm	2050	2060	2030	2060	2086	2020	2051	23.6
	30 mm	1965	1953	1933	1980	1953	1948	1955	15.9
Bearing inlet	Maximum	538	539	535	534	534	534	536	2.3
temperature [ºC]	Minimum	428	430	430	430	431	434	431	2.0
	170 mm	525	527	524	523	523	525	525	1.5
	100 mm	538	537	533	533	533	534	535	2.3
	30 mm	532	530	527	527	527	527	528	2.2
Bearing outlet	Maximum	-	-	-	-	-	-	-	-
temperature [ºC]	Minimum	-	-	-	-	-	-	-	-
	170 mm	-	-	-	-	-	-	-	-
	100 mm	-	-	-	-	-	-	-	-
	30 mm	-	-	-	-	-	-	-	-
Die face pressure	196 mm	235	242	233	230	-	239	236	4.8
avg. value [MPa]	170 mm	201	202	196	196	-	199	199	2.7
for all 3 sensors	100 mm	185	188	183	183	-	184	184	2.2
	30 mm	215	220	213	214	-	215	215	2.5
Die face pressure	196 mm	6.8	6.1	6.7	7.6	-	12.3	7.9	-
st. dev. value [MPa]	170 mm	7.5	6.3	4.5	5.0	-	9.4	6.5	-
for all 3 sensors	100 mm	8.3	6.7	4.7	4.4	-	9.4	6.7	-
	30 mm	7.7	7.6	7.7	8.2	-	12.5	8.7	-
Container / liner force	196 mm	1356	1241	-	-	1195	1163	1239	84.5
avg. value [kN]	170 mm	1008	946	-	-	884	866	926	64.5
	100 mm	563	550	-	-	504	497	529	32.9
	30 mm	217	206	-	-	163	156	186	30.5
Liner friction [MPa]		20.2	18.0	-	-	-	16.8	18.1	1.8

Table 5.12. Case 17 – input and output data

SPECIFICATION	CASE	17						
Nominal extrusion ratio		40	-	Die outlet diameter		15.8	mm	
Nominal bearing length		12	mm					
Nominal ram velocity		10	mm/s	Profile velocity		400	mm/s	
Nominal billet temperature		500	ºC					
INPUT DATA	Day/run #	D04	D05	-	-	Avg.	St.dev.	C17 - C5
Actual velocity [mm/s]	Ram	10.0	10.0	-	-	10.0	0.0	5.0
	Profile	400	400	-	-	400	0.0	200.0
Initial billet surface	Front	496	493	-	-	495	2.1	50.1
temperature [ºC]	Back	487	486	-	-	487	0.7	44.1
	Average	492	490	-	-	491	1.4	47.1
Ram temperature [ºC]	Front	169	136	-	-	153	23.3	16.5
RESPONSE		1	2	3	4	Avg.	St.dev.	C17 - C5
Ram force [kN]	Maximum	3341	3448	-	-	3395	75.7	55
	Minimum	2208	2240	-	-	2224	22.6	51
Effect C17 - C5:	196 mm	3020	3133	-	-	3077	79.9	40
Pressure [MPa]	170 mm	2650	2700	-	-	2675	35.4	33
	100 mm	2330	2385	-	-	2358	38.9	39
	30 mm	2255	2300	-	-	2278	31.8	41
Bearing inlet	Maximum	557	557	-	-	557	0.0	21
temperature [ºC]	Minimum	431	431	-	-	431	0.0	1
	170 mm	552	551	-	-	552	0.7	27
	100 mm	556	557	-	-	557	0.7	22
	30 mm	547	547	-	-	547	0.0	19
Bearing outlet	Maximum	563	564	-	-	564	0.7	-
temperature [ºC]	Minimum	431	431	-	-	431	0.0	-
	170 mm	556	555	-	-	556	0.7	-
	100 mm	562	563	-	-	563	0.7	-
	30 mm	556	557	-	-	557	0.7	-
Die face pressure	196 mm	284	279	-	-	282	3.7	45
avg. value [MPa]	170 mm	225	228	-	-	227	1.8	27
for all 3 sensors	100 mm	213	216	-	-	215	1.9	30
	30 mm	244	249	-	-	246	3.5	31
Die face pressure	196 mm	10.4	9.6	-	-	10.0	-	2.0
st. dev. value [MPa]	170 mm	6.5	7.9	-	-	7.2	-	0.3
for all 3 sensors	100 mm	7.5	9.1	-	-	8.3	-	1.0
	30 mm	8.4	10.6	-	-	9.5	-	0.6
Container / liner force	196 mm	-	-	-	-	-	-	-
avg. value [kN]	170 mm	-	-	-	-	-	-	-
	100 mm	-	-	-	-	-	-	-
	30 mm	-	-	-	-	-	-	-
Liner friction [MPa]		-	-	-	-	-	-	-

.

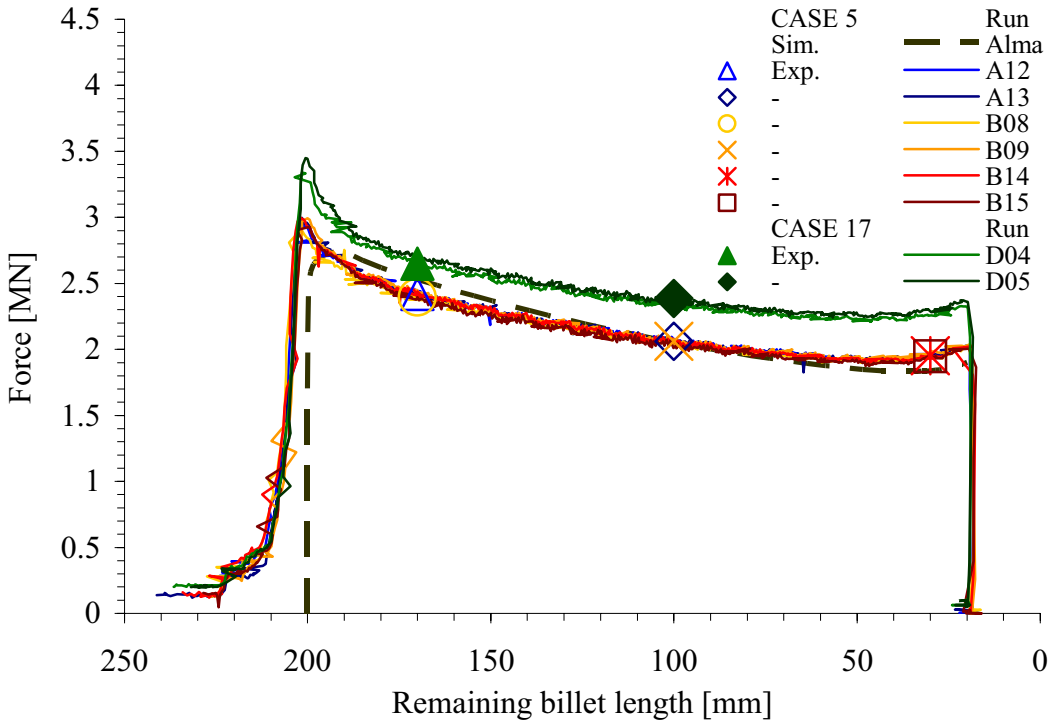

Figure 5.55. Measurement of the ram force - cases 5 and 17 (zero/long bearing).

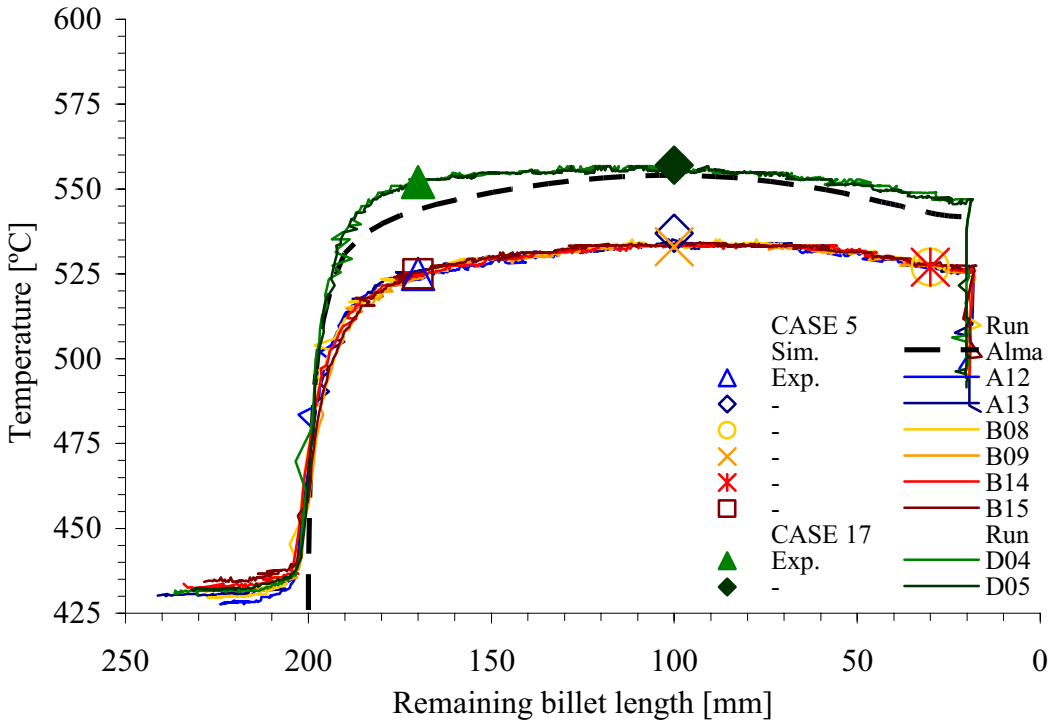

Figure 5.56. Measurement of the outlet temperature (bearing inlet) - cases 5 and 17.

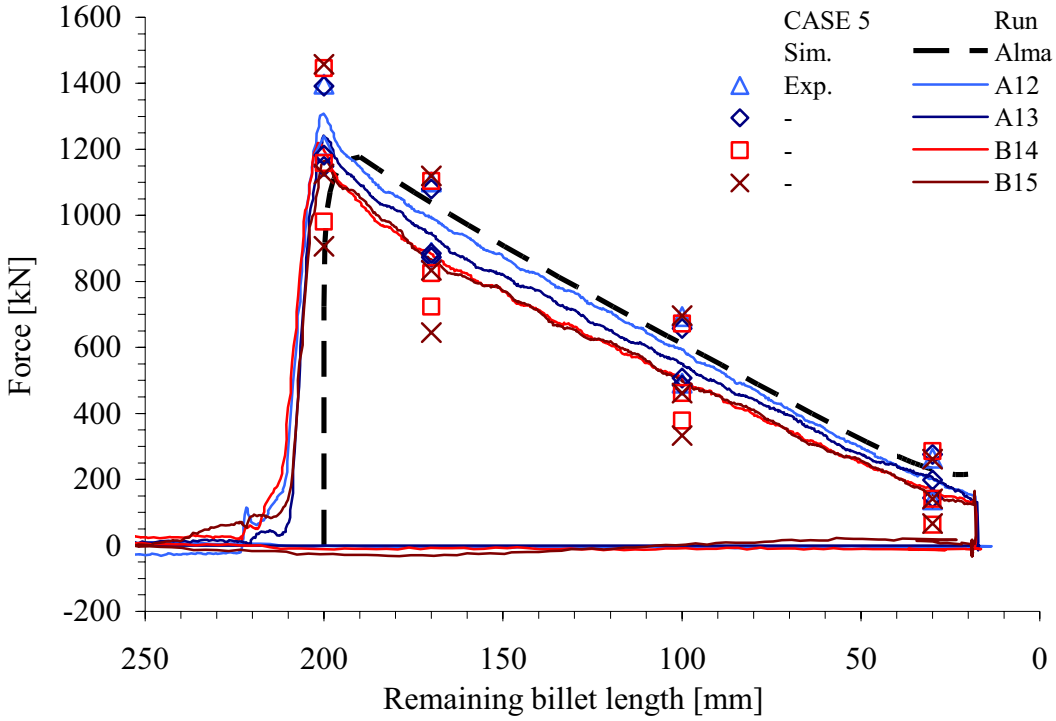

Figure 5.57. Measurement of the average container liner force – case 5.

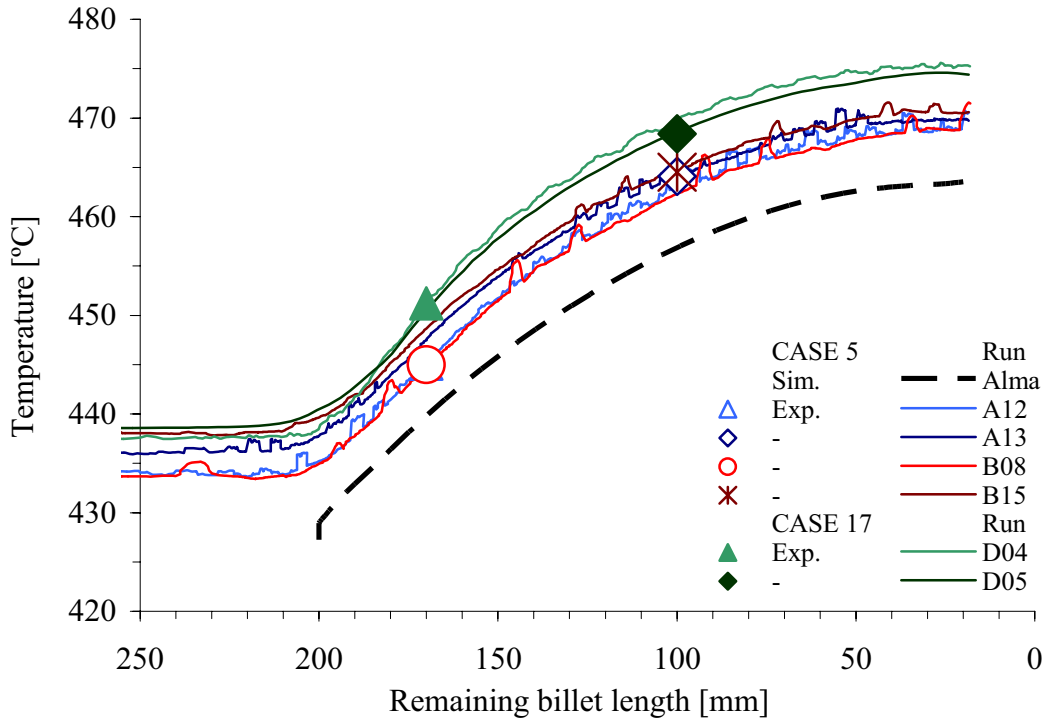

Figure 5.58. Measurement of the die face temperature - cases 1 and 13.

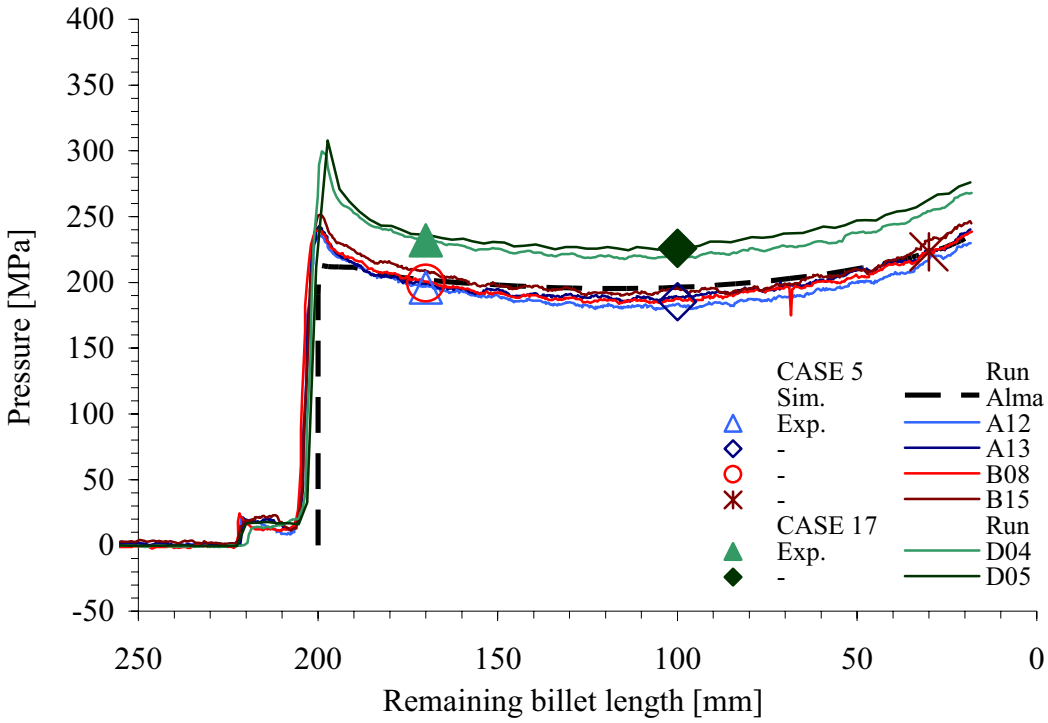

Figure 5.59. Measurement of the die face pressure by sensor 1 - cases 5 and 17.

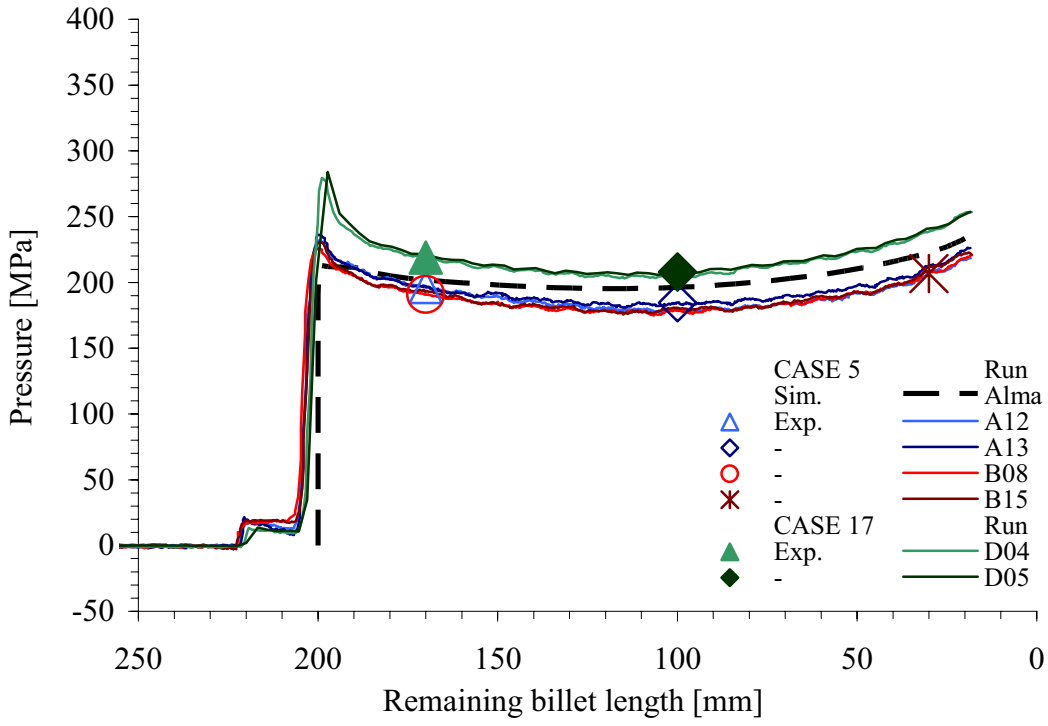

Figure 5.60. Measurement of the die face pressure by sensor 2 - cases 5 and 17.

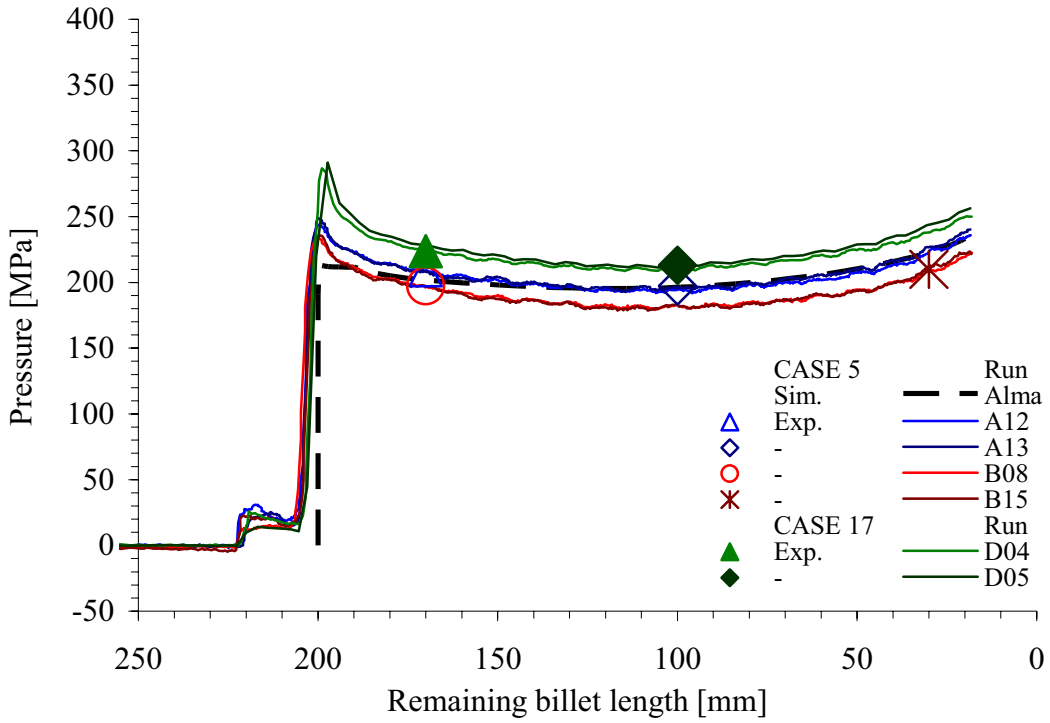

Figure 5.61. Measurement of the die face pressure by sensor 3 - cases 5 and 17.

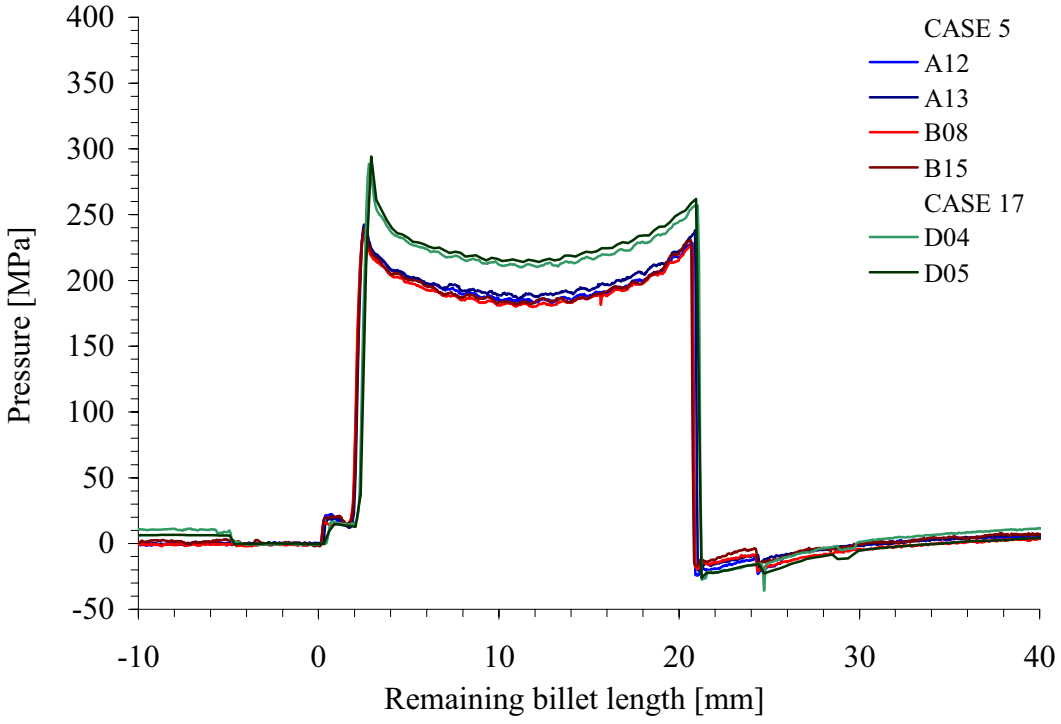

Figure 5.62. Measurement of the average die face pressure - cases 5 and 17.

Table 5.13. Case 6 – input and output data

SPECIFICATION	CASE	6							
Nominal extrusion ratio		40	-		Die outlet diameter			15.8	mm
Nominal bearing length		0	mm						
Nominal ram velocity		20	mm/s		Profile velocity			800	mm/s
Nominal billet temperature		500	ºC						
INPUT DATA	Day/run #	B10	B11	-	-	-	-	Avg.	St.dev.
Actual velocity [mm/s]	Ram	20.3	20.3	-	-	-	-	20.3	0.0
	Profile	812	812	-	-	-	-	812	0.0
Initial billet surface	Front	495	495	-	-	-	-	495	0.0
temperature [ºC]	Back	491	490	-	-	-	-	491	0.7
	Average	493	493	-	-	-	-	493	0.4
Ram temperature [ºC]	Front	123	120	-	-	-	-	122	2.1
RESPONSE		1	2	3	4	5	6	Avg.	St.dev.
Ram force [kN]	Maximum	3184	3224	-	-	-	-	3204	28.3
	Minimum	2000	1997	-	-	-	-	1999	2.1
	196 mm	3050	3100	-	-	-	-	3075	35.4
	170 mm	2570	2575	-	-	-	-	2573	3.5
	100 mm	2140	2140	-	-	-	-	2140	0.0
	30 mm	2090	2100	-	-	-	-	2095	7.1
Bearing inlet	Maximum	555	555	-	-	-	-	555	0.0
temperature [ºC]	Minimum	433	432	-	-	-	-	433	0.7
	170 mm	533	532	-	-	-	-	533	0.7
	100 mm	552	553	-	-	-	-	553	0.7
	30 mm	553	553	-	-	-	-	553	0.0
Bearing outlet	Maximum	-	-	-	-	-	-	-	-
temperature [ºC]	Minimum	-	-	-	-	-	-	-	-
	170 mm	-	-	-	-	-	-	-	-
	100 mm	-	-	-	-	-	-	-	-
	30 mm	-	-	-	-	-	-	-	-
Die face pressure	196 mm	256	257	-	-	-	-	257	0.8
avg. value [MPa]	170 mm	220	218	-	-	-	-	219	1.5
for all 3 sensors	100 mm	199	197	-	-	-	-	198	1.3
	30 mm	226	225					225	0.3
Die face pressure	196 mm	9.2	10.5	-	-	-	-	9.9	-
st. dev. value [MPa]	170 mm	7.1	8.0	-	-	-	-	7.5	-
for all 3 sensors	100 mm	4.3	4.8	-	-	-	-	4.6	-
	30 mm	6.4	8.4	-	-	-	-	7.4	-
Container / liner force	196 mm	-	-	-	-	-	-	-	-
avg. value [kN]	170 mm	-	-	-	-	-	-	-	-
	100 mm	-	-	-	-	-	-	-	-
	30 mm	-	-	-	-	-	-	-	-
Liner friction [MPa]		-	-	-	-	-	-	-	-

Table 5.14. Case 18 – input and output data

SPECIFICATION	CASE	18						
Nominal extrusion ratio		40	-		Die outlet diameter		15.8	mm
Nominal bearing length		12	mm					
Nominal ram velocity		20	mm/s		Profile velocity		800	mm/s
Nominal billet temperature		500	ºC					

INPUT DATA	Day/run #	D07	D10	D20	-	Avg.	St.dev.	C18 - C6
Actual velocity [mm/s]	Ram	20.3	20.3	20.3	-	20.3	0.0	0.0
	Profile	812	812	812	-	812	0.0	0.0
Initial billet surface	Front	499	496	494	-	496	2.5	1.3
temperature [ºC]	Back	491	489	489	-	490	1.2	-0.8
	Average	495	493	492	-	493	1.8	0.3
Ram temperature [ºC]	Front	137	143	134	-	138	4.6	16.5

RESPONSE		1	2	3	4	Avg.	St.dev.	C18 - C6
Ram force [kN]	Maximum	3575	3586	3621	-	3594	24.0	50
	Minimum	2281	2257	2252	-	2263	15.5	34
Effect C18 - C6:	196 mm	3321	3263	3260	-	3281	34.4	26
Pressure [MPa]	170 mm	2809	2780	2812	-	2800	17.7	29
	100 mm	2420	2380	2405	-	2402	20.2	33
	30 mm	2370	2370	2360	-	2367	5.8	35
Bearing inlet	Maximum	582	582	580	-	581	1.2	26
temperature [ºC]	Minimum	431	432	434	-	432	1.5	0
	170 mm	568	568	568	-	568	0.0	36
	100 mm	581	580	578	-	580	1.5	27
	30 mm	578	578	576	-	577	1.2	24
Bearing outlet	Maximum	589	588	586	-	588	1.5	-
temperature [ºC]	Minimum	431	432	434	-	432	1.5	-
	170 mm	571	570	570	-	570	0.6	-
	100 mm	587	586	583	-	585	2.1	-
	30 mm	588	584	583	-	585	2.6	-
Die face pressure	196 mm	308	304	315	-	309	5.3	52
avg. value [MPa]	170 mm	237	245	246	-	243	5.1	24
for all 3 sensors	100 mm	220	228	231	-	226	5.8	28
	30 mm	248	260	255	-	254	6.5	29
Die face pressure	196 mm	4.3	11.4	12.6	-	9.5	-	-0.4
st. dev. value [MPa]	170 mm	2.7	9.4	9.2	-	7.1	-	-0.5
for all 3 sensors	100 mm	3.6	10.4	12.6	-	8.9	-	4.3
	30 mm	4.0	6.6	9.6	-	6.7	-	-0.7
Container / liner force	196 mm	-	-	-	-	-	-	-
avg. value [kN]	170 mm	-	-	-	-	-	-	-
	100 mm	-	-	-	-	-	-	-
	30 mm	-	-	-	-	-	-	-
Liner friction [MPa]		-	-	-	-	-	-	-

.

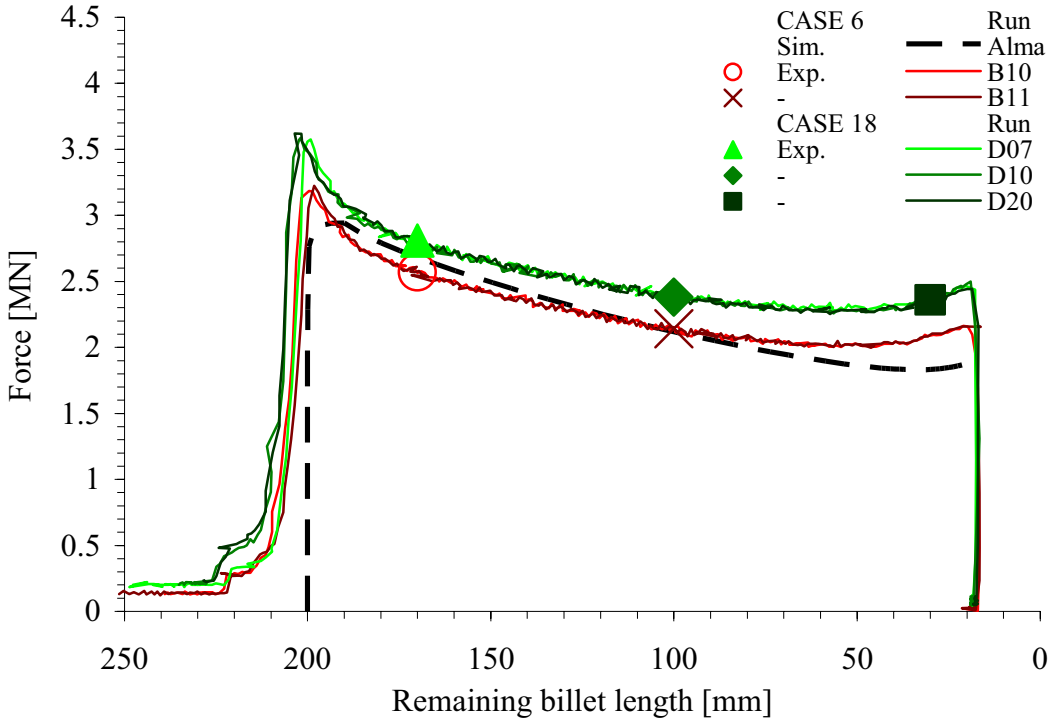

Figure 5.63. Measurement of the ram force - cases 6 and 18 (zero/long bearing).

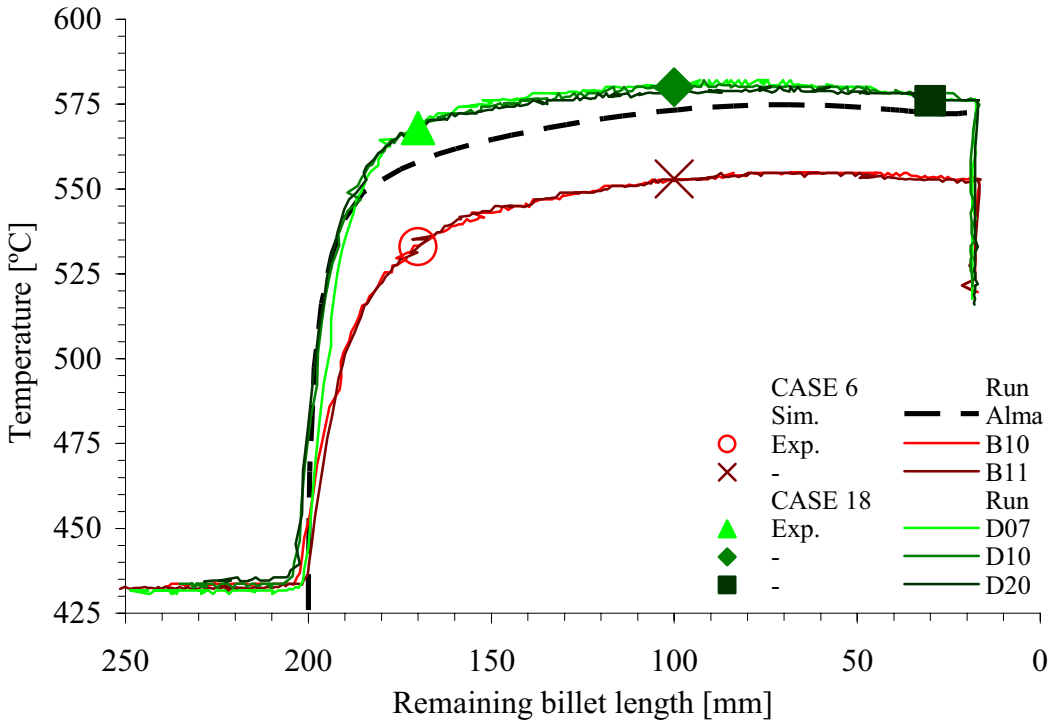

Figure 5.64. Measurement of the outlet temperature (bearing inlet) - cases 6 and 18.

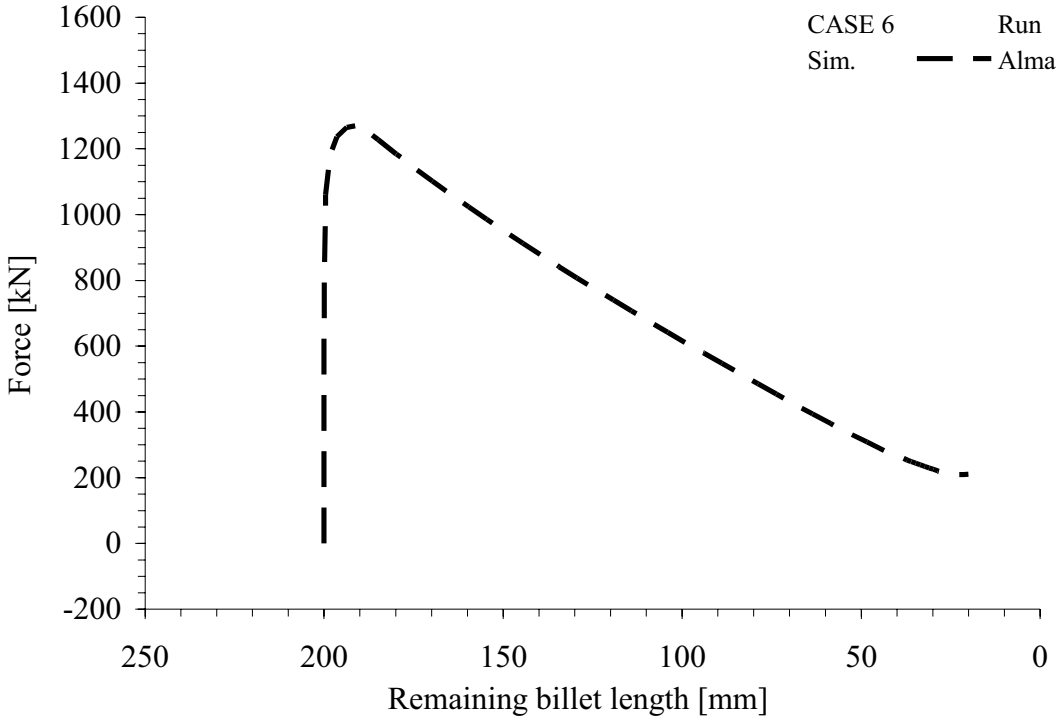

Figure 5.65. Measurement of the average container liner force - case 6.

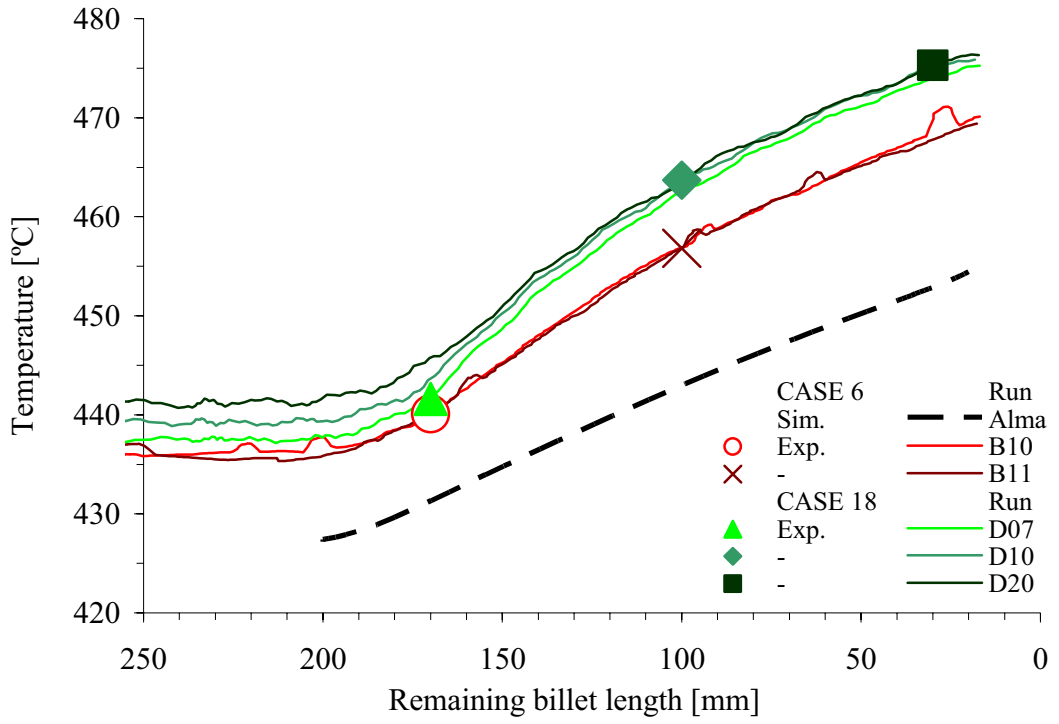

Figure 5.66. Measurement of the die face temperature - cases 6 and 18.

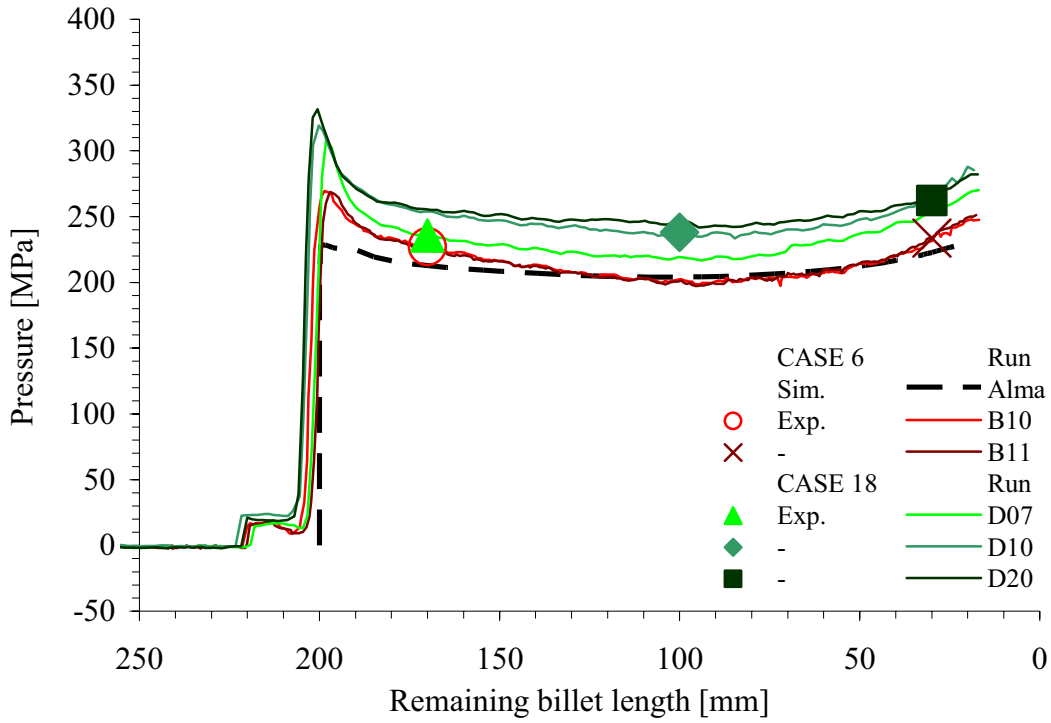

Figure 5.67. Measurement of the die face pressure by sensor 1 - cases 6 and 18.

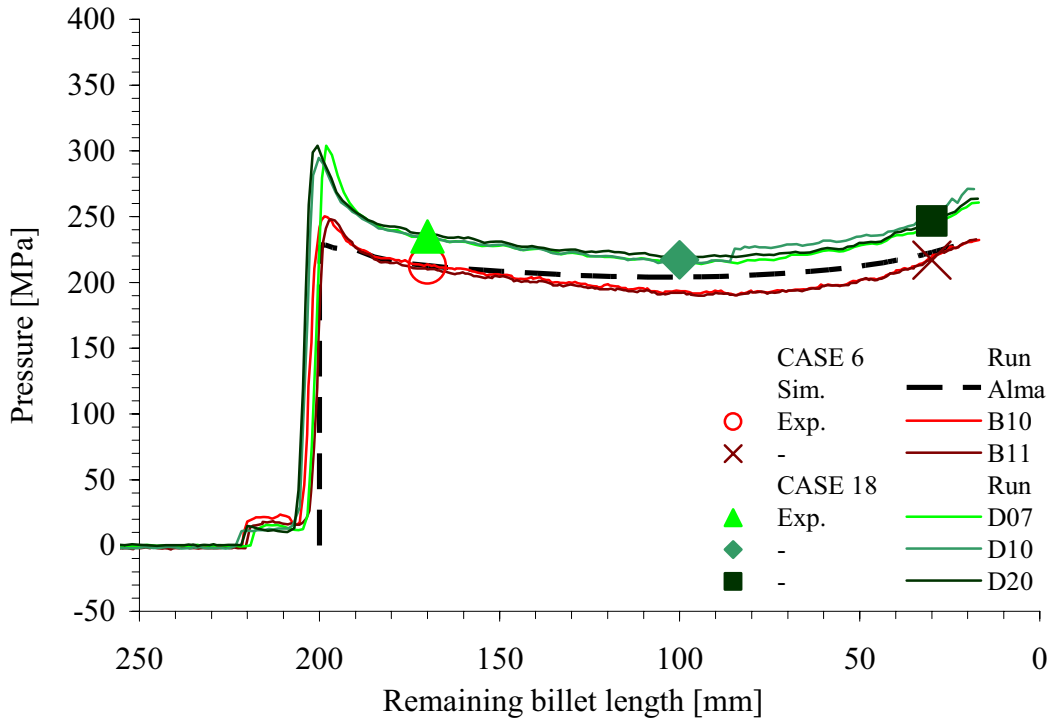

Figure 5.68. Measurement of the die face pressure by sensor 2 - cases 6 and 18.

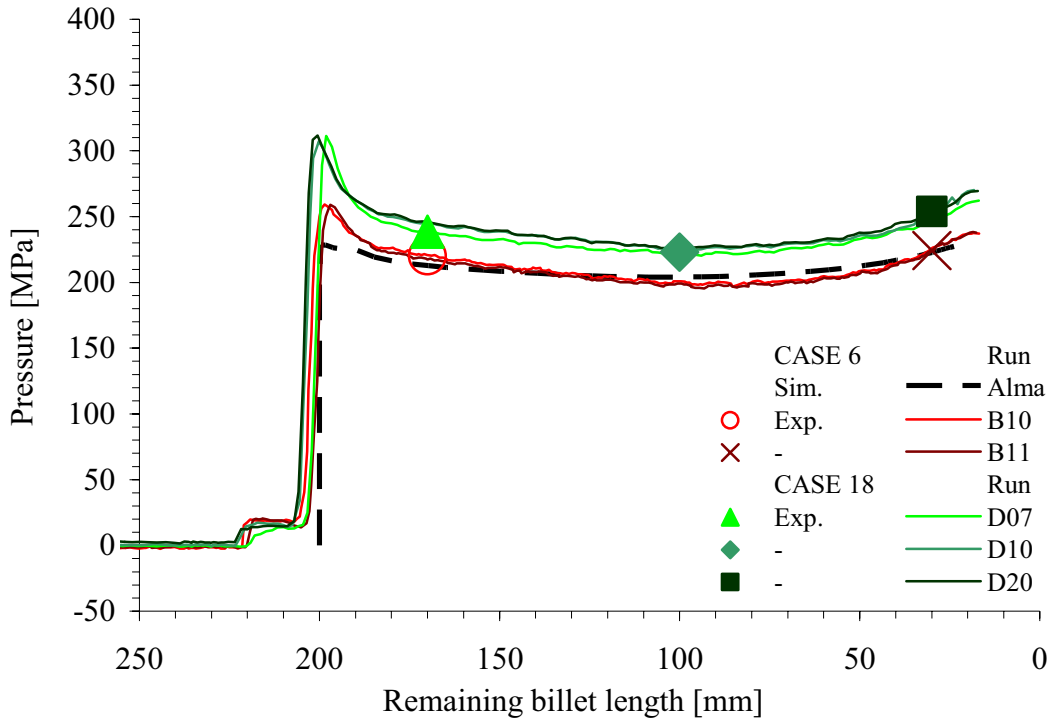

Figure 5.69. Measurement of the die face pressure by sensor 3 - cases 6 and 18.

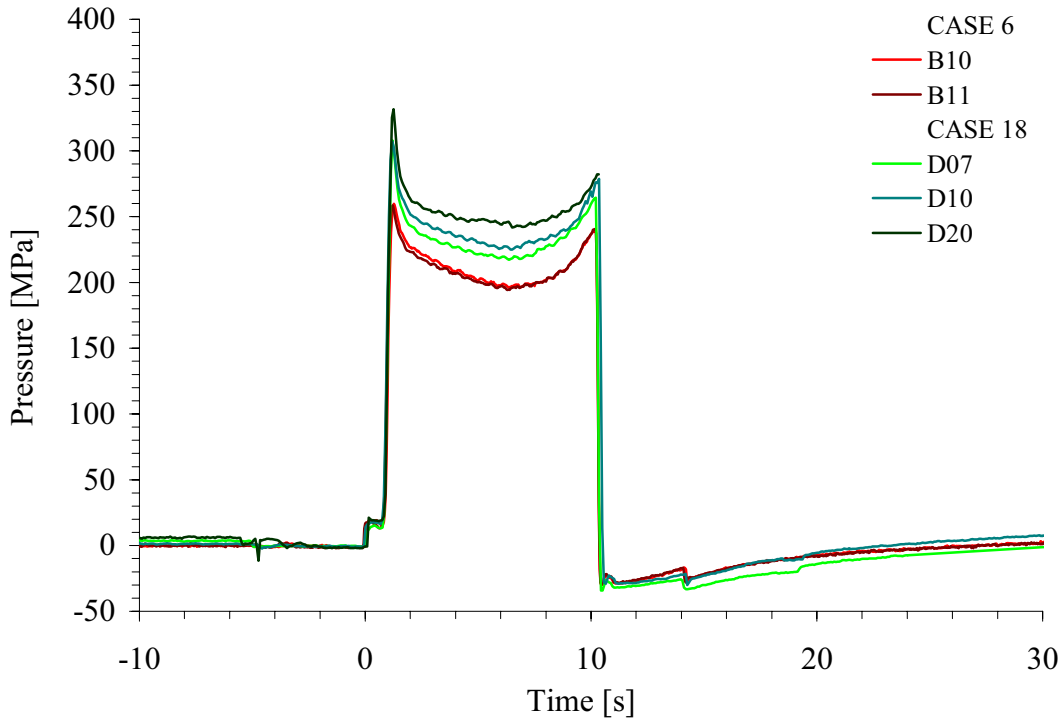

Figure 5.70. Measurement of the average die face pressure - cases 6 and 18.

Table 5.15. Case 7 – input and output data

SPECIFICATION	CASE	7						
Nominal extrusion ratio		80	-		Die outlet diameter		11.2	mm
Nominal bearing length		0	mm					
Nominal ram velocity		2.5	mm/s		Profile velocity		200	mm/s
Nominal billet temperature		450	ºC					

INPUT DATA	Day/run #	C02	C03	C04	-	Avg.	St.dev.	C7 - C1
Actual velocity [mm/s]	Ram	2.4	2.4	2.4	-	2.4	0.0	-2.6
	Profile	192	192	192	-	192	0.0	-8.0
Initial billet surface	Front	449	451	449	-	450	1.2	5.3
temperature [ºC]	Back	443	444	444	-	444	0.6	1.3
	Average	446	448	447	-	447	0.8	3.3
Ram temperature [ºC]	Front	136	122	126	-	128	7.2	-8.0

RESPONSE		1	2	3	4	Avg.	St.dev.	C7 - C1
Ram force [kN]	Maximum	3074	3051	3077	-	3067	14.2	6
	Minimum	1988	2046	2037	-	2024	31.2	27
Effect C7 - C1:	196 mm	2996	3005	3040	-	3014	23.2	8
Pressure [MPa]	170 mm	2700	2719	2700	-	2706	11.0	15
	100 mm	2305	2300	2280	-	2295	13.2	23
	30 mm	2060	2055	2057	-	2057	2.5	22
Bearing inlet	Maximum	499	500	500	-	500	0.6	-5
temperature [ºC]	Minimum	428	428	427	-	428	0.6	0
	170 mm	497	497	497	-	497	0.0	-1
	100 mm	498	498	498	-	498	0.0	-5
	30 mm	489	489	489	-	489	0.0	-6
Bearing outlet	Maximum	-	-	-	-	-	-	-
temperature [ºC]	Minimum	-	-	-	-	-	-	-
	170 mm	-	-	-	-	-	-	-
	100 mm	-	-	-	-	-	-	-
	30 mm	-	-	-	-	-	-	-
Die face pressure	196 mm	239	238	240	-	239	1.1	7
avg. value [MPa]	170 mm	227	227	225	-	227	0.9	13
for all 3 sensors	100 mm	236	236	235	-	235	0.8	31
	30 mm	253	254	254	-	254	0.6	25
Die face pressure	196 mm	4.0	3.0	4.0	-	3.7	-	-3.6
st. dev. value [MPa]	170 mm	4.7	3.2	3.5	-	3.8	-	-3.3
for all 3 sensors	100 mm	7.8	6.9	7.1	-	7.3	-	0.0
	30 mm	8.3	7.4	7.8	-	7.8	-	-2.0
Container / liner force	196 mm	-	-	1165	-	1165	-	-138
avg. value [kN]	170 mm	-	-	875	-	875	-	-125
	100 mm	-	-	455	-	455	-	-96
	30 mm	-	-	193	-	193	-	12
Liner friction [MPa]		-	-	19.1	-	19.1	-	-1.3

Table 5.16. Case 19 – input and output data

SPECIFICATION	CASE	19						
Nominal extrusion ratio		80	-		Die outlet diameter		11.2	mm
Nominal bearing length		8.5	mm					
Nominal ram velocity		2.5	mm/s		Profile velocity		200	mm/s
Nominal billet temperature		450	ºC					

INPUT DATA	Day/run #	E01	E03	E13	-	Avg.	St.dev.	C19 - C7
Actual velocity [mm/s]	Ram	2.3	2.6	2.6	-	2.5	0.2	0.1
	Profile	184	208	208	-	200	13.9	8.0
Initial billet surface	Front	448	451	442	-	447	4.6	-2.7
temperature [ºC]	Back	442	443	440	-	442	1.5	-2.0
	Average	445	447	441	-	444	3.1	-2.3
Ram temperature [ºC]	Front	140	139	122	-	134	10.1	5.7

RESPONSE		1	2	3	4	Avg.	St.dev.	C19 - C7
Ram force [kN]	Maximum	3430	3534	3621	-	3528	95.6	59
	Minimum	2439	2489	2509	-	2479	36.1	58
Effect C19 - C7:	196 mm	3378	3488	3563	-	3476	93.1	59
Pressure [MPa]	170 mm	3078	3153	3230	-	3154	76.0	57
	100 mm	2660	2720	2800	-	2727	70.2	55
	30 mm	2450	2500	2535	-	2495	42.7	56
Bearing inlet	Maximum	513	519	519	-	517	3.5	17
temperature [ºC]	Minimum	430	432	433	-	432	1.5	4
	170 mm	511	515	515	-	514	2.3	17
	100 mm	509	515	515	-	513	3.5	15
	30 mm	501	505	506	-	504	2.6	15
Bearing outlet	Maximum	521	528	528	-	526	4.0	-
temperature [ºC]	Minimum	430	432	433	-	432	1.5	-
	170 mm	518	525	522	-	522	3.5	-
	100 mm	520	525	526	-	524	3.2	-
	30 mm	512	517	516	-	515	2.6	-
Die face pressure	196 mm	285	315	316	-	305	17.6	66
avg. value [MPa]	170 mm	273	297	303	-	291	15.9	64
for all 3 sensors	100 mm	282	303	304	-	296	12.4	61
	30 mm	299	321	316	-	312	11.5	58
Die face pressure	196 mm	16.9	22.6	34.7	-	24.7	-	21.1
st. dev. value [MPa]	170 mm	18.0	22.8	34.1	-	25.0	-	21.1
for all 3 sensors	100 mm	24.3	24.7	38.4	-	29.1	-	21.9
	30 mm	23.7	23.2	32.2	-	26.4	-	18.5
Container / liner force	196 mm	-	-	1273	-	1273	-	108
avg. value [kN]	170 mm	-	-	1133	-	1133	-	258
	100 mm	-	-	706	-	706	-	251
	30 mm	-	-	359	-	359	-	166
Liner friction [MPa]		-	-	19.4	-	19.4	-	0.3

.

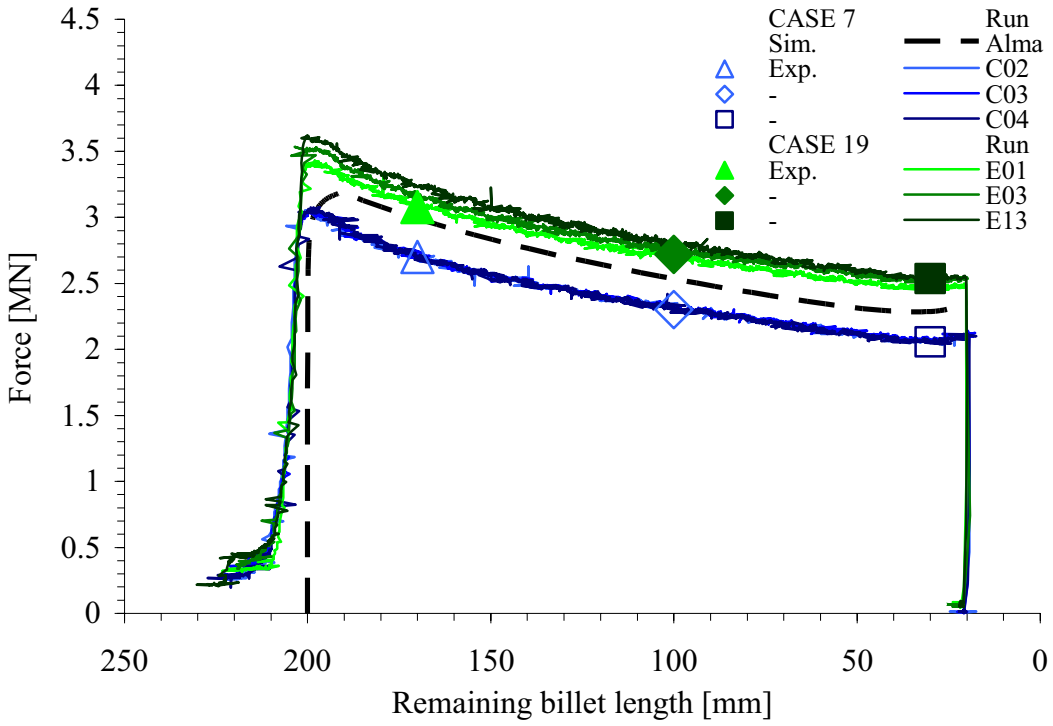

Figure 5.71. Measurement of the ram force - cases 7 and 19 (zero/long bearing).

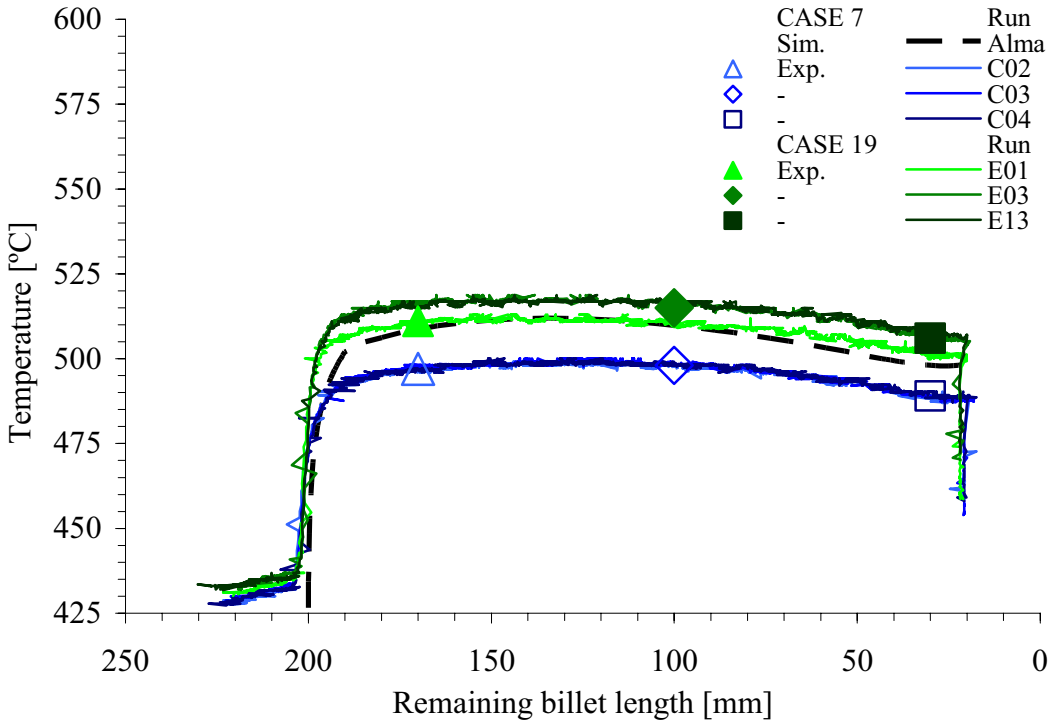

Figure 5.72. Measurement of the outlet temperature (bearing inlet) - cases 7 and 19.

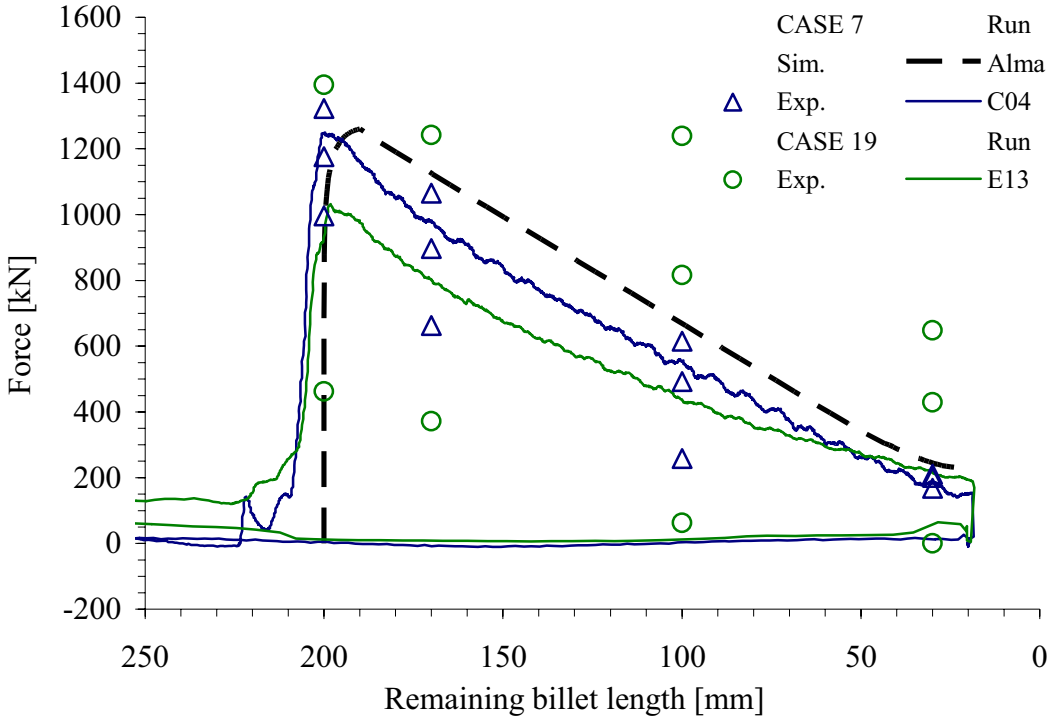

Figure 5.73. Measurement of the average container liner force - cases 7 and 19.

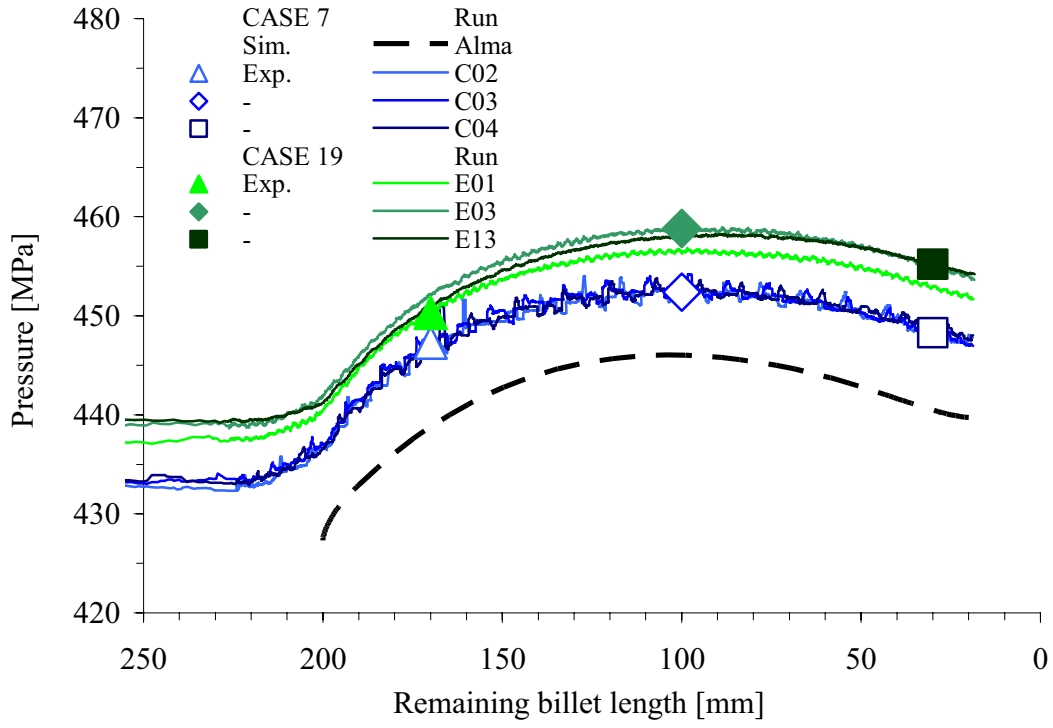

Figure 5.74. Measurement of the die face temperature - cases 7 and 19.

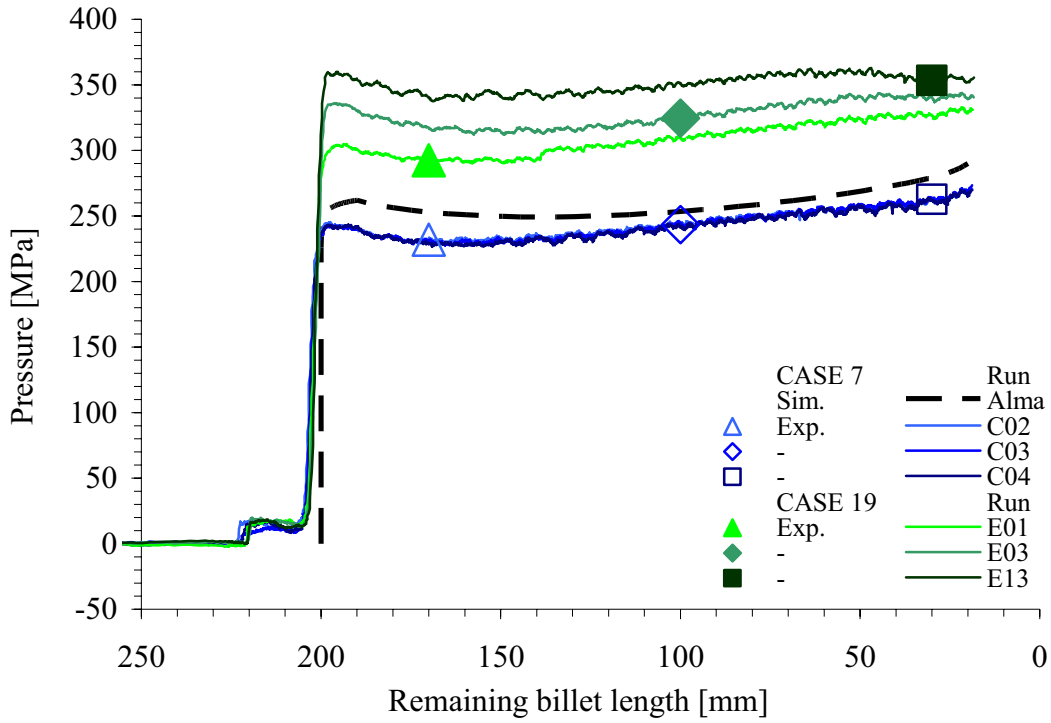

Figure 5.75. Measurement of the die face pressure by sensor 1 - cases 7 and 19.

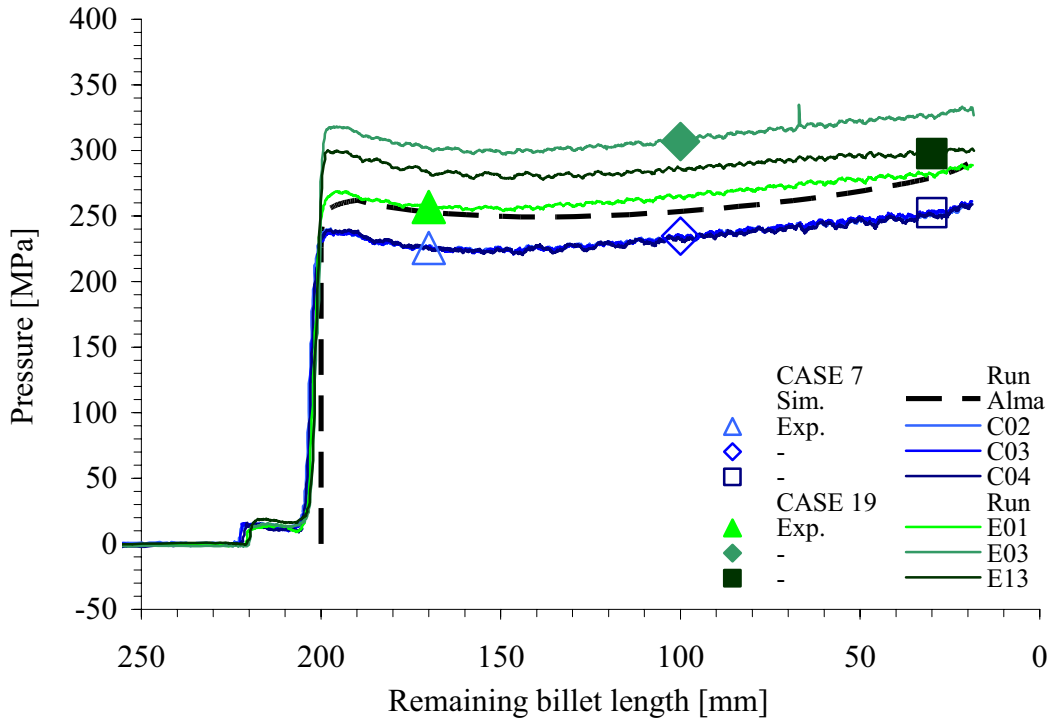

Figure 5.76. Measurement of the die face pressure by sensor 2 - cases 7 and 19.

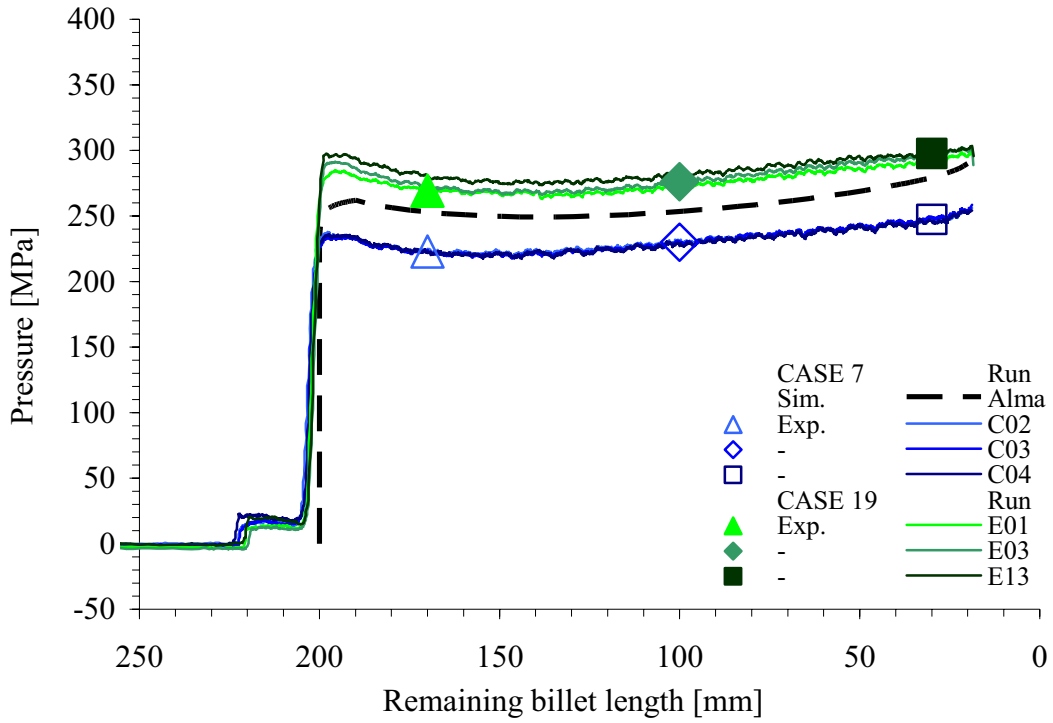

Figure 5.77. Measurement of the die face pressure by sensor 3 - cases 7 and 19.

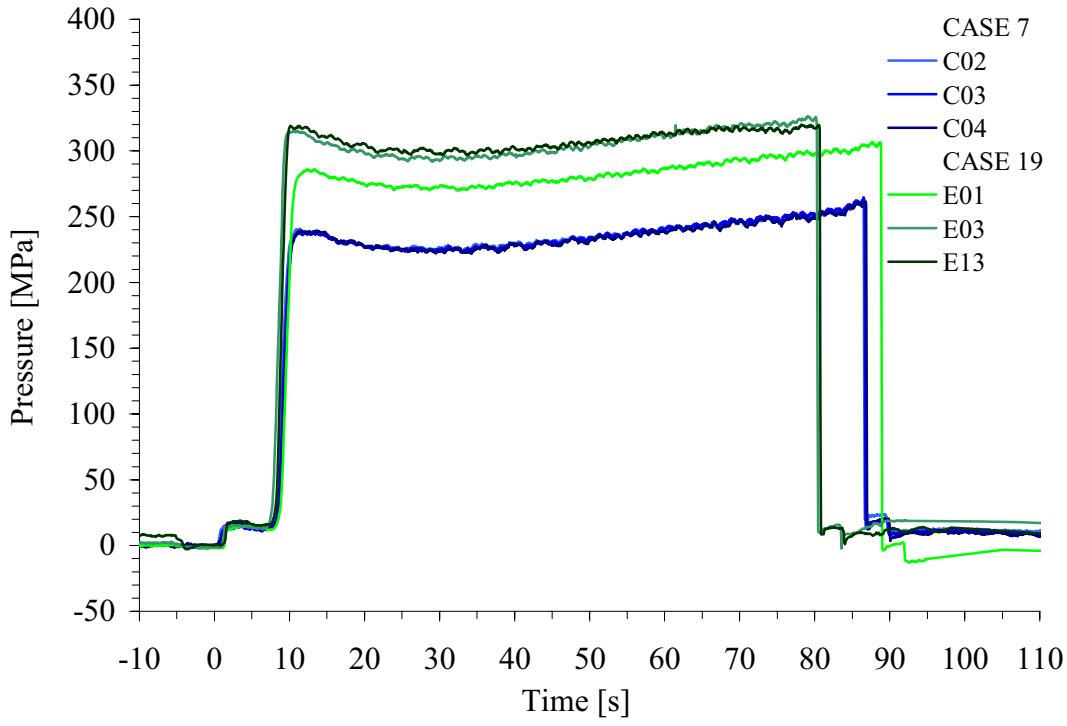

Figure 5.78. Measurement of the average die face pressure - cases 7 and 19.

Table 5.17. Case 8 – input and output data

SPECIFICATION	CASE	8						
Nominal extrusion ratio		80	-		Die outlet diameter		11.2	mm
Nominal bearing length		0	mm					
Nominal ram velocity		5	mm/s		Profile velocity		400	mm/s
Nominal billet temperature		450	ºC					

INPUT DATA	Day/run #	C05	C06	C15	C16	Avg.	St.dev.	C8 - C2
Actual velocity [mm/s]	Ram	5.0	5.0	5.0	5.0	5.0	0.0	-5.1
	Profile	400	400	400	400	400	0.0	-4.0
Initial billet surface	Front	452	449	451	450	451	1.3	1.7
temperature [ºC]	Back	445	444	445	443	444	1.0	0.6
	Average	449	447	448	447	447	1.0	1.1
Ram temperature [ºC]	Front	120	119	116	123	120	2.9	-15.8

RESPONSE		1	2	3	4	Avg.	St.dev.	C8 - C2
Ram force [kN]	Maximum	3392	3409	3456	3412	3417	27.3	12
	Minimum	2222	2231	2185	2164	2201	31.4	29
Effect C8 - C2:	196 mm	3320	3331	3285	3317	3313	19.8	15
Pressure [MPa]	170 mm	2950	2950	2927	2960	2947	14.0	21
	100 mm	2480	2490	2490	2480	2485	5.8	30
	30 mm	2257	2254	2280	2280	2268	14.2	29
Bearing inlet	Maximum	521	522	524	522	522	1.3	-2
temperature [ºC]	Minimum	428	428	430	428	429	1.0	1
	170 mm	516	515	518	518	517	1.5	5
	100 mm	521	520	522	520	521	1.0	-2
	30 mm	513	514	514	514	514	0.5	-4
Bearing outlet	Maximum	-	-	-	-	-	-	-
temperature [ºC]	Minimum	-	-	-	-	-	-	-
	170 mm	-	-	-	-	-	-	-
	100 mm	-	-	-	-	-	-	-
	30 mm	-	-	-	-	-	-	-
Die face pressure	196 mm	270	268	276	272	272	3.5	12
avg. value [MPa]	170 mm	248	250	252	253	250	2.3	16
for all 3 sensors	100 mm	239	243	244	246	243	3.1	31
	30 mm	263	266	266	275	268	5.2	35
Die face pressure	196 mm	4.3	5.8	7.9	5.5	5.9	-	-1.7
st. dev. value [MPa]	170 mm	3.1	3.4	6.4	4.1	4.3	-	-3.2
for all 3 sensors	100 mm	4.0	6.8	9.3	5.2	6.3	-	-0.4
	30 mm	6.5	8.8	3.0	8.4	6.7	-	-2.9
Container / liner force	196 mm	-	-	1295	1300	1302	10.9	-29
avg. value [kN]	170 mm	-	-	994	995	996	18.9	-57
	100 mm	-	-	536	570	547	21.6	-40
	30 mm	-	-	172	204	181	24.9	-14
Liner friction [MPa]		-	-	20.8	19.3	20.4	1.1	-0.8

Table 5.18. Case 20 – input and output data

SPECIFICATION	CASE	20						
Nominal extrusion ratio		80	-	Die outlet diameter		11.2	mm	
Nominal bearing length		8.5	mm					
Nominal ram velocity		5	mm/s	Profile velocity		400	mm/s	
Nominal billet temperature		450	ºC					
INPUT DATA	Day/run #	E17	E18	-	-	Avg.	St.dev.	C20 - C8
Actual velocity [mm/s]	Ram	5.0	5.0	-	-	5.0	0.0	0.0
	Profile	400	400	-	-	400	0.0	0.0
Initial billet surface	Front	450	449	-	-	450	0.7	-1.0
temperature [ºC]	Back	443	449	-	-	446	4.2	1.8
	Average	447	449	-	-	448	1.8	0.4
Ram temperature [ºC]	Front	127	135	-	-	131	5.7	11.5
RESPONSE		1	2	3	4	Avg.	St.dev.	C20 - C8
Ram force [kN]	Maximum	3921	3748	-	-	3835	122.3	53
	Minimum	2610	2575	-	-	2593	24.7	50
Effect C20 - C8:	196 mm	3771	3618	-	-	3695	108.2	49
Pressure [MPa]	170 mm	3320	3193	-	-	3257	89.8	39
	100 mm	2840	2770	-	-	2805	49.5	41
	30 mm	2620	2601	-	-	2611	13.4	44
Bearing inlet	Maximum	538	538	-	-	538	0.0	16
temperature [ºC]	Minimum	433	434	-	-	434	0.7	5
	170 mm	535	534	-	-	535	0.7	18
	100 mm	537	536	-	-	537	0.7	16
	30 mm	527	527	-	-	527	0.0	13
Bearing outlet	Maximum	551	552	-	-	552	0.7	-
temperature [ºC]	Minimum	433	434	-	-	434	0.7	-
	170 mm	543	543	-	-	543	0.0	-
	100 mm	548	548	-	-	548	0.0	-
	30 mm	543	540	-	-	542	2.1	-
Die face pressure	196 mm	333	316	-	-	324	12.2	53
avg. value [MPa]	170 mm	294	283	-	-	288	8.0	38
for all 3 sensors	100 mm	288	275	-	-	282	9.0	38
	30 mm	309	302	-	-	305	5.3	38
Die face pressure	196 mm	29.5	5.7	-	-	17.6	-	11.7
st. dev. value [MPa]	170 mm	28.8	5.2	-	-	17.0	-	12.7
for all 3 sensors	100 mm	31.7	7.2	-	-	19.4	-	13.1
	30 mm	28.7	5.2	-	-	17.0	-	10.3
Container / liner force	196 mm	1342	1376	-	-	1359	45.3	57
avg. value [kN]	170 mm	1148	1086	-	-	1117	77.8	121
	100 mm	736	702	-	-	719	46.7	172
	30 mm	247	375	-	-	311	101.8	130
Liner friction [MPa]		18.7	17.5	-	-	18.1	0.9	-2.3

.

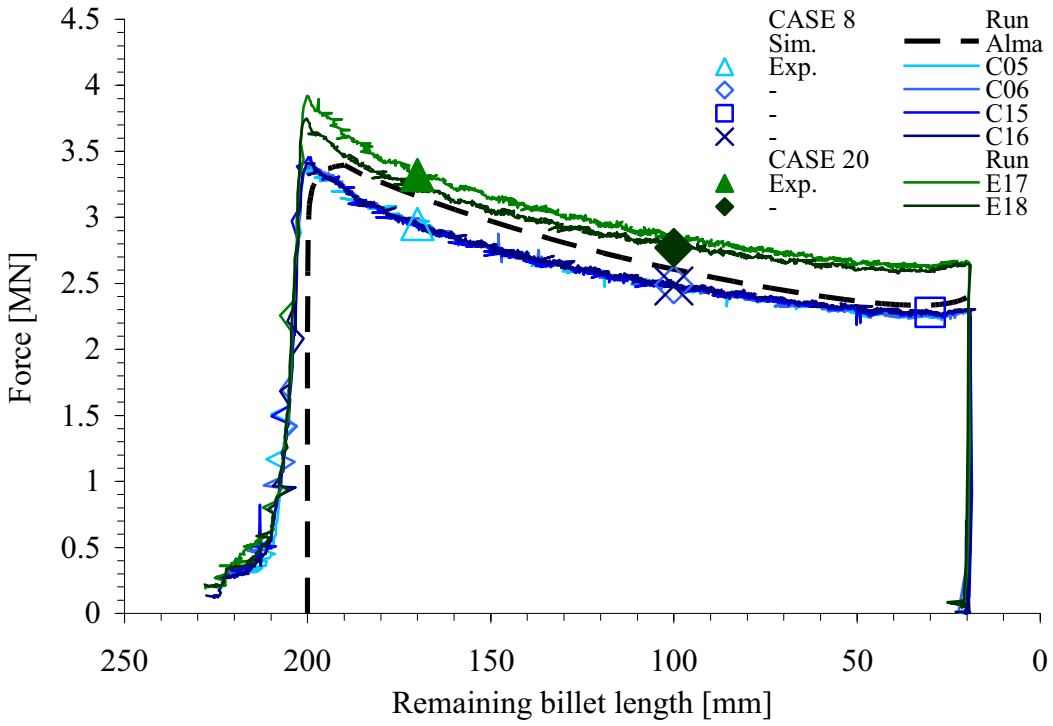

Figure 5.79. Measurement of the ram force - cases 8 and 20 (zero/long bearing).

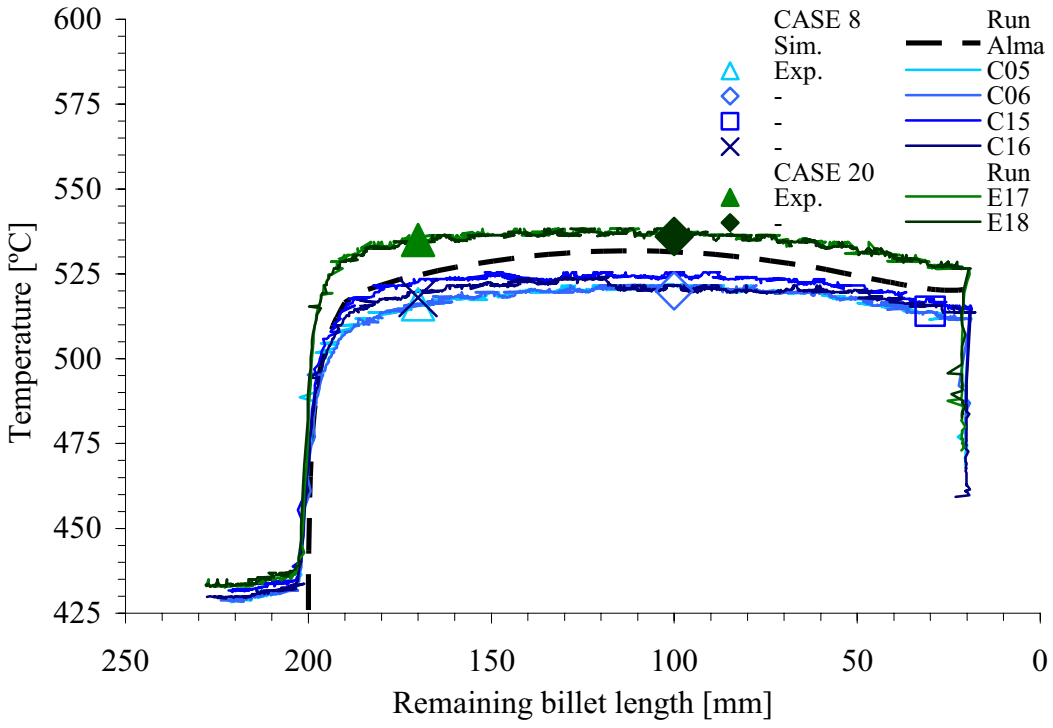

Figure 5.80. Measurement of the outlet temperature (bearing inlet) - cases 8 and 20.

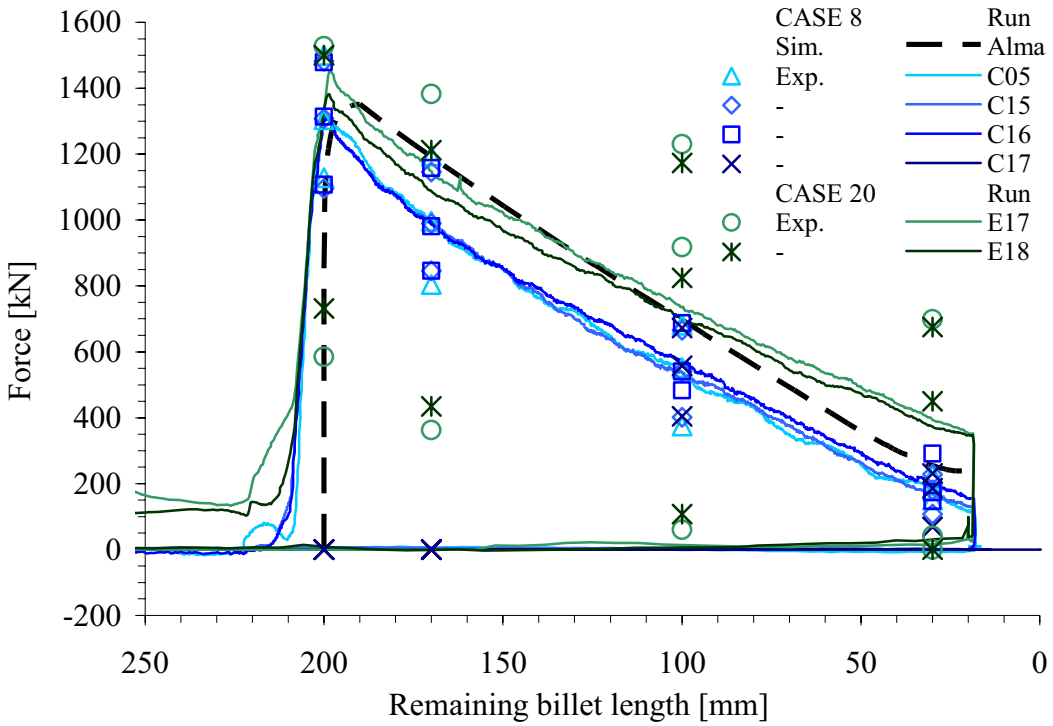

Figure 5.81. Measurement of the average container liner force - cases 8 and 20.

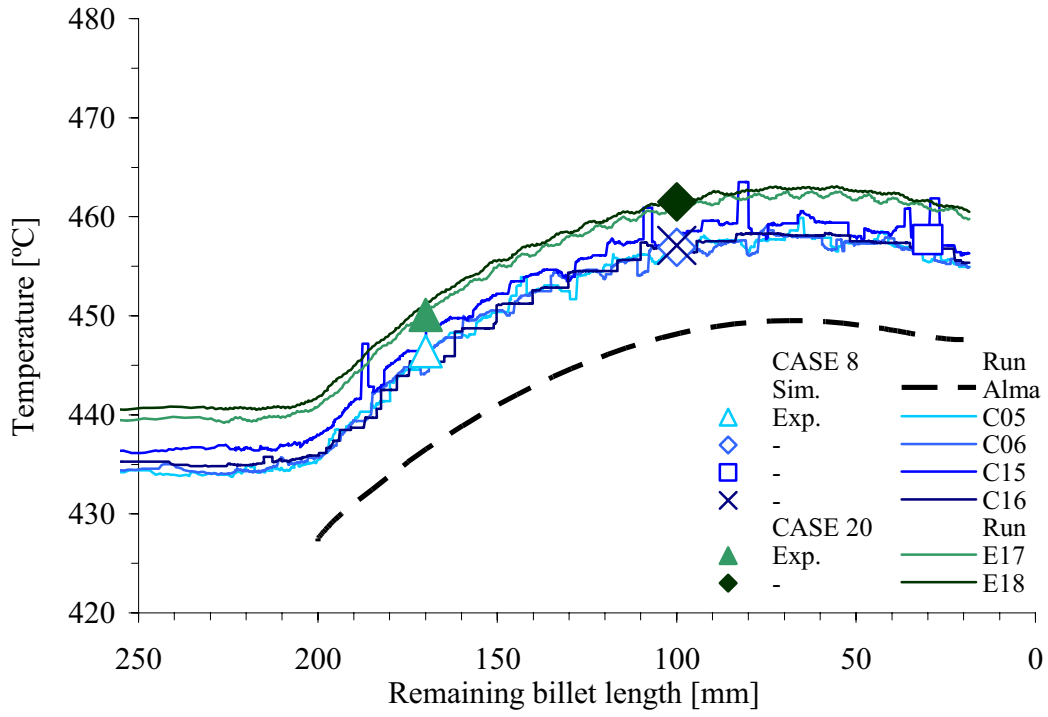

Figure 5.82. Measurement of the die face temperature - cases 8 and 20.

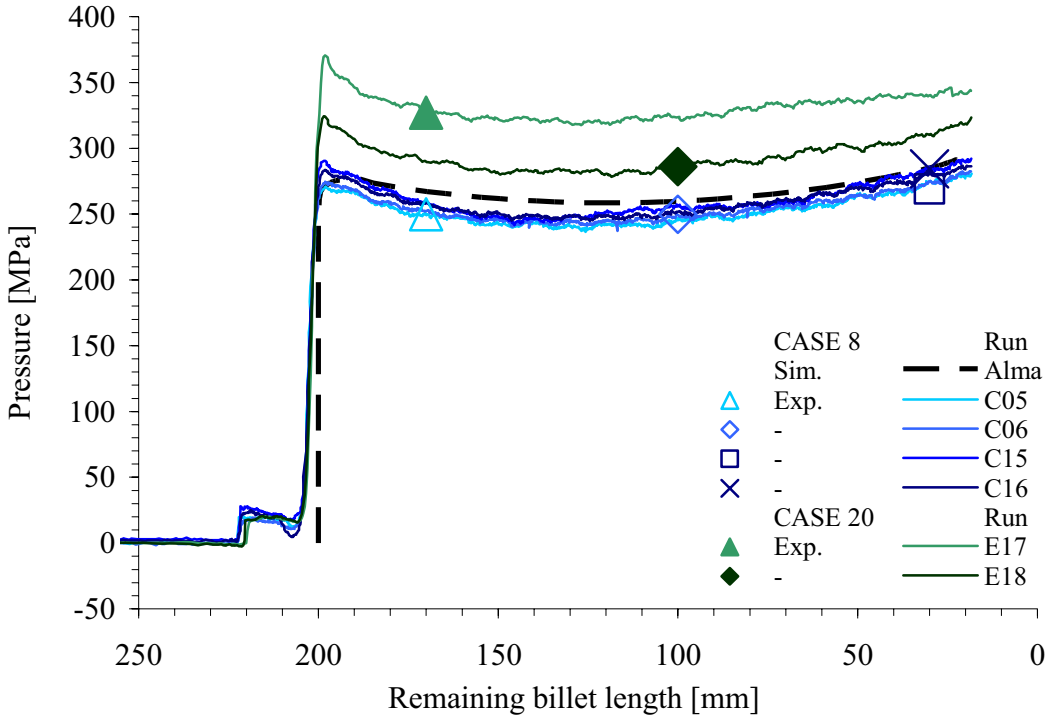

Figure 5.83. Measurement of the die face pressure by sensor 1 - cases 8 and 20.

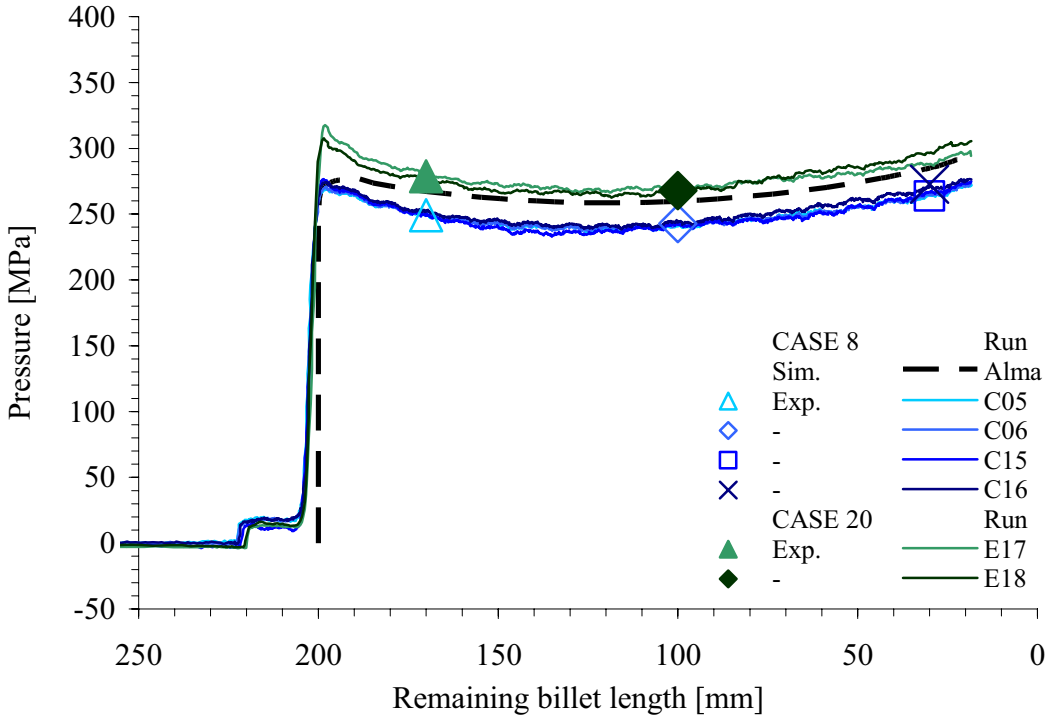

Figure 5.84. Measurement of the die face pressure by sensor 2 - cases 8 and 20.

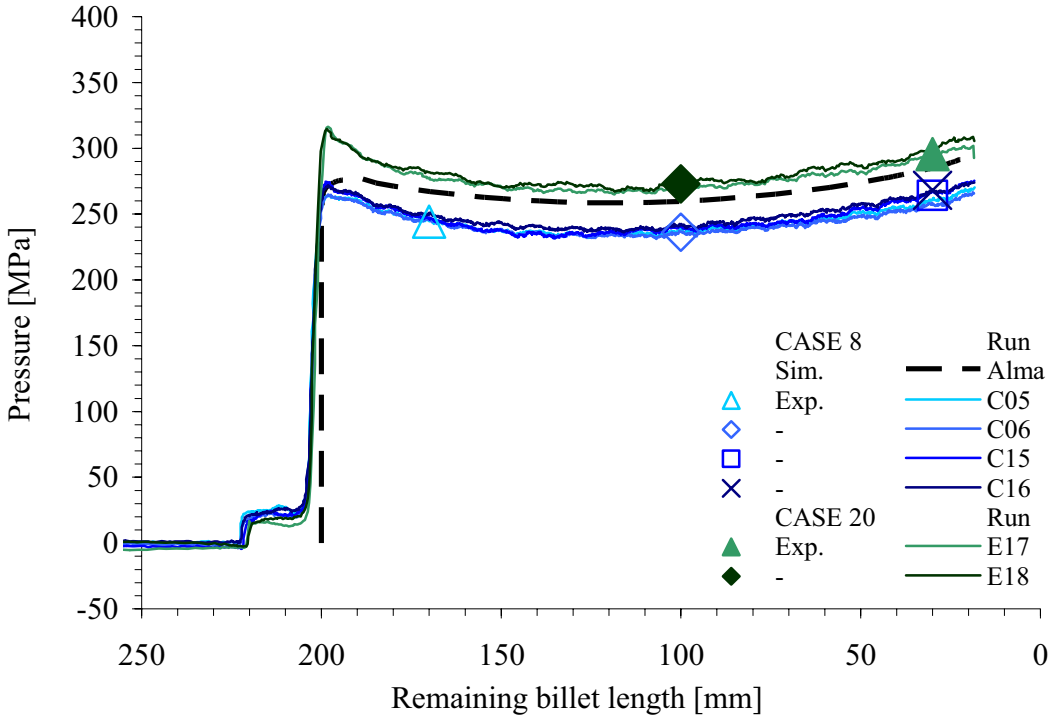

Figure 5.85. Measurement of the die face pressure by sensor 3 - cases 8 and 20.

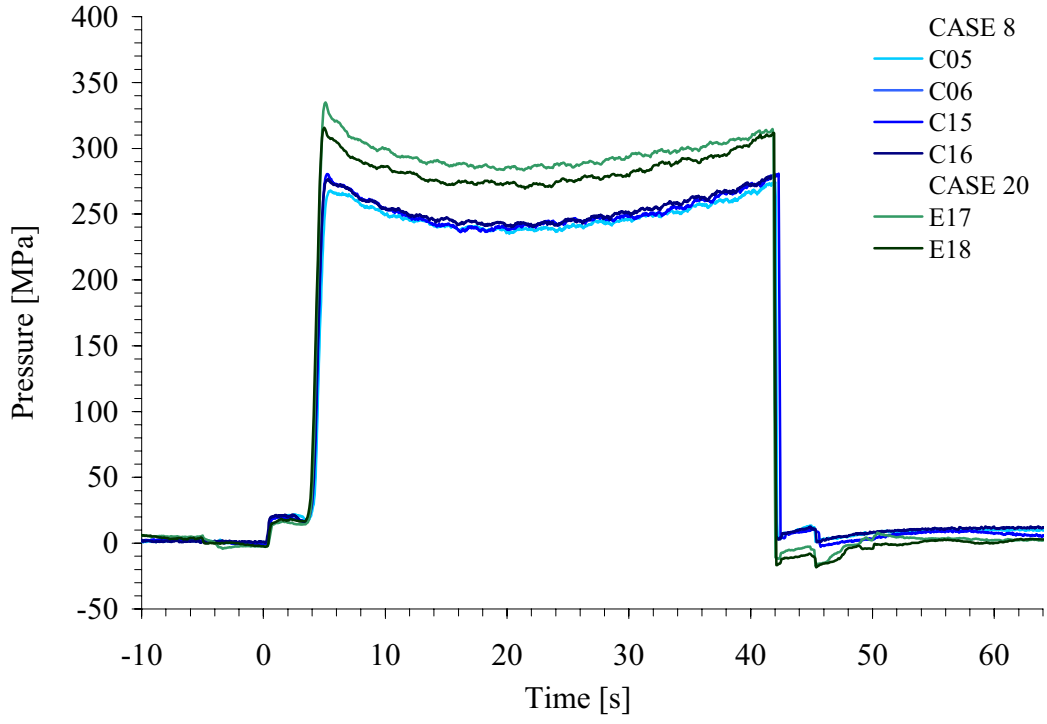

Figure 5.86. Measurement of the average die face pressure - cases 8 and 20.

Table 5.19. Case 9 – input and output data

SPECIFICATION	CASE	9						
Nominal extrusion ratio		80	-	Die outlet diameter		11.2	mm	
Nominal bearing length		0	mm					
Nominal ram velocity		10	mm/s	Profile velocity		800	mm/s	
Nominal billet temperature		450	ºC					
INPUT DATA	**Day/run #**	**C07**	**C08**	**-**	**-**	**Avg.**	**St.dev.**	**C9 - C3**
Actual velocity [mm/s]	Ram	10.1	10.1	-	-	10.1	0.0	-10.3
	Profile	808	808	-	-	808	0.0	-8.0
Initial billet surface	Front	452	449	-	-	451	2.1	1.1
temperature [ºC]	Back	444	445	-	-	445	0.7	-0.3
	Average	448	447	-	-	448	0.7	0.4
Ram temperature [ºC]	Front	127	120	-	-	124	4.9	-7.7
RESPONSE		**1**	**2**	**3**	**4**	**Avg.**	**St.dev.**	**C9 - C3**
Ram force [kN]	Maximum	3690	3733	-	-	3712	30.4	20
	Minimum	2364	2393	-	-	2379	20.5	29
Effect C9 - C3:	196 mm	3606	3640	-	-	3623	24.0	19
Pressure [MPa]	170 mm	3167	3180	-	-	3174	9.2	24
	100 mm	2620	2635	-	-	2628	10.6	31
	30 mm	2421	2425	-	-	2423	2.8	28
Bearing inlet	Maximum	545	547	-	-	546	1.4	-1
temperature [ºC]	Minimum	426	428	-	-	427	1.4	0
	170 mm	537	537	-	-	537	0.0	11
	100 mm	544	545	-	-	545	0.7	2
	30 mm	541	540	-	-	541	0.7	-5
Bearing outlet	Maximum	-	-	-	-	-	-	-
temperature [ºC]	Minimum	-	-	-	-	-	-	-
	170 mm	-	-	-	-	-	-	-
	100 mm	-	-	-	-	-	-	-
	30 mm	-	-	-	-	-	-	-
Die face pressure	196 mm	294	302	-	-	298	5.4	19
avg. value [MPa]	170 mm	272	270	-	-	271	1.5	15
for all 3 sensors	100 mm	250	251	-	-	251	0.8	21
	30 mm	269	270	-	-	269	1.0	23
Die face pressure	196 mm	5.5	7.1	-	-	6.3	-	-2.0
st. dev. value [MPa]	170 mm	4.5	3.0	-	-	3.7	-	-4.1
for all 3 sensors	100 mm	4.5	6.6	-	-	5.6	-	-1.0
	30 mm	5.9	8.0	-	-	6.9	-	-1.3
Container / liner force	196 mm	-	1312	-	-	1312	-	-125
avg. value [kN]	170 mm	-	1029	-	-	1029	-	-133
	100 mm	-	527	-	-	527	-	-85
	30 mm	-	168	-	-	168	-	-21
Liner friction [MPa]		-	22.8	-	-	22.8	-	-2.2

.

Table 5.20. Case 21 – input and output data

SPECIFICATION	CASE	21						
Nominal extrusion ratio		80	-		Die outlet diameter		11.2	Mm
Nominal bearing length		8.5	mm					
Nominal ram velocity		10	mm/s		Profile velocity		800	mm/s
Nominal billet temperature		450	ºC					

INPUT DATA	Day/run #	E02	E12	E19	-	Avg.	St.dev.	C21 - C9
Actual velocity [mm/s]	Ram	10.0	10.1	10.1	-	10.1	0.1	0.0
	Profile	800	808	808	-	805	4.6	-2.7
Initial billet surface	Front	450	449	449	-	449	0.6	-1.2
temperature [ºC]	Back	441	444	442	-	442	1.5	-2.2
	Average	446	447	446	-	446	0.6	-1.7
Ram temperature [ºC]	Front	134	146	140	-	140	6.0	16.5

RESPONSE		1	2	3	4	Avg.	St.dev.	C21 - C9
Ram force [kN]	Maximum	4161	4303	4161	-	4208	82.0	63
	Minimum	2789	2728	2714	-	2744	39.9	46
Effect C21 - C9:	196 mm	4080	4037	4011	-	4043	34.8	53
Pressure [MPa]	170 mm	3540	3490	3480	-	3503	32.1	42
	100 mm	2975	2940	2905	-	2940	35.0	40
	30 mm	2810	2740	2730	-	2760	43.6	43
Bearing inlet	Maximum	564	564	562	-	563	1.2	17
temperature [ºC]	Minimum	432	432	434	-	433	1.2	6
	170 mm	554	558	555	-	556	2.1	19
	100 mm	561	563	561	-	562	1.2	17
	30 mm	556	557	556	-	556	0.6	16
Bearing outlet	Maximum	578	577	578	-	578	0.6	-
temperature [ºC]	Minimum	432	432	434	-	433	1.2	-
	170 mm	565	570	567	-	567	2.5	-
	100 mm	578	577	575	-	577	1.5	-
	30 mm	578	575	573	-	575	2.5	-
Die face pressure	196 mm	354	379	360	-	365	13.0	67
avg. value [MPa]	170 mm	322	325	319	-	322	2.9	52
for all 3 sensors	100 mm	301	304	298	-	301	2.9	50
	30 mm	322	318	317	-	319	2.5	50
Die face pressure	196 mm	33.3	38.0	19.3	-	30.2	-	23.9
st. dev. value [MPa]	170 mm	31.6	31.9	18.2	-	27.2	-	23.5
for all 3 sensors	100 mm	34.1	33.9	18.9	-	29.0	-	23.4
	30 mm	35.3	38.1	19.6	-	31.0	-	24.1
Container / liner force	196 mm	-	-	1449	-	1449	-	137
avg. value [kN]	170 mm	-	-	1173	-	1173	-	144
	100 mm	-	-	726	-	726	-	199
	30 mm	-	-	362	-	362	-	194
Liner friction [MPa]		-	-	20.3	-	20.3	-	-2.5

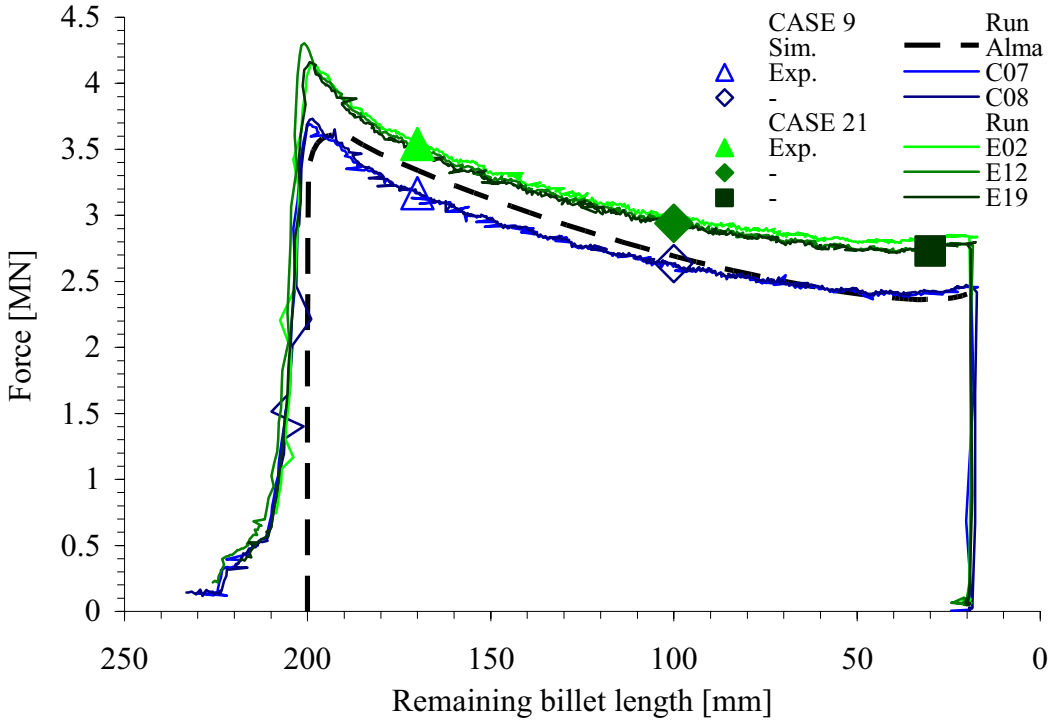

Figure 5.87. Measurement of the ram force - cases 9 and 21 (zero/long bearing).

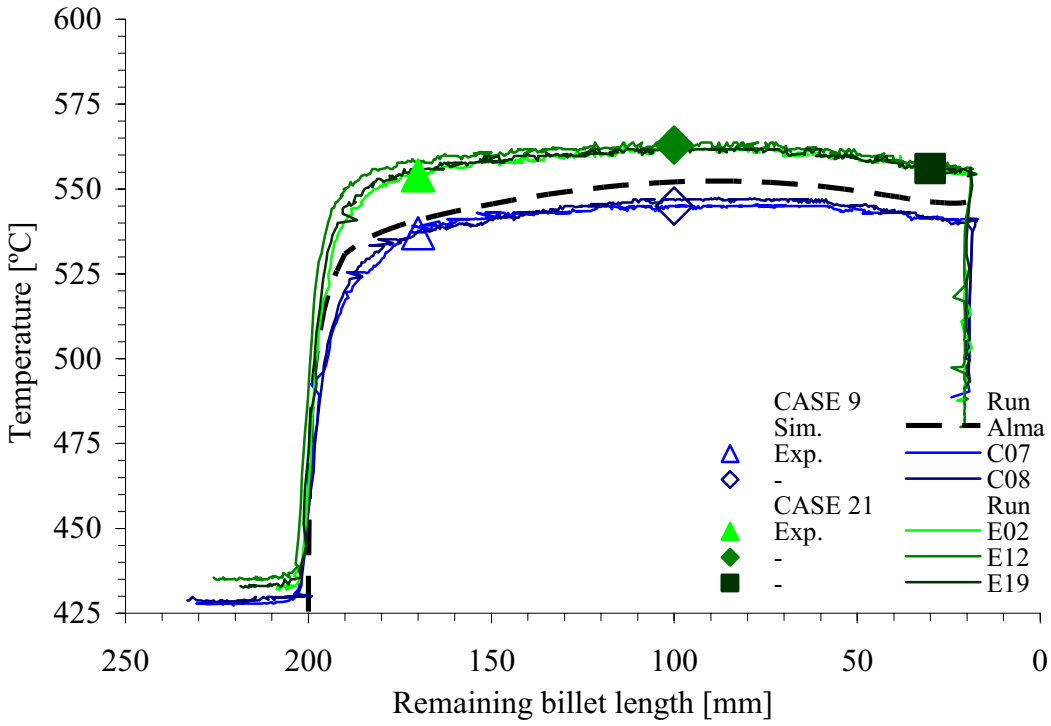

Figure 5.88. Measurement of the outlet temperature (bearing inlet) - cases 9 and 21.

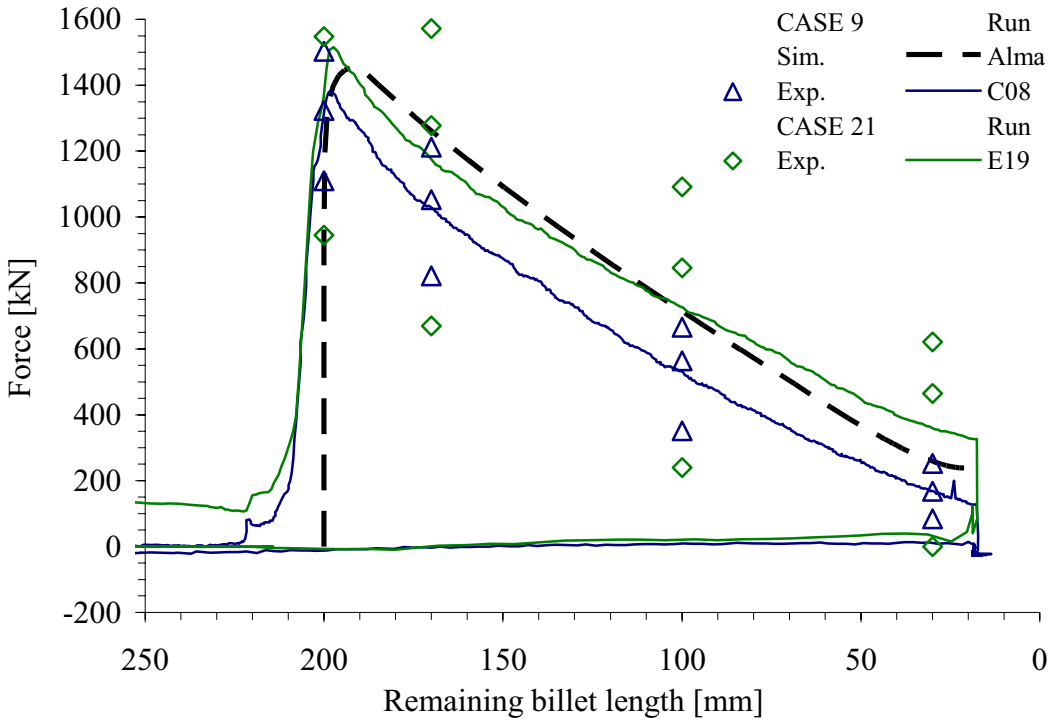

Figure 5.89. Measurement of the average container liner force - cases 9 and 21.

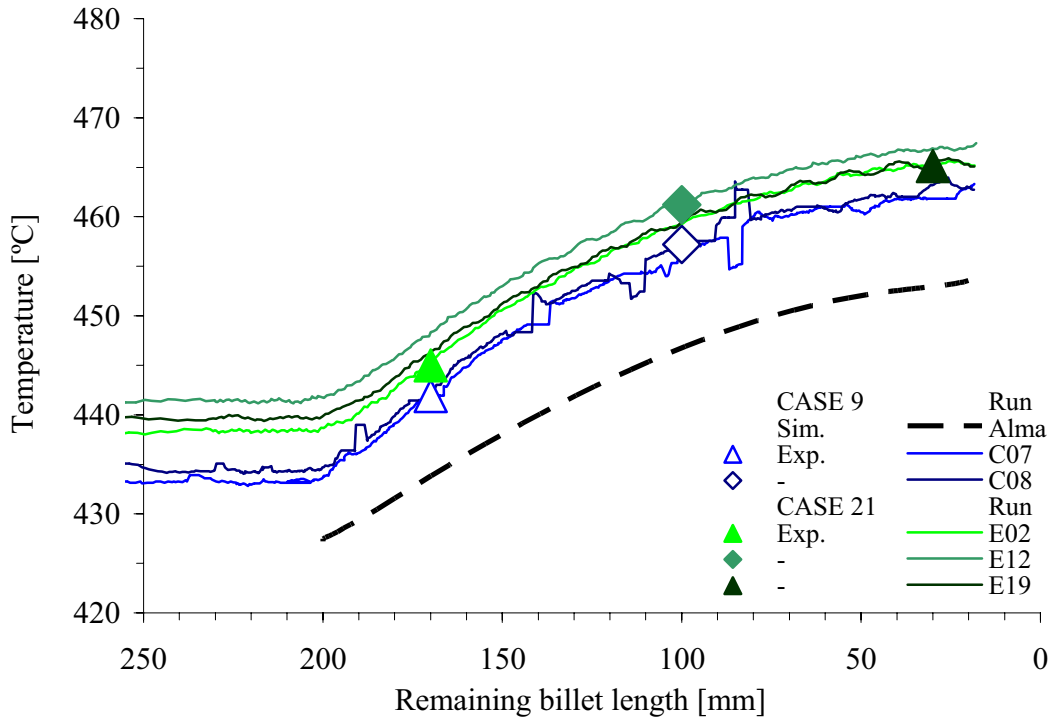

Figure 5.90. Measurement of the die face temperature - cases 9 and 21.

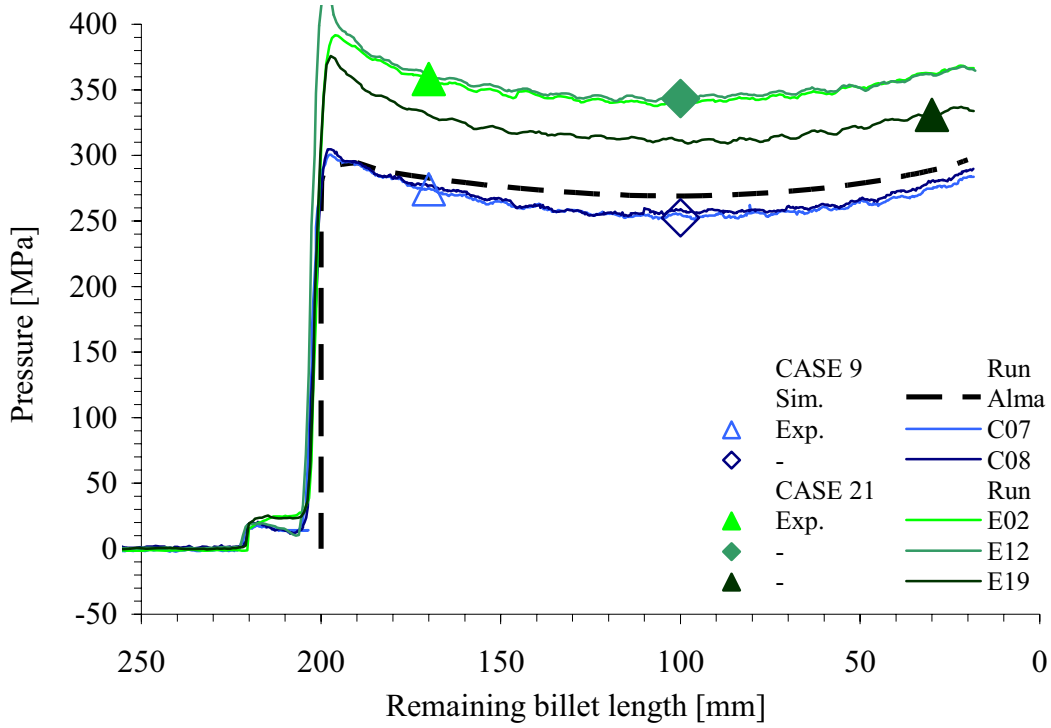

Figure 5.91. Measurement of the die face pressure by sensor 1 - cases 9 and 21.

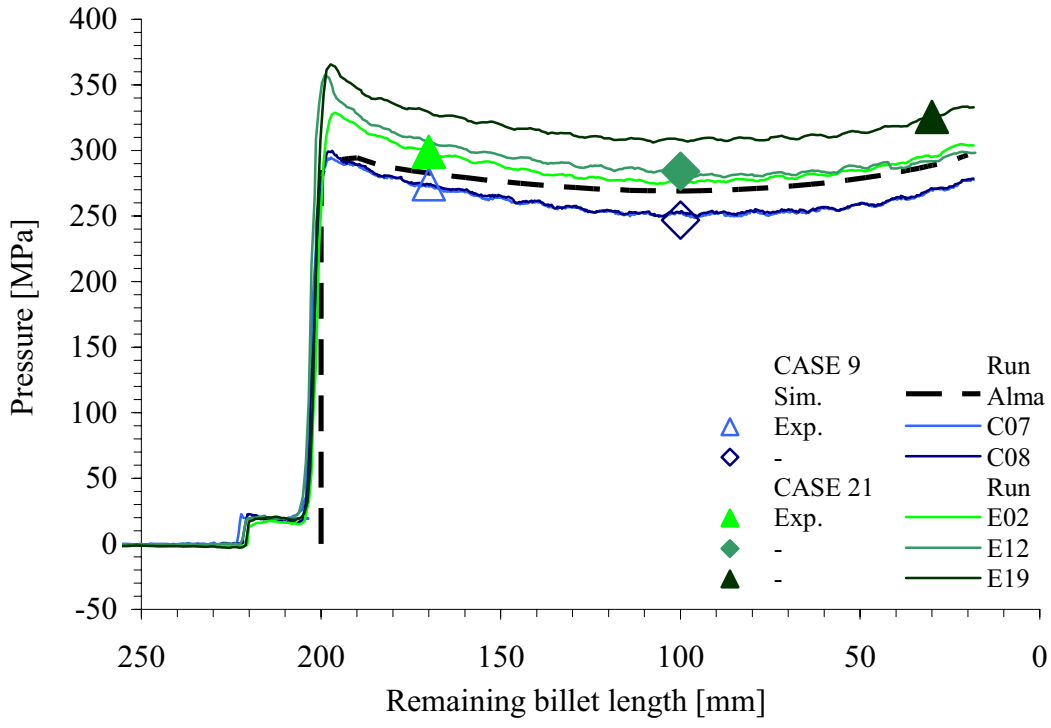

Figure 5.92. Measurement of the die face pressure by sensor 2 - cases 9 and 21.

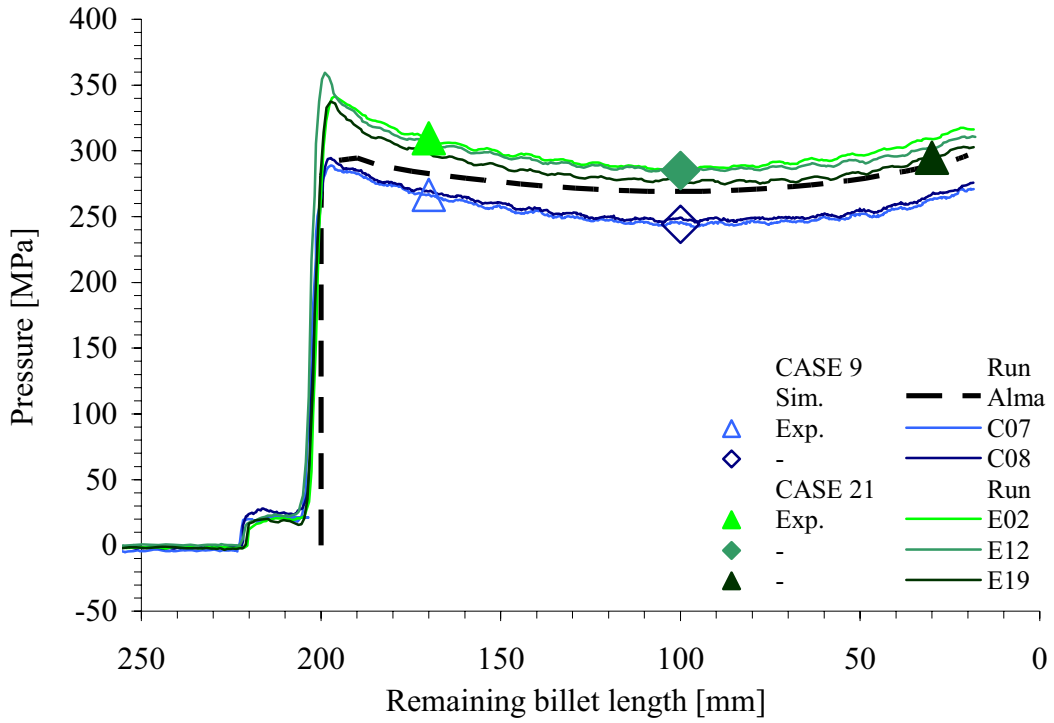

Figure 5.93. Measurement of the die face pressure by sensor 3 - cases 9 and 21.

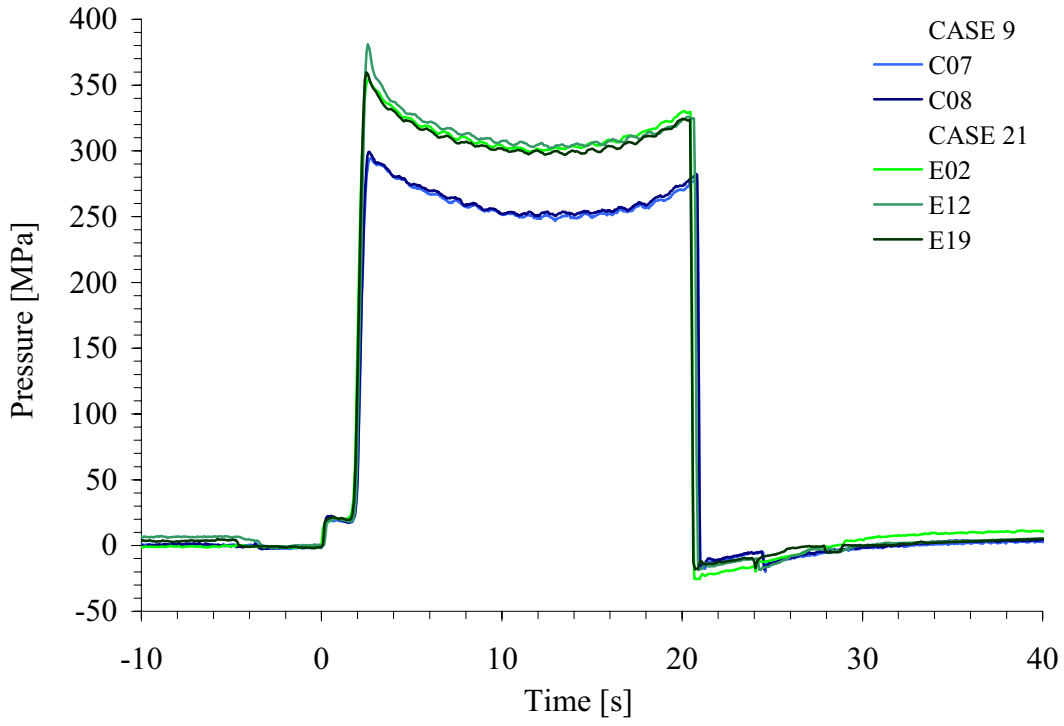

Figure 5.94. Measurement of the average die face pressure - cases 9 and 21.

Table 5.21. Case 10 – input and output data

SPECIFICATION	CASE	10						
Nominal extrusion ratio		80	-		Die outlet diameter		11.2	mm
Nominal bearing length		0	mm					
Nominal ram velocity		2.5	mm/s		Profile velocity		200	mm/s
Nominal billet temperature		500	ºC					
INPUT DATA	Day/run #	C09	C10	-	-	Avg.	St.dev.	C10 - C4
Actual velocity [mm/s]	Ram	2.3	2.3	-	-	2.3	0.0	-2.7
	Profile	184	184	-	-	184	0.0	-16.0
Initial billet surface	Front	495	494	-	-	495	0.7	2.5
temperature [ºC]	Back	492	490	-	-	491	1.4	3.5
	Average	494	492	-	-	493	1.1	3.0
Ram temperature [ºC]	Front	126	125	-	-	126	0.7	-1.0
RESPONSE		1	2	3	4	Avg.	St.dev.	C10 - C4
Ram force [kN]	Maximum	2719	2748	-	-	2734	20.5	3
	Minimum	2000	1899	-	-	1950	71.4	22
Effect C10 - C4:	196 mm	2671	2696	-	-	2684	17.7	15
Pressure [MPa]	170 mm	2470	2482	-	-	2476	8.5	24
	100 mm	2222	2225	-	-	2224	2.1	32
	30 mm	2023	2023	-	-	2023	0.0	25
Bearing inlet	Maximum	512	510	-	-	511	1.4	-5
temperature [ºC]	Minimum	430	430	-	-	430	0.0	0
	170 mm	510	509	-	-	510	0.7	-4
	100 mm	508	508	-	-	508	0.0	-7
	30 mm	498	498	-	-	498	0.0	-7
Bearing outlet	Maximum	-	-	-	-	-	-	-
temperature [ºC]	Minimum	-	-	-	-	-	-	-
	170 mm	-	-	-	-	-	-	-
	100 mm	-	-	-	-	-	-	-
	30 mm	-	-	-	-	-	-	-
Die face pressure	196 mm	216	218	-	-	217	1.8	7
avg. value [MPa]	170 mm	212	211	-	-	211	1.0	29
for all 3 sensors	100 mm	234	233	-	-	234	0.8	48
	30 mm	259	256	-	-	258	1.8	38
Die face pressure	196 mm	5.2	3.9	-	-	4.6	-	-1.9
st. dev. value [MPa]	170 mm	5.9	4.7	-	-	5.3	-	1.2
for all 3 sensors	100 mm	8.5	9.3	-	-	8.9	-	2.7
	30 mm	10.5	9.6	-	-	10.0	-	-1.4
Container / liner force	196 mm	1031	-	-	-	1031	-	-
avg. value [kN]	170 mm	794	-	-	-	794	-	-
	100 mm	449	-	-	-	449	-	-
	30 mm	148	-	-	-	148	-	-
Liner friction [MPa]		15.7	-	-	-	15.7	-	-

Table 5.22. Case 22 – input and output data

SPECIFICATION	CASE	22						
Nominal extrusion ratio		80	-		Die outlet diameter		11.2	mm
Nominal bearing length		8.5	mm					
Nominal ram velocity		2.5	mm/s		Profile velocity		200	mm/s
Nominal billet temperature		500	ºC					

INPUT DATA	Day/run #	E05	E06	E20	-	Avg.	St.dev.	C22 - C10
Actual velocity [mm/s]	Ram	2.3	2.3	2.5	-	2.4	0.1	0.1
	Profile	184	184	200	-	189	9.2	5.3
Initial billet surface	Front	500	500	499	-	500	0.6	5.2
temperature [ºC]	Back	488	487	493	-	489	3.2	-1.7
	Average	494	494	496	-	495	1.3	1.8
Ram temperature [ºC]	Front	148	135	117	-	133	15.6	7.8

RESPONSE		1	2	3	4	Avg.	St.dev.	C22 - C10
Ram force [kN]	Maximum	3162	3202	3110	-	3182	28.3	57
	Minimum	2405	2393	2460	-	2419	35.7	60
Effect C22 - C10:	196 mm	3020	3084	-	-	3052	45.3	47
Pressure [MPa]	170 mm	2824	2820	2812	-	2819	6.1	44
	100 mm	2600	2580	2600	-	2593	11.5	47
	30 mm	2420	2415	2470	-	2435	30.4	52
Bearing inlet	Maximum	529	528	534	-	530	3.2	19
temperature [ºC]	Minimum	435	437	433	-	435	2.0	5
	170 mm	527	527	532	-	529	2.9	19
	100 mm	523	523	525	-	524	1.2	16
	30 mm	511	512	511	-	511	0.6	13
Bearing outlet	Maximum	535	536	540	-	537	2.6	-
temperature [ºC]	Minimum				-			-
	170 mm	532	532	535	-	533	1.7	-
	100 mm	532	531	535	-	533	2.1	-
	30 mm	521	522	523	-	522	1.0	-
Die face pressure	196 mm	267	270	-	-	268	2.2	51
avg. value [MPa]	170 mm	247	247	238	-	244	5.1	33
for all 3 sensors	100 mm	274	274	273	-	273	0.7	40
	30 mm	296	295	305	-	299	5.7	41
Die face pressure	196 mm	12.4	12.4	-	-	12.4	-	7.8
st. dev. value [MPa]	170 mm	12.9	13.1	25.5	-	17.2	-	11.9
for all 3 sensors	100 mm	19.2	20.6	34.3	-	24.7	-	15.8
	30 mm	19.8	23.4	29.8	-	24.3	-	14.3
Container / liner force	196 mm	-	-	-	-	-	-	-
avg. value [kN]	170 mm	-	-	938	-	938	-	144
	100 mm	-	-	637	-	637	-	188
	30 mm	-	-	336	-	336	-	188
Liner friction [MPa]		-	-	13.7	-	13.7	-	-2.0

.

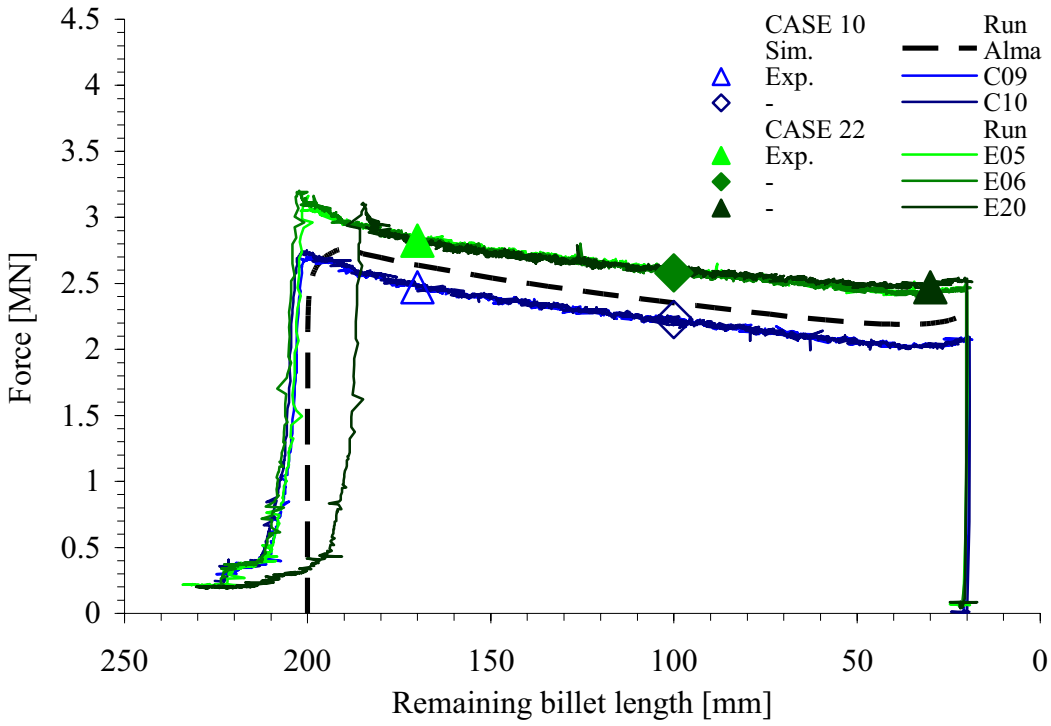

Figure 5.95. Measurement of the ram force - cases 10 and 22 (zero/long bearing).

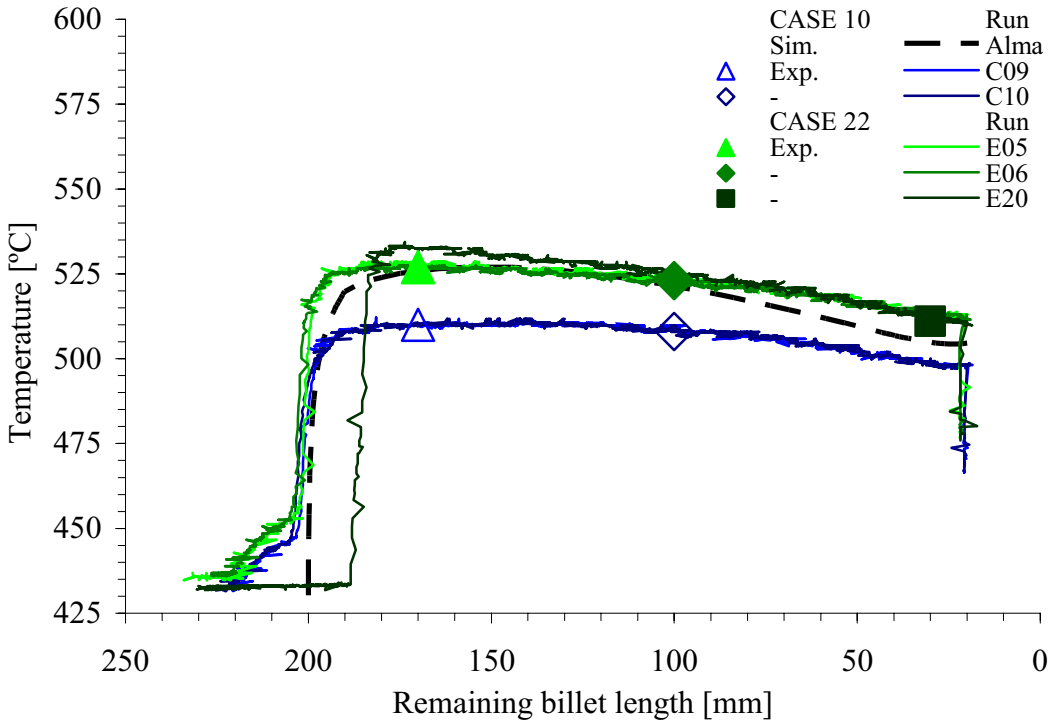

Figure 5.96. Measurement of the outlet temperature (bearing inlet) - cases 10 and 22.

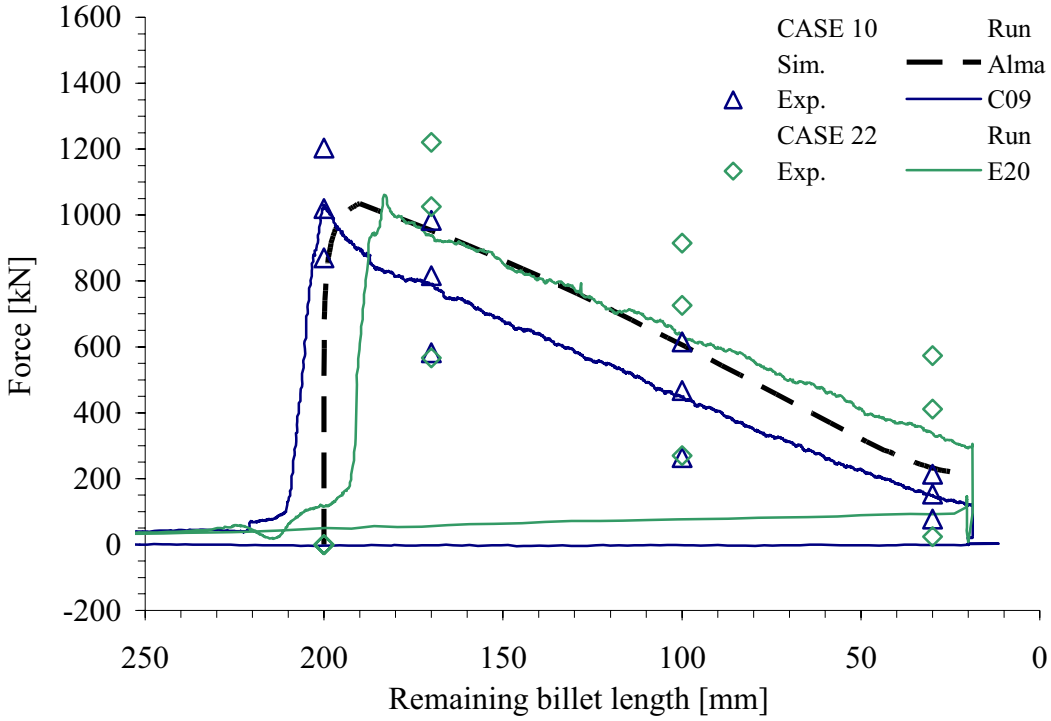

Figure 5.97. Measurement of the average container liner force - cases 10 and 22.

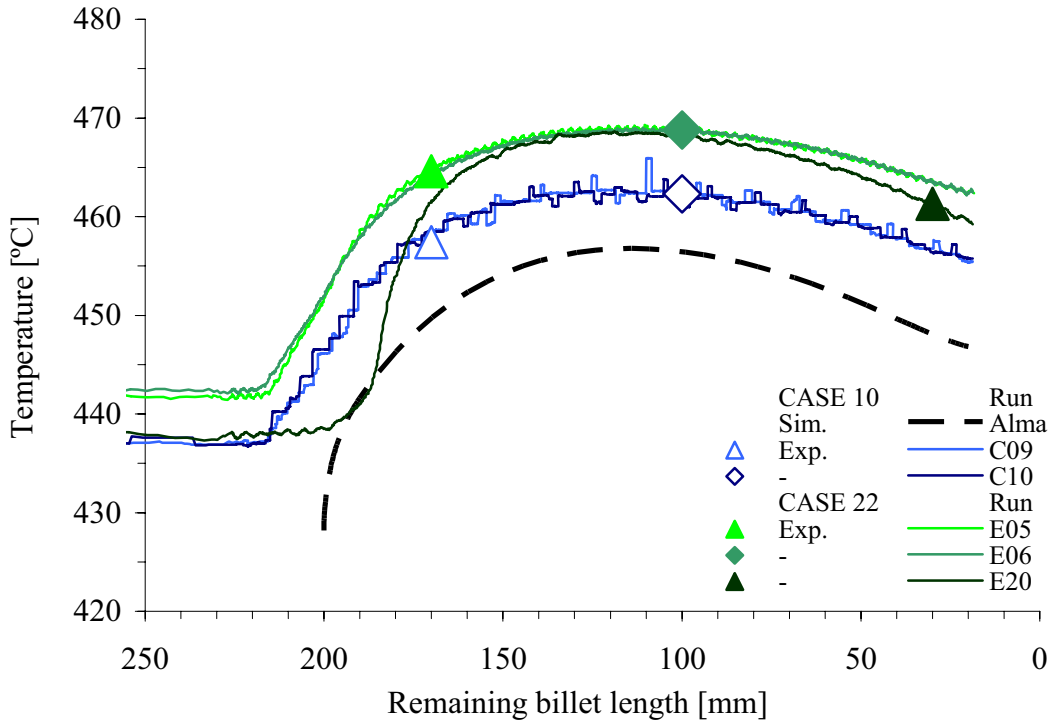

Figure 5.98. Measurement of the die face temperature - cases 10 and 22.

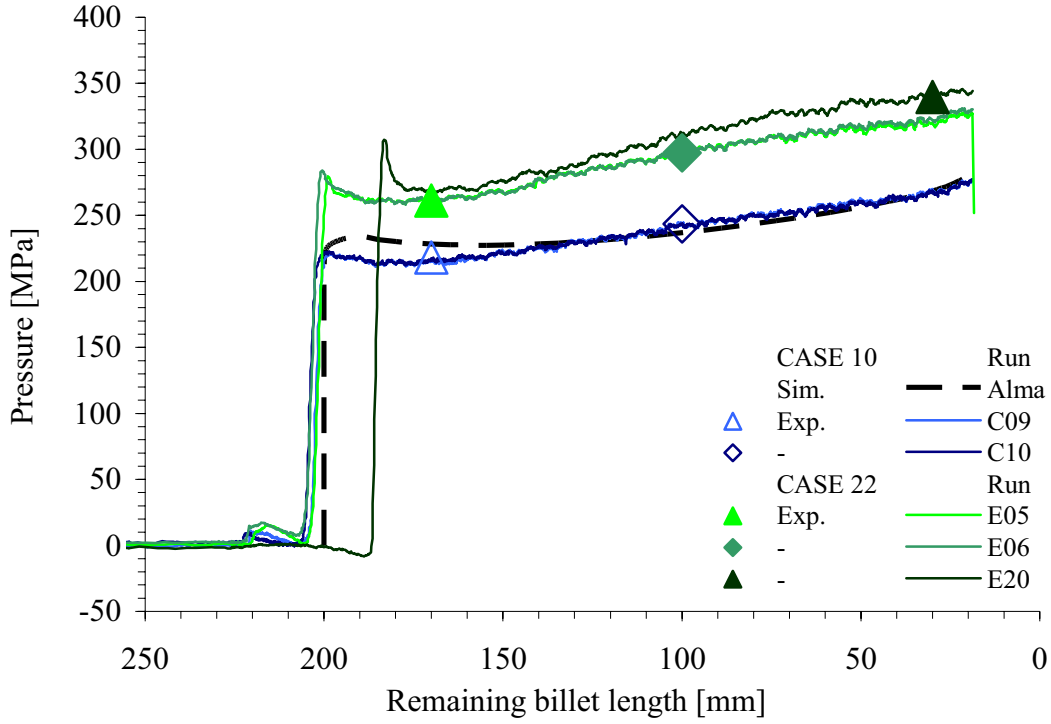

Figure 5.99. Measurement of the die face pressure by sensor 1 - cases 10 and 22.

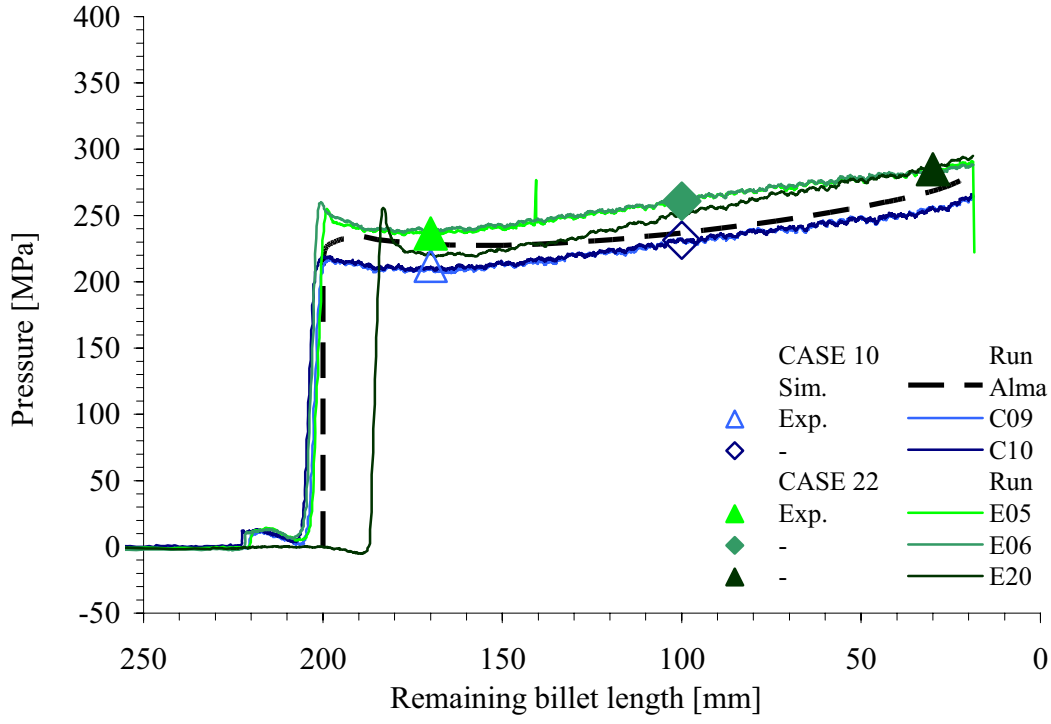

Figure 5.100. Measurement of the die face pressure by sensor 2 - cases 10 and 22.

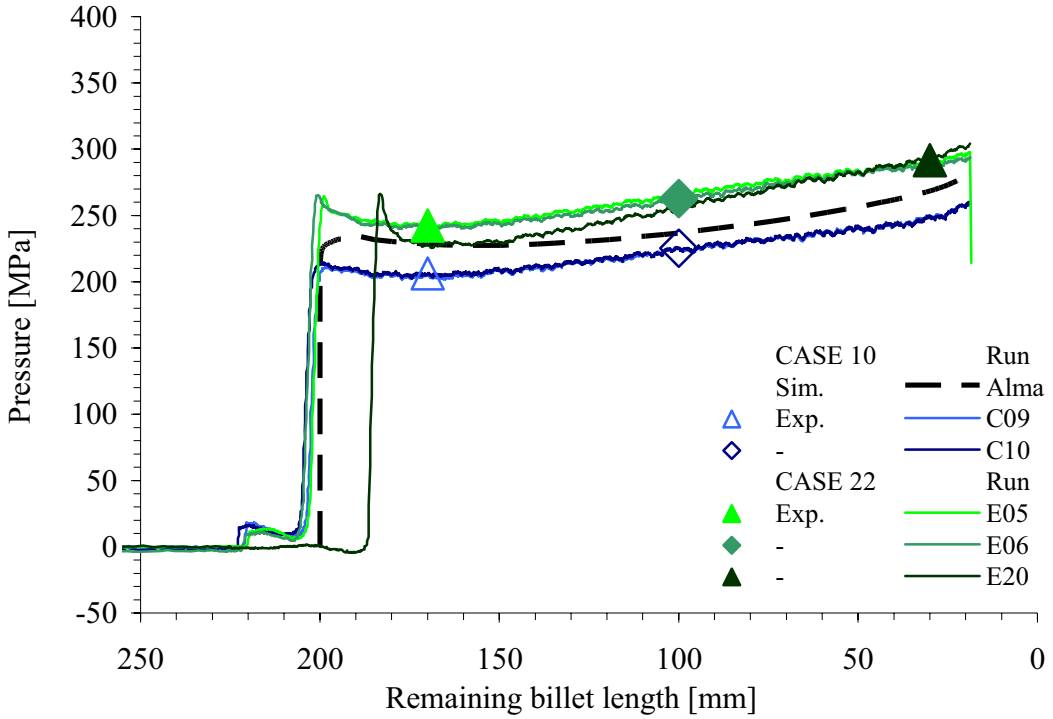

Figure 5.101. Measurement of the die face pressure by sensor 3 - cases 10 and 22.

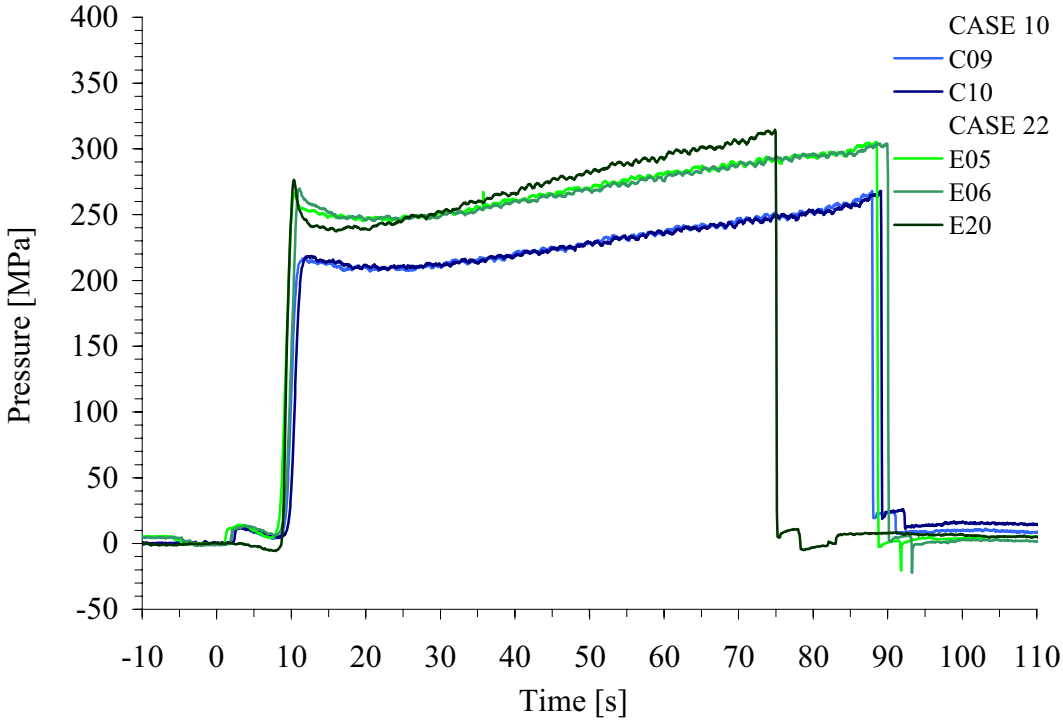

Figure 5.102. Measurement of the average die face pressure - cases 10 and 22.

Table 5.23. Case 11 – input and output data

SPECIFICATION	CASE	11						
Nominal extrusion ratio		80	-	Die outlet diameter		11.2	mm	
Nominal bearing length		0	mm					
Nominal ram velocity		5	mm/s	Profile velocity		400	mm/s	
Nominal billet temperature		500	ºC					
INPUT DATA	Day/run #	C11	C12	-	-	Avg.	St.dev.	C11 - C5
Actual velocity [mm/s]	Ram	5.0	5.0	-	-	5.0	0.0	-5.1
	Profile	400	400	-	-	400	0.0	-4.0
Initial billet surface	Front	496	496	-	-	496	0.0	2.5
temperature [ºC]	Back	491	490	-	-	491	0.7	-0.8
	Average	494	493	-	-	493	0.4	0.8
Ram temperature [ºC]	Front	133	123	-	-	128	7.1	-3.0
RESPONSE		1	2	3	4	Avg.	St.dev.	C11 - C5
Ram force [kN]	Maximum	3042	3063	-	-	3053	14.8	12
	Minimum	2118	2133	-	-	2126	10.6	39
Effect C11 - C5:	196 mm	2892	2915	-	-	2904	16.3	18
Pressure [MPa]	170 mm	2627	2615	-	-	2621	8.5	26
	100 mm	2300	2305	-	-	2303	3.5	32
	30 mm	2150	2170	-	-	2160	14.1	26
Bearing inlet	Maximum	534	534	-	-	534	0.0	-2
temperature [ºC]	Minimum	431	431	-	-	431	0.0	1
	170 mm	529	530	-	-	530	0.7	5
	100 mm	532	533	-	-	533	0.7	-2
	30 mm	524	524	-	-	524	0.0	-4
Bearing outlet	Maximum	-	-	-	-	-	-	-
temperature [ºC]	Minimum	-	-	-	-	-	-	-
	170 mm	-	-	-	-	-	-	-
	100 mm	-	-	-	-	-	-	-
	30 mm	-	-	-	-	-	-	-
Die face pressure	196 mm	246	246	-	-	246	0.2	9
avg. value [MPa]	170 mm	218	219	-	-	219	0.2	19
for all 3 sensors	100 mm	224	223	-	-	223	0.8	39
	30 mm	255	254	-	-	255	0.5	39
Die face pressure	196 mm	1.7	1.3	-	-	1.5	-	-6.5
st. dev. value [MPa]	170 mm	1.4	1.9	-	-	1.7	-	-5.3
for all 3 sensors	100 mm	3.9	3.0	-	-	3.5	-	-3.8
	30 mm	5.6	7.4	-	-	6.5	-	-2.4
Container / liner force	196 mm	-	1117	-	-	1117	-	-83
avg. value [kN]	170 mm	-	845	-	-	845	-	-54
	100 mm	-	484	-	-	484	-	-33
	30 mm	-	169	-	-	169	-	-6
Liner friction [MPa]		-	16.4	-	-	16.4	-	-0.9

Table 5.24. Case 23 – input and output data

SPECIFICATION	CASE	23						
Nominal extrusion ratio		80	-		Die outlet diameter		11.2	mm
Nominal bearing length		8.5	mm					
Nominal ram velocity		5	mm/s		Profile velocity		400	mm/s
Nominal billet temperature		500	ºC					
INPUT DATA	Day/run #	E11	E14	-	-	Avg.	St.dev.	C23 - C11
Actual velocity [mm/s]	Ram	4.9	5.0	-	-	5.0	0.1	0.0
	Profile	392	400	-	-	396	5.7	-4.0
Initial billet surface	Front	495	501	-	-	498	4.2	2.0
temperature [ºC]	Back	490	494	-	-	492	2.8	1.5
	Average	493	498	-	-	495	3.5	1.8
Ram temperature [ºC]	Front	127	162	-	-	145	24.7	16.5
RESPONSE		1	2	3	4	Avg.	St.dev.	C23 - C11
Ram force [kN]	Maximum	3479	3468	-	-	3474	7.8	54
	Minimum	2520	2465	-	-	2493	38.9	47
Effect C23 - C11:	196 mm	3280	3190	-	-	3235	63.6	42
Pressure [MPa]	170 mm	2940	2916	-	-	2928	17.0	39
	100 mm	2630	2610	-	-	2620	14.1	40
	30 mm	2532	2475	-	-	2504	40.3	44
Bearing inlet	Maximum	552	550	-	-	551	1.4	17
temperature [ºC]	Minimum	435	435	-	-	435	0.0	4
	170 mm	550	547	-	-	549	2.1	19
	100 mm	550	548	-	-	549	1.4	17
	30 mm	537	537	-	-	537	0.0	13
Bearing outlet	Maximum	562	560	-	-	561	1.4	-
temperature [ºC]	Minimum	435	435	-	-	435	0.0	-
	170 mm	557	553	-	-	555	2.8	-
	100 mm	560	558	-	-	559	1.4	-
	30 mm	562	550	-	-	556	8.5	-
Die face pressure	196 mm	310	301	-	-	306	6.5	60
avg. value [MPa]	170 mm	267	251	-	-	259	11.1	41
for all 3 sensors	100 mm	274	261	-	-	267	9.5	44
	30 mm	307	283	-	-	295	17.5	40
Die face pressure	196 mm	34.9	13.5	-	-	24.2	-	22.7
st. dev. value [MPa]	170 mm	32.6	13.6	-	-	23.1	-	21.4
for all 3 sensors	100 mm	36.3	15.1	-	-	25.7	-	22.2
	30 mm	37.6	16.1	-	-	26.9	-	20.3
Container / liner force	196 mm	-	1214	-	-	1214	-	97
avg. value [kN]	170 mm	-	958	-	-	958	-	113
	100 mm	-	651	-	-	651	-	167
	30 mm	-	356	-	-	356	-	187
Liner friction [MPa]		-	14.0	-	-	14.0	-	-2.5

.

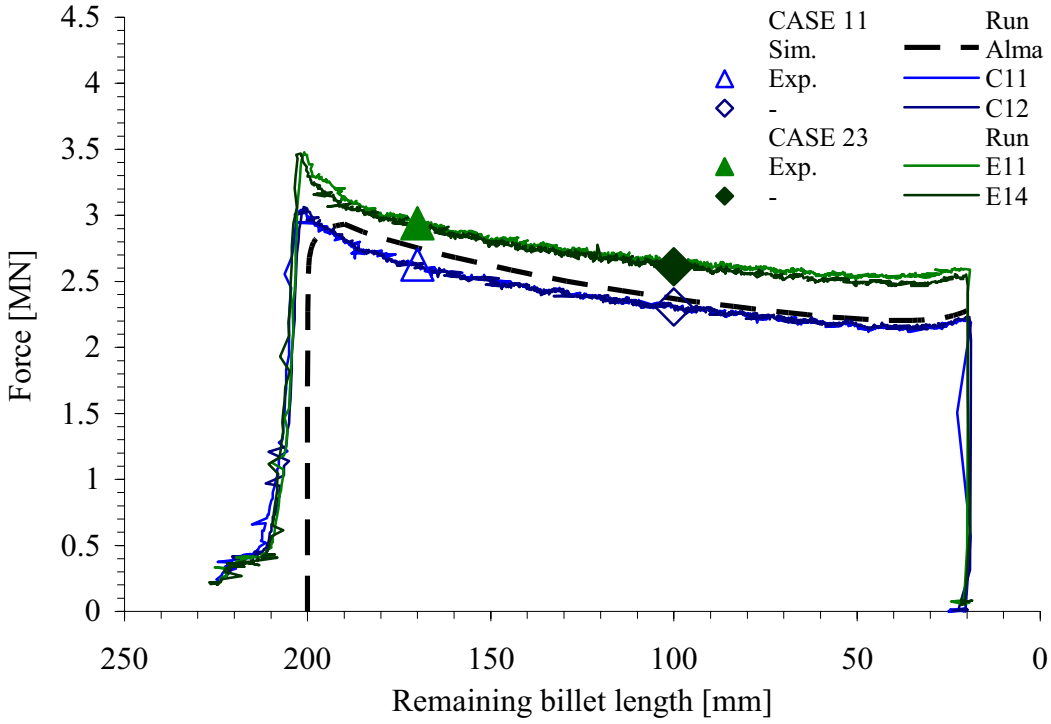

Figure 5.103. Measurement of the ram force - cases 11 and 23 (zero/long bearing).

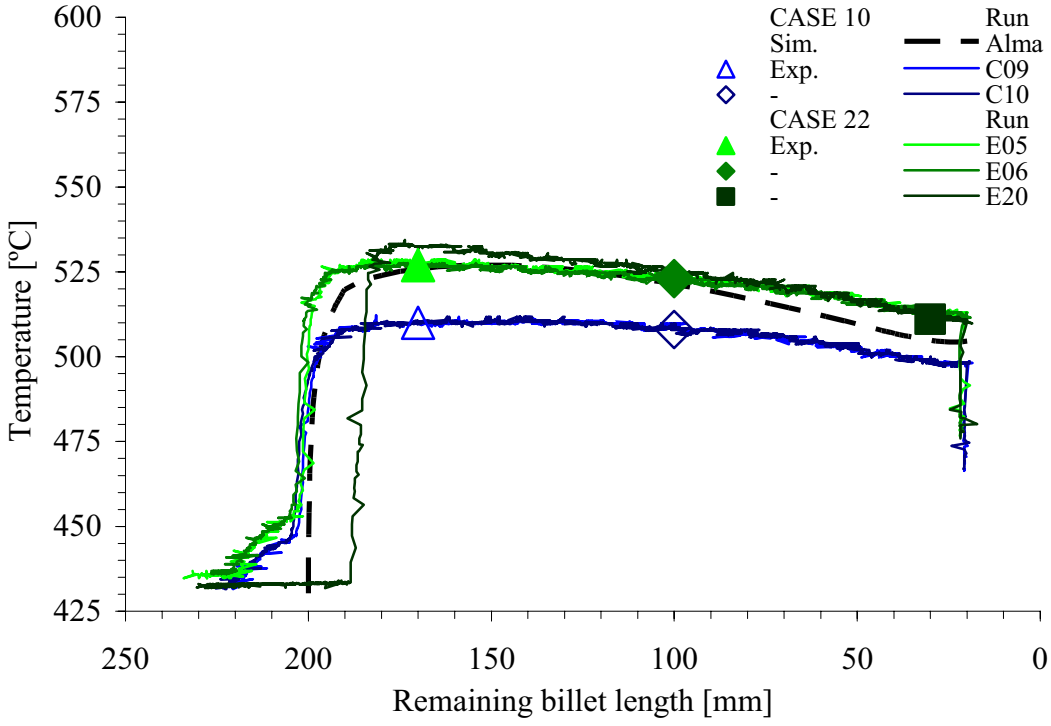

Figure 5.104. Measurement of the outlet temperature (bearing inlet) - cases 10 and 22.

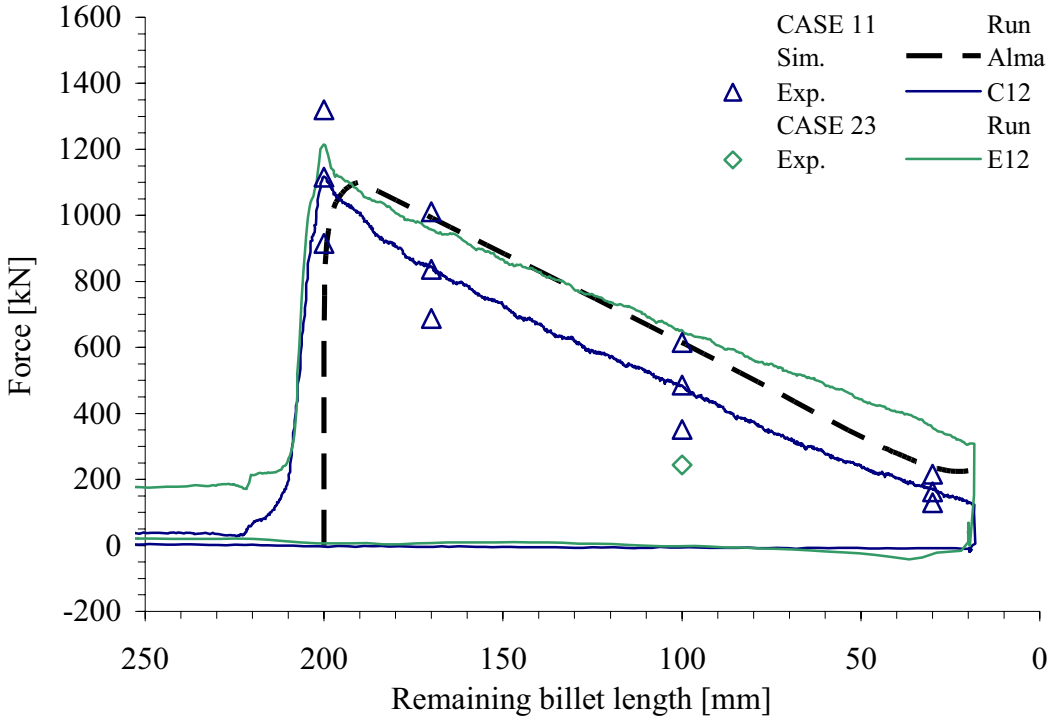

Figure 5.105. Measurement of the average container liner force - cases 11 and 23.

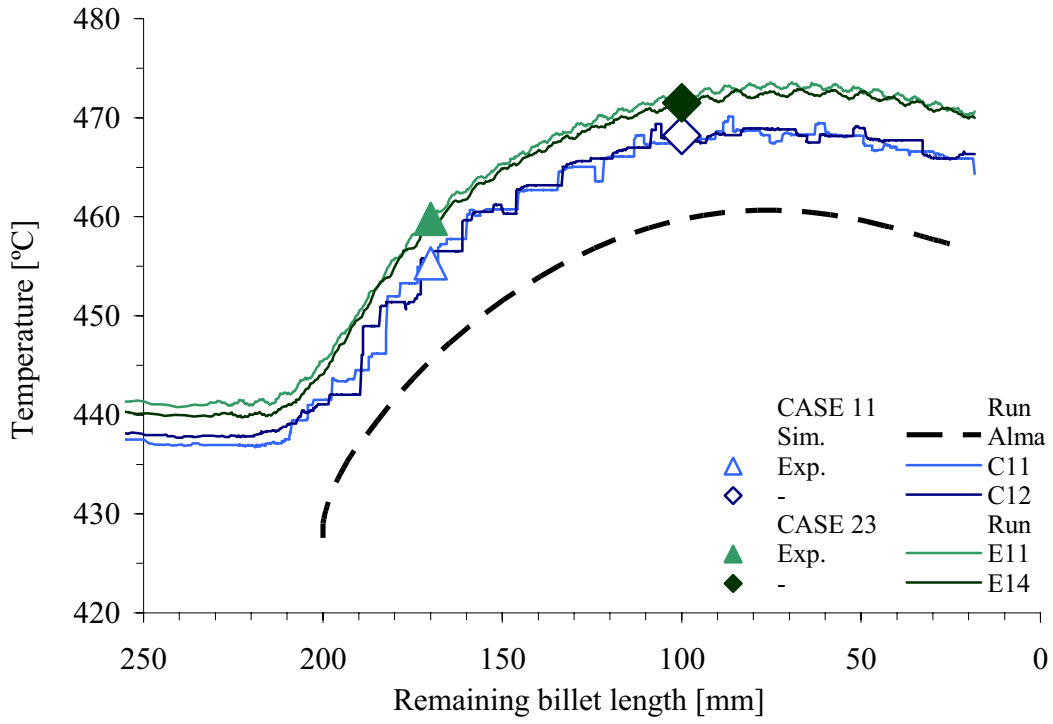

Figure 5.106. Measurement of the die face temperature - cases 11 and 23.

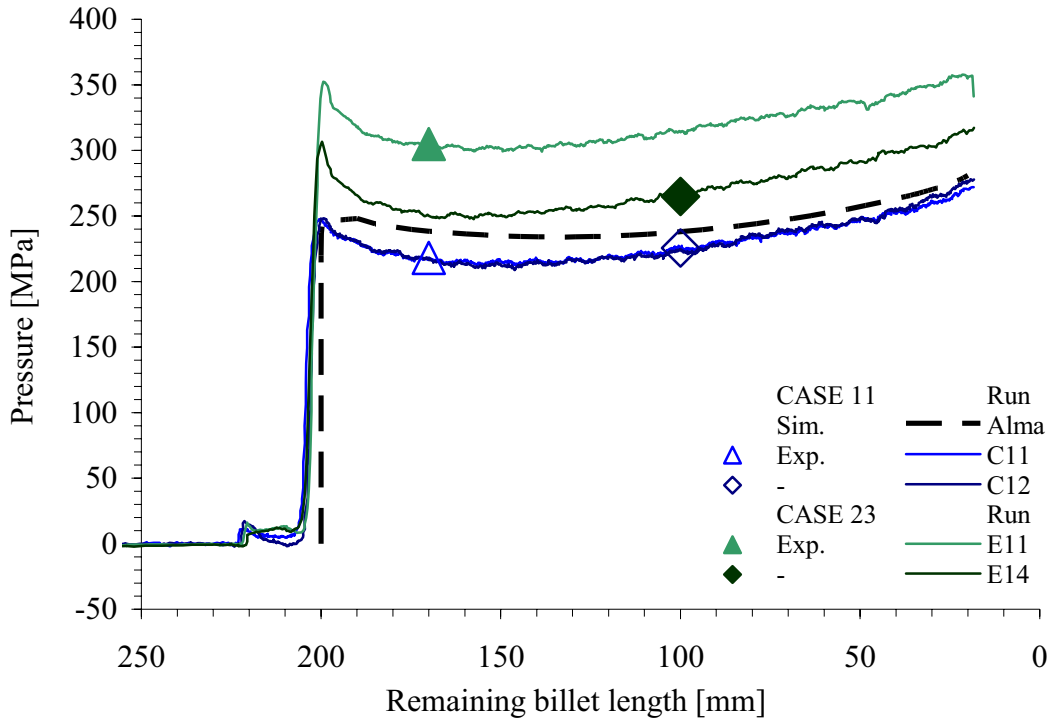

Figure 5.107. Measurement of the die face pressure by sensor 1 - cases 11 and 23.

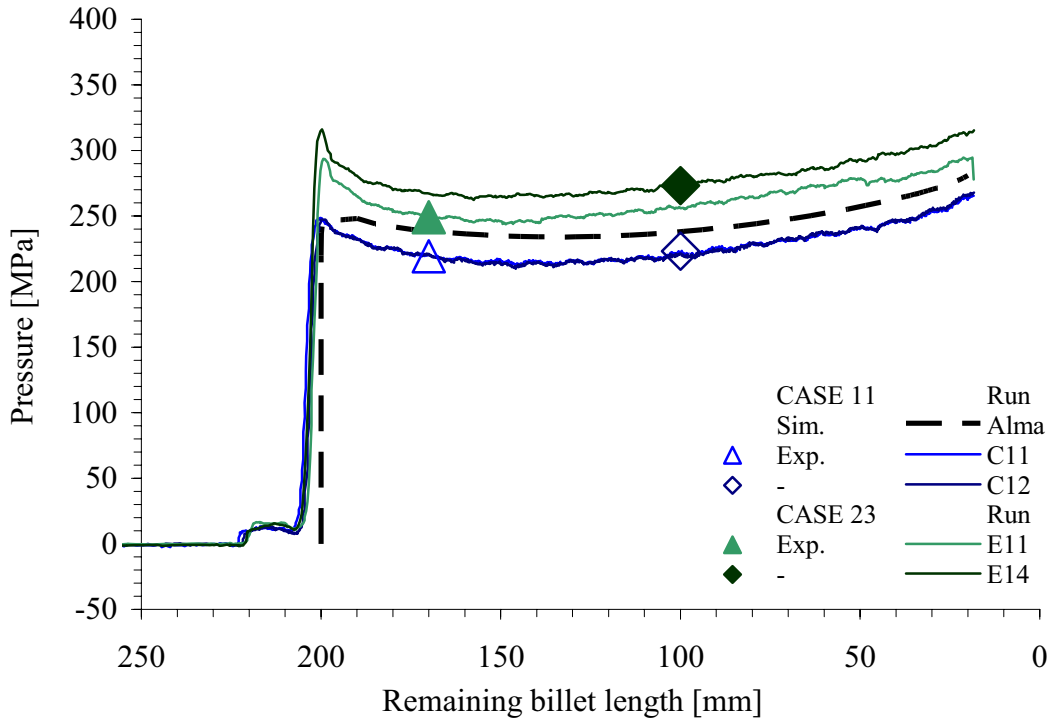

Figure 5.108. Measurement of the die face pressure by sensor 2 - cases 11 and 23.

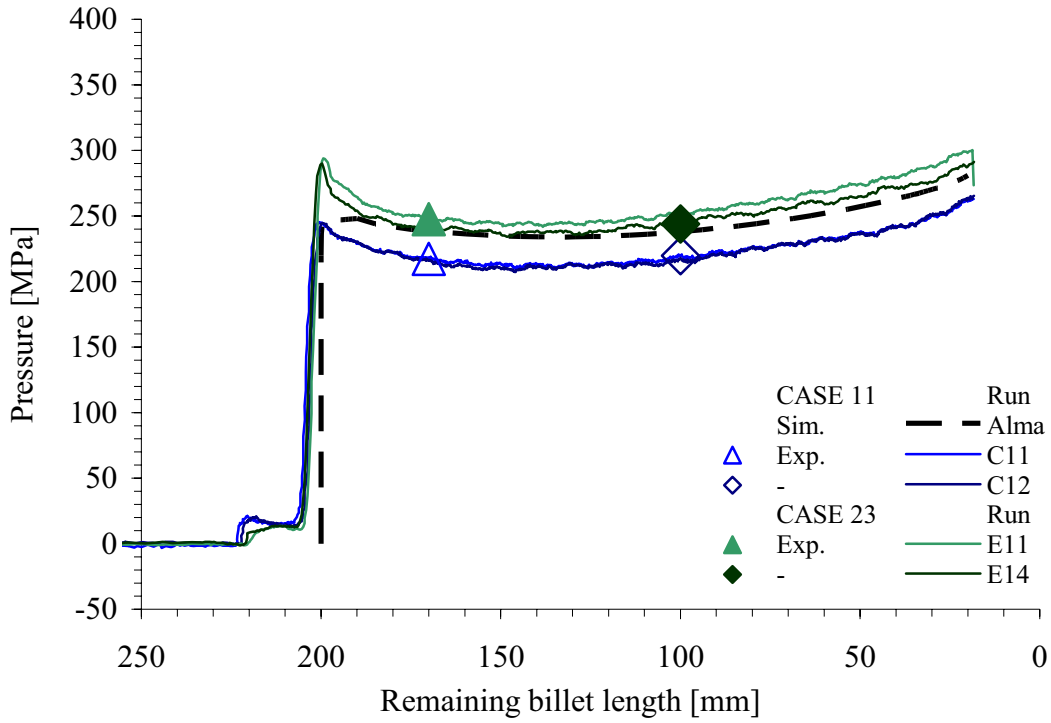

Figure 5.109. Measurement of the die face pressure by sensor 3 - cases 11 and 23.

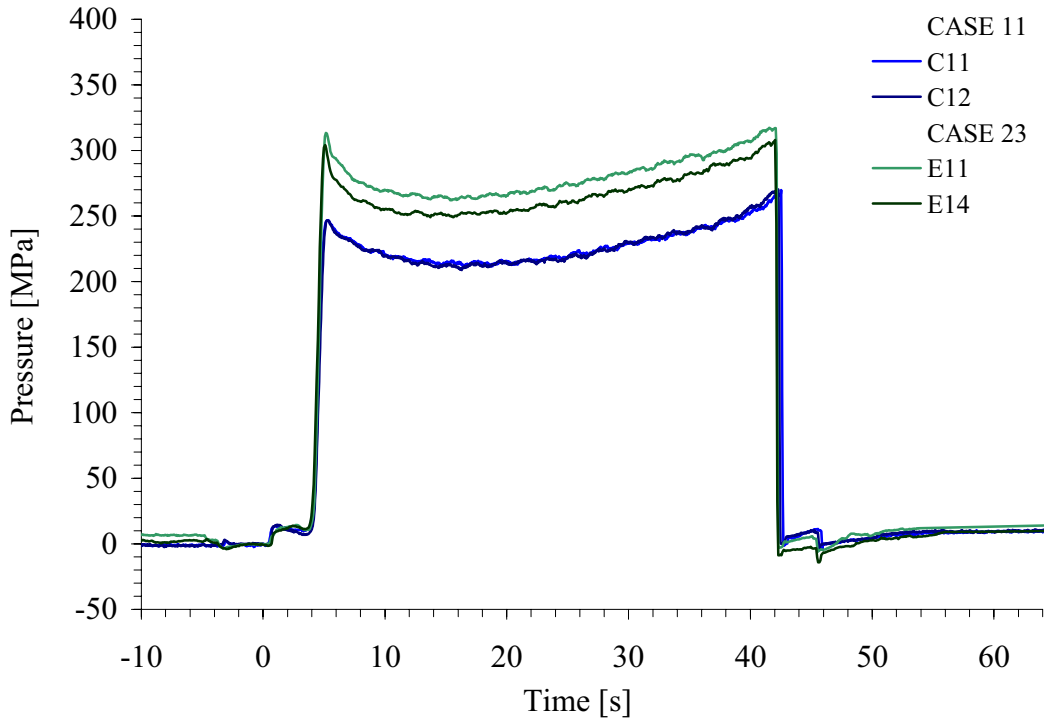

Figure 5.110. Measurement of the average die face pressure - cases 11 and 23.

Table 5.25. Case 12 – input and output data

SPECIFICATION	CASE	12						
Nominal extrusion ratio		80	-	Die outlet diameter		11.2	mm	
Nominal bearing length		0	mm					
Nominal ram velocity		10	mm/s	Profile velocity		800	mm/s	
Nominal billet temperature		500	ºC					
INPUT DATA	Day/run #	C13	C14	-	-	Avg.	St.dev.	C12 - C6
Actual velocity [mm/s]	Ram	10.1	10.1	-	-	10.1	0.0	-10.2
	Profile	808	808	-	-	808	0.0	-4.0
Initial billet surface	Front	495	491	-	-	493	2.8	-2.0
temperature [ºC]	Back	491	489	-	-	490	1.4	-0.5
	Average	493	490	-	-	492	2.1	-1.3
Ram temperature [ºC]	Front	116	118	-	-	117	1.4	-4.5
RESPONSE		1	2	3	4	Avg.	St.dev.	C12 - C6
Ram force [kN]	Maximum	3409	3432	-	-	3421	16.3	28
	Minimum	2257	2254	-	-	2256	2.1	33
Effect C12 - C6:	196 mm	3200	3227	-	-	3214	19.1	18
Pressure [MPa]	170 mm	2771	2800	-	-	2786	20.5	27
	100 mm	2395	2430	-	-	2413	24.7	35
	30 mm	2310	2326	-	-	2318	11.3	28
Bearing inlet	Maximum	558	557	-	-	558	0.7	3
temperature [ºC]	Minimum	431	429	-	-	430	1.4	-3
	170 mm	548	548	-	-	548	0.0	16
	100 mm	556	556	-	-	556	0.0	4
	30 mm	550	551	-	-	551	0.7	-3
Bearing outlet	Maximum	-	-	-	-	-	-	-
temperature [ºC]	Minimum	-	-	-	-	-	-	-
	170 mm	-	-	-	-	-	-	-
	100 mm	-	-	-	-	-	-	-
	30 mm	-	-	-	-	-	-	-
Die face pressure	196 mm	287	286	-	-	287	0.9	30
avg. value [MPa]	170 mm	238	239	-	-	238	0.6	19
for all 3 sensors	100 mm	225	226	-	-	225	0.3	27
	30 mm	255	256	-	-	256	0.5	30
Die face pressure	196 mm	3.0	3.2	-	-	3.1	-	-6.8
st. dev. value [MPa]	170 mm	2.3	0.8	-	-	1.5	-	-6.0
for all 3 sensors	100 mm	1.5	1.3	-	-	1.4	-	-3.2
	30 mm	3.7	5.8	-	-	4.8	-	-2.7
Container / liner force	196 mm	1199	-	-	-	1199	-	-
avg. value [kN]	170 mm	868	-	-	-	868	-	-
	100 mm	496	-	-	-	496	-	-
	30 mm	142	-	-	-	142	-	-
Liner friction [MPa]		16.9	-	-	-	16.9	-	-

Table 5.26. Case 24 – input and output data

SPECIFICATION	CASE	24						
Nominal extrusion ratio		80	-		Die outlet diameter		11.2	mm
Nominal bearing length		8.5	mm					
Nominal ram velocity		10	mm/s		Profile velocity		800	mm/s
Nominal billet temperature		500	ºC					

INPUT DATA	Day/run #	E04	E09	E15	-	Avg.	St.dev.	C24 - C12
Actual velocity [mm/s]	Ram	10.1	10.1	10.1	-	10.1	0.0	0.0
	Profile	808	808	808	-	808	0.0	0.0
Initial billet surface	Front	500	499	500	-	500	0.6	6.7
temperature [ºC]	Back	486	488	495	-	490	4.7	-0.3
	Average	493	494	498	-	495	2.5	3.2
Ram temperature [ºC]	Front	141	116	125	-	127	12.7	10.3

RESPONSE		1	2	3	4	Avg.	St.dev.	C24 - C12
Ram force [kN]	Maximum	3742	3745	3783	-	3757	22.9	43
	Minimum	2558	2569	2558	-	2562	6.4	39
Effect C24 - C12:	196 mm	3433	3445	3430	-	3436	7.9	28
Pressure [MPa]	170 mm	2995	2995	2994	-	2995	0.6	27
	100 mm	2650	2670	2650	-	2657	11.5	31
	30 mm	2610	2630	2625	-	2622	10.4	39
Bearing inlet	Maximum	574	575	575	-	575	0.6	17
temperature [ºC]	Minimum	433	434	435	-	434	1.0	4
	170 mm	567	570	571	-	569	2.1	21
	100 mm	573	573	575	-	574	1.2	18
	30 mm	565	565	565	-	565	0.0	15
Bearing outlet	Maximum	585	586	587	-	586	1.0	-
temperature [ºC]	Minimum	433	434	435	-	434	1.0	-
	170 mm	578	575	578	-	577	1.7	-
	100 mm	584	585	585	-	585	0.6	-
	30 mm	580	582	580	-	581	1.2	-
Die face pressure	196 mm	329	341	333	-	335	6.1	48
avg. value [MPa]	170 mm	267	275	264	-	269	5.6	31
for all 3 sensors	100 mm	259	265	258	-	261	3.8	35
	30 mm	293	303	297	-	298	5.0	42
Die face pressure	196 mm	15.7	32.2	18.8	-	22.2	-	19.1
st. dev. value [MPa]	170 mm	12.2	24.1	16.3	-	17.5	-	16.0
for all 3 sensors	100 mm	18.1	28.2	19.4	-	21.9	-	20.5
	30 mm	20.9	31.2	21.6	-	24.6	-	19.8
Container / liner force	196 mm	-	-	1322	-	1322	-	123
avg. value [kN]	170 mm	-	-	982	-	982	-	114
	100 mm	-	-	679	-	679	-	183
	30 mm	-	-	386	-	386	-	244
Liner friction [MPa]		-	-	13.8	-	13.8	-	-3.1

.

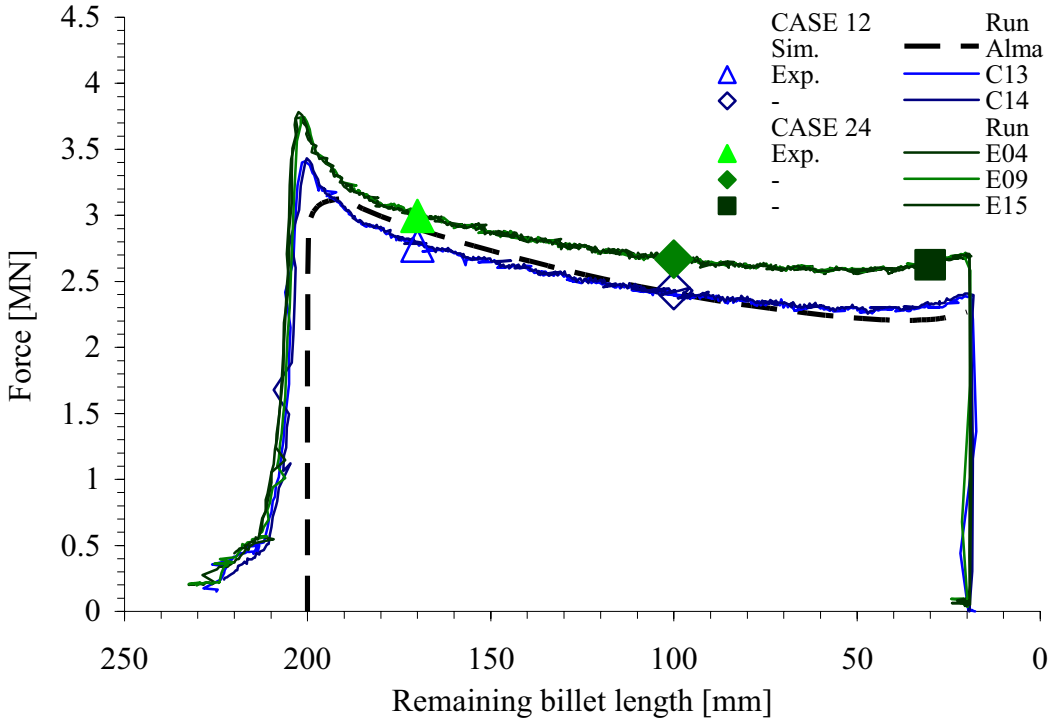

Figure 5.111. Measurement of the ram force - cases 12 and 24 (zero/long bearing).

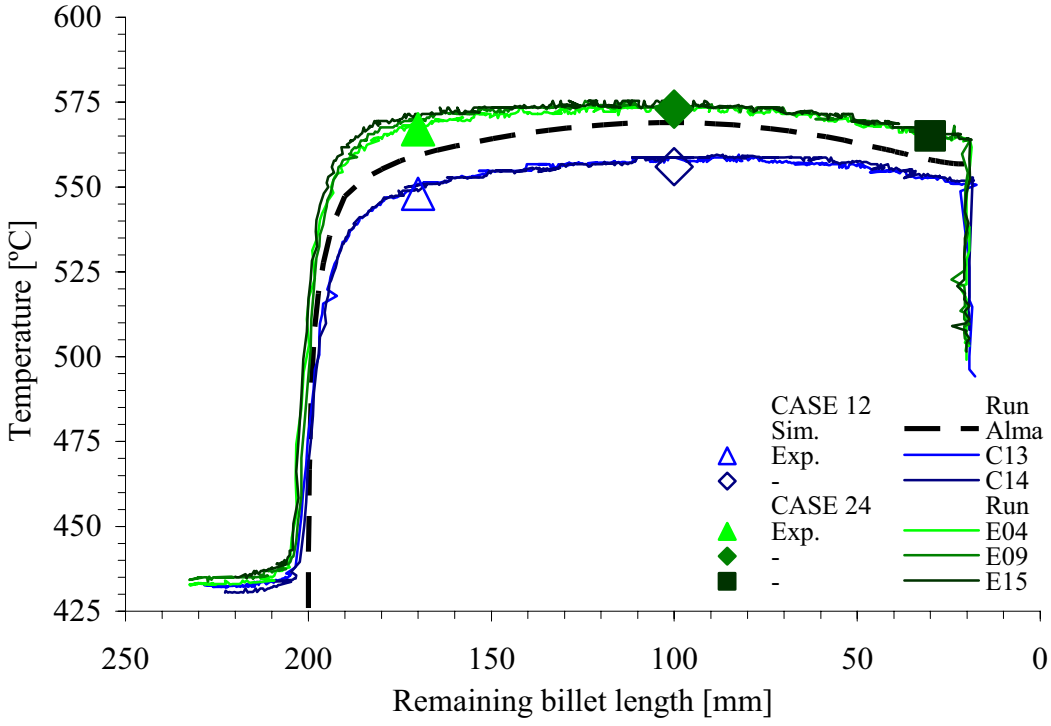

Figure 5.112. Measurement of the outlet temperature (bearing inlet) - cases 12 and 24.

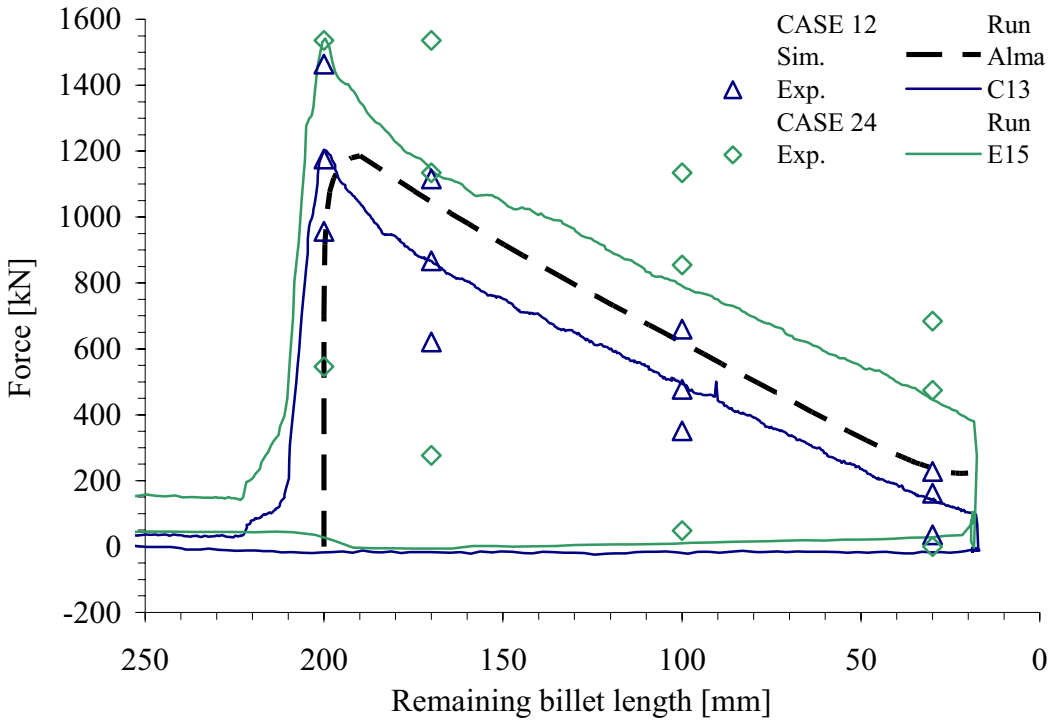

Figure 5.113. Measurement of the average container liner force - cases 12 and 24.

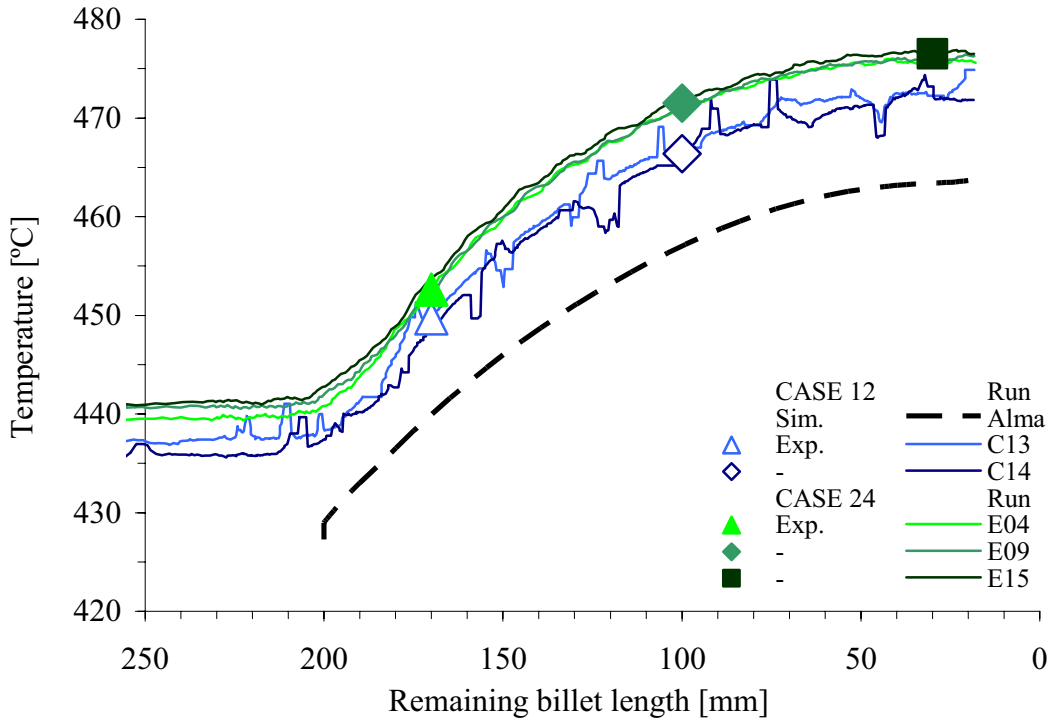

Figure 5.114. Measurement of the die face temperature - cases 12 and 24.

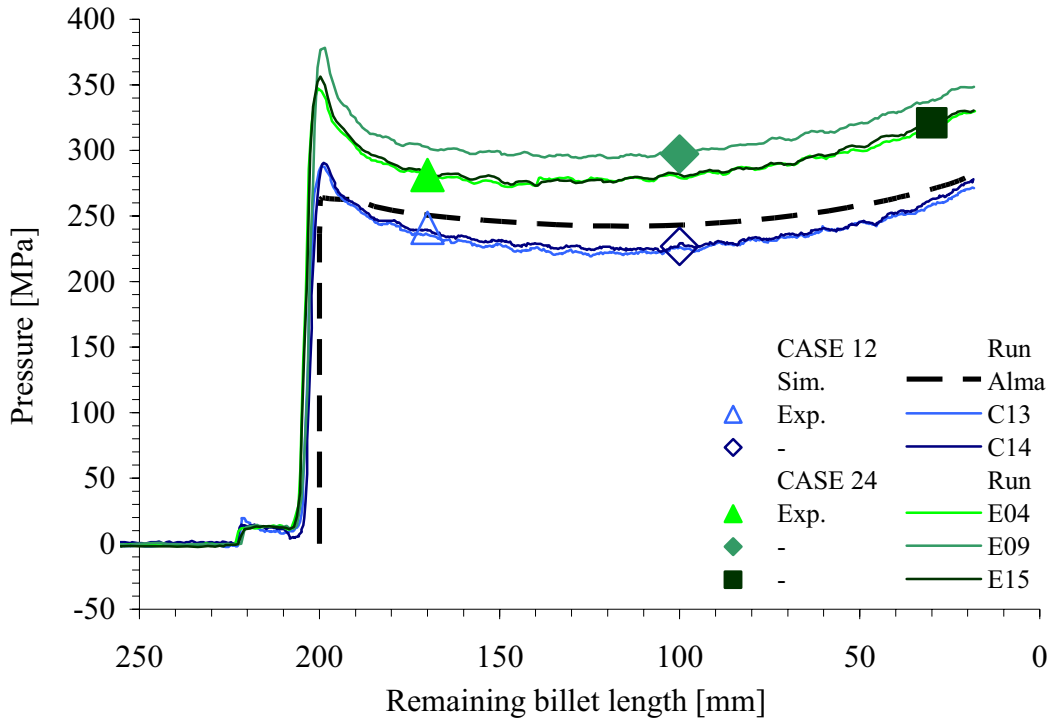

Figure 5.115. Measurement of the die face pressure by sensor 1 - cases 12 and 24.

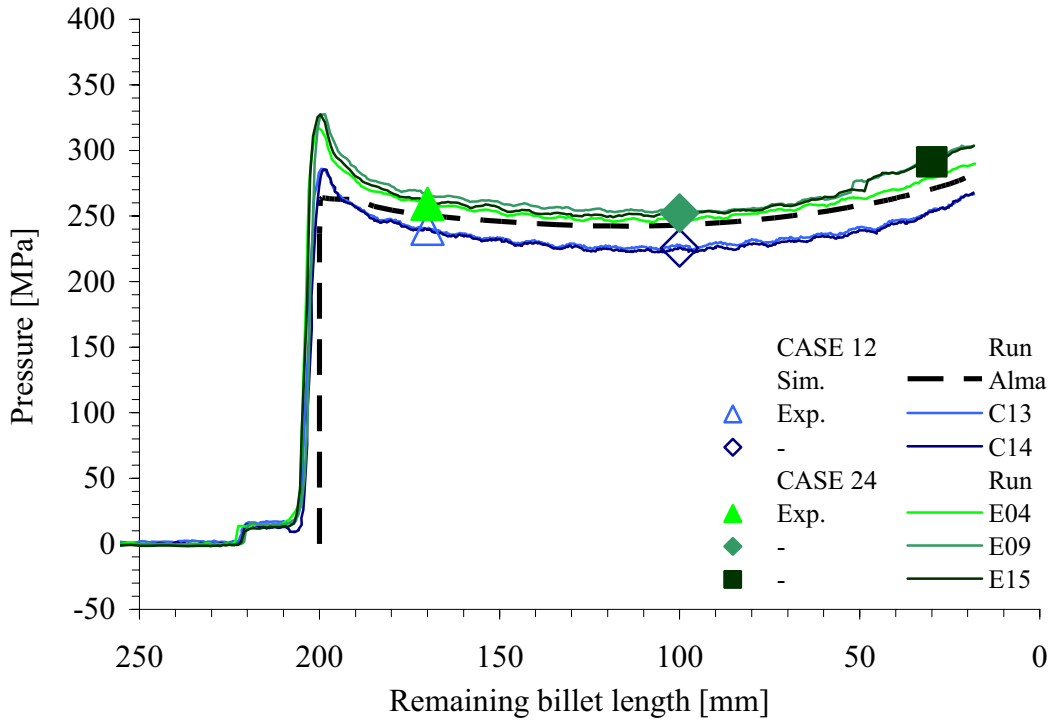

Figure 5.116. Measurement of the die face pressure by sensor 2 - cases 12 and 24.

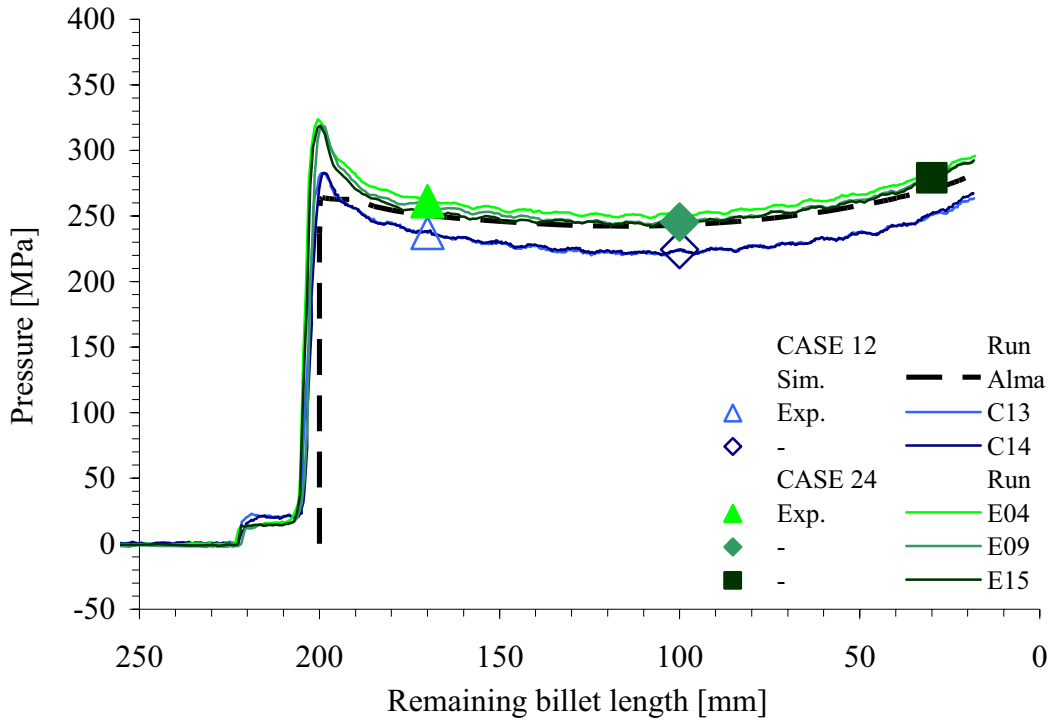

Figure 5.117. Measurement of the die face pressure by sensor 3 - cases 12 and 24.

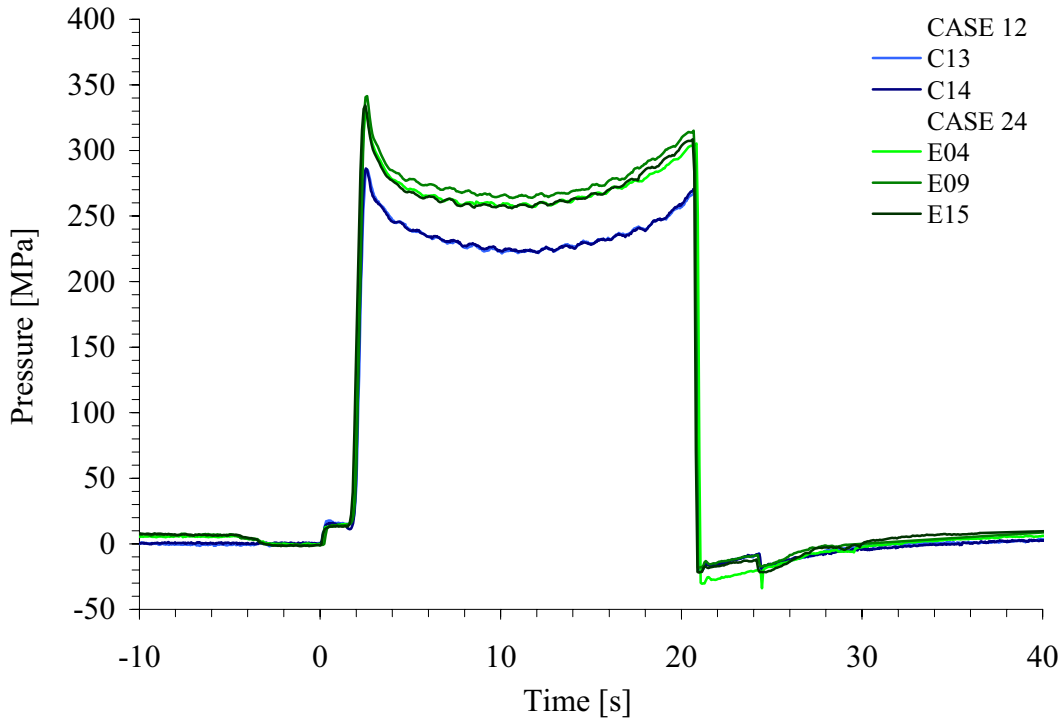

Figure 5.118. Measurement of the average die face pressure - cases 12 and 24.

Table 5.27. Cases 25, 26 and 27 – input and output data

SPECIFICATION	CASES	25	26	27					
Nominal extrusion ratio		80	80	80	-				
Nominal bearing length		8.5	8.5	8.5	mm				
Nominal ram velocity		20	20	30	mm/s				
Nominal billet temperature		450	500	500	ºC				
INPUT DATA	Day/run #	E21	E22	E23	-	C26 - C25		C27 - C26	
Actual velocity [mm/s]	Ram	20.3	20.3	31.7	-	0.0	-	11.4	-
	Profile	1624	1624	2536	-	0	-	912	-
Initial billet surface	Front	446	502	500	-	56	-	-2	-
temperature [ºC]	Back	443	488	493	-	45	-	5	-
	Average	445	495	497	-	50.5	-	2	-
Ram temperature [ºC]	Front	107	123	109	-	16	-	-14	-
RESPONSE		1	2	3	-	C26 - C25		C27 - C26	
Ram force [kN]	Maximum	4407	3930	4092	-	-477	-61	162	21
	Minimum	2855	2616	2581	-	-239	-30	-35	-4
Effects:	196 mm	4313	3800	3850	-	-513	-65	50	6
Force [kN]	170 mm	3725	3160	3200	-	-565	-72	40	5
Pressure [MPa]	100 mm	3050	2740	2720	-	-310	-39	-20	-3
	30 mm	2905	2730	2720	-	-175	-22	-10	-1
Bearing inlet	Maximum	589	598	614	-	9	-	16	-
temperature [ºC]	Minimum	431	434	434	-	3	-	0	-
	170 mm	577	585	593	-	8	-	8	-
	100 mm	587	596	610	-	9	-	14	-
	30 mm	586	595	613	-	9	-	18	-
Bearing outlet	Maximum	600	606	618	-	6	-	12	-
temperature [ºC]	Minimum	431	434	434	-	3	-	0	-
	170 mm	590	590	593	-	0	-	3	-
	100 mm	601	605	611	-	4	-	6	-
	30 mm	602	607	615	-	5	-	8	-
Die face pressure	196 mm	386	354	370	-	-32	-	16	-
avg. value [MPa]	170 mm	344	289	292	-	-55	-	4	-
for all 3 sensors	100 mm	312	271	276	-	-41	-	5	-
	30 mm	330	303	305	-	-26	-	2	-
Die face pressure	196 mm	19.8	35.2	35.0	-	15.4	-	-0.2	-
st. dev. value [MPa]	170 mm	15.3	28.1	26.8	-	12.8	-	-1.3	-
for all 3 sensors	100 mm	15.2	28.2	30.5	-	13.0	-	2.3	-
	30 mm	19.4	35.7	35.1	-	16.4	-	-0.6	-
Container / liner force	196 mm	-	-	-	-	-	-	-	-
avg. value [kN]	170 mm	-	-	-	-	-	-	-	-
	100 mm	-	-	-	-	-	-	-	-
	30 mm	-	-	-	-	-	-	-	-
Liner friction [MPa]		-	-	-	-	-	-	-	-

.

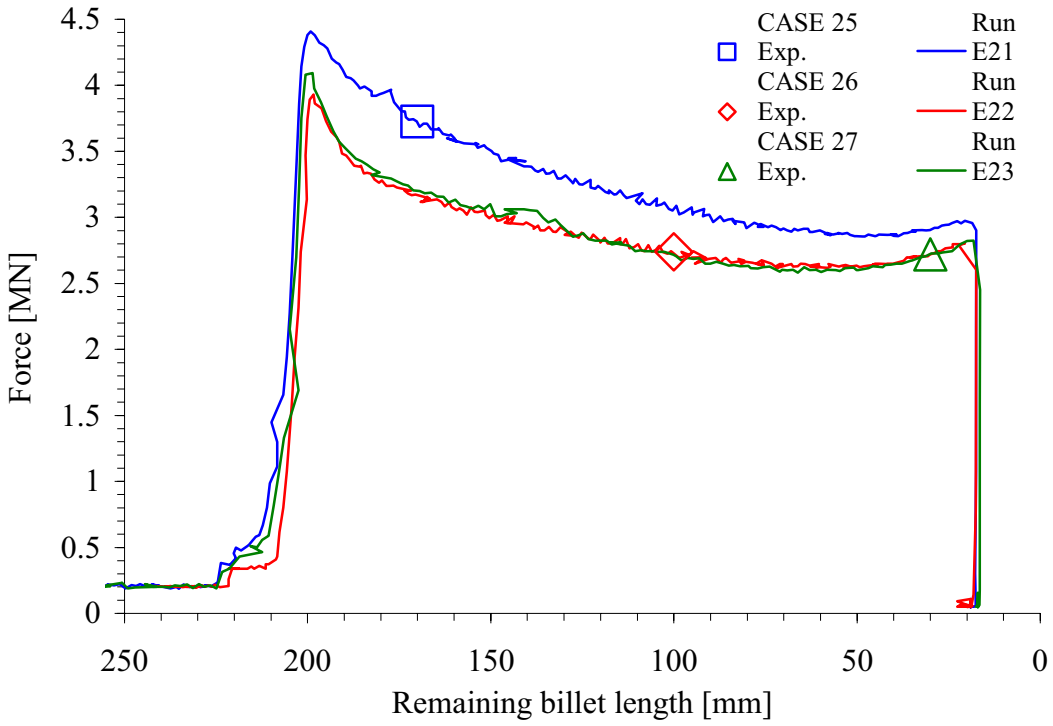

Figure 5.119. Measurement of the ram force – cases 25, 26 and 27 (long bearing).

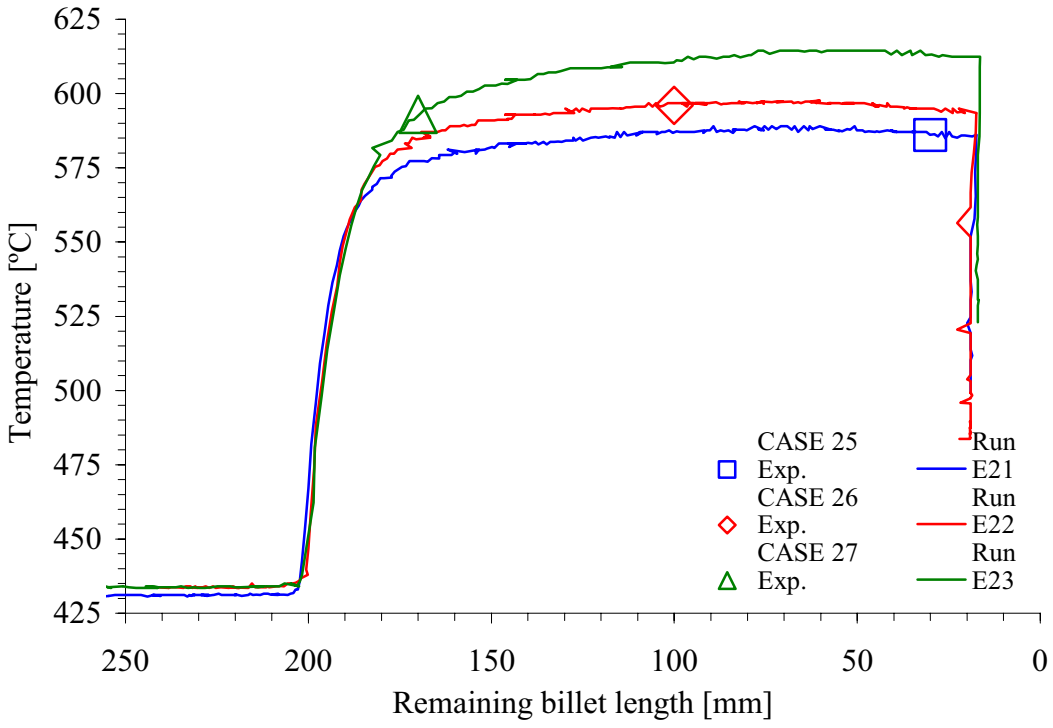

Figure 5.120. Measurement of the outlet temperature (bearing inlet) - cases 25, 26, 27.

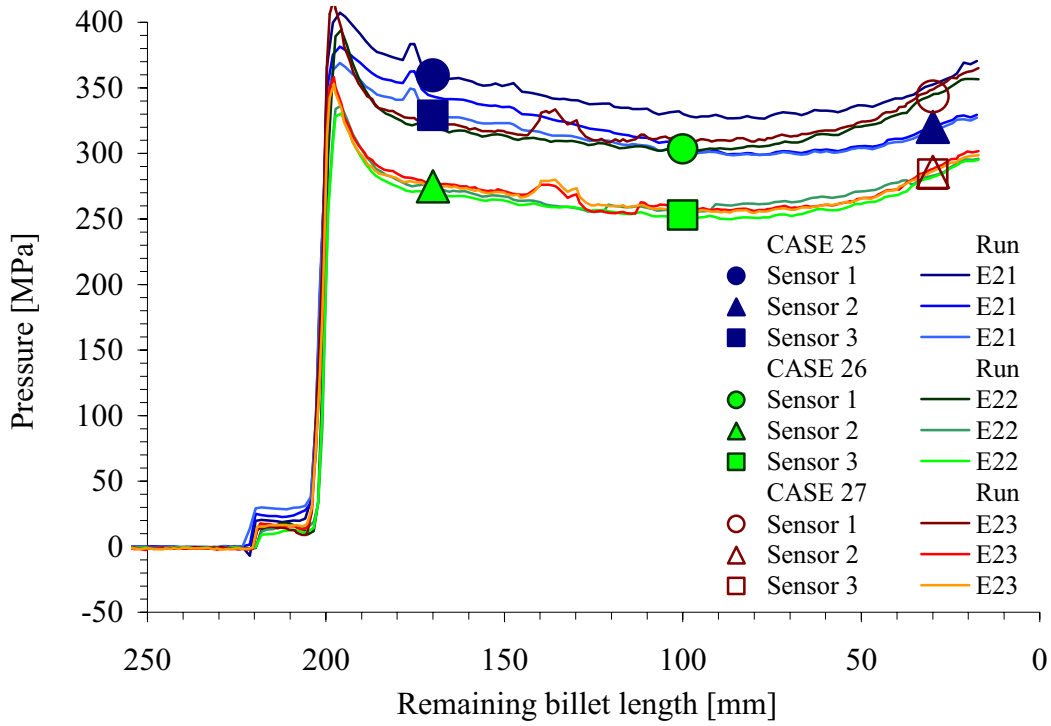

Figure 5.121. Measurement of the die face pressure - cases 25, 26 and 27.

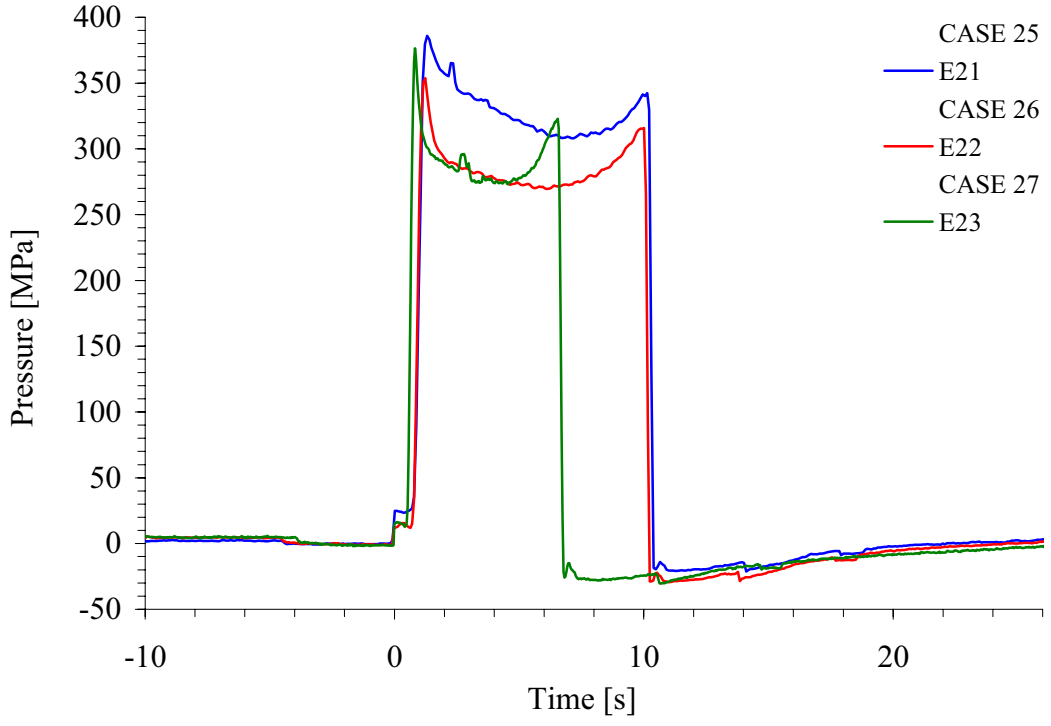

Figure 5.122. Measurement of the average die face pressure - cases 25, 26 and 27.

Table 5.28. Case 28 – input and output data

SPECIFICATION	CASE	28						
Nominal extrusion ratio		40	-		Die outlet diameter		15.8	mm
Nominal bearing length		12	mm					
Nominal ram velocity		12.5	mm/s		Profile velocity		500	mm/s
Nominal billet temperature		475	ºC					

INPUT DATA	Day/run #	D03	D12	D18	D19	Avg.	St.dev.	Effect BL
Actual velocity [mm/s]	Ram	12.6	12.6	12.6	12.6	12.6	0.0	-0.1
	Profile	504	504	504	504	504	0.0	-3
Initial billet surface	Front	474	474	472	472	473	1.2	3
temperature [ºC]	Back	461	462	468	467	465	3.5	-2
	Average	468	468	470	470	469	1.2	1
Ram temperature [ºC]	Front	133	137	140	135	136	3.0	7

RESPONSE		1	2	3	4	Avg.	St.dev.	Effect BL
Ram force [kN]	Maximum	3592	3722	3364	3696	3594	163.0	60
	Minimum	2341	2315	2301	2312	2317	16.9	49
Effect BL:	196 mm	3344	3471	3436	3500	3438	67.8	54
Pressure [MPa]	170 mm	2928	2959	2950	2960	2949	14.9	43
	100 mm	2489	2470	2480	2480	2480	7.8	41
	30 mm	2395	2365	2360	2370	2373	15.5	47
Bearing inlet	Maximum	557	559	557	558	558	1.0	27
temperature [ºC]	Minimum	427	434	432	434	432	3.3	2
	170 mm	547	551	549	549	549	1.6	32
	100 mm	557	557	557	557	557	0.0	29
	30 mm	550	553	552	551	552	1.3	27
Bearing outlet	Maximum	566	568	566	566	567	1.0	-
temperature [ºC]	Minimum	427	434	432	434	432	3.3	-
	170 mm	555	558	556	555	556	1.4	-
	100 mm	565	566	564	566	565	1.0	-
	30 mm	562	563	562	562	562	0.5	-
Die face pressure	196 mm	295	317	306	310	307	9.2	63
avg. value [MPa]	170 mm	250	258	255	255	254	3.3	37
for all 3 sensors	100 mm	228	239	235	235	234	4.5	30
	30 mm	254	260	259	257	258	2.7	27
Die face pressure	196 mm	4.9	7.3	3.9	3.8	5.0	-	-3.0
st. dev. value [MPa]	170 mm	4.4	4.5	3.1	2.9	3.7	-	-2.9
for all 3 sensors	100 mm	4.5	0.5	0.8	1.2	1.7	-	-4.4
	30 mm	1.9	0.7	4.9	1.0	2.1	-	-7.1
Container / liner force	196 mm	-	-	-	-	-	-	-
avg. value [kN]	170 mm	-	-	-	-	-	-	-
	100 mm	-	-	-	-	-	-	-
	30 mm	-	-	-	-	-	-	-
Liner friction [MPa]		-	-	-	-	-	-	-

.

Table 5.29. Case 29 – input and output data

SPECIFICATION	CASE	29						
Nominal extrusion ratio		80	-		Die outlet diameter		11.2	mm
Nominal bearing length		8.5	mm					
Nominal ram velocity		6.25	mm/s		Profile velocity		500	mm/s
Nominal billet temperature		475	ºC					

INPUT DATA	Day/run #	E07	E08	E10	E16	Avg.	St.dev.	Effect BL
Actual velocity [mm/s]	Ram	6.5	6.5	6.3	6.3	6.4	0.1	0.2
	Profile	520	520	504	504	512	9.2	14
Initial billet surface	Front	477	477	478	478	478	0.6	6
temperature [ºC]	Back	464	469	465	471	467	3.3	0
	Average	471	473	472	475	473	2.0	3
Ram temperature [ºC]	Front	137	133	127	122	130	6.6	6

RESPONSE		1	2	3	4	Avg.	St.dev.	Effect BL
Ram force [kN]	Maximum	3808	3745	3789	3826	3792	34.8	71
	Minimum	2575	2578	2607	2627	2597	24.8	57
Effect BL:	196 mm	3601	3546	3595	3621	3591	31.8	58
Pressure [MPa]	170 mm	3113	3120	3167	3200	3150	41.1	46
	100 mm	2728	2720	2750	2800	2750	36.0	46
	30 mm	2600	2605	2630	2640	2619	19.3	53
Bearing inlet	Maximum	554	554	555	554	554	0.5	26
temperature [ºC]	Minimum	435	435	434	434	435	0.6	6
	170 mm	552	550	552	551	551	1.0	28
	100 mm	553	552	552	553	553	0.6	26
	30 mm	543	543	542	543	543	0.5	23
Bearing outlet	Maximum	568	567	566	567	567	0.8	-
temperature [ºC]	Minimum	435	435	434	434	435	0.6	-
	170 mm	562	560	563	562	562	1.3	-
	100 mm	566	566	565	566	566	0.5	-
	30 mm	558	558	558	560	559	1.0	-
Die face pressure	196 mm	358	342	342	332	343	10.9	83
avg. value [MPa]	170 mm	305	290	291	283	292	9.1	56
for all 3 sensors	100 mm	298	283	284	280	286	8.1	50
	30 mm	328	312	310	305	314	10.1	55
Die face pressure	196 mm	40.6	28.9	35.3	25.2	32.5	-	28.1
st. dev. value [MPa]	170 mm	41.6	23.5	31.6	22.9	29.9	-	26.3
for all 3 sensors	100 mm	41.6	26.8	36.0	29.3	33.4	-	27.7
	30 mm	38.1	28.0	34.4	33.0	33.4	-	26.0
Container / liner force	196 mm	-	-	-	-	-	-	-
avg. value [kN]	170 mm	-	-	-	-	-	-	-
	100 mm	-	-	-	-	-	-	-
	30 mm	-	-	-	-	-	-	-
Liner friction [MPa]		-	-	-	-	-	-	-

.

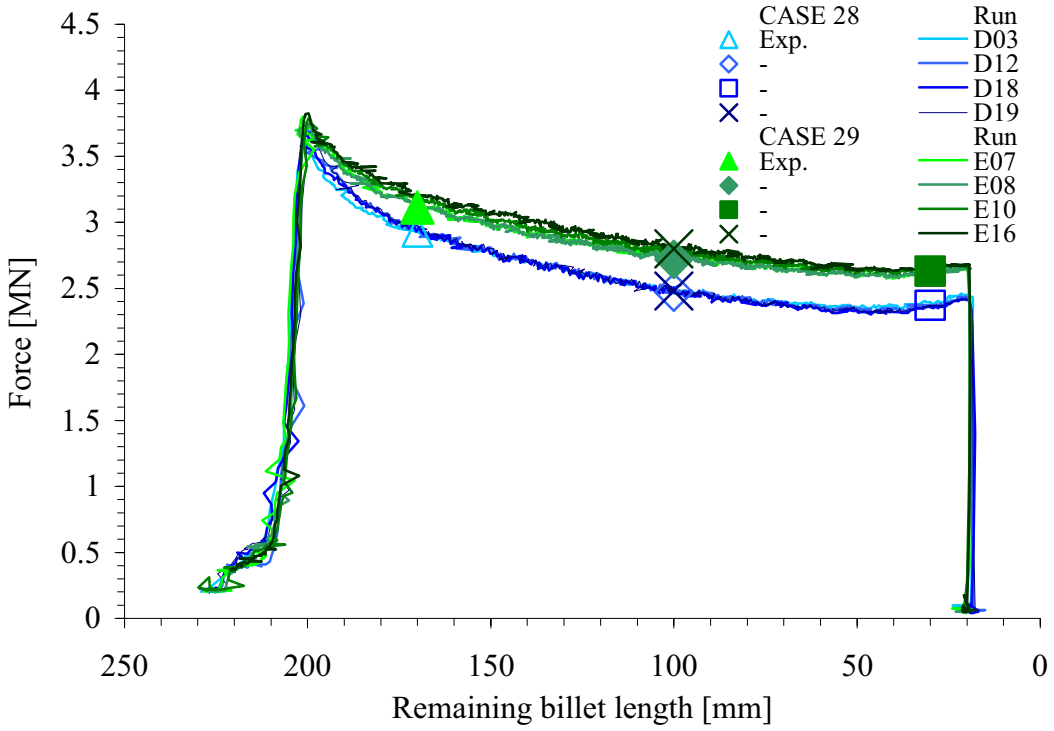

Figure 5.123. Measurement of the ram force - cases 28 and 29 (zero/long bearing).

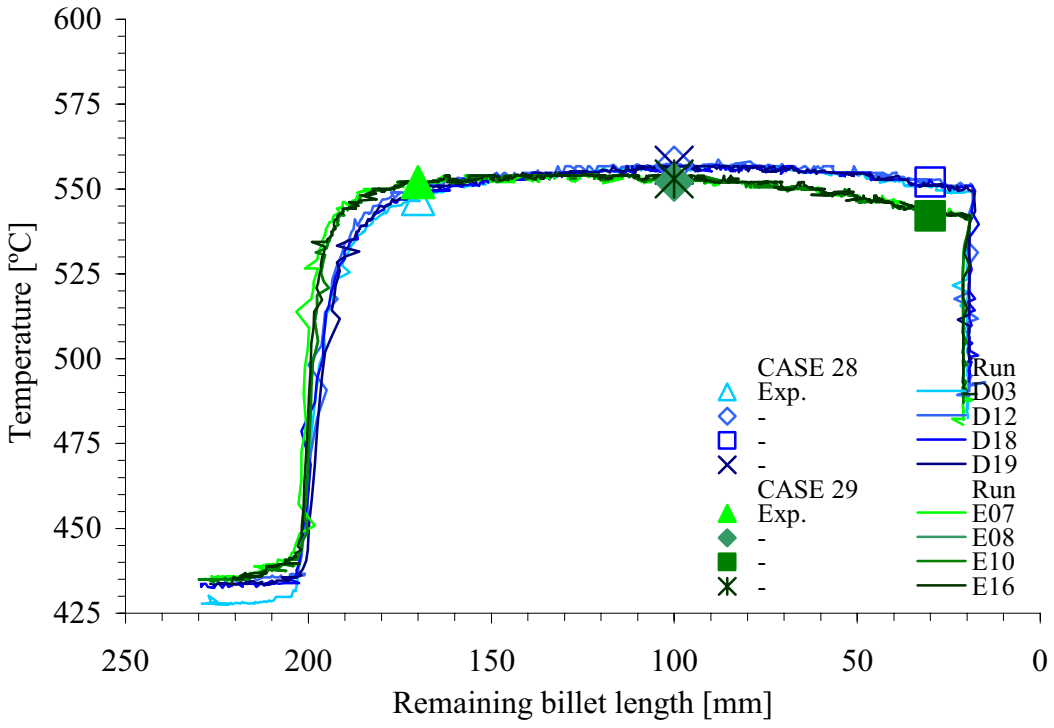

Figure 5.124. Measurement of the outlet temperature (bearing inlet) - cases 28 and 29.

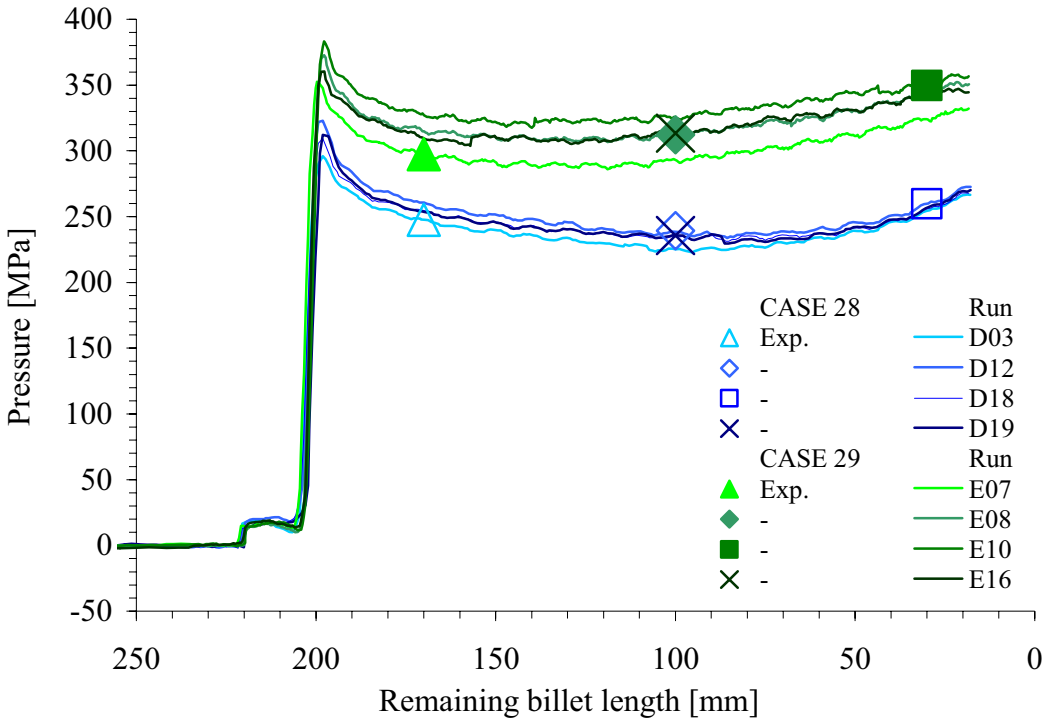

Figure 5.125. Measurement of the die face pressure by sensor 1 - cases 28 and 29.

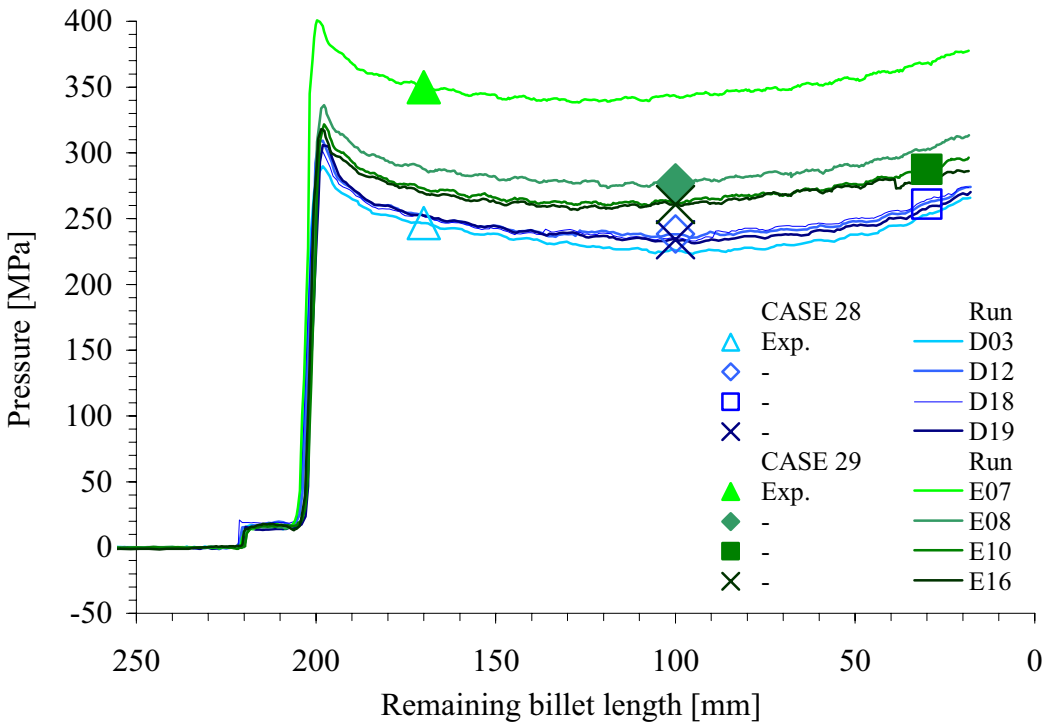

Figure 5.126. Measurement of the die face pressure by sensor 2 - cases 28 and 29.

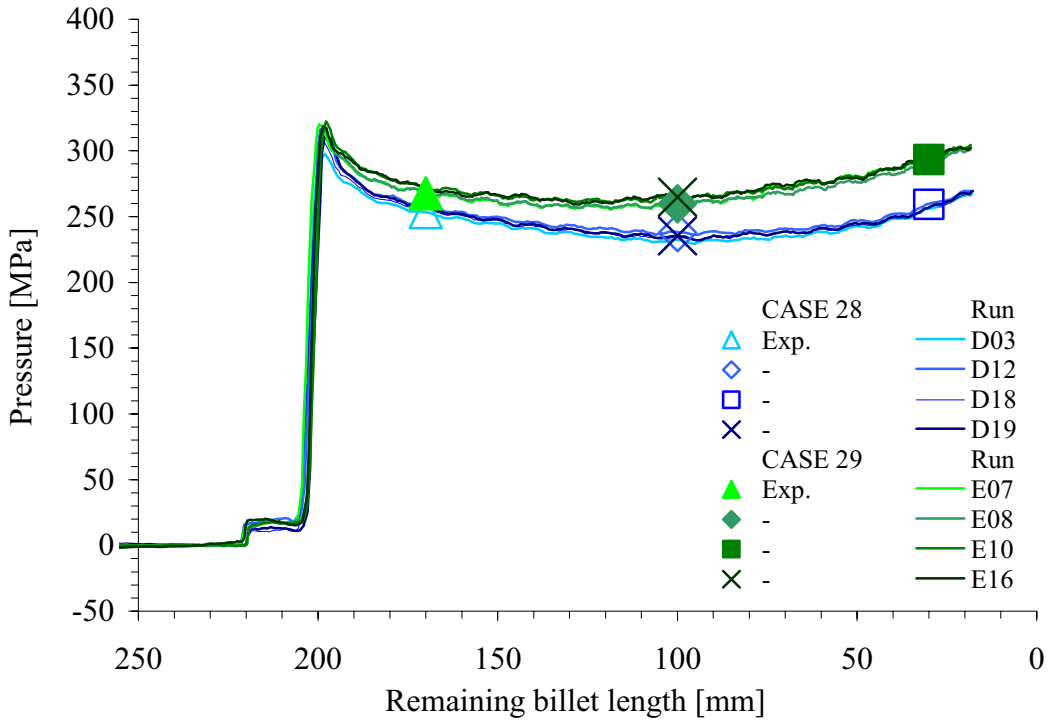

Figure 5.127. Measurement of the die face pressure by sensor 3 - cases 28 and 29.

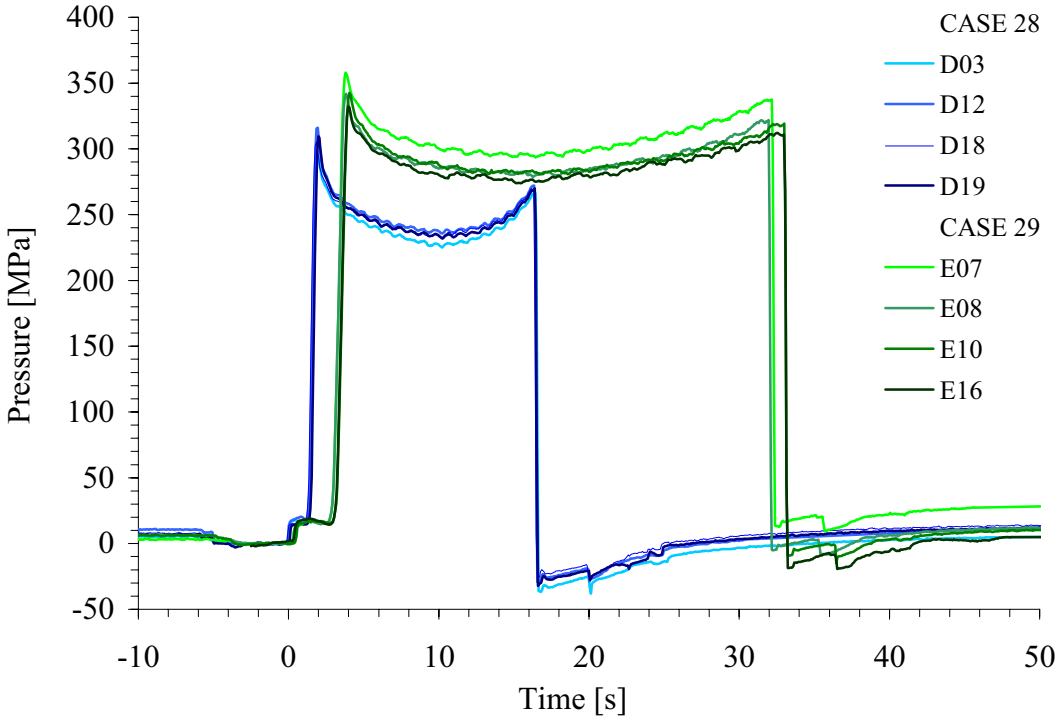

Figure 5.128. Measurement of the average die face pressure - cases 28 and 29.

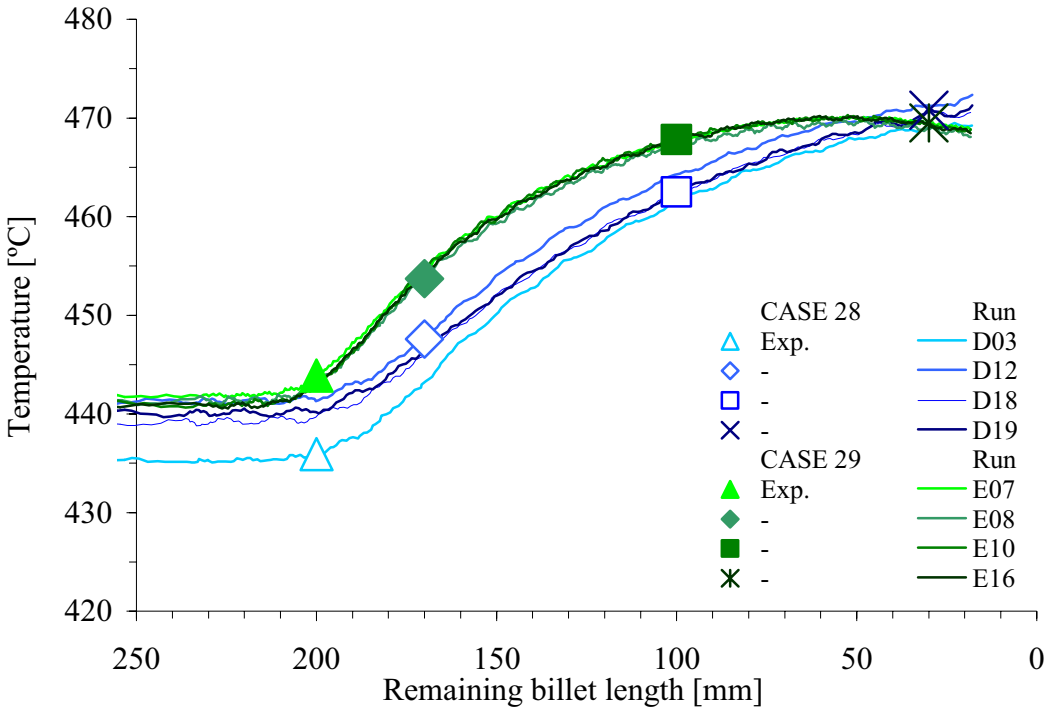

Figure 5.129. Measurement of the die face temperature - cases 28 and 29.

Chapter 6

Analysis and discussion

The main objective of this section is to shed more light on the capabilities and use of the capacitive pressure sensors presented in the earlier sections of this report. The properties of the greatest importance to the users of the sensors are most likely the accuracy and repeatability of measurement. For this reason experiments were run at many pressure levels, and various types of replicate measurements were performed. Experiments were also run with die outlet geometries of the simplest kind in order to simplify analysis. The results presented in the previous sections constitute the starting point of the analysis of this section. The ability of the sensors to measure the effects of small changes in input variables is also assessed. The final part of the analysis treats the pressure sensors' temperature sensitivity and possible schemes for temperature compensation.

An important, but probably less well-defined property of the sensors, is their usefulness. This characteristic certainly is strongly related to both the accuracy and the repeatability of measurement, but it mainly depends on the objectives and requirements of the user. In this PhD study, the results from the rod extrusion experiments have been used to assess the predictions of the flow relation [Moe04b]. The ram force and the outlet temperature have so far been the main sources of quantitative information about the extrusion process. The die face pressure and liner load measurements may potentially provide very valuable new knowledge about the extrusion process. The main reason for performing an inverse study was simply to establish estimates of the Zener-Hollomon flow relation parameters that give optimal predictions of ram force, outlet temperature and die face pressure. This would allow a careful evaluation of the response of the pressure sensors. It should be added that in this study, the inverse parameter estimation relies mainly on the ram force and outlet temperature measurements. Obviously, flow calculations performed with parameters inversely determined on the basis of a sensor's response cannot be used to evaluate the sensor's accuracy. However, if the model has proven to be satisfactory and estimates of the ram force and the outlet temperature are accurate, the die face pressure estimate should be of some value if it is compared with other responses of the system. The study is an iterative one. The sensors may also be useful for evaluating the quality of simulation codes. No thorough study of the quality of the simulation code ALMA2π has been performed. When material data based on compression testing are used, the ram force prediction is quite accurate, while the outlet temperature prediction may be somewhat too high. The issue is further discussed below.

6.1 Analysis of variance

6.1.1 The nature and limits of variability

Measurement results are affected by both random and systematic errors. It is not always possible to draw a clear distinction between the two types. Measurement errors related to recalibration may be regarded as systematic when results from only a few rounds of experiments are compared with simulation data. The results may be expected to be biased due to the systematic errors from the calibration and due to the variability in the sensor response. However, if a large number of measurement rounds are performed, a part of the error related to recalibration may be regarded as purely random.

This sub-section seeks to produce an estimate of the random errors or variability of die face pressure measurement. The focus is on two types of variability. First, the users of sensors need an estimate of the variability related to genuinely replicated runs. In the current report a genuinely replicated run is regarded as one that has essentially been performed with a new and re-calibrated sensor in a new round of experiments. It is here assumed that an estimate of the true or total variability of the die face pressure measurement may be established if disassembly, reassembly, recalibration and extrusion are performed many times with the same pressure sensor. The second type of variability may be experienced during a single round of experiments with only one sensor. It may be related to changes in the extrusion conditions or to changes in sensor behaviour. In a study of sensor behaviour the focus should be on the variability in the sensor behaviour. Systematic undesired changes in the input data and the ram force measurement may give an indication of how successfully runs are repeated. One component of the change in sensor response during a round of measurement may be of a systematic kind. In the harsh extrusion environment, the behaviour of the sensors may degrade or change during a round of experiments. The sample standard deviation calculated in the previous and this chapter may not directly disclose the degradation, but it may be further studied by assessing responses from each run. Measures of variability are first established.

There are relatively few examples of genuine replications in the experiments presented in previous sections. Reassembly and recalibration was only performed before each day or round of experiment. The experimental set-up was not altered during the round. After an extrusion run the temperature distribution was merely re-established before the new billet was loaded. The variability was then essentially linked to changes in the input variables and boundary conditions of the process, and to a possible deterioration of the sensor behaviour during the round. The capacitive probe may move and loosen, as was indeed observed on day E. The definition of the zero point may be poor. When the die was disassembled and reassembled, there were additional sources of variability. Each capacitive probe behaved according to a unique calibration curve with a non-linearity of typically ± 0.5 μm (Chapter 4). Sensors may also respond somewhat differently to changes in temperature, and experimental conditions may change after reassembly.

One of the reasons why on-line calibration was introduced was to reduce the effect of systematic errors related to sensor design and mounting. There are certain limits in the accuracy of the calibration technique. The most important one is that the press force measurement is of an accuracy no better than ± 50 kN. This corresponds to a pressure of

± 6.4 MPa and disc deflections of approx ± 0.5 μm and ± 0.8 μm for sensors 1 and 2 respectively. When a large number of genuine replications are performed, the random error related to calibration and measurement should be at least as large as this lower limit. The exact nature of the ram force measurement error is not known. Sufficiently systematic replication of calibration experiments has not been performed to evaluate repeatability. There may also be additional deviations during dynamic loading. In future experiments, a load cell should be introduced to measure the ram force accurately on-line. However, according to Chapter 4, most of the variability of measurement is related to the deficiencies of the sensor design rather than the limitations of the extrusion press.

An important objective of the experiments was to produce pressure effects as a result of parameter changes that could be assessed with the help of the die face pressure sensor. When assessing small effects a large variance may complicate the analysis and make the conclusions less certain. In such cases it may be advantageous not to perform genuine replications, but rather to perform all experiments under the very same conditions. It has already been stated that all pressure measurements are relative measurements. If all runs were genuine replications, effects could probably not be determined more accurately than the absolute values. However, the estimates of effects calculated from only one round should be less affected by the variability in measurement related to calibration and mounting. The issue of accuracy is further discussed in the next sub-section. Here, the importance of assessing different kinds of measurement variability is stressed.

6.1.2 An example of a variability study – case 2

Table 6.1 presents results from the experimental runs of case 2, performed on days A and B. The values of pressure shown in the upper part of the table have been calculated using the calibration factors established by on-line calibration. The values in Table 6.2 are also based on experimental data from the same experiments, but calibration factors calculated by the ANSYS® 7.1 finite element model have been used. The calibration factor of sensor 1 was 11.8 MPa/μm·50 μm/V, while a factor of 7.6 MPa/μm·50 μm/V was used for sensors 2 and 3. As earlier discussed, the finite element calibration factors have been established with the assumption that the capacitive displacement sensors measure the maximum deflection of the sensor disc. In reality, some sort of averaging is performed during capacitive measurement, and the maximum disc deflection is larger than indicated. Thus, the numerical calibration approach produces pressure estimates that are too low. The analysis of calibration revealed that the effect was approximately 10 %. However, this sub-section focuses only on the variability, and Table 6.2 gives an indication of the variability in the raw data from the extrusion experiments.

The pressure response from a single extrusion run is denoted p_{cdrs}. One adheres to the convention that a large letter describes a random (stochastic) variable that may assume any value, while a small letter refers to a real number, a measurement result [Box78]. The indices *c*, *d*, *r* and *s* completely define the measurement result:

- *c* shows which case the run belongs to (1-29)
- *d* indicates the day on which the run was performed (A, B, C, D or E)
- *r* gives the run number of the case on a specific day (1: A02, 2: A04, 3: A14, etc)
- *s* indicates which sensor that produced the result (1,2 or 3)

Table 6.1. Results from case 2 (runs A02, A04, A14, B02, B03, B16) for a remaining billet length of 170 mm. The values have been calculated with calibration factors established with an on-line technique. All values are in [MPa].

On-line calibration		Run				
Day	Sensor	1	2	3	Average	St. dev
	1	230.4	231.7	230.4	230.8	0.8
A	2	230.6	230.6	230.6	230.6	0.0
	3	248.1	243.2	242.4	244.6	3.1
	1	243.1	237.8	239.1	240.0	2.7
B	2	230.5	225.7	224.1	226.8	3.3
	3	234.4	231.8	231.0	232.4	1.8
Average day A		236.4	235.2	234.5	235.3	1.0
Average day B		236.0	231.8	231.4	233.0	2.5
Average case 2					234.4	1.6
St.dev. day A		10.1	7.0	6.9	7.0	
St.dev. day B		6.4	6.0	7.5	6.7	
St.dev. case 2					6.9	

Table 6.2. Results from case 2 (runs A02, A04, A14, B02, B03, B16) for a remaining billet length of 170 mm. The values have been calculated with calibration factors established with a finite element technique. All values are in [MPa].

FE calibration		Run				
Day	Sensor	1	2	3	Average	St. dev
	1	205.3	206.5	205.3	205.7	0.7
A	2	206.0	206.0	206.0	206.0	0.0
	3	233.3	228.8	228.0	230.0	2.9
	1	217.1	212.4	213.6	214.4	2.5
B	2	221.2	216.6	215.1	217.6	3.2
	3	211.3	209.0	208.2	209.5	1.6
Average day A		214.9	213.7	213.1	213.9	0.9
Average day B		216.5	212.7	212.3	213.8	2.3
Average case 2					213.9	
St.dev. day A		16.0	13.0	12.9	12.2	
St.dev. day B		5.0	3.8	3.6	4.2	
St.dev. case 2					9.6	
Ram pressure day A		363.3	356.5	350.7	355.6	5.7
Ram pressure day B		359.2	356.9	351.3	355.8	4.1

Table 6.3 provides a description of the various data presented in Table 6.1 and Table 6.2. The measurement results in Table 6.1 are all in the series p_{2Ars} and p_{2Brs} where r and s may be 1, 2 or 3. Cases 1 to 6 were run on two occasions (rounds), while cases 7 to 29 were only run on one. The responses of cases 7 to 29 are denoted p_{7Crs}, p_{13Drs} and p_{19Ers} etc. The value of greatest interest in the study of system responses is the mean pressure of a case, here denoted $\overline{p}_{c\ldots}$. It has earlier been called also $p(x_1, x_2, x_3, x_4)$, where x_1, x_2,

x_3 and x_4 are the factors of the study. Table 3.5 relates the case number to a combination of the four factors of the current study. $\overline{p}_{c\bullet\bullet\bullet}$ is calculated in a straightforward manner. The average pressure values for case c and for each day d, $\overline{p}_{cd\bullet\bullet}$, are first calculated (Equation (6.1)). Ns is the number of sensors, which is usually 3, and Nr_{cd} is the number of runs for the case c and day d ($Nr_{2A} = 3$, $Nr_{2B} = 3$).

$$\overline{p}_{cd\bullet\bullet} = \frac{1}{Ns \cdot Nr_{cd}} \sum_{s=1}^{Ns} \sum_{r=1}^{Nr_{cd}} p_{cdrs} \tag{6.1}$$

The values of $\overline{p}_{cd\bullet\bullet}$ are equal to $\overline{p}_{c\bullet\bullet\bullet}$ for all cases except those performed on the first two days of experiments. A weighted average is applied in the latter case:

$$\overline{p}_{2\bullet\bullet\bullet} = \frac{Nr_{2A}\overline{p}_{2A\bullet\bullet} + Nr_{2B}\overline{p}_{2B\bullet\bullet}}{Nr_{2A} + Nr_{2B}} \tag{6.2}$$

Table 6.1 also shows average values of pressure for each of the sensors during a day of experiments (Equation (6.3)) and the average value of pressure for each of the runs on a specific day (Equation (6.4)):

$$\overline{p}_{cd\bullet s} = \frac{1}{Nr_{cd}} \sum_{r=1}^{Nr_{cd}} p_{cdrs} \tag{6.3}$$

$$\overline{p}_{cdr\bullet} = \frac{1}{Ns} \sum_{s=1}^{Ns} p_{cdrs} \tag{6.4}$$

These expressions may be used to estimate various types of measurement variance. The column on the right-hand side of Table 6.1 presents the sample standard variation for all runs and each of the sensors $s_{cd\bullet s}$ (Equation (6.5)):

$$s_{cd\bullet s} = \sqrt{\sum_{r=1}^{Nr_{cd}} \frac{\left(p_{cdrs} - \overline{p}_{cd\bullet s}\right)^2}{Nr_{cd} - 1}} \tag{6.5}$$

The sample standard deviations of the sensor outputs (sensors 1, 2 and 3) are also calculated for each of the runs of a day:

$$s_{cdr\bullet} = \sqrt{\sum_{s=1}^{Ns} \frac{\left(p_{cdrs} - \overline{p}_{cdr\bullet}\right)^2}{Nr_{cd} - 1}} \tag{6.6}$$

The estimates $s_{cd\bullet s}$ indicate that the differences in pressure from one run to another were fairly small. The variance in the average ram pressure is a suitable reference. The variation from one run to the next may be larger if results from measurements with a remaining billet length of 196 mm are assessed. $s_{cdr\bullet}$ should give a good indication of

the true measurement variability when performing genuine replications. Although the same calibration experiments were performed to calibrate the die's three sensors, the responses of the sensors should be regarded as fairly close to independent of each other. The fact that measurements were performed in the same environment, and that sensors were exposed the same loads, makes the results comparable. Two different sensor solutions were used, and the estimate of variance, $s_{cdr\bullet}$, is perhaps more characteristic of the calibration procedure than of the pressure sensor design. Weighted averages of the sample variances on a specific day and for a specific case are calculated and used in the assessment of measurement results. The expressions for the estimates of variances for case 2 and days A and B are:

$$s_{2A\bullet\bullet}^2 = \frac{\nu_{2A1}s_{2A1\bullet}^2 + \nu_{2A1}s_{2A2\bullet}^2 + \nu_{2A1}s_{2A3\bullet}^2}{\nu_{2A1} + \nu_{2A2} + \nu_{2A3}} \tag{6.7}$$

$$s_{2B\bullet\bullet}^2 = \frac{\nu_{2B1}s_{2B1\bullet}^2 + \nu_{2B1}s_{2B2\bullet}^2 + \nu_{2B1}s_{2B3\bullet}^2}{\nu_{2B1} + \nu_{2B2} + \nu_{2B3}} \tag{6.8}$$

$$s_{c\bullet\bullet\bullet}^2 = \frac{\nu_{2A}s_{2A\bullet\bullet}^2 + \nu_{2B}s_{2B\bullet\bullet}^2}{\nu_{2A} + \nu_{2B}} \tag{6.9}$$

ν_{2A1} is the degrees of freedom for the estimates of standard variation for round A ($\nu_{2A1} = Ns - 1$). ν_{2A} is the sum of the degrees of freedom for case 2 (round A and B). It should be remembered that the variance for each run, $s_{cdr\bullet}$, is not independent, because the runs were not genuine replications. There are therefore relatively few degrees of freedom.

Table 6.3. Description of results in Tables 6.1 and 6.2. $\overline{s}_{2A\bullet\bullet}$ is the average of $s_{2A\bullet1}$, $s_{2A\bullet2}$ and $s_{2A\bullet3}$. The other symbols have been presented above.

On-line calibration		Run				
Day	Sensor	1	2	3	Average	St. dev
A	1	p_{2A11}	p_{2A21}	p_{2A31}	$\overline{p}_{2A\bullet1}$	$s_{2A\bullet1}$
	2	p_{2A12}	p_{2A22}	p_{2A32}	$\overline{p}_{2A\bullet2}$	$s_{2A\bullet2}$
	3	p_{2A13}	p_{2A23}	p_{2A33}	$\overline{p}_{2A\bullet3}$	$s_{2A\bullet3}$
B	1	p_{2B11}	p_{2B21}	p_{2B31}	$\overline{p}_{2B\bullet1}$	$s_{2B\bullet1}$
	2	p_{2B12}	p_{2B22}	p_{2B32}	$\overline{p}_{2B\bullet2}$	$s_{2B\bullet2}$
	3	p_{2B13}	p_{2B23}	p_{2B33}	$\overline{p}_{2B\bullet3}$	$s_{2B\bullet3}$
Average day A		$\overline{p}_{2A1\bullet}$	$\overline{p}_{2A2\bullet}$	$\overline{p}_{2A3\bullet}$	$\overline{p}_{2A\bullet\bullet}$	$\overline{s}_{2A\bullet\bullet}$
Average day B		$\overline{p}_{2B1\bullet}$	$\overline{p}_{2B2\bullet}$	$\overline{p}_{2B3\bullet}$	$\overline{p}_{2B\bullet\bullet}$	$\overline{s}_{2B\bullet\bullet}$
Average case 2					$\overline{p}_{2\bullet\bullet\bullet}$	$\overline{s}_{2\bullet\bullet\bullet}$
St.dev. day A		$s_{2A1\bullet}$	$s_{2A2\bullet}$	$s_{2A3\bullet}$	$s_{2A\bullet\bullet}$	
St.dev. day B		$s_{2B1\bullet}$	$s_{2B2\bullet}$	$s_{2B3\bullet}$	$s_{2B\bullet\bullet}$	
St.dev. case 2					$s_{2\bullet\bullet\bullet}$	

6.1.3 An evaluation of data from all rounds

Table 6.4 and Table 6.5 present the average values of the sample standard deviation for all the cases and days of the experiment, $s_{c\ldots}$. Overall estimates of the sample standard deviation for each day and for the complete experiment have also been calculated. Formulas similar to those of Equation (6.7) have been used. Whereas Table 6.4 treats results obtained by using the on-line calibration coefficients, Table 6.5 shows the results established by three-dimensional finite element calculations.

Table 6.4. The sample standard deviation for all days and cases, $\overline{p}_{cdr\bullet}$, $\overline{p}_{cd\bullet\bullet}$ – with on-line calibration. All values are in [MPa]

Cases	Day				
A, B, C, D	A	B	C	D	Average
1, 7, 13, 19	8.7	5.7	3.9	5.4	
2, 8, 14, 20	7.0	6.7	4.5	5.0	
3, 9, 15, 21	8.3	7.4	3.8	10.7	
4, 10, 16, 22		4.3	5.3	6.2	
5, 11, 17, 23	6.9	6.7	1.7	7.3	
6, 12, 18, 24		7.6	1.7	7.7	
28				3.8	
Average	7.6	6.5	3.8	6.6	6.2

Table 6.5: The sample standard deviation for all days and cases, $\overline{p}_{cdr\bullet}$, $\overline{p}_{cd\bullet\bullet}$ – with finite element calibration. All values are in [MPa]

Cases	Day				
A, B, C, D	A	B	C	D	Average
1, 7, 13, 19	13.9	3.9	1.3	15.3	
2, 8, 14, 20	12.2	4.2	1.9	14.3	
3, 9, 15, 21	14.7	5.0	2.9	21.7	
4, 10, 16, 22		3.9	1.7	11.8	
5, 11, 17, 23	12.0	3.5	3.5	16.1	
6, 12, 18, 24		3.0	4.3	16.1	
28				11.7	
Average	13.0	3.9	2.6	15.1	10.4

The true variability in the disc displacement measurements is somewhat larger than may be expected if it was only related to the non-linearity of the displacement measurement (1 µm / 50 µm = 4 MPa / 200 MPa = 2 % of FS). The average value of the calculated sample standard deviation of pressure from calibrated sensors is larger than the reported inaccuracy in ram force measurement. ± 50 kN corresponds to ± 6.4 MPa. When pressure sensor calibration is performed on a range of days, the effect of the ram force measurement inaccuracy may be hard to determine and can be an important cause of variability during calibration. The range of ± 50 kN, is as indicated in Chapter 4, also not a clearly defined characteristic value of variability. Most of the data from replicated

measurements lie within ± 50 kN. The calibrated output of the three pressure sensors deviated by as much as 20 MPa or 10 % of full scale, but differences were usually significantly smaller. The characteristic data for the ram force is a natural lower bound, and it seems that the full potential of the calibration technique has not been used. The calibration experiments gave a similar indication (Chapter 4). When calibration curves were reproduced, the standard deviation calculated was 0.3 MPa/μm. This corresponds to a standard deviation of pressure measurement of typically 10 MPa. Data deviated significantly more from the average value during the calibration. There are several reasons for the relatively large variability. No standard procedure for calibration had been developed, and further experiments are required to evaluate calibration procedures. More focus should, as earlier indicated, be put on controlling the environment during calibration. A significant part of the variability in the experiments and during calibration was probably due to the sensor design deficiencies and more specifically to the capacitive probe mounting solution. The possibility that there were unaccounted-for probe displacements during extrusion or calibration cannot be disregarded. Furthermore, the task of evaluating data and determining the exact zero point of measurement must be very carefully carried out. Finally, it should be remembered that an error of 6 MPa corresponds to a relative displacement of approx 0.5 μm ((6 MPa /200 MPa)·20 μm = 0.6 μm). The task of accurately reproducing displacement measurements of less than 1 μm in the high-temperature and high-pressure environment of extrusion is a most exacting task. Still, when sensors are repeated in a randomised manner during a round of experiments, the sample standard deviation was in fact only 2 to 3 MPa. This gives an indication of the potential of the measurement technique.

6.1.4 Evaluation of the variability on day D and the effect of on-line calibration

The variability is generally larger for pressure estimates that have been based on the calibration factors established by finite element modelling than by the on-line method. It may therefore seem as if the on-line calibration approach has been effective. Table 6.5 treats the results established by finite element calibration factors and gives an indication of the scatter in the raw data. A large amount of the variability is caused by the differences between the results produced by sensors 2 and 3, which make use of the same mounting solution and sensor disc dimensions. Relatively few experiments have been conducted, and it is possible to view the differences in results as insignificant, at least from a statistical point of view. The raw data from the different sensors seem to be in better accordance than calibrated data on both days B and C, while the variability in the responses is very large on days A and D. On day D, the experiments (or runs) were performed in a completely randomised manner, but this is probably not the main cause of the large sample standard variation. The variability assessed here is the one related to the responses of the different sensors for a particular run, s_{2Ar}. .

It is possible to evaluate the probability that the results of Table 6.4 and Table 6.5 originate from the very same population. If S^2 is the variance of a random sample of size n taken from a normal population of variance σ^2, then the χ^2 is chi-squared distributed:

$$\chi^2 = \frac{(n-1)S^2}{\sigma^2} \qquad (6.10)$$

Two questions are of interest:

1. What is the probability that results from day D are from the same population as the results from days B and C? If it seems likely that they are not, the conclusion may be drawn that the measurements have not been fully controlled.
2. What is the probability that results obtained with on-line and finite element calibration are from the very same distribution? If the sample standard deviation obtained with the finite element calibration technique is significantly larger than that of the on-line technique, the conclusion may be drawn that the on-line calibration technique contributes to a reduction in the variability.

The chi-squared distribution should only be used if the sample is truly random and taken from a normal distribution. The distribution of P_{cdrs} is not known, but the central limit theorem of statistics indicates that $\overline{P}_{cdr}$. at least approximates the normal distribution. Since there are only three independent measurements, there are, however, only two degrees of freedom for each run. Although a number of cases were run repeatedly on any specific day, the runs were not truly genuine replications. All the estimates of the sample variations are therefore not completely independent pieces of information. As for the first question, it should probably be assumed that the data have been gathered from populations with only two degrees of freedom (three independent measurements). If it is assumed that the real population variance for all days is $(6.4 \text{ MPa})^2$, $S^2 = (15.1 \text{ MPa})^2$ and $\chi^2 = 2 \cdot (15.1/6.4)^2 = 11.13$. Thus, the probability that an average sample standard deviation of 15.1 MPa or larger may be observed for a population of $\sigma = 6.4$ MPa is $P(\chi^2 > 11.13) = 0.4$ %. On the other hand, if on-line calibration is performed, the probability $P(\chi^2 > 2 \cdot (6.6/6.4)^2) = P(\chi^2 > 2.06) = 35$ %. Thus, by using on-line calibration, the results on day D became significantly less scattered. Note also that the variability in data from day C is very small when finite element calibration is used. This may at first seem to be an advantage, but it may also be regarded as a symptom of lack of control. However, if the standard variation of measurement is in fact $\sigma^2 = (6.4 \text{ MPa})^2$, the probability of a sample standard deviation of 2.6 MPa or smaller is as large as $P(\chi^2 < 2 \cdot (2.6/6.4)^2) = P(\chi^2 < 0.33) = 15.2$ %. Thus, it is not improbable that the three pressure sensors produce results with a sample standard deviation of 2.6 MPa.

When the average values of sample random deviation from all runs are assessed, it should be realised that experiments are not only performed with 3 sensors, but also that the sensors have been calibrated four times. It is here assumed that there are in all eight degrees of freedom. At the same time, one wishes to refute a hypothesis claiming that the on-line calibration technique is of limited value because it causes no reduction in the variability. The initial assumption is that the standard variance was 6.4^2 MPa^2 for data obtained with both calibration techniques. When finite element based calibration rather than the on-line calibration is performed, however, the observed overall standard deviation is 10.4 MPa. The probability of observing such a value or a larger one is only 2 % ($= P(\chi^2 > 8 \cdot (10.4/6.4)^2) = P(\chi^2 > 21.125)$). It is therefore reasonable to conclude that the on-line calibration technique may significantly reduce variability and increase the reproducibility of the die face pressure measurement. The effect of the calibration on the measurement accuracy is treated more thoroughly in the next subsection.

6.1.5 A presentation of raw data from the experimental sequence

A further insight into the variability of the die face pressure measurement technique may be obtained by evaluating the plots of the sample standard variation in the output of the three pressure sensors for each of the runs (Figure 6.1). The standard deviation is usually in the range from 5 to 10 MPa. On the last day of experiments, day E, only one of the sensors seemed to work satisfactorily. The variability in results was artificially large. As will be shown later in this section, estimates of the mean pressure for the cases run on day E were also much poorer than the estimates from the other days. This applies to both the average value of the sensor output data and to the output data of each of the sensors. During calibration experiments, it was obvious that one of the sensors, sensor 2, was not properly fastened. Sensor 1, which used the spring solution to hold the probe in place, also produced poor results during calibration and extrusion. The output data of sensor 3 were in line with what was observed on the other days, but estimates were probably somewhat too low.

A further important piece of information shown in Figure 6.1 is that there was no very significant changes in the variability of pressure measurements during a round of experiments, s_{cdr}. If a sensor loosens and/or stops working properly, the variability should increase or in some rare cases decrease. The changes in the sample random deviation for all sensors from one run to the next may be explained by random variation. Further information about the trends in the sensor behaviour may be obtained from plots of data from each of the runs of a round (Figure 6.2 to Figure 6.6). The calibration factors obtained with the on-line technique have been used. The low quality of the results on day E is again obvious. Only sensor 3 produced fairly repeatable results.

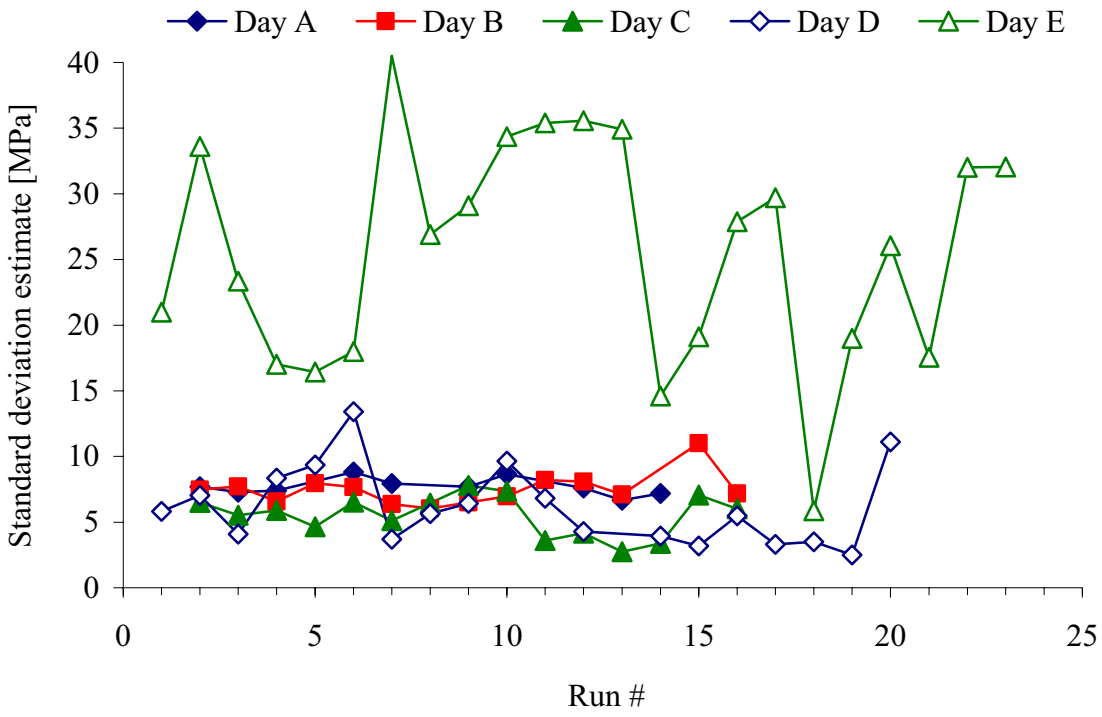

Figure 6.1. The sample standard variation for the output of three pressure sensors

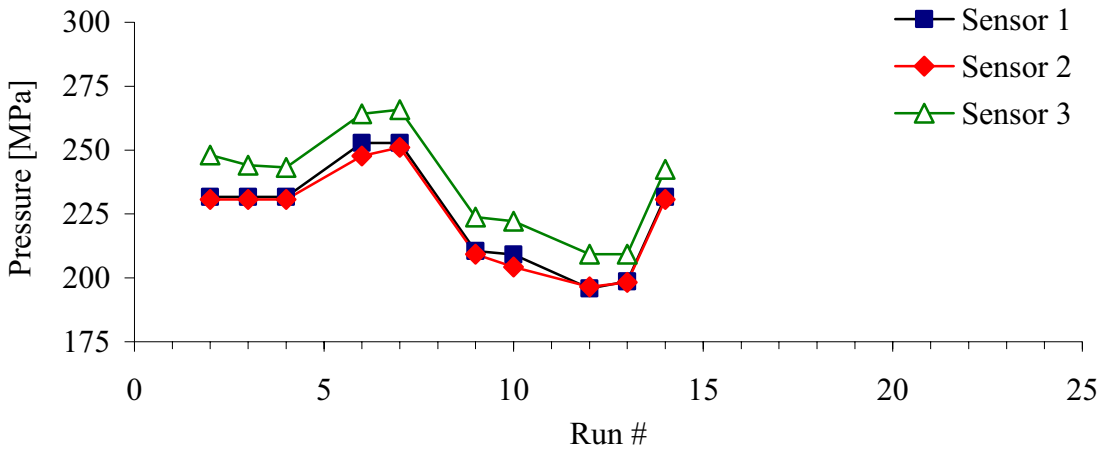

Figure 6.2. Die face pressure measurement results – day A.

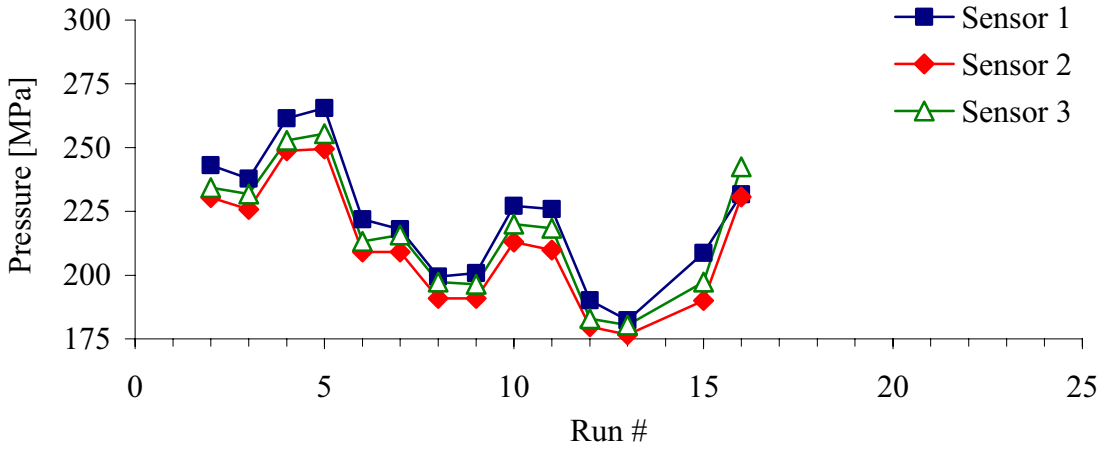

Figure 6.3. Die face pressure measurement results – day B.

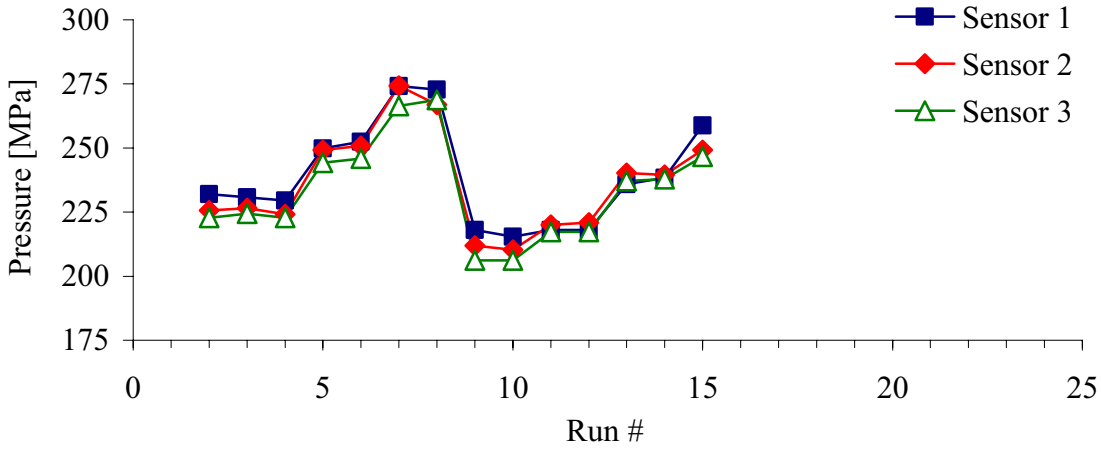

Figure 6.4. Die face pressure measurement results – day C.

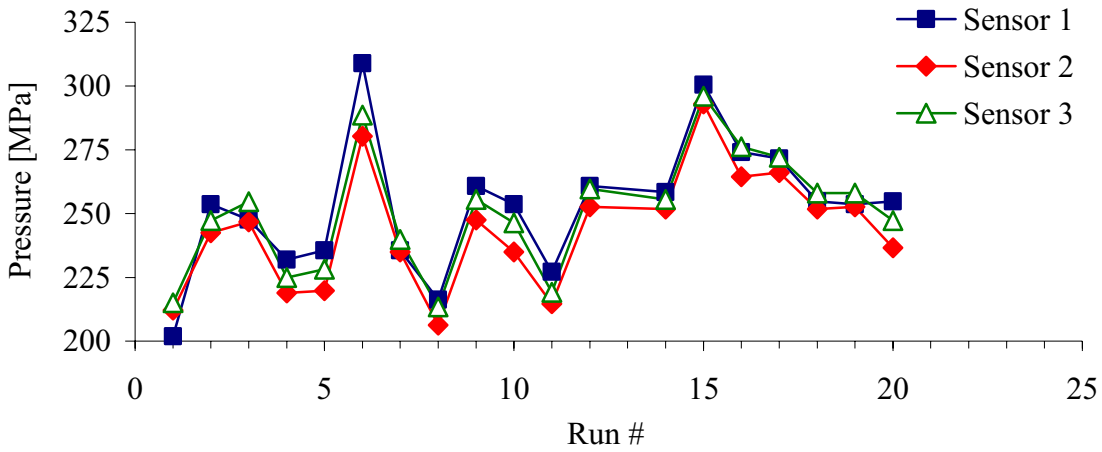

Figure 6.5. Die face pressure measurement results – day D.

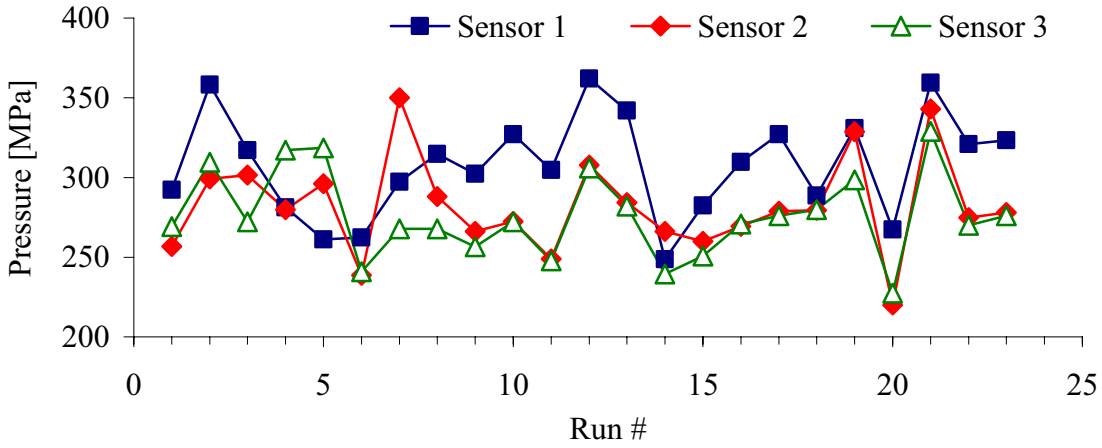

Figure 6.6. Die face pressure measurement results – day E.

6.2 An evaluation of the accuracy of measurement

The accuracy of measurement is a measure of the difference between the true and the measured value of a response. The accuracy is here regarded as the difference between the actual value and the average value of the response of a set of measurements. For example, it is possible to assess the overall accuracy of the measurement and calibration technique by studying results from all rounds and all sensors. Such a calculation should reveal systematic errors related to the calibration experiments. Also results from only one sensor during a round of experiments may be assessed. Estimates of this type are more affected by the variability related to calibration and the randomness in the die face pressure measurement in general. Nevertheless, the estimate should give an indication of the accuracy that may be expected for the individual sensors.

As was discussed in relation to calibration, the true value of a response is generally not known and can never be exactly determined. The measurement accuracy should improve when the measurement and calibration techniques improve. It is quite possible,

however, to use alternative measurement methods or modelling approaches to establish estimates of the response with which the sensor output may be compared. The results from the die face pressure sensors are here compared with those from the finite element program ALMA2π, and the ram and liner force measurements are used to estimate the mean pressure at the die face. As was discussed in relation to the analysis of flow, the sensor pressure is in general 5 % higher than the average die face pressure (Chapter 3). It should be kept in mind that none of the alternative estimates of the die face pressure may be expected to be significantly more accurate than those of the capacitive die face pressure sensors. The inaccuracies of numerical modelling have been assessed. Results from the liner load cell are scarce, and a careful examination of the data in the previous sections shows that the measurement method may be somewhat inaccurate (±10 %).

If the pressure measurement is to be accurate, calibration has to be properly performed and the calibration case should be similar to that of extrusion. The on-line calibration technique has the potential of producing calibration factors that may be used to perform very accurate measurements. The fundamental assumption of the technique is that the state of stress in the container is homogenous and isotropic during calibration and that the pressure at the die face is uniform. During extrusion, the state of stress is much more complex, but the load at the die face should be similar to the one experienced during compression testing. It is important that the shear stresses at the die face are small compared to the pressure, and that the sensor is fairly insensitive to shear loading. It is also important that the sensor behaviour be similar for a uniform and a non-uniform load distribution. This applies to loads applied locally at the sensor disc as well as at the complete die face. The described effects have been studied with a finite element model, and the sensor responses for uniform and non-uniform loads have been found to be quite similar [Moe04c]. The general deformation of the die affects only to a small extent the sensor response. Furthermore, the pressure calibration should be performed at the same temperature as the measurements. Methods for compensating for temperature changes during measurement have been treated in [Moe04c] and are also assessed in this report. The fact that calibration was usually performed at a lower temperature than the one measured at the onset of extrusion should also be considered. Finally, friction between the dummy block and container during calibration may cause a systematic error, which is believed to be small (Chapter 4).

A distinction should be made between the accuracy of measurement of the effects of changes to input variables and the accuracy of absolute measurements. The effect of a change in a variable is often more interesting than the absolute value of the response. All measurements of die face pressure are based on relative displacement readings. Yet, the estimation of the effects of parameter changes need not require a new calibration to be performed. In such cases, a part of the random error related to calibration may be avoided, and estimates of effects may be more accurate than absolute measurements of pressure. If recalibration must be performed in order to determine an effect, however, the random part of the error of calibration is added to the measurement inaccuracy. The effects of changes of ram velocity and billet temperature are more accurately determined than those of extrusion ratio and bearing length changes. Some of the main effects are, as indicated, confounded with the batch effects in the current study. The issue will be further treated below.

6.2.1 Absolute values of pressure and liner force

The flow simulation code ALMA2π was used in Chapter 3 to establish estimates of ram force, outlet temperature, die face pressure and liner load. In order to evaluate how well the simulation code describes the physics of extrusion, data from the measurement and simulation of the ram force and outlet temperature are compared here.

Ram force and outlet temperature measurements

Figure 6.7 and Figure 6.8 present responses for remaining billet heights of 196, 170, 100 and 30 mm. The calculated outlet temperature is generally approximately 10 ºC higher than the measured one. The corresponding calculated and measured ram forces differ by less than ± 5 %, and there appears to be only a small systematic error. The following observations have been made:

- ALMA2π estimates for remaining billet length of 196 mm should be too low since the simulated ram speed is too low until the billet height is 190 mm. Figure 6.7 indicates that the ram force is accurately predicted for a billet length of 196 mm. At the same time, however, it appears that it may be slightly too high for billet lengths of 170 and 100 mm. A traditional start-up effect is therefore present.
- When the remaining billet is short (30 mm), ALMA2π predicts that the magnitude of the force will be nearly independent of the velocity and the initial billet temperature. This is not completely unreasonable, but the accuracy of simulation is at this stage very dependent on a satisfactory description of boundary conditions. Predictions by ALMA2π may be too low when the remaining billet is short.
- The measured ram force should be somewhat higher than the simulated ram force due to the interaction between the dummy block (ram) and the container liner. At the same time, however, there may be additional modelling errors related to back extrusion and improper geometry descriptions (ram and die outlet). The errors are generally small, but not completely insignificant compared to the difference between the measured and simulated results (10 % of full scale).
- The initial conditions of the simulation may deviate from those of the experiment. The measured initial temperature of the billet, for example, was systematically 3 to 5 ºC lower than the nominal value. Furthermore, the billet temperature was at no stage precisely uniform. During induction heating the billet surface may have been hotter than the core. After heating, the situation was the opposite, since heat was lost to the surroundings (the air and the container).
- Die outlet temperature measurements may be inaccurate. Although the technique has been thoroughly tested, and the positioning of the thermocouples is performed in order to secure accurate measurements, it is not possible to rule out systematic errors. It is important both in relation to modelling and measurements to note that the ALMA2π predictions appear to be systematically too high. The task of linking numerical and measured results is a most difficult one. There may be very large temperature gradients close to the outlet, and errors related to data acquisition have the potential to be large. The average calculated temperature of the flow and wall has earlier been found to be in better accordance with the measured temperature [Moe03b]. This is not at all unreasonable given the nature of measurement. The finite response time of the thermocouples should also be considered.

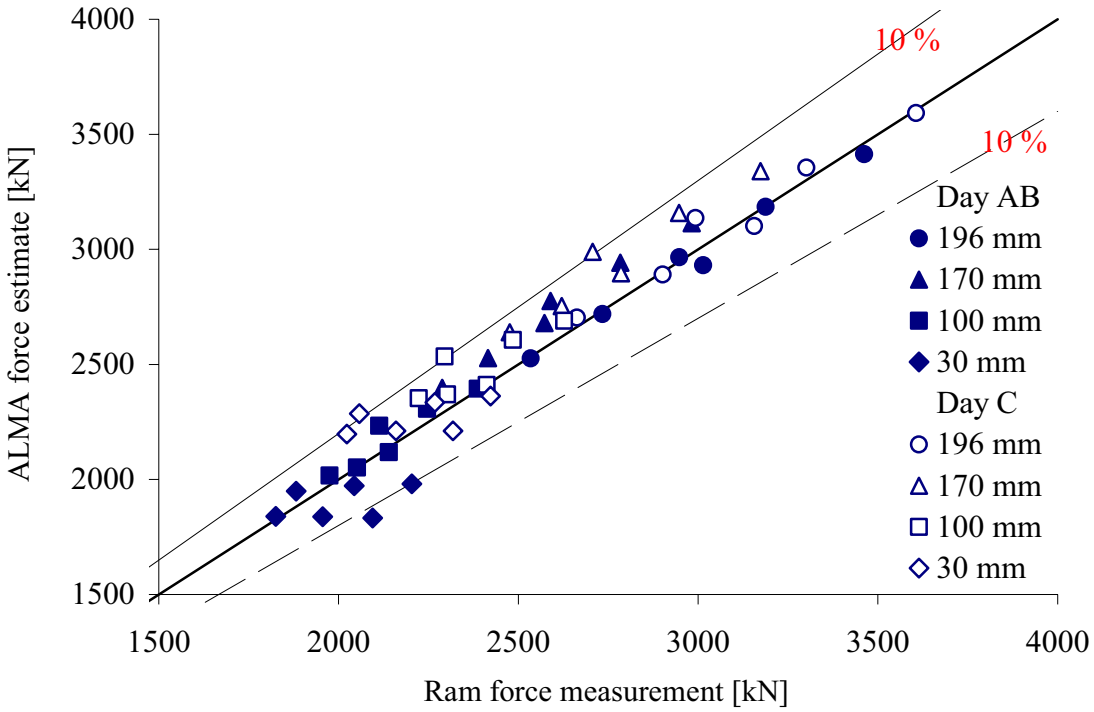

Figure 6.7. A comparison of ram force estimates by ALMA2π and measured forces. Results are for cases 1 to 12.

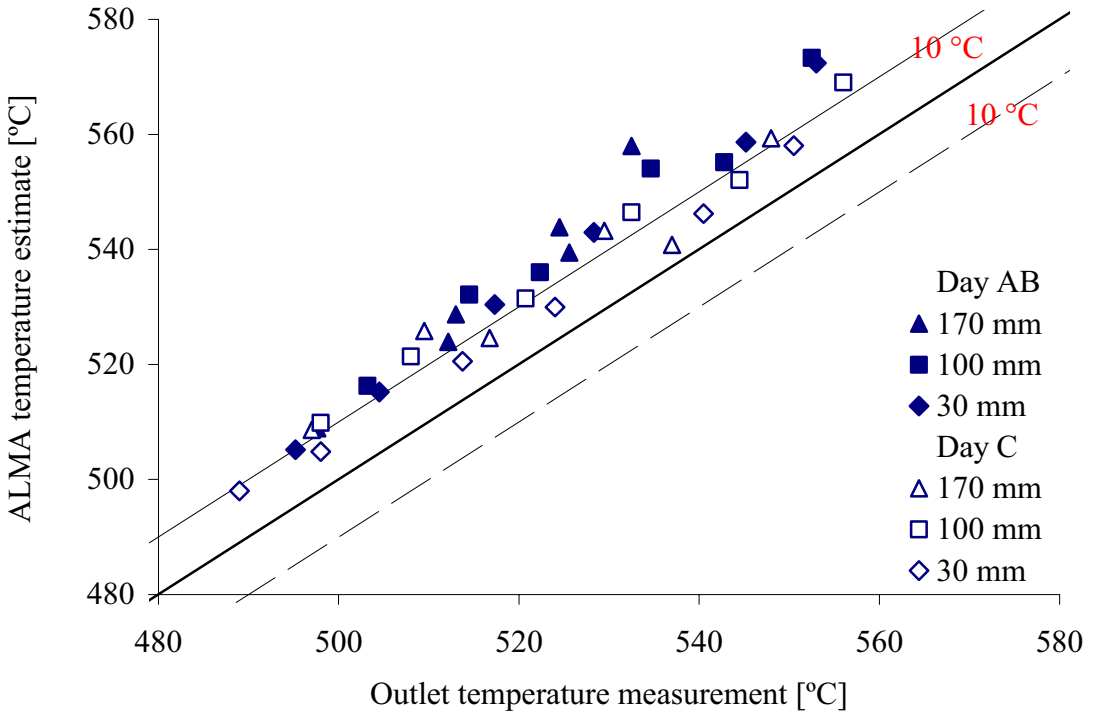

Figure 6.8. A comparison of outlet temperature estimates by ALMA2π and measured outlet temperatures. Results are for cases 1 to 12.

Figure 6.9 and Figure 6.10 provide further information concerning the nature of the temperature and force errors. The error is here defined as the measured value minus the calculated one. It should again be observed that the measured force is generally lower than the calculated, but that there is an exception for short billet heights. The calculated ram force is particularly too low when the profile/ram velocity is high. One of many possible causes may be that the extrusion model underestimates the heat transfer from the billet to the surroundings. The billet is too hot and flows too easily. Figure 6.10 also indicates that the outlet temperature errors are largest when the ram velocity and the initial billet temperatures are high. At extrusion ratio 80 the die outlet temperatures are better predicted, while the overestimation of the ram force is more significant.

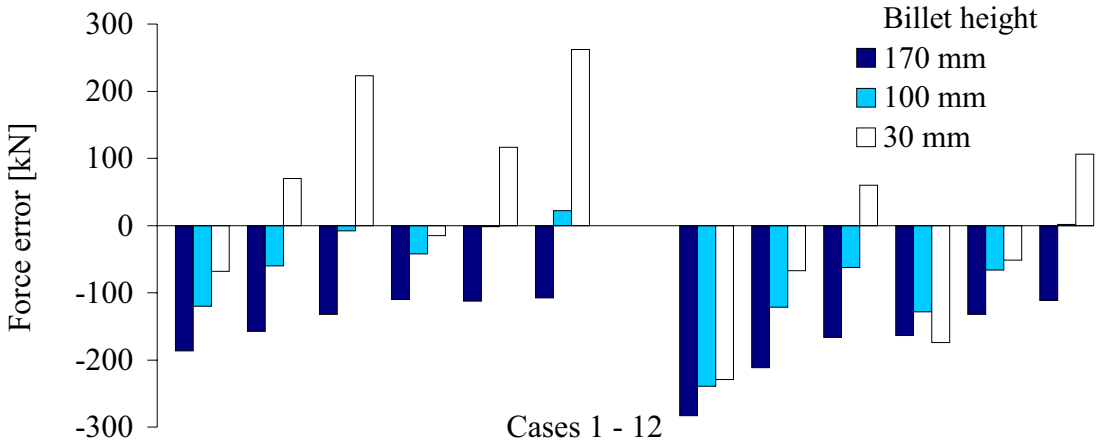

Figure 6.9. Deviation between ram force measurement and estimate by ALMA2π.

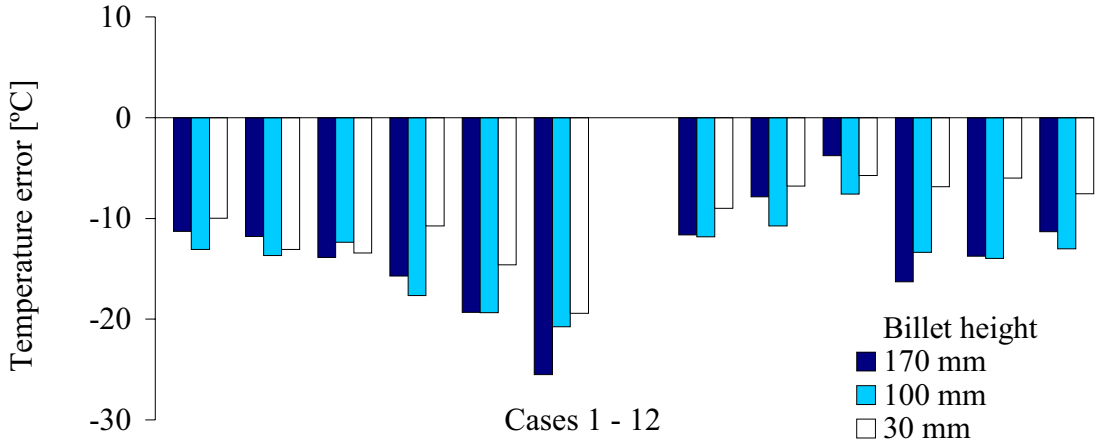

Figure 6.10. Deviation between die outlet temperature measurement and estimate.

The force and temperature errors may not only be due to improper initial and boundary conditions or to measurement, but also to the constitutive relations used in the model and to the numerical calculation scheme. All aspects of the model should be checked. Friction between the container and billet is assumed to be of the sticking type, and the magnitude of the shear stresses is therefore determined by the flow rule. The flow rule also governs the material flow in the interior of the billet. The parameters of the flow

rule have been estimated in an inverse analysis of the results from a set of compression tests [Moe04b].

An inverse analysis of aluminium extrusion on the basis of the ram force and outlet temperature results obtained from the current set of experiments has been described in [Waj04] [Moe04b]. An important objective of the inverse study was to improve the understanding of the nature of the extrusion system. It is not claimed that an inverse analysis of the extrusion process is the best way to establish material data, but the inverse analysis is a natural and perhaps necessary method to check models. It is not at all obvious that material data obtained by essentially a low-rate testing method may be used in the study of high-rate deformation. The second objective of the inverse analysis was to determine the parameters that would give the smallest force and temperature error for all cases of rod extrusion presented. This would at least be of some value to the current study of sensor behaviour. Since there are in all four parameters in the Zener-Hollomon model (A, n, α and Q), optimisation must be performed in a four-dimensional space. Measurement errors seriously complicate the task, as does the nature of the extrusion system. The coupling between the thermal and mechanical aspects renders the extrusion system less sensitive to changes in input variables than a purely mechanical system would have been. Thus, the analysis revealed no distinct and obvious point of minimum error, but rather a band of minima (a valley). The best choice of parameters cannot be easily established. This is both an advantage and a disadvantage of the extrusion system. If extrusion models are insensitive to parameter choice, parameter estimation is obviously an easier task. There seem to be many combinations of parameters that may be used to produce force and temperature estimates within ±5 to 10 % of the measured results. This may be acceptable accuracy for many purposes, given the uncertainties related to many other aspects of the extrusion model. However, if parameters cannot be easily determined, it may also be most difficult to establish a proper understanding of more complex features of extrusion. There may, for example, be much stricter requirements for the flow models that are used to study the nature of flow instability than for those that are merely used to establish force and temperature estimates for rod extrusion. A further experimental and numerical study of the problem is necessary if proper understanding is to be established. It may be concluded that an ALMA2π simulation with a set of parameters established through compression testing with inverse parameter estimation produces ram force and outlet temperature estimates that are reasonably accurate (within 10 %). The model is of the simplest kind. It should be noted that the accuracy of the estimation of die face pressure and liner load is also limited to approximately 10 % of the signal magnitude with this technique.

Liner force measurements

The liner load cell made possible the establishment of purely experimentally based estimates of the average die face pressure which may be used in the evaluation of the response of the die face pressure sensors. Here, changes in ram and liner force recorded as the billet height was reduced from 170 to 100 mm, are compared. If the container had been infinitely long and the extrusion had been a steady-state process, the friction between the billet and container could have been determined merely from the ram force curve. As the ram moves, the ram force decreases. The decrease is in an ideal situation only due to the reduction of the area of the billet-container interface. Aluminium

extrusion is, however, a transient process. The billet temperature increases due to plastic dissipation, and the material flow pattern changes as the billet becomes shorter. A part of the reduction in force may initially be due to micro-structural changes. If the ram force curve is used to estimate friction, results from the early and late phases of the run should not be assessed. The billet height interval from 170 to 100 mm is probably the most appropriate choice, although flow changes may affect the magnitude of force even in the quasi-steady state. Figure 6.11 indicates that the changes in ram and liner force measurements are in fair agreement in cases 1 to 12. The absolute values of the changes in ram and liner force have been determined from measured and simulated data. The liner force measurements seem to be less affected by changes of the input variables than the measurements of ram force. Deviations in the force differences of 50 to 100 kN are no better than may be expected, given the measurement inaccuracy. A calibration factor of 30 kN/µm·50 µm/V was used to calculate the liner forces, but the real calibration factor should be somewhat higher (Chapter 4). Figure 6.11 seems to confirm this observation. Subsequent shear stress estimates have been increased by 3 %.

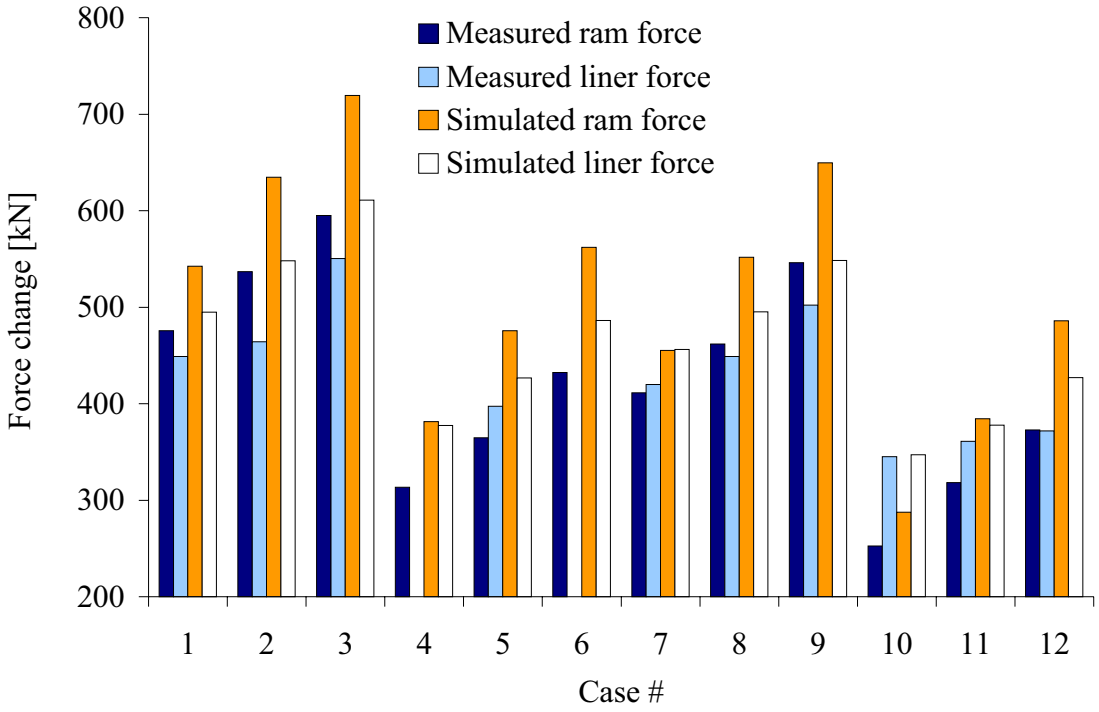

Figure 6.11. A comparison of changes in the ram and the liner force from billet height 170 to 100 mm - measured changes and estimates by ALMA2π.

No liner force measurements have been obtained for the cases 4 and 6. The liner force data are generally based on data from all three sensors of the liner load cell. In Figure 6.12 results from runs 13 to 24 have been shown in addition to those from cases 1 to 12. An estimate of the average container shear stress has been calculated. Relatively few liner load measurements were performed on day D (cases 13 to 18), and the results have to a large extent been estimated on the basis of liner load measurements from other runs and the available ram force data. The friction factors presented are based on liner load data, and are used later in the study to estimate the die face pressure.

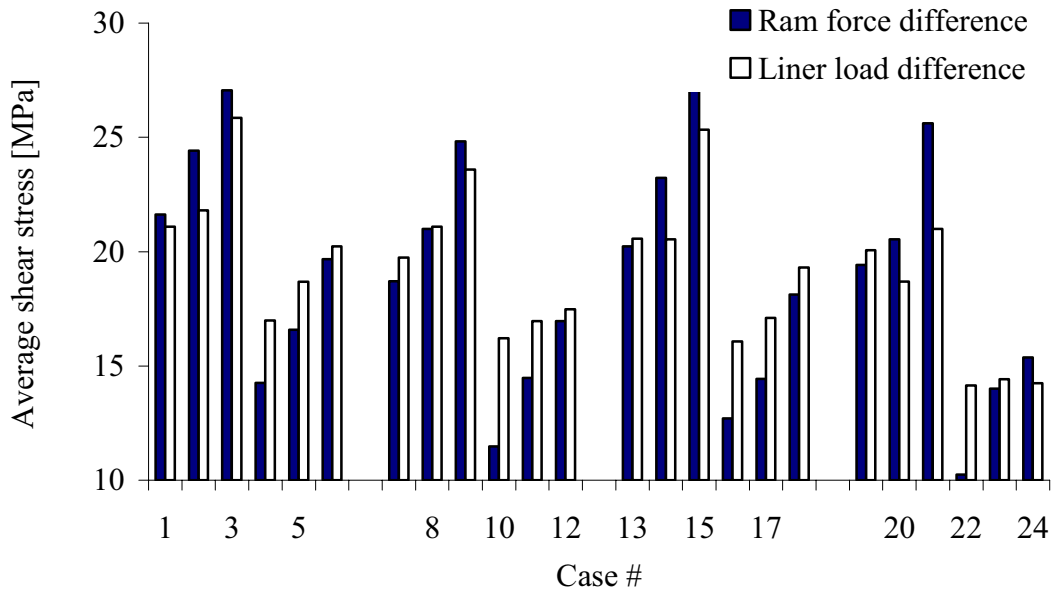

Figure 6.12. A comparison of changes in the ram and the liner force from billet height 170 to 100 mm. Only measured changes are shown.

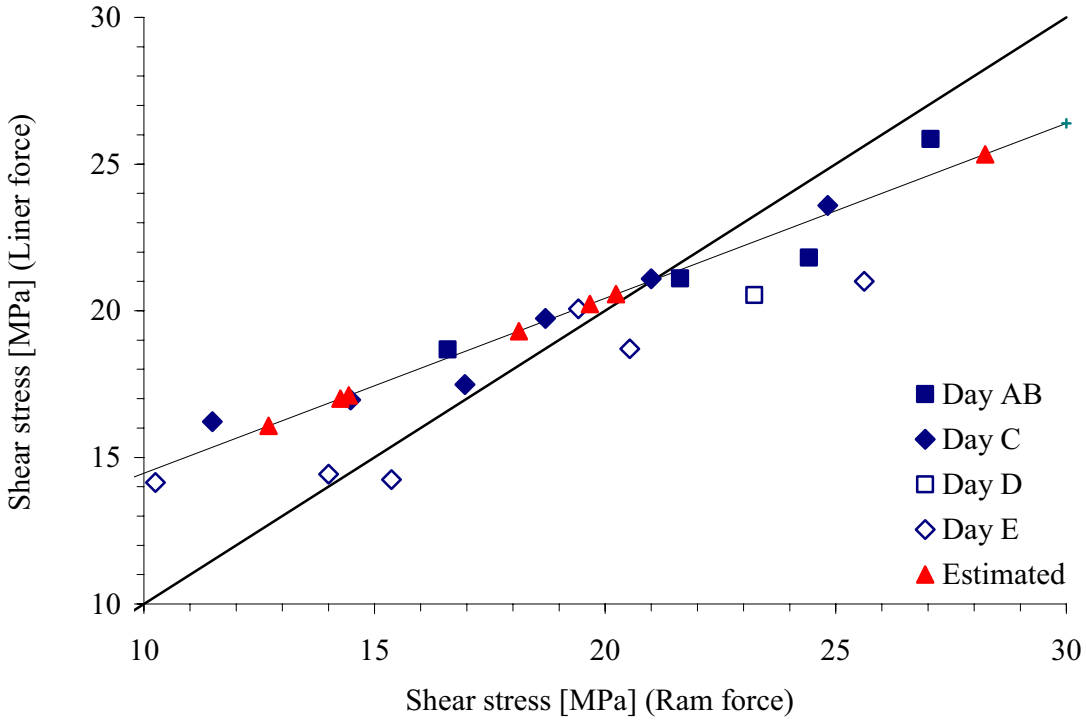

Figure 6.13. A comparison of container shear stress estimates based on both the ram and the liner force measurements.

Figure 6.11 also includes estimates of ram and liner force changes calculated with ALMA2π. The liner force estimate is here based on the ram force and the integrated die

face force. The main reason for deviations in the ram and liner force differences is most probably that the change in ram force is not only due to the reduction of the area of the surface between the liner and aluminium, but also due to flow and temperature changes. The simulated force change is generally larger than the measured one (10 to 20 % for both types of measurement). Errors related to absolute measurements are less important, for only ram and liner force differences are evaluated. The interaction between the dummy block and the container should not change significantly during extrusion. Difficulties related to the determination of the zero point for the measurement of liner load should also be unimportant.

Figure 6.13 provides further information about the correlation between the shear stress measured by the ram load sensor and liner load cell. A straight line corresponding to a one-to-one relationship ($y = x$) has been added. The figure seems to confirm that the decrease in ram force from position 170 to 100 mm is more affected by changes in the input parameters than the liner force decrease. A linear regression curve giving the best fit for the results of day A, B and C has been added. The data points that have been estimated on the basis of this curve have been plotted as filled triangles. There is a large amount of variability in the data (typically ±2 MPa or 10 %), and one simply cannot reject the assumption that the changes in liner load and ram load are truly proportional. Note also that the results obtained during the two last rounds of experiment (D and E) appear to differ from the other results (the average liner shear stress is 10 % lower).

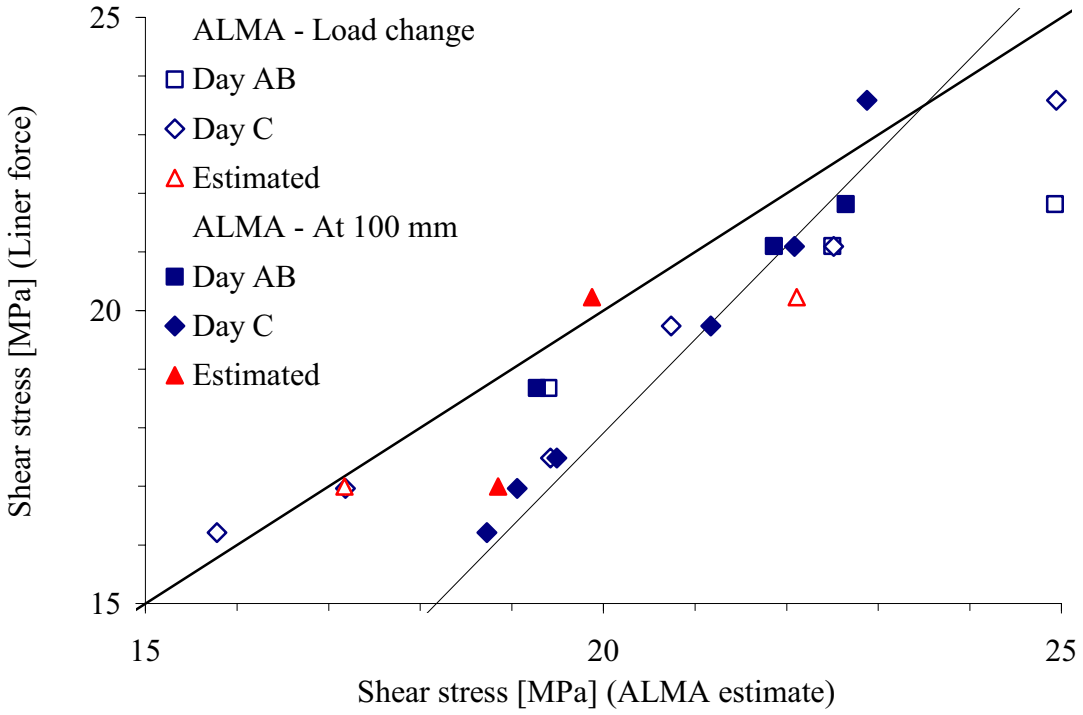

Figure 6.14. A comparison of container shear stress estimates deduced from ALMA2π and from liner force measurements.

Figure 6.14 compares measured and simulated liner load data. Two somewhat different types of comparisons are made. In the first, the average simulated shear stresses are deduced from the liner load change from 170 to 100 mm. In the second, the simulated shear stress is calculated by dividing the liner load at 100 mm by the remaining surface area of the billet. The measured shear stress is in both cases based on the load change from 170 to 100 mm. Conclusions cannot easily be drawn due to the variability and lack of data. The data based on load changes are in fairly good agreement. The simulated data based on point measurements at billet height 100 mm are less sensitive to changes in input variables. The two methods for liner shear stress estimation are not completely comparable. One of them assumes that there is an incremental change, while the other calculates an average for the whole surface. Figure 6.15 shows how the point estimate increases as the billet becomes shorter and the deviations from steady state become more important. The results have been calculated numerically. As long as the billet is relatively long the friction value obtained with the incremental approach may generally be used, but it need not work as well when billets are short and the flow is mainly in the radial direction. The details for the data application and the development of a regression equation relating friction and input variables are treated in the next sub-section.

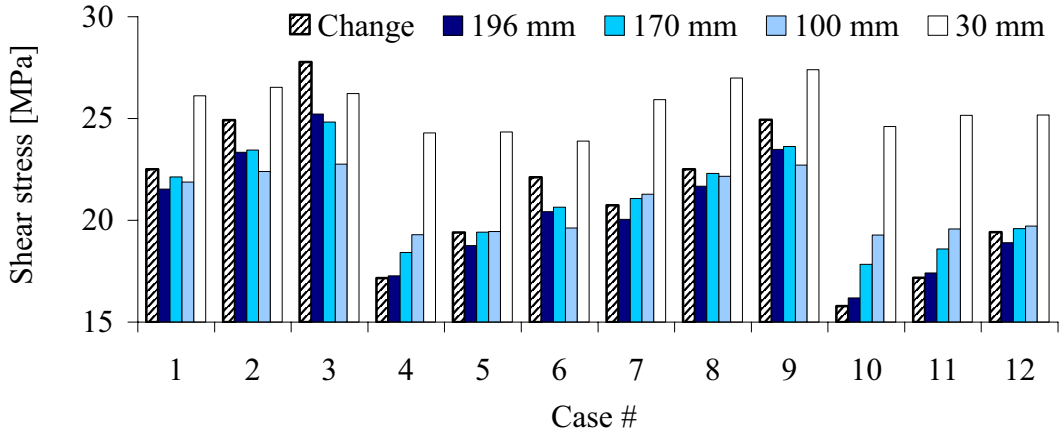

Figure 6.15. Container shear stress estimates by ALMA2π. Estimates are deduced from liner force differences (the change in force from a billet height of 170 and 100 mm) and from absolute values of liner force at given billet heights.

Die face pressure measurements

Figure 6.16 to Figure 6.18 compare simulated and measured die face pressures for runs 1 to 12. The first figure presents the data from pressure sensor 1, the second the data from pressure sensor 2 and the third data from pressure sensor 3. The average output for all sensors are compared with ALMA2π estimates in Figure 6.19. Almost all data points are positioned between lines showing -10 and +10 % deviation from linearity (approx -20 to +20 MPa). This applies both to single sensor measurements and to average data. The pressure has at the same time been varied within the range from approx 175 to 300 MPa. A pressure of 20 MPa corresponds to a disc deflection (sensor deformation) of approximately 2 μm. The calibration factors have been presented in earlier sections.

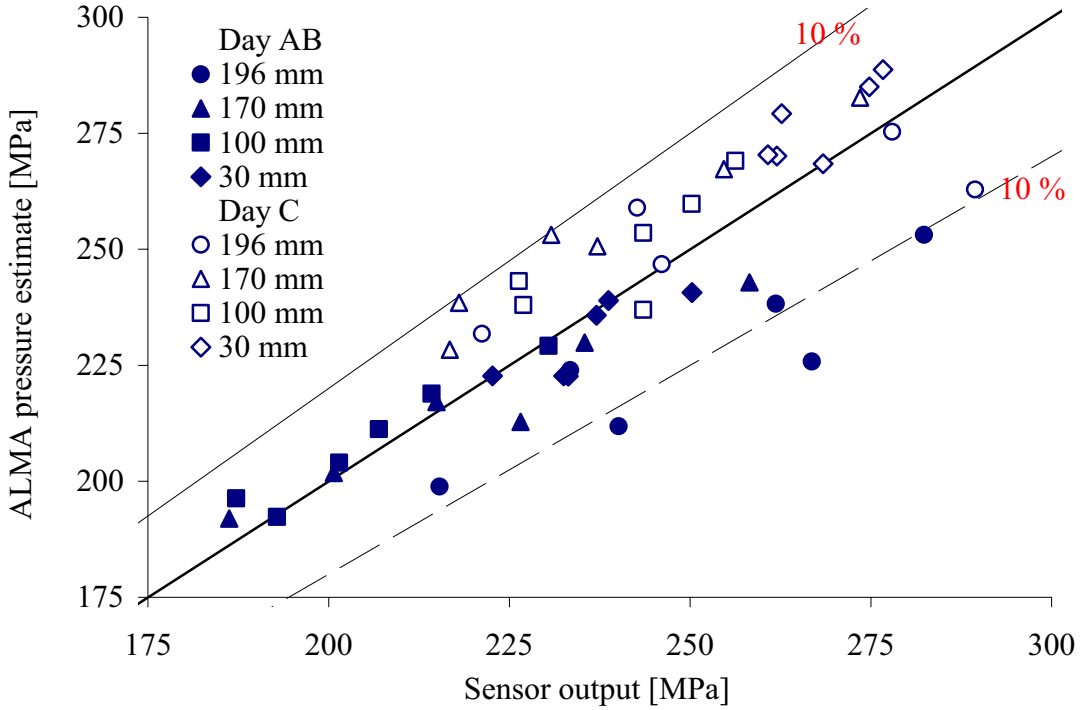

Figure 6.16. A comparison of ALMA pressure estimates and non-corrected data from sensor 1. The straight lines indicate proportionality and errors of ±10 %.

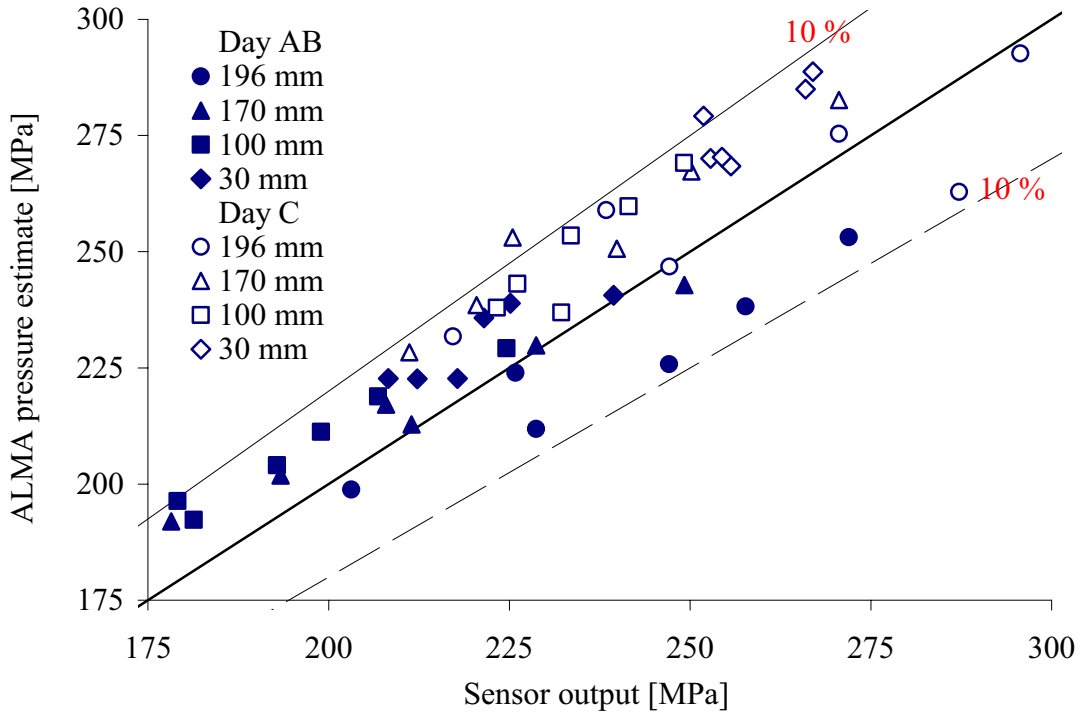

Figure 6.17. A comparison of ALMA pressure estimates and non-corrected data from sensor 2. The straight lines indicate proportionality and errors of ±10 %.

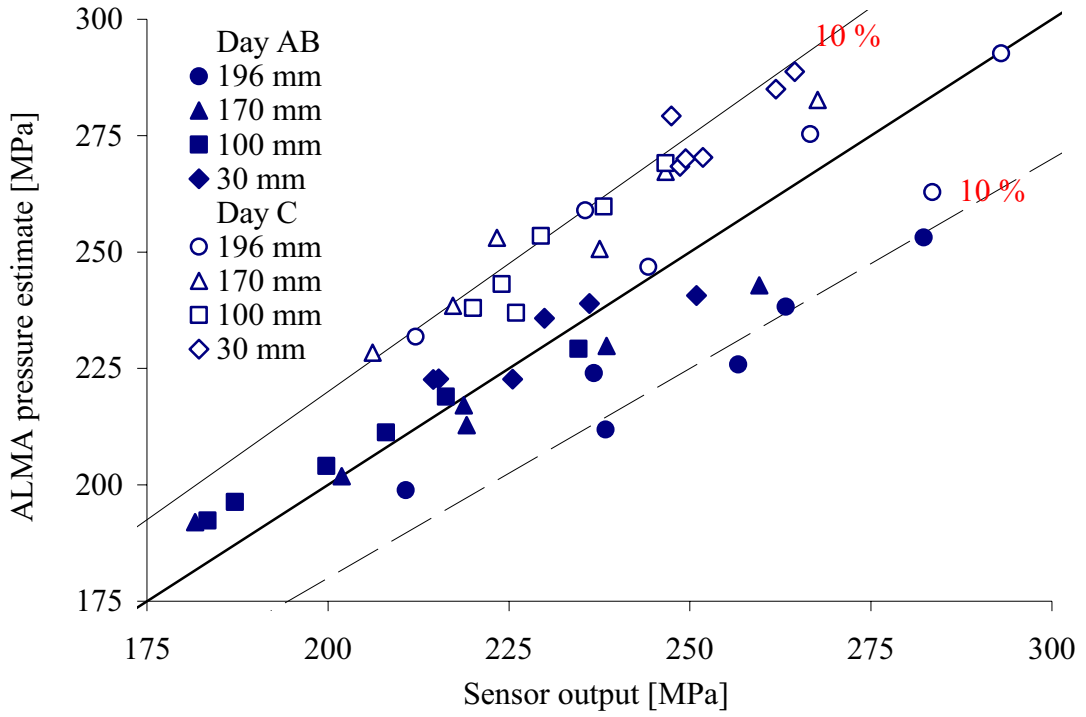

Figure 6.18. A comparison of ALMA pressure estimates and non-corrected data from sensor 3. The straight lines indicate proportionality and errors of ±10 %.

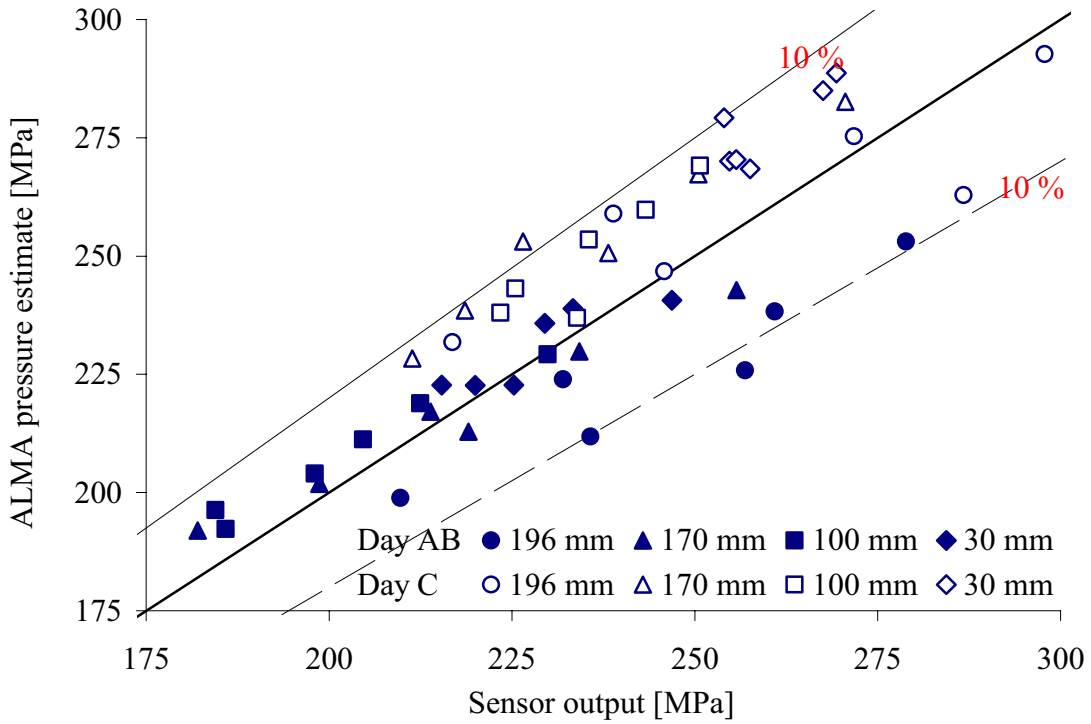

Figure 6.19. A comparison of ALMA pressure estimates and non-corrected averaged data from all sensors. The straight lines indicate proportionality and errors of ±10 %.

The figures should be compared with similar figures for ram force (Figure 6.7). Data from the force measurements are systematically somewhat lower than the predictions of ALMA2π. The systematic error is not as easy to spot for the die face pressure data, and there may be a number of reasons. The ram force data may be in error. The flow model may predict ram forces that are too high while the die face pressures may be more or less correct. However, a significant part of the variability in both figures is probably due to modelling errors. It is known that the ram force measurements are quite accurate (within ± 50 kN or approx 2 %), while the estimates by ALMA2π may deviate as much as 10 % in either direction. Thus, the scatter of the die face pressure correlation graphs should be of a similar magnitude. Even if the measurements were perfectly repeated and very accurate, there would probably have been significant deviations. Modelling errors and experimental errors of pressure measurement seem to be of similar magnitude. In the previous sub-section it was clearly demonstrated that the variability of pressure measurement was of significant magnitude for the genuine replications. The standard deviation is approximately 7 MPa, and almost all data are within ±20 MPa.

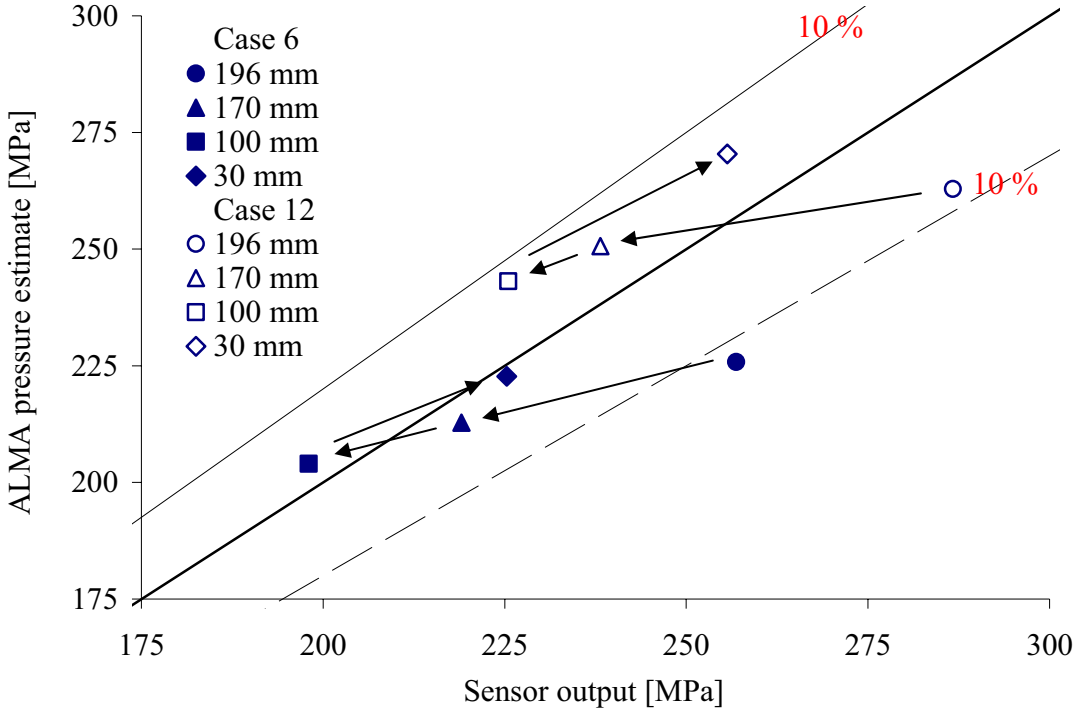

Figure 6.20. A comparison of ALMA2π pressure estimates and non-corrected data from all pressure sensors. Only results from cases 6 and 12 are shown.

When the figures showing the measured and estimated die face pressures are assessed, it should be remembered that the ram speed was too low in the initial part of the runs (from 200 to 190 mm). Furthermore, ALMA2π does not properly model hardening and softening mechanisms in the early parts of the extrusion. Thus, the symbols representing the data points for a billet height of 196 mm should be positioned higher in all plots. The ram force figure gives an indication of how large the error is (3-5 %). Figure 6.20 shows the results for cases 6 and 12, which are quite typical ones. ALMA2π predictions

for a billet height of 196 mm are manifestly significantly lower than the corresponding measurement data. When billets are shorter, calculated and measured responses agree more closely. As will be discussed more thoroughly below, however, temperature changes due to heat dissipation may affect the responses in a systematic manner. The measurement point least affected by the thermal effect is in fact the one at billet height 196 mm. At the early stages of extrusion, the heat flow has not yet reached the sensor. It will be shown that the temperature increase normally causes a decrease in the pressure indicated by the sensor. Thus, the symbols in the figure should be moved to the right.

Figure 6.16 to Figure 6.20 reveal the systematic differences in sensor output. The results from sensors 1 and 3 from the first two days (A and B) are some percent higher than the results from all other sensors, and apparently in better agreement with simulated results. The average sensor responses from day A and B are based on results from two rounds of experiments and six independent sensors, while the responses from day C were recorded only during one round with three sensors. It is likely that the average results from day A and B are more accurate than the average results from day C, but this need not always be correct. In any case, the figures reveal that a single measurement may easily be as much as 5 % in error even though on-line calibration has been performed. Average measurements may also differ by 3 %. These values should be seen in relation to the variability in data for the calibration factors. As indicated above, the sample standard deviation in the data for a calibration factor for a specific sensor recorded on a single day is approx ± 0.3 MPa/μm. This corresponds to approx 3 % or 6 MPa at 200 MPa.

Thus far only results that have not been corrected for errors related to differences in the environment of the sensors during calibration and modelling have been presented. The fact that the temperature during calibration was lower than at the onset of extrusion may be the cause of a small error (1 %). The pressure acting at the die face is higher during calibration than extrusion for a given voltage output, as the sensor disc does not deform as easily. The error is a systematic one and comes in addition to transient temperature effects. The issue is treated in relation to the discussion on temperature compensation.

The accuracy of measurement may alternatively be evaluated by comparing results from the die face pressure sensors with estimates of the die face pressure, p_{Sensor}, based on ram and liner force measurements, F_{Ram}, F_{Liner}:

$$p_{Sensor} = 1.05 \cdot \left(\frac{F_{Ram} - F_{Liner}}{A_{Die\ face}} \right) = 1.05 \cdot \left(\frac{F_{Ram} - \tau_{Liner} A_{Container}}{A_{Die\ face}} \right) \qquad (6.11)$$

$A_{Dieface}$ is the area of the die face. $A_{Container}$ is the area of the container-billet interface, and τ_{Liner} is the average shear stress acting on the interface. Since the pressure sensors generally measure a pressure that is approximately 5 % higher than the average pressure at the die face, the average pressure has been multiplied by 1.05. There are two alternative methods for estimating the liner force. One may either calculate τ_{Liner} from the change in liner force from 170 mm to 100 mm, or one may use the measured liner force directly. Figure 6.21 compares data from the die face pressure sensor with data obtained by the first estimation technique. Figure 6.22 presents the alternative plot. The

different liner force estimation approaches produce quite similar results, and only results obtained with the first technique are assessed in the following discussion. The liner load cell is better suited to measure changes in the liner load than absolute values. Hence, the die face pressure estimates based on absolute values may in fact be poorer than those based on incremental values and assumptions of constant shear stress. The difficulty related to the use of incremental changes is to determine the minimum liner force that was measured during the run. The sensors do not provide very satisfactory estimates.

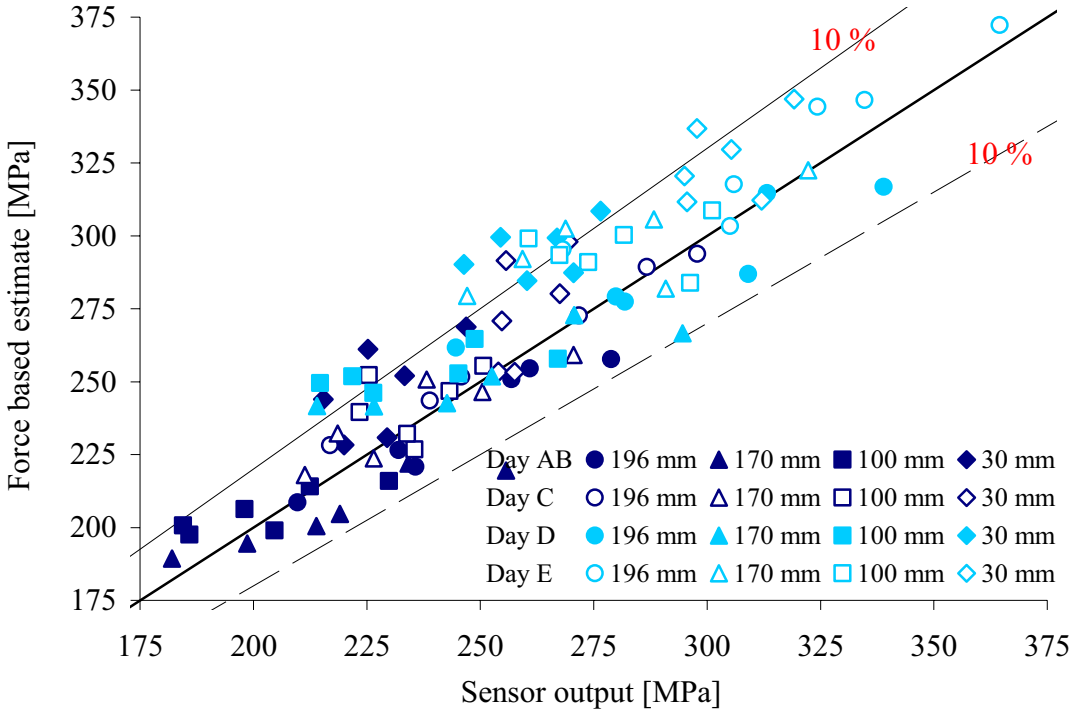

Figure 6.21. A comparison of the estimates on ram and liner force (based on friction factor) and the non-corrected averaged data from all pressure sensors.

The data in Figure 6.21 and Figure 6.22 are average measured values for all three die pressure sensors and for all the runs of a case. Results from cases 1 to 24 are treated. The pressure estimates obtained during rounds D and E were somewhat offset from the data obtained during the earlier rounds. There are systematic errors of approx ± 5 %, which must be expected given the accuracy of the calibration procedure. The data from the last round are also based on results from the sensors that did not work properly, i.e. sensors 1 and 2. Measurement results have been carefully and objectively evaluated to deduce the most of data. The best agreement between directly measured values and estimates should be obtained for a billet height of 196 mm. The temperature effects are at this stage of the run less important. Since the estimate is based on the ram force measurement, there should be no systematic error related to the material flow behaviour, but an assumption of constant liner shear stress may be incorrect.

Figure 6.23 provides an indication of the limitation of the techniques for checking sensor accuracy. The two alternative estimates of the die face pressure (simulated and indirectly measured) deviate by as much as 10 % of full scale.

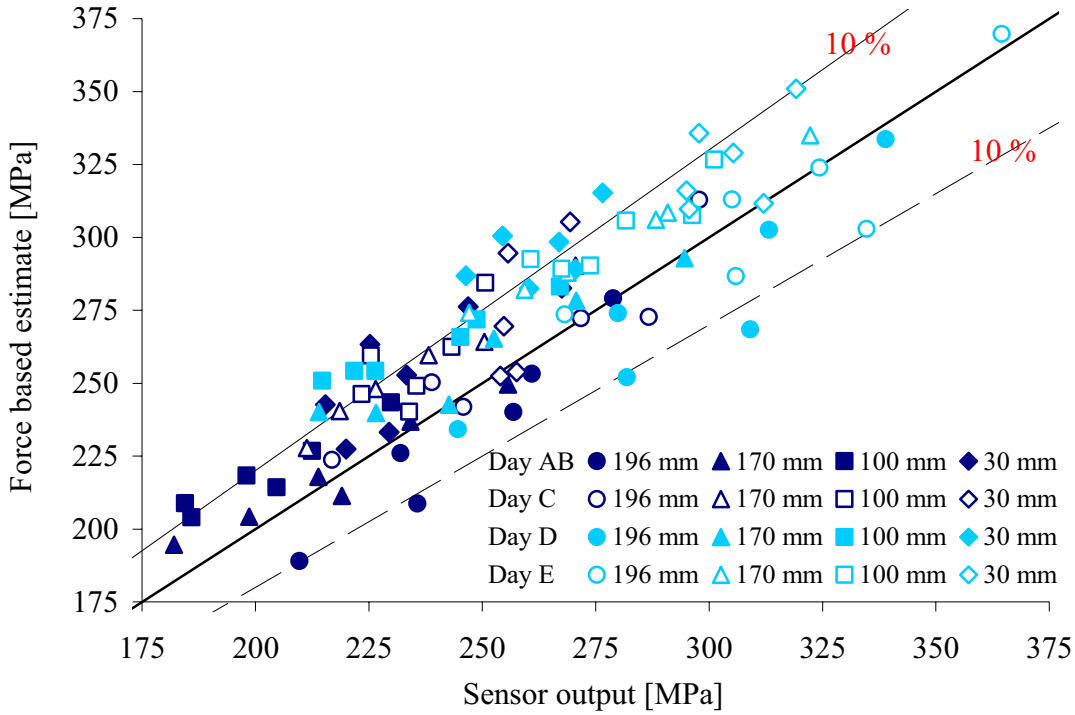

Figure 6.22. Estimates on ram and liner force (based on actual liner force) and the non-corrected averaged data from all pressure sensors.

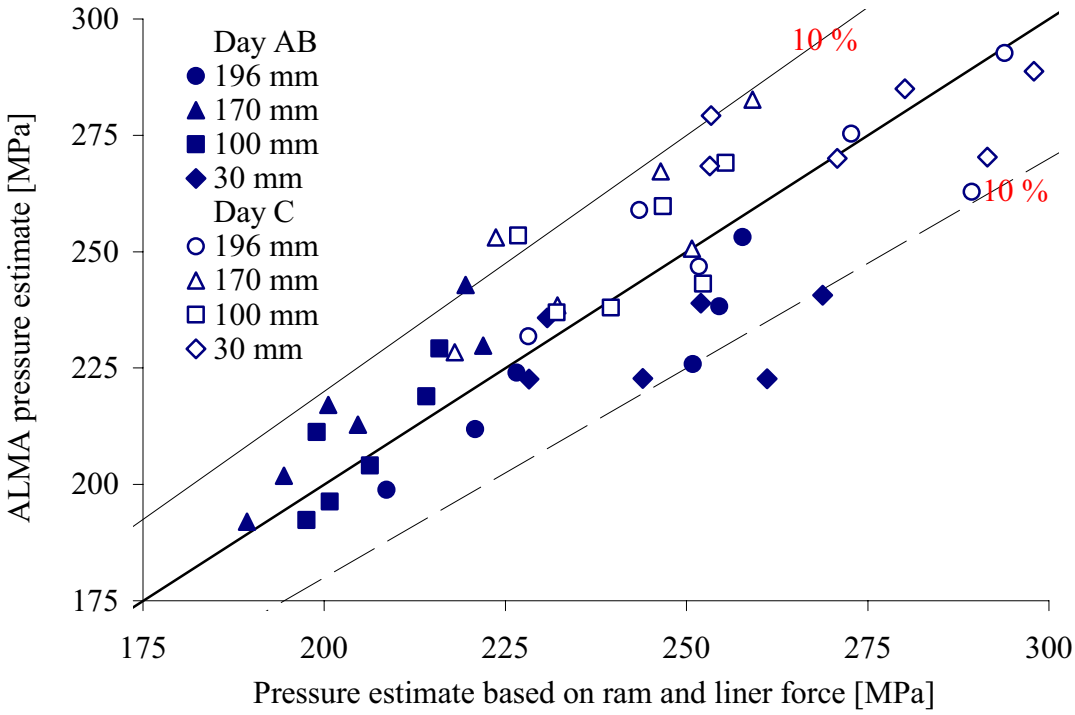

Figure 6.23. A comparison of the pressure estimate based on force measurements and the estimate of ALMA2π. Results are from cases 1 to 12.

6.2.2 Sensitivity study

As previously discussed, the accuracy may be better for relative measurements than for absolute measurements. This is particularly the case if the effect of a change of an input variable is sought, and if no recalibration of the system is necessary. Examples of relevant input variables in the current study are the profile/ram velocity and the initial profile temperature. If one wishes to determine the effect of a ram velocity change and only may perform two runs, there may be at least two causes of inaccuracy. First, there is the random variation from one run to the next (typically ± 3 MPa). Then, there may be error related to the calibration factors or non-linearity of the calibration curve. The first type of error may be reduced by performing some type of replication or by using factorial designs with randomisation of runs. The second type of error is not very significant when the response is only moderately changed, as has been done in the present case. For example, the sensor disc deflection might be 25 μm in one case and 30 μm in another. If the calibration factor is 8 MPa/μm, the pressures are 200 and 240 MPa. The factor may erroneously be set to 8.5 MPa/μm, in which case pressures are assumed to be 212.5 and 255 MPa. The real effect of a change is 40 MPa while the perceived one is 42.5 MPa. The absolute difference of 2.5 MPa is in fact smaller than the random measurement error even in such a fairly extreme case. However, if the outlet insert has to be changed and recalibration performed in order to change an input variable, additional block or calibration related errors of 10 to 20 MPa may appear. In the previous example, one would assume that the effect of changing an input variable was for example 55 rather than 40 MPa. This may be regarded as either a systematic or random error, depending on the number of recalibrations and runs that are performed and on the objectives of the study.

In the current sub-section, the effects of changes of the various input parameters of the extrusion system and model are determined and evaluated. The exercise may provide some insight into the extrusion system. The main objective, however, is to evaluate the accuracy and variability of measurement and to perform a first test of the usefulness of the pressure sensors. The essential question was whether the sensors may be used to assess effects of changes to input parameters. Average values of die face pressure for all die sensors of the die and runs of a case are used in the current study. Better predictions of effects should be obtained when estimates are based on average values than when they are based on results from individual sensors. Data from simulation of cases 1 to 12 have been presented in Chapter 3. Die face pressure results estimated from the ram and liner force measurements are also used.

In order to evaluate the significance of an effect, the variance related to the estimate of the effect must be determined. If N independent runs had been performed in accordance with a two-level factorial design and the variance of the response of a run was σ^2, the variance of the effect would have been $(4/N)\ \sigma^2$. The variance of the mean value of all runs would at the same time have been σ^2 / N [Box78]. In the present case, the criterion of independence is not fulfilled, and the case is more complex. The block effect of the main effects of a change in bearing length, A, and extrusion ratio, B, are confounded, and there is unfortunately no very simple way to compensate for the errors. In order for one of these main effects to be significant, they should be significantly larger than the

blocking effect, which in the case of pressure measurement may be 10 to 20 MPa. The blocking (division into groups of cases or rounds) affects all the results of a round of experiments, and the blocking effect must be regarded in this context as a systematic one. Effects that are not affected by the blocking, however, may more easily be found significant. This applies to the main effects of billet temperature, C, and profile velocity, D. In this relation it should be noted that it may be possible to distinguish block effects by comparing the results from simulation and all kinds of measurement. The previous section revealed the effects of blocking. It is also important to note that block effects are generally more significant for pressure and liner load measurements than for the ram force and outlet temperature measurements. The block effects are in this study mainly related to the calibration of sensors. When there are other types of block effects, such as changes in the constitution of the material or systematic errors related to input variables, they may be much more difficult to spot in all types of measurements.

In the first part of the study the bearing length was kept constant and almost equal to zero. This corresponded to the situation in which the input variable x_1 was equal to -1. Measurement data were obtained on days A, B and C. There were essentially two reasons for focusing on only a limited set of experimental data. First, a similar study of simulation data from zero bearing length extrusion was performed in the final part of Chapter 3. Second, the pressure and friction data from days A to C were better quality than data from later days. In fact, the results obtained during round E are known to be in error. In the next subsection, however, the effect of adding a long bearing channel is considered. A 2^3 full factorial design may easily be converted to a 2^4 design, as was done during the experiments. The various effects of the 2^4 design are here denoted *A, B, C, D, AB, AC* etc. The effects of the 2^3 design with $x_1 = -1$ are similarly denoted *A*, B*, C*, D*, AB*, AC** etc. The average values are *AVG* and *AVG**. The effects are the coefficients of linear relations of the type.

$$P_{170} = AVG^* + \frac{B^*}{2}x_2 + \frac{C^*}{2}x_3 + \frac{D^*}{2}x_4 + \frac{BC^*}{2}x_2x_3 + \frac{BD^*}{2}x_2x_4 + \frac{CD^*}{2}x_3x_4 + \frac{BCD^*}{2}x_2x_3x_4 \qquad (6.12)$$

P_{170} is the extrusion pressure for a remaining billet length of 170 mm. The expression for the 2^4 design includes the main effect *A* and the interaction effects *AB*, *AC*, *AD*, *ABC* etc. The relations between *B* and *B**, *C* and *C** are as follows: $AVG^* = AVG - A/2$, $B^* = B - AB$, $C^* = C - AC$, $D^* = D - AD$, $BC^* = BC - ABC$, $BD^* = BD - ABD$, $BCD^* = BCD - ABCD$. As earlier indicated, it would have been possible to develop a second-order expression with regard to the profile velocity and billet temperature, but here only two levels are used to establish regression relations. The other data points are rather used as test points to check if there is any lack of fit. If factor x_4 is expressed as a logarithm of the profile velocity, the regression equation should perform very well. A demonstration is given below, and Chapter 3 also gave such indications. Finally, the profile velocity is again regarded as the primary input variable rather than the ram velocity. The choice is most natural when the objective is to study bearing friction, but the regression equations may obviously be expressed either in terms of ram or profile velocity.

Ram force and outlet temperature

Figure 6.24 and Figure 6.25 present average values of ram force and outlet temperature increase for different levels of remaining billet length. The initial outlet temperature was approx 430 ºC (the temperature of the die). The average values should apply in the case $x_2 = x_3 = x_4 = 0$. Exactly how the interpolation for the extrusion ratio should be performed is not known and cannot be easily checked, since no runs with intermediate ratios of extrusion have been performed. x_1 should probably be a function of the logarithm of the extrusion ratio as is predicted by analytical expressions. For simplicity, it may here be assumed that the data presented in the figures correspond to an initial billet temperature of 475 ºC and a profile velocity 400 mm/s.

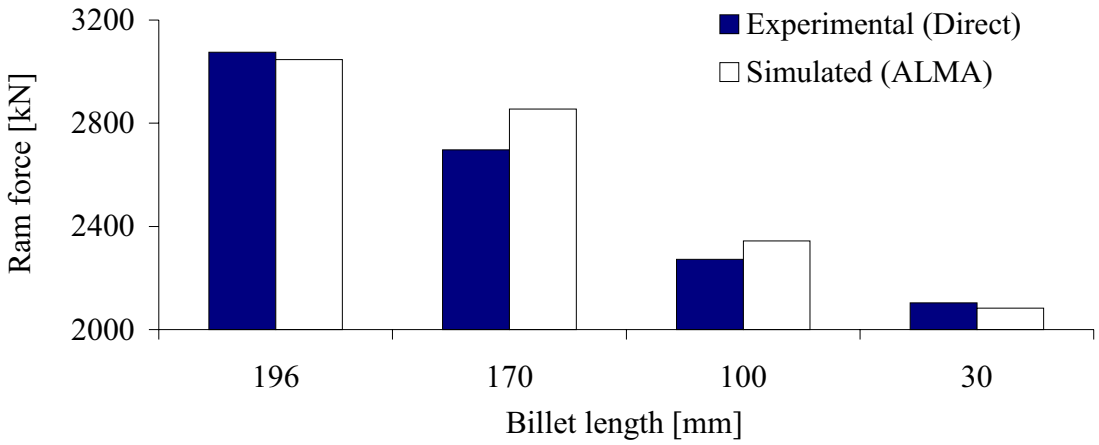

Figure 6.24. A comparison of simulated (ALMA2π) and measured average ram forces. The data are based on results from cases 1 to 12.

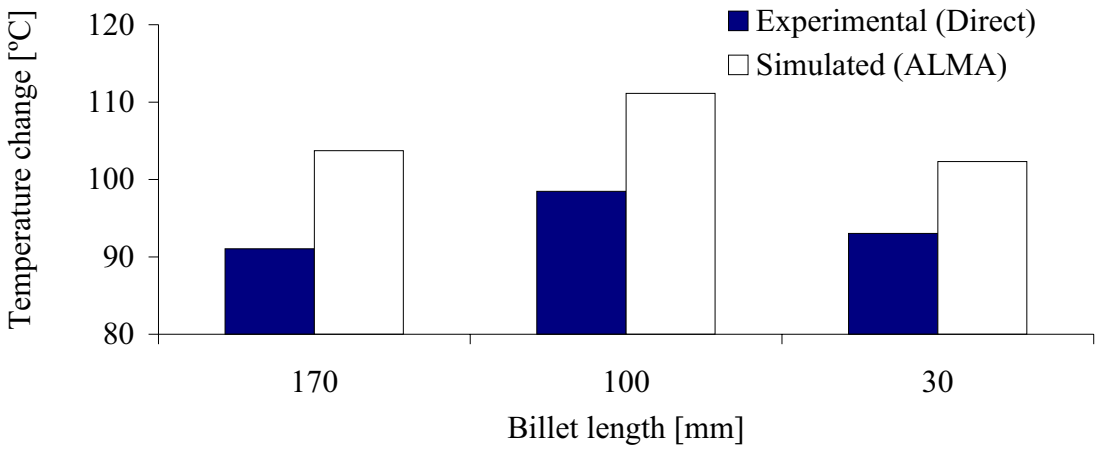

Figure 6.25. A comparison of simulated (ALMA2π) and measured average die outlet temperatures. The data are based on results from cases 1 to 12.

The advantage of average values is that they give a kind of overall estimate of the deviation between results from experiments and simulation. The conclusions, however, are no different than those drawn in relation to the study of the individual cases. Both the calculated ram forces and outlet temperatures are too high, typically 100 kN and 15

ºC. At the onset of extrusion the simulated force is artificially low. Towards the end of the press modelling errors may be of great significance.

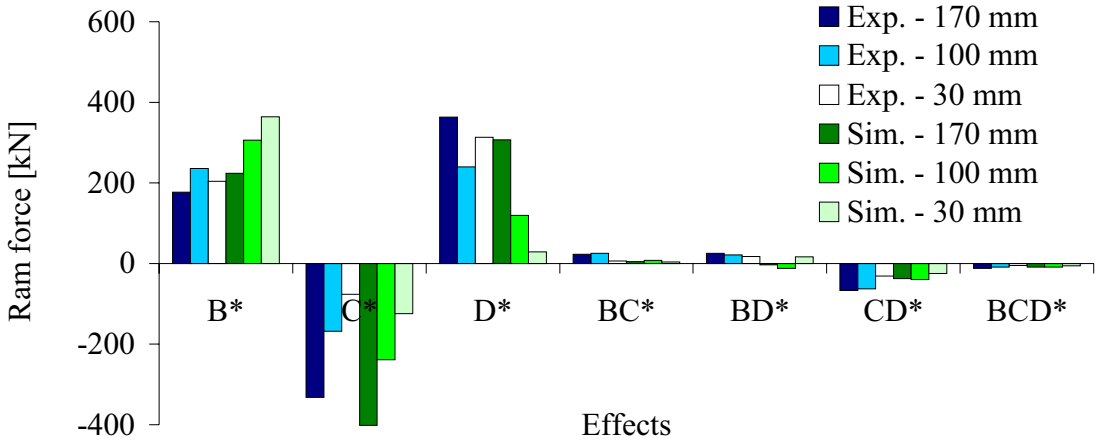

Figure 6.26. A comparison of estimates of the ram force effects of input data changes based on the simulated (ALMA2π) and measured average ram force. The data are based on results from cases 1 to 12.

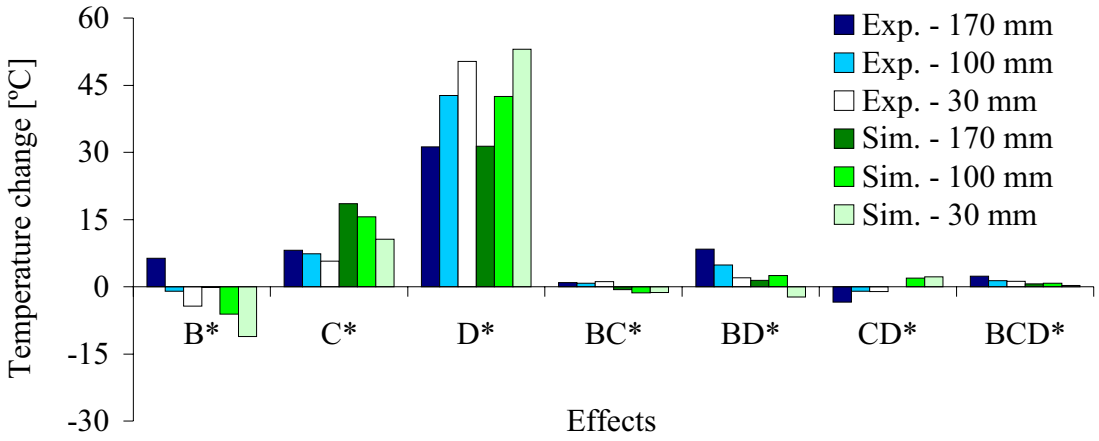

Figure 6.27. A comparison of estimates of the outlet temperature effects of input data changes based on the simulated (ALMA2π) and measured average ram force. The data are based on results from cases 1 to 12.

Figure 6.26 and Figure 6.27 show the various effects of changes to the input variables. Some of the main conclusions to be drawn are obvious. If the initial billet temperature (*C**) is increased, the ram force should decrease and the outlet temperature increase. If the profile velocity (*D**) is increased, both the ram force and outlet temperature should increase. A 50 ºC increase in the initial billet temperature causes only a 10 to 15 ºC increase in the outlet temperature. The effect of the profile velocity increase from 200 to 800 mm/s is larger. The effect of a change in the extrusion ratio may not easily be predicted. If the profile velocity is kept constant while ER is increased, the ram velocity must necessarily decrease. This may cause less dissipation and in fact a ram force that is lower. If one compares the effect of an increase in the extrusion ratio with a constant

ram velocity, one has to consider both effects *B** and *D**. An increase in ER for a constant profile velocity (B*) causes the force to increase, but has no significant effect on the temperature. Most of the interaction effects are small and probably insignificant. The most interesting information to be drawn from the effect plots is that simulation and measurement predict similar effects. Absolute values may at the same time deviate significantly. Even relatively small effects may be reproduced by the simulation.

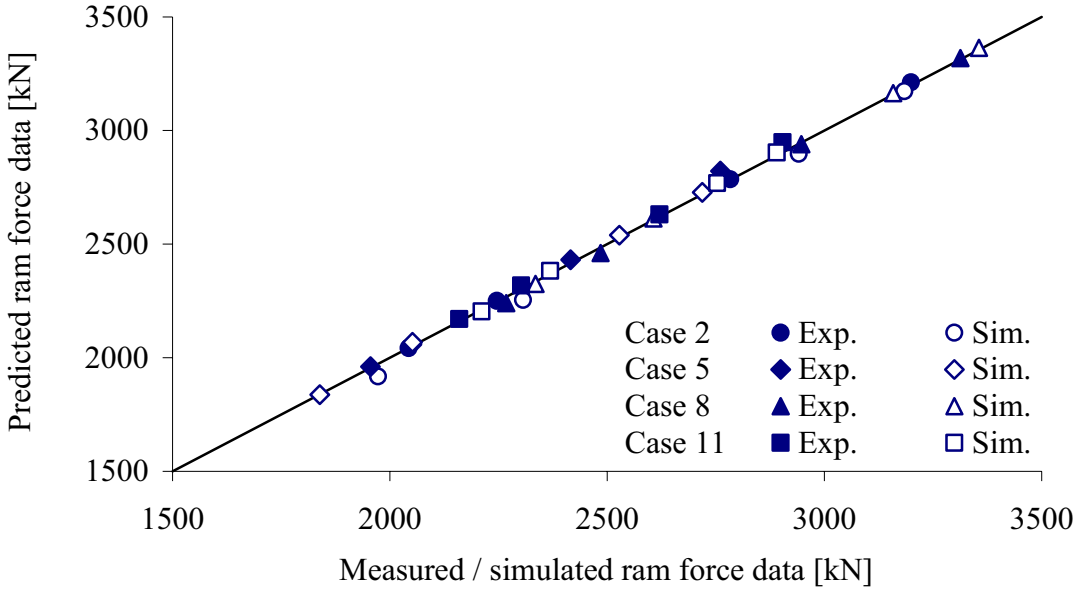

Figure 6.28. A check of linear regression curves for experimental and simulated ram force. The coefficients of the curve are shown in Table 6.6.

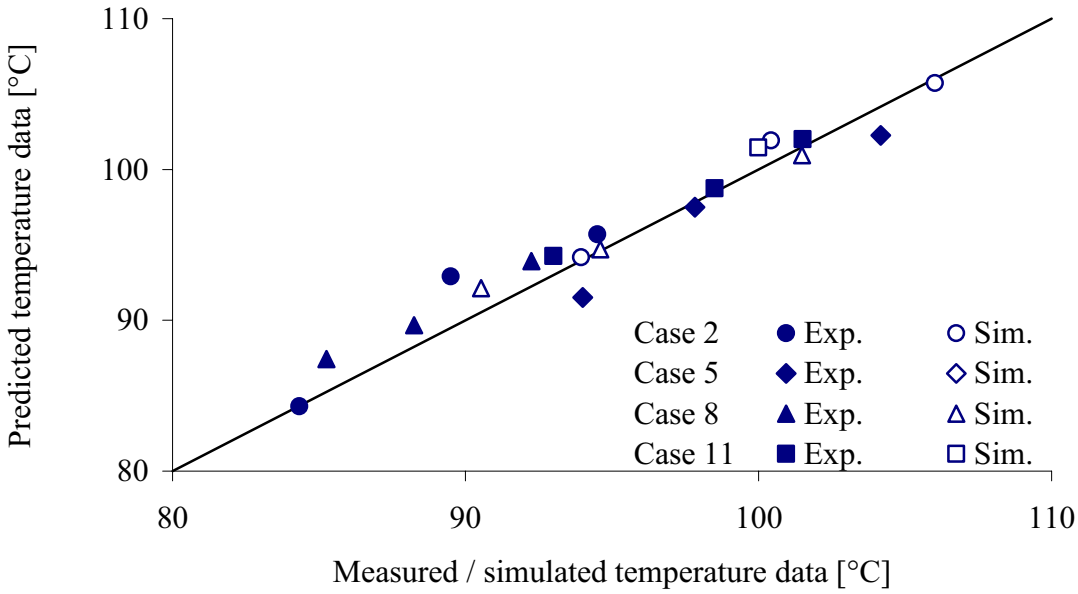

Figure 6.29. A check of linear regression curves for experimental and simulated die outlet temperature. The coefficients of the curve are shown in Table 6.7.

Table 6.6. Ram force [kN] – average values and effects (cases 1 to 12).

POS [mm]	AVG*	B*	C*	D*	BC*	BD*	CD*	BCD*
Max	3177	111	-319	589	7	76	0	22
196	3075	117	-380	542	10	28	-23	-16
170	2697	177	-332	363	23	25	-67	-12
100	2272	236	-168	240	25	21	-63	-9
30	2103	204	-76	313	7	17	-31	-5

Table 6.7. Outlet temperature change [°C] - average values and effects.

POS [mm]	AVG*	B*	C*	D*	BC*	BD*	CD*	BCD*
Max	101	-1	7	43	1	3	-2	2
170	91	6	8	31	1	8	-3	2
100	98	-1	7	43	1	5	-1	1
30	93	-4	6	50	1	2	-1	1

Table 6.6 and Table 6.7 contain information about the experimentally based force and temperature effects. The values may be inserted into regression relations. Cases 2, 5, 8 and 11 are test cases that have not been used to determine effects. The data from these cases may be used to check how accurately the output of an additional run may be predicted by first-order regression relations of the type presented above. In Figure 6.28, the actual measured force of each test case is compared to the force predicted by the regression relation. Data from measurements and simulations have been plotted. It is assumed that $x_4 = 0$ corresponds to a profile velocity of 400 mm/s. All points are positioned close to the straight line $y = x$. Hence, the regression relation performs well. The points based on experimental and simulation data are in most cases quite closely positioned, which means that simulations and measurements are in fair agreement. A similar set of data for the outlet temperature is shown in Figure 6.29. In this case, the regression relation performs somewhat poorly when used for interpolation.

Liner force

Table 6.8 and Figure 6.30 present the estimates of the average container-billet interface shear stress and the effects of extrusion ratio, billet temperature and velocity changes. The estimates of the shear stresses are based on calculations of the force change from billet length 170 to 100 mm.

Table 6.8. Container shear stress [MPa] – average value and effects (cases 1 to 12).

POS [mm]	AVG*	B*	C*	D*	BC*	BD*	CD*	BCD*
Exp.	20.1	-1.8	-4.8	3.3	0.0	-0.7	-1.0	-0.3
Est.	19.3	-2.7	-7.5	5.6	-0.1	0.2	-0.2	-0.2
Sim.	20.8	-0.4	-3.1	1.3	0.2	0.0	-0.4	-0.1

Only the main effects are of significant magnitude. The error in measurement must be expected to be as large as ± 2 MPa, which corresponds to 10 % of full scale. The main effects *C** and *D** seem to be correct. The higher the initial billet temperature, the lower the shear stress. The higher the profile velocity, the higher the shear stress. Simulated effects are somewhat more moderate than ones based on liner load and ram force measurements. Figure 6.31 provides further information about the accuracy of predictions of the regression equations. Cases 2, 5, 8 and 11 are again test cases, and it again seems as the interpolation technique is quite good.

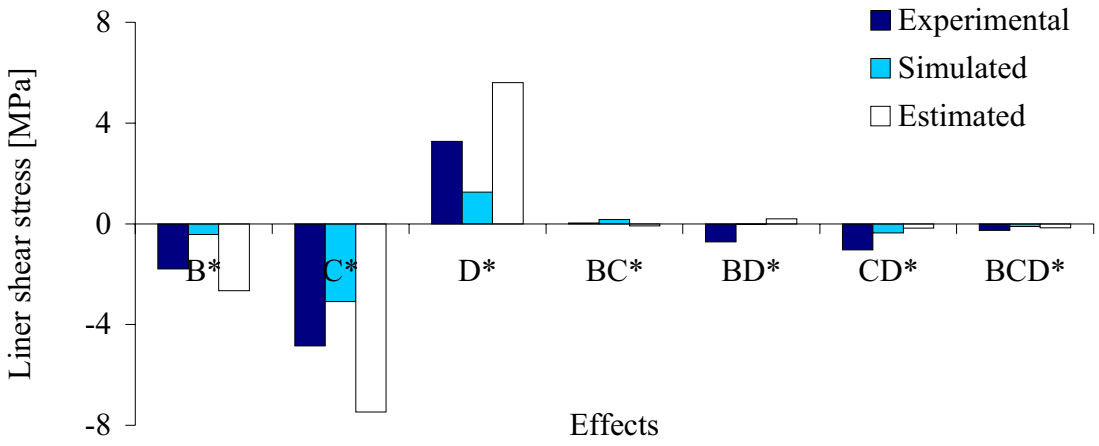

Figure 6.30. Container liner friction shear stress - the effects of changes in process parameters for cases 1 to 12.

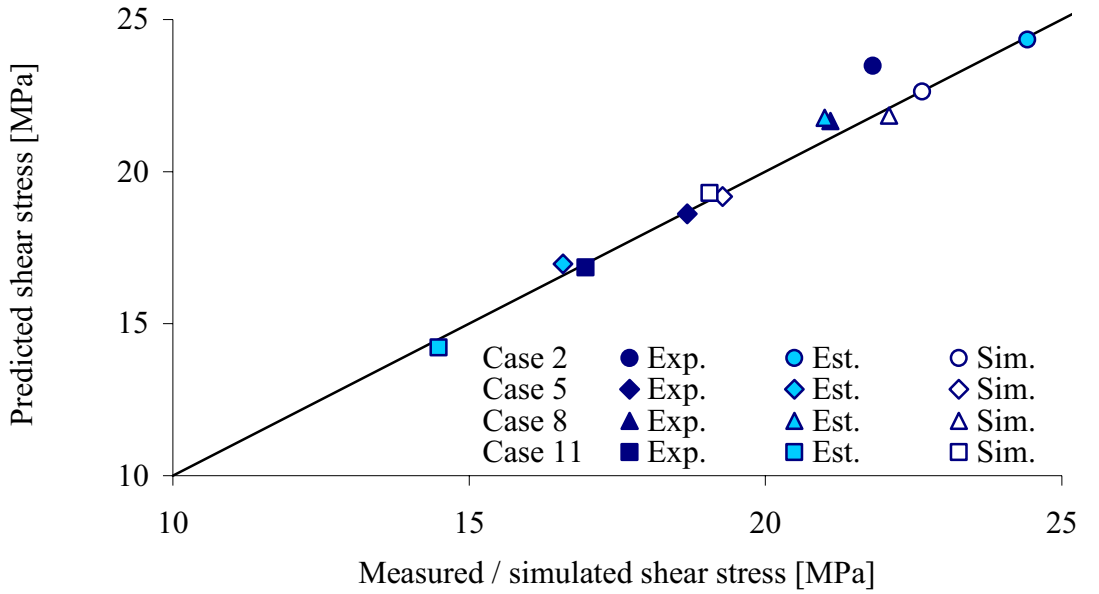

Figure 6.31. A check of the linear regression curves for experimental, estimated and simulated container friction.

Die face pressure

Table 6.9 and Table 6.10 and Figure 6.32 provide information about the average value of pressure and the effects of parametric changes. Data provided by the pressure sensors have been compared to pressure data estimated on the basis of the force and liner load measurement. The calculation approach described in the previous sub-section has been applied. The average values and effects calculated on the basis of simulation data were first presented in Chapter 3. The calculated die face pressure is the pressure applied in the centre of the sensor disc. The die face pressure was non-uniform. Shear stresses have not been considered since they are relatively small (Chapter 3 and Volume I).

Table 6.9. Measured pressure [MPa] – average value and effects (cases 1 to 12).

POS [mm]	AVG*	B*	C*	D*	BC*	BD*	CD*	BCD*
196	252	16	-19	56	3	9	3	3
170	227	19	-29	37	5	-2	-6	-3
100	220	32	-19	11	6	-8	-9	-3
30	245	29	-10	9	5	-2	-7	-1

Table 6.10. Estimated pressure [MPa] – average value and effects (cases 1 to 12).

POS [mm]	AVG*	B*	C*	D*	BC*	BD*	CD*	BCD*
196	262	29	-12	48	1	10	6	0
170	231	36	-11	27	3	9	-2	0
100	234	39	-2	20	3	6	-4	0
30	273	28	-4	40	1	3	-3	0

The conclusions to be drawn from the plot of average values of pressure are very much the same as those of the previous sub-section. At a billet length of 196 mm ALMA2π simulations produce estimates that are too low. As extrusion continues, the measured pressure is somewhat lower than the corresponding simulated and estimated pressures. This may be due to the response of the sensor to heating due to plastic dissipation in the billet. Pressure estimates based on ram and liner force are generally in better agreement with the direct measurements than the simulation. When the billets are very short, however, the container friction is most likely underestimated if a constant shear stress value is used. The force-based estimate of pressure is therefore too high. On the basis of the data presented it seems reasonable to assume that the systematic error of the pressure measurement should not be much larger than 20 MPa or 10 % of full scale. Results from individual cases and runs may differ more from the true values.

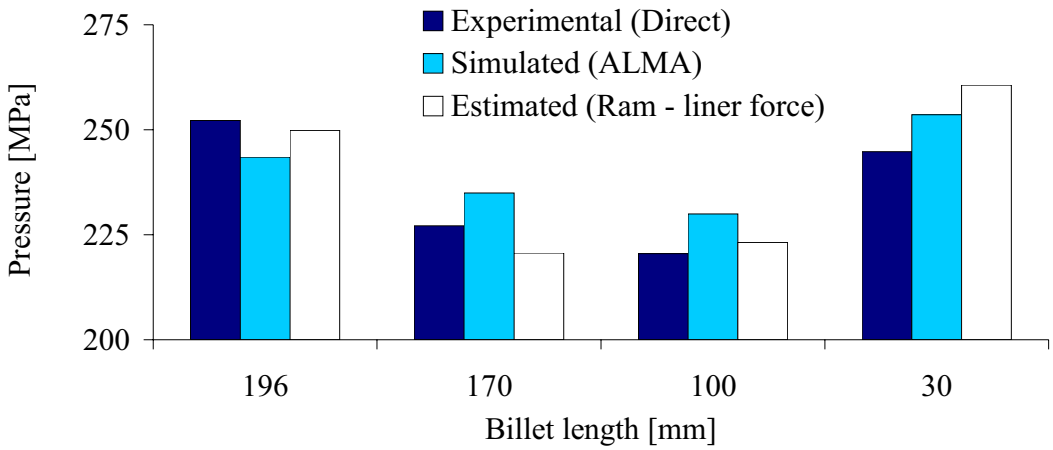

Figure 6.32. The average value of die face pressure – a comparison of experimental, estimated and simulated data for cases 1 to 12.

Two types of effect plots are shown. The first (Figure 6.33) compares experimental data from the die face pressure sensors with experimentally based estimates. The second (Figure 6.34) compares experimental and simulated data. The effects of temperature and velocity changes are significant and logical. It should be noted that as the billet length decreases, the effects become smaller. This conclusion was also drawn directly after the study of raw data and seems reasonable. The most important conclusions to be drawn

from the graphs are that the sensors are able to distinguish effects and that measurement and simulation are in fair agreement. There are some deviations that may be of a purely random nature or related to thermal response of the sensor. The issue is further treated in relation to the analysis of the thermal response of the sensors. Both the pressure sensor output and the ram force based estimate respond to a change in the extrusion ratio, but the magnitudes of the effects differ. The analysis of raw data (Figure 6.19) indicated that there was a block error of some 5 to 10 MPa related mainly to calibration. This may be the reason why the measured effects are smaller than the calculated ones.

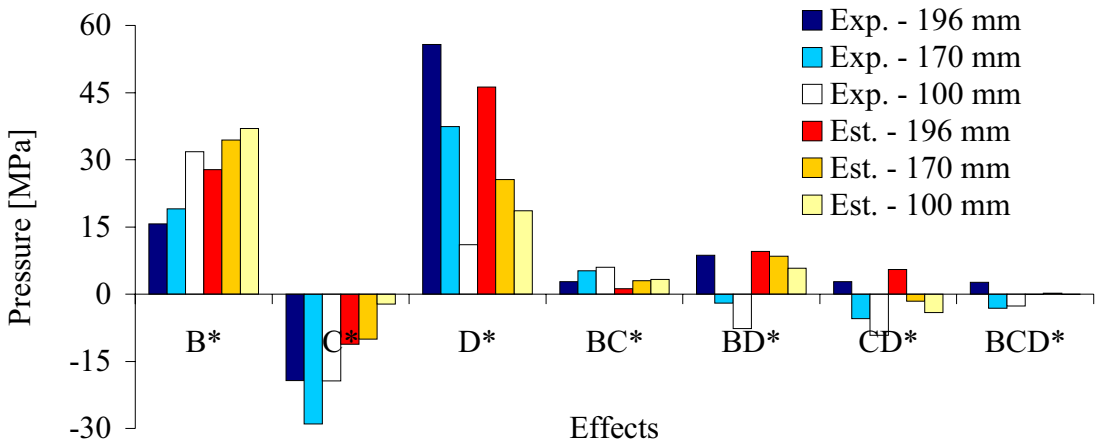

Figure 6.33. The die face pressure – the effects of changes in factors. A comparison of experimental and estimated data for cases 1 to 12.

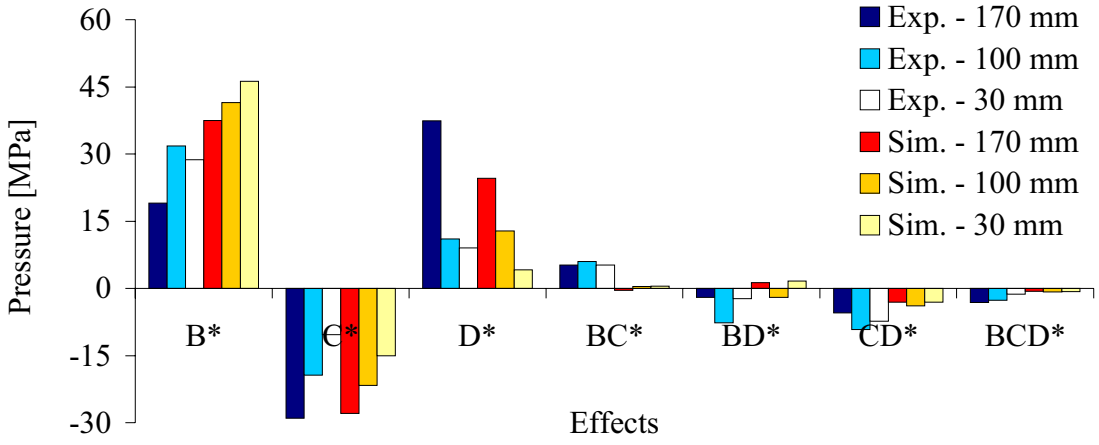

Figure 6.34. The die face pressure – the effects of changes in factors. A comparison of experimental and simulated data for cases 1 to 12.

The interaction effects are also in the case of pressure measurement relatively small and probably insignificant in a statistical sense. This does not mean, however, that they are not physical. The interaction between the profile velocity and the initial temperature of the billet is an example. If the profile velocity is increased, the die face pressure should also increase. Yet, the increase may be smaller if the initial billet temperature is high than if it is low. This is due to the coupled nature of the extrusion process and the fact

that the strain rate sensitivity of the material and the system is smaller at higher billet temperatures. *CD** should therefore be negative. If x_3 is equal to -1 (low temperature), the effect of a velocity change *D'* is *D*-CD**/2. If x_3 is equal to 1 (high temperature) the effect *D''* is *D*+CD**/2. *D'* is larger than *D''* if *CD** is negative. The interaction effect should be smaller when the billet is short, since the temperature is then less affected by the initial conditions. In practice it is not possible to distinguish such a trend with the pressure sensors. Changes that are as small as 5 MPa are generally not recognisable. This is an important conclusion for those interested in using the sensor to evaluate flow relations and bearing channel friction. A better sensor design and a better experimental plan may improve matters. Temperature compensation of data is also important. In the present case it will be shown that the effect is not large.

Finally, the quality of the regression relations is tested in Figure 6.35. All effects have been used although strictly speaking, some of them are not significant in a statistical sense and therefore probably should have been disregarded. However, the predicted and measured data are in fair agreement for all test cases. Furthermore, the figure gives an indication of the accuracy of measurement or at least of the deviation between results from simulation and measurement. The main conclusion of the study of effects is that the sensors may successfully be used to evaluate effects of magnitude larger than approximately 10 MPa if they are not confounded with block effects. If they are confounded, there may easily be pressure deviations larger than 20 MPa.

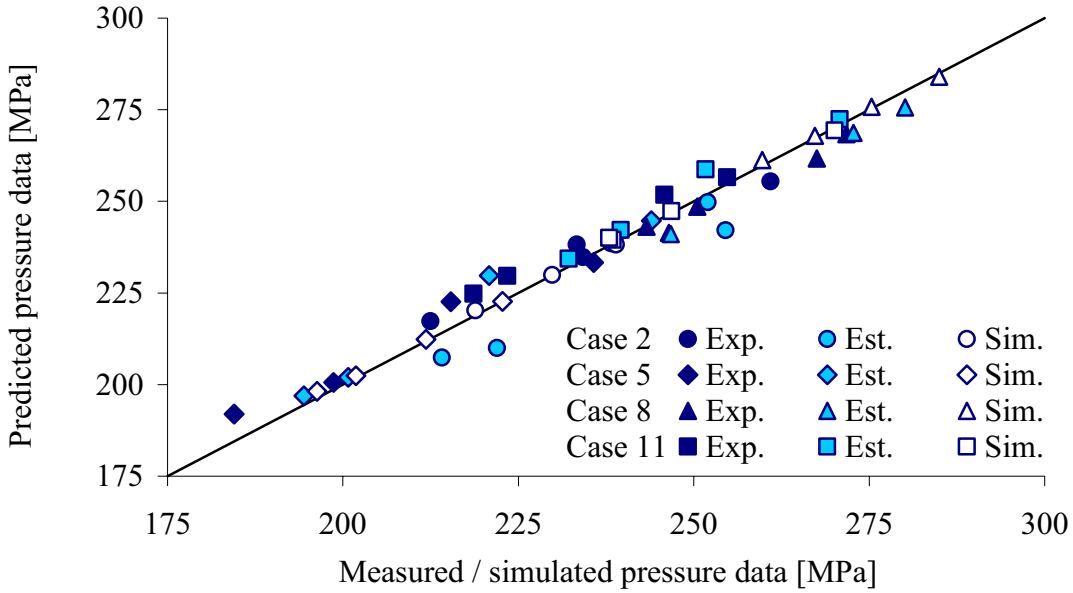

Figure 6.35: A check of the linear regression curves for experimental, estimated and simulated die face pressure. If the symbols lie along the proportionality line predicted by the linear regression, relations are accurate. If the symbols indicating experimental, estimated and simulated data are closely positioned, measurement and modelling errors are small.

6.3 The effect of a bearing channel

Cases 13 to 24 were run with die outlets of a bearing length-to-diameter ratio *L/D* of approximately 0.76. All other nominal input data to the process were otherwise equal to those of cases 1 to 12. The relatively long and slightly choked bearing channels (40') were introduced mainly in order to test the sensor principle and the approach. However, the study of bearing channel friction is also of more general interest. The main results of the analysis of the long bearing channel data are therefore presented, and conclusions on the pressure sensors' ability to measure pressure are drawn. Although the behaviour of the sensors on the last day of experiments (day E) was by no means optimal, the study still has the potential of being most useful.

Since only the length of the bearing channel was altered, the temperature of the sensor and the container wall should not differ much for cases such as 1 and 13, 2 and 14 etc. Hence, the container friction and probably also the container flow should be similar for cases with and without bearings. This simplifies a comparison of the extrusion pressure (average ram pressure) and die face pressure changes due to bearing length increases. The temperature and the thermal responses of the sensors should also be comparable for the cases of zero and long bearing channel. In Chapter 5 results from cases 13 to 24 were directly compared with the results from the cases 1 to 12. One should be very careful when assessing such estimates of the bearing friction. The main reason is that the temperature at the inlet may differ for the cases with and without a bearing channel. The heat generation at the outlet is larger when there is a bearing channel. Most of the heat is transported with the profile. However, the die also heats up, and there may be some heat transfer in the direction opposite that of extrusion. The consequence is that the temperature level at the bearing channel inlet is higher for the long bearing channel cases. The temperature increase may also cause systematic measurement errors.

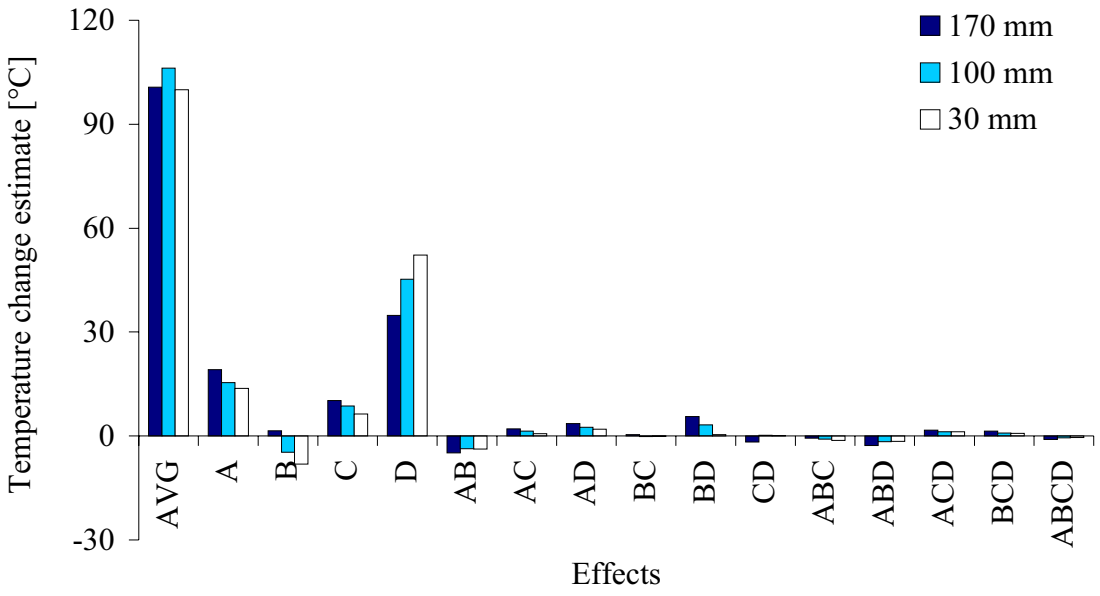

Figure 6.36. Bearing inlet temperature minus initial billet temperature – average value and effects of factor changes. Effects are based on data for cases 1 to 24.

Figure 6.36 indicates that the temperature increase at the outlet may be 15 ºC or 15 % higher for extrusion with a long rather than with a short bearing channel (effect *A*). Similar results were obtained during all rounds of the experiment (effect *AB* << effect *A*). Note that the comparison of temperatures is made at the inlet of the bearing channel. Data on the temperature increase through the bearing channel may also be obtained by assuming that $x_1 = 1$ (long bearing channel) and by comparing results from measurement of temperatures at the inlet and outlet of the channel. Figure 6.37 presents data on the average temperature increase and the effects of changes of different input variables. The temperature at the outlet is generally 6 to 13 ºC higher than at the inlet. The main effects are not very significant compared to the variability in measurement. Still, the effects appear to be physically reasonable. If the initial billet temperature (C*) is high, the temperature increase in the bearing channel should be small. If the profile velocity (D*) is high, it seems reasonable that the temperature increase is large. If the extrusion ratio (B*) is high, the temperature increase should also be large. The last two observations may imply a velocity-dependent friction model, but no clear conclusions may be drawn. Two factor interactions are generally small and even harder to assess.

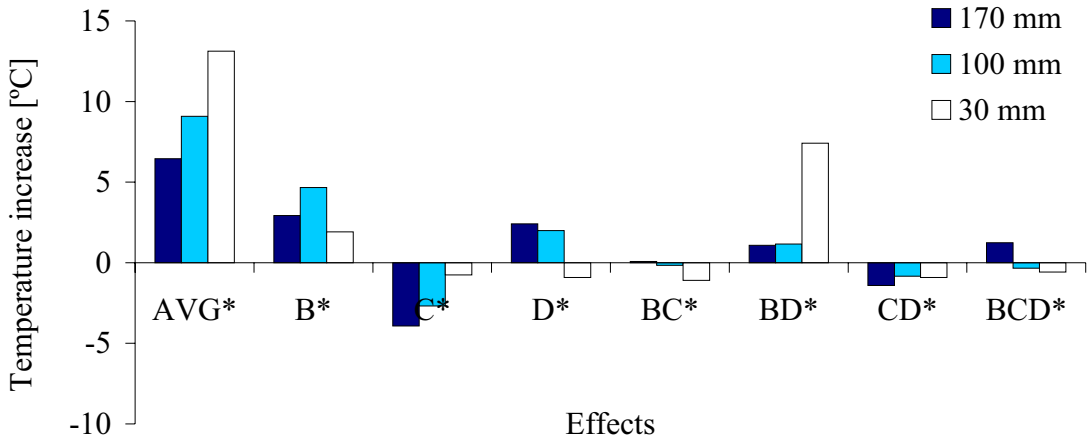

Figure 6.37. Bearing channel temperature increase – average value and effects of changes in parameters. The effects are based on experimental data for cases 1 to 24. The effects are evaluated for various billet heights.

Two approaches for evaluating the pressure difference for extrusion with long and zero bearing channels are evaluated here. First, the effects of the full 2^4 factorial design are assessed. Second, the individual differences in pressure for cases 13 and 1, 14 and 2, 15 and 3 and so on, are evaluated.

Figure 6.38 presents the average values of pressure for the full design (cases 1 to 24). Figure 6.39 shows the various effects of input variable changes. Both data as based on direct pressure measurement and estimates based measurement of ram force and liner load are presented. The estimates are of larger magnitude than those presented earlier due to the addition of cases where long bearing channels were used. Otherwise there are no significant differences. The effect of the bearing length (*A*) is obviously significant. According to ram force and pressure sensor measurements it should be from 30 to 50 MPa. The estimated effects presented earlier were somewhat larger (50 – 60 MPa). The

causes of deviation and variation may not easily be found without a closer study of measurement data. It is not necessary to evaluate the estimated die face pressure when comparing results from cases performed under very similar conditions. As it probably may be assumed that the container shear stress and flow are similar for corresponding cases of zero and long bearings, it is sufficient and better to evaluate only differences in the average ram pressure. The liner force is similar for cases 1 and 13, etc.

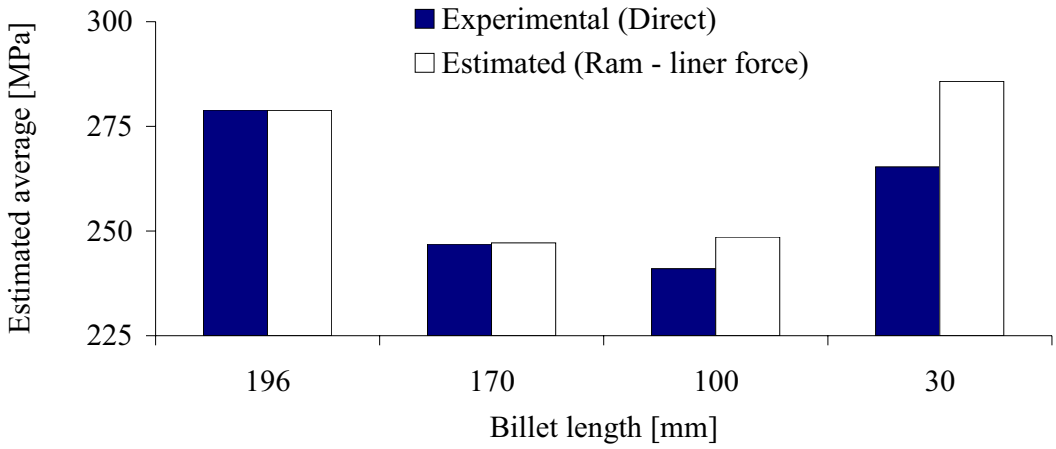

Figure 6.38. Average value of die face pressure – a comparison of experimental data and force-based estimates for cases 1 to 24.

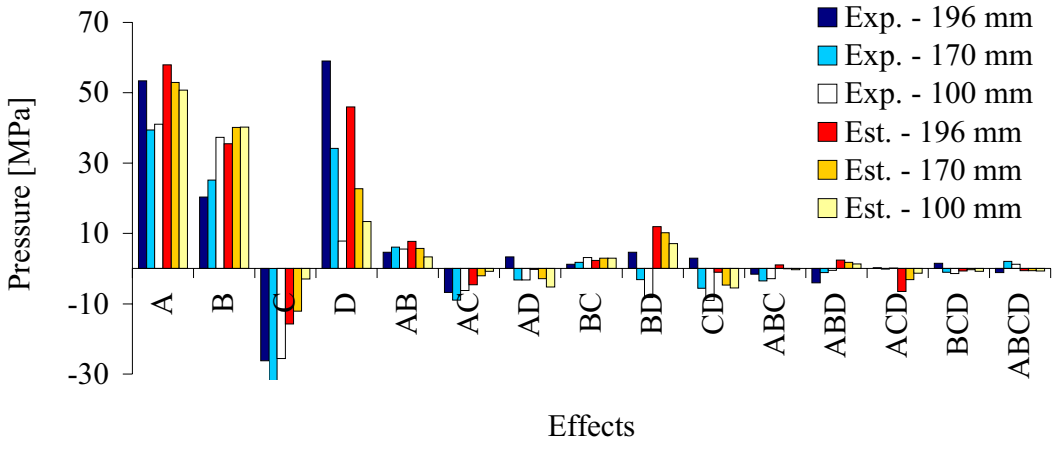

Figure 6.39. Die face pressure – the effects of parameter changes. A comparison of experimental data and force-based estimates for cases 1 to 24.

The changes in average ram and die face pressure due to bearing length changes are shown in Figure 6.40. "Day D – AB" results are from the cases run with die outlets with an extrusion ratio of 40. There are two different presentations of the other results. The first, "Day E1 – C", assumes that only the results from sensor 3 are worth evaluating on day E. The second, "Day E3 – C", takes into account results from all three sensors from the very last day. The calibration factor of sensor 3 on day E was probably too low. It should therefore be expected that the estimates of pressure and bearing channel pressure increase are too low. Note that sensors 1 and 2 did not function properly on day E.

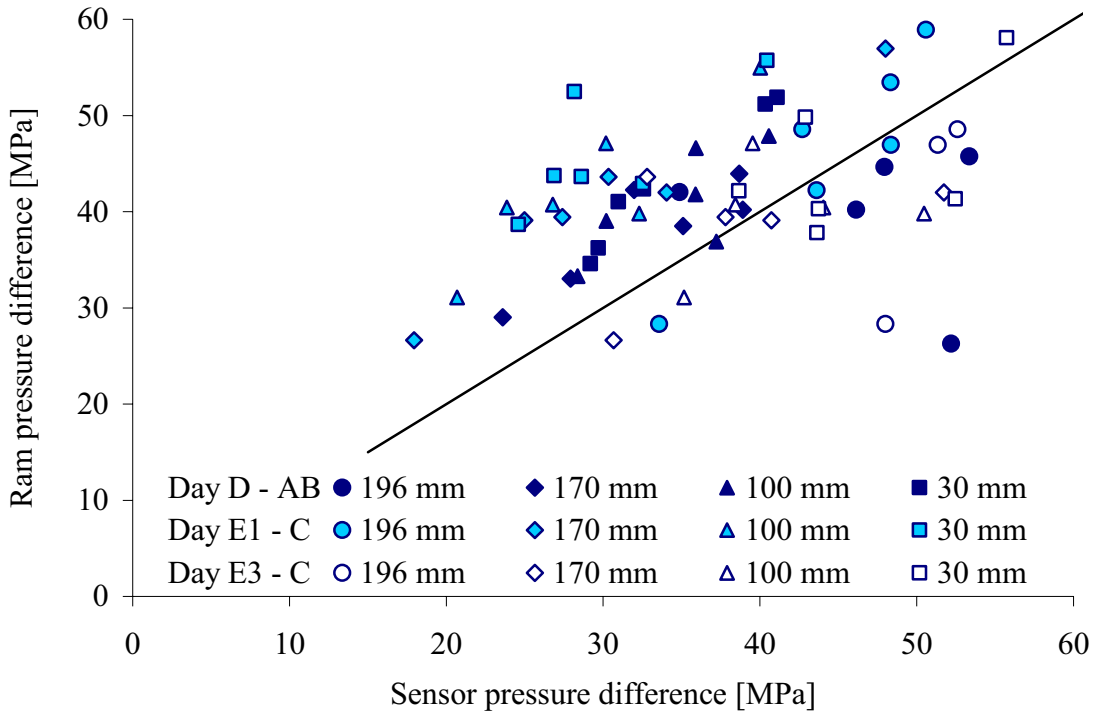

Figure 6.40. Bearing channel pressure increase estimates - calculated from the results cases 13 to 24, minus results from cases 1 to 12.

A straight line, $y = x$, has been added to allow a simpler comparison of results. Since the bearing effect is confounded with a block / calibration effect, it cannot be expected the accuracy of measurement be very much better than ±15 MPa. Results are also scattered within the range from 20 to 60 MPa. The correlation coefficient of the data is generally better than 0.6, and for results obtained at billet length 30, it is in fact better than 0.9. Results obtained with an extrusion ratio of 40 are somewhat better than those obtained with an extrusion ratio of 80. However, there is a large amount of variability in the results. The value of the pressure sensors in the study of bearing channel friction is therefore limited. A couple of fundamental observations are here identified.

A number of researchers have studied the nature of the bearing channel friction [Abt95] [Tve97] [She99] [Val94] [Wel96]. An important question is if the friction in the outer parts of slightly choked bearing channels is slipping and pressure-dependent. An earlier assumption has been that there is intimate contact and no relative movement of surfaces. It would be interesting to check if data from the rod extrusion experiments and the pressure sensors in particular give an indication of the nature of the friction in the bearing channel. The 40’ nominal bearing channel choke angle used in the current study is a relatively large one, so it may be that the observations made here are not valid for most industrial cases. The actual choke angle was probably some 3 to 5’ smaller.

A first step is to establish rough estimates of the shear stresses in the bearing channel. If one neglects the established fact that outlet temperatures of long and zero bearing cases may be different, the average shear stress at the aluminium-steel interface is given by the equilibrium equation. The average wall shear stress, τ_w, causes pressure to build-up

in the bearing channel in the direction opposite that of extrusion. The average wall shear stress may then be related to the build-up of hydrostatic pressure Δp, the bearing channel diameter D and the bearing channel length Δz, as in Equation (6.13).

$$\tau_w = \frac{\Delta\sigma_z}{4}\frac{D}{\Delta z} = \frac{\Delta p}{4}\frac{D}{\Delta z} \qquad (6.13)$$

The simple slab model used to deduce the expression has been presented in [Moe03b]. The hydrostatic pressure and the average value of the coordinate stress in the axial direction are assumed equal. This need not be correct at low pressures. If the pressure increase in the bearing channel is 20 to 60 MPa, the average shear stress should be in the range from 6.6 to 19.7 MPa. It is natural to assume that if a long bearing channel extrusion had been performed at the same die outlet temperature as the zero bearing extrusion, the pressure increase would have been larger than indicated by effect A. A temperature increase usually reduces forces and pressures required to initiate flow. However, the following evaluation of flow and friction should indicate that the effect of a die inlet temperature change of even 15 ºC should be quite moderate.

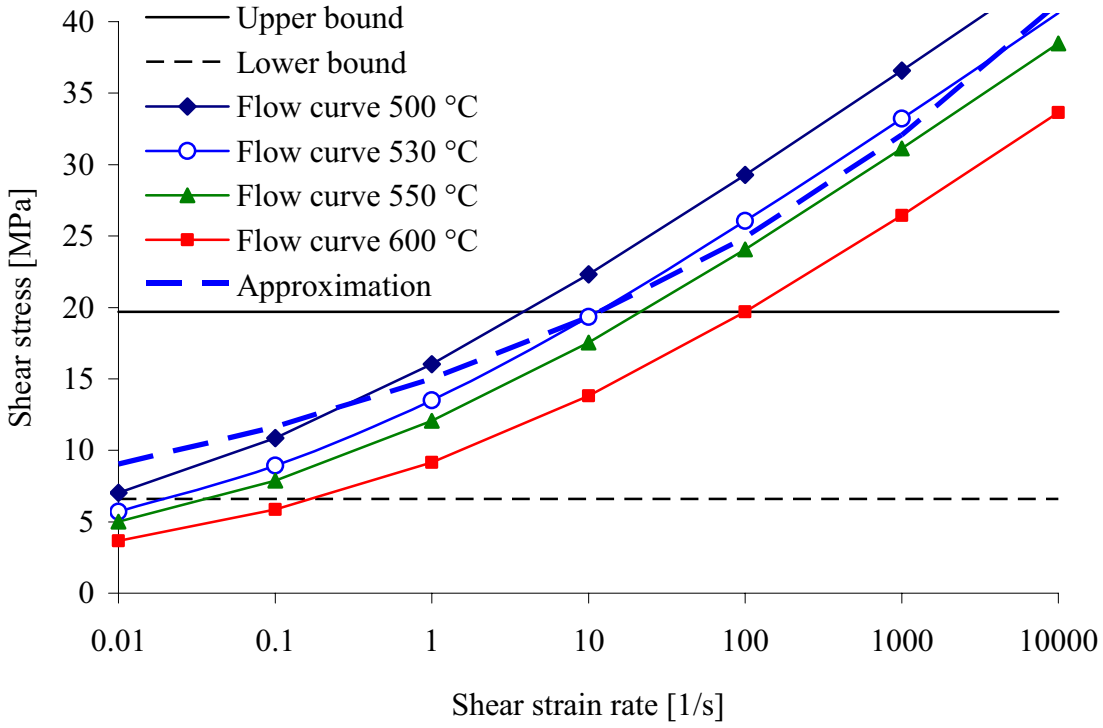

Figure 6.41. The Zener-Hollomon flow shear stress curves for temperatures 500, 530, 550 and 600 ºC. The approximation is of a Power-Law fluid.

If it is first assumed that the friction is of the sticking type in the bearing channel, the wall shear stresses may be determined directly from the geometry of the bearing channel and the flow properties of the material. Figure 6.41 shows how shear strains and shear stresses are related for AA6060 in the case of pure shear deformation. Material data were obtained by compression testing [Moe04b] and fitted to the Zener-Hollomon

flow relation by an inverse modelling technique. Lower and upper limits of 6.6 and 19.7 MPa have been added to the figure. If the outlet temperature is 530 ºC, the shear strain rate should be smaller than 10 s^{-1}. This must be regarded as a very low strain rate for the shear or plug flow in the bearing channel. The curves also render possible an assessment of the effect of temperature on the pressure build-up. The flow shear stress at 500 ºC is only approx 3 MPa higher than the flow shear stress at 530 ºC. Thus, for a full sticking bearing channel of *L/D* ratio (length-to-diameter) 0.76, the pressure build-up should be approximately 10 MPa higher than indicated by estimates (Equation (6.13)). Such a difference is not statistically significant. Furthermore, even if the maximum shear stress was 23 MPa, the maximum allowed shear strain rate should be moderate (< 50 s^{-1}).

In order to determine the actual strain rate and stress the flow problem with the relevant boundary conditions must be solved. Numerical solution techniques exist, but need not produce more accurate results than simplified analytical approaches. Only a steady state analytical analysis with a temperature independent flow relation is used here. An expression for the pressure increase through a length of the bearing channel has been deduced [Moe03b]. It is assumed that the bearing channel choke is small and that the material flow is only in the extrusion direction. The bearings are assumed to be infinitely long. Transient effects related to the flow of material into the bearing channel are disregarded, and the details of flow close to the exit of the bearing channel are also not considered. Equation (6.14) presents an expression for the increase in the isotropic or hydrostatic pressure, Δp, over a length Δz in the extrusion direction.

$$\Delta p = 2mF\left(n, A\right)\frac{\Delta z}{R} = 2m\left[\frac{v_{uni}}{AR}\frac{1+3n}{n}\right]^{n}\frac{\Delta z}{R} \qquad (6.14)$$

$m \cdot F(n,A)$ is here the wall shear stress. A, n and m are the parameters of the Power-Law flow relation. An approximate flow curve is compared to the flow curves of the Zener-Hollomon relation at a range of temperatures in Figure 6.41. If n = 0.11, m = 15 MPa and A = 1 s^{-1} the flow curve is quite similar to the Zener-Hollomon curve valid at 530 ºC. Δz is the length of the bearing channel in the flow direction and R is the radius. v_{uni} is the uniform outlet velocity. The pressure increase in the bearing channel for profile speeds from 50 to 800 mm/s is presented in Figure 6.42.

The model predicts a pressure increase through the bearing channel in the range from 75 to 105 MPa. The measured pressure differences are at the same time in the range from 20 to 60 MPa. With the proposed temperature compensation, the upper limit of the pressure build-up is approx 70 MPa. There may be further systematic errors related to measurement, the model and the many simplifications that have been introduced. There may also be a very small build-up of pressure in the short bearing channel of the zero bearing die. However, given all earlier observations it seems that a rejection of the full-sticking hypothesis may be justified. The full-sticking model predicts shear strain rates in the range from 300 to 1700 s^{-1} at the bearing surfaces (200 and 800 mm/s outlet speed). It is not likely that calculations with the Zener-Hollomon model would have produced estimates that were much lower. With such strain rates, the average wall shear stress at the bearing surface should be higher than 25 MPa (Figure 6.41).

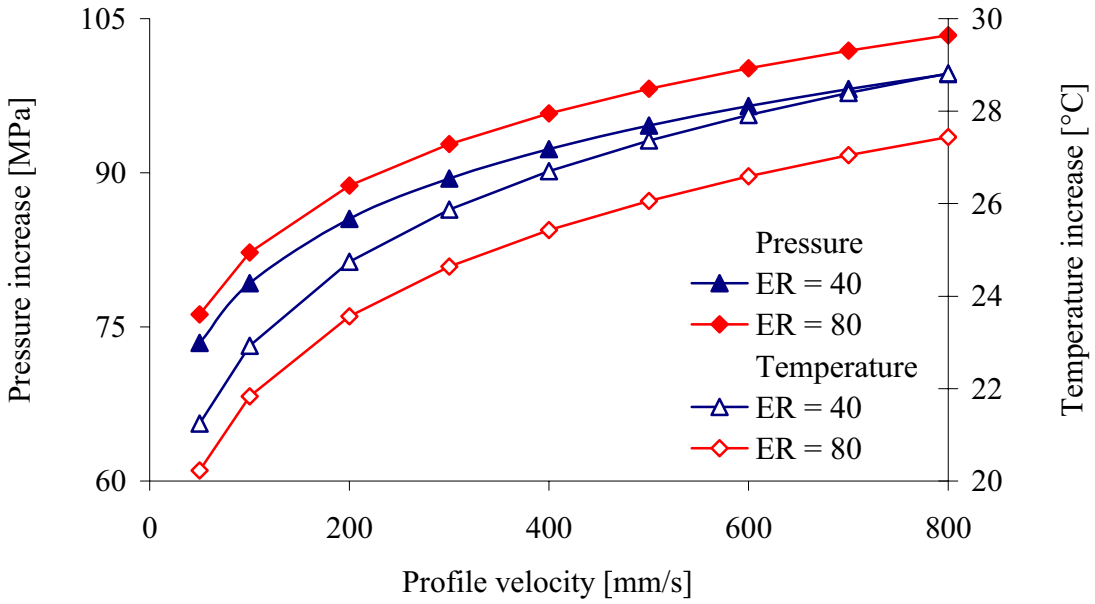

Figure 6.42. The bearing channel pressure build-up and temperature change between measurements points in the bearing channel.

The die outlet temperature measurements provide some support for the rejection of the sticking hypothesis. Figure 6.42 presents data on the temperature increase from the thermocouple placed at the inlet of the bearing channel to the one placed at the outlet. The model is a simplified one and has also been treated more thoroughly in reference [Moe03b]. It assumes that the heat is generated only at the boundary between the profile and the die, and flows into the profile. If the profile velocity is as high as in the current study, there will be very little flow of heat into the material or to the die while the profile is in the bearing channel. In this case one should use the heat conduction model proposed in [Moe03b]. If it is assumed, however, that heat is still conducted extremely fast to the centre of the profile, one may establish some sort of a lower estimate of the temperature increase at the surface of a profile flowing through the bearing channel. The values presented in Figure 6.42 are of this kind. The estimated values are as much as three to four times higher than the measured temperature increases in the bearing channel. This may not be regarded as a solid proof of the inappropriateness of the full-sticking model, but it is a strong indication of a model error. Errors may also be related to the modelling of flow at very high rates and temperatures. When use is made of the continuum approach, a clear distinction between flow and friction should be drawn, but in a study of the thin boundary layer in the bearing channel, such a distinction may be less appropriate. There may be deformation both by dislocation movement and by surface sliding. The shear resistance may be affected by the intimacy of the contact and deviate from Zener-Hollomon behaviour at high strain rates. Before advancing further, the possibility of errors also in temperature measurements should be considered. There is a certain possibility that measurements may be as much as 10 ºC in error. However, parallel measurements have been performed, and the results were in fair agreement. The fact that the sensors in the middle and at the outlet of the bearing channel produced similar responses during all rounds is an indication of low shear resistance and supports the rejection of the full-sticking model (although it is no proof).

An alternative bearing shear stress hypothesis advocated by Abtahi [Abt95] and Tverlid [Tve97] is that of a pressure-dependent friction stress. The simplest type of relation that has been used is that of Coulomb ($\tau_w = \mu\sigma_n$). σ_n is the component of stress normal the wall. The friction factor μ has been found to be most appropriate, but Tverlid notes that there may be a rate dependency. The real mechanisms of bearing friction are probably much more complex, but the Coulomb relation is here used as some kind of a first order approximation. The Coulomb relation proposes that close to the outlet of the bearing channel, there will be less intimate contact even in the case of choked bearings.

An analytical expression for the pressure build-up may also be developed in the case of Coulomb friction. A number of simplifications must be made. First, it is assumed that the material flows as a plug and that all deformation occurs in a thin layer modelled only by the Coulomb relation. Second, the component of stress normal to the wall must in a simple way be related to the component of stress in the extrusion direction. It is here assumed that the components are proportional even though this must result in a contradiction. The proportionality factor B is set to 1. The coordinate stresses are also assumed to be equivalent to the hydrostatic pressure, p, even though this may not be correct for low stresses. Finally, the determination of the pressure through integration requires that the minimum shear stress, τ_0, in the bearing channel is determined. Abtahi and Tverlid have found that the value 5 MPa is an appropriate one, but this is only a rough (but still important) assumption. For a friction factor of 0.4, the minimum contact stress, p_0, is then 12.5 MPa. The contact stress is here regarded as the fundamental parameter. The increase in the pressure, Δp, over a distance Δz = 12 mm in the case of ER = 40 (bearing channel of radius R = 7.9 mm) is then given by Equation (6.15).

$$\Delta p = p_0 \exp\left(2\mu B \frac{\Delta z}{R}\right) = 12.5 \cdot \exp\left(2 \cdot 0.4 \cdot 1 \cdot \frac{12\ \text{mm}}{7.9\ \text{mm}}\right) \text{MPa} = 42\ \text{MPa} \qquad (6.15)$$

Precisely the same result is obtained for an extrusion ratio of 80. The maximum shear stress is in this case 0.4· 42 MPa = 17 MPa. As a comparison, the full-sticking friction model predicts a shear stress of approx 28 MPa for a profile velocity of 200 mm/s. This implies that there should be a state of slipping friction in the entire bearing channel. The temperature increase should also be in better agreement with measurements.

Based on the ram force and die face pressure measurement data, one is not able to reject the hypothesis of a pressure dependent friction model in the bearing channel. The model seems to better describe friction than the full-sticking model. However, no verification of the Coulomb model or the idea of a stick-slip friction mechanism has been presented. As indicated earlier, there may be other, more appropriate models. Furthermore, the variability in measurement results and the errors and simplifications of the model make it hard to draw clear conclusions. The data available may for example not be used to accurately determine a friction factor (if it may at all be used). Pressure increases of 20 and 60 MPa correspond to friction factors of 0.16 and 0.52 respectively. A minimum contact normal stress is of 12.5 MPa has been assumed for both cases. Finally, one should not forget that the conditions at the outlet for the zero bearing and long bearing cases were somewhat different.

Pressure build-up effects

In order to better understand the effects of changes on the process parameters, a factorial design including three factors, extrusion ratio (B), initial billet temperature (C) and profile velocity (D) may be defined. The main response is the difference in pressure for comparable cases with long and zero length bearing channels (for example cases 1 and 13). This is the change in pressure due to a bearing channel increase as used above. The estimates of the average pressure differences are shown in Figure 6.43. Estimates of pressure changes based on data from one and all three of the sensors that were used on day E are presented. Again, it should be remembered that the calibration factor used for sensor 3 on day E was probably too low and that the sensor behaviour of the other two pressure sensors was highly questionable. Still data from ram force measurements are in fair agreement with the estimate of the average pressure for all sensors.

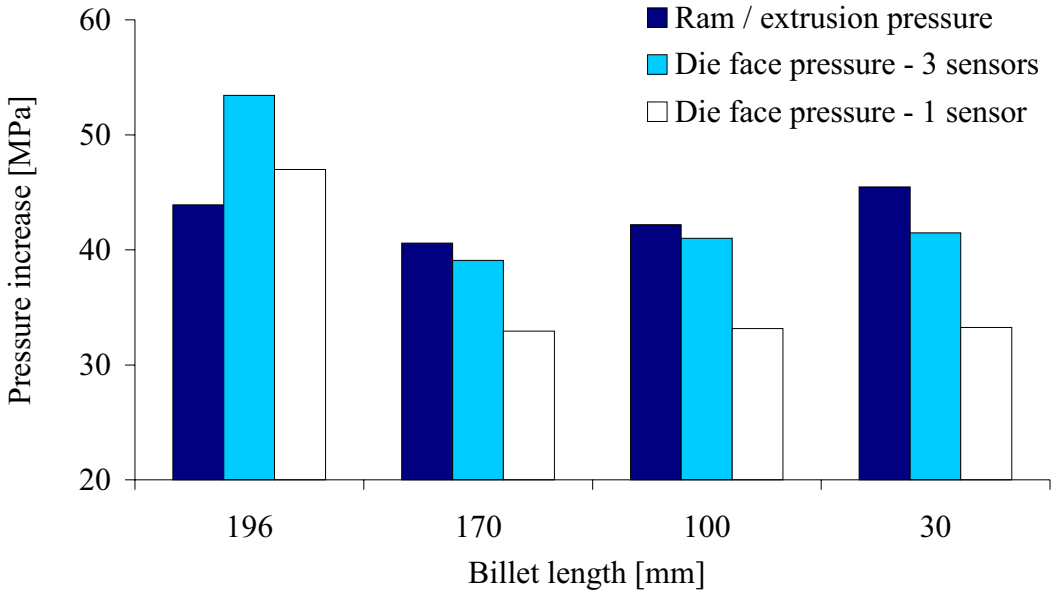

Figure 6.43. Bearing channel pressure increases – average values calculated from the results from cases 13 to 24 minus results from cases 1 to 12.

Figure 6.44 presents the effects of changes in input parameters. The main effect B is affected by blocking / calibration to a relatively large extent. Still, there is an indication that the pressure build-up may be somewhat larger at higher as opposed to lower extrusion ratios. This is the case for the traditional full-sticking model and for most other velocity- dependent models. The effect is far from statistically significant for the pressure sensors, and is mainly supported by the ram force measurements. The ram force data are the most reliable, but simplifications have been made.

The main effects C and D are not confounded with the block effects, and they are of considerable magnitude. Results from ram force and die face pressure measurements are also fairly consistent. Hence, there is an indication that the pressure build-up is lower for higher initial billet temperatures. The effect is, as should be expected, strongest when the remaining billet length is large. The pressure build-up also seems to be lower at higher profile velocities. The result is an indication of the complexity related to the

recording and analysis of data. The extrusion system is strongly coupled and non-linear. A higher profile velocity is the cause of higher strain rates and often also higher stresses. The stresses may also be affected by heating, which may occur both in the container and the bearing channel. The physical mechanisms of deformation in the bearing channel are not properly understood, and the temperature field has not been thoroughly studied here. Finally and probably most importantly, there is also a relatively large possibility of measurement and modelling/interpretation errors. The interaction effects can simply not be easily interpreted. In the main, they probably give an indication of variability related to the estimates.

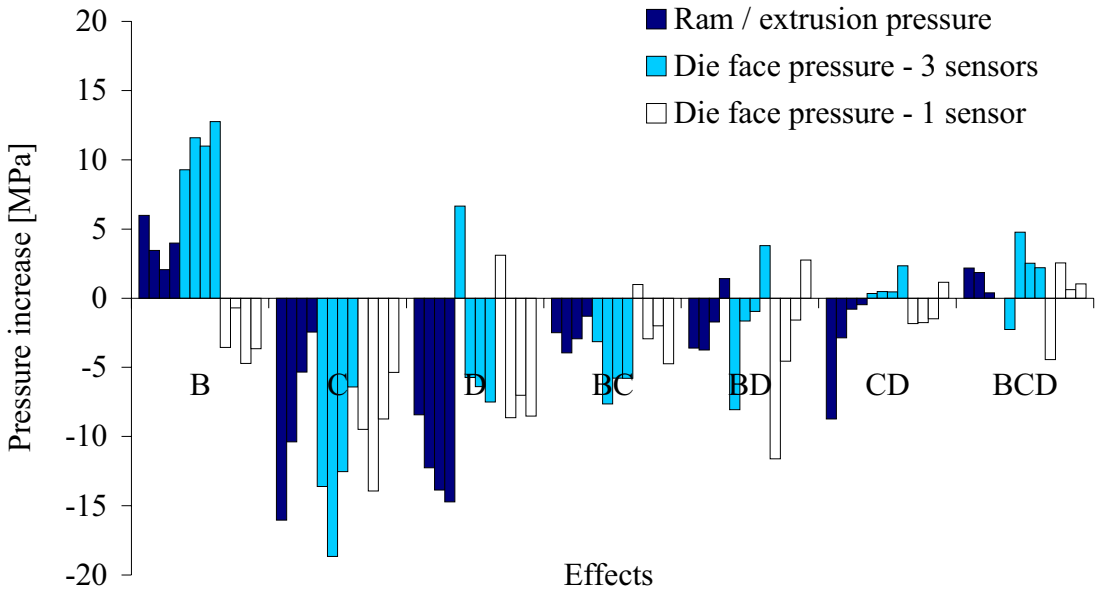

Figure 6.44. Bearing channel pressure increases – effects calculated from the results from cases 13 to 24 minus results from cases 1 to 12. The four leftmost columns of each effect reveal the ram force based estimates (R). The four central columns are estimates based on pressure sensor measurement with all sensors (3). The four rightmost columns are estimates that have also been based on data from pressure sensors. The outputs of the sensors that did not work properly on day E have not been considered (1).

6.4 Temperature compensation

6.4.1 An evaluation of data from experiments

The results presented in the previous sub-sections clearly indicate that the responses of the capacitive die face pressure sensors may be affected by sensor temperature changes. Average results for cases 1 to 6 are shown in Figure 6.45. Results from the die sensors are compared with the estimates based on the ram and liner force measurements.

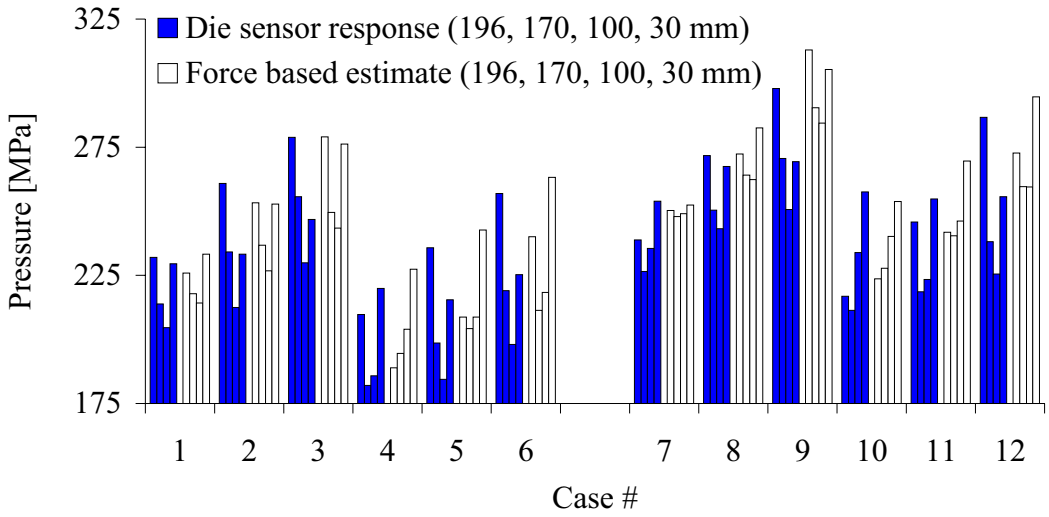

Figure 6.45. Die face pressure – a comparison of non-corrected experimental data and estimated results based on ram and liner force measurements.

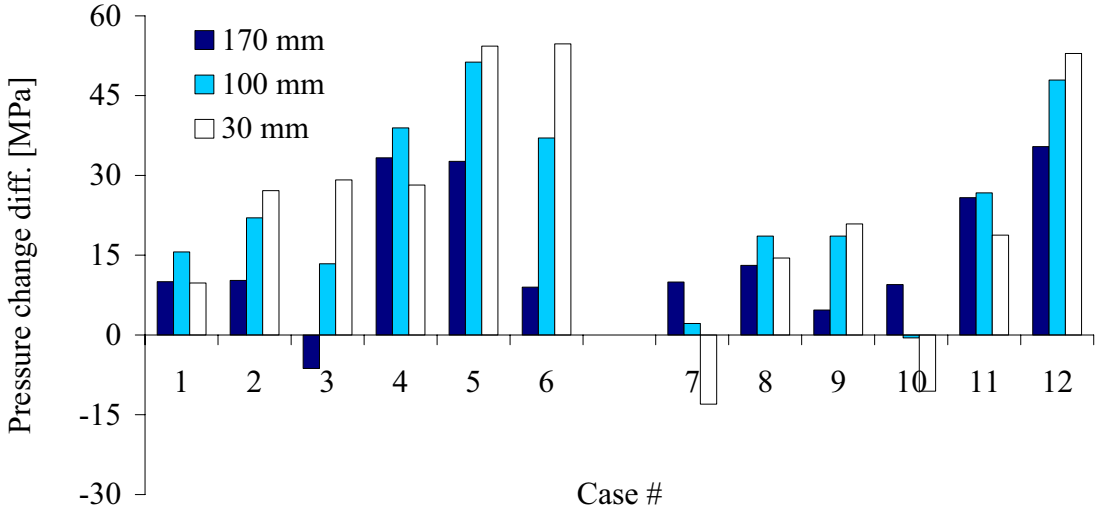

Figure 6.46. Directly measured change minus estimated force-based pressure changes $(dP_{170})^{exp} - (dP_{170})^{est}$ – a comparison of non-corrected experimental data and estimated results based on ram and liner force measurements.

As first discussed in Chapter 4, there are systematic errors related to calibration. It is more useful to assess pressure changes during a run than absolute values when assessing

the effects of temperature changes. The pressure changes or differences are $dP_{170} = P_{196} - P_{170}$, $dP_{100} = P_{196} - P_{100}$ and $dP_{30} = P_{196} - P_{30}$. P_{196}, P_{170}, P_{100} and P_{30} are the values of die face pressure for billet lengths of 196, 170, 100 and 30 mm respectively. Figure 6.45 indicates that the sensor (exp.) pressure difference values dP_{170} and dP_{100} generally are somewhat larger than the corresponding estimates. The estimated dP_{30} may in some cases be negative, which means that the pressure increases towards the end of the run. Figure 6.46 displays the difference between the experimental and estimated values of dP_{170}, dP_{100} and dP_{30}. A positive value indicates that the output of the pressure sensors decreases more than the estimates during the run. If extrusion is performed at high speed, the response of the sensors may differ significantly from the estimated values. Errors are probably not only related to the direct die face pressure measurement. Since estimates are based on average friction values obtained from liner force measurement, they may be in error, especially at small billet lengths. The aim is here, however, to evaluate to what extent the responses of the pressure sensors are systematically affected by temperature changes during an extrusion run.

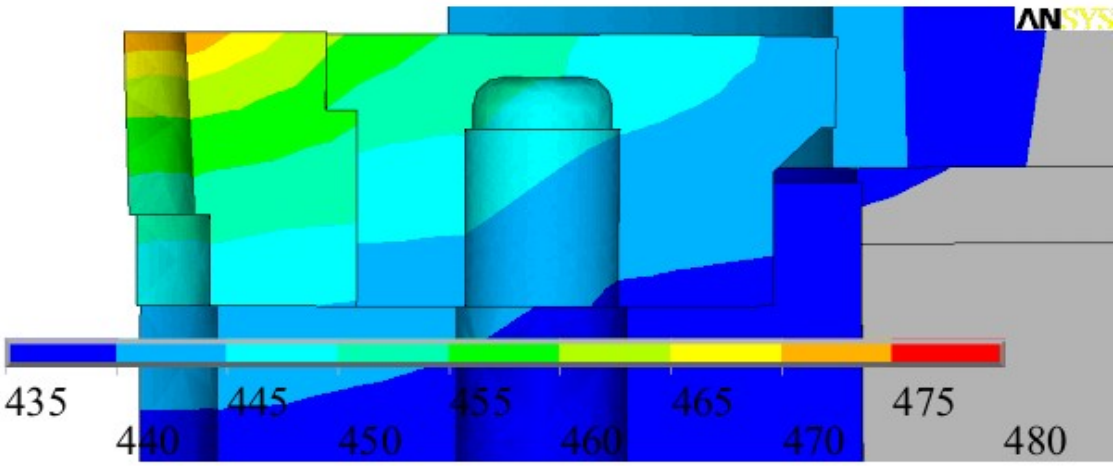

Figure 6.47. Temperature distribution at end of extrusion – case 6. The distribution is highly non-uniform. The experiment was run at profile velocity (800 mm/s). The calculation has been performed with a coupled ANSYS® 7.1 and ALMA2π flow model (Chapter 3). The material data that have been used may be inaccurate (±10 %).

ALMA2π flow calculations (Chapter 3) and experimental results have also shown that the sensor disc and die temperatures may increase by 30 to 50 ºC. The temperature field is not uniform. Figure 6.47 shows that the temperature is highest close to the source of heat, the die outlet. The temperature of the capacitive probe may also be estimated. However, the closeness of contact between the die, probe holder and probe is not known and may be a cause of heat transfer coefficient variability. In any case, the temperature of the probe changes much slower than the temperature of the die. The heat transfer from the die to the probe by convection through air or radiation is insignificant. Thus, the heat mainly flows through the probe holder and into the probe.

6.4.2 A description of various types of thermal effects

One should distinguish the temperature effects that are related to the thermo-mechanical response of the sensor from the effects related to the temperature sensitivity of the capacitive probe. The thermo-mechanical response of the sensor is usually the most significant one. As indicated in Chapter 2, Capacitec reports a temperature sensitivity of only 4 to 6 mV / 10 ºC in the relevant temperature range. This corresponds to deflections of approx 0.2 to 0.3 µm / 10 ºC and pressures of approx 2 to 3 MPa / 10 ºC. The effect may in fact be twice as large, but it is still quite small. The temperature of the probe seldom increases by as much as 10 ºC during measurement.

The thermo-mechanical effect is difficult to analyse due to the complex geometry and the many parts of the sensor and the non-uniform temperature distribution. There are two main causes of the thermo-mechanical effect, thermal expansion and temperature dependent material properties (elasticity modulus). It should be noted, however, that if the sensor has not been properly designed, connections may loosen during either heating or loading. Furthermore, when a material is heated, plastic properties are also altered. There may be stress relaxation. Even if a first run with overloading has been performed, there may be additional and undesirable plastic deformations during later cycles. It is always relevant to evaluate plastic effects for sensors that must work in the high-temperature surroundings of the extrusion process, but it is believed that the sensors of the current study have been designed and tested so that permanent deformations are largely avoided during extrusion experiments [Moe03b]. Plastic deformation of a more fragile sensor exposed to larger loads has been evaluated in [Moe04d].

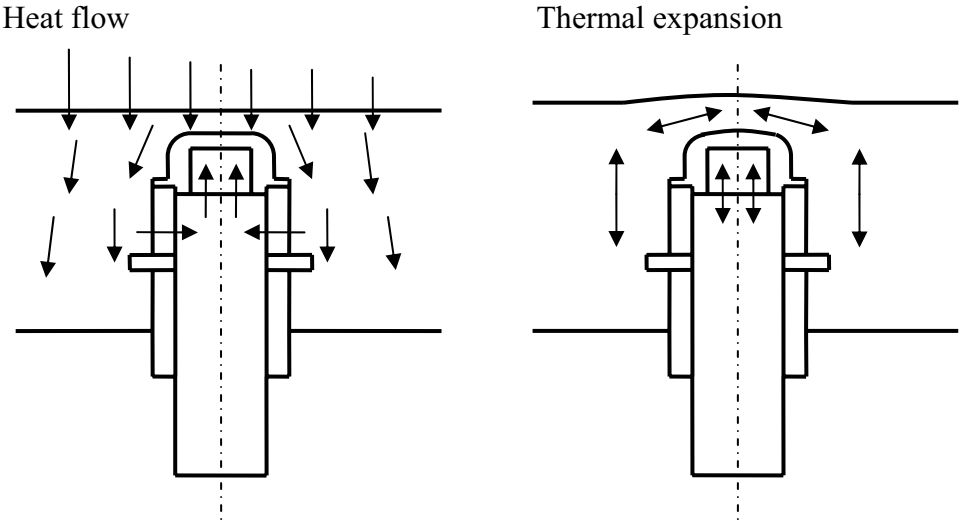

Figure 6.48. The principal mechanisms of thermal expansion during extrusion.

Figure 6.48 indicates that there are three aspects of thermal expansion that should be considered. First, there is the pure elongation of the die and consequently sensor cavity in the extrusion direction. The magnitude of the elongation is different for the two sensor mounting solutions. Sensor 1 is connected to the die quite close to the sensor disc

(3 mm), while the distance from the connection point to the disc is 9 mm for sensors 2 and 3. Figure 6.49 shows how the temperature effects may differ for the two sensor designs. The second issue that must be treated by the model is the thermal expansion of the probe. The probe is made of an Inconel® alloy with thermal expansion properties not very different from those of steel [HigW]. There are, however, insulation materials whose properties are also not known. More importantly, the actual temperature of the probe is not exactly known during measurement. Temperatures were measured in the die and close to the probe. In other experiments, the temperature of the probe holder was determined. However, accurate measurements are hard to perform. There are two extreme cases. One may either assume that the probe is not affected by the temperature changes or that it is at the same temperature as the surrounding die material. The expansion is in the latter case similar to that of the die (Figure 6.49). An assessment of the two possibilities is included in the presentation of experimental results.

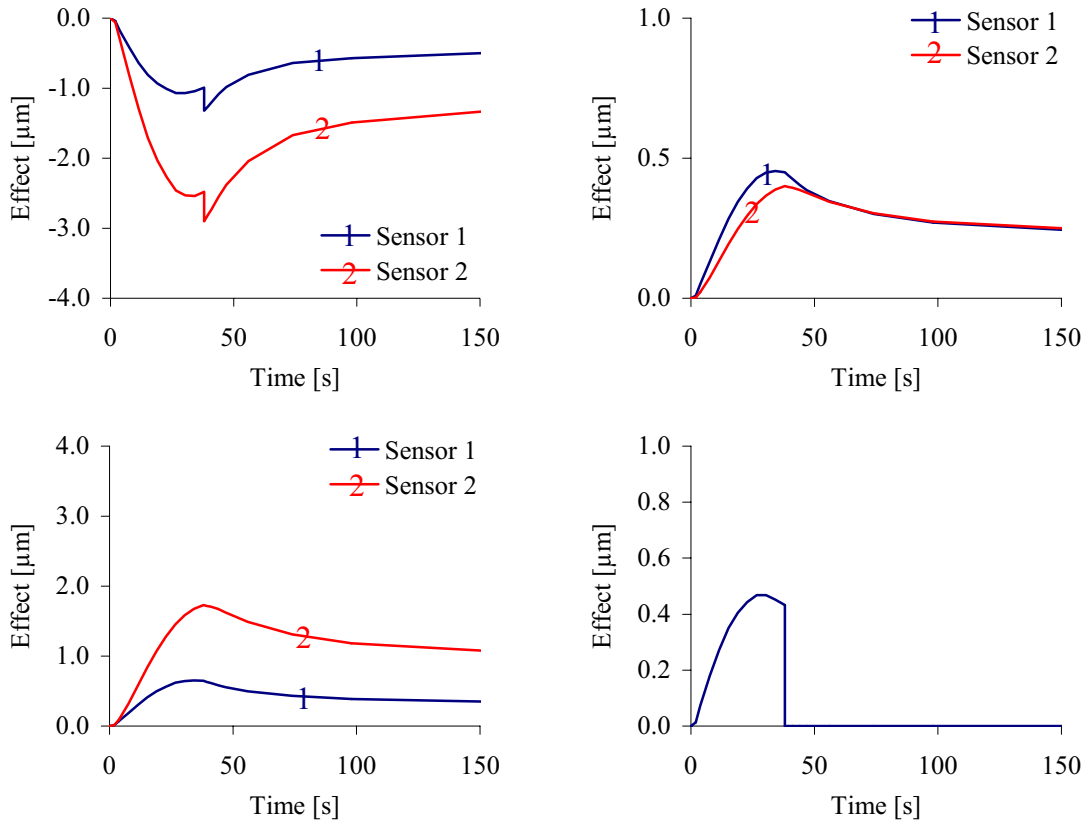

Figure 6.49. The various effects of thermal sensor response (ALMA2π and ANSYS®).
Upper left figure: The total thermo-mechanical response
Upper right figure: The effect of electromagnetic property changes.
Lower left figure: The thermal expansion of the probe
Lower right figure: The effect of changes of the elastic disc properties

The last part of the thermal expansion effect is a slight upwards bending of the sensor disc during measurement. During extrusion, the sensor disc temperature is higher than the temperature of the surrounding die. The reason is that the heat from the billet cannot effectively be transported in the extrusion direction. It has to be transferred sideways.

As a result, the disc expands more than the rest of the die and bulges upwards. During cooling after extrusion an opposite effect may be expected. Figure 6.49 does not present the bending effects. They are integral parts of the total thermal sensor deformation.

The effect that temperature has on the elastic modulus appears in two curves of Figure 6.49. First, directly after unloading there is an increase in the magnitude of the total thermal response of the sensor. The effect that concerns the elastic modulus is only relevant as long as there is an externally applied load. When extrusion ends, the load is relaxed and the disc springs back. The curve showing the thermal effect as a function of time is based on approximate temperature data. Similar curves that have been calculated for cases of materials with and without temperature-dependent elastic properties are presented in [Moe04c]. When the pressure is in the range from 200 to 300 MPa, the temperature effects should cause disc deformations larger than 0.5 µm. Note that all property-related effects work in a direction opposite to that of the pure thermal expansion effect. The thermal expansion makes it appear as if the disc deflection is somewhat smaller than it really is. The indicated pressure is therefore too low.

The curves of Figure 6.49 have been calculated with the finite element code ANSYS® as described in Chapter 3. Thermal loads from ALMA2π have been applied at the upper die face. A uniform pressure of 200 MPa has also been applied in order to provoke the thermal effect related to temperature-dependent material properties. There are large uncertainties related to the flow of heat from the billet to the die after extrusion. Rather rough assumptions have been made. There is no more heat generation in the billet, but the butt end is at an elevated temperature. However, the billet is in close contact with the colder dummy block, and the assembly looses heat to the surrounding air after the ram is retracted. In the current study a simplification has been made, and it has been assumed that there is only forced convection to air after extrusion. Experimental and simulated results for the cooling phase should be carefully assessed.

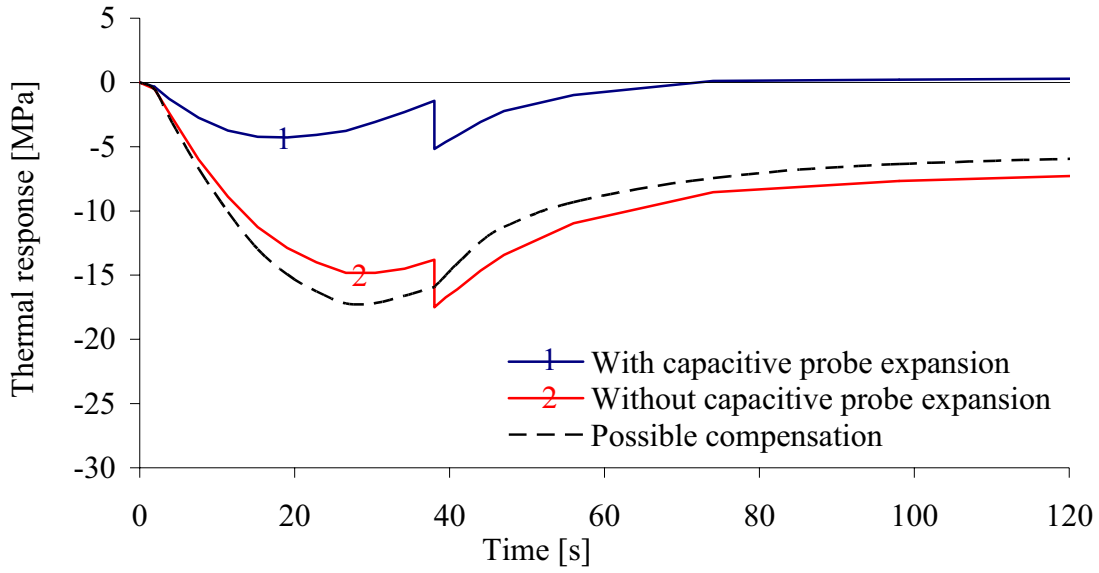

Figure 6.50. The simulated temperature effect – the effects are weighted averages of the responses of sensors 1 and 2 for case 1 (profile speed: 200 mm/s).

Figure 6.50 and Figure 6.51 present estimated temperature effects for cases of low- and high-rate extrusion (outlet velocity 200 and 800 mm/s). One of the curves of each figure has been calculated with the assumption that the capacitive probe expands during measurement. The other curve includes no such expansion since it is assumed that the temperature of the probe changes very little. Both curves assume that there is an effect of changes in the electromagnetic properties of the probes. The effect is probably in all cases exaggerated, since it is based on the temperatures of the bottom side of the sensor disc rather than of the probe. The error is greatest in the early parts of the run, but should never correspond to a pressure effect larger than 5 to 6 MPa. The error is probably largest if extrusion is performed at high rate.

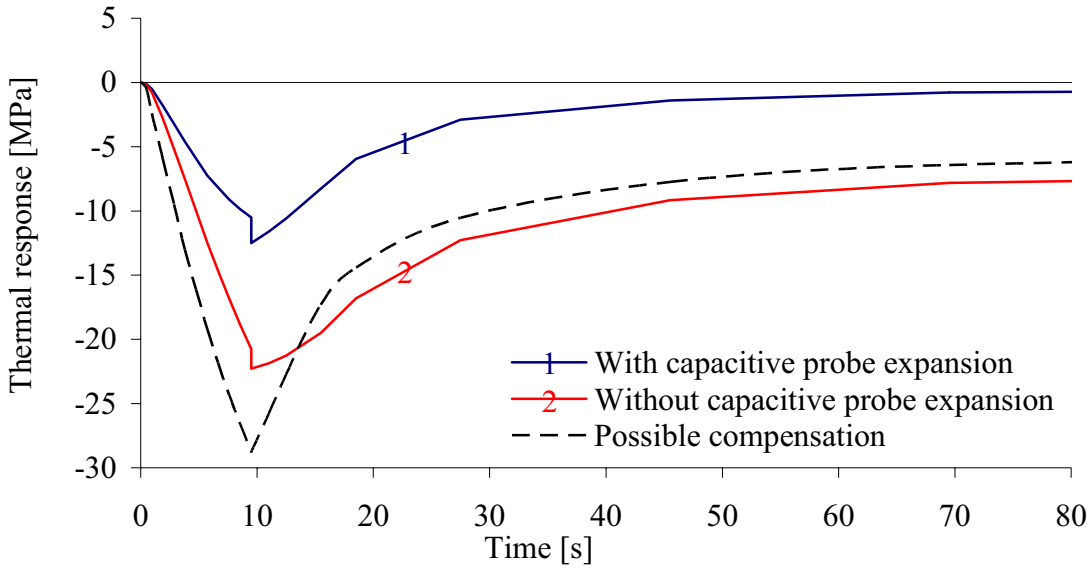

Figure 6.51. The simulated temperature effect – the effects are weighted averages of the responses of sensors 1 and 2 for case 6 (profile speed: 800 mm/s).

Possible compensation curves are also proposed in the Figure 6.50 and Figure 6.51. The curves are based on single temperature measurements at the bottom point of the sensor disc. It is assumed that only the die deforms by more or less uniform expansion over the distance from the bottom of the sensor disc to the point where the sensors are fixed. The temperature expansion of the probe and electromagnetic effects are disregarded. Also overlooked is the fact that the temperature at the bottom face of the sensor disc may be artificially high, especially if extrusion is performed at a high rate and there are large temperature gradients. Still, the compensation curve is a relatively good approximation for the thermal effect curve based on a more accurate analysis. The advantage of the compensation approach is that it is easy to use and based on inputs that may be easily gathered on-line. The temperature change at different distances from the die surface was measured continuously during experiments. Note that the curves in Figure 6.50 and Figure 6.51 and all other similar curves presented in this section are based on average values for all three sensors. The temperature effect of sensor 1 is smaller than that of sensors 2 and 3, since much of the difference in thermal expansion of the die and probe is not included in the measurement. However, only average values of pressure have been studied, and the temperature effect is here treated in a similar way.

6.4.3 A comparison of calculated and simulated data

The aim of the current sub-section is to evaluate the quality of the simulated thermal responses and the temperature compensation technique in two ways. Measurement results (die face pressure and ram and liner force based estimate) from some individual cases are first compared with the corresponding calculated results. An evaluation of the quality and usefulness of the compensation curves is then performed. It is based on both the study of all absolute values of data and on the study of effects presented in the previous sub-section.

Figure 6.52 and Figure 6.54 show experimental and numerical results from extrusion performed at relatively low velocity (200 mm/s). Figure 6.53 and Figure 6.55 show similar results for high-velocity cases (800 mm/s). The data were recorded for two levels of the initial billet temperature (450 and 500 ºC). The calculated curves are based on the assumption that the capacitive probe temperature does not change. The main reason why the sensor output deviates from zero after unloading is probably the thermal effect. The thermal effect is most likely also the major cause of the systematic deviation between curves of directly measured and estimated die face pressure. Note that there are sensor responses related to the loosening and retraction of the ram after extrusion. It is for that reason not always easy to determine the magnitude of the systematic change due to the temperature or thermal effect. Some important observations should be made.

The temperature effect seems to be larger for low than for high profile velocities. This is also predicted by finite element calculations. The effect of a ram velocity change seems to be underestimated by the finite element model. To some extent, this may be related to erroneous assumptions with regard to the thermal expansion of the capacitive probe and to the capacitive sensor response. The probe temperature increases to a relatively small extent during high-rate extrusion. During low-rate extrusion the temperature change of the probe may be so large that the thermal expansion should be considered. This seems to be particularly important in the later phases of the run. The fact that the sensor response after extrusion in some cases is larger than zero may actually indicate that the changes in the electromagnetic properties of the sensor may be more important than the net thermal expansion effects. The possibility that there are permanent displacements should be evaluated since the sensor mounting solution is imperfect.

In any case, the curves give a proper indication of the time scales of measurement. If extrusion lasts 10 seconds or less, temperature gradients are large and the heating of the probes is moderate. After extrusion, it takes another 10 to 15 seconds to establish more uniform thermal conditions. The relatively small remaining deviation from zero output corresponds to the thermal elongation of the initial gap between the capacitor plates of approx 0.4 mm. When the disc has been heated 50 ºC, the effect should be smaller than $50\ \mathrm{K} \cdot 12 \cdot 10^{-6}\ \mathrm{K}^{-1} \cdot 400\ \mu\mathrm{m} = 0.24\ \mu\mathrm{m}$. The pressure effect is in such a case approx 2 to 3 MPa. The thermal expansion effect is smaller than the effect related to electromagnetic properties. Sometimes the pressure response of the sensor is also larger than +10 MPa. Permanent deformations and capacitive probes with an artificially large sensitivity to temperature changes are possible causes. However, there may also be an inverse sensor bending effect. If the tool surface is cooled quickly after extrusion the disc may in fact contract and consequently bend slightly downwards.

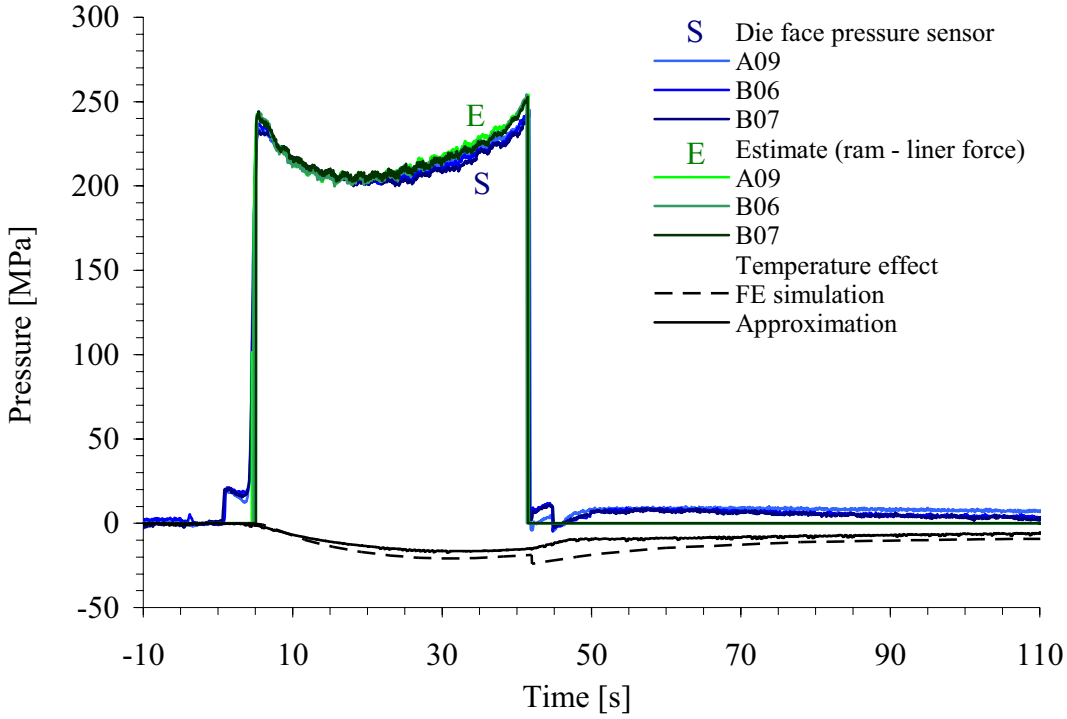

Figure 6.52. The die face pressure – average non-corrected results from case 1. Simulated and estimated temperature effect curves have been added.

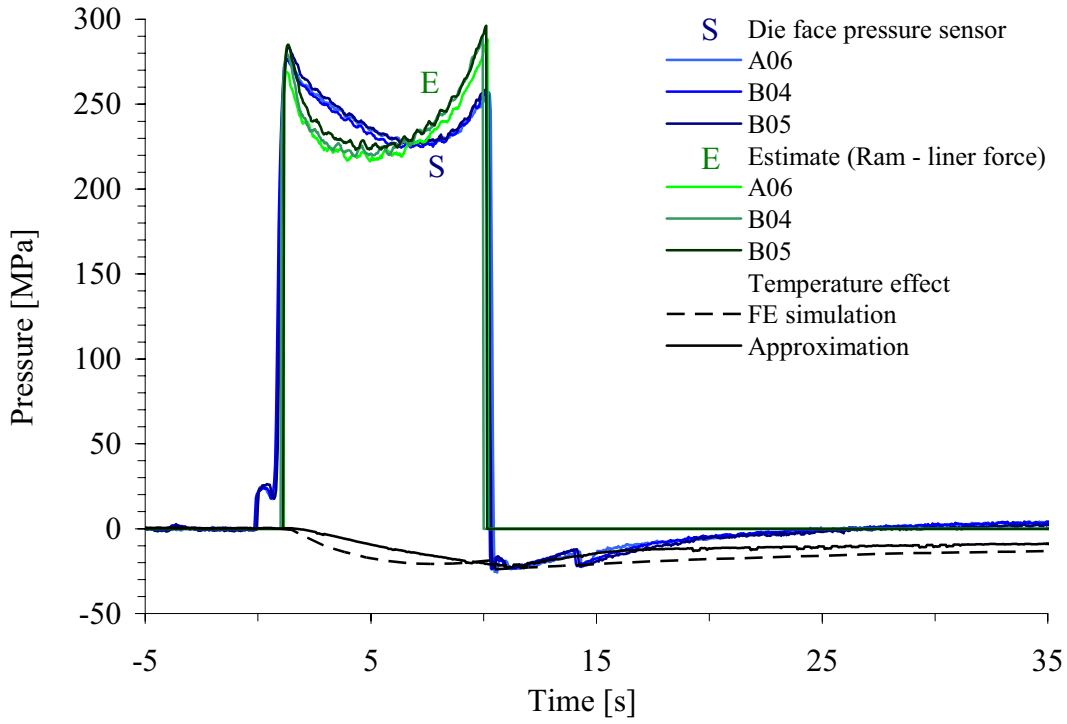

Figure 6.53. The die face pressure – average non-corrected results from case 3. Simulated and estimated temperature effect curves have been added.

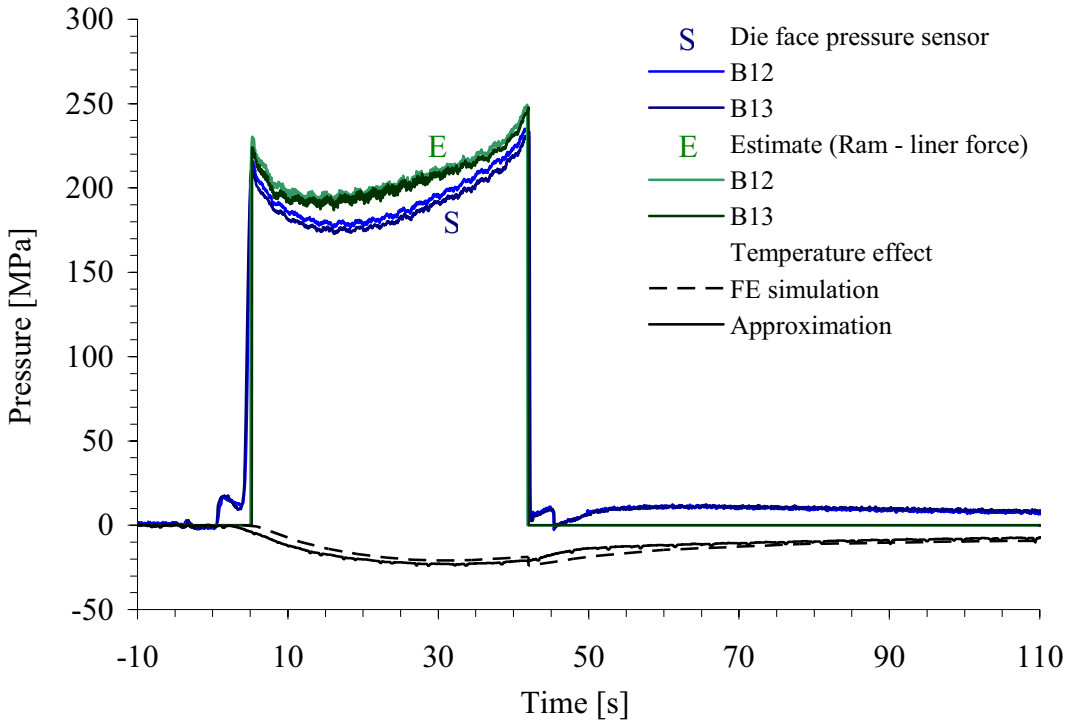

Figure 6.54. The die face pressure – average non-corrected results from case 4. Simulated and estimated temperature effect curves have been added.

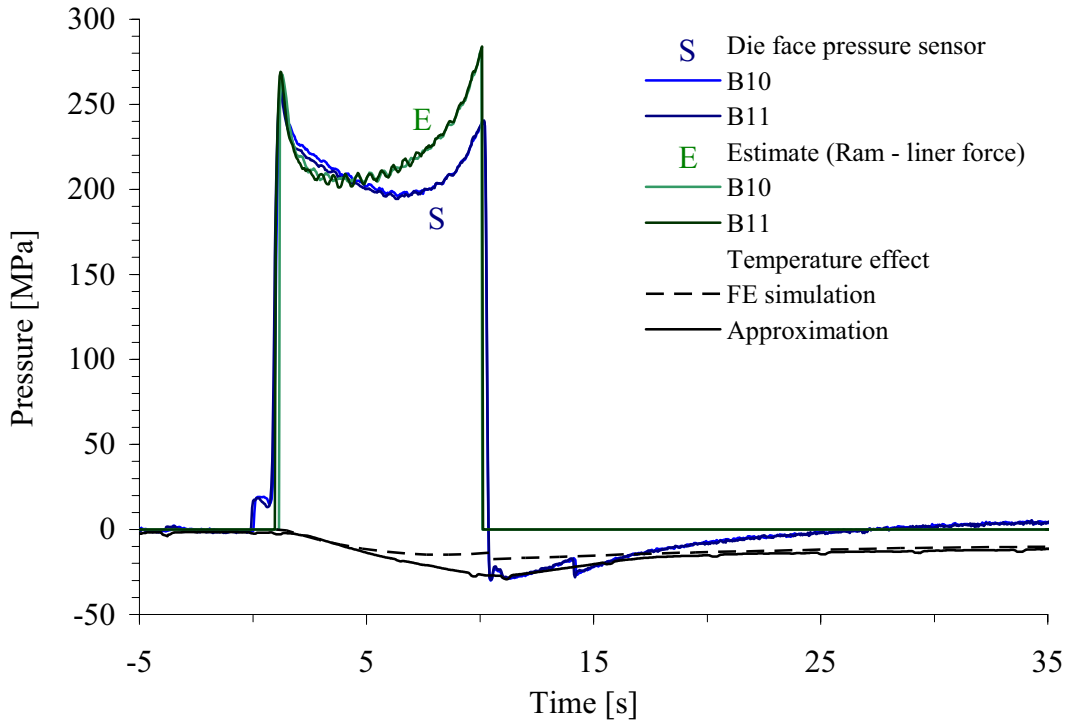

Figure 6.55. The die face pressure – average non-corrected results from case 6. Simulated and estimated temperature effect curves have been added.

The inability of the simulation to describe the cooling phase after extrusion should be expected and should probably not be regarded as a weakness of the model as a whole. The boundary conditions during the cooling phase have not been properly defined. A general conclusion from the finite element analysis is that a more refined model is needed to reproduce the temperature effects observed, particularly after extrusion. It is also necessary to more closely study the thermal effects experimentally. The variability in results is excessive. The fact that the approximate estimate of the temperature effect based on temperature measurement seems to be in better agreement with the output from sensor than the estimates based on the more exact models is probably incidental.

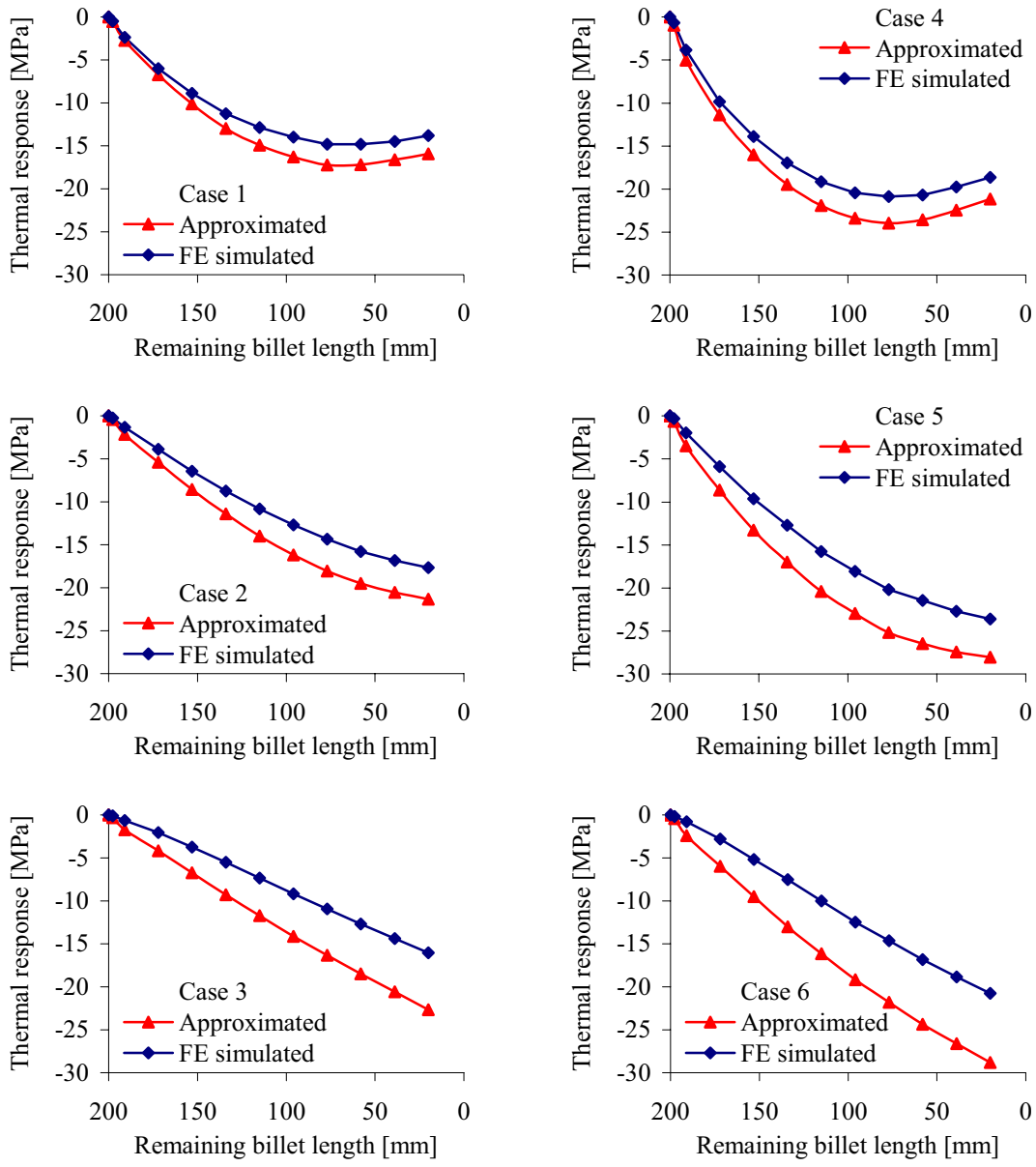

Figure 6.56. The pressure compensation curves for cases 1 to 6. The approximated curves are based on simulated temperature data from the sensor disc.

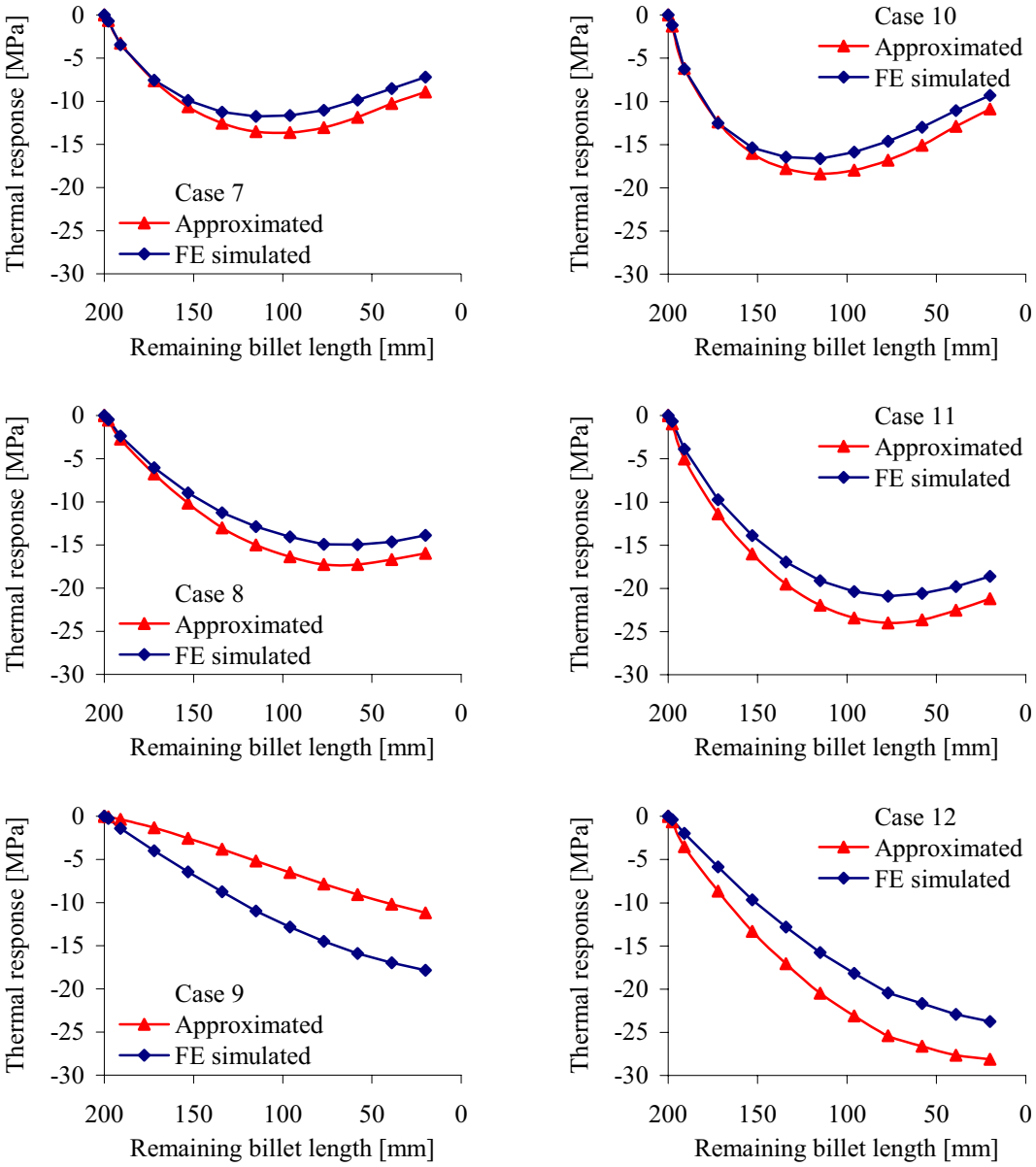

Figure 6.57. The pressure compensation curves for cases 6 to 12. The approximated curves are based on simulated temperature data from the sensor disc.

The second evaluation approach consists of applying the sensor compensation based on finite element calculations to modify sensor output results. The modified results are then compared with force-based estimates and pressure estimates obtained from ALMA2π. Both absolute values and effects are considered. Figure 6.56 and Figure 6.57 present the compensation curves as well as approximate curves based on temperature data. The figures have been positioned so that it is possible to directly compare the effects of initial billet temperature and profile velocity. When extrusion is performed at low-rate, temperature differences are smaller towards the end of the runs. The finite element simulation and the rough approximation produce thermal effects of similar magnitude. In [Moe04c] compensation has been performed with the data from the approximation.

6.4.4 An evaluation of temperature compensated data

Temperature compensation may be performed by subtracting the calculated values of the temperature response (negative values) from the measurement data. The temperature compensation curves for cases 1 to 12 have also been used for cases 13 to 24. The addition of a bearing channel did not significantly affect the temperature of the pressure sensor. The pressure data have also been temperature compensated in another sense. As calibration was generally performed at a temperature some 10 to 20 ºC lower than at the onset of extrusion, compensation should be performed for the elastic modulus change. The modulus decreases by approximately 2 GPa or 1 % per 10 ºC [UddW]. During measurement die face pressures were initially 1 % lower than indicated by the raw data.

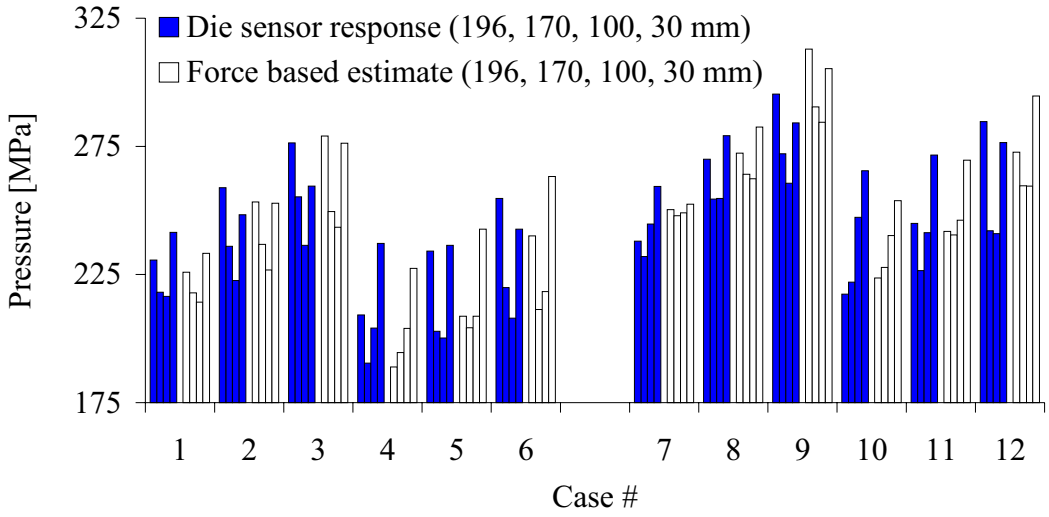

Figure 6.58. The die face pressure – a comparison of temperature compensated data and estimated results based on ram and liner force measurements.

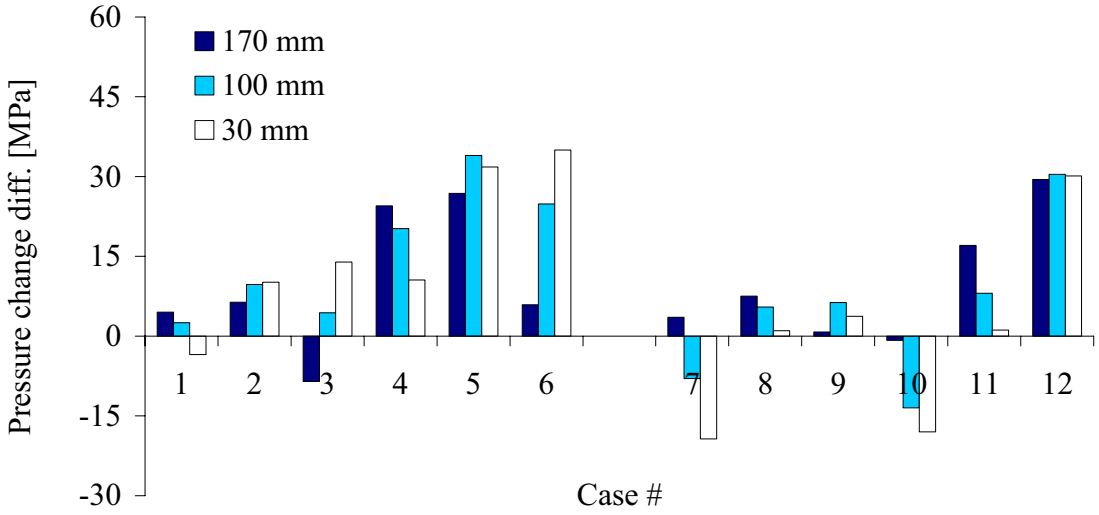

Figure 6.59. Directly measured change minus estimated force-based pressure change $(dP_{170})^{exp} - (dP_{170})^{est}$ – temperature corrected data and estimated results based on ram and liner force data.

Figure 6.58 and Figure 6.59 are of the same type as Figure 6.45 and Figure 6.46. The temperature modification has reduced the deviation between the directly measured and estimated pressure differences. The compensation again seems to be less satisfactory at high temperatures and profile velocity. In order to assess whether the modified results are in better agreement with the flow simulation, similar figures showing differences in pressure changes for both measured and simulated results are introduced. The pressure change differences before and after modification are presented in Figure 6.60 and Figure 6.61. The same trend towards an improvement of results is observed.

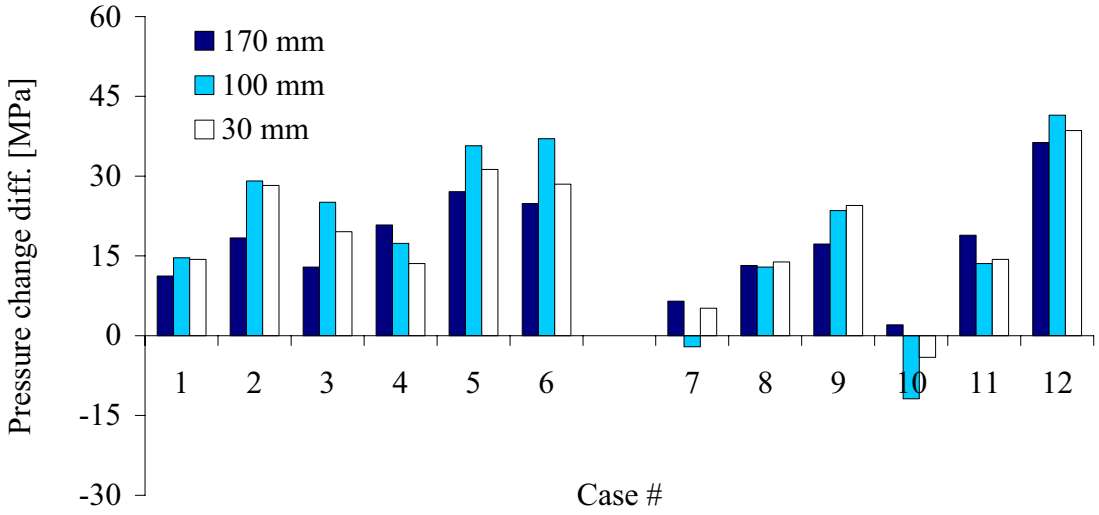

Figure 6.60. Directly measured change minus simulated (ALMA2π) die face pressure change $(dP_{170})^{exp}$ – $(dP_{170})^{sim}$ – a closer comparison of non-corrected experimental data and simulated results.

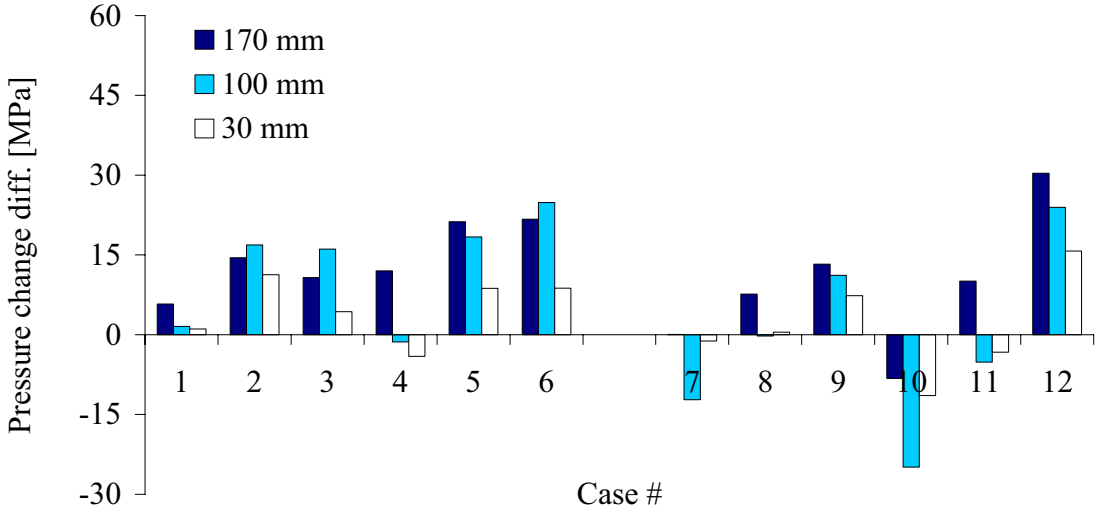

Figure 6.61. Directly measured change minus simulated (ALMA2π) die face pressure change $(dP_{170})^{exp}$ – $(dP_{170})^{sim}$ – a comparison of temperature compensated data and simulated results.

Figure 6.62, Figure 6.63 and Figure 6.64 provide information about the average values and effects of input data changes for the temperature compensated pressure values. The average values of the temperature compensated die face pressure data do not differ significantly from the simulated data. There may be an exception for billet length 196 mm. The estimated values are too low for billet lengths of 170 and 100 mm. There may be systematic errors that cause the estimated pressure to be too low in general. The differences are not large. A pressure of 10 MPa corresponds to a disc deflection only of approximately 1 µm. The effects calculated on the basis of the modified pressure data do not differ significantly from the effects based on raw data. Thus, the conclusions from the previous section may still be regarded as relevant. Note again that the main effects *B** (extrusion ratio) differ, as calculated from the measured and simulated data. The deviation may be attributed to blocking, because the temperature compensation has not reduced systematic errors related to the variability in the calibration procedure.

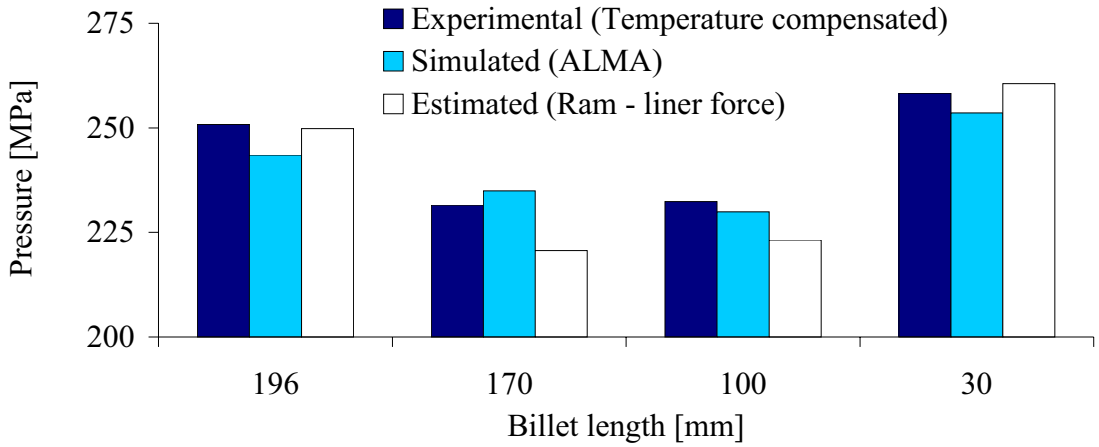

Figure 6.62. The average values of the temperature compensated die face pressure – experimental, estimated and simulated data for cases 1 to 12.

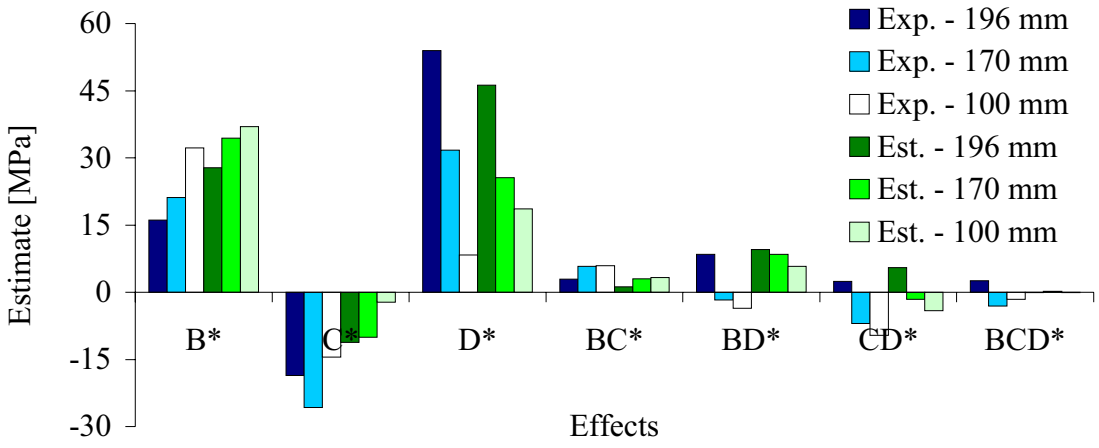

Figure 6.63. The temperature compensated die face pressure – the effects of parameter changes. Experimental and estimated data for cases 1 to 12.

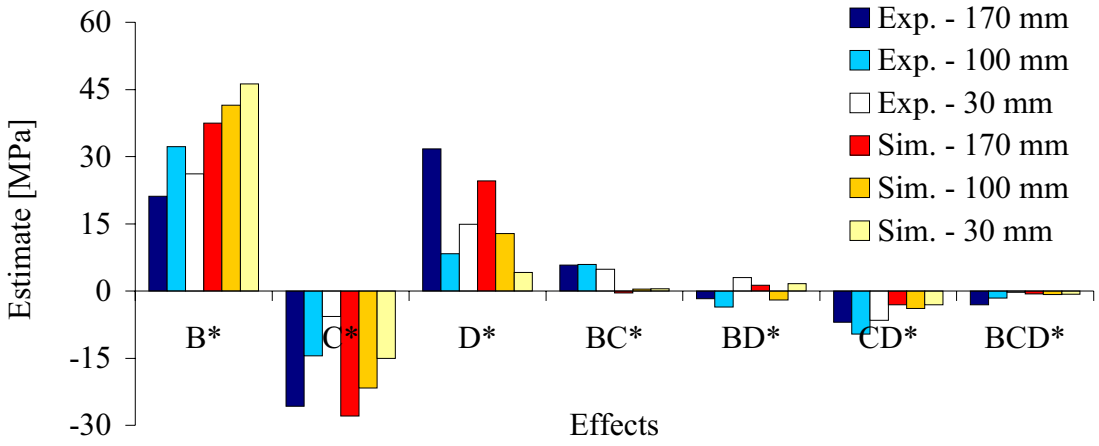

Figure 6.64. The temperature compensated die face pressure – the effects of parameter changes. Experimental and simulated data for cases 1 to 12.

The temperature compensated pressure measurement data and pressure estimates from ALMA2π are further compared in Figure 6.65. Only zero bearing length cases (1 to 12) are treated. The figure is similar to Figure 6.19. The measured results from days A and B are now systematically too high, while the measured results from day C are too low. This explains why the average error is very small, and why the main extrusion ratio effect, B*, differs for the measured and simulated cases. The error is here defined as the deviation between the measured and estimated values.

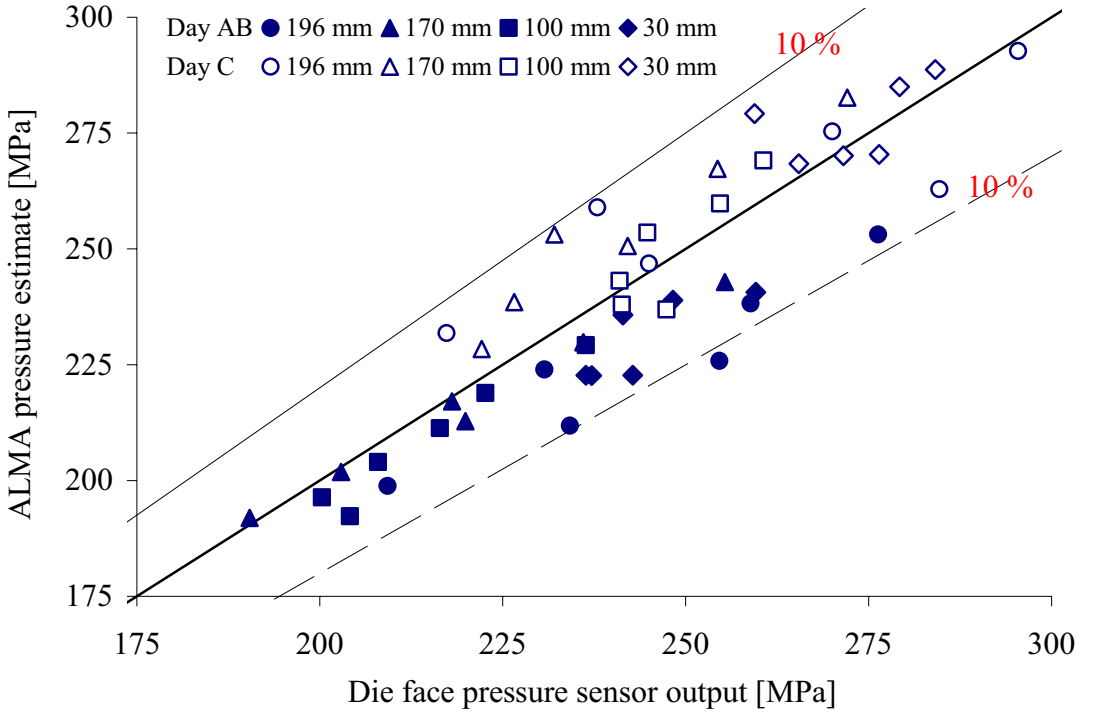

Figure 6.65. A comparison of ALMA2π die face pressure estimates and temperature compensated averaged data from all pressure sensors (cases 1 to 12).

Table 6.11. Average values and standard deviation of measured minus simulated values

	Average values [MPa]					Standard deviation [MPa]				
Pos [mm]	196	170	100	30	ALL	196	170	100	30	ALL
Measured values										
Day AB	20.4	1.2	-6.1	-2.2	10.7	9.0	8.2	4.0	5.5	6.1
Day C	-1.8	-17.5	-14.7	-17.2	-5.2	15.6	5.4	5.9	4.9	8.1
Day ABC	9.3	-8.1	-10.4	-9.7	2.7	16.8	11.7	6.6	9.2	10.0
Measured and temperature compensated values										
Day AB	18.7	4.4	6.0	13.7	3.3	8.4	5.2	3.1	5.5	6.5
Day C	-3.0	-11.9	-1.8	-4.3	-12.8	14.9	5.1	7.5	8.8	5.2
Day ABC	7.8	-3.7	2.1	4.7	-4.7	16.2	9.8	6.8	11.7	9.2

Table 6.11 presents the main statistics for the error, based on both corrected and non-corrected data. The measurement data still seem to indicate a pressure that was too high for a billet height of 30 mm after temperature compensation. Furthermore, there is no significant reduction in the absolute values and the standard deviations for the errors. The errors are, however, relatively small for the measurement data that have not been edited, and there are limits to the size of the improvements that may be achieved. The standard deviation for all error data is significantly larger than the standard deviation for replicate measurements (10 MPa vs. 6.4 MPa). This is partly due to the temperature effect, for which no completely satisfactory compensation has been introduced. The data for billet height 196 mm have not been included in the estimates of the overall average and standard deviations of the errors.

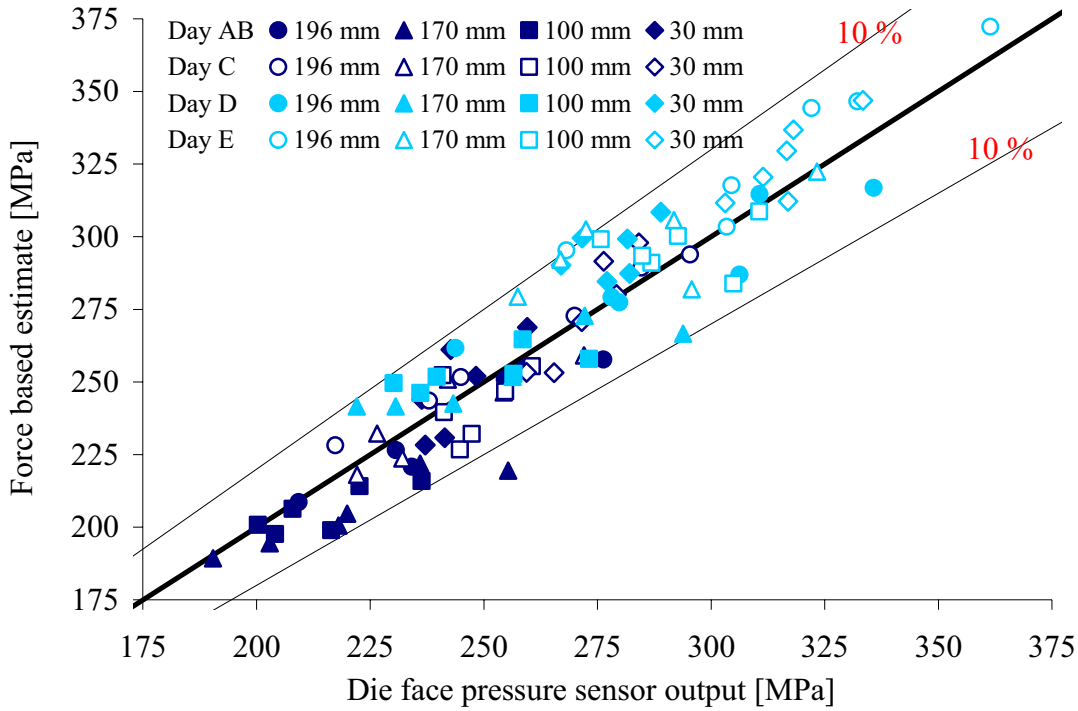

Figure 6.66. A comparison of force based estimates of the die face pressure and the temperature compensated averaged data from all pressure sensors. Cases 1 to 24 are evaluated at billet heights 196, 170, 100 and 30 mm.

The improvements due to temperature compensation are more obvious when the data are compared with the ram and liner force based pressure estimates. Thus, Figure 6.66 may be compared with Figure 6.21. The systematic errors related to calibration are still present, but the temperature compensation has brought the values recorded at billet heights of 100 and 30 mm closer to the proportionality line. Deviations between measurement and model are smaller than 10 % even for the data from day E. Table 6.12 gives a further indication of the improvements both to the accuracy and variability.

Table 6.12. Average values and standard deviation of measured minus estimated values

	Average values [MPa]					Standard deviation [MPa]				
Pos [mm]	196	170	100	30	ALL	196	170	100	30	ALL
Measured values										
Day AB	9.2	12.2	-3.0	-19.1	-0.2	7.4	14.3	11.4	12.7	16.7
Day C	-3.6	-2.4	-6.8	-14.7	-6.9	5.1	10.1	12.8	15.8	11.9
Day ABC	2.8	4.9	-4.9	-16.9	-3.5	9.0	14.0	11.7	13.9	14.7
Measured and temperature compensated values										
Day AB	7.5	15.4	9.0	-3.2	7.2	6.9	11.6	8.4	11.2	11.4
Day C	-4.8	3.2	6.1	-1.8	0.7	4.1	8.5	10.5	10.8	9.4
Day ABC	1.3	9.3	7.6	-2.5	3.9	8.4	11.6	9.2	10.5	10.8

6.5 Final remarks on the main observations of the study

The objective of the current section has been to estimate the accuracy and repeatability of the pressure measurement. Also the potential usefulness of the sensors was evaluated. The most important findings are here restated, and they are linked to a more general evaluation. Comments on both the resolution and the reliability of the approach are also provided.

The accuracy of the technique cannot be exactly determined, as the exact pressure at the die face during extrusion is never known. Two alternative semi-independent techniques for estimating the die face pressure have been used, finite element flow simulation and load difference measurement. The accuracy of the material flow simulation may be evaluated by comparing estimates of ram force with actual measured values. The systematic error in the force estimates of the simulation code is usually smaller than 5 %, but there is also a significant amount of scatter in results (± 5 % or approx ± 125 kN from the average value). The accuracy of the force measurement itself is not better than ± 50 kN. Reproduction of measurements should be possible within $\pm 3\sigma = \pm 50$ kN. The corresponding die face pressure of approx ± 6.4 MPa represents the absolute minimum accuracy and repeatability of pressure measurement in the current study. The reason is that the ram force measurements have been used during calibration of the pressure sensors. The variability of the calibration data is in practice significantly larger than the lower limit. The standard deviation (σ) of the calibration data from a single round of experiments and for one sensor is approx 6 MPa. Only five rounds of experiments have been performed with pressure sensors that were calibrated by on-line hydrostatic compression. In each of the experimental rounds three sensors were used to perform genuinely replicated measurements of pressure. Since there are so few independent measurements, very accurate estimates of the repeatability of measurement for genuine replications have not been produced. The repeatability of measurement also depends on the sensor design.

When the ram and liner force measurements are used to estimate the die face pressure during extrusion, further errors of systematic nature may be introduced. As a result the estimates of the alternative die face pressure measurement techniques may deviate from the actual die face pressure by 5 or even 10 % of the full scale pressure (200-300 MPa). It is known that the computer simulation produces poor estimates of force at the first measurement point (196 mm), while the force-based estimate is probably not acceptable at low billet heights (30 mm). The two estimates generally differ by less than 20 MPa or 10 % of full scale at the other measurement points (170 and 100 mm). Thus, even if measurements were performed very accurately, the verification approach cannot be used to demonstrate that the accuracy of measurement is much better than 10 % of full scale. Both measurement results from the individual pressure sensors and averages of all sensor outputs generally deviate by less than 10 % from estimated and simulated results. Systematic errors are believed to be smaller than 10 % of full scale (20 MPa), but there is also a significant amount of scatter. In order to bring the responses of the pressure sensors in acceptable agreement with the pressure estimates, temperature compensation should be applied. Finite element calculation may be used to assess the thermo-mechanical behaviour of sensors. However, the sensor deformation is quite complex,

and the temperature distribution is seldom exactly known. For that reason, only a model that compensates for approximately half of the thermal effect has been established. It should be added that a not insignificant part of the thermal effect is related to changes in the electromagnetic properties of the capacitive probe and coax cable. The problem has only been studied qualitatively.

The resolution or the capability of the sensor to measure small changes in the die face pressure during a run has not been systematically evaluated. Chapter 5 presents some examples of successful measurement of pressure variations smaller than 5 MPa. It is not known whether such measurements may be accurately reproduced. The resolution of the capacitive sensor system is very high. The resolution of the data logging equipment was a more serious limitation (1 mV / 0.05 μm / 0.5 MPa), but may probably be further improved. However, it is not realistic to expect that valuable information may be deduced from pressure changes smaller than 1 MPa. It is very difficult to avoid unaccounted-for deformations in the sensor that are smaller than 0.1 μm. If the pressure changes occur at a high rate, the dynamic response of the sensor needs to be much more carefully assessed. The capacitive sensor has a low-pass filter that eliminates signals of frequencies higher than 200 Hz. There are, however, limits to how fast the sensor disc and the surrounding viscoplastic medium may respond.

Pressure sensors for the extrusion environment based on capacitance measurements may potentially be extremely reliable. It is important, however, that the probes and cables are satisfactorily protected. Proper mounting of the sensors is important, and design details that prevent overloading from occurring should be evaluated. For example, when too high a pressure is applied, elastic sensor disc movement may be prevented by an edge that arrests it during overloading. In the current study, sensors were mounted and used 15 times. The sensors did not work properly on two of these occasions. In both cases, the reason was improper mounting, and in one of the cases, the error could probably have been spotted at an early stage (even during mounting). The weaknesses of both the die design and the mounting procedures were also the cause of some variability and inaccuracy during measurement. In an industrial high-temperature environment, the use of permanently fixed probes should seriously be considered [Moe04d]. A new insert sensor design with a more satisfactory mounting solution has been presented (Volume I). Further development is possible and has been seriously considered.

Chapter 7

Conclusions

Measurement of the extrusion pressure with Capacitec high-temperature capacitive probes and a deflecting disc construction is feasible. A rod extrusion sensitivity study with three parallel measurements of die face pressure and liner force proved useful for evaluating the sensor characteristics. In most cases, the pressure estimates deviated by less than 10 % from the actual value of pressure. The accuracy is probably better, but this has not been demonstrated. The accuracy of the ram force measurements used in an on-line calibration procedure was within ±50 kN or ± 7 MPa. When the measurements are genuinely replicated, the repeatability is better than ±10 % of full scale of 200 to 300 MPa. In most cases, experiments may also be more accurately repeated. The sample standard deviation of results from different sensors is typically 6 to 7 MPa. When measurements are repeated and no dismantling and recalibration has been done, more accurate reproduction is possible. The sample standard deviation is then in most cases better than 3 MPa. The variability in measurement for genuinely replicated runs is to a large extent related to the accuracy of the on-line calibration technique. Improvements to both this technique and the sensor design may improve both the accuracy and repeatability of measurement. The resolution of measurement is better than 1 MPa, and die face pressure changes as small as approximately 3 MPa have been successfully identified. The sensor system has the potential of being useful. It may be used to evaluate container friction during extrusion as well as to evaluate the nature of material flow and to study deformation related pressure oscillations. It may also be used to assess whether the process is out of control, and it provides information about flow conditions for an on- or off-line actuator system. It may also be used to assess die overloading.

A challenge related to further use of the sensor is that of designing a sensor system that is sufficiently reliable and versatile. A more compact sensor which deforms as one piece is in high demand. Focus should also be on the use of the sensors. The cost needs to be low, and sensors must be used effectively. Sensors should probably be placed in parts that are not as frequently shifted as the dies, and they should be permanently mounted. Better methods of calibration and testing suited for industrial environments should also be developed. Finally, it is important that the use of sensors be combined with the use of flow simulation codes in order to establish a better understanding of the physics of extrusion. The conclusion of Volume I presents a more thorough discussion concerning the objectives for future work.

References

[Abt95] Abtahi S., Friction and interface reactions on the die land in thin-walled extrusion, Doctoral thesis, Norwegian Institute of Technology, Trondheim, 1995.

[Abt96] Abtahi S., Welo T., Støren S., *Interface mechanisms on the bearing surface in extrusion*, Proc. 6th Int. Alu. Extr. Techn. Sem., Chicago (Ill.), 1996, Vol II pp. 125-131.

[Abt03] Personal communication

[Ans00] ANSYS® Inc., Theory Reference – ANSYS® Release 7.1, 2003.

[AnsW] www.ansys.com

[Bax97] Baxter L.K., *Capacitive Sensors – Design and Applications*, IEEE Press, New York, 1997.

[Ber99] Berge J., Varmsmiiing av messing, M.Sc.-thesis, Norwegian University of Science and Technology, 1999.

[Box78] Box G.E.P., Hunter W.G., Hunter J.S., Statistics for Experimenters: An Introduction to Design, Data Analysis and Model Building, Wiley, 1978.

[Cap97] Capacitec Inc., Non-contact displacement standard products catalogue, Ayer, Mass. 1997.

[Cap98] Capacitec Inc., Operation / Maintenance Manual for Series 4000 Capacitec Amplifiers and Rack Accessories, Ayer, Mass. 1998.

[CapW] www.capacitec.com

[Den02] Dennis S., Vajda S., J. Comput Chem, 23 (2002), 1-16.

[Flu94] Fluke Cooperation, Fluke 2640A/2645A NETDAQ® Networked Data Acquisition Unit Users Manual, 1994.

[FluW] www.fluke.com

[Fra96] Fraden J., Handbook of Modern Sensors 2nd ed., Springer-Verlag, New York, 1996.

[Gra92] Grasmo G., Holthe K., Støren S., Valberg H., Flatval R., Hanssen L., Lefstad M., Lohne O., Welo T., Herberg J., Ørsund R., *Modelling of Two-Dimensional Extrusion*, Proc. 5th Int. Alu. Extr. Techn. Sem., Chicago, Ill., 1992, Vol II pp. 367-376.

[Gra95] Grasmo G., Friction and Flow Behaviour in Aluminium Extrusion, Doctoral thesis, Norwegian University of Science and Technology, 1995.

[Han91] Hansen A.W., Temperatursensor Project: Båndstøping EXPOMAT. SINTEF Project Memo 1991-09-27.

[HeiW] www.heidenhein.com

[HigW] www.hightempmetals.com/techdata/hitempInconelX750data.php

[Hol92] Holthe K., Hanssen L., Støren S., *Numerical simulation of the aluminium extrusion process in a series of press cycles*, Proc. NUMIFORM'92, Rotterdam 1992, pp. 611-618.

[Moe02] Moe P.T., S. Støren, *A technique for measuring pressure on the die face during extrusion*, Proc. 5th ESAFORM Conf. on Material Forming, April 2002, Kraków, pp. 463-466.

[Lef93] Lefstad M., Metallurgical Speed Limitations during the Extrusion of AlMgSi-Alloys, Doctoral thesis, University of Trondheim, 1993.

[Lef01a] Lefstad M., Laboratorieprosedyrer for 800-tonns hydraulisk presse ved SINTEF Materialteknologi. SINTEF Project Memo (248011.00) 2001-02-21.

[Lef01b] Lefstad M., Kalibrering av 8MN hydraulisk presse for år 2001, Report STF F24 F01533, SINTEF Materials Technology, Trondheim, Norway.

[Lef01c] Private communication.

[Lef02a] Lefstad M., Moe P.T., Flatval R., Støren S., *Thin strip aluminium extrusion – pressure, temperature and deflection recordings of the extrusion die*, Proc. 5th ESAFORM Conf. on Material Forming, April 2002, Kraków, pp. 471-474.

[Lof02] Lof J., Blokhuis Y., J. Mater. Process. Technol. 122, 2002, pp. 344–354.

[MatW] www.mathworks.com

[Moe03a] Moe P.T., Lange H.I., Hansen A.W., Wajda W., Støren S., *Experiments with die deflection during hot extrusion of hollow profiles*, Proc. 6th ESAFORM Conf. on Material Forming, April 2003, Salerno, pp. 119-122.

[Moe03b] Moe P.T., Lefstad M., Flatval R., Støren S., Intern. J. Forming Processes Vol. 6 (2003), No. 3, pp. 241-270.

[Moe04a] Moe P.T., *An analysis of forge welding of steel rods – Heating phase modeling*, Proc. 7th ESAFORM Conf. on Material Forming, April 2004, Trondheim, pp. 399-402.

[Moe04b] Moe P.T., Wajda W., Szeliga D., Madej L., Pietrzyk M., Støren S., *An Approach for Evaluating Constitutive Models for Hot Aluminium Extrusion – Rod Extrusion of AA6060 as a Case Study*, Proc. Metal Forming 2004, Sept. 2004, Kraków, pp.

[Moe04c] Moe P.T., Wajda W., Støren S., *A study of the thermomechanical response of a die face pressure sensor for hot aluminium extrusion,* Proc. Metal Forming 2004, Sept. 2004, Kraków, pp.

[Moe04d] Moe P.T., Wajda W., Couweleers F., Støren S., *Visions of a system for shape control during thin-strip aluminium extrusion*, Proc. 12th Int. Conf. on Experimental Mechanics, Sept. 2004, Bari, pp. 570-571.

[Pin96] Pinto G.A., Lawhite L.E., Eggleston G., Carr R.B., Frusztajer B.B., Capacitive melt pressure measurement with center mounted electrode post, US Patent 5,492,016, 1996.

[She99] Sheppard T., Extrusion of Aluminium Alloys, Kluwer, 1999.

[Stø03] Støren S., Moe P.T., *Ch 8. Extrusion,* pp. 385-480, In: Totten G.E., Scott MacKenzie D. (Ed.), *Handbook of Aluminium*, Marcel Dekker, 2003, New York.

[Sva89] Svaasand L.O., Elektrisitet og Magnetisme Vol I and II 6th print, Tapir trykk 1989.

[Swa02] Swanson J., Programming in ANSYS, ANSYS 2002 Conference – Professional Development Seminar, Pittsburgh, Pennsylvania, 2002.

[TheW] www.thermocoax.com

[TraW] www.transvalor.com

[TubW] www.tu-berlin.de/fak3/wewi/metallische_werkstoffe/html_ger/Forschung

[Tve97] Tverlid S., Modelling of Friction in the Bearing Channel of Dies for Extrusion of Aluminium Sections, Doctoral thesis, Norwegian University of Science and Technology, 1997.

[UdeW] www.uddeholm.com/utab/pdf/facts/orvar_supreme english_020602.pdf

[Val88] Valberg H., The profile surface formation during the extrusion of metals, Doctoral Thesis, Norwegian Institute of Technology, Trondheim, 1988.

[Val94] Valberg H., Malvik T., *An Experimental Investigation of the Material Flow inside the Bearing Channel in Aluminium Extrusion*, Int. J. Mat. Prod. Techn. 9, 1994, 4/5/6, pp. 428-463.

[Waj03] Wajda W., Moe P.T., Lefstad M., Støren S., *A study of the limits of self-stabilization during extrusion of thin strips*, Proc. 6th ESAFORM Conf. on Material Forming, April 2003, Salerno, pp. 267-270.

[Waj04] Wajda W., Moe P.T., Abtahi S., Støren S., *An evaluation of material behaviour during extrusion of AA6060 rods*, Proc. 7th ESAFORM Conf. on Material Forming, April 2004, Trondheim, pp. 245-248.

[Wal91] Walters F.H., Parker L.R., Morgan S.L., Deming S.N., Sequential Simplex Optimisation, CRC Press, Boca Raton, Florida, 1991.

[Wel96] Welo T., Abtahi S. and Skauvik I., *An Experimental and Numerical Investigation of the Thermo-Mechanical Conditions on the Bearing Surface of Extrusion Dies*, Proc. 6th Int. Al. Extr. Techn. Sem., Chicago (Ill.), 1996, Vol. II pp. 101-106.

[Yon87] Yoneyama T., Hatamura Y., *Development of a die-sensor*. JSME Int. 30(262) 1987, pp. 670-677.

[Yon93] Yoneyama T., Kitagawa M., *Measurement of the contacting stress in extrusion*, Proc. 4th ICTP, Bejing, 1993, Vol II pp. 553-558.